Springer Climate

Chaitanya B. Pande · Kanak N. Moharir · Sudhir Kumar Singh · Quoc Bao Pham · Ahmed Elbeltagi *Editors*

Climate Change Impacts on Natural Resources, Ecosystems and Agricultural Systems

Springer

Springer Climate

Series Editor

John Dodson, Institute of Earth Environment, Chinese Academy of Sciences, Xian, Shaanxi, China

Springer Climate is an interdisciplinary book series dedicated to climate research. This includes climatology, climate change impacts, climate change management, climate change policy, regional climate studies, climate monitoring and modeling, palaeoclimatology etc. The series publishes high quality research for scientists, researchers, students and policy makers. An author/editor questionnaire, instructions for authors and a book proposal form can be obtained from the Publishing Editor. **Now indexed in Scopus® !**

Chaitanya B. Pande
Kanak N. Moharir • Sudhir Kumar Singh
Quoc Bao Pham • Ahmed Elbeltagi
Editors

Climate Change Impacts on Natural Resources, Ecosystems and Agricultural Systems

Springer

Editors
Chaitanya B. Pande
Indian Institute of Tropical
Meteorology (IITM)
Pune, Maharashtra, India

Kanak N. Moharir
Department of Earth Science
Banasthali University
Aliyabad, Rajasthan, India

Sudhir Kumar Singh
K. Banerjee Centre of Atmospheric
and Ocean Studies
University of Allahabad
Allahabad, Uttar Pradesh, India

Quoc Bao Pham
Faculty of Natural Sciences, Institute
of Earth Sciences
University of Silesia in Katowice
Sosnowiec, Poland

Ahmed Elbeltagi
Department of Agricultural Engineering
Mansoura University
Al Manşūrah, Egypt

ISSN 2352-0698 ISSN 2352-0701 (electronic)
Springer Climate
ISBN 978-3-031-19058-2 ISBN 978-3-031-19059-9 (eBook)
https://doi.org/10.1007/978-3-031-19059-9

This Springer imprint is published by the registered company Springer Nature Switzerland AG
The registered company address is: Gewerbestrasse 11, 6330 Cham, Switzerland

Dedicated to my parents

Preface

This book on the impact of climate change on natural resources, landscape and agricultural ecosystems describes the contributing aspects of climate change related to natural resources, soil erosion, irrigation planning, water, landscape, sustainable crop yield agriculture, biomass estimation, problems of climate change and discusses the related resulting mitigation system. Natural resources and agricultural ecosystems include factors from nearby regions where climate change, landscape, and agricultural practices directly or indirectly interface with the water, vegetation, irrigation planning, and ecology present. Changes in climatic situations impact all natural resources, ecology, and landscape of agricultural systems, which can possibly poorly affect their productivity. This book covers the various aspects of soil erosion, soil compaction, soil nutrients, aquifer, water of climate change in respect to vegetation's, crops, pest, water and sustainable yield for the development of the climate change factors and agricultural sector, sustainable development and management for the future. It also focuses on the use of precision techniques, remote sensing, GIS technologies, IoT, and climate-related technology for sustainability of ecology, natural resources, and agricultural area along with the capacity and flexibility of natural resources, ecology, and agricultural societies under climate change. Climate change, natural resources, landscape, irrigation planning, water, sustainable yield, and agricultural ecosystems include both theoretical and applied aspects, and help as guideline information for future research. This is a very important book for researchers, scientists, NGOs, and academicians working in the fields of climate change, environmental sciences, agricultural engineering, remote sensing, natural resources management, GIS, hydrology, soil sciences, agricultural microbiology, plant pathology, and agronomy.

This volume comprises 29 chapters contributed by various researchers, scientists, and professors from around the world. It includes research work by professors, planners, scientists, and research scholars from various universities, international organizations, and institutions of India as well as of other countries. The chapters provide an in-depth analysis of climate change, impact analysis, sustainability of agroecosystems, vulnerability assessment of stakeholders, climate-smart farming, land use and land cover change detection, precision farming, land surface

temperature, flood impact analysis, crop yield, irrigation to mitigate agriculture, and climate change impacts on natural resources, agriculture, and ecosystems.

We sincerely thank Robert Doe, Publishing Editor, Springer, and Fairle T Thattil (Ms.) for their generous assistance, constant support, and patience in finalizing this book.

Pune, Maharashtra, India — Chaitanya B. Pande

Aliyabad, Rajasthan, India — Kanak N. Moharir

Allahabad, Uttar Pradesh, India — Sudhir Kumar Singh

Sosnowiec, Poland — Quoc Bao Pham

Al Manşūrah, Egypt — Ahmed Elbeltagi

Contents

About the Editors

Chaitanya B. Pande (IITM, Pune) received his PhD from Sant Gadge Baba Amravati University, Amravati. He has more than a decade of university, research, and industrial experience. Dr. Pande is a reviewer of *Earth Science Research Journal*, *American Journal of Geophysics, Geochemistry and Geosystems*, *Sustainable Water Resources Management* (Springer journal), *Modeling Earth Systems and Environment* (Springer journal), *Applied Geomatics*, (Springer journal), *Journal of Agriculture Sciences* (Bioinfo Publication), *Applied Water Science* (Springer), *Journal of the Institution of Engineers (India): Series A* (Springer), *Groundwater Sustainable Development* (Elsevier journal), and *Environmental Sustainable Development* (Springer journal). He has published 40 research papers in international journals with Springer, Taylor and Francis, and Elsevier with more than 1280 citations. He has published two books with Springer Nature. He has presented more than 20 research papers in national and international conferences. His research interests include remote sensing, GIS, machine learning, Google Earth Engine, climate change, drone applications, watershed management, hydrological modeling, land use and land cover analysis, groundwater quality, urban planning, hydro-geochemistry, groundwater modeling, geology, hyperspectral remote sensing, remote sensing and GIS application in natural resources management, watershed management, and environmental monitoring and assessment subjects.

Kanak N. Moharir works in the Department of Earth Science, Banasthali University, Aliyabad, Rajasthan. With more than 8 years of teaching and research experience, she has published more than 45 research papers in various national and international journals and has presented 15 research papers in national and international conferences with more than 700 citations. Her research interests include remote sensing, watershed management hydrology, land use and land cover, aquifer mapping, groundwater modeling, hydrogeology, geomorphology, and geology. She is a reviewer of eight Springer journals and other journals.

Sudhir Kumar Singh, PhD, offers basics of remote sensing and GIS, and remote sensing and satellite meteorology courses to MTech students at K. Banerjee Centre of Atmospheric and Ocean Studies, University of Allahabad, Prayagraj, India. He has worked on the application of geochemical and hydrological model (SWAT) to study the impact of land use/land cover change on water quality and quantity of drought-affected river basin. He has opted for a challenge to study land use and land cover in a north-eastern part of Punjab using multi-date satellite data. He has also studied the impact of land use and land cover change on groundwater quality in the Lower Shiwalik hills: remote sensing and GIS-based approach. These studies also have socio-economic and environmental implications in achieving the objectives of sustainability. Sudhir has worked as PI and co-PI funded by University Grants Commission, Department of Science and Technology, New Delhi, India, and Ministry of Earth Sciences, Government of India. He has published his results in peer-reviewed journals with high impact factors. Also, he is part of the BRICS international team studying the impact of land use/land cover and climate change on river basins. His research focuses on remote sensing and geographical information system applications in the environment with special reference to land use/land cover change and water resource management. Sudhir has published more than 167 research papers in international journals with Springer, Elsevier, and Taylor and Francis with more than 5535 citations. He has published two edited books and one reference book. He has worked as an associate editor with the *Arabian Journal of Geoscience* and *Water Science Conservation and Engineering* and has been the guest editor of many leading journals such as Physics, Chemistry and Earth, Remote Sensing and Water.

Quoc Bao Pham obtained his master's and PhD degrees from the Department of Hydraulic and Ocean Engineering, National Cheng Kung University, Taiwan. He has been reviewing for many journals such as *Science of the Total Environment*, *Renewable & Sustainable Energy Reviews*, *Irrigation and Drainages*, *Ain Shams Engineering Journal*, *WATER*, *Stochastic Environmental Research and Risk Assessment*, *Geocarto Internationa*l, *Environmental Science and Research Pollution*, *Natural Hazards*, *Atmosphere* (was also invited to be the topic editor), *Applied Sciences*, *Arabian Journal of Geosciences*, *Alexandria Engineering Journal*, *Remote Sensing Applications: Society and Environment*, *Journal of Environmental Quality*, *Frontiers in Water*, *Acta Geophysica*, and *Journal of Engineering Science & Technology*. He is currently serving as topic editor of *Frontiers in Water* (*Special Issue: Transitional Areas, Interactions, Feedbacks, Cascading Effects and Management Challenges*). He had published more than 60 ISI research papers in international journals with Springer, Taylor and Francis, MDPI, IEEE, Nature, Wiley, and Elsevier with more than 1500 citations. His research interest includes remote sensing, GIS, drought analysis, climate change, watershed management, hydrological modeling, and water quality. Email: phambaoquoc@tdmu.edu.vn.

Ahmed Elbeltagi is a researcher in the Agricultural Engineering Department, Faculty of Agriculture, Mansoura University, Egypt. He obtained his Master of Agricultural Engineering in the use of remote sensing for predicting moisture and nitrogen status for crops and PhD in applications of remote sensing, GIS, and artificial intelligence methods for water management, scheduling, and future planning from Zhejiang University, Hangzhou, China. He is currently serving as a guest editor for a special issue on water pollution and treatment of the *American Journal of Agricultural and Biological Sciences*. Simultaneously, he is serving as an editorial board member of the *Journal of Agricultural Studies*, *American Journal of Agricultural and Biological Sciences*, *Agricultural Water Management*, *Computers and Electronics in Agriculture*, *Advances in Water Resources*, *Journal of Hydrology*, and *Water Resources Management*. Ahmed has published many research papers in various national and international journals in the areas of water footprint, water management, hydrologic modeling – machine learning, deep learning, and GIS and RS techniques.

The original version of the book has been revised. A correction to this book can be found at https://doi.org/10.1007/978-3-031-19059-9_30

Chapter 1
Impact of Climate Change on Livelihood Security and Biodiversity – Issues and Mitigation Strategies

Gyanaranjan Sahoo, Prasannajit Mishra, Afaq Majid Wani, Amita Sharma, Debasis Mishra, Dharitri Patra, Ipsita Mishra, and Monalisa Behera

Abstract Climate change is one of the most pressing issues of our day, posing a threat to the lives and livelihoods of billions of people worldwide. Natural disasters, biodiversity loss, and rising temperatures destroy crops, diminish ecosystems, put livelihoods in jeopardy, and accelerate the spread of fatal diseases. Climate change mixes population trends, migration, and greater urbanisation, putting the most vulnerable people at risk. Climate change is the most important impediment to achieving sustainable development through biodiversity conservation, and it threatens to impoverish millions of people. Species distributions have changed to higher altitudes at a median pace of 11.0 m and 16.9 km per decade to higher latitudes as a result of climate change. As a result, under migration scenarios, extinction rates for 1103 species range from 21–23% with unrestricted migration to 38–52% with no migration. When an environmental change happens on a period shorter than the plant's life, a plastic phenotypic may emerge as a reaction. Phenotypic flexibility, on

G. Sahoo (✉)
Krishi Vigyan Kendra, Odisha University of Agriculture & Technology, Angul, Odisha, India

Extension Education, Odisha University of Agriculture and Technology, Bhubaneswar, Odisha, India

P. Mishra
Extension Education, Odisha University of Agriculture and Technology, Bhubaneswar, Odisha, India

A. M. Wani
Department of Forest Biology and Tree Improvement, Sam Higginbottom University of Agriculture, Technology and Sciences, Prayagraj, Uttar Pradesh, India

A. Sharma
Krishi Vigyan Kendra, Rajmata Vijayaraje Scindhia Krishi Viswa Vidyalaya, Gwalior, Madhya Pradesh, India

D. Mishra · D. Patra · I. Mishra · M. Behera
Krishi Vigyan Kendra, Odisha University of Agriculture & Technology, Angul, Odisha, India

C. B. Pande et al. (eds.), *Climate Change Impacts on Natural Resources, Ecosystems and Agricultural Systems*, Springer Climate,
https://doi.org/10.1007/978-3-031-19059-9_1

the other hand, might protect species against the enduring impacts of climate change. Climate change also has an impact on food security, especially in people and areas that rely on rainfed agriculture. Crops and plants have growth and yield limits that must be respected. As a result, agricultural productivity in Africa alone might plummet by more than 30% by 2050. Climate change is already wreaking havoc on people's lives, especially the impoverished. Because rural people rely on natural resources, their livelihoods are jeopardised by frequent climate change. The impact of climate change on natural resource-based rural livelihoods is anticipated to be uneven and ecosystem resilience will be strengthened as a result of biodiversity conservation, and ecosystems will be better able to deliver critical functions in the face of increasing climate stresses. Moreover, as a consequence of global influence, the warming trend has changed significantly over the years. In addition to ensuring the livelihood security of rural people, a number of adaptation approaches species and ecosystems in a changing climate may be recommended.

Keywords Biodiversity · Climate change · Livelihood security · Mitigation · Rural · Strategies · Sustainable development

Introduction

Global warming has become commonplace, with heads of state, scientists, and environmental activists frequently making dire pronouncements. Extreme weather events, unpredictably changing global weather patterns, epidemics, and devastating infernos are all examples of climate change and the spread of exotic classes of flora and fauna in new regions is undoubtedly changing global climate (Trew and Maclean 2021; Chinnasamy and Srivastava 2021). Changes in weather patterns, according to sceptics of global warming, are a natural component of the Earth's temperature fluctuation, while the majority of scientists say they are most likely as a result of human-caused imbalances in heat-trapping greenhouse gases (GHG) in the atmosphere (Sahoo et al. 2021). Climate change is a worldwide subject that scientists have been concerned about since the nineteenth century, and its effects may still be seen today. Regional Circulation Models (RCM) project the average yearly temperature is anticipated to rise by 1.4 °C by 2030, 2.8 °C by 2060, and 4.7 °C by 2090 (IPCC 2021). Tropical countries have a high reliance on agriculture and related activities for their livelihoods and household economies, making them particularly susceptible to climate change. Climate change might affect food production, resulting in an increase in hunger, poverty, malnutrition, food insecurity, and food availability (IPCC 2019). Coastal subsistence farming is particularly susceptible to heat and water stress, and as a result, growing seasons will be shortened (Ajit et al. 2013; FAO 2019; Pande et al. 2021a; Orimoloye et al. 2022). Because of global warming, rising temperatures are becoming more common and intense, destabilising food prices, and hindering the region's growth and development (Inder et al. 2018). Rapid land usage, ineffective land management, overexploitation, and increased

fossil fuel burning for industrial and residential purposes are all key causes of climate change in tropical countries (Pande et al. 2021b).

The United Nations Framework Convention on Climate Change (UNFCCC) has yet to define what constitutes harmful interference with the climate system as a result of human activity, as well as allowed constraints for ecological implications, food supply, and cost-effective growth (Trew and Maclean 2021). However, arbitrary stabilising limits ranging from 450 ppm to 750 ppm have developed as a result of this. In 1990, the Advisory Group on Greenhouse Gases (AGGG) of the World Meteorological Organization (WMO), the International Council on Science (ICSU), and the United Nations Environment Programme (UNEP) developed two primary temperature indications or verges, each with diverse degrees of hazard (Barnosky et al. 2011). It was claimed that a temperature intensification of more than 1.0 °C higher than before the industrial revolution "may elicit rapid, unpredictable, and nonlinear responses that could lead to extensive ecosystem damage," with the current rise in temperatures of more than 0.1 °C per span. A temperature increase of 2.0 °C was also gritty to be "an upper limit beyond which the odds of severe ecological harm, as well as nonlinear reactions, are expected to rapidly develop." One of the key findings of the IPCC TAR is that global warming would almost certainly result in significant lost revenues in many poor nations, notably in Africa, at all degrees of warming, with these losses increasing as temperatures rise (IPCC 2021). Global temperature and rainfall are anticipated to increase, conferring to the IPCC (2021) statement, and climate change is anticipated to be one of the most noteworthy causes of habitat destruction at all stages over the next 50–100 years, compounding the consequences of prior actions challenges to habitat destruction. Climate change, global warming, economic crises, deforestation, and other factors are all threatening to rural livelihoods. This fact demonstrates the detrimental impact on rural livelihoods, forcing people to relocate to other areas, particularly cities (Ali and Erenstein 2017). People in rural and urban areas may contribute to the creation of a sustainable society by engaging in constructive activities (Brito-Morales et al. 2018). Rural and urban residents should maintain an interdependent connection in which city residents provide specialists to rural areas to educate and train them, while rural residents provide diverse food products to meet the needs of metropolitan society (Midgley and Bond 2015).

"A livelihood comprises the capacities, assets (stores, resources, claims, and access) and activities essential for a means of living," including one of the next interpretations of livelihood by Chambers and Conway. A livelihood is justified if it can withstand and sustainable when it can cope, retain or increase its functions, and provide viable income-generating possibilities (IUCN 2016). Other concerns such as agriculture policy, market conditions, other economic opportunities, other factors and position families with different asset access in a variety of scenarios affecting and complicating their livelihood choices. Diversified strategies in terms of flexibility must be viewed as a wide variety of options for actors with varied resource availability starting points, as well as for the same families over the course of their lifetimes or demographic cycles (Verma 2019). These decision-making processes may also be thought of as a blend of free will and necessity, as well as a duality of

structure vs. agency. Selections are made, but they are frequently "given" or constrained by significant preconditions or constraints (Trull et al. 2018).

Environment alteration, depletion of resources, environmental issues, species extinction, and habitat loss events, sometimes known as the "evil five" biodiversity intimidations, are the primary causes of contemporary biodiversity loss (Brook et al. 2005; Sonwa et al. 2017). The loss of biodiversity has an ecological impact (Gusli et al. 2020), with environmental change being the primary cause. Environmental factors, in combination with other factors, play a vital role in determining how organisms operate and spread. Environmental changes have had and will continue to have a major influence on species distributions, both now and in the future (Fardila et al. 2017). Only a few studies, on the other hand, have directly quantified biodiversity extinctions as a result of climate change. As a consequence, predictions may be able to provide light on the many components of climate change, as well as the dangers to global biodiversity that they pose (IPCC 2020). Despite the difficulty of distinguishing the effects of climate change from those of other multiple impacts for a variety of species, expectations may give insight into climate change's numerous constituents and their concept which refers intimidations to species diversity (Trull et al. 2018). Tubiello and Rosenzweig (2008) provide a paradigm for analysing vulnerability in the agricultural sector based on exposure, sensitivity, and adaptability. Table 1.1 shows the agriculture sector's vulnerability indicators. The exposure relates to biophysical markers, as shown in the Table. Soil and climate (temperature/precipitation), crop calendar, water availability, and yields can all be used as exposure indicators. On the subject of exposure, history and current climatic drifts and inconsistency in Asia reveal that they are often characterised by rising surface air temperatures, which are more prominent during the winter than during the summer (IPCC 2007). Increasing temperature movements have been recorded across Asia's sub-regions. In various places of Asia, the pragmatic rise over the last few decades have ranged from less than 10 °C to 30 °C per century. The increase in surface temperatures is reported to be more dramatic in North Asia. Inter-annual, inter-seasonal, and regional variability in rainfall patterns has been

Table 1.1 Framework for vulnerability criteria

Categories	Vulnerability criteria	Measurement class
Biophysical indicators	Exposure	Soil and climate Crop calendar Water availability and storage Biomass/yield
Agricultural system characteristics	Sensitivity	Land resources Inputs and technology Irrigation share Production
Socio-economic data	Adaptive capacity	Rural welfare Poverty and nutrition Protection and trade Crop insurance

Source: Adapted from Tubiello and Rosenzweig (2008)

documented in Asia in recent decades. It should be noted that annual mean rainfall is dropping in North-East and North China, Pakistan's coastal belts and dry plains, sections of North-East India, Indonesia, the Philippines, and some areas of Japan. Annual mean rainfall, nevertheless, is increasing in Western China, the South-East coast of China, the Changjiang Valley, Bangladesh, the Arabian Peninsula, and the western shores of the Philippines (IPCC 2007). The frequency of more severe rainfall events has increased in many parts of Asia, resulting in significant floods and landslides, although rainfall intensity and total annual precipitation have reduced as a result of changes in extreme climatic events. Global warming, as well as other shocks and perturbations, is critical for the agricultural industry, as well as for individuals seeking to safeguard and improve their livelihoods. Effective climate change adaptation requires adaptive ability, knowledge, and skills, as well as the resilience of livelihoods and alternatives, resources, and access to suitable frameworks (Sahoo and Wani 2020). While farm-level climate change adaptation requires more public- and private-sector expenditure, technology advancements, government initiatives, and insurance schemes all require additional public- and private-sector spending (Brown et al. 2018a, b). Climate change, at its current rate and severity, will almost probably outstrip the ability of a wide range of plants to acclimate to new weather conditions, subsequent in growing loss of habitat (Keith et al. 2008; Loarie et al. 2009; Bellard et al. 2012). In the face of climate change, climate velocity is defined as the rate and direction at which a species must migrate to preserve its current climatic conditions (Brito-Morales et al. 2018). This is seen in Africa, where environmental degradation, climate change, and rapid population growth all pose serious threats, expanding populations have unanticipatedly serious negative effects (Midgley et al. 2002; Barlow et al. 2018). As a result of this transition, a higher environmental issue is in growing market, leading to land use changes and the use of unsustainable species (Sahoo et al. 2020a). Furthermore, these variations have a major impact on biodiversity and ecological processes. This article focuses on how climate change impacts people's livelihoods, as well as biodiversity loss and the strategic actions taken to protect biodiversity and offer livelihood stability for rural people (Ali and Erenstein 2017). Framework for Vulnerability Criteria is shown in Table 1.1.

Influence of Environmental Change

Agriculture may be jeopardised by global climate change, social protection, and subsistence agriculture for a variety of people, including the impoverished in Asian countries. The negative impact on small-scale farmers will be amplified. Farmers, fishermen, and people who rely on the forest for their livelihood, who are already fragile and food insecure, are anticipated to suffer as a result of global climate change (Sahoo et al. 2020a). Farmers may benefit from agriculture adaptation and mitigation. The surviving methods might be useful in developing long-term

adaption strategies. Farmers have a lot of potential to store carbon in the soil provided appropriate legislative reforms are implemented.

The Issue of Water

In agricultural production, water is the most valuable element. Improving rural living conditions necessitates the development of groundwater resources management (Khadri and Pande 2016). Agriculture must contend with urbanisation, water, and industry for water. As previously said, small-scale farmers rely on water more than large-scale farms (Abdisa et al. 2017; Kouadri et al. 2022). The World Health Organization has extra canal water access. Several parts of the Asian country are running out of water. In the future, marginal and small farmers will confront more water-related challenges. As a result, water management will become increasingly important for these farmers (Barrios et al. 2018).

Diversification

Indian diets have shifted away from cereals and towards high-priced items such as milk and meat, as well as vegetables and fruits. Diet diversity in India is mostly due to rising conservatism as a result of rapid urbanisation, rising greater women's participation in employment generation, increased household earnings, and the effect of globalisation (Sahoo et al. 2021). Hi-value goods have bloomed with the rise of the middle class, with the consequences apparent in the increased demand for high-value processed foods (Matata and Adan 2018). In India, there is an increasing demand for non-food grain products. In Asian countries, physical property expenditure on non-cereal food items continues to be relatively high. In rural regions, it is three times higher than grains, while in urban areas, it is almost ten times higher. Fruit and vegetable intake increased the most per capita, followed by edible oils.

Susceptibility and Hazard

There is ample evidence to indicate that the poorest of the poor are exposed to a variety of hazards that might affects people, groups, or entire populations, all of which can have devastating consequences for their livelihoods and well-being. They need greater individual or family exposure to a variety of hazards. (a) Morbid obesity, sickness, accidents, and incapacity are all examples of nutrition disruptions; (b) many people labour in the informal economy, which has a substantial threat of wage stagnation; (c) crop hazards, life cycle dangers, cultural threats, and unique threats for disadvantaged teams are all factors to consider (Barrios et al. 2018). Droughts,

floods, cyclones, structural change policies, and other community risks must also be addressed. These dangers are particularly dangerous for small and marginal farms. Borrowing, asset sales, savings defrayal, family and government help, swelling labour supply, child labour, healthy labour, demand reduction, migration, and so on are some of the household heading processes. To deal with the negative impacts of risks and vulnerabilities, comprehensive social protection programmes are required (Pande and Moharir 2021).

The Impacts on Urban Livelihoods

Climate change affects urban livelihoods in both direct and indirect ways. Urban populations are overly reliant on services like water and electricity being delivered on time. When these amenities are threatened by climate change, city inhabitants are more powerless than their rural counterparts, who can at least dig wells and gather firewood for cooking. Furthermore, reduced/disrupted water and energy supplies have an influence on industrial productivity and profitability; livelihoods based on low-input market gardening, particularly among the urban poor; human health; and overall living standards (Abdisa et al. 2017).

Heavy Rainfall and Floods

Extreme occurrences such as cyclones and the storm surges and inland flooding that accompany them have a significant impact on infrastructure and livelihoods, particularly in the informal sector in metropolitan areas. Flooding caused by cyclones and severe rainfall causes damage to highways, bridges, stores, homes, and other infrastructure (Chen et al. 2011). Floods cause business losses when trade is interrupted, items are lost, and flood and water damage is repaired. Furthermore, strong rains and floods have a negative impact on the informal sector, notably street selling, as they are unable to conduct their enterprises (Sahoo et al. 2019). Their livelihood and food security are frequently reliant on revenue obtained from daily commodity transactions (Brook et al. 2008). Climate change adaptation, as well as other shocks and perturbations, is essential for the agricultural business, as well as for people trying to protect and enhance their livelihoods. Environmental management requires responsiveness, awareness, and competencies, as well as the resilience of incomes and options, resources, and exposure to suitable authorities (Bezabih et al. 2014). Climate change adaptation requires increased public and private sector spending, technological breakthroughs, and legislative reforms, whereas farm-level climate change adaptation provides a range of solutions, including floods and private sector expenditures (Paavola 2004). Agricultural and animal management practices, the usage and control of forests, and a wide range of on-farm and off-farm integrated or globalised survival options, as well as variations in agricultural and animal

management practices, land use and land management, and a range of on-farm and off-farm integrated or a variety of sources of income are all options. People and families are already adjusting to changing climatic circumstances, despite the fact that climate change has yet to be assimilated into mainstream advance strategies in European countries (FAO 2020).

Around 85% of the world's agrarians are smallholder farmers. The preponderance of these people is common in poor countries in South Asia and sub-Saharan Africa, but they also control rural areas of a number of higher-income countries, counting CEEC, Western Balkan countries, and Bosnia and Herzegovina (OECD 2014). These regions are characterised by poverty is pervasive in rural areas, with a significant rural population, widespread poverty, and enormous expanses of low agricultural output due to perpetually declining a limited supply of resources, and a constricted market, and major climate threats. Small-scale farmers are reliant on subsistence farming and existence, and many lack the means and capacity to adapt to climate change's consequences (Sahoo et al. 2020a). Lower agricultural productivity may have an influence on food security, nutrition, income, and happiness. As a result of climate change, farmers will face greater risks and uncertainties. Modern agricultural alterations have a direct and indirect influence on food security, and also income creation and dissemination, and hence farm produce demand (Verma 2019).

Several alternative approaches will be necessary to minimise the intensity of climate change impacts. Both in relation to the perceived socio-economic choices and agricultural increased efficiency. The most significant drivers of adaptation, according to empirical research across disciplines, are resource, institutional, informational, and financial limitations (Rahman and Hickey 2019). Modifications can also be planned (public) or unplanned (private), with the latter dependent on how climate change perspectives are agriculture outcome. Furthermore, due to conflicting social backgrounds and societal goals, independent adaptations will almost likely be insufficient to address the climate change which has the potential to cause damage and even maladaptation (Swaminathan and Kesavan 2012). As a result, policies must "mainstream" climate change response strategy and resource development in order to allow and encourage successful climate change adaptation development and capacity building. Agriculture can acclimatise to climate change through a variety of management approaches and the adoption of new technology. When it comes to adapting and embracing new techniques and technologies, there is no "one-size-fits-all" solution (OECD 2014). Effective variation should be based on appropriate, regional, and empirical data that is regularly changed as a result of fresh research. Because of the scale of climate change and its unpredictability, as well as the ability to respond to these changes, the degree of sustainable adaptation is directly linked to vulnerability, whether for assessment or implementation. Poverty and, as a result, a lack of agility are frequently shaped by restricted access to assets and capacities for earning a living (Abdisa et al. 2017). Unfortunately, depending just on financial resources may exaggerate people's adaptable capacity, and socio-cognitive factors should be included to generate more realistic adaption simulations and societal consequences.

Combined Effect Between Food Security and Climate Change Mitigation

Climate change vindication has never been a vital driver of agricultural activities, and it is unlikely to be in the future. Rural households are plainly uninterested in carbon sequestration on farms for climate change mitigation, especially if mitigation approaches do not result in immediate financial or welfare improvements (Workie and Debella 2017). Smallholder ranchers might be reluctant to surrender any of their frequently pitiful homestead benefits to sequester carbon. Carbon-sequestering land use procedures should either be financed to the degree that they are comparable to inevitable benefits from elective land uses, or they should be beneficial by their own doing – with no pay – if such ranchers are to add to relief regardless (IPCC 2013). With biocarbon projects actually attempting to defeat monetary, institutional, and administration hindrances, the most obvious opportunity with regards to sequestering carbon for an enormous scope on Africa's ranches is through advancements that further develop food security while likewise giving supportability administrations (for example, expanded parkland tree cover, diverse cultivating, intercropping, and land sharing practices) (Ignaciuk and Mason-D'Croz 2014). Agroforestry is one of the few land use practices that can help with food security as well as climate change mitigation. It is also less likely to have a detrimental impact on non-carbon ecosystem services like water cycle regulation and biodiversity protection, both of which are important components of "climate-smart agriculture," than other options (Rahman and Hickey 2019). Agriculture and forestry are responsible for approximately a third of all human greenhouse gas emissions. As a result, mitigation initiatives should concentrate on these industries. However, it should be remembered that seas, lakes, forests, and agricultural areas all trap and store huge amounts of carbon, helping to mitigate climate change (FAO 2020). Agricultural methods may contribute significantly to raising soil carbon sinks and reducing GHG emissions at a cheap cost. In other words, in agriculture, forestry, and fisheries, sustainable production and consumption should be the driving factors for lowering GHG emissions.

Mitigating Methane Emissions Through New Irrigation Schemes (Bohol, Philippines)

Bohol Island is one of the major rice-growing areas in the Philippines' Visayas region. Two older reservoirs (Malinao and Capayas Dams) were beset by issues and unable to produce adequate water for the second crop season (November to April) prior to the construction of the Bohol Integrated Irrigation System (BIIS) in 2007. Farmers' penchant for permanently flooded rice-growing conditions exacerbated the situation, as did the practice of uneven water distribution. In response to deteriorating rice yield, the National Irrigation Administration (NIA) devised an action

plan for the BIIS (FAO 2009). Among the projects were the construction of a new dam (Bayongan Dam; funded by a loan from the Japan Bank for International Cooperation) and the adoption of Alternate-Wetting and Drying (AWD), a water-saving technology developed by the International Rice Research Institute (IRRI) in collaboration with national research institutes. The apparent efficacy of AWD on pilot farms, along with specific farmer training programmes, was able to debunk the widely held idea that non-flooded rice fields would result in output losses. Because of the extensive usage of AWD, irrigation water was used more efficiently, allowing cropping intensity to be increased from 119% to 160% (related to the maximum of 200% in these double cropping systems). Furthermore, as compared to continuous flooding of rice fields, the new IPCC methodology (IPCC 2007) states that "multiple aeration," to which the AWD adheres, can reduce methane emissions by up to 48%. As a consequence, AWD offers several benefits, including lower methane emissions (mitigation), decreased water usage (adaptation in water-scarce locations), enhanced output, and contribution to food security. Source: FAO 2010

Challenges

Substantial rising temperatures provide both difficulties and solutions for rethinking sustainability aspirations that do not appear to be simple to comprehend. Despite the fact that conservation concepts and practices have evolved through time, there are major institutional and cognitive barriers to shifting ecological perspectives and reconfiguring goals (Harvey et al. 2014). The following are some of the institutional impediments to rethinking and reconfiguring objectives: (1) laws and principles; (2) rules and procedures for leadership; (3) people and economic investment; and (4) science and information (Montoya and Raffaelli 2010). Lawful obligations and rules, in specific, may extant problematic obstacles. Several current regulations, such as the Endangered Species Act, impose certain techniques on managers, limiting their freedom to change aims and management objectives. Several recent legal studies (Matocha et al. 2012; Mora et al. 2011) provide some insight into the complexities of Federal conservation rules as they pertain to global climate change variation. Psychological impediments, on the other hand, will be challenging to eliminate. Due to a strong aversion to making trade-offs, which are referred to in the scientific literature as "protected values," many conservationists, according to Nye et al. (2010), find it tough to progress the well-known aims of regenerating and safeguarding current patterns of richness, as well as sustainability goals chosen in advance. Doney et al. (2012) further speculated that conservationists' general aversion to "giving up on anything" might explain the restricted range of transformational adaptation techniques as comparison to keeping the current order.

Several environmentalists think that using the high conservation value (HCV) method is a good way to identify and mitigate the negative consequences of unmanaged natural resource use (Monzon et al. 2011). However, as its reach has broadened and diversified, HCV users and assessors have speculated, scrutinised, and

criticised its appropriateness for biodiversity conservation (OECD 2014). The HCV idea is evolving from a heuristic learning-by-experience model to a comprehensive management tool that allows for improved prioritising of components such as ecosystem services, biodiversity, and socio-economic-cultural values.

Some of the major research problems in this area include the following:

1. Primary and secondary research are covered in a comprehensive spatiotemporal, contextual, and particular manner
2. Development of HCV component, category, and definition interpretations at the federal provincial, regional, and municipal levels
3. Difficulties in putting a management plan in place at the landscape level
4. Participation of the public and FPIC implementation
5. HCVs are prioritised for retention depending on their human significance and vulnerabilities.

Environmental and economic NGOs, as well as wealthy individuals, have backed the HCV method. This community of partners demonstrates how the HCV approach may benefit a wide number of stakeholders while simultaneously balancing ethical, cultural, and political concerns (Pacifici et al. 2015). However, in agricultural settings, it is frequently misappropriated, resulting in low-quality HCV assessments (Mora et al. 2011). This makes distinguishing between technique flaws and those induced by bad application more challenging.

Climate Change's Impact on Biodiversity

As a consequence of a wide range of human-caused activities, biodiversity is disappearing and becoming increasingly vulnerable around the world (Fardila et al. 2017; Barlow et al. 2018). "A semi-permanent or permanent qualitative or quantitative decline in elements of biodiversity and their potential to produce products and services, to be restricted at world, regional, and national levels," according to the Convention on Biological Diversity (CBD COP VII/30). According to fossil records, a private vertebrate species went extinct after an average of one million years (Lambin and Meyfroidt 2011). Therefore, only one species out of a million ought to go inexistent. Nevertheless, the present ascertained elimination rate is 2.6 vertebrate species per 10,000 per year (Whiteside and Ward 2011). Environmental change is one of the most genuine dangers to the locale's biodiversity and biological system administrations (Workie and Dabella 2017; Matata and Adan 2018). One of the most serious dangers to biodiversity is climate change, as per the United Nations Framework Convention on Climate Change and thus the CBD. As indicated by a review distributed in Nature (Thomas et al. 2004), worldwide environmental change may bring about the termination of a greater magnitude 1,000,000 earthbound species in the following fifty years. The most powerless are uncommon species, divided environments, and districts previously upset by contamination and deforestation.

Populations of Species Fluctuations

According to scientific investigations, some taxa have shifted their species ranges in response to rapid changes in temperature and precipitation regimes, primarily towards higher elevations and temperature inversions (Nye et al. 2010; Burrows et al. 2011; Chen et al. 2011; Doney et al. 2012). According to Groffman et al., plants and animals in terrestrial ecosystems migrated at a rate of 0.011 km per decade towards various altitudes and 16.9 km per decade towards warmer temperatures (2014). The spatial bounds of east African species and habitats have shifted dramatically as a result of climate change. To adapt to rising temperatures, current migration rates must be significantly greater than those observed in previous postglacial periods (Bajramovic et al. 2014, Bland et al. 2015). Climate change is influencing Africa's natural variety. For example, the Ethiopian wolf (Canis simensis) is struggling to adapt to prolonged droughts and diminishing water and other resource availability. Ecologists are particularly vulnerable and respond as a result of their relatively restricted nutritional, thermal, and habitat niche breadths (Lowder et al. 2016; Montoya and Raffaelli 2010) and associated with generally stable ecosystems (Walther 2010). Extreme weather events threaten the habitats that support Ethiopia's endangered and distinctive species. Climate change, for example, is expected to enhance the likelihood of local extinction of the Ethiopian wolf (*C. simensis*), Africa's most endangered species, according to study. According to Rosenzweig and Parry (1994), *C. simensis* was discovered about 2500 metres above sea level in Gojjam and northern Showa in the early twentieth century. In recent decades, the species' distribution has migrated to higher heights, and it is now known to exist at elevations of over 3000 metres above sea level, with the tallest peaks reaching up to 3700 metres (Rosenzweig and Parry 1994). Prospective conservation area classifications and preservation of environmental specialising groups in Ethiopia must include estimates of future climate change and associated changes in plant and animal species' geographic ranges to assure adequacy. Unquestionably, the environment has the power to change the migration patterns (and timings) of species that depend on seasonal wetlands (like migratory birds) and keep track of seasonal changes in vegetation (like herbivores), leading to increased interactions with people, particularly in regions where rainfall is significant (Kumar and Verma 2017). Wild animals that cannot migrate or travel are endangered in Africa. In Ethiopia, land use patterns can hinder animals from altering their migratory pathways, according to Pacifici et al. (2015). Big-scale agricultural growth, for example, has been shown to disrupt migratory routes, resulting in a reduction in large animal populations (Williams and Jackson 2007).

Responses from Various Populations

Global warming causes the depletion of non-renewable ecosystems and the relocation of habitat ranges to more appropriate areas, altering the number of species populations (Erasmus et al. 2002; Walther 2010). In response to fast changes in temperature and precipitation regimes, *C. simensis* has already extended its geographic distribution to higher altitudes. New combinations of taxa, unusual interspecific interactions, and, in the worst-case scenario, extinction might arise from these changes (Paudel Khatiwada et al. 2017). Like a consequence, the shift in *C. simensis* habitat might signal a population decrease. Further, if climate change decreases a species' range to a few key areas and a severe weather event occurs, the population decline and destruction of the species would likely increase in the future. When it comes to climate change, species kinds are less likely to move in large groupings and are more likely to split apart (Walther 2010; Barnosky et al. 2011).

Changes in Phenology

Variations in plant morphology, or the periodic sequencing of life circumstances, have been seen in Africa as a function of temperature, humidity, and sunshine variations (Workie and Debella 2017). Variations in plant leaf development, blossoming, and blooming, as well as changes in animal spawning, reproduction, and migratory periods, are examples of phenological occurrences (Whiteside and Ward 2011; Burrows et al. 2011). Extreme weather has a more nuanced impact on biodiversity. Elephants (*Loxodonta africana*) reproduce all year in Africa, with powerful males mating in the rainy season and inferior males mating in the dry. Changes in the severity or duration of rainy and dry seasons may have an impact on relative breeding rates and, as a result, genetic patterns in these populations (Butchart et al. 2010) Longer growing seasons would entail higher crop production expenses because food crop farming is Africa's most significant agricultural business. Many formerly vulnerable species are projected to experience an increased risk of population loss and extinction due to the time it takes for many species to adjust to climate change (Thomas et al. 2004). While the influence of environmental issues on the possibility of extinction is still debated, environmentalists are particularly concerned about this effect (de Coninck and Puig 2015). Outside of nature conservation, there is rising worry about climate change's possible negative consequences for biodiversity, which directly threaten biodiversity-based ecosystem services. Ecosystem "tipping points," in which ecosystem thresholds may result in ecosystem loss or permanent changes, as well as a catastrophic disaster, are a major cause of concern.

Climate Change, Biodiversity, and Ecosystem Services

Climate changes, natural resource conservation, and environmental productivity, biodiversity is the broad range of goods and services that people can obtain from the nature (Sahoo and Wani 2020; Sahoo et al. 2021; Brown et al. 2018a, b). Because of environmental resources, at least 40% of the globalised trade and 80% of the GDP of emerging regions comes directly from biological capital. Reduced or declining biodiversity in any component that does not already contribute to habitat conjugation would have a major influence on the perceived importance of ecological services (Bommarco et al. 2018).

Feedbacks to Climate

Without natural ecosystems, the carbon cycle is incomplete. The consequences of climate change on natural ecosystems can have large positive feedback effects on the temperature system, and weather patterns and habitat have a nonlinear connection (Sharma and Mishra 2011). According to the IPCC, land use change accounts for 20% of total anthropogenic emissions, a proportion that may rise as a result of climate change. This linkage is not typically included in climate models, but it is a burgeoning subject of study, particularly in light of the IPCC 4AR's concerns about ecosystems' ability to withstand global warming. Increased soil respiration when temperatures rise, particularly in the arctic (IPCC 2013), will be substantial feedback to the climate system, perhaps adding 200 ppm CO_2 to the atmosphere by 2100. Even though the precise dynamics are unknown, according to new study, the two principal soil carbon storage mechanisms have positive feedback, permafrost and peatland, which may be significant (Gusli et al. 2020). Permafrost warming emissions, for example, have been projected to vary from a worldwide increase of lOOPgC by 2100 to a rise of 40–100 Pg from Canada and Alaska alone by 2100 (FAO 2020). A 10% warming of Siberian permafrost is expected to release 40 Pg by 2050, an increase that will not be reduced by the projected advance of the treeline into the tundra. Changes in natural systems brought on by the demise of soil invertebrates in low-diversity environments can also affect carbon flows (IUCN 2016).

Peat emissions are linked to the state of the water table, which is extremely vulnerable to climate change (Brown et al. 2018a, b). Moreover, according to an experimental research, climate change will alter peat diversity and abundance, with photosynthetic organisms predominating at the expense of peat generating species, lowering peat's carbon storage potential (Dhyani et al. 2020). Such feedbacks can be generated by a number of causes other than rising temperatures. One subject that has gotten little consideration in the literature is the potential effects of sea level rise.

Sustainable Biodiversity Management in the Face of Climate Impacts

The Next Steps

An essential first step was the establishment of the Ad Hoc Technical Expert Group (AHTEG) on Biodiversity and Climate Change-A COP proposal. Its mandate suggests ways to improve the combination of biodiversity concerns and ancient and local biodiversity-related data, with explicit relevance for communities and sectors affected by climate change, to recognise opportunities and potential detrimental effects on biodiversity, sustainability, and long-term usage, as well as communities for biodiversity conservation and sustainable use (Butchart et al. 2010; Barnosky et al. 2011).

Climate Change's Effects on Livelihoods and Resilience Measures

Adaptation Approaches

In the non-agricultural sector, events as well as the implementation of farming methods and technology, the questioned families indicated a variety of adaptation strategies (Abebe et al. 2013). The variations in agricultural methods used show that, in terms of both the quantity and types of practices employed, geography has a major influence in climate (and climate change) variation in nations. However, despite considerable variations in overall earnings availability, there was no difference in agricultural practices adoption depending on wealth group (FAO 2020). The most prevalent non-agricultural method was off-farm employment, with one or more family members working off-farm in 57.7% of the families questioned. Off-farm activities was the strongest in the centre area due to stronger monetary implications. Other non-agricultural occupations were tolerated to varying degrees depending on region and income level (Inder et al. 2018). Certain families chose to lease out sections of their property, either due to a lack of labour and interest in farming, or because some plots were too far away from their farm. Household members from the central region are more likely to relocate to urban areas, particularly those who are younger and more educated. Low-income households were also much more likely to migrate to cities. While migration is an essential adaptive technique. The most vulnerable individuals of society may lack the power to flee deteriorating conditions and instead opt to remain put (Gusli et al. 2020). These populations are referred to be "stuck" and "vulnerable" in two ways. The usage of both organic and mineral fertilisers, which was embraced by 94.9% of the families in this research, is particularly noteworthy. Increased fertilisation is clearly one of

the important causes of an overall improvement in yields of the major crops in the nations during the preceding couple of generations (Verma 2017), even though we did not measure the actual amounts employed. In contrast, most agricultural outputs in Europe are still much lower when compared to more industrialised countries (Midgley and Bond 2015). While subsistence needs remain a key role in crop and animal selection, there is an increasing quantity of commercial crops cultivated on fields and a trend towards a larger emphasis on the economics. A large proportion of families (68.7%) reported modifying their crops in response to market needs or using more productive crop types to boost yields (78%). Certain households, particularly in the centre area, have chosen drought-tolerant crops (IPCC 2021).

Global Warming, Habitat, and Economics

Poverty is a difficult matter that encompasses more than a lack of economic assets. A limited or risky asset base, low quality or insecure housing, and weak safety nets to guarantee basic consumption are maintained when income declines or crops fail, and a lack of authority and voice are all significant variables to consider (Verma 2019). As a result, shock vulnerability is an important aspect of poverty. Poor individuals rely on ecosystem services and goods for a greater portion of their income than rich people. Multiple livelihood activities are frequently used by disadvantaged families to generate money and fulfil their basic requirements (Verma 2016). Fish, grazing land, and forests are examples of common property resources that may supply money, nutrition, medication, skills, energy, livestock, and building materials which are all examples of need, among other things. Poor people suffer disproportionately when the environment is destroyed or their access to it is restricted (Workie and Debella 2017). Poverty and environmental degradation have long been linked. Because of this dependency, any impact of climate change on natural systems poses a threat to the livelihoods (Sahoo and Wani 2019), food intake, and health of impoverished people. As a consequence of global warming, many semi-arid regions of the developing world may become hotter and drier, with less constant rainfall. Changes in agricultural yields, ecological constraints, and animal distributions will all have a substantial influence on the lives of many impoverished people as a result of climate change (Sahoo and Wani 2020). Climate change affects the poorest people in the world's poorest countries the most. This is due to the fact that they live in areas prone to flooding, cyclones, droughts, and other natural catastrophes, and their capacity to respond to these occurrences is restricted. They rely heavily on climate-sensitive industries like fishing and agriculture (Wittig et al. 2007), and their countries lack the financial, institutional, and human resources needed to foresee and respond to the direct and indirect consequences of climate change (Sahoo et al. 2019). The preservation of biodiversity and ecological veracity may be a significant goal for strengthening such communities' adaptability to deal with climate change. Climate change and variability may be better adapted by functionally diversified systems than by functionally impoverished systems (Paavola 2004). The

development of genotypes that are more suited to changing climatic circumstances will be aided by a bigger gene pool. As biodiversity declines, changing choices grow fewer, and human society becomes more fragile. Risky weather disasters put the poor in an especially vulnerable position. In recent years, developing nations have accounted for almost 96% of disaster-related mortality. Extreme climatic measures are becoming more regular, and in 2001, 170 million people worldwide were affected by disasters, with climate change being responsible for 97% of them (FAO 2019). Women and children are especially at risk. When a storm devastated Bangladesh in 1991, for example, 90% of the casualties were women and children. This was due to a number of variables, such as their ability to survive (such as swimming) and socio-cultural norms prohibiting women and children from gathering in tropical storm shields available to the general public.

Concerning Climate Change, Biodiversity Protection, and Poverty Reduction Is the Way Forward

Indigenous activities are routinely overlooked – or devalued – in the fight against global warming, conservation of natural resources, and economic reform. International issues, such as the protection of endangered and charismatic creatures, have driven biodiversity conservation to the forefront of the conservation agenda (IPCC 2020). Local biodiversity values, such as livelihood assistance or risk reduction in the face of climatic shocks, have frequently been overshadowed by this technique. National Communications, National Adaptation Plans of Action, National Biodiversity Strategies and Action Plans, National Conservation Strategies, National Environmental Action Plans, and Poverty Rationing (often spawned by environmental conventions spawned at the United Nations Earth Summit in Rio in 1992) are receiving a lot of attention and funding right now (FAO 2020). In general, such programmes pose a significant challenge to impoverished nations by putting undue demand on already overburdened institutions with limited resources. Supporting local solutions takes multiple initiatives. Climate change vulnerability will be reduced through actions to alleviate poverty and inequality on a global scale (Sahoo et al. 2020b), as well as by reducing unsustainable natural resource use. Increased availability of the product for refined raw materials; based on strategic and untied aid (to foster responsible local processes); financial assistance; and a high-income nations' interest to change feeding patterns and thereby reduce greenhouse gas emissions are examples of such programmes (Workie and Debella 2017). The effectiveness of the Climate Change Convention and the Convention on Biological Diversity, as well as linkages to national development goals like Poverty Reduction Strategy Papers, must be investigated. Because each approach has its own constituency, administrative structure, negotiators, and scientific advisory organisations, this is an issue (Abdisa et al. 2017).

Some argue that it would be beneficial to encourage nations to form a single organisation to handle their duties under all international environmental treaties. Climate-related catastrophe management techniques, for example, may include the impact on local ecosystems as well as vulnerable human populations (Ali and Erenstein 2017). The importance of ecosystems in local livelihoods as well as biodiversity hotspots will be recognised. Two possible techniques for combining species diversity, subsistence, and climate change concerns are the ecosystem approach, which may include climatic issues, and environmental assessments, which may be changed to allow for wider adoption of environmental, social, and economic concerns (Barrios et al. 2018). The value of environmental services must be quantified in order to establish the real worth of environmental products and services. Collaborative methods and a comprehensive approach to sustainable development that considers all elements of the issue should be encouraged (Bustamante et al. 2014).

National policies that promote biodiversity, adaptation and mitigation to climate change, and poverty reduction must be supported. Development projects should include solutions to climatic hazards in order to reduce the effects of climate change. Development organisations, national governments, and other stakeholders should address climate change (Burrows et al. 2011). Many adaptation programmes, on the other hand, are implemented by environment ministries, which are often weak and have little influence over line ministries (such as those responsible for agriculture or water management). The importance of good governance must be recognised in light of the intricacies of local and national political systems. Decentralised administration with more authority can be beneficial, but a well-functioning national government with vision and responsibility is also necessary (Harvey et al. 2014). Actions that promote fair and responsible local governance, successful land tenure reform, and common property resource management that respects the rights of disadvantaged people are critical at the local level. In the hunt for solutions, building on the huge quantity of knowledge currently owned by disadvantaged people is a top focus. Adaptation initiatives should take this information into consideration because disadvantaged people have been dealing with climate change for a long time (Guo et al. 2017). Local solutions and bottom-up methods that are accountable to low-income people should be promoted through capacity-building programmes. Rather than labelling the poor as recipients of charity, assistance should be offered so that they may focus on their own efforts to decrease climate-related vulnerability through conservation planning and restoration operations that sustain and diversify local livelihoods.

Future Scope of the Study

Climate changes are the dynamic in nature that has direct impact on rural livelihoods. The changes cannot be stopped but can be controlled through smart and realistic system. There should a combination effort of government, scientists, and general public to build a protective wall against the threats of climate changes. The

study was the initiative towards the building a productive system that may support the great initiatives of Government of India. The future scope of the study can be commenced like:

Government Project
The research study and its suggestions can be implemented by Government of India towards Integrated Nutrient Management in rural areas, National Watershed Development Project for Rainfed Areas and Promoting use of Informatics in Agriculture in rural areas. National Rural Livelihood Mission: The NGOs and the local government can improve the rural livelihoods associate with national rural livelihoods mission. The organisations take initiative of building self confidence among the rural livelihoods by recognising their contribution to the society and nation. The main concept behind this initiative is to organise the destitute into SHGs (Self Help Groups) and prepare them for employment. The method aids in the reduction of poverty by providing impoverished households with possibilities for lucrative work for a living and self-employment, resulting in a significant enhancement in their livelihoods on a long-term basis. Government initiative for rural development: The Indian Government has taken initiative for retaining the villagers with their current profession and activities. The financial institutions are assigned the supporting role and assistance as per requirements of the rural livelihoods.

Policy Recommendations

The guidelines, based on the research findings and the literature cited above, provide a path forward for enhancing climate change adaptation measures to protect rural livelihoods. Because the whole continent faces similar environmental issues, the suggestions emerging from this study are pertinent to certain areas.

The Emphasis Is on Smallholders, Sensitive Spots, and the Community at Large

In order to have policies that are climate-change-aware and pro-poor, small farmers must be prioritised. The policies include the following: (a) increasing price incentives and public investment quantity and quality; (b) improving product markets; (c) increasing access to financial services and lowering the danger of becoming sick; (d) enhancing the effectiveness of producer organisations; f) encouraging entrepreneurship via science and technology; and g) establishing agriculture healthier and a source of ecological remediation. Agricultural mitigation may benefit small farmers. If relevant legislative reforms are enacted, small farmers have a tremendous potential to store soil carbon. The new market for pricing carbon emissions opens up new opportunities for farmers to profit from carbon-sequestering land usage.

Collaboration is widely recognised as vital for climate change adaptation and mitigation. According to research and practice, collective action institutions are crucial for technology transfer in agriculture and natural resource management among smallholders and resource-dependent communities.

Climate-Smart Agriculture, Green Agriculture, and Rural Nonfarm Activities Must All Be Prioritised

The implications on agricultural and food systems would have a direct impact on billions of people's major source of revenue, livelihoods, and food security. Food costs would also rise as a result of climate change. It would be detrimental to food security, as well as human growth as measured by nutrient levels. Because of all of the negative consequences, all stakeholders, notably governments, must concentrate on mitigating the negative consequences of climate change by concentrating on agriculture production. Environment and sustainable agriculture technologies must be adopted while jeopardising the food security and lives of the population, especially the poor. Organic farming and green agriculture, for example, are two of the most important paths for the evergreen revolution. Improved national research and extension programmes are required to achieve climate-smart, green, and sustainable agriculture.

Opportunities for Adaptation

It should be mentioned that public policy plays a substantial role in aiding climate change adaptation. Most governments in underdeveloped countries would be unable to plan for adaptation and implement well-targeted adaptation strategies due to a lack of resources. Investments and incentives are required to develop and supply better technology and management practices. Important ongoing development projects must be enhanced in order to mitigate climate change vulnerability. However, neither private sector or individual adaptation plans, nor public sector development policies, would be adequate to assist poor nations in Asia and the Pacific to adjust to climate change. Adaptation will necessitate novel policies.

Opportunities for Mitigation

Improved crop and grazing land management (e.g., increased agronomic methods, fertiliser usage, tillage, and residue management), regeneration of organic soils drained for crop production, and rehabilitation of marginal forests are the most

major mitigating alternatives. To reduce CH_4 emissions, rice production techniques, as well as livestock and manure management, have been improved; nitrogen fertiliser application techniques have been improved to reduce N_2O emissions; specialised energy crops have been developed to replace fossil fuel consumption; and thermal efficiency has been upgraded. Improved water and rice management, as well as set-asides and land use changes, can all assist to reduce the problem to a lesser but still significant extent (e.g., conversion of crop land to grassland). Various mitigation opportunities are now available and can be adopted right away, but technology advancement will be a vital factor in assuring the success of future mitigation efforts. Improved yield technologies would be beneficial. Other benefits include synergising with adaptability, livelihood strategies, and long-term growth. Furthermore, with the introduction of carbon markets, agricultural and forestry mitigation techniques have the potential to produce revenue in rural regions, hence increasing adaptive capacity.

Collaboration on a Broad Basis

Strengthening regional cooperation among Asian and Pacific governments is another important tactic. This partnership must address climate change concerns by supporting the successful implementation of national adaptation and mitigation programmes, as well as current and future climate change financing tools. Regional organisations such as ASEAN (Association of Southeast Asian Nations) and SAARC (South Asian Association for Regional Cooperation) should play a key role in technology and knowledge transfer, in addition to regional cooperation initiatives such as CACILM (Central Asian Countries Initiatives for Land Management) and GMS (Greater Mekong Sub-region) (ADB and IFPRI 2009). Agriculture and food security, livelihoods, and environmental services, for example, might be the focus of regional projects, all of which contribute to climate change mitigation and adaptation.

Conclusion

Several global and national development programmes have focused on the increasing poverty gap between industrialised and developing nations. Climate change has the potential to undermine decades of progress and poverty alleviation initiatives, notably the failure to meet the Millennium Development Goals set in 2000. Climate change is the most passionate problem facing the world community in the twenty-first century, particularly for rural lives. This, like the difficulties of poverty reduction, economic growth, and development, is the task. Climate change is threatening the livelihoods, health, and well-being of millions of people throughout the world, particularly the poorest and economically weakest sections of the Indian

population. Adaptation to climate change has a significant influence in emerging economies like India. The urban population may take more initiative in organising training programmes, health-related awareness camps, and effective resource management, while the rural population can take more effort in implementing sustainable agriculture operations. The categories of activities towards sustainable development are being reworked on the influence of managing water resources in the face of climate change. The significant equilibrium that exists between rural livelihoods and climatic circumstances is poised to be disrupted by a rapid change in climate. Climate change is also linked to sea level rise, and it poses a significant danger to coastal regions. It is critical to figure out how to mitigate the effects of climate change through strategic management planning. Decision-makers' views and understanding at the provincial level will have a substantial impact on India's climate change adaptation. Global warming is seen as the most serious issue of climate change, posing the greatest comprehensive fitness hazards of the twenty-first century and posing a danger to achieving sustainable development. However, players in a sustainable society, such as disaster management and agriculture graduates, doctors, teachers, vocational trainers, non-governmental organisations, and local governments, can take the lead in strengthening rural livelihoods. It is critical to recognise that biodiversity is a huge, complex, and interconnected phenomenon with no one overarching influence on production or sustainability. It is critical to recognise that biodiversity is a huge, complex, and interconnected phenomenon with no one overarching influence on production or stability. The actual impacts will be greatly influenced by the context in which they are researched as well as the time frame over which they are analysed. However, it is apparent that biodiversity is crucial for both managed and wild ecosystems, even though the proportional contributions of diversity and composition are still unknown. In order to keep diversity at its current levels, politicians must grasp fundamental science. If present human growth and resource management practices do not alter, many key species will certainly perish, and the world's ecosystems would likely never recover. Humans are just another type of natural organism that should not be considered alien to other living forms. We have no moral right to destroy the planet's ecosystem or other living creatures. Kindness should be shown to all animals and plants. Every individual may play a little but critical role in the fight to save our planet and preserve biodiversity. As a result, if catastrophic climate change is to be avoided, developed countries must increase their efforts to reduce greenhouse gas emissions. Variations in species diversity can alter the physical and trophic structure of ecosystems, influencing system function and constitution even more. One example is the spread of woody plants into temperate grasslands. Drought may cause trees to die in many environments. Warmer temperatures and growing pressures on ocean acidification are particularly harmful to coral reefs, causing bleaching and illnesses. Many coral species that create reefs are on the verge of extinction. This has far-reaching ramifications for coral reefs' vast biological communities. Ecosystems that give human values and services are a significant characteristic of ecosystems that may be affected by climate change. Ecosystems that are valued by humans and provide services are a key part of ecosystems that may be damaged by climate change.

Fisheries, which may grow in the short term in boreal regions while dropping elsewhere, and wood production, which is impacted by population characteristics as well as local circumstances and may result in significant output losses, are two examples of provisioning services. The important biological services that coral reefs provide, such as fisheries, coastal protection, building materials, new biochemical compounds, and tourism, are all under threat. Climate change affects terrestrial ecosystems' ability to manage water flows, as well as many ecosystems' ability to absorb and/or retain carbon, all of which can contribute to climate change.

References

Abdisa A, Dirba K, Muktar M (2017) Impacts of various ENSO phases on cereal crop productivity in the Upper Awash Basin, Central High Land of Ethiopia. Haramaya University, Ethiopia

Abebe D, Randall B, Alemu M (2013) Community controlled forests, carbon sequestration and REDD+: some Evidence from Ethiopia. Environment for Development, Addis Ababa

ADB and IFPRI (2009) Building climate resilience in the agricultural sector of Asia and the Pacific. Asian Development Bank, Manila

Ajit DSK, Newaj R, Handa AK, Prasad R, Alam B, Rizvi RH, Gupta G, Pandey KK, Jain A, Uma (2013) Modelling analysis of potential carbon sequestration under existing agroforestry systems in three districts of Indo-Gangetic plains in India. Agrofor Syst 87(5):1129–1146

Ali A, Erenstein O (2017) Assessing farmer use of climate change adaptation practices and impacts on food security and poverty in Pakistan. Clim Risk Manag 16:183–194

Bajramovic S, Nikolic A, Butkovic J (2014) Agriculture and agricultural policy in Bosnia and Herzegovina. In: Volk T, Erjavec E, Mortensen K (eds) Agricultural policy and European integration in Southeastern Europe. Food and Agriculture Organization of the United Nations, Budapest, pp 73–94

Barlow J, França F, Gardner T, Hicks C, Lennox GD, Berenguer E, Castello L et al (2018) The future of hyperdiverse tropical ecosystems. Nature 559:517–526. https://doi.org/10.1038/s41586-018-0301-1

Barnosky AD, Matzke N, Tomiya S, Wogan GOU, Swartz B, Quental C, Marshall TB et al (2011) Has the Earth's sixth mass extinction already arrived? Nature 471:51–57. https://doi.org/10.1038/nature09833

Barrios E, Valencia V, Jonsson M, Brauman A, Hairiah K, Mortimer PE, Okubo S (2018) Contribution of Trees to the conservation of biodiversity and ecosystem services in agricultural landscapes. Int J Biodiv Sci Ecosys Servi Manage 14:1–16. https://doi.org/10.1080/21513732.2017.1399167

Bellard C, Bertelsmeier C, Leadley P, Thuiller W, Courchamp F (2012) Impacts of climate change on the future of biodiversity. Ecol Lett 15:365–377. https://doi.org/10.1111/j.1461-0248.2012.01764.x

Bezabih M, DiFalco S, Mekonnen A (2014) On the impact of weather variability and climate change on agriculture, evidence from Ethiopia. Published by Sida Environment for Development and Resource for the Future, Addis Ababa

Bland LM, Collen B, Orme CDL, Bielby J (2015) Predicting the conservation status of data-deficient species. Conserv Biol 29:250–259. https://doi.org/10.1111/cobi.12372

Bommarco R, Vico G, Hallin S (2018) Exploiting ecosystem services in agriculture for increased food security. Global Food Security 17:57–63. https://doi.org/10.1016/j.gfs.2018.04.001

Brito-Morales I, Molinos J, Schoeman DS, Burrows MT, Poloczanska ES, Brown CJ et al (2018) Climate velocity can inform conservation in a warming world. Trends Ecol Evol 33:441–457. https://doi.org/10.1016/j.tree.2018.03.009

Brook BW, Sodhi NS, Bradshaw CJA (2008) Synergies among extinction drivers under global change. Trends Ecol Evol 23:453–460. https://doi.org/10.1016/j.tree.2008.03.011

Brooks N, Adger WN, Kelly PM (2005) The determinants of vulnerability and adaptive capacity at the national level and the implications for adaptation. Glob Environ Chang 15:151–163

Brown B, Nuberg I, Llewellyn R (2018a) Constraints to the utilisation of conservation agriculture in Africa as perceived by agricultural extension service providers. Land Use Policy 73:331–340. https://doi.org/10.1016/j.landusepol.2018.02.009

Brown SE, Miller DC, Ordonez PJ, Baylis K (2018b) Evidence for the impacts of agroforestry on agricultural productivity, ecosystem services, and human well-being in high-income countries: a systematic map protocol. Environ Evid 7:24

Burrows MT, Schoeman DS, Buckley LB, Moore P, Poloczanska ES, Brander KM, Brown C et al (2011) The pace of shifting climate in marine and terrestrial ecosystems. Science 334:652–655

Bustamante M, Robledo-Abad C, Harper R, Mbow C, Ravindranat NH, Sperling F, Haberl H, de Pinto AS, Smith P (2014) Co-benefits, trade-offs, barriers and policies for greenhouse gas mitigation in the agriculture, forestry and other land use (AFOLU) Sector. Glob Chang Biol 20:3270–3290

Butchart SHM, Walpole M, Collen B, van Strien A, Scharlemann PW, Almond REA, Baillie JEM et al (2010) Global biodiversity: indicators of recent declines. Science 328:1164–1168. https://doi.org/10.1126/science.1187512

Chen IC, Hill JK, Ohlemüller R, Roy DB, Thomas CD (2011) Rapid range shifts of species associated with high levels of climate warming. Science 333:1024–1026. https://doi.org/10.1126/science.1205623

Chinnasamy P, Srivastava A (2021) Revival of traditional cascade tanks for achieving climate resilience in drylands of South India. Front Water 3:35. https://doi.org/10.3389/frwa.2021.639637

de Coninck H, Puig D (2015) Assessing climate change mitigation technology interventions by international institutions. Clim Chang 131:417–433

Dhyani S, Bartlett D, Kadaverugu R, Dasgupta R, Pujari P, Verma P (2020) Integrated climate sensitive restoration framework for transformative changes to sustainable land restoration. Restor Ecol 28:1026–1031

Doney SC, Ruckelshaus M, Duffy JE, Barry P, Chan F, English CA, Galindo HM et al (2012) Climate change impacts on marine ecosystems. Ann Rev Marine Sci 4:11–37. https://doi.org/10.1146/annurev-marine-041911-111611

Erasmus BFN, Van Jaarsveld AS, Chown SL, Kshatriya M, Wessels KJ (2002) Vulnerability of South African animal Taxa to climate change. Glob Chang Biol 8:679–693. https://doi.org/10.1046/j.1365-2486.2002.00502.x

FAO (2009) FAO: profile for climate change. Food and Agricultural Organization, Rome

FAO (2010) Climate-Smart agriculture: policies, practices and financing for food security, adaptation and mitigation. Food and Agricultural Organization, Rome

FAO (2019) The state of the world's biodiversity for food and agriculture. In: Bélanger J, Pilling D (eds) FAO commission on genetic resources for food and agriculture assessments. FAO, Rome. 572 pp. http://www.fao.org/3/CA3129EN/CA3129EN.pdf

FAO (2020) The state of food and agriculture. Overcoming water challenges in agriculture. Food and Agriculture Organization of the United Nations, Rome, pp 111–120

Fardila D, Kelly LT, Moore JL, McCarth MA (2017) A systematic review reveals changes in where and how we have studied habitat loss and fragmentation over 20 years. Biol Conserv 212:30–138. https://doi.org/10.1016/j.biocon.2017.04.031

Groffman PM, Kareiva P, Carter S, Grimm NB, Lawler J, Mack M, Matzek V, Tallis H (2014) "Ecosystems, Biodiversity, and Ecosystem Services. Climate change impacts in the United States: the Third National Climate Assessment, J. M. Melillo, Terese (T.C.) Richmond, and G. W. Yohe, Eds., U.S." Glob Chang Res Prog 200–201

Guo D, Desmet PG, Powrie LW (2017) Impact of the future changing climate on the Southern Africa biomes, and the importance of geology. J Geosci Environ Protec 5:1–9. https://doi.org/10.4236/gep.2017.57001

Gusli S, Sumeni S, Sabodin R, Muqfi IH, Nur M, Hairiah K, Useng D, van Noordwijk M (2020) Soil organic matter, mitigation of and adaptation to climate change in Cocoa–based agroforestry systems. Land 9:323

Harvey CA, Rakotobe ZL, Rao NS, Dave R, Razafimahatratra H, Rabarijohn RH, Rajaofara H, MacKinnon JL (2014) Extreme vulnerability of smallholder farmers to agricultural risks and climate change in Madagascar. Philos Trans Royal Soc B Biol Sci 369:20130089

Ignaciuk A, Mason-D'Croz D (2014) Modelling adaptation to climate change in agriculture, OECD Food, Agriculture and Fisheries Papers 70: 58.7. OECD Publishing, Paris

Inder D, Ram A, Bhaskar S, Chaturvedi OP (2018) Role of agroforestry in current scenario. In: Agroforestry for climate resilience and rural livelihood. Scientific Publishers, Jodhpur, pp 1–10

Intergovernmental Panel on Climate Change (IPCC) (2020) Centre for climate and energy Solutions. 5th Assessment report- Kerstin Stendahl, Deputy Secretary, IPCC. Geneva, Switzerland

Intergovernmental Panel on Climate Change (IPCC) (2021) Climate Change. Impacts, Adaptation, and. Vulnerability. Mitigation of. Climate Change. 6th Assessment report- Kerstin Stendahl, Deputy Secretary, IPCC. Geneva, Switzerland

International Union for Conservation of Nature (IUCN) (2016) The IUCN Red List of Threatened Species. IUCN, Gland

IPCC (2007) Working Group III. Mitigation of Climate Change. Intergovernmental Panel on Climate Change. Fourth Assessment Report. Ed. by Metz, B. O.R. Davidson, P.R. Bosch, R. Dave, L.A. Meyer. New York: Cambridge University Press.

IPCC (2013) Climate change 2013: the physical science basis. In: Stocker TF, Qin D, Plattner G-K, Tignor M, Allen SK, Boschung J, Nauels A, Xia Y, Bex V, Midgley PM (eds) Contribution of Working Group I to the fifth assessment report of the intergovernmental panel on climate change. Cambridge University Press, Cambridge/New York

IPCC (2019) Summary for policymakers. In Climate change and land: an Ipcc special report on climate change, desertification, land degradation, sustainable land management, food security, and greenhouse gas fluxes in terrestrial ecosystems; Shukla PR, Skea J, Calvo Buendia E, Masson-Delmotte V, Pörtner H-O, Roberts DC, Zhai P, Slade R, Connors S, van Diemen R, et al Eds.; IPCC Press Office: Geneva, p. 36.

Keith DA, Akcakaya HR, Thuiller W, Midgley GF, Pearson RG, Phillips SJ, Regan HM, Araujo MB, Rebelo TG (2008) Predicting extinction risks under climate change: coupling stochastic population models with dynamic bioclimatic habitat models. Biol Lett 4:560–563. https://doi.org/10.1098/rsbl.2008.0049

Khadri SFR, Pande C (2016) Ground water flow modeling for calibrating steady state using MODFLOW software: a case study of Mahesh River basin, India. Model Earth Syst Environ 2:39. https://doi.org/10.1007/s40808-015-0049-7

Kouadri S, Pande CB, Panneerselvam B et al (2022) Prediction of irrigation groundwater quality parameters using ANN, LSTM, and MLR models. Environ Sci Pollut Res 29:21067–21091. https://doi.org/10.1007/s11356-021-17084-3

Kumar A, Verma AK (2017) Biodiversity loss and its ecological impact in India. Int J Biol Sci 8(2):156–160

Lambin EF, Meyfroidt P (2011) Global land use change, economic globalization, and the looming land scarcity. Proc Natl Acad Sci 108:3465–3472. https://doi.org/10.1073/pnas.1100480108

Loarie SR, Duffy PB, Hamilton H, Asner GP, Field CB, Ackerly DD (2009) The velocity of climate change. Nature 462:1052–1055. https://doi.org/10.1038/nature08649

Lowder SK, Skoet J, Raney T (2016) The number, size, and distribution of farms, smallholder farms, and family farms worldwide. World Dev 87:16–29

Matata AC, Adan A (2018) Causes of climate change and its impact in the multi-sectoral areas in africa-need for enhanced adaptation policies. Curr J App Sci Tech 27:1–10. https://doi.org/10.9734/CJAST

Matocha J, Schroth G, Hills T, Hole D (2012) Integrating climate change adaptation and mitigation through agroforestry and ecosystem conservation. In: Nair PKR, Garrity D (eds) Agroforestry—the future of global land use, Advances in Agroforestry. Springer, Dordrecht, pp 105–126, ISBN 978-94-007-4676-3

Midgley G, Bond WJ (2015) Bond future of african terrestrial biodiversity and ecosystems under anthropogenic climate change. Nat Clim Chang 5:823–829. https://doi.org/10.1038/nclimate2753

Midgley GF, Hannah L, Millar D, Rutherford MC, Powrie LW (2002) Assessing the vulnerability of species richness to anthropogenic climate change in a biodiversity hotspot. Glob Ecol Biogeogr 11:445–451. https://doi.org/10.1046/j.1466-822X.2002.00307.x

Montoya JM, Raffaelli D (2010) Climate change, biotic interactions and ecosystem services. Philos Trans R Soc B 365:2013–2018. https://doi.org/10.1098/rstb.2010.0114

Monzon J, Moyer-Horner L, Palama MB (2011) Climate change and species range dynamics in protected areas. Bioscience 61:752–761. https://doi.org/10.1525/bio.2011.61.10.5

Mora C, Tittensor DP, Adl S, Simpson AGB, Worm B (2011) How Many Species are There on Earth and in the Ocean? PLoS Biology 9:1–12. https://doi.org/10.1371/journal.pbio.1001127

Nye JA, Bundy A, Shackell NL, Friedland KD, Link JS (2010) Coherent trends in contiguous survey time-series of major ecological and commercial fish species in the Gulf of Maine Ecosystem. ICES J Mar Sci 67:26–40. https://doi.org/10.1093/icesjms/fsp216

OECD (2014) Climate change, water and agriculture: towards resilient agricultural and water systems. https://doi.org/10.1787/9789264209138-e

Orimoloye IR, Olusola AO, Belle JA et al (2022) Drought disaster monitoring and land use dynamics: identification of drought drivers using regression-based algorithms. Nat Hazards. https://doi.org/10.1007/s11069-022-05219-9

Paavola J (2004) Livelihoods, vulnerability and adaptation to climate change in the Morogoro Region, Tanzania. CSERGE Working Paper EDM 04-12. http://www.cserge.ac.uk/sites/default/files/edm_2004_12.pdf. Accessed on 22 Aug 2015

Pacifici M, Foden WB, Visconti P, Watson EM, Butchart HM, Kovacs KM et al (2015) Assessing species vulnerability to climate change. Nat Clim Chang 5:215–225. https://doi.org/10.1038/nclimate2448

Pande CB, Moharir KN (2021) Groundwater resources development and planning in the semi-arid region, vol 1. Springer, Cham, p XIV, 571. https://doi.org/10.1007/978-3-030-68124-1

Pande CB, Moharir KN, Panneerselvam B et al (2021a) Delineation of groundwater potential zones for sustainable development and planning using analytical hierarchy process (AHP), and MIF techniques. Appl Water Sci 11:186. https://doi.org/10.1007/s13201-021-01522-1

Pande CB, Moharir KN, Singh SK, Varade AM, Ahmed Elbeltagie SFR, Khadri PC (2021b) Estimation of crop and forest biomass resources in a semi-arid region using satellite data and GIS. J Saudi Soc Agric Sci 20(5):302–311

Paudel Khatiwada S, Deng W, Paudel B, Khatiwada J, Zhang J, Su Y (2017) Household livelihood strategies and implication for poverty reduction in rural areas of central Nepal. Sustain For 9:612

Rahman HMT, Hickey GM (2019) What does autonomous adaptation to climate change have to teach public policy and planning about avoiding the risks of Maladaptation in Bangladesh? Front Environ Sci 7, 2

Rosenzweig C, Parry ML (1994) Potential impact of climate-change on world food supply. Nature 367:133–138

Sahoo GR, Wani AM (2019) Multifunctional agroforestry systems in India for Livelihoods. Ann Hortic 12(2):139–149

Sahoo GR, Wani AM (2020) Effect of climate change on land degradation. Int J Innov Engin Manage Res SSRN Elsevier 09(12):483–494

Sahoo GR, Wani AM, Kishore P, Vijay R (2019) Biodiversity conservation and climate change approach. Int Arch App Sci Technol 10(4):01–09. https://doi.org/10.15515/iaast.0976-4828.10.4.19

Sahoo GR, Wani AM, Satpathy B (2020a) Greening wastelands for environmental security through agroforestry. Int J Adv Res Sci Technol 7:2581–9429

Sahoo GR, Wani AM, Sharma A (2020b) Enhancing food security through agroforestry for sustainability – a review. Int J Curr Microbiol App Sci Special Issue-11:2001–2020

Sahoo GR, Wani AM, Prusty M, Ray M (2021) Effect of globalisation and climate change on forest- a review. Material Today Proceedings. Article in Press. https://doi.org/10.1016/j.matpr.2021.06.113.

Sharma DK, Mishra JK (2011) Impact of environmental changes on biodiversity. Indian J Sci Res 2(4):137–139

Sonwa DJ, Dieye A, Mzouri EH, Majule A, Mugabe FT, Omolo N, Wouapi H, Obando J, Brooks N (2017) Drivers of climate risk in african agriculture. Clim Dev 9:383–398. https://doi.org/10.1080/17565529.2016.1167659

Swaminathan MS, Kesavan PC (2012) Agricultural research in an era of climate change. Agribiol Res 1(1):3–11

Thomas CD, Cameron A, Green RE, Bakkenes M, Beaumont LJ, Collingham YC, Erasmus BFN et al (2004) Extinction risk from climate change. Nature 427:145–148. https://doi.org/10.1038/nature02121

Trew BT, Maclean IMD (2021) Vulnerability of global biodiversity hotspots to climate change. Glob Ecol Biogeogr 30:768–783

Trull N, Böhm M, Carr J (2018) Patterns and biases of climate change threats in the IUCN red list. Conserv Biol J Socie Conser Biol 32:135–147. https://doi.org/10.1111/cobi.13022

Tubiello FN, Rosenzweig C (2008) Developing climate change impact metrics for agriculture‖. Inte Assess J 8(1):165–184

Verma AK (2016) Biodiversity: its different levels and values. Int J Environ Sci 7(2):143–145

Verma AK (2017) Necessity of ecological balance for widespread biodiversity. Ind J Biol 4(2):158–160. https://doi.org/10.21088/ijb.2394.1391.4217.15

Verma AK (2019) Sustainable development and environmental ethics. Int J Environ Sci 10(1):1–5

Walther GR (2010) Community and ecosystem responses to recent climate change. Philos Trans R Soc B Biol Sci 365:2019–2024. https://doi.org/10.1098/rstb.2010.0021

Whiteside JH, Ward PD (2011) Ammonoid diversity and disparity track episodes of chaotic carbon cycling during the early Mesozoic. Geology 39:99–102. https://doi.org/10.1130/G31401.1

Williams JW, Jackson ST (2007) Novel climates, no-analog communities, and ecological surprises. Front Ecol Environ 5:475–482. https://doi.org/10.1890/070037

Wittig R, Konig K, Schmidt M, Szarzynski J (2007) A study of climate change and anthropogenic impacts in West Africa. Environ Sci Pollut Res 14:182–189

Workie TG, Debella HJ (2017) Climate change and its effects on vegetation phenology across ecoregions of Ethiopia. Glob Ecol Conser 13:e00366. https://doi.org/10.1016/j.gecco.2017.e00366

Chapter 2
Desertification Intensity Assessment Within the Ukraine Ecosystems Under the Conditions of Climate Change on the Basis of Remote Sensing Data

Vadym I. Lyalko, Alexandr A. Apostolov, Lesya A. Elistratova, Inna F. Romanciuc, and Iuliia V. Zakharchuk

Abstract The study of the climate conditions modern transformations in the different countries acquires theoretical and practical significance that is determined by the high activity of climate changes in natural and social processes of the region. Many climate scenarios and forecasts make accent on increasing the frequency of adverse events, including the drought processes under the conditions of climate change. One of the most pronounced manifestations of modern climate change in Ukraine is the growing aridity. It is manifested in the increasing duration and intensity of droughts. This process is associated with the significant reduction of moisture content, leading to consequences that affect functioning of both natural environment and society. Among the landscape components, biota, water (surface and groundwater), and soil cover undergo to the greatest changes due to intensification of arid phenomena. Steady tendencies to gradual changes within the boundaries of natural zones of the studied area are already visible. Ukraine's economy faces serious challenges due to this fact. The illustrative impact of climate changes is demonstrated by the negative consequences for agriculture. An effective tool for monitoring of the natural environment processes under the influence of climate change, in particular the arid phenomena, is the applying the remote sensing data. This study uses the data from the TERRA/MODIS satellites along with the drought indices. The detailed maps of arid-zonation were developed. Such studies represent the basis of justifying measures for adapting of society to the existing climate change.

Keywords Desertification · Climate change · Desertification index (ID) · Physiographic regions · TERRA/MODIS · Remote sensing · Ukraine

V. I. Lyalko · A. A. Apostolov · L. A. Elistratova · I. F. Romanciuc (✉) · I. V. Zakharchuk
Scientific Centre for Aerospace Research of the Earth of the Institute of Geological Sciences of the National Academy of Sciences of Ukraine, Kyiv, Ukraine

C. B. Pande et al. (eds.), *Climate Change Impacts on Natural Resources, Ecosystems and Agricultural Systems*, Springer Climate,
https://doi.org/10.1007/978-3-031-19059-9_2

Introduction

Desertification is one of the most hazard processes that lead to the environment degradation. The United Nation Convention to Combat Desertification adopted in 1994 is aimed on the desert lands development organization. According to the Convention, desertification of land degradation occurs in arid, semi-arid, and arid sub-humid regions (UNEP 1994). To implement the convention, the great studies have appeared, dedicated to the methodological problems of the desertification. The main accent in such researches is focused on the climate fluctuations and changes as one of the most important factor that provoke the land degradation. The importance of climsate change as the main factor affecting the land degradation is reflected in numerous international research works (Webb et al. 2017; Sivakumar and Stefanski 2007; Srivastava and Chinnasamy 2021). These works include the global coverage of desertification issues, applied and thematic studies from all arid continents, and provide promising policy recommendations for arid land monitoring and sustainable resource management (Pande et al. 2021a, Zdruli et al. 2010). Researches are focused on highlighting the aspects of land degradation and desertification around the world; the most modern methods of erosion measurement; past and present knowledge of soil conservation and analysis of climate change impacts on ecosystems (Pande et al. 2020, 2022). Among the works devoted to regional problems of desertification should be mentioned the following, describe situation in Mediterranean region, Africa. Middle East, etc. (Rubio et al. 2009; Ci and Yang 2010; Heshmati and Squires 2013). The main problems of arid land desertification in Russia are considered in the collective monographs (Alekseev et al. 2014; Kust et al. 2011). One of the first large-scale desertification monitoring projects is CAMELEO (Changes in Arid Mediterranean Ecosystems on the Long term through Earth Observation), launched in 1998. The project participant's consortium brought together scientists from Italy, France, Algeria, Egypt, Morocco, and Tunisia. According to CAMELEO, the test sites in Morocco, Algeria, Tunisia, and Egypt were studied. Images obtained from NOAA AVHRR and SPOT for the period 1987–2000 were used as remote sensing data (Escadafal and Megier 1998).

The DeMon project (Desertification Mapping and Monitoring in the Mediterranean Basin) was aimed at studying of desertification processes in the European Mediterranean. Areas of study were located on the European coast of the Mediterranean—in Spain, France, Greece, and Crete. The studies were conducted on the basis of Landsat MSS and TM satellite data with the involvement of ground and laboratory measurements (Archer and Stokes 2000). The MEDALUS project (Mediterranean Desertification and Land Use Monitoring), which was carried out with the participation of United Kingdom, Italy, and Netherlands, was also devoted to the desertification studying within the Mediterranean (Lamqadem et al. 2018). The main goal of the DEMOS project (Desertification in the Mediterranean Drylands: Developing a Monitoring System Based on Plant Ecophysiology), carried out in 1997–2000, covered the control desertification processes in the Turkey

and Lebanon ecosystems. Representatives of scientific institutes from Italy, Greece, Turkey, and Lebanon took part in the project (Salleo and Nardini 2003).

As a result, the number of methods for remote monitoring of land degradation processes has been developed: automated classification of eroded lands based on the development of various algorithms for unsupervised (Zizala et al. 2018; Pande et al. 2018) or supervised classification, combining data from different sensors (Meng et al. 2021; Pande et al. 2021b) regression models for determining erosion and its intensity by the spectral reflection values (Chang et al. 2020; Chen et al. 2020), multifractal image analysis (Krupiński et al. 2020), analysis of surface changes by methods of comparing differences in spectral images, principal component analysis, spectral mixture analysis, and analysis of spectral changes in multi-time images (Zhang et al. 2017; Salih et al. 2017). The world's first human-induced soil degradation map was published in 1991 by the Global Assessment of Human-induced Soil Degradation (GLASOD). The project was funded and implemented by the United Nations Environment Program (UNEP) in collaboration with the International Soil Reference and Information Center (ISRIC). This has demonstrated the first approximate estimate of the land degradation on the global scale. However, the map had to be constructed in a very short time, and the recommendations proposed by ISRIC (GLASOD 1988) for this work could not be applied in all countries. Recent years, Ukraine is not developed and implemented the measures to combat the land degradation and desertification due to the lack of continuous satellite monitoring of the land use systems. Given this negative trend, as well as the implementation of the United Nations Convention to Combat Desertification, signed by Ukraine, the country has committed itself to the rehabilitation of degraded lands and soils by 2030 and to achieve a neutral level of land degradation in the world. For Ukraine, the fight against desertification is one of the priorities of the state environmental policy.

Background

In the twenty-first century, global climate change has become one of the most negative environmental problems facing human attention. Its consequences are dangerous weather disasters, including droughts, as one of the factors commonly associated with desertification that leads to significant environmental and economic losses worldwide. The problem of monitoring and forecasting droughts remains relevant both in research and in application assignments. According to UN estimations, the economic losses caused by droughts exceed 20% of the total losses belonging to all natural disasters in general. The problem of aridity increasing in many agricultural regions of the globe under the influence of climate change is particularly acute, because currently the crops and stockbreeding production account for 70% of the total water consumed by major sectors of the economy (Orimoloye et al. 2022). Global food demand is projected to increase with 70% by 2050, with agricultural water consumption rising by about 19% and the main costs falling on regions already suffering from the water scarcity (Van Dijk et al. 2021). Ukraine is one of

the main agricultural regions of Eastern Europe due to the favorable combination of temperate climate and fertile soils. However, this area is often under the influence of large-scale circulatory systems, which leads to the long periods of the precipitation deficit that provokes the arid phenomena formation, such as dry. According to scientists, due to climate change, Ukraine is moving to zone of extremely high temperatures and weather cataclysms (Lyalko et al. 2015a, 2020; Apostolov et al. 2020). In the next 30–40 years, the country is already threatened by desertification of large areas. According to the World Resources Institute, Ukraine is one of the countries of drought risk both with the Middle East, North Africa, and Asia (Buchholz 2021).

The most studies of drought are based on precipitation, evaporation, humidity, air temperature, and radiation balance data. The individual meteorological variables cannot describe the complexity of drought phenomenon. For this purpose, the various drought coefficients or indices are needed, which usually consider the humidity and temperature conditions. All existing quantitative indicators have both advantages and disadvantages, so it is desirable to use several parameters and compare them assessing the intensity and prevalence of drought in a particular area. Along with simple estimates related to the precipitation or their anomalies determination, the complex of numerical indicators or drought indices is widely used, which can detect the phenomenon of drought itself and its intensity, as well as the level of adverse effects. As a single indicator has not been found yet, the problem of finding the new one and optimizing and adapting existing indices for the territory of Ukraine is relevant. The aim of this study is to estimate the aridity change of Ukrainian climate by the satellite drought index—ID and their impact on vulnerable ecosystems, their possible transformation, and identification of areas predisposed to desertification according to satellite data. The proposed study is based on the concept developed by assessing and minimizing the negative impact of the desertification process in the context of climate change in Ukraine. Its scientific substantiation is based on the analysis of the results of national and international studies of the climate change impact to the environment, including drought and other extreme processes intensification that negatively affect the functioning of various sectors of economy and society (agriculture, construction, transport, industry, energy, and others). An effective tool for studying the processes occurring in the natural environment under the climate change influence, in particular droughts, is the use of remote sensing data. Computer thematic interpretation of remote sensing data and their ground validation give possibilities for quickly and economic assessing and forecasting of aridity changes. It will serve as a basis for recommendations development for the governmental, managerial, and economic structures to implement the measures minimizing the negative impacts and implementing conditions for sustainable society development. Ukraine has the experience in conducting the researches of aridity and desertification with the usage of remote sensing data (Groisman and Lyalko 2012; Lyalko et al. 2009, 2017). The obtained results can be included in the international databases, providing complementarity to the forecasts of environmental management probability in the climate change conditions.

Materials and Methods

Since desertification is a dynamic process in time and space, a permanent system of observations—monitoring—is needed for control, forecasting, and timely prevention. For ecological control of this process, the remote sensing technologies are important. They possess the wide spatial coverage based on periodicity and systematicity of data receiving. Recent years, the great advantage of remote sensing is also referred to the high spatial, temporal, and spectral resolution. The remote sensing data allow analyzing and detecting the time changes and trends. The main methods of desertification analysis according to the remote sensing data are as follows: visual interpretation of space images, mathematical processing, and creation of drought maps that based on indices estimation.

Visual Interpretation of Remote Sensing Data

Visual interpretation of remote sensing data is based on perception and analysis of textures, shapes, and other characteristics of studied objects (Pande et al. 2018, 2021a). It also requires an understanding of the geological, ecological, and climatic components of the study area. In this study, the methods of visual interpretation were used to assess the possible transformation of ecosystems in typical landscape and climatic zones of Ukraine in modern climate conditions. This was done in GIS programs MapInfo Professional, ArcGIS by vectorization of the obtained images and comparison them with the boundaries of physiographical zoning of Ukraine (Marynych et al. 2003; National Atlas of Ukraine, 2007).

The Drought Map Creation by Using Indexes

The extreme climate conditions are increasingly manifested in the recurrence of droughts than in excessive moisture. The search for criteria and the development of drought indicators in scientific research in different countries has been conducted since the twentieth and thirtieth of the last century, which has led to the emergence of a large number of successful, convenient, and accurate numerical criteria. (Lyalko et al. 2015b). From the second half of the eightieth, the indices based on remote sensing data began to be introduced into the world practice of drought monitoring. Currently, there are about 100 satellite drought indices nowadays (Zolotokrylin et al. 2013). Attention to the droughts analysis according to satellite data in Ukraine has intensified after a fairly significant drought in 2007, as well as quite warm and arid periods in 2009 and 2010. To determine more accurately the time of drought and the area of its spread, it was proposed to use the Index of Drought (ID), which is directly proportional to the sum of night and day temperatures and inversely

proportional to the value of normalized vegetation index (NDVI). During drought events, the value of the NDVI index drops down, and the temperature of the underlying surface increases.

Index of Drought (ID) is calculated by the following equation:

$$\mathrm{ID} = \left(\mathrm{T}_{\mathrm{day}} + \mathrm{T}_{\mathrm{night}}\right) \Big/ \mathrm{NDVI} \tag{2.1}$$

where, T_{day}—day temperature, T_{night}—night temperature, and NDVI—normalized vegetation index. The increase of ID index values reflected the expectance of drought in the studied area.

The years 2000–2020 were chosen to study the aridity changes on the Ukraine territory. For each year during the vegetation season from April till October, the MOD11C3 and MOD13C2 products were received from the TERRA/MODIS satellite. The product data have 294 files for the entire studied period (USGS, 2021). Product MOD11C3 has the day and night monthly temperature data in Kelvin degrees, with a spatial resolution of 0.05 degrees. Product MOD13C2 has monthly data of two vegetation indices NDVI and EVI, as well as monthly spectral data bands: blue, red, NIR, and MIR, with spatial resolution of 0.05 degrees in *hdf* format. Thus, the estimation of the monthly drought index for the TERRA / MODIS satellite has the following form:

$$\mathrm{ID} = \left(MOD11C3_{day} + MOD11C3_{night}\right) \Big/ MOD13C2_{NDVI} \tag{2.2}$$

The MOD11C3 and MOD13C2 products were estimated by using Erdas Imagine software for remote sensing data processing. The Erdas Imagine software performed the following algorithm: 1) conversion data from *hdr* to *img* format; 2) conversion of MOD11C3 day and MOD11C3 night input data into monthly values of day and night temperature from K to °C; 3) calculation of ID index valued according to Eq. (2.2) for each month of the vegetation season; and 4) calculation of ID index valued according to Eq. (2.2) on average per period. The performed algorithm was implemented by Spatial Modeler/Model Maker module of Erdas Imagine software (Fig. 2.1).

The Meteorological Observations

The ground observation data of the near-surface layers' air temperature and the precipitation amount on the network of Ukraine ground meteorological stations are used in this study. Dataset from the stations was used in this study with a single continuous series of observations: 26 stations (1901–2020) and 48 stations (1946–2020), which are evenly distributed throughout the country. The averaging was carried out in order to identify the general patterns of air temperature and

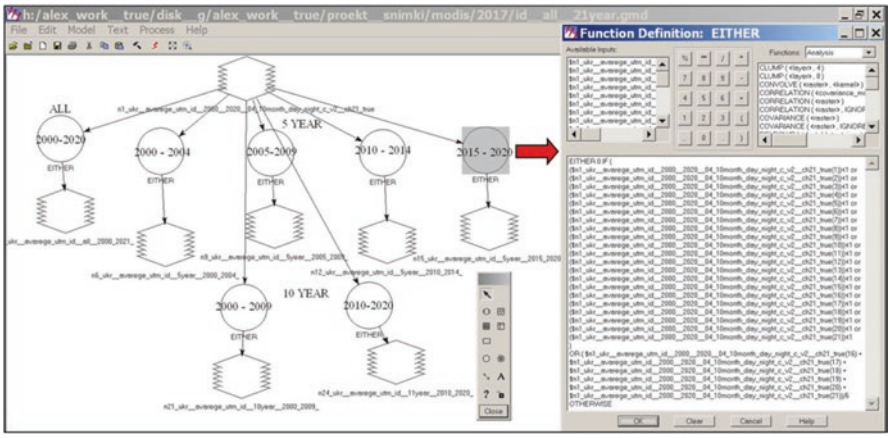

Fig. 2.1 Model built in the Erdas Imagine for ID index average values of 5 years' estimation, for decades and for the entire period 2000–2020

precipitation distribution over the Ukraine territory. Estimation of meteorological dataset in space and time was carried out using statistical methods. The location of ground meteorological stations is illustrated in Fig. 2.2.

Results and Discussions

Forecasting the environment modifications in the context of climate change requires the use of empirical and statistical meteorological information. There are no systematic data on the climate information analysis issues related to this problem. Analysis of the obtained results regarding the ecosystems changing in typical physiographic zones of Ukraine at fast process of warming was carried by applying the remote sensing estimated by the modern mathematical methods. Since 2000 till now, the characteristic feature of climate change in Ukraine is the increase of aridity.

Physiographic Conditions

Ukraine is characterized by a complex spatial differentiation of physical and geographical conditions. Geological structure and relief, climate, water, soils, vegetation, and fauna being in a complicated relationship and interaction, form natural–territorial complexes of different rank. The landscape-genetic principle serves as a basis of physical and geographical zoning, which determine the natural-territorial complexes and their boundaries. For this purpose, a comprehensive analysis is needed of the relationship and interaction of major landscape-forming

Fig. 2.2 Map of the Ukrainian physiographical zoning (National Atlas of Ukraine, 2007) completed with ground meteorological stations. I—zone of mixed (coniferous-deciduous) forests, II—zone of temperate broad-leaf forests, III—forest-steppe zone, IV—steppe zone, V—Ukrainian Carpathians, VI—Crimean Mountains

factors—solar radiation and Earth internal energy, processes occurring in lithosphere, hydrosphere, atmosphere, and biosphere, as well as considering natural components—lithogenic basis, earth's surface, air, surface and groundwater, soils, and biota (flora and fauna). In Fig. 2.2 is illustrated the map of physiographical zoning of Ukraine (National Atlas of Ukraine, 2007) combined with the location of ground meteorological stations used in this study.

Within Ukraine, there are two classes of landscapes in terms of common morphostructural features: plain and mountain. The main features of the Ukraine landscape structure are determined mainly by its location in the temperate zone. Only the southern coast of Crimea has the features of the subtropical zone characteristic. The Ukraine occupies the southwestern part of the Eastern European physiographical area, belonging to the Carpathian and Crimean mountain physiographical territory. Within the framework of the Eastern European physiographical area, Ukraine has four physical-geographical zones' categories in accordance with the predominance of certain landscape types and subtypes. According to the continental climate, the general relief nature, and the history of the geological and geomorphological basis of the natural complexes' formation, zones are divided into provinces. The provinces are divided into the physiographical areas (by position of the tectonic structures, topography, geomorphology et al.); regions—due to local differences in the manifestation, intensity and distribution of modern natural processes (National Atlas of Ukraine, 2007).

Climate Conditions

Climate changes in some parts of the globe, including Ukraine, are characterized by the annual air temperature. Temperature is an integral characteristic of all processes. Constant monitoring of air temperature from year to year gives statistical characteristic of the age course of the annual regional air temperature. It is well demonstrated in Fig. 2.3. The shown curve indicates that the warming process in Ukraine is quite active, despite the fluctuations. All this confirms that the warming is taking place throughout Ukraine and its intensity does not differ much. During twenty-first century (2000–2020) on the territory of Ukraine, the air temperature increased by 1.5 °C. Last 5 years, since 2015, the specific abnormal warm period was detected in Ukraine (Lyalko et al. 2015b, 2020).

Considering the various models is expected continuation of the temperature rising in Ukraine. By the end of the twenty-first century, it may increase by 0.7–3.0 °C compared to the period of 2001–2010 (soft "scenario B1") or 2.6–4.6 °C ("hard" scenario A2) (Nakicenovic and Swat 2000). The processes taking place in the global climate system and in the European territory determine the peculiarities of Ukraine's climate due to the general circulation processes. Ambiguous causes of climate change in Ukraine are characterized by distribution of precipitation. The formation of precipitation in Ukraine is a consequence of complex of macrocirculatory processes that provoke the heat and moisture exchange in the atmosphere. The essence of these processes is transferring the heat and moisture from the Atlantic Ocean and the Mediterranean Sea, as well as the large-scale vertical movements development under the cyclonic activity influence that leads to the precipitation process (Martazinova 2019; Martazinova et al. 2009).

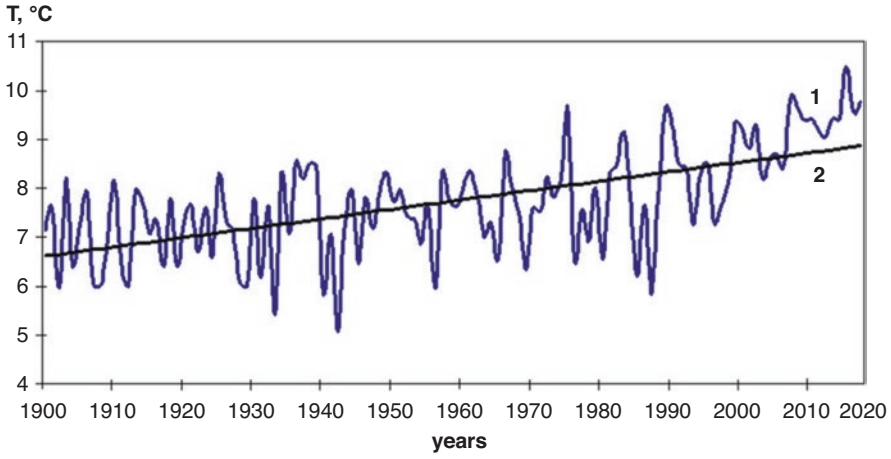

Fig. 2.3 Multiannual course of annual air temperature (°C) in Ukraine in accordance with the meteorological stations data: 1—actual course; 2—age course (trend)

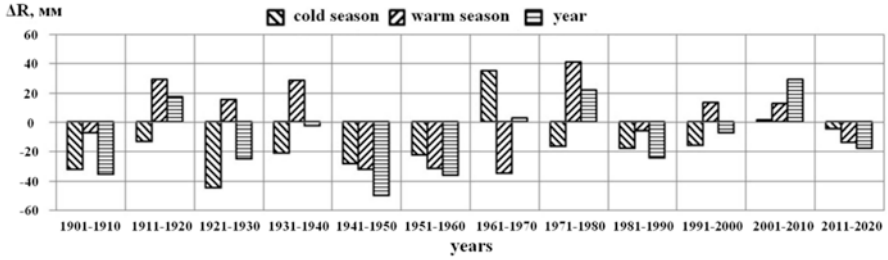

Fig. 2.4 Deviation of the precipitation average amount from the norm in Ukraine according to decades (1901–2020)

Figure 2.4 represents the estimated deviation of precipitation average amount in Ukraine for the 1901–2020 periods.

In Fig. 2.4 is shown the fluctuation of precipitations relatively to the "norm". The slight tendency of rainfalls reducing is visible. During the decades 1981–1990, 1991–2000, 2001–2010, 2010–2020, there is a decrease in precipitation fluctuations. According to the precipitations' measurement, the beginning of the precipitation-forming processes weakening is observed. Thus, the increase of air temperature average and uneven distribution of precipitation caused by the global climate change can lead to significant transformation of Ukrainian climatic and agricultural zones. It is known that the long-term fluctuations of climatic conditions on the planet significantly affect the state of ecosystems and lead to considerable displacement of natural areas. This process has the long-term period and cannot be observed by one or two generations of people. But even now, with the current trend of climate change in Ukraine, the slow changes were observed, not so much within the zones boundaries themselves, but relocations of the plants and animals' sets have begun that may lead to the zoning changes. To determine the boundaries of the plant group transition, it must be considered the temperature regime characteristics, the mode of humidification, as well as to make the analysis of parameter that characterizes the state of plants. In this study, this is characterized by the Index of Drought (ID).

Drought Estimation

Drought information based on the remote sensing technologies can be considered extremely valuable in two main reasons. First, the modern means of environmental monitoring based on satellite technologies allow the quick assess of vegetation and soil moisture content within the large areas and therefore warn in advance about the irrigation needs, or to apply other measures against the drought. Secondly, based on remote sensing data, it is possible the quickly mapping of crop losses area affected by drought and most accurately assess the damage caused by drought. This makes it possible to take the necessary measures in the agricultural sector. The parameters

that indicate the onset of drought, which can be detected by remote sensing data, are as follows: increase of the underlying surface temperature; deterioration of vegetation during the vegetation season. Drought monitoring tasks can be divided into the following levels. The first level is related to the drought occurred areas identification, the second level—monitoring the condition of crops during the drought. The method of vegetation indices is the main one that allows quantifying the dynamics of plants during the vegetation season. Traditionally, this method is used to determine the state of vegetation, its growing, and death. During the growing season, the application of NDVI, which is based on the visible and NIR band combination of the spectrum, does not provide complete information about the onset of drought. This happened because of two problems. First, the plant may be deteriorated for reasons unrelated to drought (soaking, disease, etc.). Second, each current year, the territory can be used in a way that is not typical for it, for example, it could not be planted with crops, and as a result, the vegetation is represented by wild grass. Since the drought is characterized by increased temperatures of the underlying surface, one of the important parameters of this phenomenon is the course of temperature curves during the vegetation season. But it is impossible to make judgments about the onset of agricultural drought based on the temperature elevation only, because not every meteorological drought grows into an agricultural one. Therefore, for more reliable detection of the drought-affected areas, it is better to use the underlying surface temperatures along with the vegetation index. Temperature indicators, along with vegetation indices, are widely used in the dry monitoring practice (Siqi et al. 2020; Mehravar et al. 2021). The temperature changes were characterized by product MOD11C3 obtained from the TERRA/MODIS satellite as the values. Analysis of the night and day images during the drought season and in the wet year showed that the agricultural drought is characterized by rising the daytime and nighttime temperatures. Probably lower temperatures at night lead to the formation of dew and fog, i.e., condensation of water vapor on the plants, which avoids moisture loss. In this case, the onset of atmospheric and soil droughts will not lead to agricultural drought. As higher are the values of the drought index, as greater is the probability of the drought appearance in the studied area. For the first signs of drought evaluation within the studied are, the monitoring of the vegetation conditions is necessary. Continuation of arid conditions can lead to deterioration of plants, and may not affect the harvest. For example, the May–June drought will mostly lead to the oppression of plants, and in extreme cases—to their death. The June drought is less severe, as the plants still have time to pass the growth stage, and at the stage of ripening, they are not so sensitive to the presence of moisture. Timely rain or watering can remove the threat of crop death and drought can stop by itself. But to react on time to the possible crop loss, it is necessary once a decade before the drought disappearance or even before the end of the growing season to analyze the condition of crops. In regions with the stable hot climate, the crops that are stable to drought are grown, or a set of irrigation measures is carried out that does not lead to crop loss. In regions with the normal weather conditions, the various crops are growing, including more demanding to moisture without additional reclamation measures, but during the dry years, considerable part of crop loss is possible. Such

areas with unstable weather conditions from year to year are called areas of critical agriculture. Such areas are the interest of our study. Ukraine is a region with favorable conditions for growing many crop types. This is ensured by a favorable balance of heat and moisture in most parts of the country. At the same time, a significant part of the Ukraine territory (steppe zone) is characterized by insufficient rainfalls. This presupposes the existence of territories of risky agriculture. Therefore, even the minor climate changes can lead to worsening the agro-climatic conditions.

Index of Drought

The proposed Index of Drought allows the estimation of the degree of drought development for Ukraine. In Fig. 2.5 is shown the spatio-temporal distribution of droughts within Ukraine for the 2000–2020 period. The gradations of the drought index ID values are shown in different colors. For period of 21 years, we have seen the satellite ID index changes at the subzones level of physiographical regions and districts. Starting the analysis from the Steppe zone (IV), where the largest ID values were observed in the territories of the middle steppe and south-steppe (dry-steppe) subzones. It was demonstrated that the agro-landscapes can undergo the significant changes. Figure 2.5 illustrates an acute shortage of moisture within the steppe zone. In fact, these areas are dominated by brown, orange, yellow, and pink colors: the range of ID values vary from 32 to 70 and more. According to our data,

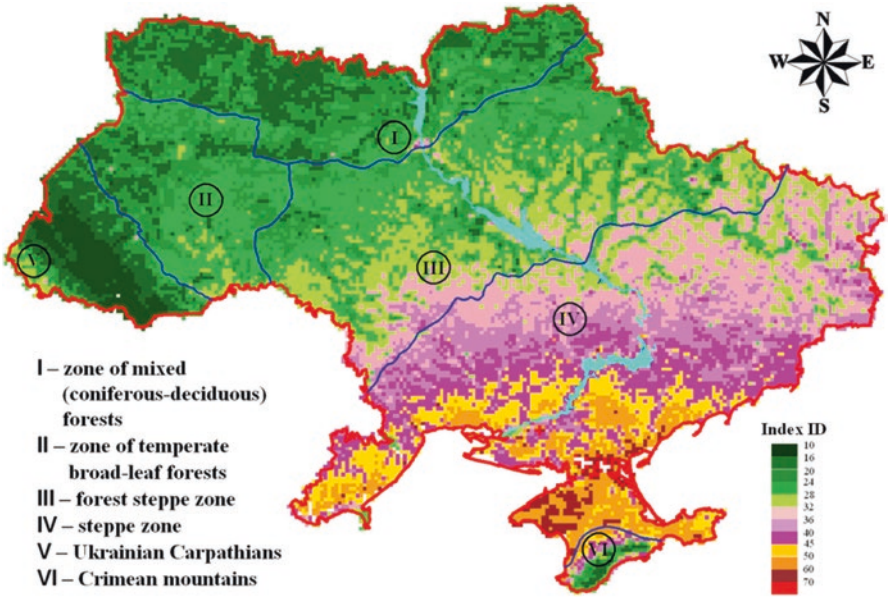

Fig. 2.5 Long-term values average (2000–2020) of the drought index ID in Ukraine

when the values of ID are more than 60, it indicates an acute shortage of moisture, where is recorded both the severe drought, and danger of possible plants death, in particular agricultural ones. In addition, the steppe zone may be affected by processes of climatic desertification (Lyalko et al. 2020; Apostolov et al. 2020) and by growth of physiological soil dryness due to its progressive salinization and increasing prevalence in the steppe zone of landscape species, which have saline and saline soils.

The main cause of droughts in Ukraine is the Arctic invasions with the subsequent transformation of air masses, as result of which the air mass moves away from the state of saturation. This leads to the cloudless hot weather establishing. Mainly drought appears due to the movement of a powerful anticyclone on the cold Arctic front. It becomes longer when one anticyclone is followed by another. There may be several days of cool weather between them, sometimes even light rains, but the moisture evaporates quickly. The main source of anticyclone, which causes drought in Ukraine, is the two main centers of action—the Arctic and the Azores (Martazinova and Sologub 2000). Also found that changes in the nature of circulation beginning in Eastern and Central Europe have led to number of southern cyclones increase. They are characterized by extremely high temperatures (more than 30-35 °C) and an increase of the precipitation amount that evaporates. During the climate change of the late twentieth and twenty-first century, the circulatory processes causing droughts have their own characteristics. It is described in detail by V.F. Martazinova (Martazinova and Sologub 2000). For a more detailed analysis of drought changing in space and time, the studied 21 years were divided into 4 periods (Fig. 2.6). It was established that each period was characterized by a gradual increase of the areas affected by droughts. During that time the entire southern, central and southeastern territory of Ukraine was covered by drought processes. In addition to drought intensity from period to period, there was detected an increase of the drought index values. Comparing the first period of 2000–2004 (Fig. 2.6a) and the last period of 2015–2021 (Fig. 2.6e) within the studied twenty-one-year period, it was found that for zone I (zone of mixed (coniferous-deciduous) forests, the ID index increased by 1.78 or 8.44%, for zone II (zone of temperate broad-leaf forests)–by 1.51 or 6.38%, for zone III (forest-steppe zone)–by 4.19 or 16.41%, and for zone IV (steppe zone)–by 6.5 or 17.58%.

In the twenty-first century, the crop yield reductions were observed in 2003 and 2007 due to the adverse weather conditions. The drought of 2007 was severe and prolonged, which has not been observed for the last 60 years. For about the same number of years, there was no such low grain yield per hectare (Semenova and Ovcharuk 2017). For comparison and analysis, the year 2007 was proposed, which was covered by a prolonged drought, in particular during the active vegetation period of plants (Fig. 2.6d). As already mentioned, the prolonged drought of 2007 has become a particularly threatening phenomenon for crop yields. According to the time of onset, there were spring, summer, and autumn drought observed. Spring drought is characterized, as a rule, by low air temperatures at low relative humidity, insignificant reserves of productive moisture in the soil and dry winds. Prolonged drought in the spring significantly reduces crop yields, even in favorable summer

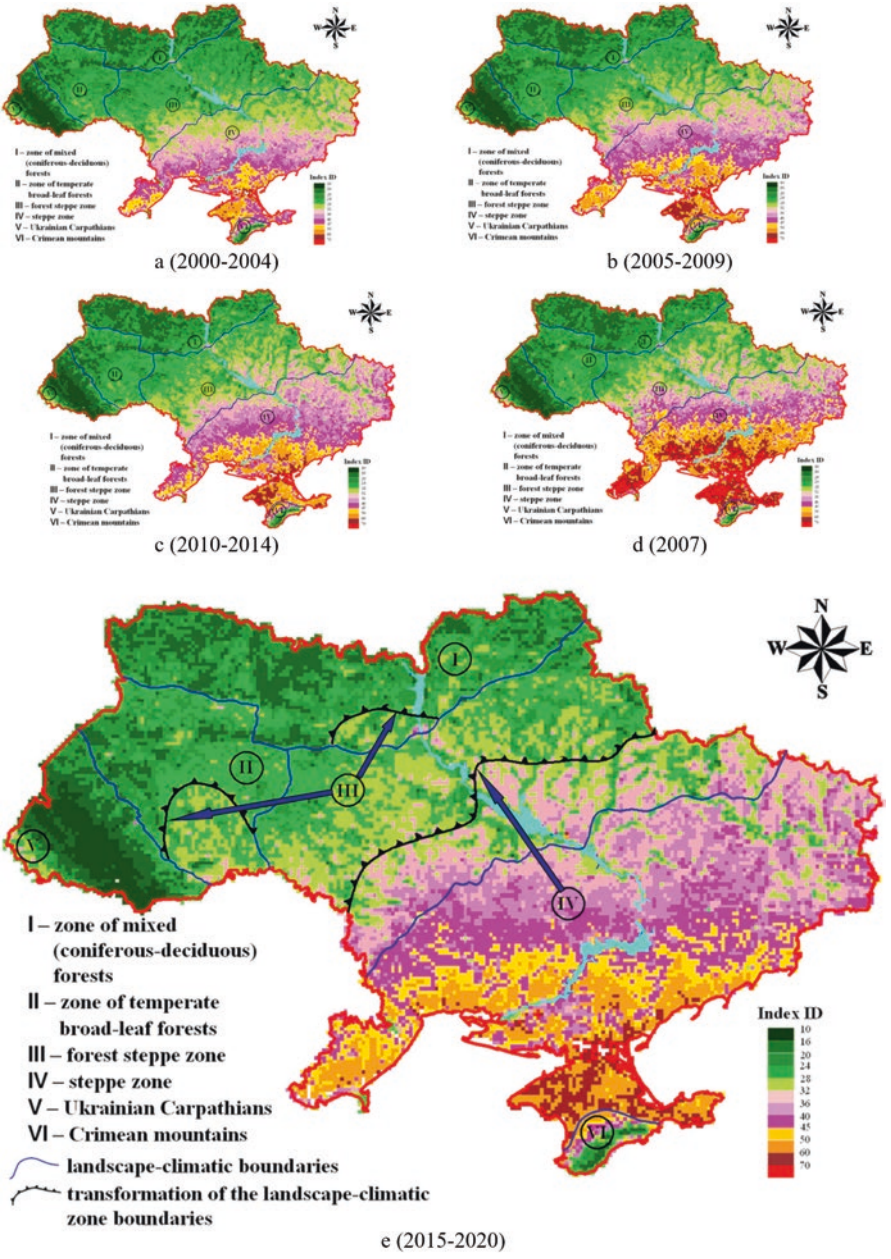

Fig. 2.6 Monitoring of the land cover state based on the drought index ID use on the Ukraine territory for the periods: (**a**) 2000–2004, (**b**) 2005–2009, (**c**) 2010–2014, (**d**) 2007, (**e**) 2015–2020

conditions for the degree of moisture. Summer drought is characterized by high air temperatures, hot dry winds, which cause increased evaporation. The effects of summer drought are manifested in a sharp decline in crop yields, etc. Autumn drought is characterized by low temperatures; it is the most dangerous for winter crops that do not have time to take root, go through the tillering phase and very often die in the winter (Walz et al. 2018; Lyalko et al. 2015c). In Fig. 2.6d is shown that in 2007 a prolonged drought began in May, including the active growing season of crops and lasted until September. The driest periods were July and August. Territorially, the most widespread drought was observed in July. In addition to these gradations of the ID index in 2007 is observed very active red color (ID value >70) in zone IV, indicating a catastrophic moisture deficit. Such a long period of drought in 2007 led to the death of crops. That year showed the scenario of the drought process development in Ukraine (catastrophic situation), if climate change occurs in the direction of warming. In Fig. 2.6e, the last 5 years 2015–2020 in terms of spatial distribution of the arid area already coincided with the model year-2007, so far there is no such intensity (no red color). In Fig. 2.6e is shown the possible transformation of the physiographical zones of Ukraine based on the drought index ID analysis. There is a gradual shift to semi-deserts, which previously was not detected in Ukraine in the steppe zone (IV), steppe zone (IV) to forest-steppe zone (III); forest-steppe zone (III) in the zone of deciduous forests (II); and in the zone of mixed (coniferous-deciduous) forests (I). This can lead to undesirable consequences, as ecosystems do not have time for adapting to rapid climate change. In addition, it will significantly complicate the agricultural activities in the southern and south-eastern regions of Ukraine (steppe zone).

Besides, this process may be accompanied by depletion of freshwater resources in these regions. This effect is quite unfavorable from ecology, as it will lead to a catastrophic state of natural ecosystems. The nature of species biodiversity can change significantly. It should be noted that the biota reaction to the new climatic conditions may happen due to both natural and anthropogenic factors, leading to appearance of the new varieties of plants. Already now such regional climate changes observed in the twenty-first century, in particular the changes in aridity, are manifested not only in the sudden replacement of one species of plant group to another, but in the gradual growth of one type of landscape features to the another type of landscape.

Due to global warming, the intensity of which is not decreasing, but rather increasing, the main issue of the world community is to maintain the food balance on Earth as a whole and at the individual regions as well. Therefore, any climate change in the direction of warming or cooling requires addressing the issue of agriculture adaptation to current and future climate change conditions. In the twenty-first century, the areas where the frequency of droughts may increase could expand. Further climate change is possible, and as a result of droughts in Ukraine, the agricultural sector may be significantly affected. At the same time, there are concerns

about the low level of readiness for these changes. Strategies for agriculture adapting to the negative climate change need to be developed now. In this situation, early notification of droughts and the true information of the drought extent is extremely important.

Conclusions

The use of remote sensing data, especially drought indices, opens up the new possibilities in understanding of the drought causes, identifying the peculiarities of its spread, especially detailing its intensity within the different territories. The advantage of the drought index ID use makes possible the consideration of the underlying surface, which cannot be sufficiently investigated and taken into account when studying drought according to the meteorological data only. The obtained results show the possibility of effective use the remote sensing data to determine drought, assessing the ecosystems moisture supply and phytocenoses within large regions. This approach can be used to conduct environmental monitoring studies within the different landscapes and climatic zones throughout Ukraine and is applicable for other countries, considering their physical and geographical features.

Recommendations

The research data obtained and methodology proposed to consider the drought index ID for the drought of agricultural areas monitoring should be considered by the State Agencies and Public Authorities responsible for the agricultural sector sustainable maintenance and development. Ensuring the food and environmental safety in arid and semi-arid areas of Ukraine and other countries affected by arid processes, it is necessary to provide a number of measures for further development of irrigated agriculture, modernization of irrigation systems based on modern technologies. In addition, organizational and economic measures should include the monetary compensation to agricultural producers who have suffered significant losses from drought, exemption from agricultural tax due to crop failure, increase in purchase prices for agricultural products, risk insurance, payment of insurance losses, creation of state agencies for agricultural risk insurance services, leasing companies and investment projects, forecasting yields and gross grain harvest, drought monitoring, development and approval of a state program to protect agricultural plants from drought, scientific support, and implementation, etc. Therefore, the control of soil moisture is extremely important for assessing the condition of crops. It is desirable that the government, as well as decision-makers in the field of logistics, pay attention to the negative effects of climate changes and the conditions of food security in Ukraine and other countries.

References

Alekseev GV, Ananicheva MD, Anisimov et al (2014) The second Roshydromet assessment report on climate change and its consequences in the Russian Federation. General Summary, Rosgidromet, Moscow, p 54

Apostolov OA, Elistratova LO, Romanchuk IF, Chekhniy VM (2020) Assessment of desertification areas in Ukraine by estimation of water indexes using remote sensing data. Ukrainian Geog J 1:16–25. https://doi.org/10.15407/ugz2020.01.016

Archer S, Stokes C (2000) Stress, disturbance and change in rangeland ecosystems. In: Amalds O, Archer S (eds) Rang e-land desertification. Kluwer Academic Publishers, pp 17–38

Buchholz K (2021) The World map of drought risk. https://www.statista.com/chart/25101/countries-by-drought-risk/

Chang C, Lin F, Zhou X, Zhao G (2020) Hyper-spectral response and estimation model of soil degradation in Kenli County, the Yellow River Delta. PLoS One 15(1):e0227594. https://doi.org/10.1371/journal.pone.0227594

Chen X, Wang T, Liu S, Peng F, Kang W, Guo Z, Feng K, Liu J, Tsunekawa A (2020) Spectral response assessment of Moss-dominated biological soil crust coverage under dry and wet conditions. Remote Sens 12(7):1158. https://doi.org/10.3390/rs12071158

Ci L, Yang X (2010) Desertification and its control in China. Springer, p 513. https://doi.org/10.1007/978-3-642-01869-5

Escadafal R, Megier J (1998, November 23–27) CAMELEO: a Concentrated Research Effort to Develop Validated Desertification Monitoring Techniques in Northern Africa. Proc. of International Symposium Satellite-Based Observation: A Tool for Study of the Mediterranean Basin. Tunis

GLASOD (1988) Global assessment of human-induced soil degradation. https://www.isric.org/projects/global-assessment-human-induced-soil-degradation-glasod

Groisman P, Lyalko V (2012) Earth systems change over Eastern Europe. Akademperiodyka, Kiev, p 488

Heshmati GA, Squires V (2013) Combating desertification in Asia, Africa and the Middle East. Springer, Dordrecht, p 476. https://doi.org/10.1007/978-94-007-6652-5

Krupiński M, Wawrzaszek A, Drzewiecki W, Jenerowicz M, Aleksandrowicz S (2020) What can multifractal analysis tell us about hyperspectral imagery? Remote Sens 12(24):4077. https://doi.org/10.3390/rs12244077

Kust GS, Andreeva OV, Dobrynin DV (2011) Desertification assessment and mapping in the Russian Federation. Arid Ecosyst 1:14–28. https://doi.org/10.1134/S2079096111010057

Lamqadem AA, Pradhan B, Saber H, Rahimi A (2018) Desertification sensitivity analysis using MEDALUS model and GIS: a case study of the Oases of Middle Draa Valley. Morocco Sensors 18(7):2230. https://doi.org/10.3390/s18072230

Lyalko VI, Kostyuchenko YV, Marton L (2009, June 9–12). EO capabilities for analysis of climate related socio ecological risks: bio productivity, desertification, and natural disasters. In: Using Satellite and In Situ Data to Improve Sustainability. Proc. of Advanced Research Workshop. Kiev. pp. 56–58

Lyalko VI, Elistratova LA, Kul'bida MI, Apostolov AA, Bararash MB (2015a) Climate changes in Ukraine at the end of XX – beginning of XXI century according to ground and remote sensing data. Ukrainian J Remote Sens Earth 6:33–63

Lyalko VI, Elistratova LA, Apostolov AA (2015b) Use of ID-index for revealing a probable transformation of ecosystems in typical landscape-climatic zones of Ukraine at the modern climate. Rep NAS Ukraine 3:94–99

Lyalko VI, Elistratova LA, Apostolov AA (2015c) Comparative researches of a drought using satellite and meteorological indexes for 2007 within Ukraine as example. Space Sci Technol 21(3):27–30

Lyalko V, Ivanov S, Starodubtsev V, Palamarchuk J (2017) The effects of institutional changes on landscapes in Ukraine. In: Gutman G, Radeloff V (eds) Land-cover and land use changes in Eastern Europe after the collapse of the Soviet Union in 1991. Springer International Publishing, Switzerland, p 119O147. https://doi.org/10.1007/978O3O319O42638O9_6

Lyalko VI, Romanciuc IF, Yelistratova LA, Apostolov AA, Chekhniy VM (2020) Detection of changes in terrestrial ecosystems of Ukraine using remote sensing data. J Geol Geogr Geoecology 1(29):102–110. https://doi.org/10.15421/112010

Martazinova VF (2019) Instability of daily summer air temperature from the beginning of the XXI century at Kyiv Weather Station. Ukrainian Geogr J 3:15–21. https://doi.org/10.15407/ugz2019.03.015

Martazinova VF, Sologub TA (2000) The atmospheric circulation forming dry conditions in Ukraine in the late twentieth century. Sci works UkrNDGMI Iss 248:36–47

Martazinova VF, Tymofeyev VE, Ivanova EK, Chayka DY (2009) The present day climate of Eastern Europe as viewed in the context of atmospheric circulation change. Bulletin of Geography 1:7–18

Marynych OM, Parkhomenko HO, Petrenko OM, Shyshchenko PH (2003) Improved physical and geographical zoning of the Ukraine. Ukrainian Geogr J 1:16–20

Mehravar S, Amani M, Moghimi A, Dadrass Javan F, Samadzadegan F, Ghorbanian A, Stein A, Mohammadzadeh A, Mirmazloumi SM (2021) Temperature-vegetation-soil moisture-precipitation drought index (TVMPDI); 21-year drought monitoring in Iran using satellite imagery within Google earth engine. Adv Space Res. https://doi.org/10.1016/j.asr.2021.08.041

Meng X, Gao X, Li S, Li S, Lei J (2021) Monitoring desertification in Mongolia based on Landsat images and Google earth engine from 1990 to 2020. Ecol Indic 129:107908. https://doi.org/10.1016/j.ecolind.2021.107908

Nakicenovic N, Swart R (2000) Special Report on Emissions Scenarios (SRES) – a Special Report of Working Group III of the Intergovernmental Panel on Climate Change

National Atlas of Ukraine (2007) Institute of Geography of National Academy of Sciences, Intelligence Systems Geo Ltd. & Ukrainian branch of World data center in Kiev Polytechnic Institute. http://wdc.org.ua/atlas/en/default.html

Orimoloye, I.R., Olusola, A.O., Belle, J.A. et al. (2022). Drought disaster monitoring and land use dynamics: identification of drought drivers using regression-based algorithms. Nat Hazards 112(2), 1085–1106. https://doi.org/10.1007/s11069-022-05219-9

Pande CB, Moharir KN, Khadri SFR et al (2018) Study of land use classification in an arid region using multispectral satellite images. Appl Water Sci 8:123. https://doi.org/10.1007/s13201-018-0764-0

Pande CB, Moharir KN, Singh SK et al (2020) An integrated approach to delineate the groundwater potential zones in Devdari watershed area of Akola district, Maharashtra, Central India. Environ Dev Sustain 22:4867–4887. https://doi.org/10.1007/s10668-019-00409-1

Pande CB, Moharir KN, Singh SK, Varade AM, Ahmed Elbeltagie SFR, Khadri PC (2021a) Estimation of crop and forest biomass resources in a semi-arid region using satellite data and GIS. J Saudi Soc Agric Sci 20(5):302–311

Pande CB, Moharir KN, Khadri SFR (2021b) Assessment of land-use and land-cover changes in Pangari watershed area (MS), India, based on the remote sensing and GIS techniques. Appl Water Sci 11:96. https://doi.org/10.1007/s13201-021-01425-1

Pande CB, Kadam SA, Jayaraman R, Gorantiwar S, Shinde M (2022) Prediction of soil chemical properties using multispectral satellite images and wavelet transforms methods. J Saudi Soc Agric Sci 21(1):21–28

Rubio JL, Safriel U, Daussa R, Blum WEH, Pedrazzini F (eds) (2009) Water scarcity, land degradation and desertification in the Mediterranean region, NATO science for peace and security series C: environmental security. Springer Science + Business Media, p 73

Salih AAM, Ganawa E-T, Elmahi AA (2017) Spectral mixture analysis (SMA) and change vector analysis (CVA) methods for monitoring and mapping land degradation/desertification in arid and semiarid (Sudan), using Landsat imagery. Egypt J Remote Sens Space Sci 20(1):S21–S29. https://doi.org/10.1016/j.ejrs.2016.12.008

Salleo S, Nardini A (2003) Some guidelines for monitoring desertification of Mediterranean drylands on the basis of plant water status: methodological problems and results from the DEMOS project. Manag Environ Qual 14(1):39–50. https://doi.org/10.1108/14777830310460379

Semenova IG, Ovcharuk VA (2017, May 9–13). Droughts of the last centenary period in Ukraine. PAGES – OSM 2017. Zaragoza, Spain. https://doi.org/10.13140/RG.2.2.35578.34245

Siqi S, Fengmei Y, Jia-Hua Z, Shanshan Y (2020) Evaluation of temperature vegetation dryness index on drought monitoring over Eurasia. IEEE Access 8:30050–30059. https://doi.org/10.1109/ACCESS.2020.2972271

Sivakumar MVK, Stefanski R (2007) Climate and land degradation — an overview. In: Sivakumar MVK, Ndiang'ui N (eds) Climate and land degradation. Environmental science and engineering (environmental science). Springer, Berlin, Heidelberg. https://doi.org/10.1007/978-3-540-72438-4_6

Srivastava A, Chinnasamy P (2021) Developing village-level water management plans against extreme climatic events in Maharashtra (India)—A case study approach. In: Vaseashta A, Maftei C (eds) Water safety, security and sustainability. Advanced sciences and Technologies for Security Applications. Springer, Cham. https://doi.org/10.1007/978-3-030-76008-3_27

UNEP (1994, June 17) Development of guidelines for assessment and mapping of desertification and degradation in Asia/Pacific. Proceedings of the Draft Report of the Expert Panel Meeting. Paris, France. United Nations Environment Programme: Robbie, Kanyana

USGS (2021, October) Earth Explorer. sUnited States Geological Survey. https://earthexplorer.usgs.gov/

Van Dijk M, Morley T, Rau ML, Saghi Y (2021) A meta-analysis of projected global food demand and population at risk of hunger for the period 2010–2050. Nat Food 2:494–501. https://doi.org/10.1038/s43016-021-00322-9

Walz Y, Dall K, Graw V, Villagran de Leon JC, Haas S, Kussul N, Jordaan A (2018) Understanding and reducing agricultural drought risk: Examples from South Africa and Ukraine. Policy Report No.3. Bonn: United Nations University. Institute for Environment and Human Security (UNU-EHS)

Webb NP, Marshall NA, Stringer LC, Reed MS, Chappell A, Herrick JH (2017) Land degradation and climate change: building climate resilience in agriculture. Front Ecol Environ 15(8):450–459. https://doi.org/10.1002/fee.1530

Zdruli P, Pagliai M, Kapur S, Cano FA (eds) (2010) Land degradation and desertification: assessment, Mitigation and Remediation. Springer, p 660. https://doi.org/10.1007/978-90-481-8657-0

Zhang Z, Ouyang Z, Xiao Y, Xiao Y, Xu W (2017) Using principal component analysis and annual seasonal trend analysis to assess karst rocky desertification in southwestern China. Environ Monit Assess 189(6):269. https://doi.org/10.1007/s10661-017-5976-5

Zizala D, Juricova A, Zadorova T, Zelenkova K, Minarik R (2018) Mapping soil degradation using remote sensing data and ancillary data: south-East Moravia, Czech Republic. European J Remote Sens 52(3):1–15. https://doi.org/10.1080/22797254.2018.1482524

Zolotokrylin AN, Titkova TB, Cherenkova EA, Vinogradova VV (2013) Comparative study of droughts 2010 and 2012 in the European Russia for meteorological and MODIS data. Sovr Probl DZZ Kosm 10(1):246–253

Chapter 3
Climate Change Effect on the Urbanization: Intensified Rainfall and Flood Susceptibility in Sri Lanka

M. D. K. Lakmali Gunathilaka and W. T. S. Harshana

Abstract Climate change is inevitable with the interference made by various anthropogenic activities. Urbanization and development are two main processes that affect climate change. Thus, urbanization and climate change are like two sides of the same coin. The conjunction between climate change and urbanization already has created several issues in urban areas. Such issues are more common in developing countries due to unsustainable development, rapid urbanization, and population growth. The Sri Lankan scenario is also the same. The increased intensity and frequency of rainfall and increased land surface temperature are observable in urban areas in Sri Lanka. Colombo is the main administrative city and the largest urban area lies within the lower Kelani River basin. Due to the frequent flooding, the low lands usually inundate for days. Along with the wetland shrinkage and unsustainable development, the inundation period has increased creating a higher magnitude of flooding disaster. The damage due to frequent flooding usually creates an economic burden which in turn affects the development of the country. Sustainable development and greening cities are highly recommended to reduce the impacts of climate change in urban areas.

Keywords Flood · Greening cities · Urban Heat Island · Rainfall · Urbanization

Introduction

Climate is defined as the long-term weather conditions that prevail over an area. Climate change is the change in long-term normal climate or climate variability (Rieddy 2020). Long-term changes in meteorological factors based on climate or

M. D. K. L. Gunathilaka (✉)
Department of Geography, University of Colombo, Colombo, Sri Lanka

W. T. S. Harshana
Urban Development Authority, Battaramulla, Sri Lanka

C. B. Pande et al. (eds.), *Climate Change Impacts on Natural Resources, Ecosystems and Agricultural Systems*, Springer Climate,
https://doi.org/10.1007/978-3-031-19059-9_3

human activity are called climate change, and these changes are measured over several decades and observed by statistical data to determine these changes (UN 2011). The atmosphere, oceans, and landmasses have warmed due to human influence and as a result, wide and rapid changes have taken place in those systems. Accordingly, research has shown that the concentration of greenhouse gases on human activity has increased since about 1750 and that the atmospheric concentration of carbon dioxide has increased from 410 ppm from 2011 to 2019, the rise of methane has risen to 1866 ppm, and the atmospheric concentration of nitrous oxide has been observed to be 332 ppb. The study also estimates that carbon dioxide emissions (Appendix 1) from human activity have increased by 56% annually over the past six decades, with regional variations (Appendix 2) (IPCC Climate change 2021). In the discussion of global warming, the last four decades from 1850 onwards have consistently recorded higher than the magnitude of global warming represented in the previous decade. That is, in the first two decades of the twenty-first century, the quantitative value of global warming represented by the year 2001–2020 has increased by 0.99 °C, over the period from 1850 to 1900 (IPCC Climate change 2021, 2017). Thus, the intensity of global warming is clear. Further research shows that global surface temperatures increased by 1.09 Celsius between 2011 and 2020, compared to 1850–1900. According to the researchers' observations and data analysis, the total global surface temperature increase caused by the human intervention was 0.8 °C between 1850 and 1900 and increased to 1.3 °C between 2010 and 2019. Variations in global precipitation can be identified as another global climate change that coincides with global warming. That is, there has been a gradual increase in global rainfall since the 1950s, and its growth rate intensified by the 1980s. Many variations on this condition have been observed by the twentieth century (IPCC Climate change 2021, 2017).

When discussing extreme conditions of temperature, the likelihood of heatwaves intensifying more frequently or in the long run is highly underestimated, and it is predicted that winter chances will be very low in the future during those triangular hot seasons. Also, the current daily temperature range is decreasing everywhere. Considering the moderate rainfall, the forecasts are that the rainfall will be maximum in the tropical and subtropical regions representing the tropical regions. It is estimated that with the intensification of the global hydrological cycle, rainfall will gradually increase in the upper latitudes as well. In the case of extreme rainfall and droughts, the intensity of rainfall increases, while the mean of the tropical and sublatitudes increases. Also, even in regions that receive less rainfall, the intensity of rainfall will increase, but the time interval between rainfall events will increase slightly. Drought conditions are predicted to be severe in the central continental regions during the summer. When discussing carbon cycles, future climate change reduces the efficiency of these carbon cycles. Also, by 2100, the atmospheric extra carbon concentration will change by 20 ppm. It is also predicted that this era will represent a value in the range of 730 ppm to 1020 ppm by 2100 (The standard value here is 836 ppm). Among the predictions made in considering the El Nino situation is that the southern oscillation of El Nino is predicted to be violently active. Forecasts for monsoon rainfall include an increase in rainfall over the Asian monsoon season

and the southern part of the West African monsoon with some decrease in the Sahel in the Northern summer, as well as an increase in the Australian monsoon in the southern summer in a warmer climate. Forecasts for its pressure at sea level show that regions above the subtropics and centers increase sea level pressure and lower it above high latitudes. Predictions of an increase in tornado patterns in the Arctic and Antarctic regions at higher latitudes have also been made. Forecasts for tropical cyclones include forecasts of future tropical cyclones that are expected to intensify and show a decrease in the number of hurricanes as a whole. The forecast for mid-latitude storms shows a decrease in the number of mid-latitude storms. In this way, its variations can be clearly defined based on global weather conditions as well as meteorological factors.

Climatic influences on climate variability are active in a variety of ways, both globally and regionally. That is, the effects of climate change, good or bad, are now clearly visible around the world. Climate change is currently causing several meteorological effects around the world, many of which appear to have adverse effects, a handful of which are expected to have a positive effect. Among these effects, it must be said that the impact of global warming is very high. That is to say, it can be seen that adverse effects have been created in many fields through this. These include increased glacial melting rates, premature eruptions of ice sheets on rivers and lakes, changes in flora and fauna, rapid flowering of plants, loss of sea ice, and rising sea levels, and intensification of heatwaves as a result of global warming (NASA 2021a, b). Sea level rise is a direct effect of climate change. This sea level rise is continuously measured by NASA and is 3.4 mm per year. That is, the gradual rise in sea level from 1995 to 2020 is as follows (NASA 2021b). Changes in rainfall patterns can also be pointed out as a result of this climate change. In 1977, NASA and JAXA used active and passive microwave equipment for the Tropical Rainfall Measurement Operation (TRMM) to observe variations in these rainfall patterns. The Arctic's ice sheet has intensified, and NASA says the Arctic Ocean is expected to be ice-free by the middle of this century. The melting of the ice is a direct result of global warming, with NASA estimates that the Arctic ice melting rate will be 13.1 km^2 per decade. Recent data shows the decrease in the mass of the ice sheet caused by the melting of ice according to satellite data from 1984 to 2016 (NASA 2021b). Accordingly, the mass of ice in 1984 was 6.81 million square kilometers, and in 1992 it was 7.47 million square kilometers, during which time the ice sheet has grown. However, by the year 2000, the mass of the ice sheet had dropped back to 6.25 million square kilometers, and in 2008 it dropped further to 4.69 million square kilometers. The size of the ice sheet is further declining, and in 2016 it reached 4.53 million square kilometers (NASA 2021b). The most demanding challenge of climate change and its intensified impacts directly targeted small island nations as well as developing countries. Coastal developing countries; Bangladesh, Thailand, India, Maldives, Micronesia and Melanesia, Pacific Island nations, Sri Lanka, countries at the zone of Sahel are among them. Climate change threatens sustainable development and all eight Millennium Development Goals. Providing a better and safe life with the shrinking environment is the greatest challenge

emerging through the disturbing economic development occurring concerning climate change.

Relationship Between Urbanization and Climate Change

Urbanization is the process by which cities grow, and a higher percentage of the population comes to live in the city. That is to say, the increase in the migration of people living outside the so-called urban areas can be further interpreted as the urbanization of an area. Most of the people living in rural areas leave the rural areas where they used to live and move to the so-called urban areas based on certain objectives. As it gradually grows, the population concentration in these areas will increase and based on these factors, there will be an increase in urban areas and at the same time, there will be an increase in infrastructure and services in those areas. Globally, the growth of the global urbanization process can be examined as follows. That is, around 1800, 3% of the world's population lived in urban areas, and by the end of the twentieth century, that number had grown to 47%. Further analysis shows that in 1950, there were 83 cities with a population of over 1 million, and by 2010 it had grown to 460 cities. That is to say, it is better to say that the growth in the so-called urban areas is very fast. Globally, the most urbanized areas in terms of urban growth are North America at 82%, Latin America and the Caribbean at 80%, Europe at 74%, and Oceania at 71% (Bolay 2019) (Fig. 3.1). In Africa and Asia, 49% and 41% of the population, respectively, live in urban areas. Further analysis reveals that most of the population live in rural areas in Africa, such as Nigeria, Ethiopia, Tanzania, and Kenya, as well as China, India, Indonesia, and Myanmar in Asia (Pande and Moharir 2017; Rajesh et al. 2021). That is, UN reports predict that by the year 2050, two-thirds of the world's population will live in urban areas, and UN forecasts show that these urban areas will gradually shift away from Europe, that is, to Asia and West Africa. Urban Population Growth, the United Nations estimates that by 2050, 65% of the population of developing countries and nearly 90% of the population of developed countries will live in urban areas (Dagmav et al. 2018). As the urban population grows, so does the urban land area. Also, the land use of the land is adapted to urban patterns. Considering the last 30 years, the coastal areas can be pointed out as the main urbanized land areas. At present, urbanization is based on South Asia, Southeast Asia, Southeast China, the United States, Eastern and Western Europe, Japan, West Africa, and the Latin American Atlantic region. That is, at the beginning of the twenty-first century, the study revealed that 11% of the urban land area, or more than 70,000 km^2, is located along this coastal zone (Dagmav et al. 2018).

Figure 3.1 shows that by 2050, most of the world's landmass will be urbanized. With the growth of urbanization, it is becoming more and more common globally that most areas are being industrialized to meet the needs of the urban population. That is, as the needs of the people in the urban areas increase, a variety

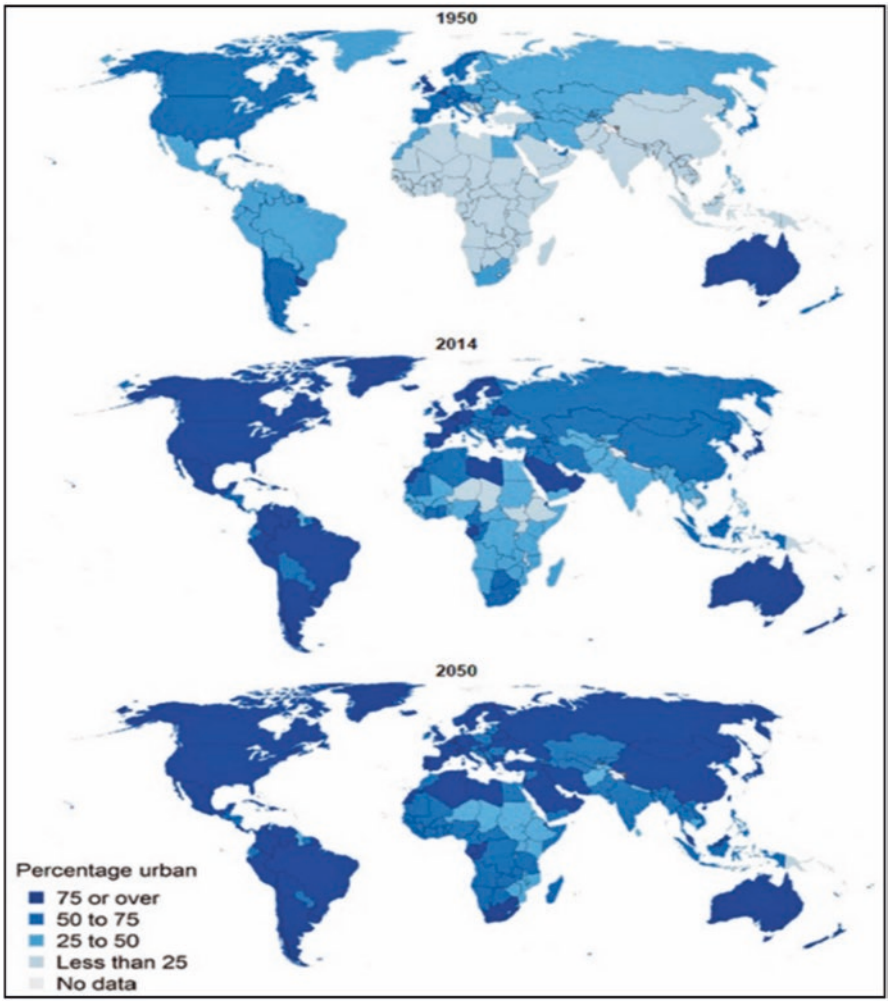

Fig. 3.1 Percentage of the population residing in urban areas in 1950, 2014, and 2050. (Reproduced from UN-HABITAT 2018. Source: Bolay 2019)

of products are created. To maintain this production process, industrial estates will be centralized in parallel with these areas.

Among the countries that were industrialized during the 1850s, the Americas were the most important region around the United States, and the most important countries in Europe were the United Kingdom, Germany, France, and Poland. That is, during the 1850s, industrialization was limited to a few parts of the world. It appears to have strongly penetrated the United States, the European region, and Asia, as well as Australia by late 1900. Later, this has led to classifying the countries into developed, developing, emerging developed, and less-developed likewise (Fig. 3.2). The bottom line is that as urbanization expands, so does industrialization

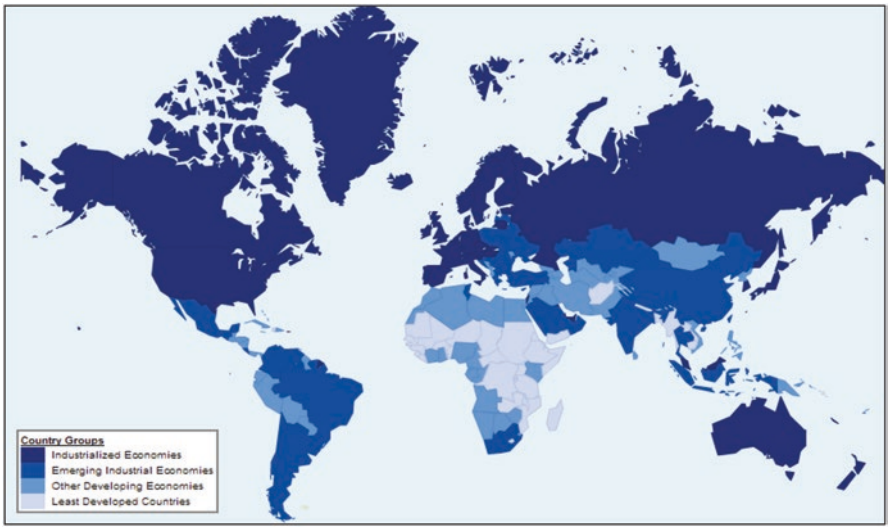

Fig. 3.2 Country groups by stage of industrialization on the world map. (Source: Upadhyaya 2013)

around the world. Today, the growth of these urban areas is rapidly occurring in almost every country in the world, and it is clear in this competitive world that the process continues to grow. The growth of these urban areas, directly and indirectly, influences many of the active processes taking place in the world, one of the major factors of which is climate change. The current changes in climatic conditions based on this urbanization can be discussed as follows. It is now clear how this effect is active globally, or even within a recognized region. With the gradual growth of the population, many of the physical features of those urban areas also grow in proportion. For example, urbanization is growing and converging building density in urban as well as suburban areas, intensification of activities such as the rise of industrialization can be seen in urban areas. It is also possible to observe the processes that take place in reverse with the growth of this urbanization. By the time, reducing forest cover and decreasing in the area of lands such as wetlands which are considered as protected areas can be pointed out. When discussing urbanization, deforestation can be pointed out as a process that works in reverse. Land-use patterns that have emerged with the expansion of urbanization include the allocation of land for residential factories, highways, terminals, parks, and playgrounds. However, with the abundance of these requirements, there is a relative shortage of land available for this purpose in the so-called urban areas. As a result, the existing territory in the semi-urban areas will be annexed to these urban areas. Accordingly, deforestation increased globally in line with urbanization.

In 1950, there was a global increase in forest cover, while forest cover in 2010 showed a significant decrease in forest cover over the years. Deforestation was more rapid in 2010 than in 1950. Urbanization was slow compared to 1950 and its

distribution was minimal, but it is clear that urbanization had grown rapidly by 2014. Thus, when these two major processes, urbanization and deforestation, are discussed together, it appears that as urbanization increases, this forest population is gradually declining. As discussed above, the processes of deforestation and increasing industrialization have become dependent on urbanization. That is, the impact on the climate process based on the industrialization that takes place with the growth of urbanization. The formation of climatic variations by greenhouse gases can be summarized as follows. That is, these gases cause changes in the clouds and also cause variations in the nuclear concentration during the condensation process. It has a direct effect on rainfall, affecting the size of the clouds (Chan n.d.). The United States, for example, currently reducing their greenhouse gas emissions to 0, but that they are currently experiencing the effects of climate change. It has been pointed out that cities like San Francisco have been affected by this climate impact and that the impact has also directly affected their income level. That is to say, they have had to experience a higher level of heat in the summer, for example. The city of Los Angeles is similarly affected by climate change. In Los Angeles, the average temperature in August was about 23.8 °C, and by the end of the twenty-first century, the average temperature in this region is expected to reach 32.2 °C due to the global warming created by this greenhouse gas release. It is no secret that this climate is a direct result of urbanization. Based on these conditions, these regions also suffer economic losses. For example, in the year 2000, the average house price in Los Angeles was $ 286632.8 and now it has dropped to 128,773. It is a detrimental effect of the climate change created on urbanization. That is the impact of greenhouse gases created on this urbanization on the climate. This shows that there is a direct link between urbanization and climate change (Kahn 2009). Further examining the relationship between urbanization and climate change globally, the impact of climate change on the effects of deforestation with the expansion of urbanization can be explained as follows. That is to say, forested areas provide great help in maintaining the ecological and atmospheric balance. That is, it absorbs greenhouse gases such as carbon dioxide and prevents them from being released into the atmosphere. This prevents global warming, which in turn helps to prevent climate change caused by global warming. Generally, plants absorb carbon dioxide released through urbanization and thus reduce the risk of climate change. Research shows that deforestation triples global warming (De Zoysa 2021). It is well-known that forest cover on urbanization has been gradually removed and the most accurate solution to the climate change caused by this global warming is to protect the forest. That is to protect the untouched forests and replant. The pattern of land use in the country changed rapidly through urbanization, and when viewed globally, irregular constructions could be seen in many areas, and the formation of tropical heat islands in those suburbs intensified. A tropical heat island is defined as a time when the average air temperature in an urbanized area is higher than in a suburban area. Heat absorption by surfaces is a major factor in the formation of these islands (NASA 2021a). These areas become thermal islands due to the irregular constructions that take place in urban areas and the raw material that maintains the high heat absorption used for such constructions. In such areas, the hot air particles do not leave the

area due to wind disturbances, and the blowing winds are confined to that area due to large construction obstructions. This creates heatwaves and the heated air particles and heat waves that are created contribute to the creation of atmospheric heat. Atmospheric warming on this contribution leads to the creation of climatic variations. That is, rainfall and temperature changes are common in such areas. Many people who have made urban tropical islands their habitat suffer from these climate changes. A good example of this is that between 1979 and 2010, about 8000 Americans died from heatstroke. The peak of this situation was in 2006 when it was named the second warmest year on record in 48 states in the United States. This means that the tropical islands that are created based on urbanization are directly affected by the variation in climatic factors (EPA 2021). Globally, it is clear that there is a strong correlation between the urbanization process and climate change. These processes are some of the most common processes in almost every country where the rate of urbanization is high (De Zoysa 2021), and these processes directly or indirectly affect climate change.

Climate Change and Sri Lanka

Sri Lanka is a small island nation lying between North 7° 52′ & East 80° 6′ in the Indian ocean. There are also three main climatic zones of the island mainly consisting of three topographic zones, namely as wet zone, dry zone, and interzone (Asian Development Bank 2020a). When discussing the prevailing temperature and precipitation in these zones, the mean temperature of the three zones is 24 °C, the dry zone is 28 °C, and the interzone is 24–26 °C. Also, when looking at the mean precipitation values of these major climatic zones, the precipitation values are more than 1750 mm in the wet zone, less than 2500 mm in the dry zone, and between 1750 mm and 2500 mm in the intermediate zone. Climatic conditions are created by meteorological elements that operate with variations based on these three regions. It is noteworthy that the climate base in Sri Lanka is based primarily on monsoon rainfall. These two monsoon showers of rain can be seen to be active during two periods of the year. That is, the southwest monsoon is active from May to September and the northeast monsoon is active from November to February. These two monsoon drops of rain have had a direct impact on Sri Lanka becoming an agricultural country. That is, the "Maha" season is based on the northeast monsoon and the "Yala" season is based on the southwest monsoon. Despite being fed by two major monsoon spots of rain; Sri Lanka is one of the hottest countries in the world. Its basis is the equatorial location of the island (Asian Development Bank 2020a). Considering the long-term climatic conditions that will be created based on these climatic conditions, several clear changes in meteorological features can be seen globally as well as within this island. Climate change in Sri Lanka is manifest through a slow but steadily rising temperature and erratic and unpredictable rainfall seasons. Although total annual rainfall (past 10 years compared to the 30-year average) remains steady (Punyawardena 2012), climate-induced changes are already

observed in the increased variability of monsoonal behavior, about on-set time, duration, nature of rainfall, and seasonal rainfall. The impacts of climate change on weather patterns in Sri Lanka can be identified with temperature and rainfall variability. Summarizing significant phenomena observed (1) Average air temperature has increased by 0.64 °C over the past 40 years and 0.97 °C over the last 72 years, revealing a trend of 0.14 °C per decade, (2) An assessment of a more recent time band has shown a 0.45 °C increase over 22 years, suggesting a rate of 0.2 °C per decade, (3) Ambient mean minimum and mean maximum temperatures have increased, (4) The number of warm days and warm nights have increased, while the number of cold days and cold nights have decreased, (5) Though precipitation patterns have changed, conclusive trends are difficult to establish, (6) A trend indicating decreased overall rainfall has been observed over the past 30–40 years, but the change is not statistically significant, and (7) Increasing trend of one-day heavy rainfall events across the country where the frequency of extreme rainfall events is anticipated, leading to more droughts, floods, and landslides. According to the National Adaptation Strategy (2011–2016), while the increased frequency of dry periods caused by consecutive dry and droughts is expected, the general warming trend is expected to increase the frequency of extremely hot days. One of the most recognizable features is the variation in the timing and intensity of the two major monsoon showers of rain, which occurred about 30–35 years ago. Variations in temperature, which are a major component of meteorological factors in discussing the prevailing climate in Sri Lanka, can be explained as follows. Research based on the Berkeley earth data set from 1900 to 1917 and from 2000 to 2017 observed clear temperature variations during this period. That is to say, during the twentieth century, the temperature in Sri Lanka has risen by about 0.8 °C (Asian Development Bank 2020a). It has also been found that Nitrous oxide recorded a record rise of 0.16 °C in temperature between 1961 and 1990. This indicates that by the end of the twentieth century that the rate of gradual increase has increased (Eriyagama and Smakhtin 2010). When discussing rainfall in Sri Lanka, monsoonal rainfall is one of the most Important rainfall patterns on the island and convection rainfall is also important. Based on its location in the tropics, it receives high levels of sunlight, indicating a certain complexity of rainfall patterns in the island. Recent variations in patterns revealed by research on variations in rainfall patterns can be analyzed as follows. Research conducted by Iriyagama and Smakthin in 2010 has observed a decrease in rainfall in the twentieth century. This is a decrease of about 7% from 1931 to 1960 (Eriyagama and Smakhtin 2010). Furthermore, Esham and Garforth (2013) identified climate change and precipitation as an increase in the extreme case (Esham and Garforth 2013). Researchers have also observed that the El Nino South Oscillation has a positive effect on the northeast monsoon rains that are active around Sri Lanka, thereby increasing rainfall on the island (Zubair and Ropelewski 2006). When examining the weather forecasts based on Sri Lanka, the following is a commentary on temperature. That is, these observations and forecasts are based on data from the World Bank Group's Climate Change Knowledge Portal (CCKP). Thus, the future average temperature variation in Sri Lanka is projected to be slower than the global warming average, with the average temperature rising in Sri Lanka

(Asian Development Bank 2020a). Researchers have also predicted an increase in mid-year rainfall in Sri Lanka based on data from the World Bank Group's Climate Change Knowledge Portal (CCKP) on climate change. It is also predicted that the intensity of rainfall will increase with the increase in temperature. It is also projected that heavy rains will continue for more than 5 days. In summary, the behavior of rainfall in future projections is that the magnitude and intensity of rainfall also increase (Silva et al. 2016). This research reveals that the impact of global climate change is also active in Sri Lanka. Also, the climate of Sri Lanka in the past has changed a lot from the past to the present. From the above, it is clear that this situation is likely to change further in the future. Rainfall, meanwhile, takes precedence over potential variations.

Being an island nation, subjected to the tropical climate system, Sri Lanka has experienced several challenges in several key thrust areas of Sri Lanka's development framework, such as agricultural, transport, health, power, environment, and settlement and vulnerable populations. The challenges are straightforward toward the economy and development where the failure in the economic sector is the ultimate challenge due to climate change and its impacts. The full extent of climate change impacts on Sri Lanka is still being studied, but there is growing recognition that climate change may threaten the significant achievements the country has made in the last 20 years in increasing incomes and reducing poverty (MoE/ADB 2010; NCSD and Presidential Secretariat 2009; MoENR 2008). Climate change exacerbates existing inequalities faced by vulnerable groups particularly women, children, and the elderly. The consequences of climate change and poverty are not distributed uniformly within the country. Coping with climate change has become a challenge due to the unawareness of climate change. There is a lack of awareness about climate change impacts on livelihood among farmers and local government officials especially those engaged in water management and agriculture extension. As such, farmers are not supported to adapt to changing rainfall patterns and seasons with proper advice on crop choice, water-saving methods or diversification of livelihoods so that dependence on rainfall is minimized. Year after year, farmers cultivate the same crop combinations, depending on seeds imported by the private sector and on agrochemical suppliers to provide them with information and advice for managing threats to their crops. This trend has resulted in deep indebtedness among rural households and a lack of disposable income for capital investments needed for a durable change in resilience. In this respect, it is clear that climate change has to become the most challenging issue that must pay much more broader attention to cope with unless the adaptation and mitigation would be beyond our hands. It is important to take note what are the consequences of climate change. Many of the natural disasters that are taking place today have confirmed that the effects of climate change are well-known and have spread throughout the world. This situation is active globally as well as regionally, and in Sri Lanka, which is located in the tropics, which represents the Asian region, the meteorological effects that have been created based on this climate change can be identified with examples at present. European Commission (2019) Inform Index for risk management observes that Sri Lanka represents a moderate level of disaster levels affected by climate change. It

also points out that Sri Lanka ranks 97th out of 191 countries. On further analysis, it is positioned as follows. That is, it represents a moderate to 56th position in riverine flood conditions, 45th with some exposure to tropical cyclones and associated hazards, and 76th in drought exposure, i.e., slightly lower. It can be said that all these processes are based on the adverse effects of climate change (The World Bank Group and the Asian Development Bank 2020). Research on the effects of heatwaves has shown that Sri Lanka currently averages about 32 °C per month. IWMI has also observed that Sri Lankans are directly affected by these heatwaves. According to their research, about 23% of the population of Sri Lanka is exposed to these dangerous heat waves. The underlying effect of this is an increase in climate variability. It appears that these heatwaves occasionally contribute to the development of high temperatures in Sri Lanka (Asian Development Bank 2020a). Floods, another consequence of climate change, are now a common sight in Sri Lanka. That is, it is possible to better observe how the intensity and duration of flooding have changed almost completely today, based on variations in rainfall patterns in the past. That is to say, research conducted to identify climate change has revealed that from time to time these floods are more likely to be reported due to the increase in rainfall intensity around the island. Landslides and epidemics are exacerbated as side effects of these floods. According to the United Nations Office for the Doctrine of the Faith, about 59,000 people in Sri Lanka are affected by floods each year, and the impact of the floods on GDP is estimated at $ 267 million. UNISDR has decided to increase its flood relief funding in Sri Lanka by 2030, indicating that the risk of floods will increase further in Sri Lanka by 2030. That is, it proves that the effects of climate change are exacerbated and that their form is severe (Asian Development Bank 2020a). Climate change in Sri Lanka can be attributed to the behavior of hurricanes. These hurricanes create conditions of heavy rainfall as well as high winds. Foreign research has shown that the intensity and frequency of hurricanes in Sri Lanka are slightly lower, but the potential for extremes has increased. Therefore, it is clear that the effects of the hurricane may be active on this island (Asian Development Bank 2020a). Real droughts can be pointed out as another possible effect of the gradual variation in climatic conditions. Thus, two possible drought conditions in Sri Lanka are identified as Meteorological Drought and Hydrological Drought. Research by IWMI has identified that about 10% of Sri Lanka‘s population was affected by drought between 2001 and 2013 (Asian Development Bank 2020a).

Climate Change and Urbanization in Sri Lanka

Compared to the United Nations estimated 60% urban population in Asia, the urban population in Sri Lanka will remain 40% by 2050. The UN-Habitat III Country Report on Sri Lanka shows the urban population growth from 2,848,116 in 1971 to 3,704,470 in 2012 while reducing the percentage of urban population from 24.4 in 1971 to 18.2 in 2012 (Ministry of Housing & Construction 2016). Urbanization has also altered traditional livelihoods’ strategies in Sri Lanka. Although Sri Lanka is

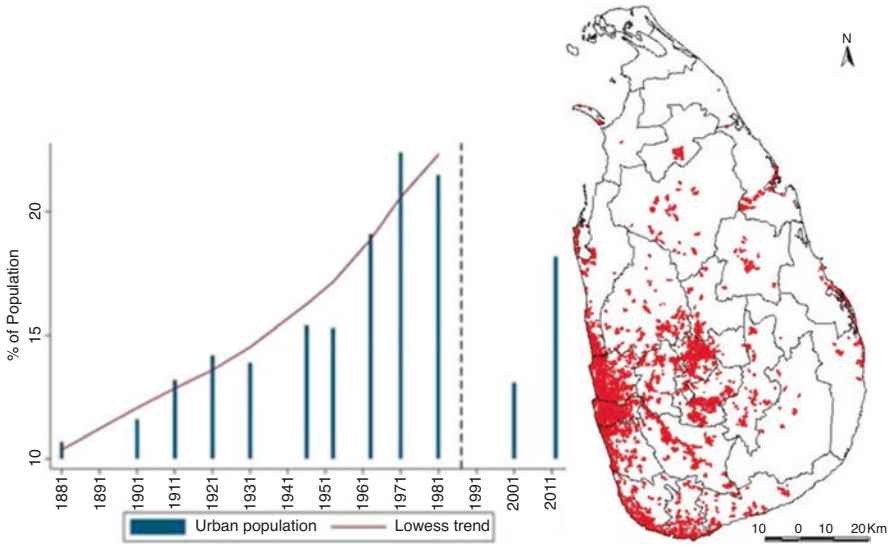

Fig. 3.3 Urban population (1881–2011) and urban areas (2012) in Sri Lanka. (Source: Weeraratne 2016)

comparatively experiencing a low level of urbanization, the urban population is heavily concentrated in the Greater Colombo area, the commercial capital where 43% of them live in slum and shanty settlements (Ministry of Environment 2012).

The present situation of urbanization in Sri Lanka can be graphically presented in Fig. 3.3.

According to the census, the urbanized areas of Sri Lanka can be identified by the map. According to the 2012 census, five districts can be identified as the main urbanized areas. Colombo, Gampaha, Kalutara, Kandy, and Galle can be listed in this order and the urban population in all these four districts is more than 50%. The urbanization of the Colombo district can be pointed out as an extreme opportunity. That is, 90.51% of the total population of the Colombo District live in urban areas, which gives a good idea of the level of urbanization in the city of Colombo. Further, focusing on the growing urban-based construction in Sri Lanka, the urban construction in the city of Colombo was 142.87 km^2 in the year 1990 and it is 67% by percentage. However, by 2015, it was 172.23 km^2, representing 81% of the total area (De Zoysa 2021). Accordingly, it appears that the building density in the city of Colombo has increased rapidly. Also, the water resources in the city of Colombo represented 5.41 km^2 in 1990 as a percentage of 3% and by 2015 it had dropped to 3.67 km^2. It is a percentage of 2%. That is, it shows how land use is changing unfavorably with this urbanization. The direct and indirect effects of this urbanization make it clear that the climatic cycle is currently operating in a different form around Sri Lanka as well (De Zoysa 2021). Accordingly, in line with the expansion of this urbanization, it appears that processes such as industrialization and deforestation have had an impact on the urban areas around Sri Lanka, as discussed earlier.

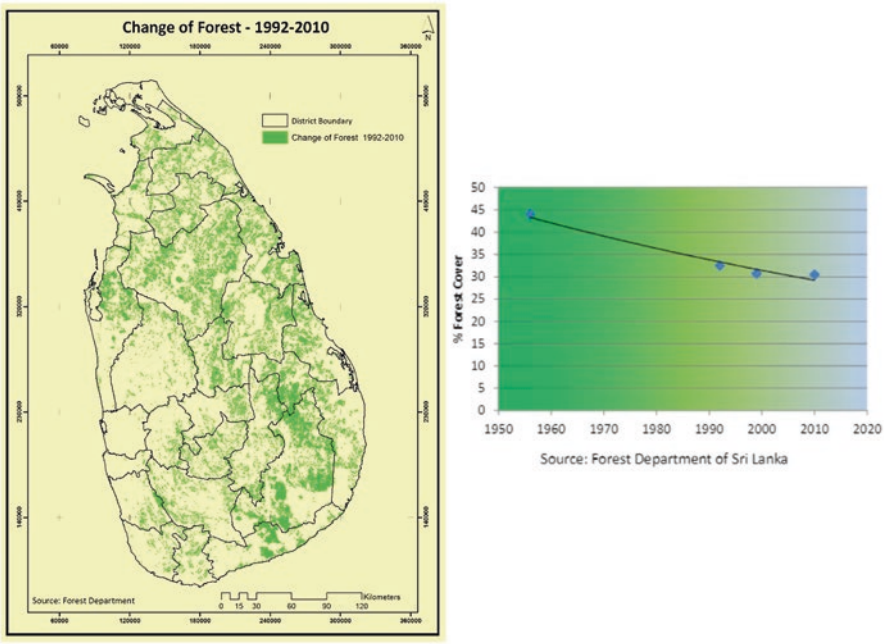

Fig. 3.4 Change of forest cover in Sri Lanka (Source: Forest Department 2010)

Figure 3.4 shows the gradual decline of Sri Lanka's forest cover from 1956 to 2000. That is a gradual decrease from 44.1% in 1956, 35% in 1992, 32% in 1999, and 29% in 2010. That is, it appears that deforestation has taken place rapidly. Simultaneously, the implication is that urbanization has grown and, accordingly, the extent of deforestation has increased. That is, it is much clearer that forest cover is rapidly disappearing in urbanized areas. With the growth of this urbanization, industrialization grew globally as well as in Sri Lanka and with the growth of this industrialization, the greenhouse gas emissions also increased significantly in Sri Lanka.

Overall, research has shown that Sri Lanka contributes 0.10% to global greenhouse gas emissions by 2011. Global greenhouse gas emissions are 46,906 metric tons, while Sri Lanka emits an average of 45 metric tons. There is no doubt that this is an indirect result of urbanization. Overall, urban areas in Sri Lanka expand by 9.5% to 7% annually, and at the same time, according to the 2100 Climate Forecast, the average temperature in Sri Lanka is expected to rise to 2.40 °C annually. In the face of all these urban conditions, it seems that the climate patterns of the past in Sri Lanka today are operating in a completely different form. By analyzing those cases as follows, it is possible to identify how climate change works under the influence of this urbanization. One example that illustrates this interrelationship is the phenomenon of tropical islands currently facing urbanized cities in Sri Lanka. Variations in the climatic process are also responsible for the formation of these tropical islands. A good example of this is the surface temperature in the Nuwara Eliya

District which was 18.90 °C in 1996 and 17.9 °C in 2006 but it has increased to 21 °C in 2017 (De Zoysa 2021). The main reason for this effect is that buildings are made of heat storage structures. Furthermore, the temperature difference between urban and rural areas in Sri Lanka is steadily increasing, from 1 °C in 1996, 1.3 °C in 2006, and 3.5 °C in 2017. The city of Colombo in Sri Lanka is also facing this experience due to multistoried buildings, widen roads and lanes, concrete roofs. Research shows that the city of Kandy in Sri Lanka is also gradually facing this situation (De Zoysa 2021). Further discussion of climate change shows clear changes in the annual rainfall in the Colombo district. That is, research (Lo and Koralegedara 2015) has shown that annual rainfall has increased and marginal opportunities have increased with it. This shows that the annual rainfall in the city of Colombo was 2000 mm in 1981 and 2000 mm in 2002 but by 2010 it was around 3000 mm. This means that the annual rainfall in the city of Colombo has increased rapidly. The conclusion that can be drawn from this is that there has been an increase in rainfall as urbanization has increased. It can also be assumed that marginal events in rainfall have increased (Margok 2020).

Case Study: Climate Change and Urbanization in Colombo

The changing pattern of land use has given birth to several suburban areas surrounding the Colombo city while expanding the urban zone further. The pressure of the Colombo primacy has filtered to these suburbs. Suburban growth has accelerated in recent years due to the interplay of demographic factors; the natural increase of population and diversion of city-ward migration to suburbs, economic factors; the spiraling cost of limited land resources in the city and the availability of cheap land in suburbs along with facilitated technological changes in the field of transportation, electricity and power, water supply have been paramount in causing suburbanization around Colombo. Location rent in these suburbs was relatively lower than in the city. The introduction of various land policy measures and statutory provisions to control land use increased its supply for urban usage. The horizontal expansion was majored to avoid physical constraints thus suburban frontier extended along the transportation lines while avoiding paddy and marshy lands liable to regulate flooding. Resulting ribbon development along the roads generally followed infilling of interstices which created more compact build-up areas in some older suburbs (Ranaweera 2016). Though “lung space” or “green belts” avoided in the past, the population expansion has had to invade those green patches as well. About 18.6% of urbanization level has been reported by 2011 which will multiply by threefold size by 2030 as projected by the urban development authority (Fig. 3.5). In 1971, two crescents of suburbs were identified. Battaramulla and Maharagama towns were among the second crescent. The relocation of administrative functions intensified the rate of suburbanization to the East of Colombo. The new capital of Sri Jayawardenepura extends over 12,200 ha including suburbs; Maharagama, Battaramulla, Kaduwela, Kesbewa, etc. Today, nearly 25% of the Sri Lankan

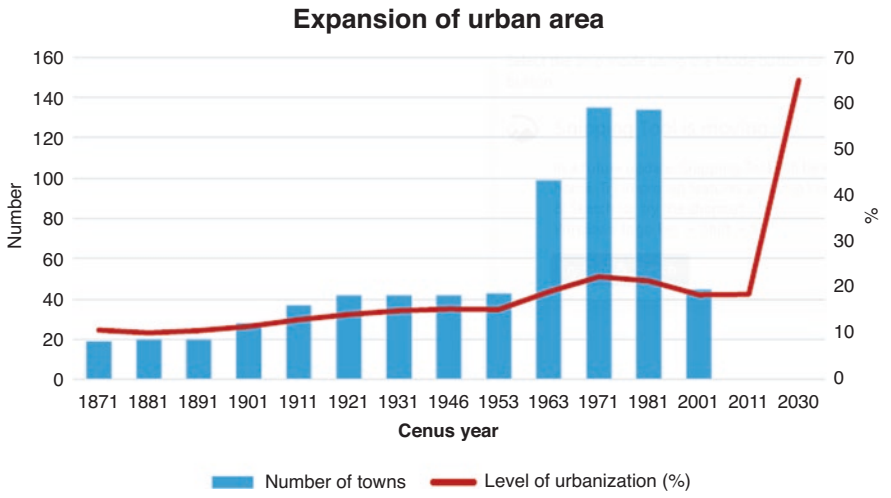

Fig. 3.5 Urban expansion in Sri Lanka from 1871 to 2030 (Source: Ranaweera 2016)

population live in urban areas and it is expected that 65% of the population will live in urban areas by 2030 (Amarawickrama et al. 2015). This will make cities grow both in number and in physical size than experienced in the past, aggravating urban sprawl-related problems in the future. A study carried out to identify urban sprawl has stated paddy lands and eco-sensitive areas have been threatened by the conversion of land into various urban uses. Eco-sensitive areas in the immediate surroundings of the urban core have decreased by 80% from 1986 to 2015. Similarly, paddy lands in the peripheral areas have decreased and they show a higher correlation with density factors, built-up density, and population density (Amarawickrama et al. 2015). As a whole, it is apparent that the vegetation cover in Colombo's EUA is diminishing throughout the year. Also, Amarawickrama et al. (2015) analyzed the commuting pattern by privately owned vehicles confirms the dominance of the Colombo core area as an employment center. Kaduwela and Nugegoda areas have recorded the highest number of work-based trips in the urban areas (Fig. 3.5).

Climate change may create hundreds of millions of urban residents increasingly vulnerable to extreme weather and other natural disasters in the next 10 years. According to the World Health Organization (WHO), the urban population in the world is expected to grow approximately 1.84% per year between 2015 and 2020, 1.63% per year between 2020 and 2025, and 1.44% per year between 2025 and 2030. South Asia with an area of about 4.5 million km^2 represents 3.31% of the world's landmass and has 22% of the world's population which has increased from 1.13 billion to 1.76 billion from 1990 to 2016 as one of the fastest and leading urbanizing zones in the world (Saparamadu et al. 2018). According to the UN, estimates revealed at the World Economic Forum on ASEAN, over half of the population in Asia (4.5 billion) will live in cities by 2026 (World Economic Forum 2018). Unplanned urbanization has many traffic congestions, increased waste resources,

vehicle emissions, limited social services, disorder, and confusion in land-use patterns and contributes to environmental challenges including natural disasters and environmental pollution. With the agglomeration of population and infrastructure in urban areas, the vulnerability of urban populations to events of higher temperatures, sea-level rise, and reductions in freshwater availability in major cities have become a common feature in many locations in the world. The local warming caused by the overall tendency of urbanization has induced a proportion of global warming during the last century, as a key issue from the climate change perspective (Paranunzio et al. 2019). The impacts of climate and land-use changes driven by urbanization effectively reduce the trade-offs and increase losses of ecosystem services (Pande et al. 2018, 2021). Hence, urban planning to enhance ecosystem services under future climate change impacts has great importance in ecosystem management and policymaking for environment resilience urbanization (Lyu et al. 2018).

With the rapid urbanization, the land-use changes are visible (Table 3.1). Connecting land-use change and urbanization is already being identified as a coming threat under climate change. Spatial analysis studies showed, the urban built-up area in Colombo, the capital city of Sri Lanka, increased from 41 km^2 in 1995 to 281 km^2 in 2017 diminishing the nonbuilt-up areas from 125 km^2 to 10 km^2 (UN-HABITAT 2018). Another study has proved that the land-use change where the built-up area has increased by 29.36 km^2 while decreased in other cultivation (−11.75 km^2), paddy (−8.46 km^2), boggy (−5.11 km^2), water (−1.74 km^2), and sand land use (−1.51 km^2) in Colombo city from 1990 to 2015 (Saparamadu et al. 2018). The green space in Colombo city in Sri Lanka has remarkably changed with "annual reduction rate of 0.46 km^2 (1980–1988), 0.39 km^2 (1988–1997), 0.37 km^2 (1997–2001), 1.37 km^2 (2001–2011), and 0.71 km^2 (2011–2015)" due to a higher rate of increasing population density and economic development of the country (Li and Pussella 2017) (Table 3.1). The vegetation extent decreased from 600 km^2 to 400 km^2 with a decrease rate of 33% in the Colombo metropolitan area alone (Fonseka et al. 2019).

The increasing intensity of impacts of climate change is further fueled by triggering and uses conversions for urban expansion. The increasing temperature and rainfall are significantly identified in Colombo. The increasing surface temperature and creation of heat islands within the urban zones are also evidenced. Transportation

Table 3.1 Land-use changes in Colombo

	Area km^2		%		Land-use changes km^2
Land use	1990	2015	1990	2015	
Built-up	142.87	172.23	67	81	29.36
Boggy	8.99	3.88	4	2	−5.11
Water	5.41	3.67	3	2	−1.74
Paddy	29.89	21.43	14	10	−8.46
Other cultivation	23.87	12.12	11	5	−11.75
Sand land use	1.51	0	1	0	−1.51

Source: Saparamadu et al. (2018)

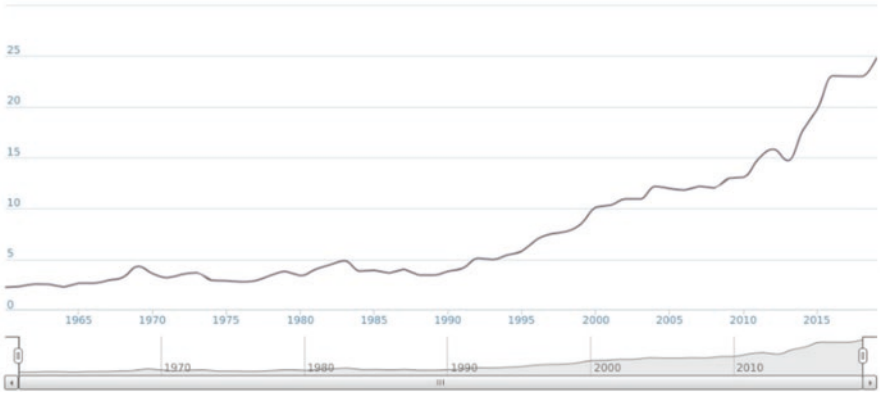

Fig. 3.6 Carbon dioxide emission Mt. from 1960 to 2019 in Sri Lanka (Source: Global carbon atlas, 2021)

development is also a consequence of urbanization. Where the transportation facilities are developed highly concentrated with population. Thus, the urban traffic congestion causes extra emissions of carbon dioxide and carbon monoxide, etc. So, fossil fuel consumption which is recognized as one of the main causes of global warming is evidenced in Colombo. It is known methane and nitrous oxide are commonly found in Colombo urban zone; however, carbon dioxide is the most prominent (Fig. 3.6).

It has been measured that Methane gas emission was 1507.681 m^3 and CO_2 gas emission was 9474.516 m^3 in Colombo Metropolitan Region in 2003. The carbon emission is changed with the changes in urbanization level particularly in response to the changes in energy consumption, and economic levels. A study in Sri Lanka confirms that urbanization has a significant effect on carbon emissions in the long-term as well as in the short-term with the increase in energy consumption (Gasimli et al. 2019). Urban areas are mainly responsible for more than 70% of CO_2 emissions related to global energy consumption and increase with the continuous trends of urbanization (Hegazy et al. 2017). According to a study conducted in Pettah division predominantly a commercial area of Colombo city in 2012, the vehicle is the highest CO_2 emitting source contributing 47737.69 ton CO2 about 95% of the total annual emission of 50352.05 ton CO_2. The contribution of CO_2 emission from firewood (41.85 tons) is not significantly high compared to vehicle emission and commuting population (Sugathapala and Jayathilake 2012). The increasing surface temperature and heat island effect are recently well documented (Fonseka et al. 2019) where most suburban centers were identified as heat islands while the severity of surface temperature increase is prominent in Colombo city and peripheral areas. The urban vegetation has converted to a concrete forest in most areas identified for high temperature and loss of soil moisture along with plant water stress. The relationship between surface temperature and urban land-use changes was well documented recently (Ahmad et al. 2013; Sultana and Satyanarayana 2018; Hoan

et al. 2018). Significant surface temperature changes were identified concerning high-rise development. The heat islands are intensified by the mixture of "mid-rise" and "high-rise" blocks (Herath et al. 2018). The greatest difference in Urban Heat Island intensity (UHI) of the Colombo city of 4.09 °C is seen when Local Climate Zones (LCZ) with lightweight low-rise (0.310 °C) are transformed into LCZ with compact high-rise areas (4.40 °C). High-rise housing complexes are rapidly spreading especially where the marshlands existed before. The conversion of marshy lands into urban apartments and other commercial centers is common in Colombo which is identified as a triggering factor to intensity urban floods. Architectural buildings and construction materials in urban areas absorb more heat than vegetation and soils, and minimize the cooling effect of evapotranspiration making urban areas warmer than their surroundings, causing the UHI effect (Oleson et al. 2013). Land cover changes from natural or agricultural lands to build environments due to rapid urbanization increase air and surface temperatures in the urban area as compared to its rural surroundings, transform cities into urban heat islands UHI (Middel et al. 2015). The empirical finding of a study indicates the reductions in green space in high-density residential areas and town centers in 10% will increase surface temperatures by 7–8.2 °C by 2080 (Dulal, 2017). Not only surface temperature but also the rainfall pattern has changed and the number of weather extremes have also increased due to climate change. Currently, it is evidenced Sri Lanka also become vulnerable to climate change. The analysis of long-term trends of rainfall as climatic variables in Colombo city of Sri Lanka indicates that the average annual dry days (193.41) and average annual wet days (171.84) are changing with a large standard deviation annually (Chen and De Costa 2017). High intensity and frequent rainfall have been recorded in wet-zone cities particularly Ratnapura, Ratmalana, and Colombo by El Niño-Southern Oscillation (ENSO) as the primary climate driver in Sri Lanka (Naveendrakumar et al. 2018). The long-term trend of the annual rainfall records in Colombo, the capital city of Sri Lanka for the 30 years from 1981 to 2010 shows that there was an increase ($R^2 = 0.146$) slightly from the average annual rainfall of 2302 mm with some recorded high rainfall values. Further analysis with simulated rainfall data from 2011to 2099 of Colombo city in Sri Lanka has revealed that very heavy rainfall as an extreme weather event may occur in the future particularly during 2080~2099 (Lo and Koralegedara 2015). Contrary, a study has shown that the periphery of urban areas experienced a higher probability of heavy rainfall while the urban areas have a decrease in rainfall with climate change impacts (Niyogi et al. 2017). A recent study has demonstrated the decreasing trend in annual rainfall in 13 stations (Allai, Puttalam, Higurakgoda, Angamedilla, Chilaw, Kurunegala, Gampaha, Katunayake, Colombo, Rathnapura, Nuwaraeliya, Kalutara, and Awissawella), but none of their trends was significant at 5% significance level (Nisansala et al. 2020). There is increase in rainfall during North Eastern Monsoon at Ratmalana and Colombo at a rate of 4.4 and 5.5 mm $year^{-1}$, respectively. Besides, this study has demonstrated an increase in rainfall during the first-inter monsoon, second-inter monsoon, and north-eastern monsoon while reporting a decrease in rainfall during the south-west monsoon. In contrast, another study demonstrated that there is a significant tendency to increase the rainfall in all

climatic zones in the country. Further, this study concluded for likely consequence of increased rainfall thus the risk of floods in the southern and western provinces in the future (Alahakoon and Edirisinghe 2021). It is also evidenced that increased rainfall intensity has resulted in severe floods in Colombo (Jayawardena et al. 2018; CHA, 2016). Due to the rapid urbanization and unplanned city development, floods in urban areas constitute a high risk and have become more frequent and increased the severity (Dammalage and Jayasinghe 2019). Colombo district is a low-lying terrain majorly covered from the lower river Kelani River basin and its extended wetlands. The overflow of the river has impacted as flooding in Colombo city. The increase in received precipitation over the upper catchment and at the same time to the lower parts of the river increased the river water level results in overflow. The 1989 and 2016 flood events were identified as such severe incidents in Colombo (Dammalage and Jayasinghe 2019). In 2016, flood hazards were identified for the creation of an additional flooded area than previous years. The changes in urban land use due to urbanization and flood area enhancement is well identified with the hazard. Sharp increase of built-up areas combined with the reduction in agricultural and green spaces are the main causes of increased flood inundation incidents in Colombo. The interesting finding done by Dammalage and Jayasinghe (2019) is 23% of urban areas in the Colombo district are distributed within the Kelani River watershed while the land use changed flood inundation covered an area of 37.7% within the watershed area of the Colombo district. The vulnerability and the severity of urban floods in the area further intensified with the urban poor. Though Sri Lanka was recognized as an upper-middle income country in 2019, where the largest portion of national gross domestic product (more than 50%) comes from Colombo city, there are 5874 families identified under extreme poverty (Hewawasam and Matsui 2020). These communities are inhabited mostly in marshy flood-prone areas especially in Kolonnawa, Dematagoda, Mattakkuliya, Wellampitiya, and Modara. Another study also showed (Patankar 2017) more than four times per year urban dwellings have been directly affected by floodwater. Even for a small amount of rainfall, 61% of families who live in urban flood-prone areas have to cope with floodwater where the average depth of flooding is ranged between two and three feet while the inundation period is almost 24 h or more. The recurrent floods have caused significant health and economic issues. Among the health effects of Dengue, viral fever and chronic cold and cough become prominent during the rainy flooding period. Apart from them, typhoid, diarrhea, fungi, asthma, and malaria in less than three cases were also reported. A significant economic loss has been caused by the infrastructure damages, which include homes, obstructed waterways, roads, and energy outage. Flood relief a government has to pay attention is also an extra burden due to unplanned urban development.

Conclusion

Climate change and its effects are visible all over the world. Sri Lanka is also the same. Rainfall and temperature changes have been significantly identified especially in urban Colombo areas. The intensified intensity and frequency of rainfall and frequent flooding have become a typical incidence in Colombo due to climate change. The magnitude and the severity of flooding have increased as a result of unplanned rapid urbanization related developments in Colombo while the population density in those of flood-prone areas further intensified the flood disaster severity. The study has demonstrated how climate is changing and the effects of climate change global scenario and then climate change in Sri Lanka. The relationship between climate change and urbanization has also been discussed with relevant literature. Finally, the study emphasized how climate change affects urbanization and what are the impacts of urbanization that trigger urban floods in Colombo urban zones. It is noteworthy to mention changes in urban land use is one of the key factors that affect climate change (Appendix 3) and urban flooding which can be controlled with a sustainable development approach. Greening the cities decrease the surface temperature while promoting safe and comfortable public transportation facilities to reduce the number of vehicles that enter Colombo possible help to reduce CO_2 emissions. Sustainable planned urban dwellings or appropriate urban housing should be initiated.

Appendixes

Appendix 1: World CO_2 Data

Sri Lanka

Year	$MtCO_2$	Year	$MtCO_2$	Year	$MtCO_2$	Year	$MtCO_2$	Year	$MtCO_2$	Year	$MtCO_2$
1960	2.2567	1970	3.5931	1980	3.3886	1990	3.8295	2000	10.1338	2010	13.0503
1961	2.3336	1971	3.1935	1981	4.0056	1991	4.137	2001	10.3273	2011	14.8866
1962	2.5608	1972	3.5379	1982	4.4669	1992	5.106	2002	10.9467	2012	15.798
1963	2.5315	1973	3.6843	1983	4.8549	1993	4.9756	2003	10.9521	2013	14.6781
1964	2.2714	1974	2.9293	1984	3.8521	1994	5.4358	2004	12.1462	2014	17.6899
1965	2.656	1975	2.893	1985	3.9166	1995	5.8155	2005	11.9352	2015	19.8301
1966	2.6597	1976	2.7988	1986	3.6603	1996	6.9701	2006	11.7937	2016	23.0284
1967	2.9451	1977	2.911	1987	4.0269	1997	7.5196	2007	12.1513	2017	22.9844
1968	3.2381	1978	3.4355	1988	3.4566	1998	7.7363	2008	11.9878	2018	22.9732
1969	4.3151	1979	3.809	1989	3.447	1999	8.5175	2009	12.9435	2019	24.8412

Afganisthan

Year	$MtCO_2$	Year	$MtCO_2$	Year	$MtCO_2$	Year	$MtCO_2$	Year	$MtCO_2$	Year	$MtCO_2$
1960	0.41388	1970	1.6704	1980	1.7565	1990	2.6032	2000	0.75767	2010	8.3978
1961	0.4908	1971	1.8936	1981	1.9787	1991	2.4274	2001	0.79796	2011	12.1058
1962	0.68859	1972	1.5304	1982	2.0949	1992	1.3795	2002	1.0516	2012	10.2185
1963	0.70674	1973	1.6356	1983	2.52	1993	1.3331	2003	1.186	2013	8.4408
1964	0.83855	1974	1.9133	1984	2.822	1994	1.2816	2004	0.88917	2014	7.7743
1965	1.0069	1975	2.1216	1985	3.5018	1995	1.2305	2005	1.3033	2015	7.9041
1966	1.0912	1976	1.9812	1986	3.1341	1996	1.1649	2006	1.6354	2016	6.7446
1967	1.2819	1977	2.3845	1987	3.1144	1997	1.0841	2007	2.2686	2017	6.8598
1968	1.2234	1978	2.1536	1988	2.8575	1998	1.0292	2008	4.1995	2018	10.4527
1969	0.94123	1979	2.2332	1989	2.7655	1999	0.80951	2009	6.74	2019	10.7203

Albania

Year	$MtCO_2$	Year	$MtCO_2$	Year	$MtCO_2$	Year	$MtCO_2$	Year	$MtCO_2$	Year	$MtCO_2$
1960	2.0225	1970	3.7409	1980	5.1662	1990	5.4447	2000	3.0045	2010	4.4481
1961	2.279	1971	4.3492	1981	7.3353	1991	4.2283	2001	3.2207	2011	5.0307
1962	2.4622	1972	5.6389	1982	7.3024	1992	2.4952	2002	3.7483	2012	4.6679
1963	2.0812	1973	5.2872	1983	7.6248	1993	2.3156	2003	4.2319	2013	4.9281
1964	2.0152	1974	4.3418	1984	7.819	1994	1.9126	2004	4.1037	2014	5.6206
1965	2.1728	1975	4.591	1985	7.8739	1995	2.0665	2005	4.1989	2015	4.5324
1966	2.5501	1976	4.9464	1986	8.0498	1996	1.9932	2006	3.8435	2016	4.4957
1967	2.6784	1977	5.7158	1987	7.4379	1997	1.5316	2007	3.8289	2017	5.4044
1968	3.0704	1978	6.4889	1988	7.3207	1998	1.7441	2008	4.2722	2018	5.403
1969	3.2426	1979	7.5808	1989	8.9768	1999	2.9752	2009	4.2539	2019	5.579

Algeria

Year	$MtCO_2$	Year	$MtCO_2$	Year	$MtCO_2$	Year	$MtCO_2$	Year	$MtCO_2$	Year	$MtCO_2$
1960	6.1512	1970	15.059	1980	66.4165	1990	76.7366	2000	87.4427	2010	117.8141
1961	6.0559	1971	18.6495	1981	46.342	1991	78.8054	2001	83.7807	2011	119.8069
1962	5.661	1972	28.3226	1982	39.173	1992	79.8818	2002	89.4067	2012	128.11
1963	5.4192	1973	38.2774	1983	52.5039	1993	81.9424	2003	91.0482	2013	132.4346
1964	5.643	1974	31.8767	1984	70.9465	1994	86.1467	2004	87.8531	2014	143.2208
1965	6.5885	1975	32.0012	1985	72.6091	1995	94.982	2005	106.4732	2015	150.8176
1966	8.4209	1976	39.1311	1986	76.0804	1996	96.7861	2006	100.2012	2016	148.839
1967	8.4316	1977	41.8449	1987	83.8835	1997	87.0043	2007	108.4	2017	153.4484
1968	9.0502	1978	62.4553	1988	83.708	1998	106.6208	2008	109.0318	2018	164.3093
1969	11.263	1979	45.5456	1989	79.8083	1999	91.6679	2009	120.1859	2019	171.707

Andorra

Year	$MtCO_2$	Year	$MtCO_2$	Year	$MtCO_2$	Year	$MtCO_2$	Year	$MtCO_2$	Year	$MtCO_2$
1960		1970		1980		1990	0.4067	2000	0.52395	2010	0.51662
1961		1971		1981		1991	0.4067	2001	0.52395	2011	0.49098
1962		1972		1982		1992	0.4067	2002	0.53128	2012	0.48731
1963		1973		1983		1993	0.41037	2003	0.53494	2013	0.47632
1964		1974		1984		1994	0.4067	2004	0.56059	2014	0.46166
1965		1975		1985		1995	0.42502	2005	0.57525	2015	0.46533
1966		1976		1986		1996	0.45434	2006	0.54594	2016	0.46899
1967		1977		1987		1997	0.46533	2007	0.53861	2017	0.46533
1968		1978		1988		1998	0.49098	2008	0.53861	2018	0.46421
1969		1979		1989		1999	0.51296	2009	0.51662	2019	0.47049

Angola

Year	$MtCO_2$	Year	$MtCO_2$	Year	$MtCO_2$	Year	$MtCO_2$	Year	$MtCO_2$	Year	$MtCO_2$
1960	0.54895	1970	3.5779	1980	5.3344	1990	5.0887	2000	9.5151	2010	28.8645
1961	0.45371	1971	3.4054	1981	5.2668	1991	5.0629	2001	9.6715	2011	30.3297
1962	1.1791	1972	4.5005	1982	4.6352	1992	5.165	2002	12.5975	2012	33.8006
1963	1.1497	1973	4.8737	1983	5.1005	1993	5.7484	2003	8.9884	2013	33.2285
1964	1.2229	1974	4.8664	1984	4.9858	1994	3.8656	2004	18.7019	2014	44.2488
1965	1.1862	1975	4.4088	1985	4.6761	1995	10.9483	2005	19.0064	2015	33.979
1966	1.5525	1976	3.28	1986	4.6338	1996	10.4248	2006	22.1024	2016	34.1109
1967	0.99181	1977	3.5275	1987	5.786	1997	7.3478	2007	24.9761	2017	37.4708
1968	1.6695	1978	5.3998	1988	5.0493	1998	7.2696	2008	25.486	2018	37.6786
1969	2.7831	1979	5.4892	1989	4.9227	1999	9.1298	2009	27.5655	2019	38.0203

Anguilla

Year	$MtCO_2$	Year	$MtCO_2$	Year	$MtCO_2$	Year	$MtCO_2$	Year	$MtCO_2$	Year	$MtCO_2$
1960		1970		1980		1990	0.051296	2000	0.087936	2010	0.15022
1961		1971		1981		1991	0.051296	2001	0.095264	2011	0.1429
1962		1972		1982		1992	0.05496	2002	0.095264	2012	0.1429
1963		1973		1983		1993	0.065952	2003	0.10259	2013	0.11725
1964		1974		1984		1994	0.065952	2004	0.12091	2014	0.13923
1965		1975		1985		1995	0.065952	2005	0.12824	2015	0.15389
1966		1976		1986		1996	0.069616	2006	0.1429	2016	0.15389
1967		1977		1987		1997	0.069616	2007	0.15022	2017	0.1429
1968		1978		1988		1998	0.076944	2008	0.15022	2018	0.14714
1969		1979		1989		1999	0.080608	2009	0.14656	2019	0.14329

Antigua and Barbuda

Year	$MtCO_2$	Year	$MtCO_2$	Year	$MtCO_2$	Year	$MtCO_2$	Year	$MtCO_2$	Year	$MtCO_2$
1960	0.03664	1970	0.46166	1980	0.1429	1990	0.21984	2000	0.29312	2010	0.45434
1961	0.047632	1971	0.42502	1981	0.10626	1991	0.21251	2001	0.29678	2011	0.44334
1962	0.10259	1972	0.37373	1982	0.29312	1992	0.20885	2002	0.32976	2012	0.458
1963	0.084272	1973	0.32976	1983	0.084272	1993	0.21618	2003	0.35174	2013	0.46166
1964	0.0916	1974	0.42869	1984	0.14656	1994	0.21618	2004	0.3664	2014	0.46166
1965	0.15022	1975	0.70715	1985	0.24915	1995	0.2235	2005	0.37373	2015	0.47998
1966	0.34808	1976	0.40304	1986	0.24915	1996	0.23816	2006	0.38472	2016	0.49098
1967	0.56426	1977	0.46533	1987	0.2748	1997	0.25648	2007	0.4067	2017	0.49098
1968	0.98928	1978	0.49098	1988	0.28579	1998	0.27114	2008	0.4177	2018	0.50557
1969	1.2568	1979	0.4067	1989	0.28579	1999	0.28213	2009	0.44334	2019	0.49234

Argentina

Year	$MtCO_2$	Year	$MtCO_2$	Year	$MtCO_2$	Year	$MtCO_2$	Year	$MtCO_2$	Year	$MtCO_2$
1960	48.7645	1970	82.648	1980	108.6569	1990	112.0791	2000	142.3583	2010	186.7331
1961	51.1267	1971	88.8472	1981	101.9693	1991	117.5057	2001	134.0039	2011	190.2738
1962	53.6401	1972	90.0668	1982	103.3518	1992	121.2306	2002	124.3923	2012	191.7148
1963	50.0327	1973	93.9761	1983	105.1428	1993	117.7775	2003	134.631	2013	190.1517
1964	55.67	1974	95.4806	1984	106.4525	1994	122.229	2004	157.0434	2014	188.6974
1965	58.8048	1975	94.8458	1985	100.5319	1995	127.7649	2005	161.4342	2015	192.3657
1966	63.0727	1976	99.6995	1986	104.151	1996	134.7621	2006	174.609	2016	190.9296
1967	65.476	1977	100.7063	1987	114.8783	1997	137.6415	2007	174.2458	2017	187.4159
1968	69.0092	1978	102.5561	1988	121.4059	1998	139.4519	2008	188.106	2018	185.0299
1969	77.2489	1979	110.6168	1989	117.0213	1999	147.2851	2009	178.9492	2019	178.9395

Armenia

Year	$MtCO_2$	Year	$MtCO_2$	Year	$MtCO_2$	Year	$MtCO_2$	Year	$MtCO_2$	Year	$MtCO_2$
1960	7.2941	1970	11.8788	1980	17.5998	1990	18.2119	2000	3.4914	2010	4.2527
1961	7.5223	1971	12.6098	1981	17.2694	1991	18.92	2001	3.5327	2011	4.9689
1962	7.895	1972	13.2715	1982	17.5968	1992	5.8599	2002	3.0768	2012	5.7483
1963	8.4668	1973	13.8367	1983	17.8517	1993	2.5736	2003	3.4556	2013	5.535
1964	9.0044	1974	14.3684	1984	18.0147	1994	2.7147	2004	3.6912	2014	5.5599
1965	9.552	1975	15.1083	1985	19.4292	1995	3.4323	2005	4.3762	2015	5.0724
1966	10.0875	1976	15.6931	1986	19.4863	1996	2.5927	2006	4.4016	2016	5.1588
1967	10.548	1977	16.2301	1987	19.4133	1997	3.2662	2007	5.1002	2017	5.4848
1968	10.8443	1978	16.7895	1988	19.9355	1998	3.3966	2008	5.5748	2018	6.2966
1969	11.2936	1979	16.9305	1989	19.4961	1999	3.0481	2009	4.3633	2019	6.0059

Aruba

Year	$MtCO_2$	Year	$MtCO_2$	Year	$MtCO_2$	Year	$MtCO_2$	Year	$MtCO_2$	Year	$MtCO_2$
1960	0.61856	1970	0.92876	1980	0.58543	1990	0.48731	2000	2.3779	2010	2.5062
1961	0.64555	1971	0.80832	1981	0.55762	1991	0.53128	2001	2.4072	2011	2.4988
1962	0.70894	1972	0.78378	1982	0.62347	1992	0.53861	2002	2.4366	2012	1.3484
1963	0.67909	1973	0.86946	1983	0.32042	1993	0.64853	2003	2.5611	2013	0.86104
1964	0.66028	1974	0.78808	1984	0.80014	1994	0.65952	2004	2.6161	2014	0.87203
1965	0.59239	1975	0.57071	1985	0.93653	1995	0.70715	2005	2.7187	2015	0.89768
1966	0.55394	1976	1.2191	1986	0.17954	1996	0.72547	2006	2.715	2016	0.88302
1967	0.68236	1977	0.63676	1987	0.44701	1997	0.75845	2007	2.8213	2017	0.916
1968	0.63451	1978	0.54229	1988	0.61189	1998	0.80608	2008	2.6564	2018	0.94323
1969	0.83041	1979	0.56887	1989	0.64853	1999	0.80974	2009	2.6271	2019	0.91855

Australia

Year	$MtCO_2$	Year	$MtCO_2$	Year	$MtCO_2$	Year	$MtCO_2$	Year	$MtCO_2$	Year	$MtCO_2$
1960	88.1189	1970	147.4798	1980	220.531	1990	278.4247	2000	350.195	2010	405.5028
1961	90.5039	1971	152.6295	1981	230.1326	1991	279.8727	2001	357.6692	2011	404.1728
1962	94.8235	1972	157.3355	1982	233.8886	1992	284.9124	2002	362.2095	2012	406.5062
1963	100.9343	1973	170.8274	1983	224.785	1993	289.2352	2003	369.726	2013	397.9432
1964	108.8758	1974	172.1894	1984	236.3612	1994	294.015	2004	383.2051	2014	394.1169
1965	120.8527	1975	175.7139	1985	240.988	1995	305.4102	2005	386.5135	2015	401.5548
1966	120.2193	1976	174.0747	1986	239.7222	1996	312.3616	2006	392.6806	2016	411.0315
1967	129.1442	1977	187.6049	1987	255.8502	1997	320.7951	2007	399.8425	2017	415.0974
1968	134.4969	1978	201.8202	1988	260.8788	1998	334.6845	2008	404.4174	2018	415.9539
1969	142.1238	1979	204.8696	1989	277.4856	1999	344.0638	2009	407.4633	2019	411.0157

Austria

Year	$MtCO_2$	Year	$MtCO_2$	Year	$MtCO_2$	Year	$MtCO_2$	Year	$MtCO_2$	Year	$MtCO_2$
1960	30.7845	1970	50.6317	1980	52.0257	1990	62.1247	2000	66.1629	2010	72.0118
1961	31.824	1971	52.0692	1981	55.8338	1991	65.7255	2001	70.1026	2011	69.8982
1962	33.865	1972	56.0714	1982	53.5662	1992	60.2041	2002	71.9188	2012	67.2091
1963	36.9491	1973	60.0158	1983	51.6692	1993	60.6354	2003	77.5543	2013	67.7457
1964	38.8964	1974	57.2945	1984	54.2151	1994	61.0024	2004	77.6744	2014	64.0844
1965	38.1406	1975	54.2141	1985	54.3673	1995	64.0653	2005	79.1924	2015	66.2832
1966	39.2086	1976	58.2043	1986	53.7296	1996	67.4216	2006	76.8983	2016	67.1123
1967	39.9156	1977	55.9943	1987	57.3751	1997	67.2328	2007	74.2626	2017	69.6289
1968	42.2971	1978	57.2272	1988	52.9385	1998	66.8751	2008	73.5884	2018	66.7197
1969	44.6384	1979	61.3221	1989	53.6976	1999	65.5627	2009	67.4939	2019	68.4951

Azerbaijan

Year	$MtCO_2$	Year	$MtCO_2$	Year	$MtCO_2$	Year	$MtCO_2$	Year	$MtCO_2$	Year	$MtCO_2$
1960	20.8952	1970	34.0246	1980	50.3189	1990	51.9472	2000	29.5063	2010	30.6329
1961	21.5482	1971	36.11	1981	49.366	1991	51.1657	2001	28.7927	2011	32.9757
1962	22.6155	1972	37.9967	1982	50.2976	1992	56.1831	2002	29.6419	2012	35.0484
1963	24.2528	1973	39.6063	1983	51.0162	1993	48.4131	2003	30.6267	2013	35.2147
1964	25.7922	1974	41.1199	1984	51.4731	1994	41.9498	2004	32.0781	2014	36.9752
1965	27.3607	1975	43.2284	1985	55.5106	1995	33.3122	2005	34.2864	2015	37.1986
1966	28.8946	1976	44.8933	1986	55.6589	1996	31.2426	2006	39.1086	2016	37.2784
1967	30.2132	1977	46.4212	1987	55.4359	1997	29.8049	2007	30.4584	2017	36.4979
1968	31.0615	1978	48.0155	1988	56.9194	1998	31.6655	2008	35.4506	2018	37.4884
1969	32.348	1979	48.4129	1989	55.6526	1999	28.5704	2009	31.8566	2019	39.8201

Bahamas

Year	$MtCO_2$	Year	$MtCO_2$	Year	$MtCO_2$	Year	$MtCO_2$	Year	$MtCO_2$	Year	$MtCO_2$
1960	0.41037	1970	2.5688	1980	7.9721	1990	1.8393	2000	1.9492	2010	2.3889
1961	0.54594	1971	6.7237	1981	2.7984	1991	1.843	2001	1.8686	2011	1.8027
1962	0.72547	1972	6.4813	1982	2.2585	1992	1.8503	2002	1.9273	2012	1.9089
1963	0.70715	1973	7.8627	1983	2.0144	1993	1.7587	2003	1.9639	2013	2.8836
1964	1.0845	1974	7.3798	1984	1.854	1994	1.7477	2004	1.9712	2014	2.3633
1965	1.3154	1975	8.2461	1985	1.5096	1995	1.7404	2005	1.8283	2015	2.0408
1966	1.0919	1976	6.4574	1986	1.4106	1996	1.7294	2006	1.777	2016	1.7954
1967	1.701	1977	9.7087	1987	1.4216	1997	1.5279	2007	1.7954	2017	1.9712
1968	1.6277	1978	6.597	1988	1.5389	1998	1.9089	2008	2.3596	2018	2.03
1969	1.7408	1979	6.9157	1989	1.9456	1999	1.9529	2009	1.6085	2019	1.9791

Bahrain

Year	$MtCO_2$	Year	$MtCO_2$	Year	$MtCO_2$	Year	$MtCO_2$	Year	$MtCO_2$	Year	$MtCO_2$
1960	0.57525	1970	2.5904	1980	7.8813	1990	12.4054	2000	18.7938	2010	29.0748
1961	1.7697	1971	3.0375	1981	8.5188	1991	11.8553	2001	14.0775	2011	28.6367
1962	1.5902	1972	3.6787	1982	9.8305	1992	10.8738	2002	15.8677	2012	27.3276
1963	1.1945	1973	5.518	1983	8.222	1993	14.6098	2003	16.7706	2013	31.1869
1964	1.5975	1974	5.4007	1984	9.2003	1994	14.7556	2004	17.8825	2014	31.1479
1965	1.2274	1975	5.7488	1985	10.1859	1995	14.7871	2005	19.803	2015	32.6721
1966	0.64853	1976	6.5696	1986	11.003	1996	15.5896	2006	19.4201	2016	31.3975
1967	1.0039	1977	7.4636	1987	11.4207	1997	17.2877	2007	26.7701	2017	32.7714
1968	1.1029	1978	7.7604	1988	12.1426	1998	18.3655	2008	29.6824	2018	31.5945
1969	1.2714	1979	8.1268	1989	11.7167	1999	17.9881	2009	28.0975	2019	34.3543

Bangladesh

Year	$MtCO_2$	Year	$MtCO_2$	Year	$MtCO_2$	Year	$MtCO_2$	Year	$MtCO_2$	Year	$MtCO_2$
1960	2.2119	1970	3.8032	1980	7.5972	1990	14.0819	2000	26.5245	2010	53.9916
1961	2.2904	1971	3.6058	1981	7.8861	1991	14.7411	2001	31.035	2011	56.5563
1962	2.5168	1972	3.5059	1982	8.5523	1992	15.3796	2002	31.9808	2012	60.6913
1963	2.8932	1973	4.5497	1983	8.1883	1993	16.0621	2003	33.4589	2013	61.7816
1964	2.9746	1974	4.6531	1984	9.0772	1994	17.5379	2004	35.945	2014	65.9787
1965	3.1213	1975	4.8567	1985	10.1892	1995	21.0416	2005	37.6765	2015	72.8346
1966	3.1763	1976	5.5558	1986	11.4058	1996	21.4921	2006	41.6892	2016	75.8574
1967	3.3711	1977	5.7847	1987	11.7997	1997	23.1262	2007	42.6421	2017	80.3238
1968	3.8657	1978	5.9844	1988	13.4784	1998	23.1983	2008	45.3009	2018	85.7188
1969	3.7493	1979	6.6126	1989	13.3824	1999	25.0755	2009	49.1481	2019	102.1617

Barbados

Year	$MtCO_2$	Year	$MtCO_2$	Year	$MtCO_2$	Year	$MtCO_2$	Year	$MtCO_2$	Year	$MtCO_2$
1960	0.17221	1970	0.42869	1980	0.67418	1990	1.0702	2000	1.1516	2010	1.464
1961	0.19419	1971	0.48365	1981	0.68517	1991	1.2021	2001	1.1862	2011	1.5157
1962	0.26014	1972	0.50197	1982	0.64486	1992	0.97497	2002	1.1996	2012	1.4595
1963	0.19053	1973	0.47998	1983	0.68517	1993	1.0993	2003	1.2453	2013	1.4383
1964	0.17954	1974	0.49098	1984	0.74742	1994	0.74033	2004	1.2695	2014	1.2625
1965	0.20518	1975	0.56792	1985	0.84639	1995	0.80628	2005	1.3192	2015	1.2625
1966	0.26747	1976	0.53128	1986	0.91606	1996	0.82474	2006	1.3428	2016	1.2847
1967	0.33709	1977	0.5899	1987	0.94177	1997	0.89094	2007	1.3628	2017	1.1709
1968	0.43968	1978	0.63021	1988	0.94547	1998	1.1001	2008	1.6123	2018	1.2071
1969	0.47998	1979	0.6009	1989	0.98952	1999	1.1625	2009	1.5971	2019	1.1866

Belarus

Year	$MtCO_2$	Year	$MtCO_2$	Year	$MtCO_2$	Year	$MtCO_2$	Year	$MtCO_2$	Year	$MtCO_2$
1960	45.6884	1970	74.4069	1980	109.884	1990	103.6897	2000	54.8774	2010	63.1564
1961	47.1178	1971	78.9544	1981	107.786	1991	96.6471	2001	54.9679	2011	62.1067
1962	49.453	1972	83.0662	1982	109.8111	1992	88.662	2002	55.0777	2012	63.0083
1963	53.0347	1973	86.5711	1983	111.3581	1993	76.38	2003	56.485	2013	63.7434
1964	56.4022	1974	89.8653	1984	112.3329	1994	62.3679	2004	60.0765	2014	63.0836
1965	59.833	1975	94.4578	1985	121.1327	1995	57.3755	2005	61.3671	2015	58.6331
1966	63.1878	1976	98.081	1986	121.428	1996	58.2148	2006	64.1572	2016	60.2849
1967	66.072	1977	101.4044	1987	120.8916	1997	58.7206	2007	63.5699	2017	60.7429
1968	67.928	1978	104.8783	1988	124.1034	1998	57.3725	2008	65.6948	2018	61.8717
1969	70.7418	1979	105.7357	1989	121.3119	1999	54.9845	2009	61.4027	2019	62.4839

Belgium

Year	$MtCO_2$	Year	$MtCO_2$	Year	$MtCO_2$	Year	$MtCO_2$	Year	$MtCO_2$	Year	$MtCO_2$
1960	90.9081	1970	125.4905	1980	134.8366	1990	120.3093	2000	126.7353	2010	114.561
1961	92.6983	1971	121.3706	1981	123.5745	1991	123.3821	2001	126.0847	2011	105.0461
1962	98.0183	1972	130.6378	1982	117.1028	1992	122.5078	2002	126.8786	2012	102.4288
1963	105.6764	1973	138.6394	1983	101.2027	1993	121.4442	2003	128.2753	2013	102.6744
1964	103.554	1974	134.9504	1984	104.9675	1994	124.8169	2004	128.8053	2014	96.8113
1965	105.3308	1975	121.8234	1985	104.0054	1995	125.9565	2005	125.6617	2015	100.9813
1966	105.0967	1976	129.6781	1986	102.3678	1996	129.4966	2006	123.9058	2016	99.8069
1967	107.361	1977	126.2	1987	102.5898	1997	124.0018	2007	120.4962	2017	99.4563
1968	118.4376	1978	135.451	1988	99.7441	1998	130.2271	2008	120.2029	2018	100.2078
1969	123.4918	1979	139.7873	1989	106.7935	1999	124.7189	2009	107.7434	2019	99.7089

Belize

Year	$MtCO_2$	Year	$MtCO_2$	Year	$MtCO_2$	Year	$MtCO_2$	Year	$MtCO_2$	Year	$MtCO_2$
1960	0.043968	1970	0.12091	1980	0.19053	1990	0.31144	2000	0.39571	2010	0.53861
1961	0.03664	1971	0.1429	1981	0.1832	1991	0.4067	2001	0.44701	2011	0.55693
1962	0.069616	1972	0.15755	1982	0.17221	1992	0.35541	2002	0.43235	2012	0.45067
1963	0.062288	1973	0.14656	1983	0.17221	1993	0.37739	2003	0.43235	2013	0.47632
1964	0.084272	1974	0.15389	1984	0.17221	1994	0.37373	2004	0.39205	2014	0.46899
1965	0.084272	1975	0.17587	1985	0.19053	1995	0.37739	2005	0.42136	2015	0.6412
1966	0.080608	1976	0.17587	1986	0.20518	1996	0.30778	2006	0.44334	2016	0.60822
1967	0.12091	1977	0.19786	1987	0.22717	1997	0.38838	2007	0.47632	2017	0.61555
1968	0.10259	1978	0.21618	1988	0.24915	1998	0.37006	2008	0.43602	2018	0.61221
1969	0.13557	1979	0.20885	1989	0.30045	1999	0.34808	2009	0.51662	2019	0.6328

Benin

Year	$MtCO_2$	Year	$MtCO_2$	Year	$MtCO_2$	Year	$MtCO_2$	Year	$MtCO_2$	Year	$MtCO_2$
1960	0.16122	1970	0.28213	1980	0.50746	1990	0.68068	2000	1.574	2010	4.9389
1961	0.12824	1971	0.29312	1981	0.41765	1991	0.79213	2001	1.7898	2011	4.8868
1962	0.13557	1972	0.38838	1982	0.47734	1992	0.86494	2002	2.0532	2012	4.6387
1963	0.12091	1973	0.38106	1983	0.43965	1993	1.0867	2003	2.3276	2013	4.8832
1964	0.1429	1974	0.4067	1984	0.4856	1994	1.2223	2004	2.4811	2014	5.2166
1965	0.15022	1975	0.44334	1985	0.72574	1995	1.2736	2005	2.3671	2015	6.0764
1966	0.11358	1976	0.26014	1986	0.66543	1996	1.2311	2006	3.7113	2016	6.74
1967	0.1429	1977	0.29678	1987	0.51719	1997	1.1982	2007	4.3196	2017	7.4249
1968	0.15389	1978	0.36274	1988	0.53805	1998	1.1944	2008	4.2548	2018	7.7598
1969	0.20152	1979	0.3664	1989	0.60965	1999	1.5423	2009	4.5079	2019	7.9981

Bermuda

Year	$MtCO_2$	Year	$MtCO_2$	Year	$MtCO_2$	Year	$MtCO_2$	Year	$MtCO_2$	Year	$MtCO_2$
1960	0.15755	1970	0.22717	1980	0.43602	1990	0.50197	2000	0.51662	2010	0.51662
1961	0.17587	1971	0.23083	1981	0.38838	1991	0.53861	2001	0.52762	2011	0.52762
1962	0.15755	1972	0.25282	1982	0.39571	1992	0.46166	2002	0.55693	2012	0.55693
1963	0.15022	1973	0.42502	1983	0.45067	1993	0.53861	2003	0.56059	2013	0.56059
1964	0.20152	1974	0.44334	1984	0.44334	1994	0.53128	2004	0.58258	2014	0.58258
1965	0.17954	1975	0.458	1985	0.45067	1995	0.53128	2005	0.58258	2015	0.58258
1966	0.20152	1976	0.46899	1986	0.42136	1996	0.52762	2006	0.65219	2016	0.65219
1967	0.21251	1977	0.45434	1987	0.57158	1997	0.52395	2007	0.72914	2017	0.72914
1968	0.2235	1978	0.42502	1988	0.64486	1998	0.52029	2008	0.64853	2018	0.64853
1969	0.19786	1979	0.46166	1989	0.78043	1999	0.51296	2009	0.47632	2019	0.47632

Bhutan

Year	$MtCO_2$	Year	$MtCO_2$	Year	$MtCO_2$	Year	$MtCO_2$	Year	$MtCO_2$	Year	$MtCO_2$
1960		1970	0.003664	1980	0.021984	1990	0.12824	2000	0.38169	2010	0.46416
1961		1971	0.003664	1981	0.025648	1991	0.17612	2001	0.36911	2011	0.66746
1962		1972	0.003664	1982	0.032976	1992	0.20538	2002	0.40171	2012	0.77225
1963		1973	0.003664	1983	0.029312	1993	0.17303	2003	0.36113	2013	0.85325
1964		1974	0.003664	1984	0.051296	1994	0.20146	2004	0.29048	2014	0.94799
1965		1975	0.003664	1985	0.062288	1995	0.23614	2005	0.37812	2015	0.96621
1966		1976	0.003664	1986	0.05496	1996	0.28519	2006	0.37301	2016	1.1531
1967		1977	0.007328	1987	0.10259	1997	0.37675	2007	0.37203	2017	1.2568
1968		1978	0.010992	1988	0.10992	1998	0.36716	2008	0.40072	2018	1.6622
1969		1979	0.021984	1989	0.062288	1999	0.37076	2009	0.3678	2019	1.7068

Bolivia

Year	$MtCO_2$	Year	$MtCO_2$	Year	$MtCO_2$	Year	$MtCO_2$	Year	$MtCO_2$	Year	$MtCO_2$
1960	1.0038	1970	2.4837	1980	4.659	1990	5.7268	2000	11.0047	2010	14.6407
1961	1.0404	1971	3.0589	1981	4.781	1991	5.974	2001	8.5606	2011	16.0381
1962	1.099	1972	3.5681	1982	4.3379	1992	6.622	2002	10.3281	2012	18.1193
1963	1.2125	1973	3.4545	1983	4.2781	1993	7.7918	2003	11.0112	2013	18.4259
1964	1.48	1974	3.5129	1984	4.0293	1994	8.5925	2004	11.0183	2014	19.6182
1965	1.5093	1975	4.055	1985	4.1098	1995	9.799	2005	12.0705	2015	19.421
1966	1.6888	1976	4.5748	1986	3.7637	1996	9.7745	2006	14.9209	2016	20.6933
1967	1.8904	1977	4.4749	1987	4.0118	1997	10.8831	2007	12.1768	2017	21.8106
1968	2.1761	1978	5.0201	1988	4.2868	1998	10.9238	2008	13.0406	2018	22.3455
1969	2.5462	1979	4.7301	1989	4.9684	1999	10.376	2009	13.4977	2019	22.5749

Bonaire, Saint Eustatius and Saba

Year	$MtCO_2$	Year	$MtCO_2$	Year	$MtCO_2$	Year	$MtCO_2$	Year	$MtCO_2$	Year	$MtCO_2$
1960	0.47065	1970	0.70668	1980	0.44544	1990	0.24388	2000	0.25228	2010	0.20499
1961	0.49119	1971	0.61503	1981	0.42429	1991	0.19461	2001	0.2569	2011	0.26151
1962	0.53942	1972	0.59636	1982	0.47438	1992	0.16033	2002	0.24767	2012	0.31144
1963	0.5167	1973	0.66155	1983	0.2438	1993	0.2475	2003	0.24783	2013	0.32243
1964	0.50239	1974	0.59963	1984	0.60881	1994	0.23729	2004	0.26003	2014	0.32243
1965	0.45073	1975	0.43424	1985	0.71259	1995	0.23482	2005	0.25772	2015	0.3261
1966	0.42148	1976	0.92761	1986	0.13661	1996	0.21966	2006	0.2686	2016	0.32976
1967	0.51919	1977	0.4845	1987	0.12145	1997	0.22987	2007	0.30238	2017	0.33342
1968	0.48279	1978	0.41262	1988	0.11963	1998	0.012688	2008	0.29084	2018	0.34334
1969	0.63184	1979	0.43284	1989	0.22773	1999	0.09508	2009	0.2976	2019	0.33435

Bosnia and Herzegovina

Year	$MtCO_2$	Year	$MtCO_2$	Year	$MtCO_2$	Year	$MtCO_2$	Year	$MtCO_2$	Year	$MtCO_2$
1960	5.2623	1970	10.6464	1980	16.1415	1990	19.4137	2000	13.7013	2010	21.1457
1961	5.5158	1971	11.4738	1981	17.5672	1991	13.7351	2001	13.2638	2011	23.7613
1962	5.6602	1972	10.7535	1982	16.1367	1992	15.0276	2002	14.1726	2012	22.1363
1963	6.2968	1973	12.8453	1983	17.3766	1993	12.5794	2003	14.3502	2013	21.801
1964	7.1339	1974	12.9007	1984	18.3251	1994	3.2044	2004	15.4625	2014	19.311
1965	7.34	1975	13.4603	1985	18.6927	1995	3.4028	2005	16.046	2015	18.4607
1966	7.2734	1976	13.8918	1986	19.5213	1996	4.2385	2006	17.3868	2016	21.7329
1967	7.3468	1977	13.5081	1987	19.0575	1997	8.3653	2007	17.4743	2017	21.7915
1968	7.8578	1978	15.0941	1988	19.6644	1998	10.5513	2008	19.9586	2018	22.0861
1969	8.1472	1979	16.4168	1989	19.604	1999	10.3339	2009	20.5371	2019	26.6211

Botswana

Year	$MtCO_2$	Year	$MtCO_2$	Year	$MtCO_2$	Year	$MtCO_2$	Year	$MtCO_2$	Year	$MtCO_2$
1960		1970		1980	0.98562	1990	2.7004	2000	3.7776	2010	4.5363
1961		1971		1981	1.0076	1991	2.6344	2001	3.8472	2011	4.0287
1962		1972	0.021984	1982	1.0992	1992	2.7773	2002	3.9754	2012	5.0766
1963		1973	0.051296	1983	1.0296	1993	3.195	2003	3.8252	2013	5.6629
1964		1974	0.087936	1984	1.0442	1994	3.0301	2004	3.8948	2014	6.8501
1965		1975	0.18686	1985	1.1578	1995	3.0448	2005	4.0927	2015	5.4248
1966		1976	0.59357	1986	1.0662	1996	2.7553	2006	4.133	2016	6.3334
1967		1977	0.78043	1987	1.2384	1997	2.7993	2007	4.2283	2017	7.0589
1968		1978	0.83173	1988	1.3007	1998	3.3416	2008	4.5031	2018	6.8154
1969		1979	0.94165	1989	1.429	1999	3.1584	2009	3.8555	2019	6.3164

Brazil

Year	$MtCO_2$	Year	$MtCO_2$	Year	$MtCO_2$	Year	$MtCO_2$	Year	$MtCO_2$	Year	$MtCO_2$
1960	0.33342	1970	8.2037	1980	6.8773	1990	6.1885	2000	4.591	2010	8.0608
1961	0.30411	1971	7.5112	1981	1.4693	1991	5.3055	2001	4.3895	2011	9.5447
1962	0.37006	1972	9.4531	1982	2.0921	1992	5.2102	2002	4.2539	2012	9.4935
1963	0.35541	1973	9.9734	1983	2.704	1993	4.9647	2003	4.4702	2013	7.6284
1964	0.34075	1974	8.178	1984	1.9163	1994	4.6899	2004	4.8731	2014	8.9255
1965	0.33342	1975	7.0752	1985	2.5941	1995	4.7852	2005	4.8695	2015	6.9543
1966	0.49098	1976	6.02	1986	2.2973	1996	4.7413	2006	4.7376	2016	7.5441
1967	0.43968	1977	6.39	1987	3.3159	1997	4.9317	2007	8.31	2017	9.552
1968	0.42869	1978	9.5337	1988	5.7122	1998	5.1589	2008	8.9915	2018	9.5604
1969	0.48731	1979	7.4343	1989	6.3424	1999	3.8032	2009	7.7457	2019	9.0887

British Virgin Islands

Year	$MtCO_2$	Year	$MtCO_2$	Year	$MtCO_2$	Year	$MtCO_2$	Year	$MtCO_2$	Year	$MtCO_2$
1960	46.8518	1970	93.5305	1980	185.7584	1990	206.9211	2000	324.226	2010	411.2402
1961	49.1445	1971	102.3579	1981	170.4679	1991	217.2277	2001	332.9874	2011	429.9594
1962	53.6314	1972	114.0143	1982	170.7893	1992	218.3833	2002	327.4348	2012	460.098
1963	55.5509	1973	132.0196	1983	165.4269	1993	228.3332	2003	317.5083	2013	495.0468
1964	56.6667	1974	142.9273	1984	167.6056	1994	239.4706	2004	333.6751	2014	523.894
1965	56.3296	1975	150.5137	1985	179.9368	1995	255.5835	2005	342.0865	2015	495.2137
1966	64.2116	1976	154.3981	1986	197.2262	1996	281.1948	2006	341.9464	2016	478.4428
1967	66.0794	1977	162.0783	1987	205.7887	1997	296.5854	2007	356.9188	2017	484.5881
1968	77.2714	1978	175.9315	1988	207.563	1998	308.3055	2008	380.3447	2018	466.6493
1969	84.1327	1979	187.1551	1989	212.1136	1999	316.2824	2009	360.0908	2019	465.7158

Brunei Darussalam

Year	$MtCO_2$	Year	$MtCO_2$	Year	$MtCO_2$	Year	$MtCO_2$	Year	$MtCO_2$	Year	$MtCO_2$
1960		1970	0.01832	1980	0.029312	1990	0.065952	2000	0.12458	2010	0.19786
1961		1971	0.021984	1981	0.043968	1991	0.07328	2001	0.12824	2011	0.20152
1962	0.003664	1972	0.021984	1982	0.03664	1992	0.084272	2002	0.13557	2012	0.20152
1963	0.003664	1973	0.025648	1983	0.040304	1993	0.087936	2003	0.14656	2013	0.20152
1964	0.007328	1974	0.025648	1984	0.040304	1994	0.098928	2004	0.16122	2014	0.21251
1965	0.007328	1975	0.025648	1985	0.047632	1995	0.10992	2005	0.17954	2015	0.21251
1966	0.010992	1976	0.025648	1986	0.05496	1996	0.11725	2006	0.1832	2016	0.21251
1967	0.003664	1977	0.029312	1987	0.062288	1997	0.11725	2007	0.18686	2017	0.16854
1968	0.014656	1978	0.029312	1988	0.065952	1998	0.12091	2008	0.19053	2018	0.17356
1969	0.01832	1979	0.029312	1989	0.065952	1999	0.12091	2009	0.19053	2019	0.16901

Bulgaria

Year	$MtCO_2$	Year	$MtCO_2$	Year	$MtCO_2$	Year	$MtCO_2$	Year	$MtCO_2$	Year	$MtCO_2$
1960	22.2707	1970	61.174	1980	77.2506	1990	76.699	2000	45.305	2010	47.8629
1961	25.945	1971	64.2216	1981	80.0868	1991	61.2326	2001	49.0141	2011	53.178
1962	30.704	1972	66.0789	1982	89.8442	1992	57.0104	2002	46.2586	2012	48.349
1963	34.3741	1973	68.7173	1983	90.0613	1993	57.6756	2003	50.5097	2013	42.6495
1964	42.8181	1974	71.1365	1984	87.0449	1994	56.0835	2004	49.5707	2014	45.1693
1965	46.2691	1975	72.9222	1985	89.2213	1995	57.7164	2005	50.6564	2015	48.1943
1966	48.716	1976	72.9648	1986	91.1723	1996	58.108	2006	51.8952	2016	45.3537
1967	55.1077	1977	75.7959	1987	91.2732	1997	55.8613	2007	55.7408	2017	47.5052
1968	59.4635	1978	81.2071	1988	86.9133	1998	53.2752	2008	54.0796	2018	43.5516
1969	66.3077	1979	78.9279	1989	86.4822	1999	46.37	2009	45.7738	2019	42.0065

Burkina Faso

Year	$MtCO_2$	Year	$MtCO_2$	Year	$MtCO_2$	Year	$MtCO_2$	Year	$MtCO_2$	Year	$MtCO_2$
1960	0.043968	1970	0.1429	1980	0.43235	1990	0.58258	2000	1.0309	2010	2.0368
1961	0.0916	1971	0.15022	1981	0.55693	1991	0.62654	2001	0.99169	2011	2.1302
1962	0.084272	1972	0.16122	1982	0.57525	1992	0.63021	2002	1.0011	2012	2.62
1963	0.087936	1973	0.16854	1983	0.59357	1993	0.62654	2003	1.0743	2013	2.8642
1964	0.10992	1974	0.20518	1984	0.46533	1994	0.64486	2004	1.0999	2014	2.912
1965	0.10259	1975	0.21984	1985	0.47632	1995	0.62387	2005	1.1218	2015	3.2976
1966	0.10259	1976	0.20885	1986	0.47998	1996	0.70446	2006	1.3562	2016	3.3814
1967	0.10259	1977	0.24915	1987	0.51662	1997	0.80269	2007	1.5906	2017	3.9384
1968	0.10259	1978	0.34808	1988	0.55326	1998	0.85763	2008	1.7345	2018	4.1403
1969	0.12091	1979	0.4067	1989	0.82074	1999	0.91417	2009	1.8302	2019	4.3013

Burundi

Year	$MtCO_2$	Year	$MtCO_2$	Year	$MtCO_2$	Year	$MtCO_2$	Year	$MtCO_2$	Year	$MtCO_2$
1960	0.03643	1970	0.06229	1980	0.14656	1990	0.20885	2000	0.27114	2010	0.29678
1961	0.04774	1971	0.07328	1981	0.15755	1991	0.23816	2001	0.20518	2011	0.35481
1962	0.04397	1972	0.07328	1982	0.15755	1992	0.21618	2002	0.21251	2012	0.37987
1963	0.04763	1973	0.07328	1983	0.20518	1993	0.22717	2003	0.16122	2013	0.39914
1964	0.04763	1974	0.09160	1984	0.21984	1994	0.23450	2004	0.19786	2014	0.37656
1965	0.03664	1975	0.07694	1985	0.23083	1995	0.23816	2005	0.15389	2015	0.39164
1966	0.04763	1976	0.08794	1986	0.23450	1996	0.24182	2006	0.18320	2016	0.44293
1967	0.04763	1977	0.09893	1987	0.24915	1997	0.24915	2007	0.20152	2017	0.54918
1968	0.05496	1978	0.10259	1988	0.22717	1998	0.24915	2008	0.20885	2018	0.56803
1969	0.07328	1979	0.10992	1989	0.26747	1999	0.25282	2009	0.16854	2019	0.57979

Cambodia

Year	$MtCO_2$	Year	$MtCO_2$	Year	$MtCO_2$	Year	$MtCO_2$	Year	$MtCO_2$	Year	$MtCO_2$
1960	0.2345	1970	1.1723	1980	0.28579	1990	1.2604	2000	1.9749	2010	5.0305
1961	0.28579	1971	0.24891	1981	0.30045	1991	1.3044	2001	2.2497	2011	5.1053
1962	0.30778	1972	0.11704	1982	0.33709	1992	1.3484	2002	2.2057	2012	5.3335
1963	0.38838	1973	0.12791	1983	0.3664	1993	1.385	2003	2.3779	2013	5.4758
1964	0.34072	1974	0.073072	1984	0.41037	1994	1.4671	2004	2.4439	2014	6.5164
1965	0.40283	1975	0.073072	1985	0.4177	1995	1.5403	2005	2.7736	2015	8.4463
1966	0.46875	1976	0.072774	1986	0.43235	1996	1.5972	2006	2.9972	2016	9.724
1967	0.41746	1977	0.072476	1987	0.43602	1997	1.5251	2007	3.4525	2017	11.186
1968	0.49074	1978	0.051139	1988	0.45067	1998	1.9354	2008	3.805	2018	15.479
1969	1.3444	1979	0.029312	1989	0.45067	1999	1.8943	2009	4.5663	2019	16.027

Cameroon

Year	$MtCO_2$	Year	$MtCO_2$	Year	$MtCO_2$	Year	$MtCO_2$	Year	$MtCO_2$	Year	$MtCO_2$
1960	0.27114	1970	0.63742	1980	3.8859	1990	0.62663	2000	3.3458	2010	6.662
1961	0.28213	1971	0.80918	1981	5.3191	1991	0.056431	2001	3.325	2011	6.5212
1962	0.28946	1972	0.86036	1982	6.3159	1992	2.726	2002	3.324	2012	6.1582
1963	0.30045	1973	0.89691	1983	6.5545	1993	2.8795	2003	3.6985	2013	5.0692
1964	0.33709	1974	0.97376	1984	6.0529	1994	2.8404	2004	3.8501	2014	6.8503
1965	0.31144	1975	1.1605	1985	6.4706	1995	3.2035	2005	3.5913	2015	7.7439
1966	0.34442	1976	1.089	1986	1.9932	1996	3.5924	2006	3.7524	2016	8.2596
1967	0.458	1977	1.559	1987	1.843	1997	3.1564	2007	5.7019	2017	7.5305
1968	0.50563	1978	1.9932	1988	2.154	1998	3.1371	2008	5.4263	2018	7.5668
1969	0.57158	1979	1.8153	1989	7.5777	1999	2.9981	2009	6.5949	2019	7.5927

Canada

Year	$MtCO_2$	Year	$MtCO_2$	Year	$MtCO_2$	Year	$MtCO_2$	Year	$MtCO_2$	Year	$MtCO_2$
1960	192.716	1970	341.177	1980	442.817	1990	462.117	2000	572.162	2010	555.550
1961	194.001	1971	352.285	1981	429.598	1991	452.495	2001	564.946	2011	566.741
1962	206.991	1972	380.787	1982	414.426	1992	467.037	2002	570.845	2012	569.737
1963	210.911	1973	381.265	1983	408.310	1993	467.406	2003	587.178	2013	576.327
1964	237.578	1974	389.605	1984	425.199	1994	482.437	2004	585.703	2014	575.942
1965	251.917	1975	396.773	1985	421.676	1995	494.920	2005	576.435	2015	575.907
1966	259.074	1976	398.946	1986	404.660	1996	510.737	2006	570.950	2016	564.033
1967	281.637	1977	407.771	1987	430.922	1997	524.789	2007	594.221	2017	572.834
1968	303.261	1978	415.505	1988	455.608	1998	533.640	2008	575.587	2018	586.505
1969	307.119	1979	441.647	1989	462.818	1999	549.553	2009	542.550	2019	576.651

Cape Verde

Year	$MtCO_2$	Year	$MtCO_2$	Year	$MtCO_2$	Year	$MtCO_2$	Year	$MtCO_2$	Year	$MtCO_2$
1960	0.02195	1970	0.03658	1980	0.12091	1990	0.09526	2000	0.21618	2010	0.55693
1961	0.02195	1971	0.03661	1981	0.03298	1991	0.09893	2001	0.23450	2011	0.61555
1962	0.01829	1972	0.05127	1982	0.03664	1992	0.10626	2002	0.27480	2012	0.50197
1963	0.01463	1973	0.06223	1983	0.03664	1993	0.10992	2003	0.30778	2013	0.49464
1964	0.02925	1974	0.06595	1984	0.08427	1994	0.11358	2004	0.32976	2014	0.48731
1965	0.02559	1975	0.07694	1985	0.08427	1995	0.12091	2005	0.43968	2015	0.49098
1966	0.02198	1976	0.07328	1986	0.05862	1996	0.14290	2006	0.47266	2016	0.53861
1967	0.01832	1977	0.08061	1987	0.08061	1997	0.14656	2007	0.50563	2017	0.57891
1968	0.02928	1978	0.20854	1988	0.07328	1998	0.15755	2008	0.46899	2018	0.60951
1969	0.03658	1979	0.24915	1989	0.08061	1999	0.18320	2009	0.52029	2019	0.63389

Central African Republic

Year	$MtCO_2$	Year	$MtCO_2$	Year	$MtCO_2$	Year	$MtCO_2$	Year	$MtCO_2$	Year	$MtCO_2$
1960	0.087936	1970	0.20885	1980	0.10626	1990	0.19786	2000	0.26747	2010	0.26381
1961	0.087936	1971	0.1832	1981	0.13557	1991	0.20518	2001	0.24549	2011	0.27846
1962	0.07328	1972	0.16854	1982	0.1429	1992	0.21618	2002	0.24549	2012	0.29312
1963	0.07328	1973	0.16122	1983	0.14656	1993	0.2235	2003	0.2345	2013	0.28579
1964	0.07328	1974	0.11358	1984	0.15022	1994	0.2345	2004	0.2345	2014	0.28946
1965	0.087936	1975	0.10259	1985	0.16122	1995	0.2345	2005	0.2345	2015	0.29312
1966	0.084272	1976	0.12824	1986	0.16122	1996	0.2345	2006	0.24915	2016	0.29678
1967	0.0916	1977	0.12824	1987	0.26014	1997	0.24549	2007	0.25282	2017	0.29678
1968	0.1832	1978	0.14656	1988	0.23083	1998	0.24915	2008	0.25282	2018	0.30048
1969	0.18686	1979	0.10259	1989	0.24915	1999	0.26381	2009	0.25282	2019	0.30765

Chad

Year	$MtCO_2$	Year	$MtCO_2$	Year	$MtCO_2$	Year	$MtCO_2$	Year	$MtCO_2$	Year	$MtCO_2$
1960	0.0550	1970	0.1246	1980	0.2089	1990	0.3774	2000	0.4873	2010	0.9966
1961	0.0513	1971	0.1502	1981	0.2089	1991	0.3847	2001	0.5020	2011	1.1175
1962	0.0843	1972	0.1209	1982	0.2052	1992	0.4067	2002	0.5093	2012	0.6140
1963	0.0916	1973	0.1612	1983	0.2052	1993	0.4030	2003	0.7438	2013	0.6549
1964	0.0989	1974	0.1502	1984	0.2162	1994	0.4067	2004	0.7475	2014	0.9893
1965	0.1063	1975	0.1832	1985	0.1795	1995	0.4214	2005	0.7658	2015	0.6961
1966	0.0843	1976	0.1832	1986	0.1869	1996	0.4360	2006	0.7914	2016	0.9929
1967	0.1173	1977	0.1979	1987	0.1979	1997	0.4507	2007	0.8537	2017	0.9966
1968	0.1246	1978	0.1942	1988	0.0660	1998	0.4617	2008	0.9270	2018	1.0080
1969	0.1612	1979	0.2015	1989	0.1026	1999	0.4763	2009	0.9417	2019	1.0303

Chile

Year	$MtCO_2$	Year	$MtCO_2$	Year	$MtCO_2$	Year	$MtCO_2$	Year	$MtCO_2$	Year	$MtCO_2$
1960	13.4765	1970	24.6358	1980	25.0905	1990	32.8822	2000	58.1137	2010	71.3298
1961	14.4582	1971	27.055	1981	24.335	1991	31.1366	2001	52.5765	2011	78.0838
1962	16.7074	1972	28.1373	1982	20.4672	1992	32.2023	2002	54.4903	2012	79.7038
1963	17.337	1973	27.586	1983	20.6644	1993	34.2594	2003	54.8842	2013	81.6916
1964	17.5051	1974	25.8746	1984	21.993	1994	37.7401	2004	59.0475	2014	77.4228
1965	17.7473	1975	22.9437	1985	21.2795	1995	41.09	2005	60.9471	2015	81.6332
1966	18.7725	1976	24.0254	1986	22.0088	1996	47.6284	2006	63.9716	2016	84.1537
1967	19.2383	1977	23.0122	1987	22.394	1997	55.4502	2007	70.7069	2017	84.0621
1968	21.2022	1978	22.8364	1988	26.5798	1998	56.8073	2008	70.8187	2018	85.8291
1969	22.5315	1979	24.7224	1989	31.9951	1999	60.9073	2009	65.9199	2019	84.2666

China

Year	$MtCO_2$	Year	$MtCO_2$	Year	$MtCO_2$	Year	$MtCO_2$	Year	$MtCO_2$	Year	$MtCO_2$
1960	778.9795	1970	770.1672	1980	1458.887	1990	2420.789	2000	3349.295	2010	8500.543
1961	550.9585	1971	874.0164	1981	1442.782	1991	2538.03	2001	3426.144	2011	9388.199
1962	439.3421	1972	928.894	1982	1570.468	1992	2653.192	2002	3782.439	2012	9633.899
1963	435.5176	1973	965.6466	1983	1655.811	1993	2835.796	2003	4452.31	2013	9796.527
1964	435.7037	1974	985.0852	1984	1802.317	1994	3010.242	2004	5125.894	2014	9820.36
1965	474.6806	1975	1142.102	1985	1951.773	1995	3265.057	2005	5771.168	2015	9683.201
1966	521.4589	1976	1190.965	1986	2052.242	1996	3408.347	2006	6377.748	2016	9552.517
1967	432.2236	1977	1304.403	1987	2191.053	1997	3414.549	2007	6861.751	2017	9750.726
1968	467.8056	1978	1455.258	1988	2347.764	1998	3265.903	2008	7375.19	2018	9956.569
1969	575.9447	1979	1487.113	1989	2386.885	1999	3258.135	2009	7758.812	2019	10174.68

Colombia

Year	$MtCO_2$	Year	$MtCO_2$	Year	$MtCO_2$	Year	$MtCO_2$	Year	$MtCO_2$	Year	$MtCO_2$
1960	16.3905	1970	28.3701	1980	44.1742	1990	56.8977	2000	56.2588	2010	76.2784
1961	18.1963	1971	30.2814	1981	44.2603	1991	56.6541	2001	55.9389	2011	76.0798
1962	19.4195	1972	31.4252	1982	45.6793	1992	61.4947	2002	55.4304	2012	79.7272
1963	21.2328	1973	33.6308	1983	49.2096	1993	63.3378	2003	57.0939	2013	89.9888
1964	21.6829	1974	36.3944	1984	48.7015	1994	66.7906	2004	54.5693	2014	90.9523
1965	22.8587	1975	35.809	1985	48.0795	1995	58.7754	2005	60.0596	2015	86.0711
1966	23.4742	1976	37.9797	1986	48.7543	1996	59.7709	2006	62.0045	2016	100.800
1967	24.6868	1977	39.241	1987	50.124	1997	64.4965	2007	60.1788	2017	91.6698
1968	26.5728	1978	41.5342	1988	52.0174	1998	65.1577	2008	66.6501	2018	92.2282
1969	28.0163	1979	44.2669	1989	52.7928	1999	54.7612	2009	72.5567	2019	102.202

Comoros

Year	$MtCO_2$	Year	$MtCO_2$	Year	$MtCO_2$	Year	$MtCO_2$	Year	$MtCO_2$	Year	$MtCO_2$
1960	0.010992	1970	0.029312	1980	0.047632	1990	0.062288	2000	0.10259	2010	0.16122
1961	0.010992	1971	0.029312	1981	0.047632	1991	0.065952	2001	0.10259	2011	0.13557
1962	0.010992	1972	0.029312	1982	0.047632	1992	0.065952	2002	0.10259	2012	0.1429
1963	0.010992	1973	0.029312	1983	0.047632	1993	0.069616	2003	0.1319	2013	0.17587
1964	0.010992	1974	0.029312	1984	0.047632	1994	0.069616	2004	0.1429	2014	0.15389
1965	0.014656	1975	0.032976	1985	0.047632	1995	0.07328	2005	0.13923	2015	0.16854
1966	0.01832	1976	0.040304	1986	0.043968	1996	0.076944	2006	0.16122	2016	0.20152
1967	0.01832	1977	0.040304	1987	0.047632	1997	0.080608	2007	0.10259	2017	0.23816
1968	0.01832	1978	0.029312	1988	0.051296	1998	0.087936	2008	0.10626	2018	0.24593
1969	0.01832	1979	0.021984	1989	0.051296	1999	0.0916	2009	0.1319	2019	0.25311

Congo

Year	$MtCO_2$	Year	$MtCO_2$	Year	$MtCO_2$	Year	$MtCO_2$	Year	$MtCO_2$	Year	$MtCO_2$
1960	0.2235	1970	0.57158	1980	0.40553	1990	1.0072	2000	0.56585	2010	1.9621
1961	0.26747	1971	0.68517	1981	0.47072	1991	1.0828	2001	0.76578	2011	2.2412
1962	0.23816	1972	0.66318	1982	1.3431	1992	1.2902	2002	0.57525	2012	2.9434
1963	0.2345	1973	1.2201	1983	1.1425	1993	1.1619	2003	0.916	2013	3.208
1964	0.26747	1974	1.6232	1984	1.1395	1994	1.7691	2004	0.94898	2014	3.1034
1965	0.24549	1975	1.0992	1985	1.2752	1995	1.1859	2005	0.99726	2015	3.451
1966	0.30778	1976	1.2348	1986	1.0624	1996	1.34	2006	1.1286	2016	3.7018
1967	0.32243	1977	0.47998	1987	1.3201	1997	1.9216	2007	1.2123	2017	3.5259
1968	0.45067	1978	0.32243	1988	1.4929	1998	0.35541	2008	1.3292	2018	3.5183
1969	0.50197	1979	0.34808	1989	1.4956	1999	0.36274	2009	1.7242	2019	3.457

Cook Islands

Year	$MtCO_2$	Year	$MtCO_2$	Year	$MtCO_2$	Year	$MtCO_2$	Year	$MtCO_2$	Year	$MtCO_2$
1960		1970	0.01099	1980	0.02931	1990	0.03664	2000	0.04763	2010	0.05130
1961		1971	0.01099	1981	0.06595	1991	0.03664	2001	0.03298	2011	0.05862
1962		1972	0.01099	1982	0.05130	1992	0.03664	2002	0.02198	2012	0.06229
1963		1973	0.01099	1983	0.05130	1993	0.04030	2003	0.02931	2013	0.06229
1964		1974	0.01099	1984	0.02198	1994	0.04030	2004	0.04763	2014	0.06595
1965		1975	0.01466	1985	0.02198	1995	0.04030	2005	0.05496	2015	0.06229
1966		1976	0.01466	1986	0.02198	1996	0.04763	2006	0.04763	2016	0.06229
1967		1977	0.02931	1987	0.02198	1997	0.04763	2007	0.04763	2017	0.06962
1968		1978	0.02931	1988	0.02198	1998	0.04763	2008	0.04763	2018	0.07271
1969	0.01099	1979	0.02565	1989	0.02198	1999	0.04763	2009	0.04397	2019	0.07746

Costa Rica

Year	$MtCO_2$	Year	$MtCO_2$	Year	$MtCO_2$	Year	$MtCO_2$	Year	$MtCO_2$	Year	$MtCO_2$
1960	0.49098	1970	1.2487	1980	2.4485	1990	2.912	2000	5.3945	2010	7.4937
1961	0.49098	1971	1.527	1981	2.2362	1991	3.2873	2001	5.6659	2011	7.3094
1962	0.5496	1972	1.7613	1982	2.0706	1992	3.7412	2002	6.2448	2012	7.2589
1963	0.6009	1973	2.0434	1983	2.0888	1993	3.891	2003	6.5832	2013	7.6327
1964	0.67406	1974	1.9041	1984	1.9809	1994	5.2003	2004	6.8416	2014	7.7486
1965	0.84591	1975	2.0358	1985	2.2425	1995	4.8019	2005	6.7234	2015	7.4071
1966	0.99247	1976	2.0819	1986	2.5775	1996	4.6867	2006	7.0056	2016	7.9237
1967	0.87525	1977	2.6074	1987	2.7239	1997	4.9167	2007	7.9613	2017	8.2352
1968	1.0364	1978	2.912	1988	2.9059	1998	5.2355	2008	7.9911	2018	8.2491
1969	1.1462	1979	2.781	1989	2.9333	1999	5.439	2009	7.7489	2019	8.5075

Côte d'Ivoire

Year	$MtCO_2$	Year	$MtCO_2$	Year	$MtCO_2$	Year	$MtCO_2$	Year	$MtCO_2$	Year	$MtCO_2$
1960	0.46166	1970	2.2424	1980	5.5693	1990	4.7815	2000	6.4633	2010	6.0639
1961	0.55326	1971	2.4549	1981	3.8655	1991	4.3089	2001	7.3976	2011	6.3424
1962	0.58624	1972	2.7114	1982	5.5546	1992	3.8435	2002	6.9579	2012	8.3393
1963	0.62288	1973	2.8762	1983	4.5177	1993	5.093	2003	5.1331	2013	9.5264
1964	0.76211	1974	3.2426	1984	5.1333	1994	4.133	2004	7.3353	2014	9.7389
1965	1.1725	1975	3.9864	1985	6.9836	1995	6.1155	2005	7.4965	2015	9.4055
1966	1.2384	1976	3.9608	1986	5.5766	1996	7.3353	2006	6.8114	2016	11.7981
1967	1.3593	1977	4.0524	1987	7.35	1997	7.0127	2007	6.5366	2017	11.8604
1968	1.5975	1978	4.8145	1988	8.8046	1998	6.5842	2008	6.5915	2018	12.5141
1969	1.8906	1979	5.4191	1989	8.266	1999	5.9395	2009	5.5143	2019	12.9465

Croatia

Year	$MtCO_2$	Year	$MtCO_2$	Year	$MtCO_2$	Year	$MtCO_2$	Year	$MtCO_2$	Year	$MtCO_2$
1960	5.6749	1970	11.5282	1980	17.4567	1990	23.3292	2000	19.6944	2010	21.0509
1961	5.9504	1971	12.4185	1981	18.9747	1991	17.1823	2001	20.8067	2011	20.6824
1962	6.1063	1972	11.6263	1982	17.4282	1992	16.5061	2002	21.9127	2012	19.1148
1963	6.7938	1973	13.9033	1983	18.7672	1993	16.9598	2003	23.2682	2013	18.4546
1964	7.7017	1974	13.9584	1984	19.7928	1994	16.2142	2004	22.9168	2014	17.705
1965	7.931	1975	14.5586	1985	20.1916	1995	16.9263	2005	23.3301	2015	17.8408
1966	7.8614	1976	15.0228	1986	21.0923	1996	17.5153	2006	23.5295	2016	18.105
1967	7.9471	1977	14.6031	1987	20.5885	1997	18.5759	2007	24.8438	2017	18.7377
1968	8.501	1978	16.324	1988	21.2505	1998	19.2789	2008	23.6286	2018	17.7186
1969	8.8157	1979	17.7589	1989	21.1838	1999	20.1155	2009	21.8378	2019	17.8822

Cuba

Year	$MtCO_2$	Year	$MtCO_2$	Year	$MtCO_2$	Year	$MtCO_2$	Year	$MtCO_2$	Year	$MtCO_2$
1960	13.6871	1970	18.6541	1980	31.3043	1990	32.7356	2000	25.9442	2010	33.9146
1961	12.1683	1971	19.5884	1981	32.6273	1991	28.899	2001	25.3322	2011	29.1693
1962	14.1545	1972	20.7763	1982	34.4206	1992	21.0203	2002	25.9656	2012	29.5222
1963	13.0259	1973	22.3737	1983	30.697	1993	19.787	2003	25.3551	2013	27.7483
1964	14.279	1974	22.8853	1984	32.4373	1994	21.2867	2004	24.8659	2014	27.426
1965	14.5941	1975	27.0356	1985	32.4051	1995	25.5862	2005	25.8476	2015	29.0528
1966	15.1694	1976	27.181	1986	33.3752	1996	26.8725	2006	26.3268	2016	27.9999
1967	15.7369	1977	29.345	1987	33.7334	1997	24.5091	2007	25.762	2017	25.1312
1968	16.0195	1978	30.6191	1988	35.3987	1998	24.3574	2008	27.7472	2018	26.0844
1969	17.2433	1979	31.6321	1989	35.513	1999	25.183	2009	28.0161	2019	25.9885

Curaçao

Year	$MtCO_2$	Year	$MtCO_2$	Year	$MtCO_2$	Year	$MtCO_2$	Year	$MtCO_2$	Year	$MtCO_2$
1960	8.9423	1970	13.4268	1980	8.4635	1990	4.6337	2000	4.7934	2010	3.8948
1961	9.3326	1971	11.6857	1981	8.0614	1991	3.6976	2001	4.881	2011	4.9687
1962	10.249	1972	11.3309	1982	9.0133	1992	3.0463	2002	4.7057	2012	5.9174
1963	9.8174	1973	12.5695	1983	4.6323	1993	4.7026	2003	4.7088	2013	5.1003
1964	9.5454	1974	11.393	1984	11.5674	1994	4.5085	2004	4.9405	2014	5.7561
1965	8.564	1975	8.2506	1985	13.5392	1995	4.4615	2005	4.8967	2015	6.2508
1966	8.0082	1976	17.6246	1986	2.5955	1996	4.1735	2006	5.1033	2016	5.3897
1967	9.8647	1977	9.2054	1987	2.3075	1997	4.3676	2007	5.7452	2017	5.093
1968	9.1729	1978	7.8397	1988	2.273	1998	0.24108	2008	5.526	2018	5.2694
1969	12.0049	1979	8.224	1989	4.3269	1999	1.8065	2009	5.6544	2019	5.1958

Cyprus

Year	$MtCO_2$	Year	$MtCO_2$	Year	$MtCO_2$	Year	$MtCO_2$	Year	$MtCO_2$	Year	$MtCO_2$
1960	0.88633	1970	1.7027	1980	3.2599	1990	4.6569	2000	7.1459	2010	8.089
1961	0.86432	1971	1.8835	1981	3.095	1991	5.1466	2001	7.0214	2011	7.7595
1962	0.90462	1972	2.4059	1982	3.1564	1992	5.5229	2002	7.2108	2012	7.2349
1963	0.98523	1973	2.5035	1983	3.1506	1993	5.767	2003	7.6056	2013	6.5544
1964	0.99997	1974	1.9287	1984	3.2338	1994	6.0111	2004	7.8409	2014	6.9346
1965	1.1501	1975	1.9906	1985	3.1444	1995	5.8823	2005	8.0313	2015	6.9601
1966	1.2417	1976	2.4873	1986	3.6052	1996	6.2332	2006	8.2232	2016	7.3682
1967	1.3623	1977	2.6989	1987	4.1841	1997	6.321	2007	8.5389	2017	7.5157
1968	1.6222	1978	2.8445	1988	4.1966	1998	6.6146	2008	8.7073	2018	7.3328
1969	1.6698	1979	3.0448	1989	4.4285	1999	6.8825	2009	8.4538	2019	7.3157

Czech Republic

Year	$MtCO_2$	Year	$MtCO_2$	Year	$MtCO_2$	Year	$MtCO_2$	Year	$MtCO_2$	Year	$MtCO_2$
1960	99.0815	1970	154.4755	1980	184.6904	1990	164.2042	2000	127.0665	2010	117.5007
1961	107.5398	1971	162.0302	1981	182.6561	1991	148.8941	2001	126.9576	2011	115.0603
1962	114.601	1972	163.5033	1982	180.8599	1992	144.619	2002	123.8956	2012	110.9552
1963	120.5546	1973	164.1514	1983	181.0857	1993	138.6373	2003	127.3828	2013	106.4275
1964	125.4635	1974	166.0289	1984	187.1865	1994	132.3761	2004	128.1138	2014	104.0499
1965	122.2494	1975	173.7007	1985	184.6214	1995	131.6083	2005	125.6719	2015	104.8154
1966	121.5591	1976	180.4472	1986	185.8769	1996	134.9625	2006	126.4495	2016	106.629
1967	121.3051	1977	185.8315	1987	183.658	1997	130.7331	2007	128.2643	2017	105.6417
1968	126.915	1978	187.4934	1988	180.6114	1998	125.3177	2008	122.9414	2018	104.4112
1969	134.7347	1979	182.5758	1989	172.3122	1999	116.6234	2009	115.1937	2019	101.0098

Democratic Republic of the Congo

Year	$MtCO_2$	Year	$MtCO_2$	Year	$MtCO_2$	Year	$MtCO_2$	Year	$MtCO_2$	Year	$MtCO_2$
1960	2.3185	1970	2.7097	1980	3.485	1990	4.2499	2000	0.89277	2010	1.9633
1961	2.3554	1971	2.9587	1981	3.7554	1991	3.1326	2001	0.76877	2011	2.4387
1962	2.1719	1972	3.0172	1982	3.047	1992	2.8092	2002	0.84996	2012	2.3558
1963	2.2927	1973	3.1892	1983	3.998	1993	2.6615	2003	1.0372	2013	3.5381
1964	1.974	1974	3.3647	1984	3.9316	1994	1.6995	2004	1.1502	2014	4.6313
1965	2.4685	1975	3.2328	1985	3.6119	1995	2.1037	2005	1.4453	2015	2.7919
1966	2.4025	1976	3.4049	1986	3.3457	1996	2.3118	2006	1.5533	2016	1.996
1967	2.2888	1977	3.477	1987	3.8159	1997	1.8754	2007	1.6962	2017	2.2049
1968	3.366	1978	3.526	1988	3.978	1998	1.6548	2008	1.8108	2018	2.2313
1969	3.648	1979	3.7401	1989	4.352	1999	1.3186	2009	1.6953	2019	2.2827

Denmark

Year	$MtCO_2$	Year	$MtCO_2$	Year	$MtCO_2$	Year	$MtCO_2$	Year	$MtCO_2$	Year	$MtCO_2$
1960	29.7495	1970	62.0393	1980	60.3479	1990	53.5528	2000	54.2767	2010	49.1523
1961	31.7019	1971	57.0095	1981	51.7726	1991	64.1694	2001	55.8652	2011	44.1971
1962	36.8899	1972	59.5939	1982	53.6838	1992	58.3613	2002	55.5274	2012	39.8236
1963	40.6679	1973	59.2218	1983	50.1673	1993	60.6078	2003	60.6137	2013	41.7295
1964	43.1469	1974	55.0415	1984	50.8558	1994	64.6698	2004	55.0657	2014	37.5273
1965	44.2934	1975	55.7446	1985	60.0646	1995	61.5816	2005	51.4954	2015	35.1815
1966	50.0784	1976	60.1023	1986	58.9062	1996	74.8299	2006	59.417	2016	36.9887
1967	49.0264	1977	61.8174	1987	58.3455	1997	65.4296	2007	54.6427	2017	34.7222
1968	53.2727	1978	61.0958	1988	55.1114	1998	61.1995	2008	51.223	2018	34.6514
1969	59.3426	1979	62.9776	1989	48.8077	1999	58.6193	2009	48.8206	2019	32.0755

Djibouti

Year	$MtCO_2$	Year	$MtCO_2$	Year	$MtCO_2$	Year	$MtCO_2$	Year	$MtCO_2$	Year	$MtCO_2$
1960	0.040304	1970	0.13923	1980	0.34808	1990	0.32243	2000	0.3664	2010	0.51662
1961	0.043968	1971	0.16122	1981	0.30045	1991	0.33709	2001	0.3664	2011	0.47266
1962	0.047632	1972	0.19053	1982	0.34808	1992	0.33709	2002	0.39938	2012	0.47998
1963	0.065952	1973	0.17954	1983	0.34808	1993	0.33709	2003	0.42136	2013	0.55554
1964	0.084272	1974	0.19419	1984	0.35174	1994	0.32976	2004	0.4067	2014	0.3733
1965	0.12091	1975	0.19786	1985	0.35907	1995	0.32976	2005	0.41403	2015	0.44577
1966	0.13923	1976	0.19786	1986	0.37739	1996	0.33342	2006	0.41037	2016	0.39814
1967	0.087936	1977	0.19786	1987	0.38838	1997	0.34808	2007	0.46166	2017	0.37982
1968	0.12091	1978	0.20152	1988	0.34808	1998	0.34075	2008	0.4983	2018	0.38997
1969	0.084272	1979	0.36274	1989	0.38838	1999	0.34075	2009	0.458	2019	0.39937

Dominica

Year	$MtCO_2$	Year	$MtCO_2$	Year	$MtCO_2$	Year	$MtCO_2$	Year	$MtCO_2$	Year	$MtCO_2$
1960	1.0399	1970	3.1051	1980	6.427	1990	9.1517	2000	19.5937	2010	20.5744
1961	1.0286	1971	3.5187	1981	6.1352	1991	9.9526	2001	19.5938	2011	21.3193
1962	1.2411	1972	4.6689	1982	6.3035	1992	10.8223	2002	21.4624	2012	21.4937
1963	1.2485	1973	5.959	1983	7.8656	1993	11.6672	2003	21.6227	2013	21.0497
1964	1.7465	1974	6.4096	1984	7.3905	1994	12.3768	2004	17.8425	2014	21.6457
1965	1.5453	1975	6.3327	1985	7.2415	1995	15.7714	2005	17.9041	2015	23.4879
1966	1.6697	1976	6.3224	1986	8.1211	1996	17.1977	2006	19.0867	2016	24.6291
1967	1.5669	1977	5.5989	1987	9.6873	1997	17.9046	2007	19.9504	2017	24.255
1968	2.3473	1978	5.4303	1988	9.7398	1998	18.2485	2008	20.269	2018	25.3052
1969	2.6512	1979	6.7856	1989	10.2579	1999	18.3839	2009	19.8137	2019	27.3788

Dominican Republic

Year	$MtCO_2$	Year	$MtCO_2$	Year	$MtCO_2$	Year	$MtCO_2$	Year	$MtCO_2$	Year	$MtCO_2$
1960	0.01099	1970	0.02565	1980	0.03664	1990	0.05862	2000	0.10259	2010	0.17221
1961	0.01099	1971	0.02565	1981	0.03664	1991	0.05862	2001	0.10992	2011	0.15389
1962	0.01099	1972	0.02565	1982	0.04030	1992	0.05862	2002	0.10259	2012	0.16488
1963	0.01466	1973	0.02565	1983	0.04030	1993	0.06229	2003	0.11725	2013	0.16854
1964	0.01466	1974	0.02931	1984	0.04397	1994	0.06595	2004	0.14290	2014	0.17587
1965	0.01466	1975	0.02931	1985	0.04763	1995	0.08061	2005	0.14290	2015	0.17587
1966	0.01466	1976	0.02931	1986	0.04763	1996	0.07328	2006	0.14290	2016	0.17954
1967	0.02198	1977	0.02565	1987	0.04763	1997	0.08061	2007	0.18320	2017	0.16122
1968	0.02198	1978	0.02565	1988	0.05496	1998	0.07694	2008	0.16488	2018	0.16601
1969	0.01832	1979	0.03298	1989	0.05862	1999	0.08061	2009	0.16122	2019	0.16166

Ecuador

Year	$MtCO_2$	Year	$MtCO_2$	Year	$MtCO_2$	Year	$MtCO_2$	Year	$MtCO_2$	Year	$MtCO_2$
1960	1.7616	1970	4.2782	1980	13.4072	1990	16.4578	2000	20.5626	2010	34.8254
1961	1.6442	1971	4.2194	1981	16.6528	1991	16.1578	2001	22.9394	2011	37.398
1962	1.5637	1972	4.589	1982	19.2351	1992	21.9596	2002	24.7531	2012	37.1528
1963	1.7943	1973	5.2559	1983	19.5026	1993	24.0874	2003	26.7478	2013	39.3619
1964	2.1423	1974	6.0836	1984	21.1895	1994	13.5385	2004	28.7858	2014	43.2078
1965	2.274	1975	7.3549	1985	19.3527	1995	22.6979	2005	29.9701	2015	40.6398
1966	2.4167	1976	8.1006	1986	15.1941	1996	24.0255	2006	28.8947	2016	39.5051
1967	2.5889	1977	7.4722	1987	15.0223	1997	18.2051	2007	33.6851	2017	39.2376
1968	3.1126	1978	10.4064	1988	17.1686	1998	22.3147	2008	29.573	2018	41.818
1969	3.5889	1979	12.1405	1989	20.1537	1999	21.365	2009	32.5026	2019	40.5403

Egypt

Year	$MtCO_2$	Year	$MtCO_2$	Year	$MtCO_2$	Year	$MtCO_2$	Year	$MtCO_2$	Year	$MtCO_2$
1960	16.0327	1970	21.654	1980	45.176	1990	75.2189	2000	140.3476	2010	198.8077
1961	17.0659	1971	23.0124	1981	50.9027	1991	77.2948	2001	124.2928	2011	211.0375
1962	18.5711	1972	25.475	1982	56.4312	1992	79.9395	2002	125.7814	2012	210.3549
1963	21.5269	1973	23.7611	1983	56.9805	1993	92.2776	2003	146.4621	2013	206.8676
1964	25.4912	1974	26.0891	1984	63.7043	1994	84.5565	2004	149.1437	2014	221.9423
1965	27.6095	1975	31.0599	1985	63.8072	1995	94.8884	2005	165.0417	2015	219.304
1966	26.5322	1976	34.4504	1986	74.3929	1996	93.5675	2006	176.0195	2016	233.5156
1967	19.6499	1977	37.8151	1987	74.6135	1997	107.512	2007	185.9052	2017	250.2401
1968	22.8726	1978	39.261	1988	74.3095	1998	121.4653	2008	195.2854	2018	251.4609
1969	19.6648	1979	42.8895	1989	71.9046	1999	124.4974	2009	202.7097	2019	246.6429

El Salvador

Year	$MtCO_2$	Year	$MtCO_2$	Year	$MtCO_2$	Year	$MtCO_2$	Year	$MtCO_2$	Year	$MtCO_2$
1960	0.61886	1970	1.4283	1980	2.1194	1990	2.4745	2000	5.6719	2010	6.317
1961	0.58228	1971	1.5088	1981	1.8187	1991	3.1532	2001	5.8581	2011	6.5005
1962	0.64826	1972	1.6772	1982	1.7521	1992	3.3168	2002	6.0737	2012	6.4691
1963	1.1245	1973	1.9666	1983	1.8854	1993	3.9753	2003	6.4343	2013	6.0936
1964	1.2307	1974	1.97	1984	1.5883	1994	4.5139	2004	6.2537	2014	6.1475
1965	1.0402	1975	2.1055	1985	1.9653	1995	4.9982	2005	6.298	2015	6.7154
1966	1.3038	1976	2.2067	1986	1.9675	1996	4.4147	2006	6.7169	2016	6.6384
1967	1.1573	1977	2.2817	1987	2.4145	1997	5.4166	2007	6.8459	2017	6.0156
1968	1.2598	1978	2.3814	1988	2.4331	1998	5.7317	2008	6.405	2018	6.0183
1969	1.1902	1979	2.3767	1989	2.5472	1999	5.5872	2009	6.3126	2019	6.2073

Equatorial Guinea

Year	$MtCO_2$	Year	$MtCO_2$	Year	$MtCO_2$	Year	$MtCO_2$	Year	$MtCO_2$	Year	$MtCO_2$
1960	0.021984	1970	0.03664	1980	0.058624	1990	0.062288	2000	0.46533	2010	6.8663
1961	0.021984	1971	0.065952	1981	0.069616	1991	0.065952	2001	4.5397	2011	8.8815
1962	0.021984	1972	0.087936	1982	0.07328	1992	0.065952	2002	6.1812	2012	7.5368
1963	0.025648	1973	0.029312	1983	0.062288	1993	0.069616	2003	6.6612	2013	7.72
1964	0.025648	1974	0.051296	1984	0.080608	1994	0.076944	2004	7.5185	2014	7.306
1965	0.029312	1975	0.062288	1985	0.065952	1995	0.084272	2005	7.5149	2015	6.434
1966	0.025648	1976	0.062288	1986	0.080608	1996	0.12824	2006	6.9616	2016	6.2068
1967	0.025648	1977	0.062288	1987	0.098928	1997	0.30411	2007	5.6279	2017	5.9796
1968	0.029312	1978	0.069616	1988	0.10626	1998	0.2235	2008	7.0166	2018	5.9058
1969	0.043968	1979	0.062288	1989	0.11725	1999	0.37006	2009	6.7528	2019	5.6338

Eritrea

Year	$MtCO_2$	Year	$MtCO_2$	Year	$MtCO_2$	Year	$MtCO_2$	Year	$MtCO_2$	Year	$MtCO_2$
1960		1970		1980		1990		2000	0.60408	2010	0.497
1961		1971		1981		1991		2001	0.62599	2011	0.56017
1962		1972		1982		1992		2002	0.60027	2012	0.61843
1963		1973		1983		1993		2003	0.71012	2013	0.63832
1964		1974		1984		1994	0.70683	2004	0.76501	2014	0.67171
1965		1975		1985		1995	0.79041	2005	0.76494	2015	0.65217
1966		1976		1986		1996	0.86067	2006	0.54493	2016	0.6595
1967		1977		1987		1997	0.76768	2007	0.55935	2017	0.68881
1968		1978		1988		1998	0.58581	2008	0.40535	2018	0.70877
1969		1979		1989		1999	0.6151	2009	0.49697	2019	0.72723

Estonia

Year	$MtCO_2$	Year	$MtCO_2$	Year	$MtCO_2$	Year	$MtCO_2$	Year	$MtCO_2$	Year	$MtCO_2$
1960	13.165	1970	21.3207	1980	31.514	1990	36.9072	2000	15.2442	2010	18.785
1961	13.5667	1971	22.6233	1981	30.8855	1991	33.9018	2001	15.5767	2011	18.8551
1962	14.2242	1972	23.8006	1982	31.4823	1992	24.3705	2002	15.0905	2012	17.685
1963	15.2469	1973	24.7993	1983	31.929	1993	18.9104	2003	16.9372	2013	19.552
1964	16.2088	1974	25.7348	1984	32.22	1994	19.734	2004	17.201	2014	18.7559
1965	17.1882	1975	27.0513	1985	34.7987	1995	18.0488	2005	16.9216	2015	15.8134
1966	18.1443	1976	28.1006	1986	34.9028	1996	18.7595	2006	16.2088	2016	17.3777
1967	18.9575	1977	29.0582	1987	34.8	1997	18.3173	2007	19.8386	2017	18.6359
1968	19.4757	1978	30.0475	1988	35.743	1998	16.8172	2008	17.6681	2018	17.711
1969	20.2732	1979	30.3051	1989	34.9376	1999	15.6533	2009	14.339	2019	13.8884

Ethiopia

Year	$MtCO_2$	Year	$MtCO_2$	Year	$MtCO_2$	Year	$MtCO_2$	Year	$MtCO_2$	Year	$MtCO_2$
1960	0.35163	1970	1.6517	1980	1.8175	1990	2.9858	2000	3.4638	2010	6.3371
1961	0.34063	1971	1.8495	1981	1.86	1991	2.9571	2001	4.2634	2011	7.402
1962	0.39553	1972	1.4062	1982	1.4739	1992	2.9373	2002	4.4305	2012	8.1099
1963	0.42121	1973	1.7509	1983	1.8348	1993	2.9948	2003	4.8711	2013	9.7808
1964	0.40653	1974	1.7363	1984	1.6503	1994	2.1969	2004	5.1586	2014	12.0174
1965	0.64448	1975	1.2085	1985	1.7987	1995	2.5057	2005	4.9551	2015	12.6934
1966	0.82398	1976	1.1747	1986	2.1952	1996	2.7947	2006	5.3169	2016	14.4321
1967	1.073	1977	1.0468	1987	2.5544	1997	2.9793	2007	5.8393	2017	15.5936
1968	1.725	1978	1.3685	1988	2.6401	1998	3.1474	2008	6.4164	2018	16.1849
1969	1.6664	1979	1.8441	1989	2.7941	1999	3.095	2009	6.4546	2019	16.2551

Faeroe Islands

Year	$MtCO_2$	Year	$MtCO_2$	Year	$MtCO_2$	Year	$MtCO_2$	Year	$MtCO_2$	Year	$MtCO_2$
1960	0.058624	1970	0.25648	1980	0.42136	1990	0.70349	2000	0.68883	2010	0.63021
1961	0.11358	1971	0.26014	1981	0.43968	1991	0.65586	2001	0.76211	2011	0.56792
1962	0.11725	1972	0.2345	1982	0.458	1992	0.64853	2002	0.72547	2012	0.5899
1963	0.12458	1973	0.25282	1983	0.48731	1993	0.58258	2003	0.7328	2013	0.67784
1964	0.12091	1974	0.30045	1984	0.4983	1994	0.57525	2004	0.74746	2014	0.59723
1965	0.13557	1975	0.34808	1985	0.51662	1995	0.57158	2005	0.72181	2015	0.60822
1966	0.13923	1976	0.32976	1986	0.49098	1996	0.6009	2006	0.67784	2016	0.63021
1967	0.16854	1977	0.4067	1987	0.4983	1997	0.5899	2007	0.68883	2017	0.70715
1968	0.1832	1978	0.39938	1988	0.52762	1998	0.62288	2008	0.63021	2018	0.70545
1969	0.21251	1979	0.47998	1989	0.57891	1999	0.63021	2009	0.57525	2019	0.715

Fiji

Year	$MtCO_2$	Year	$MtCO_2$	Year	$MtCO_2$	Year	$MtCO_2$	Year	$MtCO_2$	Year	$MtCO_2$
1960	0.19419	1970	0.52005	1980	0.79242	1990	0.80604	2000	0.83358	2010	1.2012
1961	0.16854	1971	0.54927	1981	1.0772	1991	0.66312	2001	1.046	2011	1.0679
1962	0.23083	1972	0.57856	1982	0.83512	1992	0.74	2002	0.87945	2012	1.0411
1963	0.24182	1973	0.62985	1983	0.70893	1993	0.74364	2003	1.0361	2013	1.316
1964	0.42491	1974	0.67019	1984	0.57721	1994	0.7386	2004	1.34	2014	1.6228
1965	0.34427	1975	0.62258	1985	0.57299	1995	0.75389	2005	1.081	2015	2.1304
1966	0.32225	1976	0.483	1986	0.59809	1996	0.81317	2006	1.2014	2016	2.0188
1967	0.35523	1977	0.76463	1987	0.472	1997	0.78246	2007	1.1411	2017	2.0371
1968	0.3955	1978	0.70908	1988	0.54977	1998	0.76108	2008	0.87776	2018	2.1238
1969	0.43215	1979	0.83646	1989	0.6252	1999	0.77502	2009	0.77856	2019	2.2571

Finland

Year	$MtCO_2$	Year	$MtCO_2$	Year	$MtCO_2$	Year	$MtCO_2$	Year	$MtCO_2$	Year	$MtCO_2$
1960	15.0869	1970	40.355	1980	58.1395	1990	56.9719	2000	57.0382	2010	64.0995
1961	14.9217	1971	40.5368	1981	51.4035	1991	55.2304	2001	62.5362	2011	56.6657
1962	16.7903	1972	44.1061	1982	42.9767	1992	54.2855	2002	65.0598	2012	51.2221
1963	19.3365	1973	49.3202	1983	41.4636	1993	56.3526	2003	72.6578	2013	51.751
1964	22.8277	1974	46.6085	1984	42.1474	1994	61.7162	2004	68.9608	2014	47.6439
1965	25.3001	1975	46.0258	1985	49.5493	1995	58.1454	2005	57.0429	2015	44.1137
1966	29.4888	1976	51.1986	1986	53.2146	1996	64.0624	2006	68.3844	2016	47.2275
1967	28.5877	1977	50.1371	1987	57.5337	1997	62.723	2007	66.7603	2017	44.6731
1968	33.2815	1978	51.8252	1988	52.0584	1998	59.3733	2008	58.6096	2018	45.8493
1969	37.8968	1979	54.2372	1989	52.4483	1999	58.8948	2009	55.9244	2019	41.6526

France

Year	$MtCO_2$	Year	$MtCO_2$	Year	$MtCO_2$	Year	$MtCO_2$	Year	$MtCO_2$	Year	$MtCO_2$
1960	271.3608	1970	439.6251	1980	506.255	1990	400.9833	2000	416.2659	2010	389.3863
1961	281.3733	1971	463.1314	1981	455.6496	1991	426.5009	2001	420.8481	2011	362.5039
1962	298.8665	1972	481.588	1982	438.0556	1992	415.7089	2002	415.8383	2012	363.8091
1963	334.2264	1973	517.5423	1983	423.9971	1993	394.9725	2003	422.6412	2013	365.8312
1964	345.5381	1974	499.9684	1984	407.3412	1994	390.8153	2004	423.6306	2014	333.9221
1965	352.1116	1975	447.7482	1985	402.4876	1995	397.4555	2005	426.7792	2015	338.5007
1966	347.6048	1976	506.6147	1986	387.4457	1996	413.1973	2006	416.0038	2016	341.0257
1967	372.4753	1977	481.9079	1987	379.7093	1997	406.1874	2007	405.1944	2017	345.9213
1968	385.101	1978	506.7407	1988	374.6746	1998	425.465	2008	397.7251	2018	331.7254
1969	413.7595	1979	530.2807	1989	392.9246	1999	421.705	2009	381.5991	2019	323.7471

French Polynesia

Year	$MtCO_2$	Year	$MtCO_2$	Year	$MtCO_2$	Year	$MtCO_2$	Year	$MtCO_2$	Year	$MtCO_2$
1960	0.03664	1970	0.19419	1980	0.29312	1990	0.43968	2000	0.57158	2010	0.80608
1961	0.05862	1971	0.22717	1981	0.32976	1991	0.43602	2001	0.6815	2011	0.77677
1962	0.04763	1972	0.21618	1982	0.33709	1992	0.4177	2002	0.68517	2012	0.75478
1963	0.06595	1973	0.20885	1983	0.42136	1993	0.42869	2003	0.74013	2013	0.76211
1964	0.06595	1974	0.21618	1984	0.46166	1994	0.44334	2004	0.72547	2014	0.74013
1965	0.08427	1975	0.21251	1985	0.5899	1995	0.43235	2005	0.7841	2015	0.76944
1966	0.12091	1976	0.26381	1986	0.60822	1996	0.43602	2006	0.78043	2016	0.74379
1967	0.13923	1977	0.2748	1987	0.61189	1997	0.45434	2007	0.76944	2017	0.74746
1968	0.15389	1978	0.31144	1988	0.57525	1998	0.45067	2008	0.79509	2018	0.78063
1969	0.16122	1979	0.28213	1989	0.54227	1999	0.4983	2009	0.79875	2019	0.83168

Gabon

Year	$MtCO_2$	Year	$MtCO_2$	Year	$MtCO_2$	Year	$MtCO_2$	Year	$MtCO_2$	Year	$MtCO_2$
1960	0.1319	1970	2.0812	1980	6.6247	1990	4.4854	2000	4.6699	2010	4.7823
1961	0.16488	1971	2.8433	1981	6.564	1991	4.522	2001	4.773	2011	4.931
1962	0.087936	1972	2.737	1982	6.5436	1992	4.9176	2002	4.544	2012	5.0333
1963	0.07328	1973	5.3091	1983	5.5086	1993	4.9748	2003	4.6132	2013	5.2687
1964	0.19053	1974	5.4484	1984	5.9795	1994	4.3745	2004	4.6568	2014	5.3123
1965	0.21618	1975	5.3641	1985	6.2985	1995	4.6063	2005	4.8579	2015	5.2489
1966	0.38106	1976	5.7038	1986	4.9508	1996	4.7537	2006	4.1424	2016	5.2985
1967	1.0113	1977	6.3065	1987	4.0095	1997	4.7742	2007	4.0893	2017	4.7929
1968	1.9602	1978	7.5549	1988	4.3207	1998	4.9573	2008	4.162	2018	4.8031
1969	1.4326	1979	6.7468	1989	5.7575	1999	4.787	2009	4.2328	2019	4.7049

Gambia

Year	$MtCO_2$	Year	$MtCO_2$	Year	$MtCO_2$	Year	$MtCO_2$	Year	$MtCO_2$	Year	$MtCO_2$
1960	0.01832	1970	0.047632	1980	0.15755	1990	0.19786	2000	0.2748	2010	0.43235
1961	0.021984	1971	0.05496	1981	0.15755	1991	0.19786	2001	0.30045	2011	0.44701
1962	0.025648	1972	0.065952	1982	0.16122	1992	0.19786	2002	0.30045	2012	0.45434
1963	0.029312	1973	0.062288	1983	0.16122	1993	0.20885	2003	0.30045	2013	0.43235
1964	0.029312	1974	0.062288	1984	0.17221	1994	0.20885	2004	0.32243	2014	0.51296
1965	0.029312	1975	0.098928	1985	0.17221	1995	0.21618	2005	0.3261	2015	0.52395
1966	0.032976	1976	0.098928	1986	0.16122	1996	0.21984	2006	0.35174	2016	0.53128
1967	0.032976	1977	0.11358	1987	0.17954	1997	0.2235	2007	0.35174	2017	0.53494
1968	0.03664	1978	0.13923	1988	0.1832	1998	0.24182	2008	0.3664	2018	0.56324
1969	0.047632	1979	0.14656	1989	0.17954	1999	0.2748	2009	0.38106	2019	0.58571

Georgia

Year	$MtCO_2$	Year	$MtCO_2$	Year	$MtCO_2$	Year	$MtCO_2$	Year	$MtCO_2$	Year	$MtCO_2$
1960	11.1212	1970	18.1122	1980	26.7828	1990	27.629	2000	4.4994	2010	6.2091
1961	11.4692	1971	19.2237	1981	26.2734	1991	21.471	2001	3.7337	2011	7.8037
1962	12.0377	1972	20.2294	1982	26.7673	1992	15.277	2002	3.3514	2012	8.2511
1963	12.9096	1973	21.0876	1983	27.1473	1993	9.9163	2003	3.7355	2013	8.0087
1964	13.7293	1974	21.8949	1984	27.3878	1994	6.069	2004	4.2762	2014	8.7871
1965	14.5644	1975	23.019	1985	29.5342	1995	2.2914	2005	5.017	2015	9.5887
1966	15.381	1976	23.9033	1986	29.61	1996	4.0551	2006	6.0961	2016	9.9052
1967	16.0831	1977	24.7145	1987	29.4872	1997	4.4251	2007	6.3648	2017	9.8319
1968	16.535	1978	25.561	1988	30.2735	1998	4.9386	2008	5.3082	2018	9.8622
1969	17.2199	1979	25.7704	1989	29.5963	1999	4.3097	2009	6.1349	2019	10.2867

Germany

Year	$MtCO_2$	Year	$MtCO_2$	Year	$MtCO_2$	Year	$MtCO_2$	Year	$MtCO_2$	Year	$MtCO_2$
1960	813.9502	1970	1026.022	1980	1100.059	1990	1052.349	2000	899.7802	2010	832.6697
1961	834.8396	1971	1037.236	1981	1048.517	1991	1014.2	2001	916.3661	2011	809.4269
1962	883.1686	1972	1041.48	1982	1015.727	1992	965.8898	2002	899.8211	2012	813.8931
1963	945.498	1973	1085.736	1983	1011.597	1993	956.2331	2003	900.8664	2013	831.3163
1964	968.9175	1974	1062.724	1984	1033.237	1994	939.6303	2004	886.966	2014	792.6849
1965	960.1022	1975	1002.444	1985	1044.11	1995	939.1767	2005	866.3885	2015	795.8164
1966	951.422	1976	1090.837	1986	1047.463	1996	959.1241	2006	877.9974	2016	800.5103
1967	936.2294	1977	1052.604	1987	1032.434	1997	931.2301	2007	851.3833	2017	786.6546
1968	984.7908	1978	1079.127	1988	1029.014	1998	923.2759	2008	854.7063	2018	755.3623
1969	1052.001	1979	1117.882	1989	1008.782	1999	895.6429	2009	790.1957	2019	701.9551

Ghana

Year	$MtCO_2$	Year	$MtCO_2$	Year	$MtCO_2$	Year	$MtCO_2$	Year	$MtCO_2$	Year	$MtCO_2$
1960	1.4619	1970	2.6216	1980	2.5481	1990	3.7915	2000	6.1005	2010	9.7107
1961	1.3447	1971	2.2915	1981	3.0299	1991	4.2095	2001	6.7326	2011	11.2263
1962	1.4326	1972	2.4202	1982	3.0284	1992	3.6609	2002	7.2315	2012	14.3164
1963	1.7221	1973	2.4714	1983	3.639	1993	4.3107	2003	7.4373	2013	14.1798
1964	1.6488	1974	2.9328	1984	2.5671	1994	5.0887	2004	7.1521	2014	14.7545
1965	1.7038	1975	2.7416	1985	3.3017	1995	5.1542	2005	6.8034	2015	16.1147
1966	1.44	1976	2.4266	1986	3.0303	1996	5.4686	2006	9.16	2016	16.547
1967	1.4949	1977	2.9915	1987	3.2636	1997	6.2042	2007	9.6193	2017	13.817
1968	1.7615	1978	2.9574	1988	3.4112	1998	6.2459	2008	8.9259	2018	14.48
1969	1.6875	1979	2.6492	1989	3.295	1999	6.3695	2009	7.4978	2019	14.9599

Greece

Year	$MtCO_2$	Year	$MtCO_2$	Year	$MtCO_2$	Year	$MtCO_2$	Year	$MtCO_2$	Year	$MtCO_2$
1960	9.3915	1970	24.1262	1980	50.8883	1990	83.4255	2000	102.999	2010	97.3615
1961	9.8084	1971	27.7495	1981	50.1249	1991	83.4011	2001	105.385	2011	94.5496
1962	10.1488	1972	31.4773	1982	51.5082	1992	84.9827	2002	105.021	2012	91.4301
1963	12.2395	1973	37.1311	1983	54.7887	1993	84.2964	2003	109.089	2013	81.7351
1964	13.2016	1974	36.0617	1984	56.2843	1994	86.4422	2004	109.546	2014	78.6598
1965	16.999	1975	38.6696	1985	59.7712	1995	86.9791	2005	113.931	2015	74.9579
1966	18.6206	1976	42.6554	1986	58.2737	1996	89.132	2006	112.472	2016	71.3684
1967	19.5042	1977	46.6569	1987	62.5756	1997	93.8209	2007	114.592	2017	74.8528
1968	22.2863	1978	47.6778	1988	67.0511	1998	98.6415	2008	111.125	2018	71.7979
1969	25.4343	1979	50.8183	1989	73.23	1999	97.9584	2009	104.354	2019	67.184

Greenland

Year	$MtCO_2$	Year	$MtCO_2$	Year	$MtCO_2$	Year	$MtCO_2$	Year	$MtCO_2$	Year	$MtCO_2$
1960	0.2235	1970	0.38106	1980	0.56426	1990	0.34808	2000	0.45434	2010	0.66318
1961	0.29312	1971	0.46899	1981	0.52762	1991	0.34808	2001	0.4067	2011	0.70715
1962	0.26381	1972	0.55326	1982	0.51662	1992	0.3261	2002	0.37739	2012	0.56792
1963	0.32976	1973	0.55693	1983	0.36274	1993	0.32243	2003	0.42869	2013	0.53494
1964	0.3151	1974	0.55693	1984	0.56792	1994	0.29678	2004	0.58258	2014	0.4983
1965	0.34442	1975	0.50563	1985	0.5093	1995	0.32243	2005	0.60822	2015	0.4983
1966	0.38838	1976	0.21984	1986	0.3261	1996	0.36274	2006	0.62654	2016	0.4983
1967	0.4177	1977	0.72181	1987	0.2345	1997	0.38472	2007	0.63754	2017	0.51296
1968	0.54227	1978	0.39205	1988	0.54594	1998	0.35907	2008	0.65952	2018	0.51173
1969	0.4067	1979	0.57158	1989	0.47266	1999	0.37373	2009	0.57525	2019	0.51866

Grenada

Year	$MtCO_2$	Year	$MtCO_2$	Year	$MtCO_2$	Year	$MtCO_2$	Year	$MtCO_2$	Year	$MtCO_2$
1960	0.021984	1970	0.043968	1980	0.047632	1990	0.10626	2000	0.19053	2010	0.26014
1961	0.01832	1971	0.047632	1981	0.058624	1991	0.10992	2001	0.19419	2011	0.25282
1962	0.025648	1972	0.047632	1982	0.062288	1992	0.11725	2002	0.20518	2012	0.27114
1963	0.014656	1973	0.05496	1983	0.062288	1993	0.12091	2003	0.21618	2013	0.30411
1964	0.021984	1974	0.03664	1984	0.062288	1994	0.1429	2004	0.20518	2014	0.2345
1965	0.021984	1975	0.047632	1985	0.062288	1995	0.15022	2005	0.21618	2015	0.26014
1966	0.029312	1976	0.047632	1986	0.065952	1996	0.15389	2006	0.23083	2016	0.26747
1967	0.03664	1977	0.047632	1987	0.07328	1997	0.16854	2007	0.23816	2017	0.27846
1968	0.040304	1978	0.051296	1988	0.095264	1998	0.17587	2008	0.25282	2018	0.2786
1969	0.047632	1979	0.047632	1989	0.10259	1999	0.19419	2009	0.25282	2019	0.28795

Guatemala

Year	$MtCO_2$	Year	$MtCO_2$	Year	$MtCO_2$	Year	$MtCO_2$	Year	$MtCO_2$	Year	$MtCO_2$
1960	1.3442	1970	2.2964	1980	4.4926	1990	4.9702	2000	9.7658	2010	11.0977
1961	1.4065	1971	2.4393	1981	3.9495	1991	4.9521	2001	10.2332	2011	11.2384
1962	1.3809	1972	2.7066	1982	3.6068	1992	5.9179	2002	10.7216	2012	11.5586
1963	1.5199	1973	2.9336	1983	3.1599	1993	5.5772	2003	10.4479	2013	12.5823
1964	1.769	1974	3.0655	1984	3.4011	1994	6.7508	2004	11.1797	2014	13.5686
1965	1.9739	1975	3.5195	1985	3.4968	1995	7.0793	2005	12.108	2015	15.4263
1966	1.7396	1976	3.3049	1986	3.6646	1996	6.5703	2006	12.1753	2016	16.3759
1967	1.9813	1977	3.8045	1987	3.9184	1997	7.5016	2007	12.1446	2017	17.2143
1968	2.1391	1978	4.1171	1988	4.0753	1998	8.6394	2008	10.8931	2018	19.4113
1969	2.2781	1979	4.678	1989	4.1882	1999	8.807	2009	11.442	2019	20.5134

Guinea

Year	$MtCO_2$	Year	$MtCO_2$	Year	$MtCO_2$	Year	$MtCO_2$	Year	$MtCO_2$	Year	$MtCO_2$
1960	0.41037	1970	0.79142	1980	0.96363	1990	1.0039	2000	1.4912	2010	2.4842
1961	0.61555	1971	0.81341	1981	0.98928	1991	1.0259	2001	1.5609	2011	2.5941
1962	0.65952	1972	0.83173	1982	0.98195	1992	1.0589	2002	1.6232	2012	2.4219
1963	0.69616	1973	0.80242	1983	0.95264	1993	1.0882	2003	1.7001	2013	2.1105
1964	0.69982	1974	0.83906	1984	0.97829	1994	1.1248	2004	1.7624	2014	2.1654
1965	0.69616	1975	0.84272	1985	0.99294	1995	1.1652	2005	1.8247	2015	2.4512
1966	0.71814	1976	0.88669	1986	0.99661	1996	1.2348	2006	1.8906	2016	2.7443
1967	0.72547	1977	0.90134	1987	0.99294	1997	1.2897	2007	1.9676	2017	2.8799
1968	0.74746	1978	0.90134	1988	1.0259	1998	1.363	2008	1.9969	2018	3.0321
1969	0.74746	1979	0.94531	1989	1.0442	1999	1.4326	2009	2.1105	2019	3.1534

Guinea-Bissau

Year	$MtCO_2$	Year	$MtCO_2$	Year	$MtCO_2$	Year	$MtCO_2$	Year	$MtCO_2$	Year	$MtCO_2$
1960	0.01832	1970	0.069616	1980	0.14656	1990	0.17221	2000	0.14656	2010	0.23816
1961	0.029312	1971	0.07328	1981	0.1429	1991	0.17587	2001	0.15022	2011	0.24549
1962	0.040304	1972	0.065952	1982	0.1429	1992	0.17954	2002	0.15389	2012	0.25282
1963	0.047632	1973	0.10992	1983	0.1429	1993	0.1832	2003	0.19419	2013	0.25648
1964	0.058624	1974	0.10259	1984	0.16122	1994	0.1832	2004	0.20152	2014	0.27114
1965	0.065952	1975	0.11358	1985	0.17221	1995	0.1832	2005	0.21251	2015	0.27846
1966	0.065952	1976	0.095264	1986	0.1832	1996	0.1832	2006	0.21618	2016	0.29312
1967	0.047632	1977	0.10259	1987	0.19419	1997	0.20152	2007	0.23083	2017	0.29312
1968	0.062288	1978	0.10259	1988	0.21618	1998	0.17221	2008	0.22717	2018	0.30861
1969	0.058624	1979	0.10992	1989	0.23083	1999	0.19419	2009	0.2345	2019	0.32096

Guyana

Year	$MtCO_2$	Year	$MtCO_2$	Year	$MtCO_2$	Year	$MtCO_2$	Year	$MtCO_2$	Year	$MtCO_2$
1960	0.65952	1970	1.5792	1980	1.788	1990	1.1285	2000	1.7477	2010	1.887
1961	0.73646	1971	1.4986	1981	1.799	1991	1.1065	2001	1.7441	2011	1.9602
1962	0.67784	1972	1.5609	1982	1.4033	1992	1.0406	2002	1.7148	2012	1.9602
1963	0.61555	1973	1.8027	1983	1.2458	1993	1.0442	2003	1.8576	2013	1.9053
1964	0.64853	1974	1.5535	1984	1.4033	1994	1.4583	2004	1.9273	2014	1.9712
1965	1.0772	1975	1.8247	1985	1.418	1995	1.5719	2005	1.6195	2015	2.0045
1966	1.1798	1976	1.7514	1986	1.0442	1996	1.6561	2006	1.5096	2016	2.344
1967	1.3227	1977	1.898	1987	1.308	1997	1.8064	2007	1.7807	2017	2.3183
1968	1.33	1978	2.0555	1988	1.4033	1998	1.8283	2008	1.7074	2018	2.3426
1969	1.3667	1979	1.5206	1989	1.1835	1999	1.832	2009	1.9089	2019	2.3904

Haiti

Year	$MtCO_2$	Year	$MtCO_2$	Year	$MtCO_2$	Year	$MtCO_2$	Year	$MtCO_2$	Year	$MtCO_2$
1960	0.28558	1970	0.38448	1980	0.74507	1990	0.99436	2000	1.341	2010	2.0934
1961	0.29661	1971	0.40274	1981	0.75893	1991	0.97613	2001	1.5527	2011	2.0866
1962	0.30387	1972	0.39172	1982	0.8173	1992	0.88788	2002	1.8022	2012	2.1903
1963	0.24894	1973	0.42091	1983	0.88603	1993	0.68546	2003	1.7097	2013	2.2934
1964	0.30021	1974	0.47209	1984	0.90315	1994	0.1832	2004	1.9604	2014	2.7847
1965	0.30393	1975	0.48302	1985	0.92952	1995	0.8757	2005	2.0474	2015	3.1914
1966	0.30396	1976	0.67218	1986	0.83022	1996	1.0186	2006	2.0841	2016	3.2353
1967	0.26	1977	0.70414	1987	0.89879	1997	1.3484	2007	2.361	2017	3.272
1968	0.26363	1978	0.75064	1988	1.0077	1998	1.2311	2008	2.3658	2018	3.367
1969	0.3149	1979	0.7499	1989	1.0231	1999	1.3117	2009	2.237	2019	3.2809

Honduras

Year	$MtCO_2$	Year	$MtCO_2$	Year	$MtCO_2$	Year	$MtCO_2$	Year	$MtCO_2$	Year	$MtCO_2$
1960	0.6154	1970	1.388	1980	2.0443	1990	2.4227	2000	4.9781	2010	7.9585
1961	0.73629	1971	1.3294	1981	1.812	1991	2.445	2001	5.6528	2011	8.6345
1962	0.69959	1972	1.5344	1982	1.7531	1992	2.6931	2002	5.913	2012	8.9886
1963	0.71058	1973	1.5086	1983	1.9824	1993	2.8343	2003	6.6643	2013	9.2447
1964	0.72151	1974	1.5563	1984	1.9635	1994	3.1748	2004	7.247	2014	9.3387
1965	0.75073	1975	1.6659	1985	1.8894	1995	3.7825	2005	7.5767	2015	10.082
1966	0.80566	1976	1.7749	1986	1.8286	1996	3.8394	2006	6.863	2016	9.5544
1967	0.87525	1977	1.9974	1987	2.1485	1997	3.9755	2007	8.5984	2017	9.8991
1968	1.2232	1978	2.0437	1988	2.4699	1998	4.7657	2008	8.5177	2018	10.4707
1969	1.1756	1979	1.9262	1989	2.6856	1999	4.6459	2009	8.0727	2019	10.9284

Hong Kong

Year	$MtCO_2$	Year	$MtCO_2$	Year	$MtCO_2$	Year	$MtCO_2$	Year	$MtCO_2$	Year	$MtCO_2$
1960	2.9526	1970	8.3925	1980	16.6002	1990	27.1471	2000	40.2839	2010	40.0637
1961	3.3701	1971	9.1506	1981	18.6167	1991	28.4627	2001	37.8018	2011	43.1496
1962	3.6815	1972	9.2756	1982	19.6228	1992	32.9171	2002	39.485	2012	42.7426
1963	4.2457	1973	9.2865	1983	20.9121	1993	34.7782	2003	43.2034	2013	44.3056
1964	4.2201	1974	10.6673	1984	22.2248	1994	31.079	2004	41.5683	2014	45.4907
1965	4.8025	1975	11.008	1985	22.8814	1995	31.2664	2005	43.7313	2015	42.3909
1966	5.1616	1976	12.4904	1986	25.5259	1996	28.9096	2006	41.9137	2016	43.3875
1967	6.0521	1977	14.2039	1987	28.0856	1997	30.4975	2007	43.5724	2017	42.5521
1968	6.198	1978	15.7141	1988	29.2848	1998	38.924	2008	42.7907	2018	42.5057
1969	7.7515	1979	15.8376	1989	30.1412	1999	42.55	2009	41.5798	2019	41.5364

Hungary

Year	$MtCO_2$	Year	$MtCO_2$	Year	$MtCO_2$	Year	$MtCO_2$	Year	$MtCO_2$	Year	$MtCO_2$
1960	45.3283	1970	69.9346	1980	86.709	1990	73.4649	2000	58.6083	2010	52.1237
1961	48.9299	1971	69.2094	1981	86.4616	1991	69.7845	2001	60.2388	2011	50.3221
1962	50.5122	1972	69.3544	1982	86.7135	1992	62.4159	2002	59.197	2012	46.7767
1963	56.2278	1973	72.9817	1983	88.9748	1993	63.6328	2003	61.9815	2013	43.7048
1964	62.3412	1974	74.0102	1984	90.6861	1994	61.9735	2004	60.4899	2014	43.8627
1965	61.2341	1975	75.2883	1985	85.947	1995	61.6908	2005	60.6065	2015	46.6276
1966	61.6729	1976	79.8971	1986	83.2408	1996	63.2575	2006	59.9154	2016	47.3957
1967	58.7708	1977	83.075	1987	84.1365	1997	61.8131	2007	58.6886	2017	49.6848
1968	61.0932	1978	88.0461	1988	78.0548	1998	61.415	2008	57.5308	2018	49.6285
1969	62.3582	1979	86.0818	1989	75.9172	1999	61.9116	2009	51.775	2019	49.101

Iceland

Year	$MtCO_2$	Year	$MtCO_2$	Year	$MtCO_2$	Year	$MtCO_2$	Year	$MtCO_2$	Year	$MtCO_2$
1960	1.2125	1970	1.3883	1980	1.8609	1990	2.2478	2000	2.9465	2010	3.6601
1961	1.0916	1971	1.4721	1981	1.747	1991	2.1284	2001	2.8752	2011	3.5106
1962	1.1977	1972	1.4826	1982	1.5927	1992	2.2743	2002	3.0005	2012	3.5029
1963	1.304	1973	1.7497	1983	1.5414	1993	2.4322	2003	2.9946	2013	3.4928
1964	1.3076	1974	1.738	1984	1.8085	1994	2.3733	2004	3.1169	2014	3.4697
1965	1.3955	1975	1.6129	1985	1.6213	1995	2.4767	2005	2.986	2015	3.5453
1966	1.4944	1976	1.7007	1986	1.7789	1996	2.532	2006	3.1644	2016	3.4975
1967	1.4431	1977	1.9019	1987	1.8434	1997	2.6275	2007	3.5121	2017	3.6149
1968	1.5934	1978	1.9201	1988	1.8394	1998	2.6479	2008	3.8249	2018	3.6745
1969	1.2637	1979	1.9822	1989	1.8948	1999	2.854	2009	3.7402	2019	3.3217

India

Year	$MtCO_2$	Year	$MtCO_2$	Year	$MtCO_2$	Year	$MtCO_2$	Year	$MtCO_2$	Year	$MtCO_2$
1960	111.5	1970	182.0	1980	292.1	1990	578.7	2000	978.4	2010	1678.5
1961	120.6	1971	192.2	1981	315.4	1991	616.1	2001	992.5	2011	1766.1
1962	132.8	1972	203.3	1982	325.8	1992	656.2	2002	1022.8	2012	1941.3
1963	142.7	1973	209.4	1983	352.6	1993	678.1	2003	1059.4	2013	2033.4
1964	139.7	1974	216.1	1984	362.0	1994	717.1	2004	1125.3	2014	2184.4
1965	153.9	1975	234.5	1985	398.1	1995	762.3	2005	1185.8	2015	2253.4
1966	159.6	1976	245.1	1986	426.8	1996	826.1	2006	1259.5	2016	2392.4
1967	159.8	1977	259.3	1987	455.9	1997	859.9	2007	1357.9	2017	2456.8
1968	174.3	1978	263.5	1988	492.3	1998	877.9	2008	1462.6	2018	2591.3
1969	177.6	1979	276.6	1989	541.3	1999	951.7	2009	1612.5	2019	2616.4

Indonesia

Year	$MtCO_2$	Year	$MtCO_2$	Year	$MtCO_2$	Year	$MtCO_2$	Year	$MtCO_2$	Year	$MtCO_2$
1960	21.3852	1970	35.7914	1980	94.873	1990	150.2859	2000	265.8034	2010	428.1743
1961	26.0016	1971	38.9553	1981	100.2972	1991	180.6221	2001	297.5303	2011	508.0733
1962	22.9749	1972	43.3063	1982	105.5842	1992	203.5774	2002	307.3615	2012	526.3831
1963	22.7631	1973	49.0981	1983	105.1841	1993	219.7623	2003	316.6547	2013	411.191
1964	22.3743	1974	51.2265	1984	112.4605	1994	222.8542	2004	339.8479	2014	416.8232
1965	24.6682	1975	53.9325	1985	121.5977	1995	226.5452	2005	343.3365	2015	507.012
1966	23.375	1976	61.7883	1986	122.1665	1996	255.0688	2006	346.4433	2016	568.1939
1967	24.54	1977	82.4164	1987	123.8789	1997	280.7363	2007	376.8653	2017	531.012
1968	27.5626	1978	93.9382	1988	132.7217	1998	215.97	2008	417.5618	2018	576.5844
1969	33.3622	1979	95.1371	1989	131.6742	1999	243.9519	2009	447.0988	2019	617.5126

Iran

Year	$MtCO_2$	Year	$MtCO_2$	Year	$MtCO_2$	Year	$MtCO_2$	Year	$MtCO_2$	Year	$MtCO_2$
1960	37.3586	1970	91.7875	1980	120.5645	1990	209.2383	2000	369.2635	2010	564.0345
1961	36.5088	1971	101.6278	1981	112.5286	1991	225.9542	2001	394.9314	2011	579.04
1962	37.4284	1972	106.0152	1982	137.515	1992	226.957	2002	397.7983	2012	600.684
1963	41.3049	1973	129.4753	1983	149.2134	1993	235.5766	2003	413.9935	2013	608.7101
1964	47.5191	1974	143.7754	1984	149.9427	1994	263.5204	2004	442.0897	2014	641.9164
1965	53.7184	1975	139.214	1985	159.9471	1995	271.1475	2005	463.5299	2015	640.8112
1966	64.1034	1976	156.4591	1986	147.536	1996	274.0078	2006	503.7906	2016	648.0607
1967	67.8809	1977	163.7319	1987	158.6074	1997	267.0993	2007	513.3138	2017	724.5785
1968	82.3296	1978	162.1039	1988	175.1078	1998	306.0063	2008	534.9101	2018	755.4022
1969	83.0387	1979	163.6733	1989	190.098	1999	379.627	2009	546.885	2019	779.5265

Iraq

Year	$MtCO_2$	Year	$MtCO_2$	Year	$MtCO_2$	Year	$MtCO_2$	Year	$MtCO_2$	Year	$MtCO_2$
1960	8.2562	1970	23.8838	1980	45.3582	1990	49.0568	2000	71.7154	2010	110.985
1961	8.7092	1971	28.8319	1981	31.9015	1991	45.1853	2001	84.5559	2011	135.274
1962	9.0208	1972	29.5205	1982	30.3744	1992	58.8893	2002	86.3209	2012	152.814
1963	9.3834	1973	30.6127	1983	38.4651	1993	63.1298	2003	90.7866	2013	163.676
1964	9.064	1974	30.9095	1984	39.771	1994	71.0892	2004	113.635	2014	165.150
1965	19.2931	1975	33.1203	1985	44.1964	1995	74.0842	2005	112.980	2015	165.646
1966	27.6761	1976	48.7355	1986	47.2296	1996	69.2844	2006	98.1811	2016	194.361
1967	18.373	1977	43.6295	1987	52.1838	1997	68.0788	2007	61.4918	2017	208.713
1968	19.6957	1978	42.1931	1988	67.1274	1998	72.1015	2008	92.167	2018	211.270
1969	22.6013	1979	52.8231	1989	72.2418	1999	71.6813	2009	103.489	2019	221.383

Ireland

Year	$MtCO_2$	Year	$MtCO_2$	Year	$MtCO_2$	Year	$MtCO_2$	Year	$MtCO_2$	Year	$MtCO_2$
1960	11.1685	1970	19.3937	1980	26.2708	1990	32.9443	2000	45.249	2010	41.7479
1961	12.3526	1971	22.4761	1981	26.0607	1991	33.674	2001	47.6074	2011	38.0522
1962	13.1067	1972	22.0363	1982	25.5656	1992	33.4949	2002	46.082	2012	38.2096
1963	13.4473	1973	22.8462	1983	25.728	1993	33.7162	2003	45.684	2013	37.2353
1964	14.2161	1974	23.293	1984	25.5487	1994	34.8382	2004	46.1669	2014	36.7853
1965	13.7174	1975	22.0474	1985	26.749	1995	35.8527	2005	48.1555	2015	38.5453
1966	15.0949	1976	22.293	1986	28.5495	1996	37.4691	2006	47.6039	2016	40.0298
1967	16.3948	1977	23.5683	1987	30.2254	1997	38.8052	2007	47.6651	2017	38.9102
1968	17.8016	1978	23.5791	1988	29.8825	1998	40.7088	2008	47.3662	2018	38.8034
1969	18.4944	1979	27.402	1989	30.0599	1999	42.4401	2009	42.1795	2019	37.1177

Israel

Year	$MtCO_2$	Year	$MtCO_2$	Year	$MtCO_2$	Year	$MtCO_2$	Year	$MtCO_2$	Year	$MtCO_2$
1960	6.46	1970	16.5594	1980	20.9845	1990	35.8231	2000	59.5194	2010	68.2869
1961	7.0608	1971	16.2189	1981	21.0175	1991	36.1486	2001	63.0224	2011	68.5947
1962	7.9324	1972	16.8909	1982	23.8547	1992	42.083	2002	59.2997	2012	74.7846
1963	8.1996	1973	19.2611	1983	23.7089	1993	44.2342	2003	62.4147	2013	64.9747
1964	9.1373	1974	19.3689	1984	23.4983	1994	47.4745	2004	58.6792	2014	62.2791
1965	12.9288	1975	19.5404	1985	24.6128	1995	49.8652	2005	56.5241	2015	64.9498
1966	13.5814	1976	19.4967	1986	26.3481	1996	51.9358	2006	62.149	2016	63.9072
1967	13.5279	1977	19.7658	1987	27.0687	1997	54.8639	2007	62.7999	2017	62.4673
1968	13.7942	1978	21.0316	1988	29.7024	1998	56.0093	2008	67.9802	2018	62.2126
1969	14.8009	1979	20.8643	1989	31.394	1999	54.7545	2009	63.8609	2019	64.1721

Italy

Year	$MtCO_2$	Year	$MtCO_2$	Year	$MtCO_2$	Year	$MtCO_2$	Year	$MtCO_2$	Year	$MtCO_2$
1960	109.203	1970	296.365	1980	386.433	1990	438.009	2000	468.442	2010	433.688
1961	124.375	1971	311.049	1981	375.301	1991	437.539	2001	468.643	2011	422.040
1962	146.255	1972	328.238	1982	366.880	1992	437.830	2002	476.251	2012	401.555
1963	164.556	1973	353.349	1983	358.410	1993	430.180	2003	494.183	2013	367.569
1964	175.721	1974	358.253	1984	364.602	1994	424.582	2004	499.619	2014	347.861
1965	189.528	1975	341.053	1985	368.983	1995	448.333	2005	500.006	2015	360.088
1966	213.982	1976	365.796	1986	363.188	1996	442.277	2006	495.124	2016	356.556
1967	234.130	1977	354.418	1987	380.099	1997	448.045	2007	487.693	2017	351.474
1968	249.172	1978	371.274	1988	385.963	1998	460.049	2008	476.230	2018	348.085
1969	269.661	1979	385.256	1989	404.743	1999	464.549	2009	422.624	2019	337.086

Jamaica

Year	$MtCO_2$	Year	$MtCO_2$	Year	$MtCO_2$	Year	$MtCO_2$	Year	$MtCO_2$	Year	$MtCO_2$
1960	1.4684	1970	4.9886	1980	8.4454	1990	7.5271	2000	10.314	2010	7.6773
1961	2.1279	1971	5.7472	1981	7.4086	1991	7.7506	2001	10.5764	2011	8.2556
1962	2.117	1972	6.2824	1982	6.2142	1992	7.7108	2002	10.2026	2012	7.9128
1963	2.3955	1973	8.2904	1983	6.4451	1993	8.0003	2003	10.6671	2013	8.4922
1964	4.0622	1974	7.5944	1984	5.1408	1994	8.191	2004	10.5742	2014	7.6791
1965	2.9886	1975	8.1808	1985	5.0419	1995	9.1734	2005	10.4165	2015	7.9366
1966	3.516	1976	7.276	1986	4.5474	1996	9.6876	2006	11.5772	2016	8.1414
1967	3.8642	1977	7.441	1987	5.3793	1997	10.0682	2007	10.7492	2017	7.7975
1968	3.8785	1978	9.112	1988	4.5258	1998	9.694	2008	10.7796	2018	8.0097
1969	4.2669	1979	8.5296	1989	6.7245	1999	9.9582	2009	7.9338	2019	8.0142

Japan

Year	$MtCO_2$	Year	$MtCO_2$	Year	$MtCO_2$	Year	$MtCO_2$	Year	$MtCO_2$	Year	$MtCO_2$
1960	232.4996	1970	767.9631	1980	944.8703	1990	1158.391	2000	1264.844	2010	1214.069
1961	282.7869	1971	796.5444	1981	926.8374	1991	1170.066	2001	1250.211	2011	1264.155
1962	292.8644	1972	852.1705	1982	897.4097	1992	1179.74	2002	1279.453	2012	1305.433
1963	324.8355	1973	914.2657	1983	880.9115	1993	1172.647	2003	1287.642	2013	1314.703
1964	358.8911	1974	914.3068	1984	937.0721	1994	1227.567	2004	1282.872	2014	1263.05
1965	386.4712	1975	868.5114	1985	912.403	1995	1239.928	2005	1290.056	2015	1222.781
1966	419.2451	1976	907.1454	1986	912.2622	1996	1251.868	2006	1266.829	2016	1203.167
1967	489.3074	1977	933.2387	1987	902.5328	1997	1245.112	2007	1302.524	2017	1187.662
1968	561.9126	1978	901.5914	1988	985.4671	1998	1205.416	2008	1231.91	2018	1135.688
1969	653.2154	1979	953.0729	1989	1021.685	1999	1242.015	2009	1162.648	2019	1106.664

Jordan

Year	$MtCO_2$	Year	$MtCO_2$	Year	$MtCO_2$	Year	$MtCO_2$	Year	$MtCO_2$	Year	$MtCO_2$
1960	0.74314	1970	1.5557	1980	4.6958	1990	10.4779	2000	15.2	2010	20.6143
1961	0.9774	1971	1.6544	1981	5.8252	1991	9.903	2001	15.6105	2011	21.2438
1962	1.047	1972	1.9136	1982	6.2557	1992	11.9831	2002	16.4207	2012	23.8131
1963	1.219	1973	2.1996	1983	7.2999	1993	11.7741	2003	16.982	2013	23.8126
1964	1.2408	1974	2.2253	1984	8.2469	1994	13.2495	2004	18.6695	2014	25.8939
1965	1.4204	1975	2.4892	1985	8.4215	1995	13.2077	2005	20.4361	2015	25.27
1966	1.5813	1976	2.9446	1986	9.1651	1996	13.8264	2006	20.5274	2016	23.9943
1967	1.413	1977	3.1539	1987	9.506	1997	14.0736	2007	21.437	2017	25.4672
1968	1.504	1978	3.6273	1988	9.177	1998	14.2519	2008	20.7179	2018	24.9238
1969	1.7568	1979	3.7769	1989	9.0798	1999	14.2654	2009	21.3363	2019	26.0716

Kazakhstan

Year	$MtCO_2$	Year	$MtCO_2$	Year	$MtCO_2$	Year	$MtCO_2$	Year	$MtCO_2$	Year	$MtCO_2$
1960	91.874	1970	149.6398	1980	220.1724	1990	281.214	2000	148.7562	2010	250.897
1961	94.7491	1971	158.7323	1981	215.791	1991	271.741	2001	142.9239	2011	240.6512
1962	99.4464	1972	166.9406	1982	219.7972	1992	246.7414	2002	160.8042	2012	246.7504
1963	106.6505	1973	173.9172	1983	222.7578	1993	219.39	2003	178.7746	2013	254.5474
1964	113.4238	1974	180.4566	1984	224.5884	1994	185.8353	2004	188.4759	2014	278.7756
1965	120.3236	1975	189.5953	1985	242.2487	1995	178.2075	2005	202.3262	2015	288.5781
1966	127.0707	1976	196.7938	1986	242.7351	1996	163.5438	2006	221.6493	2016	288.4214
1967	132.8732	1977	203.3784	1987	241.5543	1997	155.5722	2007	227.9611	2017	307.9265
1968	136.6081	1978	210.2611	1988	247.8811	1998	150.5412	2008	229.0963	2018	319.6474
1969	142.2691	1979	211.9163	1989	242.1091	1999	124.9524	2009	224.1456	2019	313.7978

Kenya

Year	$MtCO_2$	Year	$MtCO_2$	Year	$MtCO_2$	Year	$MtCO_2$	Year	$MtCO_2$	Year	$MtCO_2$
1960	2.4241	1970	3.0782	1980	6.1515	1990	5.6861	2000	10.3016	2010	11.746
1961	2.3986	1971	3.6791	1981	6.4731	1991	4.7104	2001	9.2357	2011	12.9281
1962	2.622	1972	3.8659	1982	4.6338	1992	5.4021	2002	7.8196	2012	11.9868
1963	2.8529	1973	3.9136	1983	4.5947	1993	6.2152	2003	6.5856	2013	12.7704
1964	2.8233	1974	4.943	1984	4.2531	1994	6.4204	2004	7.438	2014	13.7732
1965	2.4639	1975	4.9684	1985	3.716	1995	7.4055	2005	8.3386	2015	16.3006
1966	2.6801	1976	4.5962	1986	4.073	1996	9.155	2006	9.3366	2016	17.1518
1967	2.6984	1977	5.0352	1987	5.0759	1997	8.1198	2007	9.5404	2017	16.5325
1968	2.8154	1978	5.2968	1988	4.69	1998	9.896	2008	9.9117	2018	17.1367
1969	3.1265	1979	5.0119	1989	5.0885	1999	10.0293	2009	11.9677	2019	17.3153

Kiribati

Year	$MtCO_2$	Year	$MtCO_2$	Year	$MtCO_2$	Year	$MtCO_2$	Year	$MtCO_2$	Year	$MtCO_2$
1960		1970	0.02198	1980	0.02931	1990	0.02198	2000	0.03298	2010	0.05862
1961	0.00733	1971	0.02931	1981	0.02931	1991	0.02198	2001	0.02931	2011	0.05496
1962	0.01099	1972	0.02565	1982	0.02565	1992	0.02565	2002	0.04030	2012	0.05130
1963	0.01832	1973	0.03664	1983	0.02198	1993	0.02931	2003	0.04397	2013	0.05130
1964	0.01832	1974	0.03298	1984	0.02198	1994	0.02931	2004	0.04763	2014	0.05862
1965	0.01099	1975	0.03298	1985	0.02198	1995	0.02931	2005	0.05862	2015	0.06229
1966	0.01099	1976	0.03298	1986	0.01832	1996	0.02931	2006	0.06595	2016	0.06595
1967	0.02198	1977	0.02198	1987	0.02198	1997	0.02931	2007	0.05862	2017	0.06595
1968	0.03298	1978	0.02198	1988	0.02198	1998	0.02931	2008	0.06595	2018	0.06888
1969	0.01099	1979	0.02565	1989	0.02198	1999	0.02931	2009	0.05496	2019	0.07338

Kosovo

Year	$MtCO_2$	Year	$MtCO_2$	Year	$MtCO_2$	Year	$MtCO_2$	Year	$MtCO_2$	Year	$MtCO_2$
1960		1970		1980		1990		2000		2010	8.3722
1961		1971		1981		1991		2001		2011	8.31
1962		1972		1982		1992		2002		2012	7.8739
1963		1973		1983		1993		2003		2013	8.0058
1964		1974		1984		1994		2004		2014	7.1265
1965		1975		1985		1995		2005		2015	8.3393
1966		1976		1986		1996		2006		2016	8.8596
1967		1977		1987		1997		2007		2017	8.0938
1968		1978		1988		1998		2008	7.3866	2018	8.1919
1969		1979		1989		1999		2009	8.1304	2019	9.7414

Kuwait

Year	$MtCO_2$	Year	$MtCO_2$	Year	$MtCO_2$	Year	$MtCO_2$	Year	$MtCO_2$	Year	$MtCO_2$
1960	7.797	1970	25.0215	1980	24.6162	1990	37.8058	2000	53.3841	2010	89.2722
1961	9.9734	1971	27.1173	1981	25.1396	1991	14.9154	2001	57.4847	2011	86.2626
1962	14.2786	1972	27.6119	1982	21.0903	1992	29.6469	2002	57.9799	2012	100.073
1963	17.012	1973	24.2227	1983	21.5412	1993	49.1294	2003	59.6229	2013	93.5828
1964	25.3146	1974	19.312	1984	28.2852	1994	55.2258	2004	63.1079	2014	91.0333
1965	35.3906	1975	16.8129	1985	29.0702	1995	54.589	2005	71.1664	2015	96.2649
1966	35.1231	1976	18.4562	1986	35.2303	1996	49.9136	2006	73.3891	2016	101.5743
1967	25.4208	1977	17.2014	1987	31.3779	1997	54.6706	2007	74.8748	2017	104.784
1968	22.4237	1978	20.9716	1988	32.8251	1998	51.5606	2008	82.2983	2018	104.2176
1969	26.8095	1979	17.6277	1989	35.7716	1999	53.8222	2009	86.9549	2019	107.532

Kyrgyzstan

Year	$MtCO_2$	Year	$MtCO_2$	Year	$MtCO_2$	Year	$MtCO_2$	Year	$MtCO_2$	Year	$MtCO_2$
1960	8.4661	1970	13.7919	1980	20.397	1990	21.1073	2000	4.6025	2010	6.3129
1961	8.7314	1971	14.6383	1981	20.01	1991	18.4945	2001	3.8623	2011	7.5535
1962	9.1647	1972	15.4042	1982	20.3858	1992	11.0821	2002	4.9193	2012	9.9998
1963	9.8287	1973	16.0581	1983	20.6757	1993	8.5016	2003	5.3816	2013	9.6585
1964	10.453	1974	16.6732	1984	20.8592	1994	6.1458	2004	5.8068	2014	10.0946
1965	11.0892	1975	17.5295	1985	22.4932	1995	4.511	2005	5.5136	2015	10.2775
1966	11.7114	1976	18.2032	1986	22.5518	1996	5.6642	2006	5.419	2016	9.6403
1967	12.2464	1977	18.8215	1987	22.4591	1997	5.573	2007	6.5183	2017	9.2629
1968	12.5908	1978	19.4664	1988	23.0581	1998	5.9131	2008	7.5483	2018	10.1689
1969	13.1125	1979	19.626	1989	22.5428	1999	4.6468	2009	6.7374	2019	11.4826

Laos

Year	$MtCO_2$	Year	$MtCO_2$	Year	$MtCO_2$	Year	$MtCO_2$	Year	$MtCO_2$	Year	$MtCO_2$
1960	0.08061	1970	0.57158	1980	0.18686	1990	0.51296	2000	0.95818	2010	3.00030
1961	0.11358	1971	0.42136	1981	0.15022	1991	0.54594	2001	1.06060	2011	3.16700
1962	0.13190	1972	0.48731	1982	0.15755	1992	0.59289	2002	1.16320	2012	3.39790
1963	0.14656	1973	0.51662	1983	0.17954	1993	0.60755	2003	1.21700	2013	4.00660
1964	0.17221	1974	0.29312	1984	0.18320	1994	0.63319	2004	1.27880	2014	4.32930
1965	0.17954	1975	0.25282	1985	0.20518	1995	0.66983	2005	1.33700	2015	8.80580
1966	0.23450	1976	0.22350	1986	0.20885	1996	0.75090	2006	1.75250	2016	14.26140
1967	0.31877	1977	0.23083	1987	0.21251	1997	0.79115	2007	1.83090	2017	17.91440
1968	0.16854	1978	0.23083	1988	0.21251	1998	0.82042	2008	2.12650	2018	32.26250
1969	0.31877	1979	0.22350	1989	0.23083	1999	0.84605	2009	2.66430	2019	32.81480

Latvia

Year	$MtCO_2$	Year	$MtCO_2$	Year	$MtCO_2$	Year	$MtCO_2$	Year	$MtCO_2$	Year	$MtCO_2$
1960	6.7342	1970	10.9672	1980	16.2685	1990	19.5041	2000	7.0647	2010	8.5489
1961	6.9447	1971	11.6437	1981	15.9656	1991	17.7831	2001	7.4744	2011	7.8054
1962	7.2888	1972	12.2564	1982	16.2695	1992	14.0798	2002	7.5026	2012	7.5152
1963	7.8169	1973	12.7799	1983	16.5076	1993	11.8186	2003	7.7226	2013	7.382
1964	8.3133	1974	13.2727	1984	16.6607	1994	10.2968	2004	7.7278	2014	7.1826
1965	8.8188	1975	13.9581	1985	17.9696	1995	9.0903	2005	7.8067	2015	7.2727
1966	9.3131	1976	14.5001	1986	18.025	1996	9.1703	2006	8.3057	2016	7.2208
1967	9.7383	1977	14.9981	1987	17.9616	1997	8.646	2007	8.632	2017	7.2228
1968	10.012	1978	15.5166	1988	18.4471	1998	8.2807	2008	8.1928	2018	7.8593
1969	10.4269	1979	15.6484	1989	18.0438	1999	7.696	2009	7.4519	2019	8.2623

Lebanon

Year	$MtCO_2$	Year	$MtCO_2$	Year	$MtCO_2$	Year	$MtCO_2$	Year	$MtCO_2$	Year	$MtCO_2$
1960	2.576	1970	3.9407	1980	5.8898	1990	7.8679	2000	15.4663	2010	19.9972
1961	2.6785	1971	5.3006	1981	5.8443	1991	8.1149	2001	16.4063	2011	20.2641
1962	2.8508	1972	5.6534	1982	5.7195	1992	9.727	2002	16.2445	2012	22.3316
1963	3.0228	1973	7.0667	1983	6.9422	1993	10.355	2003	18.5276	2013	22.1634
1964	3.2611	1974	7.0879	1984	6.7132	1994	11.1108	2004	17.2081	2014	23.7808
1965	3.312	1975	6.2651	1985	7.765	1995	12.2546	2005	16.6541	2015	25.7698
1966	3.6229	1976	5.924	1986	7.4785	1996	12.7527	2006	14.7924	2016	26.5024
1967	3.5646	1977	5.3855	1987	7.6704	1997	15.0994	2007	13.7499	2017	27.9353
1968	3.6933	1978	5.4959	1988	7.3457	1998	16.2862	2008	17.4191	2018	27.5654
1969	4.3441	1979	5.7852	1989	7.7208	1999	16.4289	2009	20.9579	2019	28.2021

Lesotho

Year	$MtCO_2$	Year	$MtCO_2$	Year	$MtCO_2$	Year	$MtCO_2$	Year	$MtCO_2$	Year	$MtCO_2$
1960		1970		1980		1990	1.4729	2000	1.8503	2010	2.2753
1961		1971		1981		1991	1.5279	2001	1.876	2011	2.3266
1962		1972		1982		1992	1.5865	2002	1.9053	2012	2.3963
1963		1973		1983		1993	1.6341	2003	1.9309	2013	2.4219
1964		1974		1984		1994	1.6744	2004	1.9822	2014	2.4292
1965		1975		1985		1995	1.7074	2005	2.0115	2015	2.3266
1966		1976		1986		1996	1.7367	2006	2.0372	2016	2.3596
1967		1977		1987		1997	1.7697	2007	2.0738	2017	2.5282
1968		1978		1988		1998	1.8027	2008	2.1251	2018	2.4256
1969		1979		1989		1999	1.8247	2009	2.2167	2019	2.2232

Liberia

Year	$MtCO_2$	Year	$MtCO_2$	Year	$MtCO_2$	Year	$MtCO_2$	Year	$MtCO_2$	Year	$MtCO_2$
1960	0.16488	1970	1.4506	1980	2.0376	1990	0.46814	2000	0.42177	2010	0.76115
1961	0.16122	1971	1.5239	1981	1.9349	1991	0.37006	2001	0.44801	2011	0.85167
1962	0.25282	1972	1.5055	1982	0.59741	1992	0.38773	2002	0.43468	2012	0.96379
1963	0.35541	1973	1.4799	1983	0.70652	1993	0.42436	2003	0.46681	2013	0.87683
1964	0.48365	1974	1.7217	1984	0.69543	1994	0.42136	2004	0.54511	2014	1.1912
1965	0.55693	1975	1.4836	1985	0.71608	1995	0.42436	2005	0.65551	2015	1.205
1966	0.61189	1976	1.4756	1986	0.72288	1996	0.43467	2006	0.6725	2016	1.3581
1967	0.61189	1977	1.4714	1987	0.75846	1997	0.45366	2007	0.6277	2017	1.2152
1968	0.88282	1978	1.5032	1988	0.80918	1998	0.48297	2008	0.53507	2018	1.2745
1969	1.2711	1979	1.9419	1989	0.65959	1999	0.39067	2009	0.47532	2019	1.3217

Libya

Year	$MtCO_2$	Year	$MtCO_2$	Year	$MtCO_2$	Year	$MtCO_2$	Year	$MtCO_2$	Year	$MtCO_2$
1960	0.6925	1970	32.3051	1980	26.7806	1990	36.513	2000	46.793	2010	61.1217
1961	1.1945	1971	21.6283	1981	28.668	1991	42.6192	2001	47.7738	2011	39.2646
1962	1.0479	1972	15.22	1982	30.5651	1992	37.025	2002	47.4722	2012	52.4087
1963	1.4619	1973	14.5751	1983	30.146	1993	38.709	2003	48.781	2013	55.3391
1964	0.66318	1974	9.3376	1984	28.2762	1994	43.753	2004	49.9558	2014	58.3613
1965	1.0149	1975	11.5684	1985	31.0022	1995	45.6911	2005	51.6963	2015	50.8444
1966	2.6271	1976	17.8879	1986	33.8955	1996	43.7968	2006	52.6663	2016	42.8392
1967	18.4922	1977	20.0517	1987	32.3483	1997	44.7065	2007	49.3397	2017	43.7294
1968	30.1144	1978	21.1554	1988	36.1604	1998	45.1589	2008	55.3415	2018	45.206
1969	35.5222	1979	25.9264	1989	37.0685	1999	44.3033	2009	57.1956	2019	46.4278

Liechtenstein

Year	$MtCO_2$	Year	$MtCO_2$	Year	$MtCO_2$	Year	$MtCO_2$	Year	$MtCO_2$	Year	$MtCO_2$
1960		1970		1980		1990	0.19897	2000	0.21685	2010	0.19081
1961		1971		1981		1991	0.20633	2001	0.21466	2011	0.17678
1962		1972		1982		1992	0.20695	2002	0.22001	2012	0.18531
1963		1973		1983		1993	0.21503	2003	0.22935	2013	0.19254
1964		1974		1984		1994	0.20111	2004	0.22938	2014	0.16124
1965		1975		1985		1995	0.2042	2005	0.22897	2015	0.15971
1966		1976		1986		1996	0.20596	2006	0.2311	2016	0.14988
1967		1977		1987		1997	0.21837	2007	0.20077	2017	0.15628
1968		1978		1988		1998	0.22923	2008	0.21951	2018	0.14375
1969		1979		1989		1999	0.22656	2009	0.20535	2019	0.1458

Lithuania

Year	$MtCO_2$	Year	$MtCO_2$	Year	$MtCO_2$	Year	$MtCO_2$	Year	$MtCO_2$	Year	$MtCO_2$
1960	12.5815	1970	20.4915	1980	30.6223	1990	35.7718	2000	11.8739	2010	13.9267
1961	12.976	1971	21.7744	1981	30.0765	1991	37.8516	2001	12.6214	2011	14.2711
1962	13.6197	1972	22.9396	1982	30.6587	1992	21.2006	2002	12.69	2012	14.3308
1963	14.6055	1973	23.9401	1983	31.1376	1993	16.348	2003	12.6799	2013	13.3403
1964	15.5326	1974	24.8847	1984	31.455	1994	15.7883	2004	13.2723	2014	13.0875
1965	16.4783	1975	26.1931	1985	33.9365	1995	15.0845	2005	14.0911	2015	13.2971
1966	17.4031	1976	27.2308	1986	34.0844	1996	15.7576	2006	14.408	2016	13.3275
1967	18.1972	1977	28.1871	1987	34.0198	1997	15.1822	2007	15.7978	2017	13.5458
1968	18.7079	1978	29.1725	1988	34.9605	1998	16.0397	2008	15.1792	2018	13.6695
1969	19.482	1979	29.4354	1989	34.2341	1999	13.477	2009	13.0228	2019	13.4834

Luxembourg

Year	$MtCO_2$	Year	$MtCO_2$	Year	$MtCO_2$	Year	$MtCO_2$	Year	$MtCO_2$	Year	$MtCO_2$
1960	11.5078	1970	13.7354	1980	11.0821	1990	11.8476	2000	8.7316	2010	11.2193
1961	11.581	1971	13.1947	1981	9.496	1991	12.4658	2001	9.2264	2011	11.1146
1962	11.5407	1972	13.4948	1982	8.9351	1992	12.2322	2002	10.003	2012	10.8514
1963	11.4382	1973	14.1782	1983	8.3762	1993	12.3728	2003	10.476	2013	10.3039
1964	12.2956	1974	14.4279	1984	9.0167	1994	11.5639	2004	11.8443	2014	9.8252
1965	12.1929	1975	11.8685	1985	9.2485	1995	9.1703	2005	12.1054	2015	9.3332
1966	11.6104	1976	11.8666	1986	9.1276	1996	9.2199	2006	11.9363	2016	9.0803
1967	11.3503	1977	10.9594	1987	8.8351	1997	8.5731	2007	11.3336	2017	9.2504
1968	12.259	1978	11.8874	1988	9.1267	1998	7.6951	2008	11.1952	2018	9.5685
1969	13.1822	1979	12.1698	1989	9.8758	1999	8.148	2009	10.6478	2019	9.7849

Macao

Year	$MtCO_2$	Year	$MtCO_2$	Year	$MtCO_2$	Year	$MtCO_2$	Year	$MtCO_2$	Year	$MtCO_2$
1960	0.051296	1970	0.20518	1980	0.52762	1990	1.0332	2000	1.6305	2010	1.2348
1961	0.069616	1971	0.22717	1981	0.53494	1991	1.0919	2001	1.6854	2011	1.4557
1962	0.095264	1972	0.23083	1982	0.48365	1992	1.0809	2002	1.5169	2012	1.2912
1963	0.10626	1973	0.2235	1983	0.6815	1993	1.1798	2003	1.5316	2013	1.204
1964	0.12824	1974	0.26747	1984	0.60456	1994	1.2714	2004	1.7148	2014	1.5069
1965	0.1319	1975	0.29678	1985	0.7328	1995	1.2311	2005	1.8283	2015	2.0291
1966	0.15022	1976	0.25282	1986	0.8757	1996	1.407	2006	1.6195	2016	1.9998
1967	0.16488	1977	0.30778	1987	0.97096	1997	1.4876	2007	1.363	2017	2.15
1968	0.16854	1978	0.41403	1988	0.96363	1998	1.5572	2008	1.1322	2018	2.2165
1969	0.16854	1979	0.41403	1989	1.0296	1999	1.5169	2009	1.8906	2019	2.0647

Madagascar

Year	$MtCO_2$	Year	$MtCO_2$	Year	$MtCO_2$	Year	$MtCO_2$	Year	$MtCO_2$	Year	$MtCO_2$
1960	0.39938	1970	0.97066	1980	1.6139	1990	0.92916	2000	1.8675	2010	1.9383
1961	0.35541	1971	1.0256	1981	1.0245	1991	1.0097	2001	1.7355	2011	2.3769
1962	0.39565	1972	1.2858	1982	1.0133	1992	0.98038	2002	1.2319	2012	2.7399
1963	0.46149	1973	1.0733	1983	0.65039	1993	1.006	2003	1.6805	2013	3.1445
1964	0.48347	1974	1.1869	1984	0.86637	1994	1.2461	2004	1.7894	2014	3.1022
1965	0.55678	1975	1.6925	1985	1.053	1995	1.2864	2005	1.7254	2015	3.5199
1966	0.5787	1976	0.99223	1986	1.1371	1996	1.3406	2006	1.6662	2016	3.3586
1967	0.84248	1977	0.8456	1987	1.2824	1997	1.6234	2007	1.7834	2017	3.8863
1968	0.91207	1978	1.0172	1988	1.2858	1998	1.7107	2008	1.8686	2018	4.1878
1969	0.84975	1979	1.1302	1989	0.9258	1999	1.8169	2009	1.7539	2019	4.0148

Malawi

Year	$MtCO_2$	Year	$MtCO_2$	Year	$MtCO_2$	Year	$MtCO_2$	Year	$MtCO_2$	Year	$MtCO_2$
1960	0.43835	1970	0.45407	1980	0.708	1990	0.73902	2000	0.86484	2010	1.0264
1961	0.37332	1971	0.5017	1981	0.60154	1991	0.78472	2001	0.79213	2011	1.1399
1962	0.36061	1972	0.54564	1982	0.59135	1992	0.78527	2002	0.84665	2012	1.1334
1963	0.34671	1973	0.57123	1983	0.57167	1993	0.87914	2003	0.90368	2013	1.1623
1964	0.32964	1974	0.54924	1984	0.55294	1994	0.9047	2004	0.91151	2014	1.0214
1965	0.34796	1975	0.5785	1985	0.55343	1995	0.90696	2005	0.90607	2015	1.1195
1966	0.42851	1976	0.58173	1986	0.54845	1996	0.90426	2006	0.91779	2016	1.263
1967	0.36622	1977	0.63608	1987	0.54071	1997	0.94737	2007	0.96885	2017	1.4021
1968	0.38815	1978	0.66836	1988	0.5372	1998	0.92206	2008	1.0871	2018	1.4703
1969	0.38076	1979	0.63484	1989	0.55821	1999	0.92081	2009	1.0945	2019	1.4663

Malaysia

Year	$MtCO_2$	Year	$MtCO_2$	Year	$MtCO_2$	Year	$MtCO_2$	Year	$MtCO_2$	Year	$MtCO_2$
1960	4.2015	1970	14.5859	1980	28.0324	1990	55.2772	2000	126.5143	2010	216.5373
1961	4.6849	1971	16.6626	1981	30.8774	1991	66.7304	2001	134.9481	2011	217.4275
1962	4.7765	1972	17.9006	1982	30.6416	1992	72.961	2002	136.3381	2012	215.8124
1963	5.828	1973	17.5051	1983	38.048	1993	86.7186	2003	157.2664	2013	234.4188
1964	7.3994	1974	19.0446	1984	34.7941	1994	90.2243	2004	171.6946	2014	241.1278
1965	8.3802	1975	19.4451	1985	36.3294	1995	113.9337	2005	181.7549	2015	233.2682
1966	9.8344	1976	23.8976	1986	40.1014	1996	112.8995	2006	178.9297	2016	246.7224
1967	10.1276	1977	22.6207	1987	40.8772	1997	120.817	2007	182.832	2017	248.8695
1968	10.5302	1978	23.2603	1988	42.8687	1998	114.2375	2008	202.4981	2018	249.1445
1969	9.1378	1979	27.3058	1989	50.0832	1999	108.2914	2009	196.9484	2019	250.0947

Maldives

Year	$MtCO_2$	Year	$MtCO_2$	Year	$MtCO_2$	Year	$MtCO_2$	Year	$MtCO_2$	Year	$MtCO_2$
1960		1970		1980	0.043968	1990	0.17221	2000	0.45067	2010	0.93432
1961		1971	0.003664	1981	0.047632	1991	0.15389	2001	0.46166	2011	0.98562
1962		1972	0.003664	1982	0.047632	1992	0.23083	2002	0.59357	2012	1.1102
1963		1973	0.003664	1983	0.051296	1993	0.19786	2003	0.50563	2013	1.0919
1964		1974	0.003664	1984	0.058624	1994	0.19786	2004	0.66685	2014	1.3154
1965		1975	0.007328	1985	0.065952	1995	0.24915	2005	0.6009	2015	1.3007
1966		1976	0.010992	1986	0.080608	1996	0.28946	2006	0.75845	2016	1.4436
1967		1977	0.014656	1987	0.080608	1997	0.32976	2007	0.78043	2017	1.4986
1968		1978	0.021984	1988	0.095264	1998	0.30045	2008	0.84272	2018	1.5651
1969		1979	0.029312	1989	0.12458	1999	0.42136	2009	0.88302	2019	1.6674

Mali

Year	$MtCO_2$	Year	$MtCO_2$	Year	$MtCO_2$	Year	$MtCO_2$	Year	$MtCO_2$	Year	$MtCO_2$
1960	0.12091	1970	0.20152	1980	0.39134	1990	0.42309	2000	0.83173	2010	1.9749
1961	0.11725	1971	0.22717	1981	0.39488	1991	0.43407	2001	0.83906	2011	2.1581
1962	0.13923	1972	0.24549	1982	0.36513	1992	0.44871	2002	0.85738	2012	2.2973
1963	0.17587	1973	0.26729	1983	0.41662	1993	0.45969	2003	0.85738	2013	2.6486
1964	0.17587	1974	0.30393	1984	0.43482	1994	0.46766	2004	0.89035	2014	2.9055
1965	0.19786	1975	0.34054	1985	0.40538	1995	0.47132	2005	0.916	2015	3.0956
1966	0.19053	1976	0.34026	1986	0.37961	1996	0.49329	2006	1.0809	2016	3.1066
1967	0.2235	1977	0.41347	1987	0.3575	1997	0.52857	2007	1.2971	2017	3.1213
1968	0.19786	1978	0.39495	1988	0.38303	1998	0.76944	2008	1.5572	2018	3.2733
1969	0.16122	1979	0.42791	1989	0.41588	1999	0.80242	2009	1.7844	2019	3.3944

Malta

Year	$MtCO_2$	Year	$MtCO_2$	Year	$MtCO_2$	Year	$MtCO_2$	Year	$MtCO_2$	Year	$MtCO_2$
1960	0.34075	1970	0.66318	1980	1.0223	1990	2.4085	2000	2.5455	2010	2.5818
1961	0.29312	1971	0.65952	1981	1.1432	1991	2.2554	2001	2.6652	2011	2.5781
1962	0.32976	1972	0.83906	1982	1.3117	1992	2.3149	2002	2.7075	2012	2.7621
1963	0.41037	1973	0.80608	1983	0.99661	1993	2.8911	2003	2.9793	2013	2.4378
1964	0.4983	1974	0.74379	1984	1.363	1994	2.6697	2004	2.8464	2014	2.4424
1965	0.47266	1975	0.66685	1985	1.1981	1995	2.4603	2005	2.6543	2015	1.7353
1966	0.41403	1976	0.76211	1986	1.4839	1996	2.5784	2006	2.6659	2016	1.3995
1967	0.52029	1977	0.80242	1987	1.854	1997	2.5862	2007	2.7357	2017	1.553
1968	0.63754	1978	0.93432	1988	2.0115	1998	2.5451	2008	2.7471	2018	1.5316
1969	0.65219	1979	0.90501	1989	2.1691	1999	2.6276	2009	2.5326	2019	1.5538

Marshall Islands

Year	$MtCO_2$	Year	$MtCO_2$	Year	$MtCO_2$	Year	$MtCO_2$	Year	$MtCO_2$	Year	$MtCO_2$
1960		1970		1980		1990		2000	0.098928	2010	0.13557
1961		1971		1981		1991		2001	0.10259	2011	0.13923
1962		1972		1982		1992	0.076944	2002	0.10992	2012	0.13557
1963		1973		1983		1993	0.084272	2003	0.10626	2013	0.13923
1964		1974		1984		1994	0.084272	2004	0.11725	2014	0.1429
1965		1975		1985		1995	0.087936	2005	0.11358	2015	0.1429
1966		1976		1986		1996	0.087936	2006	0.12091	2016	0.1429
1967		1977		1987		1997	0.087936	2007	0.12458	2017	0.14656
1968		1978		1988		1998	0.0916	2008	0.12824	2018	0.15307
1969		1979		1989		1999	0.087936	2009	0.1319	2019	0.16307

Mauritania

Year	$MtCO_2$	Year	$MtCO_2$	Year	$MtCO_2$	Year	$MtCO_2$	Year	$MtCO_2$	Year	$MtCO_2$
1960	0.03664	1970	0.42869	1980	0.63021	1990	0.85371	2000	1.1139	2010	1.9602
1961	0.04763	1971	0.39938	1981	0.63371	1991	0.86837	2001	1.1725	2011	2.1105
1962	0.06228	1972	0.44701	1982	0.88302	1992	0.90501	2002	1.2494	2012	2.3303
1963	0.08793	1973	0.46899	1983	0.93798	1993	0.92699	2003	1.2897	2013	2.0445
1964	0.11725	1974	0.48365	1984	0.87203	1994	0.9563	2004	1.385	2014	2.4988
1965	0.16122	1975	0.5093	1985	0.65586	1995	1.0149	2005	1.4363	2015	2.8872
1966	0.17954	1976	0.51662	1986	0.37373	1996	1.0626	2006	1.4216	2016	2.7627
1967	0.19786	1977	0.55693	1987	3.2426	1997	1.0772	2007	1.6378	2017	3.7373
1968	0.2345	1978	0.58258	1988	3.184	1998	1.0699	2008	1.7734	2018	3.9348
1969	0.2748	1979	0.60456	1989	2.803	1999	1.0955	2009	1.9602	2019	4.0922

Mauritius

Year	$MtCO_2$	Year	$MtCO_2$	Year	$MtCO_2$	Year	$MtCO_2$	Year	$MtCO_2$	Year	$MtCO_2$
1960	0.17954	1970	0.4983	1980	0.5899	1990	1.4619	2000	2.6894	2010	3.9132
1961	0.18686	1971	0.39571	1981	0.54227	1991	1.5206	2001	2.8616	2011	3.9168
1962	0.25282	1972	0.68883	1982	0.50197	1992	1.7074	2002	2.8836	2012	3.9644
1963	0.20885	1973	0.67784	1983	0.59723	1993	1.7734	2003	3.0594	2013	4.067
1964	0.30778	1974	0.6925	1984	0.62654	1994	1.6232	2004	3.0888	2014	4.2063
1965	0.30411	1975	0.5899	1985	0.70715	1995	1.8283	2005	3.2939	2015	4.2099
1966	0.2748	1976	0.61922	1986	0.79875	1996	1.9492	2006	3.6274	2016	4.3455
1967	0.4983	1977	0.6412	1987	0.93066	1997	1.9969	2007	3.686	2017	4.536
1968	0.63754	1978	0.63021	1988	0.85371	1998	2.1691	2008	3.7666	2018	4.9016
1969	0.57158	1979	0.65952	1989	1.0516	1999	2.4256	2009	3.708	2019	4.6868

Mexico

Year	$MtCO_2$	Year	$MtCO_2$	Year	$MtCO_2$	Year	$MtCO_2$	Year	$MtCO_2$	Year	$MtCO_2$
1960	63.0523	1970	113.9507	1980	267.8175	1990	317.0424	2000	396.0664	2010	463.7825
1961	65.2399	1971	126.1901	1981	283.7971	1991	330.1332	2001	410.6979	2011	484.1648
1962	63.7437	1972	132.2791	1982	304.0101	1992	332.7801	2002	411.9677	2012	496.2996
1963	66.2922	1973	144.0717	1983	277.6665	1993	338.0672	2003	437.7575	2013	490.1297
1964	74.2001	1974	154.7465	1984	276.7657	1994	351.5282	2004	438.8567	2014	481.1288
1965	75.1679	1975	164.1654	1985	287.5112	1995	331.5966	2005	463.9932	2015	481.9746
1966	80.8446	1976	183.7738	1986	293.5555	1996	345.7661	2006	476.5652	2016	484.6289
1967	90.0055	1977	192.4362	1987	306.1944	1997	368.6448	2007	479.7868	2017	461.238
1968	93.8872	1978	222.1673	1988	305.8494	1998	388.3569	2008	492.9797	2018	451.0808
1969	102.1762	1979	240.3207	1989	360.5553	1999	390.5165	2009	475.9031	2019	438.4976

Micronesia (Federated States of)

Year	$MtCO_2$	Year	$MtCO_2$	Year	$MtCO_2$	Year	$MtCO_2$	Year	$MtCO_2$	Year	$MtCO_2$
1960		1970		1980		1990		2000	0.12824	2010	0.10259
1961		1971		1981		1991		2001	0.1429	2011	0.11725
1962		1972		1982		1992	0.10259	2002	0.13557	2012	0.12458
1963		1973		1983		1993	0.10259	2003	0.14656	2013	0.13557
1964		1974		1984		1994	0.10626	2004	0.1429	2014	0.13557
1965		1975		1985		1995	0.11358	2005	0.12091	2015	0.1429
1966		1976		1986		1996	0.11358	2006	0.12091	2016	0.1429
1967		1977		1987		1997	0.12091	2007	0.1319	2017	0.1429
1968		1978		1988		1998	0.12091	2008	0.10992	2018	0.14924
1969		1979		1989		1999	0.12458	2009	0.14656	2019	0.159

Moldova

Year	$MtCO_2$	Year	$MtCO_2$	Year	$MtCO_2$	Year	$MtCO_2$	Year	$MtCO_2$	Year	$MtCO_2$
1960	10.942	1970	17.8212	1980	26.3434	1990	27.779	2000	3.573	2010	4.8309
1961	11.2844	1971	18.9128	1981	25.8425	1991	22.3727	2001	3.7866	2011	4.945
1962	11.8438	1972	19.9	1982	26.3294	1992	20.9781	2002	4.0517	2012	4.7657
1963	12.7017	1973	20.742	1983	26.7033	1993	15.8458	2003	4.4043	2013	4.8994
1964	13.5084	1974	21.5335	1984	26.9403	1994	12.427	2004	4.6134	2014	4.7478
1965	14.33	1975	22.6364	1985	29.053	1995	11.4054	2005	4.9375	2015	4.7851
1966	15.1335	1976	23.507	1986	29.1281	1996	11.6871	2006	5.0297	2016	4.8963
1967	15.8245	1977	24.3057	1987	29.0074	1997	7.3013	2007	4.9786	2017	5.2916
1968	16.2692	1978	25.1397	1988	29.7816	1998	6.4438	2008	5.1904	2018	5.8778
1969	16.9434	1979	25.3468	1989	29.1156	1999	4.6845	2009	4.5395	2019	5.9578

Mongolia

Year	$MtCO_2$	Year	$MtCO_2$	Year	$MtCO_2$	Year	$MtCO_2$	Year	$MtCO_2$	Year	$MtCO_2$
1960	1.2934	1970	2.8465	1980	6.8552	1990	9.89	2000	7.4868	2010	13.82
1961	1.3923	1971	3.0324	1981	6.6147	1991	12.121	2001	7.8699	2011	21.4265
1962	1.9712	1972	3.2759	1982	6.7123	1992	10.9939	2002	8.2625	2012	35.0309
1963	1.6012	1973	3.4721	1983	6.9691	1993	9.2626	2003	8.0079	2013	43.5588
1964	2.0445	1974	3.7408	1984	6.4247	1994	7.9271	2004	8.5707	2014	29.586
1965	1.9566	1975	4.0546	1985	8.9979	1995	7.8994	2005	8.5737	2015	23.2436
1966	1.9529	1976	4.39	1986	9.5951	1996	8.0233	2006	9.4058	2016	25.3239
1967	2.1251	1977	4.9607	1987	10.4825	1997	7.6884	2007	12.0787	2017	34.1542
1968	2.4802	1978	5.7638	1988	11.4928	1998	7.6875	2008	12.0167	2018	64.5083
1969	2.6818	1979	6.2773	1989	10.459	1999	7.5352	2009	13.074	2019	65.5137

Montenegro

Year	$MtCO_2$	Year	$MtCO_2$	Year	$MtCO_2$	Year	$MtCO_2$	Year	$MtCO_2$	Year	$MtCO_2$
1960	0.51928	1970	1.0506	1980	1.5939	1990	1.9155	2000	1.5208	2010	2.4219
1961	0.5443	1971	1.1323	1981	1.7346	1991	1.3551	2001	1.6673	2011	2.4072
1962	0.55855	1972	1.0612	1982	1.5936	1992	1.4833	2002	1.7662	2012	2.2131
1963	0.62136	1973	1.2677	1983	1.716	1993	1.2936	2003	1.8892	2013	2.1508
1964	0.70397	1974	1.2733	1984	1.8097	1994	1.2567	2004	2.0413	2014	2.1068
1965	0.72431	1975	1.3286	1985	1.846	1995	1.3273	2005	1.7508	2015	2.2387
1966	0.71773	1976	1.3713	1986	1.9279	1996	1.553	2006	2.0628	2016	2.0152
1967	0.72497	1977	1.3335	1987	1.8823	1997	1.6698	2007	2.0555	2017	2.1031
1968	0.77538	1978	1.4902	1988	1.9422	1998	1.7576	2008	2.6051	2018	2.1231
1969	0.80394	1979	1.6209	1989	1.9363	1999	1.2119	2009	1.6818	2019	2.4614

Montserrat

Year	$MtCO_2$	Year	$MtCO_2$	Year	$MtCO_2$	Year	$MtCO_2$	Year	$MtCO_2$	Year	$MtCO_2$
1960		1970	0.014656	1980	0.014656	1990	0.029312	2000	0.025648	2010	0.065952
1961		1971	0.014656	1981	0.01832	1991	0.029312	2001	0.025648	2011	0.040304
1962	0.003664	1972	0.014656	1982	0.01832	1992	0.029312	2002	0.03664	2012	0.043968
1963	0.003664	1973	0.014656	1983	0.021984	1993	0.029312	2003	0.03664	2013	0.051296
1964	0.007328	1974	0.014656	1984	0.021984	1994	0.032976	2004	0.03664	2014	0.047632
1965	0.003664	1975	0.010992	1985	0.025648	1995	0.032976	2005	0.03664	2015	0.058624
1966	0.007328	1976	0.010992	1986	0.029312	1996	0.03664	2006	0.03664	2016	0.029312
1967	0.007328	1977	0.025648	1987	0.029312	1997	0.032976	2007	0.040304	2017	0.029312
1968	0.007328	1978	0.025648	1988	0.029312	1998	0.029312	2008	0.047632	2018	0.030184
1969	0.007328	1979	0.025648	1989	0.029312	1999	0.029312	2009	0.047632	2019	0.029393

Morocco

Year	$MtCO_2$	Year	$MtCO_2$	Year	$MtCO_2$	Year	$MtCO_2$	Year	$MtCO_2$	Year	$MtCO_2$
1960	3.636	1970	7.282	1980	15.9152	1990	22.5276	2000	33.6099	2010	56.2696
1961	3.7714	1971	8.1903	1981	15.8269	1991	24.0219	2001	37.452	2011	56.7116
1962	3.0749	1972	8.0361	1982	17.0279	1992	25.118	2002	38.1074	2012	59.0277
1963	3.9541	1973	9.6259	1983	17.7637	1993	27.1805	2003	37.5315	2013	58.7347
1964	4.415	1974	11.1195	1984	17.783	1994	28.5428	2004	43.3988	2014	59.6426
1965	4.2544	1975	11.0933	1985	17.8337	1995	29.157	2005	45.5691	2015	61.0279
1966	5.4595	1976	11.5279	1986	18.8482	1996	29.9264	2006	47.4388	2016	61.0315
1967	5.4083	1977	12.6796	1987	20.0825	1997	30.3983	2007	50.2889	2017	63.8308
1968	5.6202	1978	13.0535	1988	21.1392	1998	31.2927	2008	52.916	2018	65.3674
1969	5.8174	1979	15.9312	1989	22.8796	1999	32.3852	2009	52.6482	2019	71.9289

Mozambique

Year	$MtCO_2$	Year	$MtCO_2$	Year	$MtCO_2$	Year	$MtCO_2$	Year	$MtCO_2$	Year	$MtCO_2$
1960	1.8824	1970	2.9809	1980	3.1985	1990	1.0152	2000	1.3228	2010	2.6339
1961	2.6299	1971	3.611	1981	2.479	1991	1.0151	2001	1.5539	2011	3.1074
1962	1.9852	1972	3.2957	1982	2.5239	1992	1.0013	2002	1.5386	2012	2.9808
1963	1.6591	1973	3.5589	1983	1.9545	1993	1.0752	2003	1.8567	2013	4.057
1964	2.139	1974	3.1455	1984	1.5109	1994	1.0572	2004	1.8645	2014	8.2593
1965	2.0033	1975	2.8824	1985	1.1349	1995	1.1085	2005	1.7707	2015	6.3056
1966	2.1242	1976	2.5554	1986	0.97714	1996	1.0904	2006	1.9148	2016	7.726
1967	1.8713	1977	2.7064	1987	0.97675	1997	1.1705	2007	2.1872	2017	8.1473
1968	2.7762	1978	2.8658	1988	1.0062	1998	1.1124	2008	2.1799	2018	8.3835
1969	3.2378	1979	2.6346	1989	1.0345	1999	1.1672	2009	2.4399	2019	8.7058

Myanmar

Year	$MtCO_2$	Year	$MtCO_2$	Year	$MtCO_2$	Year	$MtCO_2$	Year	$MtCO_2$	Year	$MtCO_2$
1960	2.7148	1970	4.6123	1980	5.5088	1990	4.2348	2000	10.0425	2010	13.0838
1961	2.5903	1971	5.0995	1981	5.623	1991	4.1367	2001	8.6802	2011	15.0679
1962	2.8797	1972	4.8943	1982	5.5795	1992	4.8416	2002	9.1538	2012	11.8919
1963	2.6339	1973	4.1066	1983	5.7538	1993	5.3018	2003	9.7802	2013	12.9362
1964	2.8574	1974	4.6709	1984	6.5485	1994	6.1962	2004	12.3712	2014	16.1695
1965	2.7255	1975	4.5829	1985	6.6755	1995	6.9063	2005	11.529	2015	22.0764
1966	2.8061	1976	4.8928	1986	6.7563	1996	7.2036	2006	12.7804	2016	25.4688
1967	3.6158	1977	5.1657	1987	4.9434	1997	7.4445	2007	12.7951	2017	23.6698
1968	2.9268	1978	5.1461	1988	4.0867	1998	8.0371	2008	9.7225	2018	26.0956
1969	3.2126	1979	5.086	1989	4.4253	1999	8.93	2009	10.1555	2019	26.2316

Namibia

Year	$MtCO_2$	Year	$MtCO_2$	Year	$MtCO_2$	Year	$MtCO_2$	Year	$MtCO_2$	Year	$MtCO_2$
1960		1970		1980		1990		2000	1.6415	2010	3.0961
1961		1971		1981		1991	1.0552	2001	2.0152	2011	2.7648
1962		1972		1982		1992	1.1505	2002	1.7587	2012	3.3639
1963		1973		1983		1993	1.3887	2003	1.8723	2013	2.6012
1964		1974		1984		1994	1.5719	2004	1.9602	2014	3.7087
1965		1975		1985		1995	1.6195	2005	2.3083	2015	3.8857
1966		1976		1986		1996	1.7221	2006	2.3303	2016	4.1236
1967		1977		1987		1997	1.7697	2007	2.3596	2017	4.0982
1968		1978		1988		1998	1.8173	2008	3.3232	2018	4.1543
1969		1979		1989		1999	1.6635	2009	3.0668	2019	4.168

Nauru

Year	$MtCO_2$	Year	$MtCO_2$	Year	$MtCO_2$	Year	$MtCO_2$	Year	$MtCO_2$	Year	$MtCO_2$
1960		1970	0.065952	1980	0.12458	1990	0.12458	2000	0.08427	2010	0.04396
1961		1971	0.087936	1981	0.12458	1991	0.12458	2001	0.08060	2011	0.04030
1962		1972	0.076944	1982	0.12458	1992	0.12091	2002	0.07694	2012	0.04396
1963		1973	0.084272	1983	0.12458	1993	0.11358	2003	0.06595	2013	0.04763
1964	0.02931	1974	0.098928	1984	0.12458	1994	0.10992	2004	0.06595	2014	0.05129
1965	0.03297	1975	0.10259	1985	0.12458	1995	0.10626	2005	0.06228	2015	0.05496
1966	0.03297	1976	0.10259	1986	0.16122	1996	0.10259	2006	0.04396	2016	0.04396
1967	0.04763	1977	0.11358	1987	0.15755	1997	0.10259	2007	0.04396	2017	0.04763
1968	0.04763	1978	0.11358	1988	0.15755	1998	0.098928	2008	0.04396	2018	0.04974
1969	0.06595	1979	0.11358	1989	0.15755	1999	0.0916	2009	0.04030	2019	0.05299

Nepal

Year	$MtCO_2$	Year	$MtCO_2$	Year	$MtCO_2$	Year	$MtCO_2$	Year	$MtCO_2$	Year	$MtCO_2$
1960	0.080608	1970	0.22717	1980	0.5413	1990	0.76674	2000	3.038	2010	4.8244
1961	0.080608	1971	0.19786	1981	0.45319	1991	1.0725	2001	3.2368	2011	5.2215
1962	0.087936	1972	0.26747	1982	0.44236	1992	1.2902	2002	2.5951	2012	5.4698
1963	0.098928	1973	0.42136	1983	0.49242	1993	1.4698	2003	2.81	2013	6.2188
1964	0.15022	1974	0.42488	1984	0.70142	1994	1.7001	2004	2.5829	2014	7.5924
1965	0.17954	1975	0.35171	1985	0.67602	1995	2.4064	2005	2.9855	2015	6.0141
1966	0.19053	1976	0.28184	1986	0.69701	1996	2.4553	2006	2.4561	2016	8.8411
1967	0.21251	1977	0.3364	1987	0.86068	1997	2.7595	2007	2.5707	2017	10.1235
1968	0.25282	1978	0.32898	1988	0.97597	1998	2.2233	2008	3.3513	2018	13.4104
1969	0.39938	1979	0.51236	1989	0.89356	1999	3.1898	2009	4.1288	2019	13.9135

Netherlands

Year	$MtCO_2$	Year	$MtCO_2$	Year	$MtCO_2$	Year	$MtCO_2$	Year	$MtCO_2$	Year	$MtCO_2$
1960	73.4376	1970	141.8033	1980	176.6319	1990	162.3851	2000	171.8874	2010	182.1179
1961	75.8188	1971	140.6662	1981	164.1099	1991	170.7964	2001	176.7985	2011	169.0657
1962	83.2819	1972	157.4954	1982	133.4873	1992	170.6302	2002	176.113	2012	165.827
1963	91.1446	1973	165.2599	1983	137.3575	1993	170.8176	2003	179.565	2013	165.7179
1964	96.7766	1974	159.9852	1984	144.073	1994	171.4014	2004	181.3818	2014	158.768
1965	100.4036	1975	152.5255	1985	146.9802	1995	172.9662	2005	177.459	2015	166.3667
1966	103.5575	1976	169.1309	1986	144.0146	1996	182.1483	2006	172.6865	2016	166.2821
1967	106.6822	1977	163.6058	1987	151.4805	1997	175.0196	2007	172.5872	2017	164.4448
1968	113.4455	1978	169.7932	1988	145.603	1998	176.1369	2008	175.4815	2018	160.1701
1969	115.8021	1979	187.0072	1989	161.6645	1999	170.7273	2009	170.1677	2019	154.8266

New Caledonia

Year	$MtCO_2$	Year	$MtCO_2$	Year	$MtCO_2$	Year	$MtCO_2$	Year	$MtCO_2$	Year	$MtCO_2$
1960	0.86104	1970	2.3926	1980	1.9986	1990	1.5768	2000	2.2216	2010	3.5572
1961	0.88669	1971	2.4182	1981	1.3903	1991	1.758	2001	1.8777	2011	3.5401
1962	0.56426	1972	1.7038	1982	1.2618	1992	1.5747	2002	2.3934	2012	3.6379
1963	0.61922	1973	2.5976	1983	1.1512	1993	1.8275	2003	2.7267	2013	3.8482
1964	1.0992	1974	2.7807	1984	1.2022	1994	1.9704	2004	2.5161	2014	4.8721
1965	1.2311	1975	2.5279	1985	1.451	1995	2.0642	2005	2.809	2015	4.7357
1966	1.5096	1976	2.3884	1986	1.4008	1996	2.1851	2006	2.706	2016	5.3118
1967	1.4729	1977	2.139	1987	1.4545	1997	1.8187	2007	2.928	2017	5.3448
1968	1.8393	1978	1.5413	1988	1.5012	1998	1.81	2008	2.849	2018	8.209
1969	1.5572	1979	1.6399	1989	1.6395	1999	2.0555	2009	2.9332	2019	8.4516

New Zealand

Year	$MtCO_2$	Year	$MtCO_2$	Year	$MtCO_2$	Year	$MtCO_2$	Year	$MtCO_2$	Year	$MtCO_2$
1960	11.5318	1970	14.18	1980	17.479	1990	25.4463	2000	32.2814	2010	34.9578
1961	11.7551	1971	15.049	1981	16.5611	1991	26.1104	2001	34.4574	2011	34.2496
1962	11.1983	1972	16.1896	1982	18.2703	1992	28.1051	2002	34.6381	2012	36.0004
1963	12.2165	1973	18.2004	1983	17.9982	1993	27.6995	2003	36.3519	2013	35.2409
1964	13.092	1974	18.76	1984	19.3367	1994	27.8803	2004	35.9401	2014	35.4578
1965	13.6853	1975	18.2704	1985	21.8581	1995	28.0018	2005	37.571	2015	35.8392
1966	14.0003	1976	19.2486	1986	22.9461	1996	29.2951	2006	37.4663	2016	34.2676
1967	13.6268	1977	20.3135	1987	24.1654	1997	31.2893	2007	36.5599	2017	36.1533
1968	13.4731	1978	18.0241	1988	25.4495	1998	29.8828	2008	37.5923	2018	35.0803
1969	14.257	1979	16.4945	1989	25.4534	1999	31.4723	2009	34.7624	2019	36.541

Nicaragua

Year	$MtCO_2$	Year	$MtCO_2$	Year	$MtCO_2$	Year	$MtCO_2$	Year	$MtCO_2$	Year	$MtCO_2$
1960	0.53116	1970	1.4028	1980	2.0223	1990	1.9552	2000	3.7211	2010	4.469
1961	0.56044	1971	1.5054	1981	2.1349	1991	1.9879	2001	3.922	2011	4.8053
1962	0.65934	1972	1.6044	1982	2.1107	1992	2.3736	2002	3.9908	2012	4.5452
1963	0.84251	1973	1.8276	1983	1.9967	1993	2.2834	2003	4.3353	2013	4.3514
1964	0.94874	1974	1.9483	1984	1.846	1994	2.5179	2004	4.3783	2014	4.598
1965	0.78016	1975	1.9266	1985	1.9848	1995	2.7548	2005	4.2697	2015	5.2502
1966	0.95964	1976	2.2222	1986	2.2555	1996	2.8474	2006	4.4178	2016	5.448
1967	1.0805	1977	2.8331	1987	2.431	1997	3.1136	2007	4.5504	2017	5.3747
1968	1.2307	1978	2.6275	1988	2.24	1998	3.3919	2008	4.3653	2018	5.3772
1969	1.2856	1979	1.7093	1989	1.4683	1999	3.5984	2009	4.4448	2019	5.5486

Niger

Year	$MtCO_2$	Year	$MtCO_2$	Year	$MtCO_2$	Year	$MtCO_2$	Year	$MtCO_2$	Year	$MtCO_2$
1960	0.02931	1970	0.003664	1980	0.57017	1990	0.60262	2000	0.69268	2010	1.1692
1961	0.05496	1971	0.003664	1981	0.6838	1991	0.56963	2001	0.65164	2011	1.3224
1962	0.06595	1972	0.003664	1982	0.74588	1992	0.52866	2002	0.69481	2012	1.7539
1963	0.08793	1973	0.003664	1983	0.96184	1993	0.60194	2003	0.75337	2013	1.8911
1964	0.09526	1974	0.003664	1984	0.99095	1994	0.57992	2004	0.80824	2014	2.075
1965	0.0916	1975	0.003664	1985	0.9944	1995	0.5616	2005	0.70848	2015	2.0351
1966	0.13551	1976	0.003664	1986	0.89895	1996	0.64217	2006	0.68628	2016	2.0645
1967	0.13181	1977	0.003664	1987	0.99766	1997	0.64582	2007	0.7169	2017	2.0058
1968	0.16113	1978	0.003664	1988	0.98703	1998	0.69711	2008	0.80306	2018	2.0938
1969	0.19044	1979	0.003664	1989	1.0382	1999	0.68241	2009	0.9623	2019	2.1353

Nigeria

Year	$MtCO_2$	Year	$MtCO_2$	Year	$MtCO_2$	Year	$MtCO_2$	Year	$MtCO_2$	Year	$MtCO_2$
1960	3.4032	1970	21.52	1980	68.0352	1990	38.8572	2000	78.8231	2010	112.314
1961	4.1096	1971	32.2515	1981	65.8105	1991	41.9291	2001	86.7175	2011	129.5684
1962	4.175	1972	41.3876	1982	65.3936	1992	46.2651	2002	94.3047	2012	116.3306
1963	5.3436	1973	49.5323	1983	59.7052	1993	44.8134	2003	100.0086	2013	122.0978
1964	7.2667	1974	62.2355	1984	69.4059	1994	34.9337	2004	98.6858	2014	127.8226
1965	11.7501	1975	47.3517	1985	69.636	1995	33.4172	2005	105.7571	2015	113.5395
1966	12.8932	1976	55.1896	1986	73.1922	1996	36.7882	2006	97.8094	2016	116.7736
1967	12.8245	1977	50.5046	1987	59.0244	1997	41.0096	2007	94.2691	2017	130.2755
1968	6.6259	1978	48.2229	1988	70.4213	1998	37.7453	2008	94.772	2018	136.0783
1969	12.0999	1979	70.1856	1989	42.1194	1999	39.5868	2009	74.8849	2019	140.0265

Niue

Year	$MtCO_2$	Year	$MtCO_2$	Year	$MtCO_2$	Year	$MtCO_2$	Year	$MtCO_2$	Year	$MtCO_2$
1960		1970	0.003664	1980	0.003664	1990	0.007328	2000	0.007328	2010	0.003664
1961		1971	0.003664	1981	0.003664	1991	0.007328	2001	0.007328	2011	0.007328
1962		1972	0.003664	1982	0.003664	1992	0.007328	2002	0.007328	2012	0.007328
1963		1973	0.003664	1983	0.003664	1993	0.007328	2003	0.003664	2013	0.007328
1964		1974	0.003664	1984	0.003664	1994	0.007328	2004	0.003664	2014	0.010992
1965		1975	0.003664	1985	0.003664	1995	0.007328	2005	0.003664	2015	0.007328
1966		1976	0.003664	1986	0.003664	1996	0.007328	2006	0.003664	2016	0.007328
1967		1977	0.003664	1987	0.003664	1997	0.007328	2007	0.003664	2017	0.007328
1968		1978	0.003664	1988	0.003664	1998	0.007328	2008	0.007328	2018	0.007653
1969		1979	0.003664	1989	0.003664	1999	0.007328	2009	0.003664	2019	0.008154

North Korea

Year	$MtCO_2$	Year	$MtCO_2$	Year	$MtCO_2$	Year	$MtCO_2$	Year	$MtCO_2$	Year	$MtCO_2$
1960	23.7884	1970	73.4763	1980	114.0822	1990	122.4	2000	69.166	2010	50.0236
1961	26.4266	1971	107.453	1981	114.3949	1991	117.2266	2001	71.665	2011	36.1844
1962	30.6874	1972	89.5049	1982	116.8921	1992	102.9626	2002	68.6429	2012	37.566
1963	32.8265	1973	97.3253	1983	125.1631	1993	94.8685	2003	70.1365	2013	27.0146
1964	35.6182	1974	101.6115	1984	134.6616	1994	86.7195	2004	71.722	2014	30.5443
1965	44.2221	1975	107.6238	1985	144.2847	1995	81.2599	2005	74.9187	2015	24.6207
1966	47.5999	1976	110.0309	1986	156.8353	1996	71.6379	2006	76.1728	2016	27.4666
1967	52.392	1977	113.6652	1987	175.6187	1997	65.1583	2007	63.4792	2017	21.754
1968	59.269	1978	108.2129	1988	200.8081	1998	58.7688	2008	70.3281	2018	38.1629
1969	64.0794	1979	110.263	1989	213.0715	1999	64.0994	2009	53.5653	2019	38.7622

North Macedonia

Year	$MtCO_2$	Year	$MtCO_2$	Year	$MtCO_2$	Year	$MtCO_2$	Year	$MtCO_2$	Year	$MtCO_2$
1960	3.8456	1970	7.7803	1980	11.8039	1990	14.1855	2000	11.9959	2010	8.5005
1961	4.0309	1971	8.3852	1981	12.8463	1991	10.0358	2001	11.9263	2011	9.1966
1962	4.1364	1972	7.8592	1982	11.8019	1992	10.9847	2002	10.8674	2012	8.735
1963	4.6016	1973	9.3885	1983	12.7085	1993	10.1236	2003	11.2265	2013	7.7713
1964	5.2134	1974	9.4296	1984	13.4021	1994	10.2482	2004	11.1056	2014	7.4599
1965	5.3641	1975	9.8392	1985	13.6711	1995	10.6366	2005	11.1789	2015	7.0239
1966	5.3153	1976	10.1554	1986	14.2777	1996	11.6845	2006	10.8344	2016	6.9872
1967	5.3689	1977	9.8759	1987	13.9394	1997	10.578	2007	9.3835	2017	7.5075
1968	5.7423	1978	11.0362	1988	14.3836	1998	12.5712	2008	9.2956	2018	6.9809
1969	5.9537	1979	12.0041	1989	14.3397	1999	11.6662	2009	8.5921	2019	8.0414

Norway

Year	$MtCO_2$	Year	$MtCO_2$	Year	$MtCO_2$	Year	$MtCO_2$	Year	$MtCO_2$	Year	$MtCO_2$
1960	13.0868	1970	27.9787	1980	31.8978	1990	35.3213	2000	42.5186	2010	46.2317
1961	13.3355	1971	27.1662	1981	31.9425	1991	33.8165	2001	43.8664	2011	45.5134
1962	14.0604	1972	29.3954	1982	31.0626	1992	34.7347	2002	42.9857	2012	45.0383
1963	14.9653	1973	30.4923	1983	32.1199	1993	36.2242	2003	44.3057	2013	44.9824
1964	16.1703	1974	27.7057	1984	34.0109	1994	38.089	2004	44.6226	2014	44.9166
1965	16.3899	1975	30.6358	1985	32.4946	1995	38.7075	2005	43.9232	2015	45.3505
1966	19.5401	1976	33.3869	1986	35.0292	1996	41.8303	2006	44.4848	2016	44.4727
1967	19.3042	1977	33.3821	1987	33.4575	1997	41.97	2007	46.2313	2017	43.5625
1968	21.1137	1978	32.7134	1988	35.8789	1998	42.2202	2008	45.3777	2018	43.8177
1969	22.1938	1979	34.738	1989	34.4416	1999	42.974	2009	43.89	2019	42.4408

Occupied Palestinian Territory

Year	$MtCO_2$	Year	$MtCO_2$	Year	$MtCO_2$	Year	$MtCO_2$	Year	$MtCO_2$	Year	$MtCO_2$
1960		1970		1980		1990	0.86104	2000	1.6598	2010	2.0335
1961		1971		1981		1991	0.88302	2001	1.3484	2011	2.246
1962		1972		1982		1992	0.916	2002	1.1542	2012	2.1984
1963		1973		1983		1993	0.93432	2003	1.2787	2013	2.4366
1964		1974		1984		1994	0.9673	2004	2.1947	2014	2.8359
1965		1975		1985		1995	0.94531	2005	2.7407	2015	3.0045
1966		1976		1986		1996	1.0369	2006	2.2644	2016	3.2316
1967		1977		1987		1997	0.8647	2007	2.323	2017	3.2683
1968		1978		1988		1998	1.4619	2008	2.0518	2018	3.2198
1969		1979		1989		1999	1.3667	2009	2.0885	2019	3.3032

Oman

Year	$MtCO_2$	Year	$MtCO_2$	Year	$MtCO_2$	Year	$MtCO_2$	Year	$MtCO_2$	Year	$MtCO_2$
1960		1970	0.2345	1980	6.0419	1990	11.2224	2000	21.5345	2010	46.7501
1961		1971	2.0921	1981	6.0126	1991	11.5937	2001	20.1059	2011	53.2631
1962		1972	2.0885	1982	5.7305	1992	11.893	2002	25.2344	2012	58.6907
1963		1973	2.1105	1983	7.5259	1993	13.2247	2003	32.0275	2013	61.1207
1964	0.010992	1974	2.334	1984	8.0535	1994	15.0535	2004	27.5912	2014	60.4098
1965	0.025648	1975	7.2511	1985	8.6185	1995	15.7188	2005	29.4666	2015	61.604
1966	0.029312	1976	8.3209	1986	9.8249	1996	14.8827	2006	39.0464	2016	60.0331
1967	0.13557	1977	8.5005	1987	9.4018	1997	15.2481	2007	43.9704	2017	65.5108
1968	0.16122	1978	7.7897	1988	10.5166	1998	16.2998	2008	42.1107	2018	71.0299
1969	0.2345	1979	7.7164	1989	9.9857	1999	20.5579	2009	40.5146	2019	71.6846

Pakistan

Year	$MtCO_2$	Year	$MtCO_2$	Year	$MtCO_2$	Year	$MtCO_2$	Year	$MtCO_2$	Year	$MtCO_2$
1960	11.9264	1970	20.5044	1980	31.9316	1990	67.8285	2000	105.4184	2010	154.1447
1961	12.3496	1971	19.4407	1981	34.2328	1991	67.4779	2001	107.1262	2011	154.6585
1962	13.5699	1972	18.903	1982	37.1896	1992	72.015	2002	112.9036	2012	153.8759
1963	15.6002	1973	20.0085	1983	40.0222	1993	77.1766	2003	117.4907	2013	150.4513
1964	16.039	1974	21.3874	1984	42.5573	1994	84.0193	2004	129.9595	2014	154.2908
1965	16.8296	1975	23.1878	1985	46.8135	1995	83.6151	2005	134.7562	2015	170.1753
1966	17.1257	1976	22.7885	1986	49.0586	1996	93.5374	2006	143.7267	2016	203.1458
1967	18.1759	1977	24.3199	1987	52.9885	1997	93.7876	2007	155.8442	2017	232.4248
1968	20.8418	1978	26.0506	1988	57.6074	1998	96.7421	2008	155.3562	2018	247.4254
1969	20.2134	1979	28.1345	1989	60.3166	1999	99.3905	2009	155.219	2019	248.8439

Palau

Year	$MtCO_2$	Year	$MtCO_2$	Year	$MtCO_2$	Year	$MtCO_2$	Year	$MtCO_2$	Year	$MtCO_2$
1960		1970		1980		1990		2000	0.20885	2010	0.20885
1961		1971		1981		1991		2001	0.21618	2011	0.21618
1962		1972		1982		1992	0.19786	2002	0.21251	2012	0.21618
1963		1973		1983		1993	0.19786	2003	0.21251	2013	0.21984
1964		1974		1984		1994	0.19786	2004	0.21618	2014	0.2235
1965		1975		1985		1995	0.19786	2005	0.21984	2015	0.2235
1966		1976		1986		1996	0.19786	2006	0.22717	2016	0.2235
1967		1977		1987		1997	0.19786	2007	0.25282	2017	0.23083
1968		1978		1988		1998	0.19786	2008	0.20518	2018	0.24108
1969		1979		1989		1999	0.19786	2009	0.19786	2019	0.25684

Panama

Year	$MtCO_2$	Year	$MtCO_2$	Year	$MtCO_2$	Year	$MtCO_2$	Year	$MtCO_2$	Year	$MtCO_2$
1960	0.99616	1970	2.2011	1980	3.1076	1990	2.6328	2000	5.7277	2010	9.0727
1961	1.1024	1971	2.6003	1981	3.3227	1991	3.1053	2001	6.9546	2011	9.9521
1962	1.1903	1972	2.7982	1982	3.2785	1992	4.1124	2002	5.8109	2012	9.7676
1963	1.1829	1973	3.2372	1983	3.4797	1993	3.786	2003	6.0903	2013	11.366
1964	1.2416	1974	3.0175	1984	2.8674	1994	4.1784	2004	5.7117	2014	10.8558
1965	1.5272	1975	3.6592	1985	2.6133	1995	3.6541	2005	6.7411	2015	10.877
1966	1.6555	1976	3.6067	1986	2.7348	1996	4.4468	2006	7.3671	2016	10.463
1967	1.6957	1977	3.4554	1987	3.1796	1997	4.6296	2007	7.1963	2017	11.9615
1968	2.0182	1978	2.8346	1988	2.9147	1998	5.9005	2008	7.3136	2018	12.0963
1969	2.0511	1979	3.1808	1989	2.5103	1999	5.6211	2009	8.4194	2019	12.5031

Papua New Guinea

Year	$MtCO_2$	Year	$MtCO_2$	Year	$MtCO_2$	Year	$MtCO_2$	Year	$MtCO_2$	Year	$MtCO_2$
1960	0.17954	1970	0.6925	1980	1.8283	1990	2.1544	2000	2.6637	2010	4.6606
1961	0.20152	1971	0.8244	1981	1.9309	1991	2.1691	2001	3.206	2011	5.2249
1962	0.19786	1972	1.2677	1982	1.9456	1992	2.1911	2002	3.4845	2012	4.9757
1963	0.25648	1973	1.3447	1983	2.0079	1993	2.1911	2003	3.9425	2013	5.3311
1964	0.26747	1974	1.5865	1984	2.0445	1994	2.1801	2004	4.4847	2014	6.0493
1965	0.30411	1975	1.5316	1985	2.1251	1995	2.0592	2005	4.3821	2015	6.3643
1966	0.34075	1976	1.5719	1986	2.0628	1996	2.1874	2006	4.3052	2016	6.6794
1967	0.43602	1977	1.5792	1987	2.334	1997	2.5758	2007	6.1152	2017	6.5476
1968	0.50197	1978	1.6744	1988	2.1984	1998	2.8616	2008	4.7925	2018	6.7861
1969	0.55693	1979	1.7954	1989	2.0335	1999	2.4439	2009	5.0893	2019	7.0869

Paraguay

Year	$MtCO_2$	Year	$MtCO_2$	Year	$MtCO_2$	Year	$MtCO_2$	Year	$MtCO_2$	Year	$MtCO_2$
1960	0.30405	1970	0.74344	1980	1.4858	1990	2.1356	2000	3.6061	2010	5.0218
1961	0.36268	1971	0.63348	1981	1.3834	1991	2.1034	2001	3.6955	2011	5.1987
1962	0.39199	1972	0.71379	1982	1.3626	1992	2.5799	2002	3.8573	2012	5.1733
1963	0.41031	1973	0.86747	1983	1.4083	1993	2.9141	2003	4.0315	2013	5.1721
1964	0.43226	1974	0.95111	1984	1.4903	1994	3.4043	2004	4.0613	2014	5.4582
1965	0.54948	1975	0.8366	1985	1.5479	1995	3.9371	2005	3.7799	2015	6.051
1966	0.51284	1976	1.0301	1986	1.6551	1996	3.7188	2006	3.9087	2016	7.1538
1967	0.48725	1977	1.1533	1987	1.8774	1997	4.128	2007	4.0416	2017	8.0149
1968	0.58981	1978	1.4539	1988	2.1447	1998	4.3839	2008	4.278	2018	8.103
1969	0.52014	1979	1.3257	1989	2.2245	1999	4.3759	2009	4.5315	2019	8.2723

Peru

Year	$MtCO_2$	Year	$MtCO_2$	Year	$MtCO_2$	Year	$MtCO_2$	Year	$MtCO_2$	Year	$MtCO_2$
1960	8.1646	1970	17.7658	1980	24.0627	1990	21.3666	2000	30.0783	2010	57.1505
1961	8.6336	1971	18.5926	1981	24.0193	1991	20.7242	2001	26.9287	2011	48.9588
1962	9.9596	1972	18.1522	1982	23.59	1992	20.9559	2002	26.9306	2012	54.1558
1963	10.2232	1973	19.7321	1983	20.3822	1993	23.852	2003	26.1046	2013	42.9289
1964	12.2528	1974	21.3351	1984	20.619	1994	23.7202	2004	31.5555	2014	49.0534
1965	11.9515	1975	21.9397	1985	19.4399	1995	24.6276	2005	36.7331	2015	48.6962
1966	13.2411	1976	22.4103	1986	21.7533	1996	24.184	2006	28.2627	2016	52.3601
1967	13.6403	1977	23.3028	1987	25.6642	1997	27.2456	2007	34.5236	2017	52.4886
1968	14.4866	1978	22.4169	1988	24.9858	1998	27.572	2008	40.6693	2018	54.2103
1969	15.2853	1979	22.2186	1989	21.7319	1999	29.1468	2009	51.2072	2019	54.5332

Philippines

Year	$MtCO_2$	Year	$MtCO_2$	Year	$MtCO_2$	Year	$MtCO_2$	Year	$MtCO_2$	Year	$MtCO_2$
1960	8.3251	1970	24.7514	1980	36.8686	1990	41.3495	2000	72.3464	2010	82.9512
1961	8.7125	1971	27.5517	1981	34.5282	1991	43.4712	2001	70.3045	2011	83.7437
1962	10.3359	1972	26.4094	1982	34.8385	1992	48.2938	2002	70.1551	2012	88.4068
1963	11.4718	1973	31.5013	1983	35.2391	1993	48.9292	2003	70.2147	2013	95.7926
1964	12.8228	1974	30.4923	1984	30.8313	1994	54.1233	2004	72.7708	2014	101.1821
1965	13.9646	1975	32.4824	1985	27.8991	1995	59.9488	2005	73.2713	2015	112.1425
1966	16.1041	1976	35.0662	1986	29.0247	1996	61.2537	2006	66.5219	2016	122.2368
1967	18.2089	1977	36.6761	1987	32.4958	1997	70.0626	2007	70.7641	2017	134.5185
1968	22.2228	1978	37.3802	1988	37.4847	1998	68.253	2008	77.3	2018	138.9244
1969	22.8295	1979	38.031	1989	38.9065	1999	68.1767	2009	76.4925	2019	144.2628

Poland

Year	$MtCO_2$	Year	$MtCO_2$	Year	$MtCO_2$	Year	$MtCO_2$	Year	$MtCO_2$	Year	$MtCO_2$
1960	199.577	1970	304.1434	1980	463.3291	1990	376.5465	2000	317.338	2010	334.606
1961	207.235	1971	312.8808	1981	408.997	1991	373.7933	2001	313.647	2011	333.952
1962	216.607	1972	329.5064	1982	420.9704	1992	364.6779	2002	306.403	2012	326.348
1963	230.998	1973	335.59	1983	421.0238	1993	365.3707	2003	319.406	2013	322.225
1964	242.880	1974	346.2366	1984	432.4674	1994	360.4168	2004	324.146	2014	309.920
1965	246.980	1975	374.7801	1985	444.5079	1995	362.7613	2005	323.161	2015	313.099
1966	252.431	1976	398.1187	1986	451.8487	1996	377.4078	2006	337.037	2016	324.011
1967	259.025	1977	417.955	1987	463.7326	1997	367.3853	2007	336.368	2017	337.340
1968	275.801	1978	430.8701	1988	444.23	1998	339.1329	2008	330.145	2018	337.705
1969	293.365	1979	441.3086	1989	422.1751	1999	329.1673	2009	316.607	2019	322.626

Portugal

Year	$MtCO_2$	Year	$MtCO_2$	Year	$MtCO_2$	Year	$MtCO_2$	Year	$MtCO_2$	Year	$MtCO_2$
1960	8.2135	1970	15.2365	1980	26.7737	1990	45.083	2000	65.5266	2010	52.9894
1961	9.078	1971	16.3757	1981	27.0007	1991	46.9603	2001	65.1493	2011	51.7927
1962	9.2899	1972	18.3073	1982	29.0001	1992	50.8892	2002	69.5561	2012	49.9626
1963	10.0116	1973	19.9451	1983	29.9019	1993	49.3919	2003	64.4193	2013	48.1619
1964	11.0074	1974	20.645	1984	28.794	1994	50.2464	2004	67.2553	2014	47.9484
1965	11.5825	1975	21.2753	1985	27.1299	1995	54.4508	2005	69.484	2015	52.2941
1966	11.8351	1976	22.3258	1986	30.2214	1996	51.7032	2006	64.7677	2016	50.4556
1967	12.3916	1977	22.6051	1987	31.1986	1997	54.5976	2007	62.2804	2017	54.72
1968	12.9924	1978	22.5849	1988	32.5679	1998	59.1384	2008	59.9731	2018	51.4825
1969	14.5928	1979	24.8557	1989	40.8226	1999	66.7632	2009	57.2003	2019	48.5978

Qatar

Year	$MtCO_2$	Year	$MtCO_2$	Year	$MtCO_2$	Year	$MtCO_2$	Year	$MtCO_2$	Year	$MtCO_2$
1960	0.17587	1970	7.5615	1980	13.0817	1990	11.7437	2000	34.5662	2010	71.9199
1961	0.16122	1971	9.1443	1981	12.8407	1991	17.6453	2001	41.2145	2011	79.6476
1962	0.19053	1972	10.7754	1982	12.3349	1992	26.9966	2002	40.7019	2012	92.3035
1963	6.1335	1973	12.4572	1983	11.2426	1993	30.985	2003	41.2994	2013	82.6979
1964	6.2691	1974	10.4785	1984	12.298	1994	30.7044	2004	42.7103	2014	105.9796
1965	6.2874	1975	10.9474	1985	12.3778	1995	31.7171	2005	50.6901	2015	105.7561
1966	6.2728	1976	10.3749	1986	13.267	1996	32.2038	2006	63.1962	2016	102.1726
1967	6.6831	1977	9.916	1987	11.4705	1997	37.3935	2007	62.8994	2017	105.5691
1968	7.0752	1978	10.519	1988	11.8977	1998	32.271	2008	64.2571	2018	109.2447
1969	7.1666	1979	14.3424	1989	14.2924	1999	31.2711	2009	68.5969	2019	109.3447

Republic of South Sudan

Year	$MtCO_2$	Year	$MtCO_2$	Year	$MtCO_2$	Year	$MtCO_2$	Year	$MtCO_2$	Year	$MtCO_2$
1960	0.1132	1970	0.40398	1980	0.31184	1990	0.43389	2000	0.45982	2010	1.3133
1961	0.11534	1971	0.41466	1981	0.30299	1991	0.40642	2001	0.52908	2011	1.2812
1962	0.12357	1972	0.44762	1982	0.31855	1992	0.3634	2002	0.67432	2012	1.33
1963	0.13975	1973	0.45158	1983	0.32526	1993	0.25051	2003	0.75335	2013	1.4473
1964	0.1547	1974	0.47294	1984	0.2917	1994	0.34448	2004	0.95198	2014	1.5352
1965	0.20199	1975	0.35272	1985	0.33899	1995	0.35608	2005	0.91201	2015	1.9419
1966	0.21999	1976	0.31245	1986	0.35364	1996	0.36737	2006	0.99867	2016	1.7257
1967	0.26515	1977	0.31672	1987	0.27888	1997	0.44975	2007	1.1732	2017	1.4912
1968	0.25844	1978	0.28621	1988	0.40337	1998	0.38995	2008	1.2391	2018	1.5399
1969	0.34815	1979	0.29719	1989	0.31275	1999	0.4229	2009	1.2907	2019	1.5849

Romania

Year	$MtCO_2$	Year	$MtCO_2$	Year	$MtCO_2$	Year	$MtCO_2$	Year	$MtCO_2$	Year	$MtCO_2$
1960	53.3941	1970	119.9815	1980	196.199	1990	169.2859	2000	95.4558	2010	84.2897
1961	55.7161	1971	125.6815	1981	197.7302	1991	139.3703	2001	100.3571	2011	89.5182
1962	63.8128	1972	132.2542	1982	195.3292	1992	131.0723	2002	101.7353	2012	86.2557
1963	69.4555	1973	144.765	1983	200.1164	1993	122.8323	2003	105.2952	2013	76.8759
1964	72.037	1974	150.7203	1984	188.8166	1994	121.9615	2004	104.2698	2014	77.4324
1965	78.6369	1975	162.0064	1985	193.9069	1995	127.0329	2005	102.6945	2015	77.7256
1966	84.0907	1976	174.472	1986	201.6413	1996	130.0959	2006	105.0828	2016	75.8128
1967	92.0288	1977	178.0767	1987	211.6316	1997	121.0747	2007	108.4405	2017	78.0775
1968	100.0794	1978	193.5394	1988	212.2216	1998	107.5615	2008	105.5346	2018	76.9512
1969	111.5274	1979	195.6764	1989	213.5994	1999	90.7782	2009	86.0241	2019	75.0841

Russian Federation

Year	$MtCO_2$	Year	$MtCO_2$	Year	$MtCO_2$	Year	$MtCO_2$	Year	$MtCO_2$	Year	$MtCO_2$
1960	885.8611	1970	1442.53	1980	2132.301	1990	2525.294	2000	1471.052	2010	1612.885
1961	913.5253	1971	1530.889	1981	2091.653	1991	2395.978	2001	1507.501	2011	1664.953
1962	958.7569	1972	1610.796	1982	2131.136	1992	1957.659	2002	1495.484	2012	1679.866
1963	1028.218	1973	1678.915	1983	2161.338	1993	1859.46	2003	1525.39	2013	1619.173
1964	1093.519	1974	1742.934	1984	2180.496	1994	1641.399	2004	1530.474	2014	1622.349
1965	1159.985	1975	1832.155	1985	2351.675	1995	1612.928	2005	1547.376	2015	1622.861
1966	1224.976	1976	1902.632	1986	2357.643	1996	1580.161	2006	1606.313	2016	1618.304
1967	1280.896	1977	1967.275	1987	2347.912	1997	1475.157	2007	1604.324	2017	1646.18
1968	1316.893	1978	2034.807	1988	2410.627	1998	1458.157	2008	1636.694	2018	1691.36
1969	1371.484	1979	2051.615	1989	2356.63	1999	1486.09	2009	1528.765	2019	1678.367

Rwanda

Year	$MtCO_2$	Year	$MtCO_2$	Year	$MtCO_2$	Year	$MtCO_2$	Year	$MtCO_2$	Year	$MtCO_2$
1960	0.06982	1970	0.058624	1980	0.49464	1990	0.52332	2000	0.51971	2010	0.5734
1961	0.09149	1971	0.062288	1981	0.6009	1991	0.47179	2001	0.52145	2011	0.64702
1962	0.08427	1972	0.065952	1982	0.60822	1992	0.47895	2002	0.5195	2012	0.71846
1963	0.08427	1973	0.069616	1983	0.69616	1993	0.48241	2003	0.50816	2013	0.78227
1964	0.03664	1974	0.07328	1984	0.63387	1994	0.46103	2004	0.51513	2014	0.81274
1965	0.04763	1975	0.17587	1985	0.61555	1995	0.45367	2005	0.51477	2015	0.92648
1966	0.04396	1976	0.26747	1986	0.59723	1996	0.46486	2006	0.51442	2016	1.0469
1967	0.04030	1977	0.26747	1987	0.61138	1997	0.4816	2007	0.54218	2017	1.0505
1968	0.05496	1978	0.28946	1988	0.69227	1998	0.48139	2008	0.52782	2018	1.0801
1969	0.05862	1979	0.29678	1989	0.6842	1999	0.50243	2009	0.55826	2019	1.1109

Saint Helena

Year	$MtCO_2$	Year	$MtCO_2$	Year	$MtCO_2$	Year	$MtCO_2$	Year	$MtCO_2$	Year	$MtCO_2$
1960		1970		1980		1990	0.007328	2000	0.010992	2010	0.010992
1961		1971		1981	0.007328	1991	0.007328	2001	0.010992	2011	0.010992
1962		1972		1982	0.003664	1992	0.007328	2002	0.010992	2012	0.010992
1963		1973		1983	0.003664	1993	0.010992	2003	0.010992	2013	0.010992
1964		1974		1984	0.003664	1994	0.010992	2004	0.010992	2014	0.010992
1965		1975		1985	0.003664	1995	0.010992	2005	0.010992	2015	0.010992
1966		1976		1986	0.003664	1996	0.010992	2006	0.010992	2016	0.010992
1967		1977		1987	0.003664	1997	0.010992	2007	0.010992	2017	0.010992
1968	0.003664	1978		1988	0.007328	1998	0.010992	2008	0.010992	2018	0.011319
1969		1979		1989	0.007328	1999	0.010992	2009	0.010992	2019	0.011023

Saint Kitts and Nevis

Year	$MtCO_2$	Year	$MtCO_2$	Year	$MtCO_2$	Year	$MtCO_2$	Year	$MtCO_2$	Year	$MtCO_2$
1960		1970		1980		1990	0.10626	2000	0.17221	2010	0.21984
1961		1971		1981	0.05496	1991	0.10626	2001	0.17587	2011	0.23083
1962		1972		1982	0.065952	1992	0.10992	2002	0.19786	2012	0.21984
1963		1973		1983	0.051296	1993	0.11358	2003	0.19786	2013	0.2235
1964		1974		1984	0.051296	1994	0.12091	2004	0.21251	2014	0.23083
1965		1975		1985	0.051296	1995	0.12824	2005	0.19786	2015	0.2345
1966		1976		1986	0.058624	1996	0.1319	2006	0.20152	2016	0.23816
1967		1977		1987	0.05496	1997	0.1429	2007	0.21618	2017	0.24182
1968		1978		1988	0.065952	1998	0.15022	2008	0.21618	2018	0.24901
1969		1979		1989	0.065952	1999	0.16122	2009	0.2235	2019	0.2425

Saint Lucia

Year	$MtCO_2$	Year	$MtCO_2$	Year	$MtCO_2$	Year	$MtCO_2$	Year	$MtCO_2$	Year	$MtCO_2$
1960	0.01465	1970	0.065952	1980	0.11358	1990	0.16122	2000	0.34808	2010	0.3664
1961	0.01832	1971	0.069616	1981	0.095264	1991	0.16854	2001	0.34808	2011	0.33342
1962	0.01832	1972	0.076944	1982	0.11358	1992	0.15022	2002	0.28946	2012	0.32976
1963	0.02198	1973	0.080608	1983	0.10259	1993	0.23083	2003	0.37006	2013	0.30778
1964	0.02198	1974	0.07328	1984	0.11358	1994	0.25648	2004	0.37006	2014	0.34808
1965	0.02564	1975	0.076944	1985	0.12824	1995	0.30778	2005	0.33709	2015	0.35907
1966	0.02931	1976	0.084272	1986	0.1319	1996	0.32243	2006	0.3664	2016	0.33342
1967	0.03297	1977	0.069616	1987	0.14656	1997	0.30411	2007	0.29312	2017	0.35174
1968	0.03664	1978	0.098928	1988	0.16488	1998	0.29312	2008	0.30045	2018	0.3622
1969	0.06228	1979	0.15022	1989	0.16488	1999	0.33342	2009	0.32976	2019	0.35272

Saint Pierre and Miquelon

Year	$MtCO_2$	Year	$MtCO_2$	Year	$MtCO_2$	Year	$MtCO_2$	Year	$MtCO_2$	Year	$MtCO_2$
1960	0.03664	1970	0.03664	1980	0.03664	1990	0.0916	2000	0.05496	2010	0.069616
1961	0.047632	1971	0.047632	1981	0.040304	1991	0.10259	2001	0.05496	2011	0.069616
1962	0.032976	1972	0.069616	1982	0.040304	1992	0.095264	2002	0.058624	2012	0.069616
1963	0.03664	1973	0.040304	1983	0.032976	1993	0.07328	2003	0.065952	2013	0.07328
1964	0.047632	1974	0.043968	1984	0.03664	1994	0.069616	2004	0.062288	2014	0.076944
1965	0.040304	1975	0.032976	1985	0.032976	1995	0.069616	2005	0.065952	2015	0.076944
1966	0.043968	1976	0.047632	1986	0.047632	1996	0.069616	2006	0.065952	2016	0.076944
1967	0.051296	1977	0.03664	1987	0.051296	1997	0.047632	2007	0.065952	2017	0.076944
1968	0.040304	1978	0.032976	1988	0.065952	1998	0.05496	2008	0.065952	2018	0.079232
1969	0.032976	1979	0.03664	1989	0.10259	1999	0.05496	2009	0.065952	2019	0.077158

Saint Vincent and the Grenadines

Year	$MtCO_2$	Year	$MtCO_2$	Year	$MtCO_2$	Year	$MtCO_2$	Year	$MtCO_2$	Year	$MtCO_2$
1960	0.010992	1970	0.029312	1980	0.03664	1990	0.080608	2000	0.14656	2010	0.21984
1961	0.010992	1971	0.029312	1981	0.03664	1991	0.084272	2001	0.17954	2011	0.19786
1962	0.010992	1972	0.03664	1982	0.040304	1992	0.084272	2002	0.18686	2012	0.25282
1963	0.014656	1973	0.040304	1983	0.047632	1993	0.10259	2003	0.19786	2013	0.20885
1964	0.01832	1974	0.032976	1984	0.065952	1994	0.12091	2004	0.21984	2014	0.2748
1965	0.014656	1975	0.032976	1985	0.065952	1995	0.12824	2005	0.21984	2015	0.21251
1966	0.01832	1976	0.032976	1986	0.065952	1996	0.1319	2006	0.21618	2016	0.25282
1967	0.01832	1977	0.032976	1987	0.076944	1997	0.1319	2007	0.26014	2017	0.25648
1968	0.021984	1978	0.03664	1988	0.065952	1998	0.16122	2008	0.19053	2018	0.26411
1969	0.029312	1979	0.029312	1989	0.076944	1999	0.16488	2009	0.31144	2019	0.25719

Samoa

Year	$MtCO_2$	Year	$MtCO_2$	Year	$MtCO_2$	Year	$MtCO_2$	Year	$MtCO_2$	Year	$MtCO_2$
1960	0.01465	1970	0.029312	1980	0.098928	1990	0.10259	2000	0.1429	2010	0.18686
1961	0.01832	1971	0.03664	1981	0.10259	1991	0.10626	2001	0.14656	2011	0.20152
1962	0.01832	1972	0.03664	1982	0.11358	1992	0.10992	2002	0.14656	2012	0.19786
1963	0.02198	1973	0.03664	1983	0.11358	1993	0.10992	2003	0.15389	2013	0.19786
1964	0.02564	1974	0.032976	1984	0.11358	1994	0.11358	2004	0.15022	2014	0.20885
1965	0.02931	1975	0.058624	1985	0.11358	1995	0.11725	2005	0.16122	2015	0.2345
1966	0.02564	1976	0.047632	1986	0.11358	1996	0.12458	2006	0.16488	2016	0.24549
1967	0.02564	1977	0.080608	1987	0.11358	1997	0.12824	2007	0.17221	2017	0.25648
1968	0.02931	1978	0.10626	1988	0.11358	1998	0.1319	2008	0.17954	2018	0.26786
1969	0.02931	1979	0.095264	1989	0.12091	1999	0.13557	2009	0.18686	2019	0.28538

Sao Tome and Principe

Year	$MtCO_2$	Year	$MtCO_2$	Year	$MtCO_2$	Year	$MtCO_2$	Year	$MtCO_2$	Year	$MtCO_2$
1960	0.010992	1970	0.014656	1980	0.040304	1990	0.047632	2000	0.047632	2010	0.098928
1961	0.010992	1971	0.010992	1981	0.043968	1991	0.047632	2001	0.051296	2011	0.10259
1962	0.010992	1972	0.010992	1982	0.047632	1992	0.047632	2002	0.058624	2012	0.11358
1963	0.007328	1973	0.014656	1983	0.05496	1993	0.047632	2003	0.065952	2013	0.11358
1964	0.010992	1974	0.01832	1984	0.051296	1994	0.047632	2004	0.07328	2014	0.11358
1965	0.010992	1975	0.01832	1985	0.05496	1995	0.047632	2005	0.076944	2015	0.11358
1966	0.010992	1976	0.029312	1986	0.051296	1996	0.047632	2006	0.084272	2016	0.12091
1967	0.010992	1977	0.029312	1987	0.051296	1997	0.047632	2007	0.084272	2017	0.12458
1968	0.014656	1978	0.032976	1988	0.047632	1998	0.047632	2008	0.084272	2018	0.12613
1969	0.014656	1979	0.032976	1989	0.047632	1999	0.047632	2009	0.0916	2019	0.12914

Saudi Arabia

Year	$MtCO_2$	Year	$MtCO_2$	Year	$MtCO_2$	Year	$MtCO_2$	Year	$MtCO_2$	Year	$MtCO_2$
1960	2.6744	1970	45.2513	1980	169.2398	1990	185.4853	2000	296.3533	2010	517.7159
1961	3.5683	1971	59.7566	1981	175.3034	1991	267.3862	2001	296.5749	2011	497.659
1962	6.25	1972	70.2817	1982	157.8914	1992	285.0741	2002	325.6812	2012	563.1795
1963	6.9388	1973	95.0535	1983	160.8347	1993	313.3274	2003	326.5171	2013	540.8052
1964	7.0412	1974	98.7018	1984	155.5102	1994	307.4732	2004	394.5849	2014	601.8959
1965	4.2163	1975	83.2608	1985	172.4185	1995	234.712	2005	395.8548	2015	645.4086
1966	6.4073	1976	101.4595	1986	204.6006	1996	258.2636	2006	431.292	2016	565.7507
1967	25.4855	1977	118.0703	1987	190.4437	1997	215.7967	2007	386.5071	2017	579.4166
1968	29.0791	1978	115.0243	1988	202.2477	1998	207.2305	2008	432.3364	2018	576.7578
1969	35.271	1979	138.0043	1989	203.4192	1999	225.9765	2009	465.8443	2019	582.1496

Senegal

Year	$MtCO_2$	Year	$MtCO_2$	Year	$MtCO_2$	Year	$MtCO_2$	Year	$MtCO_2$	Year	$MtCO_2$
1960	0.82738	1970	1.3071	1980	3.3364	1990	3.139	2000	3.9009	2010	7.2801
1961	0.81267	1971	1.351	1981	3.2799	1991	3.378	2001	4.2577	2011	7.8193
1962	0.81267	1972	1.4532	1982	3.0366	1992	3.4234	2002	4.4369	2012	7.3629
1963	0.86027	1973	1.5487	1983	2.6114	1993	3.538	2003	4.9263	2013	7.8535
1964	0.9225	1974	1.849	1984	3.2842	1994	3.8367	2004	5.2377	2014	8.796
1965	1.692	1975	2.578	1985	2.6505	1995	3.429	2005	5.5396	2015	9.8463
1966	1.7176	1976	1.7697	1986	2.6364	1996	3.6632	2006	4.4218	2016	9.859
1967	0.69914	1977	2.2373	1987	2.4246	1997	3.1823	2007	4.8633	2017	9.3643
1968		1978	2.6196	1988	2.7108	1998	3.3331	2008	4.739	2018	9.6904
1969	0.49014	1979	2.8881	1989	3.6619	1999	3.6036	2009	4.713	2019	9.8227

Serbia

Year	$MtCO_2$	Year	$MtCO_2$	Year	$MtCO_2$	Year	$MtCO_2$	Year	$MtCO_2$	Year	$MtCO_2$
1960	15.3025	1970	30.962	1980	46.833	1990	56.4484	2000	44.9502	2010	45.6964
1961	16.0382	1971	33.3625	1981	50.9624	1991	39.9836	2001	49.2661	2011	48.9571
1962	16.4592	1972	31.2687	1982	46.7929	1992	43.6843	2002	52.147	2012	43.7245
1963	18.3108	1973	37.342	1983	50.383	1993	38.0957	2003	55.716	2013	44.5458
1964	20.7438	1974	37.4943	1984	53.1292	1994	37.0401	2004	60.212	2014	37.1891
1965	21.3437	1975	39.1106	1985	54.1876	1995	39.1408	2005	51.6341	2015	43.7471
1966	21.1519	1976	40.3541	1986	56.5792	1996	45.8247	2006	60.8614	2016	45.0357
1967	21.3669	1977	39.2283	1987	55.2231	1997	49.2646	2007	59.6302	2017	45.4827
1968	22.8559	1978	43.8209	1988	56.9738	1998	51.8821	2008	51.6801	2018	46.0531
1969	23.6988	1979	47.6476	1989	56.7923	1999	35.7907	2009	45.8582	2019	54.6667

Seychelles

Year	$MtCO_2$	Year	$MtCO_2$	Year	$MtCO_2$	Year	$MtCO_2$	Year	$MtCO_2$	Year	$MtCO_2$
1960		1970	0.029312	1980	0.095264	1990	0.15022	2000	0.57158	2010	0.44334
1961		1971	0.032976	1981	0.098928	1991	0.17221	2001	0.63387	2011	0.3261
1962		1972	0.043968	1982	0.084272	1992	0.17221	2002	0.53861	2012	0.42136
1963	0.007328	1973	0.047632	1983	0.098928	1993	0.1832	2003	0.5496	2013	0.32976
1964	0.007328	1974	0.05496	1984	0.098928	1994	0.20152	2004	0.73646	2014	0.48731
1965	0.007328	1975	0.058624	1985	0.15022	1995	0.19786	2005	0.68883	2015	0.47998
1966	0.007328	1976	0.080608	1986	0.16488	1996	0.2345	2006	0.7328	2016	0.59357
1967	0.007328	1977	0.084272	1987	0.20152	1997	0.34075	2007	0.6412	2017	0.58624
1968	0.007328	1978	0.076944	1988	0.19786	1998	0.43235	2008	0.6925	2018	0.60536
1969	0.007328	1979	0.12091	1989	0.2345	1999	0.5093	2009	0.52395	2019	0.62305

Sierra Leone

Year	$MtCO_2$	Year	$MtCO_2$	Year	$MtCO_2$	Year	$MtCO_2$	Year	$MtCO_2$	Year	$MtCO_2$
1960	0.71448	1970	0.85738	1980	0.60822	1990	0.53861	2000	0.38838	2010	0.57525
1961	0.28946	1971	0.80242	1981	0.6925	1991	0.6009	2001	0.4177	2011	0.74379
1962	0.3261	1972	0.67784	1982	0.55326	1992	0.45067	2002	0.53456	2012	0.86104
1963	0.37006	1973	0.53861	1983	0.68883	1993	0.45434	2003	0.56792	2013	1.0332
1964	0.30411	1974	0.52029	1984	0.61555	1994	0.47998	2004	0.55326	2014	1.1395
1965	0.28213	1975	0.52395	1985	0.66318	1995	0.24915	2005	0.46166	2015	0.90501
1966	0.30045	1976	0.45067	1986	0.67418	1996	0.29312	2006	0.61555	2016	0.93066
1967	0.25282	1977	0.51296	1987	0.4983	1997	0.2235	2007	0.51662	2017	0.93798
1968	0.36274	1978	0.71082	1988	0.458	1998	0.25648	2008	0.53494	2018	0.98756
1969	1.0845	1979	0.67784	1989	0.37373	1999	0.14656	2009	0.53494	2019	1.0271

Singapore

Year	$MtCO_2$	Year	$MtCO_2$	Year	$MtCO_2$	Year	$MtCO_2$	Year	$MtCO_2$	Year	$MtCO_2$
1960	1.3923	1970	18.1925	1980	31.3433	1990	44.2906	2000	48.8563	2010	56.6198
1961	2.0921	1971	16.5771	1981	26.7406	1991	45.0494	2001	49.4421	2011	30.272
1962	2.5753	1972	22.2181	1982	29.6058	1992	48.2127	2002	47.1727	2012	48.145
1963	3.3958	1973	21.1994	1983	34.8104	1993	50.8711	2003	49.4968	2013	54.3664
1964	3.6998	1974	21.9468	1984	33.2169	1994	61.3446	2004	46.8589	2014	55.2092
1965	2.5273	1975	24.5178	1985	33.2666	1995	41.8418	2005	36.4678	2015	62.1304
1966	0.67259	1976	29.9985	1986	34.8765	1996	49.3492	2006	43.0447	2016	40.2747
1967	3.0539	1977	28.2649	1987	32.4605	1997	58.0718	2007	47.5184	2017	39.0656
1968	5.4131	1978	33.1082	1988	35.9492	1998	48.3564	2008	57.5724	2018	38.2881
1969	7.1972	1979	36.0573	1989	41.7087	1999	49.8705	2009	90.0978	2019	38.9448

Slovakia

Year	$MtCO_2$	Year	$MtCO_2$	Year	$MtCO_2$	Year	$MtCO_2$	Year	$MtCO_2$	Year	$MtCO_2$
1960	31.6416	1970	49.3314	1980	59.1112	1990	61.6335	2000	41.2891	2010	38.5232
1961	34.3427	1971	51.7534	1981	58.4749	1991	53.4379	2001	43.3783	2011	38.112
1962	36.5977	1972	52.2334	1982	57.9094	1992	49.0291	2002	42.1124	2012	36.0212
1963	38.4981	1973	52.4515	1983	57.9966	1993	46.4842	2003	42.4381	2013	35.5778
1964	40.0659	1974	53.0645	1984	59.9588	1994	43.8787	2004	42.9247	2014	33.6545
1965	39.0398	1975	55.5274	1985	59.1478	1995	44.3224	2005	42.9109	2015	34.4842
1966	38.8198	1976	57.6949	1986	59.5624	1996	44.1861	2006	42.6873	2016	34.9218
1967	38.7391	1977	59.4281	1987	58.8684	1997	44.3137	2007	41.0951	2017	36.0873
1968	40.5304	1978	59.9753	1988	57.922	1998	44.0731	2008	41.5032	2018	36.0878
1969	43.0275	1979	58.4188	1989	55.2857	1999	43.2006	2009	37.7551	2019	33.3148

Slovenia

Year	$MtCO_2$	Year	$MtCO_2$	Year	$MtCO_2$	Year	$MtCO_2$	Year	$MtCO_2$	Year	$MtCO_2$
1960	4.3408	1970	8.7896	1980	13.2445	1990	15.0938	2000	15.4449	2010	16.3764
1961	4.551	1971	9.4667	1981	14.3972	1991	14.0012	2001	16.3783	2011	16.3603
1962	4.6695	1972	8.8601	1982	13.2097	1992	14.0067	2002	16.5253	2012	15.8218
1963	5.1945	1973	10.5855	1983	14.2263	1993	14.3035	2003	16.289	2013	15.1889
1964	5.8864	1974	10.6234	1984	15.004	1994	14.6427	2004	16.651	2014	13.5319
1965	6.0572	1975	11.0765	1985	15.3045	1995	15.2543	2005	16.9481	2015	13.6175
1966	6.0018	1976	11.4233	1986	15.983	1996	15.9166	2006	17.1425	2016	14.4167
1967	6.0631	1977	11.0963	1987	15.5792	1997	16.2449	2007	17.281	2017	14.2648
1968	6.4841	1978	12.3979	1988	16.147	1998	15.9611	2008	18.22	2018	14.4878
1969	6.7229	1979	13.4827	1989	16.067	1999	15.3372	2009	16.3298	2019	13.6964

Solomon Islands

Year	$MtCO_2$	Year	$MtCO_2$	Year	$MtCO_2$	Year	$MtCO_2$	Year	$MtCO_2$	Year	$MtCO_2$
1960	0.010992	1970	0.040304	1980	0.10259	1990	0.14656	2000	0.2235	2010	0.32976
1961	0.014656	1971	0.047632	1981	0.13557	1991	0.15755	2001	0.2345	2011	0.34442
1962	0.014656	1972	0.05496	1982	0.12091	1992	0.16122	2002	0.24549	2012	0.34808
1963	0.014656	1973	0.065952	1983	0.1429	1993	0.17221	2003	0.25648	2013	0.37373
1964	0.01832	1974	0.065952	1984	0.1429	1994	0.1832	2004	0.2748	2014	0.32976
1965	0.025648	1975	0.058624	1985	0.15022	1995	0.19053	2005	0.28213	2015	0.29312
1966	0.025648	1976	0.062288	1986	0.15389	1996	0.19786	2006	0.28946	2016	0.28946
1967	0.032976	1977	0.080608	1987	0.16122	1997	0.20518	2007	0.30045	2017	0.28579
1968	0.03664	1978	0.062288	1988	0.15755	1998	0.21618	2008	0.30778	2018	0.29848
1969	0.03664	1979	0.10992	1989	0.16122	1999	0.21618	2009	0.31877	2019	0.31799

Somalia

Year	$MtCO_2$	Year	$MtCO_2$	Year	$MtCO_2$	Year	$MtCO_2$	Year	$MtCO_2$	Year	$MtCO_2$
1960	0.084272	1970	0.21618	1980	0.81341	1990	0.72957	2000	0.47998	2010	0.61189
1961	0.087936	1971	0.18686	1981	0.2748	1991	0.7065	2001	0.50197	2011	0.61189
1962	0.10626	1972	0.2345	1982	0.71814	1992	0.67954	2002	0.58624	2012	0.60822
1963	0.10259	1973	0.26381	1983	0.93432	1993	0.63922	2003	0.59357	2013	0.63021
1964	0.13557	1974	0.32976	1984	0.71448	1994	0.62822	2004	0.59357	2014	0.63021
1965	0.1319	1975	0.50197	1985	0.85738	1995	0.5879	2005	0.59357	2015	0.63021
1966	0.13923	1976	0.47998	1986	0.92333	1996	0.56792	2006	0.59357	2016	0.63754
1967	0.22717	1977	0.79875	1987	0.99294	1997	0.53861	2007	0.60822	2017	0.63754
1968	0.15389	1978	0.55693	1988	1.0037	1998	0.51296	2008	0.6009	2018	0.65833
1969	0.16122	1979	0.48731	1989	0.95207	1999	0.49098	2009	0.59723	2019	0.67757

South Africa

Year	$MtCO_2$	Year	$MtCO_2$	Year	$MtCO_2$	Year	$MtCO_2$	Year	$MtCO_2$	Year	$MtCO_2$
1960	97.8435	1970	149.6182	1980	228.2175	1990	312.9722	2000	378.254	2010	466.93
1961	102.119	1971	168.4051	1981	257.0996	1991	326.0689	2001	371.516	2011	473.949
1962	105.67	1972	171.5569	1982	280.4596	1992	301.3682	2002	356.357	2012	461.139
1963	109.725	1973	173.3578	1983	291.9301	1993	320.3899	2003	404.173	2013	455.865
1964	119.546	1974	176.5523	1984	315.6243	1994	338.6248	2004	449.078	2014	481.884
1965	128.14	1975	185.011	1985	323.8902	1995	361.6414	2005	415.924	2015	451.590
1966	128.234	1976	192.9166	1986	330.5265	1996	363.6731	2006	446.622	2016	460.043
1967	133.760	1977	199.7472	1987	328.696	1997	385.4583	2007	464.800	2017	466.103
1968	137.953	1978	201.8908	1988	342.6964	1998	377.3122	2008	494.642	2018	472.001
1969	143.142	1979	218.6841	1989	340.7527	1999	374.8301	2009	502.259	2019	478.608

South Korea

Year	$MtCO_2$	Year	$MtCO_2$	Year	$MtCO_2$	Year	$MtCO_2$	Year	$MtCO_2$	Year	$MtCO_2$
1960	12.5401	1970	53.7164	1980	134.8886	1990	247.4382	2000	445.4407	2010	565.9608
1961	14.4487	1971	58.5498	1981	139.7775	1991	262.0383	2001	448.5506	2011	588.4039
1962	17.2616	1972	60.2773	1982	141.9832	1992	282.1943	2002	463.628	2012	583.6319
1963	21.0832	1973	73.0319	1983	151.0378	1993	321.8378	2003	462.4073	2013	591.5399
1964	22.1952	1974	75.6331	1984	164.0488	1994	344.2638	2004	478.6058	2014	586.5479
1965	24.9783	1975	81.784	1985	178.4848	1995	373.9924	2005	459.3457	2015	595.3939
1966	29.9822	1976	93.2708	1986	182.6718	1996	401.5296	2006	465.6059	2016	617.9601
1967	35.1132	1977	105.6916	1987	192.9399	1997	427.7861	2007	493.3534	2017	620.61
1968	37.1971	1978	113.4017	1988	222.3078	1998	363.5483	2008	505.7826	2018	634.9341
1969	42.4682	1979	133.2189	1989	236.2482	1999	398.3253	2009	506.7644	2019	611.2632

Spain

Year	$MtCO_2$	Year	$MtCO_2$	Year	$MtCO_2$	Year	$MtCO_2$	Year	$MtCO_2$	Year	$MtCO_2$
1960	48.8656	1970	116.7665	1980	213.9115	1990	231.2136	2000	311.267	2010	283.725
1961	53.6069	1971	128.4585	1981	206.0957	1991	240.953	2001	313.1198	2011	284.5438
1962	59.9758	1972	144.7162	1982	208.598	1992	249.8132	2002	333.3795	2012	278.8507
1963	58.7429	1973	154.9572	1983	203.4345	1993	241.1952	2003	337.5889	2013	252.7638
1964	64.3238	1974	172.6656	1984	197.6667	1994	253.6614	2004	354.4856	2014	255.1002
1965	71.0205	1975	181.0534	1985	199.9308	1995	267.4167	2005	369.4921	2015	271.6873
1966	77.617	1976	197.7457	1986	189.1121	1996	254.7953	2006	360.5786	2016	260.7596
1967	86.394	1977	194.8288	1987	189.5075	1997	267.3064	2007	368.4327	2017	274.6713
1968	97.0172	1978	199.5135	1988	197.4572	1998	276.0216	2008	336.6242	2018	269.6543
1969	96.7369	1979	202.7462	1989	224.8846	1999	299.4987	2009	297.2412	2019	252.6832

Sudan

Year	$MtCO_2$	Year	$MtCO_2$	Year	$MtCO_2$	Year	$MtCO_2$	Year	$MtCO_2$	Year	$MtCO_2$
1960	1.2458	1970	4.4467	1980	3.427	1990	4.7689	2000	5.0554	2010	14.3976
1961	1.2694	1971	4.5641	1981	3.3299	1991	4.4665	2001	5.8171	2011	14.0169
1962	1.36	1972	4.927	1982	3.4989	1992	3.9893	2002	7.4179	2012	14.5387
1963	1.538	1973	4.9705	1983	3.571	1993	2.7463	2003	8.2846	2013	16.1755
1964	1.7027	1974	5.2053	1984	3.2016	1994	3.785	2004	10.4708	2014	16.6448
1965	2.2233	1975	3.8822	1985	3.7204	1995	3.9029	2005	10.0281	2015	20.1626
1966	2.4214	1976	3.4383	1986	3.8834	1996	4.0276	2006	10.9837	2016	19.3113
1967	2.9185	1977	3.4844	1987	3.0612	1997	4.94	2007	12.9047	2017	21.7149
1968	2.8445	1978	3.1468	1988	4.4298	1998	4.2853	2008	13.6341	2018	22.3724
1969	3.832	1979	3.2669	1989	3.4308	1999	4.6452	2009	14.1889	2019	22.9807

Suriname

Year	$MtCO_2$	Year	$MtCO_2$	Year	$MtCO_2$	Year	$MtCO_2$	Year	$MtCO_2$	Year	$MtCO_2$
1960	0.43235	1970	1.6085	1980	2.3694	1990	1.738	2000	2.1918	2010	2.3954
1961	0.42869	1971	1.7145	1981	2.0283	1991	2.0238	2001	2.3634	2011	2.1796
1962	0.49464	1972	1.7438	1982	1.8706	1992	2.0311	2002	1.5606	2012	2.6364
1963	0.53128	1973	2.1066	1983	1.3721	1993	2.0384	2003	1.5383	2013	2.7449
1964	0.60456	1974	1.601	1984	1.552	1994	2.0417	2004	1.5564	2014	2.8361
1965	0.79509	1975	2.0187	1985	1.5959	1995	2.06	2005	1.589	2015	2.7328
1966	1.0955	1976	1.9965	1986	1.7569	1996	2.082	2006	1.7391	2016	2.3261
1967	1.3337	1977	1.8975	1987	1.7568	1997	2.1039	2007	1.7569	2017	2.5203
1968	1.4509	1978	2.3919	1988	1.8739	1998	2.1039	2008	1.9357	2018	2.5518
1969	1.5206	1979	2.2928	1989	1.8518	1999	2.1222	2009	1.9953	2019	2.606

Swaziland

Year	$MtCO_2$	Year	$MtCO_2$	Year	$MtCO_2$	Year	$MtCO_2$	Year	$MtCO_2$	Year	$MtCO_2$
1960	0.032976	1970	0.3664	1980	0.46533	1990	0.96363	2000	1.2128	2010	1.0149
1961	0.003664	1971	0.39938	1981	0.43602	1991	0.8757	2001	1.0955	2011	1.0259
1962		1972	0.38106	1982	0.43602	1992	0.83539	2002	1.0809	2012	1.1908
1963		1973	0.37006	1983	0.27114	1993	0.71082	2003	1.0039	2013	1.5462
1964	0.010992	1974	0.31144	1984	0.33342	1994	1.0809	2004	1.0003	2014	0.90134
1965	0.080608	1975	0.33709	1985	0.43968	1995	1.0626	2005	1.0149	2015	0.97829
1966	0.20152	1976	0.33342	1986	0.458	1996	0.79142	2006	1.0149	2016	1.1798
1967	0.22717	1977	0.34075	1987	0.43602	1997	1.1468	2007	1.0516	2017	0.98562
1968	0.27846	1978	0.43968	1988	0.43602	1998	1.1652	2008	1.0332	2018	0.98795
1969	0.30411	1979	0.44701	1989	0.43602	1999	1.2421	2009	1.0736	2019	0.97385

Sweden

Year	$MtCO_2$	Year	$MtCO_2$	Year	$MtCO_2$	Year	$MtCO_2$	Year	$MtCO_2$	Year	$MtCO_2$
1960	49.1705	1970	92.287	1980	71.7142	1990	57.3488	2000	54.6844	2010	53.0422
1961	48.7995	1971	84.509	1981	69.3891	1991	57.7072	2001	55.6171	2011	49.1669
1962	51.2726	1972	84.7034	1982	62.2574	1992	57.4515	2002	56.5725	2012	46.692
1963	55.3131	1973	87.2898	1983	58.269	1993	57.4934	2003	57.1606	2013	45.0863
1964	60.3681	1974	79.8231	1984	57.3088	1994	59.9538	2004	56.4759	2014	43.3376
1965	62.5622	1975	80.7605	1985	62.3647	1995	59.3662	2005	53.8529	2015	43.3368
1966	72.5174	1976	88.2412	1986	62.0105	1996	63.3028	2006	53.6743	2016	42.9726
1967	68.9297	1977	85.7408	1987	59.6956	1997	58.2126	2007	52.9409	2017	42.3068
1968	77.606	1978	79.4769	1988	57.426	1998	58.6967	2008	50.856	2018	41.7662
1969	86.3811	1979	84.8691	1989	55.5218	1999	55.8202	2009	47.2311	2019	42.7666

Switzerland

Year	$MtCO_2$	Year	$MtCO_2$	Year	$MtCO_2$	Year	$MtCO_2$	Year	$MtCO_2$	Year	$MtCO_2$
1960	19.4949	1970	40.2443	1980	40.49	1990	44.1544	2000	43.6176	2010	45.0496
1961	20.3573	1971	41.8879	1981	38.8117	1991	46.1338	2001	45.0824	2011	40.9855
1962	24.1197	1972	42.9158	1982	36.585	1992	46.0097	2002	43.4676	2012	42.2547
1963	29.0667	1973	46.2024	1983	40.0221	1993	43.601	2003	44.6519	2013	43.1858
1964	28.1257	1974	41.4268	1984	39.1279	1994	42.6759	2004	45.2364	2014	39.2344
1965	30.3289	1975	39.0511	1985	39.78	1995	43.4128	2005	45.7882	2015	38.7332
1966	31.4856	1976	40.4371	1986	42.2456	1996	44.0988	2006	45.3737	2016	39.1926
1967	32.5194	1977	41.0377	1987	40.2041	1997	43.0373	2007	43.3684	2017	38.1823
1968	35.9813	1978	42.1698	1988	40.6612	1998	44.6148	2008	44.7143	2018	36.8955
1969	38.047	1979	39.8645	1989	39.4176	1999	44.4458	2009	43.5347	2019	37.6815

Syria

Year	$MtCO_2$	Year	$MtCO_2$	Year	$MtCO_2$	Year	$MtCO_2$	Year	$MtCO_2$	Year	$MtCO_2$
1960	3.2187	1970	6.6499	1980	20.7267	1990	37.0453	2000	50.4815	2010	60.7164
1961	3.0609	1971	8.8742	1981	26.5346	1991	42.2007	2001	48.1407	2011	56.1393
1962	3.1999	1972	7.7563	1982	24.3644	1992	42.5611	2002	38.4386	2012	43.7901
1963	3.6063	1973	7.8852	1983	27.7745	1993	45.2217	2003	53.5814	2013	35.809
1964	4.3613	1974	9.6544	1984	32.849	1994	46.1898	2004	50.3846	2014	30.112
1965	3.6723	1975	11.1712	1985	29.3894	1995	41.2002	2005	49.8808	2015	28.6755
1966	4.9109	1976	13.7371	1986	31.0732	1996	42.3223	2006	52.8404	2016	28.5082
1967	4.6032	1977	14.6324	1987	35.9429	1997	45.3772	2007	65.7185	2017	26.4014
1968	5.9539	1978	15.1814	1988	36.6791	1998	49.7575	2008	66.8774	2018	25.8777
1969	7.2326	1979	22.4846	1989	34.2713	1999	51.7714	2009	61.5622	2019	26.9607

Taiwan

Year	$MtCO_2$	Year	$MtCO_2$	Year	$MtCO_2$	Year	$MtCO_2$	Year	$MtCO_2$	Year	$MtCO_2$
1960	11.8739	1970	28.734	1980	83.1194	1990	120.4397	2000	221.919	2010	264.819
1961	12.5285	1971	31.4754	1981	74.567	1991	130.616	2001	224.030	2011	266.485
1962	14.1648	1972	35.8725	1982	74.854	1992	139.1358	2002	235.360	2012	255.476
1963	15.1086	1973	40.2464	1983	82.4673	1993	152.1717	2003	241.630	2013	257.707
1964	16.9072	1974	39.3118	1984	84.1396	1994	157.8755	2004	250.259	2014	261.243
1965	17.8448	1975	43.4569	1985	83.9175	1995	165.6482	2005	255.803	2015	257.156
1966	19.4616	1976	56.0537	1986	93.411	1996	173.7284	2006	248.964	2016	265.283
1967	21.9699	1977	61.0163	1987	97.1234	1997	186.9362	2007	273.733	2017	272.450
1968	24.1406	1978	70.8362	1988	111.8178	1998	197.6516	2008	260.072	2018	273.104
1969	26.291	1979	75.4992	1989	121.6922	1999	205.3138	2009	246.906	2019	262.639

Tajikistan

Year	$MtCO_2$	Year	$MtCO_2$	Year	$MtCO_2$	Year	$MtCO_2$	Year	$MtCO_2$	Year	$MtCO_2$
1960	4.068	1970	6.6257	1980	9.8	1990	10.1331	2000	2.2321	2010	2.5104
1961	4.1953	1971	7.0323	1981	9.614	1991	9.1224	2001	2.2855	2011	2.3164
1962	4.4033	1972	7.4003	1982	9.795	1992	7.2946	2002	1.8729	2012	2.9041
1963	4.7223	1973	7.7143	1983	9.9345	1993	5.1614	2003	2.0622	2013	2.8692
1964	5.0222	1974	8.0097	1984	10.0229	1994	2.3474	2004	2.5473	2014	4.4855
1965	5.3276	1975	8.421	1985	10.8086	1995	2.4429	2005	2.4212	2015	5.1628
1966	5.6264	1976	8.7449	1986	10.8369	1996	2.8225	2006	2.6341	2016	6.3054
1967	5.8833	1977	9.0421	1987	10.7925	1997	2.1489	2007	3.2043	2017	6.8727
1968	6.0486	1978	9.3523	1988	11.0807	1998	2.4944	2008	2.8816	2018	7.4733
1969	6.2993	1979	9.4292	1989	10.8333	1999	2.5155	2009	2.431	2019	8.9799

Tanzania

Year	$MtCO_2$	Year	$MtCO_2$	Year	$MtCO_2$	Year	$MtCO_2$	Year	$MtCO_2$	Year	$MtCO_2$
1960	0.82806	1970	1.7654	1980	1.8736	1990	2.111	2000	2.5709	2010	6.9249
1961	0.70349	1971	2.4615	1981	2.1068	1991	2.2536	2001	3.0396	2011	7.7521
1962	0.76578	1972	2.1645	1982	2.1483	1992	2.1763	2002	3.487	2012	9.0622
1963	0.80242	1973	3.1827	1983	2.1963	1993	2.425	2003	3.6862	2013	9.9081
1964	1.0332	1974	2.3035	1984	2.347	1994	2.0636	2004	4.2317	2014	9.9003
1965	1.1615	1975	2.2816	1985	2.3379	1995	2.4337	2005	5.3601	2015	10.6375
1966	1.3701	1976	2.786	1986	2.2776	1996	2.5275	2006	5.879	2016	10.5353
1967	1.7581	1977	2.0076	1987	2.3675	1997	2.823	2007	5.7103	2017	11.0186
1968	1.6518	1978	2.1973	1988	2.2717	1998	2.4815	2008	5.9154	2018	11.5019
1969	1.7947	1979	2.0628	1989	2.1616	1999	2.4579	2009	5.7709	2019	11.6263

Thailand

Year	$MtCO_2$	Year	$MtCO_2$	Year	$MtCO_2$	Year	$MtCO_2$	Year	$MtCO_2$	Year	$MtCO_2$
1960	3.7095	1970	15.3525	1980	39.9562	1990	87.9172	2000	170.697	2010	256.422
1961	4.1407	1971	19.2211	1981	37.8168	1991	96.7461	2001	182.484	2011	253.800
1962	5.0268	1972	21.8055	1982	37.6356	1992	106.0945	2002	192.054	2012	270.174
1963	5.5616	1973	24.4202	1983	42.1173	1993	121.2135	2003	203.237	2013	286.068
1964	7.4703	1974	24.2105	1984	45.5558	1994	134.5066	2004	218.514	2014	279.994
1965	7.4402	1975	24.3715	1985	48.2304	1995	156.6361	2005	224.346	2015	283.293
1966	9.4654	1976	28.7162	1986	49.2234	1996	173.7286	2006	227.716	2016	281.704
1967	12.1501	1977	32.0649	1987	56.3062	1997	179.0595	2007	230.761	2017	286.336
1968	17.0757	1978	34.947	1988	66.2029	1998	159.2394	2008	228.116	2018	292.453
1969	14.54	1979	36.5865	1989	77.7842	1999	166.1435	2009	243.279	2019	288.279

Timor-Leste

Year	$MtCO_2$	Year	$MtCO_2$	Year	$MtCO_2$	Year	$MtCO_2$	Year	$MtCO_2$	Year	$MtCO_2$
1960		1970		1980		1990		2000		2010	0.2345
1961		1971		1981		1991		2001		2011	0.24549
1962		1972		1982		1992		2002	0.16122	2012	0.29312
1963		1973		1983		1993		2003	0.16122	2013	0.44334
1964		1974		1984		1994		2004	0.17587	2014	0.51296
1965		1975		1985		1995		2005	0.17587	2015	0.50197
1966		1976		1986		1996		2006	0.17954	2016	0.49464
1967		1977		1987		1997		2007	0.1832	2017	0.4983
1968		1978		1988		1998		2008	0.20152	2018	0.52042
1969		1979		1989		1999		2009	0.22717	2019	8.9799

Togo

Year	$MtCO_2$	Year	$MtCO_2$	Year	$MtCO_2$	Year	$MtCO_2$	Year	$MtCO_2$	Year	$MtCO_2$
1960	0.065952	1970	0.2748	1980	0.7933	1990	0.97267	2000	1.3314	2010	2.5957
1961	0.0916	1971	0.3151	1981	0.7053	1991	1.0485	2001	1.1589	2011	2.5039
1962	0.087936	1972	0.40486	1982	0.81661	1992	1.0307	2002	1.3225	2012	2.2156
1963	0.10626	1973	0.41151	1983	0.62247	1993	1.0689	2003	1.8047	2013	2.1287
1964	0.1319	1974	0.39027	1984	0.6933	1994	1.0049	2004	1.7439	2014	2.2381
1965	0.1319	1975	0.31144	1985	0.65741	1995	1.1747	2005	1.7216	2015	2.6864
1966	0.17954	1976	0.32243	1986	0.84583	1996	1.2652	2006	1.5005	2016	3.0976
1967	0.19786	1977	0.46166	1987	0.92262	1997	0.87899	2007	1.5168	2017	3.0492
1968	0.19419	1978	0.35541	1988	0.96091	1998	1.29	2008	1.5228	2018	3.1673
1969	0.24182	1979	1.3813	1989	1.0214	1999	1.8504	2009	2.7408	2019	3.2614

Tonga

Year	$MtCO_2$	Year	$MtCO_2$	Year	$MtCO_2$	Year	$MtCO_2$	Year	$MtCO_2$	Year	$MtCO_2$
1960	0.01099	1970	0.025648	1980	0.040304	1990	0.076944	2000	0.09526	2010	0.11725
1961	0.01099	1971	0.01832	1981	0.047632	1991	0.095264	2001	0.08793	2011	0.10259
1962	0.01099	1972	0.021984	1982	0.043968	1992	0.069616	2002	0.10259	2012	0.10626
1963	0.01099	1973	0.025648	1983	0.047632	1993	0.084272	2003	0.11725	2013	0.11358
1964	0.01099	1974	0.021984	1984	0.047632	1994	0.0916	2004	0.10992	2014	0.11358
1965	0.01099	1975	0.032976	1985	0.047632	1995	0.095264	2005	0.11358	2015	0.12091
1966	0.01099	1976	0.029312	1986	0.047632	1996	0.076944	2006	0.12824	2016	0.12824
1967	0.01465	1977	0.029312	1987	0.05496	1997	0.098928	2007	0.11358	2017	0.15755
1968	0.01465	1978	0.03664	1988	0.069616	1998	0.087936	2008	0.12091	2018	0.16455
1969	0.01099	1979	0.040304	1989	0.069616	1999	0.10992	2009	0.1319	2019	0.1753

Trinidad and Tobago

Year	$MtCO_2$	Year	$MtCO_2$	Year	$MtCO_2$	Year	$MtCO_2$	Year	$MtCO_2$	Year	$MtCO_2$
1960	2.5787	1970	8.9904	1980	16.9194	1990	16.9825	2000	24.191	2010	46.9586
1961	4.5979	1971	8.0964	1981	17.2424	1991	16.9683	2001	26.57	2011	46.6787
1962	7.2321	1972	8.2355	1982	18.4052	1992	19.1042	2002	28.5906	2012	45.556
1963	1.3074	1973	9.3898	1983	16.2755	1993	17.4118	2003	32.2505	2013	45.2357
1964	3.7915	1974	10.042	1984	17.5044	1994	17.0232	2004	32.5742	2014	46.3448
1965	5.1911	1975	9.6133	1985	20.7231	1995	16.4602	2005	37.943	2015	45.121
1966	4.0515	1976	15.9108	1986	17.3548	1996	20.7683	2006	42.4141	2016	40.0521
1967	4.6342	1977	16.1593	1987	17.4891	1997	20.5602	2007	45.2356	2017	39.9678
1968	4.0369	1978	15.3119	1988	15.8331	1998	19.7511	2008	44.0949	2018	37.8656
1969	3.9012	1979	16.7071	1989	16.105	1999	22.4658	2009	44.2193	2019	37.8639

Tunisia

Year	$MtCO_2$	Year	$MtCO_2$	Year	$MtCO_2$	Year	$MtCO_2$	Year	$MtCO_2$	Year	$MtCO_2$
1960	1.7241	1970	3.7387	1980	9.4653	1990	13.1271	2000	19.6703	2010	27.1025
1961	1.7647	1971	4.2076	1981	9.8002	1991	15.3629	2001	20.5453	2011	25.5243
1962	1.7939	1972	4.7314	1982	9.4929	1992	14.8918	2002	20.5586	2012	26.3064
1963	1.9441	1973	4.8234	1983	11.2497	1993	16.3539	2003	20.9255	2013	26.8655
1964	2.7535	1974	5.3912	1984	11.4885	1994	15.7761	2004	21.9266	2014	27.8921
1965	2.4604	1975	5.5411	1985	11.8709	1995	15.5488	2005	22.2687	2015	29.2746
1966	2.8816	1976	5.8414	1986	11.9924	1996	16.5808	2006	22.6025	2016	29.0081
1967	3.0832	1977	6.7487	1987	11.6633	1997	16.7478	2007	23.6844	2017	29.62
1968	3.5923	1978	7.4779	1988	12.3768	1998	17.8085	2008	24.3334	2018	30.3571
1969	3.8521	1979	8.7503	1989	13.1404	1999	18.1202	2009	24.3216	2019	31.0129

Turkey

Year	$MtCO_2$	Year	$MtCO_2$	Year	$MtCO_2$	Year	$MtCO_2$	Year	$MtCO_2$	Year	$MtCO_2$
1960	16.7985	1970	42.5792	1980	75.2124	1990	151.5085	2000	229.790	2010	314.38
1961	17.3408	1971	47.6382	1981	79.1862	1991	157.982	2001	213.486	2011	339.482
1962	21.6045	1972	53.7219	1982	86.2102	1992	163.9222	2002	220.977	2012	353.666
1963	22.6399	1973	59.31	1983	89.8124	1993	171.0112	2003	236.483	2013	345.220
1964	26.303	1974	60.9287	1984	94.9063	1994	167.4331	2004	244.464	2014	361.675
1965	27.353	1975	65.4194	1985	105.6626	1995	180.903	2005	264.200	2015	381.331
1966	31.5058	1976	73.3595	1986	115.6182	1996	199.5219	2006	281.649	2016	401.239
1967	33.4791	1977	81.1208	1987	128.4426	1997	212.0056	2007	312.736	2017	425.329
1968	36.2655	1978	76.714	1988	124.728	1998	212.0403	2008	309.321	2018	419.194
1969	38.7527	1979	75.038	1989	137.5705	1999	207.8042	2009	315.359	2019	405.126

Turkmenistan

Year	$MtCO_2$	Year	$MtCO_2$	Year	$MtCO_2$	Year	$MtCO_2$	Year	$MtCO_2$	Year	$MtCO_2$
1960	16.5798	1970	26.997	1980	39.8942	1990	41.1621	2000	37.4656	2010	57.1089
1961	17.098	1971	28.6526	1981	39.1318	1991	35.6167	2001	37.9998	2011	62.1823
1962	17.9449	1972	30.1513	1982	39.8646	1992	31.9954	2002	39.8896	2012	64.5329
1963	19.2437	1973	31.4303	1983	40.4271	1993	27.5175	2003	44.5201	2013	66.3741
1964	20.4647	1974	32.6331	1984	40.7827	1994	33.4425	2004	46.4471	2014	68.0321
1965	21.7093	1975	34.3083	1985	43.9769	1995	33.9322	2005	48.2316	2015	70.231
1966	22.9266	1976	35.621	1986	44.0842	1996	30.6037	2006	49.3721	2016	70.1638
1967	23.9727	1977	36.8252	1987	43.901	1997	30.5559	2007	55.8901	2017	70.1931
1968	24.6456	1978	38.082	1988	45.0702	1998	32.025	2008	56.6657	2018	78.0347
1969	25.6661	1979	38.3901	1989	44.0591	1999	37.605	2009	50.1707	2019	85.6465

Turks and Caicos Islands

Year	$MtCO_2$	Year	$MtCO_2$	Year	$MtCO_2$	Year	$MtCO_2$	Year	$MtCO_2$	Year	$MtCO_2$
1960		1970		1980		1990	0.029312	2000	0.069616	2010	0.1832
1961		1971		1981		1991	0.029312	2001	0.07328	2011	0.1832
1962		1972		1982		1992	0.032976	2002	0.098928	2012	0.1832
1963		1973		1983		1993	0.040304	2003	0.10259	2013	0.18686
1964		1974		1984		1994	0.043968	2004	0.10259	2014	0.19786
1965		1975		1985		1995	0.047632	2005	0.12091	2015	0.20518
1966		1976		1986		1996	0.047632	2006	0.1429	2016	0.21618
1967		1977		1987		1997	0.05496	2007	0.16488	2017	0.23083
1968		1978		1988		1998	0.058624	2008	0.17221	2018	0.2377
1969		1979		1989		1999	0.065952	2009	0.17954	2019	0.23147

Tuvalu

Year	$MtCO_2$	Year	$MtCO_2$	Year	$MtCO_2$	Year	$MtCO_2$	Year	$MtCO_2$	Year	$MtCO_2$
1960		1970		1980		1990	0.007328	2000	0.00732	2010	0.00732
1961		1971		1981		1991	0.007328	2001	0.00732	2011	0.00732
1962		1972		1982		1992	0.007328	2002	0.01099	2012	0.01092
1963		1973		1983		1993	0.007328	2003	0.01099	2013	0.01099
1964		1974		1984		1994	0.007328	2004	0.01099	2014	0.01099
1965		1975		1985		1995	0.007328	2005	0.01099	2015	0.01099
1966		1976		1986		1996	0.007328	2006	0.00732	2016	0.01099
1967		1977		1987		1997	0.007328	2007	0.01099	2017	0.01099
1968		1978		1988		1998	0.007328	2008	0.01099	2018	0.01148
1969		1979		1989		1999	0.007328	2009	0.01099	2019	0.01223

Uganda

Year	$MtCO_2$	Year	$MtCO_2$	Year	$MtCO_2$	Year	$MtCO_2$	Year	$MtCO_2$	Year	$MtCO_2$
1960	0.42106	1970	1.4428	1980	0.62602	1990	0.76171	2000	1.3608	2010	3.5696
1961	0.40644	1971	1.4377	1981	0.52704	1991	0.7803	2001	1.4175	2011	3.8241
1962	0.42845	1972	1.3784	1982	0.54469	1992	0.79827	2002	1.4461	2012	3.627
1963	0.43214	1973	1.1764	1983	0.61354	1993	0.79792	2003	1.5124	2013	3.7545
1964	0.49068	1974	1.1897	1984	0.58041	1994	0.70841	2004	1.6069	2014	4.097
1965	0.62601	1975	1.1286	1985	0.61691	1995	0.92648	2005	2.0179	2015	4.5219
1966	0.73232	1976	0.98537	1986	0.70185	1996	1.0179	2006	2.3834	2016	4.8051
1967	0.80918	1977	0.80195	1987	0.76857	1997	1.0607	2007	2.71	2017	5.2264
1968	0.98133	1978	0.69515	1988	0.86287	1998	1.2093	2008	2.7796	2018	5.3848
1969	1.1754	1979	0.67086	1989	0.80048	1999	1.254	2009	2.9998	2019	5.5313

Ukraine

Year	$MtCO_2$	Year	$MtCO_2$	Year	$MtCO_2$	Year	$MtCO_2$	Year	$MtCO_2$	Year	$MtCO_2$
1960	267.4304	1970	435.6509	1980	642.992	1990	705.83	2000	285.3372	2010	294.0783
1961	275.8111	1971	462.2622	1981	630.6241	1991	632.5366	2001	303.5592	2011	307.9528
1962	289.4974	1972	486.3162	1982	642.4406	1992	589.0603	2002	295.6735	2012	303.9526
1963	310.4692	1973	506.814	1983	651.4437	1993	510.1995	2003	307.0175	2013	297.2943
1964	330.1882	1974	526.0687	1984	657.1193	1994	419.2663	2004	310.3627	2014	257.5847
1965	350.2842	1975	552.9187	1985	708.6647	1995	389.8646	2005	313.1181	2015	223.9119
1966	369.9364	1976	574.0917	1986	710.3668	1996	351.4088	2006	332.6703	2016	234.2003
1967	386.8343	1977	593.5025	1987	707.3431	1997	340.2427	2007	336.364	2017	223.2322
1968	397.7108	1978	613.7679	1988	726.1392	1998	328.5789	2008	325.5327	2018	231.6942
1969	414.1898	1979	618.7449	1989	709.7377	1999	298.204	2009	277.2935	2019	223.2294

United Arab Emirates

Year	$MtCO_2$	Year	$MtCO_2$	Year	$MtCO_2$	Year	$MtCO_2$	Year	$MtCO_2$	Year	$MtCO_2$
1960	0.01099	1970	15.2349	1980	36.8234	1990	51.7026	2000	111.788	2010	155.977
1961	0.01099	1971	21.1669	1981	36.7669	1991	56.6723	2001	100.592	2011	169.174
1962	0.01832	1972	23.4349	1982	36.7528	1992	57.7577	2002	83.698	2012	217.361
1963	0.02198	1973	30.6054	1983	35.2205	1993	65.5654	2003	105.618	2013	221.836
1964	0.01832	1974	31.3016	1984	46.1556	1994	72.6046	2004	111.801	2014	215.906
1965	0.02198	1975	31.0451	1985	49.6525	1995	70.0127	2005	114.477	2015	239.670
1966	0.02564	1976	39.617	1986	47.0301	1996	72.7748	2006	121.737	2016	228.583
1967	0.916	1977	38.7513	1987	47.4504	1997	73.1007	2007	133.263	2017	186.623
1968	1.2421	1978	44.7536	1988	48.0956	1998	80.6825	2008	153.968	2018	188.541
1969	20.5074	1979	36.5465	1989	54.1861	1999	77.5426	2009	165.500	2019	190.683

United Kingdom

Year	$MtCO_2$	Year	$MtCO_2$	Year	$MtCO_2$	Year	$MtCO_2$	Year	$MtCO_2$	Year	$MtCO_2$
1960	584.02	1970	652.5774	1980	579.036	1990	600.4795	2000	567.5039	2010	512.0237
1961	588.6148	1971	660.3883	1981	560.555	1991	608.5792	2001	576.1954	2011	469.8038
1962	592.9315	1972	648.0264	1982	548.241	1992	593.0927	2002	560.3006	2012	487.7958
1963	603.3857	1973	659.5773	1983	545.4858	1993	578.8422	2003	571.7706	2013	477.901
1964	607.866	1974	617.1839	1984	529.1089	1994	575.1079	2004	573.2158	2014	439.0575
1965	622.1116	1975	603.2474	1985	559.6281	1995	566.8113	2005	569.9274	2015	422.4906
1966	618.0747	1976	598.5263	1986	568.5548	1996	588.4442	2006	567.5277	2016	399.1096
1967	592.057	1977	604.3621	1987	571.6685	1997	562.5613	2007	559.2488	2017	388.0884
1968	606.4883	1978	604.714	1988	570.2949	1998	567.8137	2008	544.812	2018	380.1386
1969	628.3825	1979	644.5133	1989	581.5773	1999	560.9515	2009	494.2942	2019	369.8784

United States of America

Year	$MtCO_2$	Year	$MtCO_2$	Year	$MtCO_2$	Year	$MtCO_2$	Year	$MtCO_2$	Year	$MtCO_2$
1960	2887.82	1970	4325.501	1980	4716.716	1990	5128.301	2000	5998.07	2010	5698.056
1961	2877.37	1971	4351.309	1981	4530.37	1991	5078.89	2001	5900.437	2011	5565.294
1962	2984.002	1972	4558.453	1982	4301.971	1992	5182.707	2002	5942.652	2012	5367.569
1963	3116.022	1973	4762.452	1983	4335.917	1993	5283.438	2003	5991.96	2013	5514.029
1964	3252.755	1974	4592.958	1984	4468.262	1994	5377.033	2004	6107.618	2014	5561.719
1965	3388.193	1975	4400.795	1985	4484.338	1995	5438.906	2005	6131.893	2015	5412.432
1966	3559.179	1976	4607.168	1986	4487.856	1996	5626.912	2006	6051.051	2016	5292.268
1967	3693.298	1977	4735.366	1987	4680.834	1997	5703.707	2007	6128.43	2017	5253.606
1968	3828.306	1978	4882.964	1988	4885.591	1998	5751.052	2008	5930.54	2018	5424.882
1969	4021.503	1979	4894.043	1989	4948.021	1999	5830.298	2009	5491.036	2019	5284.697

Uruguay

Year	$MtCO_2$	Year	$MtCO_2$	Year	$MtCO_2$	Year	$MtCO_2$	Year	$MtCO_2$	Year	$MtCO_2$
1960	4.3145	1970	5.7358	1980	5.8185	1990	3.9671	2000	5.2671	2010	6.2967
1961	4.1168	1971	5.8019	1981	5.356	1991	4.5275	2001	5.0306	2011	7.6538
1962	4.0069	1972	6.0694	1982	4.8538	1992	5.1429	2002	4.5577	2012	8.5931
1963	4.3148	1973	5.7687	1983	3.8035	1993	4.4392	2003	4.5279	2013	7.4935
1964	4.5527	1974	5.677	1984	3.4382	1994	4.0299	2004	5.5638	2014	6.6563
1965	5.5163	1975	5.9624	1985	3.2838	1995	4.5585	2005	5.7258	2015	6.6552
1966	5.3988	1976	5.8871	1986	3.1649	1996	5.4044	2006	6.5961	2016	6.5253
1967	4.8788	1977	5.6396	1987	3.5425	1997	5.5132	2007	5.9465	2017	6.1735
1968	4.8784	1978	5.7293	1988	4.786	1998	5.6401	2008	8.2007	2018	6.2518
1969	5.5894	1979	6.2624	1989	4.8526	1999	6.681	2009	7.9473	2019	6.3781

Uzbekistan

Year	$MtCO_2$	Year	$MtCO_2$	Year	$MtCO_2$	Year	$MtCO_2$	Year	$MtCO_2$	Year	$MtCO_2$
1960	44.5398	1970	72.5449	1980	106.6222	1990	109.9389	2000	120.994	2010	103.3433
1961	45.9351	1971	76.93	1981	104.5426	1991	112.7555	2001	122.5864	2011	112.8219
1962	48.2136	1972	80.8919	1982	106.4895	1992	110.9843	2002	127.5183	2012	114.924
1963	51.7042	1973	84.2586	1983	107.948	1993	115.6172	2003	125.936	2013	109.3234
1964	54.9859	1974	87.4163	1984	108.8654	1994	107.98	2004	125.1182	2014	103.4952
1965	58.3315	1975	91.8339	1985	117.3962	1995	102.6637	2005	116.5762	2015	101.7913
1966	61.6035	1976	95.3138	1986	117.6026	1996	105.546	2006	119.3649	2016	105.2219
1967	64.416	1977	98.499	1987	117.0915	1997	106.6296	2007	119.1132	2017	109.2815
1968	66.2253	1978	101.8351	1988	120.1952	1998	118.4989	2008	123.0388	2018	113.9384
1969	68.9679	1979	102.6365	1989	117.4423	1999	121.7392	2009	106.2518	2019	110.246

Vanuatu

Year	$MtCO_2$	Year	$MtCO_2$	Year	$MtCO_2$	Year	$MtCO_2$	Year	$MtCO_2$	Year	$MtCO_2$
1960		1970	0.040304	1980	0.062288	1990	0.065952	2000	0.084272	2010	0.12091
1961		1971	0.058624	1981	0.051296	1991	0.065952	2001	0.087936	2011	0.1319
1962	0.040304	1972	0.062288	1982	0.051296	1992	0.062288	2002	0.084272	2012	0.11358
1963	0.032976	1973	0.05496	1983	0.05496	1993	0.062288	2003	0.084272	2013	0.10626
1964	0.062288	1974	0.062288	1984	0.05496	1994	0.062288	2004	0.058624	2014	0.15389
1965	0.047632	1975	0.05496	1985	0.12091	1995	0.065952	2005	0.058624	2015	0.1319
1966	0.076944	1976	0.043968	1986	0.058624	1996	0.084272	2006	0.047632	2016	0.14656
1967	0.084272	1977	0.051296	1987	0.047632	1997	0.084272	2007	0.098928	2017	0.13923
1968	0.062288	1978	0.058624	1988	0.065952	1998	0.080608	2008	0.095264	2018	0.14541
1969	0.043968	1979	0.062288	1989	0.062288	1999	0.084272	2009	0.12091	2019	0.15492

Venezuela

Year	$MtCO_2$	Year	$MtCO_2$	Year	$MtCO_2$	Year	$MtCO_2$	Year	$MtCO_2$	Year	$MtCO_2$
1960	57.0168	1970	74.4894	1980	90.6406	1990	121.822	2000	151.871	2010	184.083
1961	51.8798	1971	62.5002	1981	91.7916	1991	115.0525	2001	171.974	2011	170.400
1962	54.0561	1972	62.5141	1982	93.201	1992	105.5781	2002	192.746	2012	190.974
1963	56.1517	1973	66.4329	1983	92.9079	1993	123.9679	2003	191.456	2013	182.850
1964	56.55	1974	75.0576	1984	93.0029	1994	129.5309	2004	151.268	2014	184.136
1965	60.7296	1975	63.7504	1985	101.0265	1995	132.8747	2005	163.823	2015	170.899
1966	56.974	1976	57.2734	1986	109.2398	1996	122.3396	2006	160.160	2016	163.190
1967	65.7524	1977	63.6501	1987	110.6611	1997	133.4835	2007	149.923	2017	146.673
1968	65.5721	1978	68.5914	1988	115.7518	1998	166.8022	2008	168.69	2018	129.596
1969	68.9332	1979	76.4474	1989	108.5711	1999	172.5625	2009	169.571	2019	116.687

Vietnam

Year	$MtCO_2$	Year	$MtCO_2$	Year	$MtCO_2$	Year	$MtCO_2$	Year	$MtCO_2$	Year	$MtCO_2$
1960	7.4839	1970	28.173	1980	16.7857	1990	21.1999	2000	52.3321	2010	136.1131
1961	7.9783	1971	24.5054	1981	17.6907	1991	21.2629	2001	59.5292	2011	145.0478
1962	9.3377	1972	23.0372	1982	18.3319	1992	21.3237	2002	68.6613	2012	135.6859
1963	9.1104	1973	25.0733	1983	19.2553	1993	22.7106	2003	76.277	2013	140.8932
1964	11.7878	1974	19.0646	1984	17.4744	1994	26.0186	2004	87.8002	2014	159.5828
1965	13.1499	1975	21.7797	1985	21.0685	1995	28.5235	2005	94.8591	2015	184.4356
1966	19.1811	1976	13.9049	1986	20.7513	1996	34.0229	2006	99.1304	2016	185.4322
1967	22.9622	1977	15.251	1987	24.096	1997	44.3092	2007	100.5773	2017	182.584
1968	23.6009	1978	15.389	1988	23.0087	1998	46.5548	2008	113.2445	2018	211.7741
1969	27.0556	1979	16.2484	1989	17.326	1999	46.658	2009	122.8329	2019	247.7089

Wallis and Futuna Islands

Year	$MtCO_2$	Year	$MtCO_2$	Year	$MtCO_2$	Year	$MtCO_2$	Year	$MtCO_2$	Year	$MtCO_2$
1960		1970		1980		1990		2000		2010	0.029312
1961		1971		1981		1991		2001	0.014656	2011	0.025648
1962		1972		1982		1992		2002	0.025648	2012	0.025648
1963		1973		1983		1993		2003	0.025648	2013	0.021984
1964		1974		1984		1994		2004	0.025648	2014	0.021984
1965		1975		1985		1995		2005	0.029312	2015	0.021984
1966		1976		1986		1996		2006	0.029312	2016	0.025648
1967		1977		1987		1997		2007	0.029312	2017	0.025648
1968		1978		1988		1998		2008	0.021984	2018	0.026786
1969		1979		1989		1999		2009	0.029312	2019	0.028538

Yemen

Year	$MtCO_2$	Year	$MtCO_2$	Year	$MtCO_2$	Year	$MtCO_2$	Year	$MtCO_2$	Year	$MtCO_2$
1960	3.631	1970	2.5098	1980	3.3135	1990	9.5214	2000	14.4742	2010	23.1519
1961	2.6637	1971	1.9712	1981	4.2254	1991	9.1286	2001	16.0167	2011	20.1907
1962	3.8838	1972	1.4949	1982	5.9336	1992	9.8742	2002	15.5535	2012	18.2675
1963	2.9165	1973	2.7296	1983	6.2856	1993	8.626	2003	17.0825	2013	24.9767
1964	3.631	1974	2.2458	1984	7.097	1994	8.9826	2004	18.6462	2014	24.1852
1965	3.9278	1975	2.1689	1985	8.5734	1995	10.3522	2005	19.7948	2015	13.0063
1966	3.4625	1976	2.5643	1986	8.192	1996	10.5269	2006	21.0851	2016	10.4258
1967	3.0521	1977	2.978	1987	8.6267	1997	11.316	2007	20.719	2017	10.1071
1968	11.6369	1978	3.1021	1988	9.5502	1998	12.0635	2008	22.025	2018	9.9453
1969	4.6753	1979	3.2185	1989	9.9351	1999	13.7247	2009	24.2512	2019	10.255

Zambia

Year	$MtCO_2$	Year	$MtCO_2$	Year	$MtCO_2$	Year	$MtCO_2$	Year	$MtCO_2$	Year	$MtCO_2$
1960	4.3553	1970	3.7659	1980	3.5233	1990	2.4058	2000	1.7851	2010	2.5626
1961	3.709	1971	3.7867	1981	3.358	1991	2.3821	2001	1.8849	2011	2.7814
1962	3.5827	1972	4.0614	1982	3.5108	1992	2.4241	2002	1.9601	2012	3.4891
1963	3.4445	1973	4.5857	1983	3.2608	1993	2.4672	2003	2.0756	2013	3.7561
1964	3.275	1974	4.1972	1984	2.8044	1994	2.393	2004	2.1043	2014	4.2557
1965	3.9123	1975	4.0762	1985	2.7327	1995	2.141	2005	2.2421	2015	4.2956
1966	3.4982	1976	4.0194	1986	2.8656	1996	1.837	2006	2.2317	2016	4.8378
1967	4.7876	1977	3.7349	1987	2.6738	1997	2.3537	2007	1.8676	2017	6.5196
1968	4.5676	1978	3.4709	1988	3.109	1998	2.2792	2008	2.1056	2018	6.9301
1969	4.2709	1979	3.5965	1989	2.57	1999	1.7782	2009	2.4063	2019	6.7205

Zimbabwe

Year	$MtCO_2$	Year	$MtCO_2$	Year	$MtCO_2$	Year	$MtCO_2$	Year	$MtCO_2$	Year	$MtCO_2$
1960	5.9431	1970	8.1541	1980	9.614	1990	15.5693	2000	13.8182	2010	7.8642
1961	5.0613	1971	8.7327	1981	9.4054	1991	15.8653	2001	12.5092	2011	9.4803
1962	4.889	1972	8.2158	1982	8.7799	1992	16.9174	2002	11.897	2012	7.6589
1963	4.7004	1973	9.2709	1983	10.4251	1993	16.2591	2003	10.6083	2013	11.6166
1964	4.4691	1974	9.047	1984	9.8796	1994	17.6845	2004	9.4286	2014	11.9726
1965	5.2092	1975	8.3109	1985	10.2137	1995	15.0294	2005	10.6996	2015	12.1705
1966	6.0409	1976	10.8549	1986	13.068	1996	14.8906	2006	10.3649	2016	10.8148
1967	5.2945	1977	9.2844	1987	15.1701	1997	14.2942	2007	9.834	2017	10.2468
1968	6.3777	1978	9.2797	1988	16.0295	1998	14.1396	2008	7.7189	2018	11.3406
1969	6.7439	1979	9.4317	1989	16.1137	1999	15.7277	2009	5.4759	2019	10.3743

Appendix 2: Region CO_2 Data

EU27

Year	$MtCO_2$	Year	$MtCO_2$	Year	$MtCO_2$	Year	$MtCO_2$	Year	$MtCO_2$	Year	$MtCO_2$
1960	2067.81	1970	3298.380	1980	4056.047	1990	3868.052	2000	3613.122	2010	3442.0
1961	2157.634	1971	3382.078	1981	3843.272	1991	3807.339	2001	3669.487	2011	3336.5
1962	2312.447	1972	3509.603	1982	3752.486	1992	3681.107	2002	3671.263	2012	3260.9
1963	2500.409	1973	3693.407	1983	3712.335	1993	3611.340	2003	3755.270	2013	3179.9
1964	2611.538	1974	3674.085	1984	3741.947	1994	3597.386	2004	3765.850	2014	3044.6
1965	2655.791	1975	3586.972	1985	3799.637	1995	3648.794	2005	3746.530	2015	3098.9
1966	2715.403	1976	3879.810	1986	3790.143	1996	3732.12	2006	3755.001	2016	3103.5
1967	2777.134	1977	3832.649	1987	3823.892	1997	3668.239	2007	3716.530	2017	3127.4
1968	2949.083	1978	3965.622	1988	3781.32	1998	3659.816	2008	3630.984	2018	3054.4
1969	3150.778	1979	4095.180	1989	3821.090	1999	3600.88	2009	3340.520	2019	2916.9

Canada

Year	$MtCO_2$	Year	$MtCO_2$	Year	$MtCO_2$	Year	$MtCO_2$	Year	$MtCO_2$	Year	$MtCO_2$
1960	192.72	1970	341.18	1980	442.82	1990	462.12	2000	572.16	2010	555.55
1961	194.00	1971	352.29	1981	429.60	1991	452.49	2001	564.95	2011	566.74
1962	206.99	1972	380.79	1982	414.43	1992	467.04	2002	570.84	2012	569.74
1963	210.91	1973	381.26	1983	408.31	1993	467.41	2003	587.18	2013	576.33
1964	237.58	1974	389.61	1984	425.20	1994	482.44	2004	585.70	2014	575.94
1965	251.92	1975	396.77	1985	421.68	1995	494.92	2005	576.43	2015	575.91
1966	259.07	1976	398.95	1986	404.66	1996	510.74	2006	570.95	2016	564.03
1967	281.64	1977	407.77	1987	430.92	1997	524.79	2007	594.22	2017	572.83
1968	303.26	1978	415.51	1988	455.61	1998	533.64	2008	575.59	2018	586.50
1969	307.12	1979	441.65	1989	462.82	1999	549.55	2009	542.55	2019	576.65

China

Year	$MtCO_2$	Year	$MtCO_2$	Year	$MtCO_2$	Year	$MtCO_2$	Year	$MtCO_2$	Year	$MtCO_2$
1960	778.98	1970	770.17	1980	1458.89	1990	2420.79	2000	3349.30	2010	8500.54
1961	550.96	1971	874.02	1981	1442.78	1991	2538.03	2001	3426.14	2011	9388.20
1962	439.34	1972	928.89	1982	1570.47	1992	2653.19	2002	3782.44	2012	9633.90
1963	435.52	1973	965.65	1983	1655.81	1993	2835.80	2003	4452.31	2013	9796.53
1964	435.70	1974	985.09	1984	1802.32	1994	3010.24	2004	5125.89	2014	9820.36
1965	474.68	1975	1142.10	1985	1951.77	1995	3265.06	2005	5771.17	2015	9683.20
1966	521.46	1976	1190.96	1986	2052.24	1996	3408.35	2006	6377.75	2016	9552.52
1967	432.22	1977	1304.40	1987	2191.05	1997	3414.55	2007	6861.75	2017	9750.73
1968	467.81	1978	1455.26	1988	2347.76	1998	3265.90	2008	7375.19	2018	9956.57
1969	575.94	1979	1487.11	1989	2386.89	1999	3258.14	2009	7758.81	2019	10174.68

India

Year	$MtCO_2$	Year	$MtCO_2$	Year	$MtCO_2$	Year	$MtCO_2$	Year	$MtCO_2$	Year	$MtCO_2$
1960	111.49	1970	181.95	1980	292.08	1990	578.68	2000	978.42	2010	1678.48
1961	120.58	1971	192.20	1981	315.36	1991	616.10	2001	992.52	2011	1766.07
1962	132.78	1972	203.29	1982	325.78	1992	656.22	2002	1022.84	2012	1941.31
1963	142.65	1973	209.35	1983	352.64	1993	678.11	2003	1059.41	2013	2033.40
1964	139.69	1974	216.13	1984	361.99	1994	717.12	2004	1125.26	2014	2184.44
1965	153.92	1975	234.51	1985	398.07	1995	762.33	2005	1185.75	2015	2253.43
1966	159.59	1976	245.07	1986	426.82	1996	826.15	2006	1259.52	2016	2392.36
1967	159.78	1977	259.29	1987	455.89	1997	859.92	2007	1357.91	2017	2456.85
1968	174.30	1978	263.48	1988	492.29	1998	877.93	2008	1462.57	2018	2591.32
1969	177.64	1979	276.62	1989	541.29	1999	951.67	2009	1612.51	2019	2616.45

Iran

Year	$MtCO_2$	Year	$MtCO_2$	Year	$MtCO_2$	Year	$MtCO_2$	Year	$MtCO_2$	Year	$MtCO_2$
1960	37.36	1970	91.79	1980	120.56	1990	209.24	2000	369.26	2010	564.03
1961	36.51	1971	101.63	1981	112.53	1991	225.95	2001	394.93	2011	579.04
1962	37.43	1972	106.02	1982	137.52	1992	226.96	2002	397.80	2012	600.68
1963	41.30	1973	129.48	1983	149.21	1993	235.58	2003	413.99	2013	608.71
1964	47.52	1974	143.78	1984	149.94	1994	263.52	2004	442.09	2014	641.92
1965	53.72	1975	139.21	1985	159.95	1995	271.15	2005	463.53	2015	640.81
1966	64.10	1976	156.46	1986	147.54	1996	274.01	2006	503.79	2016	648.06
1967	67.88	1977	163.73	1987	158.61	1997	267.10	2007	513.31	2017	724.58
1968	82.33	1978	162.10	1988	175.11	1998	306.01	2008	534.91	2018	755.40
1969	83.04	1979	163.67	1989	190.10	1999	379.63	2009	546.89	2019	779.53

Japan

Year	$MtCO_2$	Year	$MtCO_2$	Year	$MtCO_2$	Year	$MtCO_2$	Year	$MtCO_2$	Year	$MtCO_2$
1960	232.50	1970	767.96	1980	944.87	1990	1158.39	2000	1264.84	2010	1214.07
1961	282.79	1971	796.54	1981	926.84	1991	1170.07	2001	1250.21	2011	1264.16
1962	292.86	1972	852.17	1982	897.41	1992	1179.74	2002	1279.45	2012	1305.43
1963	324.84	1973	914.27	1983	880.91	1993	1172.65	2003	1287.64	2013	1314.70
1964	358.89	1974	914.31	1984	937.07	1994	1227.57	2004	1282.87	2014	1263.05
1965	386.47	1975	868.51	1985	912.40	1995	1239.93	2005	1290.06	2015	1222.78
1966	419.25	1976	907.15	1986	912.26	1996	1251.87	2006	1266.83	2016	1203.17
1967	489.31	1977	933.24	1987	902.53	1997	1245.11	2007	1302.52	2017	1187.66
1968	561.91	1978	901.59	1988	985.47	1998	1205.42	2008	1231.91	2018	1135.69
1969	653.22	1979	953.07	1989	1021.68	1999	1242.02	2009	1162.65	2019	1106.66

Russian Federation

Year	$MtCO_2$	Year	$MtCO_2$	Year	$MtCO_2$	Year	$MtCO_2$	Year	$MtCO_2$	Year	$MtCO_2$
1960	885.86	1970	1442.53	1980	2132.30	1990	2525.29	2000	1471.05	2010	1612.88
1961	913.53	1971	1530.89	1981	2091.65	1991	2395.98	2001	1507.50	2011	1664.95
1962	958.76	1972	1610.80	1982	2131.14	1992	1957.66	2002	1495.48	2012	1679.87
1963	1028.22	1973	1678.91	1983	2161.34	1993	1859.46	2003	1525.39	2013	1619.17
1964	1093.52	1974	1742.93	1984	2180.50	1994	1641.40	2004	1530.47	2014	1622.35
1965	1159.99	1975	1832.16	1985	2351.68	1995	1612.93	2005	1547.38	2015	1622.86
1966	1224.98	1976	1902.63	1986	2357.64	1996	1580.16	2006	1606.31	2016	1618.30
1967	1280.90	1977	1967.28	1987	2347.91	1997	1475.16	2007	1604.32	2017	1646.18
1968	1316.89	1978	2034.81	1988	2410.63	1998	1458.16	2008	1636.69	2018	1691.36
1969	1371.48	1979	2051.61	1989	2356.63	1999	1486.09	2009	1528.76	2019	1678.37

Saudi Arabia

Year	$MtCO_2$	Year	$MtCO_2$	Year	$MtCO_2$	Year	$MtCO_2$	Year	$MtCO_2$	Year	$MtCO_2$
1960	2.67	1970	45.25	1980	169.24	1990	185.49	2000	296.35	2010	517.72
1961	3.57	1971	59.76	1981	175.30	1991	267.39	2001	296.57	2011	497.66
1962	6.25	1972	70.28	1982	157.89	1992	285.07	2002	325.68	2012	563.18
1963	6.94	1973	95.05	1983	160.83	1993	313.33	2003	326.52	2013	540.81
1964	7.04	1974	98.70	1984	155.51	1994	307.47	2004	394.58	2014	601.90
1965	4.22	1975	83.26	1985	172.42	1995	234.71	2005	395.85	2015	645.41
1966	6.41	1976	101.46	1986	204.60	1996	258.26	2006	431.29	2016	565.75
1967	25.49	1977	118.07	1987	190.44	1997	215.80	2007	386.51	2017	579.42
1968	29.08	1978	115.02	1988	202.25	1998	207.23	2008	432.34	2018	576.76
1969	35.27	1979	138.00	1989	203.42	1999	225.98	2009	465.84	2019	582.15

South Korea

Year	$MtCO_2$	Year	$MtCO_2$	Year	$MtCO_2$	Year	$MtCO_2$	Year	$MtCO_2$	Year	$MtCO_2$
1960	12.54	1970	53.72	1980	134.89	1990	247.44	2000	445.44	2010	565.96
1961	14.45	1971	58.55	1981	139.78	1991	262.04	2001	448.55	2011	588.40
1962	17.26	1972	60.28	1982	141.98	1992	282.19	2002	463.63	2012	583.63
1963	21.08	1973	73.03	1983	151.04	1993	321.84	2003	462.41	2013	591.54
1964	22.20	1974	75.63	1984	164.05	1994	344.26	2004	478.61	2014	586.55
1965	24.98	1975	81.78	1985	178.48	1995	373.99	2005	459.35	2015	595.39
1966	29.98	1976	93.27	1986	182.67	1996	401.53	2006	465.61	2016	617.96
1967	35.11	1977	105.69	1987	192.94	1997	427.79	2007	493.35	2017	620.61
1968	37.20	1978	113.40	1988	222.31	1998	363.55	2008	505.78	2018	634.93
1969	42.47	1979	133.22	1989	236.25	1999	398.33	2009	506.76	2019	611.26

United States of America

Year	$MtCO_2$	Year	$MtCO_2$	Year	$MtCO_2$	Year	$MtCO_2$	Year	$MtCO_2$	Year	$MtCO_2$
1960	2887.82	1970	4325.50	1980	4716.72	1990	5128.30	2000	5998.07	2010	5698.06
1961	2877.37	1971	4351.31	1981	4530.37	1991	5078.89	2001	5900.44	2011	5565.29
1962	2984.00	1972	4558.45	1982	4301.97	1992	5182.71	2002	5942.65	2012	5367.57
1963	3116.02	1973	4762.45	1983	4335.92	1993	5283.44	2003	5991.96	2013	5514.03
1964	3252.76	1974	4592.96	1984	4468.26	1994	5377.03	2004	6107.62	2014	5561.72
1965	3388.19	1975	4400.80	1985	4484.34	1995	5438.91	2005	6131.89	2015	5412.43
1966	3559.18	1976	4607.17	1986	4487.86	1996	5626.91	2006	6051.05	2016	5292.27
1967	3693.30	1977	4735.37	1987	4680.83	1997	5703.71	2007	6128.43	2017	5253.61
1968	3828.31	1978	4882.96	1988	4885.59	1998	5751.05	2008	5930.54	2018	5424.88
1969	4021.50	1979	4894.04	1989	4948.02	1999	5830.30	2009	5491.04	2019	5284.70

Appendix 3: Landuse Emitted CO_2 Data

Canada

Year	$MtCO_2$	Year	$MtCO_2$	Year	$MtCO_2$	Year	$MtCO_2$	Year	$MtCO_2$	Year	$MtCO_2$
1960	111.5096	1970	148.5686	1980	168.1168	1990	96.6678	2000	53.04728	2010	36.56384
1961	110.3195	1971	146.3471	1981	156.491	1991	87.83631	2001	36.80386		
1962	146.9886	1972	143.1117	1982	125.2439	1992	256.0776	2002	40.59827		
1963	147.5292	1973	157.1652	1983	133.4731	1993	238.7394	2003	21.87173		
1964	148.4875	1974	148.5043	1984	132.411	1994	250.8148	2004	37.41198		
1965	147.9572	1975	131.0509	1985	130.1756	1995	238.6652	2005	27.823		
1966	151.1009	1976	147.2265	1986	133.3355	1996	217.8494	2006	7.19687		
1967	142.9784	1977	150.6898	1987	139.3646	1997	78.85656	2007	−46.2662		
1968	145.4964	1978	169.1143	1988	133.2929	1998	61.97786	2008	34.83124		
1969	149.271	1979	175.9101	1989	125.0358	1999	58.313	2009	10.0591		

Caribbean

Year	$MtCO_2$	Year	$MtCO_2$	Year	$MtCO_2$	Year	$MtCO_2$	Year	$MtCO_2$	Year	$MtCO_2$
1960	−7.3280	1970	−10.043	1980	−8.4996	1990	−12.532	2000	−10.428	2010	−6.7448
1961	−8.9030	1971	−10.836	1981	−9.2137	1991	−13.683	2001	−9.7767		
1962	−8.0595	1972	−9.6483	1982	−8.6822	1992	−13.203	2002	−11.325		
1963	−7.9850	1973	−7.9048	1983	−11.883	1993	−12.495	2003	−9.0106		
1964	−8.3999	1974	−7.0837	1984	−13.165	1994	−11.771	2004	−8.3712		
1965	−9.2273	1975	−7.0361	1985	−15.217	1995	−10.097	2005	−7.3969		
1966	−8.5263	1976	−8.5440	1986	−14.707	1996	−10.376	2006	−7.8399		
1967	−9.1324	1977	−8.1065	1987	−14.829	1997	−10.109	2007	−7.3178		
1968	−9.4438	1978	−7.7831	1988	−13.475	1998	−11.430	2008	−7.6148		
1969	−9.8281	1979	−7.8713	1989	−12.844	1999	−10.372	2009	−6.9302		

Central Africa

Year	$MtCO_2$	Year	$MtCO_2$	Year	$MtCO_2$	Year	$MtCO_2$	Year	$MtCO_2$	Year	$MtCO_2$
1960	287.0916	1970	367.6628	1980	440.3328	1990	275.9077	2000	231.4603	2010	216.7678
1961	295.7209	1971	373.9976	1981	440.378	1991	248.208	2001	233.0872		
1962	304.4915	1972	381.4084	1982	441.7183	1992	226.8864	2002	234.8051		
1963	313.287	1973	384.9074	1983	436.7021	1993	222.1003	2003	232.8186		
1964	321.8432	1974	389.8788	1984	434.3236	1994	221.385	2004	238.2913		
1965	329.1825	1975	392.2199	1985	433.8769	1995	228.8814	2005	231.8849		
1966	337.8154	1976	400.3122	1986	433.3929	1996	232.0794	2006	218.9309		
1967	343.4951	1977	409.0751	1987	434.0373	1997	233.8252	2007	216.7447		
1968	352.916	1978	419.6546	1988	434.4223	1998	237.0666	2008	217.4057		
1969	359.3403	1979	429.7364	1989	433.4435	1999	238.7709	2009	222.9565		

Central America & Mexico

Year	$MtCO_2$	Year	$MtCO_2$	Year	$MtCO_2$	Year	$MtCO_2$	Year	$MtCO_2$	Year	$MtCO_2$
1960	139.9749	1970	191.8401	1980	162.3546	1990	239.3857	2000	199.1995	2010	128.8346
1961	170.0605	1971	206.9909	1981	175.9949	1991	261.3767	2001	186.7487		
1962	153.9481	1972	184.2968	1982	165.8429	1992	252.2072	2002	216.3293		
1963	152.5259	1973	150.9922	1983	226.9913	1993	238.6796	2003	172.1157		
1964	160.4495	1974	135.3089	1984	251.4713	1994	224.8473	2004	159.9015		
1965	176.2547	1975	134.4005	1985	290.6787	1995	192.8838	2005	141.2917		
1966	162.8651	1976	163.2023	1986	280.9407	1996	198.1998	2006	149.7544		
1967	174.4421	1977	154.845	1987	283.2712	1997	193.1081	2007	139.7804		
1968	180.3908	1978	148.6684	1988	257.3955	1998	218.3389	2008	145.4535		
1969	187.7315	1979	150.3529	1989	245.3402	1999	198.1301	2009	132.3769		

China

Year	$MtCO_2$	Year	$MtCO_2$	Year	$MtCO_2$	Year	$MtCO_2$	Year	$MtCO_2$	Year	$MtCO_2$
1960	1301.469	1970	1003.436	1980	733.2899	1990	38.67776	2000	−175.56	2010	−392.84
1961	1212.751	1971	996.2703	1981	586.9446	1991	13.8337	2001	−198.36		
1962	1139.186	1972	991.8263	1982	426.687	1992	18.54561	2002	−199.72		
1963	1056.75	1973	991.685	1983	273.0062	1993	−9.92221	2003	−233.77		
1964	1046.165	1974	989.1953	1984	197.8541	1994	−34.9883	2004	−264.02		
1965	1040.017	1975	984.0672	1985	163.5712	1995	−52.2883	2005	−287.32		
1966	1035.99	1976	985.6086	1986	136.4352	1996	−79.9113	2006	−309.24		
1967	1024.403	1977	983.4649	1987	109.0148	1997	−108.372	2007	−336.32		
1968	1018.607	1978	979.2099	1988	78.66131	1998	−128.146	2008	−355.91		
1969	1007.137	1979	876.4331	1989	54.76264	1999	−156.206	2009	−371.93		

East Africa

Year	$MtCO_2$	Year	$MtCO_2$	Year	$MtCO_2$	Year	$MtCO_2$	Year	$MtCO_2$	Year	$MtCO_2$
1960	208.7558	1970	198.652	1980	197.4394	1990	195.6994	2000	204.7475	2010	231.6823
1961	202.0739	1971	195.88	1981	192.7348	1991	206.6904	2001	193.6534		
1962	200.8419	1972	194.219	1982	188.8142	1992	221.3689	2002	192.5755		
1963	203.4215	1973	198.2068	1983	165.1001	1993	223.6612	2003	191.2066		
1964	207.9323	1974	194.6678	1984	158.9484	1994	228.7265	2004	199.3893		
1965	211.3689	1975	192.083	1985	154.3716	1995	234.8444	2005	219.9266		
1966	217.7906	1976	185.1533	1986	164.8447	1996	233.761	2006	224.324		
1967	219.8113	1977	187.2258	1987	173.1308	1997	242.9125	2007	233.7096		
1968	210.9013	1978	187.9165	1988	172.1696	1998	246.6879	2008	238.6318		
1969	205.3923	1979	193.8322	1989	172.8522	1999	253.1955	2009	236.439		

East Asia

Year	$MtCO_2$	Year	$MtCO_2$	Year	$MtCO_2$	Year	$MtCO_2$	Year	$MtCO_2$	Year	$MtCO_2$
1960	205.4774	1970	95.29375	1980	−57.757	1990	−119.811	2000	−138.728	2010	−159.471
1961	208.5004	1971	82.23626	1981	−61.639	1991	−122.513	2001	−140.213		
1962	159.3653	1972	51.87068	1982	−56.029	1992	−106.045	2002	−156.215		
1963	149.2952	1973	33.05202	1983	−59.965	1993	−100.403	2003	−162.273		
1964	147.6063	1974	22.44609	1984	−69.679	1994	−114.984	2004	−180.282		
1965	143.7697	1975	6.99869	1985	−75.335	1995	−124.251	2005	−184.429		
1966	142.7913	1976	−3.73569	1986	−81.871	1996	−128.29	2006	−184.328		
1967	136.6745	1977	−12.7833	1987	−89.137	1997	−130.285	2007	−187.652		
1968	117.8209	1978	−41.3712	1988	−108.49	1998	−125.503	2008	−157.394		
1969	106.5218	1979	−53.0843	1989	−117.62	1999	−128.248	2009	−148.127		

Europe

Year	$MtCO_2$	Year	$MtCO_2$	Year	$MtCO_2$	Year	$MtCO_2$	Year	$MtCO_2$	Year	$MtCO_2$
1960	56.86995	1970	−63.917	1980	−172.416	1990	−191.43	2000	−224.51	2010	−177.08
1961	56.35432	1971	−78.507	1981	−179.299	1991	−198.85	2001	−233.64		
1962	44.36443	1972	−98.066	1982	−182.352	1992	−184.43	2002	−232.84		
1963	40.56378	1973	−113.31	1983	−203.684	1993	−181.90	2003	−233.25		
1964	36.27318	1974	−116.04	1984	−186.15	1994	−181.42	2004	−235.63		
1965	31.52016	1975	−127.21	1985	−184.415	1995	−171.90	2005	−223.27		
1966	−6.68417	1976	−144.62	1986	−187.524	1996	−200.74	2006	−226.21		
1967	−27.1936	1977	−146.59	1987	−190.812	1997	−215.67	2007	−216.89		
1968	−40.3983	1978	−149.47	1988	−192.498	1998	−223.90	2008	−206.67		
1969	−55.4365	1979	−166.01	1989	−188.935	1999	−225.99	2009	−199.26		

Former Soviet Union

Year	$MtCO_2$	Year	$MtCO_2$	Year	$MtCO_2$	Year	$MtCO_2$	Year	$MtCO_2$	Year	$MtCO_2$
1960	832.4753	1970	309.0015	1980	−66.8336	1990	−148.355	2000	−457.699	2010	−542.885
1961	832.1967	1971	241.0438	1981	−67.822	1991	−167.388	2001	−500.034		
1962	830.3992	1972	166.1196	1982	−70.6622	1992	−193.059	2002	−515.969		
1963	755.6475	1973	80.65412	1983	−83.9351	1993	−241.337	2003	−536.293		
1964	752.0623	1974	54.59198	1984	−87.1673	1994	−273.386	2004	−544.926		
1965	724.7718	1975	20.85037	1985	−91.7893	1995	−280.916	2005	−581.793		
1966	638.4171	1976	2.504408	1986	−104.658	1996	−333.449	2006	−582.484		
1967	539.5953	1977	−24.1119	1987	−104.345	1997	−346.388	2007	−591.483		
1968	467.4963	1978	−30.2837	1988	−113.075	1998	−393.463	2008	−585.465		
1969	388.7323	1979	−44.0209	1989	−139.944	1999	−415.688	2009	−569.498		

NonTropical S. America

Year	$MtCO_2$	Year	$MtCO_2$	Year	$MtCO_2$	Year	$MtCO_2$	Year	$MtCO_2$	Year	$MtCO_2$
1960	114.2005	1970	194.5151	1980	78.9072	1990	90.42623	2000	65.0324	2010	39.25102
1961	141.6073	1971	148.5825	1981	117.974	1991	84.68635	2001	79.20044		
1962	149.7063	1972	132.3288	1982	94.16229	1992	60.51096	2002	56.37597		
1963	154.6476	1973	133.7509	1983	127.5964	1993	64.12811	2003	63.24328		
1964	159.2674	1974	120.6891	1984	85.01628	1994	39.4136	2004	58.38676		
1965	166.8756	1975	112.7039	1985	116.4238	1995	60.67097	2005	74.85075		
1966	172.9506	1976	96.55293	1986	111.1867	1996	55.37957	2006	79.87461		
1967	178.0655	1977	74.67422	1987	112.513	1997	59.56483	2007	78.32954		
1968	189.6902	1978	69.40154	1988	106.4594	1998	37.68686	2008	16.41224		
1969	196.0294	1979	76.663	1989	100.4431	1999	53.03701	2009	41.51321		

North Africa & Middle East

Year	$MtCO_2$	Year	$MtCO_2$	Year	$MtCO_2$	Year	$MtCO_2$	Year	$MtCO_2$	Year	$MtCO_2$
1960	11.555	1970	5.075977	1980	−6.05844	1990	3.890567	2000	−9.9537	2010	−5.8048
1961	8.623399	1971	17.75142	1981	−2.3532	1991	3.237674	2001	−10.660		
1962	3.793679	1972	8.304109	1982	−1.99685	1992	13.25347	2002	−10.393		
1963	1.767472	1973	8.960305	1983	−3.51292	1993	11.53444	2003	−3.4611		
1964	1.937393	1974	4.734667	1984	2.705891	1994	5.228649	2004	−8.4083		
1965	5.497293	1975	5.124054	1985	−1.73408	1995	2.138509	2005	−8.6461		
1966	6.393874	1976	5.139468	1986	−0.92337	1996	3.403925	2006	−9.7185		
1967	5.552343	1977	1.746186	1987	1.234955	1997	−2.70699	2007	−12.347		
1968	3.533476	1978	0.407737	1988	−1.77848	1998	−3.57972	2008	−10.184		
1969	3.732023	1979	−4.10123	1989	3.527971	1999	−5.683	2009	−9.1217		

Oceania

Year	$MtCO_2$	Year	$MtCO_2$	Year	$MtCO_2$	Year	$MtCO_2$	Year	$MtCO_2$	Year	$MtCO_2$
1960	231.3803	1970	170.8535	1980	127.5171	1990	45.05696	2000	11.30654	2010	96.91736
1961	228.7353	1971	163.7084	1981	121.4267	1991	50.77665	2001	−2.99949		
1962	245.7263	1972	142.9762	1982	109.5469	1992	59.64117	2002	34.14935		
1963	250.2665	1973	130.7118	1983	101.8399	1993	55.76382	2003	39.52884		
1964	255.5043	1974	144.1704	1984	51.94445	1994	79.99793	2004	36.97598		
1965	256.6673	1975	139.3477	1985	37.55768	1995	81.34849	2005	33.92621		
1966	257.9823	1976	134.5727	1986	22.25928	1996	81.23765	2006	66.41416		
1967	251.9873	1977	120.2762	1987	20.28996	1997	77.02853	2007	65.20306		
1968	202.8989	1978	133.246	1988	19.31448	1998	65.01038	2008	83.23413		
1969	187.4089	1979	128.8526	1989	18.92105	1999	58.92992	2009	78.12549		

South Asia

Year	$MtCO_2$	Year	$MtCO_2$	Year	$MtCO_2$	Year	$MtCO_2$	Year	$MtCO_2$	Year	$MtCO_2$
1960	100.0937	1970	7.339266	1980	−12.102	1990	−47.8777	2000	−23.8884	2010	−73.7956
1961	98.33435	1971	1.86436	1981	−12.669	1991	−57.9574	2001	−28.3886		
1962	96.74487	1972	−3.56651	1982	−16.553	1992	−65.0687	2002	−36.7745		
1963	53.59741	1973	−9.38823	1983	−20.313	1993	−73.8532	2003	−47.0039		
1964	40.95647	1974	−15.0345	1984	−23.782	1994	−64.5604	2004	−60.5532		
1965	30.83094	1975	−12.0963	1985	−26.903	1995	−56.0339	2005	−56.3848		
1966	22.66409	1976	−11.3667	1986	−23.783	1996	−51.6828	2006	−61.198		
1967	19.6756	1977	−11.6963	1987	−26.993	1997	−31.039	2007	−72.1247		
1968	16.04744	1978	−8.93535	1988	−32.120	1998	−25.9161	2008	−70.9224		
1969	10.70172	1979	−11.035	1989	−35.618	1999	−21.388	2009	−74.3425		

Southeast Asia

Year	$MtCO_2$	Year	$MtCO_2$	Year	$MtCO_2$	Year	$MtCO_2$	Year	$MtCO_2$	Year	$MtCO_2$
1960	487.3268	1970	630.8576	1980	916.6001	1990	1230.001	2000	1907.158	2010	1164.185
1961	483.3405	1971	683.2274	1981	1003.639	1991	1412.26	2001	1893.909		
1962	453.2263	1972	703.3951	1982	1086.775	1992	1692.256	2002	2482.048		
1963	442.2526	1973	721.9	1983	1106.945	1993	1939.527	2003	1506.625		
1964	443.0274	1974	755.3095	1984	1146.693	1994	2249.312	2004	1475.699		
1965	474.6411	1975	730.4621	1985	1128.291	1995	2490.987	2005	1490.453		
1966	493.4421	1976	713.1522	1986	1043.388	1996	2601.024	2006	2357.698		
1967	543.1035	1977	737.964	1987	976.9074	1997	5920.389	2007	1045.493		
1968	585.2002	1978	790.6509	1988	1029.539	1998	2599.888	2008	1120.382		
1969	616.2337	1979	857.6996	1989	1067.395	1999	2029.166	2009	1515.536		

Southern Africa

Year	$MtCO_2$	Year	$MtCO_2$	Year	$MtCO_2$	Year	$MtCO_2$	Year	$MtCO_2$	Year	$MtCO_2$
1960	158.061	1970	219.7112	1980	264.0881	1990	284.7146	2000	291.082	2010	321.9996
1961	154.4384	1971	235.2455	1981	281.4824	1991	292.8521	2001	311.2142		
1962	167.3208	1972	244.6209	1982	273.6594	1992	308.3982	2002	326.1577		
1963	171.6756	1973	248.7038	1983	266.74	1993	304.9286	2003	365.8693		
1964	177.217	1974	256.6255	1984	259.7795	1994	310.6149	2004	377.7036		
1965	190.0348	1975	268.637	1985	255.3421	1995	323.9039	2005	399.9948		
1966	192.5047	1976	271.5815	1986	247.4318	1996	306.7988	2006	393.1777		
1967	196.4507	1977	278.2502	1987	249.9101	1997	304.4008	2007	377.9572		
1968	204.6649	1978	281.0141	1988	250.7072	1998	299.8852	2008	352.5688		
1969	213.1411	1979	278.4429	1989	254.5072	1999	289.4037	2009	337.9597		

Tropical S. America

Year	$MtCO_2$	Year	$MtCO_2$	Year	$MtCO_2$	Year	$MtCO_2$	Year	$MtCO_2$	Year	$MtCO_2$
1960	1350.744	1970	1795.862	1980	1284.542	1990	2107.146	2000	1576.328	2010	1269.565
1961	1343.977	1971	1819.265	1981	1289.31	1991	2172.687	2001	1494.054		
1962	1334.51	1972	1752.701	1982	1228.485	1992	2153.583	2002	1530.779		
1963	1524.797	1973	1507.329	1983	1210.761	1993	1795.117	2003	1481.419		
1964	1604.577	1974	1452.894	1984	1605.312	1994	1738.368	2004	1595.247		
1965	1613.251	1975	1432.227	1985	1906.159	1995	1594.538	2005	1481.575		
1966	1669.365	1976	1359.174	1986	2017.089	1996	1585.134	2006	1447.226		
1967	1755.21	1977	1320.703	1987	2044.318	1997	1539.826	2007	1395.328		
1968	1731.451	1978	1332.527	1988	1917.468	1998	1574.098	2008	1343.552		
1969	1806.265	1979	1277.165	1989	2007.195	1999	1527.5	2009	1291.378		

USA

Year	$MtCO_2$	Year	$MtCO_2$	Year	$MtCO_2$	Year	$MtCO_2$	Year	$MtCO_2$	Year	$MtCO_2$
1960	−98.9278	1970	49.40994	1980	105.4362	1990	1.214036	2000	−101.81	2010	−152.869
1961	−137.291	1971	−77.5258	1981	88.85914	1991	81.91073	2001	−100.12		
1962	−124.228	1972	−52.4204	1982	121.7772	1992	−21.8684	2002	−104.07		
1963	−137.445	1973	−104.211	1983	83.61545	1993	−45.7161	2003	−104.92		
1964	−154.726	1974	−101.117	1984	62.17164	1994	−72.6851	2004	−104.22		
1965	−133.428	1975	−57.3551	1985	45.25073	1995	−81.2641	2005	−108.52		
1966	−33.1012	1976	−19.7736	1986	52.96654	1996	−82.3276	2006	−113.42		
1967	−18.7214	1977	−1.04889	1987	50.21808	1997	−97.0168	2007	−117.24		
1968	−22.1631	1978	27.64611	1988	51.1576	1998	−98.3516	2008	−128.83		
1969	33.23002	1979	36.39466	1989	40.63864	1999	−100.871	2009	−139.32		

West Africa

Year	$MtCO_2$	Year	$MtCO_2$	Year	$MtCO_2$	Year	$MtCO_2$	Year	$MtCO_2$	Year	$MtCO_2$
1960	269.0143	1970	312.4253	1980	279.0514	1990	344.519	2000	353.6016	2010	486.457
1961	263.4877	1971	322.4051	1981	275.3983	1991	370.5658	2001	344.3227		
1962	266.0155	1972	319.9678	1982	272.227	1992	390.6469	2002	342.2789		
1963	270.0496	1973	311.728	1983	278.4524	1993	404.4656	2003	349.1278		
1964	275.8482	1974	300.5737	1984	265.1766	1994	402.0382	2004	342.4499		
1965	276.0471	1975	293.9758	1985	281.2648	1995	411.3626	2005	402.3124		
1966	273.7897	1976	279.5637	1986	278.1563	1996	411.8492	2006	417.3524		
1967	273.0014	1977	272.8583	1987	289.5854	1997	399.4846	2007	437.1521		
1968	301.5144	1978	272.4325	1988	292.4495	1998	399.485	2008	448.8516		
1969	300.6948	1979	280.8871	1989	301.6043	1999	411.3989	2009	467.7191		

References

Ahmad B et al (2013) Simulating land cover changes and their impacts on land surface temperature in Dhaka, Bangladesh. Remote Sens 5:5969–5998

Alahakoon N, Edirisinghe M (2021) Variability of rainfall trends in Sri Lanka from 1989 to 2019 as an indicator of climate change. Int J Geoinform 10(84)

Amarawickrama S, Singhapathirana P, Rajapaksha N (2015) Defining urban sprawl in the Sri Lankan context: with special reference to the Colombo metropolitan region. J Asian Afr Stud:1–25

Asian Development Bank (2020a) Climate risk country profile Sri Lanka: Asian Development Bank

Asian Development Bank (2020b) Climate risk country profile Sri Lanka: Asian Development Bank. Cited in: Eriyagama, N. and Smakhtin, V. 2010.Observed and Projected Climate Changes. Their Impacts and Adaption Options for Sri Lanka: a review.in Proceedings of the National Conference on Water. Food Security and Climate Change in Sri Lanka. Volume 2. International Water Management Institute. Colombo. 99–117

Asian Development Bank (2020c) Climate risk country profile Sri Lanka: Asian Development Bank. Cited in: Esham, M., & Garforth, C. 2013. Climate change and agricultural adaptation in Sri Lanka: a review. Climate and Development.5(1). 66–76.

Asian Development Bank (2020d) Climate risk country profile Sri Lanka: Asian Development Bank. Cited in: Silva, G. De, Weerakoonb, S. & Herath, S. 2016. Event-Based Flood Inundation Mapping Under the Impact of Climate Change: A Case Study in Lower Kelani River Basin, Sri Lanka. Hydrology: Current Research 7(1). 7–10

Asian Development Bank (2020e) Climate Risk country profile Sri Lanka: Asian Development Bank. Cited in: Zubair, L. & Ropelewski, C. F. 2006. The strengthening relationship between ENSO and northeast monsoon rainfall over Sri Lanka and southern India. Journal of Climate. 19(8). 1567–1575

Bolay J-C (2019) Urban planning against poverty. pp 7–55. Cited in: UN DESAPD United Nations. 2015. Department of Economic and Social Affairs, Population Division. World urbanization prospects: the 2014 revision, (ST/ESA/SER.A/366). United Nations, New York. [Online]. Available at https://link.springer.com/chapter/10.1007/978-3-030-28419-0_2#fig2. Accessed 20 Sept 2021

CHA (2016) Impacts of disasters in Sri Lanka. Colombo: The consortium of humanitarian agencies

Chan J (n.d.) Relationship between urbanization and climate change in South China, City University of Hong Kong

Chen LG, De Costa G (2017) Climate change impacts on water resources case of Sri Lanka. Environ Ecol Res 5(5):347–356

Dagmav H, Bharat D, Burak G, Xuemei B (2018) Global urbanization: perspectives & trends

Dammalage T, Jayasinghe N (2019) Land-use change and its impact on urban flooding: a case study on Colombo district on May 2016. Eng Technol Appl Sci Res 9(2):3887–3891

De Zoysa M (2021) Urbanization, climate change and environmental resilience: experiences in Sri Lanka. Accessed 23 Sept 2021

Dulal HB (2017) Making cities resilient to climate change: identifying "win-win" interventions. Local Environ 22(1):106–125

EPA (2021) Climate change indicators-heat related deaths. Retrieved https://www.epa.gov/climate-indicators/climate-change-indicators-heat-related-deaths#ref10. Accessed 10 Aprl 2021

Fonseka H et al (2019) Urbanization and its impact on land surface temperature in Colombo metropolitan area, Sri Lanka from 1988 to 2016. Remote Sens 11(957):1–18

Forest Department (2010) Sri Lanka forest cover 1992–2010 and 1950–2010, Battaramulla

Gasimli O, Ul Haq I, Gamage SKN, Shihadeh F, Rajapakshe PSK, Shafiq M (2019) Energy, trade, urbanization and environmental degradation nexus in Sri Lanka: bounds testing approach. Energies 12:1655

Hegazy I, Seddik W, Ibrahim H (2017) Towards green cities in developing countries: Egyptian new cities as a case study. Int J Low Carbon Technol 12:358–368

Herath HMPIK, Halwatura RU, Jayasinghe GY (2018) Evaluation of green infrastructure effects on tropical Sri Lankan urban context as an urban heat island adaptation strategy. Urban For Urban Green 29:212–222

Hewawasam V, Matsui K (2020) Equitable resilience in flood-prone urban areas in Sri Lanka: a case study in Colombo divisional secretariat division. Glob Environ Chang 62:102091

Hoan N et al (2018) Assessing the effects of land-use types in surface urban heat islands for developing comfortable living in Hanoi city. Remote Sens 10(1965)

IPCC (Intergovernmental Panel on Climate Change) (2021) Climate change, the physical science basis, a summary of policymakers. Accessed 11 Sept 2021

Jayawardena L, Darshika D, Herath H (2018) Recent trends in climate extreme indices over Sri Lanka. Am J Clim Chang 7:586–599

Kahn ME (2009) Urban growth and climate change. Accessed 23 Sept 2021

Li L, Pussella PGRN (2017) Is Colombo city, Sri Lanka secured for urban green space standards? Appl Ecol Environ Res 15(3):1789–1799

Lo KFA, Koralegedara SB (2015) Effects of climate change on urban rainwater harvesting in Colombo City, Sri Lanka. Environments 2:105–124

Lyu R, Clarke KC, Zhang J, Jia X, Feng J, Li J (2018) Impacts of urbanization on ecosystem services and their temporal relations: a case study in Northern Ningxia, China. Land Use Policy 77:163–173

Margok DZ (2020) Urbanization, climate change, and environmental resilience. Accessed 23 Sep 2021

Middel A, Chhetri N, Quay R (2015) Urban forestry and cool roofs: assessment of heat mitigation strategies in Phoenix residential neighbourhoods. Urban For Urban Green 14:178–186

Ministry of Environment (2012) Sri Lanka's middle path to sustainable development through Mahinda Chintana-vision for the future. Country Report of Sri Lanka. United Nations Conference on Sustainable Development/(Rio+20) 20–22 June 2012, Rio de Janeiro, Brazil. Retrieved from https://sustainabledevelopment.un.org/content/documents/1013SriLankaRio+20.pdf. Accessed 15 Mar 2013

Ministry of Housing & Construction (2016) UN-Habitat III Country report-Sri Lanka. Retrieved from: https://uploads.habitat3.org/hb3/Sri-Lanka-%EF%BC%88Final-in-English%EF%BC%89.pdf. Accessed 05 Aug 2018

MoE/ADB (2010) NCSD and presidential secretariat, 2009; MoENR, 2008

NASA (2021a). What is an urban heat island? https://climatekids.nasa.gov/heat-islands/. Accessed 23 Sept 2021

NASA (2021b) Global Climate Change. Vital signs of the planet. [online]. Available at https://climate.nasa.gov/vital-signs/sealevel/. Accessed 23 Sept 2021

Naveendrakumar G, Vithanage M, Kwon H, Iqbal MCM, Pathmarajah S, Obeysekera J (2018) Five decadal trends in averages and extremes of rainfall and temperature in Sri Lanka. Adv Meteorol 2018:1

Nisansala W, Abesingha N, Islam A, Bandara A (2020) Recent rainfall trend over Sri Lanka (1987–2017). Int J Climatol 40:3417–3435

Niyogi D, Lei M, Kishtawal C, Schmid P (2017) Urbanization impacts on the summer heavy rainfall climatology over the Eastern United States. Earth Interact 21:1

Oleson KW, Monaghan A, Wilhelmi O, Barlage M, Brunsell N, Feddema J, … Steinhoff DF (2013) Interactions between urbanization, heat stress, and climate change. Article in Climatic Change

Pande CB, Moharir K (2017) GIS-based quantitative morphometric analysis and its consequences: a case study from Shanur River Basin, Maharashtra India. Appl Water Sci 7:861–871. https://doi.org/10.1007/s13201-015-0298-7

Pande CB, Moharir KN, Khadri SFR et al (2018) Study of land use classification in an arid region using multispectral satellite images. Appl Water Sci 8:123. https://doi.org/10.1007/s13201-018-0764-0

Pande CB, Moharir KN, Singh SK, Varade AM, Ahmed Elbeltagie SFR, Khadri PC (2021) Estimation of crop and forest biomass resources in a semi-arid region using satellite data and GIS. J Saudi Soc Agric Sci 20(5):302–311

Paranunzio R, Ceola S, Laio F, Montanari A (2019) Evaluating the effects of urbanization evolution on air temperature trends using nightlight satellite data. Atmos 10(3):117

Patankar A (2017) Colombo exposure, vulnerability and ability to respond to floods, Sri Lanka. World Bank Group, Washington, DC

Punyawardena BVR (2012) Climate change: challenges and opportunities in Sri Lanka, natural resources management center. Department of Agriculture Sri Lanka

Rajesh J, Pande CB, Kadam SA et al (2021) Exploration of groundwater potential zones using analytical hierarchical process (AHP) approach in the Godavari river basin of Maharashtra in India. Appl Water Sci 11:182. (2021). https://doi.org/10.1007/s13201-021-01518-x

Ranaweera D (2016) Changing pattern of land use in Kaduwela municipal council. Dissertation submitted

Rieddy C (2020) Climate change: institute for sustainable futures, University of Technology Sydney. Accessed 11 Sept 2021

Saparamadu S, Yi Z, Zongping Z (2018) Temporal changes of land use land cover and environmental impacts: a case study in Colombo, Sri Lanka. Int J Earth Environ Sci 3:150

Silva TM, Medeiros AN de, Oliveira RL, Gonzaga Neto S, Queiroga R de CR do E, Ribeiro RDX, Leão AG, Bezerra LR (2016) Carcass traits and meat quality of crossbred Boer goats fed peanut cake as a substitute for soybean meal. J Anim Sci 94(7):2992–2300

Sugathapala KC, Jayathilake KADSB (2012) A green area ratio for Sri Lankan urban areas. Retrieved from https://www.nbro.gov.lk/images/content_image/publications/symposia/2010/a_green_area_ratio-for_sri_lankan.pdf

Sultana S, Satyanarayana A (2018) Urban heat island intensity during winter over metropolitan cities of India using remote-sensing techniques: impact urbanization. Int J Remote Sens 39:6692–6730

The World Bank Group and the Asian Development Bank (2020) Climate Risk Country Profile: Sri Lanka

UN-HABITAT (2018) The state of Sri Lankan cities report. Colombo, Sri Lanka. Retrieved from https://unhabitat.org/is-sri-lanka-one-of-the-least-urbanised-countries-on-earth

United Nations (2011) United Nations framework convention on climate change fact sheet: climate change-the status of climate change science today. Accessed 10 Sept 2021

Upadhyaya S (2013) Country grouping in UNIDO statistics. Statistic unit, UNIDO, Vienna

Weeraratne B (2016) Re-Defining Urban Areas in Sri Lanka. Working Paper Series No.23, Institute of Policy Studies of Sri Lanka, Colombo

World Economic Forum (2018) These 10 Asian cities are the most prepared for the future. Retrieved from https://www.weforum.org/agenda/2018/09/these-asian-cities-are-best-equipped-for-the-future/ on 18 Sept 2020. www.climateurope.eu/what-is-climate-and-climate-change/. Accessed 10 Sept 2021

Chapter 4
Climate Change, a Strong Threat to Food Security in India: With Special Reference to Gujarat

Diwakar Kumar

Abstract Gujarat contributes to around 16% of industrial and 12% of agricultural production in India (GoI, India: greenhouse gas emissions 2007. Technical report. Ministry of Environment and Forests, Government of India, New Delhi, 2010b). The Government of Gujarat acknowledges that Climate Change is not just a threat to the environment; it has profound implications for economic expansion, social progress, and nearly all other aspects of human wellbeing (Grafton et al., Nat Clim Chang 3:315–321, 2013). A Department of Climate Change has been established by the government of Gujarat to deal with climate change (GoI, Twelfth five year plan (2012–2017). Economic sectors. Government of India, New Delhi, 2013). It includes Missions on Solar Energy, Augmented Power Efficiency, Resilient Ecosystems, Water, Green procurement India, Climate resilient Agriculture, and Collaborative Knowledge for Climate Change (Bring et al., Earth's Future 3:206–217, 2015). The state of Gujarat has put in place a variety of policies and programs to address some of the issues associated with Climate Change while also assuring the attainment of sustainable development goals (Doll and Bunn, The impact of climate change on freshwater ecosystems due to altered river flow regimes. In: Climate change 2014. Assessment report of the Intergovernmental Panel on Climate Change, pp 143–146, 2014). Efforts are being taken to make farming more environmentally friendly, like setting up agro-meteorological field stations, setting up automatic weather stations, and studying Climate Change in State agriculture universities (Douglas et al., Glob Planet Chang 67:117–128, 2009). According to the Department of Agriculture, Gujarat, about 51% of the state's land is used for farming. Agriculture makes up about 18.3% of India's most populous state's GDP (GoI, Climate change and India: a 44 assessment a sectoral and regional analysis for 2030s. Technical report. Ministry of Environment and Forests, Government of India, New Delhi, 2010a). Despite the Government's efforts to address climate change, challenges persist. Agriculture in India faces numerous difficulties, one of

D. Kumar (✉)
Centre for Studies in Science, Technology & Innovation Policy, Central University of Gujarat, Gandhinagar, Gujarat, India

C. B. Pande et al. (eds.), *Climate Change Impacts on Natural Resources, Ecosystems and Agricultural Systems*, Springer Climate,
https://doi.org/10.1007/978-3-031-19059-9_4

which includes environmental unpredictability (Gosling et al., Hydrol Earth Syst Sci 7:279–294, 2011). A report from the IPCC says that by 2080–2100, India could lose 10%–40% of its crop production due to climate change. The cumulative result is expected to be a reduction in the viability of terrain for agriculture in arid and semi-arid regions. Salt concentrations' infiltration is an issue in Gujarat due to its lengthy shoreline (Garduno et al., India groundwater governance case study. Technical report. World Bank, Washington, DC, 2011). An increase in CO2 will increase the output of rice, wheat, legumes, and oilseeds by 10–20%. With each degree Celsius increase in temperature, yields of grains such as wheat, soybeans, mustard, peanuts, and potato are expected to fall by 3%–7%. There is a probability that yields of chickpeas, rabi, maize, millets, and coconuts will increase on the west coast of India (Hsu et al., J Geophys Res Atmos 118:1247–1260, 2013). In particular, to the state of Gujarat, there are not nearly enough data on the impacts of climate change on agriculture. It is anticipated that irrigated rice production in some parts of Gujarat will go down by 2030 (Gordon et al., Natl Acad Sci 102:7612–7617, 2005). According to the most recent available information, climate change will almost certainly result in more people at threat of going hungry. In 2080, the number of people who are not well-fed could rise by 5%–26% because of climate change. Agriculture, according to some assessments, is likely to be impacted in coastal regions since agriculturally productive areas are subject to flooding and soil salinity (Ghose, J Sci Ind Res 60:40–47, 2001). Climate change will have different impacts on food security in different regions of the state of Gujarat. Climate change will make it more difficult for people living in poor socio-economic regions to get their food and make food insecurity even more important (Hoff, Understanding the nexus. Background paper for the Bonn 2011. Stockholm Environment Institute, Stockholm, 2011). The future policy environment will have a significant impact on the long-term effects of climate change (GRDC, Long-term mean monthly discharges and annual characteristics of GRDC stations/online provided by the Global Runoff Data Centre of WMO 3 19. http://www.bafg.de/GRDC/EN/01_GRDC/grdc_node.html, 2020).

Keywords Climate change · Agriculture · CO_2 · India

Introduction to Climate Change Measures in Gujarat

Gujarat distinguishes out, amongst all the Indian territories, for its economic progress. With only five percent of the country's population and six percent of the country's geographical area, Gujarat contributes to around 16% of industrial and 12% of agricultural production in India and is prominent in the manufacturing and infrastructure sectors (FAO 2002a, b; Jarvis et al. 2018). However, given the context of rising international importance regarding potential risks of climate impacts, there is a need to guarantee that Gujarat's economic performance and socioeconomic development maintains robust and competent of withstanding climatic stress and shocks

(IPCC 2007a, b). The sophistication of the climate-economy association has been made apparent by countless studies and the Government of Gujarat acknowledges that Climate Change is not just a threat to the environment; it has profound implications for economic expansion, social progress, and nearly all other aspects of human wellbeing (Tubiello et al. 2007). Correspondingly, the Government of Gujarat undertaken a series of processes, involving external partners at numerous levels, representative of all segments of society, to work cooperatively and begin creating a framework that results to the realization of a growing, low-emitting, and productive economy with a much more climate adaptation population in Gujarat (IPCC 2007a, b). The Government of India published a National Action Plan on Climate Change (NAPCC) in 2008, highlighting eight primary concern deployments: Missions on Solar Energy, Augmented Power Efficiency, Resilient Ecosystems, Water, Maintaining the Eastern Himalayas Environment, Green procurement India, Climate resilient Agriculture, and Collaborative Knowledge for Climate Change-that outline a comprehensive plan aimed at promoting development goals while also achieving co-benefits for acknowledging Climate Change (IPCC 2000; IEA 2015a). To bring about the implementation of these planned steps at the subnational level, the Hon'ble Prime Minister of India requested each state government to develop its own State level plan of action that was compatible with the policies outlined in the National Plan in August 2009 (Rosenzweig et al. 2002).

Gujarat has taken a pro-active commitment to climate change, and in 2009, the hon'ble Chief minister announced that the government has decided to establish a special Department of Climate Change (IINCD 2015). With a purpose to operate as a bridge inside the public and policymakers, the Gujarat Government's Climate Change Department was established on September 17, 2009 (Fischer et al. 2002). A Department of Climate Change has been established in Gujarat. "Convenient Action – Gujarat's Response to the Challenges of Climate Change" is a book written by the current Prime Minister of India, Shri Narendra Modi who was earlier chief minister of the Gujarat state (CEA 2015). Published document addresses policy-based responses to climate change impacts and mitigation (FAO 2015). Gujarat has indeed proved its commitment through a variety of policies and programs that have the ability to address some of the issues associated with Climate Change while also assuring the attainment of sustainable development goals (FAO 2002a, b). Economy, mass transit, and households/services sectors are all being investigated and benefited from energy efficient technologies such as energy efficiency investigations, the use of alternate fuels, the introduction of a Bus Rapid Transit System, and the establishment of unified State-wide gas grids (IEA 2015b). Thrust has been on renewable energy in Gujarat during last two decades (Goi 2014). In 2009, the state put in place an optimistic solar power policy and a wind energy policy in 2007 (IPCC 2001). Apart from that, numerous interventions, such as the Smart Grid Project, the formation of a Solar Park, and the development of Gandhinagar as a Solar City, and the introduction of fiscal incentives to encourage private investment in renewables, are being implemented in Gujarat to fully exploit the tremendous potential of renewable energy sources (IPCC 2007a, b).

Moreover, new initiatives like the "Green Credit Scheme," social afforestation, and urban greening help to plan for the widening of vegetation and tree shield, as well as to make sure that ecological systems like carbon sinks will continue to circulate over time (Parry et al. 2004). There are also steps being taken to make farming more environmentally friendly, like setting up agro-meteorological field stations, setting up automatic weather stations, and studying Climate Change in State agriculture universities (Tubiello and Fischer 2007). The implementation of numerous cutting-edge efforts in the areas of urban development, water conservation as well as coastal regions development and conservation efforts. The strategic planning concentrates on the involvement of underrepresented groups and women (Bruinsma 2003). The directions of the National Action Plan on Climate Change are primarily reflected in the efforts that are now underway (Lehane and Lewis 2000).

Climate Change, a Strong Threat to Agriculture Productivity

In Gujarat, there is a tropical climate that is mostly humid, but there are also parts that are arid and semi-arid. The dry climate prevails in regions of northern Gujarat such as Kutch, Banas kantha, Mehsana, and the northwestern part of Saurashtra, whereas the sub-humid climate prevails in southern Gujarat and the semi-arid climate prevails throughout the rest of the state (Hall et al. 2002). Annual rainfall ranges from 250 mm in the north to over 1500 mm in south Gujarat. Drought is a problem in 56 of the 225 talukas that exist at the time. MoEF's report on all of India's climate changes called INCCA (Hunter 2003; Kouadri et al. 2022) shows that the Gujarat State has been getting warmer over time. The report also shows that extreme rainfall could be getting worse in the future. Agriculture is a significant sector due to the fact that it represents one of the principle means of subsistence for more than half (52.0%–598%) of the total working population (labor force) in Gujarat state (Korenberg 2004). According to the Department of Agriculture, Gujarat, about 51% of the state's land is used for farming. Agriculture makes up about 18.3% of the state's GDP. Horticulture, animal husbandry, and fisheries are all key sub-sectors in the agricultural sector of Gujarat. In Gujarat, farm output increased at an annual pace of more than 11% on average (D'Souza et al. 2004; Rajesh et al. 2021). Depending on precipitation, soil composition, and crop management, the state is classified into eight agro-climatic zones (Kovats et al. 2004). The South Gujarat (an intense rainfall location south of the River Ambika), South Gujarat (between the rivers Ambika and Narmada), Middle Gujarat (between the rivers Narmada and Vishwamitri), the entire Panchamal and Vadodra districts as well as portions of Bharuch, Anand, and Kheda districts, North Gujarat (between the rivers Vishwamitri and Sabarmati and portions of Mehsana, Ahmedabad, and Banaskantha (Fleury et al. 2006). Constraints on agriculture are diverse, with the majority of them being contingent on ecology and natural resources. Despite the Government's efforts to address these, challenges persist (Checkley et al. 2000). Almost all of Gujarat's kharif crops are rainfed, which makes the state's agriculture

somewhat vulnerable on the state's monsoon. Notably in the Saurashtra and Kutch regions, as well as in the northern portion of Gujarat region, rainfall is very variable in terms of both frequency and spatial dispersion. This causes frequent droughts in certain areas (GoG). Consequently, kharif crops in Gujarat are limited by a lack of adequate rainfall. However, improvements in irrigation infrastructure in the state have contributed to strengthen the adaptability of agricultural processes to climate variability. According to research performed by the Coastal Salinity Prevention Cell (CSPC), landowners who grew groundnut and pearl millet (bajra) in the coastal parts of Rajkot district switched toward cotton and castor. Coconut plantations that once existed in certain villages have been removed. The farming community's monetary requirements have grown as a result of a growing transition toward cash crops that require a lot of investment (McMichael et al. 2003). More than half of the farmers located in such regions require loans, according to several studies conducted in those regions. Individuals are migrating to find employment of this phenomenon (Vasilev 2003). Salt concentrations' infiltration is an issue in Gujarat due to its lengthy shoreline. Additionally, a rise in the CL/CO^3 HCO_3 concentration was spotted closer to the shoreline, demonstrating extensive blending of saltwater and local underground aquifers (Schmidhuber and Shetty 2005). Saltwater infiltration was detected somewhere around 2.5 and 4.5 km from the coastline in 1971, and have between 5.0 and 7.5 km from the coastline in 1977. As a result, overall crop value and productivity (up to 90%) decreased in the coastline of Saurashtra and Kutch, which are recognized for cultivating substantial cash crops such as wheat, mango, coconut, and garden vegetables (Alexandratos 1995).

Temperature and Drought: Major Challenge to Food Security

IPCC 2007 projects that world average temperatures will rise by around 1 °C by 2030, while worldwide median rainfall and washout would climb by 1.5%–3% during the same time, respectively (FAO 2006a, b). Environmental alterations will have a disproportionate influence on world agricultural production, with adverse effects being stronger in the tropics than in temperate climates, resulting in a detrimental impact on developing nations (Fischer et al. 2005). The cumulative result is expected to be a reduction in the viability of terrain for agriculture in arid and semi-arid regions (Panneerselvam et al. 2022; Elbeltagi et al. 2022a, b; Pande et al. 2021a, 2022a). Mankind in Gujarat will have less access to water from river systems and water table because of less streamflow and underground reservoirs recovery (Reilly et al. 1995). Causing additional reliance on irrigation while simultaneously reducing irrigation capacity owing to increasingly frequent droughts (Mishra et al. 2021). It is projected that after 2030, the threat to water supply will be worse, and there may be adverse consequences on irrigation (Darwin et al. 1995; Pande et al. 2022b). Agriculture in India faces numerous difficulties, one of which includes environmental unpredictability. A report from the IPCC says that by 2080–2100, India could lose 10%–40% of its crop production due to climate change (Tubiello et al. 2006).

According to United Nations Framework Convention on Climate Change, an increase in CO_2 to 550 parts per million (ppm) will increase the output of rice, wheat, legumes, and oilseeds by 10%–20% (Tubiello 2005). With each degree Celsius increase in temperature, yields of grains such as wheat, soybeans, mustard, peanuts, and potato are expected to fall by 3%–7% (Alcamo et al. 2005). There is a probability that yields of chickpeas, rabi, maize, sorghum, millets, and coconuts will increase on the west coast. Potato, mustard, and vegetable losses in the northwest of India will be decreased due to a reduction of freezing (cold stress) (Hill et al. 2006). In particular, to the state of Gujarat, there are not nearly enough data on the impacts of temperature variation on agriculture to make a conclusion (Rosenzweig and Parry 1994). Rainfall patterns and temperature data are essential for kharif crops, which are primarily rainfed, and rabi and other summer crops, which are primarily irrigated. Monsoon data show that the western part of the state, which includes Saurashtra and Kutch, has been receiving less rain for the last 100 years by 5% per year (Arnell et al. 2002). According to studies of thermal patterns, the maximum temperature has grown by 0.2–0.90 °C per decade. According to the (IEA 2012), Saurashtra had the largest increasing trend (0.90 °C) (McKibbin et al. 2004). Temperature is the primary constraint on the yield of rabi crops such as wheat and mustard, according to GoG. As a result of a significant temperature increase at the flowering stage, wheat productivity decreased from 3013 kg per hectare in the 2007–2008 season to 2400 kg per hectare throughout the rabi period (Darwin, Climatic Change 2004).

It is anticipated that irrigated rice production in some parts of Gujarat will go down by 2030 (FAO 2006a, b). There will be a decrease in irrigated wheat production in the southern regions, particularly Saurashtra (Abeysingha et al. 2015). It is predicted that the coast would lose up to 40% of its coconut crop due to hot summers temperatures, which are expected to rise further than in the western coastal belt (Arnell 2004). Agriculture, according to some assessments, is likely to be impacted in coastal regions since agriculturally productive areas are subject to flooding and soil salinity (Elbeltagi et al. 2022a, b; Arnell and Gosling 2013). Furthermore, planted commodities in these locations are more susceptible to be harmed as a result of cyclonic activity (Asokan and Destouni 2014). According to the most recent available information, climate change will almost certainly result in more people at threat of going hungry. In 2080, the number of people who are not well-fed could rise by 5%–26% because of climate change (Asokan et al. 2010). Current studies of climate change and food security have focused exclusively on the implications on food supply and accessibility to food, despite quantifying the expected significant consequences of climate change on food quality and susceptibility (Bandyopadhyay et al. 2009). As a result, these studies do not take into account the possible negative effects of extreme weather events like drought and floods (Bhushan et al. 2015a). Similarly, they also ignore the agricultural output consequences of a probable sea-level rise, including those linked with potential declines in ocean or inland fish production (Bhushan et al. 2015b).

Climate change will have an impact on various elements of food security: food abundance (production and trade), food accessibility, food supply consistency, and

food usage (Panda et al. 2013). Climate change will have different impacts on food security in different regions of the state and over time, these consequences will rely heavily on how well the state is doing economically to handle such challenges (Siam et al. 2013). Climate change will have a negative impact on food security, according to quantitative studies. Climate change will make it more difficult for people living in poor socio-economic regions to get their food and make food insecurity even more important (Vittal et al. 2013). Differences in socioeconomic development trajectories, on the other hand, are likely to be the most important driver of food use in the long term and to determine the ability to deal with problems of food instability, driven by climate change. The future policy environment will have a significant impact on the long-term effects of climate change (UNFCCC 2021).

Issues and Challenges in Semi-Arid and Arid Regions of Gujarat

Gujarat suffers from drought/lack of irrigation water for the crops on a consistent basis (Sreeja et al. 2016). Majority of the farmlands in Gujarat are in the semi-arid regions. The Central Water Commission has classified 14 and 17 districts as "drought prone districts" for the year 2015 and 2013 (Rodell et al. 2009). These regions have a scarcity of water. Groundwater levels are too low, rainfall is minimal, and water run-off is excessive (Vitousek et al. 1997). Annual rainfall ranges between 100 and 400 millimeters (mm) or 400 and 800 millimeters (mm) (WCD 2000). There is very little water in the northern arid areas, which are mostly deserts like the Rann of Kutch, and the semi-arid areas of Gujarat. They mostly get their water from wells, tanks, ponds, and other traditional sources. In these areas, there are no rivers (Bring et al. 2014). The southern province, on the other hand, is supplied mostly by groundwater flows and monsoon rainfall by the peninsular rivers (Schellnhuber et al. 2014). Small- and medium-sized water storage facilities serve as the primary supply of water for these regions throughout the year. The tank is often the only place where people can store rainwater (Bhushan et al. 2015b).

Food security and economic opportunity for the numerous people who live in such regions pose severe concerns (Shah and Kumar 2008). The region's vulnerability has been exacerbated by poor land productivity and small landholdings, which have resulted in hidden unemployment (Prudhomme et al. 2014). Many dryland farmers cannot make a living all year round because of present agricultural irrigation constraints (Ravindranath et al. 2011). There are numerous issues that affect pastoralists or goat/cattle keepers, including water scarcity, feed scarcity, disease in the animals (Schewe et al. 2014). Reducing pasturelands and community grazing lands puts additional strain on the land. Regional residents frequently depend on a blend of rain-fed farming, animal rearing, and other revenue activities to survive (van Vliet et al. 2016). Additionally, families develop a buffer reserve of grains or liquid assets and rely on loans to survive during tough times (Rao 1995). People are

less equipped to protect themselves from large-scale shocks (Taheripour et al. 2015). Extreme weather, such as lengthy dry spells or delayed rain, has a significant negative impact on harvest yield and makes people's life considerably more difficult (Prakash et al. 2014).

Without including migration, it would be impossible to discuss dry and semi-arid regions (Shashikanth et al. 2014b). Migration is relatively common because of the nomadic and semi-nomadic lifestyles which is triggered by extreme weather conditions and lack of resources for livelihood (Purohit and Fischer 2014). It exists in numerous ways and trends, such as seasonal/distress, rural-to-rural, and rural-to-urban. For the impoverished, migration is an essential source of income and a means of ensuring their survival and well-being; in some cases, it is their sole means of doing so (Raje and Krishnan 2012). Movement to other irrigated areas is possible because of agricultural wage labor in the construction sites for building canal/dam work, road/cable construction, etc., self-employment by skilled craftsmen and talented laborers as masons, statue makers, mechanics/drivers, etc. (Salvi et al. 2013). Extreme weather events, in combination with other physical, social, and political-economic factors, contribute to economic hardship, starvation, drought, and displacement vulnerability (Pandit 2012). Food security and biodiversity are strongly intertwined. Intercropped, traditional varieties of crop have a considerably better chance of surviving a severe and irregular monsoon and provide the farmer with basic food security (Ritzema et al. 2008). Agronomists use crop diversity and mixed cropping to lessen the possibility of crop loss due to weather or pest attacks (SWBD 2005). Traditional, hardy agricultural seed banks are gradually disappearing, giving place to monocropping of commercial crops such as groundnut, sunflower, and so on. Furthermore, the failure of a single mono-cropped, high-yielding hybrid crop might bankrupt a farmer and force him or her into debt (Bouwer et al. 2006).

Climate Change Impact on Cropping Patterns

Climate change is not the only thing that is causing problems for farmers in the dryland areas. These will be amplified even further by the consequences of climate change (Sreeja et al. 2012). The rise in population will exacerbate the fragmentation of landholdings. Fragmentation impacts will worsen agricultural productivity losses caused by rainfall and temperature fluctuations (Peters et al. 2013). Reduced precipitation, coupled with water constraint, will further erode land productivity (Roxy et al. 2015). This decline will result in a reduction in the amount of food produced (Shashikanth et al. 2014a, b). More people will migrate in search of food, which will result in a reduction in the number of people available to labor on agricultural land (Saha et al. 2014). The Gujarat Institute of Desert Ecology in Kutch discovered major findings during a 3-year study (Tian et al. 2014). The institute examined the trend of climate transition over the last 5 years with a particular emphasis on Kutch, which is technically arid but is now experiencing unusual rainfall (Skaggs et al. 2012). During the study, Gujarat has been hit by three consecutive cyclones – Vayu,

Kyarr, and Maha – which have dropped massive rains on the coastal parts of Saurashtra, causing massive crop losses for farmers (Green et al. 2000). Meanwhile, the state recorded 1185 mm of rain, the most in a decade, and the biggest rainy season ever that lasted for 6 months starting June (Bobba 2002). Crops such as legumes and horticultural crops such as coconut, mango, and sitafal (custard apple) are diminishing as saline levels rise in coastal areas of Porbandar (Green et al. 2000). Cotton and castor crop areas have increased in recent years due to the shift toward groundnut crops, which are extremely sensitive to salt water (Solomon et al. 2007). In the regions of Rajkot, groundnut and bajra plantations have been replaced with cotton and castor; similarly, coconut plantations in certain villages are not cultivated/left (Tuanmu and Jetz 2014). Additionally, bajra, jowar, castor, and cotton production have all been cut in half on an average basis (Stocker et al. 2013). Farmers are not planting new mango and coconut plantations in the regions of Junagadh, and the acreage within horticulture is progressively shrinking (Vaidyanathan 1999). Whereas cotton is being cultivated in substitute of groundnut in most regions. Cropping patterns in saline villages have shifted away from horticulture and groundnut cultivation and toward cotton and fodder crops such as jowar (Sinha et al. 2015; CWC 2015). Crops such as chilli and groundnut have seen a decline in area under cultivation. Change in the agricultural season from three crops to one crop reflects the detrimental consequences of climate change in the Jamnagar region (Sundararajan and Mohan 2011). There is a decrease in the amount of land used for horticulture and land used for pulse farming in the Kutch regions of Gujarat (Sherif and Singh 1999).

Climate Change Impact on the Landscape and Irrigation

India is the biggest user of agricultural resources in the globe, both in terms of the amount of land that can be cultivated and irrigated and the amount of underground aquifers used (FAO 2015; Shiklomanov and Rodda 2004). Agriculture, the primary source of subsistence (60%) and the most important land use (42%) in the nation, utilizes the biggest share of water (80%) and a significant quantity of energy, resulting in a complex web of nexus relationships (Siebert et al. 2015). Substantial dam surface water irrigation covers 16 Mha, whereas minor irrigation covers 2 Mha (TERI 2015; MoWR 2013; CWC 2015). There has been significant growth in the use of surface water sources, but for the time being, surface water irrigation is not only confined to the paddy-growing regions (Cullet et al. 2015). Surface water irrigation through canals and other medium has a reach to many remote areas of Gujarat (Deser et al. 2012). A significant proportion (62%) of India's gross irrigated area is still reliant on groundwater supplies with considerable geographical seasonal variability, according to the latest findings (GoI 2014; Shiva et al. 1991). Irrigation exemplifies the numerous nexus relationships that exist between water resources, land, energy, and climate. Large-scale groundwater extraction and extensive surface water infrastructure have affected river basin hydrology, resulting in a loss of

groundwater reserve and availability in several regions (WCD 200; Rodell et al. 2009; CGWB 2014; Pande et al. 2021b; Glazer and Likens 2012). With a cumulative underground water irrigated area ranging from 60 to 70 million ha in India, that requires up to 120,000–150,000 GWh of power and 5–8 million m^3 of gasoline to pump up 230–250 km^3 of irrigated water yearly, according to the World Bank (Mukherji et al. 2012; Huntington 2006). Depleting groundwater aquifers, enlarging the area under groundwater irrigation, and raising the demand for energy resulted from the provision of subsidized energy for groundwater irrigation (Mukherji et al. 2012; Hirabayashi et al. 2013; GoI 2015). Significant advances in saline water intrusion are expected along coastal areas as a result of excessive groundwater removal, which may intensify as sea levels rise and water demands increase as a consequence of environmental warming (Sherif and Singh 1999; Bobba 2002; Hagemann et al. 2013). Because to this excessive extraction, majority of blocks in Gujarat are classed as semi-critical, critical, or fully exploited (Douglas et al. 2006; Pande et al. 2020). Increased irrigation, on the other hand, has resulted in salinity, alkalinity, and water logging difficulties over different regions of Gujarat (Howells et al. 2013; Ritzema et al. 2008).

Climate variability imposes additional limitations on the linkage, making the interrelations more fragile and unpredictable (Jain and Kumar 2012). Residents living nearby water reservoirs say that climate change makes it even worse because dams and water withdrawals have already cut off the natural flow of water throughout most portions of the state (Doll et al. 2012; Hawkins and Sutton 2009). The considerable rise in temperature since 2008 has been determined to have influenced the current acute water shortages in the Indo-Gangetic lowlands, which is mostly attributed to agricultural water demands (Ghosh et al. 2012). Climate change-induced increases in water demand and decreased water supply are anticipated to significantly diminish the area irrigated by 2030 (Taheripour et al. 2015; Hansen and Cramer 2015). Strengthened irrigated agriculture interventions in the water and land sectors have a major impact on regional climate through increasing evapotranspiration fluxes (Gordon et al. 2005; Asokan et al. 2010; Jaramillo and Destouni 2015; Chaturvedi et al. 2012). Agricultural adaptations have resulted in an average annual vapor flow increase with significant seasonal changes 7% during the wet season and 55% during the dry season, with irrigation accounting for 2/3 of the increase (Doll et al. 2012; Douglas et al. 2006). According to reports, the South Asian rainfall trend is more vulnerable to anthropogenic irrigation-induced flux variations than to the climate implications of land use alteration (Douglas et al. 2009; Haddeland et al. 2014). During the years 1956–2000, irrigation in the Mahanadi basin increased ET by 40 mm year-1 and decreased annual average temperature by 0.13 °C and runoff by 32 mm year-1 (Asokan and Destouni 2014; Jaramillo and Destouni 2014). Fluxes exhibit a significant degree of geographical heterogeneity as a result of differences in irrigation volume across the watershed (Asokan et al. 2010; Immerzeel et al. 2013). Evaporation rates have risen by 77% in the Krishna River basin since 1900, a result of increasing buffer accumulation and irrigation (Jaramillo and Destouni 2015; Destouni et al. 2010). Widespread land use land cover (LULC) transition, which encompasses deforestation, changes

in the amount of cultivated lands, and urbanization as a result of direct human interventions, has a negative impact on water supplies (Lambin et al. 2003; Pande et al. 2021a, b; Chattopadhyay and Hulme 1997). In India, a sixfold rise in populace over the last century, spanning 200–1200 million, along with rapid economic expansion, has resulted in considerable LULC shifts (Bouwer et al. 2006). It has been shown that the amount of forest land has decreased from 89 to 63 Mha, whereas the amount of agriculture has expanded from 92 to 140 Mha during same time period (Tian et al. 2014; Gordon et al. 2005; Hoekstra and Chapagain 2007). Additionally, it has been reported that emerging and developing clusters of urban populations, most frequently near coastal zones and key rivers, have boosted water resource requirements and consequences (Destouni et al. 2013; McDonald et al. 2011). The purity of water is also deteriorating in many regions as a result of changes in land use (Asokan et al. 2012). Surface and aquifer pollution, caused primarily by untreated sewage, industrial effluents, fertilizer runoff, and urban garbage, is a significant environmental concern, affecting not just the supply of fresh water rather the health of millions of inhabitants (Jaramillo and Destouni 2015; CGWB 2010; CWC 2011).

Climate Change Effect on Rainfall Trend

Humans have been influencing the environment for ages (MoWR 2013). However, human activities have only begun to reach a global scale since the commencement of the industrial revolution (Khare et al. 2013; CWC 2012). Today, environmental issues have surpassed all other concerns for humanity as a result of scientific facts on the increasing quantity of greenhouse gases in the atmosphere and the Earth's changing climate (Jhajharia et al. 2014). Worldwide, temperatures are rising and precipitation amounts and distributions are changing (Mujumdar and Ghosh 2008). Rainfall is an important component of the hydrological cycle, and changes in its pattern have a direct impact on water resources. The policymakers and hydrologists are now concerned about the shifting patterns of rainfall as a result of climate change (Molle and Berkoff 2006). It has been shown that variations in rainfall amounts and frequency have an immediate effect on stream flow patterns and demand, as well as the spatiotemporal allocation of runoff, ground water reserves, and soil moisture, according to Srivastava et al. and Islam et al. (Kothawale and Kumar 2005). As a response, these changes had far-reaching implications for water resources, the environment, terrestrial ecosystems, the ocean, biodiversity, agriculture, and food security (Lehner et al. 2016). Significant shifts in rainfall patterns can lead to droughts and food shortages, which can occur on a regular basis (McDonald et al. 2011). According to Gupta et al., the proportion of soil moisture available for agricultural production is entirely dependent on the amount of rainfall (Krishna et al. 2011).

Numerous initiatives to detect rainfall trends at regional and national scales have already been carried out through different policy measures (Mukherji et al. 2012). The trend detection studies have been considered a valuable instrument since it

offers meaningful insight about the probability of future changes (Lima et al. 2008). However, projecting future climatic variables is more valuable to planners because it helps them comprehend the present and historical climate changes (Joshi et al. 2011). A regional forecasting approach might be used to project future knowledge about climatic factors, in supplementary to the complex climate model that operates on a global scale (Elbeltagi et al. 2022a, b; Lambin et al. 2003). Statistical approaches and machine learning computer techniques could be used to accomplish this (Mall et al. 2006). Agriculture is heavily dependent on precipitation, and the country's whole economy depends on it (Nakamura et al. 2014). Consequently, regional and sectoral economy cannot function without ample water supply (Koirala et al. 2014). However, as a result of climate change, the regional rainfall pattern has been disrupted (Jayaraman and Murari 2014; CWC 2011). Therefore, many researches have been conducted in varied regions to measure the pattern of rainfall variations and to establish a strategic approach in accordance with the results of such studies (Jarvis 2006).

Conclusion

The climate change is forcing every individual and organization to create actionable strategies for addressing the most pressing threats, consequences, and vulnerabilities related to food security (Jhajharia et al. 2012). Thus, three key developmental transition alternatives are recognized: increasing the productivity of food grains and socioeconomic systems, developing new sustainable livelihoods, and/or shifting population from fragile to resilient habitats (Oki and Kanae 2006). Thus, developmental paths should be capable of sustaining existing ecosystems, respecting embedded socio-cultural dynamics, innovating around governance and regulatory structures, and responding to current climate-related hazards (Kraucunas et al. 2014). However, despite rapid economic growth, particularly in the recent two decades, this has not been reflected significant into poverty alleviation or proportionate improvement on other human welfare metrics (Lee and Wang 2014). Major challenges include environmental deterioration, stagnating crop production, rising regional inequality, low levels of employment, as well as insufficient access to welfare initiatives for those from lower socioeconomic strata (Nohara et al. 2006). It is also important to note that agriculture sector in India continues to be the most important source of income for the majority of people (CWC 1993). Because it is mostly dependent on rainwater, it is extremely vulnerable to changes in the climatic conditions (Joy et al. 2008). Semi-arid regions' development relies on mitigating ecosystem disintegration, integrating sustainable resource management, and enhancing the already-existing resilience capabilities of communities and organizations (Nune et al. 2014). The failure of previous initiatives to generate the promised outcomes has resulted in, regional, and national institutions deciding to divert their resources to other ecosystems, which they deem to be superior investments (CGWB 2014). Climate change will put even more strain on the livelihoods of individuals

who live in these vulnerable environments, potentially leading to increased resource scarcity (CGWB 2010). Consequently, it is essential to assure people economic access to food, to have contingency plans for crop varieties, feed for farm animals, and drinkable water, to have crop stabilization and watershed development programs, to have community-based natural resource management practices, to practice such farming that increases land productivity, to revitalize traditional crops and practices to ensure food security, and to revitalize traditional livestock breeds (Jung et al. 2010).

References

Abeysingha N, Singh M, Sehgal V, Khanna M, Pathak H (2015) Analysis of trends in streamflow and its linkages with rainfall and anthropogenic factors in Gomti River basin of North India. Theor Appl Climatol 123:785–799

Alcamo J, van Vuuren D, Ringler C, Cramer W, Masui T, Alder J, Schulze K (2005) Changes in nature's balance sheet: model-based estimates of future worldwide ecosystem services. Econ Soc 10(2):19

Alexandratos N (1995) World agriculture: toward 2010. A Food and Agriculture Organization study. The Food and Agriculture Organization of the United Nations, Rome

Arnell NW (2004) Climate change and global water resources: SRES emissions and socioeconomic scenarios. Glob Environ Chang 14:31–52

Arnell NW, Gosling SN (2013) The impacts of climate change on river flow regimes at the global scale. J Hydrol 486:351–364

Arnell NW, Cannell MGR, Hulme M, Kovats RS, Mitchell JFB, Nicholls RJ, Parry ML, Livermore MTJ, White A (2002) Climatic change. Clim Chang 53:413–446

Asokan SM, Destouni G (2014) Irrigation Effects on Hydro-Climatic Change: Basin-Wise Water Balance-Constrained Quantification and Cross-Regional Comparison. Surv Geophys 35:879–895. https://doi.org/10.1007/s10712-013-9223-5

Asokan SM, Jarsj J, Destouni G (2010) Vapor flux by evapotranspiration: effects of changes in climate, land use, and water use. J Geophys Res Atmos 115:79–82

Asokan SM, Prieto C, Bring A, Destouni G (2012) Hydrological responses to climate change conditioned by historic alterations of land-use and wateruse. Hydrol Earth Syst Sci 16:1335–1347

Bandyopadhyay A, Bhadra A, Raghuwanshi N, Singh R (2009) Temporal trends in estimates of reference evapotranspiration over India. J Hydrol Eng 14:508–515

Bhushan C, Kumarankandath A, Goswami N (2015a) The state of concentrated solar power in India: a roadmap to developing solar thermal technologies in India. Centre for Science and Environment, New Delhi

Bhushan C, Bhati P, Kumar S, Sangeetha A, Siddhartha S, Ramanathan S, Rudra A (2015b) Heat on power: green rating of coal-based power plants. Centre for Science and Environment, New Delhi

Bobba AG (2002) Numerical modelling of salt-water intrusion due to human activities and sea-level change in the Godavari Delta, India. Hydrol Sci J 47:S67–S80

Bouwer L, Aerts J, Droogers P, Dolman A (2006) Detecting the long-term impacts from climate variability and increasing water consumption on runoff in the Krishna river basin (India). Hydrol Earth Syst Sci Discuss 10:1249–1280

Bring A, Rogberg P, Asokan S, Destouni G (2014) Evolution of the hydro-climate system in the Lake Baikal basin. J Hydrol 519:1953–1962

Bring A, Asokan SM, Jaramillo F, Jarsj J, Levi L, Pietroń J, Prieto C, Rogberg P (2015) Implications of freshwater flux data from the CMIP5 multi-model output across a set of Northern Hemisphere drainage basins. Earth's Future 3:206–217

Bruinsma J (2003) World agriculture: toward 2015/2030. A Food and Agriculture Organization perspective. Earthscan, London

CEA (2015) Growth of electricity sector in India from 1947–2015, Technical report. Central Electricity Authority, Government of India, New Delhi

CGWB (2010) Groundwater quality in shallow aquifers in India, Technical report. Central Ground Water Board, Government of India, New Delhi

CGWB (2014) Dynamic groundwater resources of India, Technical report. Central Ground Water Board, Government of India, New Delhi

Chattopadhyay N, Hulme M (1997) Evaporation and potential evapotranspiration in India under conditions of recent and future climate change. Agric For Meteorol 87:55–73

Chaturvedi RK, Joshi J, Jayaraman M, Bala G, Ravindranath NH (2012) Multi-model climate change projections for India under representative concentration pathways. Curr Sci 103(7):791–802

Checkley W, Epstein LD, Gilman RH, Figueroa D, Cama RI, Patz JA, Black RE (2000) Lancet. Lancet:442–450

Cullet P, Bhullar L, Koonan S (2015) Inter-sectoral water allocation and conflicts: perspectives from Rajasthan. Econ Polit Wkly:61–69

CWC (1993) Reassessment of water resources potential of India, Technical report. Centre Water Commission, Government of India, New Delhi

CWC (2011) Report on water quality hot spots in rivers of India, Technical report. Centre Water Commission, Government of India, New Delhi

CWC (2012) National register of large dams. Central Water Commission, Government of India, New Delhi

CWC (2015) Water and related statistics, Technical report. Central Water Commission, Government of India, New Delhi

D'Souza R, Becker N, Hall G, Moodie K (2004) Epidemiology. Epidemiology 15:86–92

Darwin R (2004) Climatic change. Clim Chang 66:191–238

Darwin R, Tsigas M, Lewandrowski J, Raneses A (1995) World agriculture and climate change, economic adaptations. Department of Agriculture, Washington, DC

Deser C, Phillips A, Bourdette V, Teng H (2012) Uncertainty in climate change projections: the role of internal variability. Clim Dyn 38:527–546

Destouni G, Asokan SM, Jarsj J (2010) Inland hydro-climatic interaction: effects of human water use on regional climate. Geophys Res Lett 37:L18402. https://doi.org/10.1029/2010GL044153, 2010L184021of6

Destouni G, Jaramillo F, Prieto C (2013) Hydroclimatic shifts driven by human water use for food and energy production. Nat Clim Chang 3:213–217

Doll P, Bunn SE (2014) The impact of climate change on freshwater ecosystems due to altered river flow regimes. In: Climate change 2014. Assessment report of the Intergovernmental Panel on Climate Change. Cambridge University Press, Cambridge, pp 143–146

Doll P, Hoffmann-Dobrev H, Portmann F, Siebert S, Eicker A, Rodell M, Strassberg G, Scanlon B (2012) Impact of water withdrawals from groundwater and surface water on continental water storage variations. J Geodyn 59-60:143–156

Douglas EM, Niyogi D, Frolking S, Yeluripati J, Pielke RA, Niyogi N, Mohanty U (2006) Changes in moisture and energy fluxes due to agricultural land use and irrigation in the Indian monsoon belt. Geophys Res Lett 33:251–267

Douglas E, Beltrán-Przekurat A, Niyogi D, Pielke R, Vorosmarty C (2009) The impact of agricultural intensification and irrigation on land–atmosphere interactions and Indian monsoon precipitation: a mesoscale modeling perspective. Glob Planet Chang 67:117–128

Elbeltagi A, Pande CB, Kouadri S et al (2022a) Applications of various data-driven models for the prediction of groundwater quality index in the Akot basin, Maharashtra, India. Environ Sci Pollut Res 29:17591–17605. https://doi.org/10.1007/s11356-021-17064-7

Elbeltagi A, Kumar N, Chandel A et al (2022b) Modelling the reference crop evapotranspiration in the Beas-Sutlej basin (India): an artificial neural network approach based on different combinations of meteorological data. Environ Monit Assess 194:141. https://doi.org/10.1007/s10661-022-09812-0

FAO (2002a) Food and Agriculture Organization, World agriculture: toward 2015/2030, Summary report. Food and Agriculture Organization, Rome

FAO (2002b) The state of food insecurity in the world 2001. Food and Agriculture Organization, Rome

FAO (2006a) Food and Agriculture Organization, the state of food insecurity in the world 2006. Food and Agriculture Organization, Rome

FAO (2006b) Food and Agriculture Organization, World agriculture: toward 2030/2050. Food and Agriculture Organization, Rome

FAO (2015) AQUASTAT main database. Food and Agriculture Organization of the United Nations (FAO), Rome

Fischer G, Shah M, van Velthuizen H (2002) Climate change and agricultural vulnerability, a special report prepared as a contribution to the world summit on sustainable development. International Institute for Applied Systems Analysis, World Summit on Sustainable Development, Johannesburg 2002,e IIASA Publications

Fischer G, Shah M, Tubiello FN, Velthuizen H (2005) Philos Trans R Soc Ser B. Philos Trans R Soc Ser B 360:2067–2083

Fleury M, Charron D, Holt J, Allen O, Maarouf A (2006) Int J Biometeorol. Int J Biometeorol 50:385–391

Garduno H, Romani S, Sengupta B, Tuinhof A, Davis R (2011) India groundwater governance case study, Technical report. World Bank, Washington, DC

Ghose M (2001) Design of cost-effective coal washery effluent treatment plant for clean environment. J Sci Ind Res 60:40–47

Ghosh S, Das D, Kao SC, Ganguly AR (2012) Lack of uniform trends but increasing spatial variability in observed Indian rainfall extremes. Nat Clim Chang 2:86–91

Glazer AN, Likens GE (2012) The water table: the shifting foundation of life on land. Ambio 41:657–669

GoI (2010a) Climate change and India: a 44 assessment a sectoral and regional analysis for 2030s, Technical report. Ministry of Environment and Forests, Government of India, New Delhi

GoI (2010b) India: greenhouse gas emissions 2007, Technical report. Ministry of Environment and Forests, Government of India, New Delhi

GoI (2013) Twelfth five year plan (2012–2017). Economic sectors. Government of India, New Delhi

GoI (2014) Landuse statistics at a glance, Technical report. Directorate of Economics and Statistics, Government of India, New Delhi

GoI (2015) Annual report 2014–15, Technical report. Ministry of Mines, Government of India, New Delhi

Gordon LJ, Steffen W, Folke C, Falkenmark M, Johannessen A (2005) Human modification of global water vapor flows from the land surface. Natl Acad Sci 102:7612–7617

Gosling S, Taylor R, Arnell N, Todd M (2011) A comparative analysis of projected impacts of climate change on river runoff from global and catchment-scale hydrological models. Hydrol Earth Syst Sci 7:279–294

Grafton RQ, Pittock J, Davis R, Williams J, Fu G, Warburton M, Udall B, McKenzie R (2013) Global insights into water resources, climate change and governance. Nat Clim Chang 3:315–321

GRDC (2020) Long-term mean monthly discharges and annual characteristics of GRDC stations/online provided by the Global Runoff Data Centre of WMO 3 19. http://www.bafg.de/GRDC/EN/01_GRDC/grdc_node.html

Green P, Salisbury J, Lammers R (2000) Global water resources: vulnerability from climate change and population growth. Science 289:284–288
Haddeland I, Heinke J, Biemans H, Eisner S, Hanasaki N, Konzmann M, Ludwig F (2014) Global water resources affected by human interventions and climate change. Natl Acad Sci 111:3251–3256
Hagemann S, Chen C, Clark D, Folwell S, Gosling SN, Haddeland I, Hannasaki N, Heinke J (2013) Climate change impact on available water resources obtained using multiple global climate and hydrology models. Earth Syst Dyn 4:129
Hall GV, D'Souza RM, Kirk MD (2002) Foodborne disease in the new millennium: out of the frying pan and into the fire? Med J Aust 177(11–12):614–618. https://doi.org/10.5694/j.1326-5377.2002.tb04984.x. PMID: 12463979
Hansen G, Cramer W (2015) Global distribution of observed climate change impacts. Nat Clim Chang 5:182–185
Hawkins E, Sutton R (2009) The potential to narrow uncertainty in regional climate predictions. Bull Am Meteorol Soc 90:1095–1107
Hill J, Nelson E, Tilman D, Polasky S, Tiffany D (2006) Proc Natl Acad Sci USA. Proc Natl Acad Sci U S A 103:11206–11210
Hirabayashi Y, Mahendran R, Koirala S, Konoshima L, Yamazaki D, Watanabe S, Kim H, Kanae S (2013) Global flood risk under climate change. Nat Clim Chang 3:816–821
Hoekstra AY, Chapagain AK (2007) Water footprints of nations: water use by people as a function of their consumption pattern. Water Resour Manag 21:35–48
Hoff H (2011) Understanding the nexus. Background paper for the Bonn 2011. Stockholm Environment Institute, Stockholm
Howells M, Hermann S, Welsch M, Bazilian M, Alfstad T, Gielen D, Rogner H (2013) Integrated analysis of climate change, land-use, energy and water strategies. Nat Clim Chang 3:621–626
Hsu P-C, Li T, Murakami H, Kitoh A (2013) Future change of the global monsoon revealed from 19 CMIP5 models. J Geophys Res Atmos 118:1247–1260
Hunter PR (2003) J Appl Microbiol. J Appl Microbiol 94:37–46
Huntington TG (2006) Evidence for intensification of the global water cycle: review and synthesis. J Hydrol 319:83–95
IEA (2012) World energy outlook 2012, Technical report. International Energy Agency, London
IEA (2015a) World energy outlook 2015, Technical report. International Energy Agency, London
IEA (2015b) World energy trends 2015, Technical report. International Energy Agency, London
IINCD (2015) India's intended nationally determined contribution: working towards climate justice, Technical report. United Nations Framework Convention on Climate Change, New Delhi
Immerzeel W, Pellicciotti F, Bierkens M (2013) Rising river flows throughout the twenty-first century in two Himalayan glacierized watersheds. Nat Geosci 6:742–745
IPCC (2000) Intergovernmental Panel on Climate Change, special report on emissions scenarios, summary for policy makers, working group III. UK. Cambridge University Press, Cambridge
IPCC (2001) Intergovernmental Panel on Climate Change, climate change: impacts, adaptation and vulnerability, contribution of Working Group II to the Third assessment report of the Intergovernmental Panel on Climate Change, UK. Cambridge University Press, Cambridge
IPCC (2007a) Climate change 2007: the physical science basis, contribution of working group I to the fourth assessment report of the Intergovernmental Panel on Climate Change, UK. Cambridge University Press, Cambridge
IPCC (2007b) Intergovernmental Panel on Climate Change, climate change: impacts, adaptation and vulnerability, contribution of Working Group II to the fourth assessment report of the Intergovernmental Panel on Climate Change. Intergovernmental Panel on Climate Change, UK. Cambridge University Press, Cambridge
Jain SK, Kumar V (2012) Trend analysis of rainfall and temperature data for India. Curr Sci 102:37–49
Jaramillo F, Destouni G (2014) Developing water change spectra and distinguishing change drivers worldwide. Geophys Res Lett 41:8377–8386

Jaramillo F, Destouni G (2015) Local flow regulation and irrigation raise global human water consumption and footprint. Science 350:1248–1251
Jarvis WT (2006) Transboundary groundwater: geopolitical consequences, commons sense, and the law of the hidden sea. Oregon State University
Jarvis A, Reuter H, Nelson A, Guevara E (2018) Hole-filled SRTM for the globe, Version 4. 09 1. http://srtm.csi.cgiar.org, National Tibetan Plateau/Third Pole Environment Data Center
Jayaraman T, Murari K (2014) Climate change and agriculture: current and future trends, and implications for India. Rev Agrar Stud 4:1–49
Jhajharia D, Dinpashoh Y, Kahya E, Singh VP, Fakheri-Fard A (2012) Trends in reference evapotranspiration in the humid region of Northeast India. Hydrol Process 26:421–435
Jhajharia D, Kumar R, Dabral P, Singh V, Choudhary R, Dinpashoh Y (2014) Reference evapotranspiration under changing climate over the Thar Desert in India. Meteorol Appl 22:425–435
Joshi M, Hawkins E, Sutton R, Lowe J, Frame D (2011) Projections of when temperature change will exceed 2 °C above pre-industrial levels. Nat Clim Chang 1:407–412
Joy KJ, Gujja B, Paranjape S, Goud V, Vispute S (2008) Water conflicts in India: a million revolts in the making. Routledge, New Delhi
Jung M, Reichstein M, Ciais P, Seneviratne SI, Sheffield J, Goulden ML, Bonan G, Cescatti A (2010) Recent decline in the global land evapotranspiration trend due to limited moisture supply. Nature 467:951–954
Khare V, Nema S, Baredar P (2013) Status of solar wind renewable energy in India. Renew Sust Energ Rev 27:1–10
Koirala S, Hirabayashi Y, Mahendran R, Kanae S (2014) Global assessment of agreement among streamflow projections using CMIP5 model outputs. Environ Res Lett 9:e01611–e01614
Korenberg E (2004) Proc. Intl. Conf. Climate Change and Public Health in Russia in the 21st Century. Russian Academy of Medical Sciences - Russian Regional Committee for Cooperation with UNEP Centre for Demography and Human Ecology Russian Regional Environmental Centre Non-Governmental Organisation 'Environmental Defence', Moscow, 461 pp
Kothawale DR, Kumar R (2005) On the recent changes in surface temperature trends over India. Geophys Res Lett 32:28
Kovats RS, Edwards S, Hajat S, Armstrong B, Ebi KL, Menne B (2004) Epidemiol Infect. Epidemiol Infect 132:443–453
Kraucunas I, Clarke L, Dirks J, Hathaway J, Hejazi M, Hibbard K, Huang M, Jin C (2014) Investigating the nexus of climate, energy, water, and land at decision-relevant scales: the Platform for Regional Integrated Modeling and Analysis (PRIMA). Clim Chang 129:573–588
Krishna K, Patwardhan SK, Kulkarni A, Kamala K, Rao KK, Jones R (2011) Simulated projections for summer monsoon climate over India by a high-resolution regional climate model (PRECIS). Curr Sci 101:312–326
Kouadri S, Pande CB, Panneerselvam B et al (2022) Prediction of irrigation groundwater quality parameters using ANN, LSTM, and MLR models. Environ Sci Pollut Res 29:21067–21091. https://doi.org/10.1007/s11356-021-17084-3
Lambin EF, Geist HJ, Lepers E (2003) Dynamics of land-use and land-cover change in tropical regions. Annu Rev Environ Resour 28:205–241
Lee JY, Wang B (2014) Future change of global monsoon in the CMIP5. Clim Dyn 42:101–119
Lehane L, Lewis RJ (2000) Ciguatera: recent advances but the risk remains. Int J Food Microbiol 61(2–3):91–125. https://doi.org/10.1016/s0168-1605(00)00382-2. PMID: 11078162.5
Lehner B, Liermann C, Revenga C, Fekete B, Crouzet P, Endejan M (2016) High-resolution mapping of the world's reservoirs and dams for sustainable river-flow management. Front Ecol Environ 9:494–502
Lima IB, Ramos FM, Bambace LA, Rosa R (2008) Methane emissions from large dams as renewable energy resources: a developing nation perspective. Mitig Adapt Strateg Glob Chang 13:193–206
Mall R, Gupta A, Singh R, Rathore L (2006) Water resources and climate change: an Indian perspective. Curr Sci 90:1610–1626

McDonald RI, Douglas I, Revenga C, Hale R, Grimm N, Fekete B (2011) Global urban growth and the geography of water availability, quality, and delivery. Ambio 40:437–446
McKibbin W, Pearce D, Stegman A (2004) Can the IPCC SRES be improved? Research School of Pacific and Asian studies. Australian National University, Canberra
McMichael A, Woodruff R, Whetton P, Hennessy K, Nicholls N, Hales S, Woodward A, Kjellstrom T (2003) Human health and climate change in Oceania: risk assessment. Department of Health and Aging, Canberra
Mishra AP, Khali H, Singh S, Pande CB, Singh R, Chaurasia SK (2021) An assessment of in-situ water quality parameters and its variation with Landsat 8 level 1 surface reflectance datasets. Int J Environ Anal Chem:1. https://doi.org/10.1080/03067319.2021.1954175
Molle F, Berkoff J (2006) Cities versus agriculture: revisiting intersectoral water transfers, potential gains, and conflicts. International Water Management Institute, Colombo
MoWR (2013) Report of the standing committee on water resources, Technical report. Ministry of Water Resources, Government of India, New Delhi
Mujumdar P, Ghosh S (2008) Modeling GCM and scenario uncertainty using a possibilistic approach: application to the Mahanadi River, India. Water Resour Res 44:W06407. https://doi.org/10.1029/2007WR006137
Mukherji A, Shah T, Giordano M (2012) Managing energy-irrigation nexus in India: a typology of state interventions, IWMI-Tata water policy research highlight. IWMI-Tata Water Policy Programme, Gujarat
Nakamura H, Nishii K, Miyasaka T (2014) A diagnostic study of future evaporation changes projected in CMIP5 climate models. Clim Dyn 42:2745–2761
Nohara D, Kitoh A, Hosaka M, Oki T (2006) Impact of climate change on river discharge projected by multimodel ensemble. J Hydrometeorol 7:1076–1089
Nune R, George BA, Teluguntla P, Western AW (2014) Relating trends in streamflow to anthropogenic influences: a case study of Himayat Sagar catchment, India. Water Resour Manag 28:1579–1595
Oki T, Kanae S (2006) Global hydrological cycles and world water resources. Science 313:1068–1072
Panda DK, Kumar A, Ghosh S, Mohanty R (2013) Streamflow trends in the Mahanadi River basin (India): linkages to tropical climate variability. J Hydrol 495:135–149
Pande CB, Moharir KN, Singh SK et al (2020) Groundwater evaluation for drinking purposes using statistical index: study of Akola and Buldhana districts of Maharashtra, India. Environ Dev Sustain 22:7453–7471. https://doi.org/10.1007/s10668-019-00531-0
Pande CB, Moharir KN, Panneerselvam B et al (2021a) Delineation of groundwater potential zones for sustainable development and planning using analytical hierarchy process (AHP), and MIF techniques. Appl Water Sci 11:186. https://doi.org/10.1007/s13201-021-01522-1
Pande CB, Moharir KN, Khadri SFR (2021b) Assessment of land-use and land-cover changes in Pangari watershed area (MS), India, based on the remote sensing and GIS techniques. Appl Water Sci 11:96. https://doi.org/10.1007/s13201-021-01425-1
Pande CB, Moharir KN, Singh SK et al (2022a) Groundwater flow modeling in the basaltic hard rock area of Maharashtra, India. Appl Water Sci 12:12. https://doi.org/10.1007/s13201-021-01525-y
Pande CB, Al-Ansari N, Kushwaha NL, Srivastava A, Noor R, Kumar M, Moharir KN, Elbeltagi A (2022b) Forecasting of SPI and meteorological drought based on the artificial neural network and M5P model tree. Land 11(11):2040. https://doi.org/10.3390/land11112040
Pandit MK (2012) Potential effects of ongoing and proposed hydropower development on terrestrial biological diversity in the Indian Himalaya. Conserv Biol 26:1061–1071
Panneerselvam B, Muniraj K, Duraisamy K et al (2022) An integrated approach to explore the suitability of nitrate-contaminated groundwater for drinking purposes in a semiarid region of India. Environ Geochem Health. https://doi.org/10.1007/s10653-022-01237-5
Parry ML, Rosenzweig C, Iglesias A, Livermore M, Fischer G (2004) Global Environ Change. Glob Environ Chang 14:53–67

Peters GP, Andrew RM, Boden T, Canadell JG, Ciais P, Marland G, Raupach MR (2013) The challenge to keep global warming below 2° C. Nat Clim Chang 3:4–6
Prakash S, Sathiyamoorthy V, Mahesh C, Gairola R (2014) An evaluation of high-resolution multisatellite rainfall products over the Indian monsoon region. Int J Remote Sens 35:3018–3035
Prudhomme C, Giuntoli I, Robinson EL, Clark DB, Arnell NW, Dankers R, Franssen W (2014) Hydrological droughts in the 21st century, hotspots and uncertainties from a global multimodel ensemble experiment. Natl Acad Sci 111:3262–3267
Purohit P, Fischer D (2014) Second generation biofuel potential in India: sustainability and cost considerations. Technical report, Denmark: UNEP Risoe Centre on Energy, Climate and Sustainable Development,United Nations Environment Programme (UNEP), Nairobi
Raje D, Krishnan R (2012) Bayesian parameter uncertainty modeling in a macroscale hydrologic model and its impact on Indian river basin hydrology under climate change. Water Resour Res 48:W08522
Rajesh J et al (2021) Exploration of groundwater potential zones using analytical hierarchical process (AHP) approach in the Godavari river basin of Maharashtra in India. Appl Water Sci 11:182. https://doi.org/10.1007/s13201-021-01518-x
Rao PG (1995) Effect of climate change on streamflows in the Mahanadi river basin, India. Water Int 20:205–212
Ravindranath N, Lakshmi CS, Manuvie R, Balachandra P (2011) Biofuel production and implications for land use, food production and environment in India. Energ Policy 39:5737–5745
Reilly J, Baethgen W, Chege FE, Geikn SC, Erda L, Iglesias A, Kenny G, Petterson D, Rogasik J, Rotter R (1995) Intergovernmental Panel on Climate Change, climate change 1995: impacts, adaptations and mitigation of climate change: scientific-technical analysis. In: Watson RT, Zinyowera MC, Moss RH (eds) Scientific-technical analysis, UK. Cambridge University Press, Cambridge
Ritzema H, Satyanarayana T, Raman S, Boonstra J (2008) Subsurface drainage to combat waterlogging and salinity in irrigated lands in India: lessons learned in farmers fields. Agric Water Manag 95:179–189
Rodell M, Velicogna I, Famiglietti JS (2009) Satellite-based estimates of groundwater depletion in India. Nature 460:999–1002
Rosenzweig C, Parry M (1994) Potential impact of climate change on world food supply. Nature 367:133–138. https://doi.org/10.1038/367133a0
Rosenzweig C, Tubiello FN, Goldberg RA, Mills E, Bloomfield J (2002) Global Environ Change. Glob Environ Chang:197–202
Roxy MK, Ritika K, Terray P, Murtugudde R, Ashok K, Goswami B (2015) Drying of Indian subcontinent by rapid Indian Ocean warming and a weakening land-sea thermal gradient. Nat Commun 6:7423
Saha A, Ghosh S, Sahana AS, Rao EP (2014) Failure of CMIP5 climate models in simulating post-1950 decreasing trend of Indian monsoon. Geophys Res Lett 41:7323–7330
Salvi K, Kannan S, Ghosh S (2013) High-resolution multisite daily rainfall projections in India with statistical downscaling for climate change impacts assessment. J Geophys Res Atmos 118:3557–3578
Schellnhuber H, Frieler K, Kabat P (2014) The elephant, the blind, and the intersectoral intercomparison of climate impacts. Natl Acad Sci 111:3225–3227
Schewe J, Heinke J, Gerten D, Haddeland I, Arnell NW, Clark DB, Dankers R, Eisner S (2014) Multimodel assessment of water scarcity under climate change. Natl Acad Sci 111:3245–3250
Schmidhuber J, Shetty P (2005) The nutrition transition to 2030. Why developing countries are likely to bear the major burden. Acta Agric Scand Sect C 2(3–4):150–166. https://doi.org/10.1080/16507540500534812
Shah Z, Kumar MD (2008) In the midst of the large dam controversy: objectives, criteria for assessing large water storages in the developing world. Water Resour Manag 22:1799–1824

Shashikanth K, Madhusoodhanan C, Ghosh S, Eldho T, Rajendran K, Murtugudde R (2014a) Comparing statistically downscaled simulations of Indian monsoon at different spatial resolutions. J Hydrol 519:3163–3177

Shashikanth K, Salvi K, Ghosh S, Rajendran K (2014b) CMIP5 simulations of Indian summer monsoon rainfall differ from those of CMIP3? Atmos Sci Lett 15:79–85

Sherif M, Singh VP (1999) Effect of climate change on sea water intrusion in coastal aquifers. Hydrol Process 13:1277–1287

Shiklomanov I, Rodda J (2004) World water resources at the beginning of the twenty-first century. Cambridge University Press, Cambridge

Shiva V, Bandyopadhyay J, Hedge P, Krishnamurthy BV, Kurien J, Narendranath G, Ramprasad V (1991) Ecology and the politics of survival: conflicts over natural resources in India. Sage, New Delhi

Siam M, Demory M, Eltahir E (2013) Hydrological cycles over the Congo and Upper Blue Nile basins: evaluation of general circulation model simulations and reanalysis products. J Clim 26:8881–8894

Siebert S, Henrich V, Frenken K, Burke J (2015) Update of the global map of irrigation areas to Version 5. University of Bonn/FAO, Bonn/Rome. 08 14. http://www.fao.org/nr/water/aquastat/irrigationmap/index10.stm

Sinha A, Kathayat G, Cheng H, Breitenbach M, Berkelhammer M, Mudelsee J, Biswas J, Edwards R (2015) Trends and oscillations in the Indian summer monsoon rainfall over the last two millennia. Nat Commun 6:6309

Skaggs R, Hibbard P, Frumhoff T, Lowry R, Middleton R, Tidwell J, Arnold J (2012) Climate and energy–water–land system interactions technical report to the us department of energy in support of the national climate assessment. Technical report. Pacific Northwest National Laboratory (PNNL), Richland

Solomon S, Qin D, Manning M, Chen Z, Marquis M, Averyt KB, Tignor M, Miller H (2007) The physical science basis: contribution of working group I to the fourth assessment report of the Intergovernmental Panel on Climate Change. Cambridge University Press, Cambridge

Sreeja K, Madhusoodhanan C, Shetty P, Eldho T (2012) Inclusive spaces in integrated river basin management: discerning multiple boundaries of resource relations. Int J River Basin Manag 10:351–367

Sreeja KG, Madhusoodhanan C, Eldho T (2016) Coastal zones in integrated river basin management in the West Coast of India: delineation, boundary issues and implications. Ocean Coast Manag 119:1–13

Stocker T, Qin G, Plattner M, Tignor S, Allen J, Boschung A, Nauels Y (2013) Climate change 2013: the physical science basis. Contribution of working group I to the fifth assessment report of the Intergovernmental Panel on Climate Change. Cambridge University Press, Cambridge

Sundararajan M, Mohan A (2011) A study on the impact of coalwashery effluents along Damodar river stretch in Dhanbad District Jharkhand. Int J Eng Manag Sci 2(4):233–245

SWBD (2005) Shuttle radar topography mission water body dataset 03 3. http://www2.jpl.nasa.gov/srtm/index.html

Taheripour F, Hertel B, Gopalakrishnan S, Sahin J, Escurra J (2015) Agricultural production, irrigation, climate change, and water scarcity in India. In: 2015 AAEA & WAEA joint annual meeting, July 26–28, San Francisco, CA, No. 205591. Agricultural & Applied Economics Association & Western Agricultural Economics

TERI (2015) TERI energy and environment data diary and yearbook 2014/15, Technical report. Energy Research Institute, New Delhi

Tian H, Banger K, Dadhwal V (2014) History of land use in India during 1880–2010: large-scale land transformations reconstructed from satellite data and historical archives. Glob Planet Chang 121:78–88

Tuanmu M, Jetz W (2014) A global 1-km consensus land-cover product for biodiversity and ecosystem modelling. Glob Ecol Biogeogr 23:1031–1045

Tubiello FN (2005) Impact of climate change, variability and weather fluctuations on crops and their produce markets. Impact reports. Cambridge, pp 70–73
Tubiello FN, Fischer G (2007) Tech forecasting social change. Tech Forecasting Soc Chang 74:1030–1056
Tubiello FN, Amthor JA, Boote K, Donatelli M, Easterling WE, Fisher G, Gifford R, Howden M, Reilly J, Rosenzweig C (2006) Eur J Agron. Eur J Agron 26(3):215–223
Tubiello FN, Soussana JF, Howden SM (2007) Crop and pasture response to climate change. Proc Natl Acad Sci U S A 104(50):19686–1990. https://doi.org/10.1073/pnas.0701728104. Epub 2007 Dec 6. PMID: 18077401; PMCID: PMC2148358
UNFCCC (2021) Paris agreement, United Nations framework convention on climate change 7 9. http://unfccc.int/resource/docs/2015/cop21/eng/l09r01
Vaidyanathan A (1999) Water resource management: institutions and irrigation development in India. Oxford University Press, New Delhi
van Vliet M, Wiberg D, Leduc S, Riahi K (2016) Power-generation system vulnerability and adaptation to changes in climate and water resources. Nat Clim Chang 6:375
Vasilev V et al (2003) Variability of Shigella flexneri serotypes in Israel during a period of two years: 2000 and 2001. Epidemiol Infect 132:51–56
Vitousek P, Mooney H, Lubchenco J, Melillo J (1997) Human domination of Earth's ecosystems. Science 277:494–499
Vittal H, Karmakar S, Ghosh S (2013) Diametric changes in trends and patterns of extreme rainfall over India from pre-1950 to post-1950. Geophys Res 40:3253
WCD (2000) Dams and development: a new framework for decision-making, The report of the World Commission on Dams. Earthscan/World Commission on Dams, London

Chapter 5
Livelihood Vulnerability Assessment and Drought Events in South Africa

Israel R. Orimoloye

Abstract Livelihood and the economies of South Africa are highly vulnerable to climatic fluctuations. Drought, in particular, is one of the most significant natural factors contributing in many parts of South Africa to agricultural losses, poverty, famine, and environmental degradation. Several factors rely on the cumulative effect of drought on a given area and its ability to recover from the resulting social, economic, and environmental impacts. South Africa's vulnerability to climate variability and the risks posed by climate change and other natural disasters needs to be mitigated urgently. "This paper seeks to highlight the challenges of drought in South Africa and examines the existing livelihood vulnerability of drought, particular assets, and well-being vulnerability. This study indicates that a pragmatic strategy that incorporates innovative technology, institutional, and policy solutions to manage risks within vulnerable communities implemented by institutions operating at different levels (community, regional, and national) is considered to be the way forward for the management of drought and climate variability. This study recommends that a pragmatic strategy that incorporates innovative technology, institutional, and policy solutions to manage risks posed by recurring droughts on vulnerable communities must be continually explored. This calls for firm partnership cooperation by implementing institutions operating at different levels (community, regional, and national) as the way forward for managing drought and climate variability.

Keywords Climate change · Drought events · Vulnerability · South Africa

I. R. Orimoloye (✉)
Department of Geography, Faculty of Food and Agriculture, University of the West Indies, St. Augustine, Trinidad and Tobago

C. B. Pande et al. (eds.), *Climate Change Impacts on Natural Resources, Ecosystems and Agricultural Systems*, Springer Climate,
https://doi.org/10.1007/978-3-031-19059-9_5

Introduction

Many developing countries are currently undergoing increasing population growth with various climate-related risks including drought disasters, which contribute in turn to urban livelihood vulnerability. Though this population growth may seem to benefit these countries, it can also, if inappropriately managed, create distinct challenges for the poor or low-income groups (Pande et al. 2021a). Droughts are a common occurrence in South Africa's environment and it has impacts on society as well as agricultural production. South Africa's climate is tremendously varied over time and space due to its location in the southern tip of Africa, situated between cold and warm sea currents, as well as its topography. As a result of these attributes, the country is regarded as having one of the world's most fluctuating river flow regimes, with drought being one manifestation of this fluctuation (Haile et al. 2019; Kusangaya et al. 2021). Droughts typically occur regularly and have negative impacts on people, such as the drought disaster of 2003–2004, 2009–2010, and 2014–2019 (Gumenge 2010; Orimoloye et al. 2021). Drought risk is determined by a conjunction of drought frequency, intensity, and geographic area, as well as the degree to which a population is vulnerable to drought's impacts (UNISDR 2005). Section 1 of Act 57 of the Disaster Management Act, 2002, as revised by Act 2015 No. 16, defined vulnerability as the conditions dictated by physical, social, economic, and environmental elements or processes that raise a community's sensitivity to the effect of hazards. The act has been amended to align with widely accepted definitions used in the international context and across industries on a national level, in order to make the main act simpler and easier to comprehend (Government Gazette 2015).

Vulnerability arises as a paradigm for comprehending what it is about people's situations that allow a hazard to turn into a disaster (Adger 2006; Tapsell et al. 2005). As a result, vulnerability assessment is the process of estimating the susceptibility of elements at risk to drought disaster, which involves an evaluation of the underlying reasons for their vulnerability (Muyambo et al. 2017). Vulnerability assessment, according to Dunning and Durden (2011), defines the relationship between social traits and drought vulnerability, identifying those who are at risk. Vulnerability, according to Bogardi and Birkmann (2004), comprises exposure, susceptibility, and coping capacity. Scientists have been paying increased attention to vulnerability assessment in the context of climate change and natural disasters in recent years. Historical narrative, comparative analysis, statistical analysis, model and GIS-based (Pande et al. 2021a, b), participatory approach, indicator-based approaches, and agent-based modeling are all methods for assessing vulnerability. These methods have their strengths and weaknesses. However, the indicator-based method is one of the most extensively used methodologies for assessing susceptibility to climate change and natural catastrophes (Thao et al. 2019; Mohmmed et al. 2018). An example of the indicator-based method includes the Livelihood

Vulnerability Index (VI) (Hahn et al. 2009) among others. The Livelihood Vulnerability Index (LVI) has proved to be a useful and popular tool in assessing farmers' vulnerability to climate change and disasters around the world (Mohmmed et al. 2018; Thao et al. 2019). The livelihood vulnerability provides tools for observing potential vulnerability over time and space, identifying the processes that lead to vulnerability, prioritizing mitigation actions, and evaluating the effectiveness of these tactics in various social and ecological settings (Shah et al. 2013). According to Panthi et al. (2016), the impact of climate change and catastrophes differs by region, and vulnerability assessments must be conducted on a regional basis to be reliable. The role of environmental and social elements in drought susceptibility is yet to be well-explored or accepted in South Africa, particularly at local and regional levels. Considering the current drought occurrence in South Africa, identifying and analyzing livelihood vulnerability in accordance with drought risk reduction is a critical issue to mitigate and reduce the risk of drought (Orimoloye et al. 2022). However, all persons living in drought-stricken areas are vulnerable, and the effects of droughts disproportionately affect the most vulnerable members of society. The question is, 'who are the people in South Africa that are vulnerable to drought, and what features or systems make them vulnerable or resilient to drought?' The necessity to understand these potential vulnerabilities prompted the researchers to conduct this research in order to make effective suggestions on vulnerability reduction strategies to farmers, policymakers, and decision-makers. This study focuses on the livelihood vulnerability influenced by drought disasters in South Africa; however, more research is needed to look into the physical, economic, and environmental aspects of vulnerability as a result of recurring drought disasters in the country (Muyambo et al. 2017).

Study Area

The world, including South Africa, has been affected by disaster both human and natural disasters. Droughts, floods, landslides, and storms are common natural disasters, but climate change is increasing the frequency and severity of these weather-related risks in the Africa continent (Orimoloye et al. 2021). South Africa (Fig. 5.1) covers around 1,218,000 square kilometers and has a coastline of nearly 3000 km. Namibia, Botswana, Zimbabwe, Mozambique, Swaziland, and Lesotho share boundaries with South Africa, as well as Namibia, Botswana, Zimbabwe, Mozambique, Swaziland, and Lesotho. South Africa has a low precipitation rate, with an average annual rainfall of 497 mm which contributed to the persistent drought in the region. The climate is typically warm and dry, with winter temperatures rarely falling below 0 °C and summer maxima frequently above 35 °C (Schulze 1997).

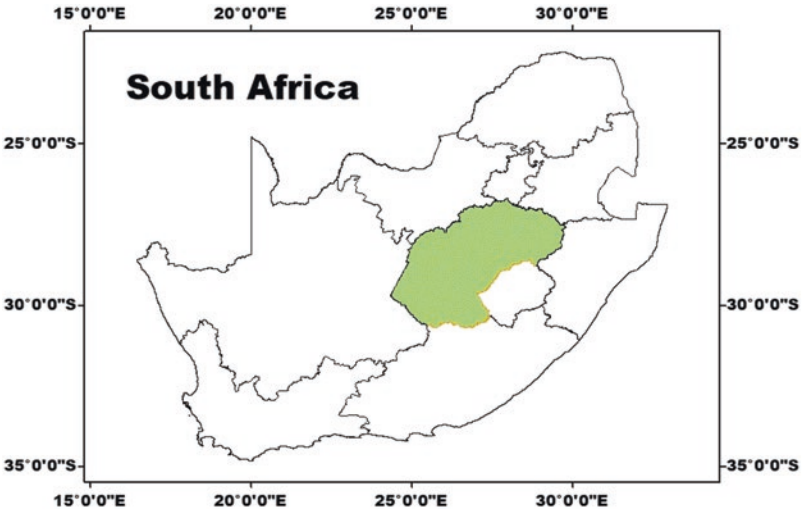

Fig. 5.1 Map showing South Africa

Impact of Drought in South Africa

Information in Table 5.1 is a list of few impacts of drought in South Africa, though these may also apply to other drought-prone places in any part of the world (Gebre and Getahun 2016). This demonstrates that, depending on the duration and severity of the drought, drought impacts are considerably more than just a food supply issue.

As the impact of drought events cannot be overemphasized, this requires government intervention in the form of emergency relief, often supported by large amounts of food or social relief. Governments' drought preparedness has generally taken the form of creating food reserves at the national level to compensate for production shortfalls and provide for possible emergency relief (Vose et al. 2016; Xulu et al. 2018). While these costly relief initiatives from the impact of drought were seen as necessary, such short-term interventions tended to prevent support for longer-term development processes, especially in locations with arid climate conditions. Because low and erratic rainfall is a key feature of these dryland areas, this fact must be reflected in government preparedness plans and in longer-term development strategies aimed at preventing future droughts from having serious consequences for the environment and people's livelihoods. This will also reduce livelihood vulnerability to drought disasters.

Table 5.1 Drought impacts

No	Impacts	Implications of livelihoods	References
1	Disrupted distribution of water resources	Communities are in grave danger due to the drought. When it gets exceedingly hot, a lack of drinking water can cause dehydration and even heat stroke. With less water available, the water's quality deteriorates. Because there is less water, the concentration of dissolved compounds rises	Olds et al. (2011)
2	Drought impact on the economy	The economic and political implications of water scarcity are significant. Drought is disastrous for affected local economies, especially those relying on agriculture; limited water can jeopardize agricultural production	Shahpari et al. (2021)
3	Marginal lands become unsustainable	The effects of government policies and further economic liberalization on the competitiveness of dryland crops in South Africa reflect the pervasiveness of poverty, as evidenced by increasing water constraints, land degradation, ongoing concerns about malnutrition, migration due to frequent droughts, lack of infrastructure, poor dissemination of improved technologies, and the effects of government policies and further economic liberalization on the competitiveness of dryland crops	Chipfupa et al. (2021)
4	Reduced grazing quality and crop yields	Drought has a negative influence on agricultural and animal farming systems in South Africa, but livestock systems, crop yields, particularly in humid temperate climates, have received less attention	Salmoral et al. (2020) and Mazibuko et al. (2021)
5	Employment lay-offs	Thousands of jobs have been shed in the agriculture industry in the Western Cape and other drought-affected provinces in South Africa, as the devastating water crisis continued. Despite interventions by all spheres of government, the looming job losses would be a further blow to the drought-stricken sector that had been under a worsening dry spell for the past few years. There were water restrictions imposed on the agricultural sector by the national government in order to find a solution or preventive measures toward combatting or reducing livelihood vulnerability to drought. Still, this place a heavy burden on one of the biggest employment sectors in the region, this will affect food production and other water-reliant industries	Cape Argus (2017)
5	Increased food insecurity	Drought conditions in South Africa resulted in lower crop yields and higher food costs. According to a recent study, this has gotten worse as a result of human-caused climate change	Piesse (2016)
6	Inequitable drought relief	Drought impacts are exacerbated by inequitable access to land. Most of the problems emanated from the inadequacy of financial resources for drought management and human development. The unavailability of drought policies and plans results in failure to adequately deal with drought impacts. These problems could be addressed with the assistance of some United Nations agencies and nations that have developed innovative drought policies	Dube (2008)

(continued)

Table 5.1 (continued)

No	Impacts	Implications of livelihoods	References
7	Increased damage to natural habitats	More than 80% of South Africa's land surface is covered by rangelands, with over 69% of these rangelands located in semi-arid areas where livestock and/or game farming are the most suited land uses. With the recurring drought events, many of these natural habitats have been affected and plantation trees suffered drought stress during the drought period	Vose et al. (2016) and Xulu et al. (2018)
8	Reduction of livestock quality	Drought caused feed prices to increase to record levels, making it unprofitable for producers to feed their own lambs for finishing. Drought in South Africa prompted producers to shrink the national commercial cattle herd by 14.4% on average between 2013 and 2016, according to research. However, certain provinces were more affected than others, and while the drought reduced the cattle herd in the Northern Cape by 34.8 percent, it also reduced the herd in the Western Cape by 4% during the same time period	Mare et al. (2018)

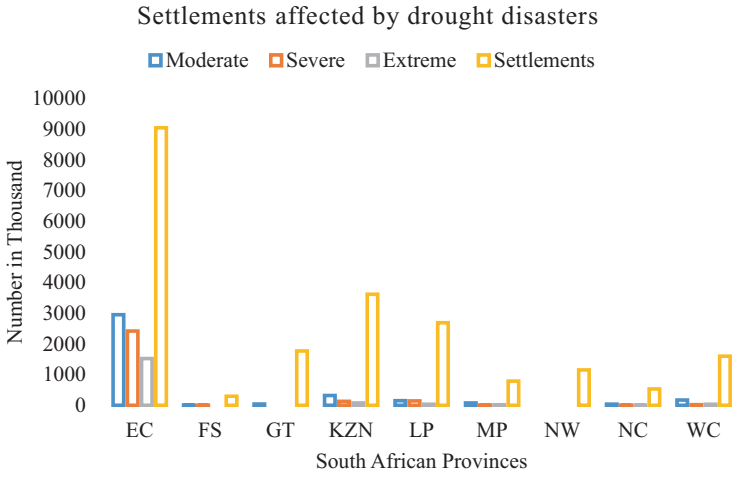

Fig. 5.2 Settlements affected by drought disasters in South Africa

Livelihood Vulnerability in South Africa

The information in Fig. 5.2 presents livelihood vulnerability to drought in South African Provinces and the number of affected settlements. The data were obtained from the National Integrated Water Information System database (https://www.dws.gov.za/NIWIS2/DroughtStatusManagement/DroughtAffectedSettlements). Eastern Cape Province was more affected by drought disaster and various settlements were vulnerable to this event. About 2952, 2421, 1524 settlements faced moderate,

severe, and extreme drought impacts as presented in Fig. 13.2. It has been shown that extensive livelihood livestock in Eastern Cape was affected mostly by the drought of which 19% of grazing areas in the province accounting for some 5600 jobs. Drought effects have caused delays in soil preparation and planting of grain crops. The Province has been officially declared as drought-stricken (Amoah 2020; Mahlalela et al. 2020). This drought has had significant socioeconomic consequences, particularly for the largely impoverished rural population as well as some metropolitan areas where water supply systems have failed in multiple instances. Both mid-latitude and tropical systems influence the region, resulting in a complicated regional climate that has received little attention compared to other parts of South Africa. Drought is one of the common disasters in the Eastern Cape, resulting in a significant socioeconomic impact on livelihood (Table 5.1), including the loss of life in some circumstances, farmland, low crop yield among others. The province is currently experiencing a severe drought (which began in 2015), with numerous settlements (Fig. 5.1) facing severe water restrictions and being on the verge of running out of potable water from the corresponding sources (Mahlalela et al. 2020). KwaZulu-Natal Province was affected by drought disaster where some regions in the province were vulnerable. This province was ranked second in South Africa with about 3619 settlements vulnerable to drought episodes. According to reports, the 2015 drought in South Africa reduced the national livestock herd by 15%, and the Red Meat Producers' Organisation projected that more than 40,000 cattle died in the KwaZulu-Natal region by the end of 2015 (Vetter et al. 2020). For example, rainfall in several parts of South Africa, particularly the Eastern Cape and neighboring KwaZulu-Natal Province, shows that there were more multi-year droughts from the late 1970s to the late 1970s than from 1950 to the late 1970s (Blamey et al. 2018). The result also revealed that Limpopo Province was ranked third vulnerable to drought in South Africa with about 148, 143, and 32 moderate, severe, and extremely vulnerable to drought, respectively. The study has shown that the current climate event in Limpopo province is dominated by drought and that as a result of the severe drought, the province has seen reduced grazing, water for cattle, and irrigation, significantly impacting agricultural livelihoods and resulting in food scarcity (Maponya and Mp 2012; Botai et al. 2020). Two thousand six hundred ninety-one settlements were affected or vulnerable to drought in Limpopo. This development required a more proactive strategy to reduce assets or well-being loss to drought in South Africa.

Western Cape and Northern Cape Provinces affected where about 1602 and 1151 settlements were vulnerable to drought disaster, respectively. In the Western Cape province's agriculture industry, drought has resulted in employment losses (Kalaba 2019; Ziervogel 2019). According to the third quarterly labor force survey from 2017, the agricultural industry lost almost 25,000 jobs across the country. In the Western Cape province, about 20,000 of these were lost and many of them were linked to the drought. The province's economy lost more than R5 billion as a result of the drought. This is significant for the country as a whole because the Western Cape accounts for 22% of the country's agricultural GDP. The citrus sector, as well as the deciduous fruit and wine industries, is important exports that contribute

significantly to South Africa's total agri-economy. More so, drought in the Northern Cape is one of the worst the province has seen in over a century. It has spread to all five districts of the Northern Cape. Drought has affected about 10,000 farms, covering more than 5.8 million hectares, with a carrying capacity of 166,000 big stock units. Droughts have become more frequent and severe in South Africa recently, particularly in water-dependent industries such as agriculture. South Africa is extremely vulnerable to new weather extremes including drought since it relies largely on climate-sensitive industries including eco-tourism, agriculture, hydropower, and fisheries. The region is already paying the price in terms of decreased food production and dam levels. Some regions of South Africa are still facing the threat of the devastating 2015/16 drought, which extended into 2018. Drought-stricken provinces such as the Eastern Cape, Northern Cape, and KwaZulu-Natal are rapidly running out of water (Amoah 2020; Mahlalela et al. 2020). Agriculture has been one of the hardest devastated sectors. As water levels decreased, crop yield and livestock numbers declined. Rural communities are particularly vulnerable in these circumstances. Winter crops become critical to family food security when the major, rainfed crops fail. However, the drought conditions are already having an adverse effect on these. Despite the fact that weather extremes are unavoidable, their impact can be mitigated via smart planning, if not, disasters can occur, leading to massive direct and indirect economic and societal costs. This has happened much too often in South Africa (Wamsler 2014; Mangani et al. 2019; Dube et al. 2020). Due to a lack of adequate early warning systems, the country is always responding to disasters rather than planning and implementing proactive measures in advance. To minimize South Africa's drought susceptibility, the Water Research Commission (WRC) policies and the findings from this study can help mitigate and reduce drought vulnerability by improving national coordination, planning, and preparation for extreme weather events.

Information in Table 5.2 presents assets vulnerability in South Africa, this is significant to livelihood stability, and the more assets vulnerable, the less the livelihood stability. South Africa recorded assets vulnerability (poor people) and non-poor people with about 70% and 64%, respectively, and access to early warning with about 607%. This development might have affected various sectors including farmers, local communities, water reliant to be vulnerable to drought disasters. According to studies, Southern Africa, particularly South Africa, is vulnerable to a number of natural and human-caused disasters that are becoming increasingly

Table 5.2 Resilience factors

Vulnerability		
Asset vulnerability, poor people (%)	Asset vulnerability, non-poor people (%)	Access to early warning (%)
70	64	60
New risk levels and socioeconomic resilience		
Risk to assets (%)	Socioeconomic resilience (%)	Risk to well-being (%)
0.39	56.01	0.69

intertwined (FAO 2018; Aryal and Marenya 2021; Branca et al. 2021). Risk levels and socioeconomic resilience in South Africa for risk to assets, socioeconomic resilience, and risk to well-being are 0.39%, 56.01%, and 0.69%, respectively. The increasing frequency and severity of disasters erode rural households' already weakened ability to forecast, cope with, and recover from risks, particularly those who rely on agriculture and are most vulnerable. Building stronger, more resilient livelihoods are critical to meeting the United Nations' 2030 Agenda for Sustainable Development's joint commitments.

Conclusion

Livelihood vulnerability to drought-related events in South Africa was exacerbated by the government's limited involvement in drought risk mitigation, the farmers' capacity, and the imbalance of decision-making authority between the experts and non-experts. People who live in drought-prone areas should build livelihood and production systems to reduce the risks posed by extreme climatic changes, such as drought disasters. Despite low returns on land, labor, and capital, farmers have long used a variety of indigenous strategies and options to manage risk and deal with poor overall productivity. However, it is widely acknowledged that low-resource agriculture may no longer be capable of meeting the livelihood demands of rising populations in these fragile dryland environments, particularly in South Africa. Land use has gotten more intensive, and land and people have become more sensitive to drought occurrences, due to the increased population in the last century and greater strain on natural resources such as land, water, and ecosystems. People, cattle, crops, and wildlife are competing for more scarce resources in a more complicated environment and through sophisticated production systems. Pressures and intensification will increase sensitivity to subsequent droughts over time, leading to increased resource degradation and output loss—a negative spiraling impact. This study recommends that a pragmatic strategy that incorporates innovative technology, institutional and policy solutions to manage risks posed by recurring droughts on vulnerable communities must be continually explored. This calls for firm partnership cooperation by implementing institutions operating at different levels (community, regional, and national) as the way forward for managing drought and climate variability.

References

Adger WN (2006) Vulnerability. Glob Environ Chang 16(3):268–281

Amoah LNA (2020) Water scarcity and food security in Ngqeleni locality in the Eastern Cape Province-South Africa

Aryal JP, Marenya P (2021) Understanding climate-risk coping strategies among farm households: evidence from five countries in Eastern and Southern Africa. Sci Total Environ 769:145236

Blamey RC, Kolusu SR, Mahlalela P, Todd MC, Reason CJC (2018) The role of regional circulation features in regulating El Niño climate impacts over southern Africa: a comparison of the 2015/2016 drought with previous events. Int J Climatol 38(11):4276–4295
Bogardi J, Birkmann J (2004) Vulnerability assessment: the first step towards sustainable risk reduction. In: Disaster and society—from hazard assessment to risk reduction, vol 1. Logos Verlag Berlin, Berlin, pp 75–82
Botai CM, Botai JO, Zwane NN, Hayombe P, Wamiti EK, Makgoale T et al (2020) Hydroclimatic extremes in the Limpopo River Basin, South Africa, under changing climate. Water 12(12):3299
Branca G, Arslan A, Paolantonio A, Grewer U, Cattaneo A, Cavatassi R et al (2021) Assessing the economic and mitigation benefits of climate-smart agriculture and its implications for political economy: a case study in Southern Africa. J Clean Prod 285:125161
Cape Argus (2017) Cape drought may lead to 17 000 job cuts. https://www.iol.co.za/capeargus/news/cape-drought-may-lead-to-17-000-job-cuts-8203391
Chipfupa U, Tagwi A, Wale E (2021) Psychological capital and climate change adaptation: empirical evidence from smallholder farmers in South Africa. Jàmbá J Disaster Risk Stud 13(1):12
Dube C (2008) The impact of Zimbabwe's drought policy on Sontala Rural community in Matabeleland South Province. Doctoral dissertation, Stellenbosch University, Stellenbosch
Dube K, Nhamo G, Chikodzi D (2020) Climate change-induced droughts and tourism: impacts and responses of Western Cape province, South Africa. J Outdoor Recreat Tour 39:100319
Dunning CM, Durden SE (2011) Social vulnerability analysis methods for corps planning. US Army Engineer Institute for Water Resources, Alexandria, VA
FAO (2018) Southern Africa Resilience strategy 2018–2021. Rome. 32 pp. License: CC BY-NC-SA 3.0 IGO
Gebre SL, Getahun YS (2016) Analysis of climate variability and drought frequency events on Limpopo River Basin, South Africa. Hydrol Curr Res 7:249
Government Gazette, 2015, Act No.16 of 2015: disaster management Amendment act, 2015. Government Gazette of Republic of South Africa, Cape Town
Gumenge P (2010) Eastern Cape reels as drought persists', Grocott's Mail, viewed 18 Sept 2015
Hahn MB, Riederer AM, Foster SO (2009) The Livelihood Vulnerability Index: a pragmatic approach to assessing risks from climate variability and change: a case study in Mozambique. Glob Environ Chang 19(1):74–88
Haile GG, Tang Q, Sun S, Huang Z, Zhang X, Liu X (2019) Droughts in East Africa: causes, impacts and resilience. Earth Sci Rev 193:146–161
International Strategy for Disaster Reduction (UNISDR) (2005) Drought, living with risk: an integrated approach to reducing societal vulnerability to drought. ISDR Ad Hoc discussion group on drought, viewed 7 July 2021, from http://www.unisdr.org/2005/task-force/tf-meetigns/7th%20TF%20mtg/tmp/Drought_information_report.pdf
Kalaba M (2019) How droughts will affect South Africa's broader economy. The Conversation, 6
Kusangaya S, Mazvimavi D, Shekede MD, Masunga B, Kunedzimwe F, Manatsa D (2021) Climate change impact on hydrological regimes and extreme events in Southern Africa. In: Climate change and water resources in Africa: perspectives and solutions towards an imminent water crisis. Springer, Cham, pp 87–129
Mahlalela PT, Blamey RC, Hart NCG, Reason CJC (2020) Drought in the Eastern Cape region of South Africa and trends in rainfall characteristics. Clim Dyn 55(9):2743–2759
Mangani R, Tesfamariam EH, Engelbrecht CJ, Bellocchi G, Hassen A, Mangani T (2019) Potential impacts of extreme weather events in main maize (Zea mays L.) producing areas of South Africa under rainfed conditions. Reg Environ Chang 19(5):1441–1452
Maponya P, Mp S (2012) Impact of drought on food scarcity in Limpopo province, South Africa. Afr J Agric Res 7(37):5270–5277
Mare F, Bahta YT, Van Niekerk W (2018) The impact of drought on commercial livestock farmers in South Africa. Dev Pract 28(7):884–898
Mazibuko SM, Mukwada G, Moeletsi ME (2021) Assessing the frequency of drought/flood severity in the Luvuvhu River catchment, Limpopo Province, South Africa. Water SA 47(2):172–184

Mohmmed A, Zhang K, Kabenge M, Keesstra S, Cerdà A, Reuben M et al (2018) Analysis of drought and vulnerability in the North Darfur region of Sudan. Land Degrad Dev 29(12):4424–4438

Muyambo F, Jordaan AJ, Bahta YT (2017) Assessing social vulnerability to drought in South Africa: policy implication for drought risk reduction. Jàmbá J Disaster Risk Stud 9(1):1–7

Olds BP, Peterson BC, Koupal KD, Farnsworth-Hoback KM, Schoenebeck CW, Hoback WW (2011) Water quality parameters of a Nebraska reservoir differ between drought and normal conditions. Lake Reserv Manag 27(3):229–234

Orimoloye IR, Zhou L, Kalumba AM (2021) Drought disaster risk adaptation through ecosystem services-based solutions: way forward for South Africa. Sustainability (Switzerland) 13(8) 10.3390/su13084132

Orimoloye IR, Olusola AO, Belle JA et al (2022) Drought disaster monitoring and land use dynamics: identification of drought drivers using regression-based algorithms. Nat Hazards 112:1085. https://doi.org/10.1007/s11069-022-05219-9

Pande CB, Moharir KN, Khadri SFR (2021a) Assessment of land-use and land-cover changes in Pangari watershed area (MS), India, based on the remote sensing and GIS techniques. Appl Water Sci (2021) Impact factor: 3.87, Five Year Impact Factor: 4.39. 11:96. https://doi.org/10.1007/s13201-021-01425-1

Pande CB, Moharir KN, Singh SK, Varade AM, Ahmed Elbeltagie SFR, Khadri PC (2021b) Estimation of crop and forest biomass resources in a semi-arid region using satellite data and GIS. J Saudi Soc Agric Sci 20(5):302–311

Panthi J, Aryal S, Dahal P, Bhandari P, Krakauer NY, Pandey VP (2016) Livelihood vulnerability approach to assessing climate change impacts on mixed agro-livestock smallholders around the Gandaki River Basin in Nepal. Reg Environ Chang 16(4):1121–1132

Piesse M (2016) South Africa: drought threatens food, energy and water security. Strategic analysis. Paper, Global Food and Water Crises Research Programme

Salmoral G, Ababio B, Holman IP (2020) Drought impacts, coping responses and adaptation in the UK outdoor livestock sector: insights to increase drought resilience. Landscape 9(6):202

Schulze RE (1997) South African Atlas of agrohydrology and climatology: contribution towards a final report to the Water Research Commission on Project 492: modelling impacts of the Agricultural Environment on Water Resources: TT82-96. Water Research Commission (WRC)

Shah KU, Dulal HB, Johnson C, Baptiste A (2013) Understanding livelihood vulnerability to climate change: applying the livelihood vulnerability index in Trinidad and Tobago. Geoforum 47:125–137

Shahpari G, Sadeghi H, Ashena M, García-León D (2021) Drought effects on the Iranian economy: a computable general equilibrium approach. Environ Dev Sustain 24:4110–4127

Tapsell S, Tunstall S, Green C, Fernández-Bilbao A (2005) Task 11 social indicator set, Floodsite Project Report

Thao NTT, Khoi DN, Xuan TT, Tychon B (2019) Assessment of livelihood vulnerability to drought: a case study in Dak Nong Province, Vietnam. Int J Disaster Risk Sci 10(4):604–615

Vetter S, Goodall VL, Alcock R (2020) Effect of drought on communal livestock farmers in KwaZulu-Natal, South Africa. Afr J Range Forage Sci 37(1):93–106

Vose J, Clark JS, Luce C, Patel-Weynand T (2016) Effects of drought on forests and rangelands in the United States: a comprehensive science synthesis, Gen. Tech. Rep. WO-93b, vol 93. US Department of Agriculture, Forest Service, Washington Office, Washington, DC, pp 1–289

Wamsler C (2014) Cities, disaster risk and adaptation. Routledge, Routledge, New York, US

Xulu S, Peerbhay K, Gebreslasie M, Ismail R (2018) Drought influence on forest plantations in Zululand, South Africa, using MODIS time series and climate data. Forests 9(9):528

Ziervogel G (2019) Unpacking the Cape Town drought: lessons learned. Cities support programme|Climate resilience paper. African Centre for Cities

Chapter 6
Possible Influence of Urbanisation on Rainfall in Recent Past

Prabhat Kumar, Archisman Barat, P. Parth Sarthi, and Devendra Kumar Tiwari

Abstract The detection of weather and climate change caused by urbanisation is an important issue to understand and future projection of local weather change due to anthropogenic activities. Observational and climatological studies of alteration in convective phenomena over and around the urban area are reviewed with a focus on urban-modified downwind enhancement of rainfall. Causative factors for the alteration of urban precipitation can be urban heat island, surface roughness and anthropogenic aerosol. Monitoring of urban climate through high-resolution datasets was found to be quite important in today's era of climate change. A detailed study through high-resolution CHIRPS-gridded data has been done for the cities of Patna and Gaya. The Mann–Kendall test and Pettitt's test also indicated a changing trend in the rainfall intensity regime in the recent past for Patna, while a decreasing rainfall over Gaya has been envisaged by time-series analysis.

Keywords Climate change · CHIRPS · Precipitation · Proba-V · Urbanisation

Introduction

Around the globe, the enormous growth of urban areas has been occurring due to the migration of people from rural areas to the city. It is estimated that by 2050 about 66% of the world population will reside in urban areas (UN 2014). According to census records of India 2011, India's population has risen from 1.02 billion in 2001 to 1.21 billion in 2011 and the urban population of India is approximately 31.20% of the total population of the country and is greater than 377.1 million. The rapid growth of urban population and economic activities implies a growing need for space. In the year 1900, only about 13% of the global population lived in urban areas, which increased to 29% and crossed the 50% in 2012 (UN 2010). It was

P. Kumar · A. Barat · P. P. Sarthi (✉) · D. K. Tiwari
Department of Environmental Science, Central University of South Bihar, Gaya, Bihar, India

C. B. Pande et al. (eds.), *Climate Change Impacts on Natural Resources, Ecosystems and Agricultural Systems*, Springer Climate,
https://doi.org/10.1007/978-3-031-19059-9_6

estimated that in 2030 approximately 70% of the world population will be living in cities. The process of urbanisation got strengthened after the industrial revolution in the western countries which led to the development of infrastructure, transportation, communication and intensified urban migration (Bhagat 2005). Basically, the growth of urbanisation in India is taking place in two ways, one is through the increase in urban population, which will be natural and the second is through the migration of people from non-urban to urban areas. The high demand for space modifies the natural land surfaces to the artificial surfaces that cause modification of microclimate and enhancement in the surface roughness, resulting in alteration of energy budget in cities and regional atmospheric parameters. Alteration in surface roughness causes a change in energy budget in cities and regional atmospheric parameters. Larger surface roughness causes the air/storm passing over a city to slow down and bifurcate and split near the upwind side of the city and the bifurcated air can remerge towards the leeward side of the city as a more powerful storm (Cotton and Pielke 1995; Tumanov et al. 1999; Miao et al. 2011). The urban heat islands, one of the most common urban climatic phenomena, induces the downwind updraft cells which initiate deep moist convection. The strong updraft cell is also responsible for downwind enhancement in precipitation (Han et al. 2014a). Another major effect of urbanisation is the lowering of albedo, which can be due to the darker surface material having high radiation trapping capacity (Heisler and Brazel 2010). Urbanisation also alters the rainfall patterns by changing the convective available potential energy (CAPE) (Shepherd and Burian 2003). Rainfall is a heterogeneous weather parameter that can be varied with space and time, and it depends on the local condition prevailing in a particular area. Increased population and emission of anthropogenic aerosols in urban areas also in turn interact as cloud condensation nuclei (CCN) and causing the cloud to store more droplets of cloud water that influence regional rainfall (Zhong and Yang 2015; Parth Sarthi et al. 2021). Heavy convective activity releases latent heat which plays an important role in extreme rainfall and thunderstorms. Due to convection warm air rises and the water vapour, it contains condenses onto cloud condensation nuclei. Rising air parcels become saturated when the water vapour condenses and forms a cloud, which releases latent heat to the atmosphere. The released latent heat warms the surrounding air and causes instability in new cloud droplets. The warmth near the cloud droplet will start to rise and condensate. That causes enhancement in cloud height and thunderstorms can be formed from these growing clouds (Kishtawal et al. 2010) in the downwind, resulting in an enhancement in rainfall in the downwind side.

Studies on the Rainfall and Urbanisation Through Observations

Many studies evaluated the relationship between urban areas and precipitation (Table 6.1). Oke (2002) states that cities have different climatology with respect to their surrounding rural area. In cities, the natural land surface (grass, crops and soil) is replaced by the artificial surface (concrete and asphalt) that have different surface

Table 6.1 Some important studies regarding urbanisation and rainfall from last two decades

Authors	Key finding
Thielen et al. (2000)	Urban rainfall is increasing with an increase in surface roughness
Shepherd et al. (2002)	Increase rainfall rate in downwind impact area by 48%–116% to the mean value of upwind control area
Rozoff et al. (2003)	Interactions associated with urban surface friction, momentum drag, and heating could induce downwind converge
Han and Baik (2008)	UHI-induced air parcel upward motion on downwind side is factor for the rainfall enhancement in the downwind side of an urban area
Shem and Shepherd (2009)	Enhancement in rainfall amount is attributed to intensify activity within the boundary layer result from UHI effect
Kishtawal et al. (2010)	Urban areas are more(less) likely to experience heavier (lighter) rainfall rate compared to non-urban areas
Niyogi et al. (2011)	Indianapolis urban area change the convective system structure, intensity and the wind split when they approach the city and converge towards the downwind side of the city
Han et al. (2012)	Aerosol concentration of urban area causes strong convective cloud development mainly due to the release of the higher amount of latent heat released in the condensation process
Hazra et al. (2017)	In a polluted atmosphere, the increased release of latent heat invigorates the cloud system to generate more ice hydrometers and cloud condensed nuclei eventually more rain at the downwind side
Sarangi et al. (2018a)	Aerosol-induced microphysical change which delay the initiation of warm rainfall (over the upwind region) but increase in ice phase particle formation (over the downwind area) resulting enhancement in downwind rainfall

roughness and thermal inertia (albedo, thermal conductivity and emissivity). These surfaces have more capacity to store solar energy and convert it to sensible heat. Urbanisation changes the rainfall patterns by the changes in convective available potential energy (CAPE) as a result of mesoscale circulation (Shepherd and Burian 2003; Niyogi et al. 2006), the larger the CAPE, the more intense the convection. This change by the formation of convective clouds causes alterations in precipitation and the hydro-meteorological environment. Convective rainfall generally depends on the vertical stratification of temperature, wind and water vapour (Pielke 2001). Huff and Changnon (1972) reported in the past that warm season rainfall increases by 9%–17% over the downwind side of the cities. An urban area is also associated with increased emission of anthropogenic aerosols which interact with cloud microphysics by serving as cloud condensation nuclei (CCN). This can be better understood with reference to the first and second indirect effects and the semi-direct effect (Tripathi et al. 2007). The first indirect effect (FIE) or Twomey effect (Twomey 1977) states that when CCN increases (mainly the fine mode aerosols like anthropogenic aerosols), in a constant cloud water content, there will be the formation of numerous small droplets. These clouds with smaller particles will not precipitate easily and the cloud lifetime will be increased (as defined by Albrecht effect/ second indirect effect (SIE)) (Albrecht 1989), further depreciation of rainfall

will happen by evaporation of these smaller cloud particles, i.e. the semi-direct effect (SDE) (Khain et al. 2005; Lohmann and Feichter 2005), and this will further influence regional rainfall (Rosenfeld and Woodley 2003; Zhong and Yang 2015; Zhong et al. 2017). Guo et al. (2014) observed the 40 years (1966–2005) data of aerosol concentration and rainfall at the seven stations during summer months over North China. They categorise hourly rainfall data into four groups: high (8 mm/h), moderate (2–8 mm/h) and low (0.6–2 mm/h and very low (0.6 mm/h). They found an enhancement in aerosol concentration causes the decreasing trend of light rainfall along with the orographic enhancement factor. They also checked the trend of environmental parameters like wind speed and direction; CAPE and vertical wind shear are responsible for the suppression of light rainfall, but they found no direct links. At the same time, the enhancement of rainfall is also widely documented by researchers across the globe. Burian and Shepherd (2005) analysed the rainfall pattern over Houston for the pre-urban time period (1940–1958) and a post-urban time period (1984–1999) to envisage the impacts of urbanisation. In this study, the average maximum 1-h rainfall intensity during warm season found to be increased by 16% from the pre- to post-urban period in the urban area. A 4% increase in rainfall over the upwind control region was also noticed. Sarangi et al. (2018b) analysed the spatial distribution of rainfall around metropolitan cities located in the central Gangetic Basin (GB). They used 4-year in situ data (2013–2016) between June and September from three automatic weather stations (AWS) in and around Kanpur. The analysis found that the amount of precipitation received in the urban area is significantly higher than the region located to the south of the city, and also the frequency of occurrence in late evening rainfall is higher in an urban area than in a rural area. In the same study, observations of TRMM-PR data at fine resolution (5 Km × 5 Km) visualised that the downwind regions of Kanpur had received heavier rainfall compared to the urban region. Sarangi et al. (2018b) also simulate a high-resolution WRF model (version .3.6.1) to the regional weather over India using three nested domains during 4–20 August 2011 (Output at the hourly frequency) on various cities of North India. The observation of the WRF dataset supported that downwind enhancement of rainfall is a prevalent phenomenon not only in Kanpur but also in other cities in North India. CCN concentration is reduced by a factor of 100 (over the Greater Kanpur region) when urban land use land covers (LULC) of Kanpur city, in all domains, are replaced with cropland LULC (Pande et al. 2018, 2021a). The LULC change affects the surface energy balance that causes the higher temperature in the near-surface layer over the urban area. Wind convergence at lower troposphere height over the city is caused by the formation of the low-pressure region due to an increase in temperature. Convergence caused an enhancement in the updraft cell that increased the water concentration in the cloud, which led to an enhancement in surface rainfall over the urban region. The Metropolitan Experiment (METROMEX) was an extensive study performed in St Louis (Midwest USA) in the 1970s to investigate the alteration in convective precipitation due to urbanisation. The observational result from METROMEX shows that urbanisation causes enhancement in rainfall amounts of 5%–25% in downwind of the cities (Changnon et al. 1977). Shepherd et al. (2002) used data from the world's first satellite-based

TRMM satellite's precipitation radar (PR) data to identify warm season rainfall patterns for the cities of Atlanta, Montgomery, Dallas, Waco and San Antonia in the USA. Results reveal that the average percentage increase in mean monthly rainfall rate is 28% towards the 30–60 km leeward side of the urban area with a 5.6% enhancement over the city. The result shows the maximum rainfall rate in downwind impact areas increased by 48%–116% to the mean value of the upwind control area (UCA). Shepherd and Burian (2003) used data from precipitation radar (PR) aboard the Tropical Rainfall Measuring Mission (TRMM) and ground-based rain gauges to quantify rainfall anomalies that they hypothesise to be linked to extensive urbanisation in the Huston River. The observational analysis of 5-year data showed a 28% enhancement in the mean rainfall rate in the downwind side of the urban-impacted region (UIR) over an upwind control region (UCR). The high amount of release of latent heat in the urban environment is also found to be quite important in earlier studies, as this may induce the cloud system to generate more ice hydrometeors and eventually resulting in more precipitation (Hazra et al. 2017; Prabha et al. 2012). In a study over Indianapolis, urban areas found to change the convective system structure, pathway and intensity; the wind found to split when they approach the city and converge towards the downwind side of the city (Niyogi et al. 2011). Kishtawal et al. (2010) investigated the in situ and satellite-based precipitation data and the population dataset to observe the relationship between urbanisation and Indian monsoon rainfall change. The urban region experiences a decreasing trend of light precipitation and a higher occurrence of intense precipitation compared to the non-urban region. They used 10-year Tropical Rainfall Measurement Mission (TRMM) combined rain rate product (3G68) at 0.5° × 0.5° resolution grids. The result from satellite data indicates that urban areas are more(less) likely to experience heavier (lighter) rainfall rates compared to rural areas. Shastri et al. (2015) analysed the impact of urbanisation on Indian summer monsoon rainfall. For this observation, they select 42 urban regions and compare their extreme rainfall characteristics with the surrounding non-urban area. They observed urban signatures on extreme precipitation are not uniformly visible at all places. They consider seven metrological homogeneous zones of India for analysis, identified by India Meteorological Department (IMD) (Parthasarathy and Yang 1995). Zonal analysis reveals that the impact of urbanisation on extreme rainfall in Southern, Central and Western India is clearly visible but in North India; this impact shows a large-scale decreasing trend. To detect the impact of urbanisation on rainfall, the most populated coastal city of Mumbai with its nearby non-urban area Alibaug has taken. Both have the same geographical area but differ in the context of urbanisation. The result reveals that urbanisation has intensified the extreme rainfall in Mumbai, which is not seen in Alibaug.

Han et al. (2014a) reviewed urban impacts on precipitation and analysed the cause for changes in convective phenomena over and around the cities with a focus on the enhancement of rainfall in downwind of cities. Thielen et al. (2000) demonstrated that rainfall is increasing with an increase in surface roughness. Han et al. (2012) explain the increased aerosol concentration of urban areas causes strong

convective cloud development mainly due to the release of the higher amount of latent heat in the condensation process (Table 6.1).

Urban Features, Processes and Mechanisms Influencing the Rainfall

Causative factors of urban climate modification are often linked to aerosol-cloud interactions, UHIs, surface roughness effect and heat fluxes (Arnfield 2003; Oke 1988). The key processes may be summarised as follows.

Aerosols, Cloud Physics and Heat Fluxes

Anthropogenic aerosols in urban areas interact with cloud microphysics by serving as CCN which interact with solar radiation and influence the regional climate (Collier 2006; Zhong et al. 2017). Urbanised areas are associated with a high rate of emission of anthropogenic aerosol. While some studies show that enhancement in aerosol number concentration suppresses rainfall from warm shallow clouds by the formation of the narrow drop size distribution (Teller and Levin 2006; Muhlbauer and Lohmann 2006; Parth Sarthi et al. 2021), other studies indicate that enhancement in aerosol concentration increases the precipitation (Rosenfeld et al. 2012; Khain et al. 2008). While summarising, a number of studies indicate that the impact of enhancement of aerosol concentration can either increase or decrease rainfall depending upon the environmental conditions, wind shear and cloud type (Fan et al. 2009). In a polluted atmosphere, the increased release of latent heat invigorates the cloud system to generate more ice hydrometers and cloud condensed nuclei, eventually more rain at the downwind side (Hazra et al. 2017). Enhancement in cloud condensed nuclei concentration is directly associated with the formation of smaller effective radios cloud droplets that lead to lower efficient collision-coalescence processes and inhibit raindrop formation processes (Rosenfeld 2000). The cloud condensed nuclei induced buoyancy that would push the lower condensates above the freezing level (Lensky and Rosenfeld 2006). Borys et al. (2003) analysed combined remote sensing and in situ mountaintop measurement data and showed that pollution in the urban areas decreases the cloud droplet size causing lower snowfall rates from mixed-phase clouds in a mountainous region by decrease in the rimming process. Some studies show the downwind shift of precipitation from the orographic clouds which is due to aerosols; aerosol inhibits the conversion of cloud ice to rainfall (Konwar et al. 2010). Heever and Cotton (2007) investigate the mechanism associated with downwind precipitation modification involving the effect of urban aerosol concentration. Studies highlight urban aerosol can directly link with the convective storm and intense rainfall. Some studies also demonstrate that high aerosol concentration is directly proportional to the summer precipitation (Lacke et al.

2009). A positive correlation between cloud to ground lightning activity and aerosol concentration is found in many areas. Choi et al. (2008) observed both surface and satellite data and found higher aerosol concentration is directly correlated with an increase in moderate rainfall events. Some studies explain the observed enhancement in rainfall in the polluted area by the mechanism of strong convection to move more cloud water to the upper atmosphere and after freezing release additional latent heat. Enhancement in aerosol concentration can increase the air humidity and intense convection occurs (Farias et al. 2014). Some previous modelling and observational studies indicate that aerosol concentration can increase or decrease the rainfall amount, which depends upon the relative humidity, wind shear, CAPE. Sarangi et al. (2019) demonstrate aerosol-induced microphysical change which delays the initiation of warm rainfall towards the upwind side but increases in ice phase particle formation over the downwind area side resulting in an enhancement in downwind rainfall. Sarangi et al. (2018a) explain enhancement in cloud condensed nuclei in urban areas is associated with the formation of more cloud droplets with a very small effective radius, which leads to a lower efficient collision-coalescence process that delays the formation of raindrops. A smaller rain droplet causes lower effective terminal velocity and enhancement in cloud droplet mobility upward. An increasing CCN concentration induces buoyancy that pushes the smaller condensates above the freezing level. The supercooled liquid above freezing liberates latent heat that exhilarates the cloud microphysics (Altaratz et al. 2014), which enhances the ice-water accretion process (Rosenfeld et al. 2008). Urban polluted areas enhance the cloud condensation nuclei that increase the convective-convergence zone, resulting in more instability and updraft. Enhancements in clouds invigorate the spatiotemporal shift of occurrence of precipitation towards the downwind region. Systematic modelling study is required to understand the mechanism for the enhancement of rainfall in the downwind side and the size distribution of aerosol particles. Also, the cloud-aerosol interactions and the mechanism involved need to be investigated. The lower collision efficiency of cloud droplets causes strong updraft under higher aerosol concentrations to result in enhancement of liquid water content (LWC) at a higher level, leading to the increased riming process that produces large ice particles. The melting of a larger amount of hail caused enhancement of rainfall in the downwind side of the urban area with increasing urban aerosol (Han et al. 2012). Changnon and Westcott (2002) documented the fast development of moving storms was observed in some urban areas which were seen in the London area. Pinto et al. (2013) demonstrate that enhancement in rainfall rate in Korean cities is directly related to the population growth in the cities. Inoue and Kimura (2004) hypothesised higher sensible heat flux causes enhancement in the mixing layer height, so the formation of the cloud is taken at the top of the enlarged thermals, and uplift and convergence of air occurred due to urban–rural temperature contrast. They saw an enhancement in a low-level cloud over Tokyo Japan. Schmid et al. (1991) demonstrate variation in solar flux across urban areas, due to the variability in building material, artificial surfaces and land use across the urban area. In cities, lower albedo is due to the darker surface material having high radiation trapping capacity and converting it to sensible heat (Heisler and Brazel 2010). These

surfaces have more capacity to store solar energy and convert it to sensible heat. Observation of previous studies of boundary layer and urban energy balance shows the flowing generic characteristic of urban areas. Harman and Belcher (2006) have discussed the different types of fluxes observed in an urban environment. These are (a) momentum flux (rural areas are less rough than the urban counterparts (Oke 2002)), (b) latent heat flux (lower in urban areas (Cleugh and Oke 1986)), (c) sensible heat flux (urban areas have higher sensible heat flux and positive sensible heat flux is found throughout the night (Oke et al. 1999) and (d) ground heat flux (artificial surfaces of urban areas stored larger ground heat flux than surrounding rural areas (Cleugh and Oke 1986)).

Urban Land Cover and Surface Roughness

Alteration in surface roughness causes a change in energy budget in cities and regional atmospheric parameters. Larger surface roughness causes the air/storm passing over a city to slow down and split near the upwind side of the city. The bifurcated air can remerge towards the leeward side of the city as a more powerful storm (Cotton and Pielke 1995; Tumanov et al. 1999; Miao et al. 2011; Pande et al. 2021b). Changes in surface roughness of urban and non-urban areas lead to a change in airflow. Enhancement in surface roughness alters the energy budget in cities and regional atmospheric parameters. Due to larger surface roughness in an urban area than the surrounding non-urban area air reaching the city to slow down nears the upwind side of the city. Larger surface roughness causes the air/storm passing over a city to slow down and bifurcate and split near the upwind side of the city. The bifurcated air can remerge towards the leeward side of the city as a more powerful storm (Cotton and Pielke 1995; Tumanov et al. 1999; Miao et al. 2011). Some studies show the downwind shift of precipitation from demonstrating that rainfall is increasing with an increase in surface roughness. Shepherd (2005) reviews the mechanism of rainfall enhancement due to urbanisation. He demonstrated that enhancement in the surface roughness in a city causes an increment in sensible heat fluxes and enhancement in aerosol concentration that works like clouds condensation nuclei. Han and Baik (2008) and Rozoff et al. (2003) used a three-dimensional model to show the upward motion of airflow will become stronger with an increase in surface roughness.

Urban Heat Island and Their Consequences on Rainfall

An urban heat island (UHI) occurs when the city experiences warmer temperatures than the nearby non-urban or rural areas. In the urban area, the natural land surface (grass, crops and soil) is replaced by the artificial surface (concrete and asphalt) that have different surface roughness, albedo and thermal properties (thermal inertia, thermal conductivity and emissivity). These surfaces have more capacity to store solar energy and convert it to sensible heat. During daytime urban areas store

radiating energy in concrete, asphalt and building material. This stored energy is used to compensate negative radiation at night, resulting the high night temperature of the urban area than the surrounding rural area. The UHI is regarded as a low-level heat source that induces airflow/circulation and modifies urban boundary layer processes. Baik (1992) carried out a two-dimensional study to investigate the characteristic of airflow past and UHI in a basic state flow with shear. Olfe and Lee (1971) also carried out two-dimensional uniform steady-state flow calculations. They analyse that upward motion in the downwind side and downward motion in the upwind side of the urban heat island. Lin and Smith (1986) solve the time-dependent problem of airflow near the hot sources. They found that air parcels descend over a heat island side and rise over the downwind side. Han and Baik (2008) and Baik et al. (2007) also suggested that UHI-induced air parcel upward motion on the downwind side is a factor for the rainfall enhancement in the downwind side of an urban area. Baik and Chun (1997) used the perturbation method to solve a weakly nonlinear problem in two dimensions. Bornstein and Lin (2000) analyse the surface precipitation data in the Atlanta area and states that convective thunderstorms were induced due to urban heat island. Baik et al. (2001) demonstrated that urban heat island induced the downwind updraft cells which initiate deep moist convection. The strong updraft cell is responsible for downwind enhancement in precipitation. Han et al. (2014b) conclude that urban heat island and the mechanism of occurrence of thunderstorms over the downwind of cities are often in the afternoon and in the morning in summer. The Indian summer monsoon is a mesoscale convective cloud system that mainly mixed-phase clouds. The above study reveals that urban heat island-induced strong updraft can produce more clouds/thunderstorms on the downwind side, resulting in an enhancement in rainfall on the downwind side. Dou et al. (2015) have investigated why somewhere show enhancement in rainfall over the urban area, while others indicate an increasing trend towards the downwind of the cities. They state that high UHI and low wind over the urban area induce convergence that causes enhancement in rainfall over the urban area or on the other hand the high wind and low urban heat island impact create a barrier effect that intensified rain downwind and around the urban area.

Modelling Studies on Rainfall and Urbanisation

Thielen et al. (2000) used a two-dimensional mesoscale model with cloud microphysics to analyse the impact of urban surfaces on urban and non-urban rainfall anomalies. This model is started with surface temperature, dew point temperature, and surface roughness. The result of this model implies that increasing near-surface temperature in the urban area is mostly due to the larger sensible heat flux in urban areas than non-urban areas; this exhibits an increase in the urban heat island effect. Kusaka et al. (2001) used a single-layer canopy model for energy and momentum exchange between the urban rough surface and surrounding. They demonstrated that the urban area leads to breaking the squall line into convective cells over the

city. By the observation of extensive previous studies, it is not clear whether surface roughness alone can initiate moist convection, also bifurcated convective systems can enhance the rainfall in the downwind side of the city or not. Rainfall can increase or decrease depending upon the flowing factor such as surface roughness and water vapour supply. Georgescu et al. (2008) used an atmospheric model and urban land cover data from 1973 to 2001 and simulated the impact of urbanisation and irrigation in the Phoenix area rainfall during monsoon seasons (Shahid et al. 2021). They found that enhancement in rainfall in the north and northeast of the phoenix urban area during the dry monsoon years. Shem and Shepherd (2009) used a three-dimensional mesoscale model to analyse the case of two studies over Atlanta. They found precipitation amounts in the downwind of the urban area to be 10%–13% higher than the city. In the simulation model, the city of Atlanta is replaced by the land use land cover type of the nearby non-urban area. Zhang et al. (2018) have investigated the impacts of urbanisation on rainfall modification by using the WRF and concluded that urbanisation causes enhancement in precipitation and flooding in the urban area. Freitag et al. (2018) have investigated rainfall modification over San Miguel De Tucuman, Argentina, by using satellite data and the WRF model and found that 20%–30% less rainfall towards the downwind of the city. Zhang et al. (2009) observed the decreasing trend of summer rainfall over Beijing, and the result reveals that urbanisation causes reduction in CAPE that is the reason for less precipitation. Previous studies indicate that some regions of the world show an increasing trend of precipitation over and downwind due to urbanisation, but some regions show a decreasing trend. To find the cause and mechanism, further in-depth analysis of the climatological model is required.

All these previous works show a close link between the impacts of urbanisation on weather events and climatic precipitation trends. Most of the observation reveals that urbanisation increases the mean rainfall rate in the downwind side of the urban area. In upcoming decades, the urban–rural ratio will be expected to increase more rapidly, so it is important to start the assessment of the impact of such urbanisation on the climate. While most of the earlier rainfall studies were based on spatial resolutions nearing quarter to half degree, which were incapable of recording precipitation for smaller cities. It is evident that the smaller cities are also showing fast increasing trends of climate modification at microscales (Barat et al. 2018, 2021) hence are needed to be studied at priority. For this purpose, in the present study, we have considered documenting the long-term changes in rainfall trends using very high-resolution gridded data for two cities from Bihar in the middle Gangetic plains of India. After a thorough review of the existing knowledge of urban–rainfall relations in Introduction (section "Introduction"), the materials (Study area and Data) and methods have been documented in section "Changes in rainfall characteristics over a typical urban centre of gangetic plain". Results are reported and discussed in section "Results and discussion" followed by conclusions, recommendations and references thereafter.

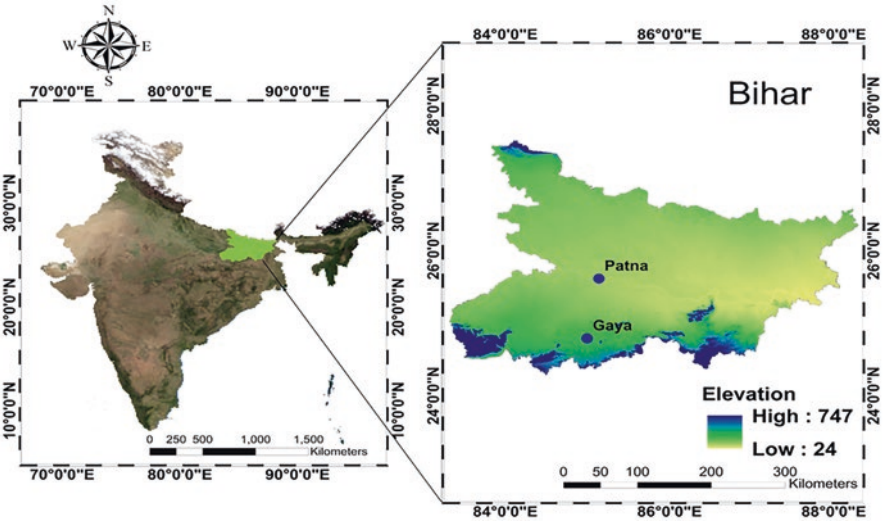

Fig. 6.1 General topography of the study area

Changes in Rainfall Characteristics Over a Typical Urban Centre of Gangetic Plain

Study Area

Two largest cities from Bihar state lying in the middle Gangetic plain (Fig. 6.1), India, are selected for the study, namely, Patna and Gaya. Both of the stations fall in the Cwa category in Köppen classification. These cities being important settlements are directly linked with fast urbanisation. The census data for these cities reflects Patna is home to 1,697,976 people and the Gaya has 394,945 residents (https://censusindia.gov.in/towns/town.aspx). The Gangetic plains is the home to the 40% people in India (Mishra et al. 2017), and due to fast urbanisation currently facing many severe issues, especially the urban centres.

Data and Methods

In the present research, it has been undertaken to analyse the characteristics of Indian Summer Monsoon Rainfall (ISMR) over the urban areas of Patna and Gaya for the months of June, July, August and September (hereafter JJAS). For this purpose, the urban areas are delineated using very high-resolution Copernicus

CGLS-LC 100 (v. 3.0.1) land cover data from Proba-V satellite (Buchhorn et al. 2020). The high-resolution (0.05° × 0.05°) daily gridded rainfall data from CHIRPS (Funk et al. 2015) dataset is considered for the present study for the period of 1981–2021. Each month of JJAS is analysed to visualise the trend of low-to-moderate rainfall events (0–35.6 mm/day) and rather heavy to extremely heavy rainfall (> = 35.6 mm) events during the last four decades. The statistical tests Mann–Kendall test (Mann 1945; Kendall 1975) and Pettitt's test (Pettitt 1979) were used to detect the trend in time series along with the change in central tendency.

Results and Discussion

All the 4 months were individually analysed for the trends in rainfall. Through the time-series analysis (Fig. 6.2a–d), we can see that the days with light rains are found to be increasing, especially over Patna (for June and August) and Gaya (for August), whereas a slight decrease in heavy rainy days was observed for Gaya (August). The Gaya falls under agro-climatic zone 3b which is infamous for the severe drought-like conditions (Kumar et al. 2019) and decrease in the heavy rainfall cases and increase in light rainy days may have a linkage with the urban aerosols and suppression of rainfall as discussed by previous researchers (Parth Sarthi et al. 2021). On the other hand, the increase in light intensity rainfall days over Patna is noticed. As Patna is situated on the riverfront and its microclimatic variability is very much influenced by the river Ganga (Barat et al. 2021), there may be an effect of localised convection intensified by urban processes. To visualise any significant trend and

Fig. 6.2 No. of light and heavy rainfall days over Patna (**a**–**b**) and no. of light and heavy rainfall over Gaya (**c**–**d**)

Table 6.2a Pettitt's test and Mann–Kendall test result for light rainfall Patna

	Pettitt's test			Mann-Kendall test($\alpha = 0.05$)		
Months	*U*	*p*-value	*K*	*S*	Tau	*p*-value
June	307	0.0006645	18	283.00	0.3601	0.0014
July	117	0.6249	17	20.84	23.1861	0.4154
August	247	0.0112	13	235.0	0.2947	0.00831
September	91	0.9895	38	14.86	15.5035	0.5722

Table 6.2b Pettitt's test and Mann–Kendall test result for heavy rainfall Patna

	Pettitt's test			Mann-Kendall test($\alpha = 0.05$)		
Months	*U*	*p*-value	*K*	*S*	Tau	*p*-value
June	104	0.7977	25	105.00	0.2085	0.104
July	123	0.5529	25	90.000	0.1262	0.2965
August	107	0.7559	28	−99.00	−0.153	0.2203
September	140	0.3781	24	19.484	24.8029	0.4207

Table 6.3a Pettitt's test and Mann–Kendall test result for light rainfall Gaya

	Pettitt's test			Mann–Kendall test ($\alpha = 0.05$)		
Months	*U*	*p*-value	*K*	*S*	Tau	*p*-value
June	142	0.3604	17	131.00	0.16605	0.1417
July	127	0.5079	28	−18.00	−0.0225	0.848
August	222	0.03034	14	171.00	0.21618	0.05484
September	120	0.5882	35	93.00	0.1169631	0.2991

Table 6.3b Pettitt's test and Mann–Kendall test result for heavy rainfall Gaya

	Pettitt's test			Mann–Kendall test ($\alpha = 0.05$)		
Months	*U*	*p*-value	*K*	*S*	Tau	*p*-value
June	78	1	23	50.00	0.1104	0.3982
July	128	0.497	33	76.00	0.1115	0.3637
August	91	0.9895	04	−39.0	−0.054	0.6576
September	102	0.8261	13	−0.423	−0.05	0.6722

possible change point in the data, Mann–Kendall test and Pettitt test have been applied for Patna (Table 6.2a and 6.2b) and Gaya (Table 6.3a and 6.3b). Mann–Kendall test showed a significant increasing trend in light rainy days for the month of June and August in Patna, the same 2 months a significant change point is observed in the 18th and 13th year, respectively, and this implies that the Patna's rainfall regime is changing in recent past, especially for the months when the monsoon peak in approaching and departing as seen from long-term climatology (Fig. 6.3). However, no significant trend was observed for Gaya, although a change point in the 14th year was found in Pettitt's test. Rainfall pattern shift was also noticed by several researchers in the past. Sadler (2002) envisaged an increment of ~20% for the precipitation over natural vegetation cover; this research also linked

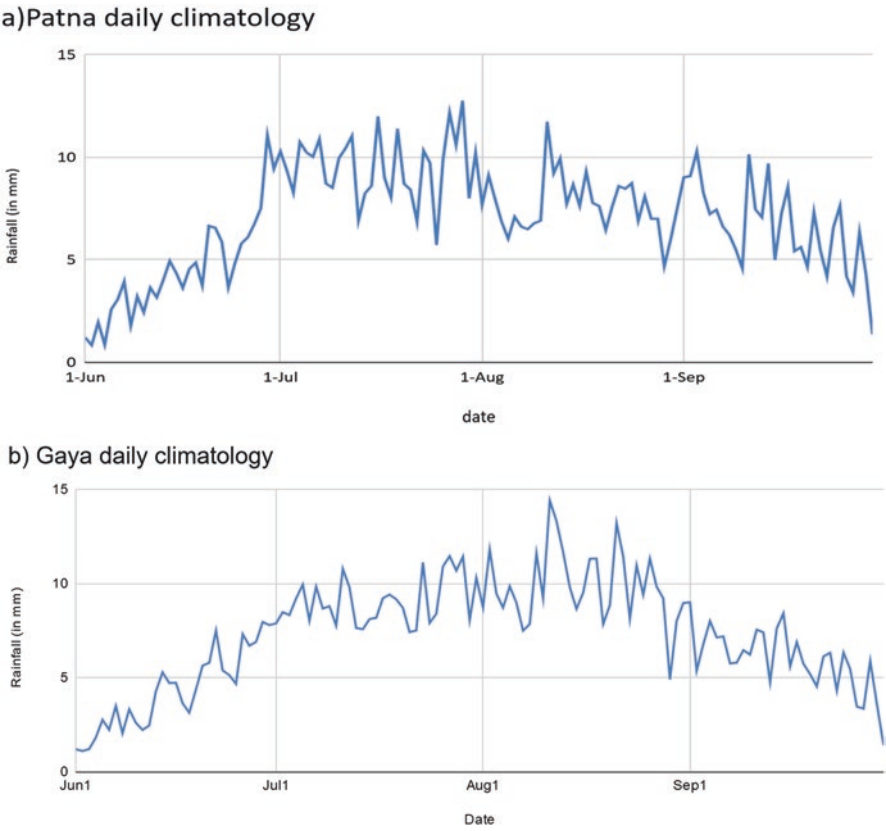

Fig. 6.3 Daily climatological JJAS rainfall for (**a**) Patna and (**b**) Gaya

this increment with the shift in the precipitation from agricultural cover towards the natural vegetation cover under a prevailing dry climate (Junkermann et al. 2009). The cities selected here are often visited by drought episodes as reported in past for this agro-climatic zone (Kumar et al. 2019); thus, the region somewhat possesses the characteristics of a drier climate. Hence, the regional influences may also cause a reduction in the precipitation amounts over non-natural covers (viz urban area) in a greater manner than the larger circulations due to change in surface roughness, moisture and energy fluxes and albedo (Ray et al. 2003; Pitman et al. 2004; Junkermann et al. 2009). We know that the impact of enhancement of aerosol concentration can trigger both enhancement and suppression of rainfall (Fan et al. 2009) depending upon the local conditions; hence, the change in the rainfall pattern over the cities may be linked with localised microclimatic variability triggered by urban aerosols. Moreover, Seifert et al. (2012) demonstrated that clouds may act as a natural buffer in larger scale-clouds systems also and cause significant

aerosol-induced change on surface rainfall. Rosenfeld (2000) indicated that both warm and cold season rainfall is inhibited in polluted clouds due to the absence of primary and secondary cloud producing nuclei. Cloud condensed nuclei may also induce more upward transportation of cloud water and suppress warm rainfall by the increase in the freezing of cloud drops to the ice phase. Lynn et al. (2007) observe the impact of aerosol on orographic precipitation by performing a two-dimensional mesoscale model over the Sierra Nevada of California. The result reveals that anthropogenic aerosols suppress the summer rainfall process by producing more cloud ice and snow that can be advected towards the downwind because of their lower sedimentation velocity. Svoma and Balling (2009) also found winter precipitation is inversely proportional to the aerosol concentration number. Muhlbauer and Lohmann (2006) demonstrated that enhancement in aerosol concentration suppresses the overall precipitation. This reduction in rainfall is due to the raindrop size distribution. Furthermore, the cities are having heavy perturbed microclimate as discussed by previous researchers, leading to formation of quite strong surface UHIs (Ghosh and Mukhopadhyay 2014; Barat et al. 2018, 2021), and thus, the urban boundary layer may also be quite modified resulting in changes regarding other meteorological characteristics. The changes in rainfall patterns over urban areas may lead to severe depletion of groundwater resources (Kumar et al. 2016; Dey et al. 2020), and under the drought conditions, the situation may get even worse. Thus, there is an exigency for monitoring the rainfall pattern changes and thus disaster preparedness to ensure a sustainable and climate smart city in the future.

Conclusions

In this research, an attempt has been made to document the urban impact on precipitation. The rainfall is very heterogeneous in nature and its spatial distribution is very unpredictable. An increase in light intensity rainfall days in early and departing months is observed, which in turn is giving rise to speculations of localised alterations in precipitation. As the microscale influences are only evident in absence of strong synoptic influences (Kumar et al. 2017; Barat et al. 2021), July may have not been showing any trend. A regional change in aerosol concentration could be an important factor for the rainfall depletion. High aerosol concentration suppresses the formation of rainfall by inhibiting the coalescence process of cloud droplets into raindrops (Rosenfeld 2000; Dave et al. 2017). Increased aerosol loading makes the atmosphere stable causing reduction in convection and enhancement in the divergence of moisture leading to aggravation of monsoon break condition and subsequently suppression of precipitation (Dave et al. 2017). In the future, cities are more likely to be influenced by regional weather conditions, so it is important to predict urban precipitation anomalies. A systematic modelling study is required to understand the mechanism for the enhancement of rainfall in the downwind side and the size distribution of aerosol particles. Also, the cloud-aerosol interactions and the mechanism involved need to be investigated.

Recommendations

The urbanisation has a well-defined impact on the rainfall distribution and amount. While the underlying causes point towards anthropogenic modifications in surface roughness, heat fluxes and aerosol loads, this is also true that all these modifications are inevitable. In this era of changing climate and fast urbanisation, the climatic vulnerability and climate resilience frameworks are matters of key concerns. To mitigate the ill impacts like heat stress, poor air quality and catastrophic hazards like urban flooding, scientific monitoring of the key precursors is utmost important. Long-term monitoring of urban environments through high-resolution meteorological data is very much important to assess the changing climatic trends. Furthermore, green town planning and strict pollution norms are much needed to manage the precursors like UHI and urban aerosols. The disaster risk assessment studies and abatement policies must also be framed in the context of urban flooding. Although urbanisation in present times seems to be inevitable, however the magnitude of the changes to local climate due to urbanisation must be minimised to the most possible extent by following sustainable development pathways to ensure a safe and sustainable environment.

References

Albrecht BA (1989) Aerosols, cloud microphysics, and fractional cloudiness. Science 245(4923):1227–1230. https://doi.org/10.1126/science.245.4923.1227

Altaratz O, Koren I, Remer LA, Hirsch E (2014) Review: cloud invigoration by aerosols—coupling between microphysics and dynamics. Atmos Res 140–141:38–60. https://doi.org/10.1016/j.atmosres.2014.01.009

Arnfield AJ (2003) Two decades of urban climate research: a review of turbulence, exchanges of energy and water, and the urban heat island. Int J Climatol 23(1):1–26. https://doi.org/10.1002/joc.859

Baik J-J (1992) Response of a stably stratified atmosphere to low-level heating — an application to the heat island problem. J Appl Meteorol Climatol 31(3):291–303. https://doi.org/10.1175/1520-0450(1992)031<0291:ROASSA>2.0.CO;2

Baik J-J, Chun H-Y (1997) A dynamical model for urban heat islands. Bound-Layer Meteorol 83(3):463–477. https://doi.org/10.1023/A:1000346229951

Baik J-J, Kim Y-H, Chun H-Y (2001) Dry and moist convection forced by an urban heat island. J Appl Meteorol Climatol 40(8):1462–1475. https://doi.org/10.1175/1520-0450(2001)040<1462:DAMCFB>2.0.CO;2

Baik J-J, Kim Y-H, Kim J-J, Han J-Y (2007) Effects of boundary-layer stability on urban heat island-induced circulation. Theor Appl Climatol 89(1):73–81. https://doi.org/10.1007/s00704-006-0254-4

Barat A, Kumar S, Kumar P, Parth Sarthi P (2018) Characteristics of Surface Urban Heat Island (SUHI) over the Gangetic plain of Bihar, India. Asia-Pacific J Atmos Sci 54(2):205–214. https://doi.org/10.1007/s13143-018-0004-4

Barat A, Parth Sarthi P, Kumar S, Kumar P, Sinha AK (2021) Surface Urban Heat Island (SUHI) over riverside cities along the Gangetic plain of India. Pure Appl Geophys 178(4):1477–1497. https://doi.org/10.1007/s00024-021-02701-6

Bhagat RB (2005) Urban growth by city and town size in India. Annual meeting of Population Association, Philadelphia

Bornstein R, Lin Q (2000) Urban heat islands and summertime convective thunderstorms in Atlanta: three case studies. Atmos Environ 34(3):507–516. https://doi.org/10.1016/S1352-2310(99)00374-X

Borys RD, Lowenthal DH, Cohn SA, Brown WOJ (2003) Mountaintop and radar measurements of anthropogenic aerosol effects on snow growth and snowfall rate. Geophys Res Lett 30(10). https://doi.org/10.1029/2002GL016855

Buchhorn M, Lesiv M, Tsendbazar N-E, Herold M, Bertels L, Smets B (2020) Copernicus global land cover layers—collection 2. Remote Sens 12(6):1044. https://doi.org/10.3390/rs12061044

Burian SJ, Shepherd JM (2005) Effect of urbanization on the diurnal rainfall pattern in Houston. Hydrol Process 19(5):1089–1103. https://doi.org/10.1002/hyp.5647

Changnon SA, Westcott NE (2002) Heavy rainstorms in Chicago: increasing frequency, altered impacts, and future implications 1. JAWRA J Am Water Resour Assoc 38(5):1467–1475. https://doi.org/10.1111/j.1752-1688.2002.tb04359.x

Changnon S, Huff F, Schickedanz P, Vogel JL (1977) Summary of METROMEX, volume 1: weather anomalies and impacts. Ill State Water Surv Bull 62:260

Choi Y-S, Ho C-H, Kim J, Gong D-Y, Park RJ (2008) The impact of aerosols on the summer rainfall frequency in China. J Appl Meteorol Climatol 47(6):1802–1813. https://doi.org/10.1175/2007JAMC1745.1

Cleugh HA, Oke TR (1986) Suburban-rural energy balance comparisons in summer for Vancouver, B.C. Bound-Layer Meteorol 36(4):351–369. https://doi.org/10.1007/BF00118337

Collier CG (2006) The impact of urban areas on weather. Q J R Meteorol Soc 132(614):1–25. https://doi.org/10.1256/qj.05.199

Cotton WR, Pielke RA (1995) Human impacts on weather and climate. Cambridge University Press, Cambridge. 288 pp

Dave P, Bhushan M, Venkataraman C (2017) Aerosols cause intraseasonal short-term suppression of Indian monsoon rainfall. Sci Rep 7(1):1–12

Dey S, Bhatt D, Haq S, Mall RK (2020) Potential impact of rainfall variability on groundwater resources: a case study in Uttar Pradesh, India. Arab J Geosci 13(3):114. https://doi.org/10.1007/s12517-020-5083-8

Dou J, Wang Y, Bornstein R, Miao S (2015) Observed spatial characteristics of Beijing urban climate impacts on summer thunderstorms. J Appl Meteorol Climatol 54(1):94–105. https://doi.org/10.1175/JAMC-D-13-0355.1

Fan J, Yuan T, Comstock JM, Ghan S, Khain A, Leung LR, Li Z, Martins VJ, Ovchinnikov M (2009) Dominant role by vertical wind shear in regulating aerosol effects on deep convective clouds. J Geophys Res Atmos 114(D22). https://doi.org/10.1029/2009JD012352

Farias WRG, Pinto O, Pinto IRCA, Naccarato KP (2014) The influence of urban effect on lightning activity: evidence of weekly cycle. Atmos Res 135–136:370–373. https://doi.org/10.1016/j.atmosres.2012.09.007

Freitag BM, Nair US, Niyogi D (2018) Urban modification of convection and rainfall in complex terrain. Geophys Res Lett 45(5):2507–2515. https://doi.org/10.1002/2017GL076834

Funk C, Peterson P, Landsfeld M, Pedreros D, Verdin J, Shukla S, Husak G, Rowland J, Harrison L, Hoell A, Michaelsen J (2015) The climate hazards infrared precipitation with stations—a new environmental record for monitoring extremes. Sci Data 2(1):150066. https://doi.org/10.1038/sdata.2015.66

Georgescu M, Miguez-Macho G, Steyaert LT, Weaver CP (2008) Sensitivity of summer climate to anthropogenic land-cover change over the Greater Phoenix, AZ, region. J Arid Environ 72(7):1358–1373. https://doi.org/10.1016/j.jaridenv.2008.01.004

Ghosh T, Mukhopadhyay A (2014) Natural hazard zonation of Bihar (India) using geoinformatics: a schematic approach. Springer Science & Business Media, Cham

Guo J, Deng M, Fan J, Li Z, Chen Q, Zhai P, Dai Z, Li X (2014) Precipitation and air pollution at mountain and plain stations in northern China: insights gained from observations and modeling. J Geophys Res Atmos 119(8):4793–4807. https://doi.org/10.1002/2013JD021161

Han J-Y, Baik J-J (2008) A theoretical and numerical study of urban heat island–induced circulation and convection. J Atmos Sci 65(6):1859–1877. https://doi.org/10.1175/2007JAS2326.1

Han J-Y, Baik J-J, Khain AP (2012) A numerical study of urban aerosol impacts on clouds and precipitation. J Atmos Sci 69(2):504–520. https://doi.org/10.1175/JAS-D-11-071.1

Han J-Y, Baik J-J, Lee H (2014a) Urban impacts on precipitation. Asia-Pac J Atmos Sci 50(1):17–30. https://doi.org/10.1007/s13143-014-0016-7

Han Z, Yan Z, Li Z, Liu W, Wang Y (2014b) Impact of urbanization on low-temperature precipitation in Beijing during 1960–2008. Adv Atmos Sci 31(1):48–56. https://doi.org/10.1007/s00376-013-2211-3

Harman IN, Belcher SE (2006) The surface energy balance and boundary layer over urban street canyons. Q J R Meteorol Soc 132(621):2749–2768. https://doi.org/10.1256/qj.05.185

Hazra A, Chaudhari HS, Ranalkar M, Chen J-P (2017) Role of interactions between cloud microphysics, dynamics and aerosol in the heavy rainfall event of June 2013 over Uttarakhand, India. Q J R Meteorol Soc 143(703):986–998. https://doi.org/10.1002/qj.2983

Heisler GM, Brazel AJ (2010) The urban physical environment: temperature and urban heat islands. Chapter 2. In: Aitkenhead-Peterson J, Volder A (eds) Urban ecosystem ecology, Agronomy monograph 55. American Society of Agronomy, Crop Science Society of America, Soil Science Society of America, Madison, pp 29–56

Huff FA, Changnon SA (1972) Climatological assessment of urban effects on precipitation at St. Louis. J Appl Meteorol Climatol 11(5):823–842. https://doi.org/10.1175/1520-0450(1972)011<0823:CAOUEO>2.0.CO;2

Inoue T, Kimura F (2004) Urban effects on low-level clouds around the Tokyo metropolitan area on clear summer days. Geophys Res Lett 31(5). https://doi.org/10.1029/2003GL018908

Junkermann W, Hacker J, Lyons T, Nair U (2009) Land use change suppresses precipitation. Atmos Chem Phys 9(17):6531–6539. https://doi.org/10.5194/acp-9-6531-2009

Kendall MG (1975) Rank correlation methods, 4th edn. Charles Griffin, London

Khain A, Rosenfeld D, Pokrovsky A (2005) Aerosol impact on the dynamics and microphysics of deep convective clouds. Q J R Meteorol Soc 131(611):2639–2663. https://doi.org/10.1256/qj.04.62

Khain A, Cohen N, Lynn B, Pokrovsky A (2008) Possible aerosol effects on lightning activity and structure of hurricanes. J Atmos Sci 65(12):3652–3677. https://doi.org/10.1175/2008JAS2678.1

Kishtawal CM, Niyogi D, Tewari M, Pielke RA Sr, Shepherd JM (2010) Urbanization signature in the observed heavy rainfall climatology over India. Int J Climatol 30(13):1908–1916. https://doi.org/10.1002/joc.2044

Konwar M, Maheskumar RS, Kulkarni JR, Freud E, Goswami BN, Rosenfeld D (2010) Suppression of warm rain by aerosols in rain-shadow areas of India. Atmos Chem Phys Discuss 10(7):17009–17027. https://doi.org/10.5194/acpd-10-17009-2010

Kumar S, Sinha A, Barat A, Kumar P, Sarthi P (2016) Changes in rainfall dynamics over Patna showing vulnerability on the groundwater regime of the area, conference on groundwater development prospects and water quality issues in Bihar. A. N. Sinha Institute, Patna, Bihar 0n 18 March 2005. Access from https://www.researchgate.net/publication/313037463_Changes_in_Rainfall_dynamics_over_Patna_showing_vulnerability_on_the_Groundwater_regime_of_the_area

Kumar R, Mishra V, Buzan J, Kumar R, Shindell D, Huber M (2017) Dominant control of agriculture and irrigation on urban heat island in India. Sci Rep 7(1):1–10

Kumar S, Kumar P, Barat A, Sinha AK, Sarthi PP, Ranjan P, Singh KK (2019) Characteristics of observed meteorological drought and its linkage with low-level easterly wind over India. Pure Appl Geophys 176(6):2679–2696. https://doi.org/10.1007/s00024-019-02118-2

Kusaka H, Kondo H, Kikegawa Y, Kimura F (2001) A simple single-layer urban canopy model for atmospheric models: comparison with multi-layer and slab models. Bound-Layer Meteorol 101(3):329–358. https://doi.org/10.1023/A:1019207923078

Lacke MC, Mote TL, Shepherd JM (2009) Aerosols and associated precipitation patterns in Atlanta. Atmos Environ 43(28):4359–4373. https://doi.org/10.1016/j.atmosenv.2009.04.022

Lensky IM, Rosenfeld D (2006) The time-space exchangeability of satellite retrieved relations between cloud top temperature and particle effective radius

Lin YL, Smith RB (1986) Transient dynamics of airflow near a local heat source. J Atmos Sci 43(1):40–49. https://doi.org/10.1175/1520-0469(1986)043<0040:TDOANA>2.0.CO;2

Lohmann U, Feichter J (2005) Global indirect aerosol effects: a review. Atmos Chem Phys 5(3):715–737. https://doi.org/10.5194/acp-5-715-2005

Lynn B, Khain A, Rosenfeld D, Woodley WL (2007) Effects of aerosols on precipitation from orographic clouds. J Geophys Res Atmos 112(D10). https://doi.org/10.1029/2006JD007537

Mann HB (1945) Nonparametric tests against trend. Econometrica 13(3):245–259. https://doi.org/10.2307/1907187

Miao S, Chen F, Li Q, Fan S (2011) Impacts of urban processes and urbanization on summer precipitation: a case study of heavy rainfall in Beijing on 1 August 2006. J Appl Meteorol Climatol 50(4):806–825. https://doi.org/10.1175/2010JAMC2513.1

Mishra A, Nizammuddin S, Mallick CB, Singh S, Prakash S, Siddiqui NA, Rai N, Carlus SJ, Sudhakar DVS, Tripathi VP, Möls M, Kim-Howard X, Dewangan H, Mishra A, Reddy AG, Roy B, Pandey K, Chaubey G, Das P, Nath SK, Singh L, Thangaraj K (2017) Genotype-phenotype study of the middle Gangetic plain in India shows association of rs2470102 with skin pigmentation. J Investig Dermatol 137(3):670–677. https://doi.org/10.1016/j.jid.2016.10.043

Muhlbauer A, Lohmann U (2006) Aerosol-cloud interactions and the effects on orographic precipitation. In: 12th conference on atmospheric radiation and cloud physics. Institute for Atmospheric and Climate Science, ETH Zurich, Zurich, Switzerland

Niyogi D, Holt T, Zhong S, Pyle PC, Basara J (2006) Urban and land surface effects on the 30 July 2003 mesoscale convective system event observed in the southern Great Plains. J Geophys Res Atmos 111(D19). https://doi.org/10.1029/2005JD006746

Niyogi D, Pyle P, Lei M, Arya SP, Kishtawal CM, Shepherd M, Chen F, Wolfe B (2011) Urban modification of thunderstorms: an observational storm climatology and model case study for the Indianapolis urban region. J Appl Meteorol Climatol 50(5):1129–1144. https://doi.org/10.1175/2010JAMC1836.1

Oke TR (1988) The urban energy balance. Prog Phys Geogr Earth Environ 12(4):471–508. https://doi.org/10.1177/030913338801200401

Oke TR (2002) Boundary layer climates. Routledge, London

Oke TR, Spronken-Smith RA, Jáuregui E, Grimmond CSB (1999) The energy balance of Central Mexico City during the dry season. Atmos Environ 33(24):3919–3930. https://doi.org/10.1016/S1352-2310(99)00134-X

Olfe DB, Lee RL (1971) Linearized calculations of urban heat island convection effects. J Atmos Sci 28(8):1374–1388. https://doi.org/10.1175/1520-0469(1971)028<1374:LCOUHI>2.0.CO;2

Pande CB, Moharir KN, Khadri SFR et al (2018) Study of land use classification in an arid region using multispectral satellite images. Appl Water Sci 8:123. https://doi.org/10.1007/s13201-018-0764-0

Pande CB, Moharir KN, Khadri SFR (2021a) Assessment of land-use and land-cover changes in Pangari watershed area (MS), India, based on the remote sensing and GIS techniques. Appl Water Sci 11:96. https://doi.org/10.1007/s13201-021-01425-1

Pande CB, Moharir KN, Singh SK, Varade AM, Ahmed E, Khadri SFR, Choudhari P (2021b) Estimation of crop and forest biomass resources in a semi-arid region using satellite data and GIS. J Saudi Soc Agric Sci 20(5):302–311

Parth Sarthi P, Kumar S, Barat A (2021) A linkage between Aerosol Optical Depth (AOD) and meteorological drought over the eastern Gangetic plain of India. Aerosol Sci Eng 5(4):440–450. https://doi.org/10.1007/s41810-021-00113-6

Parthasarathy B, Yang S (1995) Relationships between regional Indian summer monsoon rainfall and Eurasian snow cover. Adv Atmos Sci 12(2):143–150. https://doi.org/10.1007/BF02656828
Pettitt AN (1979) A non-parametric approach to the change-point problem. J R Stat Soc Ser C (Appl Stat) 28(2):126–135. https://doi.org/10.2307/2346729
Pielke RA Sr (2001) Influence of the spatial distribution of vegetation and soils on the prediction of cumulus convective rainfall. Rev Geophys 39(2):151–177. https://doi.org/10.1029/1999RG000072
Pinto JG, Ulbrich S, Parodi A, Rudari R, Boni G, Ulbrich U (2013) Identification and ranking of extraordinary rainfall events over Northwest Italy: the role of Atlantic moisture. J Geophys Res Atmos 118(5):2085–2097. https://doi.org/10.1002/jgrd.50179
Pitman AJ, Narisma GT, Pielke RA Sr, Holbrook NJ (2004) Impact of land cover change on the climate of Southwest Western Australia. J Geophys Res Atmos 109(D18). https://doi.org/10.1029/2003JD004347
Prabha TV, Patade S, Pandithurai G, Khain A, Axisa D, Pradeep-Kumar P, Maheshkumar RS, Kulkarni JR, Goswami BN (2012) Spectral width of premonsoon and monsoon clouds over Indo-Gangetic valley. J Geophys Res Atmos 117(D20). https://doi.org/10.1029/2011JD016837
Ray DK, Nair US, Welch RM, Han Q, Zeng J, Su W, Kikuchi T, Lyons TJ (2003) Effects of land use in Southwest Australia: 1. Observations of cumulus cloudiness and energy fluxes. J Geophys Res Atmos 108(D14). https://doi.org/10.1029/2002JD002654
Rosenfeld D (2000) Suppression of rain and snow by urban and industrial air pollution. Science 287:1793. https://doi.org/10.1126/science.287.5459.1793
Rosenfeld D, Woodley W (2003) Closing the 50-year circle: from cloud seeding to space and back to climate change through precipitation physics. In: Cloud systems, hurricanes, and the Tropical Rainfall Measuring Mission (TRMM), Meteorological monographs, vol 51. American Meteorological Society, Boston, pp 59–80
Rosenfeld D, Lohmann U, Raga GB, O'Dowd CD, Kulmala M, Fuzzi S, Reissell A, Andreae MO (2008) Flood or drought: how do aerosols affect precipitation? Science 321:1309. https://doi.org/10.1126/science.1160606
Rosenfeld D, Woodley WL, Khain A, Cotton WR, Carrió G, Ginis I, Golden JH (2012) Aerosol effects on microstructure and intensity of tropical cyclones. Bull Am Meteorol Soc 93(7):987–1001
Rozoff CM, Cotton WR, Adegoke JO (2003) Simulation of St. Louis, Missouri, land use impacts on thunderstorms. J Appl Meteorol Climatol 42(6):716–738. https://doi.org/10.1175/1520-0450(2003)042<0716:SOSLML>2.0.CO;2
Sadler B (2002) Climate variability and change in south West Western Australia, Indian Ocean Climate Initiative Panel, c/-Department of Environment, Water and Catchment Protection, WA
Sarangi C, Kanawade VP, Tripathi SN, Thomas A, Ganguly D (2018a) Aerosol-induced intensification of cooling effect of clouds during Indian summer monsoon. Nat Commun 9(1):3754. https://doi.org/10.1038/s41467-018-06015-5
Sarangi C, Tripathi SN, Qian Y, Kumar S, Ruby Leung L (2018b) Aerosol and urban land use effect on rainfall around cities in Indo-Gangetic Basin from observations and cloud resolving model simulations. J Geophys Res Atmos 123(7):3645–3667. https://doi.org/10.1002/2017JD028004
Sarangi B, Ramachandran S, Rajesh TA, Dhaker VK (2019) Black carbon linked aerosol hygroscopic growth: size and mixing state are crucial. Atmos Environ 200:110–118. https://doi.org/10.1016/j.atmosenv.2018.12.001
Schmid HP, Cleugh HA, Grimmond CSB, Oke TR (1991) Spatial variability of energy fluxes in suburban terrain. Bound-Layer Meteorol 54(3):249–276. https://doi.org/10.1007/BF00183956
Seifert A, Köhler C, Beheng KD (2012) Aerosol-cloud-precipitation effects over Germany as simulated by a convective-scale numerical weather prediction model. Atmos Chem Phys 12(2):709–725. https://doi.org/10.5194/acp-12-709-2012
Shahid M, Rahman KU, Haider S et al (2021) Quantitative assessment of regional land use and climate change impact on runoff across Gilgit watershed. Environ Earth Sci 80:743. https://doi.org/10.1007/s12665-021-10032-x

Shastri H, Paul S, Ghosh S, Karmakar S (2015) Impacts of urbanization on Indian summer monsoon rainfall extremes. J Geophys Res Atmos 120(2):496–516. https://doi.org/10.1002/2014JD022061

Shem W, Shepherd M (2009) On the impact of urbanization on summertime thunderstorms in Atlanta: two numerical model case studies. Atmos Res 92(2):172–189. https://doi.org/10.1016/j.atmosres.2008.09.013

Shepherd JM (2005) A review of current investigations of urban-induced rainfall and recommendations for the future. Earth Interact 9(12):1–27. https://doi.org/10.1175/EI156.1

Shepherd JM, Burian SJ (2003) Detection of urban-induced rainfall anomalies in a major Coastal City. Earth Interact 7(4):1–17. https://doi.org/10.1175/1087-3562(2003)007<0001:DOUIRA>2.0.CO;2

Shepherd JM, Pierce H, Negri AJ (2002) Rainfall modification by major urban areas: observations from Spaceborne rain radar on the TRMM satellite. J Appl Meteorol Climatol 41(7):689–701. https://doi.org/10.1175/1520-0450(2002)041<0689:RMBMUA>2.0.CO;2

Svoma BM, Balling RC (2009) An anthropogenic signal in Phoenix, Arizona winter precipitation. Theor Appl Climatol 98(3):315–321

Teller A, Levin Z (2006) The effects of aerosols on precipitation and dimensions of subtropical clouds: a sensitivity study using a numerical cloud model. Atmos Chem Phys 6(1):67–80. https://doi.org/10.5194/acp-6-67-2006

Thielen J, Wobrock W, Gadian A, Mestayer PG, Creutin J-D (2000) The possible influence of urban surfaces on rainfall development: a sensitivity study in 2D in the meso-γ-scale. Atmos Res 54(1):15–39. https://doi.org/10.1016/S0169-8095(00)00041-7

Tripathi SN, Srivastava AK, Dey S, Satheesh SK, Krishnamoorthy K (2007) The vertical profile of atmospheric heating rate of black carbon aerosols at Kanpur in northern India. Atmos Environ 41(32):6909–6915. https://doi.org/10.1016/j.atmosenv.2007.06.032

Tumanov S, Stan-Sion A, Lupu A, Soci C, Oprea C (1999) Influences of the city of Bucharest on weather and climate parameters. Atmos Environ 33(24):4173–4183. https://doi.org/10.1016/S1352-2310(99)00160-0

Twomey S (1977) The influence of pollution on the shortwave albedo of clouds. J Atmos Sci 34(7):1149–1152. https://doi.org/10.1175/1520-0469(1977)034<1149:TIOPOT>2.0.CO;2

UN (2014) World urbanization prospects, the 2011 revision. Available online at http://esa.un.org/unup/

United Nations(UN) (2010) World urbanization prospects. Department of Economic and Social Affairs United Nations. Access from: https://www.un.org/en/development/desa/publications/world-population-prospects-the-2010-revision.html

van den Heever SC, Cotton WR (2007) Urban aerosol impacts on downwind convective storms. J Appl Meteorol Climatol 46(6):828–850. https://doi.org/10.1175/JAM2492.1

Zhang CL, Chen F, Miao SG, Li QC, Xia XA, Xuan CY (2009) Impacts of urban expansion and future green planting on summer precipitation in the Beijing metropolitan area. J Geophys Res Atmos 114(D2). https://doi.org/10.1029/2008JD010328

Zhang X, Xiong Z, Zheng J, Ge Q (2018) High-resolution precipitation data derived from dynamical downscaling using the WRF model for the Heihe River Basin, Northwest China. Theor Appl Climatol 131(3):1249–1259. https://doi.org/10.1007/s00704-017-2052-6

Zhong S, Yang X-Q (2015) Ensemble simulations of the urban effect on a summer rainfall event in the Great Beijing Metropolitan Area. Atmos Res 153:318–334. https://doi.org/10.1016/j.atmosres.2014.09.005

Zhong S, Qian Y, Zhao C, Leung R, Wang H, Yang B, Fan J, Yan H, Yang X-Q, Liu D (2017) Urbanization-induced urban heat island and aerosol effects on climate extremes in the Yangtze River Delta region of China. Atmos Chem Phys 17(8):5439–5457. https://doi.org/10.5194/acp-17-5439-2017

Chapter 7
Influence of Climate Change on Crop Yield and Sustainable Agriculture

M. Aali Misaal, Syeda Mishal Zahra, Fahd Rasul, M. Imran, Rabeea Noor, and M. Fahad

Abstract Climate change (CC) is one of the serious matters regarding the global food supply, safety, and sustainability of agriculture. The population of the world is increasing at a rapid pace, especially in South Asia. To fulfill the food consumption of the growing population and encountering CC at the same time in agriculture is the toughest challenge of today's world. The events like severe hot summer and extremely cold winters, uncertain prolonged seasons, and randomness of precipitation are the biggest evidence of CC. Global warming and increased anthropogenic human activities are meant to be the cause of CC. Crops at early and even advanced

M. A. Misaal (✉)
Department of Farm Machinery & Power, Faculty of Agricultural Engineering and Technology, University of Agriculture, Faisalabad, Pakistan

Department of Farm Machinery & Precision Engineering, Faculty of Agricultural Engineering and Technology, PMAS-Arid Agriculture University, Rawalpindi, Pakistan

S. M. Zahra
Department of Irrigation & Drainage, Faculty of Agricultural Engineering and Technology, University of Agriculture, Faisalabad, Pakistan

Agricultural Remote Sensing Lab (ARSL), University of Agriculture, Faisalabad, Pakistan

Department of Agricultural Engineering, Bahauddin Zakariya University, Multan, Pakistan

F. Rasul
Department of Agriculture, University of Agriculture, Faisalabad, Pakistan

M. Imran
Department of Irrigation & Drainage, Faculty of Agricultural Engineering and Technology, University of Agriculture, Faisalabad, Pakistan

Department of Agricultural Engineering, Bahauddin Zakariya University, Multan, Pakistan

R. Noor
Department of Agricultural Engineering, Bahauddin Zakariya University, Multan, Pakistan

M. Fahad
Department of Farm Machinery & Precision Engineering, Faculty of Agricultural Engineering and Technology, PMAS-Arid Agriculture University, Rawalpindi, Pakistan

C. B. Pande et al. (eds.), *Climate Change Impacts on Natural Resources, Ecosystems and Agricultural Systems*, Springer Climate,
https://doi.org/10.1007/978-3-031-19059-9_7

stages are significantly affected by CC, the processes like photosynthesis, evapotranspiration, plant growth, metabolic activities, and other chemical reactions. The variability of climate at the specific crop period slows down reactions within the plant which results in decreased crop production. There is a wide range of farmers with different socioeconomic conditions and life experiences. The progressive farmers have conceptualized the climate in recent years and updated their farm practices, while the others are still trying to cope up with CC. Thus, this is the need of time that farmers must be educated with the ongoing environmental conditions and best cropping pattern, crop rotation, and practices are informed so that the emerging issue of food security and safety of the developing world can be overcome. The review is carried out to understand the effect of CC on crop production and sustainable agriculture.

Keywords Climate change · Agriculture · Crop Yield · Sustainability

Introduction

Climate change (CC) is one of the biggest threats of the twenty-first century creating complex environmental and social challenges for sustainable developments. It has been recognized as a major reason for the downfall of most sectors like fisheries, agriculture, livestock, tourism, and forestry (Kalele et al. 2021). CC refers to change in the average weather patterns of a region. The change in global climate is being observed continually since the pre-industrial revolution (Dissanayake et al. 2018) due to increased anthropogenic human activities and greenhouse gasses (GHGs). The anthropogenic activities have led to massive GHGs emissions through the burning of fuels and air conditioning. It is estimated that 50% of CO_2 emissions are accumulated during 1750–2011. Growing population and economy have led to changing lifestyles, increased energy use which is directly linked with CC (van der Keur et al. 2016). CC events can have a severe impact on food security such as non-availability, less utilization, and access issues with food (Nguyen and Drakou 2021). CC coupled with global warming and other environmental factors is contributing immensely to the global system. The temperature of the globe is expected to increase by 1.5 °C from 2030 to 2052 (Barry and Hoyne 2021). About 40% of the global population is living in a climate with an average daytime temperature above 30 °C (Ansah et al. 2021). The strong evidence of CC is the melting of glaciers, floods, tsunamis, rising sea levels, uncertain precipitations, shifting of seasons, and the increase in earth temperature. Currently, most of the indicators are focused on change in environmental conditions (Ziogas et al. 2021); however, factors other than the environment will allow nations to switch towards more sustainable society. Adopting mitigation and adaptation strategies has now become necessary to counter the ongoing CC. Many international and local agencies have developed mitigation and adaptation measures to deal with climate-associated risks (Anandhi 2017). The studies on adaptation strategies and CC impacts are dominated by quantifying

modeling the future of CC using relatively less socio-economic and biophysical parameters (Kalele et al. 2021). Some progressive farmers in South Africa have adopted adaptation strategies and minimized the impact of CC on food production (Ogunleye et al. 2021). Experts have said that the capacity to adopt new strategies is affected by CC, access to technology, and level of information. Estimation of vulnerability has become a prerequisite to planning adaptation technologies (Malley et al. 2021). The influence of different factors put stress on the international community to invest further in adaptation and mitigation programs for sustainable agriculture. The implementation of adaptation measures will result in a reduction in the vulnerability of agroecosystems and improve the resilience of agrosystems to CC. Most people believe that CC is a real thing while some have different perceptions about the consequences of CC effects, which ultimately plays a significant role in policy-making, mitigating, and adapting strategies. The devasting effects of CC have become more evident across geographies, and new approaches are aimed to integrate effective relations among the food system, humans, and the environment (Medina Hidalgo et al. 2021). Global warming coupled with CC has been turned into a devasting threat for global climate and sustainable development (Fu et al. 2021; Srivastava and Chinnasamy 2022). The international agencies have been paying significant attention to counteractive measures to cushion farmers for the national cause. CC often results in land degradation, soil erosion, deforestation, and desertification. Land degradation negatively affects the functionality of the ecosystem and the capacity such as water retention and nutrient cycling (Eekhout and de Vente 2022). Soil erosion is the main cause of land degradation which affects biogeochemical cycles and interacts with CC itself. Scientists have discovered that food production is at the stake of high-risk globally especially the South Asian countries (Alvi et al. 2021). Assessment of the world's food production from the ongoing CC is one of the trending research projects. The legislation and policy-making at micro- and macro-levels need time for sustainability and the provision of food for the growing population. Pakistan ranks in the fifth position of the world's most vulnerable countries to CC (Syed et al. 2022). Vulnerability is the susceptibility of being affected adversely by CC. Being an under developing and agricultural country, the agriculture sector is at the edge of food safety and security due to CC. The vulnerability coupled with other parameters like soil erosion, uncertain rainfall, erratic distribution, and change in cropping patterns led to a great hindrance in achieving high yields (Kalele et al. 2021). The vulnerability rate in low-income countries is expected to be high due to the large population, poor infrastructure, development, and weak adaptation capacity (Wilts et al. 2021). Within the countries, vulnerability differs across farms, topography, and income levels. Farming is often vulnerable to CC and results in low-crop yield and crop failure in some cases as well. Lesser supply of food can increase produce price but a direct hit for the end-user.

Pakistan's economy is based on the agriculture sector mainly. Around 60% of the country's population has direct and indirect linkage with agriculture. Pakistan stands at the 12th position among the countries where agriculture sector and livelihood of people are significantly and detrimentally affected because of CC (Syed

et al. 2022). The country is striving its best to meet the food demand due to the growing population by bringing total arable land under cultivation. The agriculture systems throughout the world have been driven by multiple factors including CC. The temperature increase due to global warming has resulted in abrupt rainfall patterns, which has directly affected agricultural production and water reserves. The effects of CC can be estimated by shifting cropping patterns in different areas around the globe (Singh and Kumar 2021). The consumption of agricultural inputs has seen an abrupt increase due to changes in fertilization, recollection of land, and alternate agricultural water use (Guo et al. 2020) which considerably affects the produce. The agriculture sector is closely related to the ecosystem and sensitive to human behaviors, and a slight change in practice can lead to unexpected results. Studies have shown that CC will ultimately affect water reserves, and water availability for agriculture and domestic use is a future threat (Guo et al. 2020). Wheat, rice, sugarcane, maize, and cotton are important crops of Pakistan. The performance of the agriculture sector seems competing as the growth was 2.77% while the set target was 2.80% (Anonymous 2021). The government has a keen eye on key crops and trying the best efforts in policy-making and other interventions to tackle important challenges like CC, temperature variation, uncertain rainfall, reducing arable lands, and water shortages as well. With the growing population at the rate of 2.6% per annum and shrinking culturable areas, the pressure for sustainable practices and development is increasing day by day (Anonymous 2017; Pande et al. 2021; Shahid et al. 2021). The production of sugarcane, rice, maize, and wheat showed an increase of 22, 13.6, 7.4, and 8.1% increase in production, However, a clear decline of 22.8% is observed in the cotton crop (Anonymous 2021). The key factors that boosted the production are certified seeds, subsidized fertilizer, pesticides, and agriculture credit. The population of the world is growing at a rapid pace, specifically in Pakistan. Urbanization, industrialization, and deforestation are the key factors that have a significant effect on reduced land for arable farming. Uncertain and erratic rainfall, long dry spell, early withdrawal of monsoon are the factors that have massively reduced the crop yields and crop failure as well in some regions. Therefore, the objective of the research is to estimate the effects of CC on crop yield in Punjab.

Materials and Methods

Study Area

The research study was carried out in Punjab, Pakistan, with 71 m elevation from minimum and 2193 m from the maximum. It falls within the coordinates of 29.30°–32.32° N and 73.55°–76.50° E. Punjab is located in the lower north-east of the country with an area of 205,344 km^2. The population of Pakistan is increasing at a rapid pace and Punjab being the most populated province contributes the largest share of agricultural produce to GDP as well. The landuse-landcover of Punjab in

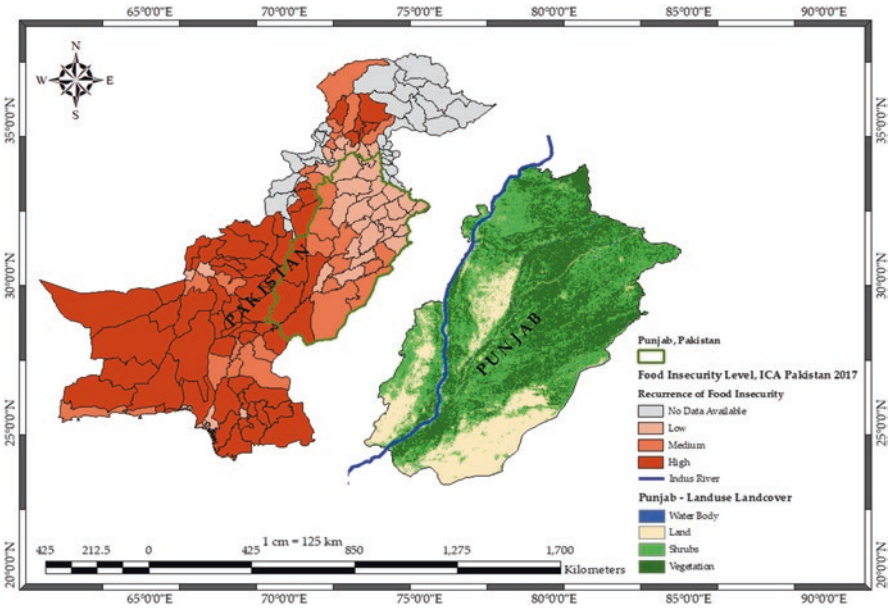

Fig. 7.1 Recurrence of food insecurity and land use land cover (LULC) of Punjab

November 2021 is shown in Fig. 7.1. Pakistan ranked 92nd out of 116 countries in Global Hunger Index (GHI) with a score of 24.7 which indicates the seriousness of hunger in the country. Increasing population poses direct pressure on food safety and security, therefore the recurrence of food insecurity of Pakistan of 2017 can be observed in Fig. 7.1. Also, Table 7.1 indicates the population increase as contrary to conducted census since partition.

Data Collection

It is estimated that 75% of Pakistan's exports are agricultural commodities and 60% of those are comprised of Punjab. About 83% geographic area of Punjab is under cultivation of important crops like wheat, cotton, rice, maize, sugarcane, millet, barley, fruits, etc. The average temperature in summer ranges from 36 °C to 49 °C and from 2 °C to 18 °C in winters. The average annual rainfall of Punjab is 650 mm. More than 16% of land in Punjab lies in the arid regions (rainfall dependent). Arid regions are characterized by uncertain rainfalls, erratic distributions, and long dry spells which makes it impossible to achieve inadequate yield levels to meet the food demand in the country.

Cotton (Gossypium), sugarcane (Saccharum officinarum), and maize (Zea mays subsp. mays) crops are frequently cultivated during the summer. During the winter, rice (Oryza sativa) and wheat (Triticum) are grown in Punjab, Pakistan, as shown in

Table 7.1 Population census of Pakistan since partition

Sr. No.	Year	Population (000's)
1	1951	33,740
2	1961	42,880
3	1972	65,309
4	1981	84,254
5	1998	132,352
6	2017	207,774

Table 7.2 Growing season of different crops in Punjab, Pakistan

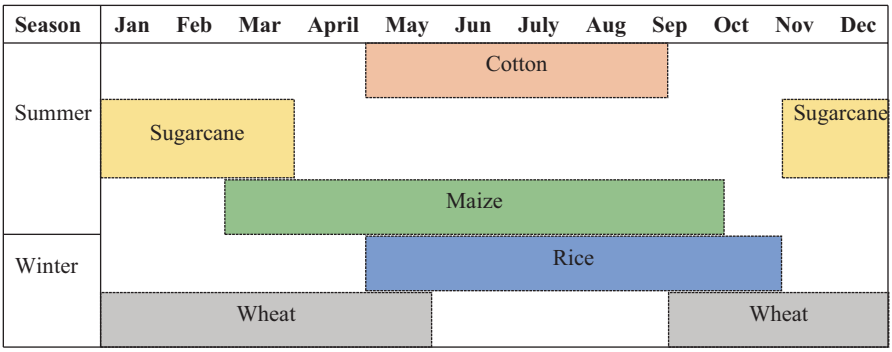

Table 7.2 above. Wheat-cotton and sugarcane-wheat are the predominant cropping patterns in the research area, with others being secondary crops. Wheat is the staple food in Pakistan, accounting for 72% of protein and calories in the overall diet. As a result, wheat is the most important crop in terms of diet. Other crops are the principal cash crops of Pakistan, and contributions to exports are heavily influenced by agricultural production from Punjab province. Pakistan Agricultural Research Council (PARC) conducted a research that indicated 120 kg per capita was wheat utilization of the nation in Pakistan. In rural areas, wheat production is the main source of income for the farmer community.

The data of five major crops, i.e., wheat, rice, cotton, sugarcane, and maize, were taken to estimate the impacts of CC on crop production and future recommendations. Historical (30 years) data of minimum, maximum, and mean temperature was collected from the Pakistan Meteorological Department (PMD), while the parameters like cultivation area, yield, and agriculture share to GDP were collected from Crop Reporting Service (CRS) Punjab and Pakistan Economic Survey (PES) since 1990–2021 and 2000–2021, respectively, as described in Table 7.3 below.

Table 7.3 Data used in the study area along with the duration and sources

Sr. No.	Data type	Details of data			Duration	Source
1	Climate	Maximum temperature			1990–2018	Pakistan meteorological department
		Minimum temperature			1990–2018	
		Rainfall			1990–2018	
2	Crops	Cotton	Yield	Area	1990–2021	Crop reporting service, Punjab
		Sugarcane	Yield	Area	1990–2021	
		Maize	Yield	Area	1990–2021	
		Rice	Yield	Area	1990–2021	
		Wheat	Yield	Area	1990–2021	

Results and Discussion

Agriculture Sector and GDP of Pakistan

Pakistan is the country with population crossing over 220 million by giving a nominal GDP (Gross Domestic Production). The main exports of country are textiles, leather and sports products, chemical, and rugs. The GDP of country has been abruptly increasing or severe declining since 2000 as seen in Fig. 7.1. Similarly, the contribution of agriculture to GDP has been fluctuating as well. The highest share of agriculture sector, i.e., 25.62%, was recorded in during 2000–01 when the growth rate was 4.3%. The highest growth rate of 7.7% was achieved in 2005–06 but the contribution of agriculture remained 22.90%. Being an agricultural, under developing and affected by CC, the predictions about growth rate of agriculture sector would not be very close to reality. During the fiscal years of least growth rate, i.e., 2008, 2010, and 2019, the agriculture contribution remained around 22.00% throughout. On the other hand, the agriculture share remained below 20% on growth rate of 5.5% and above. The sectors other than agriculture contributing to GDP are industry and services. Agriculture is directly affected by CC; long dry spells, uncertain rains, global warming, and erratic distribution of rains, which ultimately results in lower crop yields and threats like food security and safety may arose. Figure 7.2 indicates the 20 years agriculture contribution and growth rate of Pakistan.

Major Crops of Pakistan

Cotton

Cotton crop was cultivated on 5250 thousand acres with production of 8501 thousand bales and the average yield stood 22.13 maund/acre in 1990–91. However, the cultivation area was reduced by 72 and 59% in production; the net yield was decreased to 15.81 maund/acre in 2020–21. The trend of cotton cultivation and production remained very random throughout the study period. The highest yield

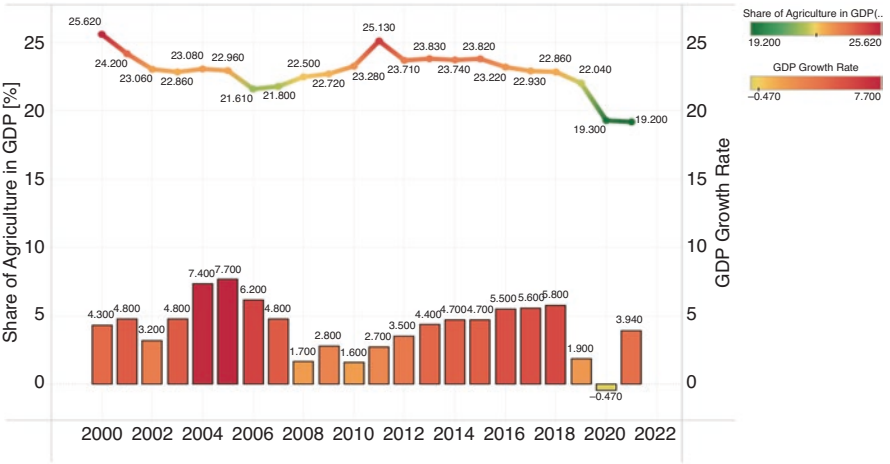

Fig. 7.2 GDP growth and agriculture share of Pakistan 2000–2021

(27.62 maund/acre) was obtained in 1991–1992 followed by 24.49 maund/acre in 2004–2005 and 21.47 maund/acre in consecutive years of 2012–2014. Cotton is the only crop that has suffered the most, and the main reasons are less competitiveness due to other major crops, low water availability, unfavorable weather conditions, uncertified seeds, stunting of crops, attack of whitefly, pink bollworm, pest infestation, localized monsoon, widespread attack of cotton leaf curl virus (CLCV), floods of 2010 and closure of canals, high temperatures, excessive fruit shedding, and less use of DAP.

Sugarcane

Sugarcane was cultivated on 1299 thousand acres with production of 19,633 thousand tonne and the average yield of Punjab stood 405 maund/acre in 1990–1991. However, the cultivation area was increased 47 and 290% increase in production; the net yield was increased to 742 maund/acre. The sugarcane yield remained very less by 1993–1994 but afterwards the linear increase was observed, and the maximum yield was obtained in 2020–2021. The extensive study of historical crop data indicates that the reasons of production shortages are payment difficulties by sugar mills, disposal of cane, shifting to other competitive crops, significant attack of pest and disease, shortage of irrigation water, less usage of DAP, and high-fertilizer prices. The factors of increased crop productions were favorable weather conditions, better cultural management, higher economic returns, timely availability of inputs, flood of 2010 increased the fertility of soil, and balanced dose of inputs.

Maize

Maize crop was cultivated on 790 thousand acres with production of 425 thousand tonne and the average yield of Punjab stood at 14.41 maund/acre in 1990–1991. However, the cultivation area was increased by 295 and 1645% increase in production; the average yield stood 80.26 maund/acre in 2019–2020. The yield of maize crop remained stagnant with slight increase up to 25.86 maund/acre till 2003–2003 afterwards a significant increase in yield was seen till 2021. The maximum yield of 84.05 maund/acre was obtained in year 2020–2021. The trend of crop yield remained linearly increasing throughout the study period. The reasons of better production were good economic return of the crop, improved seed quality, healthy grain formation, intensive use of fertilizer, favorable weather conditions and shifting from cotton and sugarcane.

Rice

Rice crop was cultivated on 3118 thousand acres with production of 1422 thousand tonne and the average yield of Punjab stood at 12.22 maund/acre in 1990–1991. However, the cultivation area was increased by 89.7% with an increase of 372% in production; the average yield remained at 22.40 maund/acre in 2020–2021. The 30 years' trend of rice yield showed a linear increase. The highest yield (22.96 maund/acre) was achieved in growing season of 2017–2018. The study of 30 years crop data evaluated that the reasons of declined production are dry weather, shortage of water, decreased in cultivation area, domestic price, less economic returns, shifting from sugarcane and maize, abundant supply during FY 2014–2015, effect of monsoon rains, devasting floods of 2010, and pest and disease attacks. The parameters effecting increased production were better unit price of commodity, increased export demand, subsidized input, high-yielding hybrid varieties, and non-payment from sugarcane mills led to shifting towards rice crop.

Wheat

Wheat crop was cultivated on 14,114 thousand acres with production of 10,514 thousand tonne and the average yield of Punjab stood at 20 maund/acre in 1990–1991. However, the cultivation area was increased by 15.6 with 25.6% increase in crop production; the net yield was increased to 31.34 maund/acre in 2020–2021. The slight increase in crop yield was observed from 1990 to 1999, but the significant increase in crop yield was seen afterwards with slight variations. The highest crop yield (33.32 maund/acre) was obtained in growing season of 2017–2018. The statistical reports and publications were studied extensively, and the reasons of decline and increase in production was find out. The reasons of low production were decline in sown area, delayed and prolonged crushing of sugarcane, late cotton picking by growers, acute shortage of water, higher prices of fertilizers, extended

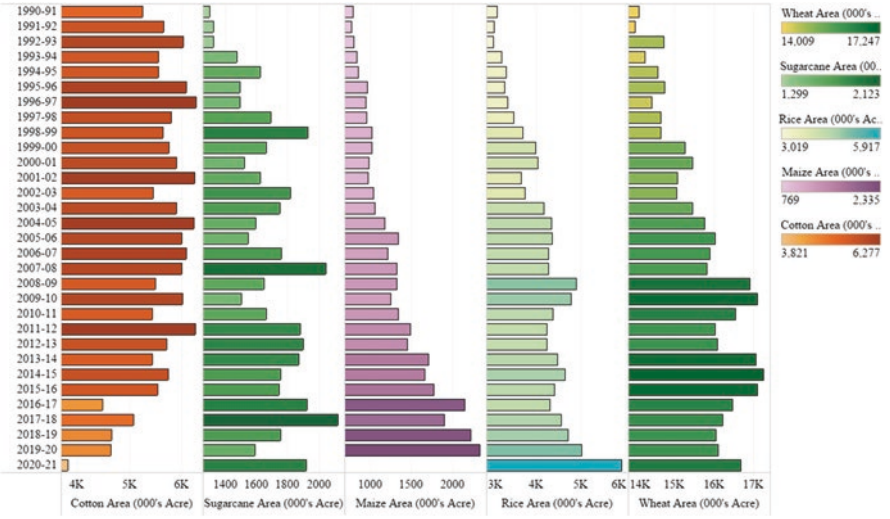

Fig. 7.3 Area cultivation of major crops in Punjab (1990–2021)

winter season, dry season, and lastly the uncertain rains of April–May which led to damage of grains at maturity stage. The significant increase in production resulted due to availability of certified seed, urea fertilizer, water availability, timely rains, high-yielding varieties, agricultural credit, better supply of inputs, and early maturity of cotton crop (Figs. 7.3 and 7.4). These figures indicate the area cultivation and average yield of major crops in Punjab.

Meteorological Parameters

Temperature

Figure 7.5 indicates the month-wise temperature (minimum and maximum) averages of Punjab from 1990 to 2021. The key months for five major crops are April, June, July, September, and November. The minimum monthly average temperature of April month remained 12.27 °C and maximum of 16.40 °C was recorded. Similarly, 20.38 °C and 24.92 °C for June, 22.71 °C and 31.52 °C for July, 18.06 °C and 22.60 °C for September and the minimum monthly average temperature was recorded 5.96 °C as minimum and 9.70 °C as maximum. The moderate increase in minimum monthly temperatures (5 °C increase) was observed in four key months, i.e., February, May, October, and December. However, the increase of up to 8 °C was observed for the 30 years data of June month. Increased temperature at initial phenological stages of crops effects pollination as it is directly affected by it. High-vapor pressure enhances the effects of temperature on pollen viability. The response

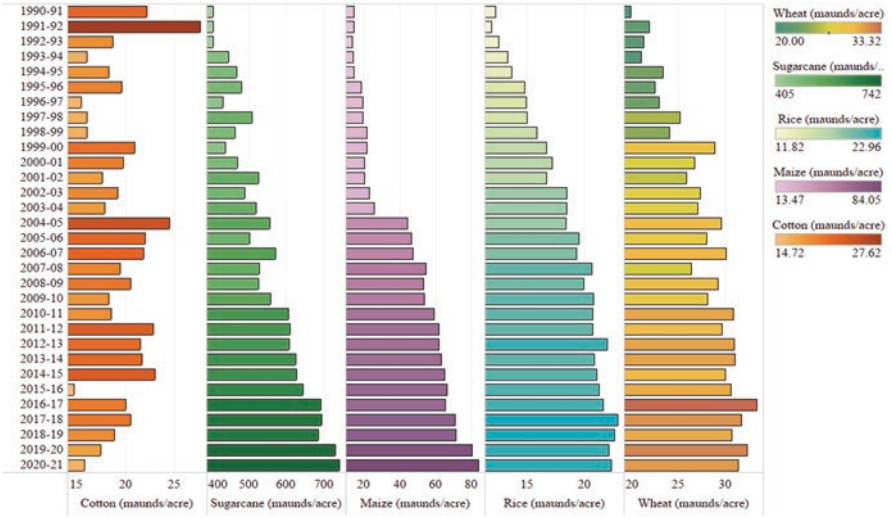

Fig. 7.4 Average yield of major crops in Punjab (1990–2021)

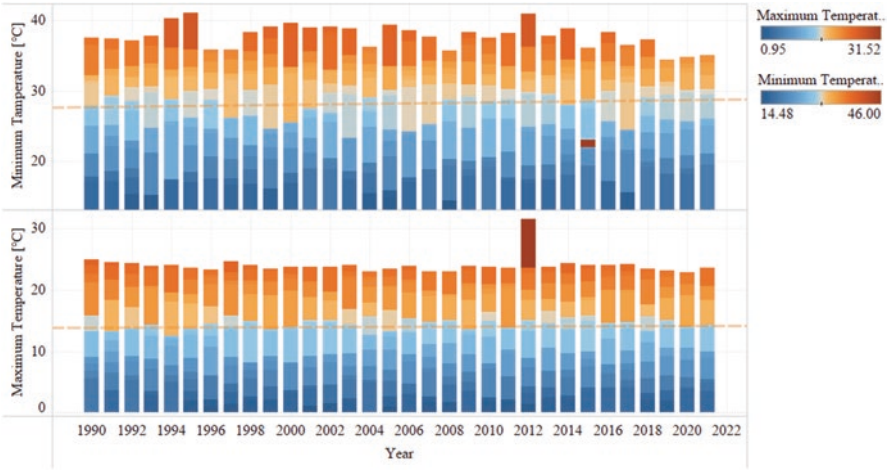

Fig. 7.5 Minimum and maximum monthly average temperature of Punjab (1990–2021)

of some crops like maize is good at high temperatures at vegetative stages. The effects of CC are most significant in maximum monthly temperature. The observation of 30 years average monthly data showed the 8 °C above increase for January–May, 6 °C increase for June, July, October, and December, and moderate increase of 4 °C for rest of month. It resulted in long dry spell and heat waves, which ultimately effects the crop production.

Rainfall

Rainfall pattern are being shifted due to CC. Low rainfall with high intensity has becoming more apparent producing floods, droughts, and off-season precipitations as well. Floods are the major cause of food security as it destroys the standing crops and extend the sowing time of other crops due to high-moisture content. The several models have predicted that rainfall during critical stage of crops leads to abrupt reduction in crop production (Asseng et al., 2019). Rainfall during winter and autumn may increase the effect of disease attack to crop which ultimately affects the crops yield. Uncertain precipitations and more intense rainfall during spring season provoke early damage of young plants in maize crop. Although drought resists the cropping area, but the production is severely affected due to hot dry spells and warmer temperature. The most damaging impact of droughts is at early growing stage. Figure 7.6 shows the average rainfall, minimum, maximum, and mean temperature of historical (1990–2021) data of Punjab.

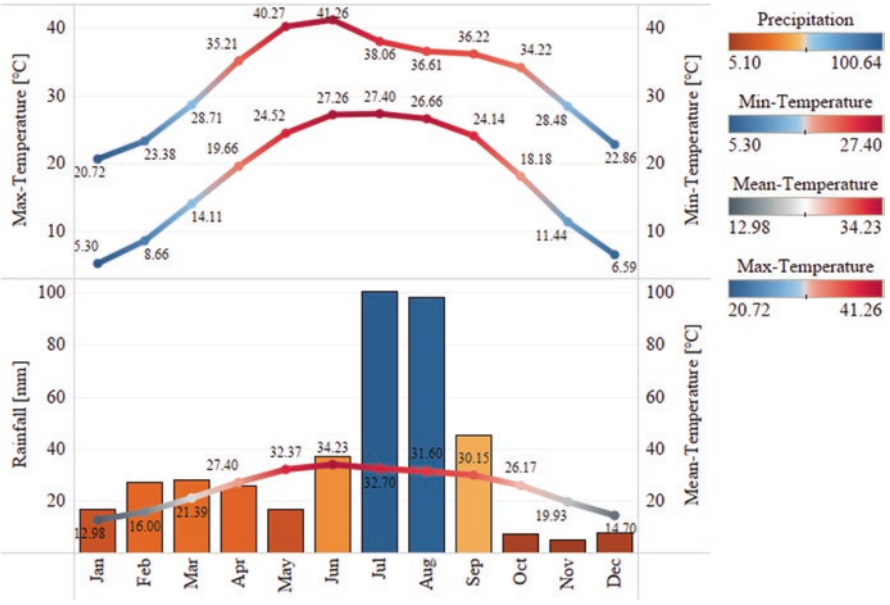

Fig. 7.6 Mean, minimum, and maximum temp with average rainfall in Punjab

Strategies and Future Recommendations

Keeping in view the condition of global climate, the yield increase started in century is now stagnant and even have a decreasing trend in some areas (Lobell and Field 2007). The effects of global warming resulted in heat shock waves. Even the slight change in ambient temperature has a profound effect on crop growth. Scientists have predicted that continued increase of temperature will result in heavy loss of production in medium latitudes (Guo et al. 2020), whereas the more fertile soils located at higher latitudes are getting worsened effects of climate (Long and Ort 2010). Higher global temperatures have shortened the crop growing seasons, allowing crops to undergo photosynthesis for a significantly shorter length of time, especially in case of irrigated and resistant crops. Heat stress has an immediate influence on photosynthesis rate. As a result, less biomass is available for anthesis and grain filling (Fahad et al. 2017). Furthermore, the rise in temperature increases evapotranspiration which reduces the soil moisture, and grain filling is ultimately affected (Sharif et al., 2017). Plants exposed to higher temperatures directly reduce the production by effecting its processes. Crop quality and composition of seed are reduced due to high temperatures. The main challenge of the century is to feed the global population in context of CC. The population of world is expected to reach 9 billion by 2050, whereas the temperature increase of 1.5–2 °C is also predicted. Elevated temperature, long dry spells, uncertain and erratic rainfalls are now becoming more common and adversely affecting the crop yield. It will result in food shortage, increased prices of agricultural commodity, increasing global hunger index, and poverty. It is necessary to adopt the improved seed to withstand the biotic and abiotic stresses. The sustainability of agriculture along with ongoing global threat (CC) is possible through improved cultural, agronomic management, use of diversified genetics of crops, temperature stress elevation by beneficial bacteria's, use of non-destructive and non-invasive methods of phenotyping.

References

Alvi S, Roson R, Sartori M, Jamil F (2021) An integrated assessment model for food security under climate change for South Asia. Heliyon 7(4):e06707

Anandhi A (2017) CISTA-A: conceptual model using indicators selected by systems thinking for adaptation strategies in a changing climate: case study in agro-ecosystems. Ecol Model 345:41–55

Anonymous. 2017. Pakistan Economic Survey 2016-17. Finance and Economic Affairs Division. Ministry of Finance, Govt. of Pakistan, Islamabad, Pakistan. https://www.finance.gov.pk/survey_1617.html

Anonymous. 2021. Pakistan Economic Survey 2020-21. Finance and Economic Affairs Division. Ministry of Finance, Govt. of Pakistan, Islamabad, Pakistan. https://www.finance.gov.pk/survey_2021.html

Ansah EW, Ankomah-Appiah E, Amoadu M, Sarfo JO (2021) Climate change, health and safety of workers in developing economies: a scoping review. J Clim Change Health 3:100034

Asseng S, Martre P, Maiorano A, Rötter RP, O'Leary GJ, Fitzgerald GJ, Girousse C, Motzo R, Giunta F, Babar MA, Reynolds MP, Kheir AMS, Thorburn PJ, Waha K, Ruane AC, Aggarwal PK, Ahmed M, Balkovič J, Basso B, Biernath C, Bindi M, Cammarano D, Challinor AJ, de Sanctis G, Dumont B, Eyshi Rezaei E, Fereres E, Ferrise R, Garcia-Vila M, Gayler S, Gao Y, Horan H, Hoogenboom G, Izaurralde RC, Jabloun M, Jones CD, Kassie BT, Kersebaum KC, Klein C, Koehler AK, Liu B, Minoli S, Martin MMS, Müller C, Kumar SN, Nendel C, Olesen JE, Palosuo T, Porter JR, Priesack E, Ripoche D, Semenov MA, Stöckle C, Stratonovitch P, Streck T, Supit I, Tao F, van der Velde M, Wallach D, Wang E, Webber H, Wolf J, Xiao L, Zhang Z, Zhao Z, Zhu Y, Ewert F (2019) Climate change impact and adaptation for wheat protein. Glob Chang Biol 25:155–173

Barry D, Hoyne S (2021) Sustainable measurement indicators to assess impacts of climate change: implications for the new green Deal era. Curr Opin Environ Sci Health 22:100259

Dissanayake S, Mahadevan R, Asafu-Adjaye J (2018) How efficient are market-based instruments in mitigating climate change in small emitter south Asian economies? Econ Model 75:169–180

Eekhout JPC, de Vente J (2022) Global impact of climate change on soil erosion and potential for adaptation through soil conservation. Earth Sci Rev 226:103921

Fahad S, Bajwa AA, Nazir U, Anjum SA, Farooq A, Zohaib A, Sadia S, Nasim W, Adkins S, Saud S, Ihsan MZ, Alharby H, Wu C, Wang D, Huang J (2017) Crop production under drought and heat stress: plant responses and management options. Front Plant Sci 8:1147

Fu L, Cao Y, Kuang SY, Guo H (2021) Index for climate change adaptation in China and its application. Adv Clim Chang Res 12:723–733

Guo C, Dai H, Liu X, Wu Y, Liu X, Liu Y (2020) Impacts of climate change mitigation on agriculture water use: a provincial analysis in China. Geogr Sustain 1:189–199

Kalele DN, Ogara WO, Oludhe C, Onono JO (2021) Climate change impacts and relevance of smallholder farmers' response in arid and semi-arid lands in Kenya. Sci Afr 12:e00814

Lobell DB, Field CB (2007) Global scale climate-crop yield relationships and the impacts of recent warming. Environ Res Lett 2(1):014002

Long SP, Ort DR (2010) More than taking the heat: crops and global change. Curr Opin Plant Biol 13:241

Malley CS, Omotosho D, Bappa B, Jibril A, Tarfa P, Roman M, Hicks WK, Kuylenstierna JCI, de la Sota Sandez C, Lefèvre EN (2021) Integration of climate change mitigation and sustainable development planning: lessons from a national planning process in Nigeria. Environ Sci Policy 125:66–75

Medina Hidalgo D, Nunn PD, Beazley H (2021) Challenges and opportunities for food systems in a changing climate: a systematic review of climate policy integration. Environ Sci Pol 124:485–495

Nguyen N, Drakou EG (2021) Farmers intention to adopt sustainable agriculture hinges on climate awareness: the case of Vietnamese coffee. J Clean Prod 303:126828

Ogunleye A, Kehinde A, Mishra A, Ogundeji A (2021) Impacts of farmers' participation in social capital networks on climate change adaptation strategies adoption in Nigeria. Heliyon 7(12):e08624

Pande CB, Moharir KN, Singh SK, Varade AM, Ahmed Elbeltagie SFR, Khadri PC (2021) Estimation of crop and forest biomass resources in a semi-arid region using satellite data and GIS. J Saudi Soc Agric Sci 20(5):302–311

Shahid M, Rahman KU, Haider S et al (2021) Quantitative assessment of regional land use and climate change impact on runoff across Gilgit watershed. Environ Earth Sci 80:743. https://doi.org/10.1007/s12665-021-10032-x

Sharif B, Makowski D, Plauborg F, Olesen JE (2017) Comparison of regression techniques to predict response of oilseed rape yield to variation in climatic conditions in Denmark. Eur J Agron 82:11–20

Singh RK, Kumar M (2021) Assessing vulnerability of agriculture system to climate change in the SAARC region. Environ Challenges 5:100398

Srivastava A, Chinnasamy P (2022) Assessing groundwater depletion in southern India as a function of urbanization and change in hydrology: a threat to tank irrigation in Madurai City. In: Kolathayar S, Mondal A, Chian SC (eds) Climate change and water security, Lecture notes in civil engineering, vol 178. Springer, Singapore. https://doi.org/10.1007/978-981-16-5501-2_24

Syed A, Raza T, Bhatti TT, Eash NS (2022) Climate impacts on the agricultural sector of Pakistan: risks and solutions. Environ Challenges 6:100433

van der Keur P, van Bers C, Henriksen HJ, Nibanupudi HK, Yadav S, Wijaya R, Subiyono A, Mukerjee N, Hausmann HJ, Hare M, van Scheltinga CT, Pearn G, Jaspers F (2016) Identification and analysis of uncertainty in disaster risk reduction and climate change adaptation in south and Southeast Asia. Int J Disaster Risk Reduct 16:208–214

Wilts R, Latka C, Britz W (2021) Who is most vulnerable to climate change induced yield changes? A dynamic long run household analysis in lower income countries. Clim Risk Manag 33:100330

Ziogas AI, Pechlivanidis IG, Romas ED, Tzimas AM (2021) Climate service derived indicators to assess the impact of climate change on local river assimilative capacity. Climate Services 23:100250

Chapter 8
Hybrid Daily Streamflow Forecasting Based on Variational Mode Decomposition Random Vector Functional Link Network-Based Ensemble Forecasting

Salim Heddam

Abstract Streamflow forecasting using advance machine learning models have received great importance during the last few years regarding its importance for water resources management, especially for facing climate change. Several approaches based on the exploitation of a wide variety of models have been proposed and successfully applied for accurately daily and monthly streamflow forecasting. However, since streamflow and rainfall are closely interconnected, they were always combined for building more robust forecasting models. While, other climatic variables, i.e., temperature and evapotranspiration, were rarely, if ever, combined for streamflow forecasting, an important part of the developed models used only the value of streamflow measured at previous time lag as input variables. Recently, the use of signal processing decomposition algorithms, i.e., wavelet decomposition (WD) and more recently the variational mode decomposition (VMD), has attracted considerable attention and its success was highlighted up to this date without serious criticism. In the present chapter, we introduce a new scheme for daily streamflow forecasting using the random vector functional link network (RVFL) combined with the VMD. The VMD was used for decomposing the streamflow signal, and then the different intrinsic mode functions (IMF) were used as input variables. For more in depth conclusions, obtained results using the RVFL were compared to those using the extreme learning machine (ELM). Models accuracies were evaluated using several performances metrics and, overall, our best estimation resulted in an overall low RMSE and MAE, and high correlation between measured and predicted streamflow. Furthermore, the best forecasting accuracies were obtained using the RVFL combined with the VMD, for which the R and NSE values were ranged from 0.922 to 0.995 and from 0.850 to 0.991 using the RVFL_

S. Heddam (✉)
Faculty of Science, Agronomy Department, Hydraulics Division, Laboratory of Research in Biodiversity Interaction Ecosystem and Biotechnology, University 20 Août 1955, Skikda, Algeria

C. B. Pande et al. (eds.), *Climate Change Impacts on Natural Resources, Ecosystems and Agricultural Systems*, Springer Climate,
https://doi.org/10.1007/978-3-031-19059-9_8

VMD compared to the values of 0.836–0.947 and 0.691–0.898 obtained using the ELM_VMD. It was found that the gained improvement in terms of model performances was more significant using the RVFL models compared to the ELM models.

Keywords Forecasting · Stream flow · RVFL · ELM · VMD · IMF

Introduction

During the last few decades, improving water resources management has attracted the interest of hydrologists worldwide, and among the hydrological cycle components, river flow is certainly the most important (Pande et al. 2021; Kilinc and Haznedar 2022). Accurate forecasting of streamflow is highly important and used for improving water resources planning, flood control, and for many hydraulic operations (Moharir et al. 2017; Khosravi et al. 2022). With the increase in human activities and climate change, the natural of streamflow has been influenced which has led to an increase if the researches having as objectives the understanding of streamflow variation over times and space (Aher and Yadav 2021). Recently, Ossandón et al. (2022) argued that the need for robust tools used for short-, mild-, and long-terms planning of flood risk is extremely related to the accurate forecasting of streamflow, and these tools are mainly based on the application of available hydrological models, i.e., physical models. While the use of physical models is well known and practiced for a long time (Pande et al. 2022; Hai Nguyen et al. 2022), the advancement in the computer science has allowed the development of robust artificial intelligence models for streamflow forecasting and other hydrological components (Shen et al. 2022). Streamflow is a dynamic hydrological variable (Chen et al. 2022) and, to deal with its potential non-stationarity and high non-linearity, has motivated the development of new modelling strategies based on preprocessing signal decomposition and a large number of applications that are available in the literature. Kisi (2011) used the generalized regression neural network coupled with the discrete wavelet transform (DWT) (WGRNN) for forecasting monthly streamflow at one time in advance using data collected at two stations in Turkey. By using streamflow measured at several previous time-lag (i.e., four lag), the authors demonstrated that the WGRNN was more accurate compared to the standalone GRNN and the multilayer perceptron neural network (MLPNN), exhibiting a root mean square errors (RMSE) and correlation coefficient (R) of approximately $\approx 5.31 m^3/s$ and ≈ 0.728 compared to the values of $\approx 6.36 m^3/s$ and ≈ 0.553 and $\approx 6.15 m^3/s$ and ≈ 0.589 obtained using the GRNN and MLPNN, respectively. Kisi and Cimen (2011) compared between the support vector regression coupled with the discrete wavelet transform (WSVR) and the standalone SVR for monthly streamflow forecasting. It was found that the WSVR was more accurate compared to the SVR with mean absolute error (MAE), RMSE, and R values of $\approx 8.14 m^3/s$, $\approx 13.9 m^3/s$, and ≈ 0.700 compared to the values of $\approx 10.0 m^3/s$, $\approx 15.7 m^3/s$, and ≈ 0.590, respectively. Danandeh Mehr et al. (2014) used the wavelet transform as preprocessing signal

decomposition for improving the performances of the MLPNN model applied for monthly streamflow forecasting. By comparing the standalone MLPNN and the hybrid WT-MLPNN, it was found that the WT-MLPNN was more accurate having RMSE and Nash–Sutcliffe efficiency (NSE) of ≈0.034m^3/s and ≈0.955 compared to the values of ≈0.037m^3/s and ≈0.948, respectively. Yarar (2014) applied the adaptive neuro fuzzy inference systems (ANFIS) coupled with WT for monthly streamflow forecasting, and a comparison with the seasonal autoregressive-integrated moving average SARIMA has been conducted showing the superiority of the WANFIS model. The obtained RMSE and R^2 values using the WANFIS at five stations were ranged from ≈0.89m^3/s to ≈5.58m^3/s and from ≈0.82 to ≈0.94, compared to the values of ≈1.93m^3/s–≈10.14m^3/s and ≈0.60–≈0.69 obtained using SARIMA model, respectively. Fouchal and Souag-Gamane (2019) used monthly streamflow, precipitation and evapotranspiration for better forecasting of multi-step ahead forecasting of monthly streamflow. A comparison between MLPNN and WT-MLPNN showing the superiority of the WT-MLPNN with RMSE and NSE ranging from ≈2.46 to ≈8.26 and from ≈0.978 to ≈0.984, compared to the values of ≈18.04–≈39.28 and ≈0.160–≈0.478 obtained using the MLPNN. In addition, it was demonstrated that increasing the forecasting horizon yielded very poor model performances, and the forecasting accuracies were dramatically decreased. A new forecasting approach for monthly streamflow was proposed by Tikhamarine et al. (2019). They introduced a hybrid model composed of SVR, WT, and the meta-heuristics grey wolf optimizer (GWO) algorithm, and the hybrid model was called WT-SVR-GWO. It was found that the use of WT contributed to an important improvement in the models' performances, and the NSE, RMSE, and NSE were significantly improved exhibiting the values of ≈0.964, ≈0.0686, and ≈0.0885, respectively.

Over the years, the issues raised by the standalone models have become more numerous and more complex (Moosavi et al. 2022), which has lead to a high application of the hybrid models based on the signal decomposition and the number of published papers has significantly increased. Recently, several kinds of signal decomposition algorithms have been successfully used among them; DWT-SVR for monthly streamflow forecasting in Indiana, United States (Liu et al. 2014), empirical mode decomposition (EMD) and singular spectrum analysis (SSA) coupled with the MLPNN and the autoregressive-moving-average (ARMA) (Zhang et al. 2015), continuous wavelet transformation coupled with multigene genetic programming (Hadi and Tombul 2018a), improved complete ensemble empirical mode decomposition with adaptive noise (ICEEMDAN), ensemble EMD, EMD, and SSA coupled with extreme learning machine (ELM) and ARIMA models (Wang et al. 2019), ICEEMDAN coupled with deep learning gated recurrent unit (GRU) (Zhao et al. 2021), bootstrap wavelet artificial neural network (Saraiva et al. 2021; Kouadri et al. 2022; Elbeltagi et al. 2022), variational mode decomposition (VMD) coupled long short-term memory (LSTM) deep learning (Zuo et al. 2020), VMD-coupled SVR (VMD-SVR) (Feng et al. 2020), M5 model tree (M5Tree) and multivariate adaptive regression spline (MARS) coupled with EEMD (Rezaie-Balf et al. 2019), the VMD and ICEEMDAN coupled with the ELM model (Wen et al. 2019), DWT, EMD, and

VMD coupled with SVR (Fang et al. 2019), continuous wavelet transformation (CWT), DWT, and discrete continuous wavelet transformation (DCWT) coupled with ANFIS and SVR models (Hadi and Tombul 2018b), and the VMD coupled deep neural network (He et al. 2019).

The literature review discussed above confirms that preprocessing signal decomposition, i.e., WT, DWT, EMD, EEMD, ICEEMDAN, and VMD, has been widely used and applied by the researchers for improving the accuracies of streamflow forecasting at different time scales, and also it was found that high number of similar studies are available in the literature, and there is no one single method that has been proven to be more accurate compared to the other, and each one possess some advantages and some disadvantages. Therefore, the present chapter was inspired from these previous studies for which the VMD signal decomposition has been successfully applied and its high robustness has been proven. Two machine learning models were applied and compared according to two modelling scenarios: (*i*) single ELM and random vector functional link network (RVFL) models without signal decomposition and (*ii*) the ELM and RVFL were combined with the VMD algorithm. In this chapter, single models, i.e., ELM and RVFL and hybrid models, i.e., ELM_VMD and RVFL_VMD, were for daily streamflow forecasting, and their performances have been compared. This chapter follows the following structure. Section "Introduction" presents introduction and discussion of the related work on streamflow forecasting using different machines learning models. Briefs description of the data used is presented in section "Materials and methods". In section "Methodology", a brief description of different modelling techniques is presented. In section "Results and discussion", obtained results are presented and deeply discussed. Conclusion is drowning in section "Summary and conclusions".

Materials and Methods

Study Site

Daily streamflow data collected at two USGS stations were used in the present study (Fig. 8.1). The two stations were: (*i*) USGS 14141500 little Sandy River near Bull Run River, Clackamas County, Oregon, USA (latitude 45°24′56″, longitude 122°10′13″ NAD27) and (*ii*) USGS 14142500 Sandy River blw Bull Run River, nr bull run, Clackamas County, Oregon, USA (Latitude 45°26′57″, Longitude 122°14′38″ NAD27). Data were measured at daily time step with different periods of record. For the USGS 14141500, we used data corresponding to the period from 01 January 2001 to 10 November 2021, with a total of 7619 patterns. In addition, for the USGS 14142500, we used the data for the period form 01 January 2003 to 10 November 2021, with a total of 6889 patterns. Daily data were measured in cubic foot per second. In the present chapter, we split the data into training and validation with splitting ratios of 70% and 30%, respectively. In Table 8.1, we report the

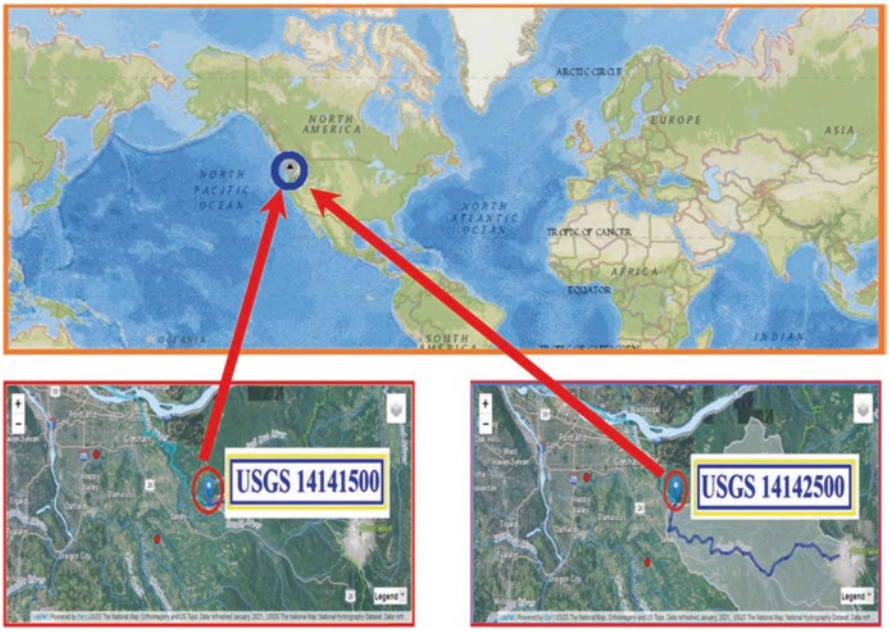

Fig. 8.1 Map showing the location of the two USGS stations

Table 8.1 The statistical parameters of the streamflow for the two stations

Variables	Subset	Unit	X_{max}	X_{mean}	X_{min}	S_x	C_v
USGS 14141500							
Q	Training	cu.ft/s	2400.000	135.924	9.750	162.599	0.836
	Validation	cu.ft/s	1470.000	129.004	9.280	169.593	0.761
	All data	cu.ft/s	2400.000	133.839	9.280	164.741	0.812
USGS 14142500							
Q	Training	cu.ft/s	38500.000	2388.490	235.000	2907.294	0.822
	Validation	cu.ft/s	22900.000	1953.557	295.000	2157.777	0.905
	All data	cu.ft/s	38500.000	2258.067	235.000	2711.609	0.833

Abbreviations: X_{mean} mean, X_{max} maximum, X_{min} minimum, S_x standard deviation, C_v coefficient of variation

statistical descriptive of the data set for the two stations. For selecting the relevant input variables, we calculate the autocorrelation function (ACF) and the partial autocorrelation function (PACF) which were depicted in Fig. 8.2. According to Fig. 8.2, six-time lag were selected and used as input variables, i.e., streamflow measured at (*t-1*), (*t-2*), (*t-3*), (*t-4*), (*t-5*), and (*t-6*), while the output variable starts from the time (*t*), and in total we have adopted six input combination (Table 8.2). Two scenarios were tested and compared, using only the streamflow without decomposition, and in a second scenario the six streamflow selected using the ACF and PACF were decomposed into several intrinsic mode functions (IMF)

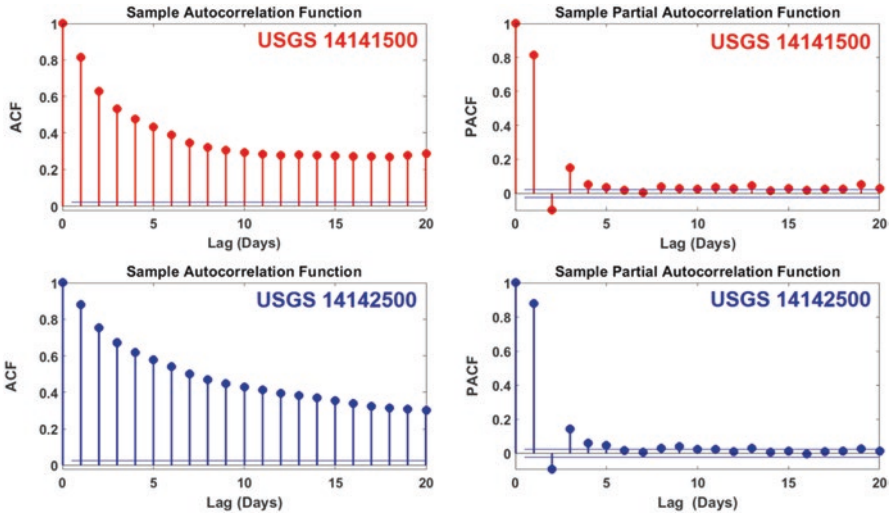

Fig. 8.2 Sample autocorrelation (ACF) and partial autocorrelation function (PACF) for daily streamflow (*Q*)

Table 8.2 The input combinations of different models

ELM	RVFL	Input combination	Output
ELM1	RVFL1	*Q(t-1)*	*Q(t)*
ELM2	RVFL2	*Q(t-2), Q(t-1)*	*Q(t)*
ELM3	RVFL3	*Q(t-3), Q(t-2), Q(t-1)*	*Q(t)*
ELM4	RVFL4	*Q(t-4), Q(t-3), Q(t-2), Q(t-1)*	*Q(t)*
ELM5	RVFL5	*Q(t-5), Q(t-4), Q(t-3), Q(t-2), Q(t-1)*	*Q(t)*
ELM6	RVFL6	*Q(t-6), Q(t-5), Q(t-4),Q(t-3), Q(t-2), Q(t-1)*	*Q(t)*

subcomponents using the VMD algorithm, and example was provided in Fig. 8.3. In the present chapter, we adopted a decomposition level of nine, and the ELM and the RVFL have in total sixty (60) input variables. Flowchart of the proposed modelling strategies adopted in the present work is depicted in Fig. 8.4.

Methodology

Extreme Learning Machine (ELM)

Extreme learning machine (ELM) is an improved training algorithm for the single-layered feedforward neural network (SLFN) proposed by Huang et al. (2006a, b). The major and principal difference between the ELM and SLFN is that the parameters of the ELM model, i.e., the hidden layer weights and biases, are chosen

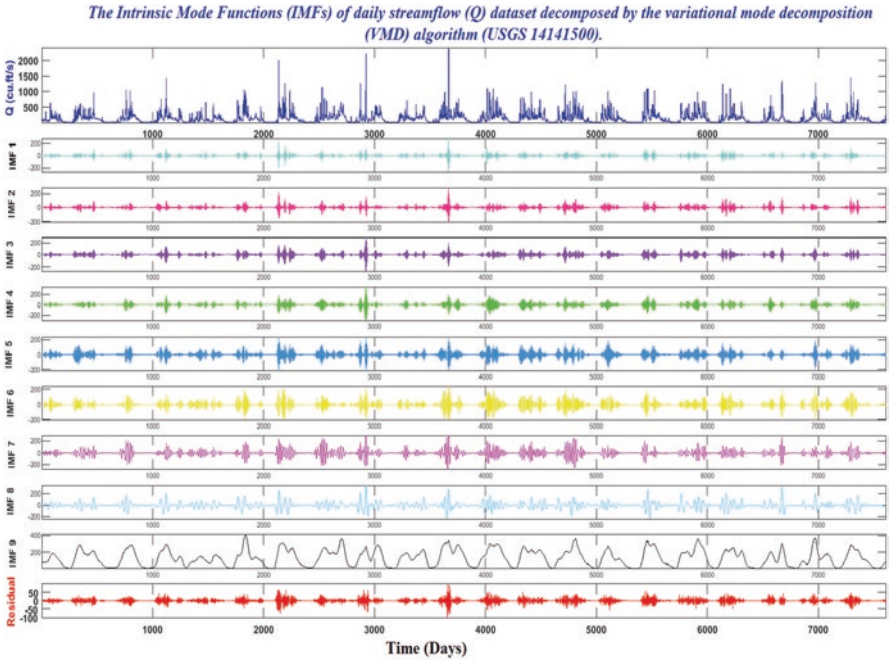

Fig. 8.3 Intrinsic mode functions (IMF) subcomponents of daily streamflow (Q) dataset obtained using the variational mode decomposition (VMD) algorithm

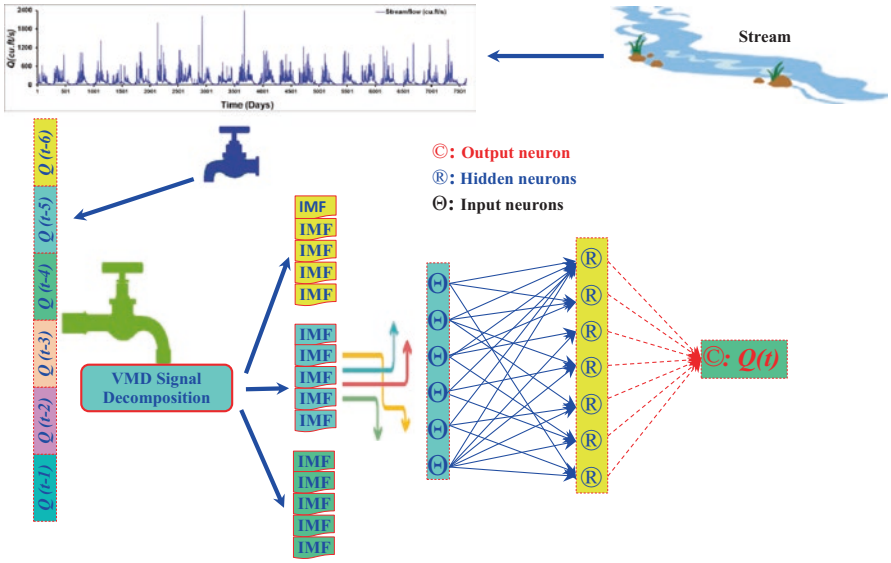

Fig. 8.4 Flowchart of the extreme learning machine (ELM) architecture based on VMD algorithm

randomly and they are not required to be tuned, while the output layer weights and biases are determined analytically. The ELM consists of three successive layers namely, input, hidden, and output layers (Fig. 8.4). The input weights matrix (W), i.e., linking the input and the hidden layer, is randomly chosen, while the output matrix (β) is analytically determined. Figure 8.4 shows the architecture of the ELM proposed for streamflow forecasting. For M samples with x_i as the input and z_i as the output:

$$N \text{ sample} : \left(x_i, z_i\right), \tag{8.1}$$

where

$$x_i = \left[x_{i1}, x_{i2}, x_{i3}, \ldots, x_{in}\right]^T \in R^n \text{ and } z_i = \left[z_{i1}, z_{i2}, z_{i3}, \ldots, z_{im}\right]^T \in R^m \tag{8.2}$$

The ELM with N hidden nodes and activating function f(x) can be expressed as follows:

$$\text{Output} = O_j = \sum_{i=1}^{N} \beta_i f_i\left(x_j\right) = \sum_{i=1}^{N} \beta_i f\left(w_i \bullet x_j + b_i\right), \tag{8.3}$$

where $w_i = [w_{i1}, w_{i2}, w_{i3}, \ldots, w_{in}]^T$ corresponds to the weights matrix linking the ith input to the ith hidden neuron, $\beta_i = [\beta_{i1}, \beta_{i2}, \beta_{i3}, \ldots, \beta_{im}]^T$ corresponds to the weights matrix linking the *ith* hidden to the single output neuron, and the b_i is the bias of the *ith* hidden node (Gan et al. 2021). More details about the ELM algorithm can be found in Huang et al. (2006a, b).

Random Vector Functional Link Network (RVFL)

Similar to the ELM, the RVFL network (RVFL) is a single hidden layer neural network with direct link between the input and output layers, for which only the output weights are required to be updated (Pao et al. 1992, 1994). The general structure of the RVFL neural network as depicted in Fig. 8.5 consists of one input layer having a direct link (i.e., functional link) to the output layer (i.e., blue-dashed line), a hidden layer having several enhancement neurons, and an output layer (Pao et al. 1992, 1994). From a mathematical point of view, the overall RVFL algorithm and its advantages can be summarized as follow: (*i*) possess high ability to avoid the overfitting because only the output weights are updated during a training process, (*ii*) the overall computational time and cost is highly reduced by the fact that the input weights are randomly generated, (*iii*) the output weights were obtained using the Moore Penrose Pseudo Inverse method (Abd Elaziz et al. 2021; Elmaadawy et al. 2021). The RVFL can be formulated as follow:

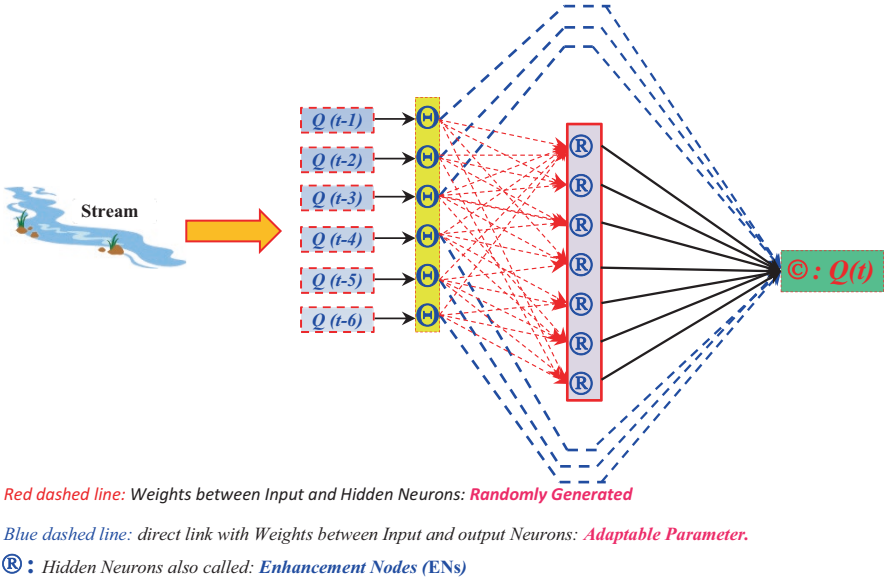

Fig. 8.5 Random vector functional link (*RVFL*) neural network architecture

$$y_i = \sum_{j=1}^{L} \beta_j f_j \left(w_j^T, b_j, x \right) + \sum_{j=L+1}^{L+m} \beta_j x_j \tag{8.4}$$

where N is the number of hidden neurons, m represents the number of input variables, w_j is the input weights, b_j corresponds to the bias of the hidden neuron, f_j is the sigmoid activation, and x is the input variable or the predictor (Majumder et al. 2021).

Variational Mode Decomposition (VMD)

The variational model decomposition (VMD) was proposed by Dragomiretskiy and Zosso (2014). The idea behind the development of the VMD is to overcome some of the disadvantages of the empirical model decomposition (EMD) algorithm by decomposing the signal into a series of band called intrinsic mode functions (IMFs) (Ali et al. 2021; Li et al. 2022). Use of the VMD is based on the idea that the optimal center frequency and limited bandwidth are determined adaptively for each IMF and are defined as follow (Chang et al. 2022):

$$u_k(t) = A_k(t) \cos\left[\varnothing_k(t) \right] \tag{8.5}$$

where u_k (t) corresponds to one IMF, A_k (t) is the instantaneous amplitude of u_k (t), and ϕ_k (t) denotes the instantaneous phase function (Chang et al. 2022). The VMD calculates the IMFs using an iterative process having as its principal objective the establishment of the best solution obtained by an effective separation of the signals from low to high frequency (Gu et al. 2022).

Results and Discussion

To verify the performances of the developed hybrid forecasting models, results are presented and discussed in this section. As stated above, two models were used and compared: the ELM and RVFL neural network model. These two models were applied and compared according to two scenarios: (*i*) standalone models without decomposition and (*ii*) hybrid models using the VMD signal decomposition. For selecting the best input variables, the ACF and the PACF were used, and in total six input combinations were selected and reported in Table 8.2. The effective decomposing technique, i.e., VMD, is adopted to decompose the six input variables into several IMFs, and then, the obtained IMFs were used as new input variables. In the present chapter, each input variable was decomposed into 10 successive IMFs as shown in Fig. 8.3. Finally, the evaluation of the models was done using four common performance criteria of forecast accuracy including, mean absolute error (MAE), root mean square error (RMSE), correlation coefficient (R), and Nash–Sutcliffe efficiency (NSE). In this chapter, the effectiveness of the proposed hybrid models is evaluated by two different datasets with data at daily time scale: the USGS 14141500 and the USGS 14142500 stations. Obtained results at the USGS 14141500 station are reported in Table 8.3. As mentioned above, six different input combinations are adopted with and without the VMD. According to the results of the six models without VMD (i.e., ELM1 to ELM6 and RVFL1 to RVFL2) reported in Table 8.3, it is observed that the ELM models have acceptable performances measured by the R and NSE values and the errors criterions, i.e., the RMSE and MAE. The six ELM models exhibited a mean R and NSE values of approximately ≈0.840 and ≈0.707, and a mean RMSE and MAE of approximately ≈86.99(cu.ft./s) and ≈36.27(cu.ft./s); in addition, the best forecasting accuracy was obtained using the ELM3 having as input variables *Q(t-3)*, *Q(t-2)*, and *Q(t-1)*, respectively. The ELM3 exhibited the high R and NSE values ≈0.847 and ≈0.718, and the lowest RMSE and MAE values of 85.124(cu.ft./s) and 35.434(cu.ft./s), respectively. It is also clear that beyond the third input combination, i.e., ELM3, the performances of the models were decreased to be the poorest for the ELM6 model, which leads to conclude that only three lag times (i.e., *Q (t-3), Q (t-2), Q (t-1)*) are necessary for better for forecasting of daily streamflow at time (t). It is clear from Table 8.3 that the R and NSE were dropped from ≈0.847 and ≈0.718 to ≈0.836 and ≈0.700 showing a decreasing rate of approximately ≈1.30%–≈2.5%, respectively. In addition, as reported in Table 8.3, the RMSE and MAE were increased from ≈85.124(cu.ft./s)

Table 8.3 Performances of different forecasting models at the USGS 14141500 station

Models	Training				Validation			
	R	NSE	RMSE	MAE	*R*	NSE	RMSE	MAE
ELM1	0.830	0.689	88.992	37.305	0.828	0.687	89.901	37.011
ELM2	0.844	0.712	85.698	35.329	0.844	0.713	86.280	35.716
ELM3	0.843	0.711	85.850	35.721	0.847	0.718	85.124	35.434
ELM4	0.845	0.713	85.476	35.364	0.844	0.712	86.179	35.707
ELM5	0.844	0.712	85.652	35.786	0.842	0.710	86.501	36.018
ELM6	0.856	0.733	82.435	35.482	0.836	0.700	87.984	37.733
ELM1_VMD	0.969	0.939	39.458	22.446	0.846	0.691	89.381	41.451
ELM2_VMD	0.987	0.975	25.282	15.689	0.947	0.898	51.417	27.625
ELM3_VMD	0.977	0.955	33.946	20.596	0.935	0.874	57.044	32.173
ELM4_VMD	0.954	0.910	47.841	27.253	0.932	0.869	58.187	33.453
ELM5_VMD	0.953	0.908	48.518	28.939	0.923	0.852	61.808	35.530
ELM6_VMD	0.961	0.924	43.878	27.159	0.918	0.841	64.061	38.195
RVFL1	0.830	0.690	88.933	37.325	0.831	0.691	89.320	36.903
RVFL2	0.841	0.707	86.349	35.293	0.847	0.718	85.317	34.812
RVFL3	0.844	0.712	85.743	35.003	0.850	0.723	84.564	34.829
RVFL4	0.846	0.716	85.096	34.819	0.851	0.724	84.382	34.667
RVFL5	0.845	0.714	85.413	35.050	0.848	0.720	84.975	35.028
RVFL6	0.846	0.716	85.102	35.128	0.849	0.721	84.963	34.880
RVFL1_VMD	0.918	0.842	63.442	29.326	0.922	0.850	62.188	30.542
RVFL2_VMD	0.997	0.994	11.889	7.409	0.993	0.987	18.602	12.068
RVFL3_VMD	0.998	0.995	10.980	6.871	0.994	0.988	17.906	11.777
RVFL4_VMD	0.999	0.998	7.425	4.812	0.995	0.990	16.107	10.691
RVFL5_VMD	0.999	0.998	6.209	4.006	0.995	0.990	15.673	10.461
RVFL6_VMD	0.999	0.999	5.745	3.721	0.995	0.990	15.678	10.564

and ≈35.434(cu.ft./s) to ≈87.98(cu.ft./s) and ≈37.73(cu.ft./s) showing an increasing rates of approximately ≈3.25%–≈6.09%, respectively. It can be seen in Table 8.3 that the proposed RVFL models were slightly more accurate compared to the ELM models, and numerical comparison revealed that the RVFL models improve the mean R, NSE, RMSE, and MAE of the ELM by ≈0.7%, ≈1.32%, ≈1.618%, and ≈2.98%, respectively. Among the six RVFL model, the best performances were obtained using the RVFL4 showing the high R (≈0.851) and NSE (≈0.724) values, and the lowest RMSE (≈84.38) and MAE (≈34.66) values, respectively. While we can see that the RVFL4 was slightly more accurate compared to the RVFL3 with negligible difference, we can conclude that the overall forecasting accuracies were captured using only the first three lag time (i.e., *Q (t-3), Q (t-2), Q (t-1)*). In the second stage of the investigation, the VMD algorithm was used for decomposing the input variables into several IMFs, and the hybrid models were designated as ELM_VMD and RVFL_VMD, respectively. From the results reported in Table 8.3, we can conclude that the use of the VMD yielded high improvement in model

performances and forecasting accuracy. The mean R, NSE, RMSE, and MAE of the ELM models were improved by ≈8.36%, ≈15.62%, ≈26.83%, and ≈4.22%, respectively, using the ELM_VMD. The best accuracies were obtained using the ELM2_VMD having a high R (≈0.947) and NSE (≈0.898) values, and lowest RMSE (≈51.41) and MAE (≈27.62) values, respectively. Beyond the second input combination, i.e., the ELM2_VMD, it is clear that the performances of the models continued to worsen, which lead to conclude that only the Q (*t-2*), Q (*t-1*) are necessary for better forecasting of daily streamflow. Numerical comparison between the models with and without VMD revealed that, the ELM2_VMD model improves the performances of the best ELM3 model by ≈10.56%, ≈20.045%, ≈39.59%, and ≈22.03%, respectively. The improvement of model performances gained using the RVFL models was more obvious. According to the Table 8.3, by using the VMD, the mean R, NSE, RMSE, and MAE of the single RVFL models were improved by ≈13.87%, ≈25.85%, ≈71.54%, and ≈59.21%, respectively, which is an excellent improvement in terms of forecasting accuracies. More specifically, we can conclude that the RVFL models were more stable in terms of model performances, and beyond the RVFL2_VMD, the performances remained fairly consistent with slightly fluctuation, and the best accuracies were obtained using the RVFL5_VMD with R, NSE, RMSE, and MAE values of approximately ≈0.995, ≈0.990%, ≈15.67, and ≈10.46, respectively, significantly higher than the values obtained using the ELM2_VMD with an improvement rate of approximately ≈4.82%, ≈9.29%, ≈69.51%, and ≈62.13%, in terms of R, NSE, RMSE and MAE values, respectively. Finally, the scatterplots measured against forecasted daily streamflow (*Q*) at the USGS 14141500 for the validation stage are depicted in Fig. 8.6. In addition, the comparison between measured and forecasted data is plotted in Fig. 8.7.

Obtained results at the USGS 14142500 station are reported in Table 8.4. The scatterplots measured against forecasted daily streamflow (*Q*) for the validation stage are depicted in Fig. 8.8. In addition, the comparison between measured and forecasted data is plotted in Fig. 8.9. According to Table 8.4, it is clear that the models without VMD were relatively acceptable with only negligible difference whether for the ELM or for the RVFL models. The ELM models worked with R and NSE values ranging from ≈0.863 to ≈0.890 (mean≈0.875) and from ≈0.754 to ≈0.799 (mean≈0.773), respectively. The best performances were obtained using the ELM3 slightly higher than the other models. In addition, the RVFL models worked with R and NSE values ranging from ≈0.871 to ≈0.891 (mean≈0.885) and from ≈0.767 to ≈0.801 (mean≈0.792), respectively. The best performances were obtained using the RVFL4 slightly higher than the RVFL3 model. It is also clear that the difference between the ELM and RVFL models was marginal and does not exceed ≈1.22%, ≈2.37%, ≈4.22%, and ≈7.18% in terms of mean R, NSE, RMSE, and MAE, respectively. It is also clear that increasing the number of input variables does not contribute to the improvement of model performances and beyond the third input combination, the performances remain constant with slightly variation.

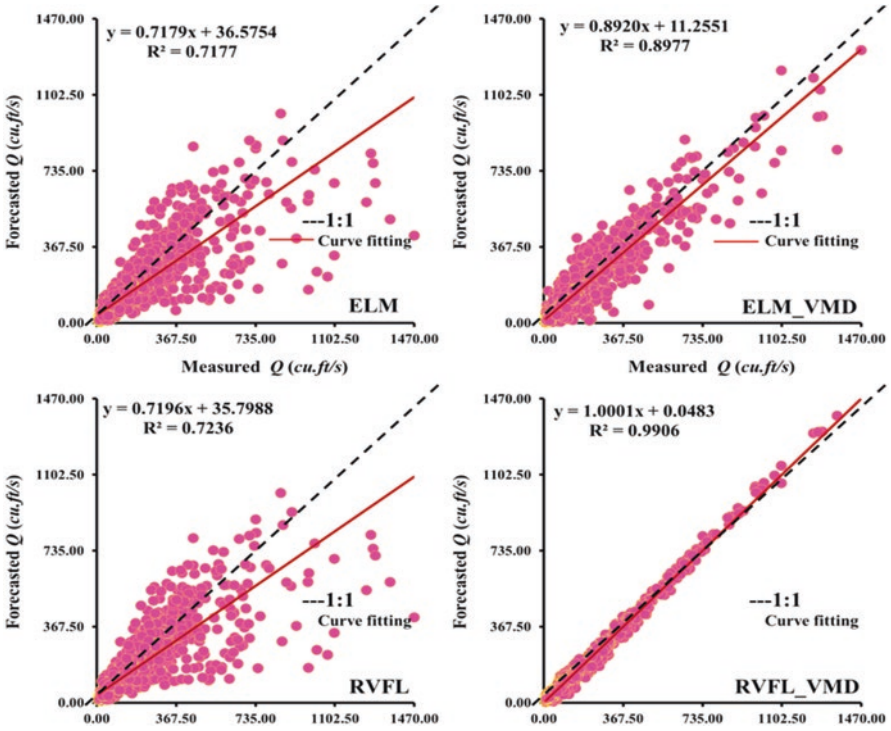

Fig. 8.6 Scatterplots measured against forecasted daily streamflow (*Q*) at the USGS 14141500 for the validation stage

According to Table 8.4, it is clear that the use of hybrid models based on the VMD decomposition contributes to the improvement of forecasting accuracies with a high degree of accuracy. Using the ELM_VMD yielded an improvement of approximately ≈3.97% and ≈6.58% in terms of mean R and NSE values compared to the ELM models. Similarly, the RVFL_VMD guaranteed high rates of improvement in terms of mean R and NSE exhibiting the values of ≈10.25% and ≈18.71%, and an improvement of approximately ≈71% and ≈52.61% in terms of mean RMSE and MAE values, respectively. The RVFL_VMD models were more accurate compared to the ELM_VMD models for which the best accuracy was obtained using the RVFL6_VMD with R, NSE, RMSE, and MAE values of ≈0.996, ≈0.992, ≈196.82, and ≈133.69, respectively. However, from RVFL2_VMD to RVFL6_VMD, it is clear that the difference between the models in terms of model performances was negligible, and beyond the second input combination, the improvement was completely marginal and only the first two time lags (Q (*t-2*) and Q (*t-1*)) contributed to the better streamflow forecasting.

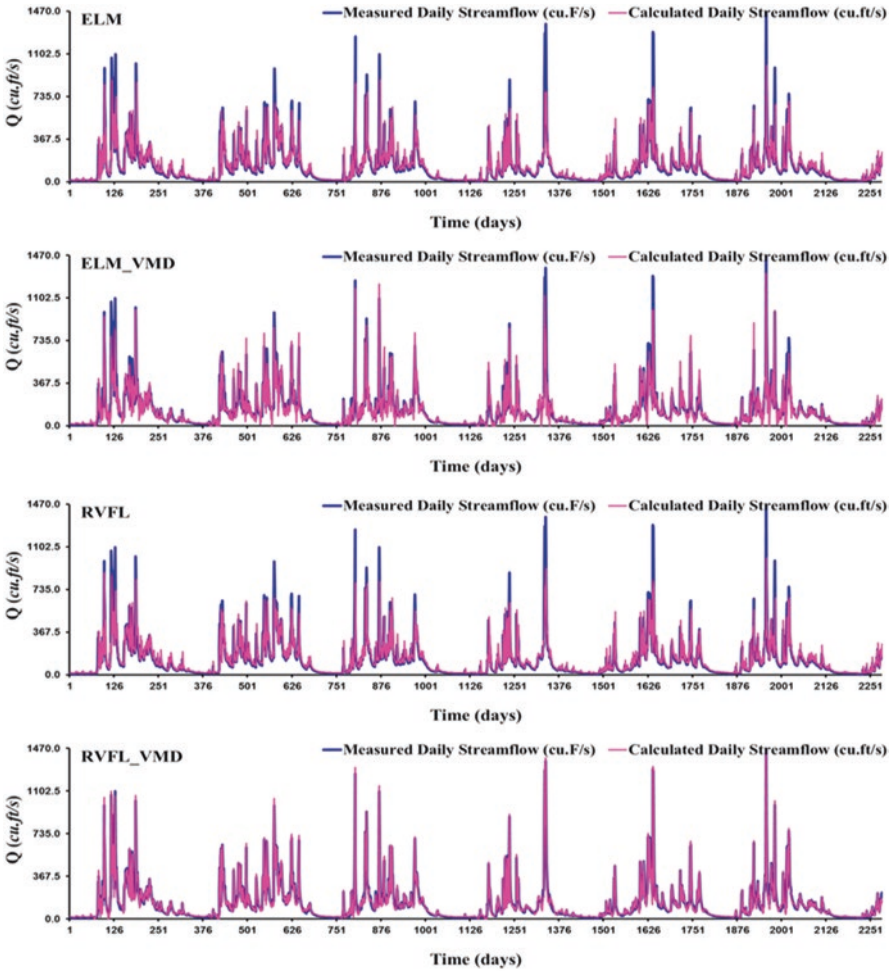

Fig. 8.7 Comparison between measured against forecasted daily streamflow (Q) at the USGS 14141500 for the validation stage

Summary and Conclusions

In the present work, an approach based on preprocessing signal decomposition was proposed for better forecasting of daily streamflow at two USGS stations. Two machine learning models were tested and found to be capable for accurately forecasting streamflow. High difference in terms of model performances was found between the RVFL and the ELM models yet whether it was calibrated with or without the VMD signals decomposition. However, the difference in terms of numerical

Table 8.4 Performances of different forecasting models at the USGS 14142500 station

Models	Training				Validation			
	R	NSE	RMSE	MAE	*R*	NSE	RMSE	MAE
ELM1	0.891	0.795	1317.512	493.477	0.863	0.754	1092.044	383.579
ELM2	0.880	0.774	1382.997	509.810	0.867	0.760	1077.100	395.762
ELM3	0.899	0.809	1270.749	464.372	0.890	0.799	985.448	356.882
ELM4	0.877	0.768	1398.975	524.913	0.871	0.767	1062.187	392.377
ELM5	0.905	0.819	1237.323	456.061	0.880	0.783	1026.153	377.796
ELM6	0.900	0.810	1266.096	491.006	0.876	0.776	1042.393	401.731
ELM1_VMD	0.947	0.898	929.545	471.537	0.923	0.848	857.846	443.046
ELM2_VMD	0.971	0.943	696.664	388.025	0.941	0.886	741.542	412.469
ELM3_VMD	0.952	0.906	890.342	509.096	0.918	0.840	879.950	491.620
ELM4_VMD	0.970	0.940	709.858	436.473	0.900	0.811	957.697	532.699
ELM5_VMD	0.975	0.950	648.718	414.530	0.890	0.789	1011.838	568.189
ELM6_VMD	0.968	0.937	731.870	467.903	0.892	0.792	1003.970	596.458
RVFL1	0.886	0.784	1349.723	507.392	0.871	0.767	1061.677	380.077
RVFL2	0.901	0.811	1263.698	457.336	0.884	0.789	1010.822	356.671
RVFL3	0.903	0.816	1247.916	450.079	0.890	0.801	982.817	348.141
RVFL4	0.904	0.818	1240.348	447.346	0.891	0.801	981.663	349.597
RVFL5	0.904	0.816	1246.018	450.376	0.888	0.797	991.717	351.941
RVFL6	0.905	0.819	1236.624	450.471	0.888	0.797	991.194	355.816
RVFL1_VMD	0.952	0.905	893.687	392.400	0.939	0.887	740.675	336.720
RVFL2_VMD	0.999	0.998	141.960	82.733	0.996	0.991	202.974	137.860
RVFL3_VMD	0.999	0.998	127.284	75.761	0.996	0.992	201.564	136.715
RVFL4_VMD	0.999	0.999	107.364	64.613	0.996	0.992	198.520	134.849
RVFL5_VMD	0.999	0.999	98.965	58.717	0.996	0.992	199.891	135.378
RVFL6_VMD	0.999	0.999	88.563	52.027	0.996	0.992	196.829	133.695

performances was especially more evident for the models based on VMD. Using the models without VMD, it was found that all ELM and RVFL models worked relatively with the same performances for which the R and NSE for the ELM models were ranged from 0.828 to 0.847 and from 0.687 to 0.718 for the first station, and from 0.863 to 0.890 and 0.754 to 0.799, for the second station, respectively. Using the RVFL models the R and NSE were ranged from 0.831 to 0.851 and 0.691 to 0.724 for the first station, and from 0.871 to 0.891 and 0.767 to 0.801, respectively, which were slightly higher than the values obtained using the ELM, and the difference was completely marginal. By using the VMD as preprocessing signal decomposition, two important conclusions can be drawn. First, using the RVFL_VMD models were found to be more appropriate and high forecasting accuracy was obtained compared to the ELM_VMD. Second, an interesting concluding remark regarding the RVFL_VMD was that, beyond the first input combination using only the Q at (t-1), all models were equal in terms of numerical performances exhibiting

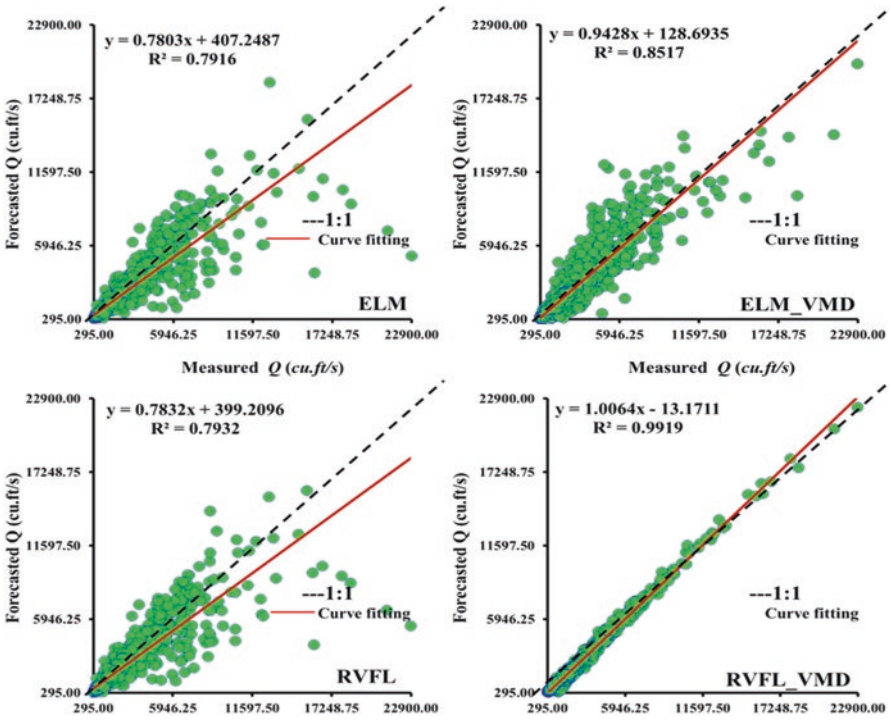

Fig. 8.8 Scatterplots measured against forecasted daily streamflow (*Q*) at the USGS 14142500 for the validation stage

very high R (≈0.99) and NSE (≈0.99) values, while for the ELM_VMD models, it was found that numerical performances have fluctuated significantly between the six input combination and increasing the number of input variables does not appear to have yielded any improvement in the achievement rate, and the performances of the models were decreased beyond the combination three (i.e., ELM3_VMD), highlighting the instability of the ELM models compared to the RVFL models. For concluding, models that aim to forecast and predict streamflow are for great interest, and they have become important tools for better monitoring and management of water resources. It is therefore very important to create robust, stable, and well-validated models that can accurately and correctly forecast streamflow at different time scales.

Acknowledgments This study could not have been possible without the support of the USGS data survey. The author would like to thank the staffs of USGS web server for providing the data that makes this research possible.

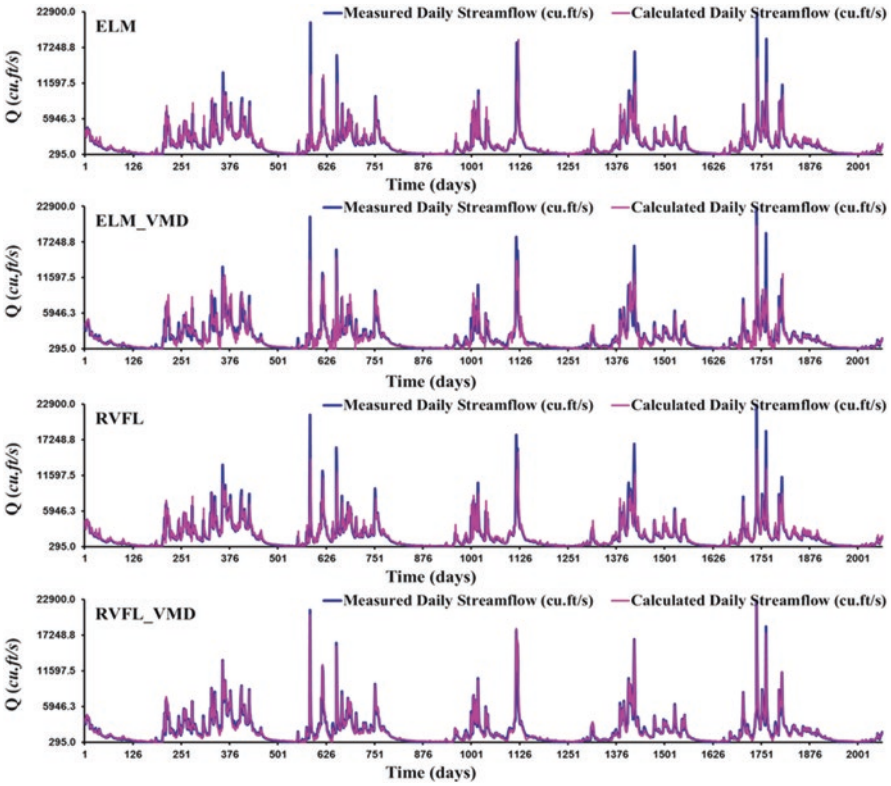

Fig. 8.9 Comparison between measured against forecasted daily streamflow (Q) at the USGS 14142500 for the validation stage

References

Abd Elaziz M, Senthilraja S, Zayed ME, Elsheikh AH, Mostafa RR, Lu S (2021) A new random vector functional link integrated with mayfly optimization algorithm for performance prediction of solar photovoltaic thermal collector combined with electrolytic hydrogen production system. Appl Therm Eng 193:117055. https://doi.org/10.1016/j.applthermaleng.2021.117055

Aher MC, Yadav S (2021) Impact of land use-land cover change on spatio-temporal trends in seasonal stream flow and suspended sediment load of Godavari basin from 1969 to 2019. J Water Clim Change. https://doi.org/10.2166/wcc.2021.184

Ali M, Prasad R, Xiang Y, Khan M, Farooque AA, Zong T, Yaseen ZM (2021) Variational mode decomposition based random forest model for solar radiation forecasting: new emerging machine learning technology. Energy Rep 7:6700–6717. https://doi.org/10.1016/j.egyr.2021.09.113

Chen C, Zhang Q, Kashani MH, Jun C, Bateni SM, Band SS et al (2022) Forecast of rainfall distribution based on fixed sliding window long short-term memory. Eng Appl Comput Fluid Mech 16(1):248–261. https://doi.org/10.1080/19942060.2021.2009374

Danandeh MA, Kahya E, Bagheri F, Deliktas E (2014) Successive-station monthly streamflow prediction using neuro-wavelet technique. Earth Sci Inf 7(4):217–229. https://doi.org/10.1007/s12145-013-0141-3

Dragomiretskiy K, Zosso D (2014) Variational mode decomposition. IEEE Trans Signal Process 62(3):531–544. https://doi.org/10.1109/TSP.2013.2288675

Elbeltagi A, Kumar N, Chandel A et al (2022) Modelling the reference crop evapotranspiration in the Beas-Sutlej basin (India): an artificial neural network approach based on different combinations of meteorological data. Environ Monit Assess 194:141. https://doi.org/10.1007/s10661-022-09812-0

Elmaadawy K, Abd Elaziz M, Elsheikh AH, Moawad A, Liu B, Lu S (2021) Utilization of random vector functional link integrated with manta ray foraging optimization for effluent prediction of wastewater treatment plant. J Environ Manag 298:113520. https://doi.org/10.1016/j.jenvman.2021.113520

Fang W, Huang S, Ren K, Huang Q, Huang G, Cheng G, Li K (2019) Examining the applicability of different sampling techniques in the development of decomposition-based streamflow forecasting models. J Hydrol 568:534–550. https://doi.org/10.1016/j.jhydrol.2018.11.020

Feng ZK, Niu WJ, Tang ZY, Jiang ZQ, Xu Y, Liu Y, Zhang HR (2020) Monthly runoff time series prediction by variational mode decomposition and support vector machine based on quantum-behaved particle swarm optimization. J Hydrol 583:124627. https://doi.org/10.1016/j.jhydrol.2020.124627

Fouchal A, Souag-Gamane D (2019) Long-term monthly streamflow forecasting in humid and semiarid regions. Acta Geophys 67(4):1223–1240. https://doi.org/10.1007/s11600-019-00312-3

Gan L, Zhao X, Wu H, Zhong Z (2021) Estimation of remaining fatigue life under two-step loading based on kernel-extreme learning machine. Int J Fatigue 148:106190. https://doi.org/10.1016/j.ijfatigue.2021.106190

Gu L, Fei Z, Xu X (2022) Enhancement method of weak Lidar signal based on adaptive variational modal decomposition and wavelet threshold denoising. Infrared Phys Technol 120:103991. https://doi.org/10.1016/j.infrared.2021.103991

Hadi SJ, Tombul M (2018a) Monthly streamflow forecasting using continuous wavelet and multigene genetic programming combination. J Hydrol 561:674–687. https://doi.org/10.1016/j.jhydrol.2018.04.036

Hadi SJ, Tombul M (2018b) Streamflow forecasting using four wavelet transformation combinations approaches with data-driven models: a comparative study. Water Resour Manag 32(14):4661–4679. https://doi.org/10.1007/s11269-018-2077-3

Hai Nguyen D, Hien Le X, Tran Anh D, Kim S-H, Bae D-H (2022) Hourly streamflow forecasting using a Bayesian additive regression tree model hybridized with a genetic algorithm. J Hydrol 606:127445. https://doi.org/10.1016/j.jhydrol.2022.127445

He X, Luo J, Zuo G, Xie J (2019) Daily runoff forecasting using a hybrid model based on variational mode decomposition and deep neural networks. Water Resour Manag 33(4):1571–1590. https://doi.org/10.1007/s11269-019-2183-x

Huang GB, Chen L, Siew CK (2006a) Universal approximation using incremental constructive feedforward networks with random hidden nodes. IEEE Trans Neural Netw 17(4):879–892. https://doi.org/10.1109/TNN.2006.875977

Huang GB, Zhu QY, Siew CK (2006b) Extreme learning machine: theory and applications. Neurocomputing 70(1–3):489–501. https://doi.org/10.1016/j.neucom.2005.12.126

Khosravi K, Golkarian A, Tiefenbacher JP (2022) Using optimized deep learning to predict daily streamflow: a comparison to common machine learning algorithms. Water Resour Manag 36(2):699–716. https://doi.org/10.1007/s11269-021-03051-7

Kilinc HC, Haznedar BA (2022) Hybrid model for streamflow forecasting in the basin of Euphrates. Water 14:80. https://doi.org/10.3390/w14010080

Kişi Ö (2011) A combined generalized regression neural network wavelet model for monthly streamflow prediction. KSCE J Civ Eng 15(8):1469–1479. https://doi.org/10.1007/s12205-011-1004-4

Kisi O, Cimen M (2011) A wavelet-support vector machine conjunction model for monthly streamflow forecasting. J Hydrol 399(1–2, 132):–140. https://doi.org/10.1016/j.jhydrol.2010.12.041

Kouadri S, Pande CB, Panneerselvam B et al (2022) Prediction of irrigation groundwater quality parameters using ANN, LSTM, and MLR models. Environ Sci Pollut Res 29:21067–21091. https://doi.org/10.1007/s11356-021-17084-3

Li G, Zheng C, Yang H (2022) Carbon price combination prediction model based on improved variational mode decomposition. Energy Rep 8:1644–1664. https://doi.org/10.1016/j.egyr.2021.11.270

Liu Z, Zhou P, Chen G, Guo L (2014) Evaluating a coupled discrete wavelet transform and support vector regression for daily and monthly streamflow forecasting. J Hydrol 519:2822–2831. https://doi.org/10.1016/j.jhydrol.2014.06.050

Majumder I, Dash PK, Dhar S (2021) Real-time energy management for PV-battery-wind based microgrid using on-line sequential kernel based robust random vector functional link network. Appl Soft Comput 101:107059. https://doi.org/10.1016/j.asoc.2020.107059

Moharir K, Pande C, Patil S (2017) Inverse modelling of Aquifer parameters in basaltic rock with the help of pumping test method using MODFLOW software. Geosci Front Elsevier J May(2017):1–13, Impact Factor 4:256. ISSN: 1674-9871

Moosavi V, Fard ZG, Vafakhah M (2022) Which one is more important in daily runoff forecasting using data driven models: input data, model type, preprocessing or data length? J Hydrol 606, 127429. https://doi.org/10.1016/j.jhydrol.2022.127429

Ossandón Á, Brunner MI, Rajagopalan B, Kleiber W (2022) A space-time Bayesian hierarchical modeling framework for projection of seasonal maximum streamflow. Hydrol Earth Syst Sci 26(1):149–166. https://doi.org/10.5194/hess-26-149-2022

Pande CB, Moharir KN, Panneerselvam B, Singh SK, Elbeltagi A, Pham QB, Varade AM, Rajesh J (2021) Delineation of groundwater potential zones for sustainable development and planning using analytical hierarchy process (AHP), and MIF techniques. Appl Water Sci 11(12):1–20. https://doi.org/10.1007/s13201-021-01522-1

Pande CB, Moharir KN, Elbeltagi SKSA, Pham QB, Panneerselvam B, Varade AM, Kouadri S (2022) Groundwater flow modeling in the basaltic hard rock area of Maharashtra, India. Appl Water Sci 12(1):1–14. https://doi.org/10.1007/s13201-021-01525-y

Pao YH, Phillips SM, Sobajic DJ (1992) Neural-net computing and the intelligent control of systems. Int J Control 56(2):263–289. https://doi.org/10.1080/00207179208934315

Pao YH, Park GH, Sobajic DJ (1994) Learning and generalization characteristics of the random vector functional-link net. Neurocomputing 6(2):163–180. https://doi.org/10.1016/0925-2312(94)90053-1

Rezaie-Balf M, Kim S, Fallah H, Alaghmand S (2019) Daily river flow forecasting using ensemble empirical mode decomposition based heuristic regression models: application on the perennial rivers in Iran and South Korea. J Hydrol 572:470–485. https://doi.org/10.1016/j.jhydrol.2019.03.046

Saraiva SV, de Oliveira Carvalho F, Santos CAG, Barreto LC, Freire PKDMM (2021) Daily streamflow forecasting in Sobradinho Reservoir using machine learning models coupled with wavelet transform and bootstrapping. Appl Soft Comput 102:107081. https://doi.org/10.1016/j.asoc.2021.107081

Shen Y, Ruijsch J, Lu M, Sutanudjaja EH, Karssenberg D (2022) Random forests-based error-correction of streamflow from a large-scale hydrological model: using model state variables to estimate error terms. Comput Geosci 159:105019. https://doi.org/10.1016/j.cageo.2021.105019

Tikhamarine Y, Souag-Gamane D, Kisi O (2019) A new intelligent method for monthly streamflow prediction: hybrid wavelet support vector regression based on grey wolf optimizer (WSVR-GWO). Arab J Geosci 12(17):1–20. https://doi.org/10.1007/s12517-019-4697-1

Wang L, Li X, Ma C, Bai Y (2019) Improving the prediction accuracy of monthly streamflow using a data-driven model based on a double-processing strategy. J Hydrol 573:733–745. https://doi.org/10.1016/j.jhydrol.2019.03.101

Wen X, Feng Q, Deo RC, Wu M, Yin Z, Yang L, Singh VP (2019) Two-phase extreme learning machines integrated with the complete ensemble empirical mode decomposition with adaptive noise algorithm for multi-scale runoff prediction problems. J Hydrol 570:167–184. https://doi.org/10.1016/j.jhydrol.2018.12.060

Yarar A (2014) A hybrid wavelet and neuro-fuzzy model for forecasting the monthly streamflow data. Water Resour Manag 28(2):553–565. https://doi.org/10.1007/s11269-013-0502-1

Zhang X, Peng Y, Zhang C, Wang B (2015) Are hybrid models integrated with data preprocessing techniques suitable for monthly streamflow forecasting? Some experiment evidences. J Hydrol 530:137–152. https://doi.org/10.1016/j.jhydrol.2015.09.047

Zhao X, Lv H, Lv S, Sang Y, Wei Y, Zhu X (2021) Enhancing robustness of monthly streamflow forecasting model using gated recurrent unit based on improved grey wolf optimizer. J Hydrol 601:126607. https://doi.org/10.1016/j.jhydrol.2021.126607

Zuo G, Luo J, Wang N, Lian Y, He X (2020) Decomposition ensemble model based on variational mode decomposition and long short-term memory for streamflow forecasting. J Hydrol 585:124776. https://doi.org/10.1016/j.jhydrol.2020.124776

Chapter 9
Climate Change and Natural Hazards in the Senegal River Basin: Dynamics of Hydrological Extremes in the Faleme River Basin

Cheikh Faye

Abstract Extreme events punctuate the climate variability that directly affects the national economies of West African countries, those of the Sahel in particular, due to the low level of water control and poor reservoir filling conditions. This paper examines the dynamics of hydrological extremes and thus droughts and floods from the Faleme basin to the Gourbassi and Kidira stations, taking into account the context of climate change. The analyses are based on daily maximum (Dmax) and minimum (Dmin) discharge data for the period 1954–2019. The XLStat and KhronoStat software made it possible to calculate a set of indices (irregularity index, drying coefficient and Myer coefficient A). These software were also used to determine trends in the temporal evolution of the data. The discharges of the Faleme River make it possible to distinguish the hydroclimatic conditions in the basin over the study period. At station level, the Dmin underwent three successive breaks, in 1966–67 and 2007–08, with a decrease in values of more than 50%. These ruptures reflect the transition from wet conditions to a marked drought. From 2007 onwards, conditions became particularly contrasted, with the return of years with excess discharges. On average, Myer's coefficient A is 7.2. This reflects a low flood strength. The annual value of the Dmax/Dmin ratio is very high, reflecting the variability of the discharge. The drying coefficient is generally low (0.06/day on average). Not all of the catastrophic floods in the study area occurred in wet years. This reflects the important role played by other factors, such as the spatial distribution of rainfall.

Keywords Drought · Flood · Risk · Dynamics · Faleme catchment area

C. Faye (✉)
Department of Geography, U.F.R. Sciences et Technologies, Assane Seck University of Ziguinchor, Laboratoire de Géomatique et d'Environnement, BP, Ziguinchor, Senegal
e-mail: cheikh.faye@univ-zig.sn

C. B. Pande et al. (eds.), *Climate Change Impacts on Natural Resources, Ecosystems and Agricultural Systems*, Springer Climate,
https://doi.org/10.1007/978-3-031-19059-9_9

Introduction

Today, hydroclimatic risks are the most recurrent and devastating in all continents (World Bank 2014; Guhasapir et al. 2016; Pande et al. 2022a). Many rivers experience the occurrence of extreme discharges (Moharir et al. 2020; Rodier 1981). Droughts are associated with low discharges and floods with high discharges (Giret 2004; Khadri and Pande 2016), with their consequences in terms of economic losses and human lives (Easterling et al. 2000). Within the framework of ongoing climate change studies, various works report the resurgence of extreme rainfall, with an impact on surface discharges (Sow 2007; Field et al. 2012; Saha et al. 2020; Srivastava and Chinnasamy 2021). In recent decades, climate change has been one of the hottest topics in climatology and hydrology. Beyond temperature, precipitation and runoff are considered to be the most important elements that can directly reflect climate change. Climate change is causing an increase in natural disasters and extreme events (drought, floods, etc. (IPCC 2014)). Extreme precipitation events often cause a series of extreme hydrological events such as droughts and floods (Xu et al. 2015; Pande et al. 2022c; Pande 2022). In this situation, areas where the main source of economic income depends on agriculture can be clearly influenced by changes in precipitation and temperature and their impact on water resources (Radinovi'c and C'uric' 2012). Since the beginning of the twenty-first century, numerous studies on extreme precipitation and runoff (Sighomnou 2004; Milly et al. 2005; Sharma and Panu 2010) at global, regional and national scales have been carried out. These studies have indicated the climatic upheaval since the 1970s, which has resulted in a general downward trend in river discharges in some regions, particularly in West Africa. Faced with a succession of extreme climatological (droughts and floods) and hydrological (floods and low water levels) episodes, it is common to invoke climate change as the basis for analysing the data to explain their increase. It is in this same wake that many studies have been carried out on the Senegal River catchment basin (Sow 2007; Faye 2013, 2017a, b; Faye et al. 2015a, b; Orimoloye et al. 2022). The Senegal River basin has experienced climatic variability since the 1970s marked by a drop in rainfall (Sow 2007; Faye et al. 2019a), which has resulted in a significant decrease in surface runoff as illustrated by the years 1983 and 1984 when runoff even stopped at Bakel. This drop in runoff has had a negative impact on many sectors of activity (agricultural production, industry, drinking water supply, navigation, etc.), placing the basin in an unprecedented ecological crisis (Tropica Environmental Consultants 2008). However, new studies have highlighted the increase in rainfall and runoff in the area, which augurs well for an improvement in the hydrological regime (Ali et al. 2008; Niang 2008; Pande et al. 2019, 2022b) and a resurgence of floods. A flood situation exists when the discharge of a river cannot be discharged within the margins of its normal channel, with water spilling over adjacent lowlands occupied by agricultural or urban land, including residential areas (Strahler and Strahler 2003; Abashiya 2006; Pande and Moharir 2017). In recent years, there has been an increase in floods that have caused enormous damage in terms of loss of life and property (Abashiya et al. 2017). However, significant floods and overflows of the

Senegal River are indicated in travellers' accounts, historical documents and old maps well before 1903 (the beginning of the first water level measurements). The major floods recorded are those of 1827, 1841, 1843 and 1853 (Kane 2002), resulting in river overflows so large that their homes were full of water up to the first floor (Hardy 1921). Devastating floods are occurring due to heavy rains in many parts of the country. Studies have shown that the Senegal River basin is prone to frequent floods and droughts due to high interannual variability in rainfall; the most devastating effects of these extreme events, particularly floods, are the leaching of agricultural land, affecting agricultural production and food security, destruction of homes, increased health risks and the spread of infectious diseases (Sawa 2002; Abashiya et al. 2017; Ahmed et al. 2022). The resource can thus become a problem because of its overabundance, as was the case with the devastating floods of 1890, 1906, and 1950 (Roche 2003). The Bafing basin was not spared and heavy rainfall often causes flooding and many inconveniences. Drought, which is characterised by a reduction or poor distribution, or even the absence of rainfall in a given area for a period of time (Bootsma et al. 1996; Orimoloye et al. 2022), is primarily meteorological. It is then hydrological and agricultural. Meteorological drought is defined as a period of reduced rainfall relative to the average over a long period of time (Esfahanian et al. 2017; Elbeltagi et al. 2022b). Soil drought is associated with soil moisture deficits leading to reduced vegetation development and crop yields (Li et al. 2016). Hydrological drought is related to changes in groundwater and surface water levels and disruption of runoff. The consequences of drought are not immediate, its effects are felt over a larger area and are more widespread over time than those of other natural phenomena (Łabędzki 2004; Pande et al. 2021, 2022a). The impact of droughts first manifests itself on the agricultural sector and then gradually on other water-dependent sectors. The risk of drought is a major concern in many parts of Senegal, particularly in the arid and semi-arid regions of the North, where climatic conditions are extremely variable in space and time (Faye 2018; Faye et al. 2019b). The combination of rainfall deficits with other climatic factors is likely to cause severe droughts in Senegal, where agriculture is the main occupation for most of the population. The impact of drought in Senegal is considerable, affecting agriculture, irrigation and the economy. In a climatic context marked by a possible increase in the occurrence and impact of floods and droughts in the coming years, it is essential to be able to analyse hydrological variables with a view to proposing adaptation measures to populations. It is within this framework that the present study was initiated in the Faleme basin, a tributary of the Senegal River, which has been subject to hydrometric surpluses and deficits in recent years. The purpose of this paper is to analyse the characteristics of extreme discharge in the Faleme basin in order to examine the implications for floods and droughts. Discharge observations are then compared with available knowledge on droughts and the frequency and magnitude of catastrophic floods. This is of paramount importance because floods (floods) and low discharges (droughts) are natural hazards that need to be protected against both through prevention and prediction. In addition, the rational management of the waters of the Senegal River basin and of the major works and the control of floods and droughts in the valley require a better knowledge of floods and low water levels throughout the basin.

Study Area

The Faleme, a tributary of the Senegal River, rises at an altitude of 800 m at the foot of the Fouta Djallon. Its watershed lies between latitudes 12°11′ and 14°27′ N and longitudes 11°12′ and 12°15′ W (Fig. 9.1). It covers an area of 28,900 km^2, i.e., 10% of the total area of the Senegal River catchment basin of which it is the last major tributary, 625 km long. The Faleme hydrographic network is made up of two "mother branches", the Koila Kabé and the Balinn Ko, enlarged by numerous tributaries: The Kouloun Ko, the Gombo, the Kounda Ko and the Khassaye. At the confluence of these two "mother branches", the Faleme is formed and stretches 625 km long to the confluence with the Senegal River. Its course is irregular and interspersed with small rapids (Faye 2013).

Data and Methods

Data

The analysis of extreme discharge characteristics in the Faleme basin and the examination of their implications on floods and droughts were assessed on the basis of hydrological data provided by the Organisation for the Development of the Senegal

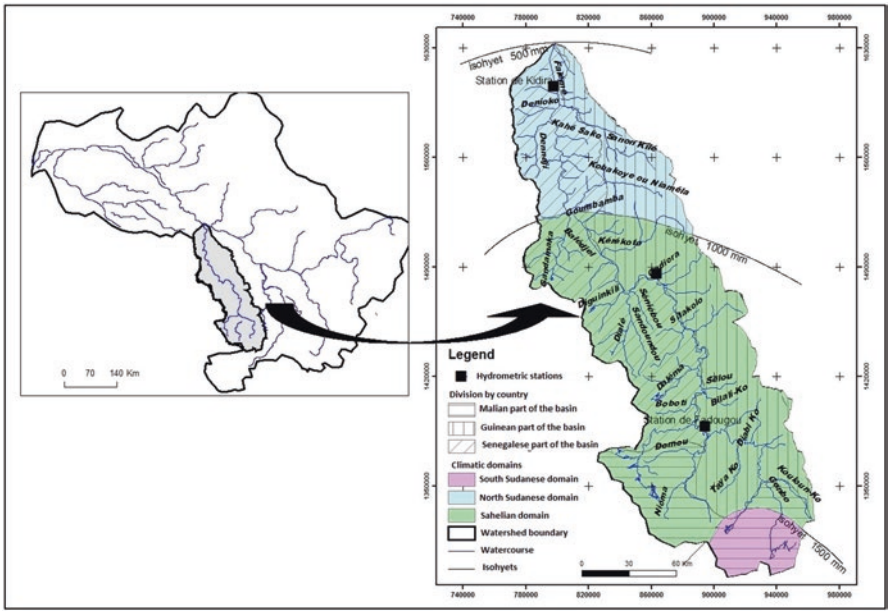

Fig. 9.1 Situation of the Faleme catchment area

River (OMVS). The hydrographic conditions of the years 1954–2019 in the Faleme catchment area were characterised on the basis of daily measurements of the discharge at the Gourbassi and Kidira stations, respectively, in the middle and lower Faleme basin.

Methods

The series of daily discharges we have processed are those for the period 1954–2019. The annual values were determined from May 1 to April 30, which corresponds to the hydrological year. The treatments and analyses (Table 9.1) specifically concern annual modules and extreme daily discharges (maximum and minimum). The interannual variability of the hydrological regime is assessed through variations in the various indices. The drying coefficient makes it possible to assess the intensity of hydrological droughts when the discharge is only sustained by the emptying of the water table (Saha et al. 2020; Elbeltagi et al. 2022a). The strength of flood discharges is translated by the Myer coefficient A (Table 9.1).

In order to detect trends in the distribution of annual data, we applied different homogeneity tests on KhronoStat 1.01 and XLStat as Hubert's rank tests. The specificity of Hubert's segmentation lies in its ability to detect several changes in the mean, unlike other procedures specialised in detecting a single break (Hubert et al. 1998; Lubès-Niel et al. 1998). The information on the droughts and floods of the Senegal River Valley comes not only from the OMVS archives and documentation but also from writings on the same theme. Major studies on floods and droughts in the Senegal River Valley have also been used. These data are analysed in relation to the hydrological extremes of the basin to highlight useful relationships for guiding early warning policies and disaster management in general.

Results

Extreme Discharges in the Faleme Basin Between Humidity and Drought

The Senegal River, some 1700 km long, drains a basin of 300,000 km^2, straddling four countries – Guinea, Mali, Senegal and Mauritania from upstream to downstream, and is made up of several tributaries, the main ones being the Bafing, Bakoye and Faleme, which have their sources in Guinea and form the upper basin (OMVS 2008). The Faleme, which is the subject of this study, produces 25% of the discharge of the Senegal River at the Bakel station (the rest coming from the Bafing (which is the main tributary) at 50%, the Bakoye with 20% and the other tributaries of the river at 5%) (OMVS 2012). The Faleme has severely suffered from the long

Table 9.1 Indices of assessment of hydrological variability

Index	Formula	Reference
Coefficient *A* of P. Myer	$A = \text{Dmax}\left(m^3/s\right)/\sqrt{S\left(\text{km}^2\right)}$	Loup (1965)
Irregularity index *R*	*R* = Dmax annuel/*D* min annuel	Nguimalet (2017)
Taring coefficient (α)	$\text{Qt} = Q_0\, e^{-\alpha t}$	Lang and Gille (2006)
Reduced centred variable	$\text{RCV} = x_i - x/\sigma$	https://www.softconcept.com/surveymag/definitionvariablecentreereduite.html
Coefficient of variation	$\text{CV} = \sigma \times 100/x$	https://www.insee.fr/fr/metadonnees/definition/c11366

S surface area of the catchment area, *Qt* discharge at time *t*, *Q0* initial discharge of the dry phase, *t* time in days, *xi* data of year, *x* average of the data series, σ standard deviation

drought that has plagued tropical Africa since 1970 (Faye 2013). If, towards the middle of the twentieth century, rainfall in the basin was abundant, analysis of the rainfall series shows breaks between 1964 and 1971. These breaks are manifested by droughts causing rainfall deficits of the order of 13.9–30.5%, which is very high and has considerable effects on water resources (Faye 2013). This trend also affects discharges and hydrological regimes that have undergone profound changes with significant discharge deficits. Analysis of the hydrological series shows that the discharge (as for rainfall) has also undergone breaks noted as early as 1970. The three hydrometric stations of the basin record a decrease (in addition to the irregularity) of the discharges of the order of 50.8% at the hydrological station of Fadougou in the upper basin, 56.4% at Gourbassi and 59.3% at Kidira, in the middle and lower course of the basin (Faye 2013). This drop also affects the extreme daily discharges at Gourbassi and Kidira in the middle and lower reaches of the basin.

Minimum Daily Discharges

The low water levels, although occurring during the low water period, are different from them. Low water is an extreme phenomenon of the discharge that occurs during the low water period, in the non-rainy season when, in tropical areas, the parameters that contribute to the discharge deficit, such as evaporation and temperatures, are high. Sow (2007) defines low discharge as the period of time over several days or months when there is low discharge. These discharges decrease to the absolute daily minimum discharge for the year (Dmin). The study of low discharges is not an easy task because of the difficulties in measuring discharges, especially for seasonally flowing rivers, but they are painful in their severity.

At the Gourbassi station in the middle Faleme basin, the mean Dmin is only 0.045 m^3/s over the period 1954–2019 (hydrological years), but with a high interannual variability (coefficient of variation of 3.2) (Fig. 9.2). The break occurs in 1968–69, the year from which the Dmin cancels out until the end of the series. In total, 55 years (85% of the series) recorded a zero Dmin. As regards the Kidira station in the lower Faleme basin, which controls the whole basin, the mean Dmin of the series (1954–2019) is slightly higher than Gourbassi with a value of 0.2 m^3/s for a coefficient of variation of 2.96. The number of years at zero Dmin remains less important and counts a total of 43 years (i.e. 66.2%). This weakness of the Dmin and its generally nil character testify to the seriousness of the drought in the basin whose socio-economic and environmental consequences are numerous and need to be evaluated. With an average of 0.045 m^3/s at Gourbassi and 0.2 m^3/s at Kidira, the Dmin is highly variable. The difference between the most sustained DMIN (1 m^3/s at Gourbassi and 4.2 m^3/s at Kidira) and the lowest that cancels out is 1 m^3/s at Gourbassi and 4.2 m^3/s at Kidira. Over the 65 years, only 10 and 24 years have not recorded zero discharges at Gourbassi and Kidira, respectively. The highest Dmin is noted at Gourbassi in 1966–67 with 1 m^3/s and in 1974–75 at Kidira with 4.2 m^3/s, as opposed to the year of the highest average discharge 1954–55, when the Dmin

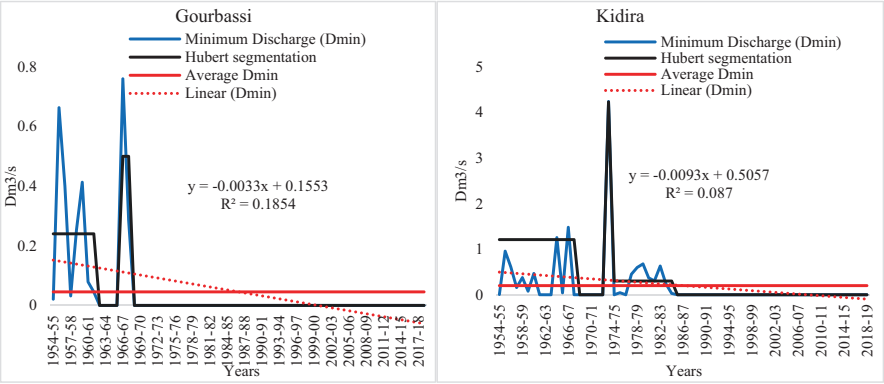

Fig. 9.2 Variability and segmentation of the Dmin of the Faleme basin at Gourbassi and Kidira from 1954 to 2019

was 0.02 m^3/s at Gourbassi and 0.01 m^3/s at Kidira. As for the year 1983–84 with the lowest average discharge, the Dmin cancels itself out.

Maximum Daily Discharges

Floods and high waters differ in frequency, duration and discharge values (Frécaut 1982). Flooding, therefore, occurs when the conditions favourable to runoff are met: saturated soil and atmosphere, low evaporation and temperatures and high precipitation (Faye 2013). It is characterised by great variability (Fig. 9.3). The Dmax (maximum daily discharge of the year) and the flood characteristic discharge (FCD) are used to study the flood. In the Faleme basin, the interannual evolution of the flood is irregular. At the Gourbassi station, annual Dmax values ranged from 148 m^3/s in 1983–84 to 1912 m^3/s in 1964–65 (Fig. 9.3). The average over the period 1954–2019 is 935 m^3/s, with a standard deviation of 429 m^3/s, a coefficient of variation of 46% and a slight general tendency to decrease over time, despite a slight increase in recent years. Hubert's segmentation method highlights a first break in 1966–69 and a second break in 2007–08, dividing the series into three phases. The average of the values increases from 1391 m^3/s over the period 1954–66, to 706 m^3/s over the period 1967–07 (representing a 49% decrease compared to the first phase), to 1240 m^3/s over the period 2008–19 (representing a 75.6% decrease compared with the first phase but a 46% increase compared with the second phase). The largest deficits are thus recorded over the 1970s, 1980s and 1990s, the "heart of the drought".

At the Kidira station, Dmax values are higher than at Gourbassi over the period 1954–2019 and vary from 152.5 m^3/s in 1983–84 to 3108 m^3/s in 1961–62 (Fig. 9.3) for an average of 1229 m^3/s, a standard deviation of 707 m^3/s, a coefficient of variation of 58% and a slight general tendency to decrease over time, despite a slight increase in recent years. As at Gourbassi, Hubert's segmentation method highlights

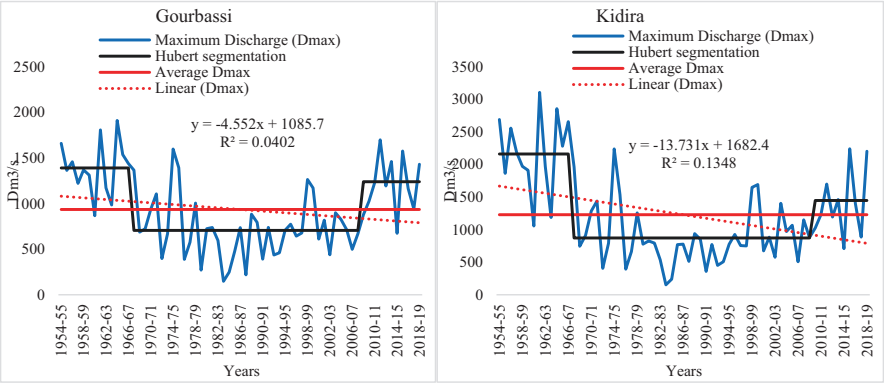

Fig. 9.3 Variability and segmentation of the Dmax of the Faleme basin at Gourbassi and Kidira from 1954 to 2019

two breaks in the series (1966–69 and 2007–08), dividing it into three phases. The first phase, from the beginning of the series (1954–55) to 1966–69, remains the wettest with an average value of 2162 m^3/s. As for the second phase, the longest and driest, it runs from 1967–68 to 2007–08 with an average value of 872 m^3/s. This phase shows a 62.4% decrease compared with the first phase. Finally, the third and last phase, which runs from 2008–09 to 2018–19, sees an increase in Dmax values and remains more or less wet, with an average value of 1447 m^3/s. This period, although registering a 33.1% decrease compared with the first phase, is experiencing a 66% increase compared with the second phase. As in Gourbassi, in Kidira, the greatest deficits are thus recorded over the 1970s, 80s and 90s, the "heart of the drought". Analysis of the Dmax indicates that the deficits affected Faleme in Gourbassi more severely than Faleme in Kidira. The downstream situation of the Kidira station, which benefits from the discharge of the entire surface of the basin, can be cited in this respect.

Dynamics of the Hydrological Extremes of the Faleme Basin Through Some Indices

Power of Peak Discharges

To characterise the flood power calculated by Myer's coefficient A, the classification of Pardé (1968) was used. According to this classification, whenever the coefficient is less than 60, it is qualified as poor. According to this classification, whenever the coefficient is less than 60, it is classified as poor. However, this criterion, in relation to the discharge of large African rivers in tropical regimes, gives values below 60, and their flood powers are classified as poor. This is why, in the Faleme basin, this classification must be evaluated with caution, especially since for

the calculation, daily maximum discharges are used instead of instantaneous maximum discharges.

At the Gourbassi station, the year 1964–65 saw the largest flood over the study period with a Myer A coefficient of 14.6 (Fig. 9.4). The years 1961–62, 2011–12, 1974–75 and 2015–16 followed, with 13.8, 12.9, 12.2 and 12.1, respectively. The lowest flood was recorded in 1983–84 with a coefficient of 1.13. For an overall average of 7.2, the coefficient A is 10.6 over the period 1954–66, 5.4 over the period 1967–07 and 9.4 over the period 2008–19. Of course, we find the same indications as those provided by the Dmax: break in 1966–67, low values over the period 1968–07, slight increase over the current period marked by the alternation of low values. At the Kidira station, the year 1961–62 saw the largest flood over the study period with a Myer A coefficient of 18.3 (Fig. 9.4). The years 1964–65, 1954–55, 1966–67 and 1974–75 followed, with 16.8, 15.8, 15.6 and 13.2, respectively. The lowest flood was recorded in 1983–84 with a coefficient of 0.90. For an overall average of 7.23, the coefficient A is 12.8 for the period 1954–66, 5.2 for the period 1967–07 and 8.4 for the period 2008–19. We find the same indications as those provided at the Gourbassi station: Dmax. According to Olivry et al. (1994a), this "poor flood performance" is a general characteristic of rivers on the African continent, both in dry Africa where rainfall remains modest and the catchment area's ability to discharge is weak, and in west Africa where more abundant rainfall only produces a flood wave that is widely spread over time due to the dense vegetation of the continent. The flood powers are very low according to Pardé's classification (which is unsuitable for characterizing flood power in the tropics). The low flood powers have become more pronounced since the 1970s with the climatic deterioration and the decrease in Dmax values.

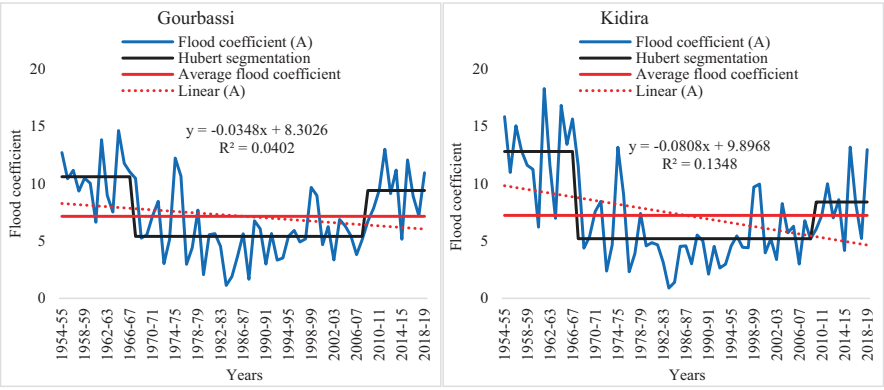

Fig. 9.4 Evolution and segmentation of the flood coefficient of the Faleme basin at Gourbassi and Kidira from 1954 to 2019

Irregularity Index

Since the calculation of the irregularity index requires values of Dmin which are not zero, for each year of the series (1954–19) whose Dmin is equal to 0, the value of the average Dmin of the series was used instead at the Gourbassi and Kidira stations, the interannual mean of the irregularity index R is 18,960. It shows a very slight upward trend (Fig. 9.5). The observation remains the same at the Kidira station, but with a much lower mean value of 6280. While the difference between Dmax and Dmin is greater over the 1950s and 1960s, it fell over the 1970s, 1960s and 1990s before rising again in the recent period. Some years stand out for their very high R values at Gourbassi (42,488 in 1964–65, 40,177 in 1961–62 and 38,187 in 1957–58) and at Kidira (4,972,800 in 1961–62, 3,139,200 in 1967–68 and 458,212 in 1954–55). These were years that saw very high floods and very severe low water levels.

With all the precautions imposed by very low coefficients of determination, there is a certain tendency for the gaps between Dmin and Dmax to widen at Gourbassi, while the opposite is observed at Kidira (beyond the 3 years reported at astronomical R values).

Taring Coefficient

Depletion represents "the phase of discharge in a river or spring corresponding to the steady decrease in discharge in the absence of meteoric inputs and human intervention" (Dacharry 1997). It begins on the day when the decrease in discharge is continuous and corresponds to the phase of emptying of the water table, thus causing a decrease in the underground reserves supporting the discharge of the watercourse during the non-rainy period. The drying up follows the temporal distribution of rainfall, which conditions the period of low water and low water levels (Faye

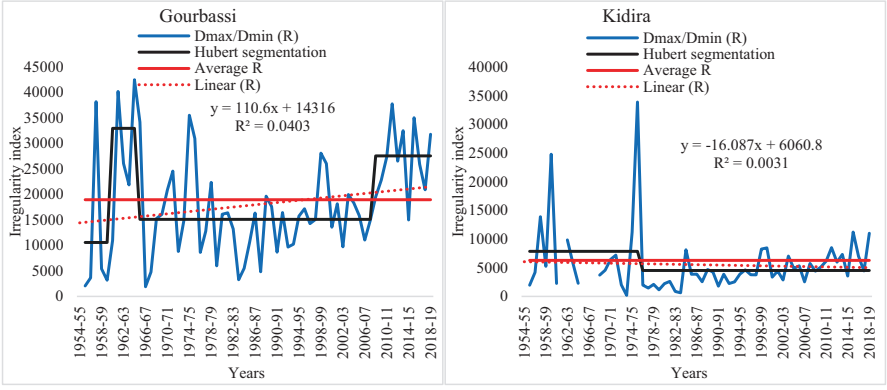

Fig. 9.5 Evolution and segmentation of the irregularity index of the Faleme basin at Gourbassi and Kidira from 1954 to 2019

2013). At the Gourbassi and Kidira stations, the beginning of the drying-up period is spread over nine decades, from September to December. The month of October is the normal month of onset of drying up (Q0) and accounts for nearly 3/4 of the frequencies, and the second dekad is the normal dekad. The end of the drydown Qt is more variable, with 12 dekad ranging from September to April, which is the normal month of the end. For this normal month, April, the third dekad is the normal end dekad. The high frequencies of this dekad reflect the perennial nature of the discharge at Kidira over certain years. The average discharge at the beginning of tapping (Q0) is 308 m^3/s at Gourbassi and 355 m^3/s at Kidira, and the average discharge at the end of tapping (Qt) is 0.2 m^3/s at Gourbassi and 4.2 m^3/s at Kidira. The average duration of tapping (t) at Gourbassi is 170 days, and the average tapping coefficient (k) is 0.062. At Kidira, the average dry period (t) is 156 days, and the average drying coefficient (k) is 0.054. At Gourbassi, if the mean inter-annual drying coefficient is 0.062/day, the maximum annual value reached 0.098/day (in 1984–85) and the minimum value 0.012/day (in 1954–55). For Kidira, the interannual average drying coefficient is 0.054/day with an annual maximum value of 0.11/day (in 1985–86) and a minimum value of 0.02/day (in 1967–68). The coefficient of variation, 29% at Gourbassi and 33% at Kidira, reflects a spread from 1954 to 2019 (Fig. 9.6).

Analysis of the extreme discharge patterns of floods and low discharges confirms the variability of the discharge. The drying up in the basin is faster and shows the severity of low water levels at Gourbassi and Kidira in the pure tropical domain.

Hydroclimatic Risks in the Faleme Basin

Water-related risks in the Faleme basin can be partly considered by taking into account hydrological extremes.

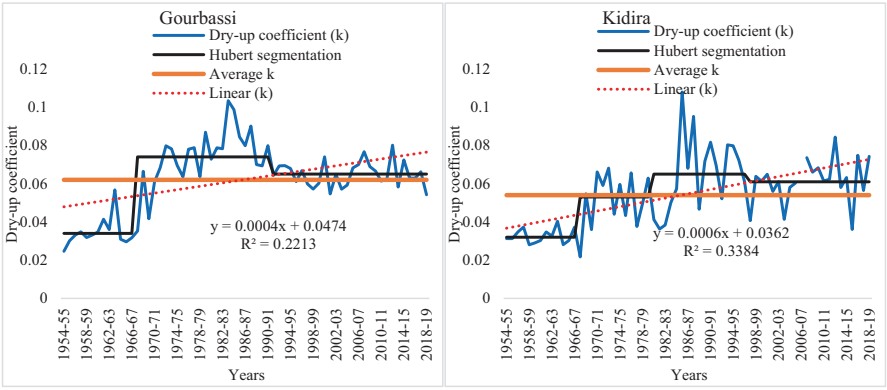

Fig. 9.6 Evolution and segmentation of the irregularity index of the flow of the Falémé basin at the Gourbassi and Kidira stations from 1954 to 2019

Different Aspects of the Hydrological Drought in the Faleme Basin

The analysis of the discharge over the period 1954–19 revealed significant fluctuations with multiple consequences on the environment, hence the interest of studying them. It shows a hydroclimatic rupture at the beginning of the 1970s marked by the beginning of a drought phase affecting all the rivers of the African Sahel. At Gourbassi, if the average interannual discharge is 105 m^3/s, the maximum annual value reached 214 m^3/s (in 1954–55) and the minimum value 20 m^3/s (in 1983–84). For Kidira, the mean interannual flow discharged is 159 m^3/s for a maximum annual value of 558 m^3/s (in 1954–55) and a minimum value of 32.6 m^3/s (in 1983–84). As with rainfall, the evolution of hydrological parameters reflected in the basin's runoff from 1954 to 2019 first showed a decrease during the 1970s before recognising an increase from 2009 onwards (Fig. 9.7). This new upward trend in the Faleme basin, although not significant, corresponds to the improvement in rainfall conditions that began in the 1990s and confirms numerous studies (Ali et al. 2008; Niang 2008).

The probability of occurrence of different categories of wet and dry periods at Gourbassi and Kidira is shown in Fig. 9.7. In Gourbassi, 53.8% of the years are dry with varying intensities, indicating the slight dominance of drought. The mild drought with the highest percentage (35.4%) has a probability of 1 in 2.8 years. It is followed by light humidity with a percentage of 29.9% and a probability of occurrence of 1 in 3.4 years. There is no such thing as an extremely dry year. Extremely wet (4.6%) and severely wet (6.1%) years showed very low percentages. The same is true for severely dry years with a percentage of 1.5% and a probability of occurrence of 1 in 65 years.

At Kidira, 61.5% of the years are dry with variable intensities, a little more than what is noted at Gourbassi. The mild drought that has the highest percentage (53.8%) has a probability of 1 in 1.8 years. It is followed by light humidity with a percentage of 24.6% and a probability of occurrence of 1 in 4.1 years. There is no

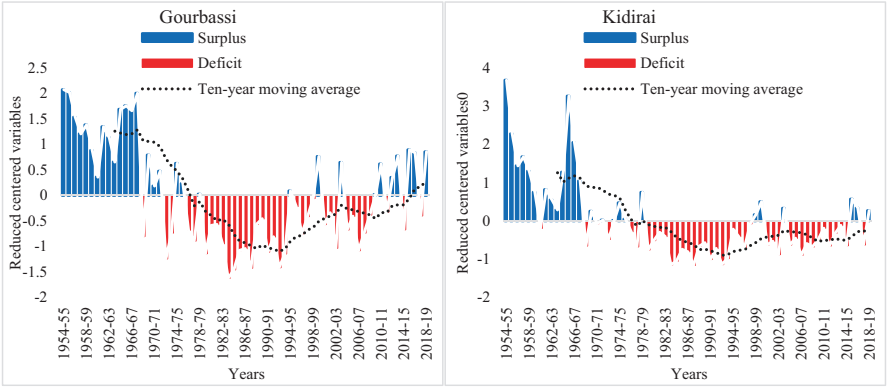

Fig. 9.7 Evolution of the reduced centred variables (RCV) of the annual modules of the Faleme basin at Gourbassi and Kidira from 1954 to 2019

such thing as an extremely and severely dry year. Extremely wet (6.2%) and severely wet (1.5%) years showed very low percentages. The same is true for moderately dry years with a percentage of 7.7% and a probability of occurrence of 1 in 13 years and moderately wet years with a percentage of 6.2% and a probability of occurrence of 1 in 16.2 years.

As regards low water levels, the situation is slightly different between the Gourbassi and Kidira stations. Indeed, the first half of the series is clearly in surplus (with values that can reach 1573% in 1966–67 at Gourbassi and 2017 in 1973–74 at Kidira) (Fig. 9.8). At Gourbassi, the year 1968–69 marks the beginning of the deficits, which reach their maximum (100%) there. For the Kidira station, beyond the years of deficits noted between 1954 and 1985, the deficits globally concern the period 1985–2019 and are at their maximum (100%).

Unlike the Dmin, which showed some deficits from the beginning of the observation series at Gourbassi and Kidira, the Dmax remained in surplus until 1967–68 (Fig. 9.9). The Dmax thus appears to be more in line with the general discharge trend in this basin. While the first phase of the series (1954–67) remains in surplus, Dmax deficits begin in 1967–68 and continue thereafter (with the exception of a few surplus years noted over the 1970s at both stations) until 2008–09, after which a return to surplus years is noted (despite the presence of a few deficit years at Kidira). All these analyses make it possible to measure the extent of the hydrological drought that affected the Faleme basin. For the most part, average, minimum and maximum discharges evolve in the same way from 1 year to the next (Saha et al. 2020), although some exceptions can be noted at the beginning and end of the drought period. Indeed, over the period 2008–19, for example, the Faleme River had a deficit Dmin, while the mean annual discharge and Dmax are in surplus and have caused flooding in several localities of the Senegal River valley. In general, many Dmax have been in surplus in years when the mean annual discharge and the Dmin were in deficit (period 2008–19). Figure 9.10 presents a synthetic drought index resulting

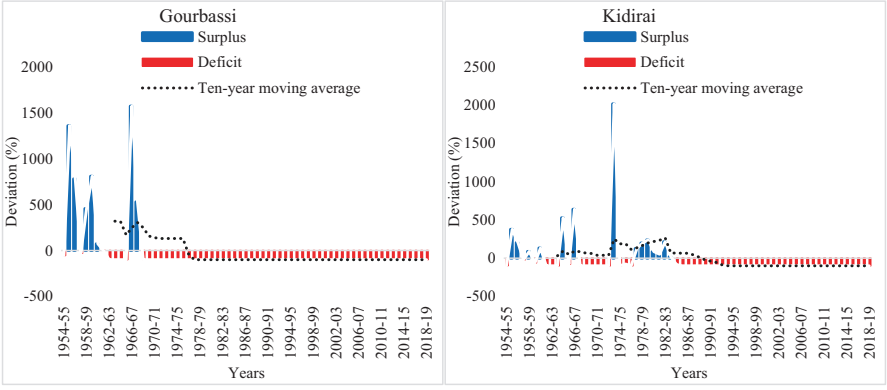

Fig. 9.8 Evolution of the Deviations (in %) of the annual Dmin of the Faleme basin at Gourbassi and Kidira compared to the interannual mean values from 1954 to 2019

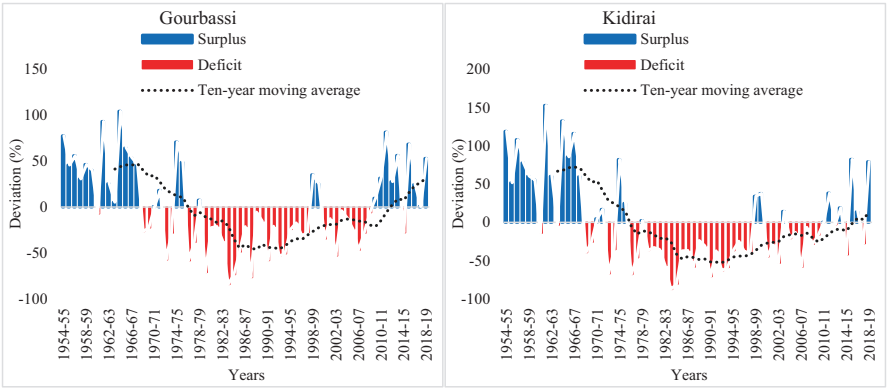

Fig. 9.9 Evolution of the deviations (in %) of the annual Dmax of the Faleme basin at Gourbassi and Kidira compared to the interannual mean values from 1954 to 2019

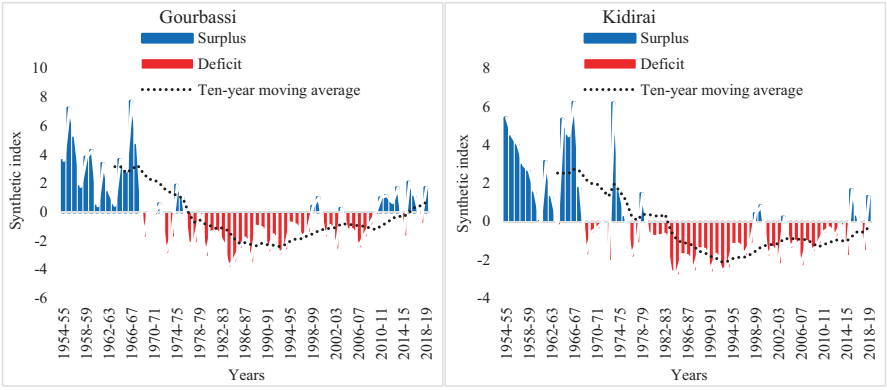

Fig. 9.10 Evolution of the values of the synthetic hydrological drought index of the Faleme basin at Gourbassi and Kidira from 1954 to 2019

from the addition of the reduced centred variables of the modules, Dmin and Dmax. Drought years are characterised by a negative result.

Based on available data, the persistent drought started in 1967–68 on Faleme and subsided in 2007–08. The socio-economic context of the Kédougou region of the Faleme basin makes it highly vulnerable to natural hazards in general and to drought in particular. Indeed, food insecurity rates are as high as in the three departments of the Kédougou region (30.4% of households in Kédougou, 30.9% in Salémata and 38.5% in Saraya are food insecure) (ANSD 2015a). Kédougou is, today, a region undergoing demographic and economic change and where 71% of the population lives below the poverty line (ESPS 2011). Given the inadequacy of water infrastructure for water supply, the Faleme and Gambia Rivers, the two major rivers, play an important role in local development (agriculture, human and livestock water supply) (ANSD 2019). The region's population growth is one of the highest in Senegal over

the last decade. Over the 2014–16 period, the annual population growth rate in Kédougou is 3.3% (ANSD 2019). However, although the labour force is abundant, many young people are fleeing to the gold panning sites. The other obstacles to agriculture are related to the lack of fertilisers, and their late implementation, the unsuitability of agricultural equipment often made available to producers, soil degradation that affects agricultural production and environmental degradation that threatens the health of the population. It is under these conditions that the hydrological deficits of the 1970s and 1980s caused real disasters in the eastern Senegal region, as evidenced by the worsening of food shortages (Faye 2013). With good rainfall and hydrography, Kédougou is one of the regions of Senegal where rainfed farming is most widespread. Indeed, according to the results of the 2013 RGPHAE, 69% of households in Kédougou practice agriculture in the broad sense, and nearly 81% of these farming households are engaged in rainfed farming. Agriculture is therefore the main economic activity of the people of Kédougou on which their livelihood is essentially based (ANSD 2015b). Thus, 69% of households were engaged in agriculture in 2013 (ANSD 2014). Similarly, livestock and fishing are also common activities practiced by the population, with a good part of the population engaged in livestock farming (49.6% in 2013). However, despite the region's multiple potentialities in agriculture and the efforts made by the State and development partners through programmes and projects, this agriculture sub-sector still faces many difficulties that prevent it from fully playing its role as the main lever in the process of poverty reduction and food security (ANSD 2015b). Indeed, according to the Kédougou Regional Development Agency, from 2005–06 to 2011–12, there is a downward trend in cereal production, and this situation is reflected in a recurrent food deficit observed during the same period. Several challenges need to be addressed to improve agricultural production, including finding solutions to livestock raiding, mechanizing local agriculture with adapted equipment, facilitating access to inputs in a timely manner, setting up model farms, helping to develop the Faleme and Gambia Rivers, strengthening livestock rangelands, supporting the valorisation of local agricultural products, strengthening the development of off-season activities, fighting bush fires and other forms of soil and environmental degradation and reducing the misuse of chemical fertilisers.

Hydrological Parameters and Flooding in the Valley

With regard to floods, the surpluses on the modules (see Fig. 9.8) and on peak discharges (see Fig. 9.9) provide elements for analysis. However, it is also useful to look at discharges equalled or exceeded for 10 days per year or flood characteristic discharges (FCD). The average FCD is 593 m^3/s on the Faleme at Gourbassi and 818 m^3/s on the Faleme at Kidira. Like the other hydrological parameters studied, the FCDs are highly variable on an interannual scale (Fig. 9.11). The most numerous and highest high values are at the beginning of the observation series. The maximum FCD values are noted in 1954–55 with 1527 m^3/s at Gourbassi and 2330 m^3/s at Kidira, and the minimum values are noted in 2006–07 at Gourbassi with 96.1 m^3/s

and in 1984–85 at Kidira with 77 m^3/s. Years of catastrophic flooding do not always correspond to average discharges above the module, nor even to daily peak discharges or FCDs above the interannual averages. Information on a few examples of catastrophic floods in the Senegal River valley in relation to hydrological variables in the upper basin (including the Faleme) shows that they have not always occurred in wet years compared with average and peak discharges in the upper basin. Most of the catastrophic floods have occurred during years of hydrological drought. The location of catastrophic floods depends both on the distribution of rainfall over the territory and on the local measures taken to avoid damage (Saha et al. 2020). An example is the floods of the 1994–95 season, which correspond to an average flood. Indeed, in 1994, 120,000 people were left homeless in the Saint-Louis region, causing the displacement of populations suffering from health problems and the flooding of farmland (Kane 2002). In that year, the maximum discharge observed during the flood at Kidira on the Faleme River was 675 m^3/s on 25 September 1994. However, higher discharges have already been observed without triggering today's catastrophic floods, such as the highest daily discharge observed on the Faleme and the Senegal River in general. The same is also true for the floods of 2003 (which caused a breach to save the city) and 2013 in the river valley and delta.

The current flooding in the valley can be explained by a combination of several facts. Firstly, it is getting wetter and wetter during the winter months. Secondly, there is also a significant inflow of water from tributaries not yet equipped with water control structures, namely the Bakoye and Faleme, which play a major role in triggering the floods. The agitation of the sea swell in the winter period on the coast, which prevents the discharge of river water and contributes to a rise in the water level in all branches of the river and in the water table, is also to be noted (Diack 2000). Thirdly, the OMVS often carries out large releases. Fourthly, the modification of the discharge regime can cause water saturation in the soil as a result of the rising roof of the water table, which is now practically flush. Finally, anarchic land use leads to the stagnation of rainwater in the absence of drainage, or to garbage

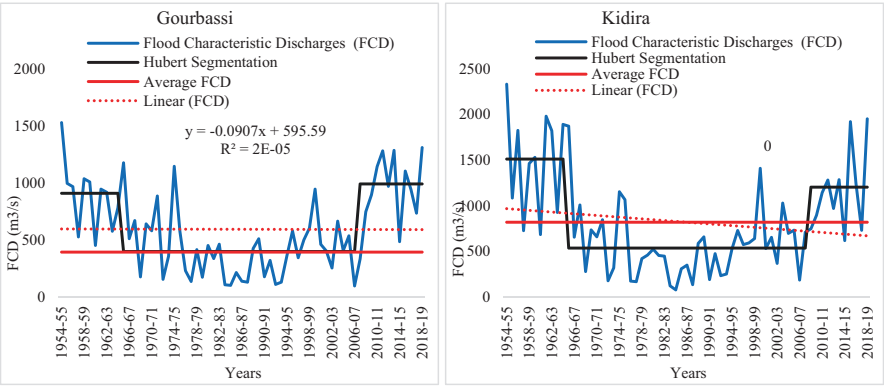

Fig. 9.11 Occurrences of surplus FCDs from the Faleme Basin at Gourbassi and Kidira from 1954 to 2019

dumps, which contribute to very slow runoff towards the river branches, etc. The damming of the delta in 1964 also modified the natural feeding conditions of the peripheral depressions, which can no longer play their buffer role in the accumulation of overflow (Kane 2002). Thus, the implementation of complex hydraulic developments in the river delta combined with the construction of a large dam was not sufficient to control flooding.

Discussion

The dynamics of extreme discharges in the Faleme basin are part of the hydrological context of the entire Sahelian zone and even beyond. In this basin, analysing data from 1954 to 2008, highlights a downward trend in Dmin and Dmax. It is accompanied by a break in hydrological conditions at the very beginning of the 1970s, which marks the transition from a wet period to a deficit period. The same trend has been observed over Senegal and all the West African basins by several authors (Faye 2013; Saha et al. 2020). It should be noted that, in general, on the large African rivers, the behaviour of Dmax is identical to the trends observed for mean annual discharges (Olivry et al. 1998). Dmin, on the other hand, is much less related to them. It should also be noted that the rivers of West Africa have suffered more severely from the deterioration of discharges compared with Central Africa (Olivry et al. 1998; Saha et al. 2020). In fact, on the Faleme, the deficits are higher than 50%, which is in line with the results of Cissé et al. (2014) on Senegal, which indicate a 57% deficit between 1971 and 1993, with an increase in humidity from 1994 onwards, and much higher than those obtained by Saha et al. (2020) on Central African rivers (25.5% on the Logone and 36% on the Chari). Hydrological indices are tools for assessing the dynamics of African rivers. Olivry et al. (1994a, b) speak of low flood power on tropical African rivers (Myer A coefficients from 6 to 28 for Niger and from 2 to 20 for Senegal). The vastness of the basins of these rivers can be cited as an explanatory factor. The year 1983–84, which had the lowest flood power on the Faleme (average discharge of 20 m^3/s at Gourbassi and 32.5 m^3/s at Kidira), is identified as the most deficient year of the dry period on several African rivers (Olivry et al. 1998). Faleme's dry periods are much slower (170 days at Gourbassi and 156 days at Kidira) than those of West African rivers where only 2 months separate Dmax from Dmin (Olivry et al. 1994a, b). In this respect, the functioning of the Faleme is increasingly different from that of rivers in equatorial Africa, such as the Oubangui (tributary of the Congo), for which Nguimalet (2017) finds practically a different average value of the drying coefficient (0.020). However, the increase in this coefficient from the early 1970s on the Faleme is noted by Nguimalet (2017) on the Oubangui and by Saha et al. (2020) on the Logone and Chari. The differences between the annual Dmin and Dmax (irregularity index) are

very pronounced in Faleme (on average 18,961 in Gourbassi and 137,840 in Kidira). This is due to the low water discharges, which are very low. Indeed, on many of their tributaries, discharges dry up a few months after the end of rainfall (Saha et al. 2020). This drying coefficient is on average 0.062 at Gourbassi and 0.054 at Kidira, which reflects a more or less significant support of the water table in the river during the low-water season.

In the Senegal River basin, Sow (2007) and Faye (2013), for example, place the onset of drought between the late 1960s and early 1970s, which corresponds to the beginning of the decline in rainfall. The hydrological parameters were not affected until a few years later. The same applies to the end of the drought, the date of which varies according to the data taken into account. The weak relationship between discharges and the occurrence of damage in the area is an exception in the case of catastrophic floods in the cities bordering the major African rivers (Saha et al. 2020). But the proximity of a river and the violence of its discharges are, of course, only two of the factors that contribute to the construction of flood risk. The negative consequences of recent hydraulic developments provide a good illustration of this.

Conclusion

Among the strong trends highlighted by this study, it should first be noted that peak daily discharges (and thus also Myer's coefficient A) decreased in the early 1970s. This is in line with observations made by other authors on rivers in tropical Africa. For the Dmin, the evolutions appear more contrasted. In the Faleme basin, after a decrease in discharges at the very beginning of the 1970s following the decades of hydrological abundance (1950 and 1960), the values started to increase again from the 2000s onwards, in phase with the increase in rainfall. In the basin, the variability of the discharge is explained by the importance of the annual values of the irregularity index R (Dmax/Dmin) (on average 18,961 at Gourbassi and 137,840 at Kidira). This can be explained by the fact that the minimum discharge can fall very low in some years or even cancel out, which explains the very high R values. The average tapping coefficient is around 0.062 at Gourbassi and 0.054 at Kidira. This coefficient had its highest values during the period of drought that hit all tropical and even equatorial Africa from the 1970s onwards. From the late 1970s to the end of the 1990s, all the variables studied (Dmin, Dmax, irregularity index and drying up coefficient) were strongly affected by the drought that hit Africa. However, conditions may have been heterogeneous in the catchment basins, so that catastrophic floods occurred on tributary rivers during this period. The return to high maximum discharges on the Faleme and other Senegal River rivers and the dyking of long sections in the valley and delta0 resulted in catastrophic floods as had not been experienced before 1971, at a time when the valley was admittedly less anthropised.

References

Abashiya M (2006) Influences of Manmade structures on floods in the Northern parts of Kaduna metropolis, Nigeria. Unpublished M.Sc. thesis, Department of Geography A.B.U, Zaria

Abashiya M, Abaje M, Iguisi IB, Bello EO, Sawa AL, Amos BA, Musa BB (2017) Randall characteristics and occurrence of floods in Gombe metropolis, Nigeria abashiya. Ethiop J Environ Stud Manag 10(1):44–54

Ahmed E, Nagy A, Mohammed S, Pande CB et al (2022) Combination of limited meteorological data for predicting reference crop evapotranspiration using artificial neural network method. Agronomy 12(2):516. https://doi.org/10.3390/agronomy12020516

Ali A, Lebel T, Amami A (2008) Signification et usage de l'indice pluviométrique au Sahel. Sécheresse 19(4):227–235

ANSD (2014) Recensement Général de la Population et de l'Habitat, de l'Agriculture et de l'Elevage (RGPHAE 2013). Rapport définitif, République du Sénégal Ministère de l'Economie, des Finances et du Plan. 19 p

ANSD (2015a) Situation Economique et Sociale régionale – 2012 Service Régionale de la Statistique et de la Démographie de Kédougou. 10 p

ANSD (2015b) Situation Economique et Sociale régionale – 2013 Service Régionale de la Statistique et de la Démographie de Kédougou. 10 p

ANSD (2019) Situation économique et sociale de la région de Kédougou, Ed. 2015–2016, Service Régionale de la Statistique et de la Démographie de Kédougou. 153 p

Bootsma A, Boisvert JB, De Jong R, Baier W (1996) La sécheresse et l'agriculture canadienne. Sécheresse 7:277–285

Cissé MT, Sambou S, Dieme Y, Diatta C, Bop M (2014) Analyse des écoulements dans le bassin du fleuve Sénégal de 1960 à 2008. Rev Sci Eau 27(2):167–187

Dacharry M (1997) Dictionnaire Français d'Hydrologie. http://www.cig.ensmp.fr/~hubert/glu/FRDIC/DICTARIS.HTM

Diack A (2000) Comment sauver Saint-Louis du péril hydraulique. Dakar, Sénégal., Walffadjri, 16 mai 2000, 2451:10

Easterling DR, Evans JL, Groisman PY, Karl TR, KunkeL KE, Ambenje P (2000) Observed variability and trends in extreme climate events: a brief review. Bull Am Meteorol Soc 81:417–425

Elbeltagi A, Kumar N, Chandel A et al (2022a) Modelling the reference crop evapotranspiration in the Beas-Sutlej basin (India): an artificial neural network approach based on different combinations of meteorological data. Environ Monit Assess 194:141. https://doi.org/10.1007/s10661-022-09812-0

Elbeltagi A, Kumar M, Kushwaha NL et al (2022b) Drought indicator analysis and forecasting using data driven models: case study in Jaisalmer, India. Stoch Environ Res Risk Assess. https://doi.org/10.1007/s00477-022-02277-0

Esfahanian E, Nejadhashemi AP, Abouali M, Adhikari U, Zhang Z, Daneshvar F, Herman MR (2017) Development and evaluation of a comprehensive drought index. J Environ Manag 185:31–43

ESPS (2011) Enquête de suivi de la pauvreté au Sénégal (2010–2011), Sénégal, 2011, Agence nationale de la Statistique et de la Démographie (ANSD)

Faye C (2013) Evaluation et gestion intégrée des ressources en eau dans un contexte de variabilité hydroclimatique: cas du bassin versant de la Faleme. Thèse de Doctorat, Université Cheikh Anta Diop de Dakar. 309 p

Faye C (2017a) Une évaluation comparative des séquences du stress hydrique et de la sécheresse par indicateurs et par échelles de temps dans le bassin du Bafing en amont de Manantali. Espace Géographique et Société Marocaine (Numéro 19), pp 171 à 188

Faye C (2017b) Variabilité et tendances observées sur les débits moyens mensuels, saisonniers et annuels dans le bassin de la Faleme (Sénégal). Hydrol Sci J J Sci Hydrol 62(2):259 à 269

Faye C (2018) Analysis of drought trends in Senegalese coastal zone on different climatic domains (1951–2010). Anallelle Uniiversiităţiii diin Oradea, Seriia Geografiie XXVIII, no. 2//2018, pp 231–244

Faye C, Diop ES, Mbaye I (2015a) Impacts des changements de climat et des aménagements sur les ressources en eau du fleuve Sénégal: caractérisation et évolution des régimes hydrologiques de sous-bassins versants naturels et aménagés. Belgeo (Numéro 4), pp 1 à 22

Faye C, Sow AA, Ndong JB (2015b) Étude des sècheresses pluviométriques et hydrologiques en Afrique tropicale: caractérisation et cartographie de la sècheresse par indices dans le haut bassin du fleuve Sénégal. Physio-Géo Géogr Phys Environ 9:17–35

Faye C, Grippa M, Wood S (2019a) Use of the Standardized Precipitation and Evapotranspiration Index (SPEI) from 1950 to 2018 to determine drought trends in the Senegalese territory. Clim Chang 5(20):327–341

Faye C, Sow AA, Diop ESD (2019b) Caractérisation des effets du barrage de Manantali sur le régime hydrologique du fleuve Sénégal. Rev Roum Géogr/Rom J Geogr 63(1):121–133

Field CB, Barros V, Stocker TF, Qin D, Dokken DJ, Ebi KL, Mastrandea MD, Mach KJ, Plattner GK, Allen SK, Tignor M, Midgley PM (2012) Résumé à l'intention des décideurs. In: Gestion des risques de catastrophes et de phénomènes extrêmes pour les besoins de l'adaptation au changement climatique, Édit. Groupe d'experts intergouvernemental sur l'évolution du climat (GIEC), rapport spécial des Groupes de travail I et II. Cambridge University Press, Cambridge (GrandeBretagne) et New York (USA). 20 p

Frécaut R (1982) Eléments d'hydrologie et de dynamique fluviale, Tome 1. Publ. Université Nancy. 147 p

Giret A (2004) Le risque hydrologique. L'information géographique 68(1):1426 p

Guhasapir D, Hoyois P, Wallemacq P, Below R (2016) Annual disaster statistical review 2016: the numbers and trends. Édit. CRED, Université catholique de Louvain, Bruxelles (Belgique). 91 p

Hardy G (1921) La mise en valeur du Sénégal de 1817 à 1854. Larose, Paris. 376 p

Hubert P, Servat E, Paturel JE, Kouame B, Bendjoudi H, Carbonnel JP, Lubès-Niel H (1998) La procédure de segmentation, dix ans après. In: Water resources variability in Africa during the XXth Century, actes de colloque (Abidjan, Côte d'Ivoire), E. Servat, D. Hughes, JM. Fritsch et M. Hulme édit., Édit. IAHS, Publication, 252, pp 267–273

IPCC (GIEC) (2014) Changements climatiques 2014: impacts, vulnérabilité et adaptation. Résumé à l'intention des décideurs. Contribution du Groupe de travail II au cinquième Rapport d'évaluation du Groupe d'experts intergouvernemental sur l'évolution du climat. 40 p

Kane A (2002) Crues et inondations dans la basse vallée du fleuve Sénégal. Gestion intégrée des zones inondables tropicales. IRD Éditions, pp 197–208

Khadri SFR, Pande C (2016) Ground water flow modeling for calibrating steady state using MODFLOW software: a case study of Mahesh River basin, India. Model Earth Syst Environ 2:39. https://doi.org/10.1007/s40808-015-0049-7

Łabędzki L (2004) Drought problems in Poland. Water Environ Rural Areas 4:47–66

Lang C, Gille E (2006) Une méthode d'analyse du tarissement des cours d'eau pour la prévision des débits d'étiage. Norois 201(4):31–43

Li Z, Hao Z, Shi X, Déry SJ, Li J, Chen S, Li Y (2016) An agricultural drought index to incorporate the irrigation process and reservoir operations: a case study in the Tarim River Basin. Glob Planet Chang 143:10–20

Loup J (1965) Pardé Maurice. Sur la puissance des crues en diverses parties du monde. Rev Géogr Alp 53(1):157–159

Lubès-Niel H, Masson JM, Paturel JE, Servat E (1998) Variabilité climatique et statistique: étude par simulation de la puissance et de la robustesse de quelques tests utilisés pour vérifier l'homogénéité de chroniques. Rev Sci Eau 11(3):383–408

Milly PCD, Dunne KA, Vecchia AV (2005) Global pattern of trends in streamflow and water availability in a changing climate. Nature 438:347–350

Moharir K, Pande C, Singh S, Del Rio RA (2020) Evaluation of analytical methods to study aquifer properties with pumping test in Deccan Basalt Region of the Morna River Basin in Akola District of Maharashtra in India. Ground water hydrology Intech Open, the world's leading publisher of Open Access books Built by scientists, for scientists. number 10.5772/intechopen.84632 published 4/3/2020 Muhammad Salik Javaid, ISBN:978-1-83880-622-4

Nguimalet CR (2017) Changements enregistrés sur les extrêmes hydrologiques de l'Oubangui à Bangui (République centrafricaine): analyse des tendances. Rev Sci Eau 30(3):183–196
Niang AJ (2008) Les processus morphodynamiques, indicateurs de l'état de la désertification dans le Sud-Ouest de la Mauritanie. Approche par analyse multisource. Thèse de Doctorat, Université de Liège (Belgique). 286 p
Olivry JC, Bricquet JP, Mahé G (1994a) De l'évolution de la puissance des crues des grands cours d'eau intertropicaux d'Afrique depuis deux décennies; Dossier de la revue de Géographie Alpine, n°12. 9 p
Olivry JC, Bricquet JP, Bamba F, Diarra M (1994b) Le régime hydrologique du Niger supérieur et le déficit des deux dernières décennies. In: Quelques données préliminaires sur l'environnement et la qualité des apports du Niger au Sahel, JC Olivry, M Diallo, JP Bricquet édit., Édit. ORSTONCNRST, p 925
Olivry JC, Bricquet JP, mahé G (1998) Variabilité de la puissance des crues des grands cours d'eau d'Afrique intertropicale et incidence de la baisse des écoulements de base au cours des deux dernières décennies. In: Water resources variability in Africa during the XXth Century, actes de colloque (Abidjan, Côte d'Ivoire), É Servat, D Hughes, JM Fritsch, M Hulme édit., Édit. IAHS, Publication no 252, pp 189–197
OMVS (2008) Plan d'Action Stratégique de Gestion des Problèmes Environnementaux Prioritaires du Bassin du Fleuve Sénégal, Version finale. 133 p
OMVS (2012) SENEGAL-HYCOS Document de projet Une composante du Système Mondial d'Observation du Cycle Hydrologique (WHYCOS). I.00585.001- DI-SFA 12-173. 110 p
Orimoloye IR, Olusola AO, Belle JA et al (2022) Drought disaster monitoring and land use dynamics: identification of drought drivers using regression-based algorithms. Nat Hazards 112:1085. https://doi.org/10.1007/s11069-022-05219-9
Pande CB (2022) Land use/land cover and change detection mapping in Rahuri watershed area (MS), India using the google earth engine and machine learning approach. Geochem Int. https://doi.org/10.1080/10106049.2022.2086622
Pande CB, Moharir K (2017) GIS based quantitative morphometric analysis and its consequences: a case study from Shanur River Basin, Maharashtra India. Appl Water Sci 7:861–871. https://doi.org/10.1007/s13201-015-0298-7
Pande CB, Moharir KN, Singh SK, Varade AM (2019) An integrated approach to delineate the groundwater potential zones in Devdari watershed area of Akola district, Maharashtra, Central India in Environment, Development and Sustainability Springer Journal. https://doi.org/10.1007/s10668-019-00409-1
Pande CB, Moharir KN, Singh SK, Varade AM, Ahmed Elbeltagie SFR, Khadri PC (2021) Estimation of crop and forest biomass resources in a semi-arid region using satellite data and GIS. J Saudi Soc Agric Sci 20(5):302–311
Pande BC, Kadam SA, Jayaraman R, Gorantiwar S, Shinde M (2022a) Prediction of soil chemical properties using multispectral satellite images and wavelet transforms methods. J Saudi Soc Agric Sci 21(1):21–28
Pande CB, Moharir KN, Singh SK et al (2022b) Groundwater flow modeling in the basaltic hard rock area of Maharashtra, India. Appl Water Sci 12:12. https://doi.org/10.1007/s13201-021-01525-y
Pande CB, Al-Ansari N, Kushwaha NL, Srivastava A, Noor R, Kumar M, Moharir KN, Elbeltagi A (2022c) Forecasting of SPI and Meteorological Drought Based on the Artificial Neural Network and M5P Model Tree. Land 11(11):2040. https://doi.org/10.3390/land11112040
Pardé M (1968) Fleuves et rivières. A. Colin, Paris. 245 p
Radinovi'c D, C'uric' M (2012) Some evidence on European monsoon existence. Theor Appl Climatol 110:11–15. https://doi.org/10.1007/s00704-012-0609-y
Roche PA (2003) L'eau, enjeu vital pour l'Afrique, Afrique contemporaine, n°205, printemps 2003. http://www.cairn.info/revue-afrique-contemporaine-2003-1-page-39.htm
Rodier JA (1981) Phénomènes hydrologiques extrêmes: sècheresses et crues exceptionnelles. Communication pour la conférence internationale sur l'hydrologie et les bases scientifiques de la gestion rationnelle des ressources en eau. UNESCO, Paris. 29 p

Saha F, Tchindjang M, Dzana J-G, Nguemadjita D (2020) Risques naturels dans la région de l'Extrême-Nord du Cameroun et dynamique des extrêmes hydrologiques du système Chari-Logone », Physio-Géo [En ligne], Volume 15 | 2020, mis en ligne le 04 janvier 2020, consulté le 14 mars 2020. URL: http://journals.openedition.org/physio-geo/10719; https://doi.org/10.4000/physio-geo.10719

Sawa BA (2002) Trend in temporal variability of occurrence of wet and dry spells north of latitude 10oN in Nigeria. In: Iguisi EO (ed) The Zaria geographer, vol 15(1), Ahmadu Bello University, Geographical Society, Nigeria, pp 34–41

Sharma TC, Panu US (2010) Analytical procedures for weekly hydrological droughts: a case of Canadian rivers. Hydrol Sci J 55(1):79–92

Sighomnou D (2004) Analyse et redéfinition des régimes climatiques et Hydrologiques du Cameroun: perspectives d'évolution des ressources en eau. Thèse Doctorat d'Etat, Université de Yaoundé 1, Département des Sciences de la Terre. 291 p

Sow AA (2007) L'hydrologie du Sud-est du Sénégal et de ses Confins guinéo-maliens: les bassins de la Gambie et de la Faleme. Thèse doctorat d'Etat Es lettres et sciences humaines, UCAD, FLSH, Département de Géographie. 1232 p

Srivastava A, Chinnasamy P (2021) Investigating impact of land-use and land cover changes on hydro-ecological balance using GIS: insights from IIT Bombay, India. SN Appl Sci 3:343. https://doi.org/10.1007/s42452-021-04328-7

Strahler AN, Strahler AH (2003) Introducing physical geography, 3rd edn. Wiley, Cambridge, pp 499–502

Tropica Environmental Consultants (2008) EIES Pipeline Eaux Faleme SMC, Rapport d'audience publique dans le cadre de l'étude d'impact environnemental du projet d'installation et d'exploitation d'une conduite de pompages d'eau de la Faleme vers la mine de la Sabodala Mining Company. 176 p

World Bank (2014) Gérer les risques de catastrophe pour protéger le développement. La Banque Mondiale, article du 11 avril 2014, en ligne: https://www.banquemondiale.org/fr/results/2013/04/12/managingdisasterriskresilientdevelopment

Xu ZX, Yang XJ, Zuo DP, Chu Q, Liu WF (2015) Spatiotemporal characteristics of extreme precipitation and temperature: a case study in Yunnan Province, China. Proc. IAHS 369:121–127. proc-iahs.net/369/121/2015/. https://doi.org/10.5194/piahs-369-121-2015

Chapter 10
Review of Various Impacts of Climate Change in South Asia Region, Specifically Pakistan

Rabeea Noor, Chaitanya B. Pande, Syeda Mishal Zahra, Aarish Maqsood, Azhar Baig, M. Aali Misaal, Rana Shehzad Noor, Qaiser Abbas, and Mariyam Anwar

Abstract Climate change is a dire and increasing crisis worldwide in South Asian region, especially Pakistan. This region is highly vulnerable to climate change, while awareness of climate change issues and adaptation strategies is very low. Pakistan faces a perpetual threat in its ecosystem, biodiversity, and oceans. Much of the country's threats stem from poverty, a lack of financial resources, and natural

R. Noor (✉) · A. Maqsood · A. Baig · Q. Abbas
Department of Agricultural Engineering, Bahauddin Zakariya University, Multan, Pakistan

C. B. Pande
Indian Institute of Tropical Meteorology (IITM), Pune, Maharashtra, India

S. M. Zahra
Department of Irrigation and Drainage, Faculty of Agricultural Engineering and Technology, University of Agriculture, Faisalabad, Pakistan

Agricultural Remote Sensing Lab (ARSL), University of Agriculture, Faisalabad, Pakistan

Department of Agricultural Engineering, Bahauddin Zakariya University, Multan, Pakistan

M. A. Misaal
Department of Farm Machinery & Power, Faculty of Agricultural Engineering and Technology, University of Agriculture, Faisalabad, Pakistan

Department of Farm Machinery & Precision Engineering, Faculty of Agricultural Engineering and Technology, PMAS-Arid Agriculture University, Rawalpindi, Pakistan

R. S. Noor
Faculty of Agricultural Engineering and Technology, PMAS-Arid Agriculture University, Rawalpindi, Pakistan

Department of Agriculture, Biological, Environment and Energy Engineering, College of Engineering, Northeast Agricultural University, Harbin, China

M. Anwar
Department of Pharmaceutical Chemistry, The Islamia University, Bahawalpur, Pakistan

C. B. Pande et al. (eds.), *Climate Change Impacts on Natural Resources, Ecosystems and Agricultural Systems*, Springer Climate,
https://doi.org/10.1007/978-3-031-19059-9_10

disasters. Pakistan endures ongoing seasonal changes, including extreme climate events, an ongoing shortage of water, pest diseases, human health issues, and more. The country has a low adaptive capacity to these threats, given its ongoing economic struggles and varying living conditions from season to season. The likely effects of climate change on the common Pakistani citizens are devastating, especially for local animals like lions, tortoises, dolphins, and vultures. These animals, regardless of their small global impact, will face extinction. In fact, the effects on local people, such as the per capita impact on global greenhouse gas emissions, are severe. The findings of this review support the theory that GHG emissions cause climate change. The effects of this global phenomenon have been seen in Pakistan in agriculture, livestock, precipitation and temperature trends and patterns, food and energy reliability, water resources, and community. According to a recent sectorial assessment, this review evaluates climate change alleviation and adaptation techniques in the sectors mentioned above, which caused a huge economic loss in Pakistan every year. A new study finds that governmental intervention is necessary for recent climate policy development. The research suggested that strict accountability of resources and regulatory actions are vital to creating climate policy.

Keywords Climate change · Greenhouse gases emissions · Adaptation · Alleviation

Introduction

The term "climate" refers to overall environmental conditions observed in a specific region—variations in temperature, precipitation, pressure, and humidity in the atmosphere. It can be altered by natural phenomenon or human interventions, resulting in "climate change." The changing climate is causing more extreme events across the world, like global warming and melting ice glaciers. These changes are caused by greenhouse gases, which are released into the atmosphere from various sources and activities (Lipczynska-Kochany 2018). Natural disasters, such as hurricanes Harvey and Irma, and the devastating wildfires burning in the western states are frequently cited as evidence of climate change by numerous researchers, scientist, and environmentalists (Orimoloye et al. 2022). The consequences of climate change are growing at an alarming rate and require immediate action. All people must now engage in actions that promote climate change adaptation, such as conserving water, reducing the use of fossil fuels, and recycling materials (Fawzy et al. 2020). The accumulation of greenhouse gases (GHGs) in the earth's natural atmosphere is the primary cause of global climate change (CO_2, CH_4, N_2O, and H_2O). This buildup of GHGs can be naturally found but raises the planet's temperature (Kweku et al. 2018). Climate change has been causing a rise in atmospheric events all over the world. In response, its claimed that this is causing global warming to be underestimated. Humanity is not the only cause of environmental degradation. Natural disasters like volcanic eruptions, earthquakes, and solar cycles also heavily impact environment (van Pelt 2018). Natural sinks, such as plants and oceans, have

historically absorbed GHGs like carbon dioxide—but human activities have increased their output. For example, the number of cars on the road, land used for agriculture, forests (Huang et al. 2016), industrial revolution, and burning fossil fuel (Udeh and Kidak 2019; Yousaf et al. 2017) is all increasing at an accelerating pace. However, water vaporization is the exception (Ceglar et al. 2019). The damage done by global warming caused by GHG emissions has been happening for decades. In the past, before the Industrial Revolution, the environment and natural atmosphere were balanced and stable (Wiedmann et al. 2020). The two main contributors of anthropogenic carbon dioxide (CO_2) emissions are human activities, i.e., the burning of fossil fuels and changes to land. These factors have contributed to global warming since the mid-twentieth century (Anderson et al. 2016; Yousaf et al. 2017; Yue and Gao 2018).

The past few Septembers have been the fourth hottest since 2000 (Leonelli et al. 2017). It was a record-setting hot summer, with ten of the warmest summers in recent times recorded since 2003 and September of 2014–2018 have been the five warmest Septembers on record (Hoy et al. 2020). This rise in temperature is not just a passing trend. It threatens the existence of civilization by way of erratic weather patterns, environmental devastation, commercial deprivation, and society destruction (Espeland and Kettenring 2018). The impacts of climate change are catastrophic, and they're felt in two discrete time periods: short period and long period. Short period, humans feel the effects of climate change through the release of GHGs, while in long term, humans face the release of harmful gases, quantities of heat, and worldwide food shortage because of extreme weather (Godde et al. 2021). Pakistan is disproportionately affected by climate change because it is in Asia and surrounded by countries facing severe challenges due to a lack of resources, industrial expansion, urbanization, and excessive economic development. These factors are making the country incapable of sustainable development (Abdul and Yu 2020; Shaffril et al. 2018). The amazing economic growth of Pakistan and much of the world relies on excessive use of natural and nonrenewable resources. But this massive exploitation is having harmful impacts over the atmosphere. The detrimental effects include permanent damage to the environment. To alleviate the negative effects of global climate change and other environmental degradation, it's important to both implement policies that reflect ecological values and integrate these into public liability, intellectual fences, behavioral intents, and esteem for nature (Islam and Kieu 2020).

In 2010, there was a 5.8% increase in global GHG emissions and Pakistan contributed to this dramatic rise with same percent (Ahmed et al. 2016; Hussain et al. 2019a, b). Pakistan is experiencing extreme climate change impacts that are damaging the economy and social and environmental development. Rapid urban development, rising transportation needs, and a rise in energy usage could cause the country to become even more susceptible to climate change by 2030 (Babar et al. 2021). Pakistan is experiencing the effects of climate change. The adverse conditions include melting glaciers at an unprecedented rate, sudden flooding, unpredictable droughts, high temperatures, lack of water sources, and intense heat waves. In addition, human healthcare issues and pest diseases such as mosquitos and other

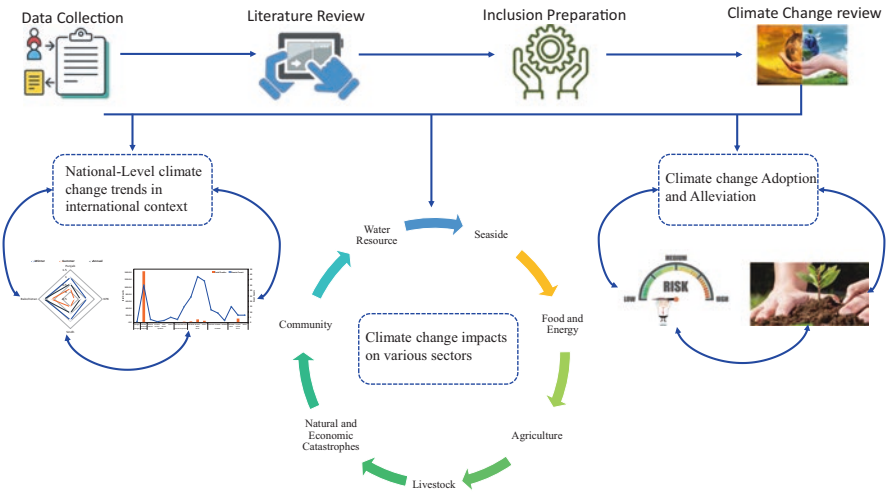

Fig. 10.1 Overview of climate change review on Pakistan

seasonal changes are occurring. Because of these issues, lifestyle changes are required (Abdul and Yu 2020; Hussain et al. 2018). Climate change is a reality with real, tangible effects. To tackle it effectively, it's necessary to take steps toward both alleviation—stopping future GHGs emissions and lessening the present level of GHGs in the atmosphere—and adaptation, changing to meet the resulting effects of climate change (Castillo et al. 2021; Enríquez-de-Salamanca et al. 2017; Shahid et al. 2021). A systematic review was conducted on the Pakistan climate change influence using multiple sources of literature. The main aim is to evaluate how climate change will affect different sectors across the country. The analysis is thorough and reveals notable climate changes that pose a threat to Pakistan. Climate change impacts on various sectors, including, but not limited to, agriculture, livestock, food security, water security, and energy security. In this review, you'll discover that numerous strategies for alleviation and adaptation practices have been implemented in Pakistan with an emphasis on socioeconomic and environmental impacts (Fig. 10.1).

National Level Climate Change Trends in International Context

In increasingly warming world, climate change is already having a significant impact on our lives. Rising sea levels and increased heat-related deaths are just two of the consequences of climate change's impact. These effects are not only visible in our own region but also throughout the world. Climate change will likely intensify these effects even further in the future (Cavicchioli et al. 2019). Climate change is a worldwide problem. However, its effects are more severe in developing

countries due to several reasons, including a lack of knowledge and understanding about effective measures, as well as limited resources and public funds exploitation (Ullah et al. 2019). The IPCC has forecasted the disastrous effects of climate change—particularly on natural resources, anthropogenic measures, and natural disasters in the future (IPCC 2021). The El Nino and La Nina have already negatively influenced reservoirs and aquifers throughout the world. The average annual temperature has increased by about 0.4 °C in the past century, from 1896 to 1995 (Hughes 2003). In the past century, the mean annual temperature in the South Asia region has increased by 0.75 °C. In Pakistan, the rate of change has been accelerating. From 1961 to 2007, the temperature rose by 0.47 °C. The warmest year before 2007 was 2004, and the most significant temperature increase was noticed during winter. The average winter temperature is typically between 0.5 and 1.1 at 2 degree centigrade. The warmest winter in Pakistan happened in Balochistan while the coolest summer was experienced in the northwestern regions. Pakistan's annual temperatures only raised by 0.87 °C (maximal) and 0.48 °C (minimal) from 1960 to 2007 (Fig. 10.2a). It can be observed that droughts have hit Pakistan the hardest in 1998 and 2004. Baluchistan, its largest province, has been severely influenced, killed 76% of its livestock and 84% of the population directly influenced, even the entire country suffered a great deal of devastation due to the massive floods (Arif et al. 2021). The flood displaced many people in both the northern and central parts of the country. Sizzling temperatures, severe droughts (Cayuela et al. 2016), pest problems, health-related issues, and lifestyles will be present in the forthcoming also (Hussain et al. 2018; Ullah et al. 2018).

Climate change is a global issue that is impacting many areas of the world. This issue includes things such as various dangerous temperatures, numerous famines, sudden rainfall patterns, and agriculture ruin (Lake et al. 2012; Rojas-Downing et al. 2017; Pande et al. 2021a, b). Agrarian countries like Pakistan will be especially harmed by climate change; this will devastate the economy. While the per unit of population revenue is low and the country deficit in sufficient infrastructure building or development, the economy is dependent on agricultural exports (Noor et al. 2021a). Agricultural exports are made possible by large irrigable land. The 80% economy relies on these products, and any decrease in either quantity or quality will have detrimental effects on Pakistan's export industry (Grote et al. 2021; Rehman et al. 2015). Pakistan's water supply relies heavily on the melting of glaciers and snow at the country's northernmost areas. These sources account for two-thirds of its irrigable land, while two-thirds of the population is involved in farming. However, Pakistan lacks an infrastructure to alleviate and acquire to climate effects (Khan et al. 2020). Pakistan is on the verge of climate change devastation. Their location, dependence on agriculture, reliance on water resources, and lack of emergency response capacity makes them the country most threatened by climate change (Noor et al. 2021b; Grote et al. 2021). The other alarming concern is that not all areas will be affected with uniform severity (Ali and Erenstein 2017b; Rehman et al. 2015). The poor farmers in rural areas are expected to be hit the hardest, which was illustrated by the 2010–2011 floods (Shah et al. 2020). Developing countries mostly depend on natural resources for their living actions, particularly people in

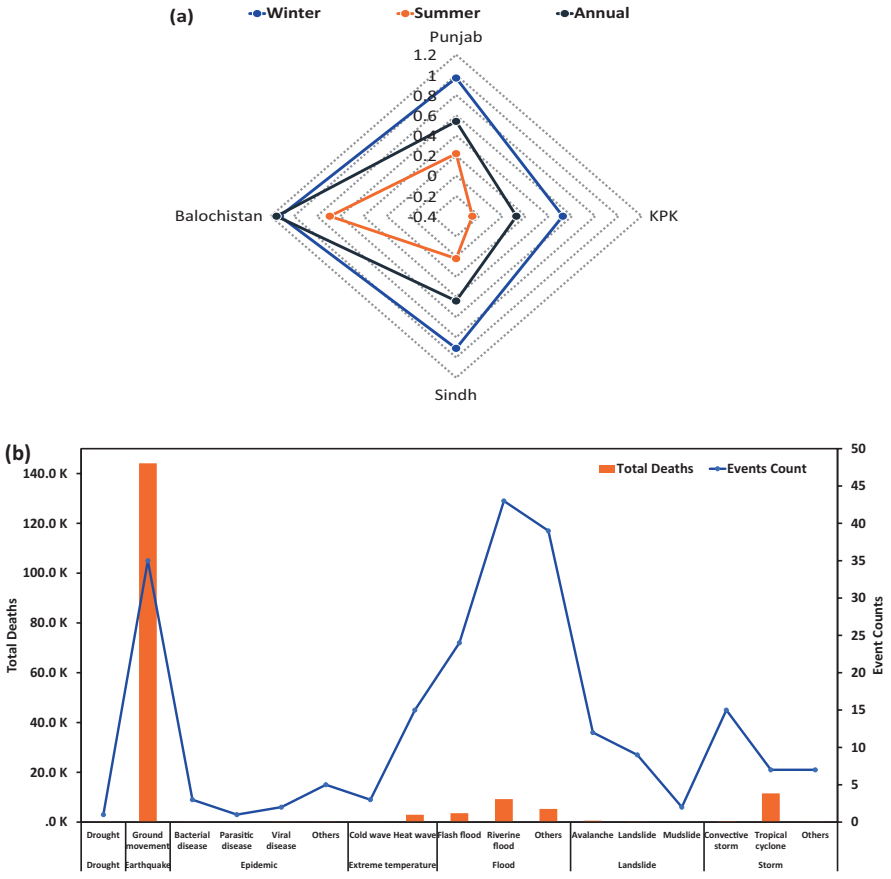

Fig. 10.2 (**a**) Change in annual temperature from 1960 to 2007. (Source: Chaudhary 2009) (**b**) Summary of Natural disaster in Pakistan from 1900 to 2020. (Source: INFORM 2020)

mountainous regions. Hence, this dependence, especially considering climate change, poses a massive economic and life-threatening danger to the country (Weiskopf et al. 2020). Despite its miniscule contribution to global greenhouse gas emissions, Pakistan ranks as one of the country's most susceptible to the impacts of climate change (Cheema 2014; Khan et al. 2016). From Fig. 10.2b, it is noted that the average number of people affected by disasters has increased since 2010. In 2012 and 2014, more than 1,000,000 people were influenced by floods alone, leaving this population in a situation of disorder the number of refugees has decreased to less than a million, since 2015, due to the hard work of persons, profitless firms, and environmentalists to alleviate the climate change.

Climate Change Impacts on Various Sectors

In this section, after the climate change impact trend over the whole country, impacts of climate change on various sectors have been discussed: i.e., natural and economic catastrophes, water resources, agriculture, livestock, energy and food reliability, and community. This article will explore the physical and ecological impacts of climate change. In the end, we have provided you with additional information (i.e., alleviation and adaptation) that may be helpful. The critical detail from the studies is also available in Table 10.2 and Fig. 10.2a.

Climate Change Impact on Water Resource Sector

Climate change is a big problem—but the water sector is one of the most overwhelmed by it. The majority of Pakistan's largest irrigation system (i.e., Indus Basin) is dependent on rainfall, melting glaciers, and groundwater (Noor et al. 2021a; Podger et al. 2021; Qureshi 2011). The key sources of water come from monsoon rain (50-million-acre feet), river inflow (142-million-acre feet), and ground water (48%). Most of the water use is for agriculture (92%), followed by industries (3%), and household and infrastructure (5%) (Anjum et al. 2021; Watto et al. 2021; Wescoat et al. 2021). The future is expected to bring an increase in water demand in sectors due to population growth and improvements in living standards. Annual river flow changes seem to be declining in (Fig. 10.3a). A particularly rapid decline was observed from 1998 to 2003, and this is attributed to the long drought that persisted throughout many of those years (Khan and Khan 2015). In a normal year, the annual flow of Kotri Barrage is lessened from 77.3 MAF to 39.2 MAF. The post-Kotri/Mangla era has caused a serious disruption in flows to the Indus Delta region (Basharat 2019). The area includes Hyderabad, Thatta, and Badin, where farmland is inundated, and groundwater quality is ruined by seawater intrusion (Khan et al. 2011; Radecki-Pawlik et al. 2015). The Indus River System will experience more substantial impacts from glacier melt because of climate change. This will cause more considerable alternations in the forthcoming water supply. The Western Himalayan glaciers, which feed the Indus River, are predicted to retreat in the next 50 years. Initially, it will enhance because of the glacier melt. But then, the glaciers will be empty and causes the river's flow to decrease by 30–40% over the course of 50 years. Depending on a study from 1997 to 2002, it is announced that there are some large glaciers in the Karakoram Range, 40–70 km in length, that have an altitude of 5–15 m (Chen et al. 2005). This finding has led to conflicting results about the effects of climate change on the Indus River flow and Karakoram glaciers. More demanding key findings related to the water sector recognized by the climate change task force are shown in Fig. 10.3b.

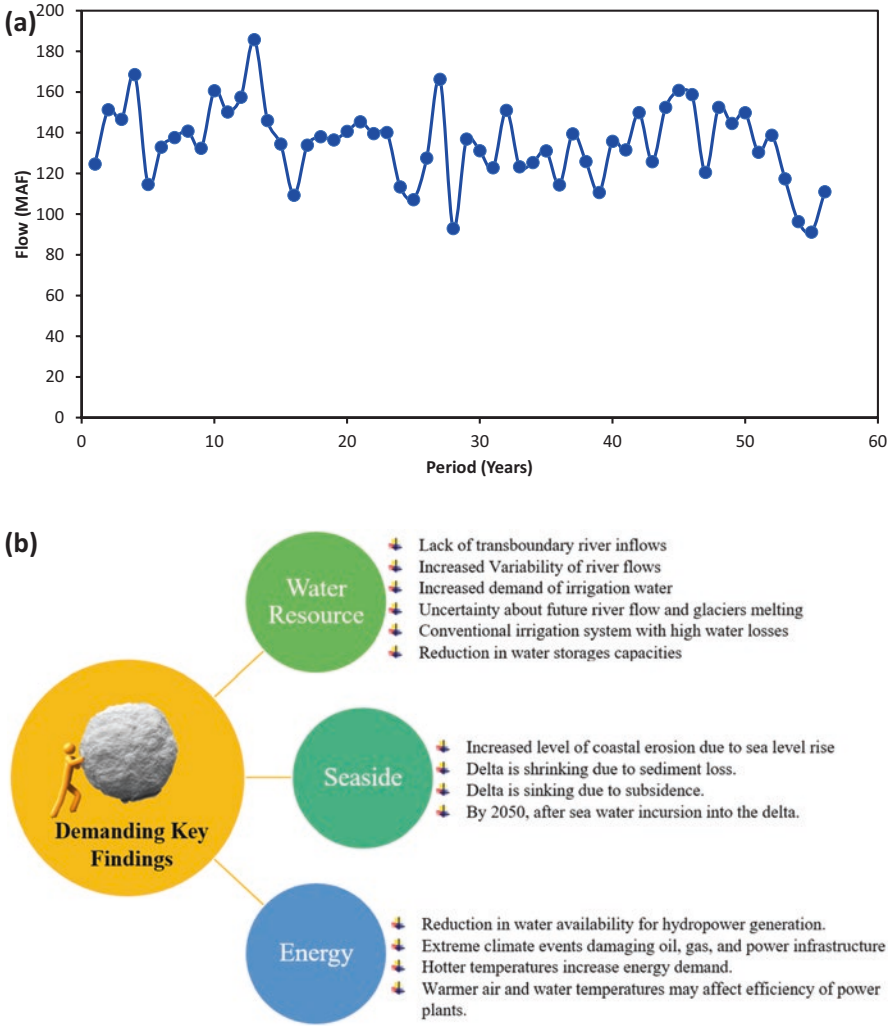

Fig. 10.3 (**a**) Indus River system annual rivers flow in MAF from 1946 to 2002. (Source: Ahmad 2009). (**b**) Demanding key findings of Water, Seaside and Energy sector. (Climate Change Ministry 2016; Hewitt 2005)

Climate Change Impact on Seaside Sector

It has been anticipated that the seaside areas and its resources will be heavily impacted as sea levels rise. Low-lying areas have been inundated, mangroves forests have been degraded, drinking water quality has diminished, and fish and shrimp productivity has reduced (Group 2012). Pakistan's 1046 km long sea line is on the border of the Arabian Sea and stretches along the provinces of Sindh and Balochistan.

Sindh seaside area is more vulnerable to sea level rise than Baluchistan due to its flat topography and higher population density. It also has many industries that contribute to a large amount of pollution to the seaside, which can affect the environment in the long run (Masood et al. 2007). An underwater survey of the Indus Delta's seabed is expected to encompass an area roughly equivalent to the size of 7500 square kilometers. The low-lying seaside areas of Baluchistan, i.e., Pasni may also be affected by SLR. The Baluchistan seaside is a seismically unsafe zone. This region experiences constant earthquake activity. Every year, this area is raised by 1–2 mm because of the subduction process (Masood et al. 2007). Additionally, rising sea levels combined with the existing coastal erosion on the delta's coastlines could worsen the extent of shoreline erosion over time. The cricks in the delta areas such as Hajamaro, Ghoro, Kaanhir, and Kahhar are areas with active shoreline erosion (Grases et al. 2020). Their erosion rate, however, ranges from 31 meters per year to 176 meters per year. On the south side of the mouth of Ghoro Creek, erosion is the highest with a rate of 176 meters per year between 2006 and 2009. The area retreated 425 m during that time. The delta region will shrink and sink even more than it already has because of lack of sedimentation. There is about an 80% depletion in the amount of river sediment due to extensive damming on the Indus River (Clift and Jonell 2021; Syvitski et al. 2009). The current rate of sediment accumulation does not exceed relative projected SLR, which is one of the main sources for worthwhile SLR in almost 70% of the world's deltas, involving the Indus Delta (Ericson et al. 2006; Tessler et al. 2015). The Indus River delta is at great risk because of the threats it faces. They are ranked third on the greater risk scale. There are many reasons for this ranking, but one of the most prominent is sinking or subsidence rates, which are natural and usually range from <1 mm/year to >10 mm/year. But this rate goes up because of humans' oil extraction and groundwater activities (Kalhoro 2016a, b). In 2006, a research study found that the Indus Delta is at high risk for sea level incursion. The population there is at risk by 0.79%, and 2.73% of the total delta area could be vanished by 2050 (Ericson et al. 2006). Demanding key findings related to seaside sector recognized by climate change task force is shown in Fig. 10.3b.

Climate Change Impact on Energy and Food Sector Reliability

Pakistan is vulnerable to climatic factors and food insecurity (Syed et al. 2022). These issues are becoming more frequent due to climate change, and the negative impacts will only worsen in the future (Manisalidis et al. 2020). In South Asia, 300 million people are classified as food insecure. This staggering number is the most in the world, and it's highly undernourished. Pakistan's high levels of poverty are the outcome of climate change variations, which have hugely impacted the economy of Pakistan (Ali and Erenstein 2017b). The present impact of climate change is

evident. The threat of water and food scarcity and extreme changes in the atmosphere, such as colder winters and hotter summers, are becoming more common in many regions. Regions with less rainfall, such as deserts, hotter summers, and colder winters are also feeling the pressure of climate change. Furthermore, Pakistan's food security is terribly affected by climate (Ali et al. 2017). A statistical comparison of the difference between crop yield (2020–2080) and actual crop yield (1961–1990) reveals that Pakistan's climate is in a downward spiral as illustrated in Fig. 10.4a. Unpredictable precipitation and changing mercury levels can have devastating effects on food crops. The main food crops are severely impacted during

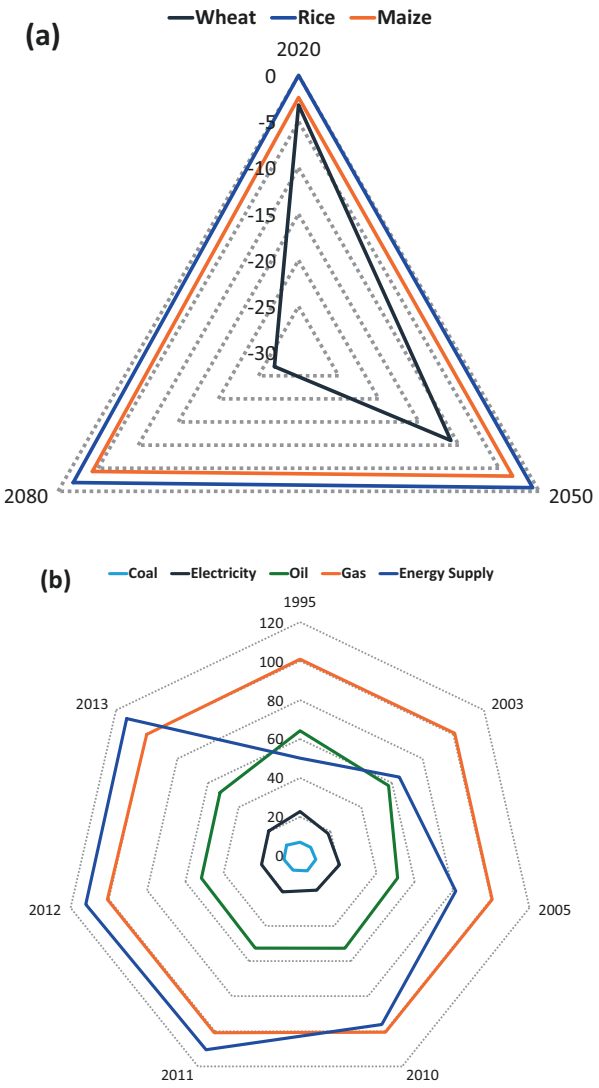

Fig. 10.4 (**a**) Statistical comparison of crop yield (2020–2080) with actual crop yield (1961–1990) by A2 Scenario. (**b**) Main Energy sources of Pakistan in 2013. (Source: Development Bank 2017)

critical growth periods. Unpredictable precipitation and changing mercury levels can have devastating impacts on food crops (Tirado et al. 2010). The hilly regions of Pakistan may be filled with natural resources, but the land is lacking proper management of agricultural activities and agricultural output in the face of erratic weather and unseasonal rainfall. Due to dry spells and flooding, Pakistan's farmers are suffering (Ullah 2016). Another problem is the increase in crop pests. The people living in hilly areas are increasingly dependent on those living in plain areas because of decreased food reliability (Aslam et al. 2017; Hussain and Mumtaz 2014). A challenge for farmers and other rural residents in the fight against climate change is implementing effective adaptation strategies. However, farmers will have to spend money on these strategies and take steps on their own (Ajani and van der Geest 2021; Ali and Erenstein 2017a). Modern agriculture is the key to effective food security, increased water efficiency, and a significant drop in CO_2 emissions. A successful modern agriculture program has shown that farmers are able to achieve higher food security and reduced poverty levels by an average of 3–6% (Abid et al. 2016b). According to a study, more educated and skilled farmers tended to take more agricultural practices than less educated and skilled farmers (FAO 2013). In the past century, rapid industrialization and urbanization encouraged the government to take action to meet energy demand in the short term. This short-term policy has had various suggestions for the environment, energy security, and stable deposits (Aslam 2017). However, the government is still struggling to grapple with the energy crisis, which has resulted in a shortage of 3000 megawatts of electricity as the main source of energy in the country were gas (48%), oil (32%), hydropower (31%), coal (7%), and nuclear energy (2%) in 2013 (Fig. 10.4b) (Lin and Ahmad 2017; Development Bank 2017). A major reason behind the shortage is that loopholes in energy planning deepened the demand–supply gap. Scientists have also pointed out that increasing demand for energy is caused by rapid urbanization, which is creating carbon emissions (Abdallah and El-Shennawy 2013; Ali and Nitivattananon 2012). In Pakistan, the situation with energy is dire. Urban centers are having a hard time keeping up with the energy demands of their citizens, who rely primarily on vehicular use for travel (Shah et al. 2020). This increase in vehicles makes them susceptible to energy shortages and environmental pollution. In the case of Pakistan, research on GHG emissions and energy security is lacking. Pakistan is in a dilemma of growing the economy and improving sustainability also energy security (Lin and Ahmad 2016; Naeem Nawaz and Alvi 2018). CO_2 emissions must be curbed in order to limit their damage. Policies should put the reduction in emissions at the forefront to alleviate the growing levels of pollution. Smart grids, smart cities, and smart buildings are important concepts to cut life-threatening greenhouse gas emissions and ensure national energy security. Some of Pakistan's crops are sensitive to climate changes, including rice, wheat, cereals, vegetables, spices, and grains. Food security is becoming a major concern. The worldwide population has increased in the recent years and productivity in staple crops, such as rice and wheat, has fallen due to extreme temperature changes and lack of rain (Saboor et al. 2019). Demanding key findings related to the energy sector recognized by the climate change task force are shown in Fig. 10.3b.

Climate Change Impact on Agriculture Sector

The agricultural sector in Pakistan not only plays an essential role in the economy but also has experienced huge ramifications because of climate change. The climate changes in the agricultural areas have a big impact on the productivity and yields of crops. Climate change can affect crop production in a variety of ways, depending on the type of agricultural practices performed in the system (Abrahão et al. 2015). The crops in tropical climates are already suffering the effects of climate change. The effects include an increase in temperature and droughts, making it difficult for crops to thrive. If the temperature rises continuously, it is predicted that Agriculture will decrease by 8–10% by 2040 (El-Beltagy and Madkour 2012). A crop simulation study conducted in Pakistan found that major crops yields would decrease, specifically for wheat and rice. Four different agroclimatic zones were simulated, and all showed that the length of the growing season would shrink as well (Table 10.1). The lowlands are likely to experience flooding, sea level rise, and an increased frequency of droughts as a result of climate change. The reduction in snowfall and the rapid melting of glaciers will both converge to decrease the amount of water available for agricultural crops (Ponting et al. 2021; Poveda et al. 2020). Agriculture is the sector most sensitive to climate change. Climate change not only affects this sector but also affects the environment as well (Bhatti et al. 2016). Variations in rainfall patterns in the Indus Basin will cause a decrease in water supply, which will impact the agriculture and the entire economy. Furthermore, the centuries-old indigenous crop varieties of Pakistan are at risk of extinction. A lack of modern irrigation techniques has led to crop field water waste as well (Qureshi and Perry 2021). In July 2015, the Chitral district of Khyber Pakhtunkhawa was hit with heavy rainfall and frequent floods. The resulting floods destroyed crops and livestock. In the Upper Indus basin, many residents saw a rise in drought during the years 2001–2011. This led to problems with agriculture and soil degradation. As a result, agricultural output decreased as well as livestock. Climate change and extreme weather have harmed rural livelihoods and cash crops around the world. As a result, millions of people have been forced to migrate to urban centers in search of a better life (Abid et al. 2015, 2016a). It is important to keep in mind that climate change poses risks to farmers. A plan

Table 10.1 Length of growing season of wheat in different climatic zones in days

Name	Length of growing season in days			
Temperature	Humid	Subhumid	Semiarid	Arid
Reference	246	161	146	137
1	232	155	140	132
2	221	149	135	127
3	211	144	130	123
4	202	138	125	118
5	194	133	121	113

Source: Muhammad Iqbal (2009)

should be in place to educate farmers about these risks to prevent further vulnerability in the future (Hussain et al. 2016).

Climate Change Impact on Livestock

Pakistan is an important region for livestock, as these animals provide an important livelihood to the residents. However, climate change has had a devastating effect on the livestock. When climates are erratic, it can cause livestock to suffer from illnesses that are adjacent and even deadly. Climate change is affecting many aspects of food production, making it hard for livestock to survive. The livestock's feed, water, and grazing land are all affected as the climate changes and as CO_2 and temperature rise (Escarcha et al. 2018). This is making meat and milk production decline (Abbas et al. 2019). Livestock is also affected by diseases, animal vectors, and biodiversity. Meanwhile, animal and plant species are at risk of extinction (Shah et al. 2020).

Climate Change Impact on Natural and Economic Catastrophes

The backlashes of climate change, i.e., water and food security, are taking their toll on the world (Aggarwal et al. 2019; Myers et al. 2017). Global warming is causing water shortages, heat strokes, and mass migrations (Mekonnen and Hoekstra 2016). Thousands of millions of people are affected by these issues. The interior regions are vulnerable to soaring temperatures because of the changing weather patterns (Mannig et al. 2017). As glaciers melt, food security is jeopardized because there will be less fresh water for crops. There is also the risk of extinction to many plant species (Gomez-Zavaglia et al. 2020). Moreover, the coastal ecosystem's health is at stake. It's being threatened by a rise in the sea level (Braun de Torrez et al. 2021; Perera et al. 2018)—as well as an increase in temperature, disease, and more seasonal and lifestyle changes. There's a vigorous likelihood that these trends will persist in the future (van den Broeke et al. 2016). Pakistan is a country with a lot of climate-related woes. Continuing the problems, there is insufficiency of environmental knowledge and understanding, lack of adaptive capacity, shortage of good infrastructure, scarcity of inducements, scarcity of regulations, and insufficiency of government attention toward climate change (Mumtaz and Ali 2019). Hence, Pakistanis' worries are constantly piling up. It's predicted that an enhancement of 2–3% in mercury and particular rainfall trends will severely affect Pakistan by 2050 (Janjua et al. 2021). If this occurs, the effects of economic and natural catastrophes will reduce agricultural outputs, rehabilitation, and rebuilding of essential infrastructure. In the past few years, Punjab has dealt with the consequences of the smog:

eye and skin infections and an enhancement in road accidents because of less distinctness (Ali and Erenstein 2017a).

Impacts of Climate Change on Community

Climate change is having a plethora of suggestions for the environment and in socioeconomic sectors and is influencing community in several ways. Community is paying the price for these suggestions in the social fabric, such as human health, clean air, food, water, and diseases (Chen et al. 2020; Pande et al. 2021b; Panneerselvam et al. 2021, 2022). Climate change has a variety of consequences for community, such as untimely deaths and human health issues. It is also influencing food and water—two things that are necessary for survival (Li and Yap 2011). Natural calamities such as droughts, floods, earthquakes, and heat strokes are a worldwide problem. They affect the population in a number of ways. One way is through the rise in global temperature caused by global warming. In Pakistan, the warmest temperature observed in history has occurred in southern regions, making it one of the countries that will see a dramatic increase in global warming. The southern part of Pakistan is most at risk from global warming due to its close proximity to the equator (Abid et al. 2021; Miyan 2015). Punjab, the central region of Pakistan, is experiencing intense waves of heat with an average temperature increase of 0.5 °C every year. Moreover, a marked increase in temperature by 31 days has been observed from 1980 to 2007 (Sultana et al. 2009). It is predicted that the northern and central parts of Pakistan are most at risk from the negative effects of climate change. These regions could see temperature increases of up to 4% by 2050 and 3% in the north and nearly 1% in the south. The detailed trend of temperature and rainfall in Pakistan are illustrated in Fig. 10.5. Climate change could have a significant impact on the global economy. In developing countries, it's expected that it will bring rising unemployment rates and a clogged job market. Because agriculture is one of the oldest forms of labor, it'll soon be second to services in terms of the number of people involved, with one billion workers engaging in agricultural activities (Ludwig et al. 2004; Olsen and International Labour Office. 2009). The agriculture sector is anticipated to be at risk in the future. The trend is expected to be worsened by nonuniform weather patterns, higher temperatures, less rainfall, and deforestation. This will negatively impact the industry and the people employed in it (Olsen and International Labour Office. 2009).

Migration is one of the many environmental approaches for alleviating and adapting to the effects of climate change. It is the act of relocating and displacing people because conditions are no longer safe for living or because jobs are no longer available. Climate change can impact our education systems not only because of increased locational impacts but also because it can affect students' performance in school (Schwerdtle et al. 2017). Extreme weather events are short-term disruptions to life. They cause unpredictable rainfall, storms, floods, and hurricanes. Many

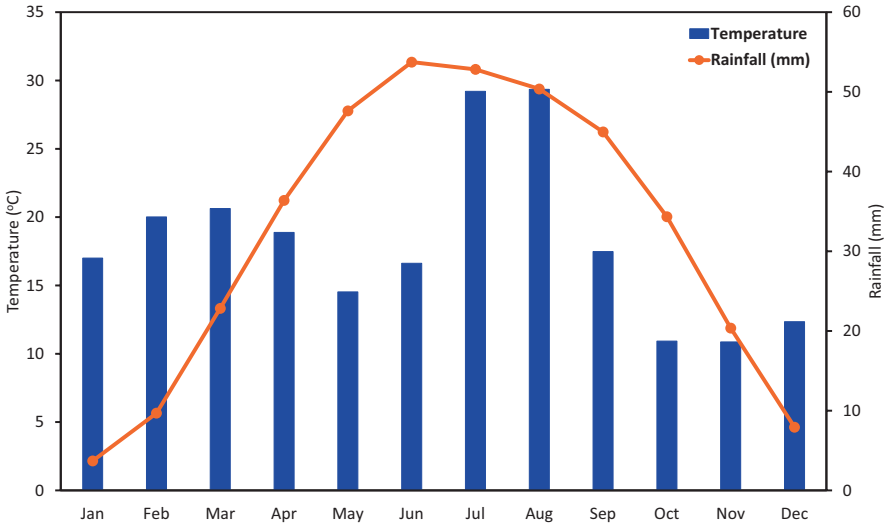

Fig. 10.5 Average monthly temperature and rainfall in Pakistan from 1991 to 2020. (Source: CCKP 2021)

people believe that if these variations in climate persist, there will be more chances of disasters such as floods (Babar et al. 2021; Kara and Yucel 2015). The long-term effects of climate change on education include undernourishment and drought, leading to an inadequate food supply and a shortage of crops. Pakistan is experiencing such effects through increased occurrences of diseases and people being forced to relocate (Cheema 2014). These consequences also lead to economic instability in the country, with many people competing for low-wage jobs. These adverse impacts to the lives of people in developing countries are the result of natural disasters, such as floods or storms. In addition to the environmental impacts, income inequality can also arise from migrations. This often results in high rates of unemployment, which can lead to malnutrition in children and a low standard of living for individuals. It may also result in a scarcity of food (Ali and Erenstein 2017a, b; Hallegatte et al. 2020). Heat waves are destroying developing countries. In Pakistan, the heat wave has been a shocking problem for citizens, with about 65,000 people needing treatment in 2015. The heat waves have spread to the northern areas of the country as well (Hanif 2017). In 2016, over 100 casualties have been reported from the northern regions due to the heat waves (Sheikh 2010). In the face of climate change, heat waves are becoming worse. Lack of adequate health facilities in developing countries makes these consequences more severe (Rauf et al. 2017). Climate changes are originating flooding and other disasters across worldwide. The effects of a flood-related disaster can include health effects, dermatological problems, and a wide range of psychological problems. A wide range of dermatological problems is rising after floods. Many infectious diseases, such as impetigo, measles, dengue fever, and

malaria, that have a skin manifestation have increased. And inflammatory conditions, such as irritant contact dermatitis are also increasing (Dayrit et al. 2018).

In addition, climatic aspects and weather variations can contribute to the spread of dengue hemorrhagic fever (DHF) (Banu et al. 2014). Variations in the weather can create conditions conducive to Aedes mosquitoes' expansion, such as more precipitation and higher temperatures. High humidity and low vapor pressure are two of the most common causes of DHF (Noor et al. 2022; Bhatt et al. 2013; Bhatti et al. 2016; Syed et al. 2022). In several districts of the Punjab province, morbidity and mortality rates were high. Faisalabad, for example, experienced the worst of these in 2011. Faisalabad has been hit the hardest by the disease. More than 300 people have died of DHF in the city alone, and it impacted more than 14,000 people in two big cities in the district: Faisalabad and Sialkot (Bakhsh et al. 2018). Given the increase in global warming and the frequency of earthquakes and seismic activities, the latter may have severe impacts. Severe impacts can include health issues, stress, anxiety, lack of sleep, and depression (Cianconi et al. 2020). It is noted that seismic activity in Pakistan increased significantly, and the average temperature changed from −19 Celsius during winter to +53 Celsius during summer (Cheema 2014; Dimri et al. 2018). Citizens of Pakistan have been faced with the existence of multiple outbreaks in the past few months. Health policymakers need to focus on raising awareness through media campaigns. This will not only lead to a more informed population but also help protect citizens from these viruses. Access to health facilities should increase, and facilities in Pakistan should be made much more extensive.

Climate Change Adoption and Alleviation

Pakistan has suffered from the impact of climate change for years. The Ministry of Climate Change has taken various necessary steps to help people in Pakistan face this reality. It's compulsory for the country's economic and social development to be able to adapt to these effects. They have worked on ensuring that the masses are aligned with the national climate policy, which pertains to alleviation and adaptation actions. To combat the climate crisis, companies in three sectors must work together. They include the agriculture, livestock, and energy industries. These sectors must help alleviate the climatic effects by collaborating to achieve zero-carbon emissions (Abbas et al. 2019; Lin and Ahmad 2017). To ease the climatic changes at the national level, ensure a coordinated plan of action. According to the Intended Nationally Determined Contributions (INDCs), Pakistan needs 6.5–13.5 dollars billion per year to alleviate the effects of climate change. The country has planted 100 million trees throughout the country to help alleviate the effects of climate change (Economic survey 2017–2018). Technology has made some massive advances in the fields of energy, forestry, and transport. The report emphasizes the eco-friendly advancements in energy, including solar power and micro-hydropower plants. Today, energy is also being generated more sustainably, with developments in forestry including viable forest governance and social forestry against deforestation,

whereas advances in transport include an advanced bus rapid transit system and high-performance vehicles (Climate Change Ministry 2016). Moreover, the study concludes that neither water nor agriculture nor energy is immune from climate change. The most vulnerable sectors are water, energy, and agriculture. The three important adaptation measures for the water sector are storm water management, harvesting of rainwater, and groundwater recharge. Suggested technologies for the agricultural sector include drip and sprinklers for efficient irrigation and drought-tolerant crops. Improved climate forecasts and early warning systems also provide important resources for farmers (Climate Change Ministry 2016). Moreover, In Table 10.2, Pakistani conservatives have begun to propose adaptation technologies and measures in response to the country's agricultural, water, and energy sectors facing the threats of climate change (Mumtaz et al. 2019). As local residents are the most affected by climate change, it is vital that they have a say in how their environment can be alleviated and adapted to. As global awareness increases, it is of utmost importance that governments avoid inconsistency in climate change policy.

The Intergovernmental Panel on Climate Change points out that the lack of knowledge and inadequate data is hindering the ability to take adaptive actions (IPCC 2021; Neil Adger et al. 2014). Because of these factors, policies have been difficult to execute and face numerous obstacles (Solomon 2007). In Pakistan, the problem is even worse. Climate change is affecting the entire world, and there is an urgent need to create a comprehensive and multifaceted strategy to adapt and alleviate. To protect the environment, it's important to minimize interventions in forests, on glaciers, wetlands, and pastures. To meet the national sustainable developmental objectives, it is important to prioritize the crucial processes for alleviation and adaptation. Pakistan, relatively new to the climate finance world, has limited resources to receive and disburse global financial resources. Pakistan's National Climate Change Policy of 2012 is the country's leading paper on climate change. It sets out aims to ensure that the country is fully ready for changes in the climate. Objectives identified for each adaptation priority area are identified in Parry (2016). These policies are quite important because Pakistan is at-risk for climate change, due to its vulnerability to natural disasters and high population density in coastal regions (Noor et al. 2022). In 2010–2014, 6% of the Pakistani federal budget was earmarked for climate-affected sectors such as energy and transportation. Pakistan has shown its commitment to the Paris Agreement in its National Determined Contribution: to reduce 20% of total greenhouse gas emissions by 2030. The country would need 40 billion USD in international grants to make up for the cost of the reduction. Pakistan requires 6.5–13.5 billion dollars in annual adaptation (Development Bank 2017). Pakistan has secured funds from the Asian Development Bank (ADB), Global Environment Facility (GFF), and the Adaptation Fund to help with climate financing. The ADB's funding to Pakistan reached 389.8 million dollars during 2010–2015. 96.4% of the 375.9 million US dollars was used for alleviation, and only 3.6% was used for adaptation. The Global Environment Facility also granted 12.5 million US dollars to be used for alleviation activities, and those funds have been completely distributed already. Pakistan's annual adaption requirement is roughly between 6.5 billion and 13.5 billion dollars. However, the accumulation of funding from

Table 10.2 Adaptation technologies and measures in response to the country's agricultural, water, and energy sectors facing the threats of climate change

Climate change threats	Adaptation techniques
Agriculture sector of Pakistan	
Reduced crop production and water shortages	New crop varieties are emerging with increased heat and drought tolerance. Such crops will help farmers better withstand heat and dryness conditions. For example, mustard is a high-yielding crop that does not need as much water. Best of all, it can be grown during any season
As a result of changing rainfall patterns, the reduction of irrigation water	A new era requires new water-saving techniques to reduce wastage and help the environment. Promote efficient irrigation methods, including sprinkler and drip irrigation, and improve the irrigation system to minimize distribution loss and land leveling to save water
Pervasive soil decline, crop productivity decline, and underground water devastation are the results of excessive pumping from the ground	You should improve water management along with legislative and awareness support
Flooding, droughts, and heat waves are causing extensive damage to the agriculture and livestock sectors	A new early warning system is developing. It will enable businesses to plan ahead and prepare for more than one disaster at once
Water sector of Pakistan	
With changing climatic patterns, such as drier winters, higher temperatures, and more precipitation in the summer, there are significant and increasing water shortages	There are many ways to promote water efficiency in urban areas. One way is to use efficient irrigation methods such as sprinkler and drip irrigation. Smart agriculture, such as recycling wastewater and promoting rainwater harvesting, can also help. An additional method is desalinating water
Water storage capacities are reduced by sedimentation	Initiate integrated watershed management efforts to restore forested areas around the country. Reforestation can help alleviate flooding and other natural disasters. Additional water storage areas can also help with flood control
A lack of awareness of climate change is affecting the availability of water in our country	Awareness-raising campaigns can help to teach people about water issues and the importance of conservation. These campaigns can engage consumers, giving them the knowledge, they need to make decisions and take action
The Indus delta has experienced severe saltwater intrusion, the result of reduced freshwater supplies from the dams	Water management is crucial for maintaining a healthy ecosystem in the delta area. Consumers must ensure that freshwater supplies are insufficient supply to the region to support a thriving ecosystem
Energy sector of Pakistan	
Sea level rise and heavy rainfall-induced landslides	To deal with the risk of natural disasters, take preventative measures. To deal with the risk of natural disasters, take preventative measures. Construct dikes and walls to contain flooding and increase vegetation cover on the earth's surface to help slow down the largely irreversible process of global warming

(continued)

Table 10.2 (continued)

Climate change threats	Adaptation techniques
Heavy rainfall and extreme weather events have a big impact on urban water supply systems	Urban storm drain channels must be enhanced to handle greater capacity of water. The city is experiencing a severe drought; improvements need to be made. They need to develop and promote rain gardens and bioswales as well as make efficient use of water. These parts of the city should especially be located in arid areas
Hotter air and water temperatures in many regions of the world could increase the cost of using thermal power plants	Invest in additional energy capacity and make it a priority to utilize renewable energy sources

Source: Development Bank (2017)

different governments is still less (Development Bank 2017). The Global Climate Risk Index shows that Pakistan suffers 141 annual uttermost events and 500 casualties, which costs up to two billion dollars per year. This makes it one of the most climate-influenced countries in the world (Eckstein et al. 2021). Pakistan has developed an initiative, "Carbon Neutral Pakistan," to reduce GHG emissions. This initiative is backed by technical support from China. The government of Pakistan commenced the initiative in June 2015 and is currently seeking foreign investment. This project has an estimated cost of 3.85 million US dollars. It is part of a public sector development program for 2016 (PSDP) (Development Bank 2017).

Pakistan's lack of capacity building in terms of climate change alleviation and adaptation measures leaves it vulnerable to the changes in climate. Updates are essential because the government, corporations, and the general population all need to know what to do in order to minimize the negative impacts of climate change. In order to take a comprehensive approach, it is necessary to take it region wise. The climate in rural, urban, and peri-urban areas changes differently, so taking a region-specific approach is necessary to plan climate policy systems. By delivering the knowledge about the timing and magnitude of climatic impacts, the acceptance of anticipated feedback options, and the expected cost of both adaptation and alleviation, a situational assessment can be made (Hussain et al. 2018, 2020). In this modern world, there is a need to understand the devastating impacts of climate change. In developing countries like Pakistan, a concrete understanding of climate change at a local and divisional level is critical for effective implementation of alleviation and adaptation policies. This requires basic information about the issue from all stakeholders (FAO 2015).

Conclusion

The past two decades have seen climate change at the forefront of research worldwide, because of its effects on global warming. It's been shown that GHG emissions (which are at their highest ever) are causing the world to heat up and the number of

hot days and nights to increase. Hot temperatures can result in intense heat waves that have led to numerous deaths in many countries each year, including Pakistan. Pakistan is suffering from high poverty and not enough economic or physical resources. This has severely limited their ability to adapt to climate change. Pakistan' climate change is causing extremely serious effects, such as an unprecedented melting of Himalayan glaciers, erratic rainfalls, unpredictable flooding, and lack of water sources. Temperatures are rising, water is scarce, heat waves are frequent, and lakes are filling up. There are more storms and hurricanes now than ever before, earthquakes happen more frequently, diseases spread more widely and rapidly, and people have to change their lifestyles because of seasonal changes. To solve the climate crisis, there is a need to build awareness from the grassroots level, educate the population about environmental issues, and implement government policies and regulations. Governments, policymakers, environmental organizations, and community members should work together to devise strategies and approaches to alleviate and adapt to climate change. The goal of the climate change review is to provide detailed information on climate change and its economic aspects. Review on the concentration on the cost of climate change, which reaches from 6.5 billion dollars to 13.5 billion dollars per year, will help to understand climate change alleviate and adaptation approaches. The study shows the present climate changes and how they may affect agriculture, livestock, forestry, food, and renewable energy. These insights are important for planning for the future. It also encourages awareness about climate change and its dangers, such as governments need to be proactive and eliminate inconsistencies. They should also establish and execute effective policies; sustainable development is important for the future of the planet. A national plan should be formulated to review and prioritize ecofriendly processes for alleviation and adaptation; beyond governmental interference, the residents should take action and share their experience with climate change. This can contribute to improved alleviation and adaptation strategies in their community; the authorities must take action to minimize human intervention in natural resources and landscapes. These landscapes include forests, oceans, wetlands, pastures, and fertile lands. Governments should develop strategies to manage the land that makes up the landscape for sustainability, and the majority of research on climate change in Pakistan focuses on hard numbers and quantitative findings. While there is a lack of in-depth studies on the effects of climate change, it is clear that it can have significant consequences on the environment.

Furthermore, there are limitations to the data on observed changes of climate change. With only a restricted pond of research and data available at the national and subnational levels, there is still a great amount of uncertainty about the effects it may have on various socioecological systems and sectors. The agriculture, water, and coastal areas are in the most need of research. The vulnerability assessments in these spaces are generally geared toward understanding the risks without considering that the economic factors are intricately connected to people's livelihoods. When this is taken into account, wealth inequality can be diminished by addressing the problems of local poverty. The Central and West Asia regions short of good knowledge of the impacts of climate change and its effects on the environment and

biodiversity because evidence on this topic is poor and inaccessible. Pakistan has many research gaps in its environment. The most significant effects of rising CO_2 on biodiversity and its interaction with climate change are that it affects how well plants and animals cope with higher temperatures. Although there is uncertainty about the effects of climate change on rice, there is extensive research on rice within this region. However, other crops like wheat, maize, and cotton are not as well studied and do not have the appropriate data to predict their risks accurately. Researchers understand that the impacts of climate change on urban areas required more study on it. This includes understanding vulnerabilities and adaptations in large and medium-sized cities. Also, it is proposed that a more in-depth evaluation of the numerous sectors that affect climate should take place. The current research on climate change tends to focus on individual aspects but lacks a real understanding of how specific causes and impacts relate to one another.

References

Abbas Q, Han J, Adeel A, Ullah R (2019) Dairy production under climatic risks: perception, perceived impacts and adaptations in Punjab, Pakistan. Int J Environ Res Public Health 16(20):4036. https://doi.org/10.3390/IJERPH16204036

Abdallah L, El-Shennawy T (2013) Reducing carbon dioxide emissions from electricity sector using smart electric grid applications. J Eng (U K) 2013:1. https://doi.org/10.1155/2013/845051

Abdul L, Yu T (2020) Resilient urbanization: a systematic review on urban discourse in Pakistan. Urban Sci 4(4):76. https://doi.org/10.3390/URBANSCI4040076

Abid M, Scheffran J, Schneider UA, Ashfaq M (2015) Farmers' perceptions of and adaptation strategies to climate change and their determinants: the case of Punjab province, Pakistan. Earth Syst Dynam 6(1):225–243. https://doi.org/10.5194/esd-6-225-2015

Abid M, Schilling J, Scheffran J, Zulfiqar F (2016a) Climate change vulnerability, adaptation and risk perceptions at farm level in Punjab, Pakistan. Sci Total Environ 547:447–460. https://doi.org/10.1016/j.scitotenv.2015.11.125

Abid M, Schneider UA, Scheffran J (2016b) Adaptation to climate change and its impacts on food productivity and crop income: perspectives of farmers in rural Pakistan. J Rural Stud 47:254–266. https://doi.org/10.1016/j.jrurstud.2016.08.005

Abid M, Hafeez M, Watto MA (2021) Sustainability analysis of irrigation water management in Punjab, Pakistan, pp 133–154. https://doi.org/10.1007/978-3-030-65679-9_8

Abrahão R, García-Garizábal I, Merchán D, Causapé J (2015) Climate change and the water cycle in newly irrigated areas. Environ Monit Assess 187(2):22. https://doi.org/10.1007/S10661-014-4260-1

Aggarwal P, Vyas S, Thornton P, Campbell BM (2019) How much does climate change add to the challenge of feeding the planet this century? Environ Res Lett 14(4). https://doi.org/10.1088/1748-9326/AAFA3E

Ahmad S (2009) Water resources and management in Pakistan n – challenges and future vision

Ahmed S, Mahmood A, Hasan A, Sidhu GAS, Butt MFU (2016) A comparative review of China, India and Pakistan renewable energy sectors and sharing opportunities. Renew Sust Energ Rev 57:216–225. https://doi.org/10.1016/J.RSER.2015.12.191

Ajani A, van der Geest K (2021) Climate change in rural Pakistan: evidence and experiences from a people-centered perspective. Sustain Sci 16(6):1999–2011. https://doi.org/10.1007/S11625-021-01036-4/FIGURES/1

Ali A, Erenstein O (2017a) Assessing farmer use of climate change adaptation practices and impacts on food security and poverty in Pakistan. Clim Risk Manag 16:183–194. https://doi.org/10.1016/J.CRM.2016.12.001

Ali A, Erenstein O (2017b) Climate risk management assessing farmer use of climate change adaptation practices and impacts on food security and poverty in Pakistan. Clim Risk Manag 16:183–194. https://doi.org/10.1016/j.crm.2016.12.001

Ali G, Nitivattananon V (2012) Exercising multidisciplinary approach to assess interrelationship between energy use, carbon emission and land use change in a metropolitan city of Pakistan. Renew Sust Energ Rev 16(1):775–786. https://doi.org/10.1016/j.rser.2011.09.003

Ali S, Liu Y, Ishaq M, Shah T, Abdullah IA, Din IU (2017) Climate change and its impact on the yield of major food crops: evidence from Pakistan. Foods 6(6):39. https://doi.org/10.3390/FOODS6060039

Anderson TR, Hawkins E, Jones PD (2016) CO2, the greenhouse effect and global warming: from the pioneering work of Arrhenius and Callendar to today's Earth System Models. Endeavour 40(3):178–187. https://doi.org/10.1016/J.ENDEAVOUR.2016.07.002

Anjum MN, Cheema MJM, Hashmi MZ u R, Azam M, Afzal A, Ijaz MW (2021) Climate change in the mountains of Pakistan and its water availability implications. In: Watto MA, Mitchell M, Bashir S (eds) Water resources of Pakistan: issues and impacts. Springer, Cham, pp 79–94. https://doi.org/10.1007/978-3-030-65679-9_5

Arif GM, Riaz M, Jamal M, Khattak K, Sathar Z (2021) Population Council Population Council climate, population, and vulnerability in Pakistan: exploring climate, population, and vulnerability in Pakistan: exploring evidence of linkages for adaptation evidence of linkages for adaptation. https://knowledgecommons.popcouncil.org/

Aslam AQ, Ahmad SR, Ahmad I, Hussain Y, Hussain MS (2017) Vulnerability and impact assessment of extreme climatic event: a case study of southern Punjab, Pakistan. Sci Total Environ 580:468–481. https://doi.org/10.1016/j.scitotenv.2016.11.155

Babar MS, Tazyeen S, Khan H, Tsagkaris C, Essar MY, Ahmad S (2021) Impact of climate change on health in Karachi, Pakistan. J Clim Chang Health 2:100013. https://doi.org/10.1016/J.JOCLIM.2021.100013

Bakhsh K, Sana F, Ahmad N (2018) Dengue fever in Punjab, Pakistan: knowledge, perception and adaptation among urban adults. Sci Total Environ 644:1304–1311. https://doi.org/10.1016/j.scitotenv.2018.07.077

Banu S, Hu W, Guo Y, Hurst C, Tong S (2014) Projecting the impact of climate change on dengue transmission in Dhaka, Bangladesh. Environ Int 63:137–142. https://doi.org/10.1016/j.envint.2013.11.002

Basharat M (2019) Water management in the Indus Basin in Pakistan: challenges and opportunities. In: Khan SI, Adams TE (eds) Indus River Basin: water security and sustainability. Elsevier, Amsterdam, pp 375–388. https://doi.org/10.1016/B978-0-12-812782-7.00017-5

Bhatt S, Gething PW, Brady OJ, Messina JP, Farlow AW, Moyes CL, Drake JM, Brownstein JS, Hoen AG, Sankoh O, Myers MF, George DB, Jaenisch T, William Wint GR, Simmons CP, Scott TW, Farrar JJ, Hay SI (2013) The global distribution and burden of dengue. Nature 496(7446):504–507. https://doi.org/10.1038/nature12060

Bhatti MT, Balkhair KS, Masood A, Sarwar S (2016) Optimized shifts in sowing times of field crops to the projected climate changes in an AGRO-climatic zone of Pakistan. Exp Agric 54(2):201–213. https://doi.org/10.1017/s0014479716000156

Braun de Torrez EC, Frock CF, Boone WW, Sovie AR, McCleery RA (2021) Seasick: why value ecosystems severely threatened by sea-level rise? Estuar Coasts 44(4):899–910. https://doi.org/10.1007/S12237-020-00850-W/TABLES/2

Castillo MD, Anenberg SC, Chafe ZA, Huxley R, Johnson LS, Kheirbek I, Malik M, Marshall JD, Naidoo S, Nelson ML, Pendleton N v, Sun Y, van den Broek d'Obrenan H, Kinney PL (2021) Quantifying the health benefits of urban climate mitigation actions: current state of the epidemiological evidence and application in health impact assessments. Front Sustain Cities 3:123. https://doi.org/10.3389/FRSC.2021.768227/BIBTEX

Cavicchioli R, Ripple WJ, Timmis KN, Azam F, Bakken LR, Baylis M, Behrenfeld MJ, Boetius A, Boyd PW, Classen AT, Crowther TW, Danovaro R, Foreman CM, Huisman J, Hutchins DA, Jansson JK, Karl DM, Koskella B, Mark Welch DB et al (2019) Scientists' warning to humanity: microorganisms and climate change. Nat Rev Microbiol 17(9):569–586. https://doi.org/10.1038/s41579-019-0222-5

Cayuela H, Arsovski D, Bonnaire E, Duguet R, Joly P, Besnard A (2016) The impact of severe drought on survival, fecundity, and population persistence in an endangered amphibian. Ecosphere 7(2). https://doi.org/10.1002/ECS2.1246

CCKP (2021) WBG climate change knowledge portal. https://climateknowledgeportal.worldbank.org/country/pakistan/climate-data-historical

Ceglar A, Zampieri M, Toreti A, Dentener F (2019) Observed northward migration of agro-climate zones in Europe will further accelerate under climate change. Earth's Futur 7(9):1088–1101. https://doi.org/10.1029/2019EF001178

Chaudhary QZ, AMGR, MA (2009) Climate change indicators of Pakistan. Technical report no. PMD-22/2009

Cheema AR (2014) Climate change: Pakistan must invest in adaptation. Nature 514(7522):305. https://doi.org/10.1038/514305A

Chen A, Fu Y, Guo H (2005) Fallow agroecosystem dynamics and socioeconomic development in China: two case studies in Xishuangbanna Prefecture, Yunnan Province. Mt Res Dev 25(4):365–371. https://doi.org/10.1659/0276-4741(2005)025

Chen J, Dahlin MJ, Luuppala L, Bickford D, Boljka L, Burns V, Johnson MS (2020) Air pollution and climate change: sustainability, restoration, and ethical implications. In: Meyers RA (ed) Encyclopedia of sustainability science and technology, pp 1–48. https://doi.org/10.1007/978-1-4939-2493-6_1082-1

Cianconi P, Betrò S, Janiri L (2020) The impact of climate change on mental health: a systematic descriptive review. Front Psych 11:74. https://doi.org/10.3389/FPSYT.2020.00074/BIBTEX

Clift PD, Jonell TN (2021) Monsoon controls on sediment generation and transport: mass budget and provenance constraints from the Indus River catchment, delta and submarine fan over tectonic and multimillennial timescales. Earth Sci Rev 220:103682. https://doi.org/10.1016/J.EARSCIREV.2021.103682

Climate Change Ministry (2016) National climate change policy Government of Pakistan Ministry of Climate Change

Dayrit JF, Bintanjoyo L, Andersen LK, Davis MDP (2018) Impact of climate change on dermatological conditions related to flooding: update from the International Society of Dermatology Climate Change Committee. Int J Dermatol 57(8):901–910. https://doi.org/10.1111/ijd.13901

Development Bank Asian (2017) Asian Development Bank sustainable infrastructure for future needs 2 President's Message 4 Board of Directors. https://doi.org/10.22617/FLS189307

Dimri AP, Kumar D, Choudhary A, Maharana P (2018) Future changes over the Himalayas: maximum and minimum temperature. Glob Planet Chang 162:212–234. https://doi.org/10.1016/j.gloplacha.2018.01.015

Eckstein D, Künzel V, Schäfer L, Germanwatch Körperschaft (2021) Global climate risk index 2021 who suffers most extreme weather events? Weather-related loss events in 2019 and 2000–2019

El-Beltagy A, Madkour M (2012) Impact of climate change on arid lands agriculture. Agric Food Secur 1(1):1–12. https://doi.org/10.1186/2048-7010-1-3/FIGURES/6

Enríquez-de-Salamanca Á, Díaz-Sierra R, Martín-Aranda RM, Santos MJ (2017) Environmental impacts of climate change adaptation. Environ Impact Assess Rev 64:87–96. https://doi.org/10.1016/j.eiar.2017.03.005

Ericson JP, Vörösmarty CJ, Dingman SL, Ward LG, Meybeck M (2006) Effective sea-level rise and deltas: causes of change and human dimension implications. Glob Planet Chang 50(1–2):63–82. https://doi.org/10.1016/J.GLOPLACHA.2005.07.004

Escarcha JF, Lassa JA, Palacpac EP, Zander KK (2018) Understanding climate change impacts on water buffalo production through farmers' perceptions. Clim Risk Manag 20:50–63. https://doi.org/10.1016/J.CRM.2018.03.003

Espeland EK, Kettenring KM (2018) Strategic plant choices can alleviate climate change impacts: a review. J Environ Manag 222:316–324. https://doi.org/10.1016/j.jenvman.2018.05.042

FAO (2013) The future of food and agriculture. FAO, Rome

FAO (2015) Climate change and food security: risks and responses. FAO, Rome

Fawzy S, Osman AI, Doran J, Rooney DW (2020) Strategies for mitigation of climate change: a review. Environ Chem Lett 18(6):2069–2094. https://doi.org/10.1007/S10311-020-01059-W

Godde CM, Mason-D'Croz D, Mayberry DE, Thornton PK, Herrero M (2021) Impacts of climate change on the livestock food supply chain; a review of the evidence. Glob Food Sec 28:100488. https://doi.org/10.1016/J.GFS.2020.100488

Gomez-Zavaglia A, Mejuto JC, Simal-Gandara J (2020) Mitigation of emerging implications of climate change on food production systems. Food Res Int (Ottawa, Ont) 134:109256. https://doi.org/10.1016/J.FOODRES.2020.109256

Grases A, Gracia V, García-León M, Lin-Ye J, Sierra JP (2020) Coastal flooding and erosion under a changing climate: implications at a low-lying coast (Ebro delta). Water (Switzerland) 12(2). https://doi.org/10.3390/w12020346

Grote U, Fasse A, Nguyen TT, Erenstein O (2021) Food security and the dynamics of wheat and maize value chains in Africa and Asia. Front Sustain Food Syst 4:317. https://doi.org/10.3389/FSUFS.2020.617009/BIBTEX

Group IE (2012) The global facility for disaster reduction and recovery. https://openknowledge.worldbank.org/handle/10986/23232

Hallegatte S, Vogt-Schilb A, Rozenberg J, Bangalore M, Beaudet C (2020) From poverty to disaster and back: a review of the literature. Econ Disasters Clim Chang 4(1):223–247. https://doi.org/10.1007/S41885-020-00060-5

Hanif U (2017) Socio-economic impacts of heat wave in Sindh. Pakistan J Meteorol 13:87–96

Hewitt K (2005) The Karakoram anomaly? Glacier expansion and the 'Elevation Effect', Karakoram Himalaya, Inner Asia. Mt Res Dev Spec Issue Clim Chang Mt 25(4):332

Hoy A, Hänsel S, Maugeri M (2020) An endless summer: 2018 heat episodes in Europe in the context of secular temperature variability and change. Int J Climatol 40(15):6315–6336. https://doi.org/10.1002/JOC.6582

Huang W, Gao QX, Cao G, Liang Ma ZY, Zhang WD, Chao QC (2016) Effect of urban symbiosis development in China on GHG emissions reduction. Adv Clim Chang Res 7(4):247–252. https://doi.org/10.1016/j.accre.2016.12.003

Hughes L (2003) Climate change and Australia: trends, projections and impacts. Austral Ecol 28(4):423–443. https://doi.org/10.1046/J.1442-9993.2003.01300.X

Hussain M, Mumtaz S (2014) Climate change and managing water crisis: Pakistan's perspective. Rev Environ Health 29(1–2):71–77. https://doi.org/10.1515/reveh-2014-0020

Hussain A, Agrawal NK, Leikanger I (2016) Action for adaptation: bringing climate change science to policy makers—a synthesis report of a conference held in Islamabad on 23–25 July 2015. Food Secur 8(1):285–289. https://doi.org/10.1007/s12571-015-0529-7

Hussain M, Liu G, Yousaf B, Ahmed R, Uzma F, Ali MU, Ullah H, Butt AR (2018) Regional and sectoral assessment on climate-change in Pakistan: social norms and indigenous perceptions on climate-change adaptation and mitigation in relation to global context. J Clean Prod 200:791–808. https://doi.org/10.1016/j.jclepro.2018.07.272

Hussain M, Butt AR, Uzma F, Ahmed R, Islam T, Yousaf B (2019a) A comprehensive review of sectorial contribution towards greenhouse gas emissions and progress in carbon capture and storage in Pakistan. Greenhouse Gases Sci Technol 9(4):617–636. https://doi.org/10.1002/ghg.1890

Hussain M, Butt AR, Uzma F, Ahmed R, Rehman A, Ali MU, Ullah H, Yousaf B (2019b) Divisional disparities on climate change adaptation and mitigation in Punjab, Pakistan: local perceptions, vulnerabilities, and policy implications. Environ Sci Pollut Res 26(30):31491–31507. https://doi.org/10.1007/s11356-019-06262-z

Hussain M, Butt AR, Uzma F, Ahmed R, Irshad S, Rehman A, Yousaf B (2020) A comprehensive review of climate change impacts, adaptation, and mitigation on environmental and natural calamities in Pakistan. Environ Monit Assess 192(1):1–20. https://doi.org/10.1007/S10661-019-7956-4/FIGURES/3

INFORM (2020) Index for risk management. Inter-agency standing committee reference group on risk, early warning and preparedness. http://www.inform-index.org/

IPCC (2021) Climate change widespread, rapid, and intensifying. https://www.ipcc.ch/2021/08/09/ar6-wg1-20210809-pr/

Iqbal M (2009) Climate change aspersions on food security of Pakistan. Sci Vis 15(1).

Islam MS, Kieu E (2020) Tackling regional climate change impacts and food security issues: a critical analysis across ASEAN, PIF, and SAARC. Sustainability 12(3):883. https://doi.org/10.3390/SU12030883

Janjua AA, Aslam M, Sultana N, Batool Z (2021) Identification of climate induced optimal rice yield and vulnerable districts rankings of the Punjab, Pakistan. Sci Rep 11(1):23393. https://doi.org/10.1038/S41598-021-02691-4

Kalhoro (2016a) The impact of sea level rise on Pakistan's coastal zones-in a climate change scenario. https://doi.org/10.13140/2.1.2353.9203

Kalhoro NA (2016b) Vulnerability of the indus river delta of the North Arabian Sea, Pakistan. GlobalNEST Int J. https://www.researchgate.net/publication/308365689_Vulnerability_of_the_indus_river_delta_of_the_North_Arabian_Sea_Pakistan

Kara F, Yucel I (2015) Climate change effects on extreme flows of water supply area in Istanbul: utility of regional climate models and downscaling method. Environ Monit Assess 187(9):580. https://doi.org/10.1007/s10661-015-4808-8

Khan AN, Khan SN (2015) Drought risk and reduction approaches in Pakistan, pp 131–143. https://doi.org/10.1007/978-4-431-55369-4_7

Khan B, Iqbal MJ, Yosufzai MAK (2011) Flood risk assessment of river Indus of Pakistan. Arab J Geosci 4(1–2):115–122. https://doi.org/10.1007/S12517-009-0110-9

Khan MA, Khan JA, Ali Z, Ahmad I, Ahmad MN (2016) The challenge of climate change and policy response in Pakistan. Environ Earth Sci 75(5):1–16. https://doi.org/10.1007/S12665-015-5127-7

Khan NA, Gao Q, Abid M (2020) Public institutions' capacities regarding climate change adaptation and risk management support in agriculture: the case of Punjab Province, Pakistan. Sci Rep 10(1):1–12. https://doi.org/10.1038/s41598-020-71011-z

Kweku D, Bismark O, Maxwell A, Desmond K, Danso K, Oti-Mensah E, Quachie A, Adormaa B (2018) Greenhouse effect: greenhouse gases and their impact on global warming. J Sci Res Rep 17(6):1–9. https://doi.org/10.9734/JSRR/2017/39630

Lake IR, Hooper L, Abdelhamid A, Bentham G, Boxall ABA, Draper A, Fairweather-Tait S, Hulme M, Hunter PR, Nichols G, Waldron KW (2012) Climate change and food security: health impacts in developed countries. Environ Health Perspect 120(11):1520–1526. https://doi.org/10.1289/EHP.1104424

Leonelli G, Coppola A, Salvatore MC, Baroni C, Battipaglia G, Gentilesca T, Ripullone F, Borghetti M, Conte E, Tognetti R, Marchetti M, Lombardi F, Brunetti M, Maugeri M, Pelfini M, Cherubini P, Provenzale A, Maggi V (2017) Climate signals in a multispecies tree-ring network from central and southern Italy and reconstruction of the late summer temperatures since the early 1700s. Clim Past 13(11):1451–1471. https://doi.org/10.5194/CP-13-1451-2017

Li D, Yap KS (2011) Climate change and its impact on food and nutrition security and food safety in China. World Rev Nutr Diet 102:175–182. https://doi.org/10.1159/000327807

Lin B, Ahmad I (2016) Energy substitution effect on transport sector of Pakistan based on translog production function. Renew Sust Energ Rev 56:1182–1193. https://doi.org/10.1016/j.rser.2015.12.012

Lin B, Ahmad I (2017) Analysis of energy related carbon dioxide emission and reduction potential in Pakistan. J Clean Prod 143:278–287. https://doi.org/10.1016/j.jclepro.2016.12.113

Lipczynska-Kochany E (2018) Effect of climate change on humic substances and associated impacts on the quality of surface water and groundwater: a review. Sci Total Environ 640–641:1548–1565. https://doi.org/10.1016/j.scitotenv.2018.05.376

Ludwig F, Terwisscha Van Scheltinga C, Verhagen J, Kruijt B, van Ierland E, Dellink R, de Bruin K, de Bruin K, Kabat P, Goossens Y (2004) Policy department economic and scientific policy climate change impacts on developing countries-EU accountability Co-operative Programme on Water and Climate (CPWC). www.waterandclimate.org

Manisalidis I, Stavropoulou E, Stavropoulos A, Bezirtzoglou E (2020) Environmental and health impacts of air pollution: a review. Front Public Health 8:14. https://doi.org/10.3389/FPUBH.2020.00014/BIBTEX

Mannig B, Pollinger F, Gafurov A, Vorogushyn S, Unger-Shayesteh K (2017) Impacts of climate change in Central Asia. In: Encyclopedia of the anthropocene, pp 1–5, 195–203. https://doi.org/10.1016/B978-0-12-809665-9.09751-2

Masood T, Khan A, Rabbani MM (2007) Sea level monitoring and study of sea level variations along Pakistan coast: a component of integrated coastal zone management

Mekonnen MM, Hoekstra AY (2016) Four billion people experience water scarcity. Sci Adv 2(2):1–7. https://doi.org/10.1126/sciadv.1500323

Miyan MA (2015) Droughts in Asian least developed countries: vulnerability and sustainability. Weather Clim Extrem 7:8–23. https://doi.org/10.1016/J.WACE.2014.06.003

Mumtaz M, Ali HS (2019) Adaptive governance and sub-national climate change policy: a comparative analysis of Khyber Pukhtunkhawa and Punjab provinces in Pakistan. Complex Gov Netw 5(1):81. https://doi.org/10.20377/CGN-68

Mumtaz M, Antonio J, de Oliveira P, Ali SH (2019) Climate change impacts and adaptation in agricultural sector: the case of local responses in Punjab, Pakistan. Clim Chang Agric. https://doi.org/10.5772/INTECHOPEN.83553

Myers SS, Smith MR, Guth S, Golden CD, Vaitla B, Mueller ND, Dangour AD, Huybers P (2017) Climate change and global food systems: potential impacts on food security and undernutrition. 38:259–277. https://doi.org/10.1146/ANNUREV-PUBLHEALTH-031816-044356

Naeem Nawaz SM, Alvi S (2018) Energy security for socio-economic and environmental sustainability in Pakistan. Heliyon 4(10):e00854. https://doi.org/10.1016/J.HELIYON.2018.E00854

Neil Adger W, Pulhin JM, Barnett J, Dabelko GD, Hovelsrud GK, Levy M, Oswald Spring Ú, Vogel CH, Adams H, Hodbod J, Kent S, Tarazona M, Aldunce P, Leichenko R, Pulhin J, Barnett J, Dabelko G, Hovelsrud G, Levy M, … Mastrandrea P (2014) 12 — human security

Noor R, Maqsood A, Inam A (2021a) Performance evaluation of various models for the assessment of reference evapotranspiration in arid and semi-arid zones of Pakistan. CEWRE/ICHWR/, pp 41–47. www.cewre.edu.pk

Noor R, Inam MA, Abbas Q, Asif M (2021b) A participatory socioeconomic environmental modelling framework for groundwater management, pp 119–124. CEWRI. www.cewre.edu.pk

Noor R, Inam A, Zahra SM, Shoaib M, Riaz R, Sarwar A, Asif M, Ahmad S (2022) A methodological framework for modeling sustainability visions: A case study of groundwater management in Faizpur distributary, Pakistan. Agric Water Manag 271. https://doi.org/10.1016/J.AGWAT.2022.107822

Olsen L, International Labour Office (2009) The employment effects of climate change and climate change responses: a role for International Labour Standards? ILO

Orimoloye IR, Olusola AO, Belle JA et al (2022) Drought disaster monitoring and land use dynamics: identification of drought drivers using regression-based algorithms. Nat Hazards 112:1085. https://doi.org/10.1007/s11069-022-05219-9

Pande CB, Moharir KN, Khadri SFR (2021a) Assessment of land-use and land-cover changes in Pangari watershed area (MS), India, based on the remote sensing and GIS techniques. Appl Water Sci 11:96. https://doi.org/10.1007/s13201-021-01425-1

Pande CB, Moharir KN, Singh SK, Varade AM, Ahmed Elbeltagie SFR, Khadri PC (2021b) Estimation of crop and forest biomass resources in a semi-arid region using satellite data and GIS. J Saudi Soc Agric Sci 20(5):302–311

Panneerselvam B, Muniraj K, Pande C et al (2021) Geochemical evaluation and human health risk assessment of nitrate-contaminated groundwater in an industrial area of South India. Environ Sci Pollut Res. https://doi.org/10.1007/s11356-021-17281-0

Panneerselvam B, Muniraj K, Duraisamy K et al (2022) An integrated approach to explore the suitability of nitrate-contaminated groundwater for drinking purposes in a semiarid region of India. Environ Geochem Health. https://doi.org/10.1007/s10653-022-01237-5

Parry J-E (2016) Review of current and planned adaptation action in Pakistan. www.idrc.ca/cariaa

Perera KARS, de Silva KHWL, Amarasinghe MD (2018) Potential impact of predicted sea level rise on carbon sink function of mangrove ecosystems with special reference to Negombo estuary, Sri Lanka. Glob Planet Chang 161:162–171. https://doi.org/10.1016/j.gloplacha.2017.12.016

Podger GM, Ahmad MUD, Yu Y, Stewart JP, Ali Shah SMM, Khero ZI (2021) Development of the indus river system model to evaluate reservoir sedimentation impacts on water security in Pakistan. Water (Switzerland) 13(7). https://doi.org/10.3390/W13070895

Ponting J, Kelly TJ, Verhoef A, Watts MJ, Sizmur T (2021) The impact of increased flooding occurrence on the mobility of potentially toxic elements in floodplain soil – a review. Sci Total Environ 754:142040. https://doi.org/10.1016/J.SCITOTENV.2020.142040

Poveda G, Espinoza JC, Zuluaga MD, Solman SA, Garreaud R, van Oevelen PJ (2020) High impact weather events in the Andes. Front Earth Sci 8:162. https://doi.org/10.3389/FEART.2020.00162/BIBTEX

Qureshi AS (2011) Water management in the Indus basin in Pakistan: challenges and opportunities. Mt Res Dev 31(3):252–260. https://doi.org/10.1659/MRD-JOURNAL-D-11-00019.1

Qureshi AS, Perry C (2021) Article managing water and salt for sustainable agriculture in the indus basin of Pakistan. Sustainability (Switzerland) 13(9). https://doi.org/10.3390/su13095303

Radecki-Pawlik A, Laszek W, Plesiński K, Khan Lashari B (2015) Dominant discharge in the Indus river from downstream of the Kotri barrage dam. Acta Sci Pol Formatio Circum 13(4):225–232. https://doi.org/10.15576/ASP.FC/2014.13.4.225

Rauf S, Bakhsh K, Abbas A, Hassan S, Ali A, Kächele H (2017) How hard they hit? Perception, adaptation and public health implications of heat waves in urban and peri-urban Pakistan. Environ Sci Pollut Res 24(11):10630–10639. https://doi.org/10.1007/s11356-017-8756-4

Rehman A, Jingdong L, Shahzad B, Chandio AA, Hussain I, Nabi G, Iqbal MS (2015) Economic perspectives of major field crops of Pakistan: an empirical study. Pac Sci Rev B Humanit Soc Sci 1(3):145–158. https://doi.org/10.1016/J.PSRB.2016.09.002

Rojas-Downing MM, Nejadhashemi AP, Harrigan T, Woznicki SA (2017) Climate change and livestock: impacts, adaptation, and mitigation. Clim Risk Manag 16:145–163. https://doi.org/10.1016/J.CRM.2017.02.001

Saboor A, Authors L, Tiwari PC, Hussain A, Chettri GB, Mazhar A, Ahmad T, Khadka MS (2019) Food and nutrition security in the Hindu Kush Himalaya: unique challenges and niche opportunities. In The Hindu Kush Himalaya assessment, pp 301–338. https://doi.org/10.1007/978-3-319-92288-1_9

Schwerdtle P, Bowen K, McMichael C (2017) The health impacts of climate-related migration. BMC Med 16(1):1–7. https://doi.org/10.1186/S12916-017-0981-7/FIGURES/1

Shaffril HAM, Krauss SE, Samsuddin SF (2018) A systematic review on Asian's farmers' adaptation practices towards climate change. Sci Total Environ 644:683–695. https://doi.org/10.1016/j.scitotenv.2018.06.349

Shah SMH, Mustaffa Z, Teo FY, Imam MAH, Yusof KW, Al-Qadami EHH (2020) A review of the flood hazard and risk management in the South Asian Region, particularly Pakistan. Sci Afr 10:e00651. https://doi.org/10.1016/J.SCIAF.2020.E00651

Shahid M, Rahman KU, Haider S et al (2021) Quantitative assessment of regional land use and climate change impact on runoff across Gilgit watershed. Environ Earth Sci 80:743. https://doi.org/10.1007/s12665-021-10032-x

Sheikh MA (2010) Energy and renewable energy scenario of Pakistan. Renew Sust Energ Rev 14(1):354–363. https://doi.org/10.1016/j.rser.2009.07.037

Solomon S (Atmospheric chemist), Intergovernmental Panel on Climate Change, & Intergovernmental Panel on Climate Change. Working Group I (2007) Climate change 2007: the physical science basis: contribution of Working Group I to the Fourth Assessment Report of the Intergovernmental Panel on Climate Change. Cambridge University Press

Sultana H, Ali N, Iqbal MM, Khan AM (2009) Vulnerability and adaptability of wheat production in different climatic zones of Pakistan under climate change scenarios. Clim Chang 94(1–2):123–142. https://doi.org/10.1007/s10584-009-9559-5

Syed A, Raza T, Bhatti TT, Eash NS (2022) Climate impacts on the agricultural sector of Pakistan: risks and solutions. Environ Chall 6:100433. https://doi.org/10.1016/J.ENVC.2021.100433

Syvitski JPM, Kettner AJ, Overeem I, Hutton EWH, Hannon MT, Brakenridge GR, Day J, Vörösmarty C, Saito Y, Giosan L, Nicholls RJ (2009) Sinking deltas due to human activities. Undefined 2(10):681–686. https://doi.org/10.1038/NGEO629

Tessler ZD, Vörösmarty CJ, Grossberg M, Gladkova I, Aizenman H, Syvitski JPM, Foufoula-Georgiou E (2015) Profiling risk and sustainability in coastal deltas of the world. Science 349(6248):638–643. https://doi.org/10.1126/SCIENCE.AAB3574

Tirado MC, Clarke R, Jaykus LA, McQuatters-Gollop A, Frank JM (2010) Climate change and food safety: a review. Food Res Int 43(7):1745–1765. https://doi.org/10.1016/j.foodres.2010.07.003

Udeh BA, Kidak R (2019) The excessive use of fossil fuel and its impact to climate change in Africa. Curr J Appl Sci Technol 32(5):1–4. https://doi.org/10.9734/CJAST/2019/41680

Ullah W (2016) Climate change vulnerability of Pakistan towards natural disasters: a review. Int J Environ Prot Pol 4(5):126. https://doi.org/10.11648/J.IJEPP.20160405.13

Ullah W, Nihei T, Nafees M, Zaman R, Ali M (2018) Understanding climate change vulnerability, adaptation and risk perceptions at household level in Khyber Pakhtunkhwa, Pakistan. Int J Clim Chang Strateg Manag 10(3):359–378. https://doi.org/10.1108/IJCCSM-02-2017-0038

Ullah W, Nafees M, Khurshid M, Nihei T (2019) Assessing farmers' perspectives on climate change for effective farm-level adaptation measures in Khyber Pakhtunkhwa, Pakistan. Environ Monit Assess 191(9):547. https://doi.org/10.1007/S10661-019-7651-5

van den Broeke MR, Enderlin EM, Howat IM, Kuipers Munneke P, Noël BPY, Jan Van De Berg W, van Meijgaard E, Wouters B (2016) On the recent contribution of the Greenland Ice Sheet to sea level change. Cryosphere 10(5):1933–1946. https://doi.org/10.5194/tc-10-1933-2016

van Pelt JC (2018) Climate change in context: stress, shock, and the crucible of livingkind. Zygon 53(2):462–495. https://doi.org/10.1111/ZYGO.12418

Watto MA, Mitchell M, Akhtar T (2021) Pakistan's water resources: overview and challenges, pp 1–12. https://doi.org/10.1007/978-3-030-65679-9_1

Weiskopf SR, Rubenstein MA, Crozier LG, Gaichas S, Griffis R, Halofsky JE, Hyde KJW, Morelli TL, Morisette JT, Muñoz RC, Pershing AJ, Peterson DL, Poudel R, Staudinger MD, Sutton-Grier AE, Thompson L, Vose J, Weltzin JF, Whyte KP (2020) Climate change effects on biodiversity, ecosystems, ecosystem services, and natural resource management in the United States. Sci Total Environ 733:137782. https://doi.org/10.1016/J.SCITOTENV.2020.137782

Wescoat JL, Muhammad A, Siddiqi A (2021) Pakistan's water resources: from retrospect to prospect, pp 13–36. https://doi.org/10.1007/978-3-030-65679-9_2

Wiedmann T, Lenzen M, Keyßer LT, Steinberger JK (2020) Scientists' warning on affluence. Nat Commun 11(1):1–10. https://doi.org/10.1038/s41467-020-16941-y

Yousaf B, Liu G, Abbas Q, Wang R, Ubaid Ali M, Ullah H, Liu R, Zhou C (2017) Systematic investigation on combustion characteristics and emission-reduction mechanism of potentially toxic elements in biomass- and biochar-coal co-combustion systems. Appl Energy 208:142–157. https://doi.org/10.1016/j.apenergy.2017.10.059

Yue XL, Gao QX (2018) Contributions of natural systems and human activity to greenhouse gas emissions. Adv Clim Chang Res 9(4):243–252. https://doi.org/10.1016/J.ACCRE.2018.12.003

Chapter 11
Future Hydroclimatic Variability Projections Using Combined Statistical Downscaling Approach and Rainfall-Runoff Model: Case of Sebaou River Basin (Northern Algeria)

Bilel Zerouali, Mohamed Chettih, Zak Abda, and Mohamed Mesbah

Abstract Due to its location in the Mediterranean basin, Algeria is one of the most countries vulnerable to the effects of climate change. The aim of this study is to assess future flow rate projections of Sebaou basin (Northern Algeria), using the coupling of statistical downscaling approach (SDSM) based on the general circulation model Hadley Centre Coupled Model version 3 (GCM-HadCM3) of the Royaume-Uni with an anthropogenic forcing SRES A2a (pessimist) and SRES B2a (optimistic) and GR2M model for rainfall-runoff transformation. The use of GR2M rainfall-runoff model has been able to control the hydrological functioning of the basin with very satisfactory performance values expressed by the Nash values over 80% for most subbasins, except for the degradation the Nash coefficient after the commissioning of the Taksebt dam in the Oued Aissi subbasin after 2001. The combining approach showed, on one hand, a decrease in rainfall ranging from 18% to

B. Zerouali (✉)
Vegetal Chemistry-Water-Energy Research Laboratory, Faculty of Civil Engineering and Architecture, Department of Hydraulic Hassiba Benbouali, University of Chlef, Chlef, Algeria

Research Laboratory of Water Resources, Soil and Environment, Department of Civil Engineering, Faculty of Civil Engineering and Architecture, Amar Telidji University, Laghouat, Algeria
e-mail: b.zerouali@univ-chlef.dz

M. Chettih · Z. Abda
Research Laboratory of Water Resources, Soil and Environment, Department of Civil Engineering, Faculty of Civil Engineering and Architecture, Amar Telidji University, Laghouat, Algeria

M. Mesbah
Earth Sciences Faculty, University of Science and Technology Houari Boumediene, Bab Ezzouar, Algeria

C. B. Pande et al. (eds.), *Climate Change Impacts on Natural Resources, Ecosystems and Agricultural Systems*, Springer Climate,
https://doi.org/10.1007/978-3-031-19059-9_11

14% and that the maximum, average, and minimum temperatures could continue to increase with a maximum of 1.1–0.65 °C, 1.1–1.25 °C, and 2.7–3.4 °C, respectively, for the H3A2 and H3B2 emission scenarios until the long-term horizon 2080. On the other hand, the model indicated that these climatic changes have an effect on decreases in the basin's water resources and that the 2050 and 2080 horizons are the most deficient with a decrease in flows estimated from −35% to −49% for A2 and from −45 to −57% for B2 scenarios, respectively, which represents approximately 500–300 Hm^3 by the end of the twenty-first century.

Keywords Rainfall · Temperatures · Flow rates · SDSM · HadCM3 · GR2M · Algeria

Introduction

Throughout the last century, water resources and climatic variables have been significantly influenced by climate change (Elbeltagi et al. 2022d; Duan et al. 2017; Meenu et al. 2013; Kanber et al. 2019; Almazroui et al. 2020). Increased levels and concentration of greenhouse gases of anthropogenic direct, indirect, or natural origin in the terrestrial atmosphere could change the local climate at particular basins and area around the world (Meenu et al. 2013). According to the report of the Intergovernmental Panel on Climate Change (IPCC 2007), the climate is changing, and that cannot be associated and explained by natural variability (Yilmaz and Imteaz 2011). Most of the studies carried out in the context of water resource show that the projections of future climate change could significantly affect the water cycle components and socioeconomic sectors of the basins around the world (Zerouali et al. 2021a, b; Bucak et al. 2017; Arnell 2004; Ragab and Prudhomme 2002). According to Somot et al. 2008, the Mediterranean basin will experience a significant rise in temperatures during the twenty-first century. For this, the downward and upward trends respectively for rainfall and temperatures will lead to the form of extreme weather phenomena. At regional scale in North Africa, the study of Tramblay et al. (2018) documented the climate change analysis and its impacts on water resources. The results indicate a reduction in most regions of northern Algeria and Morocco, but there is superior uncertainty for Tunisia, as some regional circulation models shows insignificant increase. On the contrary, all the models indicate high-temperature projections, and this change in temperature is very similar over the region with a decrease in water availability is foreseen for all basins in all scenarios. In northern Algeria, El Meddahi et al. (2014) observed significant changes in the climatic conditions, which led to a decline in annual rainfall ranging between 14% and 32%, an increase in mean temperatures by 0.9 °C compared with the reference period (1961–90). Which induced a flow deficit of 20–25% for 2050 in both scenarios "lows and high." Recently, as part of water resources management in direct relation to the water demand of populations and the forecast of their evolution, several hydrological models have been proposed, such as the following:

deterministic, probabilistic, event-driven, global or distributed, based physics, and those with reservoirs destined to comprehend the internal karst processes and physical mechanisms that manage the water cycle and incorporate the physical laws of water circulation as well as the components linked with the watershed characteristic (Meenu et al. 2013). According to the literature, among the models most used in the modeling of the rainfall-runoff transformation, we can cite the rural engineering models with daily and monthly steps (GR4J, GR2M, and GR3M), the SHYPRE method, artificial neural networks (ANN) with its hybridizations, HEC-HMS, IHACRES, and SWAT (Kouadri et al. 2021; Elbeltagi et al. 2022a, b; Pande et al. 2022). The difficulty of finding a unified classification stems from the fact that the great diversity of approaches leads to no less great diversity in the characteristics of the models (Perrin 2000). Currently, there are several tools and software to reproduce climate time series and obtain higher resolution climate change scenarios from a lower resolution general circulation model (GCM) for a given region (Wang et al. 2020; Khorshidi et al. 2019), like stochastic generators: automated statistical downscaling (ASD), statistical downscaling model (SDSM), and Long-Ashton Research Station Weather Generator (LARS-WG) (Cherkaoui 2012; Ouyang et al. 2019; Bayatvarkeshi et al. 2020). For example, the MAGICC/SCENGEN software is a coupled gas/climate cycle model, where the MAGICC is a space climate change scenario generator (SCENGEN); each generator has its own advantages and disadvantages (Galdies and Lau 2020). In the Subarnarekha River basin (India), the climate change impact was simulated by Sambaran et al. (2015) and Elbeltagi et al. (2022c) based on the regional climate projections model (RCM-PRECIS) for the A1B scenario. The outputs of this projection are inserted in HEC-HMS hydrological model. The results revealed a decrease in rainfall and flow during the period June to September for half of the coming years, while potential evapotranspiration showed an increase from February to June. Raghavan et al. (2012) used the outputs of the RCM obtained from the Weather Research and Forecasting (WRF) as input series in the SWAT hydrological model for the future assessment of flows in the Bas Mekong basin in Vietnam, where MCG-ECHAM5 T63 has been reduced under the IPCC-A2 emission scenario. Results show that flow rates are expected to increase. Hassan et al. (2015) used a coupled model to determine current and future scenarios (HadCM3-A2 and HadCM3-B2) of climate change over the northern region of Peninsular Malaysia using SDSM and ANN models to assess their future impacts on hydrology (precipitation, flow, and evaporation) using HACRES. The results show that daily precipitation and temperature will increase by 2.23 mm and 2.02 °C, respectively, during the 2080s and a maximum increase in daily flows of 52 m^3/s. the study concluded that the ANN model was unable to provide an identical trend for the annual runoff series. The water resources sector in Algeria has 94 dams and five others under construction spread across the national territory, which are under the authority of the Ministry of Water Resources (MRE). The sector's forecasts for 2030 are 139 dams. Despite that, studies carried out in the context of assessing climate change and its impacts on the protection and management of these storage facilities are not sufficient. Among the works that are carried out, we cite the research of Bouabdelli et al. (2020) and Chourghal et al. (2016). In this study,

coupling statistical downscaling approach (SDSM) based on GCM-HadCM3 scenarios and GR2M model for rainfall-runoff transformation was used to assess future climate variability impacts on flow rates of Oued Sebaou basin (Northern Algeria).

Study Area

The watershed of Sebaou River, its position between latitudes North 36°30 and 37°00 and longitudes East 03°30 and 04°30, is part of coastal watersheds Algiers code (02) according to the nomenclature of the Algerian National Agency of Water Resources (Fig. 11.1). It extends over an area of 2500 km^2 limited in the north by the Mediterranean coastal, in the south by the Djurdjura mountain chain (Wilaya of Bouira), in the East by the massif Akfadou and Beni-Ghobri (Wilaya of Bejaia), and in the west by the mountains of Sidi Ali and Jebel Bounab Bouberak (Wilaya of Boumerdes). The study area is dominated by the Mediterranean climate which characterizes by warm to hot dry summers and mild to cool wet winters and are classified in the subhumid bioclimatological stage with alternation of two seasons during the year, a wet season that starts in October and ends at the end of May (Zerouali et al. 2020), and, moreover, a dry season that begins at the end of May and ends at September. The intra-annual average of precipitation in Sebaou River basin is between 720 and 1200 mm year^{-1} (Fig. 11.1).

Materials and Methods

The rainfall, temperatures, and runoff series database collected as part of the study are taken from the Algerian National Agency of Water Resources (ANRH).

Global Climate Models (GCM)

In climatology, the choice and availability of data for the future projection of meteorological variables for a hydrological system is one of the essential elements for assessing and studying probably future water resources availability. Several models of general circulation models are proposed, which attempt to illustrate the components of the climate system by computing the properties of the Earth's atmosphere and their evolution over time. In this study, the National Centers for Environmental Prediction (NCEP) dataset was used. This center is based on the support and operational execution of numerical analyses of forecasting models and prepares NCEP data for dissemination. All of these data contain 41 years of forecast data daily observed, normalized over the entire period (1961–90) on a spatial scale of

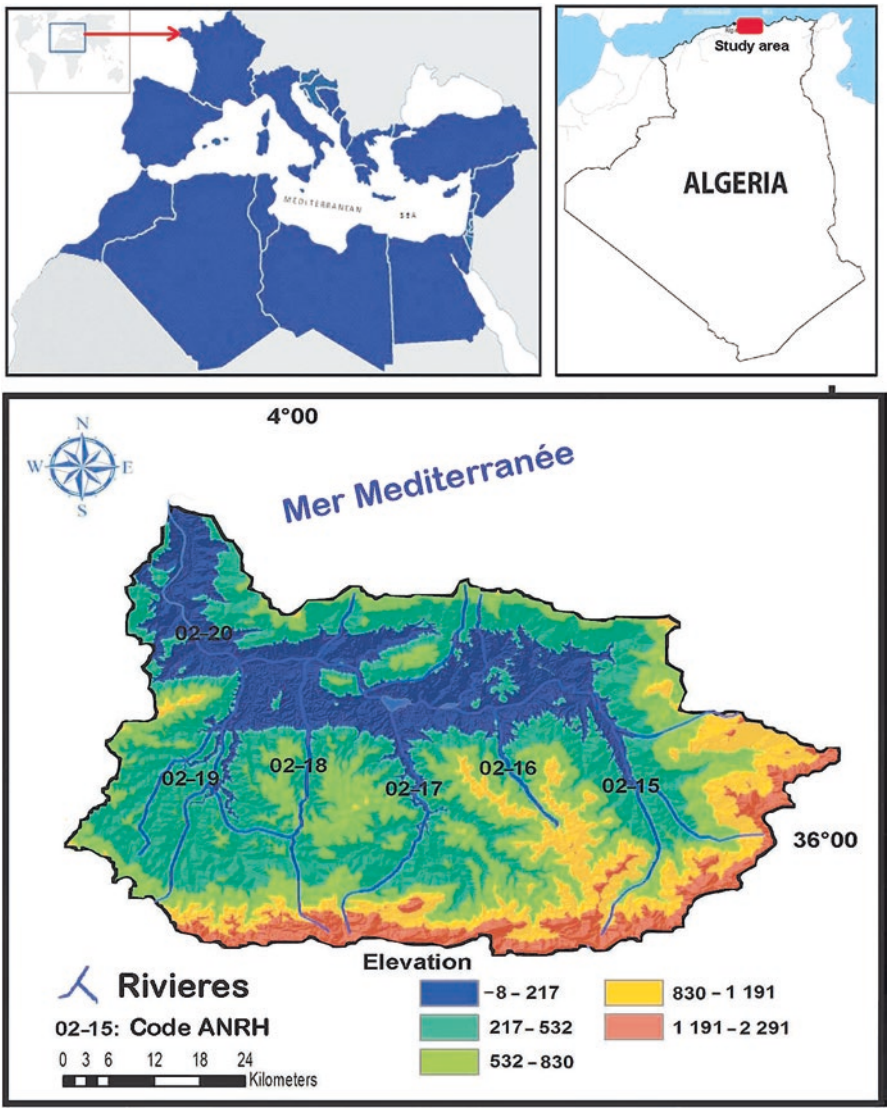

Fig. 11.1 Location map of study area

2.5° × 3.75 ° and which includes 26 atmospheric variables (see Yang et al. 2017; Sigdel and Ma 2016). These variables are used to examine the relationships observed between atmospheric and surface variables at a regional scale on a continental scale within the limits of historical meteorological data (Hassan et al. 2015).

According to Kaas and Frich (1995), these relationships are important for producing reduced climate scenarios from the outputs of other results of a climate model.

For this study, we used the climate model HadCM3 of the atmosphere-ocean global circulation model (AOGCM) type. According to Wilby and Dawson (2007), the recommended model (HadCM3) meets the following requirements:

1. Explains the atmosphere-ocean couple in three dimensions.
2. The model has been validated and published in one of the scientific journals indexed and subject to peer review.
3. The stability of the model has been verified by control simulations over several centuries.
4. AOGCM-HadCM3 is one of the models contributed to the intermodel comparison project (CMIP).
5. The model has small-scale spatial resolution of at least 4° in latitude.

According to the IPCC Data Distribution Center, the data from MCG-HadCM3 are available with free access on the website of "Canadian climate data and scenarios" (http://ccds-dscc.ec.gc.ca/index.php?page=pred-hadcm3&lang=fr).

The experiments in the HadCM3 module were carried out at au Hadley Centre for Climate Prediction and Research du Royaume-Uni for the third evaluation report, which is the successor to the HadCM2 used in the second evaluation report. The HadCM3 has a spatial resolution of 2.5 × 3.75 ° (latitude–longitude). It contains a rectangular mesh of 96 (longitude) × 73 (latitude) grid points, which reduces the surface spatial resolution from 417 km × 278 km to approximately 295 × 278 km (45° North and South (comparable with a spectral resolution of T42)). The NCEP data were also interpolated on the same grid as the HadCM3 before normalization. The HadCM3 was developed and proposed to the world of climatology by Pope et al. (2000).

Presentation of the Statistical Downscaling Model "SDSM Tool"

Statistical data reduction model 4.2 (SDSM 4.2) describes a decision support tool to assess the local impacts of climate change using a robust statistical disaggregation data technique. The SDSM facilitates the rapid development of multiple scenarios, with low cost and at a single site and with daily surface climate variables in the current framework and future climate forcing. In addition, the tool performs auxiliary data quality transformation and control tasks: predictor variable pretest, automatic model calibration, basic diagnostic tests, statistical analysis, and graphical representation of climate data (Wilby and Dawson 2007). The main stages of statistical disaggregation are summarized in the paper of Wilby and Dawson (2007).

Rainfall-Runoff Relationship Simulation Using the GR2M Model

Between the 1980s and 1990s, new versions of rainfall-runoff transformation models have been developed by the "Cemagref," with objectives of application on hydrology and water resources management, named the rural engineering models (GR). The rural engineering model (GR2M) is one of them, which is a global monthly rainfall-runoff model that includes two parameters.

Presentation of the GR2M Model

Several versions have been proposed successively to increase the performance and accuracy of the GR2M model; among them are the contributions of Mouelhi (2003) and Mouelhi et al. (2006). According to Perrin et al. (2007), the improved version by Mouelhi et al. (2006) implemented on MATLAB seems to be the most efficient. The structure of GR2M is one of the conceptual reservoir models with a procedure for monitoring the state of humidity in the basin, which appear to be the better manner to take into account prior conditions and ensure continuous operation of the model. The concept of the structure of the GR2M combines a production tank and a routing tank, as well as an opening to the outside other than the atmospheric environment. These functions make the model more flexible to simulate the hydrological behavior of the watershed (Mouelhi et al. 2006).

Assessment of the Performance, Robustness, and Uncertainties of the Model

The linear correlation coefficient is defined by

$$R^2 = \frac{\operatorname{cov}(x;y)}{\delta(y)\,\delta(y)} \tag{11.1}$$

– The root-mean-squared error

$$\mathrm{RMSE} = \sqrt{\frac{\sum_{t=1}^{n}\left(V_{obs} - V_{sim}\right)^2}{n}} \tag{11.2}$$

– Nash–Sutcliffe

$$\text{Nash} = 1 - \frac{\sum_{t=1}^{n} \left(V_{obs} - V_{sim}\right)^2}{\sum_{t=1}^{n} \left(V_{obs} - V_{avr}\right)^2} \tag{11.3}$$

where n – observation number

V_{obs} – value observed in the original series.
V_{sim} – value simulated by the model.
V_{avr} – average of the values observed in the original series.

The criterion used is the criterion of least squares of errors, presented in the dimensionless form of the bounded Nash criterion (Nash and Sutcliffe 1970). Nash criterion is one of the best performing criteria (Perrin et al. 2007) and is universally used in hydrology. The calibration operation consists of finding values of the model parameters, which minimizes the modeling error over the period, considered (Abda et al. 2022). The model is considered efficient when the modeled flows approximately equal to the observed flows, which is to say when the value of the Nash-Sutcliffe criterion is near to 100% and it can be considered satisfactory, if the performance is greater than or equal to 60% (Kouamė et al. 2013.) The difference between the observed flow in site and the modeled flow is a frequently used method for calculating errors and is no longer acceptable for better and practical use, as in the Nash criterion. The same absolute error can be minor, especially during hydrological extremes for peak flood flows and low-water flows (El Meddahi 2016). Therefore, the ratio observed flow and simulated flow is more adequate and consistent to calculate the errors. The expression of uncertainty (I) is represented by Eq. (11.4):

$$I = Q_{\text{observed}} / Q_{\text{simulated}} \tag{11.4}$$

where (Q) is the flow.

Calibration therefore consists in selecting on the chosen a set of model parameters, simulates the watershed hydrological behavior in the better possible way (Madsen 2000). The calibration phase in the rainfall-runoff transformation models requires the following conditions:

– A hydroclimatic series representative of the modeled system (input–output).
– Insert initial parameters of the models and variables representative of the system (state variables).
– Use one of the methods for adjusting and calibrating parameters (qualitative and quantitative approach).
– Choose two or more methods and performance criteria that make it possible to quantify and assess the quality between the variables observed on the site and the variables simulated by the model (Haziza 2003).

Generally, a 5-year period is used to calibrate the model (El Meddahi et al. 2014; Perrin 2000). From the moment it is decided to build a structure on an ungauged

watershed, the manager will not possess an average of 5 years of data to operate the model (Berthier 2005). However, the validation focuses on the application of the models on the data that were not used during the calibration of the models. The evaluation of the robustness of a model is carried out only at the control, therefore, according to the results obtained in validation (Haziza 2003). Generally, in the rainfall-runoff transformation models, the cutting and the choice of calibration and validation periods always take into consideration the position of the change points and the climatic trend within the climatic series, such as those of 1975, 1984, and 2001 for our case (Zerouali et al. 2020, 2022).

Another evaluation of the calibration quality and the examination of the performance values of the model has been made based on the following criteria:

- Examination and comparison of the monthly hydrographs plots observed and simulated for every subbasin in the calibration and validation phase (Nash, correlation coefficients, and determination coefficients).
- Analysis of the correlograms of the observed monthly flows compared with the simulated monthly flows.
- Analysis of the uncertainties between the observed and simulated annual flows.

The methodology adapted for this research is as follows (Fig. 11.2):

1. We chose the NCEP/NCAR data over the period (1961–2001) for the calibration and validation of the model that describes the current climate, to be better able to make the meteorological forecast.

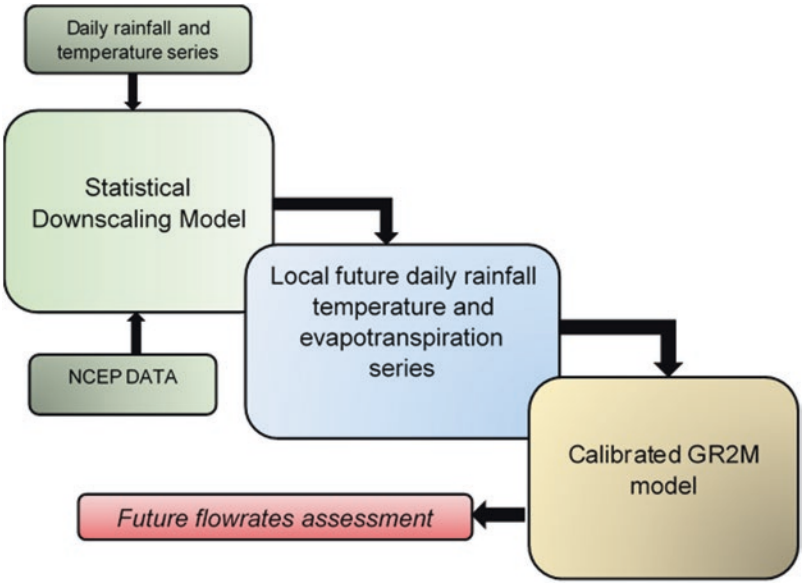

Fig. 11.2 Schematically flowchart used for the analysis combining statistical downscaling approach of Wilby and Dawson (2007) and GR2M model of Mouelhi et al. (2006)

2. We have chosen the anthropogenic emission scenarios most appropriate for the technological, socioeconomic, and industrial development of Algeria, which is the GCM-HadCM3 of the Royaume-Uni with an anthropogenic forcing SRES A2a (pessimist) and SRES B2a (optimistic).
3. Future projections in precipitation and temperatures in the Sebaou basin (northern Algeria) were made for three time horizons, 2011–40, 2041–70, and 2071–99, compared with the reference period (1961–01).
4. Finally, the series of precipitation and future temperatures for the period (2010–99) obtained from the SDSM tool will be used as input time series in GR2M rainfall-runoff transformation model to assess and study the impact of future (probable) climate change in rainfall and temperatures on the flows and water resources of the Sebaou basin.

Results and Discussions

Probable Change in Rainfall

In this part, the rainfall calibration period was 13 years between 1968 and 1980. However, the validation period was 31 years between 1981 and 2011. The results for the calibration period (Table 11.1) revealed good coincidence between the observed and simulated rainfall, particularly reasonable at seasonal and annual scale (Nash and R2 values equal to 0.99). With regard to validation with NCEP, HadCM3-A2, and HadCM3-B2 data (Table 11.1), the results show a somewhat obvious difference between the used data and the NCEP data, which clearly represents the rainfall in the study area (R^2 = 0.99, Nesh = 0.99, and RMSE=10.016) compared with the climate scenario data (R^2 = 0.99, Nesh = 0.93, RMSE=22.558 (A2), and RMSE=21.672 (B2)). The statistical parameters and the results validation are presented in Table 11.1.

Figure 11.3 indicates rainfall time series until 2099 resulting from SDSM analysis under scenarios A2 (bleu) and B2 (red). The change in totals monthly, seasonal, and annual average rainfall of stations in scenarios H3A2 and H3B2 has been

Table 11.1 Performance indicator between the values of rainfall and temperatures observed and simulated in the validation phase using NCEP, HadCM-A2, and HadCM-B2 data

			Validation stage							
		Using NCEP			Using scenario A2			Using scenario B2		
Variable		R^2	NASH	RMSE	R^2	NASH	RMSE	R^2	NASH	RMSE
Rainfall	**Total**	0.99	0.97	10.016	0.93	0.85	22.558	0.93	0.86	21.672
	Average	0.99	0.97	0.334	0.93	0.85	0.752	0.93	0.86	0.722
Temperatures	**Maximal**	0.84	0.70	4.859	0.81	0.64	5.283	0.82	0.65	5.257
	Average	0.78	0.55	4.624	0.70	0.43	5.187	0.70	0.43	5.192
	Minimal	0.98	0.95	1.227	0.97	0.89	1.799	0.97	0.89	1.786

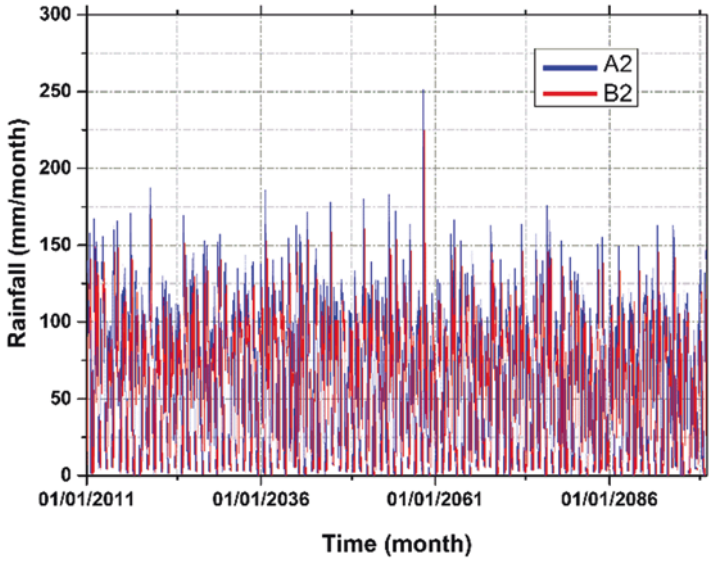

Fig. 11.3 Rainfall time series until 2099 resulting from SDSM simulations under A2 and B2 scenarios

presented in Figs. 11.3, 11.4 and 11.5. For the H3A2 scenario, we note that there is a decrease in annual rainfall for future periods 2020, 2050, and 2080, which would be 6.72, 13.9, and 18.26%, respectively (Fig. 11.5). Şen (2019) observed that a rainfall will decrease in the upper Tigris River basin (Turkey) at about 12.5% in 2030. In winter and spring, Taibi et al. (2019) observed in northern Algeria a significant upward trend of future rainfall projection (2021–50 and 2070–99). At High Atlas basins (Morocco) using CORDEX regional climate with high-resolution simulations, under representative concentration pathway (RCP 4.5 and RCP 8.5), Zkhiri et al. (2019) and Zerouali et al. (2021a, b) observed a decrease in rainfall toward the year 2100 up to −65%.

The changes in seasonal rainfall for the H3A2 and H3B2 scenarios show obvious differences between them and between seasons, especially for H3B2. For the H3A2 scenario, the seasons in which the variations in average seasonal rainfall would be most remarkable and significant in future periods with a tendency towards the driest conditions (Fig. 11.4). The decreases for the three horizons 2020, 2050, and 2080 are, respectively, as follows: in autumn, (Sep–Nov) 9.02%, −13.53%, and 9.72%; in winter (Dec–Feb), 2.98%, 6.07%, and 9.48%; in spring (March–May), 6.94%, 19.06%, and 27.29%; and in summer (June–August), 15.85%, 21.55%, and 35.69%. More or less, similar trends are observed for the results of B2 scenario with a difference in the variation of magnitude and percentage, more noted for the first period of the 2020s (Fig. 11.5). In most cases, models underestimate and overestimate the wet and the dry seasons respectively during the reference period.

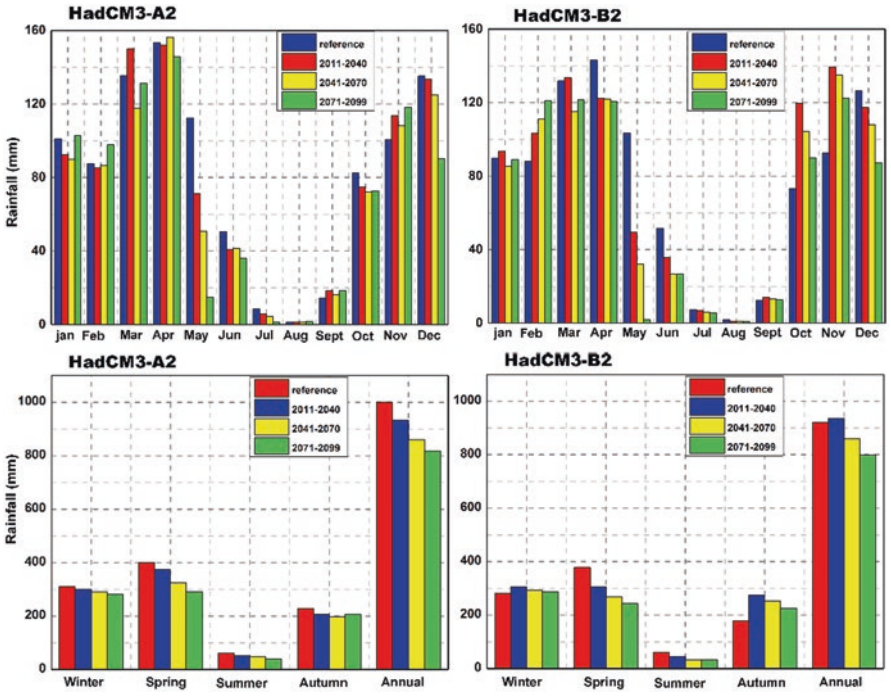

Fig. 11.4 Changes in rainfall amount for the future (2011–40, 2041–70, and 2071–99) as compared with recent periods at monthly, seasonal, and annual scale corresponding to scenarios A2 and B2

Probable Change in Minimum, Average, and Maximum Temperatures

The probable change in maximum, average, and minimum temperatures at Tizi Ouzou station were also calculated using the SDSM Tool. The Tizi Ouzou station is taken for the calculation since it is the most representative of our watershed studied. The calibration was carried out for the period from 1990 to 2001 for 12 years. The remaining series retained from 2002 to 2009 were used to validate the model. Table 11.1 and Fig. 11.6 show the validation between the simulated and observed maximum and average and minimum temperatures of the proposed model. The results indicate a good coincidence between the simulated temperatures and observed temperatures, explained by the calibration results that showed only considerable uncertainty for the maximum temperatures of December and the autumn season. According to Wilby and Dawson (2007) and Bader et al. (2008), rainfall forecasts have a greater degree of uncertainty compared with those of temperature, and rainfall varies widely in space, and GCM models are not relatively efficient for capturing this variability. The results of validation with the NCEP, H3A2, and H3B2 data also show a somewhat obvious dissimilarity concerning the data used and the

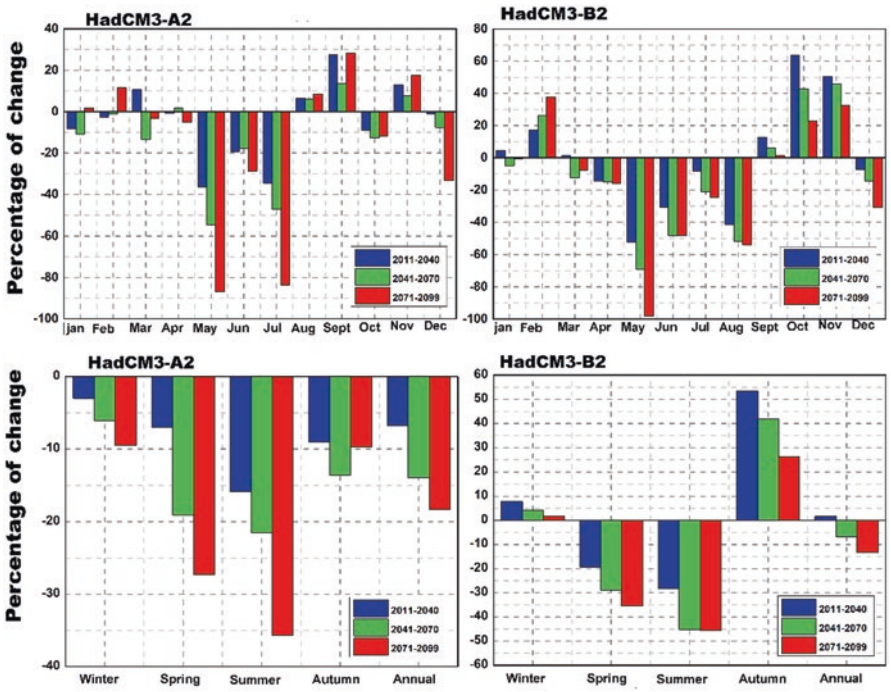

Fig. 11.5 Percentage (%) of change in rainfall for the periods (2011–40, 2041–70, and 2071–99) at monthly, seasonal, and annual scale, in millimeter corresponding to scenarios A2 and B2 compared with the reference period

NCEP data, which are the most representative of the temperature of the study area (Fig. 11.6 and Table 11.1). As shown in Figs. 11.7 and 11.9, the monthly, seasonal, and annual temperature changes (temperature difference) compared with the reference period (recent) that showed, on the one hand, an upward trend for the two scenarios H3A2 and H3B2 and the three proposed horizons 2030, 2050, and 2080. On the other hand, the growths in the H3A2 scenario are much larger than in the H3B2 scenario. Maximum annual temperatures could rise by 2, 3, 3.5 °C and by 2.5, 2.7, and 3.4 °C in 2030, 2050, and 2080, respectively, for the H3A2 and H3B2 emission scenarios (Fig. 11.7). The results of the seasonal scale indicate that winter will have experienced the highest increases under the H3A2 emission scenarios of 4.5 and 5.4 °C between 2030 and 2080 compared with H3B2, which indicated the opposite for winter, while the lowest increases were observed in autumn of nearly 0.5 and 1.5 °C. On a monthly scale, the biggest growth in maximum temperatures could appear in the months of May and October for the two scenarios H3A2 and H3B2 (approximately between 5 °C and 6 °C) (Fig. 11.7).

The average annual temperatures could increase with a maximum of 1.1 °C for the H3A2 emission scenarios and 1.25 °C for the H3B2 emission scenarios up to the long-term horizon 2080s (Fig. 11.8). The results of the seasonal scale indicate

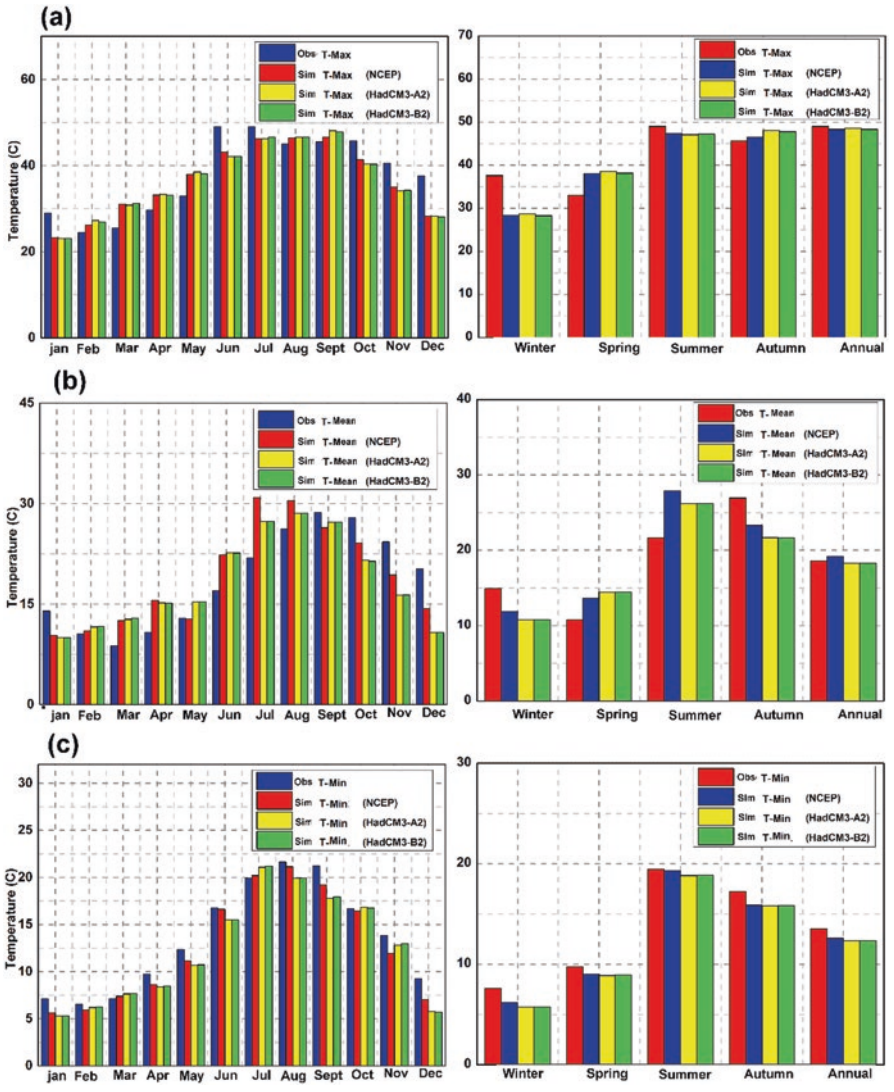

Fig. 11.6 Result of validation between the (**a**) maximum, (**b**) average, and (**c**) minimum monthly, seasonal, and annual temperatures observed and simulated at Tizi Ouzou station

homogeneous upward warming observed in all seasons under the H3A2 emission scenario from 1.1 to 1.7 °C and even on the monthly scale. However, the H3B2 emission scenario indicates a nonhomogeneous upward trend, which differs from one season to another and that autumn will have experienced the highest increases of 1.7 °C for 2030, 1.9 °C for 2060, and 2.4 °C for 2080, while summer presents the lowest increases of 0.7 °C for 2030 and 0.25 °C for 2080. On a monthly scale, the

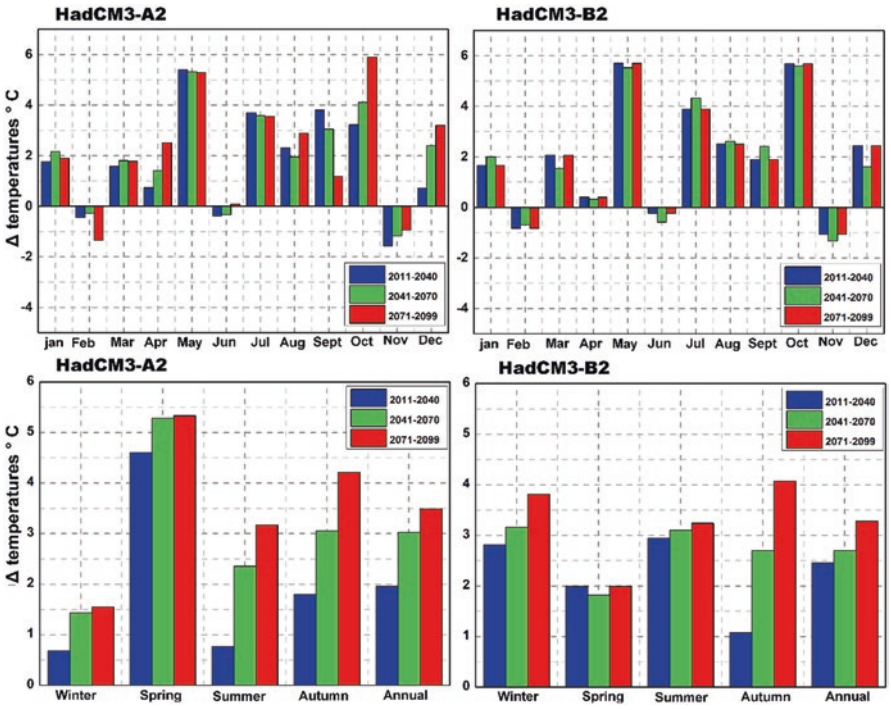

Fig. 11.7 Changes in maximum temperature for the future (2040–70 and 2071–99) as compared with recent period at monthly, seasonal, and annual scale corresponding to scenario A2 and B2

months of September and October for scenario H3B2 present the largest increase in average temperatures approximately between 1.4 and 2.4 °C (Fig. 11.8).

The minimum annual temperatures could increase with a maximum of 1.1 °C for the H3A2 emission scenarios and 0.65 °C for the H3B2 emission scenarios until 2080 (Fig. 11.9). On a seasonal scale, winter will have experienced a decrease in minimum temperatures of 0.5 °C, observed for the two scenarios H3A2 and H3B2. On the other hand, the climatic scenarios indicate that there is an upward trend in the minimum temperatures of spring compared with that of summer from 1 to 1.7 °C for H3A2 and H3B2, the autumn from 0.25 to 2.25 °C for H3A2, and from 0.7 to 1.7 °C for H3B2 (Fig. 11.9). On a monthly scale, the minimum temperatures tend to increase, with the exception of winter months (Dec, Jan, and Feb) and the month of August observed for the two scenarios H3A2 and H3B2. On the other hand, the two scenarios indicate that the months of October and November will have the highest increases reaching 3 °C until 2080 (Fig. 11.9). Those results confirm the results obtained at regional and global scale, for example, in the central region of the Arabian Peninsula (Almazroui et al. 2020) which indicate that the temperatures of all seasons will increase during the twenty-first century. Using The Coordinated Regional Downscaling Experiment (CORDEX) ensemble scenarios, Zittis et al. (2019) documented that the Mediterranean basin really at present ingoing the

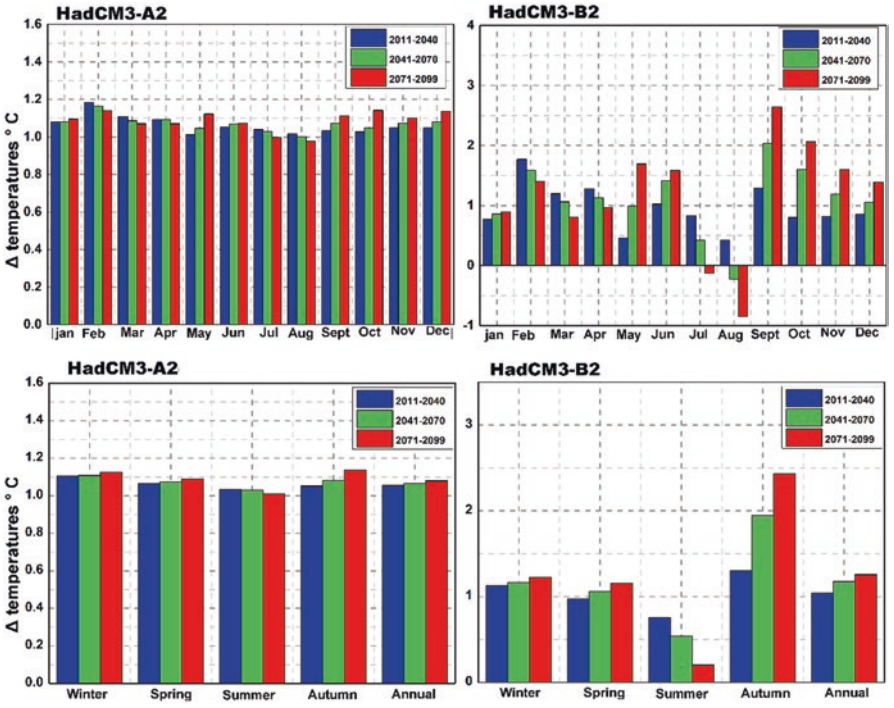

Fig. 11.8 Changes in average temperature for the future (2040–70 and 2071–99) as compared with recent period at monthly, seasonal, and annual scale corresponding to scenario A2 and B2

climate-warming epoch with 1.5 °C, which can be reached 2 °C in two decades. In the Mediterranean region, Kanber et al. (2019) indicate that the temperatures are expected to rise at +3 °C and + 5 °C by 2050 and 2100, respectively. According to Lefebvre et al. (2019), the countries of Northern Africa, such as Algeria, Morocco, and southern Europe (Portugal and Spain), are the highest risk countries of loss and wetland degradation. From the results of simulations using climatic scenarios, it can be said that the observed changes in temperatures show great agreement, homogeneity, and similarity in terms of magnitude with the results obtained on a regional and global scale from +2 °C to +5 °C on average at the end of the twenty-first century.

Rainfall-Runoff Relationship Analysis by GR2M

Table 11.2 illustrates the results of the rainfall-runoff modeling obtained from different stations on the basis of the best calibration parameters. In addition, in modeling, we tried to seek the best rainfall station, which represents the hydrometric of each subbasin area or basin area based on the comparison between the performances indicators (Table 11.2). Two calibration methods were used; the first corresponds to

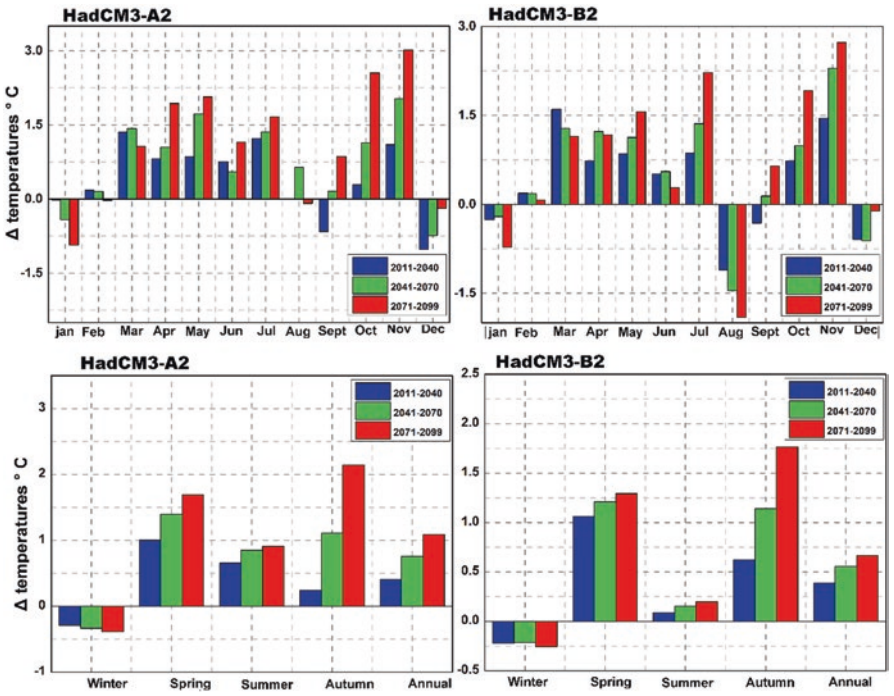

Fig. 11.9 Changes in minimum temperature for the future (2040–70 and 2071–99) as compared with recent period at monthly, seasonal, and annual scale corresponding to scenario A2 and B2

Table 11.2 Best Nash and R^2 values of the GR2M model for calibration and validation process the main subbasins and basin of Sebaou

	Nash-calibration (%)	Nash-validation (%)	R^2 calibration (%)	R^2 calibration (%)
Oued Sébaou-1- basin	87.1	84.5	0.94	0.95
Oued Sébaou-2- basin	81.0	85.0	0.80	0.91
Oued Sébaou Rabta subbasin	84.3	84.2	0.86	0.88
Oued Aissi subbasin before 2001	87.5	80.3	0.92	0.72
Oued Aissi subbasin after 2001	35.2	45.9	0.55	0.67

calibration by varying the two parameters X1 and X2 and setting S0 and R0 "initial filling level," and the second is to vary S0 and R0 and setting the values of X1 and X2 in order to seek and to optimize the Nash. The parameters X, R0, and S0 of the model are manually calibrated by changing their values.

The first observations on the values of the Nash criterion in Table 11.2 show that the GR2M was more efficient. In the Oued Sebaou basin, the values of the Nash criterion found are superior to 80% in calibration (87.1%) after optimization as in

validation (84.5%). In addition, a correlation coefficient $R^2 = 0.95$, which indicates that the correlation is very good. It is the same case for the Oued Sebaou basin (2) and the subbasin of Sebaou Rabta, which also shows Nash values in calibration and validation exceeding 80%, which translates the robustness of the GR2M model on the Sebaou River. The results of the model show that the calibration period (1991–95) is the best to explain the Sebaou River system (1) in comparison with the periods 1990–94, (1992–96, and 1993–97.

Based on the different 5-year calibration periods, in the performance results obtained in terms of the Nash criterion, correlation coefficient, and determination, from the GR2M, at the RN30 station (subbasin Oued Aissi), the Nash exceed 80%. From Table 11.2, we note that the best calibration period for this system is the period 1990–94 with a Nash value equal to 85%. As regards, the coefficient of correlation is 0.92.

However, model validation indicates results that differ from one period to another; for example, the value of Nash before the 2000s (between 1995 and 1999) reaches 80% and therefore acceptable in the calibration and validation phase. The GR2M model therefore successfully reproduces the hydrological behavior of the basin (Kouamė et al. 2013). After this period, we notice a deterioration in Nash values, which decrease to 45%between 2005 and 2009. This degradation is marked by the Nash in validation and not in calibration, which defines the robustness criterion of the model is unacceptable after the implantation and the commissioning of the Taksebt dam in 2001. The latter modifies the flow regime of the Oued Aissi and requires the search for an efficient solution for considering reservoir dams in a rainfall-runoff-reservoir model. This problem is widely discussed in several countries of the world, for example, the Aswan dam, which was put into service in 1970, with a capacity of 169 billion m^3, strongly disturbs the hydrological regime of the Nile, and poses many environmental problems. It completely eliminates floods and reduces the space of wetlands downstream (Remini 1997). Moreover, Zerouali et al. (2021a, b) have found in Sebaou River basin (northern central of Algeria) that rainfall and discharge relationship was nonlinear, which could be due to the dry periods. Moreover, the field investigation revealed that the commissioning of Taksebt dam and human activities such as the smuggling and trafficking of rocks and sands from the abdomen of the river since the year 1998 have had a negative and significant influence on the lows decline of river flows amount. Despite that, the results obtained from the hydrographs are also of good quality for all the simulated basins and that the model well respects the flow dynamics (Figs. 11.10 and 11.11).

Generally, the results are very satisfactory (Fig. 11.10); the model indicates that the simulated and observed peak flows are well located and coincide quite well over time with an overestimation in the validation phase for the Oued Sebaou basin (1) and an underestimation for Oued Sébaou Rabta, with the exception of a few peaks where the uncertainties are greater. During low-water periods, low flows are better and well reproduced than peak flows during floods, with the presence of overestimation. In the Oued Aissi subbasin, the model estimates the flows after 2000 with poor quality and with underestimates. In addition, the commissioning of the dam and the rainfall in the Oued Sébaou basin, after the year 2001, experienced surplus years

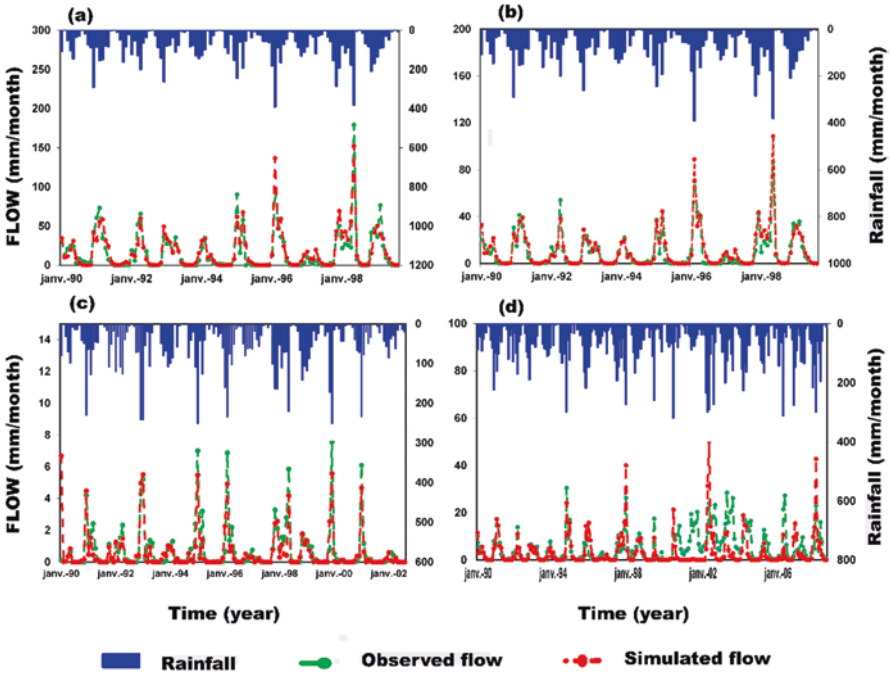

Fig. 11.10 Comparison and assessment between the observed flows and simulated monthly flows at (**a**) Oued Sebaou (1), (**b**) Oued Sebaou (2), (**c**) Oued Sebaou Rabta, and (**d**) Oued Aissi

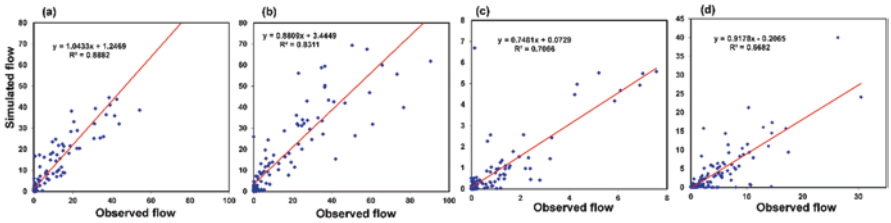

Fig. 11.11 Correlations between the observed and simulated flows at (**a**) Oued Sebaou (1), (**b**) Oued Sebaou (2), (**c**) Oued Sebaou Rabta, and (**d**) Oued Aissi

with an upward trend in comparison with the calibration period before the year 2001. This explains why the calibration parameters are not representative during this period.

Graphical analysis of the results, specifically the correlation coefficients, the uncertainties (ratios of Q_{obs} and Q_{sim}), and the residuals (difference between Q_{obs} and Q_{sim}), with monthly and annual time scales, shows that the water slides (flows) simulated by the model are good with the measured water slides (Tramblay et al. 2018).

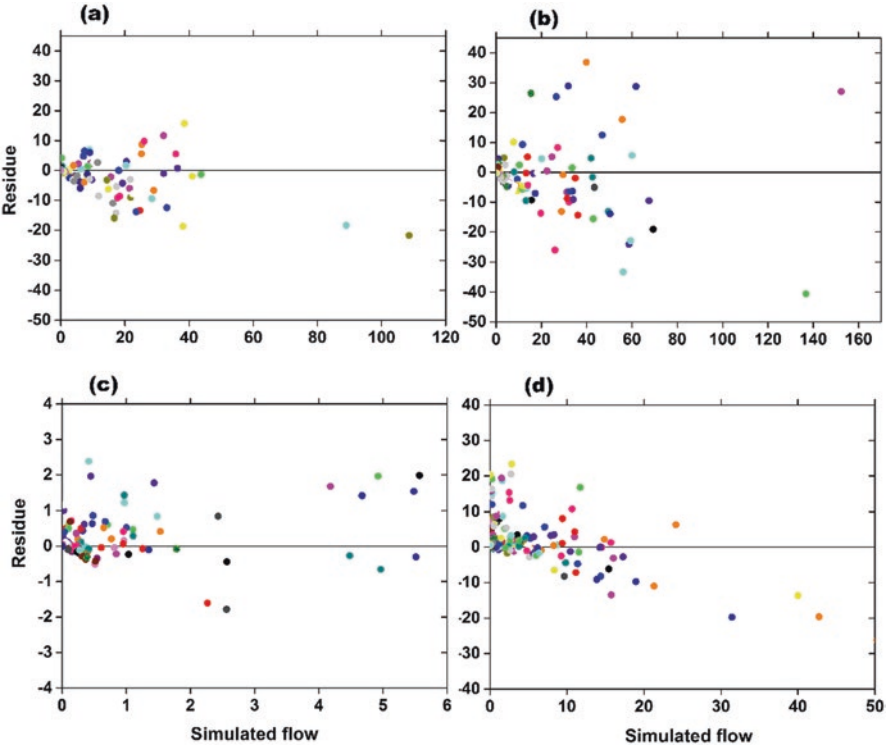

Fig. 11.12 Relations between simulated flows and residues at (**a**) Oued Sebaou (1), (**b**) Oued Sebaou (2), (**c**) Oued Sebaou Rabta, and (**d**) Oued Aissi

The residuals as a function of the simulated monthly flows and the evolution of the annual uncertainty are well illustrated in Figs. 11.13 and 11.14. The residue values were examined in three stages:

1. If the residue values are approximately zero, which indicates unbiased estimates.
2. If the residue values are greater than zero (positive). This implies estimates affected by bias with a tendency to underestimate the flows by the model.
3. If the residue values are less than zero (negative), which expresses estimates affected by bias with an overestimation of the flows by the model (Bodian et al. 2012).

Figure 11.12 shows that most of the clouds constituting the low flow peaks are concentrated around the error axis of the value 0. This observation is more marked for the Oued Sebaou basin (1) and the subbasin Sebaou Rabta. On the other hand, the high and medium values of the discharges of the different subbasins indicate errors, which are sometimes considerably greater, noted by a mixed trend toward underestimates and overestimations, with the exception of the underestimates of the model at the level of the subbasin of Oued Aissi.

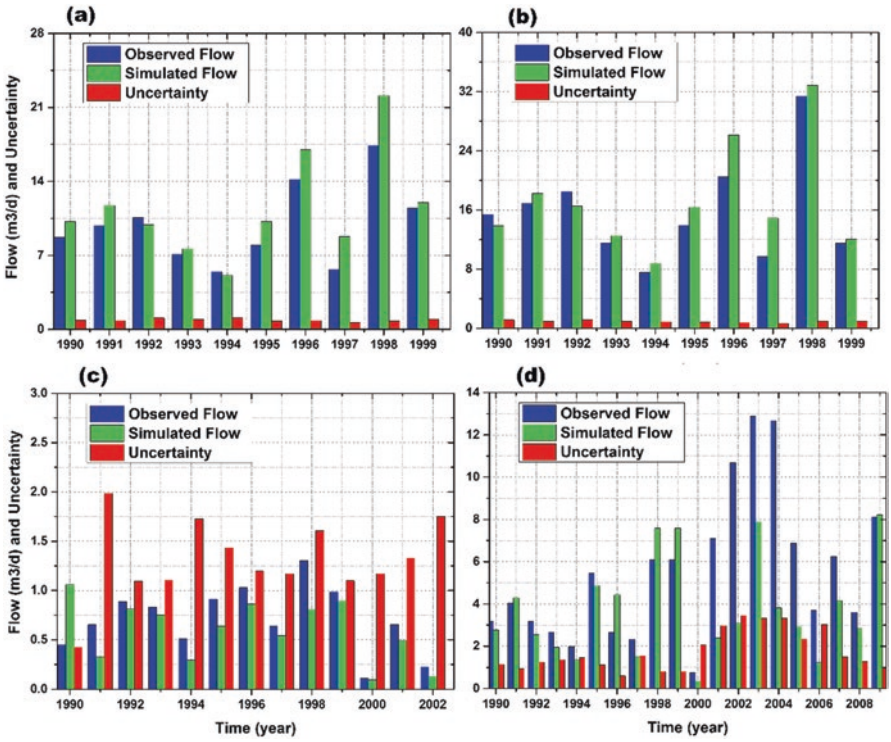

Fig. 11.13 Comparisons between the uncertainties of the observed and simulated average annual flows at (**a**) Oued Sebaou (1), (**b**) Oued Sebaou (2), (**c**) Oued Sebaou Rabta, and (**d**) Oued Aissi

Another method for better assessment of the errors remarked is the graphical representation of the evolution of the uncertainty as a function of the annual flows observed in site and simulated by the model during the calibration and validation phase. The results show the uncertainty in the calibration period around the values 0.82–1.10 for Oued Sébaou (1) and (2) and between 1.01 and 1.5 for the subbasins of Oued Sébaou Rabta and Oued Aissi. However, in the validation phase, we note an increase in the uncertainty values with a trend toward the value 1 from 1997, more marked in the Oued Sebaou 1 and 2 and the Oued Sebaou Rabta. Between the period 2001 and 2007, the Oued Aissi subbasin experienced a significant increase in uncertainty and remains too far from reality (Fig. 11.13). The monthly modeling by the conceptual model of GR2M gives a general tendency to good simulation within a tolerable margin of uncertainties. According to the literature, the GR2M model remains more sensitive to input data such as precipitation and potential evapotranspiration. In addition, changes in surface conditions (land use, vegetation cover, hydraulic structures, water pumping, modification of the minor and major bed of the river, etc.) contribute to determining the soil's water reserves (Ardoin-Bardin 2004).

The results indicate the efficiency of the GR2M model in hydrological simulation. Those models can give very satisfactory and adequate responses with a high degree of reliability for the prediction of flows in the studied subbasin.

Elaboration of Hydrological Modeling Scenarios

In this part, the different climatic parameters, precipitation, temperature, and future evapotranspiration simulated by the HadCM3 model over the periods 2011–40, 2041–70, and 2071–2099, are important for the elaboration of a hydrological impact model based on the GR2M model for better controlling and planning of water resources. The stages of the hydrological impact study caused by climate change are schematically mentioned in Fig. 11.2. This flowchart indicates the interface between the regional circulation model (RCM) and the GR2M hydrological models (Fig. 11.2). Before the implementation of the model, the databases of future variables were subjected to a bias correction based on the DELTA method (method of disturbances or anomalies). DELTA method consists of the climatic variables of the disturbances that are calculated monthly, as the ratio (or the difference in the case of the temperature) between the average monthly climate simulated under climate change and that simulated for the present climate taken as reference. These monthly disturbances are used to modify the current series observed, which if applied uniformly for the entire month considered, (R^* (j) = O (j) and S^* (j) = O (j) × (S/R)) or (+($S - R$)) (R is the reference period, S is the future RCM scenarios, and O is the actual observations to give rise to new corrected data (R * and S *)). This technique is widely used in the case of hydrological impact studies (Beldring et al. 2008). After the bias correction, the variables from the A2 and B2 scenarios were used as input datasets in the GR2M hydrological model to simulate future flows and water resources in the study basin. For our hypothesis, we keep the same parameters of the hydrological model calibrated and validated previously in the future simulation. Elmeddahi and Ragab (2019) in the Cheliff basin (North of Algeria) also applied this hypothesis.

Assessment of Future Flow Rate Projections

Figure 11.14 shows the monthly flows corresponding to the climatic scenarios A2 and B2 projected by the hydrological model GR2M in the basins of the Oued Sébaou (1) and (2).

On the other hand, a wide and big range output of future changes can be obtained from A2 and B2 climate change scenarios at scale of basin hydrology. The GR2M model shows a diminution in flow rates compared with the current or reference period according to the upward trend in rainfall and the increase in temperatures. On a seasonal scale, future flows under the H3A2 and H3B2 scenarios present slightly

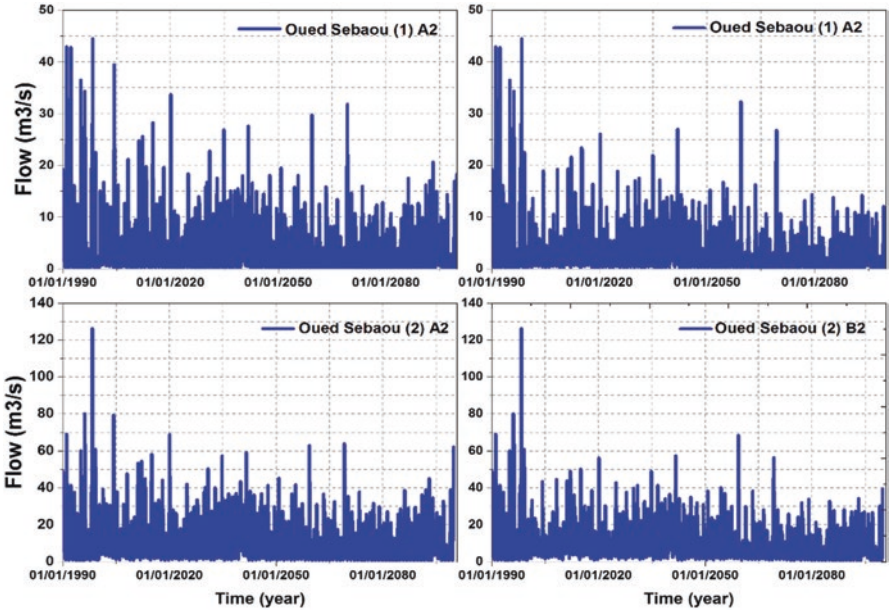

Fig. 11.14 The average monthly flows in m^3/s probably up to the horizon 2100 from the GR2M model at (**a**) Oued Sebaou (1) and (**b**) Oued Sebaou (2)

significant differences between them and are evident from one season to the other (Figs. 11.15 and 11.16). For the autumn season, it shows an increase for water flowing during the periods 2039–70 and 2071–99, of the order of 600–700% or 20–170 Mm^3/year observed at basin scale for the two scenarios. The winter and spring months show similar trends with a slight downward trend in flows but higher for the periods 2040–70 and 2071–99, between 50 and 85%. On the annual scale, it appears from the obtained results a decreasing trend in the average annual flows projected for future periods. The horizons 2050 and 2080 are the most deficit compared with horizon 2020 with a probable decrease for the end of the twenty-first century, estimated by −49% (A2) and − 57% (B2) for Oued Sébaou (1) and − 35% (A2) and 45% (B2) for Oued Sébaou basin (2) (Figs. 11.15 and 11.16). Following the surface temperature increases, evapotranspiration may too increase, so in the future, a higher rate of evapotranspiration is probable, which could directly influence the flow creation routing. Thus, during this time, the evapotranspiration variability could significantly influence the change in simulated flow, which means that it cannot stay unchanged over the operation of projecting flows (Duong 2016). Another side, according to the uncertainty, of the GCM is one of the factors that can affect the future flow projections, and this is associated with the great simplification between the interface of the MCG and the local flow simulations, which can strongly affect the hydrograph.

In general, the decreases in flows for the scenarios A2 and B2 observed in the basin of the Sebaou River are coincident with studies developed in the Mediterranean

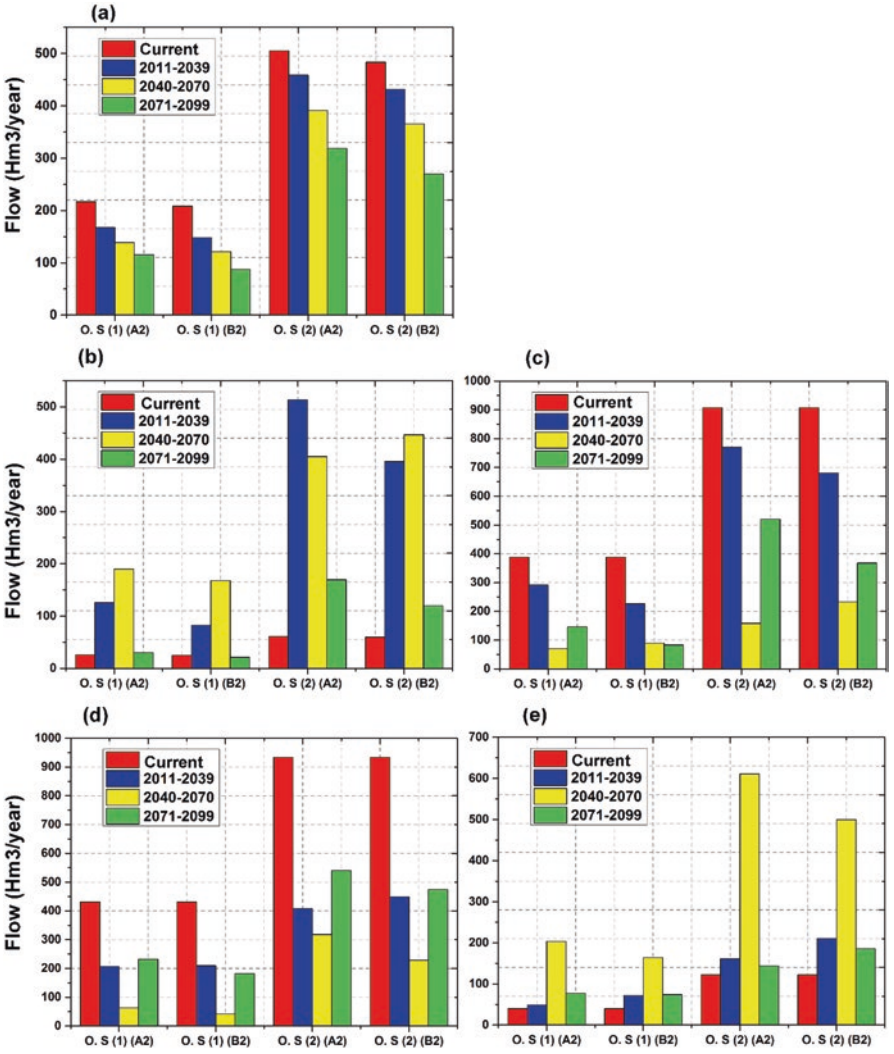

Fig. 11.15 Average annual and monthly runoff volumes probably at (**a**) annual, (**b**) autumn, (**c**) winter, (**d**) spring, and (**e**) summer over the horizons (2011–39, 2040–70, and 2071–99) in the Sebaou Oued basin (OS) (1) and (2) under scenarios A2 and B2

basin and Algeria. Our results show that climate change has a significant impact on decreases in rainfall and basin flows. For this, the Mediterranean region remains one of the most vulnerable to climatic variability. According to Duong et al. is clear that the river flow regimes variability will probably have significant impacts on ecosystems and the environment, reduced water availability and increased atmospheric temperatures during dry summer seasons will produce an increase of pressure on water resources. In addition, the shortage in water availability will lead to an additional

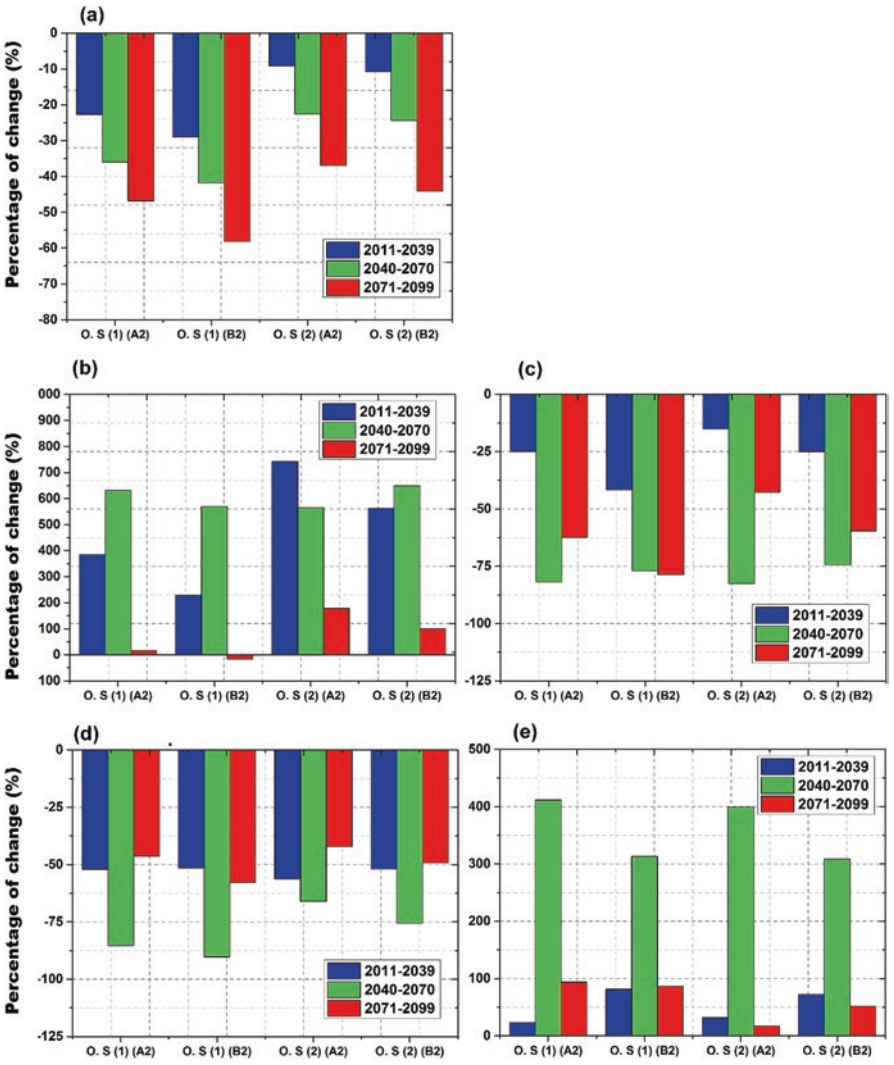

Fig. 11.16 Percentage change in the average annual and monthly runoff volumes probably at (**a**) annual, (**b**) autumn, (**c**) winter, (**d**) spring, and (**e**) summer scale over the horizons (2011–39, 2040–70, and 2071–99) in the Sebaou Oued basin (OS) (1) and (2) under scenarios A2 and B2

intrusion of the salinity of groundwater in coastal basins, which reduces the cultivable area. Kabiri (2014) also reported that agricultural production is expected to decrease and water conflicts could multiply due to increasing water scarcity. The risk of flood disasters is also expected to occur more frequently due to changes in farming methods and rapid urbanization processes.

Conclusion

In this chapter, we discussed the following:

1. The future projections of climate parameters to the horizon 2099 according to three periods, 2011–39, 2040–70, and 2071–99 from the IPCC HadCM3-A2 and HadCM3-B2 scenarios, have been assessed using the statistical disaggregation model. This tool was largely used as a decision support tool based on its simplicity.
2. The climate series resulting from future projections were used in the GR2M rainfall-runoff model to simulate the hydrological behavior of Sebaou basin. The main results obtained are summarized in the following points:

   (a) The simulation using NCEP data is better than HadCM3-A2 and HadCM3-B2 in the calibration and validation phases.
   (b) The HadCM2-A2 and HadCM2-B2 models predict a decrease in annual precipitation averages, reaching 18–14%, respectively, to the horizon 2099. However, on a seasonal scale, autumn, winter, spring, and summer, it shows a decrease of 9.72, 9.48, 27.29, and 35.69% respectively for HadCM2-A2. In addition, for the HadCM2-B2 there are similar trends except for the increasing trends in the autumn season.
   (c) Minimum, maximum, and average annual temperatures could continue to increase with a maximum of 1.1–0.65 ° C, 1.1–1.25 ° C, and 2.7–3.4 ° C, respectively, for the H3A2 and H3B2 emission scenarios until the long-term horizon 2080.
   (d) The values of the Nash criterion obtained are greater than 80% in calibration and 84.5% in validation with a correlation coefficient equal to 0.95 except for the degradation the Nash coefficient after the commissioning of the Taksebt dam in the Oued Aissi subbasin.
   (e) The hydrographs show that the simulated and observed peak flows are well located and coincide fairly well over time, with some more significant peaks of the estimate in the validation phase during flood periods.
   (f) The uncertainty shows acceptable values varying between 0.6 and 1.1. However, the values of Oued Aissi model remain too far from reality after the year 2001.
   (g) The GR2M model appears very effective in simulating the flows and the hydrological functioning of the basin. The comparison between the variables observed in the site with those simulated by the model confirm that the GR2M can be preferred as a tool for managing water resources.
   (h) The coupling between series from the HadCM-A2 and HadCM-B2 scenarios and the GR2M model has shown a wide and big range output of future changes in the basin hydrology with an upward trend in flows compared with the current period, particularly for the months between December and May for the period 2040–70.

(i) The results show that the horizons 2050 and 2080 are the most deficient compared with the current horizon 2020. With a probably decrease in flows by the end of the twenty-first century, estimated at −49% (A2) and − 57% (B2) for the Oued Sebaou (1) and − 35% (A2) and 45% (B2) for the Oued Sebaou (2) following the decreases in winter and spring during the periods 2040–70 and 2071–99 between 50 and 85%.

Currently, we are working on two emission scenarios RCP 4.5 and 8.5 scenarios of CMIP 5 to assess future water resources on some representative basins of northern Algeria by combining those output with artificial intelligence techniques and meta-heuristic algorithm to reduce and assess the uncertainty associated with predictions of climatic, hydrological, and land use conditions.

References

Abda Z, Zerouali B, Chettih M, Guimaraes Santos CA, de Farias CAS, Elbeltagi A (2022) Assessing machine learning models for streamflow estimation: A case study in Oued Sebaou watershed (Northern Algeria). Hydrol Sci J 67(9):1328–341

Almazroui M, Khalid MS, Islam MN, Saeed S (2020) Seasonal and regional changes in temperature projections over the Arabian Peninsula based on the CMIP5 multi-model ensemble dataset. Atmos Res 104913. https://doi.org/10.1016/j.atmosres.2020.104913

Ardoin-Bardin S (2004) Variabilité hydroclimatique et impacts sur les ressources en eau de grands bassins hydrogra-phiques en zone soudano-sahélienne, Doctoral dissertation, Université de Montpellier II, France, 337 p

Arnell NW (2004) Climate change and global water resources: SRES emissions and socio-economic scenarios. Glob Environ Chang 14:31–52. https://doi.org/10.1016/j.gloenvcha.2003.10.006

Bader D, Covey C, Gutowski W, Held I, Kunkel K, Miller R, Tokmakian R, Zhang M (2008) Climate models: an assessment of strengths and limitations. A report by the US Climate Change Science Program and the Subcommittee on Global Change Research, Office of Biological and Environmental Research, Department of Energy, Washington, DC

Bayatvarkeshi M, Zhang B, Fasihi R, Adnan RM, Kisi O, Yuan X (2020) Investigation into the effects of climate change on reference evapotranspiration using the HadCM3 and LARS-WG. Water 12(3):666. https://doi.org/10.3390/w12030666

Beldring S, Engen-Skaugen T, Førland EJ, Roald LA (2008) Climate change impacts on hydrological processes in Norway based on two methods for transferring regional climate model results to meteorological station sites. Tellus A Dyn Meteorol Oceanogr 60(3):439–450. https://doi.org/10.1111/j.1600-0870.2007.00306.x

Berthier C-H (2005) Quantification des incertitudes des débits calculés par un modèle pluie-débit empirique. Mémoire de Master en Sciences de la terre. Université Paris sud 11

Bodian A, Dezetter A, Dacosta H (2012) Apport de la modélisation pluie-débit pour la connaissance de la ressource en eau: application au haut bassin du fleuve Sénégal. Climatologie 9:109–125

Bouabdelli S, Meddi M, Zeroual A, Alkama R (2020) Hydrological drought risk recurrence under climate change in the karst area of Northwestern Algeria. J Water Clim Change. https://doi.org/10.2166/wcc.2020.207

Bucak T, Trolle D, Andersen HE, Thodsen H, Erdoğan Ş, Levi EE et al (2017) Future water availability in the largest freshwater Mediterranean lake is at great risk as evidenced from simulations with the SWAT model. Sci Total Environ 581:413–425. https://doi.org/10.1016/j.scitotenv.2016.12.149

Cherkaoui A (2012) Désagrégation statistique des via l'outil SDSM pour la projection des changements climatiques futurs dans la haute Moulouya. Thèse d'Ingénieur d'Etat: Génie des Procédés et d'Environnement. Université Hassan II Mohammadia –Casablanca

Chourghal N, Lhomme JP, Huard F et al (2016) Climate change in Algeria and its impact on durum wheat. Reg Environ Chang 16:1623–1634. https://doi.org/10.1007/s10113-015-0889-8

Duan W, He B, Takara K, Luo P, Nover D, Hu M (2017) Impacts of climate change on the hydroclimatology of the upper Ishikari river basin, Japan. Environ Earth Sci 76(14):490. https://doi.org/10.1007/s12665-017-6805-4

Duong PC (2016) Assessment of climate change impact on river flow regimes to support decision-making in water resources Management in the Red River Delta, Vietnam: A Case Study of Nhue-day River Basin. J Nat Resour Dev 06:81–91. https://doi.org/10.5027/jnrd.v6i0.09

El Meddahi Y (2016) Les changements climatiques et leurs impacts sur les ressources en eau, cas du bassin du Cheliff. Thèse de doctorat en Hydraulique. Universite Hassiba Ben Bouali – Chlef (245 p)

El Meddahi Y, Issaadi A, Mahmoudi H, Tahar Abbes M, Mattheus FAG (2014) Effect of climate change on water resources of the Algerian middle Cheliff basin. Desalin Water Treat 52:2073–2081. https://doi.org/10.1080/19443994.2013.8317

Elbeltagi A, Kumar N, Chandel A et al (2022a) Modelling the reference crop evapotranspiration in the Beas-Sutlej basin (India): an artificial neural network approach based on diffèrent combinations of meteorological data. Environ Monit Assess 194:141. https://doi.org/10.1007/s10661-022-09812-0

Elbeltagi A, Nagy A, Mohammed S, Pande CB, Kumar M, Bhat SA, Zsembeli J, Huzsvai L, Tamás J, Kovács E, Harsányi E, Juhász C (2022b) Combination of limited meteorological data for predicting reference crop evapotranspiration using artificial neural network method. Agronomy 12(2):516. https://doi.org/10.3390/agronomy12020516

Elbeltagi A, Pande CB, Kouadri S et al (2022c) Applications of various data-driven models for the prediction of groundwater quality index in the Akot basin, Maharashtra, India. Environ Sci Pollut Res 29:17591–17605. https://doi.org/10.1007/s11356-021-17064-7

Elbeltagi A, Zerouali B, Bailek N et al (2022d) Optimizing hyperparameters of deep hybrid learning for rainfall prediction: a case study of a Mediterranean basin. Arab J Geosci 15:933. https://doi.org/10.1007/s12517-022-10098-2

Elmeddahi Y, Ragab R (2019) Assessing the climate change impact on water resources and adaptation strategies in Al-gerian Cheliff Basin. In: Negm, A.M., Bouderbala, A., Chenchouni, H., Barceló, D. (eds) Water Resources in Algeria - Part I. The handbook of environmental chemistry, vol 97. Springer, Cham. https://doi.org/10.1007/698_2019_398

Galdies C, Lau HS (2020) Urban Heat Island effect, extreme temperatures and climate change: a case study of Hong Kong SAR. In: Climate change, hazards and adaptation options. Springer, Cham, pp 369–388. https://doi.org/10.1007/978-3-030-37425-9_20

Hassan Z, Shamsudin S, Harun S, Malek MA, Hamidon N (2015) Suitability of ANN applied as a hydrological model coupled with statistical downscaling model: a case study in the northern area of Peninsular Malaysia. Environ Earth Sci 74(1):463–477. https://doi.org/10.1007/s12665-015-4054-y

Haziza E (2003) Modélisation mensuelle pluie-débit/apports de la spatialisation: cas des données de sols. Thèse de Docto-rat en Sciences de l'Eau et de la Terre. Université Montpellier II

IPCC (2007) The physical science basis. Contribution of working group I to the fourth assessment report of the intergovernmental panel on climate change. Cambridge University Press, Cambridge/New York, p 996

Kaas E, Frich P (1995) Diurnal temperature range and cloud cover in the Nordic countries: observed trends and estimates for the future. Atmos Res 37:211–228. https://doi.org/10.1016/0169-8095(94)00078-R

Kabiri R (2014) Assessment of climate change impact on runoff and peak flow: a case study on Klang. Philosophy PhD thesis, University of Nottingham (316 p)

Kanber R, Ünlü M, Kapur B, Özekici B, Donma S (2019) Adaptation of contemporary irrigation systems to face the challenges of future climate changes in the Mediterranean region: a case study of the lower Seyhan irrigation system. In: Watanabe T, Kapur S, Aydın M, Kanber R, Akça E (eds) Climate change impacts on basin agro-ecosystems. The Anthropocene: Politik—economics—society—science, vol 18. Springer, Cham. https://doi.org/10.1007/978-3-030-01036-2_7

Khorshidi MS, Nikoo MR, Sadegh M, Nematollahi B (2019) A multi-objective risk-based game theoretic approach to reservoir operation policy in potential future drought condition. Water Resour Manag 33(6):1999–2014. https://doi.org/10.1007/s11269-019-02223-w

Kouadri S, Pande CB, Panneerselvam B, Moharir KN, Elbeltagi A (2021) Prediction of irrigation groundwater quality parameters using ANN, LSTM, and MLR models. J Environ Sci Pollut Res, Springer Publication, Impact Factor 4:22. https://doi.org/10.1007/s11356-021-17084-3

Kouamë KF, Kouassi AM et al (2013) Analyse de tendances dans la relation pluie-débit dans un con-texte de changements climatiques: cas du bassin versant du N'zo-Sassandra (Ouest de la Côte d'Ivoire). Int J Innov Appl Stud 2:92–103

Lefebvre G, Redmond L, Germain C, Palazzi E, Terzago S, Willm L, Poulin B (2019) Predicting the vulnerability of seasonally-flooded wetlands to climate change across the Mediterranean Basin. Sci Total Environ 692:546–555. https://doi.org/10.1016/j.scitotenv.2019.07.263

Madsen H (2000) Automatic calibration of a conceptual rainfall–runoff model using multiple objectives. J Hydrol 235:276–288. https://doi.org/10.1016/S0022-1694(00)00279-1

Meenu R, Rehana S, Mujumdar PP (2013) Assessment of hydrologic impacts of climate change in TungaBhadra river basin, India with HEC-HMS and SDSM. Hydrol Process 27(11):1572–1589. https://doi.org/10.1002/hyp.9220

Mouelhi S (2003) Vers une chaîne cohérente de modèles pluie-débit conceptuels globaux aux pas de temps pluriannuel, annuel, mensuel et journalier. Thèse de Doctorat, ENGREF, Cemagref Antony, France, 323, p 16

Mouelhi S, Michel C, Perrin C, Andreassian V (2006) Linking stream flow to rainfall at the annual time step: the Manabe bucket model revisited. J Hydrol 328:283–296. https://doi.org/10.1016/j.jhydrol.2005.12.022

Nash JE, Sutcliffe JV (1970) River flow forecasting through conceptual models part I—A discussion of principles. J Hydrol 10(3):282–290. https://doi.org/10.1016/0022-1694(70)90255-6

Ouyang W, Hao F, Shi Y et al (2019) Predictive ability of climate change with the automated statistical downscaling method in a freeze–thaw agricultural area. Clim Dyn 52:7013–7028. https://doi.org/10.1007/s00382-018-4560-1

Pande CB, Kadam SA, Jayaraman R, Gorantiwar S, Shinde M (2022) J Saudi Soc Agric Sci 21(1):21–28

Perrin C (2000) Vers une amélioration d'un modèle global pluie-débit (Doctoral dissertation, Institut National Polytech-nique de Grenoble-INPG)

Perrin C, Oudin L, Andreassian V, Rojas-Serna C, Michel C, Mathevet T (2007) Impact of limited streamflow data on the efficiency and the parameters of rainfall—runoff models. Hydrolog Sci J 52(1):131–151. https://doi.org/10.1623/hysj.52.1.131

Pope VD, Gallani ML, Rowntree PR, Stratton RA (2000) The impact of new physical parametrizations in the Hadley Centre climate model - HadCM3. Clim Dyn 16:123–146. https://doi.org/10.1007/s003820050009

Ragab R, Prudhomme C (2002) Climate change and water resources management in arid and semi-arid regions: Prospec-tive and challenges for the 21st century. Biosyst Eng 81(1):3–34. https://doi.org/10.1006/bioe.2001.0013

Raghavan SV, Vu MT, Liong SY (2012) Assessment of future stream flow over the Sesan catchment of the lower Mekong Basin in Vietnam. Hydrol Process 26(24):3661–3668. https://doi.org/10.1002/hyp.8452

Remini B (1997) Envasement des retenues de barrages en Algérie: importance, mécanismes et moyen de lutte par la tech-nique du soutirage. Doctorat d'état, Ecole Nationale Polytechnique d'Alger

Sambaran J, Mantu D, Debasri R, Subhasish D, Asis M (2015) Simulation of climate change impact in a river basin in Eastern India. Int J Hydrol Sci Technol 5(4):2015. https://doi.org/10.1504/IJHST.2015.072631

Şen Z (2019) Climate change expectations in the upper Tigris River basin, Turkey. Theor Appl Climatol 137:1569–1585. https://doi.org/10.1007/s00704-018-2694-z

Sigdel M, Ma Y (2016) Evaluation of future precipitation scenario using statistical downscaling model over humid, subhumid, and arid region of Nepal—a case study. Theor Appl Climatol 123(3–4):453–460. https://doi.org/10.1007/s00704-014-1365-y

Somot S, Sevault F, Déqué M, Crépon M (2008) 21st century climate change scenario for the Mediterranean using a coupled atmosphere–ocean regional climate model. Glob Planet Chang 63(2–3):112–126. https://doi.org/10.1016/j.gloplacha.2007.10.003

Taibi S, Meddi M, Mahé G (2019) Seasonal rainfall variability in the southern Mediterranean border: observations, regional model simulations and future climate projections. Atmósfera 32(1):39–54. https://doi.org/10.20937/atm.2019.32.01.04

Tramblay Y, Jarlan L, Hanich L, Somot S (2018) Future scenarios of surface water resources availability in north African dams. Water Resour Manag. https://doi.org/10.1007/s11269-017-1870-8

Wang Q, Xu Y, Wang Y, Zhang Y, Xiang J, Xu Y, Wang J (2020) Individual and combined impacts of future land-use and climate conditions on extreme hydrological events in a representative basin of the Yangtze River Delta, China. Atmos Res 236:104805. https://doi.org/10.1016/j.atmosres.2019.104805

Wilby RL, Dawson CW (2007) SDSM 4.2-A decision support tool for the assessment of regional climate change im-pacts. United Kingdom

Yang C, Wang N, Wang S (2017) A comparison of three predictor selection methods for statistical downscaling. Int J Climatol 37(3):1238–1249. https://doi.org/10.1007/s00704-016-1956-x

Yilmaz AG, Imteaz MA (2011) Impact of climate change on runoff in the upper part of the Euphrates basin. Hydrol Sci J 56(7):1265–1279. https://doi.org/10.1080/02626667.2011.609173

Zerouali B, Chettih M, Abda Z et al (2020) The use of hybrid methods for change points and trends detection in rainfall series of northern Algeria. Acta Geophys 68:1443–1460. https://doi.org/10.1007/s11600-020-00466-5

Zerouali B, Chettih M, Abda Z et al (2021a) Spatiotemporal meteorological drought assessment in a humid Mediterranean re-gion: case study of the Oued Sebaou basin (Northern Central Algeria). Nat Hazards 108:689–709. https://doi.org/10.1007/s11069-021-04701-0

Zerouali B, Chettih M, Alwetaishi M, Abda Z, Elbeltagi A, Augusto Guimarães Santos C, Hussein EE (2021b) Evaluation of karst spring discharge response using time-scale-based methods for a Mediterranean Basin of Northern Algeria. Water 13:2946. https://doi.org/10.3390/w13212946

Zerouali B, Elbeltagi A, Al-Ansari N et al (2022) Improving the visualization of rainfall trends using various innovative trend methodologies with time–frequency-based methods. Appl Water Sci 12:207. https://doi.org/10.1007/s13201-022-01722-3

Zittis G, Hadjinicolaou P, Klangidou M et al (2019) A multi-model, multi-scenario, and multi-domain analysis of regional climate projections for the Mediterranean. Reg Environ Chang 19:2621–2635. https://doi.org/10.1007/s10113-019-01565-w

Zkhiri W, Tramblay Y, Hanich L et al (2019) Spatiotemporal characterization of current and future droughts in the high atlas basins (Morocco). Theor Appl Climatol 135:593–605. https://doi.org/10.1007/s00704-018-2388-6

Chapter 12
Predication of Sugarcane Yield in the Semi-Arid Region Based on the Sentinel-2 Data Using Vegetation's Indices and Mathematical Modeling

Chaitanya B. Pande, Sunil A. Kadam, J. Rajesh, S. D. Gorantiwar, and Mukund G. Shinde

Abstract This paper is aimed at developing the model of prediction of the sugarcane yield based on the satellite data and mathematical modeling. Remote sensing satellites have been monitoring agricultural crops with regard to growing, harvesting, and other periods. Satellite data have provided accurate information on the earth surface and then easily interpreted which crop is in good health and which is unhealthy, and vegetation indices can give more valuable information for the prediction of crop yield. In this regard, if farmers can estimate the yield before harvesting this is very helpful to the farmers and countries. In this study, ground truth data were collected by farmer's fields and validated with satellite indices and predicted yield. In this model sugarcane crop is first selected for the prediction of yield because 72% of crops consist of sugarcane and the duration of this crop is 8–12 months. During the survey, information was collected on crop yield, the demonstration plots were verified and the observed yield computed. Sentinel-2 data were selected for crop yield forecasting. This crop model used three vegetation indices (Normalized Difference Vegetation Index [NDVI], Enhanced Vegetation Index [EVI], and Green Chlorophyll Vegetation Index [GCVI]), which have been computed from sentinel-2 data using Raster Calculator. To correlate the sugarcane observed crop yield, NDVI, EVI, and GCVI values were computed by linear model. Sugarcane crop yield correlated strongly with the NDVI, EVI, and GSVI (NDVI:

C. B. Pande (✉)
Indian Institute of Tropical Meteorology (IITM), Pune, Maharashtra, India
e-mail: chaitanay45@gmail.com

S. A. Kadam · J. Rajesh · S. D. Gorantiwar · M. G. Shinde
Center for Advanced Agriculture Science and Technology on Climate-Smart Agriculture and Water Management, Mahatma Phule Krishi Vidyapeeth, Rahuri, Maharashtra, India

C. B. Pande et al. (eds.), *Climate Change Impacts on Natural Resources, Ecosystems and Agricultural Systems*, Springer Climate,
https://doi.org/10.1007/978-3-031-19059-9_12

R^2 = 0.65, EVI: R^2 = 0.598 and GCVI: R^2 = 0.746). The GCVI index has a high correlation with observed yield using a linear model. Therefore, three linear correlation models have been developed by vegetation indices to determine which indices correlated best with the prediction yield. The observed yield data were compared with normalized vegetation index and other indices. The sugarcane yield is high compared with the observed yield.

Keywords Crop yield · NDVI · Linear correlation models · Sentinel-2 data

Introduction

Regularly checking and monitoring agronomy crop situations in the growing period are significant for approximation before cutting the plant yield (Dorigo et al. 2007). The manufacture of agricultural crops and the forecast of crop yields have a direct an effect every year nationwide with worldwide economic and performance a significant part of the entire sustainable food quality and security management (Wendroth et al. 2003; Sakhare 2017). In so many nations, including India and Ethiopia, crop yield assessment is dependent on conventional methods of yield and crop data accumulation and field information (CSA 2008; Anup et al. 2006; FAO 2016, 2017). The conventional techniques are very expensive, time-intensive, and inclined to many mistakes for an unfinished field report (Gulhane et al. 2022). That information was directed to poor agronomy plant yield calculations. The agronomy crop growth mathematical model is very effectively utilized to forecast crop yields before harvesting crops at the demonstration plots (Jorgensen 1994; Bastiaanssen and Ali 2003; Dorigo et al. 2007). Innovative technologies such as Geographic Information System (GIS), Global Positioning System (GPS), remote sensing, drones, machine programming language (Pande et al. 2022), image processing, and plant yield development models enabled chances of developing farming economic schemes (Jones 1982; Burke and David 2016; Pande et al. 2018). The advanced sensors and satellite data can continuously detect large single areas of agriculture land that have been enhanced to give the opportunity to observe farm production within large sections of the globe (Tucker et al. 1983; Doraiswamy et al. 2003; Pinter et al. 2003; Pande et al. 2021b; Shahid et al. 2021; Srivastava and Chinnasamy 2021). Additionally, geo-informatics with sensor techniques are able to give data on the exact varieties of plant with real-time snaps of variations under different circumstances directly affected by climate and various disaster activities (Reynolds et al. 2000; Pande et al. 2021a, 2022). The technologies can also possibly permit operators to find the agronomy crop types and evaluation crop yields. The large correlation with crop vegetation spectral values has been demarcated using unmanned aerial vehicles (UAVs) and satellite (Jones 1982; Zhao et al. 2007; Fermont and Benson 2011).

Presently, today's geo-informatics advances have been useful for evaluating crop yields in countries such as Australia, Japan, China, United States, Malaysia, and India; still, broad examinations are as yet required, because past remote detecting procedures may have been extensively used for estimating the crop yield. As accurate appraisal for agronomy crop yields through UAV and satellite pictures with various sensors is not straightforward and significantly progressively extreme in the state of African horticultural plans (FAO 2017; Orimoloye et al. 2022).

In the Normalized Difference Vegetation Index (NDVI) has been indicated the crop growth development and future yields could forecasting using computation models by different strategies from simple coordination to enormous complex change. NDVI is shown a vegetation condition and stages of agriculture crop (Groten 1993; Hayes and Decker 1996; Rosema et al. 1998); in this way, it shows levels of wellbeing and vermin in the farming improvement and adopted the digital technology that time timely identified the damage and stress in the soil then full-fill whole need of crop after farmers can get the huge yield production under climate change. Despite the fact that different vegetation yield phases of plots may differ from those of green and regular vegetation on account of human impacts, including, for example, water system, utilization of manure and pesticides, the NDVI is permitted as a significant wellspring of material for the circumstances of farming harvests. Such huge numbers of analysts and researchers have taken a shot at the different strategies (Stoikos 1995; Jones 1982) autoregressive state space models least-square relapse, according to the exponential-direct farming harvest advancement calculation and arithmetical yield model, which have been applied to the estimation of harvest yields with better achievement, and those outcomes are helpful for horticulture creation (Oroda 2001; Jackson and Huete 1991). Hence, the creation and application of an appropriate and correct crop yields assessment cycle that decreases the manpower needed for the collection of data, with differences among the observed and assessed given are needed. A comparatively correct estimation of plant yield may be determined if plant development and other stage situations are regularly monitored using GIS and geospatial techniques. These technologies and methods also could, importantly, benefit farmers, administration, and further policy results to correctly assign properties and accept timely positive observation for an improvement of sustainable food security. Suppose exact data and very fine resolution geospatial data are utilized for the assessment of the sugarcane crop yield within India. The predicted crop yield is dependent upon the different techniques and material bases such as ground field surveys, subject expert knowledge, regression analysis, trend analysis, multi-regression analysis, statistical models, and sugarcane crop growth models. In this area one sugarcane plant yielding estimation and forecasting model is established depending on the sugarcane yield evaluations, applying the NDVI, Enhanced Vegetation Index (EVI), and Green Chlorophyll Vegetation Index (GCVI). These vegetation indices can be estimated from satellite data using geospatial software. The different vegetation indices are compared with observed yield using the linear regression correlation model. The prediction of the sugarcane crop yield in the semiarid region is developed through satellite data and the linear regression model.

Study Area

The current study area is located in the Sadegaon village of Ta. Rahuri, Dist. Ahmednagar, Maharashtra, India (Fig. 12.1). The area is part of a semi-arid region and most of the land is familiar to the sugarcane crop owing to water availability and the farm land has the most cultivating agricultural demonstrations within the Sadegaon village (Fig. 12.2). The area latitude and longitude are 74° 40′ 0″ E, 19° 21′ 0″ N to 74°41′ 30″ E, 19° 20′ 00″ E. The area has a well drainage network with irrigation waterways from the Mula River dam and a surrounding area of channels such as a key canal with extremely productive farm lands in the village.

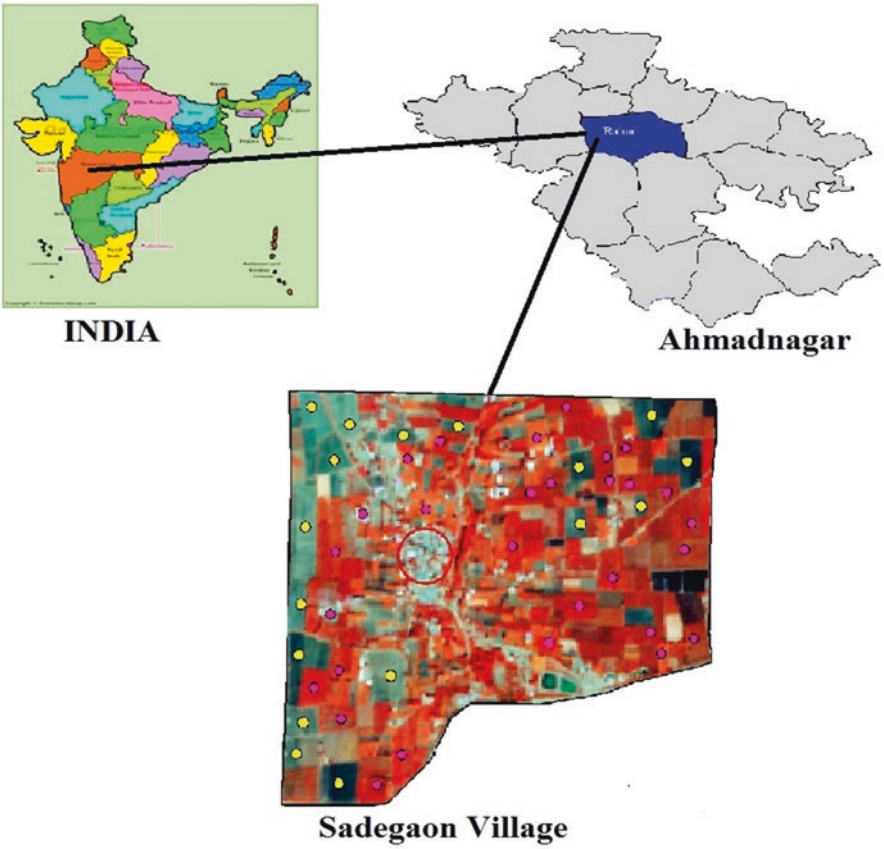

Fig. 12.1 Location map of the study area

Fig. 12.2 Photographs showing stages of the sugarcane crop. (**a**) Sugarcane crop during the months of November to December 2017. (**b**) Growth stage of the sugarcane crop during September to December 2018. (**c**) Harvested sugarcane crop during the months of January to February 2019

Materials and Methods

Data Collection

Freely available Sentinel-2 data were collected from Google earth engine platform after all the images had been pre-processed, and reflectance values were extracted by GPS observation points data; the sugarcane crop yield was calculated from observation plots. The current analysis based on the 10-m high-resolution Sentinel-2 data was acquired and in these data 13 spectral bands were combined, but the current study used of four bands, 2 to 4 and 8, which were observed for the estimation of plant yield. These three bands play an important part in the creation of the vegetation index. In this study area, most farmers are familiar with sugarcane crop for 12–14 months. For sugarcane crop modelling 12 plots were selected. From the selected 12 plots information was collected during the before and after harvesting stages of the sugarcane crop. All 12 observation areas of farm land at large locations were finally chosen and located using the GPS method, and then were regularly observed, including crop height and crop condition with yield estimation. This study's only plant yield calculation was done for sugarcane crop modeling available. The crop sowing and harvesting periods are included in Fig. 12.3.

Satellite Data Analysis

In the study area linear regression models were created for the forecasting of yield and these models were totally based on the satellite data analysis. In the satellite data pixel values to various indices were shown such as the GCVI, NDVI, and EVI. In this study the Raster Calculator of Arc GIS 10.1 was used to make the various indexes with clip point data from every index[4]. These three indices values were inserted into the models and correlated with ground yields, then forecasting the sugarcane yield (see Fig.12.6). Three vegetation indices for every pixel were estimated by two types of bands, red and near infrared (NIR) reflectance, as follows:

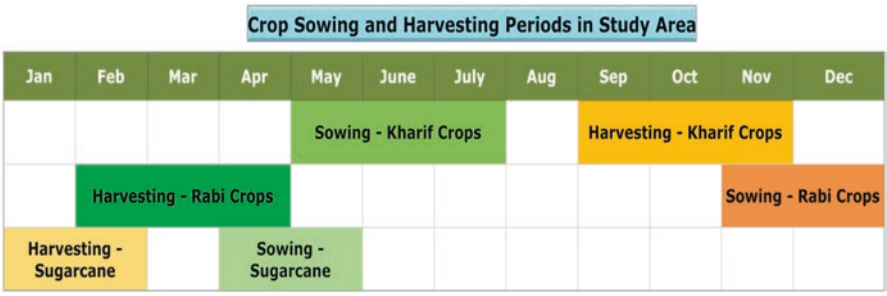

Fig. 12.3 Crop sowing and harvesting periods

In the satellite data the red (B3) and NIR (B4) bands are 0.63 to 0.69 and 0.76 to 0.90 μm respectively

$$\mathrm{NDVI} = \frac{\left(\mathrm{NIR}\left(\mathrm{band}\right) - \mathrm{RED}\left(\mathrm{band}\right)\right)}{\left(\mathrm{NIR}\left(\mathrm{band}\right) + \mathrm{Red}\left(\mathrm{band}\right)\right)}$$

$$\mathrm{GCVI} = \frac{\left(\mathrm{NIR}\left(\mathrm{band}\right)\right)}{\left(\mathrm{Green}\left(\mathrm{band}\right)\right)} - 1$$

$$\mathrm{EVI} = \mathrm{G}\left(\mathrm{band}\right) * \frac{\mathrm{NIR}\left(\mathrm{band}\right) - \mathrm{RED}\left(\mathrm{band}\right)}{\mathrm{NIR}\left(\mathrm{band}\right) + \mathrm{C1} * \mathrm{RED}\left(\mathrm{band}\right) - \mathrm{C2} * \mathrm{Blue}\left(\mathrm{band}\right) + \mathrm{L}}$$

After effective recognition of the best time for the predicted plant yield, the regression examination was completed among mean NDVI, EVI, and GCVI ranges of time with sugarcane crop information. The study area was analyzed and evaluated based on results from the linear regression model so as to observe the large appropriate model. The procedure attempted to create the future plan and the model is digitally presented in Fig. 12.4.

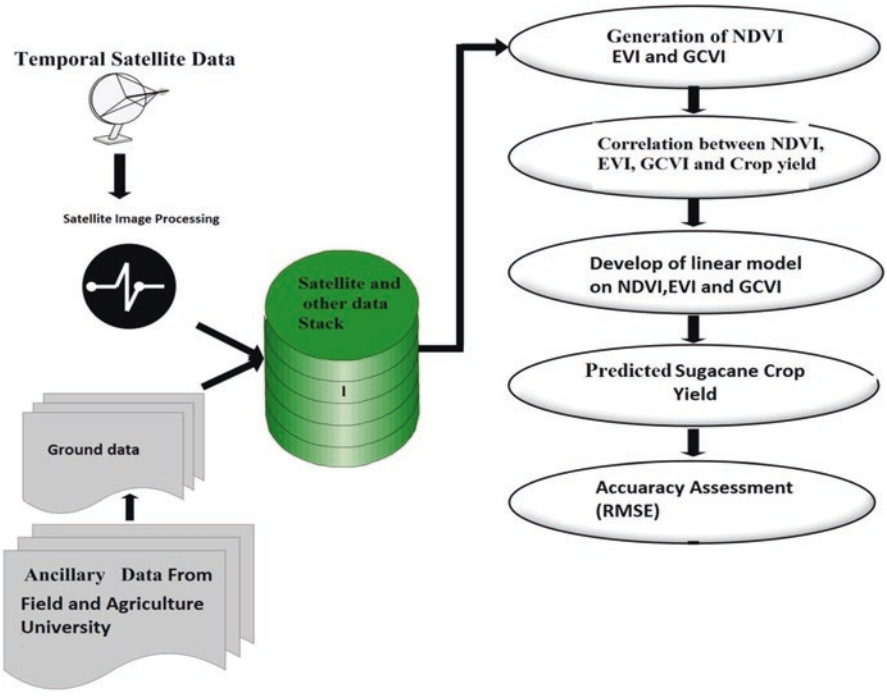

Fig. 12.4 Flow chart of methodology

Field Work

The sites of the wheat crop were given by semi-arid regions in the Maharashtra state. During the field work ten wheat plots were selected in the semi-arid regions (Fig. 12.1). Cadastral maps were used as a reference to identify the plot borders. Samples were taken from the soil in order to look at soil properties of wheat-cultivated land. The plots were located by using a GPS instrument. Wheat-cultivated land was visited and photographed ten times in the procedure until the harvest phase.

Application of Remote Sensing and the Role of GIS in Crop Yield

A common application of geoinformatics knowledge is for observing sugarcane crop yields. RS and GIS can be identified the green plant vegetation's using low reflectance wavelength and transmittance and converted them into the visible range of the spectrum (wavelength 400–700 nm) owing to the vigorous absorbance using photosynthetic crop colors. The study of reflectance and transmittance are both typically maximum values in the NIR section (700–1300 nm). The fact that the current study utilized the vegetation indexes (VIs) is significant for demarcating the green vegetation amount indication from the composite canopy spectrum. The study of plant yield estimation used various types of vegetation indices, whereas the analysis selected three major indices viz. GSVI, EVI, and NDVI and these three indices are working for a very easy and better accuracy of estimation of stressed and mature crops[2]. The common disadvantage of most approaches that use statistical associations with the NDVI and plant yield is higher empirical parameters using correlation coefficients[11].

Temporal data for growing rates and crop replies to activate the climate situations and planning practices. This is a great chance for influences such as dryness, soil nutrients, pest infestation, and diseases to directly impact the crop yield, but particularly now when today's climate change factors have affected crop yields and more pest and diseases have been observed on the plants.

Crop Yield Modeling

The generation of mathematical models for sugarcane crop yield forecasting depends on the mean NDVI and the EVI with a GCVI profile, in which the best indices correlated with observed yield under linear regression model performance and evaluation of the developed model using root mean square error (RMSE). Crop yield modeling has been very helpful to farmers and agricultural departments (Fig. 12.4).

Results

These techniques are hugely expensive and require a lot of manpower, period overriding, and are disposed to maximum mistakes owing to the imperfect environment of field explanations. However, the developed models needed various input factors, which are precise with the agriculture crop, soil properties, agronomy practices, and climatic situations. The crop model predicts the yield before harvesting of the sugarcane crop. In developed nations the crop yield model has been effectively used during climate changes and water issues. Thus, currently, every country is facing the problems of climate change factors so much, because at any time, rainfall, day-by-day temperature increases, and most importantly pollution of air and water. directly impact climate change and agricultural production. Today's new innovations are in advanced remote sensing techniques, satellite image analysis, and plant yield. The study of crop modeling and the geoinformatics framework consisted of the hopeful chances of refining farming system and farmer practices, so many climate changes affected on the crop and natural resources in the earth. The objectives consist of the data structure and are helpful for sugarcane crop yield prediction. This information may be helpful for the development of agricultural practices and change the advanced mode to development of this sector of India because agriculture sector is backbone of India and 70% peoples depend on the agriculture sector hence we can change the policy and practices as compare to climate. That time our farmers can facing any problems related to agriculture and farming system. The regression modeling based on the NDVI, EVI, and GCVI ranges are used from the sugar crop sowing within the best period and the past plant yield data within the Sadegaon village. The results from the study area are shown in Table 12.1. Regression model equations, the coefficient of determination (r^2), and the connection to the vegetation models are presented in Fig. 12.5. The connection between the sugarcane yield and NDVI ranges is denoted efficiently by using the linear model as compared with other vegetation indices in Sadegaon village. However, the coefficient of determination for the regression models associated with the linear model are found to be highly related (Fig. 12.6).

In this paper we have developed four models: logarithmic, exponential, polynomial, and linear models. The four models were compared with each other, but the linear model is best for the prediction of sugarcane crop yield. The GCVI is highly correlated with observed crop yield based on the linear model (Figs. 12.5 and 12.6).

A detailed statistical analysis was performed to examine the competence of the outcomes found by the linear model for the different vegetation indices on the current proposed methodology. In this study, statistical analysis RMSE was worked out

Table 12.1 Regression model equations for the yield estimation

Vegetation indices	Model	Equation	Coefficient determination
NDVI	Linear	$y = 46.80x + 22.68$	0.655
EVI	Linear	$y = -18.46x + 71.36$	0.598
GCVI	Linear	$y = 3.911x + 43$	0.746

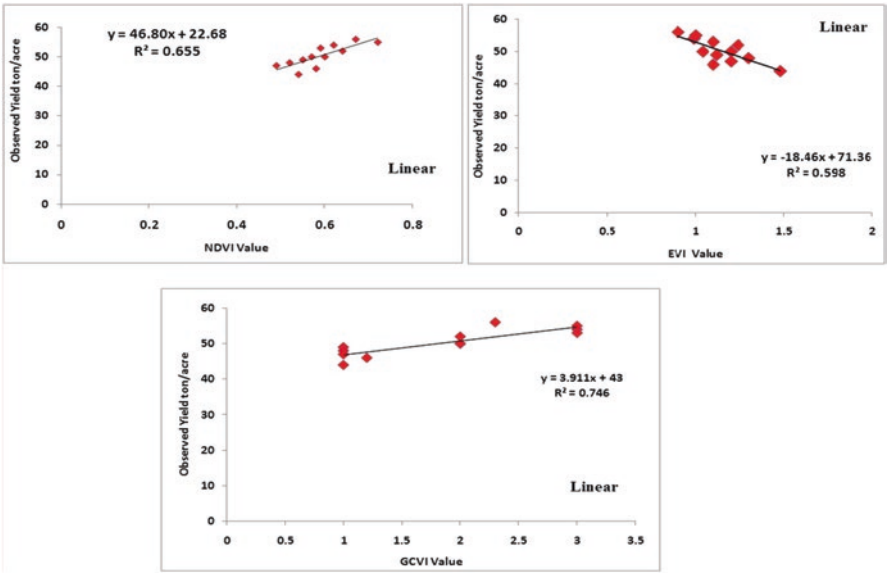

Fig. 12.5 Correlation between the observed yield with the NDVI, EVI, and GCVI indices based on the linear model

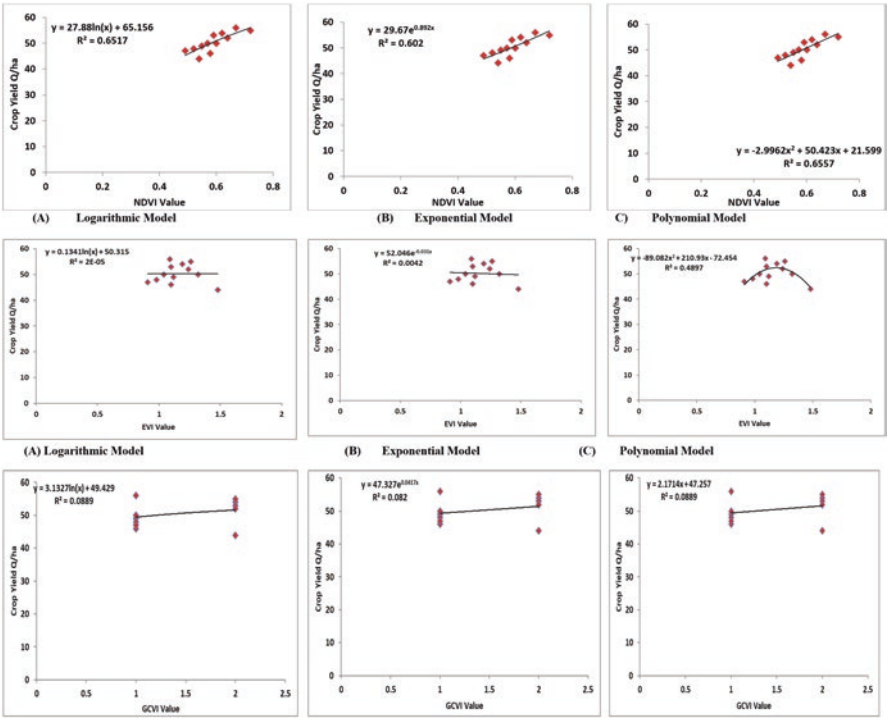

Fig. 12.6 Correlation between the observed yield with the NDVI, EVI, and GCVI indices based on logarithmic, exponential, and polynomial models

to calculate the act with the behavior of the suggested model observed, with suitable time for forecasting of the sugarcane crop yield assessment for the entire Sadegaon village.

$$\text{RMSE} = \frac{1}{n}\sqrt{\sum\left(Py_i - Oy_i\right)^2},$$

where n is the total number of observations, Py denotes estimated or predicted yield, and Oy is the observed or actual yield.

Models, which can give the more accuracy for estimation of crop yield. we have observed the yield data from 12 various farmer fields for used of development of predicted crop models. The observed information was analyzed in the differences between the forecast and experiential yield information. The outcome values were calculated using the RMSE equation and these results are shown in Table 12.2 and Fig. 12.7. The predicted sugarcane crop yield is a smallest RMSE choice for model development, which based on the model we have better forecasting of sugarcane crop yield data in the semi-arid region.

Discussion

Prediction Versus Observed Sugarcane Yield

The NDVI, EVI, and GCVI are available to respond to changes in chlorophyll content, water stress, and green biomass. Actual values are forecasting surface characteristics when the agriculture plant canopy is not so much thin or thick vegetations. Owing to the rise in NDVI, EVI, and GCVI values concurrently with increasing sugarcane crop yield, the NDVI, EVI, and GCVI ranges influence the maximum and minimum values during the development stage, and maturing growth stage of sugarcane crop. This decrease due to the detail that the sugarcane crop greenery is yellow during the maturing stage and the NDVI, EVI, and GCVI have been directly related to the chlorophyll content of sugarcane crop plants and vegetation. Soil moisture factors also increase the NDVI, EVI, and GCVI ranges during the crop growth period. The harvesting time crop has been shown the NDVI, EVI, and GCVI values decreased; accordingly, there is a good association with the sugarcane crop produce with NDVI ranges during the cutting period as they are victims of the

Table 12.2 Model validation and performance indicator using RMSE

Vegetation indices	Model	RMSE
NDVI	Linear	0.10
EVI	Linear	0.17
GCVI	Linear	0.04

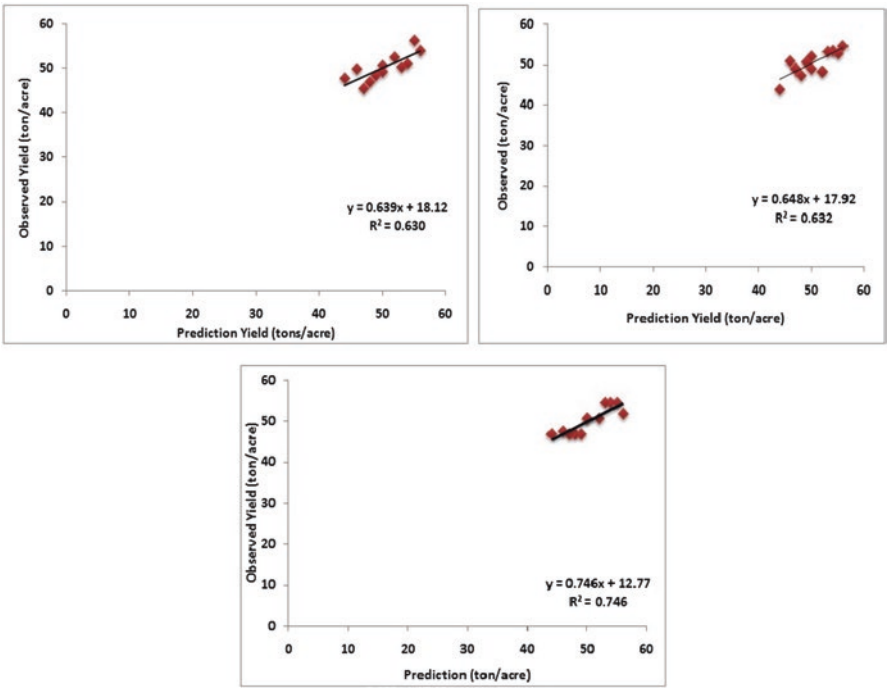

Fig. 12.7 Correlation of observed yield with predicted yield in Sadegaon village

humidity factor. Therefore, the best period for prediction of sugarcane production is around 60 days pre-harvest of sugarcane yield in the area.

Sugarcane Yield Prediction Using Linear Regression Model
Table 12.3 clearly show a summary of the statistics of sugarcane plant yield estimation in a semiarid region based on various vegetation indices of 12 plots in Sadegaon village. In this study, linear regression models were utilized to predict the sugarcane yield with the help of the available data. Average sugarcane yield is large or less similar among plots. However, much variation exists in the sugarcane yield between plots. On the whole, the results clearly show that three of the vegetation indices have been upscaled with the help of the prediction of agriculturalists' yields on small and larger scales (Fig. 12.8).

Conclusion

The study area was created to support sugarcane crop yield assessment equation by using geoinformatics methods to estimate production and support farmers of the sugarcane plant in Sadegaon village. We collected yield information data from

Table 12.3 Sugarcane crop yield predicted based on the NDVI

Plot no.	Observed yield (tonne/acre)	Predicted yield (tonne/acre) (NDVI)	Predicted yield (tonne/acre) (EVI)	Predicted yield (tonne/acre) (GCVI)
1	54	51.08	53.54	54.73
2	53	50.29	53.25	54.73
3	46	49.91	51.04	47.69
4	49	48.42	50.68	46.91
5	50	49.36	49.2	50.82
6	55	56.38	52.9	54.73
7	48	47.01	47.36	46.91
8	47	45.61	49.2	46.91
9	52	52.63	48.47	50.82
10	44	47.95	44.04	46.91
11	56	54.04	54.75	52
12	50	50.76	52.16	50.82

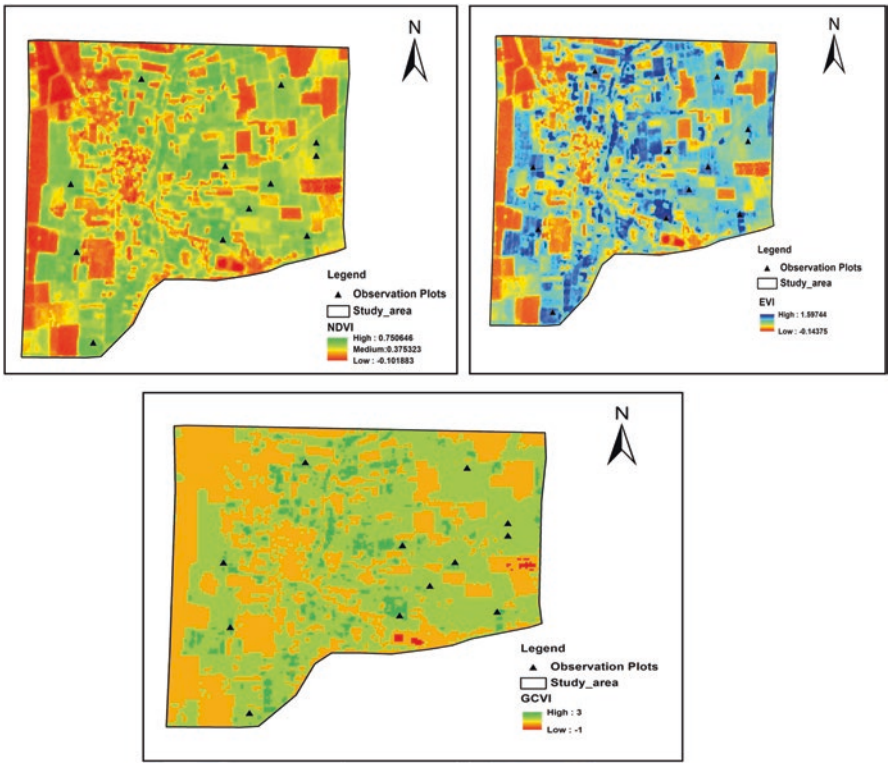

Fig. 12.8 Spatial distribution maps of (**a**) the NDVI, (**b**) the EVI, and (**c**) the GCVI at the observation of sugarcane plots

farmers' fields, agricultural experts, and satellite images to create methods of predicting and assessing sugarcane crop yield modelling. Sugarcane yields are well fitted with the NDVI ($R^2 = 0.65$) and/or the GCVI ($R^2 = 0.746$). The EVI ($R^2 = 0.0598$) is highly correlated with yield and whole indices but all vegetation indices show minimum values of RMSE. Such kinds of study so important for India, because so many farmers are facing the loss yield during last stage because heavy rainfall and climate change, hence crop insurance and government can be adopted advanced technology and models for measuring the past yield. After these responsible company and government can provide crops loss amount to farmer based on the remote sensing, GIS and ML models. We have strongly recommended whole crop losses amount provide to farmer based on the only remote sensing, GIS and ML models with verified. The linear model shows better practice than the other models. The outcome of the proposed crop yield forecasting technique demonstrates potential. Any crop model can develop that time most important input data from farmer systems and ecological parameters in the semi-arid region are included in the modeling. The comparison of observed and predicted yield is shown in Figs. 12.9, 12.10 and 12.11.

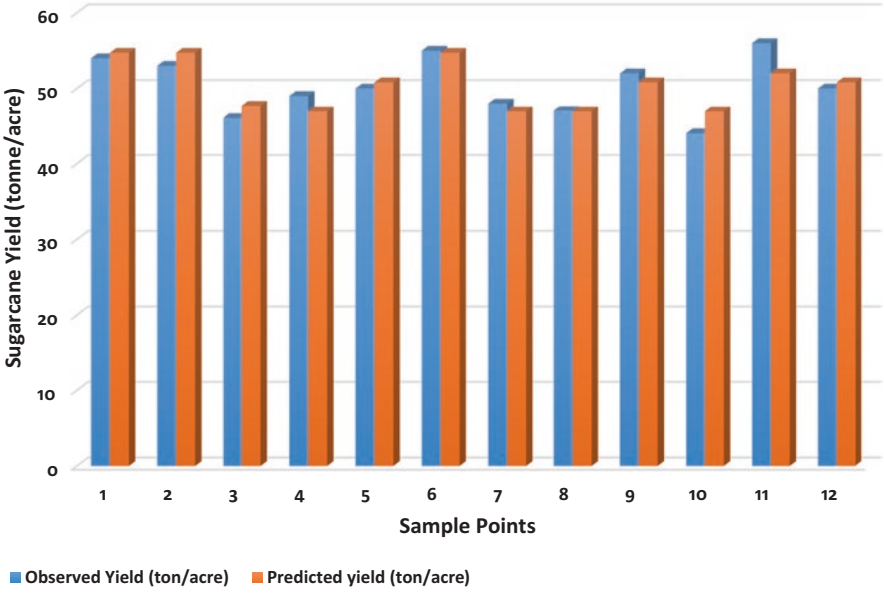

Fig. 12.9 Observed versus predicted sugarcane yield based on NDVI values

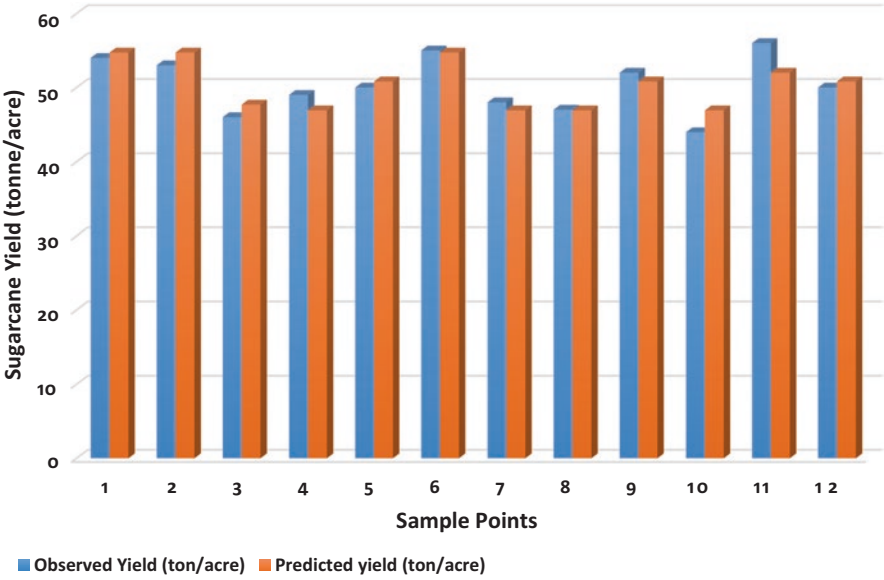

Fig. 12.10 Observed versus predicted sugarcane yield based on EVI values

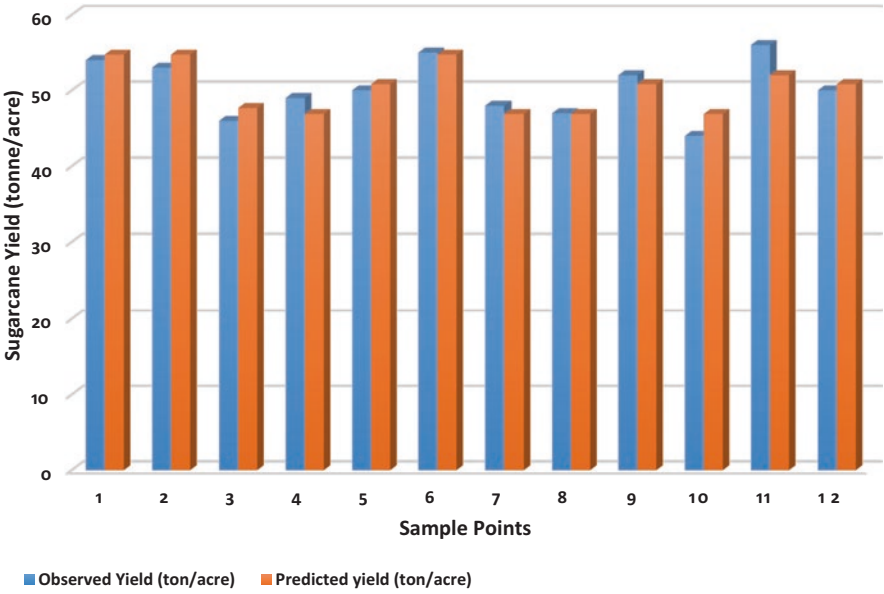

Fig. 12.11 Observed versus predicted sugarcane yield based on GCVI values

Acknowledgements We are grateful to the Principal Investigator, Center for Advanced Agriculture Science and Technology on Climate Smart Agriculture and Water Management, MPKV, Rahuri (Agricultural University) and ICAR, NAHEP, and the World Bank for providing the necessary facilities and financial support to conduct this research.

References

Anup K, Prasad LC et al (2006) Crop yield estimation model for Iowa using remote sensing and surface parameters. Int J Appl Earth Obs Geoinf 8:26–33

Bastiaanssen GM, Ali S (2003) A new crop yield forecasting model based on satellite measurements applied across the Indus Basin, Pakistan. Agric Ecosyst Environ 94:321–340

Burke M, David LB (2016) Satellite-based assessment of yield variation and its determinants in smallholder African systems. Department of Earth System Science, Stanford University, Stanford

Chaitanya B. Pande (2022) Land use/land cover and change detection mapping in Rahuri watershed area (MS), India using the google earth engine and machine learning approach. Geocarto Int. https://doi.org/10.1080/10106049.2022.2086622

CSA (2008) Agricultural sample survey 2007/2008. Volume I – Report on area and production crops (Private Peasant Holdings, Meher Season). Statistical Bulletin 417. Addis Ababa: Central Statistical Agency, (2000 E.C.)

Doraiswamy PC, Moulin S, Cook PW, Stern A (2003) Crop yield assessment from remote sensing. Photogramm Eng Remote Sens 69:665–674

Dorigo WA, Zurita-Milla R, de Wit AJ, Brazile J, Singh R, Schaepman ME (2007) A review on reflective remote sensing and data assimilation techniques for enhanced agroecosystem modeling. Int J Appl Earth Obs Geoinform 9:165–193

FAO (2016) Crop yield forecasting: methodological and institutional aspects. Food and Agriculture Organization of the United Nations, Rome

FAO (2017) Review of the available remote sensing tools, products, methodologies and data to improve crop production forecasts. Food and Agriculture Organization of the United Nations, Rome

Fermont A, Benson T (2011) Estimating yield of food crops grown by smallholder farmers. International Food Policy Research Institute

Groten SME (1993) NDVI-crop monitoring and early yield assessment of Burkina Faso. Int J Rem Sens 14:1495–1515

Gulhane VA, Rode SV et al. (2022) Correlation analysis of soil nutrients and prediction model through ISO cluster unsupervised classification with multispectral data. Multimed Tools Appl. https://doi.org/10.1007/s11042-022-13276-2

Hayes MJ, Decker WL (1996) Using NOAA AVHRR data to estimate maize production in the United States Corn Belt. Int J Remote Sens 17:3189–3200

Jackson RD, Huete AR (1991) Interpreting vegetation indexes. Prev Vet Med 11:185–200

Jones DR (1982) A statistical inquiry into crop–weather dependence. Agric Meteorol 26:91–104

Jorgensen SE (1994) Models as instruments for combination of ecological theory and environmental practice. Ecol Model 75–76:5–20

Orimoloye IR, Olusola AO, Belle JA et al (2022) Drought disaster monitoring and land use dynamics: identification of drought drivers using regression-based algorithms. Nat Hazards 112:1085. https://doi.org/10.1007/s11069-022-05219-9

Oroda A (2001) The International archives of the photogrammetry. Remote Sens Spatial Inform Sci XXXIV:66–72

Pande CB, Moharir KN, Khadri SFR, Patil S (2018) Study of land use classification in the arid region using multispectral satellite images. Appl Water Sci 8(5):1–11

Pande CB, Moharir KN, Singh SK, Varade AM, Elbeltagie A, Khadri SFR, Choudhari P (2021a) Estimation of crop and forest biomass resources in a semi-arid region using satellite data and GIS. J Saudi Soc Agric Sci 20(5):302–311

Pande CB, Moharir KN, Khadri SFR (2021b) Assessment of land-use and land-cover changes in Pangari watershed area (MS), India, based on the remote sensing and GIS techniques. Appl Water Sci 11:96. https://doi.org/10.1007/s13201-021-01425-1

Pande CB, Kadam SA, Jayaraman R, Gorantiwar S, Shinde M (2022) Prediction of soil chemical properties using multispectral satellite images and wavelet transforms methods. J Saudi Soc Agric Sci 21(1):21–28

Pinter PJ, Hatfield JL et al (2003) Photogramm Eng Remote Sens 69:647–664

Reynolds CA, Yitayew M, Slack DC et al (2000) Estimating crop yields and production by integrating FAO crop specific water balance model with real-time satellite data and ground-based auxiliary data. Int J Remote Sens 21:3487–3508

Rosema A, Roebeling RA, van Dijk A, Nieuwenhuis GJA, Huygen J, Kashasha DA (1998) ACMP agromet and crop monitoring project in the SADC region, BCRS report NRSP-2, Delft, pp 96–13

Sakhare AV (2017) Agriculture development and Indian economy. Int J Adv Std 2:1–6

Shahid M, Rahman KU, Haider S et al (2021) Quantitative assessment of regional land use and climate change impact on runoff across Gilgit watershed. Environ Earth Sci 80:743. https://doi.org/10.1007/s12665-021-10032-x

Srivastava A, Chinnasamy P (2021) Investigating impact of land-use and land cover changes on hydro-ecological balance using GIS: insights from IIT Bombay. India SN Appl Sci 3:343. https://doi.org/10.1007/s42452-021-04328-7

Stoikos G (1995) Sugar beet crop yield prediction using artificial neural networks (in Greek). In: Proceedings of the Modern Technologies Conference in Automatic Control, Athens, Greece, 120–122

Tucker CJ, Vanpraet C, Boerwinkel E, Gaston A (1983) Satellite remote sensing of total dry matter production in the Senegalese Sahel. Rem Sens Environ 13:461–474

Wendroth O, Reuter HI, Kersebaum KC (2003) Predicting yield of barley across a landscape: a state-space modeling approach. J Hydrol 272(1–4):250–263

Zhao J, Shi K, Wei F (2007) Research and application of remote sensing techniques in Chinese agricultural statistics. Paper presented at the fourth international conference on agricultural statistics, October 22–24, Beijing, China

Chapter 13
Effect of Urbanism on Land Surface Temperature (LST) in a River Basin and an Urban Agglomeration

J. Brema, Ahmed Khalid Alsalmi, C. Mayilswami, and Jenita Thinakaran

Abstract The environmental and social consequences of predicted climate change are expected to be magnified in urban regions due to the elevated temperatures, which are due to the continuous manmade processes. A research work was carried out by utilizing remote sensing and geographic information systems to explore the interactions between land surface temperatures (LST) and normalized difference vegetation index (NDVI) in an urban area and in a basin area. Increase in vegetative cover can provide microclimate formation through the process of evapotranspiration by increasing the amount of urban vegetation. This might prove to be a highly effective solution in reducing the effect of temperature toward urbanization. The results were presented based on the observations carried out using Landsat 8/ Sentinel 2 satellite imageries and from the field by deriving land-use data as input and by comparing the temperature variations, normalized difference vegetation index (NDVI), normalized differential build-up index (NDBI), and normalized differential water index (NDWI) derived from satellite imageries (2004–18) in an urban limit (Chennai City, India) and a subbasin (Noyyal River, India). The correlation revealed that both the spatial and temporal variation in vegetation sprawl and surface temperature affect the local climatic temperature. It has been suggested that

J. Brema (✉)
Department of Civil Engineering, Karunya Institute of Technology and Sciences (KITS), (Deemed to-be University), Coimbatore, Tamil Nadu, India

A. K. Alsalmi
College of Engineering, Sultan Qaboos University, Seeb, Oman

C. Mayilswami
Water Institute, Karunya Institute of Technology and Sciences (KITS), (Deemed to-be University), Coimbatore, Tamil Nadu, India

J. Thinakaran
Department of Agriculture, Karunya Institute of Technology and Sciences (KITS), (Deemed to-be University), Coimbatore, Tamil Nadu, India
e-mail: jenita@karunya.edu; hod_agri@karunya.edu

C. B. Pande et al. (eds.), *Climate Change Impacts on Natural Resources, Ecosystems and Agricultural Systems*, Springer Climate,
https://doi.org/10.1007/978-3-031-19059-9_13

future modeling studies should account for anthropogenic heating in the case of urban planning for better climatic control characteristics.

Keywords Land surface temperature · NDVI · NDWI · NDBI · Land use

Introduction

The most significant biophysical feature of a river basin is its altered surface cover, which is a major contributor to the phenomenon commonly referred to as urban heating. The excess warmth in an urban environment is due to the heating phenomenon in the urban limits when compared to the rural environment (Shahid et al. 2021). This excess warmth is estimated based on the surface cooling rates that prevail in urban and rural regions. The temperature in the surface and atmospheric region of the urban environment is generally higher when compared to the peripheries. This excess warmth is naturally due to the concrete and metal surfaces and asphalt roads, which are generally considered as nonporous and non-evaporative with high heat absorption capacity and low solar reflectivity. These materials reflect reduction in cooling rates in urban areas with respect to their surroundings. The increase in urbanization results in decrease in vegetation cover, and hence, transpiration is drastically diminished, thus causing warmer urban areas (Pande et al. 2021a, b). The most commonly observed physical phenomenon in urban region is urban heating, which can be described as elevated temperature in urban regions compared to the surroundings. Urban heat island (UHI) is of great importance for development in the field of sustainable urban planning. Anthropogenic modification of landscapes and the surroundings in the urban boundary layer results in the UHI effect. The occurrence of UHI is due to increased absorption of solar radiation, population density, vegetative cover, and the extent of built-up area (Lettenmaier et al. 2014; Meehl and Tebaldi 2004). The UHI can be monitored based on two methods, namely through air temperature and surface temperature measurements. With the advent of remote sensing, it has become quite easy to monitor the surface temperature and is being monitored globally now (Coumou and Rahmstorf 2012; Li and Bou-Zeid 2013; Arnfield 2003). The studies of land surface temperature (LST) and UHI show that surface temperature is a reflection of land cover and vegetative cover (Oke 1987; Peng et al. 2012; Zhou et al. 2013, 2014, 2015; Ma et al. 2010). Research studies envisage that increase in urban vegetation with low emissions will definitely decrease the ozone concentrations (Taha 1996). Analysis of normalized difference vegetation index (NDVI) will result in monitoring the changes in vegetation and as a result the dynamics of the ecosystem (Zaitunah et al. 2018; Streutker 2003; Chen et al. 2002; Ben et al. 2001; El-Ramady et al. 2014; Gibson 2006). In addition to the land use/land cover and LST derived from Landsat 8 were compared and the temperature difference were reckoned (Brema et al. 2019; Dagliyar et al. 2015). The changes in land surface temperature were related to many factors such as land use changes, seasonal variations, economic development, etc. (Kumar and

Shekhar 2015). Vegetation changes in large scale can be predicted by comparative analysis of trend of derived NDVI (Nicholson et al. 1990). The application of satellite imageries like Landsat 8 is highly suitable for urban planning, environmental protection, and climate studies by way of studying the correlation between LST, NDVI, and normalized difference built-up index (NDBI). In this study, the effects of UHIs and the relationship between LST, NDWI, and NDVI have been studied for the Chennai Metropolitan Area. For this purpose, Landsat 4, 5, 7, and 8 satellite imageries spreading over the period 2004–2018 have been downloaded from the USGS webpage, with an interval period of 5 years.

Multispectral Landsat-8 series imageries corresponding to the month of May corresponding to the years 2014–2017 were collected. Band 5 and Band 4 were considered for NDVI estimation. Band10, Band 11, and thermal infrared bands were considered for estimating land surface temperature in the subbasin. The observation stations have been identified as weather stations at Karunya University and Coimbatore airport. From the corresponding bands of the geocoded satellite imageries, the land surface temperature was calculated based on the emissivity and NDVI value in the Noyyal subbasin. In order to understand the variations in land surface temperature, the study area has been considered in two different regions: one in a semiarid region (Noyyal river subbasin) and the other in a coastal humid place (Chennai Metropolitan Area).

Study Area

Noyyal River basin, a tributary of river Cauvery, has a length of about 175 kms and an average width of about 25 kms. The basin sprawls over Coimbatore, Tiruppur, Erode, and Karur districts with a total extent of the basin of about 3646 sq. kms. The basin lies between the latitudes 10°53′1.06″ N–11°21′57″N and longitudes 76°37′49″E–78°12’55.06″E. The study area is shown in Fig. 13.1a, b. The subbasin

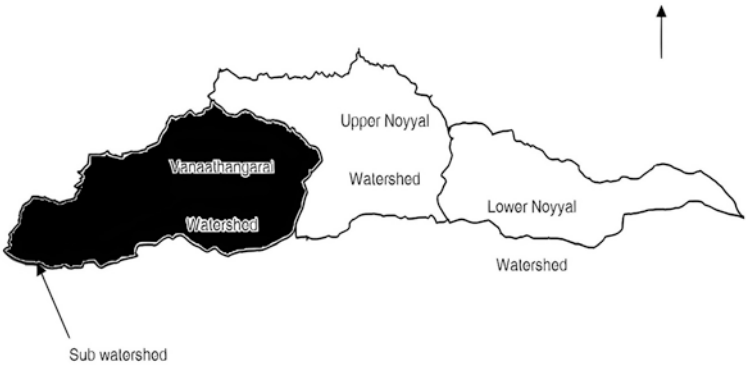

Fig. 13.1 (**a**) Noyyal River basin (**b**) Chennai Metropolitan Area

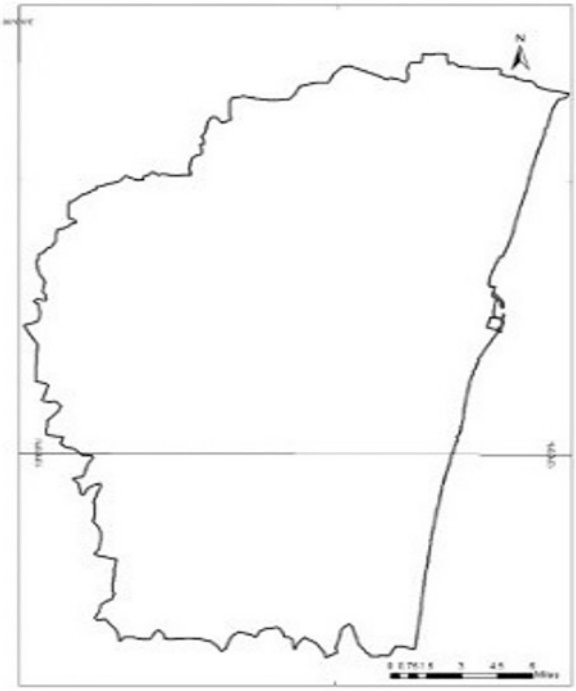

Fig. 13.1 (continued)

considered in the study is in the head region of Noyyal basin and is of 1631.54 km^2. The subbasin experiences wide spread rainfall during the northeast monsoon period from October to December. Another study area, Chennai normally receives an average annual rainfall of about 140 mm. The city experiences dry-summer tropical wet and dry climate. The region normally has maximum temperature in the range of 35–40 °C and minimum temperature with 19–25 °C.

Materials and Methods

Normalized Difference Vegetation Index (NDVI)

Generally, vegetative cover absorbs electromagnetic spectrum in the visible region. Due to the internal structure of the leaves, normally healthy vegetation has high reflectance specially in the near infrared (NIR) region between 0.7 and 1.3 μm. The plants absorb blue (0.4–0.5 μm) and Red (0.6–0.7 μm) spectrum and reflects Green (0.5–0.6 μm) spectrum. Since there is high reflectance in NIR and high absorption in red spectrum, these two bands are used to calculate NDVI. The following formula gives normalized difference vegetation index (NDVI):

$$\mathrm{NDVI} = \left(\mathrm{NIR} - \mathrm{Red}\right) / \left(\mathrm{NIR} + \mathrm{Red}\right)$$

The NDVI value varies from −1 to 1. The NDVI value increases as the reflection increases. The NDVI is categorized as: −1 to 0 represent water bodies; −0.1 to 0.1 represent Barren rocks, sand, or snow; 0.2–0.5 represent shrubs and grasslands; and 0.6–1.0 represent dense vegetation or tropical rainforest.

Land Surface Temperature(LST)

Land surface temperature is referred to as the radiation that is felt in a particular location. The land surface temperature depends on the object on the earth's surface. In a satellite imagery, it could be snow and ice, the grass on a lawn, the roof of a building, or the leaves in the canopy of a forest. Thus, land surface temperature is not the same as air temperature.

In this study, the UHI has been extracted using the following method: $UHI = \mu + \sigma/2$, in which μ is the mean LST value of the study area and σ is the standard deviation of the LST.

The estimation of land surface temperature involves the following equations:

$$L_\lambda = M_L Q_{\mathrm{cal}} + A_L \tag{13.1}$$

where L_λ = top of atmosphere spectral radiance, M_L= band-specific multiplicative rescaling factor, A_L = band-specific additive rescaling factor, and Q_{cal} = quantized and calibrated standard product pixel values.

$$T_{10} = K_2 / \ln\left(K_1 / L_\lambda + 1\right) - 273 \tag{13.2}$$

where T_{10} = top of atmosphere brightness temperature, L_λ = TOA spectral radiance, K_1 = band-specific thermal conversion constant, and K_2 = band-specific thermal conversion constant. The $K_1$and K_2, rescaling factor values used in the Eqs. 13.1 and 13.2 were obtained from the Metadata of the satellite imageries. Table 13.1 gives the values of K_1 and K_2.

$$\mathrm{LST}_{10} = T_{10} / \left(1 + \left(\lambda T_{10} / \rho\right) \ln\left(e\right)\right) \tag{13.3}$$

Table 13.1 K_1 and K_2 values

Thermal conversion constant	Band10	Band11
K_1	1321.08	1201.14
K_2	777.89	480.89

$$\text{Emissivity}, e = 0.004P_v + 0.986 \tag{13.4}$$

Normalized difference vegetation index:

$$\text{NDVI} = \text{Float}\left(\text{Band5} - \text{Band4}\right) / \text{Float}\left(\text{Band5} + \text{Band4}\right) \tag{13.5}$$

Proportion of vegetation:

$$P_v = \left(\text{NDVI} - \text{NDVI}_{\text{min}} / \text{NDVI}_{\text{max}} - \text{NDVI}_{\text{min}}\right)^2 \tag{13.6}$$

where LST is land surface temperature (in Kelvin), T_{10} is radiant surface temperature (in Kelvin), λ is the wavelength of emitted radiance (11.5 μm), ρ is h × c/s (1.438×10^{-2} m K), h is Planck's constant (6.26×10^{-34} J s), c is the velocity of light (2.998×10^{8} m/s), and s is Stefan Boltzmann's constant (1.38×10^{-23} J K).

Results and Discussions

Noyyal Subbasin

In order to assess the impact of land use changes on the meteorological parameters, the land surface temperature estimated from the satellite imageries was used. The raster image of land surface temperature, estimated based on Band 10 and Band 11 of the satellite imagery acquired on 02.05.2014 are shown in Figs. 13.2 and 13.3.

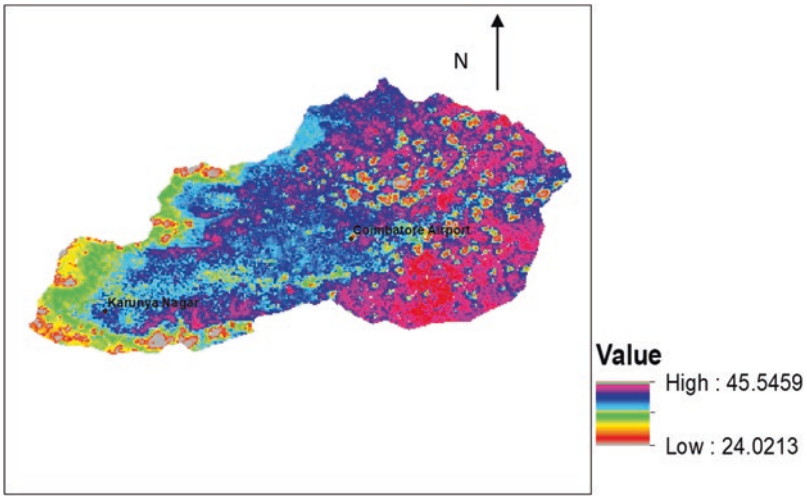

Fig. 13.2 Land surface temperature for Band 11

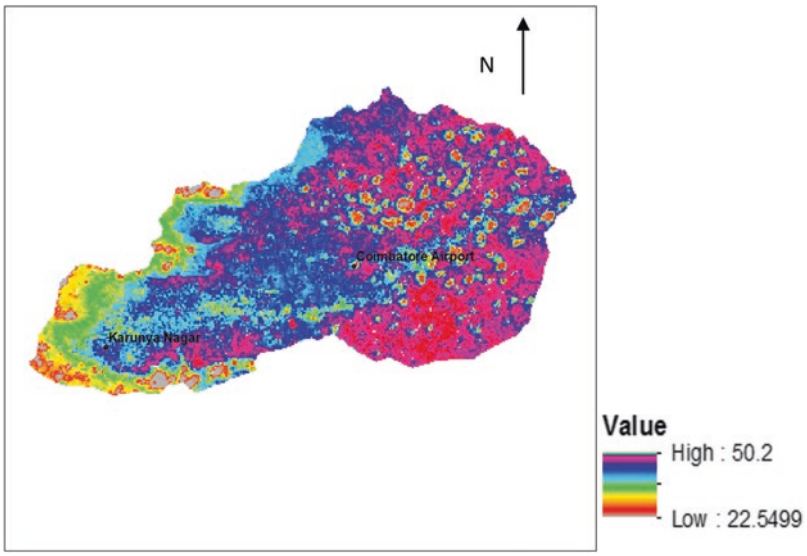

Fig. 13.3 Land surface temperature for Band 10

The temperature is very high nearer to the highly urbanized locations like Tiruppur, Coimbatore corporation, etc. In order to correlate the estimated values, the data corresponding to daily maximum and minimum temperatures from meteorological stations were used. The trends obtained for the maximum temperature showed a slight increase corresponding to the study period. The standard deviation (SD) and the coefficient of variation (C_v) for both were of less value indicating only minor variations from year to year.

The normalized difference vegetation index (NDVI) is a simple numerical indicator that can be used for analyzing the existence of vegetation by using remote sensing imageries in the study area. The NDVI is calculated as a ratio between measured reflectivity in the red and near-infrared portions of the electromagnetic spectrum. The two spectral bands, Band 4 and Band 5, were chosen as they are good indicators of the absorption of chlorophyll in leafy green vegetation and the density of green vegetation on the surface. It is also observed that in red and near-infrared bands, the contrast between vegetation and soil is exhibited to a maximum extent. The maximum NDVI value has decreased from 0.55 to 0.52 during the study period. The values of NDVI during May 2014 and May 2017 are shown in Figs.13.4 and 13.5, respectively.

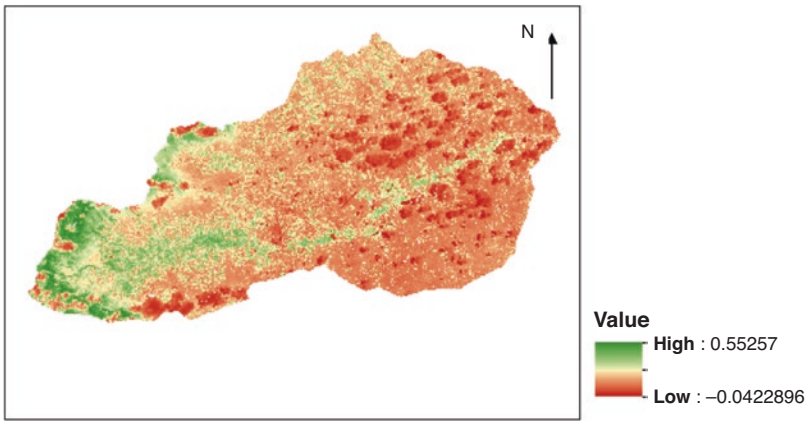

Fig. 13.4 Normalized difference vegetation index during May 2014

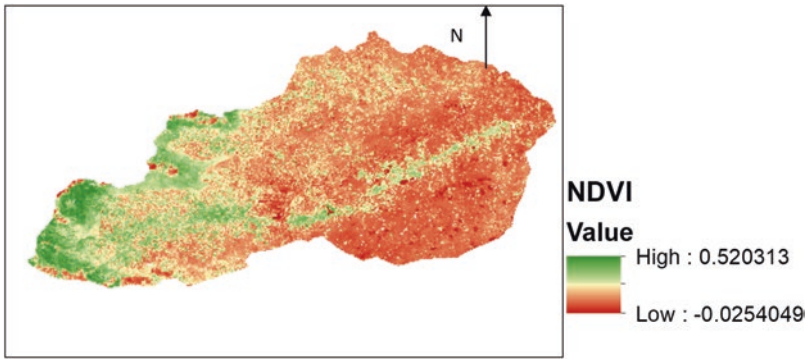

Fig. 13.5 Normalized difference vegetation index during May 2017

Statistical Analysis

The estimated land surface temperature values corresponding to both the bands were compared with the observed temperature values in two stations, namely Karunya University, Coimbatore, and Coimbatore airport. The estimated and observed values of temperature are given in Table 13.2. The correlation coefficient values were found to be 0.819 and 0.884 for Bands 10 and 11 at Karunya University, Coimbatore. The correlation values were found to be 0.432 and 0.505 corresponding to bands 10 and 11, respectively, for Coimbatore airport station.

Table 13.3 shows the estimated values of maximum and minimum temperatures in the subbasin.

From Table 13.3, it can be observed that the minimum temperature values are almost same, but there are large variations corresponding to the maximum temperature values. This may be due to increase in temperature in the highly urbanized

Table 13.2 Estimated and observed temperature values

	Years	2014	2015	2016	2017
Observed temp. °C	Karunya University	36.00	34.50	35.00	34.10
	Coimbatore Airport	35.30	32.00	34.50	34.00
Karunya University, Coimbatore	Band 10	41.58	32.91	34.99	34.39
	Band 11	38.89	29.50	34.03	30.97
Coimbatore Airport	Band 10	35.63	32.94	38.98	37.39
	Band 11	32.19	28.6	35.85	33.48

Table 13.3 Estimated temperature values in the subbasin

Category	Years	2014	2015	2016	2017
Minimum temperature °C	Band 10	22.50	9.96	23.84	16.17
	Band 11	24.04	9.68	24.12	16.32
Maximum temperature °C	Band 10	50.17	39.53	45.07	43.56
	Band 11	45.52	33.98	41.39	38.35

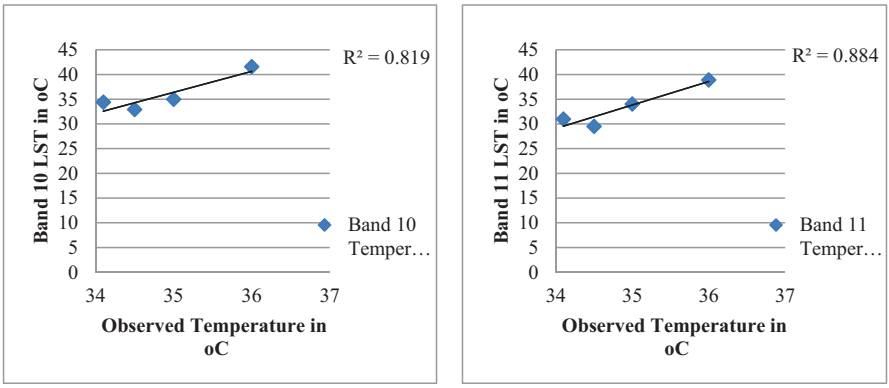

Fig. 13.6 Observed vs estimated temperature corresponding to Bands 10 and 11 at Karunya University station

locations, which is due to increased Co^2 level. Figure 13.6 shows the scatter diagram between the estimated and the observed temperatures at Karunya University, Coimbatore.

Figure 13.7 shows the scatter diagram between the estimated and the observed temperatures at Coimbatore airport.

Table 13.4 shows the estimated values of NDVI in the subbasin for the years 2014–2017.

The lowest positive and negative NDVI values are observed in the year 2017. Figure 13.8 shows the relationship between NDVI values with respect to years.

From Fig. 13.8, it can be seen that there is a decrease in NDVI value during the period of 4 years. The relationship between NDVI and surface radiance temperature was studied for the study period through correlation analysis. Surface radiant

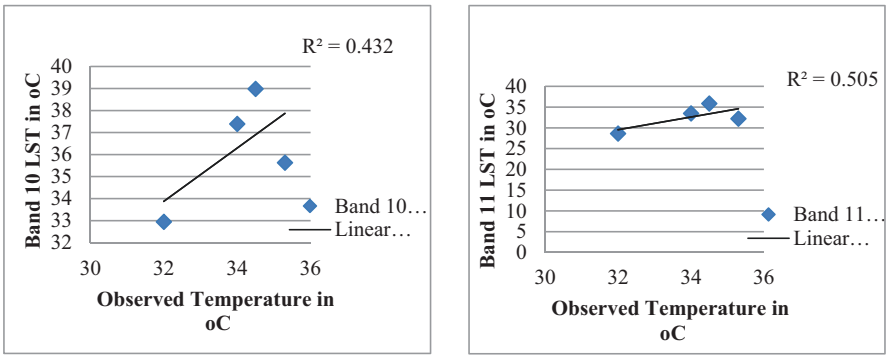

Fig. 13.7 Observed vs estimated temperature corresponding to Bands 10 and 11 at Coimbatore Airport station

Table 13.4 Estimated NDVI values in the subbasin

Category/years	2014	2015	2016	2017
Minimum	−0.42	−0.05	−0.05	−0.025
Maximum	0.552	0.547	0.547	0.52

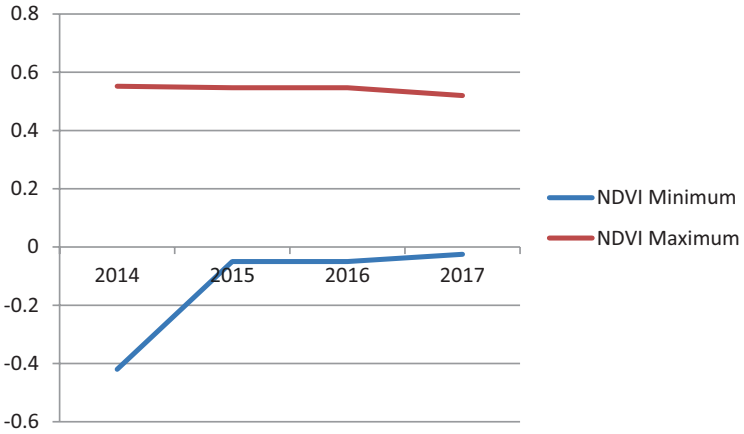

Fig. 13.8 Estimated extreme NDVI values

temperature values tend to negatively correlate with NDVI values. The methodology will help to estimate the microclimate, heat pockets, and vulnerable study aids in identifying the regions susceptible to urban heating in the study area and to take the necessary scientific actions like afforestation, reduction of vehicle pollution, construction of seepage ponds, etc., which may lead to decrease in temperature.

Chennai Metropolitan Area

Figures 13.9 and 13.10 show the variations in land surface temperature during summer corresponding to the years 2004, 2009, 2014, and 2018. The temperature values ranged from 24.6 to 42.3 °C, from 21.2 to 42.3 °C, from 22.4 to 41.0 °C, and from and 17.7 to 34.3 °C during the corresponding years. It is observed that there is a decrease in the maximum and minimum values during 2018 when compared to 2014.

Figures 13.11 and 13.12 exhibit the variation in NDVI values, which varies between −0.51 and + 0.71, −0.45 and + 0.67, −0.18 and + 0.51, and − 0.16 and + 0.50 during the years 2004, 2009, 2014, and 2018, respectively. The highest vegetative fraction is represented as +0.67 in the year 2009, and the lowest is −0.16 during 2018. Figures 13.13 and 13.14 show that the vegetation is highly distributed during 2004 and the lowest is during 2014 and 2018.

From Table 13.5 and Figs.13.13 and 13.14, it is inferred that there is an increase in fractal vegetation cover in the Chennai Metropolitan Area. It is observed that there is a reduction in forest cover in the zone XIII of the metropolitan area. In zone VIII, which consists of Anna Nagar and Kilpauk, there is a decrease in vegetative cover of 50.6% and 86% in the years 2014 and 2018, respectively. The T. Nagar location decreases in vegetative cover by 73% during 2018, when compared to 2014. A correlation coefficient between LST and NDVI has been calculated in order to explore the impact of the green land on UHI. The results from the land cover analysis showed that the vegetation area has slightly increased from 2004 to 2018

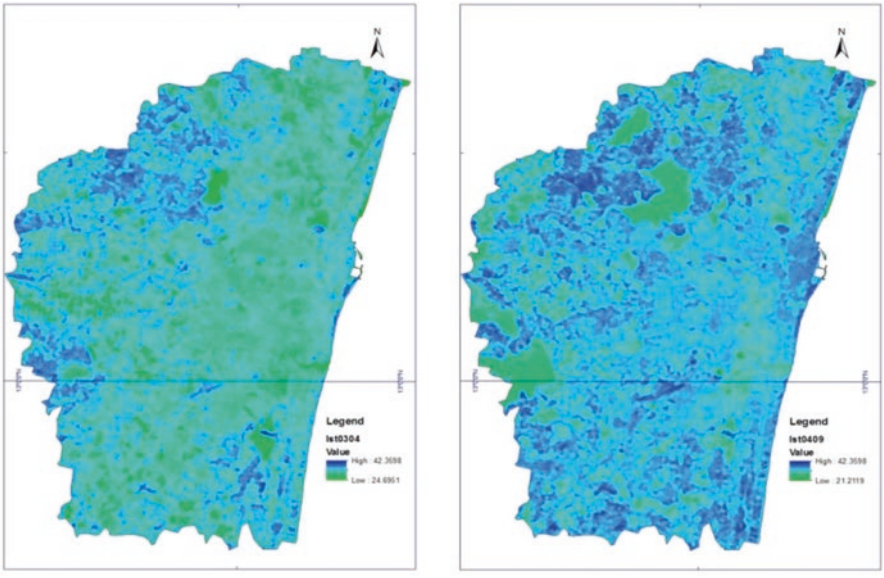

Fig. 13.9 Land surface temperature during the years 2004 and 2009 (summer)

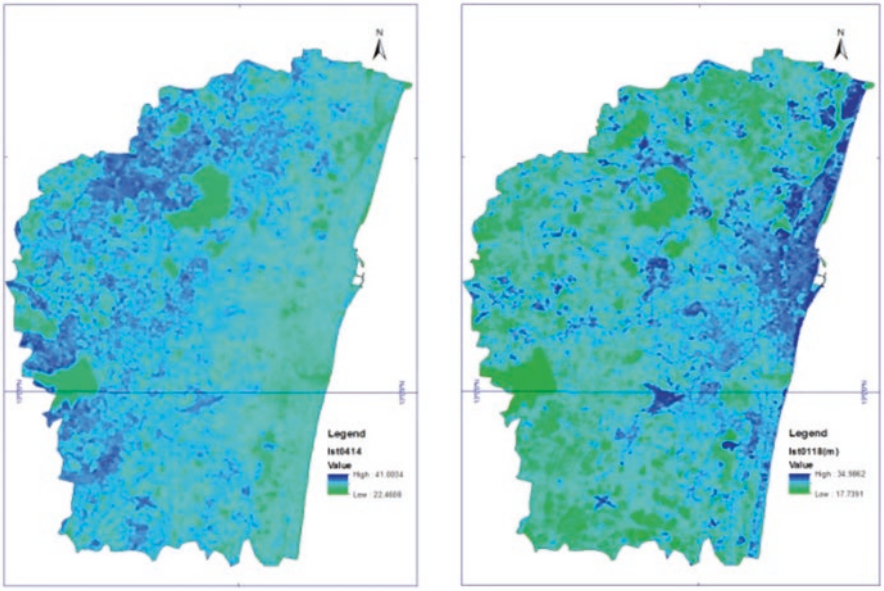

Fig. 13.10 Land surface temperature during the years 2014 and 2018 (summer)

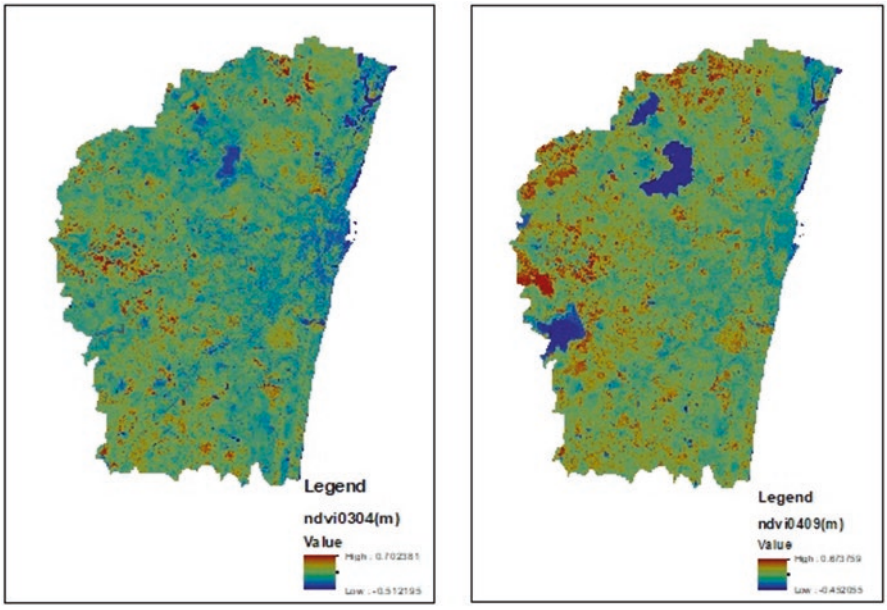

Fig. 13.11 Normalized difference vegetation index corresponding to the years 2004 and 2009 (summer)

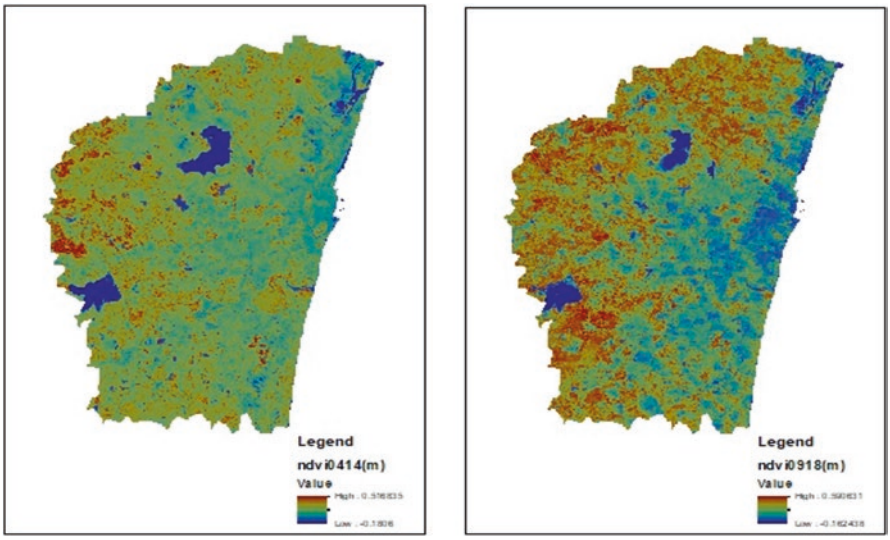

Fig. 13.12 Normalized difference vegetation index corresponding to the years 2014 and 2018 (summer)

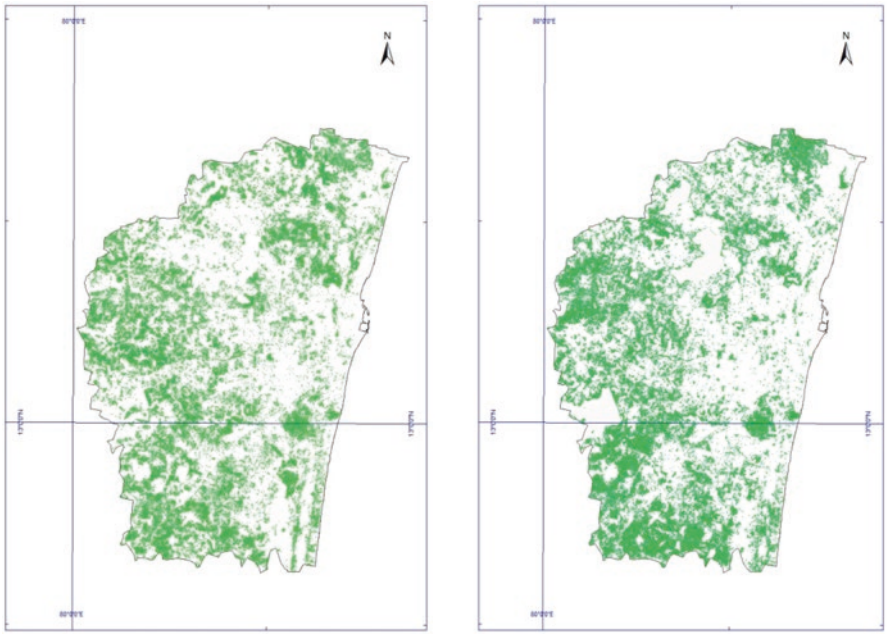

Fig. 13.13 Fractal vegetation cover 2004 and 2009

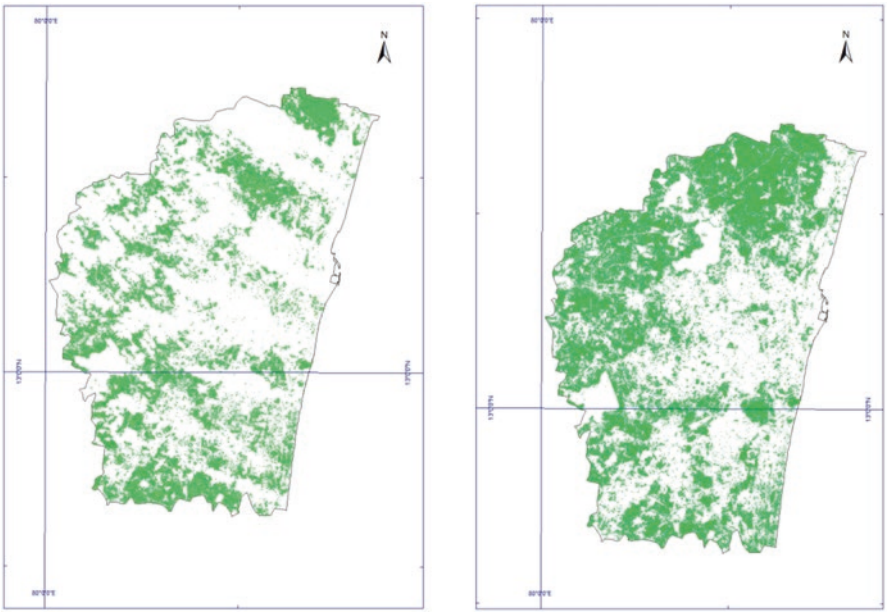

Fig. 13.14 Fractal vegetation cover 2014 and 2018

Table 13.5 Fractal vegetation cover on 2004, 2009, 2014, and 2018

Year	NDVI range	Area in km^2	Increase in %
2004	>0.2	345.72	–
2009	>0.2	356.47	3.10
2014	>0.2	484.88	40.25
2018	>0.2	457.93	32.45

and expansion of some urban areas has been noticed. The surface temperature analysis showed that the minimum and maximum temperatures in the study area were 24.69 °C and 42.35 °C for 2004 and 17.7 °C and 34.9 °C for 2018, which matches the air temperature differences from the meteorological data. Even though there is a drop in temperature, the area that experiences the urban heat effect has increased in the study area as follows 69.61, 173.26, 999.27, and 220.64 km^2, respectively.

From the NDWI maps (Fig. 13.15), it was inferred that the water spread area of the water bodies in the study area where 97.73, 156.08, 119.85, and 131.20 km^2 during the years 2004, 2009, 2014, and 2018, respectively. When the results were compared, it was observed that there is an increase in water spread area of 34.24%. This is directly proportional to the percentage increase in the fractal vegetation cover in the study area.

It is a well-known fact that water bodies regulate temperature and attenuate daily and seasonal temperature differences, as can be seen in the limited daily and annual temperature ranges in the study area.

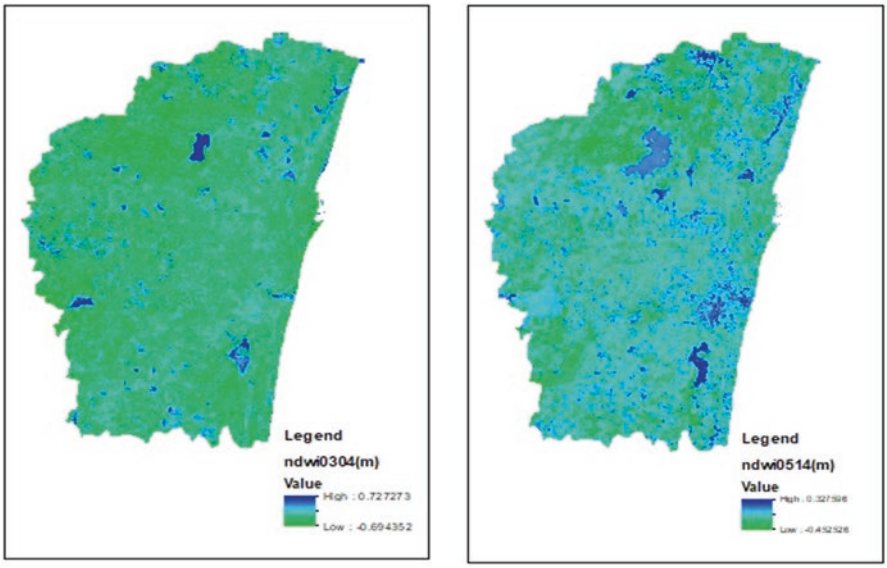

Fig. 13.15 NDWI for non-monsoon season for 2004 and 2014

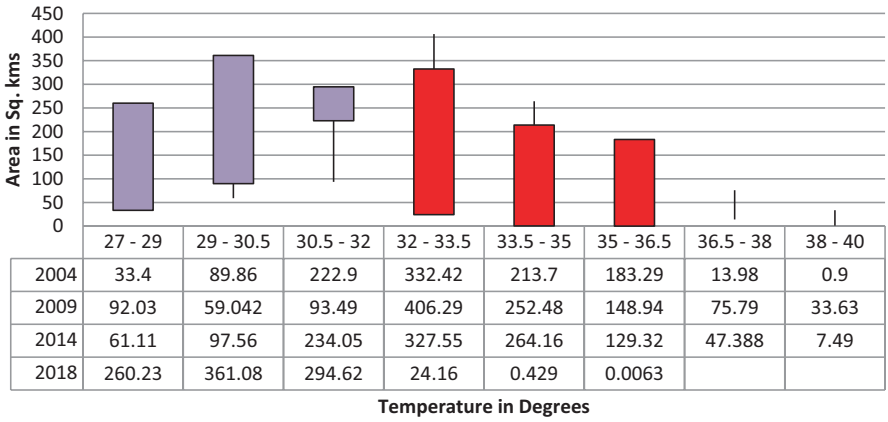

	27 - 29	29 - 30.5	30.5 - 32	32 - 33.5	33.5 - 35	35 - 36.5	36.5 - 38	38 - 40
2004	33.4	89.86	222.9	332.42	213.7	183.29	13.98	0.9
2009	92.03	59.042	93.49	406.29	252.48	148.94	75.79	33.63
2014	61.11	97.56	234.05	327.55	264.16	129.32	47.388	7.49
2018	260.23	361.08	294.62	24.16	0.429	0.0063		

Fig. 13.16 Fluctuations in land area with various ranges of temperature

Figure 13.16 shows that there is a shift in more land area from higher temperature toward lower temperature. This phenomenon is high, especially in the year 2018. The variations in temperature were studied statistically, and the mean temperature and the standard deviation are given as follows in Table 13.6.

The area of Chennai Metropolitan Area is around 1187.45 Km^2, and it is classified into four types, namely, water bodies area, built-up area, vegetation, and barren land as shown in Fig. 13.17 and Table 13.7. From Table 13.8, it is observed that the percentage of water bodies area, built-up area, and vegetation have increased by

Table 13.6 Variations in temperature values through the study period

Year/statistical values	2004	2009	2014	2018
Mean temperature (°C)	33.12	33.51	32.70	28.90
Standard deviation	1.93	2.44	1.83	2.40

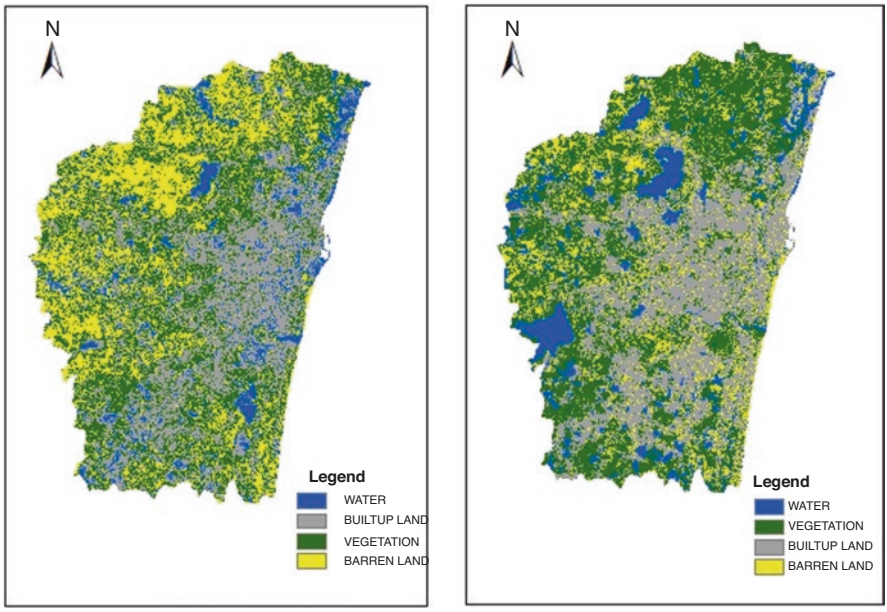

Fig. 13.17 Land use maps corresponding to 2004 and 2018

Table 13.7 Classification, area, and percentage of land use

Year	Land use type	Area (km^2)	Percentage of total area
2004	Water bodies	97.73	8.23
	Built-up area	429.51	36.17
	Vegetation	392.03	33.01
	Barren land	268.19	22.59
2018	Water bodies	131.20	11.05
	Built-up area	470.40	39.61
	Vegetation	431.11	36.31
	Barren land	154.74	13.03

2.82%, 3.44%, and 3.29%, respectively, during 2018 when compared with 2004. On the other hand, the percentage of barren land has reduced by 9.55%.

In order to understand the variations in temperature at various points with changes in land use type, profiles were taken across the study area as shown in Fig. 13.18. The line AB was considered in the longitudinal direction, and the profiles CD and EF were considered across the study area, so that the distance increases

Table 13.8 Changes in land use type from 2004 to 2018

Land use type	Change in %
Water bodies	2.82
Built-up area	3.44
Vegetation	3.29
Barren land	−9.55

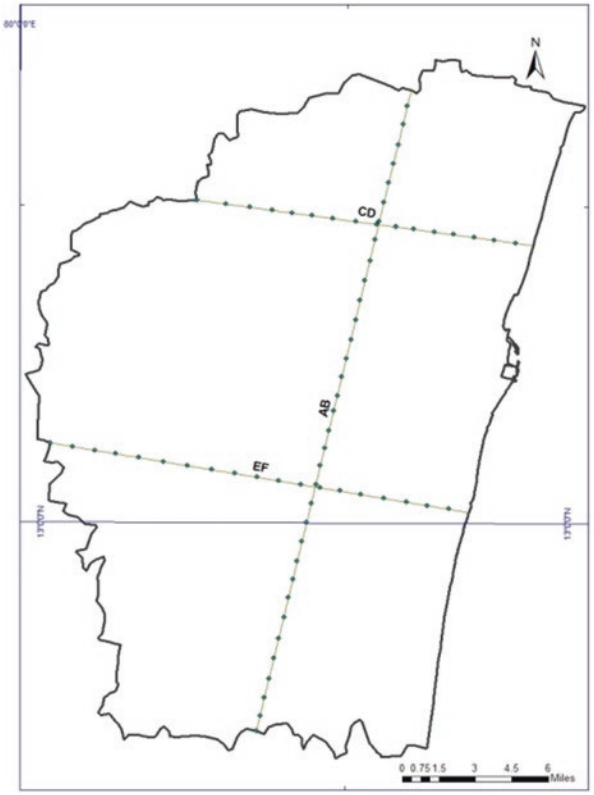

Fig. 13.18 Study area map with profiles

from the seashore. From Figs.13.19, 13.20 and 13.21, it is observed that along profile AB, there is not much variation in temperature with respect to distance, whereas in the other two profiles, the graph shows a decrease in temperature as the distance increases from the shore. It was also observed that with change in land use from barren land to vegetation and barren land to water bodies, there was a decrease in temperature. This was assured with the help of NDVI and NDWI values also.

From Fig. 13.22, the area under urban heat effect was estimated, and it was found as 69.61, 173.26, 999.27, and 220.64 during the years 2004, 2009, 2014, and 2018. The results show that the estimated UHI value for the study area was 30.91, which

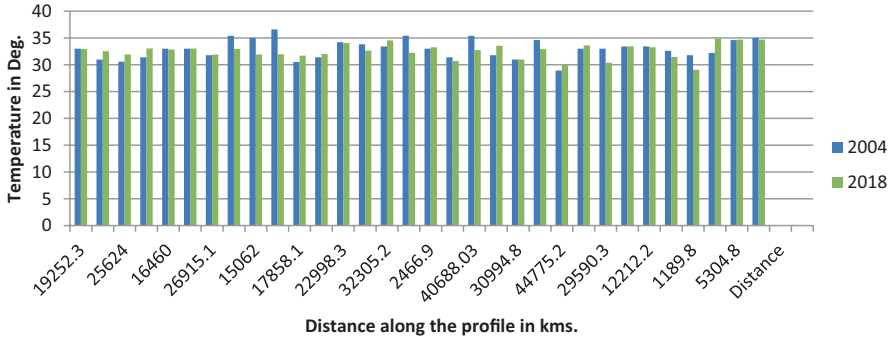

Fig. 13.19 Variations in temperature along profile AB

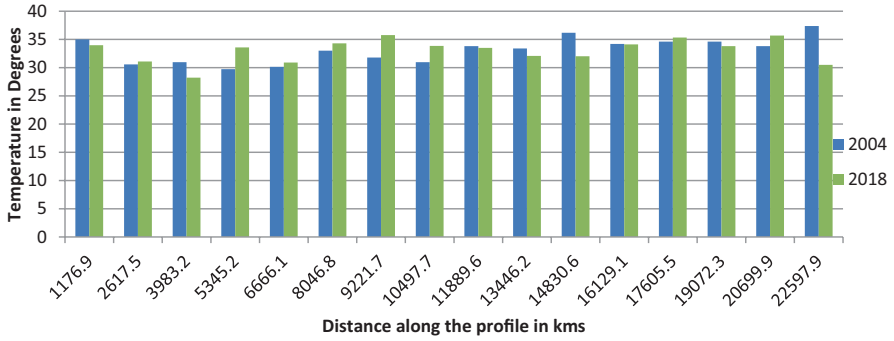

Fig. 13.20 Variations in temperature along profile CD

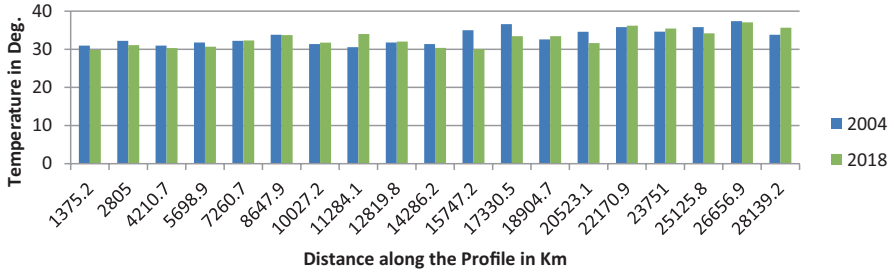

Fig. 13.21 Variations in temperature along line EF

was less when compared to that of 2004 (33.06). Even though the average annual temperature has decreased in the study area, the urban heat effect is high during the month of April. It was observed that the area under urban heat effect has increased from 69.61 km^2 to 220.64 km^2 during the period 2004–2018. From Table 13.9, it can be observed that the mean value has increased, and the standard deviation is also

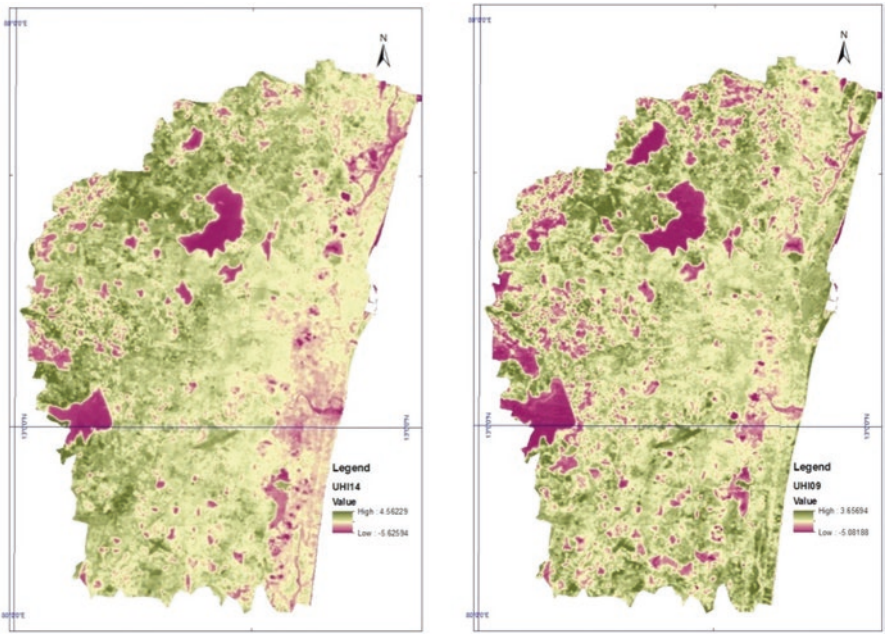

Fig. 13.22 UHI for the years 2004 and 2009

Table 13.9 Variations in the urban heat value for the land with vegetative cover and non-vegetative cover

Year	Type of land cover	Std. deviation	Mean	Maximum	Minimum
2004	Vegetative area	0.959	−0.0074	4.434	−3.647
	Non-vegetative area	1.091	−0.1446	2.203	−3.676
2018	Vegetative area	0.983	−0.638	3.424	−4.164
	Non-vegetative area	1.142	0.322	4.812	−4.387

high for the land with non-vegetative cover. As such, there are limited studies are available to understand the influence of sea in the coastal areas.

Conclusions

In this research, the potential of remote sensing to study the temperature variation and its characteristics in two different regions has been demonstrated. The heat energy radiated by the earth's surface is determined by including the factors such as different land use types, vegetation cover, and soil in the study area. Pearson correlation coefficient(R) between surface temperature and NDVI for the study area is estimated as 0.88. The result shows that the urban region experiences high temperature whereas the water bodies and the vegetative cover region area have

comparatively low temperature. In the Chennai Metropolitan Area, the area extent under water bodies, built-up area, and vegetative cover have increased compared with the barren land by 2018. The results show that even though there is an increase in vegetative cover, the maximum urban heat value are high in the case of both vegetative and non-vegetative area, respectively. Considering this, necessary steps need to be taken for solving the urban heating effect in the future scenario in the Chennai Metropolitan Area. This study proves that the increase in vegetative cover does not have immediate effect over urban heating, especially in coastal areas.

References

Arnfield AJ (2003) Two decades of urban climate research: a review of turbulence, exchanges of energy and water, and the urban heat island. Int J Climatol 23:1–26

Belal AA, El-Ramady HR, Mohamed ES et al (2014) Drought risk assessment using remote sensing and GIS techniques. Arab J Geosci 7:35–53

Ben W, Redeker EJ, Thurow TL (2001) Vegetation and water yield dynamics in an Edwards plateau watershed. J Range Manag 54(2):98–105

Brema J, Rahul TS, Julius JJ (2019) Study on drought monitoring based on spectral indices in Noyyal River Sub-watershed using Landsat-8 imageries. In: Proceedings of international conference on remote sensing for disaster management. Springer, Cham, pp 473–482

Chen Y, Wang J, Li X (2002) A study on urban thermal field in summer based on satellite remote sensing. Remote Sens Land Resour 4:55–598

Coumou D, Rahmstorf S (2012) A decade of weather extremes. Nat Clim Chang 2:1–6

Dagliyar A, Avdan U, Yildiz ND, Nefeslioglu HA (2015) Geophysical research, abstracts, vol 17. EGU, General Assembly

Gibson DJD (2006) Land degradation in the Limpopo Province, South Africa. Master of Science degree

Kumar D, Shekhar S (2015) Statistical analysis of land surface temperature-vegetation indexes relationship through thermal remote sensing. Ecotoxicol Environ Saf 121:39–44

Lettenmaier D, Mishra V, Ganguly A, Nijssen B (2014) Observed climate extremes in global urban areas. Environ Res Lett 16:14787

Li D, Bou-Zeid E (2013) Synergistic interactions between urban heat islands and heat waves: the impact in cities is larger than the sum of its parts. J Appl Meteorol Climatol 52:2051–2064

Ma Y, Kuang Y, Huang N (2010) Coupling urbanization analyses for studying urban thermal environment and its interplay with biophysical parameters based on TM/ETM+ imagery. Int J Appl Earth Obs Geoinf 12:110–118

Meehl G, Tebaldi C (2004) More intense, more frequent, and longer lasting heat waves in the 21st century. Science 305:994–997

Nicholson SE, Davenport ML, Malo AR (1990) A comparison of the vegetation response to rainfall in the Sahel and East Africa, using normalized difference vegetation index from NOAA AVHRR. Clim Chang 17:209–241

Oke TR (1987) Boundary layer climates, 2nd edn. Methuen, London

Pande CB, Moharir KN, Singh SK, Varade AM, Ahmed Elbeltagie SFR, Khadri PC (2021a) Estimation of crop and forest biomass resources in a semi-arid region using satellite data and GIS. J Saudi Soc Agric Sci 20(5):302–311

Pande CB, Moharir KN, Khadri SFR (2021b) Assessment of land-use and land-cover changes in Pangari watershed area (MS), India, based on the remote sensing and GIS techniques. Appl Water Sci 11:96. https://doi.org/10.1007/s13201-021-01425-1

Peng S et al (2012) Surface urban heat island across 419 global big cities. Environ Sci Technol 46:696–703

Shahid M, Rahman KU, Haider S et al (2021) Quantitative assessment of regional land use and climate change impact on runoff across Gilgit watershed. Environ Earth Sci 80:743. https://doi.org/10.1007/s12665-021-10032-x

Streutker DR (2003) A remote sensing study of the urban heat island of Houston, Texas. Remote Sens Environ 85:282–289

Taha H (1996) Modeling impacts of increased urban vegetation on ozone air quality in the South Coast Air Basin. Atmos Environ 30(20):3423–3430

Zaitunah A, Samsuri, Ahmad AG, Safitri RA (2018) Normalized difference vegetation index (ndvi) analysis for land cover types using Landsat 8 OLI in Besitang watershed, Indonesia. IOP Conf Series: Earth and Environmental Science 126:012112

Zhou B, Rybski D, Kropp JP (2013) On the statistics of urban heat island intensity. Geophys Res Lett 40:5486–5491

Zhou D, Zhao S, Liu S, Zhang L, Zhu C (2014) Surface urban heat island in China's 32 major cities: spatial patterns and drivers. Remote Sens Environ 152:51–61

Zhou D, Zhao S, Zhang L, Sun G, Liu Y (2015) The footprint of urban heat island effect in China. Sci Rep 5:srep11160

Chapter 14
Estimation of Land Surface Temperature and Urban Heat Island by Using Google Earth Engine and Remote Sensing Data

Komal Gadekar, Chaitanya B. Pande, J. Rajesh, S. D. Gorantiwar, and A. A. Atre

Abstract This chapter aims at the surface temperature of urbanization, nonurban heat island (NUHI), and urban heat island, an important factor for heat changes that affect the surface of the earth. Therefore, due to local and global environmental changes and man-made operations, block land surface temperatures in so many areas of Nashik town are rising. The estimation of urban heat island, NDVI, and NDBI indices was calculated using GEE, machine learning algorithm, and also remote sensing data. In this chapter, the relationship and correlation between the LST, NDVI, and NDBI indies were established for the estimation of the surface temperature of the Nashik urban area and other areas of the Maharashtra block. The NDVI and NDBI indices were estimated using the machine learning algorithm and satellite data. The GEE platform has provided easy access to all satellite data with a java script algorithm for analysis and LST relationship between the built-up area and the vegetative land. Various urban thermal islands (UHIs) have demarcated as higher temperatures in urban areas within city borders due to more man-made activities and climate change factors. The UHI value threshold for 2015 was measured at 41.03 °C and in 2019 at 43.28 °C. The relationship between LST–NDVI and LST–NDBI was identified quantitatively by a correlation analysis based on the algorithm and the GEE platform. LST shows a strong negative correlation (−0.41 for 2015 and −0.57 for 2019) with NDVI and a strong positive correlation (0.31 for 2015 and 0.71 for 2019) with NDBI throughout the Nashik region. The non-UHI zones (green areas and water bodies) remain almost unchanged if any change is assumed to be very little altered, but only the UHI zones are in severe heat stress due

K. Gadekar · J. Rajesh · S. D. Gorantiwar · A. A. Atre
Center for Advanced Agriculture Science and Technology on Climate-Smart Agriculture and Water Management, Mahatma Phule Krishi Vidyapeeth, Rahuri, Maharashtra, India

C. B. Pande (✉)
Indian Institute of Tropical Meteorology (IITM), Pune, Maharashtra, India
e-mail: chaitanay45@gmail.com

C. B. Pande et al. (eds.), *Climate Change Impacts on Natural Resources, Ecosystems and Agricultural Systems*, Springer Climate,
https://doi.org/10.1007/978-3-031-19059-9_14

to urban air pollution. The study field results can help the urban, agricultural, and ecological planners decide on the sustainable practices of ecological and climate change.

Keywords Remote sensing · LST · NDVI · NDBI · GEE · UHI

Introduction

The UHI is a very useful subject for studies on climate, atmospheric, and urban planning. The most known and contrasting climates are widely understood (Tan et al. 2010). Today, urban and industrial areas have developed, and these factors directly affect air and surface temperatures, soil water, and air pollution (Oke 1982; Pande et al. 2018). Air and land surface temperature assessments are useful for local and global surface temperatures directly related to this measurement device (typically estimated in Kelvin). LST has studied the outer layer of the earth where the heat and radiation of the sun have assimilated, mirrored, and refracted. Due to different climatic conditions and other man-made exercises, where the definite expectations are checked, the surface temperature of the day has now changed (Santamouris 2015). The overall urbanization of ozone-damaging substances has increased, and the landscape has been reshaped, which, due to the synchronous shift in the normal distribution of land and the presentation of urban resources, such as anthropogenic earth surfaces, has major climatic impacts on different scales. Ground overviews have allowed a deeply accurate land use land cover (LULC) characterization (Pande et al. 2021b; Srivastava and Chinnasamy 2021), but they are time-consuming, troublesome, and expensive, featuring remote detection and an obvious and preferred alternative. Urban heat island (UHI) identifiable evidence and representation was established on LST that fluctuates spatially due to the nonhomogeneity of land surface spread and other barometric components (Buyantuyev and Wu 2010). The main factor for calculating the maximum and lowest temperature of a given region is LST. Medium spatial target information, such as that given by LANDSAT and place, is suitable for land spread or vegetation mapping at a local nearby scale (Pande et al. 2022). OLI gathers data at a 30 m spatial target with eight groups positioned in the electromagnetic ranges of the visible and nea-infrared and shortwave infrared districts and an extra panchromatic 15 m spatial target band (Estoque et al. 2006). At a spatial target of 100 m, TIRS measures the TIR brilliance using two classes located in the air window somewhere in the range of 10–12 µm. In comparison with the twentieth period, nearly 50% of the population currently resides in the area. Since the last 5 years, fast-growing urbanization has had a direct effect on the atmosphere, water, air pollution, and soil temperatures (Shahid et al. 2021).

The Earth's surface temperature plays an important role in maintaining magnitude, ecological planning, crop yield production, and atmospheric conditions. Proper view of the different scales, i.e., local, global, and regional, has been derived. These forecasting levels were estimated using thermal sensors and satellite data (Pande et al. 2021a). Remote sensing and GIS were quantitatively analyzed by urban thermal

islands. The results of the study directly affected urban climate problems and environmental development and planning. For the study of urban thermal islands, soil moisture, air, emissions, land use, and urban spatial information, remote sensing satellites may provide several types of resolution and time data. Available soil surface temperatures have been studied by a number of researchers and scientists, but this analysis shows a very strong negative association between the different indices, i.e., the normalized vegetation difference index and soil surface temperature. During the seasons, the calculated values of NDVI and land surface changes varied widely. The UHI was estimated with data on soil surface temperatures. UHII had generally estimated single environments in the below village zone from both existing in situ locations (Earl et al. 2016). In comparison with the surrounding peri-urban region, the urban heat island (UHI) effect shows greater air pollution and LST in urban areas. The high levels of near-surface energy emissions, solar radiation absorption of ground objects, and low evapotranspiration rates were provided by this study (Small 2006). In this chapter, the main focus on the four objectives has been completed by using Google Earth Engine and remote sensing techniques. The following four are as follows: (1) to develop thematic LST maps from Landsat 8 OLI via Google Earth Engine Platform between 2015 and 2019, (2) to study the UHI and non-UHI in the Nashik block and this study during the years 2015 and 2019 based on the LST maps, (3) to measure the algorithm-based NDVI and NDBI maps over the years 2015 and 2019, and (4) to compared LST during the 2015 and 2019 cycles with NDVI and NDBI. This relative analysis of non-UHI in semiarid regions takes a broad perspective of the UHI, its behavior, and its climate-related impact in semiarid areas into account.

Study Area

The city of Nashik is the third town in the Maharashtra region located at 19°59′39″ N latitude and 73°47′50″ E with the area is 15,582 sq. km. in the Maharashtra area to the north. In contrast to other districts, the district has different croplands such as paddy, soybean, cotton, and maximum agriculture land under more horticultural crops. The surface temperature of the land is useful for calculating the semi-aerated area's soil moisture. As per 2011 census data, the population of Nashik Tehsil is 1, 317, 367. The larger eastern part of the district is situated under the Deccan rock region with larger cultivated land (Fig. 14.1).

Climate

The town has a tropical location combined with a high elevation from the mean sea level to provide it with a relatively small tropical location in wet and dry climates. The maximum temperature range is 40–42 °C in May, and the minimum temperature range is 14–15 °C in January. April and May are the hottest months in the study region, while December and January are the coldest months. Red soils are mainly found in the north-west and black soils in the south-east.

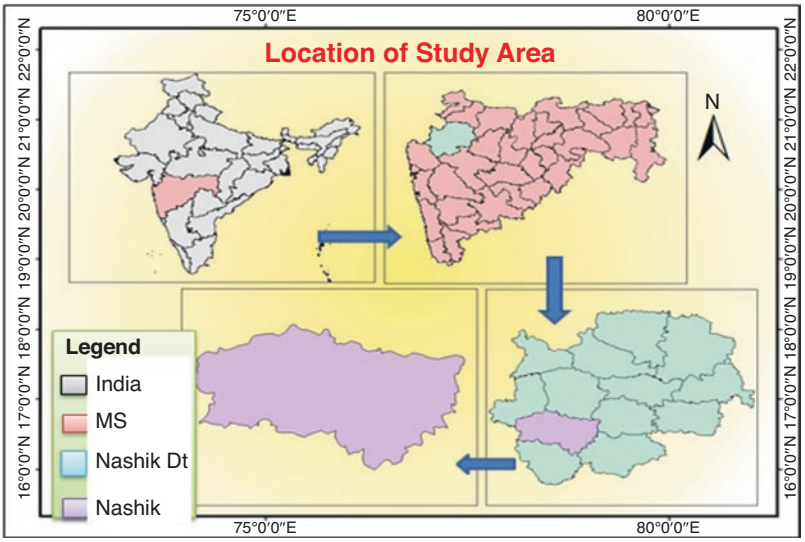

Fig. 14.1 Location map of the study area

Methodology

An efficient method of analyzing and collecting satellite data using a java script algorithm is the Google Earth Engine (Pande 2022). The data treatment is based on the GEE algorithm (Google Earth Engine). The NDVI, NDBI, and surface land temperatures measured in the semiarid zone have been determined for this platform (Majkowska et al. 2017). In Landsat 8 satellite data, two sensors, including the Operational Land Imager (OLI) and the Thermal Infrared Sensor, were selected for terrestrial surface temperatures (TIRS). For wavelength 1–7 (visible and infrared) and 9 (Cirrus), the OLI data has been formed into nine spectral ribbons with a spatial resolution of 30 m. Spatial resolution has been used for bands 8 (panchromatic) and 15 m. With a spatial resolution of 100 meters, both thermal infrared (10 and 11) bands were provided by TIRS. Urban heat and nonurban heat island surveys focus on NDVI and NDBI Landsat images, although they are widely used for LULC and UHI investigations. Evolving algorithms have been used to calculate NDVI, NDBI, and surface temperature. Terrestrial surface temperature maps were used to examine urban-heat islands and nonurban islands in the Nashik city. The temperature difference between the mean LST in urban areas and the average LST in the surrounding area (but still within urban borders) for each site was measured in order to detect the extent of the heat island (Fig. 14.3). Meteorological data sets have been used to validate the surface temperature with metrological data. The tool used can be found in Fig. 14.2.

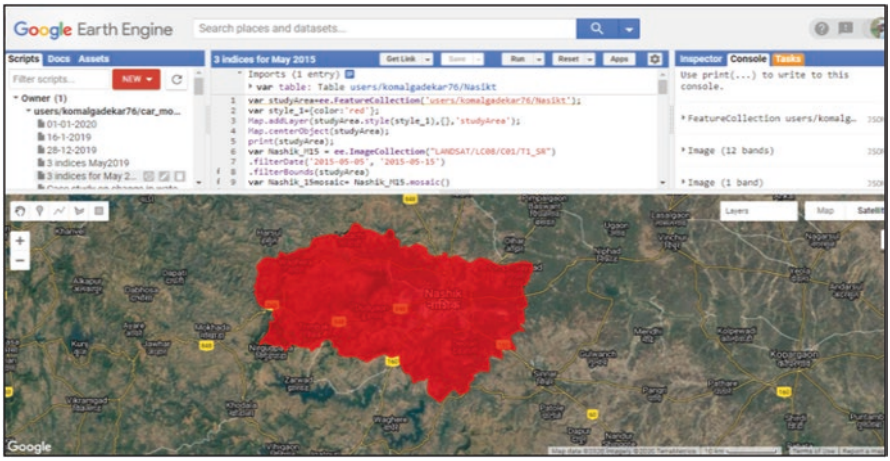

Fig. 14.2 GEE Window showing Nashik Taluka shapefile

For Extraction of Land Surface Temperature

Landsat 8 is a satellite series of Landsat launched by NASA. For the study of land surface temperature, these are the strongest satellites. The Landsat 8 data is accessible from the cost-free United States Geological Survey (USGS) Earth Explorer site (Gulhane et al. 2022). The Landsat 8 satellite images the entire planet once every 16 days. The TIRS group 10 was used in the current investigation to evaluate splendor temperature and vegetation extent, and groups 4 and 5 were used to create NDVI of the examination zone. In this study, satellite information about Nashik Taluka for May 2015 and May 2019 was used. Landsat 8 includes group metadata, such as warm and reliable factor esteem, which can be used for the computation of computers such as LST (Lin et al. 2018).

For Calculation of Indices

Landsat-8 satellite data has been collected from the data catalog and the surface reflectance data as an image collection in Google Earth Engine (Fig. 14.2). For the estimation of the NDVI and NDBI during the years 2015 and 2019, Landsat satellite data is the highest, although it is very significant for the study of land surface temperatures. Sentinel-2 data was compiled from the data catalog of Google Earth Engine and is used for calculating NDVI and NDBI indices. In the Java script and satellite data on the Google Earth cloud-based platform (Kandekar et al. 2021; Pande 2022), all indices were algorithms developed (Fig. 14.3).

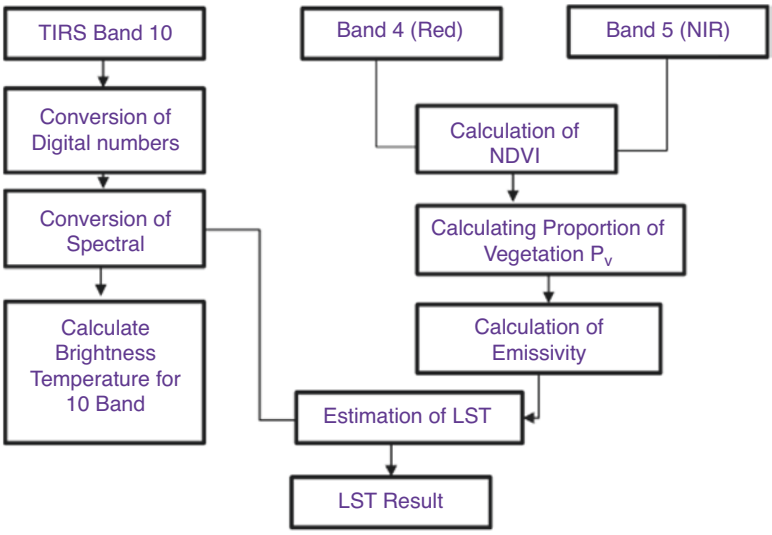

Fig. 14.3 Flow chart of the methodology

Top of Atmosphere (TOA) Radiance

The atmosphere radiance is measured by radiance rescaling factor by using thermal infrared digital numbers. It is converted to TOA spectral radiance.

$$L\lambda = \mathrm{ML}^{*}\mathrm{Qcal} + \mathrm{AL}$$

where

Lλ = TOA spectral radiance (Watts/ (m^2 * sr * μm))
ML = radiance multiplicative Band (No.)
AL = radiance Add Band (No.)
Qcal = quantized and calibrated standard product pixel values (DN).

Top of Atmosphere (TOA) Brightness Temperature

Spectral radiance data has been transformed to top of atmosphere brightness temperature using the thermal constant values in the metadata file:

$$\mathrm{BT} = \mathrm{K2} / \ln\left(\mathrm{k1} / L\lambda + 1\right) - 272.15$$

where

BT = Top of atmosphere brightness temperature (°C).
Lλ = TOA spectral radiance (Watts / (m2 * sr * μm)).
K1 = K1 constant band (no.)
K2 = K2 constant band (no.)

Land Surface Temperature (LST)

The land surface temperature (LST) is the radiative temperature calculated by using top of atmosphere brightness temperature, wavelength of emitted radiance, land surface emissivity (Peng et al. 2018):

$$\mathrm{LST} = \left(\mathrm{BT}/1\right) + \mathrm{W}^{*}\left(\mathrm{BT}/14380\right) * \ln\left(\mathrm{E}\right)$$

where

BT = Top of atmosphere brightness temperature (°C).
W = wavelength of emitted radiance.
E = land surface emissivity.

Normalized Differential Vegetation Index (NDVI)

The normalized differential vegetation index (NDVI) is a standardized vegetation index calculated using near infrared (Band 5) and red (Band 4) bands. The NDVI also shows the vegetation condition on the surface of the earth if any climate change factors affect the vegetation. In these respects, NDVI plays an important role in estimating the temperature of the surface of the land:

$$\mathrm{NDVI} = \left(\mathrm{NIR} - \mathrm{RED}\right) / \left(\mathrm{NIR} + \mathrm{RED}\right)$$

where

RED = DN values from the RED band.
NIR = DN values from Near-Infrared band.

Land Surface Emissivity (LSE)

Land surface emissivity (LSE) is the average emissivity of an element of the surface of the Earth calculated from NDVI values:

$$\mathrm{PV} = \left[\left(\mathrm{NDVI} - \mathrm{NDVI\,min}\right) / \left(\mathrm{NDVI\,max} + \mathrm{NDVI\,min}\right)\right]^{2}$$

where

PV = Proportion of vegetation.
NDVI = DN values from NDVI image.
NDVI min = Minimum DN values from NDVI image.
NDVI max = Maximum DN values from NDVI image.

Estimation of Normalized Difference Vegetation Index

NDVI is a linear combination between the near-infrared band and the red band, which is observed as the basic index for measuring the "greenness" of the earth's surface. It was calculated by NDVI formula from satellite data.

$$\mathrm{NDVI} = \left(\mathrm{NIR} - \mathrm{RED}\right) / \left(\mathrm{NIR} + \mathrm{RED}\right)$$

For Landsat 8:

$$\mathrm{NDVI} = \left(\mathrm{Band}\,5 - \mathrm{Band}\,4\right) / \left(\mathrm{Band}\,5 + \mathrm{Band}\,4\right)$$

For Sentinel 2:

$$\mathrm{NDVI} = \left(\mathrm{Band}\,8 - \mathrm{Band}\,4\right) / \left(\mathrm{Band}\,8 + \mathrm{Band}\,4\right)$$

Normalized Difference Built-Up Index (NDBI)

It is estimated as the linear combination of the near-infrared band (0.76–0.90 μm) and the short-wave infrared (SWIR) band (1.55–1.75 μm). It is used for the extraction of urban built-up land.

$$\mathrm{NDBI} = \left(\mathrm{SWIR} - \mathrm{NIR}\right) / \left(\mathrm{SWIR} + \mathrm{NIR}\right)$$

Mapping UHI

Therefore, two types of UHI and non-UHI were measured by LST according to the following equations (Guha et al. 2018):

$$\mathrm{LST} > \mu + 0:5^{*}\delta$$
$$0 < \mathrm{LST} < \mu + 0:5^{*}\delta$$

where μ and δ are the mean and standard deviation of LST in the study area, respectively.

Delineating the UHS

The analysis of LST maps was used to delineate UHS across the entire Nashik region. Unique significance has been granted to nonstop monitoring. This small section is the hottest and often established within the UHI and unfavorable for human settlement (Ranagalage et al. 2017).

UHS was demarcated as per as following equation (Guha et al. 2018):

$$\text{LST} > \mu + 2^{*}\delta$$

where μ and δ are the mean and standard deviation of LST in the study area, respectively.

Developed Algorithm

The following algorithm was developed for estimating the vegetation index and soil surface temperature for agriculture and ecological resource planning in the semi-arid region.

```
var         studyArea=ee.FeatureCollection('users/komalgadekar76/
Nasikt');
var style_1={color:'red'};
Map.addLayer(studyArea.style(style_1),{},'studyArea');
Map.centerObject(studyArea);
print(studyArea);
var Nashik_M15 = ee.ImageCollection("LANDSAT/LC08/C01/T1_SR")
.filterDate('2015-05-05', '2015-05-15')
.filterBounds(studyArea)
var Nashik_15mosaic= Nashik_M15.mosaic()
print(Nashik_15mosaic)
var rgbVis={
 min:0.0,
 max:3000,
 bands:['B4','B3','B2'],
};

Map.addLayer(Nashik_15mosaic.clip(studyArea),rgbVis,
'Nashik_15mosaic');
```

(a) **Calculation of NDVI**

```
var NDVI_M15 =Nashik_15mosaic.expression(
'(NIR-RED)/(NIR+RED)',
{'NIR':Nashik_15mosaic.select('B5'),       'RED':Nashik_15mosaic.
select('B4')}
);
var visParams = {
 min: -1,
 max:1,
 palette:['red','green'],
};
Map.addLayer(NDVI_M15.clip(studyArea),visParams, 'NDVI_M15');
print(NDVI_M15);
```

(b) **Calculation of NDBI**

```
var NDBI_M15 =Nashik_15mosaic.expression(
'(SWIR-NIR)/(SWIR+NIR)',
{'SWIR':Nashik_15mosaic.select('B6'),      'NIR':Nashik_15mosaic.
select('B5')}
);
var visParams1 = {
 min: -1,
 max:1,
 palette:['orange','blue'],
};
Map.addLayer(NDBI_M15.clip(studyArea),visParams1, 'NDBI_M15');
print(NDBI_M15);
```

Results and Discussion

More horticulture and agricultural land are the selected study area, and LST is more important for vegetation and human health. A significant factor in agriculture and ecological planning is the surface temperature of the ground. Various indices such as LST, NDVI, and NDBI for any wide area have been effectively provided to the GEE cloud-based platform (Fig. 14.4). For specific agricultural purposes and the urban heat index, this platform is useful for broad areas of extraction data. The NDVI maps showed the status of the vegetation with the amount of area occupied

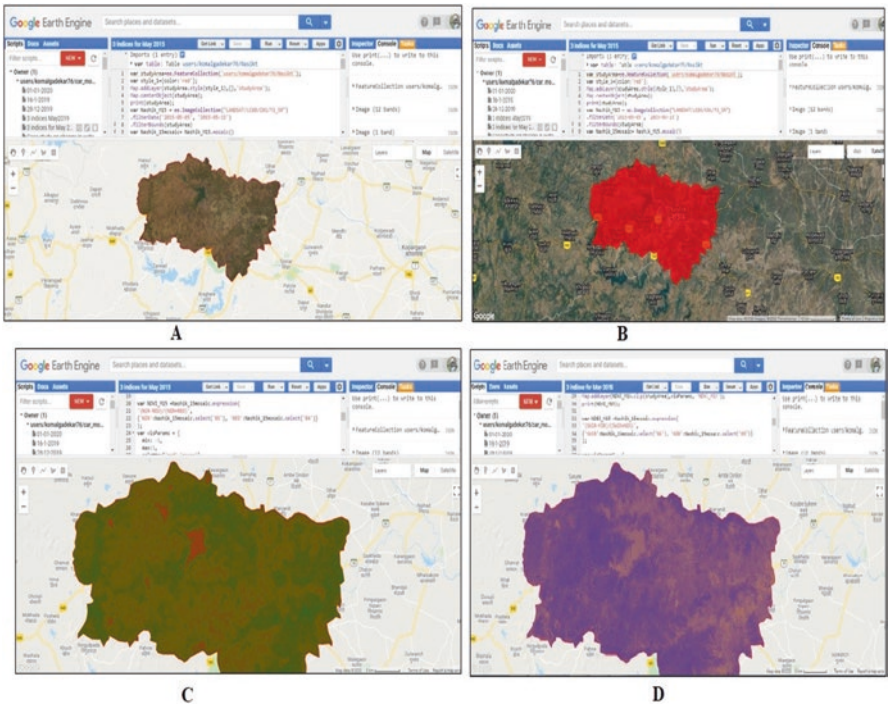

Fig. 14.4 NDVI and NDBI index in the GEE platform

by agriculture and built-up land. These NDVI maps can be useful for estimating land surface temperatures and built-in indices used to estimate city temperatures since day-to-day city temperature rises due to climate change causes and man-made activities (Rasul et al. 2015). UHI temperatures directly affect crops, food security, and other vegetation trees in agriculture. These UHI values are increased from LST, while values have an effect on crop irrigation water and decreased agricultural soil moisture during the Kharif and Rabi seasons. The Nashik Taluka shape file was uploaded from the GEE platform. This platform has acquired Landsat images for the year 2015 and sentinel images for the year 2019 for unique periods measured for analysis of the NDVI, LST, and NDBI indices at the Nashik City in 2015 and 2019. As a result, 2 years of soil surface temperature and soil moisture status, crop conditions, urban heat index, and other environmental planning in the semiarid zone have been calculated (Yao et al. 2019; Pande 2014). The values of NDVI and NDBI were compared with changes in ground surface temperatures in the years 2015 and 2019. Farmers and related regional departments will make perfect use of agro-advisory services. From satellite data, NDVI values such as −0.34–0.8 and 0.35–0.76 have

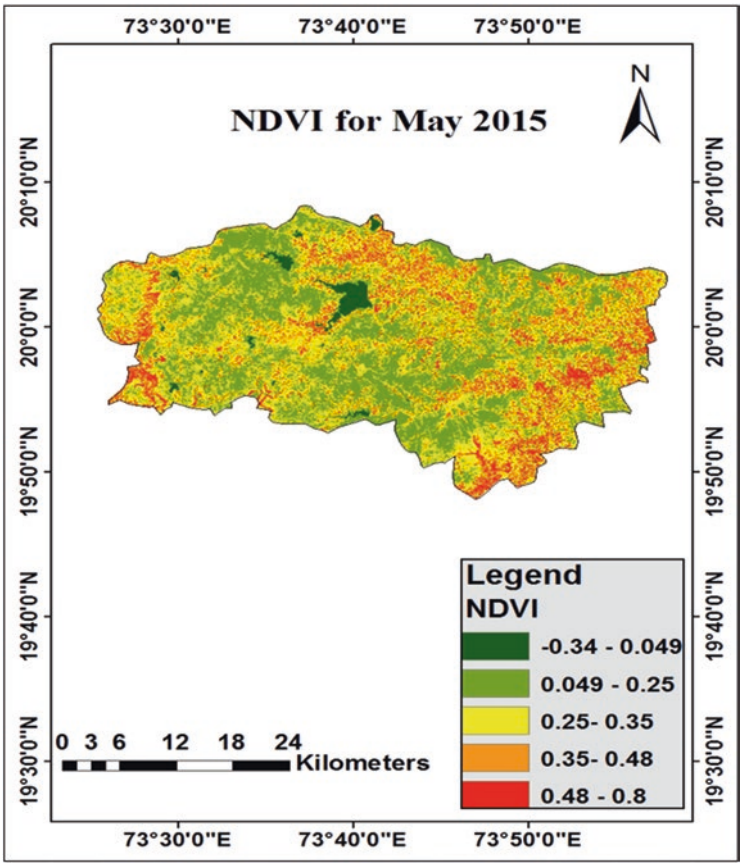

Fig. 14.5 NDVI map of Nashik Taluka for May 2015

been calculated using the GEE platform (Figs. 14.5 and 14.6). Due to drought and rising soil surface temperatures, the NDVI values were reflected in the reduced vegetation (Pande et al. 2018). The statistical effects of the two-year NDVI values are shown in Table 14.1. The NDVI of May 2015 was observed the maximum values of standard deviations (Table 14.1). There was a disparity between maximum and minimum NDVI values such as 0.043 and 0.010 on two separate days, respectively (Fig. 14.7). These NDBI values were measured for Nashik Taluka in the years 2015 and 2019 (Figs. 14.8 and 14.9). The statistical effects of NDBI values are shown in Table 14.2. While these values are shown on two different dates, the difference between the maximum and minimum NDBI values was 0.320 and 0.008 on the two dates, respectively (Figs. 14.10 and 14.11 and Table 14.2).

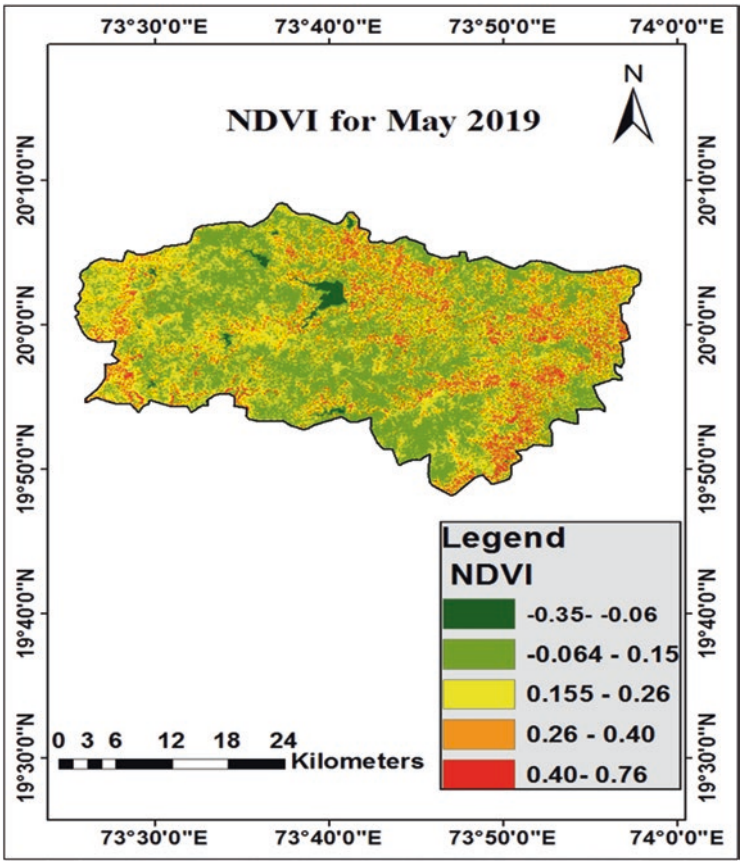

Fig. 14.6 NDVI map of Nashik Taluka for May 2019

Table 14.1 NDVI for Nashik Taluka

	Statistical results			
Year	Max.	Min.	Mean	SD
May 2015	0.8111	−0.3443	0.3021	0.1229
May 2019	0.7680	−0.3548	0.1913	0.1217

Relationship of LST–NDVI and LST–NDBI Within the UHI and the Non-UHI

The correct values of the LST are defined. The color coding of the LST theme maps within the study area was developed in accordance with the thermal pattern. Average LST values such as 39.22 °C and 41.87 °C were calculated during 2015 and 2019, respectively. The Google Earth Engine development algorithm has calculated all of

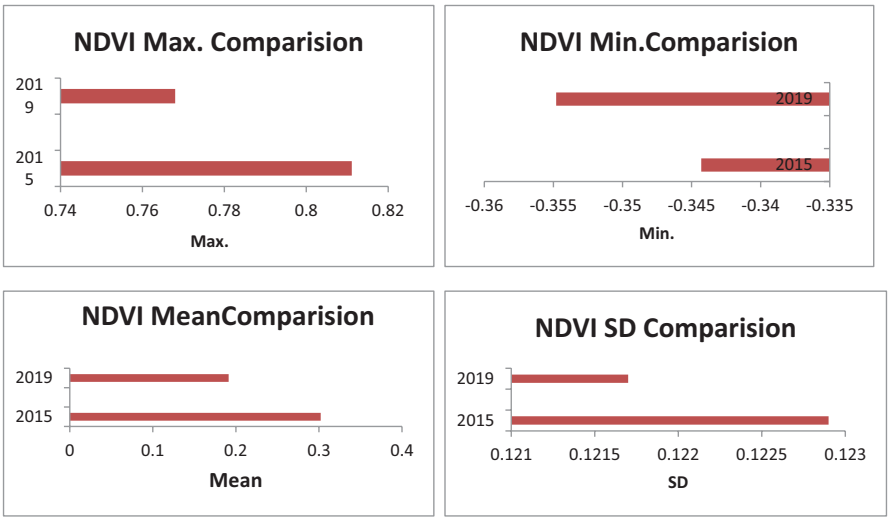

Fig. 14.7 NDVI graph for 2 years of Nashik Taluka

the LST values. It has set the UHI threshold values. UHI values such as 41.03 °C and 43.28 °C were specified in the 2015 and 2019 algorithms (Figs. 14.11 and 14.12). The LST maps are generated using Google Earth Engine algorithms and Arc GIS tools (Fig. 14.13).

LST has a good relationship between NDBI and NDVI. The LST was strongly negative in semiarid areas, −0.41 for 2015 and − 0.56 for 2019. In the region of 0.31 in 2015 and 0.71 in 2019, the positive LST correlation for NDBI was shown to be strong (Fig. 14.11). The issue of landscape composition has established this phenomenon (Pande and Moharir 2014). LST-NDVI and LST-NDBI both have a greater effect in a wide variety of natural environments (Tables 14.3 and 14.4).

Spatial Distribution of UHI and Non-UHI

The intensity of UHI is defined as the difference between average UHI and non-UHI temperatures (Table 14.3). The UHI strength in Nashik Taluka is concentrated in a big industrial area, which is Ambad industrial area and this directly play in a major part for UHI. This area has more heat waves during the summer season. The area near the Godavari River and Kashyapi Dam was taken away from the non-UHI area. The UHI threshold value is calculated for 2015 at 41.03 °C and for 2019 at 43.28 °C. For UHI, the LST standard deviation values indicate more heterogeneity in both cities (Fig. 14.14 and Table 14.5).

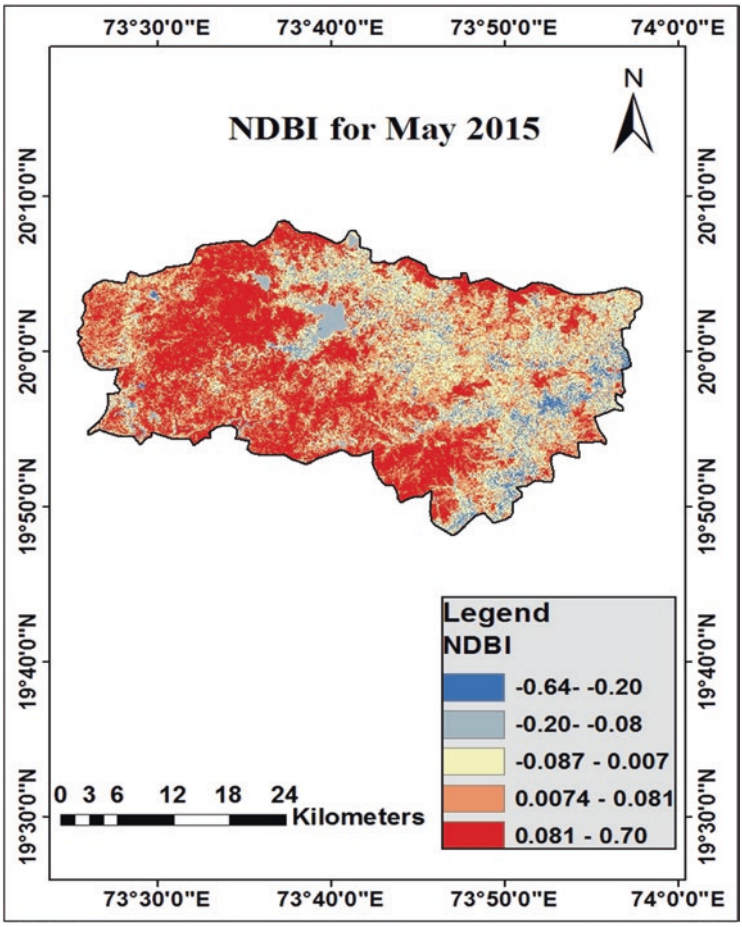

Fig. 14.8 NDBI map of Nashik for May 2015

Identification of UHS

In the built-up areas and bare land available near Devlali in the Nashik block, UHS was more abundant due to a lack of vegetation. For 2015 and 2019, the UHS was observed at a threshold of 46.44 °C and 47.52 °C, respectively. The most important locations for UHS growth are parking areas, roadways, power plants, metal roofs, and industrial factories. There are very few or small quantities of vegetation and water bodies in almost all such hot spots (Fig. 14.15).

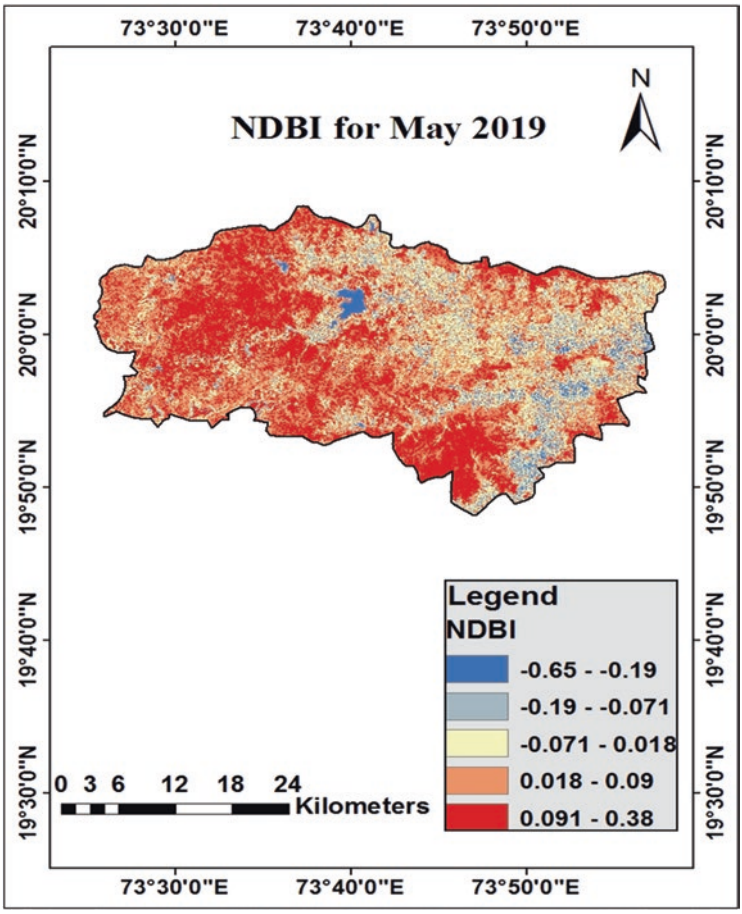

Fig. 14.9 NDBI map of Nashik for May 2019

Table 14.2 NDBI for Nashik Taluka

	Statistical results			
Year	Max.	Min.	Mean	SD
May 2015	0.7011	−0.6492	0.0252	0.1036
May 2019	0.3808	−0.6581	0.0416	0.0958

Conclusion

This research studied how urban shapes are related to the UHI by GEE and GIS software. With superior spatial resolution in the long-term sequenced TM/ETM images, the mechanisms involved in generating UHI arising from urban form could be recognized. Landsat-8 OLI and TIRS data were used for the UHI intensity effect

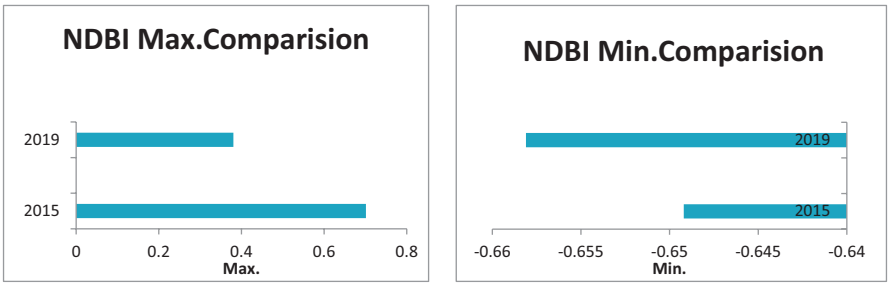

Fig. 14.10 NDBI graph of Nashik

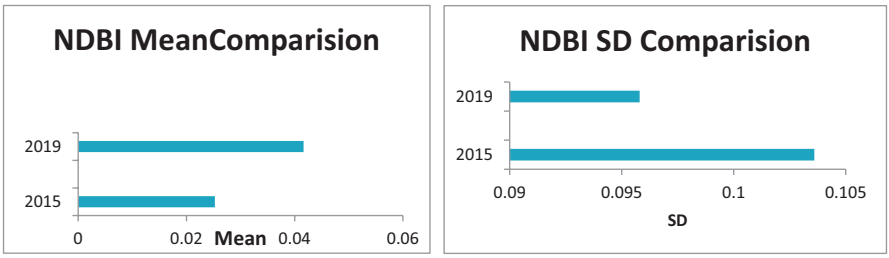

Fig. 14.11 NDBI graph of Nashik

study on the town of Nashik. With dynamic interactions with NDVI and NDBI indices, LST has interpreted them. LST maps spread through Nashik's industrial zone and city center–defined UHI areas. The primary responsibility for LST lands and built-up areas is to be established. The presence of vegetation and water has decreased LST levels. Some UHS in the UHI zones have detected elevated concentrated LST. In order to interpret the relations between LST–NDVI and LST–NDBI, correlation analysis was also used. Over the whole of Nashik, LST has a large negative correlation with the NDVI (−0.41 for 2015, −0.57 for 2019, −0.31 for 2015, and 0.71 for 2019) and a strong positive correlation with the NDBI. It demonstrates that there are practically unchanged or little altered non-UHI areas (green areas and water bodies). Only UHI areas are severely heat-stressed. The growing urban area can be used to research urban growth over time along with the area's LST material; it will help decision-makers, in particular village-level preparation specialists, to have broad concepts in management and planning processes. It was therefore proposed that predictors, technologists, and other experts involved in the processing of geographic information should follow an accurate method of generating efficient results for better performance. It shows that the Taluka area is larger than any other agricultural area in connection with most of its surroundings and can be linked to the reduction of trees and shrubs in order to accommodate farmland and other farming activities. In this context, it is suggested that planners and experts who are afraid should take action to estimate the advice given to farmers to plant trees and stop cutting down existing trees in order to have an unnecessary environmental balance.

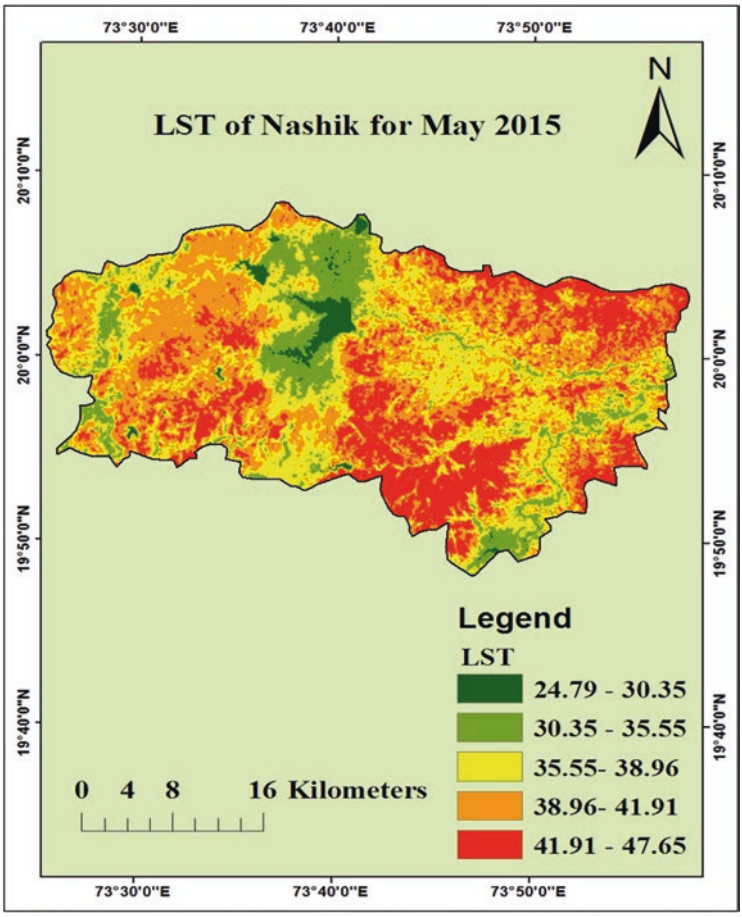

Fig. 14.12 Spatial distribution map of LST for May 2015

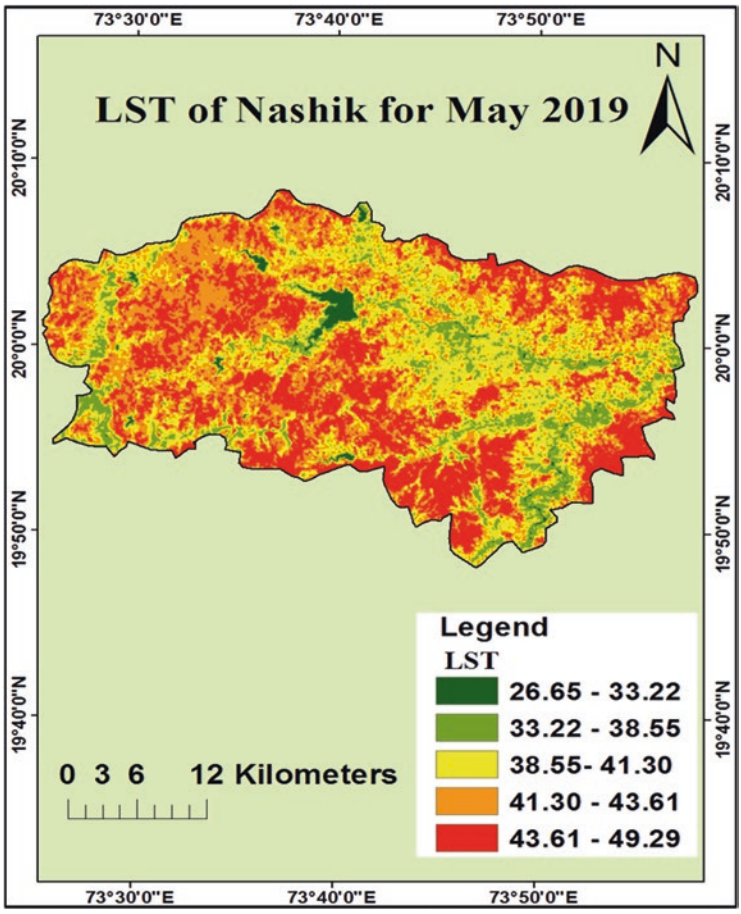

Fig. 14.13 Spatial distribution map of LST for May 2019

Table 14.3 Correlation coefficient between LST, NDVI, and NDBI

Year	LST-NDVI	LST-NDBI
2015	−0.41	0.32
2019	−0.56	0.71

Table 14.4 Statistical results of LST

	LST (Max.)		LST (Min.)		LST (Mean)		LST (SD)	
Year	UHI	NUHI	UHI	NUHI	UHI	NUHI	UHI	NUHI
May 2015	47.65	40.97	41.03	24.79	44.34	32.88	0.75	1.90
May 2019	49.29	43.27	43.28	26.65	46.28	34.96	0.82	1.35

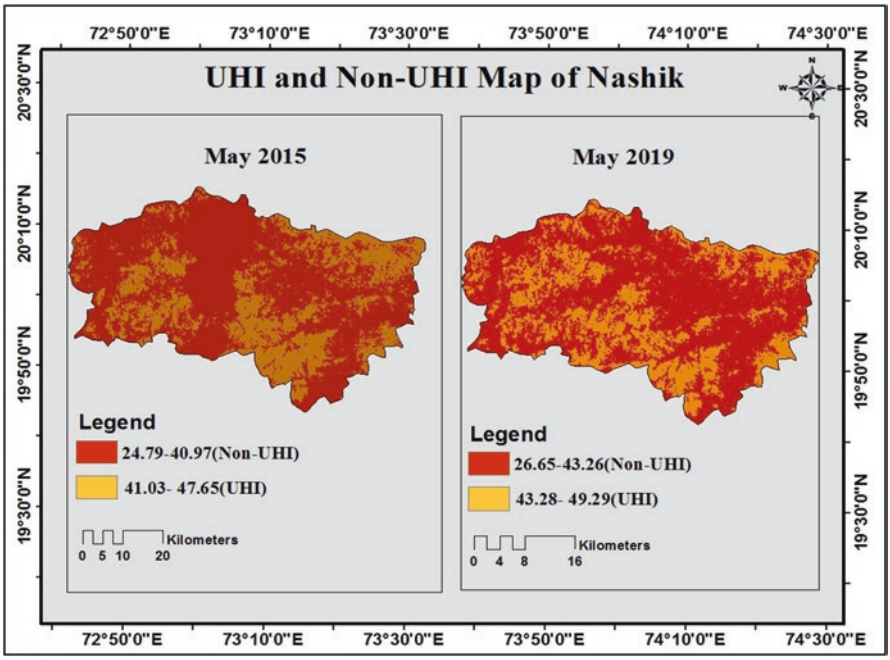

Fig. 14.14 Spatial extent of UHI and Non-UHI

Table 14.5 Variation of LST in UHI and Non-UHI

	Statistical results of LST			
Year	Max.	Min.	Mean	SD
May 2015	47.65	24.79	39.22	3.613
May 2019	49.29	26.65	41.87	2.852

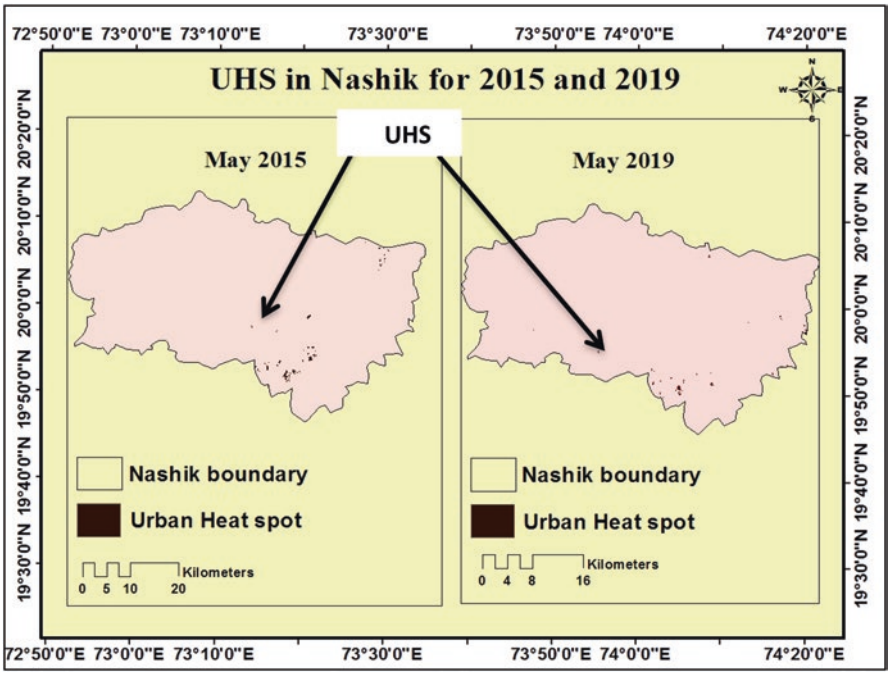

Fig. 14.15 Location of UHS within Nashik boundary

Acknowledgments We are grateful toward Principal Investigator, Center for Advance Agriculture Science and Technology on Climate-Smart Agriculture and Water Management, MPKV, Rahuri (Agricultural University) and ICAR, NAHEP, and World Bank for providing the necessary facilities and financial support for conducting this research.

Conflict of Interest The authors declare that they have no conflict of interest.

References

Aslan N, Koc-San D (2016) Analysis of relationship between urban heat island effect and land use/cover type using landsat 7 ETM+ and landsat 8 oli images. In: The international archives of the photogrammetry, remote sensing and spatial information sciences, volume XLI-B8. XXIII ISPRS Congress

Bala R, Prasad R, Yadav VP, Sharma J (2018) Comparative study of land surface temperature with different indices on heterogeneous land cover using Landsat 8 data. In: The international archives of the photogrammetry, remote sensing and spatial information sciences, volume XLII-5. https://doi.org/10.5194/isprs-archives-xlii-5-389-2018

Buyantuyev A, Wu J (2010) Urban heat islands and landscape heterogeneity: linking spatiotemporal variations in surface temperatures to land-cover and socioeconomic patterns. Landsc Ecol 25(1):17–33. https://doi.org/10.1007/s10980-009-9402-4

Carlson TN, Arthur ST (2000) The impact of land use land cover changes due to urbanization on surface microclimate and hydrology: a satellite perspective. Glob Planet Chang 25(1–2):49–65. https://doi.org/10.1016/S0921-8181(00)00021-7

Earl N, Simmonds I, Tapper N (2016) Weekly cycles in peak time temperatures and urban heat island intensity. Environ Res Lett. https://doi.org/10.1088/1748-9326/11/7/074003

Estoque RC, Murayama Y, Myint SW (2006) Effects of landscape composition and pattern on land surface temperature: an urban heat island study in the megacities of Southeast Asia. Sci Total Environ 577:349–359

Franz (2018) How to calculate land surface temperature with Landsat 8 satellite images. Remote Sensing and GIS Tutorial

Guha S, Govil H, Dey A, Gill N (2018) Analytical study of land surface temperature with NDVI and NDBI using Landsat 8 OLI and TIRS data in Florence and Naples city, Italy. Eur J Remote Sens 51(1):667–678

Gulhane VA, Rode SV et al. (2022) Correlation analysis of soil nutrients and prediction model through ISO cluster unsupervised classification with multispectral data. Multimed Tools Appl. https://doi.org/10.1007/s11042-022-13276-2

Kandekar VU, Pande CB, Rajesh J et al (2021) Surface water dynamics analysis based on sentinel imagery and Google Earth Engine Platform: a case study of Jayakwadi dam. Sustain Water Resour Manag 7:44. https://doi.org/10.1007/s40899-021-00527-7

Kaplan G, Avdan U, Avdan ZY (2018) Urban Heat Island analysis using the Landsat 8 satellite data: a case study in Skopje, Macedonia. PRO 2:358

Lin L, Ge E, Liu X, Liao W, Luo M (2018) Urbanization effects on heat waves in Fujian Province, Southeast China. Atmos Res 210:123–132. https://doi.org/10.1016/j.atmosres.2018.04.011

Majkowska A, Kolendowicz L, Półrolniczak M, Hauke J, Czernecki B (2017) The urban heat island in the city of Poznań as derived from Landsat 5 TM. Theor Appl Climatol 128:769–783. https://doi.org/10.1007/s00704-016-1737-6.N

Oke TR (1982) The energetic basis of the urban heat island. Q J Roy Meteorol Soc 108:1–24. https://doi.org/10.1002/qj.49710845502

Pande C (2014) Change detection in land use/land cover in Akola Taluka using remote sensing and GIS technique. Int J Res 1(8):1–13

Pande CB (2022) Land use/land cover and change detection mapping in Rahuri watershed area (MS). India using the google earth engine and machine learning approach, Geocarto Int. https://doi.org/10.1080/10106049.2022.2086622

Pande C, Moharir K (2014) Analysis of land use/land cover changes using remote sensing data and GIS techniques of Patur Taluka, Maharashtra, India. Int J Pure Appl Res Eng Technol 2(12):85–92

Pande CB, Moharir KN, Khadri SFR, Patil S (2018) Study of land use classification in the arid region using multispectral satellite images. Appl Water Sci 8(5):1–11. ISSN 2190-5487

Pande CB, Moharir KN, Singh SK, Varade AM, Ahmed Elbeltagie SFR, Khadri PC (2021a) Estimation of crop and forest biomass resources in a semi-arid region using satellite data and GIS. J Saudi Soc Agric Sci 20(5):302–311

Pande CB, Moharir KN, Khadri SFR (2021b) Assessment of land-use and land-cover changes in Pangari watershed area (MS), India, based on the remote sensing and GIS techniques. Appl Water Sci 11:96. https://doi.org/10.1007/s13201-021-01425-1

Pande CB, Kadam SA, Jayaraman R, Gorantiwar S, Shinde M (2022) Prediction of soil chemical properties using multispectral satellite images and wavelet transforms methods. J Saudi Soc Agric Sci 21(1):21–28

Pattanayak SP, Diwakar SK (2018) Seasonal comparative study of NDVI, NDBI and NDWI of Hyderabad City (Telangana) based on LISS-III image using remote sensing and DIP. Int J Geogr 5:78–86

Peng J, Jia J, Liu Y, Li H, Wu J (2018) Seasonal contrast of the dominant factors for spatial distribution of land surface temperature in urban areas. Remote Sens Environ 215(15):255–267. https://doi.org/10.1016/j.rse.2018.06.010

Ranagalage M, Estoque RC, Murayama Y (2017) An urban heat island study of Colombo metropolitan area, Sri Lanka, based on Landsat data (1997–2017). ISPRS Int J Geo-Inf 6:189. https://doi.org/10.3390/ijgi6070189

Rasul A, Balzter H, Smith C (2015) Spatial variation of the daytime Surface Urban Cool Island during the dry season in Erbil, Iraqi Kurdistan, from Landsat 8. Urban Clim 14:176–186

Santamouris M (2015) Analyzing the heat island magnitude and characteristics in one hundred Asian and Australian cities and regions. Sci Total Environ 512–513:582–598. https://doi.org/10.1016/j.scitotenv.2015.01.060

Shahid M, Rahman KU, Haider S et al (2021) Quantitative assessment of regional land use and climate change impact on runoff across Gilgit watershed. Environ Earth Sci 80:743. https://doi.org/10.1007/s12665-021-10032-x

Small C (2006) Comparative analysis of urban reflectance and surface temperature. Remote Sens Environ 104:168–189. https://doi.org/10.1016/j.rse.2005.10.029

Srivastava A, Chinnasamy P (2021) Investigating impact of land-use and land cover changes on hydro-ecological balance using GIS: insights from IIT Bombay, India. SN Appl Sci 3:343. https://doi.org/10.1007/s42452-021-04328-7

Tan J, Zheng Y, Tang X, Guo C, Li L, Song G et al (2010) The urban heat island and its impact on heat waves and human health in Shanghai. Int J Biometeorol 54(1):75–84. https://doi.org/10.1007/s00484-009-0256-x

Tsou J, Zhuang J, Li Y, Zhang Y (2017) Urban Heat Island assessment using the Landsat 8 data: a case study in Shenzhen and Hong Kong. Urban Sci 1:10

Yao R, Wang L, Huang X, Gong W, Xia X (2019) Greening in rural areas increases the surface urban heat island intensity. Geophys Res Lett 46:2204–2212. https://doi.org/10.1029/2018GL081816

Chapter 15
Study on Irrigated and Nonirrigated Lands in Ukraine Under Climate Change Based on Remote Sensing Data

Artur Ya. Khodorovskyi, Alexander A. Apostolov, Lesya A. Yelistratova, and Tetiana A. Orlenko

Abstract According to the UN, potential of Ukraine's agricultural sector allows feeding of 450–500 million people. However, nowadays, its capabilities are exploited only by a third. The key factors, which characterize increasing average annual temperature, are primarily related to climate change. Increasing drought and desertification caused by global warming occur against the background of almost unaltered precipitation in the steppe zone of Ukraine. Climate change will derate the condition of the humidity. Therefore, the role of irrigation and drainage in agricultural production increases. However, at present, melioration agriculture is in crisis concerning the level of use of the facilities engineering and infrastructure of irrigation and drainage in Ukraine. Irrigation system recovery is a vital tool in the present conditions. Firstly, the development of the agricultural economy sector and increasing the export potential of Ukraine. Secondary, climate impact minimizing on the processes of socioeconomic nature of the regions. Climate change monitoring is a crucial problem, in specific, due to the aridity of the climate, especially regarding regional changes on agroecosystems determining its impact on long-term development and food security. Information on moisture conditions and the occurrence of the degradation process is continuously up to date with recent developments. Obtaining of the monitoring data would necessitate integrated remote sensing at the global, regional, and local scale. In addition, high spatial resolution and low satellite revisit period will supplement the use of optical and radar data from satellite images to overcome the problem of cloud cover. Remote sensing data of the Earth allows identifying and establishing regular variation in agroecosystems structure and determining their productivity. This research is based on remote sensing of the Earth, monitoring and underpinned by international experience and internal capacity, including integrated approaches and methods for reclaimed lands. The results of

A. Y. Khodorovskyi · A. A. Apostolov · L. A. Yelistratova · T. A. Orlenko (✉)
Scientific Centre for Aerospace Research of the Earth of the Institute of Geological Sciences of the National Academy of Sciences of Ukraine, Kyiv, Ukraine
e-mail: artur@casre.kiev.ua

C. B. Pande et al. (eds.), *Climate Change Impacts on Natural Resources, Ecosystems and Agricultural Systems*, Springer Climate,
https://doi.org/10.1007/978-3-031-19059-9_15

this study will enable the effective use of reclaimed land. Furthermore, proposals based on the monitoring outcome allow improved governance in the agriculture of Ukraine.

Keywords Remote sensing data · Climate change · Irrigated agriculture · Irrigation systems · Moisture content · Moisture indices

Introduction

Nowadays, climate change and crisis processes in the environment are two main interrelated processes on a global scale. Global warming has led to a decrease in water resources and the deterioration of their quality. A significant increase in potential evaporation in recent years and the water balance deficit have been the main reasons why crop yields decline (Pande et al. 2022a). All these situations are incredibly negative phenomena and are severe challenges for the sustainable development of any country (Pande et al. 2021b; Pande 2022). They cause significant problems of environmental and socioeconomic nature and threaten the provision of society with the necessary food (Pande et al. 2020, 2021a). Irrigation is one of the main factors in the intensification of the crop industry in areas with insufficient and unstable natural moistening. That is why artificial humidification is widespread in arid regions. Over the past 20 years, the site of irrigated land has increased by 50 million hectares, or 17%, and is more than 270 million hectares. Irrigated land provides more than 40% of world crop production, occupying only 18% of agricultural land. The productivity of one irrigated hectare is more than twice the productivity of nonirrigated. During the same period, the world area under drip and other microirrigation methods increased at least 6.6 times – from 1.6 to 10.5 million hectares. However, the world's freshwater reserves make up 35 million m3, nearly 8.5% of which are the freshwater resources concentrated in rivers, lakes, and reservoirs, which are a traditional source of water supply (Khadri and Pande 2016; Pande et al. 2022b; Rajesh et al. 2021; Srivastava and Chinnasamy 2021). The unequal distribution of water resources in the world calls for transformation in agriculture and, in particular, the introduction of resource-saving technologies and methods of irrigation of crops (Elbeltagi et al. 2022). For countries with limited water resources, which Ukraine belongs to, this issue becomes of particular importance. In addition, according to the National Oceanic and Atmospheric Administration of the United States, in the region in which Ukraine is based, the rate of temperature rise is one of the highest in the world in the last 30 years.

Over the past 30 years, the average annual air temperature in Ukraine has risen by 1.2 °C as a whole, and the rate of increase is much higher compared with global and European scales (Kulbida et al. 2009). Instead, the amount of precipitation in Ukraine as a whole region remains virtually unchanged (Lyalko 2015). Due to warming in Ukraine, the conditions of natural moisture supply have significantly deteriorated. As a result, the practical cultivation of almost all crops in the steppe

and southern forest-steppe zone without irrigation has become virtually impossible (Lyalko et al. 2020). Moreover, due to climate change, even in the Polissya area, soil moisture has been deficit since July, and obtaining high and stable yields is no longer possible without additional moisture. Therefore, if we do not develop irrigation in the south and water regulation in Polissya, Ukraine will not realize its massive potential for food production (Apostolov et al. 2020).

Further changes in the temperature regime may lead to two-thirds of the territory of Ukraine becoming an area of risk agriculture. The increased temperature has already led to a change in the season durations: the cold period will be much shorter and warmer and the warm period longer and hotter. In winter, more and more snowfalls instead of snow, resulting in snow not accumulating with melted water. Thus, every year, the consequences of global warming for Ukraine become more and more destructive. That is particularly relevant in the case of Ukraine's southern regions. The steppes are gradually turning into semideserts, which many areas are at risk in becoming unsuitable for agriculture. Moreover, due to climate change, agricultural production is slowly moving from the south of steppes to the north, to forest-steppe and woodland areas. In recent years, one of the trends in the land market of Ukraine has been the loss of interest in land located in the southern regions. Due to droughts and wind erosion, the grounds of south Ukraine are gradually losing soil layer, moisture-holding capacity, and fertility. Since 1991, the area of the dry zone has increased by 7%. Today, it covers almost a third of the territory, including 11.6 million hectares of arable land. At the same time, the area with excessive and sufficient atmospheric moisture decreased by 10%, occupying only 7.6 million hectares of arable land. Thus, almost 19 million hectares of arable land require constant irrigation, and 4.8 million hectares require water regulation. According to forecasts, further climate change will worsen the conditions of natural moisture supply. As a result, the role of irrigation and drainage in agricultural production will only increase. Therefore, the only way to preserve the southern agricultural fields of Ukraine is land melioration. Based on the organizational, economic, technical measures to improve hydrological, soil, agroclimatic conditions to increase the efficiency of land and water resources for high and sustainable agriculture. Today, many Ukrainian scientists study the management of reclaimed areas, including Kovalchuk et al. (2010), Bahniuk et al. (2002). However, a single system of optimal management of reclaimed lands has not yet been developed, ensuring economic stability, social well-being, and economic security, and, as a result, sustainable development of agriculture in reclaimed territories. Therefore, today, scientists such as Moshinsky (2005), Nasiedkin et al. (2008), Cvjetova et al. (2009), and others are engaged in monitoring melioration territories.

Regarding the experience of foreign states in the development of meliorating territories, it is safe to say that a significant step forward has been taken compared with Ukraine. So abroad in most developed countries (England, Belgium, Netherlands, Germany, France, Denmark, Turkey, Israel, the United States, etc.), permanent reconstruction of drainage systems and permanent intensifying agriculture through land reclamation are being replaced by more intensive forms of land use.

The reclamation fund for the modernization and refurbishment of drainage systems is constantly evaluated, depending on their design and the technical state for systems today. And the land that is not economically viable for use is withdrawn from the land reclamation fund altogether.

Several studies have shown that many world scientists have tried to resolve problems of irrigated and nonirrigated lands, including Eberhard et al. (2013), Cosh et al. (2012), Brown and Pervez (2013), Hunt et al. (2014), Pun et al. (2017), Pervez and Brown (2010), Chance et al. (2017), Dinesh et al. (2021), Nickum and Ogura (2010), Dowgert (2010), Alon (2016), Satoh and Ishii (2021), Tabayashi (1987), Shevah (2015), Ruopu and Mahesh (2016), Wang et al. (2021), Rahmonov et al. (2016), Qiu et al. (2021), Jiang et al. (2021), Zhu et al. (2021), Isgandarov (2015), Pajic et al. (2014), Simsek and Arabacı (2021), Gunlu and Gol (2017), Guo et al. (2020), Teng et al. (2021), Johansson et al. (2009), Senturk et al. (2014), Abuzar et al. (2020), and others. Land and water resources are especially important to agriculture and rural development. They are intrinsically linked to global challenges of food insecurity and poverty, climate change adaptation and mitigation, and degradation and depletion of natural resources that affect the livelihoods of millions of rural people across the world. Studies show that much of the research work related to depleting freshwater resources stimulates and promotes collaborative actions and discussions toward sustainable water management solutions in agriculture (Orimoloye et al. 2022; Shahid et al. 2021). Today, the development of science and technology has reached a level where ignoring modern technologies in the management of reclaimed areas can lead to a loss of potential benefits from their use. The introduction of the latest GIS technologies has emerged as an important new data source for environmental applications over the past few years.

However, the creation of geospatial data infrastructure for reclaimed areas is not sufficiently addressed in our country for now. Government decrees confirm the relevance of such studies: “Irrigation and Drainage Strategy in Ukraine until 2030,” “Water Strategy for 2025,” several laws of Ukraine, regulations governing the design, construction, and operation of irrigation and drainage systems in Ukraine.

Currently, the state of melioration agriculture in terms of the use of existing irrigation and drainage engineering infrastructure is assessed as a crisis, with a further threat of deterioration. The introduction of innovative technologies is due to the worsening of environmentally friendly use of irrigated lands, which is associated with a decrease in their fertility, spreading erosion processes, and increasing the area of degraded lands for Ukraine. Furthermore, with minimal time and money, remote sensing data are essential for environmental control, thanks primarily to comprehensive spatial coverage, periodicity, and systematic data acquisition. The work aims to assess changes in the productivity of irrigated and drained lands using the analysis of remote sensing data in the monitoring mode and in nonstationary climate conditions, which will evaluate the possible impact of melioration measures on the environment. The study is based on the concept we had developed to evaluate the moisture content in lands of Ukraine using materials from regular satellite multizone surveys, which allows monitoring to conduct a variety of tasks. First, the degree of soil moisture and vegetation condition is taken based on assessing changes

in the intensity of soil brightness and vegetation in different spectral ranges under the influence of moisture content. It is known that with increasing moisture content, there is a decrease in the reflectivity of soils and vegetation, especially in the bands of water absorption, which lie in the red range. However, the curves of the spectral reflectivity of soils and vegetation are markedly different. Therefore, it is necessary to use the known relationships between the spectral brightness of soils and vegetation in different spectral ranges for their effective selection. Numerous indices are based on these ratios, which other performers successfully use. The involvement of the satellite data will make it possible to assess the degree of soil moisture and humidity changes in time and space, determine the impact of humidity on vegetation, control vegetation development, and identify crops that need fertilizing. In addition, the results of satellite data will monitor changes in water basins such as rivers, lakes, ponds, canals, and water levels in them, overgrowing with aquatic vegetation, siltation, changes in water composition, and others.

These studies can be conducted at different scale levels, from regions and regions to individual farms.

To implement the proposed concept, you need to implement the following approaches:

1. Assessment of the impact of the melioration system on the environment in the context of modern climate change in Ukraine.
2. Assessment of the impact of soil erosion processes on the reduction of their productivity.

These materials can be included in national databases, increasing the probability of forecasts of rational use of nature in melioration lands in the context of climate change.

Materials and Methods

Data basis “Assessment of the impact of the melioration system on the environment in the context of modern climate change in Ukraine.” The proposed technology is based on satellite data – the most widely used optical data of different spatial and temporal resolutions. Therefore, the recognize and classify the underlying surface spectral and textural information from satellite apply. The most efficient solution for natural resource problems is materials of multizone space imagery from the Landsat-5 TM series satellites, which regularly conducted space imagery of the Earth’s surface for more than 50 years. Such a temporary archive of images allows you to solve the problems in the monitoring mode.

Images from Landsat-5TM satellites, dated 07.07.2004, and Landsat-8 OLI/TIRS, dated 23.08.2021, with a spatial resolution of 30 m, were used for the study (Fig. 15.1).

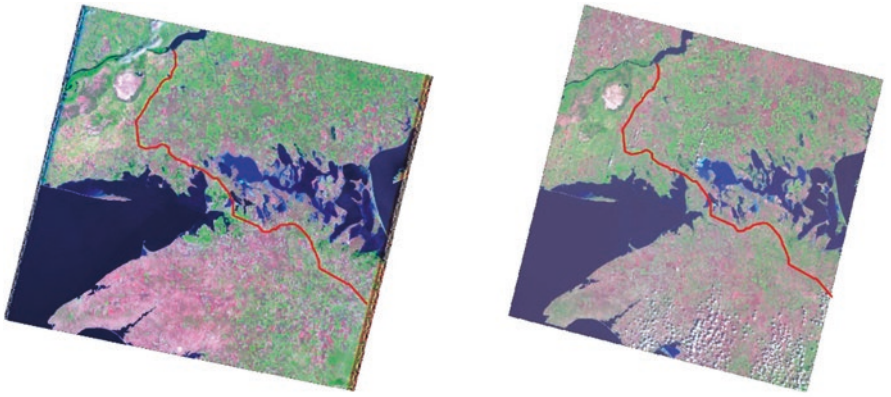

Fig. 15.1 Landsat-5TM and Landsat-8 OLI/TIRS, satellite data, path178 rows 28 to the study area

North Crimean Canal

Landsat satellites provide information in optical channels, so image quality depends on the percentage of clouds and precipitation. Therefore, synthetic aperture radar (SAR) images from the Sentinel-1 satellite, with a spatial resolution of 10 m, were used to obtain data regardless of weather conditions. Images from the Sentinel-1 satellite for August 9, 2016 and August 22, 2021 were used for the study (Fig. 15.2).

North Crimean Canal

Images from the Landsat-5TM, Landsat-8OLI/TIRS, and Sentinel-1 satellites complement each other. In addition, they are data from different ranges of electromagnetic waves, allowing you to significantly expand the list of tasks to improve the quality of the research. Using various moisture indices is an effective method for determining surface moisture by remote sensing data. These indices are designed to assess the presence of moisture in vegetation or soil. Table 15.1 shows the moisture index or water index used in our study.

Considering that the Landsat-5 TM and Lands at-8 OLI/TIRS satellites have two short-wave infrared bands (SWIR1 and SWIR2), the water indices were calculated separately for each infrared band. In addition, the authors proposed using the studied water index – WPCA1, which was calculated by the method of principal components (principal component analysis, PCA). That is one of the methods of factor analysis based on the orthogonal transformation of many observations with possibly related variables (entities, each from which it acquires different numerical values) into a set of variables without linear correlation, which is called principal

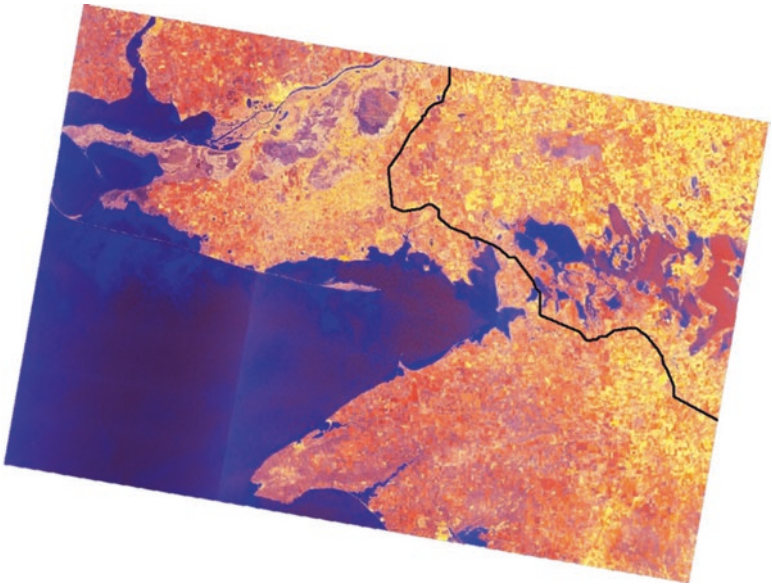

Fig. 15.2 Example of a scene from the satellite Sentinel-1 (combination of channels: vv, vh, vv/vh, polarization. C-band – wavelength 5.5 cm), for 22.08.202

Table 15.1 Water indices used to calculate the moisture content of the territory

№	Index	Equations
1	DSWI	DSWI = (NIR+GREEN)/(SWIR+RED)
2	NDII	NDII = (NIR-SWIR)/(NIR+SWIR)
3	RDI	RDI = SWIR/NIR
4	NWI	NWI = (GREEN-SWIR)/(GREEN+SWIR)

components. The proposed water index WPCA1 was calculated for four water indices considering the two infrared ranges (SWIR1 and SWIR2). For further analysis, the first component was used, which is known to contain helpful introductory information.

Thus, in the study, all the proposed water indices were calculated for SWIR1 and SWIR2. The scheme of the model for estimating water indices, DSWI, NDII, RDI, and NWI using the program for processing space images ERDAS Imagine, is shown in Fig. 15.3, and the new water index WPCA1 was calculated using the image interpreter module of the principal components function. The next step was to form a ten-band image consisting of these calculated water indices. We determined the influence of the North Crimean Canal on soil moisture within the areas of loose soil at different distances from the channel. Water index values were measured at the

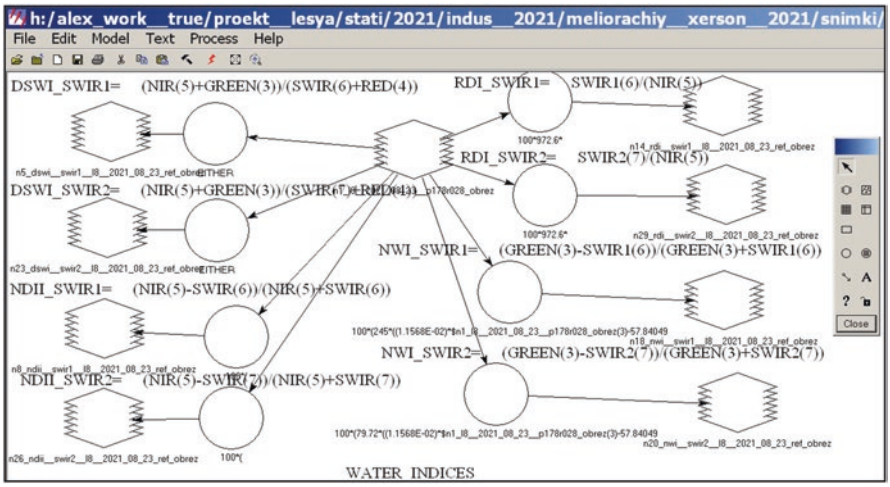

Fig. 15.3 Scheme of the model of calculation of water indices: DSWI, NDII, RDI, and NWI taking into account two infrared ranges (SWIR1 and SWIR2) using the program for processing space images Erdas Imagine

following distances from the canal: up to 240 m; from 240 to 480 m, from 990 to 1500 m, and from 2100 to 5100 m. To establish these distances in the images, the North Crimean Channel was vectorized, and the Model Maker module of the ERDAS Imagine space image processing program was used. Within each of the four established strips, areas of open ground with a homogeneous structure were identified. Within the selected regions, the values of ten water indices were determined from the generated ten-band image.

To determine the effect of irrigation on vegetation productivity, the normalized difference vegetation index (NDVI) was used, obtained by satellite sounding. The value of this index corresponds to different degrees of vegetation, its area, density, biomass, and reflectivity. The concept of the NDVI index is based on the fact that healthy vegetation generally has low reflectivity in the visible part of the electromagnetic spectrum due to absorption by plant pigments, mainly chlorophyll. At the same time, green leaves have high reflectivity in the near-infrared range. This index was demonstrated (Rouse et al. 1973) and is defined as the difference between the values of the intensity of the reflected radiation in the red R_{RED} (0.62–0.69 μm) and near-infrared R_{NIR} (0.75–0.9 μm) ranges electromagnetic waves, divided by the sum of these values:

$$\mathrm{NDVI} = \frac{R_{NIR} - R_{RED}}{R_{NIR} + R_{RED}} \tag{15.1}$$

To perform the second research stage, "Assessment of the impact of soil erosion on the reduction of their productivity," morphometric indicators characterize the

terrain's vertical and horizontal relief. They are established by analysis of digital terrain model (DEM) from the Shuttle satellite with a spatial resolution of 30 meters.

Evaluation of erosion dismemberment was performed according to the method developed and tested by the authors of this study (Lyalko et al. 2017, 2018).

Erosional dismemberment of the terrain:

$$\mathrm{ER} = \frac{\Delta H^* \left(N^* l \right)}{P^2} \tag{15.2}$$

where $(N^*l)/P$ is horizontal dissection of the relief, N is the number of pixels of the isolines in the sliding window and l is the length of the pixel.

The calculation of the vertical dissection of the terrain was performed using the spatial modeler module of the ErdasImagine program according to the following equation:

$$\frac{\Delta H}{P} = \left(H_{\max} - H_{\min} \right) / P \tag{15.3}$$

where $H_{\min}$, $H_{\max}$ are minimum and maximum values of heights in the sliding window.

To calculate the horizontal dissection of the relief, isolines were built for the whole territory of Ukraine with a height of the relief section of 5 m, firstly with the help of the Interpreter module of the ERDAS Imagine program.

The next step is the calculation in the sliding window of the horizontal dissection of the terrain. According to the equation:

$$\left(N^* l \right) / P \tag{15.4}$$

Thus, the intensity of erosional dismemberment of the territory was calculated using Eq. 15.2 in the program ErdasImagine.

Since the values of the ER index depend on the height, to compare different areas, it was proposed to scale the values of the index by the equation:

$$\mathrm{ER}_{\mathrm{new}} = 100^* \left(\frac{\mathrm{ER} - \mathrm{ER}_{\min}}{\mathrm{ER}_{\max} - \mathrm{ER}_{\min}} \right) \tag{15.5}$$

According to the radar survey data from the Sentinel-1 satellite, the method of radar interferometry was used to determine the erosional dismemberment of the relief.

A synthetic aperture interferometric radar is a geodetic method that uses two or more images from a synthetic aperture radar (SAR) to create maps of surface deformation or digital altitude using the phase differences of the waves returning to the satellite. The main idea of the proposed technique is to measure changes in the deformation of the land surface on a millimeter scale for days to years. The obtained images describe the latest geodynamic conditions in the study area. The mission of the European Space Agency (ESA) Sentinel-1 is based on a group of identical

satellites of the SAR band C. Sentinel-1A provides SAR data to the ASF Data Search (https://search.asf.alaska.edu) with a viewing time of 10–12 days. The built-in SAR tool supports four image modes that provide different resolutions and coverage.

In this research, we used the pairs of satellite images of Sentinel-1 in 2016 and 2020 August, which correlated with Landsat images. Image processing was performed entirely using the open-source Sentinel Application Platform (SNAP), applying the built-in SNAPHU module.

We have the interferogram algorithm forming: previous preprocessing, coregistration, interferogram formation, TOPS-Deburs, interferogram filtering, phase unwrapping, displacement of phase, and terrain correction (Piestova et al. 2020). The two SAR SLC Sentinel-1 interferometric products were taken in pairs with a difference between images of 12 days to determine changes in the land surface. The result of the algorithm is digital terrain models for 2016 and 2021 and changes in the height of the terrain surface (Orlenko 2021). The processing of space images was carried out in the program processing space images. Erdas Imagine, SNAP, ENVI, GIS systems were also used: ArcGIS on-line and MapInfo Professional (Gulhane et al. 2022).

The following methods were used to solve all the tasks:

- Information: bibliographic and analytical – for a detailed analysis of existing approaches to monitoring irrigated lands, the state, and technology of its implementation, accuracy, completeness, reliability, and relevance of data.
- Abstract: logical – for theoretical generalization and formation of conclusions on the possibilities of using remote sensing data for monitoring irrigated lands.
- Multidimensional analysis, methods of geoinformation processing, and geostatistical data analysis – for evaluation and verification of input data used for agricultural purposes, by different composition of lands and by types of crops and reclamation measures (irrigated/drained).
- Statistical – to identify the reliability of the results.
- Mathematical (regression, correlation, and factor) – to establish the relationships and relationships between different data sets, particularly remote sensing data of the Earth and ground information.

Results and Discussions

For the last few years, the discussion of the causes and consequences of the predicted changes in climate has continued. According to most scientists, the increase in anthropogenic greenhouse gas content in the atmosphere with high probability is the main reason for the rise in the global average temperature from the middle of the twentieth century. Therefore, it is doubtful that global climate change over the last 50 years of the twentieth century and the first years of the XXI century could challenge only internal natural variability. The noticeable influence of the economic

activity of a person is now spread to other characteristics of climate, including average temperature on continents, atmospheric conditions, and some kinds of extreme phenomena. But, unfortunately, the current policy of all countries is not fully adequate to remain within the limits of the increase in temperature of the eyelid by 0.1–0.2 °C. In the decade, the world's carbon dioxide emissions have reached a new peak, and no country has been on the way to preventing global climate change (Kostyuchenko et al. 2017, 2020; Lyalko et al. 2016; Yelistratova et al. 2021; Tymchyshyn et al. 2021). The reluctance of some countries to recognize the impact of their industrial and agricultural potential on increasing greenhouse gas emissions leads to an increase in the effects of climate change. In addition, natural disasters are enhancing in different regions of the Earth, so there is a need from forecasting the climate to develop strategies to adapt to future changes, not only global climate but also climate at the regional level. This problem is quite urgent for our country. Actual observations on the territory of Ukraine show that our annual temperature exceeds the norm for the corresponding number of degrees every year. If the temperature rise continues to keep the current trends and the government do nothing to adapt to the climate changes, Ukraine will have severe problems with food. Moreover, because a large part of the territory is located in zones of nonstatic and unstable moisture, the food provision depends on the efficiency of the irrigated lands. Finally, the analysis results allow us to assert the existence in Ukraine of economic and reclamation infrastructure, the capacity of which is used highly unsatisfactorily.

There are many methods of enhancing natural landscapes. Melioration hydrogeology studies only water reclamation: irrigation, the creation of optimal conditions for growing cultivated plants in the zone of insufficient moisture; drainage, the creation of optimal conditions for increasing cultivated plants in the location of excessive moisture; bilateral regulation, the use of humidification and drainage at different times of the year in one area in certain climatic conditions; and flooding, water supply to dry regions without irrigation. In this work, we studied only the first method of improving natural landscapes – "irrigation" – because, with modern global warming, most of the territory of Ukraine suffers from a lack of moisture.

The territory of the study consists of two test sites: the southern part of the Kherson region, south of the Kakhovka reservoir, and the north of the Crimean peninsula, which differ in natural conditions. Therefore, to compare the results, further studies were conducted separately for each test site. The area of the Kherson region, which is located south of the Kakhovka Reservoir, is characterized by fertile chernozem soils with a high humus content, from 3% to 4.5%. High yields of crops are possible on these lands, but the lack of moisture and the uneven distribution of rainfall over time significantly complicate agriculture in these areas. Getting high yields in this area is possible only with artificial irrigation. The central North-Crimean canal and other canals have solved the problem of water shortage. However, in 2014, after the annexation of the Crimean Peninsula by the Russian Federation, Ukraine blocked the North Crimean Canal on its territory with a 107 km dam (Kalanchak checkpoint) on the border with Crimea. Next to this dam, located 1 km

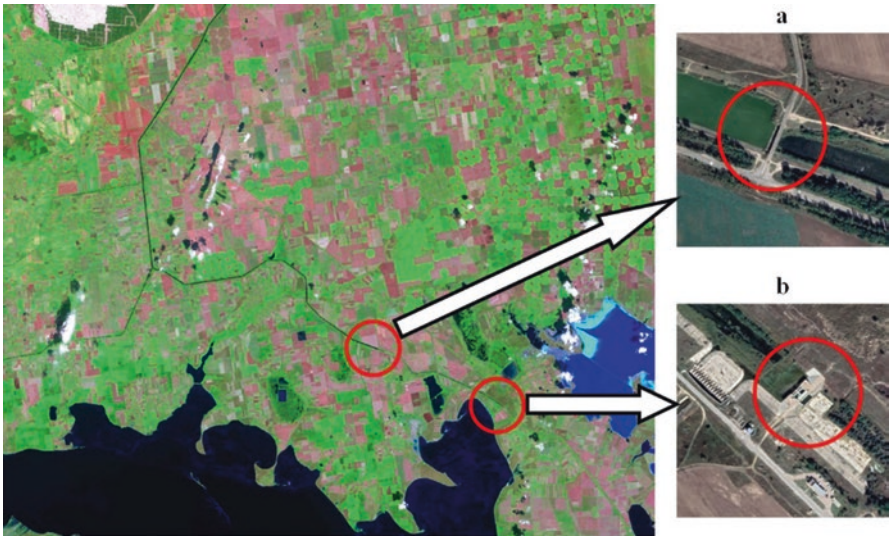

Fig. 15.4 Fragment of the study area with two dams on the North Crimean Channel on the Landsat-8 OLI/TIRS satellite, dated 2021.08.23. In the pictures from the QuckBird satellite: (**a**) "farmer's dam" and (**b**) dam near the checkpoint "Kalanchak"

from the border, another dam was built, located 16 km from the first (Fig. 15.4). As a result, a large area of the region was deprived of water, and yield losses reached 25%.

It should also be noted about the unsatisfactory technical condition of farm melioration systems in the region, due to which irrigation of land on large areas cannot be used.

All these problems influence the climatic factor, namely the climate's aridity, which is due to the onset of frequent droughts. In addition to deficits, crops are significantly affected by abrupt changes in weather conditions, particularly rainfall. In these conditions, operational control over soil moisture, its variability over time, and the vegetation-grown state are necessary. Finally, and most importantly, the loss of water from irrigation canals is due to various technical problems. Irrigation canals are designed to transport water from the water intake to irrigation. At the same time, the efficiency of most irrigation systems today is 0.85–0.87. Therefore, about 25–30% of all water transported from the water intake to the irrigated field is lost to filtration from irrigation canals. If the total losses on the system are taken as 100%, they are distributed as follows: losses on filtration, 70–75%; losses on evaporation, 3–5%; and technical losses, 20–25%. As a result of filtration from canals, there are unproductive water losses, rising groundwater levels, flooding and waterlogging of territories, secondary salinization of soils, and the creation of emergencies. Solving these problems by traditional ground methods requires significant funds and time. However, as our experience has shown, the use of multizone space images allows you to solve this problem quickly and with minimal time and money. The calculated water indices were compared using the infrared range SWIR1 and

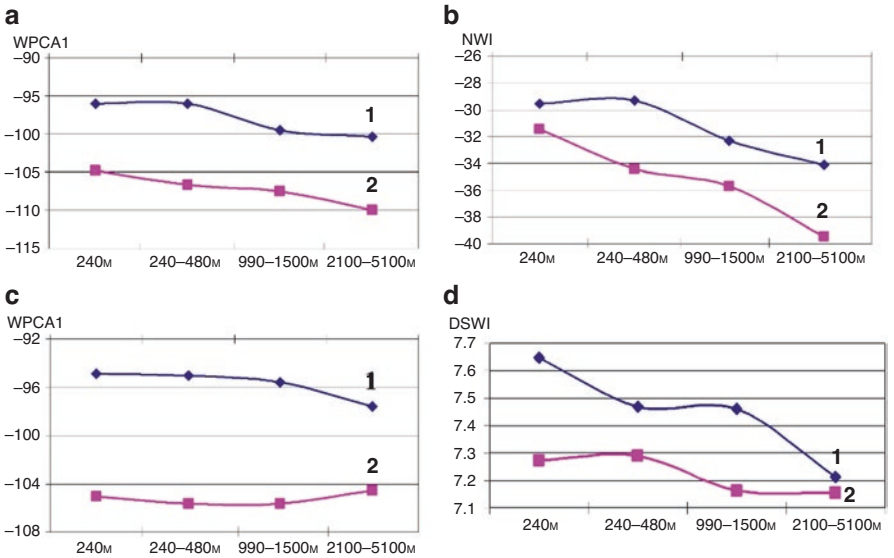

Fig. 15.5 Graph of soil moisture change according to the data from Landsat 5 satellites (2004-07-07) (1), Landsat 8 (2021-08-23) (2) depending on the distance to the North – Crimean canal for the value of water indices. The territory of the southern part of the Kherson region: (**a**) WPCA1 using SWIR-1, (**b**) NWI using SWIR-2; the territory of northern Crimea (**c**) WPCA1 using SWIR-1, and (**d**) DSWI using SWIR-1

SWIR2 according to the data from the Landsat-5TM satellite, for 07.07.2004 and according to the Landsat-8 OLI/TIRS satellite, for 23.08.2021, studying the soil moisture in the south of the Kherson region. Three water indices were selected based on the analysis, which best characterize the soil moisture (Fig. 15.5a, b). The research of these graphs shows a decrease in the values of the calculated water indices for open ground with increasing distance from the North Crimean canal. This dependence is observed for all calculated water indices, regardless of the Landsat-5TM and Landsat-8 OLI/TIRS satellite series or the year of the study. Thus, for water indices, WPCA1 was calculated using the infrared range SWIR1 (Fig. 15.5a), and NWI was calculated using the infrared range SWIR2 (Fig. 15.5b); the values of the index for 2004 outweigh the corresponding values for 2021; uneven change of values of water indices at different distances from the channel. When analyzing water indices calculated at four distances from the canal ((1) up to 240 m, (2) from 240 to 480 m, (3) from 990 to 1500 m, and (4) from 2100 to 5100 m), it was found that at the first two distances, the average values differ from the average values of water indices measured at distances 3 and 4 from the channel. For the WPCA1 index calculated using the infrared range SWIR1 (Fig. 15.5a) for 2004, the difference between the average values calculated at distances 1 and 2 and distances 3 and 4 is 4.12%, for 2021 and is 2.86%. For the NWI index computed using the infrared range SWIR2 (Fig. 15.5b) for 2004, the difference between the average values at distances 1 and 2 and distances 3 and 4 is 13.08%, for 2021 14, 11%.

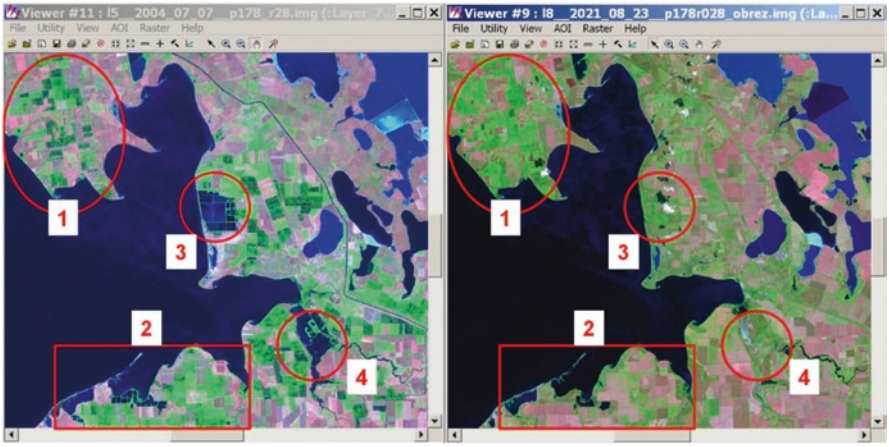

Fig. 15.6 Influence of irrigation, on the example of the North-Crimean channel, on agrocenoses

When studying the soil moisture in the test area (north of the Crimean peninsula), an analysis of the distribution of the values of the obtained water indices was also performed (Fig. 15.5c, d). A decrease the range of changes in the calculated water indices was found. Thus, the content of values for the water index WPCA1 calculated using the infrared range SWIR1 (Fig. 15.5c) for 2004 is 2.717 and for 2021 is 0.495, and for the water index DSWI calculated using the infrared range SWIR1 (Fig. 15.5d) is 0.433 and for 2021 is 0.118. Thus, the decrease in the di-range of values is from 72.74% to 81.78%.

The areas near the North Crimean Canal were analyzed until 2014 (we took 2004 years images from the Landsat-5 TM satellite) and after 2014 (2021, photos from the Landsat-8 OLI/TIRS satellite), when part of the North Crimean Canal was blocked by two dams and water supply to the Crimean Peninsula was cut off (Fig. 15.6). In Fig. 15.6, four objects were identified: the territory of the south of Kherson region, where the North-Crimean canal was not blocked, the first (№1) object corresponding to rice checks; the part of the Crimean peninsula, where the channel was blocked, the second (№2) object corresponding to the rice checks; and the third (№3) and the fourth (№4) objects correspond to the changes of the hydrological regime of the territory. The object №1 means that rice checks are well and visible, and according to the data from the Landsat 5 and Landsat 8 satellites, in 2004 and 2021, only the brightness value changes. The North Crimean Canal blockage on the border with the administrative boundary of the Autonomous Republic of Crimea did not particularly affect the situation in the Kherson region, as water supply continued there. The analysis of plot №2 means that rice checks showed that in 2004, plot №2 did not differ fundamentally from plot №1, as well as the areas near plots №3 and №4, which correspond to rice checks. On the contrary, the data analysis for 2021 showed that the closure of the North-Crimean canal in 2014 led to a significant reduction and, one might say, stops of rice cultivation in the north of the Crimean peninsula.

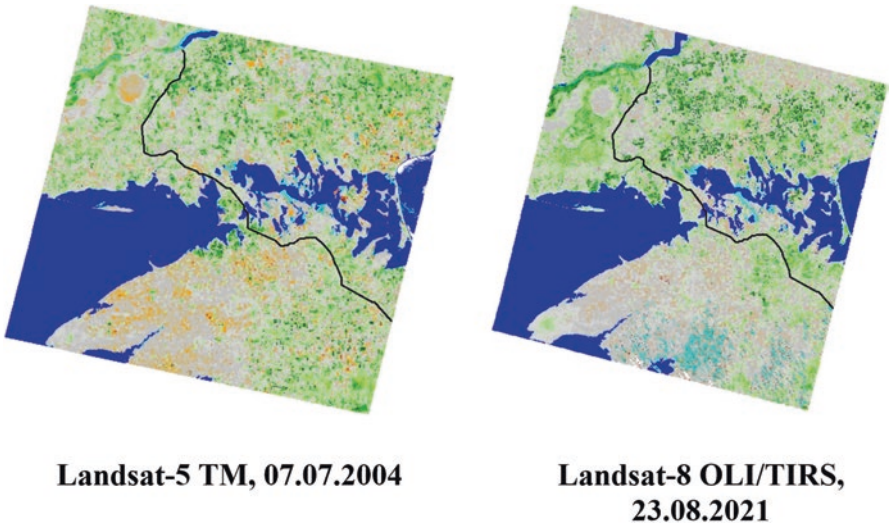

Fig. 15.7 Construction of the vegetation index NDVI to determine the impact of irrigation on vegetation

The analysis of sections №3 and №4 shows that artificial water bodies disappear without ensuring the timely and complete provision of water resources by the North Crimean Canal (Sections №3 and №4).

The effect of moisture on vegetation productivity was shown, which is established according to satellite imagery and allows to predict yields. Maps of the distribution of the NDVI index by Eq. (15.1) were constructed, and the values of the index corresponding to irrigation fields (concentric circles in the space image) and nonirrigation areas of elongated rectangular shape were analyzed (Fig. 15.7). As a result, it was found that the average NDVI value for irrigated fields is 73,821, while for nonirrigated areas is 64,859, which is almost 12% less than irrigated.

Thus, studies of soil moisture using water indices have shown that it is possible to study the distribution of soil moisture in the southern part of the Kherson region and the north of the Crimean peninsula. Moreover, according to satellites Landsat, Sentinel-2, and others, such work can be carried out quickly at various scale levels. Since the study area is determined by the uneven distribution of erosion processes, both in intensity and in the area in which they are developed, an assessment of the impact of soil erosion processes on the reduction of their productivity was given. According to Eqs. (15.2), (15.3), (15.4) and (15.5), potentially dangerous erosion areas were calculated (Fig. 15.8).

Figure 15.8 shows the danger of erosional dismemberment levels of the relief according to the ER index in color gradations from red to light green. According to the values of the index from 0 to 2 (from light to dark green), the level of danger is absent; from 2 to 7 (mustard and yellow colors), the level is weak; from 7 to 10 (light orange), level is significant; and from 10 to 13 (dark orange), the level is

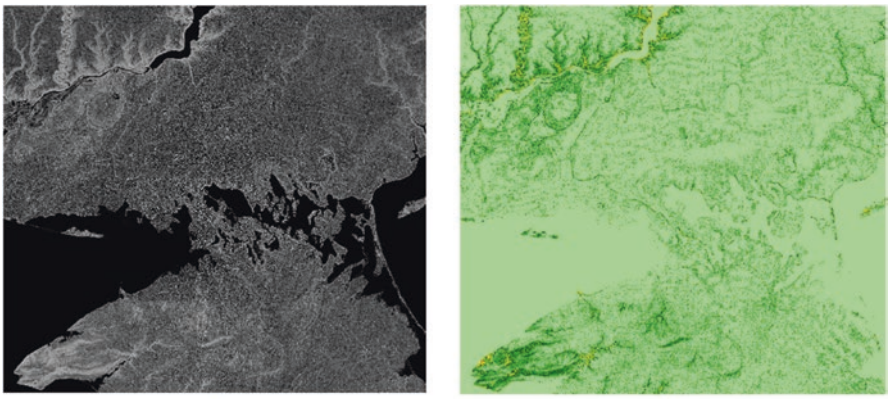

Fig. 15.8 Example of using the methodology for calculating the ER index in the area with coordinates (37.22E 47.13 N) and (35.00E 45.00 N) in the scale 1: 800000: (**a**) digital terrain model from the Shuttle satellite, spatial resolution 30 m, and (**b**) the obtained values of the ER index

strong. Analysis of the results showed that the maximum values of the index are confined to the sloping surfaces (this is the value of the ER index from 7 to 13). Thus, these relief elements are naturally affected by erosion processes, complicated by ravines and gullies of different ages and origins, and require special attention from erosion safety. Figure 15.9 shows the difference in altitude from the Sentinel-1 for 2021 and 2016. The most intense erosion processes occur in the north-right tributaries of the Dnieper River, as well as within the valley of the Dnieper River. In Fig. 15.9b, the boundary of the floodplain of the Dnieper River and the first floodplain terrace on the left bank of the Dnieper River are visible, and the borders of Oleshkiv Sands – the only sandy desert in Ukraine. In addition to large-sized erosive landforms, numerous small-sized erosive forms are observed throughout the study area.

Thus, within some small annual valleys, local areas are observed in which there is a more intensive development of erosion processes. Such processes lead to significant losses, primarily of chernozem, reduction of arable land, and a considerable reduction in soil productivity. According to our previous research [VISNYK 2017], the loss of one hectare of chernozems leads to approximately $ 500,000, and due to the relatively comprehensive development of erosion processes throughout the study, losses in monetary terms will increase rapidly.

The values of the obtained ER index make it possible to identify potentially dangerous areas of erosion. Erosion processes over time, mainly due to irrational management, can suddenly intensify in unpredictable places. The possibility of using a radar survey to determine the erosional dismemberment of the terrain and establish the loss of humus in monetary terms from erosion processes is shown. It is satellite monitoring that makes it possible to record the manifestations of negative phenomena associated with soil erosion throughout the country.

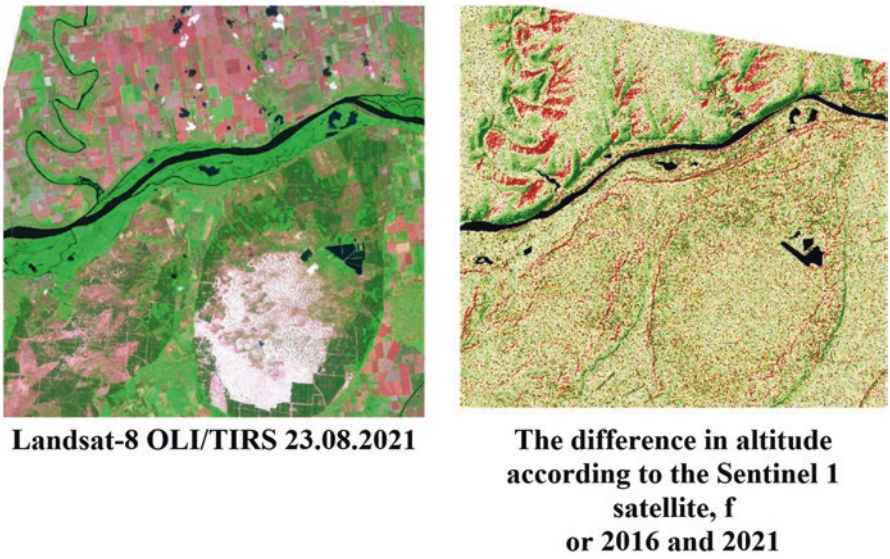

Fig. 15.9 Comparison of the space image from the Landsat-8OLI/TIRS, for 2021-08-23 and the height difference according to the data from the Sentinel-1, for 2016 and 2021 for the detection of erosion-hazardous areas

Conclusion

To sum up, the management of reclaimed areas is not an easy task. Above all, it is determined by the existence of land reclamation systems that are not in the best possible condition today. Furthermore, the lack of quality, reliable data greatly complicates managerial decision-making. Therefore, to develop melioration territories, it is necessary to introduce scientific and methodological bases based on the latest technologies, mainly using data from remote sensing of the Earth. Furthermore, remote sensing allows the identification of sites of excessive soil moisture resulting from water filtration during canal transport, which should be an action for introducing the necessary protective management measures. The technology proposed in the study, which is based on an estimation of soil moisture level and vegetation condition, can reveal the reasons for their nonsatisfactory state to prevent soil degradation and harmful effects of water. In addition, in monitoring mode, it is possible to conduct a timely assessment of the state of the meliorative system, assess the nonoperating systems, and observe the clearing of channels and water transmission systems, the organization of existing dams, strengthening of drainage.

Recommendations

Today, remote sensing provides necessary information support for the most common tasks of nature conservation and economy. For this reason, timely monitoring of rural areas is one of the requirements of food security. Information about the different components of crops, types of crops, and small-scale measures is an essential component in the assessment of yield and the determination of statistical indicators by relevant state agencies, agricultural and insurance companies, as well as contributes to the development of modern micro-, small-, and medium-sized agricultural enterprises; this will allow them to integrate into competitive Ukrainian and world markets successfully. Today, it is proved that satellite remote sensing methods in the whole world have become significant for solving problems set in the study. The results of the study can be included in the preparation of proposals on the improvement of existing legislation in Ukraine on derivative works. Their use for the environmental monitoring system can ensure rational use of land and water resources.

References

Abuzar M, McAllister A, Whitfield D, Sheffield K (2020) Remotely-sensed surface temperature and vegetation status for the assessment of decadal change in the irrigated land cover of north-Central Victoria, Australia. Land 9(9):308. https://doi.org/10.3390/land9090308

Alon T (2016) Rethinking the sustainability of Israel's irrigation practices in the drylands. Water Res 90:387–394. https://doi.org/10.1016/j.watres.2015.12.016

Apostolov OA, Elistratova LO, Romanchuk IF, Chekhniy VM (2020) Assessment of desertification areas in Ukraine by estimation of water indexes using remote sensing data. Ukr Geogr J 1:16–25. https://doi.org/10.15407/ugz2020.01.016

Bahniuk V, Movchan Y, Tsyvinskyi H (2002) Water melioration reality in Ukraine. Visnyk Natl Acad Sci Ukr 12:45–56

Brown JF, Pervez MS (2013) Variability and trends in irrigated and non-irrigated croplands in the central US. In: 2013 second international conference on agro-geoinformatics. Proceedings paper, pp 102–105

Chance EW, Cobourn KM, Thomas VA, Dawson BC, Flores AN (2017) Identifying irrigated areas in the Snake River plain, Idaho: evaluating performance across composting algorithms, spectral indices, and sensors. Remote Sens 9(6):546. https://doi.org/10.3390/rs9060546

Cosh MH, Evett SR, McKee L (2012) Surface soil water content spatial organization within irrigated and non-irrigated agricultural fields. Adv Water Resour 50:55–61. https://doi.org/10.1016/j.advwatres.2012.07.009

Cvjetova OV, Rjabceva G, Nasjedkin I, Turajeva O (2009) Monitoryng meliorovanyh zemel' v gumidnij zoni Ukrai'ny. Bulletin Turaev NUWMNRU. Coll Sci Works Rivne 3((47), Part 1):237–242

Dinesh S, Jesslyn FB, Trenton DB, Daniel MH (2021) Exploring the regional Dy-namics of U.S. irrigated agriculture from 2002 to 2017. Land 10:394. https://doi.org/10.3390/land10040394

Dowgert MF (2010) The impact of irrigated agriculture on a stable food supply. In: Proceedings of the 22nd annual central plains irrigation conference, Kearney, NE., February 24–25, 2010 available from CPIA, 760 N.Thompson, Colby, Kan-sas

Eberhard J, McHugh A, Scobie M, Schmidt E, McCarthy A, Uddin MJ, McKeering L, Poulter R (2013) Improving irrigation efficiency through precision irriga-tion in South East Queensland. National Centre for Engineering in Agriculture, pp 16–24

Elbeltagi A, Kumar N, Chandel A et al (2022) Modelling the reference crop evapotranspiration in the Beas-Sutlej basin (India): an artificial neural network approach based on different combinations of meteorological data. Environ Monit Assess 194:141. https://doi.org/10.1007/s10661-022-09812-0

Gulhane VA, Rode SV et al (2022) Correlation analysis of soil nutrients and prediction model through ISO cluster unsupervised classification with multispectral data. Multimed Tools Appl. https://doi.org/10.1007/s11042-022-13276-2

Gunlu A, Gol C (2017) The effects of catchment melioration on land cover case study: Tatlıçay catchment. In: ISFOR – international symposium on new horizons in forestry, Isparta – Turkey

Guo L, Zakari A, Tawiah V (2020) Energy resource melioration and CO_2 emissions in China and Nigeria: efficiency and trade perspectives. Resour Policy 68. https://doi.org/10.1016/j.resourpol.2020.101769

Hunt ED, Svoboda M, Wardlow B, Hubbard K, Hayes M, Arkebauer T (2014) Moni-toring the effects of rapid onset of drought on non-irrigated maize with agronomic data and climate-based drought indices. Agric For Meteorol 191:1–11. https://doi.org/10.1016/j.agrformet.2014.02.001

Isgandarov MY (2015) Melioration and ecological state of soils, based on draining de-gree of kura-Aras lowland. Sci J «Science Rise» 2/1(7). https://doi.org/10.15587/2313-8416.2015.37212

Jiang S, Xu N, Li Z, Huang C (2021) Satellite derived coastal reclamation expansion in China since the 21st century. Glob Ecol Conserv 30. https://doi.org/10.1016/j.gecco.2021.e01797

Johansson O, Aimbetov I, Jarsjo J (2009) Variation of groundwater salinity in the par-tially irrigated Amudarya River delta. Uzb J Mar Syst 76(3):287–295. https://doi.org/10.1016/j.jmarsys.2008.03.017

Khadri SFR, Pande C (2016) Ground water flow modeling for calibrating steady state using MODFLOW software: a case study of Mahesh River basin, India. Model Earth Syst Environ 2:39. https://doi.org/10.1007/s40808-015-0049-7

Kostyuchenko Y, Movchan D, Artemenko I, Kopachevsky I (2017) Stochastic approach to uncertainty control in multiphysics systems: modeling of carbon balance and analysis of GHG emissions using satellite tools. In: Ram M, Davim JP (eds) Mathematical concepts and applications in mechanical engineering and mechatronics. IGI Global, pp 350–378. https://doi.org/10.4018/978-1-5225-1639-2.ch017

Kostyuchenko Y, Yuschenko M, Elistratova L, Artemenko I (2020) Multi-model Ap-proach in the risk assessment tasks with satellite data utilization, 1st edn. CRC Press, p 27. https://doi.org/10.1201/9780429200304-3

Kovalchuk PI, Myhalska T, Pendak N, Demchuk O (2010) Ecological-economic model of integrated sustainability management of reclaimed areas. Water Economy Ukr 1:25–30

Kulbida M, Barabash M, Yelistratova L, Adamenko T, Hrebeniuk N, Tatar-chuk O, Korzh T (eds) (2009) Klimat Ukrainy: u mynulomu…i maibutnomu? 1st edn. Stal, Kyiv, pp 85–98

Lyalko VI (2015) Greenhouse effect and climate changes in Ukraine: assessments and consequences. Editor-in-Chief Academician of National Academy of Sciences of Ukraine V.I. Lyalko. Kyiv, Naukova Dumka, p 283, ISBN: 978-966-00-1526-5

Lyalko VI, Apostolov AA, Elistratova LA, Artemenko IG (2016) Analysis of the relationship between the concentration of CO_2 in the atmosphere and temperature of the air for research and forecasting of climate change in Ukraine. Ukr J Remote Sens 10:17–20

Lyalko VI, Elistratova LA, Apostolov AA, Chekhniy VM (2017) Analysis of soil erosion processes in Ukraine on the basis of remote sensing of the Earth. Visn Natl Acad Sci Ukr 10:34–41

Lyalko V, Elistratova L, Apostolov A, Khodorovsky A, Czechniy V (2018) Express-evaluation of potentially erosive soils on the territory of Ukraine, by using the re-mote sensing data with consideration of climatic factors and vegetation. Rep Natl Acad Sci Ukr 3:87–94. https://doi.org/10.15407/dopovidi2018.03.087

Lyalko VI, Romanciuc IF, Yelistratova LA, Apostolov AA, Chekhniy VM (2020) Detection of changes in terrestrial ecosystems of Ukraine using remote sensing data. J Geol Geogr Geoecol 29(1):102–110. https://doi.org/10.15421/112010

Moshinsky VS (2005) Methods of productivity management and ecological stability of drained lands. NUVGP, Rivne, p 250. ISBN: 966-327-024-1

Nasiedkin I, Tsvietova O, Riabtseva H, Yakovenko P (2008) Ekoloho-melioratyvnyi monitorynh osushuvanykh zemel. Melioratsiia i vodne hospodarstvo 96:115–123

Nickum JE, Ogura C (2010) Agricultural water pricing: Japan and Korea. In: OECD, pp 1–34

Orimoloye IR, Olusola AO, Belle JA et al (2022) Drought disaster monitoring and land use dynamics: identification of drought drivers using regression-based algorithms. Nat Hazards. https://doi.org/10.1007/s11069-022-05219-9

Orlenko T (2021) Remote sensing methods for the landslide hazard areas esti-mation and monitoring. Paper presented at the International Conference on Space Science and Technology (ICSST 2021): Ahmedabad, India. Available at: https://youtu.be/jR2I2DvC9z8

Pajic P, Andjelic L, Urosevic U, Polomcic D (2014) Evaluation of melioration area damage on the river Danube caused by the hydroelectric power plant 'Djerdap 1' backwater. Water Sci Technol 70(2):376–385

Pande CB (2022) Land use/land cover and change detection mapping in Rahuri watershed area (MS), India using the google earth engine and machine learning approach. Geocarto Int. https://doi.org/10.1080/10106049.2022.2086622

Pande CB, Moharir KN, Singh SK et al (2020) An integrated approach to delineate the groundwater potential zones in Devdari watershed area of Akola district, Maharashtra, Central India. Environ Dev Sustain 22:4867–4887. https://doi.org/10.1007/s10668-019-00409-1

Pande CB, Moharir KN, Panneerselvam B et al (2021a) Delineation of groundwater potential zones for sustainable development and planning using analytical hierarchy process (AHP), and MIF techniques. Appl Water Sci 11:186. https://doi.org/10.1007/s13201-021-01522-1

Pande CB, Moharir KN, Singh SK, Varade AM, Ahmed Elbeltagie SFR, Khadri PC (2021b) Estimation of crop and forest biomass resources in a semi-arid region using satellite data and GIS. J Saudi Soc Agric Sci 20(5):302–311

Pande CB, Kadam SA, Jayaraman R, Gorantiwar S, Shinde M (2022a) Prediction of soil chemical properties using multispectral satellite images and wavelet transforms methods. J Saudi Soc Agric Sci 21(1):21–28

Pande CB, Moharir KN, Singh SK et al (2022b) Groundwater flow modeling in the basaltic hard rock area of Maharashtra, India. Appl Water Sci 12:12. https://doi.org/10.1007/s13201-021-01525-y

Pervez MS, Brown JF (2010) Mapping irrigated lands at 250-m scale by merging MODIS data and National Agricultural Statistics. Remote Sens 2(10):2388–2412. https://doi.org/10.3390/rs2102388

Piestova I, Dugin S, Orlenko T, Svideniuk M (2020) Assessing and fore-casting landslide hazards of the right bank of the Kaniv reservoir based on radar remote sensing data with corner reflectors using. Paper presented at the XIV In-ternational Scientific Conference on Monitoring of Geological Processes and Eco-logical Condition of the Environment. https://doi.org/10.3997/2214-4609.202056082

Pun M, Mutiibwa D, Li RP (2017) Land use classification: a surface energy balance and vegetation index application to map and monitor irrigated lands. Remote Sens 9(12):1256. https://doi.org/10.3390/rs9121256

Qiu L, Zhang M, Zhou B, Cui Y, Yu Z, Liu T, Wu S (2021) Economic and ecological trade-offs of coastal reclamation in the Hangzhou Bay, China. Ecol Indic 125:107477. https://doi.org/10.1016/j.ecolind.2021.107477

Rahmonov O, Snytko VA, Szczypek T (2016) Influence of melioration in natural ecological processes of a Small River Valley (Poland). Geografiya i Prirodnye Resursy 37(4):191–197

Rajesh J, Pande CB, Kadam SA et al (2021) Exploration of groundwater potential zones using analytical hierarchical process (AHP) approach in the Godavari river basin of Maharashtra in India. Appl Water Sci 11:182. https://doi.org/10.1007/s13201-021-01518-x

Rouse JW, Haas RH, Deering DW, Schell JA, Harlan JC (1973) Monitoring the vernal advancement and Retrogradation (Green Wave Effect) of natural vegetation. In: NASA/GSFCT type III final report, p 93

Ruopu L, Mahesh P (2016) Classification of irrigated and non-irrigated cropland using object-based image analysis: a case study in south-Central Nebraska. In: IEEE 2016 5th international conference on agro-geoinformatics (Agro-geoinformatics). https://doi.org/10.1109/Agro-Geoinformatics.2016.7577619

Satoh M, Ishii A (2021) Japanese irrigation management at the crossroads. Water Altern 14(2):413–434

Senturk S, Bagis S, Ustundag BB (2014) Application of remote sensing techniques in locating dry and irrigated farmland parcels. In: Third international conference on agro-geoinformatics (Agro-Geoinformatics 2014), pp 321–324

Shahid M, Rahman KU, Haider S et al (2021) Quantitative assessment of regional land use and climate change impact on runoff across Gilgit watershed. Environ Earth Sci 80:743. https://doi.org/10.1007/s12665-021-10032-x

Shevah YI (2015) ICID – irrigation & drainage in the world – a global review. International Commission on Irrigation & Drainage | Commission Interationale des Irrigation et du Drainage, Ukrine

Simsek C, Arabacı D (2021) Simulation of the climatic changes around the coastal land reclamation areas using artificial neural networks. Urban Clim 38:1–18

Srivastava A, Chinnasamy P (2021) Investigating impact of land-use and land cover changes on hydro-ecological balance using GIS: insights from IIT Bombay, India. SN Appl Sci 3:343. https://doi.org/10.1007/s42452-021-04328-7

Tabayashi A (1987) Irrigation systems in Japan. Geogr Rev Jpn 60((Ser. B), 1):41–65

Teng L, Cheng H, Swart de HE, Dong P (2021) On the mechanism behind the shift of the turbidity maximum zone in response to reclamations in the Yangtze (Changjiang) Estuary, China. Mar Geol 440. https://doi.org/10.1016/j.margeo.2021.106569

Tymchyshyn MA, Yelistratova LA, Apostolov AA, Romanciuc IF (2021) Remote detection the CO_2 concentration within different land classes cover on the territory of Ukraine. In: Conference proceedings, Geoinformatics, Kyiv, 11–14 May, vol 2021, pp 1–5. https://doi.org/10.3997/2214-4609.20215521046

Wang F, Peng W, Zhang B, Cao Y, Zhao J, Cao H (2021) Succession of bacterial community composition in coastal agricultural soils along a 1000-year reclama-tion chronosequence in Hangzhou Bay, China. Ecol Indic 121. https://doi.org/10.1016/j.ecolind.2020.106972

Yelistratova LA, Apostolov AA, Romanciuc IF (2021) Estimation of CO_2 over the Ukraine based on GOSAT satellite data. In: Proceedings of ideas and innovations in natural sciences, pp 72–76. https://doi.org/10.30525/978-9934-26-047-6-19

Zhu X, Zhang L, Zuo Y, Liu J, Yu J, Yuan F (2021) Wetland reclamation homoge-nizes microbial properties along soil profiles. Geoderma 395. https://doi.org/10.1016/j.geoderma.2021.115075

Chapter 16
Hybrid Kernel Extreme Learning Machine-Based Empirical Wavelet Transform for Water Quality Prediction Using Only River Flow as Predictor

Salim Heddam

Abstract During the last few years, monitoring and controlling water quality in freshwater ecosystems was strongly facilitated by the increasing number of in situ stations, certainly in combination with the high number of developed models. Several water quality variables have received a great deal of attention regarding their environmental importance, while other variables have rarely been studied in detail using modeling strategies. Generally speaking, water variables were linked to building robust models and rarely are the models using fewer variables. Machine learning algorithm aiming to accurately build relationships between water quality variables are widely used and acknowledged. In the present investigation, we tried to introduce a new modeling strategy for predicting two water quality variables: water pH and specific conductance (SC) using kernel extreme learning machine models (KELM). The major contribution of our study is that we used only the river flow as relevant predictor and a single-input and single-output (SISO) model was proposed for predicting water pH and SC. Two scenarios were analyzed and compared. First, SISO models were developed and compared. Second, to greatly increase the performances of the KELM models, we have used the empirical wavelet transform (EWT) algorithm for decomposing the river flow time series into several multiresolution analysis components (MRA), which were used as new input variables. Data collected at the USG websites were used to test the proposed algorithms, and we find that the EWT clearly exhibited high accuracies compared with the SISO models, and it provides a very robust estimate of the water pH and SC. For water pH, it was found that the KELM models based on EWT were more accurate compared with the models without EWT, exhibiting R, NSE, RMSE, and MAE values ranging from 0.888 to 0.981, from 0.767 to 0.961, from 0.038 to 0.074, and

S. Heddam (✉)
Faculty of Science, Agronomy Department, Hydraulics Division, Laboratory of Research in Biodiversity Interaction Ecosystem and Biotechnology, University 20 Août 1955, Skikda, Algeria

C. B. Pande et al. (eds.), *Climate Change Impacts on Natural Resources, Ecosystems and Agricultural Systems*, Springer Climate,
https://doi.org/10.1007/978-3-031-19059-9_16

from 0.027 to 0.058, respectively. In addition, for the SC, it was found that KELM models based on EWT were more accurate exhibiting R, NSE, RMSE, and MAE values ranging from 0.897 to 0.974, from 0.804 to 0.947, from 2.352 to 5.374, and from 1.528 to 4.152, respectively.

Keywords Modeling · Water quality · pH · Electrical conductivity · KELM · EWT

Introduction

Estimation of water quality variables is a challenging task, and several factors need to be taken into account and considered to be reasonable for the evaluation, control, and monitoring of water resources (Rizo-Decelis et al. 2017). Generally speaking, water quality variables were measured and controlled individually and combined together for calculating the water quality index (Babbar and Babbar 2017; Kouadri et al. 2022). Among a large number of water quality variables, water pH and specific conductance (SC) were reported to be among the most significant water quality variables that have received great attention from researchers worldwide (Dow and Zampella 2000). During the last few years, the use of machine learning models for predicting water quality variables has received great importance, and a few of them have largely modeled and studied, i.e., dissolved oxygen concentration (Moghadam et al. 2021; Yaseen et al. 2018; Yang et al. 2021) and river water temperature (Piotrowski et al. 2021; Yousefi and Toffolon 2022), while other have been marginalized, i.e., water pH and specific conductance (SC), and few studies are available in the literature.

Lu and Ma (2020) used two hybrid decision tree models for predicting several water quality variables, i.e., water pH, specific conductance (SC), dissolved oxygen (DO), water temperature (T_w), turbidity (TU), and fluorescent dissolved organic matter (FDOM). The authors have coupled the random forest regression (RFR) and the extreme gradient boosting (XGBoost) models with the complete ensemble empirical mode decomposition with adaptive noise (CEEMDAN), i.e., RFR-CEEMDAN and the XGBoost-CEEMDAN. The two hybrid models were developed using data from the Tualatin River, the United States. For comparison, results obtained using the RFR-CEEMDAN and the XGBoost-CEEMDAN were compared to those obtained using the least-squares support-vector machine (LSSVM), long- and short-term memory deep learning (LSTM), particle swarm optimization optimized support vector regression (SVR-PSO), and the radial basis function neural network (RBFNN). The CEEMDAN was used for decomposing the water variables into several intrinsic mode functions (IMF_S), which were used as input variables. Obtained results revealed that the best performances with high numerical indexes were obtained using the RFR-CEEMDAN and the XGBoost-CEEMDAN with MAE and RMSE of approximately 0.025 and 0.02 for water pH and 1.17 and 1.27 for specific conductance, respectively. Ahmadianfar et al. (2020) adopted the same

modeling strategy of our present investigation for modeling river water SC, by selecting the river discharge as a single input variable to several machine learning models. They compared between hybrid wavelet locally weighted linear regression (W-LWLR) model and the multiple linear regression (MLR), the SVR, the LWLR, ARIMA, wavelet ARIMA (WARIMA), wavelet MLR (WMLR), and WSVR models. The wavelet decomposition WD was used for decomposing the river discharge into several subcomponents, and all models were applied and compared for monthly SC prediction. It was found that the W-LWLR model was the most accurate model and ranked in the first place with the coefficient of correlation (R), Nash-Sutcliffe coefficient of efficiency (NSE), RMSE, and MAE of 0.904, 0.785, 182.37, and 147.26, respectively, while the poorest performances were achieved by the MLR model.

Dabrowski et al. (2020) used the linear and nonlinear state space models for predicting water quality variables, i.e., water pH, DO, and T_w. The linear and nonlinear were applied with and without mean reversion, and acceptable forecasting accuracies were obtained for river water pH with normalized RMSE (NRMSE) of approximately 21.84 and 87.89 for the models with and without mean reversion. Eze et al. (2021) applied the LSTM deep learning model coupled with the ensemble empirical mode decomposition (EEMD) for predicting DO, Tw, pH, and TU. The EEMD was used as a signal preprocessing approach for decomposing the water quality variables into several IMFs, and it was found that for water pH, high forecasting accuracies were obtained with MAE and RMSE of approximately 0.0042 and 0.0092 for the EEMD-LSTM and 0.014 and 0.0074 for the LSTM models, respectively. Fu et al. (2021) used the temporal convolutional network (TCN) model for predicting DO, water pH, and T_W. They compared between the TCN, the LSTM, the recurrent neural network (RNN), the simple recurrent unit (SRU), bidirectional simple recurrent unit (BI-SRU), and the gated recurrent unit (GRU). Comparison between the models' performances was found that the best predictive accuracy was achieved using the TCN model (RMSE $\approx$ 0.050, MAE $\approx$ 0.0214), while the lowest accuracy was obtained using the GRU model with (RMSE $\approx$ 0.0678, MAE $\approx$ 0.0338), respectively. Yang and Liu (2021) used the LSTM coupled with the CEEMDAN (LSTM- CEEMDAN) for predicting river pH. The authors have reported that the use of sample entropy (SE) for better selection of the IMFs helps in better improving the model accuracies for which the RMSE and MAE were dropped from 0.0293 and 0.0307 obtained using the LSTM to the values of 0.0189 and 0.0107, obtained using the LSTM-SA-CEEMDAN, respectively. He et al. (2011) used the multilayer perceptron artificial neural network (MLPNN) for predicting several water quality variables, i.e., water SC and pH. The authors have demonstrated that the use of partial mutual information (PMI) algorithm for selecting the best input variables contributed to the improvement of the MLPNN performances, and high accuracy was obtained with RMSE, MAE, and R^2 of 0.641, 0.342, and 0.913 for water SC, and 0.087, 0.067, and 0.870 for water pH, respectively. Finally, Sahoo et al. (2006) used the MLPNN model for modeling river water pH and SC using river stage and discharge as input variables. It was found that water pH and SC were predicted with

high accuracies with R and RMSE of 0.847 and 7.180 for water SC and 0.799 and 0.068 for water pH. Consequently, in the present chapter, we propose a new modeling strategy for predicting river water pH and SC using only river discharge. The novelty of our study is that we used the empirical wavelet transform (EWT) as a preprocessing signal decomposition for decomposing the river discharge (Q) to form a series of multiresolution analysis components (MRA), which were combined together to form the input variables for the kernel extreme learning machine (KELM) models.

Materials and Methods

Study Site

In the present chapter, data used for developing the KELM were collected at two USGS stations namely: (*i*) USGS 14206241 Tualatin River at Highway 219 Near Hillsboro, Washington County, Oregon, the United States (latitude 45°30′01″, longitude 122°59′24″ NAD27), and (*ii*) USGS 14211720 Willamette River at Portland, Multnomah County, Oregon (latitude 45°31′03″, longitude 122°40′09″ NAD83). River discharge (Q), river water pH, and river water-specific conductance (SC) were measured at daily time step. For the USGS 14206241 station, data were recorded for the period ranging from 01/January/2005 to 26/May/ 2020 with a total of 5300 patterns. For the second station, i.e., the USGS 14211720 station, data were recorded for the period ranging from 21/January/2009 to 10/November/2021 with a total of 4586 patterns. Dataset was divided into training (70%) and validation (30%), hence, for the USGS 14211720 station; 3211 and 1375 were used for training and validation, respectively, and for the USGS 14206241; 3710 and 1590 were used for training and validation, respectively. In Table 16.1, we reported the statistical values of the Q, pH, and SC, i.e., the mean, maximal, minimal, standard deviation, the coefficient of variation, and the coefficient of correlation with Q, respectively. The location of the USGS stations is shown in Fig. 16.1. In this chapter, for modeling the pH and SC, we adopted two scenarios: (*i*) using only the discharge as a single input variable, and (*ii*) river discharge was decomposed into several subcomponents, i.e., the multiresolution analysis components (MRA), which were combined and used as input variables. In this chapter, at each station, we decompose the river discharge into 12 MRA subcomponents (Fig. 16.2).

Table 16.1 Summary statistics of discharge, pH, and specific conductance variables

Variables	Subset	Unit	X_{mean}	X_{max}	X_{min}	S_x	C_v	R
Daily data for USGS ID 14211720 Willamette River at Portland, Oregon, USA								
Q	Training	*Kcfs*	30.755	200.000	2.250	29.044	0.944	1.000
	Validation	*Kcfs*	31.372	176.000	3.510	28.482	0.908	1.000
	All data	*Kcfs*	30.940	200.000	2.250	28.875	0.933	1.000
pH	Training	/	7.295	8.200	6.700	0.155	0.021	−0.523
	Validation	/	7.298	8.000	6.700	0.153	0.021	−0.538
	All data	/	7.296	8.200	6.700	0.154	0.021	−0.528
SC	Training	*uS/cm*	76.603	102.000	49.000	10.262	0.134	−0.664
	Validation	*uS/cm*	76.861	107.000	50.000	10.254	0.133	−0.631
	All data	*uS/cm*	76.680	107.000	49.000	10.259	0.134	−0.654
Daily data for USGS ID 14206241 Tualatin River at HWY 219 near Hillsboro, Oregon, USA								
Q	Training	*cu.f/s*	771.483	3670.000	60.100	852.823	1.105	1.000
	Validation	*cu.f/s*	767.080	3650.000	67.200	854.384	1.114	1.000
	All data	*cu.f/s*	770.162	3670.000	60.100	853.213	1.108	1.000
pH	Training	/	7.212	7.800	6.500	0.194	0.027	−0.754
	Validation	/	7.210	7.800	6.600	0.193	0.027	−0.747
	All data	/	7.211	7.800	6.500	0.194	0.027	−0.752
SC	Training	*uS/cm*	94.936	142.000	45.000	12.230	0.129	−0.567
	Validation	*uS/cm*	94.671	142.000	53.000	12.133	0.128	−0.573
	All data	*uS/cm*	94.857	142.000	45.000	12.200	0.129	−0.569

Abbreviations: X_{mean} mean, X_{max} maximum, X_{min} minimum, S_x standard deviation, C_v coefficient of variation, R coefficient of correlation with *discharge*, Q river discharge, *SC* specific conductance, *Kcfs* thousands of cubic feet per second, *cu.f/s* cubic feet per second

Methodology

Empirical Wavelet Transform (EWT)

The empirical wavelet transform (EWT) was proposed by Gilles (2013). The EWT is a preprocessing signal decomposition method used for reducing the nonstationarity and high fluctuation of the signal in the presence of noise using a projection schema along the orthogonal subspace. As a result, the nonlinear signal becomes decomposed into a series of subcomponent called multiresolution analysis (MRA) components (Rout et al. 2022; Chen et al. 2022). From a mathematical point of view, the EWT is composed of two parts functions: the empirical wavelet and the empirical scale functions and considered as a filter for low-pass signals (Yang et al. 2022). The EWT procedure consists of several stages, which are detailed in Gilles (2013), and can be summarized as follows (Peng et al. 2022):

1. In the first stage, the Fourier transform is used for providing the Fourier spectrum of the signal and the frequency range is specified as [0,π].
2. A series of N segments is obtained by decomposing the original signal.

Fig. 16.1 Map showing the location of the two USGS stations

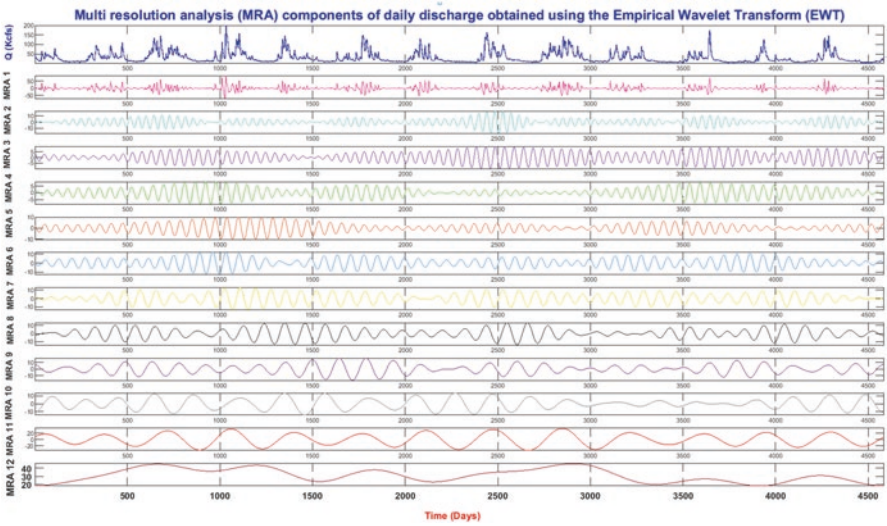

Fig. 16.2 Multiresolution analysis components (MRA) of daily discharge (Q) dataset obtained using the empirical wavelet transform (EWT) algorithm

3. By applying the Littlewood-Paley and Meyer wavelet decomposition algorithms, the EWT is constructed.
4. Calculates the detail and approximate coefficients of the EWT.

In this chapter, the EWT was applied for decomposing the single input variable, i.e., the river discharge into several multiresolution analysis (MRA) components, which were reported in Fig. 16.2.

Kernel Extreme Learning Machine (KELM)

The extreme learning machine (ELM) was introduced by Huang et al. (2006a, b) for improving the training of the single-layer feedforward neural network (SLFN). The mathematical formulation of the ELM can be expressed as follows: given N training data (x_j, y_j), $j = 1,\ldots, N$. In ELM, the weights and biases from the input to the hidden neurons are assigned arbitrarily, while the weights from the hidden to the output layer are calculated analytically (Huang et al. 2006a, b). The output of the ELM model with L hidden nodes can be calculated as follows:

$$Y_j = \sum_{i=1}^{L} \beta_j \bullet g\left(w_i x_j + b_i\right), j = 1,2,3,\ldots,L \tag{16.1}$$

For which g (.) is the sigmoid activation function, w_i corresponds to the weight vector from the input to the hidden neurons, β_i the weight vector from the hidden neurons to the single output neuron; and b_i is the biases of hidden neurons.

Equation (16.1) can be written as follows:

$$T = H.\beta \tag{16.2}$$

where H is the output matrix of the hidden layer.

$$H = \begin{bmatrix} h\left(x_1\right) \\ \vdots \\ h\left(x_L\right) \end{bmatrix} = \begin{bmatrix} g\left(w_1 \bullet x_1 + b_1\right) & \cdots & g\left(w_l \bullet x_1 + b_l\right) \\ \vdots & \cdots & \vdots \\ g\left(w_1 \bullet x_L + b_1\right) & \cdots & g\left(w_l \bullet x_L + b_l\right) \end{bmatrix}_{L \times l} \tag{16.3}$$

Huang et al. (2012) developed and improved ELM called kernel extreme learning (KELM) by replacing the sigmoidal function by new kernel functions. In this chapter, we selected three kernel functions expressed as follows (Hou et al. 2021; Xie and Wu 2021; Lu et al. 2021):

1. The radial basis function (*RBF*) kernel ELM is:

$$K_{\mathrm{RBF}}\left(x_i, x_j\right) = \left[\exp\left(-\frac{x_i - x_j^{\,2}}{2\sigma^2}\right)\right] \tag{16.4}$$

For which the σ is the width of the radial basis function.

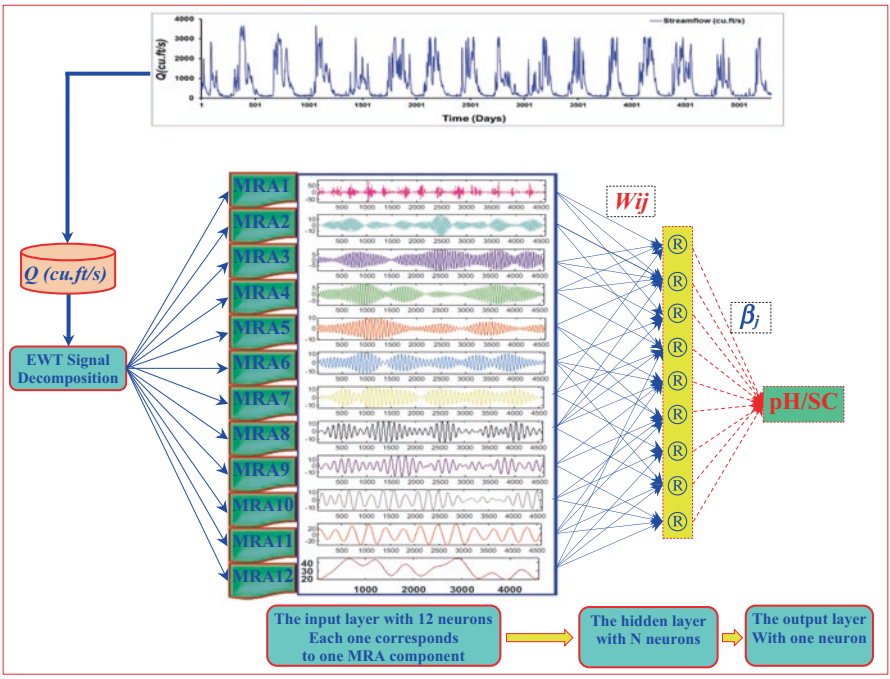

Fig. 16.3 Flowchart of the kernel extreme learning machine (KELM) based on empirical wavelet transform (EWT)

2. The polynomial kernel (*Pol*):

$$K_{\text{Pol}}\left(x_i,x_j\right)=\left[\left(\alpha_P x_i \bullet x_j+\gamma_P\right)^d\right] \tag{16.5}$$

3. The wavelet kernel (W):

$$K_w\left(x_i,x_j\right)=\left[\cos\left(\alpha_w\left(\frac{x_i-x_j}{\gamma}\right)\exp\left(-\frac{x_i-x_j^{\,2}}{2\gamma^2}\right)\right)\right] \tag{16.6}$$

For which the σ is the width of radial basis function, and α and γ are parameters of the kernel functions. Figure 16.3 shows the flowchart of the kernel extreme learning machine (KELM) proposed for better prediction of water-specific conductance and pH.

Results and Discussion

This section presents obtained results on the application of the kernel extreme learning machine (KELM) for predicting river water pH and water-specific conductance. As described above, three kernel functions, i.e., the WKELM, RBELM, and POELM, were compared with the standalone ELM having a sigmoid activation function. The four models were applied according to two scenarios: (*i*) using only river discharge (Q) and (*ii*) using the river discharge decomposed using the EWT into several multiresolution analysis (MRA) components. The evaluation of the models was done using four common performance criteria of forecast accuracy including mean absolute error (MAE), root mean square error (RMSE), correlation coefficient (R), and Nash-Sutcliffe efficiency (NSE).

Prediction of River Water pH

Table 16.2 reports the main simulation results for river water pH. At the USGS 14211720, using the first scenario with only the river discharge as input variables, it is clear that none of the four models was able to correctly predict the river pH, and

Table 16.2 Performances of different models for water pH prediction

	Training				Validation			
Models	*R*	NSE	RMSE (/)	MAE (/)	*R*	NSE	RMSE (/)	MAE (/)
Daily data for USGS ID 14211720 Willamette River at Portland, Oregon, USA								
ELM1	0.539	0.291	0.130	0.105	0.563	0.315	0.126	0.102
ELM2	0.975	0.951	0.034	0.026	0.914	0.818	0.065	0.048
WKELM1	0.537	0.289	0.131	0.105	0.560	0.313	0.127	0.103
WKELM2	0.980	0.955	0.033	0.023	0.950	0.897	0.049	0.035
RBELM1	0.538	0.290	0.131	0.105	0.561	0.313	0.127	0.102
RBELM2	0.985	0.970	0.027	0.018	0.954	0.907	0.047	0.031
POELM1	0.531	0.282	0.131	0.106	0.555	0.307	0.127	0.103
POELM2	0.927	0.859	0.058	0.044	0.880	0.767	0.074	0.058
Daily data for USGS ID 14206241 Willamette River at Portland, Oregon, USA								
ELM1	0.800	0.640	0.117	0.091	0.800	0.640	0.115	0.091
ELM2	0.980	0.961	0.038	0.029	0.964	0.928	0.052	0.039
WKELM1	0.800	0.639	0.117	0.092	0.799	0.639	0.116	0.091
WKELM2	0.990	0.978	0.029	0.021	0.980	0.955	0.041	0.030
RBELM1	0.800	0.639	0.117	0.092	0.799	0.639	0.116	0.091
RBELM2	0.992	0.984	0.024	0.017	0.981	0.961	0.038	0.027
POELM1	0.800	0.639	0.117	0.092	0.800	0.640	0.116	0.091
POELM2	0.965	0.932	0.051	0.039	0.946	0.894	0.063	0.049

very accuracy was obtained. The mean R and NSE values were approximately ≈0.560 and ≈0.312, respectively, while the mean RMSE and MAE values were approximately ≈0.127 and ≈0.103, respectively. It is also clear that the four models worked equally with the same performances. For improving the models' performances, a preprocessing signal decomposition algorithm, i.e., the EWT, was used for decomposing the river discharge into several MRA components, which yielded high improvement in models' performances. According to Table 16.2, using the EWT, the means R, NSE, RMSE, and MAE values were significantly improved reaching the values of ≈0.925, ≈0.847, ≈0.059, and ≈0.043 with improvement rates of approximately ≈39.45%, ≈63.17%, ≈53.65%, and ≈58.04% compared to the values obtained using the first scenario. The best accuracy was obtained using the RBELM2 (R ≈ 0.925, NSE ≈ 0.847), slightly higher than the WKELM2, while the POELM2 was the poorest model exhibiting the lowest R (≈0.880) and NSE (≈0.767) values, respectively. For comparison, the RBELM2 (i.e., with EWT) improve the accuracies of the RBELM1 (i.e., without EWT) by ≈41.19%, ≈65.49%, ≈62.99%, and ≈69.60%, in terms of R, NSE, RMSE, and MAE values, respectively, which clearly highlighted the high contribution of the EWT in improving the performances of the models. Scatterplots of measured against calculated river water pH at the USGS 14211720 for the validation stage are depicted in Fig. 16.4. At the USGS 14206241, using the first scenario, all four models have the same performances without any difference. The obtained means R, NSE, RMSE, and MAE were approximately ≈0.800, ≈0.640, ≈0.115, and ≈0.091, respectively. Using the second scenario, i.e., using the EWT, the performances of the models were significantly improved and the means R, NSE, RMSE, and MAE reached the values of ≈0.968, ≈0.935, ≈0.049, and ≈0.036, respectively, with improvement rates of ≈17.38%, ≈31.56%, ≈58.09%, and ≈60.16%, respectively. The best accuracy was obtained using the RBELM2 slightly better than the WKELM2, and the POELM was the poorest model. Comparison between the models with and without EWT revealed that the RBELM2 improves the performances of the RBELM1 by ≈18.55%, ≈33.50%, ≈67.24%, and ≈70.336%, in terms of R, NSE, RMSE, and MAE, respectively. Scatterplots of measured against calculated river water pH at the USGS 14206241 for the validation stage are depicted in Fig. 16.5.

Prediction of River Water-Specific Conductance

Predicting river water-specific conductance was conducted according to two scenarios similar to what is reported in the previous section for the water pH. At the USGS 14211720 station as shown in Table 16.3, for the first scenario, using only the river discharge, it is clear that none of the models was able to correctly predict the river-specific conductance showing very low performances for which the R and

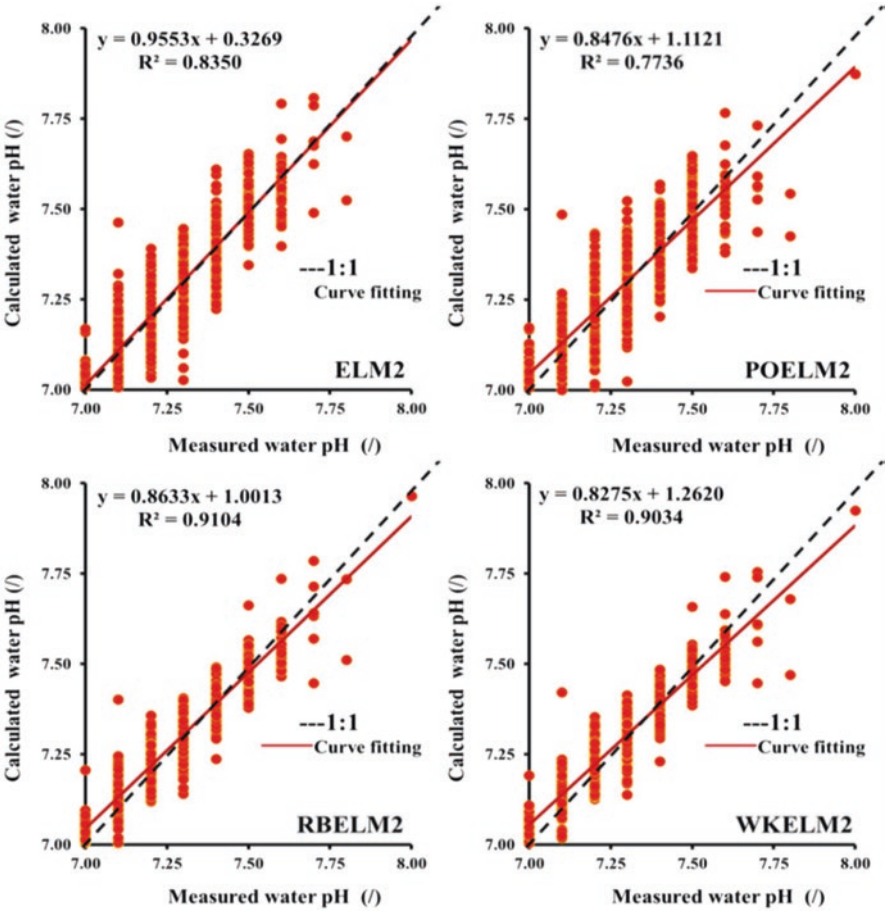

Fig. 16.4 Scatterplots of measured against calculated daily river pH (/) at the USGS 14211720 for the validation stage

NSE values were ranged from ≈0.709 to ≈0.715 (mean ≈ 0.713) and from ≈0.497 to ≈0.504 (mean ≈ 0.502), while the RMSE and MAE were ranged from ≈7.223 to ≈7.270 (mean ≈ 7.24) and from ≈5.685 to ≈5.734 (mean ≈ 5.70), respectively. The use of EWT lead to a high improvement in models' performances for which the R and NSE values ranged from ≈0.925 to ≈0.974 (mean ≈ 0.953) and from ≈0.847 to ≈0.947 (mean ≈ 0.903), while the RMSE and MAE were ranged from ≈2.352 to ≈4.014 (mean ≈ 3.122) and from ≈1.528 to ≈3.054 (mean ≈ 2.211), respectively. The best accuracies were achieved using the RBELM2 slightly lower than the WKELM2, while the POELM2 was the lowest model in terms of numerical

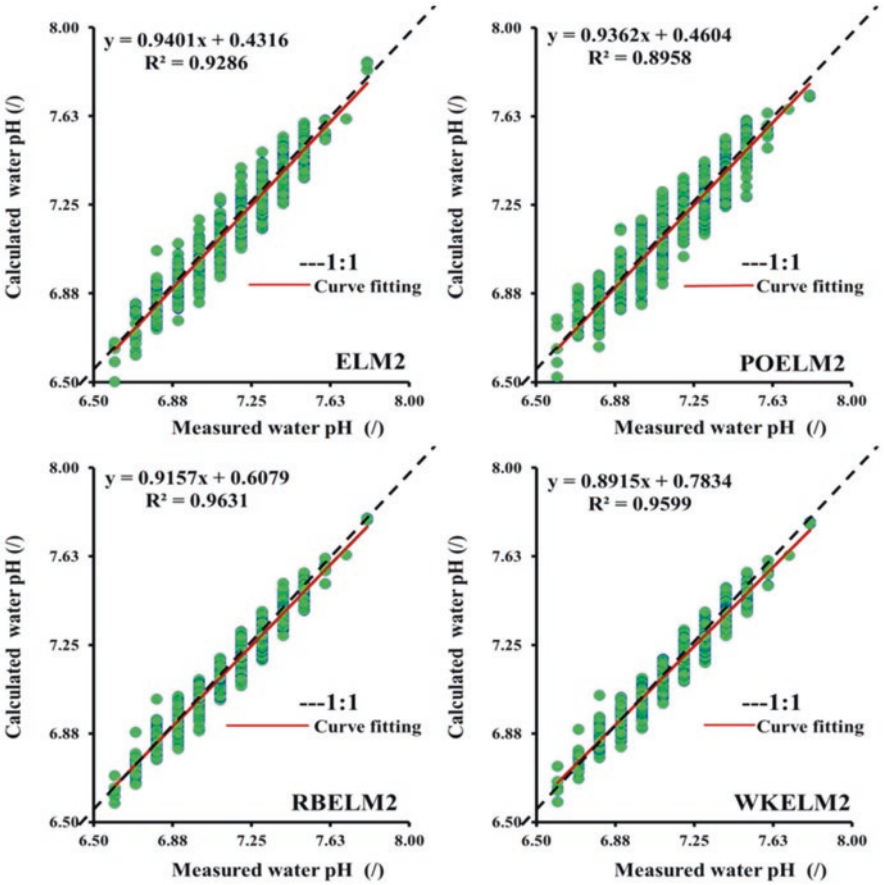

Fig. 16.5 Scatterplots of measured against predicted daily river pH (/) at the USGS 14206241 for the validation stage

performances. For numerical comparison, the RBELM2 model improves the performances of the RBELM1 by increasing the R and NSE values by ≈26.59% and ≈46.78%, respectively, and by decreasing the RMSE and MAE by≈67.43% and ≈73.12%, respectively. At the USGS 14206241 station, as shown in Table 16.3, the same concluding remarks can be drawn, by highlighting the poor predicting accuracies using only the river discharge and the high improvement in models' performances obtained using the EWT. It is clear that the best performances were obtained using the RBELM2 with R, NSE, RMSE, and MAE values of approximately ≈0.963, ≈0.925, ≈3.330, and ≈2.298, respectively, with an improvement rates of approximately ≈31.56%, ≈53.08%, ≈63.51%, and ≈67.79%, respectively.

Table 16.3 Performances of different models for water-specific conductance prediction

	Training				Validation			
Models	*R*	NSE	RMSE (*uS/cm*)	MAE (*uS/cm*)	*R*	NSE	RMSE (*uS/cm*)	MAE (*uS/cm*)
Daily data for USGS ID 14211720 Willamette River at Portland, Oregon, USA								
ELM1	0.743	0.553	6.862	5.430	0.715	0.502	7.239	5.699
ELM2	0.988	0.975	1.611	1.228	0.943	0.881	3.538	2.512
WKELM1	0.742	0.550	6.882	5.457	0.713	0.503	7.226	5.691
WKELM2	0.991	0.979	1.493	1.112	0.970	0.936	2.585	1.751
RBELM1	0.743	0.552	6.869	5.440	0.715	0.504	7.223	5.685
RBELM2	0.995	0.988	1.107	0.809	0.974	0.947	2.352	1.528
POELM1	0.737	0.543	6.934	5.509	0.709	0.497	7.270	5.734
POELM2	0.960	0.921	2.882	2.204	0.925	0.847	4.014	3.054
Daily data for USGS ID 14206241 Willamette River at Portland, Oregon, USA								
ELM1	0.683	0.466	8.933	7.000	0.668	0.446	9.032	7.030
ELM2	0.962	0.925	3.345	2.553	0.919	0.842	4.823	3.583
WKELM1	0.655	0.428	9.244	7.323	0.649	0.421	9.235	7.246
WKELM2	0.980	0.958	2.500	1.849	0.957	0.912	3.605	2.544
RBELM1	0.669	0.447	9.091	7.171	0.659	0.434	9.126	7.135
RBELM2	0.987	0.973	2.019	1.470	0.963	0.925	3.330	2.298
POELM1	0.639	0.408	9.411	7.518	0.632	0.399	9.405	7.447
POELM2	0.929	0.863	4.521	3.495	0.897	0.804	5.374	4.152

Scatterplots of measured against calculated river water-specific conductance at the two stations for the validation stage are depicted in Figs. 16.6 and 16.7.

Summary and Conclusions

Our study examined the use of signal decomposition paradigm for improving the performances of kernel extreme learning machine used for predicting river water pH and specific conductance. We compared three KELM, i.e., wavelet, radial basis, and polynomial kernel ELM and the standalone ELM models. Our modeling strategy was based on the use of river discharge as a single input variable, and our analysis indicates the potential of the EWT for decomposing the discharge into several MRA subcomponents, which has significantly contributed to the improvement of models' performances. While similar studies based on signal decomposition have been done previously, our results are particularly encouraging because the EWT was introduced for the first time, and differences in terms of numerical performances between models with and without the EWT were remarkably significant. In addition to providing a simple and easily applied algorithm for accurately

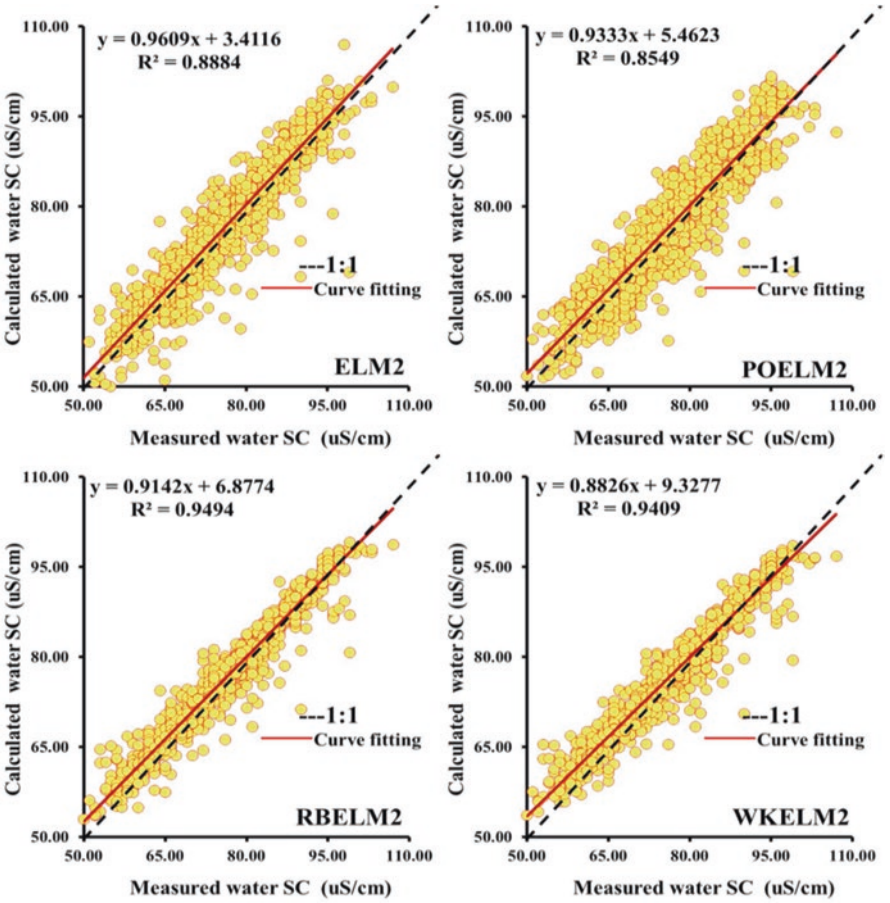

Fig. 16.6 Scatterplots of measured against calculated daily river-specific conductance (*uS/cm*) at the USGS 14211720 for the validation stage

predicting two water quality variables, with continuous investigations and an increase in the availability of in situ measured rivers discharge, our results can be an excellent tool for assessing and monitoring changes in water quality variables, and it should be more suitable to extends the developed approach for predicting other water variables.

Acknowledgments This study could not have been possible without the support of the USGS data survey. The author thanks the staffs of USGS web server for providing the data that makes this research possible.

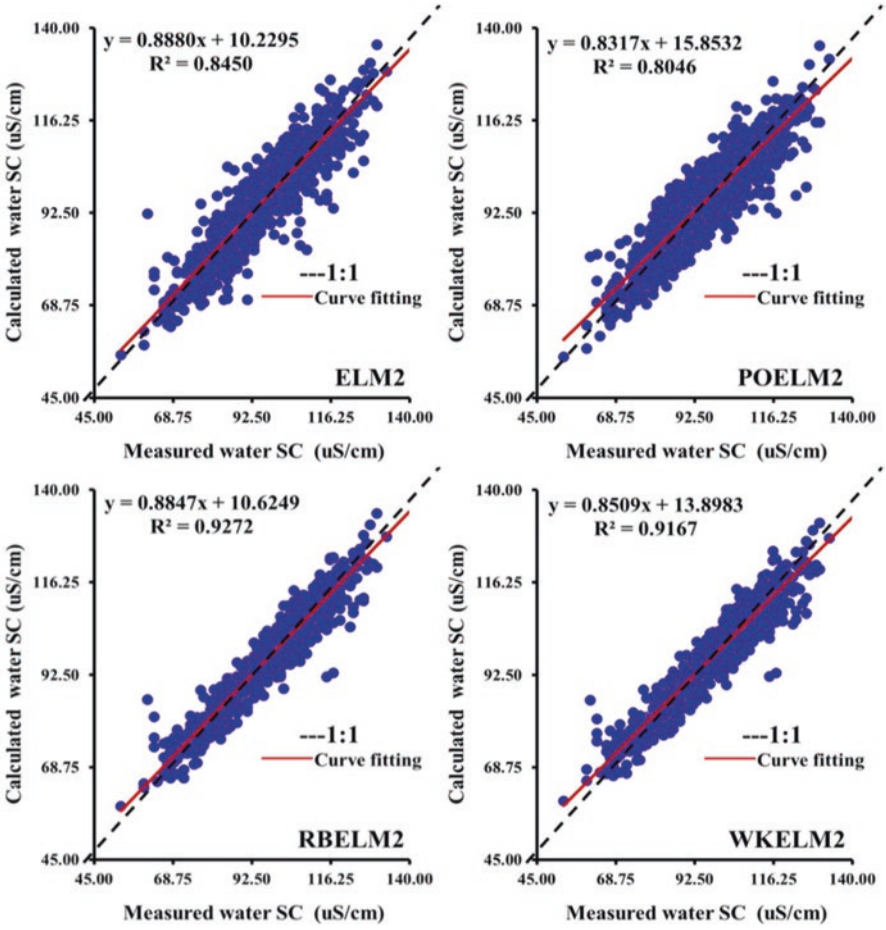

Fig. 16.7 Scatterplots of measured against calculated daily river-specific conductance (*uS/cm*) at the USGS 14206241 for the validation stage

References

Ahmadianfar I, Jamei M, Chu X (2020) A novel hybrid wavelet-locally weighted linear regression (W-LWLR) model for electrical conductivity (EC) prediction in surface water. J Contam Hydrol 232:103641. https://doi.org/10.1016/j.jconhyd.2020.103641

Babbar R, Babbar S (2017) Predicting river water quality index using data mining techniques. Environ Earth Sci 76(14):1–15. https://doi.org/10.1007/s12665-017-6845-9

Chen B, Guo R, Zeng K (2022) A nonlinear active noise control algorithm using the FEWT and channel-reduced recursive Chebyshev filter. Mech Syst Signal Process 166:108432. https://doi.org/10.1016/j.ymssp.2021.108432

Dabrowski JJ, Rahman A, Pagendam DE, George A (2020) Enforcing mean reversion in state space models for prawn pond water quality forecasting. Comput Electron Agric 168:105120. https://doi.org/10.1016/j.compag.2019.105120

Dow CL, Zampella RA (2000) Specific conductance and pH as indicators of watershed disturbance in streams of the New Jersey Pinelands, USA. Environ Manag 26(4):437–445. https://doi.org/10.1007/s002670010101

Eze E, Halse S, Ajmal T (2021) Developing a novel water quality prediction model for a South African aquaculture farm. Water 13(13):1782. https://doi.org/10.3390/w13131782

Fu Y, Hu Z, Zhao Y, Huang M (2021) A long-term water quality prediction method based on the temporal convolutional network in smart mariculture. Water 13(20):2907. https://doi.org/10.3390/w13202907

Gilles J (2013) Empirical wavelet transform. IEEE Trans Signal Process 61(16):3999–4010. https://doi.org/10.1109/TSP.2013.2265222

He J, Valeo C, Chu A, Neumann NF (2011) Prediction of event-based stormwater runoff quantity and quality by ANNs developed using PMI-based input selection. J Hydrol 400(1–2):10–23. https://doi.org/10.1016/j.jhydrol.2011.01.024

Hou Z, Lao W, Wang Y, Lu W (2021) Hybrid homotopy-PSO global searching approach with multi-kernel extreme learning machine for efficient source identification of DNAPL-polluted aquifer. Comput Geosci:104837. https://doi.org/10.1016/j.cageo.2021.104837

Huang GB, Chen L, Siew CK (2006a) Universal approximation using incremental constructive feedforward networks with random hidden nodes. IEEE Trans Neural Netw 17(4):879–892. https://doi.org/10.1109/TNN.2006.875977

Huang GB, Zhu QY, Siew CK (2006b) Extreme learning machine: theory and applications. Neurocomputing 70(1–3):489–501. https://doi.org/10.1016/j.neucom.2005.12.126

Huang GB, Zhou H, Ding X, Zhang R (2012) Extreme learning machine for regression and multiclass classification. IEEE Trans Syst Man Cybern B Cybern 42(2):513–529. https://doi.org/10.1109/TSMCB.2011.2168604

Kouadri S, Pande CB, Panneerselvam B et al (2022) Prediction of irrigation groundwater quality parameters using ANN, LSTM, and MLR models. Environ Sci Pollut Res 29:21067–21091. https://doi.org/10.1007/s11356-021-17084-3

Lu H, Ma X (2020) Hybrid decision tree-based machine learning models for short-term water quality prediction. Chemosphere 249:126169. https://doi.org/10.1016/j.chemosphere.2020.126169

Lu S, Gao W, Hong C, Sun Y (2021) A newly-designed fault diagnostic method for transformers via improved empirical wavelet transform and kernel extreme learning machine. Adv Eng Inform 49:101320. https://doi.org/10.1016/j.aei.2021.101320

Moghadam SV, Sharafati A, Feizi H, Marjaie SMS, Asadollah SBHS, Motta D (2021) An efficient strategy for predicting river dissolved oxygen concentration: application of deep recurrent neural network model. Environ Monit Assess 193(12):1–18. https://doi.org/10.1007/s10661-021-09586-x

Peng L, Wang L, Xia D, Gao Q (2022) Effective energy consumption forecasting using empirical wavelet transform and long short-term memory. Energy 238:121756. https://doi.org/10.1016/j.energy.2021.121756

Piotrowski AP, Osuch M, Napiorkowski JJ (2021) Influence of the choice of stream temperature model on the projections of water temperature in rivers. J Hydrol 601:126629. https://doi.org/10.1016/j.jhydrol.2021.126629

Rizo-Decelis LD, Pardo-Igúzquiza E, Andreo B (2017) Spatial prediction of water quality variables along a main river channel, in presence of pollution hotspots. Sci Total Environ 605:276–290. https://doi.org/10.1016/j.scitotenv.2017.06.145

Rout SK, Sahani M, Dora C, Biswal PK, Biswal B (2022) An efficient epileptic seizure classification system using empirical wavelet transform and multi-fuse reduced deep convolutional neural network with digital implementation. Biomed Signal Process Control 72:103281. https://doi.org/10.1016/j.bspc.2021.103281

Sahoo GB, Ray C, De Carlo EH (2006) Use of neural network to predict flash flood and attendant water qualities of a mountainous stream on Oahu, Hawaii. J Hydrol 327(3–4):525–538. https://doi.org/10.1016/j.jhydrol.2005.11.059

Xie Z, Wu Z (2021) Maximum power point tracking algorithm of PV system based on irradiance estimation and multi-kernel extreme learning machine. Sustain Energy Technol Assess 44:101090. https://doi.org/10.1016/j.seta.2021.101090

Yang H, Liu S (2021) A prediction model of aquaculture water quality based on multiscale decomposition. Math Biosci Eng 18(6):7561–7579. https://doi.org/10.3934/mbe.2021374

Yang F, Moayedi H, Mosavi A (2021) Predicting the degree of dissolved oxygen using three types of multi-layer perceptron-based artificial neural networks. Sustainability 13(17):9898. https://doi.org/10.3390/su13179898

Yang R, Liu H, Nikitas N, Duan Z, Li Y, Li Y (2022) Short-term wind speed forecasting using deep reinforcement learning with improved multiple error correction approach. Energy 239:122128. https://doi.org/10.1016/j.energy.2021.122128

Yaseen ZM, Ehteram M, Sharafati A, Shahid S, Al-Ansari N, El-Shafie A (2018) The integration of nature-inspired algorithms with least square support vector regression models: application to modeling river dissolved oxygen concentration. Water 10(9):1124. https://doi.org/10.3390/w10091124

Yousefi A, Toffolon M (2022) Critical factors for the use of machine learning to predict lake surface water temperature. J Hydrol:127418. https://doi.org/10.1016/j.jhydrol.2021.127418

Chapter 17
Assessment of Climate Change Impact on Land Use-Land Cover Using Geospatial Technology

Syeda Mishal Zahra, Muhammad Adnan Shahid, Rabeea Noor, M. Aali Misaal, Fahd Rasul, Sikandar Ali, M. Imran, M. Tasawar, and Sidra Azam

Abstract Monitoring land cover variations is imperative for global resource management. Climatic variation influences land use–land cover (LULC) distribution steadily. Geospatial techniques are among the most comprehensive and efficient approaches for developing LULC categorization maps, which greatly enhance the overall utilization of agricultural, industrial, and urban areas of any region. The primary causes of LU change are urbanization and variation in temperature and precipitation leading to climate change. People have the innate desire to be close to nature, which drives them to relocate from densely populated places toward less heavily populated regions. Therefore, as a result, agricultural lands are being replaced by new communities created by deforestation and disrupting overall ecology. In the perspective of urbanization and variation in climatic parameters, i.e.,

S. M. Zahra (✉)
Department of Irrigation and Drainage, Faculty of Agricultural Engineering and Technology, University of Agriculture, Faisalabad, Pakistan

Agricultural Remote Sensing Lab (ARSL), University of Agriculture, Faisalabad, Pakistan

Department of Agricultural Engineering, Bahauddin Zakariya University, Multan, Pakistan

M. A. Shahid
Department of Irrigation and Drainage, Faculty of Agricultural Engineering and Technology, University of Agriculture, Faisalabad, Pakistan

Agricultural Remote Sensing Lab (ARSL), University of Agriculture, Faisalabad, Pakistan

R. Noor
Department of Agricultural Engineering, Bahauddin Zakariya University, Multan, Pakistan

M. A. Misaal
Department of Farm Machinery & Power, Faculty of Agricultural Engineering and Technology, University of Agriculture, Faisalabad, Pakistan

Department of Farm Machinery & Precision Engineering, Faculty of Agricultural Engineering and Technology, PMAS-Arid Agriculture University, Rawalpindi, Pakistan

C. B. Pande et al. (eds.), *Climate Change Impacts on Natural Resources, Ecosystems and Agricultural Systems*, Springer Climate,
https://doi.org/10.1007/978-3-031-19059-9_17

precipitation and temperature, the present and previous LULC have been examined in this study by using geospatial techniques. Geographic information systems enable the examination of the changing patterns of LULC through monitoring by satellites. The key categorization indices in this study are the normalized difference vegetation index (NDVI) ranging between −0.28 and 0.74. As per analysis, the forthcoming trend of climate change and its impact on LULC has been detected for the better management of land resources. The outcomes of this research will aid in the formulation of mitigation as a result of climate change.

Keywords Climate change · LULC · Precipitation · Temperature · Geographic information systems

Introduction

Climate change is the major distribution of the weather pattern from decades to millions of years. It greatly influences the agriculture sector, and it leads to environmental changes (Hussain 2020; Karuppannan 2021). Due to environmental changes, shifting of the season and cropping patterns occur. Pakistan has four distinct seasons throughout the year, and in recent decades, global warming has been observed as a man-made disaster in the environment (Hussain 2020; Karuppannan 2021). Global warming is occurring due to many human activities to make their lives luxurious i.e., factories, traffic, emission of GHGs, destruction of the ozone layer, burning of fossil fuels, deforestation, solar radiation, and changes in land use–land cover (LULC) (Pande et al. 2021; Hussain 2020; Karuppannan 2021). These all factors, directly or indirectly, are affecting the physical environment and becoming the cause of the sea-level rise, heat waves, increase in the average temperature, shifting of seasons, undistributed rainfall, abnormal behavior of winds, biosphere damage, vegetation, shifting of agroecological zones, social tensions, drinking water shortage, human health effect, and urbanization (Hashim et al. 2020; Kawo et al. 2021). As per previous research (Majeed et al. 2021), it has been observed that almost annually, there is a 1 °C rise in temperature occurring, which is the main cause of the melting of glacier and generation of GLOF events (Jabbar et al. 2020). Agriculture is the foundation of Pakistan, contributing to almost 19.5% of GDP. The

F. Rasul
Department of Agriculture, University of Agriculture, Faisalabad, Pakistan

S. Ali · S. Azam
Department of Irrigation and Drainage, Faculty of Agricultural Engineering and Technology, University of Agriculture, Faisalabad, Pakistan

M. Imran · M. Tasawar
Department of Irrigation and Drainage, Faculty of Agricultural Engineering and Technology, University of Agriculture, Faisalabad, Pakistan

Department of Agricultural Engineering, Bahauddin Zakariya University, Multan, Pakistan

average production (tons) per hectare of cash crops, mainly wheat, cotton, rice, maize, and sugarcane, is 70%, 53%, 61%, 82%, and 60%, accordingly, lower than the worldwide average production per hectare (Aslam 2016). Climate change is a major cause of that decreased yield and leads to a variant economy.

The socioeconomic status of the inhabitants who live on the land is greatly influenced by LULC (Qureshi and Mahessar 2016). Extreme events such as tsunamis, earthquakes, and floods, among others, dramatically alter the structure of LULC and influence inhabitants over all aspects of life (Qureshi and Mahessar 2016). Because of the population boom, which disrupts the natural ecosystem and LULC types (Kefi et al. 2021), assessing LULC and monitoring its variations seem to have become a significant concern; however, these LULC variations are crucial; thus, land use planning is required for the development of any territory (Dhinwa et al. 1992). Analyzing the altering trends of LULC and its pattern is critical owing to massive human activities (Pasha et al. 2016), which are at a drastic level and could have a significant impact on the ecological environment, availability of food, and so these exponentially growing factors are major key drivers that convert LC from one form to another and endanger natural environment (Wakdok and Bleischwitz 2021). LULC mapping is the way by which its variation can be visualized and evaluated using remote sensing technologies.

Map-based LULC has indeed been performed effectively using satellite images at a variety of geographical, spectroscopical, and temporal resolutions (Hussain 2020); however, in arid and semiarid environments, the use of multi-temporal satellite data has just been decreased to establish and evaluate LULC variations (Maviza and Ahmed 2020). Changes in LULC could also be investigated though they have a long-term impact on the regional ecosystem, especially in major criteria with micro-global warming (Majeed et al. 2021; Srivastava and Chinnasamy 2021). Normalized difference vegetation index (NDVI) does have a high potential to convey seasonal fluctuation in vegetative covered activities and vegetation's adaptation to climatic variation (Pande et al. 2021; Hussain 2020). The NDVI scores are found to be related to the bioactivities of plants, and changes in NDVI characterize the bioactivities in plants (Qureshi and Mahessar 2016). The regular fluctuations in land surface temperature (LST) could also be easily characterized using the NDVI value, which represents the status of natural vegetation. The NDVI additionally aids in the analysis of various vegetation's annual and seasonal patterns at international and provincial levels (Ullah et al. 2019). The reaction of vegetation to climatic fluctuations, biological activities of different seasons, and the condition of native vegetation, all can be tracked using NDVI (Abdul Athick et al. 2019). NDVI can be used to track the growth-development processes of green plant cover (Kidane et al. 2019). The NDVI values are obtained by peak reflections near-infrared area and inside red area (Pande et al. 2021; Naz et al. 2017). Plant cover productivity is related to evaporation, transpiration, and precipitation, and NDVI seems to be a useful technique for assessing LULC efficiency at the global level (Rizvi et al. 2021). NDVI and LST are directly influenced by climatic variabilities.

The NDVI scale spans from −1 to 1, with the lowest value indicating total surface resources and the highest value indicating green vegetation (Ahmad 2012).

Negative NDVI value indicates places having almost no vegetation, and positive value shows pixel with moderate to high vegetation. NDVI values are symbolized as soil surface while they are close to "0" (Lambin et al. 2003). The NDVI is widely used in remote sensing (RS) studies because that gives appropriate proof for integrating and examining plants (Harris et al. 2014). Geographic information system (GIS) and RS are vital elements for researching urban proportions and densities with LULC mapping, as well as the environmental implications of urbanization planning across time (Pande et al. 2018; Näschen et al. 2019). RS enables inexpensive on-time access to LULC and vegetative coverage statistics at specified intervals (Tariq et al. 2020). GIS effectively organizes and interprets geographical data, and that is an essential and core requirement of this field of research. RS is becoming crucial for evaluating vegetation changes because it delivers up-to-date remote sensing data on vegetation. Moderate Resolution Imaging Spectroradiometer (MODIS) is just one of many RS sensors that can be used to analyze natural vegetation deterioration as it gives worldwide information (MODIS Global Land Cover products) for LULCC mapping and also NDVI data (MODIS NDVI) for vegetation variability trends evaluation (Jacquin et al. 2010). Furthermore, MODIS vegetative indicators had enhanced resolution (250 m × 250 m) and were determined to be significantly associated with in situ observed vegetative indicators than NOAA/AVHRR NDVI or SPOT VGT (Fensholt et al. 2006). Different websites are available to get access to the MODIS NDVI data.

Numerous similar initiatives to analyze and monitor LULC variations and deterioration using RS datasets have been investigated by many researchers from nations worldwide (Choudhury et al. 2019), including Malaysia (Hussain 2020), China (Fan et al. 2007), Ethiopia (SAPURO 2016), Turkey (Nowacki and Abrams 2015), Nepal (Wang et al. 2020), Zimbabwe (Maviza and Ahmed 2020), NW-Ethiopia (Tewabe and Fentahun 2020), S-Africa (Harris et al. 2014), Iran (Use et al. 2020), N-Ethiopia (Ayele et al. 2018), W-Africa (Zoungrana et al. 2018), Brazil (Lu et al. 2013), Bangladesh (Rahman et al. 2017), Iraq (Rahman et al. 2021), NW-Ethiopia (Tewabe and Fentahun 2020), S-Africa (Harris et al. 2014), Iran (Rahman et al. 2021), and N-Ethiopia (Ayele et al. 2018). Multiple types of research in Multan (Ibrahim 2017), Faisalabad (Choudhury et al. 2019), Lodhran (Akar and Güngör 2015), Vehari (Farooq and Qurat-ul-ain 2012), Khyber Pakhtunkhwa (Hussain 2020), Sindh (Hussain 2020), S-Punjab (Hussain 2020; Shahid et al. 2021), Azad Jammu and Kashmir (Hussain 2020), and Islamabad (Hassan et al. 2016) have used RS data to evaluate and control changes that have occurred in LULC. The LULC is rapidly evolving as agricultural land becomes part of urban areas as a result of the exponential increase in population. Climate variability is exacerbated by urbanization and industry. This is an alarming situation that is taking human beings to a very destructive end. There is a need to understand the climatic parameters, bring changes to improve the physical environment, and stop further destruction of natural parameters. In this study, LULC has been observed using RS and GIS techniques to fulfill the objectives of analyzing the spatiotemporal changes in LULC and developing correlations between different climatic parameters and LULC changes.

Materials and Methods

Study Area

Sindh is a province of Pakistan with an area of 140,914 km^2 and is located between 23°53′23″ N to 28°29′44″ N latitude and 67°8′39″ E to 70°42′16″ E longitude, as shown in Fig. 17.1. It is situated in the southeast of Pakistan and elevation ranges from average and maximum is 857 m and 1714 m, respectively. It is a tropical region with maximum temperatures of 46 °C and lowest temperatures of 2 °C, making it hot in the summer and mildly cold in the winter. Sindh is the second-largest province in terms of economics, with a GDP share ranging from 30% to 32.7%. Sindh is sandwiched between the monsoon seasons: SW monsoon from the Indian Ocean and the NE monsoon, which is reflected toward it by the Himalayan Mountain range, hence escaping their impact. The region's lack of precipitation is accounted for by the Indus River's flooding twice a year, produced by the melting of Himalayan glaciers in the spring and early summer and precipitation during the monsoons.

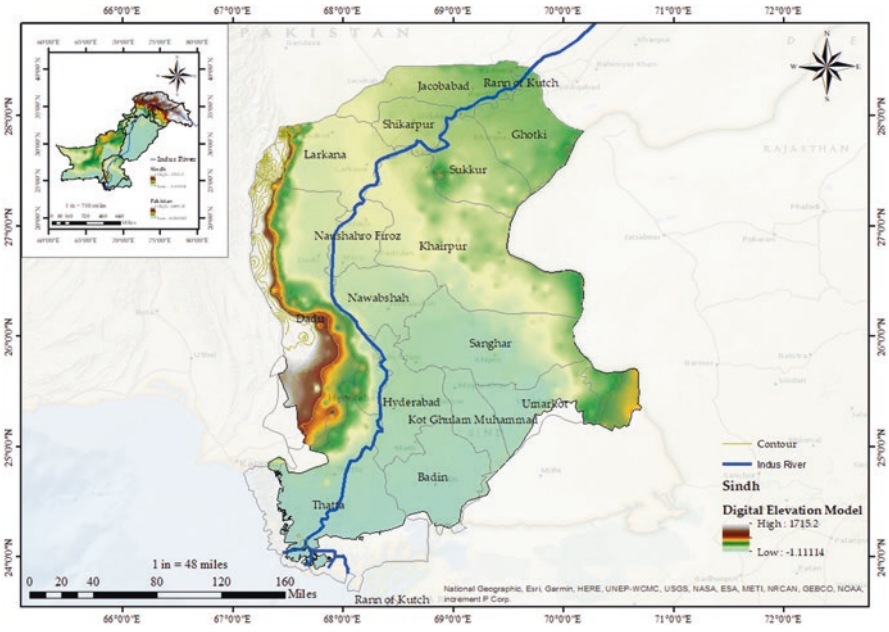

Fig. 17.1 Study area – digital elevation model (DEM) of Sindh, Pakistan

Satellite Data

The AppEEARS was used to download Tera MODIS vegetation indices (NDVI and EVI) data from 2000 to 2021. MODIS operates on a 16-day cycle with swath measurements of 2330 km (crosstracking) by 10 km (along-track at nadir). MOD13Q.006 of MODIS, with a spatial resolution of 250 m, was downloaded in GeoTIFF format. Data were projected at the geographic datum of WGS84, EPSG: 4326, and PROJ: + proj = longlat + datum = WGS84 + no_defs. The selected sublayers from Tera MODIS vegetation indices (NDVI and EVI) MOD13Q.006 were 250 m 16 days EVI, 250 m 16 days MIR reflectance, 250 m 16 days NDVI, 250 m 16 days NIR reflectance, 250 m 16 days VI quality, 250 m 16 days blue reflectance, 250 m 16 days composite day of the year, 250 m 16 days pixel reliability, 250 m 16 days red reflectance, 250 m 16 days relative azimuth angle, 250 m 16 days sun zenith angle, and 250 m 16 days view zenith angle.

Image Processing

Terra MODIS has 36 bands, although Bands 1 and 2 are just for surface reflectance. Band-1 represented the RED spectrum, whereas Band-2 represented the near-infrared (NIR) spectrum. The NDVI value was calculated using these two bands. The bands of the RED and NIR spectrum were processed in ArcGIS 10.8 and gave NDVI value of the Sindh. AppEEARS data was downloaded directly in GeoTIFF format of the designated study area (Fig. 17.2), and various supporting files in XML, txt, MD, JSON, and CSV were also provided to see the LULC change over a selected period.

Estimation of NDVI

NDVI was calculated for the estimation of vegetation cover by using MODIS Band-1 and Band-2 data. The NDVI was calculated using MODIS images and has specific values ranging from −1 to 1. The NDVI was determined by using the following formula:

$$\mathrm{NDVI} = \frac{\mathrm{NIR} - \mathrm{RED}}{\mathrm{NIR} + \mathrm{RED}} \tag{17.1}$$

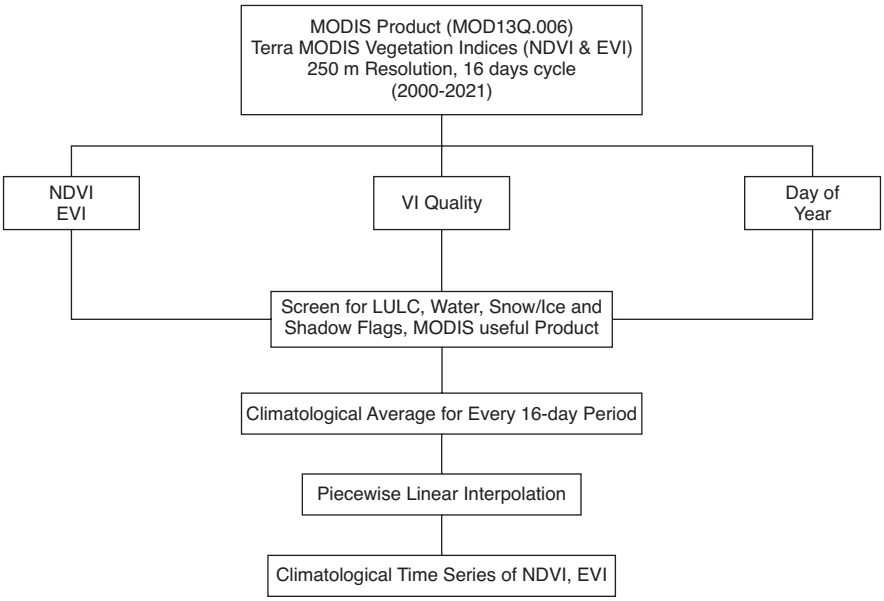

Fig. 17.2 Flow chart of MODIS processing data

Table 17.1 NDVI classes range in ArcGIS 10.8

Classes of land	NDVI ranges
Water bodies	−0.28–0.015
Built-up area	0.015–0.14
Barren land	0.14–0.18
Shrubs and grassland	0.18–0.27
Spare vegetation	0.27–0.36
Dense vegetation	0.36–0.74

or

$$\mathrm{NDVI} = \frac{\mathrm{Band\,2} - \mathrm{Band\,1}}{\mathrm{Band\,2} + \mathrm{Band\,1}} \tag{17.2}$$

where NIR is near the infrared band (Band-2) and RED is a red band (Band-1) NDVI value.

The area of Sindh was classified into six classes to see the variation in LULC. The classes were water bodies, built-up area, barren land, shrubs and grassland, sparse vegetation, and dense vegetation with the ranges as mentioned above in Table 17.1.

Climate

Temperature, humidity, evapotranspiration, and precipitation were the main climatic elements that had a direct impact on LULC. These meteorological parameters'data were obtained from the Sindh province statistics agency. Monthly data of minimum, maximum, and mean temperature in °C, relative humidity (saturated and actual humidity) in %, and rainfall in mm have been collected. The meteorological data for these factors were collected from 2000 to 2021 and compared using LULC.

Statistical Analysis of LULC

Sixteen-day data of total pixel count, minimum, maximum, range, mean, standard deviation (SD), variance, upper quartile (UQ), interquartile range (IQR), and lower quartile (LQ) of NDVI has been observed. Maximum and minimum NDVI were the maximum and minimum values of NDVI observed in the circle of 16 days, respectively. The maximum and minimum values set the range of the NDVI in a given duration.

Mean of NDVI

The mean was a variable with a quantity that was between the extreme elements of the collected data. There were several types of means and the process of determining a mean. The following was the formula for calculation of the mean of NDVI:

$$\text{Mean of NDVI} = \frac{\sum f(i) * i}{\sum f(i)} \tag{17.3}$$

where i = spectral value and $\sum f(i)$ = number of pixels.

The Standard Deviation of NVDI

The SD was a measure of the dispersion of how far apart the dataset was from the mean. A low SD indicated that data was grouped all-around mean, whereas a large SD showed that data was more dispersed. The formula for SD of NDVI is given below:

$$\text{SD of NDVI} = \frac{\sqrt{\left(\sum f(i) * (\mu - i)^2\right)}}{\sum f(i)} \tag{17.4}$$

where μ = mean of NDVI.

Variance of NDVI

The variance was a measurement of the dispersion between numbers in collected data. Further particularly, variance assessed how far every value in the set deviated from the mean and hence from every other number in the dataset. The variance of NDVI was estimated by the following formula:

$$\text{Variance of NDVI} = \frac{\Sigma\left(f\left(i\right)-\mu\right)2}{\Sigma f\left(i\right)} \tag{17.5}$$

Quartile of NDVI

The UQ, also known as the third quartile (Q_3), was the value at which 75% of data points were located when sorted in ascending order. The median or LQ was regarded as the second quartile (Q_2). The difference between the upper and lower quartiles was the IQR. The formulas for the determination of UQ, LQ, median, and IQR in NDVI are given below:

$$\text{UQ of NDVI} = \frac{3}{4}\left(f\left(i\right)+1\right)^{\text{th}}\ \text{term} \tag{17.6}$$

$$\text{LQ of NDVI} = \frac{1}{4}\left(f\left(i\right)+1\right)^{\text{th}}\ \text{term} \tag{17.7}$$

If $f(i)$ was odd:

$$\text{Median of NDVI} = \left(\frac{f\left(i\right)+1}{2}\right)^{\text{th}}\ \text{term} \tag{17.8}$$

If $f(i)$ was even:

$$\text{Median od NDVI} = \frac{\left(\frac{f\left(i\right)}{2}\right)^{\text{th}}\ \text{term} + \left(\frac{f\left(i\right)}{2}+1\right)^{\text{th}}\ \text{term}}{2} \tag{17.9}$$

$$\text{Inter Quartile Range}\left(\text{IQR}\right) = \text{UQ} - \text{LQ} \tag{17.10}$$

Results and Discussion

Change detection of LULC

LULC categories with the maximum and minimum changes in LULC were analyzed at all stages to find the optimum comparative change in Sindh Province over the previous 21 years. The classification analysis revealed that the research province was covered with various land surface features (water bodies, built-up areas, barren land, shrubs and grassland, sparse vegetation, and dense vegetation) and the LULC classification configuration was carried out using satellite data with Sindh GIS information, as shown in Fig. 17.3. Classification of LULC is done based on NDVI values as explained in Table 17.1. Food demand is a major concern as Pakistan's population is growing at an exponential rate. Agriculture is expanding to meet food demand, and cultivated land is rising in a linear pattern. The cultivated area was less in 2000, and Fig. 17.3 shows that it is rising with time. Farmers are using farm mechanization technologies to increase crop yield and maximize crop production. Sindh's built-up area is dwindling as a result of people moving from rural to urban

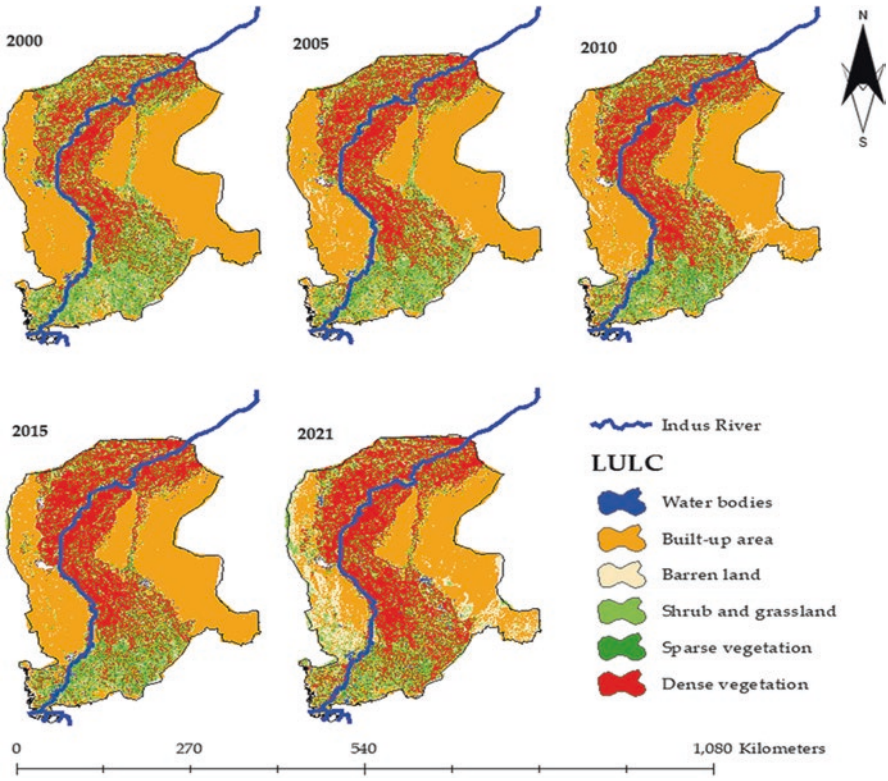

Fig. 17.3 Land use–land cover (LULC) changes occurring from 2000 to 2021

areas at a rate of 3.1%. The motives for rural-to-urban migration are to obtain better facilities, educate their children, improve their lifestyles, and find a source of revenue. Sindh's barren land is growing as a result of migration. Because water is abundantly available along the Indus River, vegetation and agricultural lands are expanding to a greater extent. Looking at the water bodies aspect, most flood events occur downstream of the Indus River when extreme glacier events occur. People are migrating from flood-affected places such as Dadu, Jamshoro, Qambar Shahadkot, and Malir, which are quickly becoming part of barren lands. Sindh is divided into four zones based on agricultural climate and soil conditions: upper Sindh (Shikarpur, Larkana, and Jacobabad), middle Sindh (Dadu, Nawabshah, and Nausherferoz), lower Sindh (Hyderabad, Mirpurkhas, and Sangar), and desert and kacho area (Dadu Larkana and Hyderabad), which is demonstrated in Fig. 17.1. Rice is grown as a major crop in Upper Sindh, with matter, mustard, rape, and sunflower as minor crops. Cotton is the most important crop in middle Sindh, whereas mustard, rape, and sunflower are minor crops. Cotton and wheat are the major crops in lower Sindh, with soybean, rape, sunflower, groundnut, and mustard as minor crops. Sindh's desert area is predominantly rainfed, and crops grown there include sesamum, sorghum, guar, caster, and millet. According to census 2017–2018 (Finance Division 2019), it has been observed that percentage change in production of Sindh was about 3.62% in 2011–12, and it was 3.81% in 2017–2018, so dense vegetation (cultivated area) has increased in the top and middle parts of Sindh, and shrubs, grassland, and spare vegetation have been replaced by dense vegetation.

Statistical Trends of NDVI Data

From 2000 to 2021, the minimum value range of NDVI is from −0.2 to −0.19, maximum value range of NDVI is from 0.5 to 0.9, mean NDVI ranges between 0.08 and 0.21, standard deviation range of NDVI is from 0.04 to 0.16, the variance of NDVI ranges between 0.0001 and 0.02, upper quartile range of NDVI is from 0.09 to 0.3, upper 1.5 IQR has the range of 0.15–0.6, lower 1.5 IQR ranges between −0.19 and 0.01, and lower quartile has the range of 0.05–0.11. The trends of MODIS NDVI values are pixel count NDVI, minimum NDVI, maximum NDVI, mean of NDVI, SD of NDVI, the variance of NDVI, LQ, and UQ of NDVI as shown in Figs. 17.4, 17.5, 17.6, 17.7, 17.8, 17.9, 17.10, and 17.11, respectively. The statistical patterns of NDVI values are revealing themselves in an abrupt manner. Table 17.2 shows the percent variation of various statistical parameters between 2000 and 2021. Minimum and maximum NDVI values are deviated upto 0.13% and 11.2%. The mean NDVI has a deviation of 25.3%, indicating that there is increase in the green vegetation in Sindh from 2000 to 2021. Farmers are practicing farm mechanization technology to increase crop production, due to which shrubs, grassland, and spare vegetation land are becoming part of dense vegetation. Sindh government is also aiding farmers in promoting new crop technology, pesticides, fertilizers, varieties, weedicide, farm machinery, and tools; providing farmers with information on

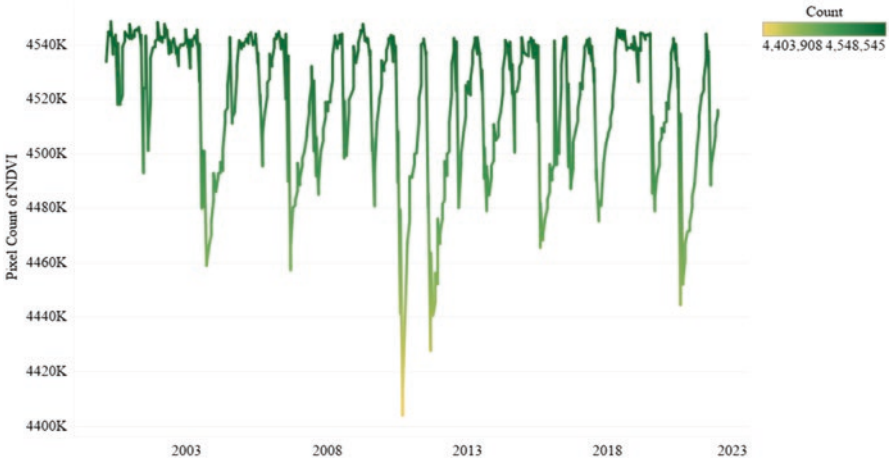

Fig. 17.4 Pixel count of NDVI from 2000 to 2021

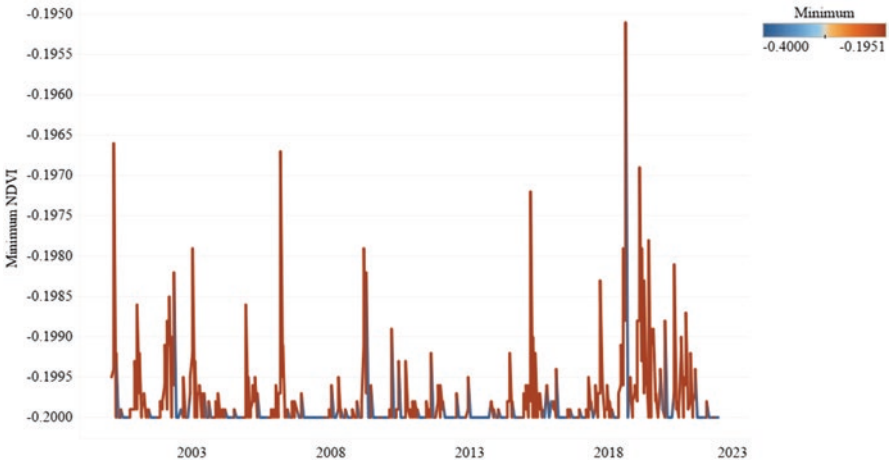

Fig. 17.5 Trend of minimum value of NDVI from 2000 to 2021

urgent issues such as insect/pest outbreaks, climate change, weather forecast, the evolution of new high-yielding and insect-, pest-, disease-resistant resistant variety of major and minor crops and providing farmers with crop subsidies. The reason behind this increase is to meet food security, fulfill the need of human beings, and get maximum profit.

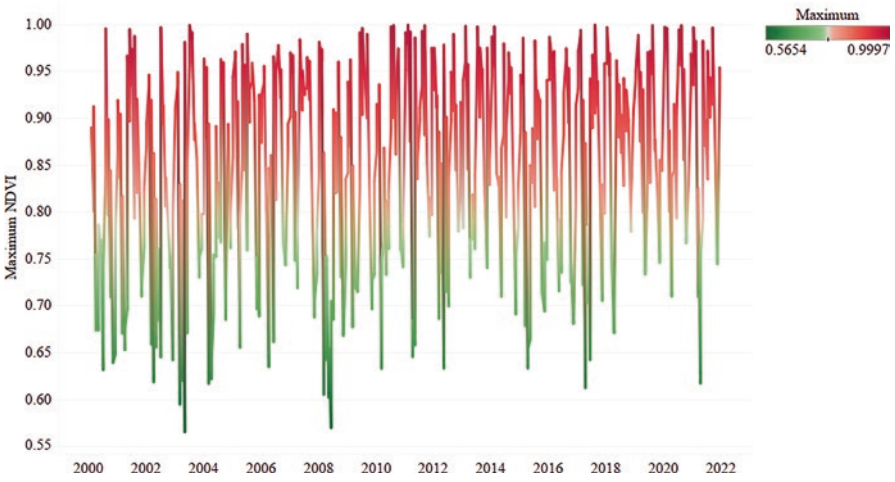

Fig. 17.6 Trend of maximum value of NDVI from 2000 to 2021

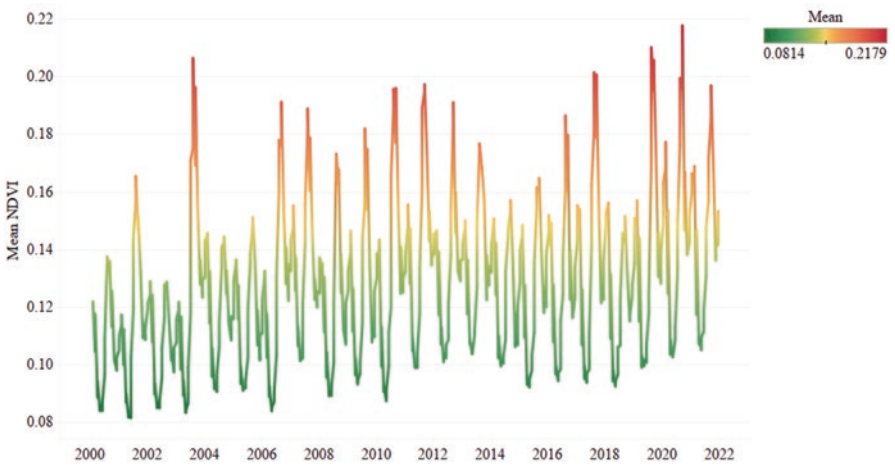

Fig. 17.7 Trend of mean value of NDVI from 2000 to 2021

Climate Factors of the Research Area

Within Pakistan, Sindh has been the hardest hit by extreme weather events, which are quintessential indications of climate change. Temperature, rainfall, and relative humidity are all climatic elements that have a direct impact on land use–land cover. The average temperature range over the last 20 years has been 14.2–28.1 °C, with a mean temperature of 21.1 °C. Figure 17.12 illustrates the trends of various temperature ranges and the five-year average smooth curve. Maximum mean temperature is recorded in 2018. Figure 17.13 depicts the relative humidity range of 52–66.7%,

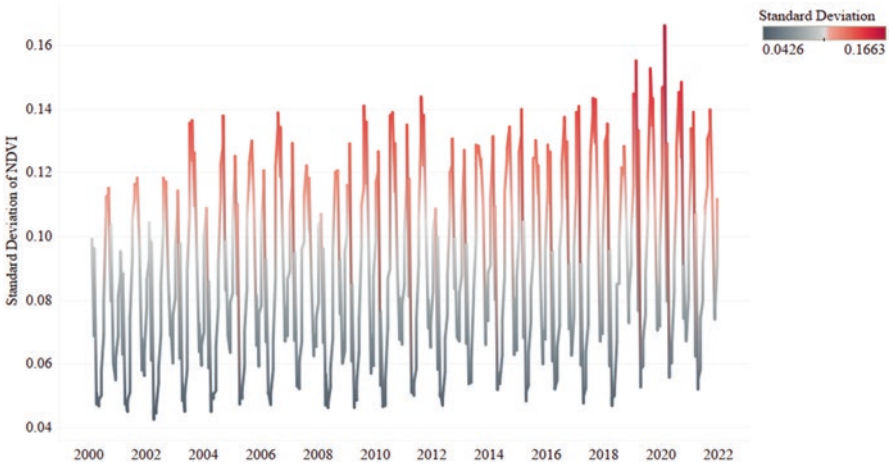

Fig. 17.8 Trend of SD of NDVI from 2000 to 2021

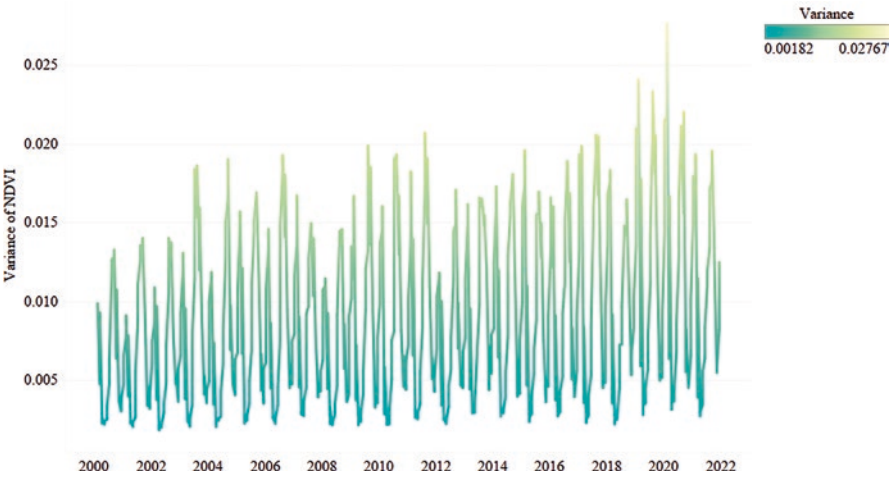

Fig. 17.9 Trend of variance of NDVI from 2000 to 2021

with a mean relative humidity of 59.3%. Rainfall ranged from 190.75 to 396.83 mm, with an average of 301 mm during the last 21 years. Figure 17.14 demonstrates the year-average and five-year average smooth curve of rainfall. Temperature and rainfall exhibit a relative increasing tendency; however, relative humidity shows the reverse pattern, with a linear declining trend.

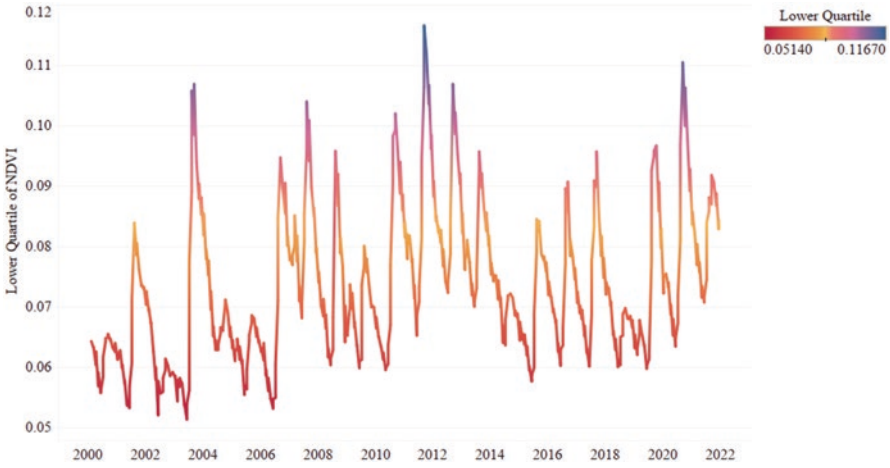

Fig. 17.10 Trend of LQ of NDVI from 2000 to 2021

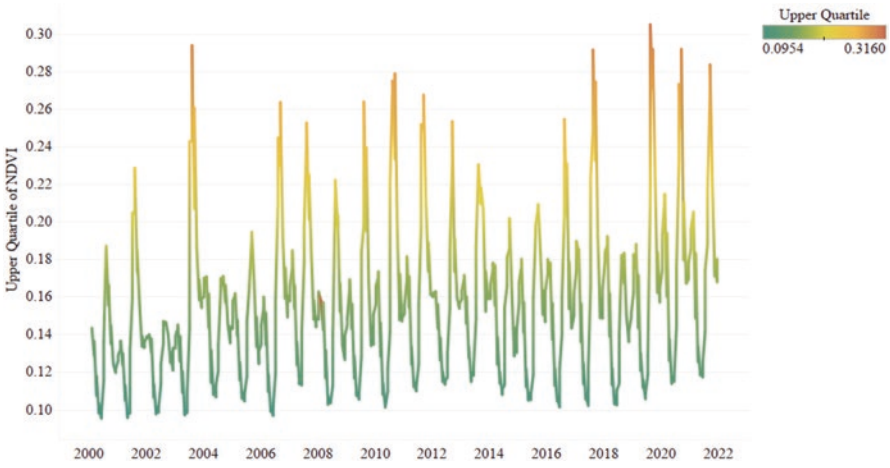

Fig. 17.11 Trend of UQ of NDVI from 2000 to 2021

Relationship Between Climatic Factors and NDVI

Temperature and NDVI have a direct relationship, as demonstrated in Fig. 17.15, as the temperature rises, so does the NDVI value. The annual mean temperature and the NDVI have a linear relationship. The following models have been developed based on the 21-year data:

$$\text{Annual mean temperature} = 0.0114416^{*}\ \text{year} \pm 1.81706 \tag{17.11}$$

$$\text{Annual mean NDVI} = 0.001131^{*}\ \text{year} \pm 2.14716 \tag{17.12}$$

Table 17.2 %Variation of different parameters of NDVI between 2000 and 2021

Statically parameters of NDVI	% variation
Minimum	0.13
Maximum	11.2
Mean	25.3
Standard deviation	23.9
Variance	40.9
Upper quartile	25.7
Upper 1.5 IQR	26.3
Median	27.5
Lower 1.5 IQR	31.6
Lower quartile	23.9

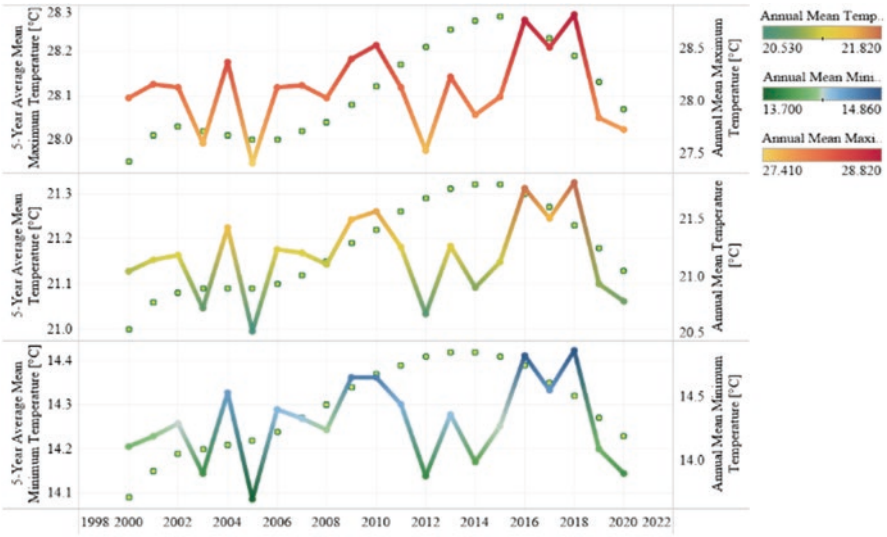

Fig. 17.12 Annual Mean Maximum, 5-Year Average Mean Maximum, Annual Mean Minimum, 5-Year Average Mean Minimum, Mean Temperature, and 5-Year Average Mean Temperature in °C from 2000 to 2020

P-value (significance) for annual mean temperature and NDVI is 0.371365 and 0.0006541, respectively. Residual degrees of freedom, sum squared error, mean squared error, and standard error for annual mean temperature trend are 19, 2.2847, 0.12, and 0.346, respectively, while residual degrees of freedom, sum squared error, mean squared error, and standard error for annual mean NDVI trend are 19, 0.0011302, 5.94 e^{-05}, 0.0077, respectively. R^2 value for annual mean temperature and NDVI is 0.042 and 0.46, which depict that there is low correlation among the data.

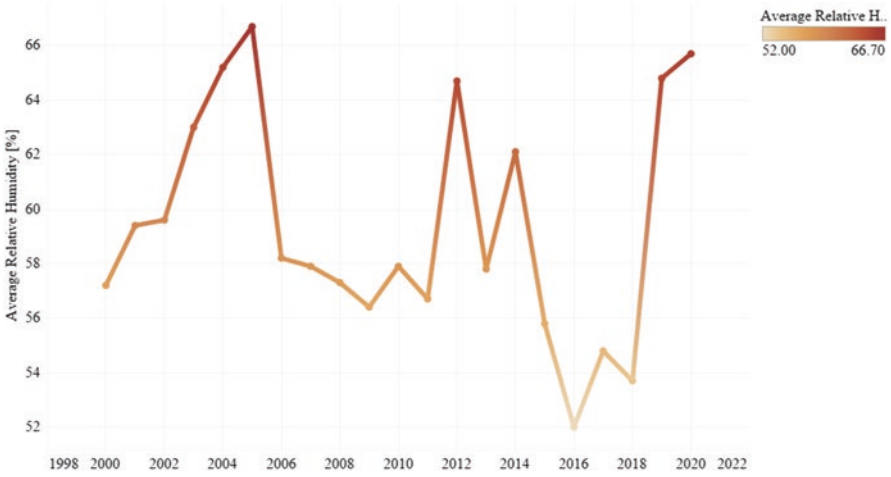

Fig. 17.13 Average Relative Humidity (%) from 2000 to 2020

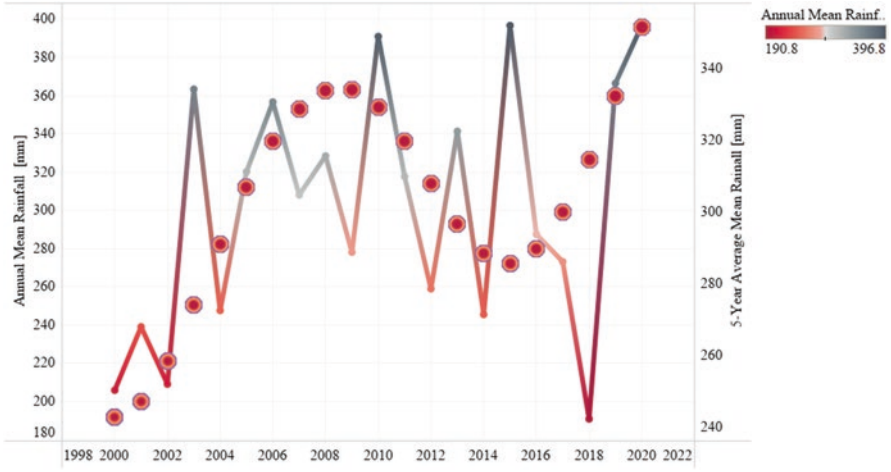

Fig. 17.14 Annual mean rainfall and five-year average rainfall from 2000 to 2020

Relative humidity and NDVI have an indirect relationship, as demonstrated in Fig. 17.16, as the relative humidity increases, the NDVI value decreases. The annual mean relative humidity and the NDVI have a linear relationship. The following model of relative humidity has been developed based on the 21-year data: Annual mean relative humidity = −0.0964935 * year + 253.328.

P-value (significance), residual degrees of freedom, sum squared error, mean squared error, and standard error for annual mean temperature trend are 0.54, 19, 352.389, 18.5468, and 4.3066, respectively. R^2 value is 0.019, which shows that the data has poor correlation (Fig. 17.17).

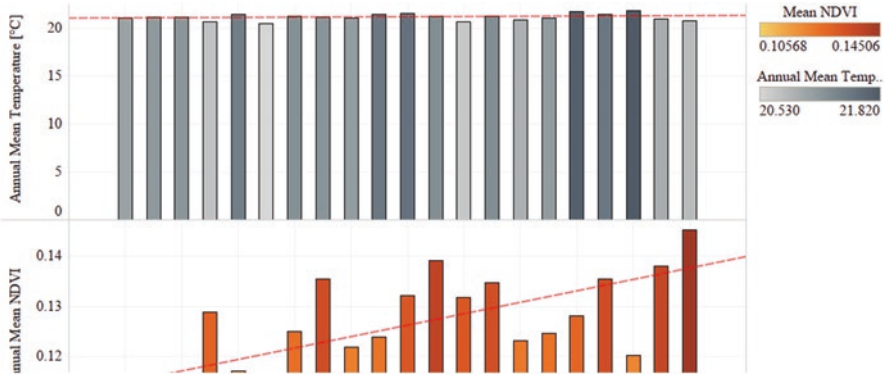

Fig. 17.15 Relationship between annual mean temperature and NDVI

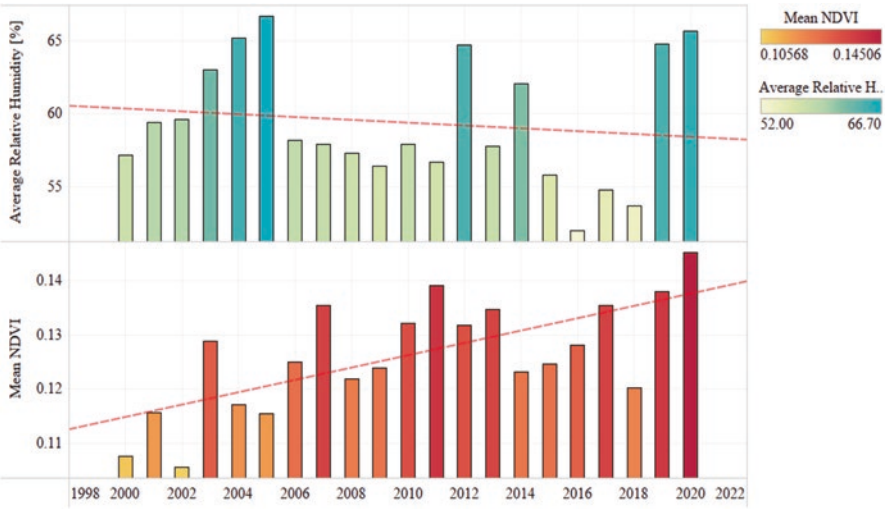

Fig. 17.16 Relationship between mean NDVI and average relative humidity

Rainfall and NDVI have a direct relationship, as demonstrated in Fig. 17.17, as the rainfall rises, so does the NDVI value. The annual mean rainfall and the NDVI have a linear relationship. The following model of rainfall has been developed based on the 21-year data:

$$\text{Annual mean temperature} = 3.19186^{*}\ \text{year} \pm 6114.58 \tag{17.13}$$

P-value (significance), residual degrees of freedom, sum squared error, mean squared error, and standard error for annual mean rainfall trend are 0.17, 19, 75735.8, 3986.09, and 63.1355, respectively. R^2 value 0.093 shows that the data has poor correlation.

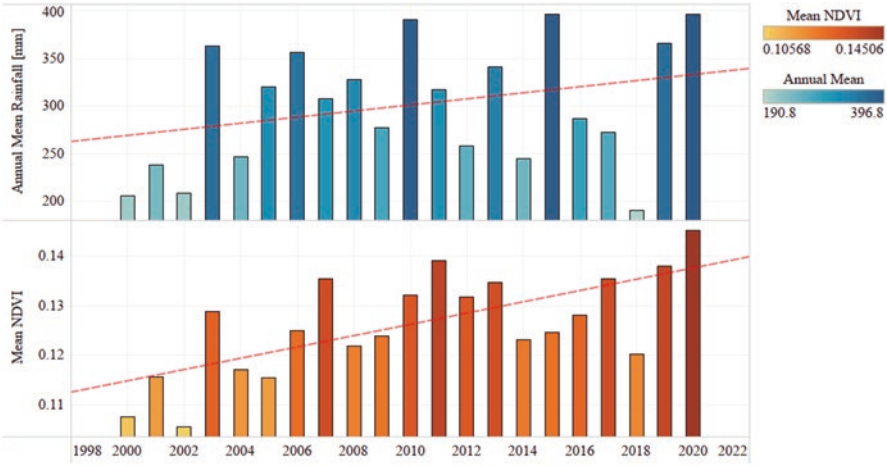

Fig. 17.17 Relationship between annual mean relative rainfall and NDVI

It has been observed from the climatic data (2000–2021) that with the increase in temperature and rainfall, NDVI value increases, and the case is opposite while having look on the relative humidity. People are switching from villages to cities, and as a result, remote areas in certain districts of Sindh are becoming barren. Increased food demand causes farmers to engage in more cultivation practices, and instead of a single cropping system, farmers are adopting multiple cropping systems to meet demand and earn a higher profit. The NDVI value in Sindh province indicates significant fluctuation in LULC because of multiple cropping. Because the environment in Sindh is conducive to this cropping system, the climate has a significant impact on LULC.

Conclusion

The research had been carried out in Sindh province, Pakistan, to assess climate change impact on land use–land cover. Farmers' livelihoods in the research region are fully dependent on agriculture and are related to average temperature and rainfall. However, average temperature changes led to a lack of rainfall, a rise in climate extremes, and a decline in the availability of water for irrigation, directly harming the agrarian population and agricultural advancements. In the research area, rising temperatures and decreased irrigation water supply due to less rainfall are regarded as severe concerns. Farmers need required government assistance as they are aware of climate variations and are reacquainting themselves with methods for mitigating their effects. The results reveal that the vegetation section gives an additional-based beneficial relationship with the NDVI at all stages, whereas built-up area have been inversely associated with LULC and the NDVI during the previous 21 years. On an

average, Sindh area was classified into water bodies, built-up areas, barren land, shrubs and grassland, sparse vegetation, and dense vegetation on the base of NDVI value ranging between −0.28 and 0.74. It has been concluded that climate change has direct impact on LULC. In the whole time period the main variation occur in barren land and dense vegetation area. The latest results provide the primary observation basis for regular inspections of variances in LULC, which will assist policymakers in improving strategies for managing land capitals effectively.

References

Abdul Athick ASM, Shankar K, Naqvi HR (2019) Data on time series analysis of land surface temperature variation in response to vegetation indices in twelve Wereda of Ethiopia using mono window, split window algorithm and spectral radiance model. Data Br 27:104773

Ahmad F (2012) A review of remote sensing data change detection algorithms: comparison of Faisalabad and Multan districts, Punjab Province, Pakistan. J Geogr Reg Plan 5:236–251

Akar, Güngör O (2015) Integrating multiple texture methods and NDVI to the random forest classification algorithm to detect tea and hazelnut plantation areas in northeast Turkey. Int J Remote Sens 36:442–464

Aslam M (2016) Agricultural productivity current scenario, constraints and future prospects in Pakistan. Sarhad J Agric 32:289–303

Ayele GT, Tebeje AK, Demissie SS, Belete MA, Jemberrie MA, Teshome WM, Mengistu DT, Teshale EZ (2018) Time series land cover mapping and change detection analysis using geographic information system and remote sensing, Northern Ethiopia. Air Soil Water Res 11:117862211775160

Choudhury D, Das K, Das A (2019) Assessment of land use land cover changes and its impact on variations of land surface temperature in Asansol-Durgapur Development Region. Egypt J Remote Sens Sp Sci 22:203–218

Dhinwa PS, Pathan SK, Sastry SVC, Rao M, Majumder KL, Chotani ML, Singh JP, Sinha RLP (1992) Land use change analysis of Bharatpur district using GIS. J Indian Soc Remote Sens 20:237–250

Fan F, Weng Q, Wang Y (2007) Land use and land cover change in Guangzhou, China, from 1998 to 2003, based on Landsat TM/ETM+ imagery. Sensors 7:1323–1342

Farooq A, Qurat-ul-ain F (2012) Algorithm and n-dimensional visualization for ETM+ image analysis: a case of district Vehari. Glob J Hum Soc Sci Arts Humanit 12:23–32

Fensholt R, Sandholt I, Stisen S (2006) Evaluating MODIS, MERIS, and VEGETATION vegetation indices using in situ measurements in a semiarid environment. IEEE Trans Geosci Remote Sens 44:1774–1786

Finance Division, G. of P (2019) Pakistan economic survey 2017–18. Pakistan Econ Surv, pp 115–131

Harris A, Carr AS, Dash J (2014) Remote sensing of vegetation cover dynamics and resilience across southern Africa. Int J Appl Earth Obs Geoinf 28:131–139

Hashim AM, Elkelish A, Alhaithloul HA, El-hadidy SM, Farouk H (2020) Environmental monitoring and prediction of land use and land cover spatio-temporal changes: a case study from El-Omayed Biosphere Reserve, Egypt. Environ Sci Pollut Res 27:42881–42897

Hassan Z, Shabbir R, Ahmad SS, Malik AH, Aziz N, Butt A, Erum S (2016) Dynamics of land use and land cover change (LULCC) using geospatial techniques: a case study of Islamabad Pakistan. Springerplus 5:812

Hussain S (2020) Land Use/Land Cover Classification by Using Satellite NDVI Tool for Sustainable Water and Climate Change in Southern Punjab By MS Thesis COMSATS University Islamabad (CUI). https://doi.org/10.13140/RG.2.2.32363.69923

Ibrahim GRF (2017) Urban land use land cover changes and their effect on land surface temperature: case study using Dohuk City in the Kurdistan Region of Iraq. Climate 5:13

Jabbar A, Othman AA, Merkel B, Hasan SE (2020) Change detection of glaciers and snow cover and temperature using remote sensing and GIS: a case study of the Upper Indus Basin, Pakistan. Remote Sens Appl Soc Environ 18:100308

Jacquin A, Sheeren D, Lacombe JP (2010) Vegetation cover degradation assessment in Madagascar savanna based on trend analysis of MODIS NDVI time series. Int J Appl Earth Obs Geoinf 12:3–10

Karuppannan S (2021) Land use/land cover changes and their impact on land surface temperature using remote sensing technique in district Khanewal, Punjab Pakistan. Geol Ecol Landscapes 00:1–13

Kawo NS, Hordofa AT, Karuppannan S (2021) Performance evaluation of GPM-IMERG early and late rainfall estimates over Lake Hawassa catchment, Rift Valley Basin, Ethiopia. Arab J Geosci 14:256

Kefi C, Mabrouk A, Halouani N, Ismail H (2021) Comparison of pixel-based and object-oriented classification methods for extracting built-up areas in coastal zone. Environ Sci Eng 8:2151–2155

Kidane M, Tolessa T, Bezie A, Kessete N, Endrias M (2019) Evaluating the impacts of climate and land use/land cover (LU/LC) dynamics on the Hydrological Responses of the Upper Blue Nile in the Central Highlands of Ethiopia. Spat Inf Res 27:151–167

Lambin EF, Geist HJ, Lepers E (2003) Dynamics of land-use and land-cover change in tropical regions. Annu Rev Environ Resour 28:205–241

Lu D, Li G, Moran E, Hetrick S (2013) Spatiotemporal analysis of land-use and land-cover change in the Brazilian Amazon. Int J Remote Sens 34:5953–5978

Majeed M, Tariq A, Anwar MM, Khan AM, Arshad F, Mumtaz F, Farhan M, Zhang L, Zafar A, Aziz M, Abbasi S, Rahman G, Hussain S, Waheed M, Fatima K, Shaukat S (2021) Monitoring of land use–land cover change and potential causal factors of climate change in Jhelum district, Punjab, Pakistan, through GIS and multi-temporal satellite data. Land 10:1026

Maviza A, Ahmed F (2020) Analysis of past and future multi-temporal land use and land cover changes in the semi-arid Upper-Mzingwane sub-catchment in the Matabeleland south province of Zimbabwe. Int J Remote Sens 41:5206–5227

Näschen K, Diekkrüger B, Evers M, Höllermann B, Steinbach S, Thonfeld F (2019) The impact of land use/land cover change (LULCC) on water resources in a tropical catchment in Tanzania under different climate change scenarios. Sustainability 11(24):7083

Nowacki GJ, Abrams MD (2015) Is climate an important driver of post-European vegetation change in the Eastern United States? Glob Chang Biol 21:314–334

Pande CB, Moharir K, Khadri SFR, Patil S (2018) Study of land use classification in Aried region using multispectral satellite images. Appl Water Sci (Springer J)., ISSN 2190-5487 8(5):1–11

Pande CB, Moharir KN, Khadri SFR (2021) Assessment of land-use and land-cover changes in Pangari watershed area (MS), India, based on the remote sensing and GIS techniques. Appl Water Sci. Impact factor: 3.87, Five Year Impact Factor: 4.39. 11:96. https://doi.org/10.1007/s13201-021-01425-1

Pasha SV, Reddy CS, Jha CS, Rao PVVP, Dadhwal VK (2016) Assessment of land cover change hotspots in Gulf of Kachchh, India using multi-temporal remote sensing data and GIS. J Indian Soc Remote Sens 44:905–913

Qureshi A, Mahessar AA (2016) Time – dependent flow through asymmetric contraction and expansion channel. Sindh Univ Res J (Sci Ser) 45:153–157

Rahman MTU, Tabassum F, Rasheduzzaman M, Saba H, Sarkar L, Ferdous J, Uddin SZ, Zahedul Islam AZM (2017) Temporal dynamics of land use/land cover change and its prediction using CA-ANN model for southwestern coastal Bangladesh. Environ Monit Assess 189:565

Rahman G, Rahman AU, Ullah S, Dawood M, Moazzam MFU, Lee BG (2021) Spatio-temporal characteristics of meteorological drought in Khyber Pakhtunkhwa, Pakistan. PLoS One 16:1–16

Rizvi SH, Fatima H, Alam K, Iqbal MJ (2021) The surface urban heat island intensity and urban expansion: a comparative analysis for the coastal areas of Pakistan. Environ Dev Sustain 23:5520–5537

Sapuro JT (2016) No 主観的健康感を中心とした在宅高齢者における 健康関連指標に関する共分散構造分析Title. Euphytica 18:22280

Shahid M, Rahman KU, Haider S et al (2021) Quantitative assessment of regional land use and climate change impact on runoff across Gilgit watershed. Environ Earth Sci 80:743. https://doi.org/10.1007/s12665-021-10032-x

Srivastava A, Chinnasamy P (2021) Investigating impact of land-use and land cover changes on hydro-ecological balance using GIS: insights from IIT Bombay, India. SN Appl Sci 3:343. https://doi.org/10.1007/s42452-021-04328-7

Tariq A, Riaz I, Ahmad Z, Yang B, Amin M, Kausar R, Andleeb S, Farooqi MA, Rafiq M (2020) Land surface temperature relation with normalized satellite indices for the estimation of spatio-temporal trends in temperature among various land use land cover classes of an arid Potohar region using Landsat data. Environ Earth Sci 79:1–15

Tewabe D, Fentahun T (2020) Assessing land use and land cover change detection using remote sensing in the Lake Tana Basin, Northwest Ethiopia. Cogent Environ Sci 6:E09267

Ullah S, Tahir AA, Akbar TA, Hassan QK, Dewan A, Khan AJ, Khan M (2019) Remote sensing-based quantification of the relationships between land use land cover changes and surface temperature over the lower Himalayan region. Sustainability 11(19):5492

Use L, Cover L, Using C (2020) CA-Markov chain analysis of seasonal land surface temperature and land use land cover change using optical multi-temporal satellite data of Faisalabad, Pakistan. Remote Sens 12:3402

Wakdok SS, Bleischwitz R (2021) Climate change, security, and the resource nexus: case study of Northern Nigeria and Lake Chad. Sustainability 13:1–18

Wang SW, Gebru BM, Lamchin M, Kayastha RB, Lee WK (2020) Land use and land cover change detection and prediction in the Kathmandu district of Nepal using remote sensing and GIS. Sustainability 12(9):3925

Zoungrana BJB, Conrad C, Thiel M, Amekudzi LK, Da ED (2018) MODIS NDVI trends and fractional land cover change for improved assessments of vegetation degradation in Burkina Faso, West Africa. J Arid Environ 153:66–75

Chapter 18
Impacts of Climate-Induced Events on the Season-Based Agricultural Cropping Pattern and Crop Production in the Southwestern Coastal Region of Bangladesh

Shimul Roy, Rezuana Afrin, Md. Younus Mia, and Sanjoy Kumar Mondol

Abstract Agricultural cropping pattern and crop production in the Southwestern coastal region of Bangladesh is affected severely by climate-induced events and climatic variability. This study shows the impacts of climatic-induced events (e.g., cyclone *Sidr* and *Aila*) on agricultural cropping patterns and crop production in two disaster-prone Southwestern coastal districts (i.e., *Khulna* and *Satkhira*) in Bangladesh. For analyzing the trend of climatic variability (e.g., temperature, rainfall, and relative humidity), 35 years (1980–2014) of climatic data were used. This study shows that the agricultural crop production in the selected Southern coastal region of the country had declined significantly when the two major cyclones (i.e., *Sidr* and *Aila*) approached in 2007 and 2009, respectively. A correlation analysis has been performed between annual average crop production and annual average climatic data to identify the influence of climatic variability on crop production.

Keywords Climate · Crop production · Climatic variability · Bangladesh

Introduction

In South Asian countries, the impacts of climate change on various sectors, including freshwater, rainfall, temperature, soil moisture, etc., have severely hindered crop yield (Arnell et al. 2016). In Bangladesh, the impact of climate change on agricultural crop production is a growing concern, especially for long-term agricultural

S. Roy (✉) · R. Afrin · M. Y. Mia · S. K. Mondol
Department of Environmental Science and Resource Management,
Mawlana Bhashani Science and Technology University, Tangail, Bangladesh
e-mail: royshimul@mbstu.ac.bd

C. B. Pande et al. (eds.), *Climate Change Impacts on Natural Resources, Ecosystems and Agricultural Systems*, Springer Climate,
https://doi.org/10.1007/978-3-031-19059-9_18

development. As the vast majority of the country's population relies on agriculture, crop production is highly vulnerable to changes in the climatic system in Bangladesh (Amin et al. 2015). Different studies (e.g., Islam et al. 2020; Chen et al. 2016; Amin et al. 2015; Zakaria et al. 2014; Rimi et al. 2009; Rokonuzzaman et al. 2018; Hossain et al. 2019; Sikder and Xiaoying 2014) reported that agricultural cropping patterns and crop productivity could be severely affected due to the changing pattern of seasonal climatic factors, including temperature, rainfall, humidity, and day length. Additionally, different climate-induced events, such as cyclones, floods, storm surges, droughts, sea level rise, coastal flooding, etc., profoundly impact agricultural cropping patterns and production in Bangladesh (Islam et al. 2020). Agriculture is the backbone of Bangladesh, which significantly influences the country's food security. Apart from food security, this sector has considerable impacts on the country's GDP and employment generation (GED 2021). Currently, this sector generates 12.65% of the country's GDP and employs around 50% of the population (World Bank 2021; Imdad 2021). Although the government of Bangladesh envisioned achieving the universal food security target by 2021, the most pressing concern is increased crop production demand for the rapidly growing population and the climate change impacts on the agricultural sector (GED 2021). It is evident that Bangladesh is one of the highly vulnerable countries worldwide in terms of climate change impacts due to its geographic location between the Himalayas and the Bay of Bengal, making it vulnerable to natural events (Ahmed 2006). The agricultural sector is the most vulnerable and affected in Bangladesh due to climate change (Islam et al. 2015).

In the coastal regions of Bangladesh, the agricultural sector is highly susceptible to climate change impacts, where a significant portion of the population relies on it for livelihood (Islam et al. 2020). Out of 2.85 million hectares of the coastal and offshore regions in Bangladesh, approximately 0.83 million hectares are arable lands, covering more than 30% of the total cultivable lands of the country (Petersen and Shireen 2001). In Bangladesh, the Southern coastal region is severely affected by climate change, notably agricultural crop production (Islam et al. 2020). For instance, two devastating cyclones (i.e., *Sidr* and *Aila*) approached in 2007 and 2009, respectively, severely damaged agricultural production in the Southern region of the country (BBS 2009). In Bangladesh, the impacts of climate change on the agricultural sector have drawn much attention in the recent decade. Some studies were conducted on this issue, primarily focusing on the climate change vulnerability and adaptation practices (Rokonuzzaman et al. 2018; Sikder and Xiaoying 2014; Abedin and Shaw 2013; Huq et al. 2015). Rimi et al. (2009) and Hossain et al. (2019) conducted a study to investigate the impacts of changing climatic variables on rice production in the Southern region of Bangladesh. Islam et al. (2020) studied the influence of climate-induced events and climatic variability on cropping patterns and crop production in the *Satkhira* region, Bangladesh. In this study, we investigate the existing agricultural cropping patterns and status of crop production in two disaster-prone Southwestern coastal districts in Bangladesh (i.e., *Khulna* and

Satkhira), the influence of climatic variability and major climate-induced events (e.g., *Sidr* and *Aila*) on annual crop production, and the correlation between annual crop production and different climatic parameters in the study areas.

Methodology

Study Area

This study was conducted in different Upazilas (i.e., *Dacope*, *Koyra*, *Paikgachha*, *Batiaghata*, *Dumuria*, *Assasuni*, and *Kalaroa*) of the *Khulna* and *Satkhira* districts located in the Southwestern coastal part of Bangladesh (Fig. 18.1). The annual average temperature and rainfall of this region range from 12.5 to 35.5 °C and 1710 to 2500 mm, respectively (Islam et al. 2020; Hossain et al. 2019). This study considered these two Southwestern coastal districts of Bangladesh to provide an overview of the impacts of climatic variability and climate-induced events on agricultural cropping patterns and annual crop production. This study selected this region as the country's Southwestern coastal part is more susceptible to climate-induced events (e.g., cyclones, saltwater intrusion due to coastal flooding or storm surge, etc.).

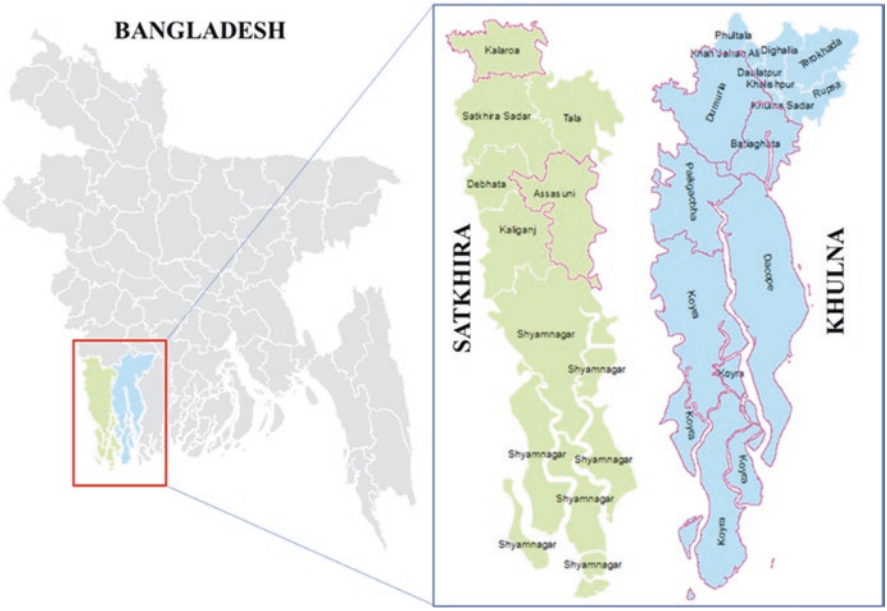

Fig. 18.1 Map of *Khulna* and *Satkhira* districts showing the selected study

Data Collection

This study was mainly conducted based on the secondary data gathered from different local and national sources. Agricultural land area, cropping pattern, and crop production data (e.g., *Aus*, *Aman*, and *Boro* rice) for different seasons (i.e., *Kharif-I*, *Kharif-II*, and *Robi*) for the selected study areas had been collected from the local Agriculture Extension Office (AEO). To analyze this region's climatic variability, 35 years (1980–2014) of climatic data (temperature, humidity, and rainfall) were collected from the Bangladesh Meteorological Department (BMD). However, primary data were also collected from the farmers, local communities, and relevant professionals for obtaining in-depth information regarding various issues relevant to the study (e.g., existing cropping patterns, the status of crop production, concept on climate change, climate-induced events and their frequency in the study areas, and adaptation practices). Primary data were collected through the questionnaire survey, key informant interview (KII) with the government officials (i.e., Upazila Agriculture Extension Officers) and NGOs (e.g., BRAC and Muslim Aid, Winrock International, Prodipon, Rupantor), and through the focus group discussion (FGD) with the farmers of selected Upazilas and local communities. A total of 10 KII had been conducted with the officials of government organizations and NGOs. For the questionnaire survey, 200 respondents (100 from each district) were selected randomly. Besides, a total of eight FGD sessions were conducted between March and October 2015.

Data Analysis

Microsoft Excel and SPSS-20 software were used for data calculation and data analysis. Based on the availability of annual crop production data in three different seasons (i.e., *Kharif-I*, *Kharif-II*, and *Robi* season) and climatic data (temperature, rainfall, and humidity) for the selected study areas, Pearson correlation has been performed among annual average crop production and annual average climatic variability.

Results and Discussion

Climate Change and Its Impacts on the Agricultural Sector in Bangladesh: An Overview

Bangladesh is one of the world's most vulnerable countries to climate change. Located as an interface of the Himalayas and the Bay of Bengal, the country is highly susceptible to natural disasters (Hossain et al. 2018; Huq and Shoaib 2013).

Climate change has increased the severity and frequency of different events, including cyclones, salinity intrusion, droughts, erratic rainfall, high temperatures, flash floods, etc. (Aggarwal et al. 2013; Huq et al. 2015; Rokonuzzaman et al. 2018). As a heavily populated deltaic region, Bangladesh is experiencing the early effects of climate change due to its geographical location, height above sea level, and floodplains (Ahmad 2019; Islam et al. 2020). The Fifth Assessment Report (AR5) of the Intergovernmental Panel on Climate Change (IPCC) mentioned that Bangladesh has already experienced these devastating impacts resulting from climate change (Hijioka et al. 2014). These climate-induced events would be more frequent and extreme in the future and would severely impact various sectors of the country, including agriculture, fisheries, livestock, health, and human livelihood (Ahmad 2019). Sikder and Xiaoying (2014) reported that in the agricultural sector, crop agriculture is highly vulnerable to climate change impacts in Bangladesh.

In Bangladesh, the coastal area covers an area of 47,201 km^2, with more than 37 million people relying on it (Dasgupta et al. 2015). The coastal regions of Bangladesh, mainly the Western and Central coastal regions, are highly vulnerable to climate change impacts (Karim and Mimura 2008). The Western coastal part of the country is surrounded by the world's largest mangrove forest (i.e., the Sundarbans). However, it is a low-lying area subjected to frequent coastal flooding caused by cyclones or storm surges (Ahmad 2019), which have significant impacts on the agricultural sector (including crop agriculture) (Islam et al. 2020). As the population in the coastal region could reach 60 million by 2050 (Dasgupta et al. 2015), the decline in agricultural yield due to climate change could severely impact food security for the growing population (Ismail 2016). Shahid (2010) reported that climate change is anticipated to result in a constant increase in temperature and a change in rainfall pattern, resulting in substantial impacts on agriculture. Table 18.1 shows the reported or possible impacts of climate-induced events in Bangladesh.

Cropping Seasons and Major Cultivated Crop Species

The climate of Bangladesh ranges from subtropical to tropical, which favors the cultivation of a large variety of crops (both rice and non-rice) in different seasons. Generally, crop cultivation has been performed in three different seasons across the country. These include *Kharif-I* (extended from mid-March to mid-July), *Kharif-II* (extended from mid-July to mid-November), and *Robi* (extended from mid-November to mid-March). The Southern region of the country is characterized by the tropical climate, where different crops have been cultivated in these seasons under two different environmental conditions (Table 18.2). The study identified that in the *Kharif-I* season, the dominant crop species is the *Aus* rice. In contrast, it has been observed that T. *Aman* (transplanted *Aman*) is the major crop species during the *Kharif-II* season in the Southern region. In *Robi* (dry season), *Boro* rice is the main cultivated rice species, along with other non-rice crops (Table 18.2).

Table 18.1 Impacts of Climate-Induced Events in Bangladesh

Events	Reported/possible impacts or changes	References
Sea level rise, storm surges, and coastal or riverine flooding	Inundation of crops and increased soil salinity, resulting in substantial loss of agricultural productivity More than 7% reduction in annual rice production during 2005–2050	Sikder and Xiaoying (2014) and Yu et al. (2010)
Cyclones	The tropical cyclone *Sidr* damaged 698,391 tons of *Aman* rice in 2007–2008 in the Southern coastal region The tropical cyclone *Sidr* damaged 1446 acres of *Boro* seedbed in 2007–2008 in the Southern coastal region Significant changes in annual rice (*Aus*, *Aman*, and *Boro*) production after 2007–2008 due to cyclone *Sidr*	Haque et al. (2016) and Islam et al. (2020)
Temperature	1.9 °C increase in temperature by 2030 Rising temperature caused by climate change resulting in lower crop production Substantial decline in cereal (rice and wheat) production, resulting from increased temperature *Boro* rice and wheat would drop by 55–62% and 61%, respectively, by 2050 due to increased temperature	IPCC (2007), Sikder and Xiaoying (2014), Stern (2006) and Mondal (2010)
Rainfall	5–6% increase in rainfall by 2030 Changes in rainfall could result in reduced crop yields in the country Substantial decline in cereal (rice and wheat) production, resulting from erratic rainfall	IPCC (2007), Sikder and Xiaoying (2014) and CDMP II (2013)

Table 18.2 Crop cultivation in different environmental conditions in the Southern coastal region

Conditions	Robi	Kharif-I	Kharif-II
Rainfed condition	Wheat/potato/pulses/oil seeds/sugarcane	*Boro* (local), *Aus*	Fallow
Irrigated condition	Wheat/*Boro*/potato/winter vegetables	Fallow/T. *Aus*	T. *Aman*/fallow

Notes: FGD and KII conducted in 2015. *T. Aus* Transplanted *Aus*, *T. Aman* Transplanted *Aman*

Status of Cropping Patterns in the Southwestern Coastal Region in Bangladesh

Cropping patterns are yearly sequences of crop production on a particular area of land (Alam 1994). In different regions of the country, a wide range of crops are grown under various cropping patterns, which vary from one location to the next.

Agricultural cropping patterns in Bangladesh and variation in crop production are heavily influenced by several factors, including climate, meteorological conditions (e.g., rainfall, temperature range), soil moisture, soil types, irrigation facilities, and availability of cultivable land (Islam et al. 2020; Rashid et al. 2017; Pande et al. 2021; Elbeltagi et al. 2022). However, in the coastal districts of Bangladesh, agricultural land usage is particularly low. For instance, in 2007–2008, the country's average cropping intensity was 179%, whereas in the Southern region, it was much lower (ranging from 128% to 147%) (BBS 2014). The study identified different cropping patterns (both rice and non-rice) that have been practiced recently in the study areas (Tables 18.3 and 18.4).

In Bangladesh, most of the regions (including the Southern coastal region) are covered by rice-based cropping patterns, with the dominance of three main rice varieties (i.e., *Aus*, *Aman*, and *Boro*) (Huq and Shoaib 2013). This study identified that the existing cropping patterns in the selected Southwestern coastal region consist of "two-crop combinations" and "three-crop combinations" (Tables 18.3 and 18.4). Islam et al. (2020) also reported similar cropping patterns for the *Satkhira* region. Rashid et al. (2017) reported that a significant portion of land area (i.e., 63%) in the *Khulna* region is covered by rice-based cropping patterns. This study shows that in *Khulna*, "Fallow land-Fallow land-T. aman" is the dominant cropping pattern, covering more than 44% of the area. "Boro-Fallow-T. aman" and "Boro-Fallow land-Ropa aman" also cover a considerable portion (i.e., 29.5% and ~15%, respectively). However, the proportion of other cropping patterns ranged from 0.2% to ~7%, as presented in Table 18.3. In *Satkhira*, the dominant cropping pattern is identified as "Boro-Fallow land-Ropa aman," covering more than 60% of the land, followed by "Boro-Aus-Ropa aman" (26.5%) and others (Table 18.3).

Apart from the existing cropping pattern of wide rice varieties, the study identified some major non-rice cropping patterns commonly practiced in the study areas

Table 18.3 Existing cropping pattern (rice) in the study area

Sl.	Cropping pattern (rice)	Land under cropping pattern (hec.)[a]	Percentage (%)
Khulna			
1.	Fallow land-Fallow land-T. aman	23,732	44.17
2.	Boro-Fallow-T. aman	15,818	29.44
3.	Boro-Fallow land-Ropa aman	8008	14.91
4.	Boro-Aus-Ropa aman	3522	6.56
5.	Boro-Fallow-Fallow	1789	3.33
6.	Boro-Aus-T. aman	452	0.84
7.	Boro-Aush-Fallow land	305	0.57
8.	Fallow-Aus-T. aman	100	0.19
Satkhira			
1.	Boro-Fallow land-Ropa aman	8008	60.26
2.	Boro-Aus-Ropa aman	3522	26.50
3.	Boro-Fallow land-Fallow land	1759	13.24

Notes: AEO (2014). [a]Total land under cropping pattern in the selected study areas in 2014

Table 18.4 Existing cropping pattern (non-rice) in the study areas

Sl.	Cropping pattern (non-rice)	Land under cropping pattern (hec.)[a]	Percentage (%)
Khulna			
1.	Vegetables-vegetables-vegetables	4423	67.70
2.	Vegetables-jute-vegetables	1050	16.07
3.	Mustard seed-vegetables-vegetables	558	8.54
4.	Vegetables-vegetables-Fallow	175	2.68
5.	Potato-vegetables-vegetables	104	1.59
6.	Potato-vegetables-Fallow	100	1.53
7.	Spices-lentil-vegetables	61	0.93
8.	Spices-vegetables-vegetables	50	0.77
9.	Wheat-vegetables-vegetables	12	0.18
Satkhira			
1.	Potato-jute	2208	41.97
2.	Mustard seed (local)	1950	37.07
3.	Vegetables-vegetables-vegetables	1103	20.97

Notes: AEO (2014). [a]Total land under cropping pattern in the selected study areas in 2014

(Table 18.4). This study shows that in *Khulna*, "vegetables-vegetables-vegetables" is the dominant cropping pattern, covering more than 68% of the land. Besides, "vegetables-jute-vegetables" and "mustard seed-vegetables-vegetables" also cover significant land under the cropping pattern (i.e., 16% and ~9%, respectively). In *Satkhira*, the dominant non-rice cropping pattern is identified as "potato-jute," covering ~42% of the land under the cropping pattern, followed by "mustard seed (local)" and "vegetables-vegetables-vegetables" (Table 18.4).

Impacts of Climate Change on Crop Production

The agricultural cropping pattern in the Southwestern coastal region of Bangladesh is largely dominated by rice, followed by non-rice crops (Rashid et al. 2017). Hence, this study emphasized the influence of climate-induced events on rice production in the selected region of the country. Different climate-induced events are frequent in this region, resulting in substantial damage in cultivable land areas and the annual crop production. Islam et al. (2020) reported that as the land areas in this region are inundated by saline water during and post-cyclone period, soil salinity increases and, therefore, makes the land unfavorable for crop cultivation. According to the Soil Resource Development Institute (SRDI), the Southwestern part of the country, mainly *Khulna*, *Satkhira*, and *Bagerhat*, are highly vulnerable to soil salinity, which has profound impacts on crops produced in this region (SRDI 2010). Islam et al. (2015) reported that due to the salinity intrusion, different local rice varieties (e.g., *kalojira*, *najirsail*, *boran*, etc.) have already been extinct from the country's coastal regions. According to Nishat and Mukherjee (2013), increased salinity triggered by climate-induced events reduces annual average rice production by around

0.2 million metric tons and affects the *Boro* and wheat production in the coastal saline soils. The estimated loss of rice due to the cyclones in 2007 and 2009 was nearly two million metric tons (CIAT 2017). In Bangladesh, climatic-induced events (e.g., floods, cyclones, etc.) are anticipated to become more frequent and intense and could affect the crop agriculture severely (CIAT 2017). For instance, it is projected that salinity intrusion due to climate-induced events could reduce rice and wheat production by 8% and 32%, respectively, in the coastal regions by 2050 (The Financial Express 2018).

The study reveals that in the Southwestern coastal regions, agricultural land areas and rice production vary considerably in different seasons (Fig. 18.2a, b), which is believed to be because of climate-induced events, mainly cyclone as reported by the majority of the respondents, that is, 60% (average) of the study areas. Figure 18.2a shows that in the *Kharif-II* season (extended from mid-July to mid-November), annual production of *T. Aman* rice per hectare during 2007–2008 in *Satkhira* reduced considerably (~15%) compared to 2006–2007 (i.e., 2.7 vs. 2.3 Mt/hec.). A significant reduction in *Boro* rice (~10%) in the *Robi* season (extended from mid-November to mid-March) had also been observed (i.e., 5.3 vs. 4.8 Mt/hec.). The production of *Aus* rice in the *Kharif-I* season (extended from mid-March to mid-July) reduced by 5% during the same period compared to 2006–2007 in this coastal part of the country. This reduction is due to cyclone Sidr, which struck Bangladesh on 15 November 2007.

In 2008–2009, the production of *Aus* rice in the *Kharif-I* reduced significantly (~50%) compared to the production rate in 2007–2008 (i.e., 18.3 vs. 9.3 Mt/hec.), which is because of the cyclone *Aila* (which struck Bangladesh on 25 May 2009). The study also identified that cyclone *Sidr* and *Aila* caused massive destruction for agricultural crop production in the *Khulna* region. For instance, in 2006–2007, the *T. Aman* high yield variety (HYV) production was 52,984 Mt, which decreased substantially (24%) in 2007–2008 (i.e., 52,984 Mt vs. 40,295.7 Mt) when cyclone *Sidr* hits at the coastal region of Bangladesh and cyclone *Aila* swept up almost all the crop fields during 2009–2010 (Fig. 18.2b).

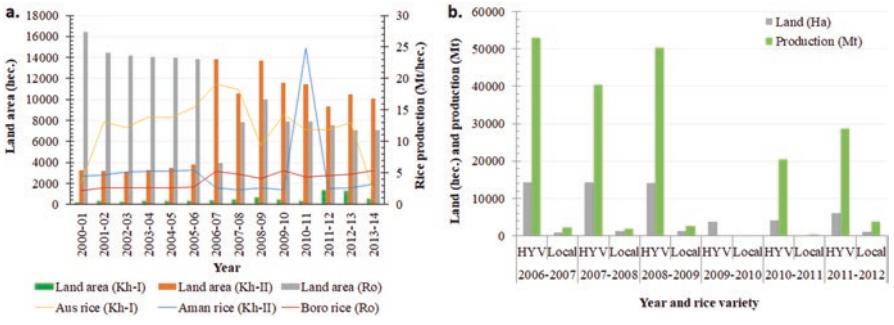

Fig. 18.2 Annual rice production with land area in different seasons: (**a**) *Assasuni* Upazila, *Satkhira*, and (**b**) production of *Aman* rice (HYV and local variety) in *Koyra* Upazila (*Khulna*). (Notes: *Kh-I* Kharif-I, *Kh-II* Kharif-II, *Ro* Robi, *HYV* high yield variety)

Trend of Variability in Climatic Parameters

The variability trends in different climatic parameters were analyzed for the *Khulna* and *Satkhira* region of Bangladesh using the average annual temperature, relative humidity, and rainfall data during the period 1980–2014 (Fig. 18.3). The study shows that in *Khulna*, the highest and lowest average annual temperatures were 26.7 °C (in 2010) and 25.2 °C (in 1981), respectively. An increasing trend (0.0254%) of average temperature was observed during this period in *Khulna*, where the coefficient of determination is 0.4908 (Fig. 18.3a). Hossain et al. (2019) reported a similar increasing temperature trend in *Khulna* during 1980–2010. In *Satkhira*, the highest and lowest average annual temperatures were recorded at 27.7 °C (in 1987) and 25.5 °C (in 1997), respectively. However, a decreasing trend (0.0371%) of average temperature was observed in this region during that period, where the coefficient of determination is 0.3666 (Fig. 18.3d). Islam et al. (2020) also reported a decreasing trend in average temperature for the *Robi* season (i.e., 0.071%) in the *Satkhira* region during 1980–2014.

The trend analysis of average annual rainfall during the study period in *Khulna* shows a slightly decreasing trend (0.7591%), where the coefficient of determination is 0.0006. The average rainfall during this period ranged from 1130 to 2594 mm, with the highest average rainfall in 2002 and the lowest in 1994 (Fig. 18.3b). Hossain et al. (2019) reported a slightly increasing trend in annual temperature during the monsoon season in the *Khulna* region. For *Satkhira*, a decreasing trend (3.3445%) was also observed during the same period, where the coefficient of determination is 0.019. The average rainfall during this period ranged from 1295 to 2195 mm, with the highest average rainfall in 1986 and the lowest in 2010 (Fig. 18.3e). Islam et al. (2020) reported a decreasing trend in average rainfall for *Robi* season (characterized by dry season) in the *Satkhira* region and a moderate trend for *Kharif-I*

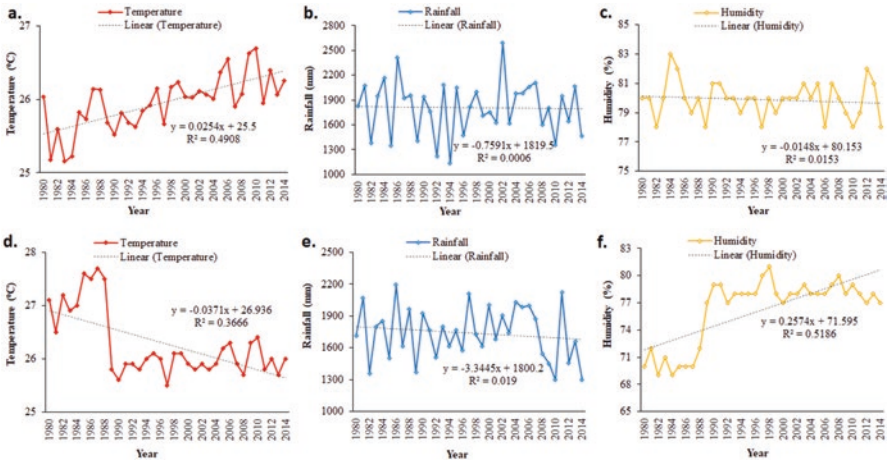

Fig. 18.3 Variability in different climatic parameters during 1980–2014 in (**a–c**), *Khulna* region, and (**d–f**), *Satkhira* region

(pre-monsoon) and *Kharif-II* (monsoon) season during 1980–2014. As variability in temperature and humidity significantly impacts the overall rainfall (Mawonike and Mandonga 2017), this erratic rainfall pattern might be occurred due to variability in temperature and relative humidity.

The average relative humidity during 1980–2014 ranged from 78% to 83% and from 69% to 81% in *Khulna* and *Satkhira*, respectively. The study identified a decreasing trend in the average relative humidity (0.0148%) in the *Khulna* region during this period, where the coefficient of determination is 0.0153 (Fig. 18.3c). However, in *Satkhira*, an increasing trend in the average relative humidity (0.2574%) was observed, where the coefficient of determination is 0.5186. A similar finding has been reported by Islam et al. (2020) for the *Satkhira* region, with an increasing trend in average relative humidity in different seasons (ranging from 0.248% to 0.431%) during 1980–2014 (Fig. 18.3f).

Correlation Between Crop Production and Climatic Parameters

Pearson correlation among annual average crop production and annual average climatic data (e.g., temperature, humidity, and rainfall) was performed in this study (Table 18.5), as we assumed that the climatic parameters influence annual crop production in the study areas. Rahman and Rahman (2019) reported that crop production in Bangladesh is largely influenced by climatic variability. It should be mentioned that the Pearson correlation has been performed based on the availability of annual crop production data. This study found a significant strong positive correlation between annual average rainfall and average crop production in *Batiaghata* Upazila in the *Khulna* region ($r = 0.961$, $p < 0.05$). A strong positive correlation between average yearly rainfall and average crop production ($r = 0.641$, $p < 0.05$) and between annual average humidity and annual average crop production ($r = 0.668$, $p < 0.05$) has been observed in *Koyra* Upazila in the *Khulna* region. However, a moderate to strong negative correlation was observed between the annual average temperature and annual average crop production (Table 18.5). For the *Satkhira* region, no significant correlation was found among annual average crop production and average annual climatic data (Table 18.5).

Local People's Perception of Climate-Induced Events, Possible Causes, and Impacts

This study used different approaches (mentioned earlier) to gather local peoples' responses regarding the climate-induced events, possible causes, and impacts in the study areas. As local people were the direct observers of different climate-induced events and the damages that occurred in the past, it was crucial to have their

Table 18.5 Pearson correlation among annual average crop production and average climatic data of *Khulna* region

	Avg. production	Avg. temperature	Avg. rainfall	Avg. humidity
Dacope Upazila, Khulna (2007–2014)[a]				
Avg. production	1			
Avg. temperature	−0.629	1		
Avg. rainfall	0.003	−0.660	1	
Avg. humidity	0.372	−0.390	0.541	1
Koyra Upazila, Khulna (2007–2012)[a]				
Avg. production	1			
Avg. temperature	−0.520	1		
Avg. rainfall	0.641	−0.704	1	
Avg. humidity	0.668	−0.391	0.342	1
Batiaghata Upazila, Khulna (2011–2014)[a]				
Avg. production	1			
Avg. temperature	−0.629	1		
Avg. rainfall	0.961*	−0.757	1	
Avg. humidity	0.407	−0.366	0.32	1
Assasuni Upazila, Satkhira (2000–2013)[a]				
Avg. production	1			
Avg. temperature	0.037	1		
Avg. rainfall	−0.222	−0.247	1	
Avg. humidity	−0.007	−0.129	−0.286	1

Notes: *Correlation is significant at the 0.05 level (two-tailed). [a]Rice production data during the period used for the correlation analysis has been considered based on data availability

responses. We believe that these findings will better understand the appearance of climate-induced events and the associated impacts on the agricultural cropping system. The result (average response rate of two regions) revealed that local people now realize that climate-induced events are approaching frequently compared to the past decades with immense impacts on the agricultural sector. Most of the respondents (~63%) reported that the Southwestern coastal areas are highly vulnerable to climate-induced events and asserted the frequency of massive cyclones that occurred every 4–5-year interval, resulting in a substantial loss in crop production. A similar finding was reported by Sikder and Xiaoying (2014) and Islam et al. (2020), with a considerable loss in the agricultural sector in Southern Bangladesh due to cyclones.

Our result shows that local people in all the study areas agreed that the cropping pattern had been changed significantly in their regions, possibly due to climatic influences. For instance, a considerable proportion of the respondents (37%) reported that the cropping pattern has changed due to unreliable rainfall in the past decades and increased soil salinity (35%) due to coastal flooding and storm surges. However, some respondents mentioned that soil fertility and productivity reduction due to increased soil salinity results in changing cropping patterns. Besides, introducing high yield varieties (HYV) to cope with climate change is another reason for cropping pattern change (Fig. 18.4).

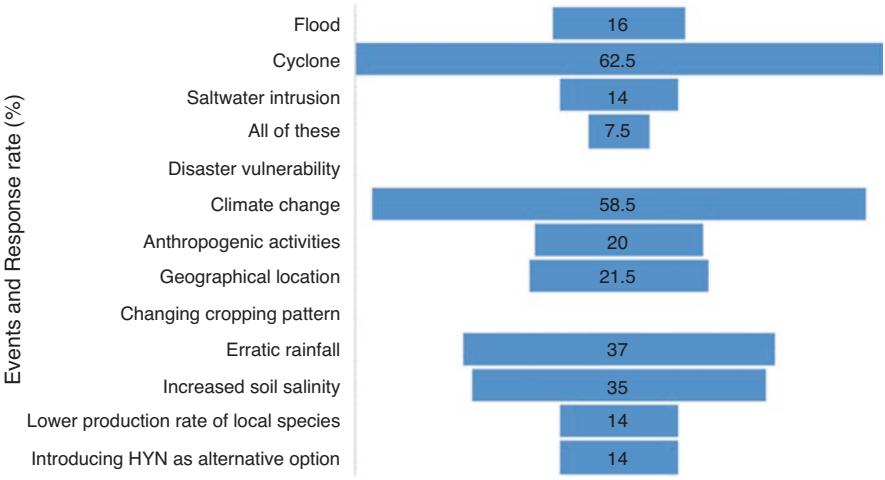

Fig. 18.4 Local peoples' responses on climate change, its causes, and impacts

Conclusions and Recommendations

In summary, climate-induced events (e.g., cyclone *Sidr* and *Aila*) significantly impact annual crop production and change cropping patterns in Southwestern coastal Bangladesh. For instance, in the *Satkhira* region, rice production of major varieties (i.e., *T. Aman*, *Aus*, and *Boro*) in different crop growing seasons reduced by 5–15% in 2007–2008 compared to the production amount in 2006–2007, which is mainly due to effects of cyclone *Sidr*. In the *Khulna* region, the loss in crop production was even more. This study shows a 24% reduction in *T. Aman* production caused by the effects of cyclone *Sidr* during that period, and *Aus* rice production reduced by ~50% due to the impact of cyclone *Aila* in 2008–2009. The study also identified the changing trend in climatic variables (temperature, rainfall, and relative humidity) in these regions, which considerably influences annual crop production. A strong positive correlation has been observed between average annual rainfall/humidity and average crop production, while average annual temperature and average crop production were found negatively correlated. As the agricultural sector is highly susceptible to climate change, this study recommends that concerned authorities of the government should adopt proper adaptation measures in the crop agricultural production system to meet the growing demand of the country's large population through policy reforms and effective implementation. For instance, salt-tolerant and flood-tolerant rice varieties could be practiced on a large scale in these climate-sensitive areas to cope with the climate change impacts. Besides, the government should prioritize the sustainable management of water resources for irrigation in the disaster-prone coastal regions of Bangladesh.

Acknowledgments The authors sincerely acknowledge the Ministry of Science and Technology (MOST) and the People's Republic of Bangladesh for funding the project.

References

Abedin MA, Shaw R (2013) Agriculture adaptation in coastal zone of Bangladesh. In: Climate change adaptation actions in Bangladesh. Springer, Tokyo, pp 207–225

AEO (2014) Agricultural production data: rice varieties and crops in Khulna and Satkhira region. Agricultural Extension office (AEO), Department of Agricultural Extension (Personal communication)

Aggarwal P, Pathak H, Kumar S, Sharma P (2013) South Asia perspectives on climate change and agriculture: adaptation options. In: Hillel D, Rosenzweig C (eds) Handbook of climate change and agroecosystems: global and regional aspects and implications. Joint Publication with the American Society of Agronomy, Crop Science Society of America, and Soil Science Society of America, pp 209–222

Ahmed AU (2006) Bangladesh climate change impacts and vulnerability: a synthesis. Climate Change Cell, Department of Environment

Ahmad H (2019) Bangladesh coastal zone management status and future trends. J Coast Zone Manag 22(1):1–7

Alam MS (1994) Optimum cropping patterns of the small farmers under risk: a micro level study in Bangladesh. PhD thesis, Department of Agricultural Economics, Bangladesh Agricultural University, Mymensingh

Amin M, Zhang J, Yang M (2015) Effects of climate change on the yield and cropping area of major food crops: a case of Bangladesh. Sustainability 7(1):898–915

Arnell NW, Brown S, Gosling SN, Gottschalk P, Hinkel J, Huntingford C et al (2016) The impacts of climate change across the globe: a multi-sectoral assessment. Clim Chang 134(3):457–474

BBS (Bangladesh Bureau of Statistics) (2009) Statistical year book of Bangladesh. Planning Division, Ministry of Planning Government of the People's Republic of Bangladesh, Dhaka

BBS (Bangladesh Bureau of Statistics) (2014) Statistical yearbook of Bangladesh. Statistics Division, Ministry of Planning, Government of the People's Republic of Bangladesh

CDMP II (Comprehensive Disaster Management Programme) (2013) Development of four-decade long climate scenario & trend temperature, rainfall, sunshine & humidity. Institute of Water and Flood Management, BUET. Study report, pp 91–101

Chen S, Chen X, Xu J (2016) Impacts of climate change on agriculture: evidence from China. J Environ Econ Manag 76:105–124

CIAT (2017) Climate-smart agriculture in Bangladesh. CSA country profiles for asia series. International Center for Tropical Agriculture (CIAT)/World Bank, Washington, DC, 28 p

Dasgupta S, Kamal FA, Khan ZH, Sharifuzzaman C, Nishat A (2015) River salinity and climate change: evidence from coastal Bangladesh. In: World scientific reference on Asia and the world economy, pp 205–242

Elbeltagi A, Kumar N, Chandel A et al (2022) Modelling the reference crop evapotranspiration in the Beas-Sutlej basin (India): an artificial neural network approach based on different combinations of meteorological data. Environ Monit Assess 194:141. https://doi.org/10.1007/s10661-022-09812-0

GED (2021) Making vision 2041 – a reality perspective plan of Bangladesh 2021–2041. General Economics Division (GED), Bangladesh. Planning Commission, Ministry of Planning, Government of the People's Republic of Bangladesh

Haque MN, Ali MH, Masum SM (2016) Climate change impacts on rice production in Bangladesh. Lambert Academic Publishing, Saarbrücken

Hijioka Y, Lin E, Pereira JJ, Corlett RT, Cui X, Insarov GE, Lasco RD, Lindgren E, Surjan A (2014) Asia. In: Climate change 2014: impacts, adaptation, and vulnerability. Part B: regional aspects. Contribution of Working Group II to the Fifth Assessment Report of the Intergovernmental Panel on Climate Change

Hossain MS, Qian L, Arshad M, Shahid S, Fahad S, Akhter J (2018) Climate change and crop farming in Bangladesh: an analysis of economic impacts. Int J Clim Change Strateg Manag 11(3):424–440

Hossain MN, Saifullah ASM, Bhuiyan SH, Uddin N, Rahman M (2019) Effects of climate change on rice production at Khulna district, Bangladesh. Environ Earth Ecol 3(1):42–54

Huq SI, Shoaib JM (2013) The soils of Bangladesh. Springer, Dordrecht

Huq N, Hugé J, Boon E, Gain AK (2015) Climate change impacts in agricultural communities in rural areas of coastal Bangladesh: a tale of many stories. Sustainability 7(7):8437–8460

Imdad MP (2021) Revitalising Bangladesh's agriculture sector. https://www.thedailystar.net/supplements/30th-anniversary supplements/news/revitalising-bangladeshs-agriculture-sector-2042629. Accessed 3 Dec 2021

IPCC (2007) Climate change 2007: the physical science basis. Agenda 6(07):333

Islam MA, Shitangsu PK, Hassan MZ (2015) Agricultural vulnerability in Bangladesh to climate change induced sea level rise and options for adaptation: a study of a coastal Upazila. J Agric Environ Int Dev 109(1):19–39

Islam MS, Roy S, Afrin R, Mia MY (2020) Influence of climate-induced disasters and climatic variability on cropping pattern and crop production in Bangladesh. Environ Dev Sustain 22(7):6709–6726

Ismail H (2016) Climate change, food and water security in Bangladesh. Future Directions International. https://www.futuredirections.org.au/publication/climate-change-food-water-security-bangladesh/. Accessed 10 Nov 2021

Karim MF, Mimura N (2008) Impacts of climate change and sea-level rise on cyclonic storm surge floods in Bangladesh. Glob Environ Chang 18(3):490–500

Mawonike R, Mandonga G (2017) The effect of temperature and relative humidity on rainfall in Gokwe region, Zimbabwe: a factorial design perspective. Br View 3(2)

Mondal MH (2010) Crop agriculture of Bangladesh: challenges and opportunities. Bangladesh J Agric Res 35(2):235–245

Nishat A, Mukherjee N (2013) Climate change impacts, scenario and vulnerability of Bangladesh. In: Climate change adaptation actions in Bangladesh. Springer, Tokyo, pp 15–41

Pande CB, Moharir KN, Singh SK, Varade AM, Ahmed Elbeltagie SFR, Khadri PC (2021) Estimation of crop and forest biomass resources in a semi-arid region using satellite data and GIS. J Saudi Soc Agric Sci 20(5):302–311

Petersen L, Shireen S (2001) Soil and water salinity in the coastal area of Bangladesh. Bangladesh Soil Resource Development Institute, Dhaka

Rahman MS, Rahman MA (2019) Impacts of climate change on crop production in Bangladesh: a review. J Agric Crops 5(1):6–14

Rashid MH, Shirazy BJ, Ibrahim M, Shahidullah SM (2017) Cropping systems and their diversity in Khulna region. Bangladesh Rice J 21(2):203–215

Rimi RH, Rahman SH, Karmakar S, Hussain SG (2009) Trend analysis of climate change and investigation on its probable impacts on rice production at Satkhira, Bangladesh. Pak J Meteorol 6(11):37–50

Rokonuzzaman M, Rahman MA, Yeasmin M, Islam MA (2018) Relationship between precipitation and rice production in Rangpur district. Progress Agric 29(1):10–21

Shahid S (2010) Recent trends in the climate of Bangladesh. Clim Res 42(3):185–193

Sikder R, Xiaoying J (2014) Climate change impact and agriculture of Bangladesh. J Environ Earth Sci 4(1):35–40

SRDI (2010) Saline soils of Bangladesh. Soil Resource Development Institute, Farmgate, Dhaka, 55p

Stern N (2006) Report of the stern review: the economics of climate change. HM Treasury, London
The Financial Express (2018) Impact of climate change on agricultural. https://www.thefinancialexpress.com.bd/views/impact-of-climate-change-on-agricultural-1518619832. Accessed 2 Dec 2021
World Bank (2021) The World Bank Data, Bangladesh. https://data.worldbank.org/indicator/NV.AGR.TOTL.ZS?locations=BD. Accessed 3 Dec 2021
Yu W, Alam M, Hassan A, Khan AS, Ruane A, Rosenzweig C, Major D, Thurlow J (2010) Climate change risks and food security in Bangladesh. Routledge
Zakaria M, Aziz M, Hossain M, Rahman N (2014) Effects of rainfall and maximum temperature on Aman rice production of Bangladesh: a case study for last decade. Int J Sci Technol 3(2):131–137

Chapter 19
Toward Smart Agriculture for Climate Change Adaptation

Rinku Moni Devi

Abstract Agriculture plays a significant role in food security and forms the backbone of the economic system of a country. The increase in population has led to an urgent need to balance demand and supply, threatening sustainability and putting pressure on agricultural systems. Furthermore, climate change challenges like extreme weather conditions, climatic changes, and environmental impact have adversely impacted agriculture and linked resources. Besides this, about 85% of Indian farmers are marginal and small landholders. About 60% of the net sown area is under rainfed agriculture, and this makes India vulnerable to climate change considerably affecting the cropping system, livestock, and soil and increasing pests and diseases. Climate change would have a serious impact on Indian agriculture in the coming years which would negatively impact some important crops leading to food insecurity. The present trend and scenario are evident that without an efficient measure, it would be very difficult to meet agro-demand of the country. Therefore, there is an urgent need of efficient measures of adaption and mitigation. Therefore, smart agriculture using IoT (Internet of Things) technology has opened up extremely productive ways for farmers, helps in managing agricultural systems, and deals with weather uncertainties and challenges improving resource management. It enables farmers to collect real-time data related to weather updates, irrigation, production, yield quality, and soil moisture and predict pest, diseases, and market information and strengthen good agricultural practices in farms. Additionally, IoT solutions along with smart practices in agriculture offer opportunities for innovation in climate adaptation reducing the ecological footprints and enhancing the livelihoods of farmers. Thus, the present paper aims to review the current and future trends of IoT in the Indian agriculture system, highlighting potential challenges and also its role in combating climate change. Additionally, the study recommends adoption of good agricultural practices, capacity building, and switching from traditional to precise farming with IoT-based technology. For future scope, institutional innovations, networking of farmers, regulatory authorities, clear policies supporting the necessary

R. M. Devi (✉)
Indian Institute of Forest Management, Bhopal, Madhya Pradesh, India

C. B. Pande et al. (eds.), *Climate Change Impacts on Natural Resources, Ecosystems and Agricultural Systems*, Springer Climate,
https://doi.org/10.1007/978-3-031-19059-9_19

legal and market architecture for smart farming, and transparent data management system will be required.

Keywords Smart agriculture · Internet of Things · Climate change · Livelihood · Adaptation

Introduction

Climate change is a global concern impacting the Earth's ecosystem and humankind. A recent report by IPCC (Intergovernmental Panel on Climate Change) (2021) provides new estimates of the chances of crossing the global warming level of 1.5 °C in the next decades and is unequivocal (IPCC 2021). There will be intensification of extreme events globally, and weather uncertainties will be natural resources including agriculture sector. Most importantly, water scarcity is also one of the greatest challenges of the twenty-first century (FAO 2011), and agriculture accounts for an estimated 70% of global water withdrawals (WWAP 2015). Therefore, it is also important to address water scarcity as well as water use efficiency (Hatfield and Dold 2019; Pande et al. 2022a). In the Indian context, agriculture is the main backbone of Indian economy and accounts for around 20% of India's gross domestic product (GDP) (Economic Survey 2020–2021). Climate change impacts will be more visible in developing countries like India as compared to developed countries as millions of populations are dependent on agriculture and natural resources for their livelihood (IPCC 2014). Additionally, the rise in population increases the demand for food security putting pressure on natural resources (Adamides et al. 2020; Pande et al. 2021a; Rajesh et al. 2021). Furthermore, developing countries are more vulnerable due to low adaptation measures, lack of financial resources, and technological constraints. Thus, these impacts in turn have significant economic, social, and environmental consequences, so a better understanding of all the changes that might arise in view of climate change and variability is essential. To meet the needs and to overcome these challenges, one has to adopt new technologies to gain a much-needed edge. New agricultural application in smart farming is precise through IoT which enables crop farmers to collect real-time data related to irrigation and plant protection processes, aiming to increase production volume, improve product quality, and predict diseases, while optimizing resources and farming processes (Adamides et al. 2020). It improves the livelihoods of farmers and helps them in tackling climate change challenges. Thus, this chapter reviews the potential of current and future trends of smart agriculture using IoT-based tools in India and challenges and role in combating climate change. The study recommends the use of good agricultural practices along with adoption of IoT-based smart agriculture in combating climate change.

Smart Farming Approach

Smart agriculture with IoT-based solution is "a group of infrastructures interconnecting connected objects and allowing their management, data mining and the access to the data they generate" (Dorsemaine et al. 2015). By utilizing data like temperature, rainfall, soil moisture, humidity, wind, pH, etc. from IoT devices in the field and using cloud computing and analytics, farmers are timely notified to proceed with such targeted activities, and proper planning is done for farming based on the real-time database (Ayaz et al. 2019; Adamides et al. 2020).

The schematic diagram below shows the use of IoT-based techniques where different sensors, microcontrollers, power supply, and cloud computing and its application in the agricultural system (Fig. 19.1).

The application of IoT in agriculture aims at empowering farmers, enhancing livelihoods of farmers, and providing decision tools and automation technologies that integrate products, knowledge, and services for increased productivity, quality improvement, and profit (Elijah et al. 2018). It utilizes advance information and communication technology (ICT) and deploys smart sensors in the field, scanning the field with drones and enhancing the use of spatial and real-time events (Walter et al. 2017). This approach improves farm productivity, quality yield, increased production, profitability, efficient irrigation, identification of pests/diseases, and precise use of pesticides. Good practice approach enhances the use of organic manure, less use of pesticides, selection of crops, timings, crop rotation, maintaining soil health, and efficient use of water in agriculture which in turn also reduces environmental footprint. Thus, for an economically and environmentally sustainable production system, there is a need to develop techniques that can increase crop

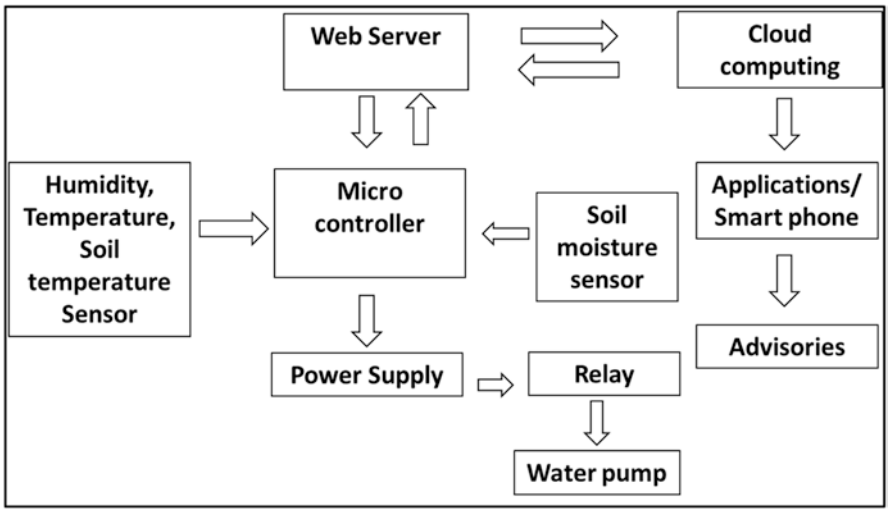

Fig. 19.1 Schematic diagram of IoT and its application

production through increased efficiency of input use and reduced environmental losses, and smart agriculture using IoT solutions is the key component of sustainable agriculture in the twenty-first century (Delgado et al. 2019; Sishodia et al. 2020). Smart agriculture is based on three important pillars: (i) better resource management, (ii) improved conservation of ecosystem and landscape, and (iii) smart farming technologies with more adequate services for farmers (Adamides et al. 2020). It is estimated that the smart agriculture market will grow by 12.7%, annually (Chen et al. 2019). In the next several years, the use of smart solutions powered by IoT will increase in agricultural operations. In fact, a few of the recent reports depicted that the IoT device installation will see a compound annual growth rate of 20% in the agriculture industry and a number of connected devices (agricultural) will grow from 13 million in 2014 to 225 million by 2024 (Machina 2017; Elijah et al. 2018). Thus, most countries are switching from traditional farming to technology-based farming in the long run.

From Data Collection to Farming Advisories

Different emerging technologies like the Internet of Things (IoT), Big Data analysis, artificial intelligence (AI), remote sensing, geographic information systems (GIS), and global positioning systems (GPS) are very important tools in agricultural operations which aimed to enhance production and reduce inputs and yield losses (Elijah et al. 2018; Delgado et al. 2019; Jha et al. 2019; Pande et al. 2021b, 2022a, b). Furthermore, IoT technology systems utilizing cloud computing, wireless sensor networks, and big data analysis have been developed for smart farming operations such as automated wireless-controlled irrigation systems and intelligent disease and pest monitoring and forecasting systems (Elijah et al. 2018; Jha et al. 2019; Shisodia et al. 2020). AI techniques, including machine learning, have been used to estimate different parameters like evapotranspiration (ET), soil moisture, soil pH, and crop predictions for automated and precise application of water, fertilizer, herbicides, and insecticides (Boursianis et al. 2020). These technologies and tools enable farmers to characterize the important crop growth parameters enabling the management of good growth and yield and avoiding losses (Koch et al. 2004).

The ecosystem of smart agricultures includes the following as mentioned below:

Internet of Things (IoT)

IoT is a technology aimed at connecting all intelligent objects within a single network, that is, the Internet. It involves all kinds of computer technologies, both (a) hardware (intelligent boards and sensors) and (b) software (advanced operating

systems and AI algorithms). Its primary target is the establishment of applications for devices, in order to enable the monitoring and control of a specific domain primarily used in agriculture for the management of agricultural products within gathered real-time data, alongside: (1) searching, (2) tracking, (3) monitoring, (4) controlling, (5) managing, (6) evaluating, and (7) operations within a supply chain.

Big Data Analytics (BDA)

It refers to the large volume of data gathered from different dataset sources over a long period of time, that is, sensor, the Internet, and business data. Thus, BDA involved the utilization of (a) tools, classification and clustering; (b) techniques, data mining, machine learning, and statistical analysis; and (c) technologies (Alreshidi 2019). The use of BDA in agriculture focusses on the management of the supply chain of agricultural products, in order to enhance decision-making and minimize the cost of production cost. It is also employed for the analysis of the properties of different types of soil for classification and further enhancement. Furthermore, it is useful for improved prediction and crop production.

Cloud Computing

It is "a model for enabling convenient, on-demand network access to a shared pool of configurable computing resources (networks, servers, storage, applications and services) that can be rapidly provisioned and released with minimal management effort or service provider interaction" (Alreshidi 2019). The cloud computing can be seen as a high virtualization method for datacenter infrastructure distributed over a wide geographical area, linked by means of high bandwidth network cables providing a variety of virtualized services. All these advanced data acquisitions and processing techniques aid the decision-making process for field crops, horticulture, pasture, and livestock (Shisodia et al. 2020).

Mobile Computing

It refers to infrastructure in which data processing and data storage take place externally to the mobile device. Systems collect and send daily data to farmers, informing them of both the production status and weather conditions.

Artificial Intelligence (AI)

AI covers many areas, including computer vision, data mining, deep learning, image processing, and neural networks (Kale and Patil 2019; Elbeltagi et al. 2022a, b). It includes robots, monitoring crops and soils, and predictive analytics, as the following:

(a) *Robots:* These are developed and programmed to handle fundamental agricultural tasks/human force.
(b) *Monitoring crop and soil:* It employs computer vision and deep learning algorithms for processing captured data by sensors monitoring crop and soil health.
(c) *Predictive analytics:* This analysis captures data, based on machine learning models capable of tracking and predicting various environmental impacts on crop harvest, that is, changes in weather. IoT/AI technologies (such as drone and satellite) that generate a large amount of data on a daily basis have the potential to enable agricultural production to forecast changes and detect opportunities (Alreshidi 2019).

Applications

Smart agriculture also includes Farm Management Systems (FMS) that assist farmers with a variety of collected information, by managing and controlling various tracking devices and sensors (Alreshidi 2019). The devices are attached to solar panel for power supply, and good network connectivity is the outmost need. Remote sensing and GIS tools can be also used for monitoring farms, crop yields, water management, nutrient management, disease management, and production spatially and temporally. Remote sensing uses sensor-based technology, and these sensors differ based on spatial, spectral, radiometric, and temporal resolution. Numerous vegetation indices like NDVI (normalized difference vegetation index), EVI (enhanced vegetation index), and statistical/machine learning approaches, such as deep convolutional neural network and random forest, have been applied to reduce the dimensionality of hyperspectral data to extract useful information on crop conditions (Zarco-Tejada et al. 2016; Chlingaryan et al. 2018; Chang et al. 2020; Elbeltagi et al. 2022a). More recently, quantification of solar-induced chlorophyll fluorescence (SIF) from hyperspectral images has increasingly been applied to estimate photosynthesis, plant nutrients, and biotic and abiotic stresses such as disease and water stress (Zarco-Tejada et al. 2016; Mohammed et al. 2019).

Additionally, special devices like automated weather stations collect weather-related data like rainfall, temperature, humidity, wind, etc. Disease models and sensor-based cameras provide accurate information on pest−/insect-related diseases in crops and help in predicting the trends. Precise information on crop pests/insects provides alerts when there is rise in pest attacks and saves the crops from further

damage. Additionally, it provides guidance in the use of appropriate pesticides/insecticides in farms. The utilization process of IoT/AI technologies aids in establishment, monitoring, management, processing, and analysis of data generated from various agricultural resources, such as field, crops, livestock, etc. and further enriches decision-making of stakeholders (Kumar et al. 2012).

Decision-Making in Farmers

The large data obtained from sensor offers learning opportunities to improve decision-making in constantly changing environmental conditions; such decision-making can be over a short, medium, or long term (Adamides et al. 2020). It allows various farms to be connected and managed on a single platform, where information on scientific advances, production, marketing, farm management, recommendations, and other related topics are disseminated to maximize productivity, yield, and revenue. Automated decisions can be made from the IoT system when certain conditions are reached, therefore requiring less or no human interventions. Such automated decision could range from regulating the temperatures to the control of water supply from an irrigation system.

Insurance

Farmers are usually exposed to extreme weather conditions which could lead to poor harvest and yield loss due to unpredictable rain and lack of storage system. However, with the implementation of IoT technology, farmers can be insured with their crops and livestock. A network of sensors can be deployed, and monitoring can be achieved by remote unmanned stations (Alreshidi 2019). The data can be sent to the cloud and analyzed. The insurance policy can be embedded with a warning system, where extreme weather conditions are predicted and the insured farmers are alerted by text messages. This can enable the farmers to take precautionary approach to protect their farms.

Advisories

With the help of various applications and interfaces in smartphones, farmers can receive advisories at regular intervals at their doorsteps. They can plan agricultural practices as per the precise information reducing the risks. Additionally, with connectivity through online interface, they get platform to connect to markets for buying and selling their produce with the right price (Fig. 19.2).

Fig. 19.2 Mobile application

Climate Change and Agriculture

India is the third highest greenhouse gas (GHG) emitter after China, and the United States accounts for 18% of gross national emissions from agriculture and livestock. The agriculture sector is the main source of CH_4 and N_2O emissions (BUR 2021). In the year 2016, the agriculture sector emitted 407,821 Gg of CO2e. Within agriculture, in 2016, 54.6% of GHG emissions were due to enteric fermentation, followed by 17.5% from rice cultivation, 19.1% from fertilizer applied to agricultural soils, and 6.7% from manure management, and 2.2% due to field burning of agricultural residues (BUR 2018). Climate change is threatening India's food security with frequent dry spells, heat waves, and erratic monsoonal rainfall, adding to farmers' woes. As the global population continues to surge, developing countries will need to double food production by 2050. Consequently, scientists and policymakers are faced with the challenge of meeting the growing demand for food while also reining in on GHG emissions. Creating sustainable and climate-resilient agricultural systems has been highlighted as part of India's plan to meet its ambitious pledge to the United Nations Framework Convention on Climate Change international treaty to reduce the emission intensity of its GDP by up to 35% by 2030, compared to 2005 levels (INDC 2015). Moreover, frequent dry spells, heat waves, and erratic monsoonal rainfall add to farmers' woes. It is very much evident that climate change has a severe impact on global food production influencing both demand and supply of food grains, globally (Srinivasarao et al. 2018); under such conditions, the program of sustainable development goals will continuously slow down, affecting the communities immensely. Besides this, about 85% of Indian farmers and marginal and small landholders (Agricultural census 2011) and about 60% of the net sown area are under rainfed agriculture. This makes India vulnerable to climate change,

considerably affecting the cropping system, livestock, fisheries, poultry, soil, pest, and diseases. Climate change would have a serious impact on Indian agriculture in the coming years which would negatively impact some important crops that would lead the country to food insecurity. The present trend and scenario are evident that without an efficient measure, it would be very difficult to meet agro-demand of the country. Thus, efficient measures of adaption and mitigation are required.

Advantages of Smart Agriculture Based on IoT and Good Agricultural Practices (GAPs)

IoT system has wide applications in the agricultural system. It can manage water content efficiency and soil health and also maintain crop growth. It has more advantages in multi-cropping agricultural system with diverse crops and huge yields. It saves time and minimizes manpower. It reduces the agriculture issues due to uncertainties in weather- or environment-related issues. It minimizes the manual works and makes a very effective farming system which promotes efficient use of water and soil management approach. It is a fast technology; increases crop production; improves crop quality, large production, and regular advisories; minimizes loss; and increases profits. To enable farm, produce to be internationally competitive innovative farming practices incorporating the concept of globally accepted good agricultural practices (GAP) within the framework of commercial agricultural production for long-term improvement and sustainability is essential. Good agricultural practices are "practices that address environmental, economic and social sustainability for on-farm processes, and result in safe and quality food and non-food agricultural products" (Hobbs 2003). The four "pillars" of GAP are economic viability, environmental sustainability, social acceptability, and food safety and quality. GAP in addition to improving the yield and quality of the products also has environmental and social dimensions. Implementation of GAP would promote optimum utilization of water resources such as pesticides, fertilizers, water, and eco-friendly agriculture. Efficient use of fertilizer not only lowers emissions at the field but also reduces the need for fertilizer and the emissions associated with production and transportation. It also represents savings for the farmer. Mitigation options would include applying fertilizer at the right time and the right place for plant uptake or using slow-release fertilizer forms or nitrification inhibitors. Adoption of zero tillage farming and residue management-maintaining crop residues on the soil surface to protect the ground from erosion in rice, wheat, maize, cotton, and sugarcane was shown to reduce emissions. The use of sprinkler or micro-sprinkler irrigation and fertigation together reduces greenhouse gas emissions. Other good practices include the use of organic manure vermicompost, farm yard manures, integrated pest management, irrigation management, neem use of drip farming, zero tillage, no crop burning after harvest, timely sowing, harvesting, storage, transportation, and knowledge of markets. The implementation of GAPs contributes to sustainable agriculture and rural development.

Key Problems Faced in Indian Agriculture System

There are numerous factors which restrain India's agricultural output. Some of them are systemic or historical in nature, while others are related to environmental or technological factors. The technological factors have emerged primarily due to lack of advancement of agricultural techniques and affordability of machinery and equipment (Dixon et al. 2004). Systemic factors include cropping pattern mono-cropping; application of obsolete cropping patterns inhibits agricultural productivity and leads to soil degradation. Small/fragmented landholdings of farmers and land tenure make it difficult to achieve economies of scale and introduce new technologies and machinery. Further, due to lack of systematic agriculture financing provision, it is unaffordable for farmers to take load at high interest, thereby making finance unaffordable for farmers. Similarly, environmental factors like unpredictable behavior of monsoons influence agricultural productivity, overuse of fertilizers, increase in tillage, abandonment of traditional organic soil revival techniques, and insufficient rotation of crops resulted in soil degradation and loss of fertility (World Bank 2012). Furthermore, the diverse topography of India's land makes it essential to identify the right crops for the various soil variants and climatic conditions. Other factors include technological factors like lack of farm equipment, new farming techniques, lack of efficient ways of water supply for irrigation, groundwater, lack of storage facilities, awareness and illiteracy among farmers, market connectivity, and the use of traditional farming system (FAO 2017). An important aspect in rural India is the dependence of all household members on single source of livelihood which makes even more necessary to tackle the problems with a comprehensive strategy. While addressing most of these factors needs policy interventions, tackling some of them can be easier through the adoption of analytics and smart farming. Some of the drawbacks of IoT comprises requirement of continuous Internet connectivity, costlier, several kinds of security issues to maintain these types of networks, and a need of equipment maintenance done regularly.

Conclusion and Recommendations

Climate change is a global challenge affecting the natural ecosystem and humankind. It has detrimental effects on natural resources by altering their natural properties. Due to altering of soil and water properties, it not only impacts agriculture but also faulty farming practices have detrimental effects on the climate. Therefore, there is a need of smarter, better, and more efficient crop growing technology which meets the growing food demand of the increasing population, promotes sustainable agriculture, and reduces emissions. Thus, the use of AI and IoT techniques can help to practice sustainable agriculture and also contribute in climate mitigation by reducing the carbon footprint. Thus, this review paper highlights the role of IoT-based technology in agriculture in order to make agriculture smarter and more

efficient to meet future expectations. Moreover, the high efficiency of integrated agriculture production systems delivers socioeconomic and ecological benefits that profit farmers as well as the whole society. There are many ways in which integrated agriculture production systems can help producers to adapt to climate change and provide important mitigation co-benefits. However, several factors hamper the effective adaptation of integrated production systems, such as lack of data on the impacts of climate change and high requirements in terms of knowledge and labor and initial investments that may pay off only over long time periods. Besides, a key area to be worked upon is the strategy to ensure economic feasibility and ease of adoption. Emphasis must be given to pilots, and after learnings from implantations, it can be further scaled up and framework could be developed. Furthermore, opportunities for entrepreneurs will arise in future in this sector. They can further help in capacity building of farmers and encourage for more adoption of such technology in their farms. Thus, the sustainable intensification of integrated agriculture production systems requires a better understanding of the impacts of changes in climate and climate variability on these systems; the generation and sharing of local and global knowledge, experiences, and practices; capacity development through research and development, dialogue, and dissemination of information; and the support and coordination of policies, particularly policies that can provide incentives and create enabling institutions. Climate-smart policies will emphasize incentives and capabilities to encourage improved decision-making at the farm level. This includes the adoption of best feasible technologies, improved input use, and post-harvest practices. Establishment of extension and improved supply chains may go a long way to meet this objective. Governments may also consider introducing insurance schemes with low transaction costs and moral hazard potential to reduce the cost of risk and risk aversion. Further, governments may provide input subsidies in short-term situations in which learning by doing is needed, as well as insured and subsidized credit. These activities should be designed to induce transition to sustainable and economically viable practices.

Thus, adopting smart agriculture IoT and practicing good agricultural practices in farms would be a boon in agriculture. It is a platform for development of new methods of improving crop yield and handling, technology, and innovation; tracking the crop growth, profit, safety, and nutrition labeling, and partnerships between growers, suppliers, and retailers and buyers. Additionally, IoT solution has bridged the gap between production and quality and quantity yield and increases profits. Real-time data provides precise information in the form of advisories related to weather updates, irrigation, production, yield quality, and soil moisture; predicts pest, diseases, and market information; and minimizes loss. The livelihoods of smallholder farmers will improve by adopting technology-based agriculture and play major role in managing food security in long run. Additionally, it acts as a viable climate change mitigation and adaptation approach to tackle climate change targets. Thus, it can be concluded that every inch of farmland is vital to maximize crop production and using of sustainable IoT-based sensors and communication technologies is not optional – it is necessary. This will further help in achieving our

sustainable development goals and development of management practices, contribute in climate adaptation, and have implications in policy aspects.

In the way forward, it can be concluded that institutional innovations would be possible, leading to networks of farmers who are more self-organized and flexible than today. Joint use of machinery and applications can promote private exchange of sowing, maintenance, and harvesting operations. Yet, because regulatory authorities need to have access to some aspects of the data gathered, clear policies and a transparent data management system will be required. ICT and data management can provide novel ways into a profitable, socially accepted agriculture that benefits the environment (e.g., soil, water, climate), species diversity, and farmers in developing and developed countries. But this can only happen with the proactive development of policies supporting the necessary legal and market architecture for smart farming, with a dialogue among farming technology supporters and skeptics, and with careful consideration of emerging ethical questions.

References

Adamides G, Kalatzis N, Stylianou A, Marianos N, Chatzipapadopoulos F, Giannakopoulou M, Neocleous D (2020) Smart farming techniques for climate change adaptation in Cyprus. Atmosphere 11(6):557

Agricultural census GoI (2011) Available online at https://agcensus.nic.in/document/agcensus2010/completereport.pdf

Alreshidi E (2019) Smart sustainable agriculture (SSA) solution underpinned by internet of things (IoT) and artificial intelligence (AI). arXiv preprint arXiv:1906.03106

Ayaz M, Ammad-Uddin M, Sharif Z, Mansour A, Aggoune EHM (2019) Internet-of-Things (IoT)-based smart agriculture: toward making the fields talk. IEEE Access 7:129551–129583

Boursianis AD, Papadopoulou MS, Diamantoulakis P, Liopa-Tsakalidi A, Barouchas P, Salahas G, Goudos SK (2020) Internet of things (IoT) and agricultural unmanned aerial vehicles (UAVs) in smart farming: a comprehensive review. Internet of Things:100187

Chang CY, Zhou R, Kira O, Marri S, Skovira J, Gu L, Sun Y (2020) An Unmanned Aerial System (UAS) for concurrent measurements of solar-induced chlorophyll fluorescence and hyperspectral reflectance toward improving crop monitoring. Agric For Meteorol 294:108145

Chen WL, Lin YB, Lin YW, Chen R, Liao JK, Ng FL, Yen TH (2019) AgriTalk: IoT for precision soil farming of turmeric cultivation. IEEE Internet Things J 6(3):5209–5223

Chlingaryan A, Sukkarieh S, Whelan B (2018) Machine learning approaches for crop yield prediction and nitrogen status estimation in precision agriculture: a review. Comput Electron Agric 151:61–69

Delgado JA, Short NM Jr, Roberts DP, Vandenberg B (2019) Big data analysis for sustainable agriculture on a geospatial cloud framework. Front Sustain Food Syst 3:54

Dixon J, Taniguchi K, Wattenbach H, Tanyeri Arbur A (2004) Food and Agriculture Organization of the United Nations, Rome

Dorsemaine B, Gaulier JP, Wary JP, Kheir N, Urien P (2015) Internet of things: a definition & taxonomy. In: 2015 9th international conference on next generation mobile applications, services and technologies. IEEE, pp 72–77

Elbeltagi A, Nagy A, Mohammed S, Pande CB, Kumar M, Bhat SA, Zsembeli J, Huzsvai L, Tamás J, Kovács E, Harsányi E, Juhász C (2022a) Combination of limited meteorological data for predicting reference crop evapotranspiration using artificial neural network method. Agronomy 12(2):516. https://doi.org/10.3390/agronomy12020516

Elbeltagi A, Pande CB, Kouadri S et al (2022b) Applications of various data-driven models for the prediction of groundwater quality index in the Akot basin, Maharashtra, India. Environ Sci Pollut Res 29:17591–17605. https://doi.org/10.1007/s11356-021-17064-7

Elijah O, Rahman TA, Orikumhi I, Leow CY, Hindia MN (2018) An overview of Internet of Things (IoT) and data analytics in agriculture: benefits and challenges. IEEE Internet Things J 5(5):3758–3773

FAO (2011) The state of the world's land and water resources for food and agriculture–managing systems at risk. Earthscan/Food and Agriculture Organization of the United Nations, London, pp 3

Food and Agriculture Organization of the United Nations (FAO) (2017) The future of food and agriculture – trends and challenges. FAO, Rome

Hatfield JL, Dold C (2019) Water-use efficiency: advances and challenges in a changing climate. Front Plant Sci 10:103

Hobbs JE (2003) Incentives for the adoption of good agricultural practices (GAPs). Food and Agriculture Organization, p 1

India's Nationally Determined Contributions (NDC), GoI (2015)

IPCC (2021) Climate change 2021: the physical science basis. Contribution of Working Group I to the Sixth Assessment Report of the Intergovernmental Panel on Climate Change [Masson-Delmotte V, Zhai P, Pirani A, Connors SL, Péan C, Berger S, Caud N, Chen Y, Goldfarb L, Gomis MI, Huang M, Leitzell K, Lonnoy E, Matthews JBR, Maycock TK, Waterfield T, Yelekçi O, Yu R, Zhou B (eds)]. Cambridge University Press

IPCC AR5 (2014) Climate change 2014: synthesis report. Contribution of Working Groups I, II and III to the Fifth Assessment Report of the Intergovernmental Panel on Climate Change [Core Writing Team, Pachauri RK, Meyer LA (eds)]. IPCC, Geneva, 151 p

Jha K, Doshi A, Patel P, Shah M (2019) A comprehensive review on automation in agriculture using artificial intelligence. Artif Intell Agric 2:1–12

Kale SS, Patil PS (2019) Data mining technology with fuzzy logic, neural networks and machine learning for agriculture. In: Data management, analytics and innovation. Springer, Singapore, pp 79–87

Koch B, Khosla R, Frasier WM, Westfall DG, Inman D (2004) Economic feasibility of variable-rate nitrogen application utilizing site-specific management zones. Agron J 96(6):1572–1580

Kumar A, Lee BG, Lee H, Kumari A (2012) Secure storage and access of data in cloud computing. In: 2012 international conference on ICT convergence (ICTC). IEEE, pp 336–339

Machina. Available https://machinaresearch.com/reports. Accessed 1 Oct 2017

Ministry of Finance, Government of India. Economic Survey Report, 2020–2021

MoEFCC (2018) India: second biennial update report to the United Nations framework convention on climate change. Ministry of Environment, Forest and Climate Change, Government of India

MoEFCC (2021) India: third biennial update report to the United Nations framework convention on climate change. Ministry of Environment, Forest and Climate Change, Government of India

Mohammed GH, Colombo R, Middleton EM, Rascher U, van der Tol C, Nedbal L, Zarco-Tejada PJ (2019) Remote sensing of solar-induced chlorophyll fluorescence (SIF) in vegetation: 50 years of progress. Remote Sens Environ 231:111177

Pande CB, Moharir KN, Panneerselvam B et al (2021a) Delineation of groundwater potential zones for sustainable development and planning using analytical hierarchy process (AHP), and MIF techniques. Appl Water Sci 11:186. https://doi.org/10.1007/s13201-021-01522-1

Pande CB, Moharir KN, Singh SK, Varade AM, Elbeltagie A, Khadri SFR, Choudhari P (2021b) Estimation of crop and forest biomass resources in a semi-arid region using satellite data and GIS. J Saudi Soc Agric Sci 20(5):302–311

Pande CB, Moharir KN, Singh SK et al (2022a) Groundwater flow modeling in the basaltic hard rock area of Maharashtra, India. Appl Water Sci 12:12. https://doi.org/10.1007/s13201-021-01525-y

Pande CB, Kadam SA, Jayaraman R, Gorantiwar S, Shinde M (2022b) Prediction of soil chemical properties using multispectral satellite images and wavelet transforms methods. J Saudi Soc Agric Sci 21(1):21–28

Rajesh J, Pande CB, Kadam SA et al (2021) Exploration of groundwater potential zones using analytical hierarchical process (AHP) approach in the Godavari river basin of Maharashtra in India. Appl Water Sci 11:182. https://doi.org/10.1007/s13201-021-01518-x

Sishodia RP, Ray RL, Singh SK (2020) Applications of remote sensing in precision agriculture: a review. Remote Sens 12(19):3136

Srinivasarao C, Shanker A, Chanker C (2018) Climate resilient agriculture-strategies and perspectives. Intech Open, Hyderabad, p 181

Walter A, Finger R, Huber R, Buchmann N (2017) Opinion: smart farming is key to developing sustainable agriculture. Proc Natl Acad Sci 114(24):6148–6150

World Bank (2012) India: issues and priorities for agriculture. https://www.worldbank.org/en/news/feature/2012/05/17/india-agriculture-issues-priorities

WWAP (2015) Water for a sustainable world. UNESCO, Paris

Zarco-Tejada PJ, González-Dugo MV, Fereres E (2016) Seasonal stability of chlorophyll fluorescence quantified from airborne hyperspectral imagery as an indicator of net photosynthesis in the context of precision agriculture. Remote Sens Environ 179:89–103

Chapter 20
Flood Impact and Damage Assessment Based on the Sentitnel-1 SAR Data Using Google Earth Engine

Sachin Shinde, Chaitanya B. Pande, V. N. Barai, S. D. Gorantiwar, and A. A. Atre

Abstract Floods, as cataclysmic events, are often commonly brought on by floods and heavy downpours or by overflowing streams, rivers or seas; this sort of destructive occurrence is one of the most frequently recognised and affects nearly every sector and Earth area. This recommended practice involves supplying vital disaster data for both short- and long-haul flood worries. The tool offers a flood scale chart using Sentinel-1 SAR (synthetic aperture radar) images, just as cropland and community focus data presentations have been affected to address the entirety of essential issues caused by floods. Remote sensing data is a valuable asset for outlining areas. As of late, the availability of free satellite data has dramatically increased in terms of form and recurrence, making it easier to build flood maps across the globe. Propose a semiautomatic flood mapping system right now with free satellite imagery and open-source tools in mind. Google Earth Engine (GEE) is given an essential platform for impact analysis and damage assessment based on the SAR data. Rapid analysis of SAR data also identified how much area was affected due to flood. The possibility of flooding causes a significant loss of life and property, leading to the instability of human civilisation. Flood risk analysis is also needed to understand flood singularities, particularly for development and mitigation determinations. The central portion of the Panchganga River was chosen for current research. The essen-

S. Shinde · V. N. Barai
Department of Soil and Water Conservation, Mahatma Phule Krishi Vidyapeeth, Rahuri, Maharashtra, India

C. B. Pande (✉)
Indian Institute of Tropical Meteorology (IITM), Pune, Maharashtra, India
e-mail: chaitanay45@gmail.com

S. D. Gorantiwar · A. A. Atre
Center for Advanced Agriculture Science and Technology on Climate-Smart Agriculture and Water Management, Mahatma Phule Krishi Vidyapeeth, Rahuri, Maharashtra, India

C. B. Pande et al. (eds.), *Climate Change Impacts on Natural Resources, Ecosystems and Agricultural Systems*, Springer Climate,
https://doi.org/10.1007/978-3-031-19059-9_20

tial purpose of the present thesis was to use Google Earth Engine mapping to determine the possible flood risk regions of the Panchganga River. A flood setup was done based on the SAR data of 5 August 2005 around the river area. The holding method was used to SAR data applied on separate flooded and non-flooded areas. Area outcomes can be significant for flood planning and damage.

Keywords Surface water dynamics · Google Earth Engine · Kolhapur flood · Water spread-out area

Introduction

Disaster hazards globally have affected cost-effective damages worth billions of US dollars and influenced millions of public faced so much disaster vulnerabilities in last and current eras (UNISDR 2012). Hazard mitigation of natural risks has been grown as an essential ecological advancement of the human nation (Wang et al. 2018a, b). While universal community urban growth is beneficial, human settlements and livelihoods must be exposed to disaster threats on a regular basis (Elbeltagi et al. 2022; Orimoloye et al. 2022). Increased natural hazards and extreme circumstances as a result of global climate change will provide rising problems for numerous countries and territories in preventing and mitigating financial and social disruptions (Huang et al. 2018; Lin and Han 2001). As a result, new research recommends that flood control should use a risk-based strategy (Feyisa et al. 2014; Zhang et al. 2014). Such techniques are designed to lower the total risk of flooding, which has a determined probability multifunction. The extent and likelihood of the flood (hazard), the potential damage (exposure) and how flood events are handled (coping capacity) can be limited (Gorelick et al. 2017; Han 2010). Various forms of floods occur, all of them result in flooding outside the river. The EU (European Union) directive covers river floods, seas, ephemeral streams, mountain torrents and water systems floods. The directive requires the Member States to develop plans for the management of flood risks before 2015 (Ji et al. 2015). A preliminary flood risk assessment took place in 2011 in preparation for this, and by 2013, flood risks and risk maps must be developed as they are essential instruments in establishing management strategies. Since the risk of flooding is not permanent over time, these maps (and the plans) have to be reviewed every six years. The mapping of floods is therefore crucial for EU countries to comply with the new Flood Directive criteria. Flood hazard mapping is not new, and many governments and commercial entities have mapped flood dangers for various objectives (Mei et al. 2016; Xu et al. 2019).

A common and accurate strategy for assessing the magnitude of significant flooding is SAR-based flood mapping. In any climate conditions, SAR can join the overcast spread and run and provide comfortable and vital details regarding one of the most successive and obliterating cataclysmic events: floods (Jiang et al. 2017). The critical way was collected from data; this recommended practice includes a virtually constant, cloud-based and easy-to-use flood grade mapping technique designed to address technological constraints (Rokni et al. 2014). This cloud-based

preferred practice completes all exams without consuming hard drive space or managing the end-computer user's strength without the need to import enormous and complicated details. This method generates in seconds what a GIS (Geographic Information System) client can take hours to finish by inserting the provided code and remote the locale of interest just as the when dates (Pande 2022). Flooding influences around each area on the globe are one of the most commonly recognised catastrophe incidents. Every year, flooding obliterates 800 crores (80,000 lakhs) beyond the 100 people who lose their lives, creating severe challenges for on-call experts and emergency chiefs to handle after a disaster hits. Not only does this suggested technique produce a simple and easy flood diagram, but it overlays it with land use and population data, such as the crop area and number of communities within the harmed regions, in instant production statistics.

Materials and Methods

Description of Study Area

The study area is located in Fig. 20.1. Nowadays, this research focuses on the flood impact and potential damage assessment analysis within the Kolhapur area in the southwest of Maharashtra state. Kolhapur area's mean sea level is 569 metres (1867 ft). The area is presented in Sahyadri mountains in the Western Ghats with a

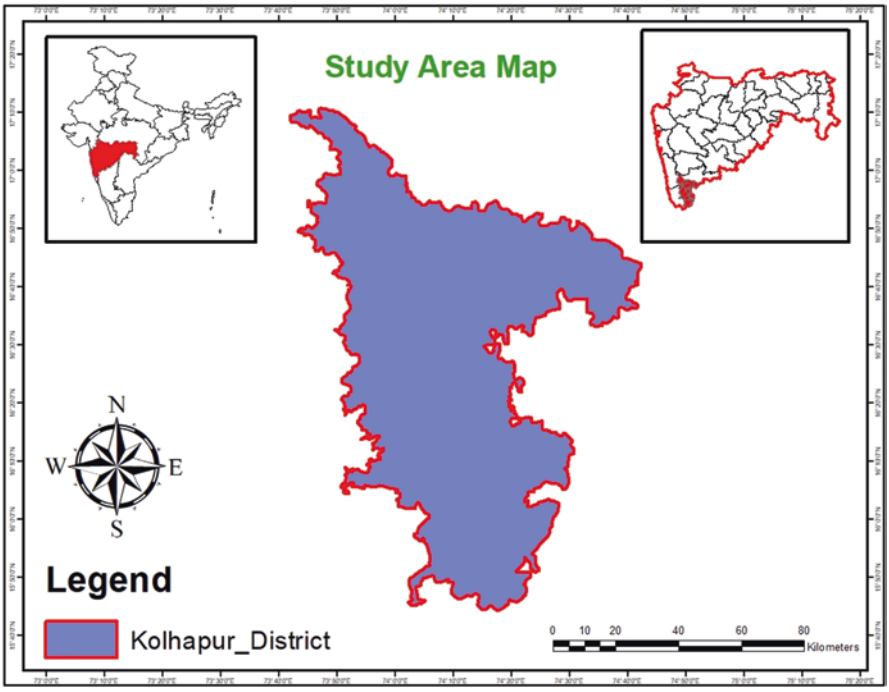

Fig. 20.1 Study area of the entire Kolhapur District

boundary between 16.5764° N and 74.1240° E with 7685 km^2. Chandgad is a coolest spot in Kolhapur area. Tambraparni waterway dam is a fabulous spot close to Umgaon town. Additionally, close by dams are Radhanagari and Kalambawadi. Kolhapur's atmosphere is a mix of beachfront and inland components normal of Maharashtra. The temperature has a moderately tight value between 10 °C and 35 °C. Kolhapur is nearly cooler in the summer period, yet significantly moister, than neighbouring inland urban areas. Most extreme temperatures infrequently surpass 40 °C and ordinarily extend somewhere between 33 °C and 35 °C. The Kolhapur gets plenteous precipitation from June to September because of its nearness towards at the Western Ghats. Years of 2005 and 2006 were floods happened.

Flood-Prone Area in Kolhapur District

Topography

The town of Kolhapur is located on the bank of the Panchganga River, which is a major Krishna River tributary. Kolhapur city's average altitude is 540.00 m on the riverbank and 560.00 m on the hilly part.

Flood-Prone Area

In the Kolhapur District, three main rivers, namely, Krishna, Warna and Panchganga, receive very high rainfall in the upper catchment. Almost all dams, including Radhanagari (automatic gates), usually release higher outflows during heavy rains. During very heavy inflows, in Kolhapur town, sections of tehsils, namely, Karvir, Panhala, Radhanagari, Hatkanangale, Shirol, Bhudargad, Gadhinglaj and Ajra, are typically flooded.

Data Used and Methodology

The purpose of phase-by-phase process of flood is to estimate the affected areas at local and regional scale. This research on flood risk analysis has used important data such as flood, elevation, built-up area and land use and cover map (Pande et al. 2018, 2021a, b). A flood scale change detection approach is established based on Sentinel-1 (SAR) data. Further datasets will be interrelated and visualised with the derived flood amount map to determine the number of potentially vulnerable residents and impacted cropland and urban areas. Google Earth Engine, a versatile web interface for cloud-based remote sensing analysis on a wide scale, is used in the

following step-by-step method (Rover et al. 2012; Kandekar et al. 2021; Srivastava and Chinnasamy 2021). The advantage lies predominantly in its computing speed (Gulhane et al. 2022). Several continuously updated datasets are supported by the platform that can be viewed directly inside the code editor. No raw imagery download is needed. Although it is free of charge, you need to trigger your Google account with the Google Earth Engine (Pande et al. 2022). Normally, an approval arrives in two or three working days (Kandekar et al. 2021).

Data Preparation/Pre-processing

Step 1

Option of Research Field

We will provide three separate techniques to determine the site of river area in the subsequent section. This knowledge is essential to restrict the complexity of the research and prevent repetitive measurements from being processed. The use of GEE feature set can be used to manually create the field of interest, upload geographical information out of a file, or import the country's borders.

Hand-Drawn Polygons

It is important to interactively establish boundaries. GEE is a shortest and simplest choice for discovering and checking the script entire various areas. In the upper-right corner of the map pane, the polygon tool can be triggered. Through left clicks, vertices are formed, and the polygon is finished by double-clicking. More than one polygon may consist of a geometry. When you are finished with background research regions, click 'Exit'. Geometry has described at the highest of the script under 'Imports'.

Shape File

The most accurate approach is to describe the spatial processing amount with a shape file (.shp). When investigating a very different research area, this is recommended (e.g. a watershed). In the top-left corner, start importing through the 'Assets'-tab. Select 'Upload the Table' from the 'New' drop-down menu, and select file. Careful: Create certain the .dbf and .shx files are still used, as shape file depends

on them. It regularly takes a little minute to transfer files. You will import the form into the script until the 'Asset ingestion' task is done (which turns blue). Click the 'Import' button under 'Assets' to list the table in the column for imports. Rename it to 'geometry' to make the script understand this new table.

In-Build Country Boundary Features

GEE gives small range of shapes, like big administrative constraints. However, if one attempts to do this analysis at the national level, if there is a sufficient dataset containing simpler features, there is an acceptable dataset.

Step 2

Time Frame and Sensor Parameter Selection

Besides the region of concern, in the first few lines of the code, the consumer is expected to identify pre- and post-flood times. The consumer allows appropriate tiles to cover the area of interest by setting intervals, not single dates. For each point on the globe, Sentinel-1 imagery is collected at least 12 days. To carry out the analysis, the operator should select amongst 'HV' and 'VV' polarisation. For flood mapping, 'HV' is commonly recommended because it is more resilient to changes on the surface of the Earth, whereas 'VV' is rather vulnerable to vertical structures and could be valuable for delineating open water from the surface of the land. To prevent false-positive signals which were generated by variations in viewing angle, it is important to choose the equal passway for the images to be associated when performing change detection. Depending on the study location, the user could select amongst the 'DESCENDING' and 'ASCENDING' permit paths. Increase 'Layers' in the top-right angle of the map viewer, and pick 'Before and After Flood' to verify if the region of interest is protected provided the chosen factors.

Step 3

Run the Script

Hit 'Run' all the factors which are chosen, and wait a little minute for results of study area to be shown.

Step 4

Visualise Results in GEE

Click the full-screen key to show flood product in the top-right angle viewer of the map. You can have checked or unchecked the maps you are involved in under 'Layers' and a screenshot of the map as a first summary.

Step 5

Export Products

Click 'Tasks' in the top-right angle of code editor to export the created items to your Google Drive account, hit 'RUN' and select where to save file. A GeoTIFF raster file was generated of the flood amount by 'Flood extent raster'. A shape file is flood extent vector, which may be useful for further research. A raster layer is used in the 'Exposed population', indicating the place and number of possible individuals exposed.

Processing Steps

The processing steps that are taken automatically while the Google Earth Engine script is running are discussed in this section.

Step 6

Data Filtering

The full Sentinel-1 GRD archive is filtered by instrument mode, polarisation, direction of passage and spatial resolution according to established parameters and trimmed to the region of interest's boundaries, which is called Image Collection in the Google Earth Engine. The ImageCollection filter's time intervals will be lowered.

Step 7

Preprocessing

- The following preprocessing processes have already been applied to data from Google Earth Engine's Sentinel-1 Level-1 Ground Range Detected (GRD) imagery:
- Apply-orbit-file.
- Removal of ARD boundary noise (which removes low-intensity noise and invalid data on the scene edges).
- Noise reduction due to thermal decrease (which removes additive noise in sub-swaths).
- Radiometry calibration (which estimates backscatter intensity by sensor calibration factors).
- Land correction (orthorectification).
- Conversion of the coefficient of backscatter (σ°) into decibels (dB).

The code of suggested exercise therefore only applies a softly filter to decrease the radar imagery's intrinsic speckle effect.

Step 8

Change Detection

In this script, the following flood mosaic is divided by the pre-flood mosaic, and a raster layer shows that the degree of change per pixel is used to detect a straightforward change. Big values show a high (luminous pixels) change; low values (dark pixels) shows a small change. A predetermined threshold of 1.25 is applied by assigning 1 to all values over 1.25 and 0 to all values below 1.25. The binary raster layer generated by this approach indicates the possible magnitude of the flood. By trial and error, the threshold of 1.25 was chosen and could be calibrated for high rates of false-positive or false-negative values.

Step 9

Refining the Flood Extent Layer

In order to remove false positives within flood extent map, multiple additional datasets are helpful. To obscure all areas that have been protected by water, Global Surface Water dataset is used. A digital elevation model by SRTM (Shuttle Radar Topography Mission) data. It is a spatial resolution of 3 arc-seconds which was selected to exclude areas with over 5% slope. In addition, to exclude those connected to eight or fewer neighbours, the jointed of the flood pixels is measured. This process minimises the noise of the flood scope product.

Assessment

Step 10

Area Calculation of Flood Extent

In order to measure the flood region, a new raster layer is formed, measuring the area in m2 for every pixel, enchanting into account the projection. The area knowledge is resulting and translated into hectares by summing up all the pixels. The outcome is shown in the map viewer's bottom-left corner in 'Results' column.

Step 11

Exposed Population Density

The code utilises global human settlement population map, which has a spatial resolution (250 m), to approximate the number of exposed individuals, which was previously revised in 2015. It provides details on the numeral of individuals residing in every cell. The flood extent raster must first be reprojected to the resolution and prediction of the population dataset in order to intersect the flood layer with the people layer. Next, a connection is measured and shown as a new raster layer between both layers. The pixel values of the showing population raster are summarised to determine the number of exposed individuals and presented in the 'Results' board on the map viewer.

Processing Platform

Google's open cloud framework for collecting and studying geoscience data is GEE (Gorelick et al., 2017). It supports web programming and an interactive display, and without downloading images, it can have procedure of satellite images available on the Internet. Its powerful computational ability facilitates remote sensing data analysis at the PB level, creating it ideal for big and long-term research sequences (Pekel et al., 2016; Kandekar et al. 2021). Furthermore, numerous greater image processing algorithms or models are consumed by GEE's rich API papers, which are friendly to individuals who concentrate on data processing rather than programming. The GEE GUI (graphical user interface) in Fig. 20.2 is shown.

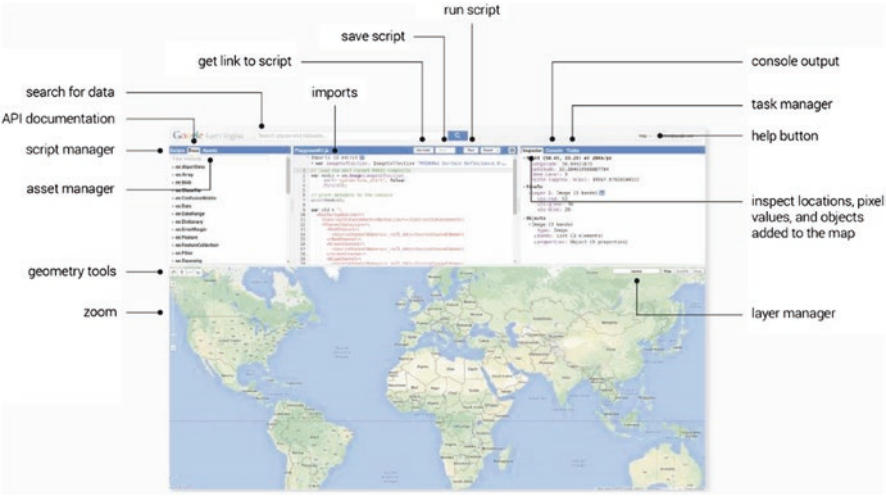

Fig. 20.2 Image showing Google Earth Engine platform

Methodology

The methodology adopted is described in Fig. 20.3. The Google Earth Platform makes satellite and population data very easy for disaster prevention and flood planning purposes. Since there have been so many floods in India for five years, many people face critical problems such as crop destruction, weak economy, increased death rate, etc. From that point of view, it is extremely easy to observe how many individuals in the Google Earth and machine learning algorithms have affected floods and damage assessments (Figs. 20.4 and 20.5). For a given year and period, Sentinel-2 data is first shown with code on the GEE platform. This image is also preprocessed for a minimum cloud coverage or cloud-free picture in GEE. After processing, the mosaic of many images was made. The water index NDWI (Normalised Difference Water Index) is calculated using a formula and is displayed in the GEE platform. It is called the Normalised Difference Water Index (Lai et al. 2019). This NDWI was then exported to a disc for a certain year using GEE java code and processed further with Arc GIS (Mcfeeters 1996; Tong et al. 2017). This raster database is further categorised to discover the real water distribution area of the dam and turned to a polygon with the Arc tool for area calculation.

Results and Discussion

Since they are widespread fiascos, floods leave disaster managers with a wide range of problems. The immediate goal during a disaster is that of human survival, and the framework is expected to have a crisis solution. Flooding can sweep away

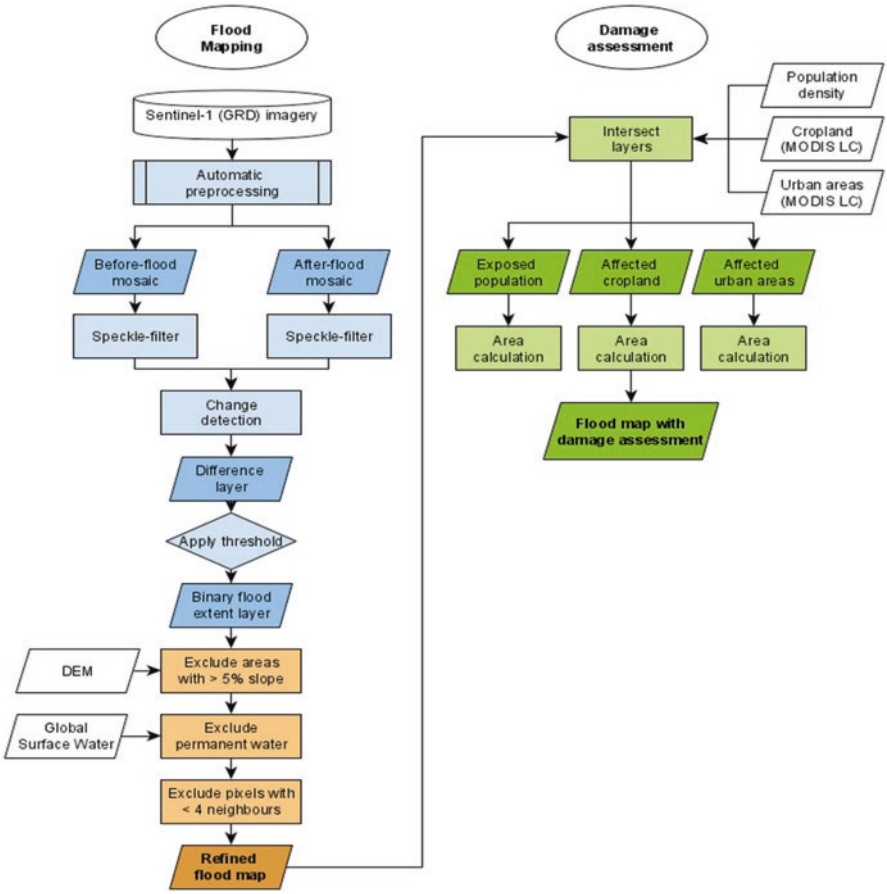

Fig. 20.3 Image showing Google Earth Engine platform

scaffolding and infrastructure, power frameworks can be devastated and bits of metropolitan centres or regional networks can even be isolated from callers that need to access them. Long-haul problems caused by massive floods focus on fundamental damage; nutrition is the most important problem regularly when harvests are crushed, and significant flood disasters suffocate domesticated animals. In general, the risk of flooding is measured using the Google Earth Engine as a function of probability and consequences. It is essential to provide comprehensive information on floods and flood zones to ensure sound planning and conservation of urban and rural land. It also provides the basic line information needed to help describe the phenomenon of floods. Luckily, this study would be valuable information to assess the damage caused by flood hazards. Planners and managers would have a significant advantage in overcoming the conflict between civilisation and the workings of the river system. It is challenging to penetrate optical sensors through clouds. It is therefore important to see an alternative way of addressing certain subjects.

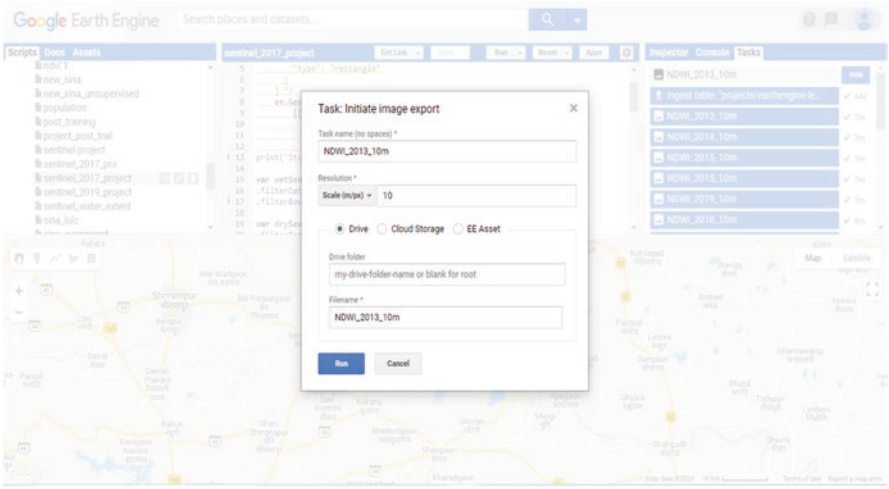

Fig. 20.4 Image showing Google Earth Engine platform

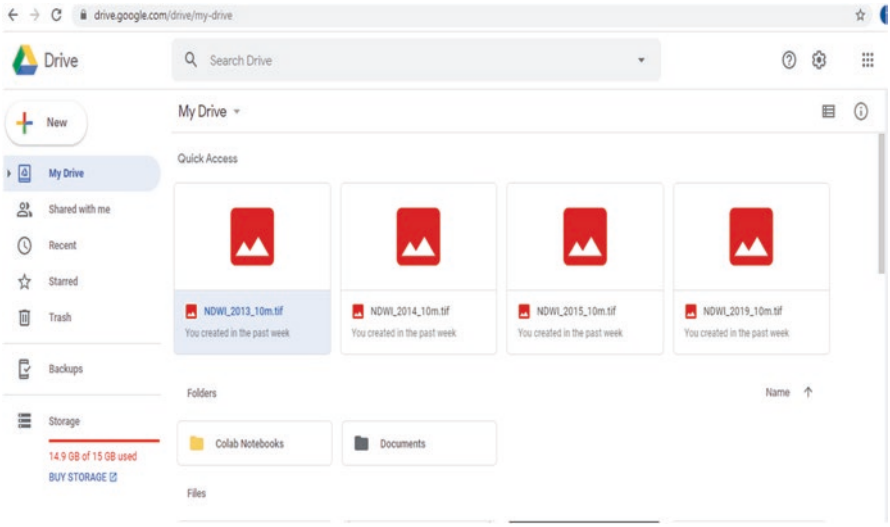

Fig. 20.5 Image showing Google Earth Engine platform

Synthetic aperture radar (SAR) is the most powerful sensor that can penetrate clouds and detect floods (Kandekar et al. 2021). In SAR, the smooth water shows the least backscattering values of the natural objects in the microwave field. The same backscattering range is available underwater for calm water and completely dissolved soil coverings. The RADARSAT image of 5 August 2019 has been used in order to create a flood inundation map. Geometrically and radiometrically, the RADARSAT image was rectified. For the picture, then, dB values were observed for land and

water. Water pixel threshold values range from 17 to 35 dB when the water pixel is removed from satellite data (Elbeltagi et al. 2022). The ERDAS modeller was used to create flood charts to delete the water pixel (Kandekar et al. 2021). The total population and population affected are defined in Table 20.1. Because of the aftereffects of the examination, we can presume that Earth observation and geospatial technologies give brief data to successful choices for exhaustive flood catastrophe of the executives for Kolhapur. Because of the prevalence of extreme climate conditions during flooding time, uninhibitedly accessible and routinely examined Sentinel-1 SAR Earth perception information has incredible potential in delivering flood data with high precision and high spatial resolution in a multi-day interim. The strategy depended on openly accessible gratis information, especially helpful for less created nations. Cloud-based calculation conditions, for example, the GEE platform, end up being especially significant for operational clients in arranging a flood-related crisis reaction and for understanding flood damage via land cover mapping (Wang et al. 2018a, b). Regular flood fiascos are normal and cannot be halted. Be that as it may, proficient instruments for flood immersion mapping and flood harm evaluation can be valuable for emergency response and disaster management.

Elevation Data Generation

The DEM (digital elevation model) research indicates that the area has a minimum and maximum elevation of 550 and 957 m. The vertical and horizontal precision of the DEM produced is approximately 6 and 3 m, respectively. The high gradient of

Table 20.1 Block-wise total populations and populations affected Taluka wise of Kolhapur District

Sr. no.	Taluka	Populations affected block-wise	Total population	Area (km^2)	Population density
1.	Chandgad	166,174	187,220	956.48	196
2.	Gadhinglaj	160,054	225,734	472.38	478
3.	Hatkanangle	642,071	807,751	612.57	1319
4.	Kagal	292,200	275,372	545.23	505
5.	Panhala	154,290	259,417	566.67	458
6.	Radhanagari	149,378	199,713	880.75	227
7.	Shahuwadi	138,633	185,661	1025.27	181
8.	Shirol	350,320	391,015	503.39	777
9.	Kolhapur	732,393	1,037,713	664.65	1561
10.	Ajra	104,210	120,265	543.96	221
11.	Gargoti	134,076	150,368	635.63	237
12.	Bavda	15,149	35,772	278.02	129

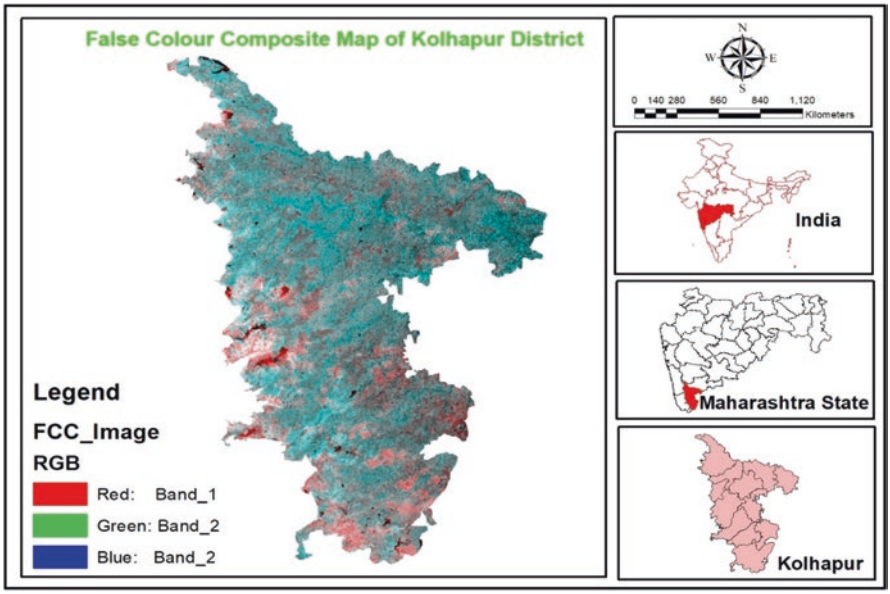

Fig. 20.6 False colour composite map of Kolhapur District

the northwest and southern portion of the catchment area is dominated by hills with rough topography, and the level surface is in the eastern part (Fig. 20.6).

Flood Inundation Maps Based on the Interpretation of RADARSAT-2 Satellite Data

While from 5 August 2019 onwards, all the banks of the Krishna, Warna, Panchganga and Dudhganga Rivers of the Sangli and Kolhapur Districts were flooded, there was still substantial flooding over large areas on 9 August 2019 (as seen in the flood map) and slowly receded until 15 August 2019.

Inundation on 9 August 2019

A total of 215 villages in nine Talukas, covering an area of 332.30 km^2 (21.20% of the area) in these villages, were affected in Kolhapur District.

Inundation on 13 August 2019

A total of 78 villages in four Talukas were affected in Kolhapur District, covering an area of 207.91 km^2 (24.47% of the area) in these villages.

Inundation on 15 August 2019

A total of 68 villages in four Talukas, covering an area of 133.59 km^2 (almost 19.28% of the area) in these villages, were affected in Kolhapur District. Due to the mixing of digital signatures of the metropolitan region with water spread and course resolution (+50–100 m) of RADARSAT-2, flooding in the town area of Kolhapur could not be obtained.

Encroachment/Blocking of Kolhapur City River and Tributaries

The Panchganga River surrounds Kolhapur, making an inverted 'U' form. Panchganga's Rajaram barrage has a river-gauging system. The study of the terrain indicates that the central portion of Kolhapur city is higher than the western, northern and eastern parts of the city. Much urbanisation has taken place in the western, northern and eastern parts of the town, where the landscape is almost flat and tributaries are deep. Such areas, especially in low-lying areas in the western, northern and eastern part of Kolhapur District, are observed at lower elevations than the high flood level of 2019. In the past ten years, these regions have been heavily urbanised.

Flood Vulnerability

Complete image of a wide variety of dam inflows. The stations in the above parts have been addressed in depth. Koyna, Dhom, Tarali, Kanher, Urmodi and Warna dams (Inundation) are located in the fragile catchment area above Sangli city, out of 10 dams. Similarly, some weak catchment areas in the Panchganga basin above Kolhapur Town are Tulsi, Kasari, Kumbhi and Radhanagari dams. The flood-affected area shown in Fig. 20.7 with block-wise flood-affected details is presented in Fig. 20.8. The flood-affected cropland and urban map are depicted in Fig. 20.9.

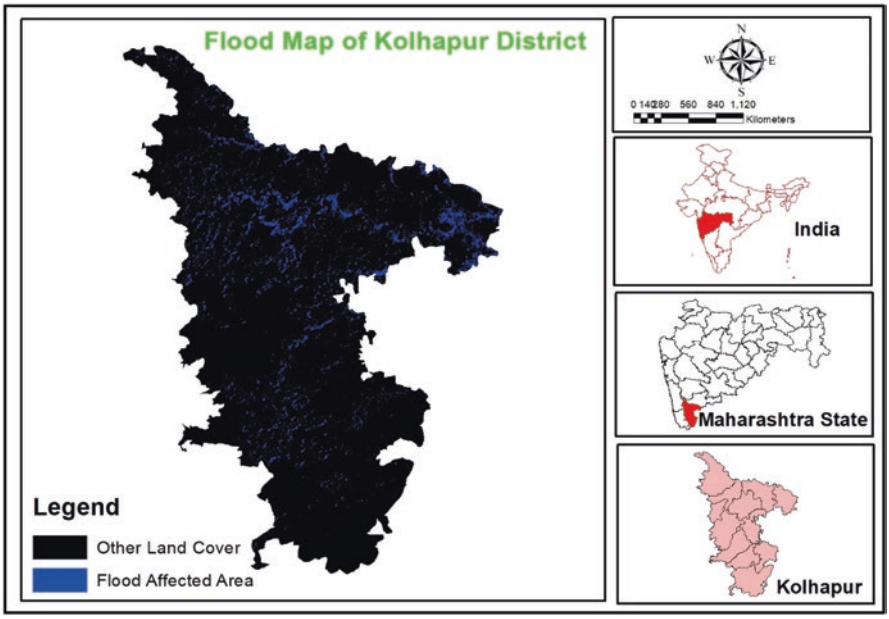

Fig. 20.7 Flood-affected area map of Kolhapur District during August 2019

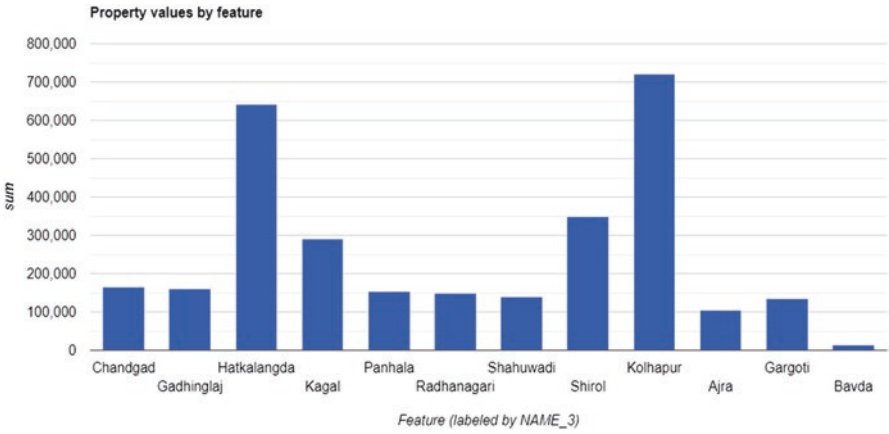

Fig. 20.8 GEE generated bar chart of population affected by Flood Taluka wise during 2019

Affected Cropland

The MODIS (Moderate Resolution Imaging Spectroradiometer) Land Cover Form product has been selected to approximate the amount of damaged cropland (Shahid et al. 2021; Pande et al. 2022). The dataset has a 500 m spatial resolution and is updated periodically. It is the only global ground cover dataset accessible on Google

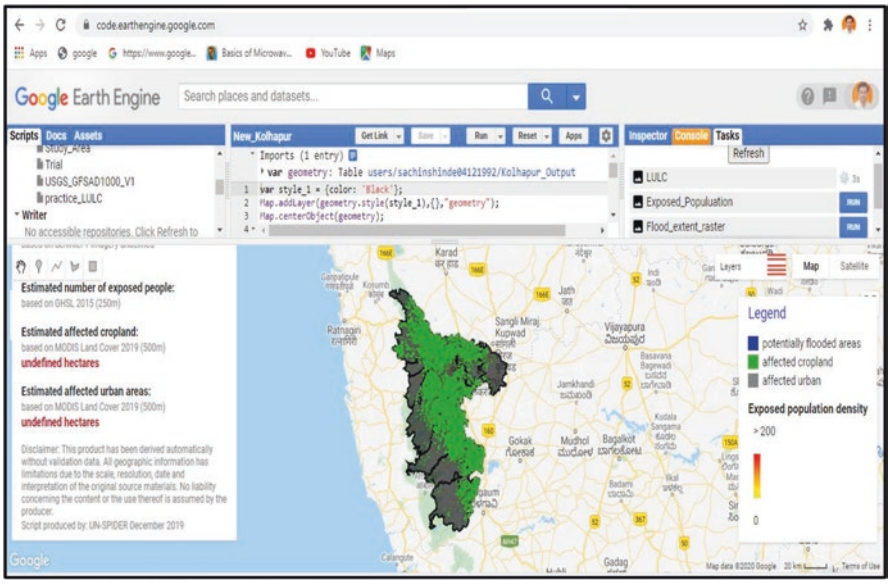

Fig. 20.9 Flood-affected cropland and urban map of Taluka wise during 2019

Earth Engine. The Type 1 band of the land cover consists of 17 classes with 2 classes of cropland (Class 12, at least 60% of the field under cultivation, and Class 14, cropland/natural vegetation mosaics, 40–60% small-scale cultivation of natural forest, shrub, or herbaceous vegetation). Both groups are removed from the dataset and intersected with the layer of flood magnitude, which was resampled to the MODIS layer scale and prediction (Fig. 20.9).

Affected Urban Areas

Using the MODIS Land Cover Style dataset, impacted urban areas are measured the same as the prior two phases. In order to determine currently impacted metropolitan areas, 'Urban Class 13' of band 'Land Cover Form 1' is extracted. Due to the complexities of water detection in build-up environments, affected urban areas are very likely to be underestimated in this process. For more info, see strengths and weaknesses.

Conclusions

For the study of climate change, the shift in surface water supplies will be fundamental. Surface water changes produced by human activities significantly affect surface temperature, soil humidity, biodiversity, the working of the ecosystem and even human well-being. Surface water monitoring is essential for health and sustainable economic development, as is the natural environment as a cloud platform for the processing and analysis of geoscience data. GEE is Google's open cloud platform for the processing and analysis of geoscience data. It offers interactive online programming and display and can handle remote data without downloading images online. Due to its high interaction capacity and computing performance, GEE reduces picture download time and significantly shores the work cycle, allowing remote sensing science to examine more than the waste in the repeated processing system. Thanks to the GEE support for remote sensing image processing, vector information on the body of water can easily and rapidly be obtained, which provides the basis for additional hydrological element removal. A change in the surface or dam of the reservoir can effectively reflect a change in the amount of water. Analysis of their changing characteristics will assist in monitoring changes in the amount of water and make scientific judgements easier for the relevant departments.

Acknowledgements We are grateful to the Principal Investigator, Center for Advance Agriculture Science and Technology on Climate-Smart Agriculture and Water Management, MPKV (Mahatma Phule Krishi Vidyapeeth), Rahuri (Agricultural University) and ICAR (Indian Council for Agricultural Research), NAHEP (National Agricultural Higher Education Project) and World Bank for providing the necessary facilities for conducting this research and the Chhatrapati Shahu Maharaj Research Training and Human Development Institute (SARTHI), Pune, for the support for financial for this research.

References

Elbeltagi A, Kumar M, Kushwaha NL et al (2022) Drought indicator analysis and forecasting using data driven models: case study in Jaisalmer. Stoch Environ Res Risk Assess, India. https://doi.org/10.1007/s00477-022-02277-0

Elbeltagi A, Pande CB, Kouadri S et al (2022) Applications of various data-driven models for the prediction of groundwater quality index in the Akot basin, Maharashtra, India. Environ Sci Pollut Res 29:17591–17605. https://doi.org/10.1007/s11356-021-17064-7

Feyisa GL, Meilby H, Fensholt R, Proud SR (2014) Automated water extraction index: a new technique for surface water mapping using Landsat imagery. Remote Sens Environ 140:23–35

Gorelick N et al (2017) Google Earth Engine: planetary-scale geospatial analysis for everyone. Remote Sens Environ 202:18–27

Gulhane VA, Rode SV et al (2022) Correlation analysis of soil nutrients and prediction model through ISO cluster unsupervised classification with multispectral data. Multimed Tools Appl. https://doi.org/10.1007/s11042-022-13276-2

Han BP (2010) Reservoir ecology and limnology in China: a retrospective comment. J Lake Sci 22(2):151–160

Huang Q et al (2018) Discharge estimation in high-mountain regions with improved methods using multisource remote sensing: a case study of the Upper Brahmaputra River. Remote Sens Environ 219:115–134

Ji HX, Fan XW, Wu GP, Liu YB (2015) Accuracy comparison and analysis of methods for water area extraction of discrete lakes. J Lake Sci 27(02):327–334

Jiang L, Nielsen K, Andersen OB, Bauer-Gottwein P (2017) Monitoring recent lake level variations on the Tibetan Plateau using CryoSat-2 SARIn mode data. J Hydrol 544:109–124

Kandekar VU, Pande CB, Rajesh J, Atre AA, Gorantiwar SD, Gavit SAKB (2021) Surface water dynamics analysis based on sentinel imagery and Google Earth Engine platform: a case study of Jayakwadi dam. Sustain Water Resour Manag 7:44. https://doi.org/10.1007/s40899-021-00527-7

Lai Y, Zhang J, Song Y, Cao Y (2019) Comparative analysis of different methods for extracting water body area of Miyun Reservoir and driving forces for nearly 40 years. J Indian Soc Remote Sens 48:451

Lin QQ, Han BP (2001) Reservoir limnology and its application in water quality management: an overview. Acta Ecol Sin 21(06):1034–1040

Mcfeeters SK (1996) The use of the normalized difference water index (NDWI) in the delineation of open water features. Int J Remote Sens 17(7):1425–1432

Mei Y, Chang CC, Dong Z, Wei L (2016) Stream, lake, and reservoir management. Water Environ Res 88(10):1533–1563

Orimoloye IR, Olusola AO, Belle JA et al (2022) Drought disaster monitoring and land use dynamics: identification of drought drivers using regression-based algorithms. Nat Hazards 112:1085–1106. https://doi.org/10.1007/s11069-022-05219-9

Pande (2022) Land use/land cover and change detection mapping in Rahuri watershed area (MS), India using the google earth engine and machine learning approach. Geocarto Int. https://doi.org/10.1080/10106049.2022.2086622

Pande CB, Moharir KN, Khadri SFR et al (2018) Study of land use classification in an arid region using multispectral satellite images. Appl Water Sci 8:123. https://doi.org/10.1007/s13201-018-0764-0

Pande CB, Moharir KN, Singh SK, Varade AM, Ahmed E, Khadri SFR, Choudhari P (2021a) Estimation of crop and forest biomass resources in a semi-arid region using satellite data and GIS. J Saudi Soc Agric Sci 20(5):302–311

Pande CB, Moharir KN, Khadri SFR (2021b) Assessment of land-use and land-cover changes in Pangari watershed area (MS), India, based on the remote sensing and GIS techniques. Appl Water Sci 11:96. https://doi.org/10.1007/s13201-021-01425-1

Pande CB, Kadam SA, Jayaraman R, Gorantiwar S, Shinde M (2022) Prediction of soil chemical properties using multispectral satellite images and wavelet transforms methods. J Saudi Soc Agric Sci 21(1):21–28

Pekel J, Cottam A, Gorelick N, Belward AS (2016) High-resolution mapping of global surface water and its long-term changes. Nature 540(7633):418

Rokni K, Ahmad A, Selamat A, Hazini S (2014) Water feature extraction and change detection using multitemporal landsat imagery. Remote Sens 6(5):4173–4189

Rover J, Ji L, Wylie BK, Tieszen LL (2012) Establishing water body areal extent trends in interior Alaska from multitemporal landsat data. Remote Sens Lett 3(7):595–604

Shahid M, Rahman KU, Haider S et al (2021) Quantitative assessment of regional land use and climate change impact on runoff across Gilgit watershed. Environ Earth Sci 80:743. https://doi.org/10.1007/s12665-021-10032-x

Srivastava A, Chinnasamy P (2021) Developing village-level water management plans against extreme climatic events in Maharashtra (India)—a case study approach. In: Vaseashta A, Maftei C (eds) Water safety, security and sustainability, Advanced sciences and technologies for security applications. Springer, Cham. https://doi.org/10.1007/978-3-030-76008-3_27

Tong LX, Yan Q, Luo CF, Du YK (2017) Water body information extraction based on NDWI segmentation and object oriented method. Geospat Inf 15(05):57–59

Wang C, Jia M, Chen N, Wang W (2018a) Long-term surface water dynamics analysis based on Landsat imagery and the Google Earth Engine platform: a case study in the middle Yangtze River Basin. Remote Sens J 10(10):1635

Wang X et al (2018b) A robust multi-band water index (MBWI) for automated extraction of surface water from Landsat 8 OLI imagery. Int J Appl Earth Obs Geoinf 68:73–91

Xu RG, Qiao G, Wu YJ, Cao YJ (2019) Extraction of rivers and lakes on Tibetan Plateau based on Google Earth Engine. The international archives of the photogrammetry, remote sensing and spatial information sciences, vol XLII-2/W13

Zhang YF, Ai HB, Du QY, Zhang L (2014) Application of water extraction algorithm based on pyramid image segmentation in automatic aerial triangulation for island and reef. Bull Surv Map 12:70–73

Chapter 21
Application of Hyperspectral Remote Sensing Role in Precision Farming and Sustainable Agriculture Under Climate Change: A Review

Chaitanya B. Pande and Kanak N. Moharir

Abstract Each year, scholars, agronomists, scientists, and engineers have implemented several technologies to improve low-cost agricultural production, but this has detrimental environmental impacts. Precision agriculture deals with the study of the use of hyperspectral remote sensing (RS) and other technologies to boost cultivation as opposed to traditional farming methods which reduce harmful environmental consequences. Hyperspectral remote sensing technology plays a significant role in agricultural precision and agricultural growth, with its use in precision agriculture providing different ways to enhance agricultural practices. The idea of precision farming has attracted significant interest from farmers and scholars in the entire globe. The decision-making method includes making the best management choices based on the knowledge on uncertainty obtained from evidence gathered in the sector. The hyperspectral remote sensing and the various field data such as slope, dimension of plant indices, soil nutrients, crop quality, and yield can be calculated. This analysis illustrates hyperspectral remote sensing technologies, GIS, RGB, and multispectral, thermal imagery and gives you an understanding of how accurate farming and agricultural development can be useful.

Keywords Remote sensing · RGB · Hyperspectral remote sensing · precision farming · GIS

C. B. Pande (✉)
Indian Institute of Tropical Meteorology (IITM), Pune, Maharashtra, India
e-mail: chaitanay45@gmail.com

K. N. Moharir
Department of Earth Science, Banasthali University, Aliyabad, Rajasthan, India

C. B. Pande et al. (eds.), *Climate Change Impacts on Natural Resources, Ecosystems and Agricultural Systems*, Springer Climate,
https://doi.org/10.1007/978-3-031-19059-9_21

Introduction

Hyperspectral Remote Sensing: A Major Role in the Precision Farming

Hyperspectral remote sensing can provide the exact and timely knowledge needed to establish preparation for the growth of agriculture and precision farming (FICCI 2012; Gowrisankar and Adiga 2001; Rock et al. 1986; Tucker 1979; Elbeltagi et al. 2022). This is precisely a planned instrument that can provide full images of hundreds of small spectral bands of observed objects. The extractable spectral signatures from the hyperspectral picture cube are utilized to categorize or identify artifacts inside the area being displayed (Agro-Informatics 2001; Aziz et al. 2008; Bairagi and Hassan 2002; Bingfng and Chenglin 2000; Burrough and McDonnell 1998). Hyperspectral imaging detectors usually absorb light in the spectrum of 400–2500 nm, spanning the frequency bands of the visible, near-infrared (NIR), and short-wave infrared (SWIR), though multispectral details were collected over fairly narrow spectral bands (< 20 nm) (Gulhane et al. 2022). Spaceborne systems appear to have weaker spatial resolution (30–150 m) relative to their equivalents in the soil (35 cm–4 m) (Thenkabail et al. 2012; Pande et al. 2022). One significant use of hyperspectral imaging technology is that of agriculture and in particular of agricultural precision and development of agriculture. Precision farming may mostly be described as the use of observations to maximize resource use and management of farming practices. Usually, a global navigation system has combined with geographic information systems (GIS) readings, and satellite data and UAV (unnamed aerial vehicles) have used to track agricultural crops on a regular basis, control and schedule resource use, and make decisions on farming activities. An illustration of a hyperspectral sensor has been used to classify crop varieties, pests, and diseases and estimate crop yields and water stress on crops, with soil characteristics such as shape, composition, physical characteristics, humidity, and nutrient rates (Goetz et al. 1985). This chapter is an overview of the technology and usage of hyperspectral remote sensing imagers, GIS, and remote sensing functions in the growth and management of agricultural production (Doad et al. 2022; Pande 2022). This would be a stupendous undertaking and a daunting obstacle for space and agricultural scientists alike, all of whom are actually positioned distant from Indian farming's ground reality. Nevertheless, alongside the financial capital available, the pace of these transitions depends largely on the degree of engagement of leaders, administrators, technocrats, and scientists. Indian agriculture is called as for providing fruit, work, livelihood, and nutritional and ecological securities with multifunctionalities (Pande et al. 2021a).

Hyperspectral Sensors and Data Processing

Hyperspectral sensors, also known as optical spectrometers, constitute the next phase of spectral imaging beyond multispectral imaging radiometers, providing existing spatial examples such as LANDSAT, Location, IKONOS, and WorldView. Spectral photography requires collecting numerous photographs over several bands of wavelengths. The data were calibrated in such a manner that all defined wavelengths include details for increasing spatial position or pixel. Thus, hyperspectral artifacts are simply a tridimensional data cube (Fig. 21.1). The importance of hyperspectral sensing resides in its capacity to collect knowledge about the spatial and spectral features of the Earth that were reproduced on the transmitted signal through contact with the Earth, which can be used to decipher a multitude of properties regarding the artifacts being studied. The difference in reflectance and wavelength at each pixel, for example, thus generates a distinctive spectral signature which can be used to differentiate artifacts observed.

Understanding Various Imageries

Different types of imaging such as color, thermal, multispectral, and hyperspectral can provide unique applications in precision agriculture (Fig. 21.2).

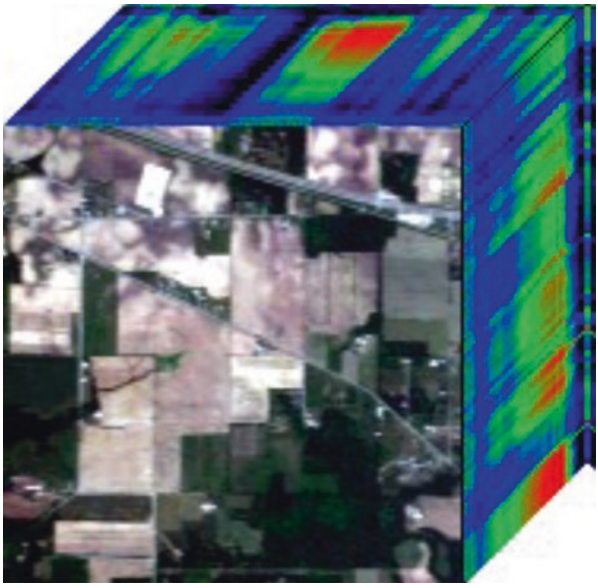

Fig. 21.1 Hyperspectral image cube

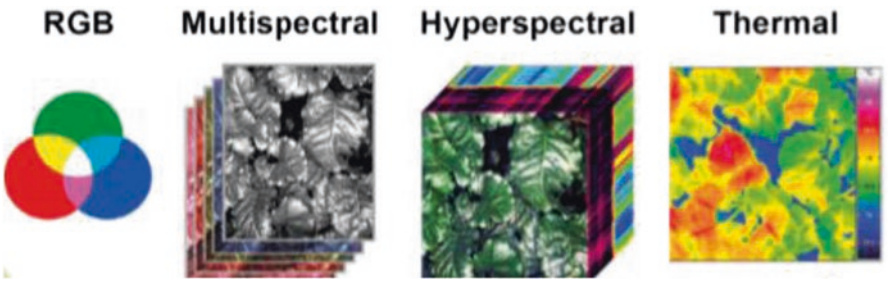

Fig. 21.2 Different types of imaging

Fig. 21.3 RGB image. (Source: Corn crop filed was captured by the Phantom 4 UAV-NDSU Research Center. (Carrington 2016))

RGB Imagery

In agronomy crop fields, color or RGB (red, green, blue) images are essential for recognizing disease indications, fertilizer shortages, damaged plants, and different weeds and plant species. For RGB pictures, the color of an object is the outcome of the light reflected from the source and its optical properties and human vision. For cultivation, RGB-based picture processing has proven useful for weed identification and field visualization, vector physiological procedures around the surface of the plants, plant height, and plant stand counting. The numerous vegetation indices (VIs) and water stress can be calculated using RGB image. The RGB picture representation is shown in Fig. 21.3.

Thermal Imagery

Thermal imaging is based on the assumption that objects release infrared (heat) energy as a function of their temperature. The warmer objects usually produce more radiation than the colder objects. Thermal cameras are essentially heat sensors that measure changes in temperature of objects. The thermal infrared camera detects radiation in the electromagnetic spectrum infrared range (800–1400 nm) and is

shown as a false color image (Grant et al. 2016). Within a thermal imaging, every pixel has a single temperature point. Thermal imaging may help track the temperatures of plants and soil over a region. Thermal imaging may help track the temperatures of plants and soil over a region. Symptoms of plant disease, water-stressed plants, and infestations of pests may all induce higher temperatures for the canopy or plant surface (Elarab et al. 2015). Farmers may use thermal imaging to track disease outbreak cycles or infestation of the insect and soil moisture in crop fields and shelter from rainout. The thermal imaging illustration is seen in Fig. 21.4.

Multispectral Imagery

Multispectral pictures consist of spectral source details in specific wavebands of spectra. Multispectral sensors typically note spectral details in the electromagnetic spectrum in red, green, and blue, as well as the violet edge and near-infrared wave ranges. From multispectral imaging, vegetation indices like the uniform normalized difference vegetation index (NDVI), SAVI (soil-adjusted vegetation index), and GCVI (green chlorophyll vegetation index) and band ratio are two important techniques for multispectral image processing (Pande et al. 2021b). Such techniques can be utilized to track crop safety, plant pests, crop damage after spraying of herbicides, and signs of diseases. Images of two forms are shown in Fig. 21.5.

Hyperspectral Imagery (Sensor)

Hyperspectral cameras assess spectral reflectance of plants in the parts of the electromagnetic spectrum visible, near-infrared, and mid-infrared (350–2500 nm) in 5–10 nm wavelengths. Spectral reflectance at the canopy or single leaf scale of

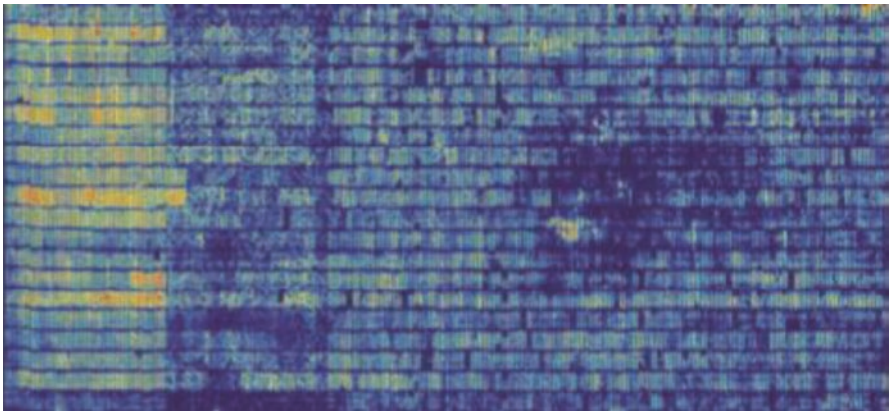

Fig. 21.4 Heat map of local leaf density

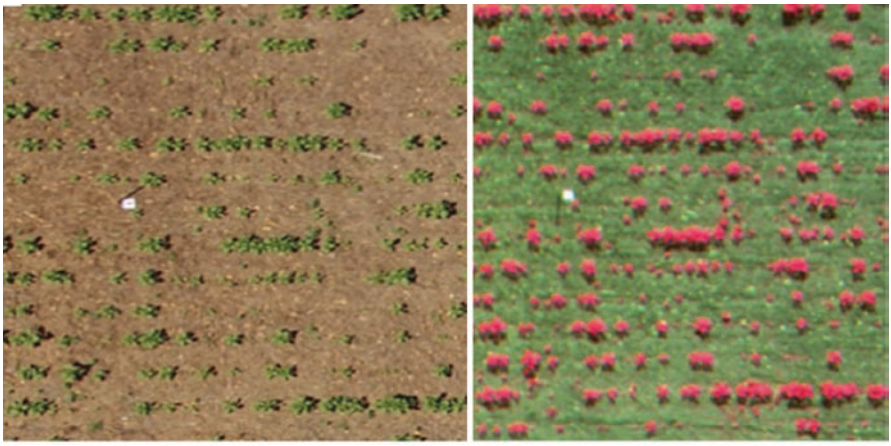

Fig. 21.5 UAV images collected by the two cameras: (**a**) RGB camera and (**b**) multispectral camera

individual plant species is special and is stated as a spectral signature. Spectral reflectance calculations may be the capacity of remote spectral data to categorize weeds and crops and to classify indicators of crop and horticultural diseases. Light absorption by plant pigments, plant composition, and leaf chemistry establishes special spectral signatures that are useful for tracking crop conditions in agronomy. Hyperspectral picture plays a significant role in climate change, food health, soil selection, calculation of crop yields, and water tension (Yu et al. 2017). There are actually two groups of hyperspectral sensors or satellite systems required for selection functions such as ground-based and airborne. Hyperion, Airborne Visible/Infrared Imaging Spectrometer (AVIRIS), and Portable Airborne Spectrographic Imager (CASI) are spacecraft with hyperspectral sensors. The illustrations of disease detection through a hyperspectral picture of the leaf are shown in Figs. 21.6 and 21.7.

Hyperspectral Vegetation Indices

With the advent of hyperspectral data, vegetation indices have been developed specifically for hyperspectral data:

1. Discrete-band normalized difference vegetation index
2. Yellowness index
3. Photochemical reflectance index
4. Discrete-band normalized difference water index
5. Red-edge position determination
6. Crop chlorophyll content prediction
7. Moment distance index (MDI)

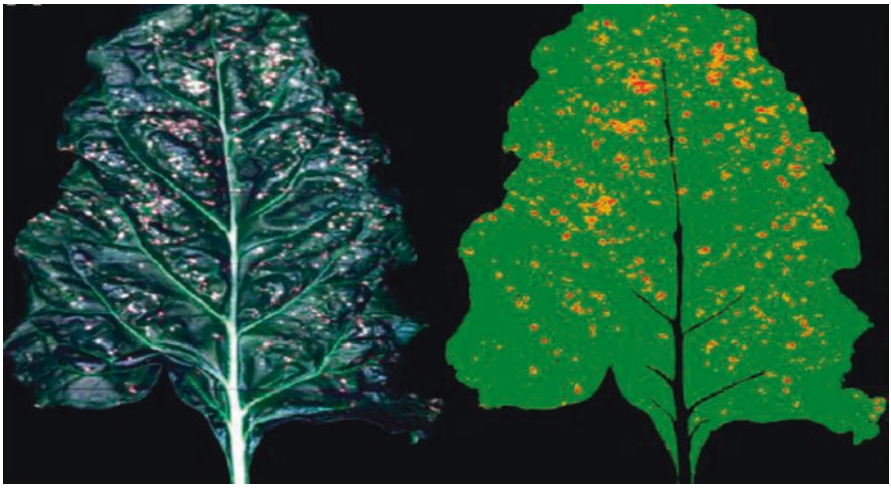

Fig. 21.6 Disease detection of fungal plant diseases based on hyperspectral images on sugar beet

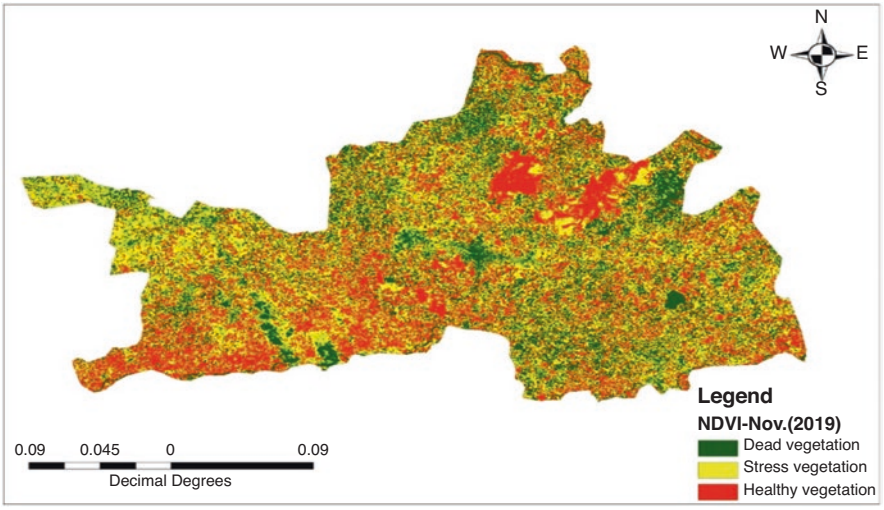

Fig. 21.7 Vegetation health detection by satellite data

Hyperspectral Remote Sensing Importance and Spectral Data Uses

Within this paper, different correct details relate to the present situation of remote sensing and advanced remote sensing, geographical information system (GIS), and agricultural Indian cameras and sensors. These techniques may be used to predict crop yield tracking, field acreage, and output prediction using detailed farming

technology activities. Their prospects and threats have been addressed as follows. Today's "Space Age" has continued to give tremendous possibilities for well-organized preparation, production, and control of agricultural tools on science concepts through machine and networking technology (Bajcsy and Groves 2004). The past hyperspectral remote sensing data has deemed vulnerable and used mainly for defense purposes, but currently, hyperspectral data is more important for the mapping of effective cultivation, growth of agriculture, urban planning, land usage, soil and natural resource properties, and sustainable farming in India. However, space scientists and researchers are now able to exchange data on the hyperspectral satellite and various image processing sensors for precession farming and agricultural development in India but on a high-cost basis. Application of agricultural smart technology in agricultural resource management is increasing due to exponential steps in ground-based sensors and spaceborne remote sensing satellites in the context of geographical, temporal, spectral, and radiometric resolutions (Govender et al. 2007). Using RS and GIS tools, many of the traditional methods to execute multi-theme knowledge to achieve maximal strategies are computerized. Precision cultivation has limited to developing countries (Bannari et al. 2006). Land tenure scheme smaller farm size (< 1 ha) and crop variety restrict India's potential for precision agriculture. However, in irrigated areas/commercial crops/fruit and vegetable crops/high-value crops, there is a broad possibility for precision farming. It is evident from the above that there is a wonderful potential for the use of hyperspectral remote sensing, GIS, and precision farming techniques in the creation of a natural resource database and farm-level decision support systems (< 1 ha).

Spectral Signatures

Remote sensing can identify interactions between the reflected, ingested, and distributed electricity. The changes in the colors of the leaves, materials, forms, or just how the leaves are bound to the plants decide how much energy can be transmitted, stored, or transferred. To establish spectral signatures of separate plants, the interaction between reflected, absorbed, and transmitted energies is employed. Spectral signatures are special to certain types of plants. Remote sensing is utilized by first starting spectral signatures of healthy plants to distinguish stressed areas in farm area. Stressed plant spectral signatures appear to be changed from those of good plant. The spectral signatures of balanced and stressed sugar beets are contrasted in Fig. 21.3. Stressed sugar beets in the visible portion of the spectrum have a higher reflectance intensity from 400 to 700 nm of stressed sugar beets; this trend is changed in the non-visible range of about 750–1200 nm. Within the higher reflectance spectrum from around 1300–2400 nm, the apparent pattern is replicated (Fig. 21.8). Interpreting the reflectance values at specific energy wavelengths can be used to determine crop health (Clark 1999).

Fig. 21.8 Handheld SVC (scalable video coding)-spectroradiometer instruments

Deficit irrigation is the practice of irrigation of crops deliberately below their water requirements. Such practice is aimed at minimizing water applied to the crop to maximize crop yield per unit of water applied. The NDVI values of wheat crop were determined from spectral reflectance data by spectroradiometer during crop growth stages at a suitable interval.

There are several indices of vegetation (VIs), all of which are functionally similar. The inverse association between red and near-infrared reflectance correlated with good green plants has included in many of the indices (Maresma et al. 2016). Scientists have been utilizing remote satellite sensing since the 1960s to track changes of plants at the surface of the Earth. Measurements of plant characteristics include index of leaf area (LAI), percentage of green cover, chlorophyll quality, green biomass, and absorbed photosynthetically active radiation (APAR) absorption (Perry et al. 2018). The analysis of reflectance ranges at numerous wavelengths is widely utilized to measure plant vigor, known as vegetative measure. The common vegetative index is uniform vegetative difference index (NDVI). NDVI measures the electromagnetic spectrum reflectance values for the red and NIR zones. The NDVI meaning for growing region on an image helps to distinguish areas inside fields of differing amounts of plant vigor. Drone images have estimated the various indices for used of precision farming and water management (Fig. 21.9).

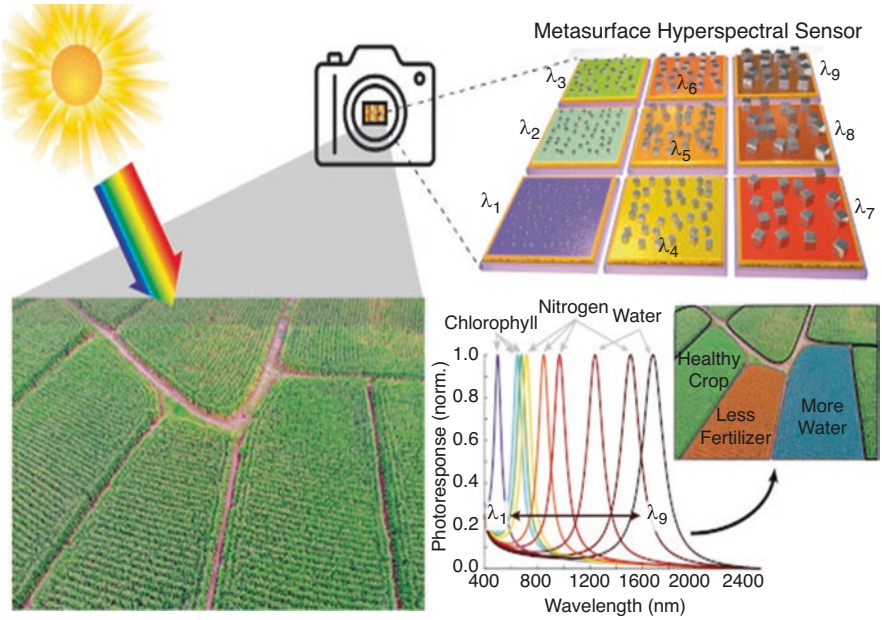

Fig. 21.9 Hyperspectral remote sensing showing field view of agriculture field

Uses of Vegetation Indices Have Been Used to Precision Farming

Important vegetation indices can be used for precision farming (Fig. 21.9):

- Examine climate trends.
- Estimate water content of soils remotely. Monitor drought. Schedule crop irrigation. Improve crop management. Monitor evaporation and plant transpiration. Assess changes in biodiversity (Kandekar 2021).
- Classify vegetation.

Hyperspectral Remote Sensing in Agriculture: Present Scenario

Remote sensing techniques play a crucial role in the identification of crops in agriculture, in the evaluation of acreage and productivity, in the finding of diseases and stress, in the characterization of soil and water supplies, and also in providing the required inputs for the following: planning of watershed growth plans, cultivation of additional land using thematic mapping and recovery of wastelands, and increase of irrigation (Pande et al. 2020, 2021a; 2022). Hyperspectral remote sensing

Table 21.1 Current and recent hyperspectral sensors and data providers

Satellite sensors	Manufacturer	Number of bands	Spectral range in μm
FTHSI on MightySat II	Air Force Research Laboratory	256	0.35–1.05
Hyperion on EO-1	NASA Goddard Space Flight Center	220	0.4–2.5
Airborne sensors	Manufacturer	Number of bands	Spectral range
AVIRIS	NASA Jet Propulsion Lab	224	0.4–2.4
HYDICE	Naval Research Lab	210	0.4–2.5
PROBE-1	Earth Search Sciences Inc.	128	0.4–2.5
CASI	ITRES Research Limited	228	0.4–1.0
HyMap 00 to 200 visible to thermal infrared	Integrated Spectronics	100–200	Visible to thermal infrared
AISA	Spectral Imaging	Up to 288	0.43–1.0 um

technologies (Table 21.1) in agriculture have evolved to a point where these observations are being used throughout the country for a range of policy-level decisions related to food protection, scarcity mitigation, and sustainable growth (Zhang et al. 2002). Decision on buffer stocks of food grains may be focused on preharvest crop acreage and estimation of growth, whereas maps of groundwater prospects act as the key source of knowledge for confirming drinking water and other requirements in rainfed and less-favored regions (Mulla 2013; Elbeltagi et al. 2022a; Kouadri et al. 2022). State desert, land usage, ground cover, and soil analysis have led to the extension and intensification of agricultural practices and to the definition of ground efficiency groups and crop adaptability indices (Fig. 21.9).

Crop Acreage and Production Estimation

The usage of spaceborne remote sensing data for crop acreage calculation and output forecasts in selected districts for wheat, rice, and groundnut was tested in India in the early 1980s. The positive and inspiring findings of this initial study led to a 1985–1986 attempt to estimate wheat acreage at state level using LANDSAT MSS data for Haryana and Punjab. The findings were encouraging, and the program, called 'Crop Acreage and Development Forecast' (CAPE), was launched in selected major rising states/districts covering wheat, rice, groundnut, and rabi sorghum. As the quality of optical data is a problem in monsoon seasons, the usage of data from active sensors, such as RADARSAT SAR, has been operationally used in 12 districts of Karnataka for kharif rice. Microwave results, which have all the weather capabilities, have displayed that the rice crop can be discriminated against at greater than 90% precision, which can help with numerous forecasting in early detection. In addition to using high-resolution single-date satellite images to give district-level

crop acreage predictions under CAPE, multi-date WiFS data (coarse resolution and strong receptivity) is utilized to understand the possibility of national-level forecasts. The Department of Agriculture and Cooperation is setting up a National Crop Forecasting Center, Government of India, to carry out the project. (As remote sensing, weather, and field observation provide complementary and supplementary crop forecasting knowledge, FASAL (Forecasting Agricultural output using Space, Agro-meteorology and Land-based observations) suggests a method that incorporates the three forms of observation into the pulses to allow forecasts of required range, precision, and timeliness.) The FASAL's definition, therefore, enhances the latest early crop season forecasting capacities from econometric and weather-based approaches with mid-season remote sensing evaluations that can be integrated with the data-based multi-temporal coarse resolution research. Direct contribution of remote sensing in the form of acreage projections and yield predictions is possible throughout the time after half of crop growth phase. However, incorporating more detailed field knowledge and forecast measurements will also improve the predictive quality in this scenario, too. India is also preparing to provide agricultural-specific data for some unique satellites (Fig. 21.10).

Fig. 21.10 Cropping pattern map

Quantifying Soil Property Variability

Hyperspectral imaging may be used to measure the soil electrical conductivity (ECa) and soil fertility rates. The data collected have been transformed to reflectance with the help of chemically modified reference tarps with eight identified rates of reflectance (Pande et al. 2022). Through a rubber sheeting process, dimensional irregularities of the push broom sensor images are rectified. Statistical analyses, including basic correlations, multiple regressions, and PCA (Principal Component Analysis), were utilized to link HSI data and LANDSAT-like bands to soil properties measured in the field (Naveen et al. 2014; Pande et al. 2022).

Weed Detection

Usually it is patchy, so UAVs have a better direction to map weeds so enabling site-specific weed control (SSWM). There are double distinct methods to identify UAV weeds. Next, spectral discrimination begins from observable shifts in the spectrum of weeds and crop plants and has a long tradition of remote sensing in non-UAV (López-Granados 2011). In UAV applications, if the weed's spectral signal varies from that of the crops, supervised classification methods may be effective, also with (modified) RGB cameras (Alexandridis et al. 2017), and permit the making of prescription maps for herbicide spraying (Castaldi et al. 2017). Nevertheless, controlled instruction is time-consuming and not necessarily promised results (Lambert et al. 2018).

Classification of Agricultural Crops

Traditionally, mapping the vegetation of a whole field involves time-intensive field surveys; however, with hyperspectral remote sensing images, particularly hyperspectral data, the classification and mapping of vegetation can be calculated with further precision farming in less time in a more cost-effective way (Govender et al. 2007). Several experiments (Dalponte et al. 2009) indicate that the precision of the sorting of agricultural crops obtained from hyperspectral narrowband data is significantly higher than that achieved with multispectral data. Hyperspectral data will be composed before seeding and during planting and harvesting to detect improvements within the region. Data collection prior to seeding offers details on soil quality, soil fertility, and soil physical properties – texture, density, mechanical intensity, moisture content, organic soil chemical properties, salinity, and water-holding capability required for soil plants (Bannari et al. 2006). LULC (land use/land cover) mapping is a very important study for changes of crops and soil (Pande 2022). Drone images have given a better resolution for mapping of LULC (Figs. 21.11 and 21.12).

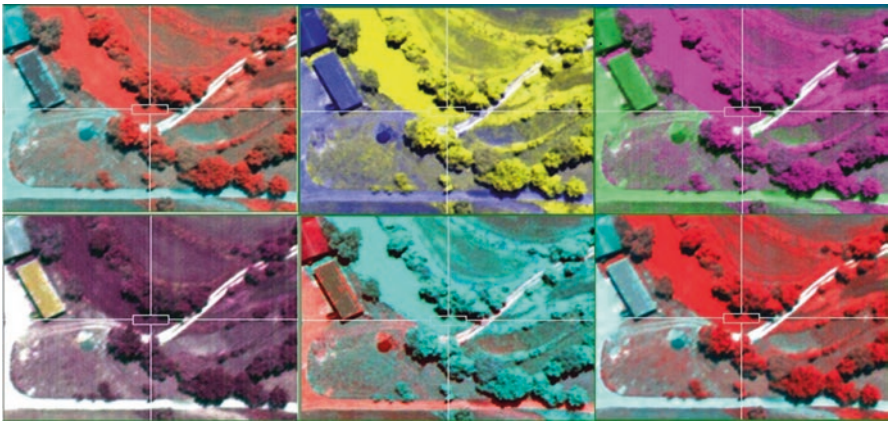

Fig. 21.11 Hyperspectral image based on the UAV. (Source: http://vespadrones.com/product/hyperspectral-camera-rikola/)

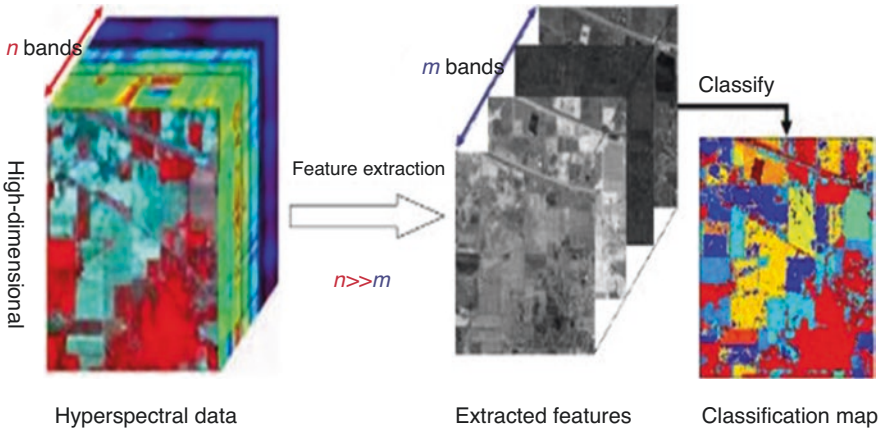

Fig. 21.12 Classification map of hyperspectral image and UAV. (Source: Boggavarapu et al. 2017)

Yield Forecasting

Accurate forecasting of early yields is as important for farmers as it is for the whole agricultural sector. RGB image could be used for measuring the plant height and canopy cover (Chu et al. 2016), multispectral imagery or VIs (Kyratzis et al. 2017) and strong crop yield forecasting correctness were found with UAVs and hyperspectral remote sensing. Multitemporal VIs, like a cumulative VI over the rising period, outperform only measurements as is the instance with satellite data (Rembold et al. 2013).

Precision Farming

Precision agriculture is a new concept of smart farming within varying conditions of climate change. It is a micromanagement framework that benefits from the use of knowledge generated by geospatial technology to arrive at better agricultural and land management decisions (Kim et al. 2017). In other terms, it is "Virtual Smart Agriculture" involving farmer-level mapping of far greater size, extensive database development of required tools prepared by space-based information and field observations, and a robust work plan to optimize yield and minimize input costs via the hyperspectral remote sensing and decision support network (Deng et al. 2018; Elbeltagi et al. 2022b). It is very important for the growth of Indian agricultural output. The period of precision farming is seen in Fig. 21.13.

Conclusion

Throughout this short study, we presented hyperspectral field photography, imaging technologies, precision cultivation software, and hyperspectral data processing techniques. Hyperspectral imaging systems enable researchers to acquire knowledge required to conduct agricultural precision practices. The regular exactness of hyperspectral imaging is increased relative to the rendering of multispectral pictures. The interest in and description of precision farming (PF) has resulted in a discrepancy between technical capacities and theoretical knowledge of the

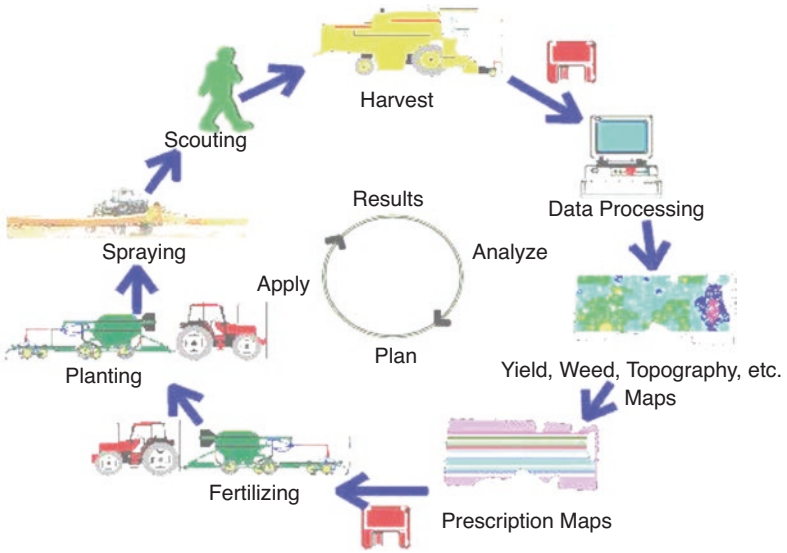

Fig. 21.13 Precision farming cycle

relationship between accessibility of inputs and outcome production. Agriculture, the energetic mechanism regulated by a grouping of biotic and abiotic forces, requires to be maintained, as it is the main function in the Indian economy. Although we are self-appropriate in food grain development, there are many gray areas that need to be developed for the ever-green revolution to be accomplished. Translation of remote sensing data, GIS innovations, and precision farming database knowledge into field-level implementable schemes and grassroot absorption of technology by the actual beneficiaries remains a bigger challenge. A short survey should act as a starting point for farm and image processing experts alike to consider the usage of hyperspectral picture processing in agriculture.

References

Agro-Informatics (2001) In: Patil VC, Dasog GS, Alagawadi AR, Shashidhara KC, Biradar DP (eds) Proceedings of the first National Conference on Agro-Informatics (NCAI). INSAIT, Dharwad

Alexandridis T et al (2017) Novelty detection classifiers in weed mapping: Silybum marianum detection on UAV multispectral images. Sensors 17:2007

Aziz FAA, Shariff ARM, Amin BM, Mohd S, Rahim AA, Jahanshiri E, Nik Norasma Che'Ya (2008) GIS based System for Paddy Precision Farming. Iaald Afita WCCA, World Conference on Agricultural Information and IT, Tokyo, University of Agriculture, Tokyo, Japan, August 24–27, pp 417–422

Bairagi GD, Hassan Z (2002) Wheat crop production estimation using satellite data. J Indian Soc Remote Sens 30(4):213–219

Bajcsy P, Groves P (2004) Methodology for hyperspectral band selection. Photogramm Eng Remote Sens 70(7):793–802

Bannari A, Pacheco A, Staenz K, McNairn H, Omari K (2006) Estimating and mapping crop residues cover on agricultural lands using hyperspectral and IKONOS data. Remote Sens Environ 104:447–459

Bingfng W, Chenglin L (2000) Crop growth monitor system with coupling of AVHRR and VGT Data, vegetation 2000, conference, Lake Maggiore – Italy

Boggavarapu LNP et al (2017) Survey on classification methods for hyper spectral remote sensing imagery, International Conference on Intelligent Computing and Control Systems (ICICCS). IEEE Xplore. https://doi.org/10.1109/ICCONS.2017.8250520

Burrough PA, McDonnell RA (1998) Principles of geographic information systems. Oxford University Press, Oxford, pp 10–16

Carrington B (2016) The Shifting Landscape of Sports Media with Dave Zirin. Contexts 15(3):8–11. https://doi.org/10.1177/1536504216662231

Castaldi F et al (2017) Assessing the potential of images from unmanned aerial vehicles (UAV) to support herbicide patch spraying in maize. Precis Agric 18:76–94

Chu T et al (2016) Cotton growth modeling and assessment using unmanned aircraft system visual-band imagery. J Appl Remote Sens 10:036018

Clark RN (1999) Spectroscopy of rocks and minerals, and principles of spectroscopy. In: Renz AN (ed) Remote sensing for the earth sciences: manual of remote sensing, vol 3, 3rd edn. Wiley, New York, pp 3–58

Dalponte M, Bruzzone L, Gianelle D (2009) The role of spectral resolution and classifier complexity in the analysis of hyperspectral images of forest areas. Remote Sens Environ 113:2345–2355

Deng L et al (2018) UAV-based multispectral remote sensing for precision agriculture: a comparison between different cameras. ISPRS J Photogramm Remote Sens 146:124–136

Doad AP, Das S, Khadse SP et al (2022) An assessment of geo-environmental quality using physical data and a geospatial approach: an example for a watershed in Central India. Environ Earth Sci 81:356. https://doi.org/10.1007/s12665-022-10480-z

Elarab M et al (2015) Estimating chlorophyll with thermal and broadband multispectral high-resolution imagery from an unmanned aerial system using relevance vector machines for precision agriculture. Int J Appl Earth Obs Geoinf 43:32–42

Elbeltagi A, Pande CB, Kouadri S et al (2022a) Applications of various data-driven models for the prediction of groundwater quality index in the Akot basin, Maharashtra, India. Environ Sci Pollut Res 29:17591–17605. https://doi.org/10.1007/s11356-021-17064-7

Elbeltagi A, Nagy A, Mohammed S, Pande CB, Kumar M, Bhat SA, Zsembeli J, Huzsvai L, Tamás J, Kovács E, Harsányi E, Juhász C (2022b) Combination of limited meteorological data for predicting reference crop evapotranspiration using artificial neural network method. Agronomy 12(2):516. https://doi.org/10.3390/agronomy12020516

Elbeltagi A, Kumar M, Kushwaha NL et al (2022) Drought indicator analysis and forecasting using data driven models: case study in Jaisalmer, India. Stoch Environ Res Risk Assess. https://doi.org/10.1007/s00477-022-02277-0

FICCI (2012) Agriculture overview. Available: http://www.ficci-b2b.com/sectoroverview-pdf/Sector-agri.pdf. Accessed 26 May 2012

Goetz AFH, Vane G, Solomon JE, Rock BN (1985) Imaging spectrometry for earth remote sensing. Science 228:1147–1153

Govender M, Chetty K, Bulcock H (2007) A review of hyperspectral remote sensing and its application in vegetation and water resource studies. Water SA 33. https://doi.org/10.4314/wsa.v33i2.49049

Gowrisankar D, Adiga S (2001) Remote sensing in agricultural applications: an overview. In: Proceedings of the first National Conference on agro-informatics (NCAI). INSAIT, Dharwad

Grant OM et al (2016) Thermal imaging to detect spatial and temporal variation in the water status of grapevine (Vitis vinifera L.). J Hortic Sci Biotechnol 91:43–54

Gulhane VA, Rode SV et al (2022) Correlation analysis of soil nutrients and prediction model through ISO cluster unsupervised classification with multispectral data. Multimed Tools Appl. https://doi.org/10.1007/s11042-022-13276-2

Kandekar VU (2021) Surface water dynamics analysis based on sentinel imagery and Google earth engine platform: a case study of Jayakwadi dam. Sustain Water Resour Manag 7:44. https://doi.org/10.1007/s40899-021-00527-7

Kim M et al (2017) Monitoring canopy growth and grain yield of paddy rice in South Korea by using the GRAMI model and high spatial resolution imagery. GISci Remote Sens 54:534–551

Kouadri S, Pande CB, Panneerselvam B et al (2022) Prediction of irrigation groundwater quality parameters using ANN, LSTM, and MLR models. Environ Sci Pollut Res 29:21067–21091. https://doi.org/10.1007/s11356-021-17084-3

Kyratzis AC et al (2017) Assessment of vegetation indices derived by UAV imagery for durum wheat phenotyping under a water limited and heat stressed Mediterranean environment. Front Plant Sci 8:1114

Lambert J et al (2018) Evaluating the potential of unmanned aerial systems for mapping weeds at field scales: a case study with Alopecurus myosuroides. Weed Res 58:35–45

López-Granados F (2011) Weed detection for site-specific weed management: mapping and real-time approaches. Weed Res 51:1–11

Maresma A et al (2016) Analysis of vegetation indices to determine nitrogen application and yield prediction in maize (Zea mays L.) from a standard UAV service. Remote Sens 8:973

Mulla DJ (2013) Twenty-five years of remote sensing in precision agriculture: key advances and remaining knowledge gaps. Biosyst Eng 114:358–371

Naveen JPA et al (2014) Modeling soil parameters using hyperspectral image reflectance in subtropical coastal wetlands. Int J Appl Earth Obs Geoinf 33:47–56

Pande CB (2022) Land use/land cover and change detection mapping in Rahuri watershed area (MS), India using the google earth engine and machine learning approach. Geocarto Int. https://doi.org/10.1080/10106049.2022.2086622

Pande CB, Moharir KN, Singh SK et al (2020) An integrated approach to delineate the groundwater potential zones in Devdari watershed area of Akola district, Maharashtra, Central India. Environ Dev Sustain 22:4867–4887. https://doi.org/10.1007/s10668-019-00409-1

Pande CB, Moharir KN, Singh SK, Varade AM, Ahmed Elbeltagie SFR, Khadri PC (2021a) Estimation of crop and forest biomass resources in a semi-arid region using satellite data and GIS. J Saudi Soc Agric Sci 20(5):302–311

Pande CB, Moharir KN, Khadri SFR (2021b) Assessment of land-use and land-cover changes in Pangari watershed area (MS), India, based on the remote sensing and GIS techniques. Appl Water Sci 11:96. https://doi.org/10.1007/s13201-021-01425-1

Pande CB, Kadam SA, Jayaraman R, Gorantiwar S, Shinde M (2022) Prediction of soil chemical properties using multispectral satellite images and wavelet transforms methods. J Saudi Soc Agric Sci 21(1):21–28

Perry EM et al (2018) Remote sensing using canopy and leaf reflectance for estimating nitrogen status in red-blush pears. HortScience 53:78–83

Rembold F et al (2013) Using low resolution satellite imagery for yield prediction and yield anomaly detection. Remote Sens 5:1704

Rock BN, Vogelmann JE, Williams DL, Vogelmann AF, Hoshizaki T (1986) Remote Detect For Damage Bio-Sci 36:439–445

Thenkabail PS, Lyon JG, Huete A (2012) Hyperspectral remote sensing of vegetation. CRC Press

Tucker CJ (1979) Red and photographic infrared linear combinations for monitoring vegetation. Remote Sens Environ 8:127–150

Yu FH et al (2017) Radiative transfer models (RTMs) for field phenotyping inversion of rice based on UAV hyperspectral remote sensing. Int J Agric Biol Eng 10:150–157

Zhang N, Wang M, Wang N (2002) Precision agriculture-a worldwide overview. Comput Electron Agric 36:113–132

Chapter 22
Tools and Solutions for Watershed Management and Planning Under Climate Change

Abbas Mirzaei, Nasser Valizadeh, and Hassan Azarm

Abstract Water resources in watersheds are severely affected by climate change, water scarcity, and frequent droughts. This leads to a conflict between different users of water, especially between agriculture and the environment sectors. Due to the multidimensional and multiscale nature of watershed management and climate change, it is necessary to provide some tools and solutions for sustainable management and planning of watersheds under climate change. In this regard, the purpose of this study was to develop a conceptual framework in the field of tools and solutions for integrated watershed management and planning to optimally allocate water resources between different sections in the watersheds. In order to achieve this goal, the literature on the watershed management was reviewed, and it was found that there are three categories of studies in this field. The first category includes studies that have managed the watershed using hydrological and economic simulation tools. The second category is studies that consider environmental aspects as well and combine hydrological, economic, and environmental simulation tools. The third category is studies that consider users' behavior very important in watershed management and employ some behavior-specific tools to simulate the behavioral complexities of users. The results showed that the combination of all hydrological, socioeconomic, environmental, and behavioral components and the use of component-specific tools to simulate these components can achieve sustainable watershed management. Furthermore, the present integrated framework can be used

A. Mirzaei (✉)
Department of Agricultural Economics, Agricultural Sciences and Natural Resources University of Khuzestan, Mollasani, Iran
e-mail: amirzaei@asnrukh.ac.ir

N. Valizadeh
Department of Agricultural Extension and Education, School of Agriculture, Shiraz University, Shiraz, Iran
e-mail: n.valizadeh@shirazu.ac.ir

H. Azarm
Department of Agricultural Economics, School of Agriculture, Shiraz University, Shiraz, Iran

C. B. Pande et al. (eds.), *Climate Change Impacts on Natural Resources, Ecosystems and Agricultural Systems*, Springer Climate,
https://doi.org/10.1007/978-3-031-19059-9_22

in various case studies around the world due to its comprehensiveness and operationality for integrated watershed management.

Keywords Climate change · Watershed management · Sustainability of water resources · Water management strategies

Introduction

Today, issues such as limited water and energy resources, unsustainable agricultural production practices, climate change, and increasing population have posed challenges in food production and sustainable management of the resources (Pande and Moharir 2021; Hoff 2011; Bizikova et al. 2013; Alloisio 2015; El-Gafy 2017; Wang et al. 2018; Nhamo et al. 2020). Water scarcity is the most important problem facing humans in the twenty-first century (Eliasson 2015; Li et al. 2017; Lu et al. 2018; Moharir et al. 2020). Population growth, the need for more food, land use change, and policy problems in developing and developed countries exacerbate this complex situation (Ward 2014). It is estimated that about 2.8 billion people in 43 countries are affected by water scarcity, of which 1.2 billion do not even have access to adequate drinking water (Pande et al. 2019; United Nations World Water Development Report 2015). In addition, it is projected that by 2050, the world's population will increase to 9.8 billion, and half of this population will live in urban areas (UN 2017). This population growth, along with economic development, will increase the need to produce more food, and as a result, water demand will grow by 40% by 2050 (UN 2015).

Changes in water resources have a dynamic trend and many factors affect the amount of water resources over time. Increased consumption and demand, population growth, climate change, and changes in ground/surface water abstraction are all factors that affect the water system of an area or watershed over time (Pande and Moharir 2015; Döll 2002; Arnell et al. 2011). Furthermore, users of water resources in the watershed are interconnected, and water use in one sector affects other sectors. Therefore, the water sector should be considered as a whole in countries' development plans, and the environmental and economic impacts of policies on this resource should be accurately examined (Fiorillo et al. 2007).

Watersheds are important components in the water cycle and water resources management (Kharrazi et al. 2016a, b). Therefore, improving the hydrological process and sustainable management of water resources through watershed management has a high feasibility. It should be mentioned that the consumption of water resources in watersheds involves a complex process of social, economic, and environmental dimensions (Cai et al. 2003).

Climate change such as precipitation and temperature changes can affect the hydrological processes of watersheds (Arnell and Gosling 2013; Jiménez Cisneros et al. 2014). Climate change is defined as statistically significant changes in climate conditions over a period of more than a decade (Intergovernmental Panel on Climate

Change (IPCC) 2007). The climate change phenomenon as one of the most threatening factors of human beings has strongly affected various sectors (Koutiva and Makropoulos 2016). Climate change in recent decades has posed many challenges for watershed planners and managers in the sustainable use of water resources, environmental protection, and adequate food production, leading to a global crisis (Wilhite 2005; OECD 2006).

Increasing competition between different sectors for the use of limited water resources in watersheds along with the climate change and drought leads to further food and water shortages (Steffen et al. 2015; Pastor et al. 2019; Abdelkader and Elshorbagy 2021). In fact, water supply scarcity due to severe droughts and increased competition for water consumption between urban-rural, agricultural, industrial, and the environmental sectors have led to imbalances between water resources capacity and consumption in many watersheds (Brinegar and Ward 2009; Mirzaei and Zibaei 2021). Although various stakeholders including urban, agricultural, industrial, tourism, energy, and financial and insurance market sectors are affected by climate change (Tol 2002; Hope 2005; Kemfert 2009), the agricultural sector as one of the most vulnerable sectors to climate change has always been prominent (Chang 2003).

The agricultural sector is the main consumer of water in the world, which has a significant contribution to the scarcity of water resources in the watersheds (Han et al. 2011). In recent years, due to the expansion of agricultural activities, the demand for surface and groundwater resources has increased significantly, and the scarcity of water resources in the watersheds has intensified (Mishra et al. 2016). Therefore, due to the scarcity of water resources for agricultural production, especially in arid and semiarid areas of the world, sustainable management of water resources at watershed level is essential (D'Odorico et al. 2019; Sadeghi et al. 2020). Watershed management decision-makers face many challenges in the field of sustainable management of water resources. They must decide on the allocation of scarce water supply in a way that leads to the achievement of economic goals of activities such as agriculture and environmental sustainability (Forni et al. 2016).

In general, due to limited water resources, increasing demand, reduced supply, complexity, conflicts in consumption systems, and dynamics of the water sector, the development of strategic planning for sustainable management of water resources in the watersheds is an inevitable necessity. In this context, the systematic, integrated, and systematic management of watershed water resources is one of the most important issues facing policy makers (Simonovic and Fahmy 1999). Different policies to manage the watersheds can result in adverse outcomes if they do not consider all potential communications in a system and in an integrated manner (FAO 2011). Integrated watershed management requires an initial description of aquatic ecosystem performance and related values and services (Bino et al. 2015; Gilvear et al. 2013; Lamers et al. 2015). Therefore, an integrated view of watershed management is necessary due to the multidimensional and multiscale nature of water resources management and climate change (Downing 2012; Mirzaei and Zibaei 2021).

Today, considering technical, socioeconomic, hydrological, environmental, and behavioral variables is essential for the integrated watershed management under the

climate change (Mirzaei and Zibaei 2021). Agents' behavioral rules and the interaction methods of them with each other's environment must be considered to make decisions about issues of the watershed management (Bonabeau 2002). In other words, for the sustainability of watershed management, it is important to pay attention to the conflicting goals among users and the need for their participation in the form of a prescriptive or optimal model (Akhbari and Grigg 2013). International efforts in recent years have added an integrated and comprehensive view of water resources to water management models. The United Nations Conference on Water in *Mar del Plata* in 1977 was the first meeting to discuss the concept of integrated water resources management (IWRM). However, the implementation of the concept of IWRM in practice was discussed after the Summit on Sustainable Development in 1992, and at the International Water and Environment Conference in Dublin in 1992, representatives of more than 100 countries agreed on four principles as follows:

- Water is a limited and vulnerable resource and plays a key role in the sustainability of life, development, and the environment.
- Water management should be based on participatory and consensual solutions between consumers, planners, and policy makers at all levels.
- The role of women in water management and safeguarding is central.
- Water must be recognized as an economic commodity because it has economic value in all its competing uses.

According to the Global Water Partnership (GWP), IWRM refers to the coordinated development and management of water, soil, and related resources in order to maximize economic and social well-being in a fair way without compromising the sustainability of ecosystems. The United Nations Development Programme (UNDP) defines IWRM as a principled process for the sustainable development and optimal allocation of water resources in the social, economic, and environmental fields. The United States Agency for International Development (USAID) defines IWRM as the cooperation of governors, communities, and stakeholders to select solutions for the proper use of freshwater and coastal resources. According to the World Bank, IWRM ensures the social, economic, and environmental dimensions of water use (Zargar and Noorzad 2010).

Efficient management of water resources at watershed levels and under climate change exposes the decision-makers of arid and semiarid regions of the world to difficult conditions in terms of designing climate-adaptive policies and strategies (Kahil et al. 2016). Impact assessment of the water resources management policies and adaptive strategies used by stakeholders should be in the form of integrated modeling at the watershed level. In other words, impact assessment and application of adaptive strategies should be done based on the economic, social, and environmental goals and according to the hydrological and behavioral conditions of watershed stakeholders (Esteve et al. 2015). Therefore, it is necessary to integrate watershed management and planning solution under the climate change conditions. In this way, a set of comprehensive and agreed solutions meeting the goals of all users in a system are developed (Mirzaei and Zibaei 2021). This chapter attempts to develop and describe the tools and solutions for sustainable watershed management under climate change.

Components of Watershed Management Under Climate Change

As mentioned earlier, climate change poses major challenges to watershed management. The literature shows that so far, five reports have been published by the Intergovernmental Panel on Climate Change (IPCC) in the context of a comprehensive analysis of the climate change, which is the main basis for climate-related studies. Currently, the fourth and fifth reports are used in various studies. In the fourth evaluation models, the Special Report on Emissions Scenarios (SRES) have been used, and in the fifth evaluation models, new scenarios based on forcing radiation (FR) have been applied. In the fourth report, the main scenarios B1, B2, A1, and A2 represented the most optimistic to the most pessimistic emissions, respectively, which were later transformed into three scenarios B1, A1B, and A2. In the fifth report, the new scenarios RCP2.6, RCP4.5, RCP6.0, and RCP8.5 replaced them. CMIP6 (Coupled Model Intercomparison Project) has recently designed many updated climate model outputs and will contribute to the IPCC. CMIP6 data makes future scenarios more rational and practical by combining the RCPs and shared socioeconomic pathways (SSPs) (Eyring et al. 2016; Nature Climate Change 2019). Some studies have focused on simulation of climate variables, climate extremes, and ocean-atmosphere systems by the CMIP6 data (Di Luca et al. 2020; Kim et al. 2020; Nie et al. 2020; Srivastava et al. 2020; Su et al. 2021). From a scale point of view, water resources management can take place at the level of a farm, a plain, a subbasin, or even a watershed (Molden et al. 2009). Water management at the watershed level results in a comprehensive framework of economic efficiency, equity (equitable distribution), and sustainability. Since the mid-1990s, many studies have been conducted on water management at the watershed level (Gurluk and Ward 2009; Ward and Pulido-Velazquez 2009; Gohar and Ward 2010; Nikouei et al. 2012; Nikouei and Ward 2013; Gohar et al. 2013, 2015; Ward 2014; Kahil et al. 2015). A review of the literature in this field shows that an integrated view of watershed management under climate change is based on four components: hydrological, socioeconomic, environmental, and behavioral components. In this section, each of the components and related studies are described in detail.

Hydrological Component

In recent decades, the assessment of the impacts of climate change on various sectors (especially the agricultural sector) at the watershed scale is mostly based on biophysical modeling with a focus on the agronomic dimension (Moriondo et al. 2010; Ventrella et al. 2012) or the hydrological dimension (Joyce et al. 2011; Rochdane et al. 2012). In other words, most water resource allocation studies at the watershed level have been based on a water supply-demand equilibrium approach and allocation optimization scenarios by using physical and hydrological aspects

(Rosegrant et al. 2000; Ringler and Huy 2004). This approach is suitable for informing planners to meet current and future demand and to show the volume of demand and water supply at a specific time at the watershed level. However, it does not provide sufficient information on the economic consequences of allocation policies.

Hydrological simulation models represent complex systems of natural hydrological communication and management of water resources and infrastructure of these resources at limited spatial and temporal scales. In some studies, it was found that integration of Earth observation datasets in geographical information system (GIS) provides more reliable parameters for hydrological simulation of the basin (Rawat and Singh 2017; Maliqi and Singh 2019). Hydrological simulation models can show the interaction of urban, agricultural, industrial, and environmental systems. In addition, they can be used to illustrate the temporal-spatial dependencies and the effects of climate change and human activities on environmental systems (Joyce et al. 2011; Girard et al. 2015; Forni et al. 2016). For example, Rawat et al. (2021) used a curve number method and then compared empirical mathematical models with SCS-CN (Soil Conservation Service-curve number) to simulate runoff as one of the main hydrological parameters of the basin.

Water Evaluation and Planning (WEAP) simulation model is an efficient tool for depicting the above characteristics and analyzing the effects of climate change in watersheds (Bhave et al. 2014; Satti et al. 2015; Forni et al. 2016). The WEAP model was first used in 1992 to simulate water supply and demand in the Russian Aral Sea region (Raskin et al. 1992). This model has been used mainly for planning water resources at the regional, local, and watershed scales (Huber-Lee et al. 2004; Groves et al. 2008; Purkey et al. 2008; Demertzi et al. 2014). Lévite et al. (2003) first used the WEAP model to allocate water resources at the watershed scale. Then, Gaiser et al. (2008) analyzed a wide range of water management models and concluded that the WEAP model is a comprehensive model for watersheds. By providing detailed details to planning officials, it can assess the long-term effects of population change and economic development. Since 2008, this model has been modified and tested in Central Asia and East Africa under various ecological, hydrological, and socioeconomic conditions. The results have revealed that the WEAP model has the potential to simulate future scenarios in strategic water resources management plans.

Today, the WEAP model is the most widely used hydrological simulation tool in the watersheds to achieve various goals (Lévite et al. 2003; Li et al. 2015; Adgolign et al. 2016; Mishra et al. 2017; Khalil et al. 2018). For example, Yaqob et al. (2015) used the WEAP model to evaluate and analyze the role of wastewater treatment in the Nablus watershed in Palestine. Esteve et al. (2015) investigated the yield and net water requirement of agricultural products in the Middle Guadiana Basin, using the WEAP model. To this end, they used hydrological simulation to articulate the climate change scenarios and adaptive strategies of farmers. Hum and Talib (2016) examined the effect of population growth scenarios in the Selangor watershed of Malaysia using the WEAP model to assess the future status of water supply. In a study by Adgolign et al. (2016), the WEAP model was applied to allocate the surface water to agricultural and environmental sectors in western Ethiopia. Mishra

et al. (2017) investigated water balance under different management scenarios in one of the watersheds of Sri Lanka using WEAP tools. Cetinkaya and Gunacti (2018) in a study created 16 different scenarios of water allocation in the watersheds of Turkey by changing and combining different irrigation and under-irrigation priorities. Then the results of these scenarios were simulated using the WEAP model, and their performance was evaluated through economic, social, and environmental indicators. Khalil et al. (2018) used the WEAP model to evaluate water supply and demand under water transfer and climate change scenarios in the Mae Klong watershed of Thailand. Furthermore, Mirzaei and Zibaei (2021) used WEAP tool to simulate the yield and net water requirement of crops in Halilrud watershed of Iran under climate change scenarios and farmers' adaptive strategies.

Socioeconomic Component

Water is a vital resource for life, but it has become a limiting factor for social and economic development in many parts of the world. Water scarcity, droughts, and increasing the pressure on water resources and the environment have led to the growth of social and economic conflicts in various sectors (Gleick et al. 2009). Water scarcity will ultimately limit economic and social development, which means that in the near future, water will be recognized as a major obstacle to world development (Kojiri et al. 2008). Therefore, considering social and economic goals in the allocation of water resources at the watershed level is very important.

Allocating water between different sectors based on economic efficiency will maximize the overall value of water. In other words, in order to achieve the economic goals of water consumption, water allocation must be shifted from low-profit activities to high-yield economic activities (Tisdell 2010; Turner et al. 2010). Another aspect of economic efficiency in water allocation is Pareto efficiency. According to this rule, any change in water allocation is appropriate when at least one beneficiary gains more prosperity and no beneficiary of this change suffers (Just et al. 2005; Thomas and Durham 2003). This principle is difficult to apply in the real world, so another criterion called the Kaldor-Hicks criterion is used to this end. According to this criterion, any change in allocations would be appropriate if the welfare interests of one group of individuals offset the losses of another group (Turner et al. 2010). In general, water engineering economics emphasizes the use of economic principles for decision-making, integrated and flexible management, profit valuation, program design, alternative evaluation, financial resources, and institutional design (Griffin 1998; Braden 2000; Lund et al. 2006).

Efforts to manage the demand for water resources between different sectors at the watershed level require knowledge of the economic value of water in crop production and changes in this value over time and space. Economic value and its changes can be due to physical differences (climate and soil type) and socioeconomic production conditions (input or output prices and regulations). Therefore, by entering water economic modeling studies, production functions evaluate the

economic effects of different policies at the watershed scale and determine the optimal allocation of water consumption between different economic sectors, environment, cities, and hydropower plants (Cai 2008; Bekchanov et al. 2015; Erfani et al. 2015; Kahil et al. 2015). For example, production functions related to watershed economic-hydrological models can provide a powerful tool for assessing the spatial and temporal conflict between agricultural profitability and environmental consequences in groundwater-based irrigation systems (Kuwayama and Brozović 2013; Foster and Brozović 2018). In general, allocating water to meet any needs at the watershed level has social and economic consequences. Therefore, it is necessary to pay attention to the socioeconomic component along with the hydrological component in the framework of integrated water management (Harou et al. 2009; George et al. 2011).

The relationship between economic issues and the hydrological process in water resources management developed from the 1960s to the 1970s in arid regions of Israel and the southwestern United States. During these years, Gisser and Mercado (1972, 1973), and Rogers and Smith (1970) used the water demands' economic curves to optimize the water resources system. The conceptual framework of economic models of integrated regional water resources management was formed by maximizing the area under water-derived demand curves (Gisser and Mercado 1973; Noel et al. 1980). Since then, researchers have used economic modeling in the water resources system under different names. For example, concepts such as economic-hydrology (Gisser and Mercado 1972), water economics (Noel and Howitt 1982), hydrological-agricultural economics (Lefkoff and Gorelick 1990), institutional economics (Booker 1995), institutional-economic-hydrological integration (Booker 1995), integrated river optimization (Ward and Lynch 1996), allocation efficiency (Diaz and Brown 1997), hydrological-economic integration (McKinney et al. 1999; Rosegrant et al. 2000), engineering economics (Newlin et al. 2002; Draper et al. 2004; Lund et al. 2006), integrated agro-hydrological economics (Cai et al. 2003), supply and demand (Griffin 2006), integrated hydrological economics (Cai et al. 2003; Ringler and Cai 2006; Pulido-Velazquez et al. 2006), and water resources economics (Volk et al. 2008) are examples of different terminologies.

There are various studies around the world that have used economic-hydrological modeling and mathematical planning methods to manage water resources at the watershed level (see Gurluk and Ward (2009), Ward and Pulido-Velazquez (2009), Gohar and Ward (2010), Nikouei et al. (2012), Blanco-Gutierrez et al. (2013), Nikouei and Ward (2013), Gohar et al. (2013, 2015), Akter et al. (2014), Ward (2014), and Kahil et al. (2015)). However, one of the main disadvantages of such modeling is that not all variables affecting hydrological conditions can be formulated in the form of mathematical programming methods. To overcome this weakness, it is necessary to perform accurate hydrological simulations using information about products, type of irrigation, soil, climate, geographical relationships, and etc. The simulation results can then be used as input to the economic model (Esteve et al. 2015; Forni et al. 2016; Mirzaei and Zibaei 2021).

Environmental Component

As water harvesting and consumption increase due to population growth and economic growth, awareness of environmental conservation is also increasing (Kahil et al. 2015). Therefore, the role of government agencies and water resources managers as decision-makers in water allocation process is very important (Johansson et al. 2002; Orubu 2006; Hanak and Lund 2012; Farhadi et al. 2016; Hu et al. 2016). In relation to water consumption, there is a conflict between the urban, agricultural, and industrial sectors on the one hand and the recovery of ecosystems on the other. Excessive exploitation of water resources destroys ecological aquatic environments in the watersheds (Abdulbaki et al. 2017). Since 1990, more than half of the world's natural wetlands have been degraded by human activities (Stacke and Hagemann 2012; Russi et al. 2013; WWAP 2018). The development of agriculture as the largest consumer of water (Siebert et al. 2010; WWAP 2012) has been a major cause of wetlands' degradation over the last hundred years (Davidson 2014; Ramsar Convention on Wetlands 2014). By emphasizing the lack of integrated water resources management policies at the watershed level, some studies have warned of wetlands' extinction (Turner 1991). Irrigation water storage in the agricultural sector to meet the environmental needs of the watersheds is one of the management policies used in this field (Peck et al. 2004; Nikouei et al. 2012; Zou et al. 2018; Mirzaei and Zibaei 2021). Other existing policies to further protect wetlands include reducing part or all of the rights to use surface water for irrigation with economic incentives for farmers (Peck et al. 2004). In general, the need for a comprehensive approach to water use and the ecological needs of wetlands in the watersheds is essential (Ringler and Cai 2006; Nikouei et al. 2012; Zou et al. 2018; Meng et al. 2019; Vinten et al. 2019; Mirzaei and Zibaei 2021).

On the other hand, paying attention to the quality of water resources in the watersheds is of special importance. Past studies have focused on the distribution, output, handling, and transfer of contaminant resources (Shen et al. 2015). A number of studies (see Centner et al. (1999), Liu et al. (2013), Strauch et al. (2013), and Strokal et al. (2015)) have also identified areas with a critical source of pollution and best management practices (including ecological and engineering measures) to control pollution from these sources. Many researchers (like Mouri et al. (2011), Wu et al. (2011), Shen et al. (2012, 2015), and Meaurio et al. (2015)) have evaluated the factors affecting temporal and spatial changes of pollution by calculating the total amount of nitrogen and phosphorus. Nitrogen overload in watersheds is one of the deepest impacts of human activities on the environment (Vorosmarty et al. 2010). In recent years, research efforts on the characteristics and methods of pollution management for agricultural resources have increased in many parts of the world (Liu et al. 2015; Villamizar and Brown 2016; Naghavi et al. 2021). Agricultural growth has consequences such as increased water consumption (Mosavi and Esmaeili 2012), increased use of chemical fertilizers (Lepistö et al. 2001), and pollution of water resources (Maillard and Santos 2008; Salehi et al. 2018). Agriculture is one of the main sources of nitrate and phosphate loading in the watersheds and aquatic

ecosystems (Vorosmarty et al. 2010). Some research (see Ongley et al. (2010) and Van Meter et al. (2018)) has been conducted in the field of simulations and providing solutions to reduce the nitrate and phosphate loads due to agricultural activities in watersheds around the world.

Studies on the environmental effects of agricultural activities on water, soil, and air have also increased (Yaqubi et al. 2016). Due to the use of pollutant inputs in the production process, a set of rebound effects is created simultaneously with the product (Zhou et al. 2014). For example, energy use in the agricultural sector leads to the release of carbon dioxide into the atmosphere (Mosavi 2016). Thus, pollutants from agriculture are released into the atmosphere and eventually transferred to water and soil resources (Rong et al. 2017). In China, since the 1990s, the need to examine environmental factors in the water resources management decision-making process has been recognized (Bao et al. 2004). In addition, the evaluation of environmental strategies has been discussed in the academic community of this country as an important decision-making element (Zhu et al. 2010; Wu et al. 2011; Gao et al. 2017).

Economic or market tools are recognized as an optimal way to reduce the harmful effects of pollution in the watersheds (Freeman 2003). In recent decades, the willingness to use the economic incentives to achieve environmental goals has increased (Eisner 2004). Taxes on input, taxes or environmental subsidies, governmental grants, licenses and rules of liability, and the creation of exchangeable liabilities and licenses are among the economic policies adopted to reduce the pollutions (Edson 2004). This type of tax, if raised enough, can be an efficient tool to achieve the desired level of pollution reduction. Of course, tax increases in this area should be politically feasible (Larson et al. 1996). Most studies in this field have focused on determining the optimal input for tax collection, and few studies have been conducted on the overall effectiveness of this policy (Shortle et al. 1998; Dowd et al. 2008). An environmental tax or subsidy sets a specific level of pollution for different pollutants. Now, if the pollution is lower than the acceptable cutoff, targeted subsidies will be paid, and if the pollutant output is more than the set amount, they will be fined (Shortle and Horan 2001). In this type of tax, due to different climatic conditions and the occurrence of accidental phenomena, the concentration of pollutants changes drastically, and as a result, these events may lead to unfair fines for people who have tried to reduce the level of pollution. In fact, in such circumstances, the problem of free riding is not detectable, and the increase in pollution by some people leaves other people's efforts to reduce the level of pollution fruitless (Shortle and Horan 2001; Shortle et al. 1998). Government grants come in the form of grants and green payments or subsidies. By financing and reducing the capital needed by taxpayers, these programs provide a favorable environment for reducing nonpoint pollution. Paying farmers for not using farmlands in the United States has been the most prominent example of these programs in recent decades. Green payments are made by the government to reduce the spread of pollution in agriculture (USDA-FSA 2007; Horan et al. 1999). According to the rules and regulations related to environmental responsibility, people related to pollution can be sued according to the amount of damage to the environment. In this method, the court

may cost more than other corrective methods. In other words, individuals seeking to convict polluters may drop their grievances due to significant costs (Shortle and Horan 2001). Another method in this type of program is to receive some money from the polluters to confiscate that if the pollution is not sufficiently controlled in the future (Lichtenberg 1992). Some scholars, for political reasons, suggest that environmental responsibility regulations and laws be combined with other instruments (Menell 1990; Wetzstein and Centner 1992). Successful implementation of the exchange permission program has become a popular policy in reducing point pollution (Salamon 2002). This method is mentioned as an effective approach in achieving environmental goals (Shortle and Horan 2001). Emission exchange of the inputs and exchange related to loading are considered as two methods in the point and nonpoint pollution sources (Horan et al. 2002). In an input-related emission exchange system, changes in the emission of point sources are exchanged against the use of input management methods by pollutants. In contrast, in the loading emission exchange system, the emission of point sources is exchanged against the nutrient charge (Horan et al. 2002). Due to the unequal ratio of contamination in point or nonpoint sources, adjusting the ratio required for exchange is a major challenge in implementing this program (Horan et al. 2002). In addition, the profitability of agricultural activity is one of the reasons that makes the exchange process a major challenge (Obropta et al. 2008; Corrales et al. 2014).

Behavioral Component

As mentioned earlier, in the field of water resources management at the watershed level, the interaction between users and the simulation of these interactions is of particular importance. It should be noted that these interactions are rooted in their behavioral characteristics. Therefore, modeling the behavior of stakeholders in the practical management of water resources is essential. Since in water resources management, due to conflicting goals between the users, the participation or nonparticipation of them in a prescriptive or optimal model is very important. Efficient communication between different users of water resources can be defined in the framework of non-compromising game theory models. In this type of games, the interaction between the actors (stakeholders) is based on their strategic goals (Carraro et al. 2007). The Stackelberg or leader-follower game is a special type of non-compromising game (Kahil et al. 2015; Hu et al. 2016). The application of leader-follower game in the field of optimal allocation of water resources was first proposed by Bhaduri and Barbier (2008) and then used in various studies of water resources management (see Bhaduri and Liebe (2002), Parsapour-Moghaddam et al. (2015), Hu et al. (2016), and Zhang et al. (2016)).

If at the watershed level, stakeholder participation is not achieved to implement an efficient management model, that model will certainly fail at the operational level. In other words, the operation and applicability of optimal models at the

watershed level should be examined. Agent-based models (ABMs) have been used to simulate these behavioral and social complexities on a large scale, especially in water resources management (Bandini et al. 2009; Farhadi et al. 2016; Mirzaei and Zibaei 2021). Today, the applications of ABMs have been considered by many researchers. For example, Kock (2008) showed that socio-hydrological systems are highly correlated with institutional capacity and conflicts. Galán et al. (2009) presented an ABM for the water management in urban areas of Valladolid, Spain. Barthel et al. (2010) proposed a multiactor model for climate adaptation. Zechman (2011) provided an ABM for analyzing management strategies in water distribution systems. Nikolic et al. (2013) used a biological-economic-socio-physical system as a management tool. Akhbari and Grigg (2013) used the ABM to investigate the resolution of consumption disputes in the San Joaquin Basin in California. In this study, they resolved water disputes between agriculture and the environment. The three objectives of maximizing water abstraction for agricultural use, maximizing water output to the wetlands, and minimizing salt loaded by water used in agriculture were considered as the objectives of the study. This study ultimately led to an optimal and workable solution at the watershed level. Zhao et al. (2013) compared the behavior of water users under the system of allocation of administrative and market-based water resources. In this study, the ABM was used to analyze the water allocation in two different allocation systems. Yuan et al. (2014) and Tamene et al. (2014) used ABM for modeling the water resources management and conflict resolution. Mulligan et al. (2014) evaluated groundwater management policies using multiagent system models and combining economic models with the physical groundwater flow model. Gorelick and Zheng (2015) also studied the challenges of groundwater management and the role of multiagent system models in this field. Akhbari and Grigg (2015) modeled the optimal allocation of water resources using a simulation and optimization model and then examined farmers' participation with this model. In this study, they simulated the behavior of farmers. Koutiva and Makropoulos (2016) employed ABM to socially model urban water demand. Farhadi et al. (2016) used an agent-based modeling framework for sustainable groundwater management in Fars Province of Iran. For this purpose, a multiobjective optimization model was used with the objectives of reducing irrigation water, increasing parity in water allocation, and reducing groundwater abstraction to achieve Pareto optimization. In addition, Nash's bargaining model was used to reach an agreement among stakeholders. Then, an ABM was implemented to examine social factors and policy mechanisms and to encourage stakeholders to participate in managerial decisions. Mirzaei and Zibaei (2021) employed an ABM to investigate the participatory behavior of farmers. The aim of this work was to identify the optimal models and to investigate the relationship between climate change adaptive strategies and the identified models in the Halilrud watershed.

Discussion

According to the review and analysis of the research literature, it can be concluded that the integrated model of watershed management and planning is an effective way to analyze the hydrological, socioeconomic, environmental, and behavioral characteristics of the users at the watershed level and under climate change. Review of the literature showed that most studies have considered only one or some influential components in watershed management. Some studies focus on integrated management at the watershed level and with regard to hydrological and socioeconomic components emphasize the optimal allocation of water resources between different sectors at the watershed level. Today, the combination of economic modeling with hydrological simulation of the watersheds is used in studies (see Gurluk and Ward (2009), Ward and Pulido-Velazquez (2009), Gohar and Ward (2010), Nikouei et al. (2012), Blanco-Gutierrez et al. (2013), Nikouei and Ward (2013), Gohar et al. (2013), Akter et al. (2014), Ward (2014), Esteve et al. (2015), Kahil et al. (2015), and Gohar et al. (2015)). These studies present the hydrological relationships and economic objectives comprehensively using mathematical programming. In such models, physical interactions between different uses at the watershed level (agricultural, urban, industrial, recreational, and environmental sectors), reserves (dams and groundwater aquifers), flows (diversion, pumping, abstraction, discharge, and return of water), and waste (at farm level and transferring and evaporation processes) are included. Economic goals also include maximizing the total economic benefits of different sectors at the watershed level (Nikouei et al. 2012; Ward 2014).

Mathematical programming framework and its use for optimal and economical allocation of water resources according to the hydrological situation is a risky and complex decision-making problem that is associated with multilevel, multistage, multisubject, multiobjective, and nonlinear correlation features (Hassan-Esfahani et al. 2015; Davijani et al. 2016; Abdulbaki et al. 2017; He et al. 2017; Lu et al. 2018). Hence, in such cases, mathematical programming methods such as nonlinear programming (Li et al. 2017; Georgakakos 2012), dynamic programming (Anvari et al. 2014), degree programming Two (Marques et al. 2010), positive mathematical programming (Esteve et al. 2015), and multiobjective programming (Mosleh et al. 2017) are used. In this regard, it should be noted that with the development of applied mathematical theories, game theory (Girard et al. 2016) and fuzzy mathematical theory (Nikoo et al. 2013) have been widely used. Given the weakness of mathematical models in simulating all variables affecting the hydrological situation, it cannot be considered a suitable tool for integrated management of watersheds (Mirzaei and Zibaei 2021). Therefore, the use of hydrological simulation tools and its integration with economic models can be effective in the integrated management of watersheds. Studies in this field have shown that the WEAP model is an effective tool to simulate the hydrological status of watersheds under climate change conditions (Lévite et al. 2003; Bhave et al. 2014; Li et al. 2015; Satti et al. 2015; Forni et al. 2016; Adgolign et al. 2016; Mishra et al. 2017; Khalil et al. 2018).

The WEAP model is a water resources planning tool based on the principle of water balance and represents the different and interrelated sectors such as water demand nodes, infrastructure, water flows, and water transmission channels (Yates et al. 2005). This model calculates the features of the hydrological cycle of watersheds by simulating rainfall-runoff processes and time series of climate data. Each watershed unit is divided into different land use classes, and the water balance is calculated under the climatic conditions of the watershed. In this model, experimental functions are used to describe and simulate evapotranspiration, runoff and surface currents, changes in soil moisture, basal river flow trends, and deep infiltration for each agricultural unit (Sieber and Purkey 2011). The MABIA method in WEAP software is a suitable tool for simulating such variables. This method simulates water requirements and crop performance and allows users to understand the effects of climate change and available water on crop growth. However, it should be noted that this method cannot evaluate the effects of CO_2 pollution on crops (Esteve et al. 2015). WEAP tool has various capabilities such as analyzing the components of surface and groundwater resources balance in different scales, evaluating quantitative and qualitative changes of water resources according to water withdrawals in different parts of the watershed, determining the share of different areas of watershed water resources, communication with remote sensing software such as GIS, calibration with existing watershed conditions, graphical display of the results of implementation of different policies in watersheds on sensitive variables, and flexibility of the model to change its components depending on the watershed conditions. The main advantage of WEAP in the integrated model of watershed management and planning approach is related to the simulation of water systems and its policy orientation. In its equations, WEAP equates issues of need (water consumption patterns, equipment efficiency, reuses, costs, and allocation) with resource issues (surface runoff, groundwater, reservoirs, and water transfers). WEAP is able to solve the water mass equilibrium equation for each node and connection in the system in different time steps.

Lack of attention to all environmental issues in watershed management is another weakness of integrated watershed management studies. Storing water resources and meeting the water needs of natural ecosystems such as wetlands in the watershed, balancing groundwater resources, reducing the withdrawal of surface water resources, paying attention to the quality of water resources, and the release of pollutants from various activities are environmental components that should be considered in watershed management and planning. Studies in this area show that most of the researchers have focused on the storage of water resources for environmental protection and environmental benefits (Nikouei et al. 2012; Nikouei and Ward 2013; Gohar et al. 2013; Akter et al. 2014; Kahil et al. 2015; Mirzaei and Zibaei 2021). In environmental economics, various methods are applied to measure the environmental benefits. These methods are classified into two general categories: revealed preferences and stated preferences. Revealed preferences are based on individuals' actual behaviors and choices, whereas the stated preferences are based on the individuals' statements about their choices in a hypothetical context (White and Lovett

1999). Contingent valuation is a method that has been used for more than 30 years to determine the preferences of consumers of environmental goods (which cannot be traded directly in the market) (MacMillan et al. 2006). Contingent valuation is one of the most widely used methods to estimate the economic value of nonmarket goods and services (Ndebele 2009; Johnston et al. 2017). This method is based on the existence of a hypothetical market in which the value assigned by each person to the product is examined (Pedroso et al. 2007). The literature on the valuation of nonmarket goods shows that contingent valuation has been widely used to estimate the benefits of the environment, especially wetlands (Bateman and Langford 1997; Loomis et al. 2000; Zhongmin et al. 2003; Wattage and Mardle 2007; Dias and Belcher 2015; Trenholm et al. 2017; Hassan 2017; Ndebele and Forgie 2017; Pueyo-Ros et al. 2018).

Some studies (see Van Meter et al. (2018) and Huang et al. (2019)) have pointed to the issue of water quality as a key environmental component in watershed management. A review of studies in this field revealed that the Soil and Water Assessment Tool (SWAT) is an effective tool in simulating the quality parameters of water resources (Malagó et al. 2019). The SWAT model is a complete watershed-scale tool developed by the US Agricultural Research Service to simulate the flow, sediment, nutrients, and chemical balance in the watersheds. This tool is provided for watersheds with soil, land use, and different management conditions in the future (Kumar et al. 2018). SWAT model inputs include hydrological information, climatic conditions, soil type, plant growth, agricultural and pesticide management, land management, and flow routing. The SWAT model is a process-oriented semi-distributed model that uses specific information in the fields of air, soil, topography, vegetation, and land cover. Also, this model enables users to simulate the parameters in long-term periods and thus is a continuous model in terms of time. In addition, this model can be schematic by incorporating GIS software and take advantage of it. The SWAT model includes key components of the US Department of Agriculture-Agricultural Research Service (USDA-ARS) models (Gassman et al. 2007).

Atmospheric pollutants from various activities in the watersheds are other environmental components that have received less attention from researchers in integrated watershed management studies. Today, the application of water-energy-food-environment nexus can overcome the weakness of integrated watershed management studies in addressing energy consumption issues and air pollution caused by these uses (González-Bravo et al. 2018; Li et al. 2019). For this purpose, mathematical programming methods are a suitable tool for formulating goals such as minimizing environmental pollution, like carbon dioxide and greenhouse gases from various activities in the watershed (González-Bravo et al. 2018; Li et al. 2019).

Recognizing and analyzing the users' behavior at the watershed level is a key component for management and planning. Therefore, it is necessary to use an efficient tool to simulate the behavior of different users in the watersheds. Various studies (Bandini et al. 2009; Akhbari and Grigg 2015; Farhadi et al. 2016; Mirzaei and

Zibaei 2021) show that ABMs are an effective and efficient tool for simulating behavioral and social complexities in water resources management in the watersheds. In ABMs, agents are recognized as independent entities that have specific knowledge and information (Parker et al. 2003). These agents can interact with each other and with a common environment. Agents are goal-oriented and can act on the environment and respond to political and market conditions (Wooldridge and Jennings 1995). Agents are identified by their intentions, rules of behavior, and decision complexities. An agent can be a software, model, individual, organization, group, etc. (Bonabeau 2002). In social processes, people or groups of people are known as agents, and agents' relationships represent the social relationships between them (Gilbert and Troitzsch 1999). Hence, in an ABM, the people and the social relations between them are modeled to achieve a specific goal (Macal and North 2006). Key factors in developing an ABM include defining the agents, accurately determining the different behaviors of the agents, defining the environment in which the agents are located, determining the relationship between the agents, developing a theory for the agents' reciprocal behavior together with the environment, developing an agent-related data set, and validating the behavioral model of the agents (Macal and North 2006).

Based on the literature analysis, it can be mentioned that integrated watershed management and planning has four dimensions: socioeconomic simulation, hydrological simulation, environmental simulation, and behavioral simulation (Fig. 22.1). It also introduces the most appropriate tools and solutions for simulating each of the components of integrated watershed management and planning.

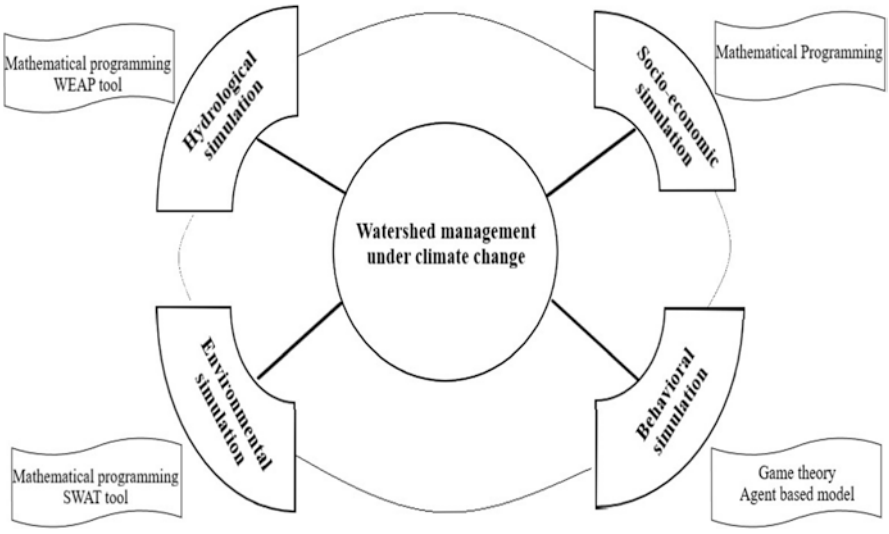

Fig. 22.1 Proposed framework for integrated management and planning of watersheds under climate change

Summary and Concluding Remarks

The main purpose of this chapter was to provide a conceptual framework in the field of tools and solutions for watershed management and planning in order to optimally allocate water resources between different sectors. To achieve this goal, the research literature was analyzed, and a conceptual framework was developed. The results demonstrated that most studies have considered the two main objectives of improving the economic efficiency of water consumption and environmental sustainability. In balance, the studies were divided into three general categories. The first group were studies that tried to help improve the economic efficiency of water consumption by simulating the hydrological components of the watershed. Most studies in this category have analyzed water resources management with respect to hydrological-economic modeling. In this category, different tools have been used for hydrological-economic modeling. The most important of these tools are simulation using mathematical functions in the form of mathematical programming software such as GAMS and WEAP software. The second group consisted of studies that estimated environmental benefits and simulated environmental factors affecting watershed management. The most widely used tools in this group of study were the use of mathematical relations to formulate the functions of environmental benefits and air pollutants resulting from various activities and the use of SWAT to simulate water pollution factors. The third category included studies that consider the users' behavior as an important component of watershed management. These studies have used tools such as game theory and ABM to simulate the behavioral complexities of the users. Finally, by summarizing the studies, a conceptual framework for sustainable watershed management tools and solutions was presented. Future researchers can use this model to study the impacts of climate change and water resources management policies in the watersheds. Given the comprehensiveness and operationality of this framework, it is suggested that it be used in integrated case studies around the world for integrated watershed management.

References

Abdelkader A, Elshorbagy A (2021) ACPAR: a framework for linking national water and food security management with global conditions. Adv Water Res 147:103809

Abdulbaki D, Al-Hindi M, Yassine A, Najm MA (2017) An optimisation model for the allocation of water resources. J Clean Prod 164:994–1006

Adgolign TB, Rao GS, Abbulu Y (2016) WEAP modeling of surface water resources allocation in Didessa Sub-Basin, West Ethiopia. Sustain Water Resour Manag 2(1):55–70

Akhbari M, Grigg NS (2013) A framework for an agent-based model to manage water resources conflicts. Water Resour Manag 27(11):4039–4052

Akhbari M, Grigg NS (2015) Managing water resources conflicts, modelling behavior in a decision tool. Water Resour Manag 29(14):5201–5216

Akter S, Grafton RQ, Merritt WS (2014) Integrated hydro-ecological and economic modeling of environmental flows: Macquarie marshes, Australia. Agric Water Manag 145:98–109

Alloisio I (2015) The water-energy-food nexus. Equilibrium 19(2):299–310
Anvari S, Mousavi SJ, Morid S (2014) Sampling/stochastic dynamic programming for optimal operation of multi-purpose reservoirs using artificial neural network-based ensemble streamflow predictions. J Hydroinf 16(4):907–921
Arnell NW, Gosling SN (2013) The impacts of climate change on river flow regimes at the global scale. J Hydrol 486:351–364
Arnell NW, van Vuuren DP, Isaac M (2011) The implications of climate policy for the impacts of climate change on global water resources. Glob Environ Chang 21(2):592–603
Bandini S, Manzoni S, Vizzari G (2009) Agent-based modeling and simulation: an informatics perspective. J Artif Soc Soc Simul 12(4):4
Bao C, Lu Y, Shang J (2004) Framework and operational procedure for implementing strategic environmental assessment in China. Environ Impact Assess Rev 24(1):27–46
Barthel R, Janisch S, Nickel D, Trifkovic A, Horhan T (2010) Using the multi actor-approach in Glowa-Danube to simulate decisions for the water supply sector under conditions of global climate change. Water Resou Manag 24:239–275
Bateman IJ, Langford IH (1997) Non-users' willingness to pay for a National Park: an application and critique of the contingent valuation method. Reg Stud 31(6):571–582
Bekchanov M, Ringler C, Bhaduri A, Jeuland M (2015) How would the Rogun Dam affect water and energy scarcity in Central Asia. Water Int 40:856–876
Bhaduri A, Barbier EB (2008) International water transfer and sharing: the case of the Ganges River. Environ Dev Econ 13(1):29–51
Bhaduri A, Liebe J (2002) Cooperation in trans boundary water sharing with issue linkage: game-theoretical case study in the Volta Basin. J Water Resour Plann Manag 139(3):235–245
Bhave AG, Mishra A, Raghuwanshi NS (2014) A combined bottom-up and top-down approach for assessment of climate change adaptation options. J Hydrol 518:150–161
Bino G, Sisson SA, Kingsford RT, Thomas RF, Bowen S (2015) Developing state and transition models of floodplain vegetation dynamics as a tool for conservation decision-making: a case study of the Macquarie Marshes Ramsar wetland. J Appl Ecol 52(3):654–664
Bizikova L, Roy D, Swanson D (2013) The water-energy-food security nexus: towards a practical planning and decision-support framework for landscape investment and risk management. The International Institute for Sustainable Development, Winnipeg
Blanco-Gutierrez I, Varela-Ortega C, Purkey DR (2013) Integrated assessment of policy interventions for promoting sustainable irrigation in semi-arid environments: a hydro-economic modeling approach. J Environ Manag 128:144–160
Bonabeau E (2002) Agent-based modelling, methods and techniques for simulating human systems. Proc Natl Acad Sci 99(3):7280–7287
Booker JF (1995) Hydrological and economic impacts of drought under alternative policy responses. J Am Water Resour Assoc 31(5):889–906
Braden JB (2000) Value of valuation: introduction. J Water Resour Plan Manag 126(6):336–338
Brinegar HR, Ward FA (2009) Basin impacts of irrigation water conservation policy. Ecol Econ 69(2):414–426
Cai X (2008) Implementation of holistic water resources-economic optimization models for river basin management – reflective experiences. Environ Model Softw 23:2–18
Cai X, McKinney DC, Lasdon LS (2003) Integrated hydrologic-agronomic- economic model for river basin management. ASCE J Water Resour Plann Manag 129(1):235–245
Carraro C, Marchiori C, Sgobbi A (2007) Negotiating on water: insights from non-cooperative bargaining theory. Environ Dev Econ 12(2):329–349
Centner T, Houston J, Keeler A, Fuchs C (1999) The adoption of best management practices to reduce agricultural water contamination. Limnologica-Ecol Manag Inland Waters 29:366–373
Cetinkaya CP, Gunacti MC (2018) Multi-criteria analysis of water allocation scenarios in a water scarce basin. Water Resour Manag 32(8):2867–2884
Chang CC (2003) The potential impact of climate change on Taiwan s agriculture. Agric Econ 27:51–64

Corrales J, Melodie G, Bhat MG, Mirrales-Wilhelm F (2014) Modeling a phosphorous credit trading program in an agricultural watershed. J Environ Manag 14:162–172
D'Odorico P, Carr J, Dalin C, Dell'Angelo J, Konar M, Laio F, Tuninetti M (2019) Global virtual water trade and the hydrological cycle: patterns, drivers, and socio-environmental impacts. Environ Res Lett 14(5):053001
Davidson NC (2014) How much wetland has the world lost? Long-term and recent trends in global wetland area. Mar Freshw Res 65:936–941
Davijani MH, Banihabib ME, Anvar AN, Hashemi SR (2016) Optimization model for the allocation of water resources based on the maximization of employment in the agriculture and industry sectors. J Hydrol 533(1):430–438
Demertzi KA, Papamichail DM, Georgiou PE, Karamouzis DN, Aschonitis VG (2014) Assessment of rural and highly seasonal tourist activity plus drought effects on reservoir operation in a semi-arid region of Greece using the WEAP model. Water Int 39(1):23–34
Di Luca A, Pitman AJ, de Elía R (2020) Decomposing temperature extremes errors in CMIP5 and CMIP6 models. Geophys Res Lett 47(14):e2020GL088031
Dias V, Belcher K (2015) Value and provision of ecosystem services from prairie wetlands: a choice experiment approach. Ecosyst Serv 15:35–44
Diaz GE, Brown TC (1997) Aquarius: an object-oriented model for efficient allocation of water in river basins. In: Warwick JJ (ed) Symposium water resources education, training, and practice: opportunities for the next century, June 29–July 3, 1997, Keystone, CO, pp 835–844
Döll P (2002) Impact of climate change and variability on irrigation requirements: a global perspective. Clim Chang 54(3):269–293
Dowd BM, Press D, Los Huertos M (2008) Agricultural nonpoint source water pollution policy: the case of California's Central Coast. Agric Ecosyst Environ 128:151–161
Downing TE (2012) Views of the frontiers in climate change adaptation economics. WIREs Clim Change 3:161–170
Draper AJ, Munevar A, Arora SK, Reyes E, Parker NL, Chung FI, Peterson LE (2004) CalSim: generalized model for reservoir system analysis. J Water Resour Plan Manag 130(6):480–489
Edson D (2004) Executive Director, National Association of Resource Districts. Brian Dowd, personal communication, September 25, 2004
Eisner MA (2004) Corporate environmentalism, regulatory reform, and industry self-regulation: toward genuine regulatory reinvention in the United States. Governance 17(2):145–167
El-Gafy I (2017) Water–food–energy nexus index: analysis of water-energy-food nexus of crop's production system applying the indicators approach. Appl Water Sci 7:2857–2868
Eliasson J (2015) The rising pressure of global water shortages. Nature 517(7532):6
Erfani T, Binions O, Harou J (2015) Protecting environmental flows through enhanced water licensing and water markets. Hydrol Earth Syst Sci 19:675–689
Esteve P, Varela-Ortega C, Gutierrez I, Downing TE (2015) A hydro-economic model for the assessment of climate change impacts and adaptation in irrigated agriculture. Ecol Econ 120:49–58
Eyring V, Bony S, Meehl GA, Senior CA, Stevens B, Stouffer RJ, Taylor KE (2016) Overview of the coupled model Intercomparison project phase 6 (CMIP6) experimental design and organization. Geosci Model Dev 9(5):1937–1958
FAO (2011) The state of the World's land and water resources for food and agriculture. Managing systems at risk. Earthscan, Abingdon
Farhadi S, Nikoo MR, Rakhshandehroo GR, Akhbari M, Alizadeh MR (2016) An agent-based-Nash modeling framework for sustainable groundwater management: a case study. Agric Water Manag 177:348–358
Fiorillo F, Esposito L, Guadagno FM (2007) Analyses and forecast of water resources in an ultracentenarian spring discharge series from Serino (Southern Italy). J Hydrol 336(1–2):125–138
Forni LG, Medellin-Azuara J, Tansey M, Young C, Purkey D, Howitt R (2016) Integrating complex economic and hydrologic planning models: an application for drought under climate change analysis. Water Resour Econ 16:15–27

Foster T, Brozović N (2018) Simulating crop-water production functions using crop growth models to support water policy assessments. Ecol Econ 152:9–21
Freeman AM (2003) The measurement of environmental and resource values: theory and methods, 2nd edn. Resources for the Future Press, Washington, DC, 496 pp
Gaiser T, Printz A, Schwarz von Raumer HG, G€otzinger J, Dukhovny VA, Barthel R, Sorokin A, Tuchin A, Kiourtsidis C, Ganoulis I, Stahr K (2008) Development of a regional model for integrated management of water resources at the basin scale. Phys Chem Earth 33(1–2):175–182
Galán JM, López-Paredes A, del Olmo R (2009) An agent-based model for domestic water management in Valladolid metropolitan area. Water Resour Res 45(5):1–17
Gao J, Christensen P, Kørnøv L (2017) Indicators' role: how do they influence strategic environmental assessment and sustainable planning – the Chinese experience. Sci Total Environ 592:60–67
Gassman PW, Reyes MR, Green CH, Arnold JG (2007) The soil and water assessment tool: historical development, applications, and future research directions. Trans ASABE 50(4):1211–1250
Georgakakos KP (2012) Water supply and demand sensitivities of linear programming solutions to a water allocation problem. Appl Math 3(10):1285–1297
George B, Malano H, Davidson B, Hellegers P, Bharati L, Massuel S (2011) An integrated hydro-economic modelling framework to evaluate water allocation strategies I: model development. Agric Water Manag 98(5):733–746
Gilbert N, Troitzsch KG (1999) Simulation for the social scientist. Open University Press
Gilvear DJ, Spray CJ, Casas-Mulet R (2013) River rehabilitation for the delivery of multiple ecosystem services at the river network scale. J Environ Manag 126:30–43
Girard C, Rinaudo J-D, Pulido-Velazquez M, Caballero Y (2015) An interdisciplinary modelling framework for selecting adaptation measures at the river basin scale in a global change scenario. Environ Model Softw 69:42–54
Girard C, Rinaudo J, Pulido-Velazquez M (2016) Sharing the cost of a river basin adaptation portfolios to climate change: insights from social justice and cooperative game theory. Water Resour Res 52(10):7945–7962
Gisser M, Mercado A (1972) Integration of the agricultural demand function for water and the hydrologic model of the Pecos basin. Water Resour Res 8(6):1373–1384
Gisser M, Mercado A (1973) Economic aspects of ground water resources and replacement flows in semiarid agricultural areas. Am J Agric Econ 55(3):461–466
Gleick HP, Cooley H, Cohen M, Morikawa M, Morrison J, Palaniappan M (2009) The world's water 2008–2009: the biennial report on freshwater resources. Island Press, Washington, DC
Gohar AA, Ward FA (2010) Gains from expanded irrigation water trading in Egypt: an integrated basin approach. Ecol Econ 69:2535–2548
Gohar AA, Ward FA, Amer SA (2013) Economic performance of water storage capacity expansion for food security. J Hydrol 484:16–25
Gohar AA, Amer SA, Ward FA (2015) Irrigation infrastructure and water appropriation rules for food security. J Hydrol 520:85–100
González-Bravo R, Sauceda-Valenzuela M, Mahlknecht J, Rubio-Castro E, Ponce-Ortega JM (2018) Optimization of water grid at macroscopic level analyzing water-energy-food nexus. ACS Sustain Chem Eng 6:12140–12152
Gorelick SM, Zheng C (2015) Global change and the groundwater management challenge. Water Resour Res 51(5):3031–3051
Griffin RC (1998) The fundamental principles of cost-benefit analysis. Water Resour Res 34(8):2063–2071
Griffin RC (2006) Water resource economics: the analysis of scarcity, policies and project. MIT Press, London
Groves DG, Yates D, Tebaldi C (2008) Developing and applying uncertain global climate change projections for regional water management planning. Water Resour Res 44:W12413
Gurluk S, Ward FA (2009) Integrated basin management: water and food policy options for Turkey. Ecol Econ 68:2666–2678

Han Y, Huang YF, Wang GQ, Maqsood I (2011) A multi-objective linear programming model with interval parameters for water resources allocation in Dalian city. Water Resou Manag 25:449–463
Hanak E, Lund JR (2012) Adapting California's water management to climate change. Clim Chang 111(1):17–44
Harou JJ, Pulido-Velazquez M, Rosenberg D, Mdellin-Azuara J, Howitt R (2009) Hydro-economic models: concepts, design, applications and future prospects. J Hydrol 375:627–643
Hassan S (2017) Environmental attitudes and preference for wetland conservation in Malaysia. J Nat Conserv 37:133–145
Hassan-Esfahani L, Torres-Rua A, Mckee M (2015) Assessment of optimal irrigation water allocation for pressurized irrigation system using water balance approach, learning machines, and remotely sensed data. Agric Water Manag 153:42–50
He L, Du P, Chen YZ, Lu HW, Cheng X, Chang B, Wang Z (2017) Advances in microbial fuel cells for wastewater treatment. Renew Sust Energ Rev 71:388–403
Hoff H (2011) Understanding the nexus. Background paper for the Bonn 2011 conference: the water, energy and food security nexus. Stockholm Environment Institute, Stockholm
Hope C (2005) Integrated assessment models. In: Helm D (ed) Climate change policy. Oxford University Press, Oxford, pp 77–98
Horan RD, Shortle JS, Abler DG (1999) Green payments for nonpoint pollution control. Am Agric Econ Assoc 81(5):1210–1215
Horan RD, Shortle JS, Abler DG (2002) Point-nonpoint nutrient trading in the Susquehanna River basin. Water Resour Res 38(5). https://doi.org/10.1029/2001WR000853
Hu Z, Wei C, Yao L, Li C, Zeng Z (2016) Integrating equality and stability to resolve water allocation issues with a multi-objective bi-level programming model. J Water Resour Plann Manag 142(7):1–12
Huang J, Zhang Y, Arhonditsis GB, Gao J, Chen Q, Wu N et al (2019) How successful are the restoration efforts of China's lakes and reservoirs? Environ Int 123:96–103
Huber-Lee A, Purkey DR, Sieber J, Swartz C, Young C (2004) Sustainable water supply planning for three US cities: contrasts in climates and stakeholder issues. In: Paper presented at the Stockholm water symposium, August 2004. Stockholm, pp 16–20
Hum NNMF, Abdul Talib SA (2016) Modeling water supply and demand for effective water management allocation in Selangor. Jurnal Teknologi 78(5–5). https://doi.org/10.11113/jt.v78.8569
IPCC (2007) Impacts, adaptation, and vulnerability. Contribution of working group II to the third assessment report. Cambridge University Press, Cambridge
Jiménez Cisneros BE, Oki T, Arnell NW, Benito G, Cogley JG, Döll P, Jiang T, Mwakalila SS (2014) Chapter 3: Freshwater resources. In: Field CB, Barros VR, Dokken DJ, Mach KJ, Mastrandrea MD, Bilir TE, Chatterjee M (eds) Climate change 2014: impacts, adaptation, and vulnerability. Part a: global and sectoral aspects. Contribution of working group II to the fifth assessment report of the intergovernmental panel on climate change. Cambridge University Press, Cambridge/New York, pp 229–269
Johansson RC, Tsur Y, Roe TL, Doukkali R, Dinar A (2002) Pricing irrigation water: a review of theory and practice. Water Policy 4(2):173–199
Johnston RJ, Boyle KJ, Adamowicz W, Bennett J (2017) Contemporary guidance for stated preference studies. J Assoc Environ Resour Econ 4(2):319–405
Joyce BA, Mehta VK, Purkey DR, Dale LL, Hanemann M (2011) Modifying agricultural water management to adapt to climate change in California's central valley. Climate Change 109:299–316
Just RE, Hueth DL, Schmitz A (2005) The welfare economics of public policy: a practical approach to project and policy evaluation. Edward Elgar Publishing
Kahil MT, Dinar A, Albiac J (2015) Modelling water scarcity and droughts for policy adaptation to climate change in arid and semiarid regions. J Hydrol 522:95–109
Kahil MT, Ward F, Albiac J, Eggleston J, Sanz D (2016) Hydro-economic modeling with aquifer–river interactions to guide sustainable basin management. J Hydrol 539:510–524

Kemfert C (2009) Climate protection requirements – the economic impact of climate change. In: Handbook utility management. Springer
Khalil A, Rittima A, Phankamolsil Y (2018) The projected changes in water status of the Mae Klong Basin, Thailand, using WEAP model. Paddy Water Environ 16(3):439–455
Kharrazi A, Akiyama T, Yu Y, Li J (2016a) Evaluating the evolution of the Heihe River basin using the ecological network analysis: efficiency, resilience, and implications for water resource management policy. Sci Total Environ 572:688–696
Kharrazi A, Fath BD, Katzmair H (2016b) Advancing empirical approaches to the concept of resilience: a critical examination of paparchy, ecological information, and statistical evidence. Sustainability 8(9):935
Kim YH, Min SK, Zhang X, Sillmann J, Sandstad M (2020) Evaluation of the CMIP6 multi-model ensemble for climate extreme indices. Weather Clim Extremes 29:100269
Kock BE (2008) Agent-based models of socio-hydrological systems for exploring the institutional dynamics of water resources conflict. Master's thesis, Massachusetts Institute of Technology
Kojiri T, Hori T, Nakatsuka J, Chong T (2008) World continental modeling for water resources using system dynamics. Phys Chem Earth Parts A/B/C 33(5):304–311
Koutiva I, Makropoulos C (2016) Modelling domestic water demand, an agent based approach. Environ Model Softw 79:35–54
Kumar N, Singh SK, Singh VG, Dzwairo B (2018) Investigation of impacts of land use/land cover change on water availability of Tons River Basin, Madhya Pradesh, India. Model Earth Syst Environ 4(1):295–310
Kuwayama Y, Brozović N (2013) The regulation of a spatially heterogeneous externality: tradable groundwater permits to protect streams. J Environ Econ Manag 66:364–382
Lamers LP, Vile MA, Grootjans AP, Acreman MC, van Diggelen R, Evans MG et al (2015) Ecological restoration of rich fens in Europe and North America: from trial and error to an evidence-based approach. Biol Rev 90(1):182–203
Larson DM, Helfand GE, House BW (1996) Second-best tax policies to reduce nonpoint source pollution. Am J Agric Econ 78(4):1108–1117
Lefkoff LJ, Gorelick SM (1990) Benefits of an irrigation water rental market in a saline stream-aquifer system. Water Resour Res 26(7):1371–1381
Lepistö A, Kenttämies K, Rekolainen S (2001) Modeling combined effects of forestry, agriculture and deposition on nitrogen export in a Northern River basin in Finland. Ambio 30:338–348
Lévite H, Sally H, Cour J (2003) Testing water demand management scenarios in a water-stressed basin in South Africa: application of the WEAP model. Phys Chem Earth Parts A/B/C 28(20–27):779–786
Li X, Zhao Y, Shi C, Sha J, Wang ZL, Wang Y (2015) Application of water evaluation and planning (WEAP) model for water resources management strategy estimation in coastal Binhai New Area, China. Ocean Coast Manag 106:97–109
Li M, Fu Q, Singh VP, Ma M, Liu X (2017) An intuitionistic fuzzy multi-objective non-linear programming model for sustainable irrigation water allocation under the combination of dry and wet conditions. J Hydrol 555:80–94
Li M, Fu Q, Singh VP, Ji Y, Liu D, Zhang C, Li T (2019) An optimal modelling approach for managing agricultural water-energy-food nexus under uncertainty. Sci Total Environ 651:1416–1434
Lichtenberg E (1992) Alternative approaches to pesticide regulation. Northeastern J Agric Resour Econ 21:83–92
Liu R, Zhang P, Wang X, Chen Y, Shen Z (2013) Assessment of effects of best management practices on agricultural non-point source pollution in Xiangxi River watershed. Agric Water Manag 117:9–18
Liu R, Xu F, Zhang P, Yu W, Men C (2015) Identifying non-point source critical source areas based on multi-factors at a basin scale with SWAT. J Hydrol 533:379–388
Loomis J, Kent P, Strange L, Fausch K, Covich A (2000) Measuring the total economic value of restoring ecosystem services in an impaired river basin: results from a contingent valuation survey. Ecol Econ 33:103–117

Lu HW, Li J, Ren LX, Chen YZ (2018) Optimal groundwater security management policies by control of inexact health risks under dual uncertainty in slope factors. Chemosphere 198:161–173
Lund JR, Cai X, Characklis GW (2006) Economic engineering of environmental and water resource systems. J Water Resour Plan Manag 132(6):399–402
Macal CM, North MJ (2006) Tutorial on agent-based modeling and simulation part 2, how to model with agents. Winter Simulation Conference, pp 73–83
MacMillan D, Hanley N, Lienhoop N (2006) Contingent valuation: environmental polling or preference engine. Ecol Econ 60:299–307
Maillard P, Santos NA (2008) A spatial-statistical approach for modeling the effect of non-point source pollution on different water quality parameters in the Velhas river watershed-Brazil. J Environ Manag 86:158–170
Malagó A, Bouraoui F, Pastori M, Gelati E (2019) Modelling nitrate reduction strategies from diffuse sources in the Po River basin. Water 11(5):1030
Maliqi E, Singh SK (2019) Quantitative estimation of soil erosion using open-access earth observation data sets and erosion potential model. Water Conserv Sci Eng 4(4):187–200
Marques GF, Lund JR, Howitt RE (2010) Modeling conjunctive use operations and farm decisions with two-stage stochastic quadratic programming. J Water Resour Plan Manag 136(3):386–394
McKinney D, Cai X, Rosegrant MW, Ringler C, Scott CA (1999) Modeling water resources management at the basin level: review and future directions, SWIM Paper 6. International Water Management Institute, Colombo
Meaurio M, Zabaleta A, Uriarte JA, Srinivasan R, Antigüedad I (2015) Evaluation of SWAT models' performance to simulate streamflow spatial origin. The case of a small forested watershed. J Hydrol 525:326–334
Menell P (1990) The limitation of legal institutions for addressing environmental risk. J Econ Perspect 5:93–114
Meng B, Liu JL, Bao K, Sun B (2019) Water fluxes of Nenjiang River Basin with ecological network analysis: conflict and coordination between agricultural development and wetland restoration. J Clean Prod 213:933–943
Mirzaei A, Zibaei M (2021) Water conflict management between agriculture and wetland under climate change: application of economic-hydrological-Behavioral modelling. Water Resour Manag 35(1):1–21
Mishra AK, Kumar B, Dutta J (2016) Prediction of hydraulic conductivity of soil bentonite mixture using Hybrid-ANN approach. J Environ Inf 27(2):98–105
Mishra BK, Regmi RK, Masago Y, Fukushi K, Kumar P, Saraswat C (2017) Assessment of Bagmati river pollution in Kathmandu Valley: scenario-based modeling and analysis for sustainable urban development. Sustain Water Qual Ecol 9:67–77
Moharir K, Pande C, Singh S, Choudhari P, Rawat K, Jeyakumar L (2020) Spatial interpolation approach-based appraisal of groundwater quality of arid regions in. Aqua J (IWA Publication) 68(6):431–447. Impact Factor: 1.05
Molden D, Oweis T, Steduto P, Bindraban P, Hanjra MA, Kijne J (2009) Improving agricultural water productivity, between optimism and caution. Agric Water Manag 97(4):528–535
Moriondo M, Bindi M, Zbigniew W, Kundzewicz Szwed M, Chorynski A, Matczak P, Radziejewski M, McEvoy D, Wreford A (2010) Impact and adaptation opportunities for European agriculture in response to climatic change and variability. Mitig Adapt Strat Glob Change 15(7):657–679
Mosavi SH (2016) Energy price reform and food markets: the case of bread supply chain in Iran. Agric Econ 47(2):169–179
Mosavi SH, Esmaeili A (2012) Self-sufficiency versus free trade: the case of rice in Iran. J Int Food Agribus Mark 24(1):76–90
Mosleh Z, Salehi MH, Fasakhodi AA, Jafari A, Mehnatkesh A, Borujeni IE (2017) Sustainable allocation of agricultural lands and water resources using suitability analysis and mathematical multi-objective programming. Geoderma 303:52–59

Mouri G, Takizawa S, Oki T (2011) Spatial and temporal variation in nutrient parameters in stream water in a rural-urban catchment, Shikoku, Japan: effects of land cover and human impact. J Environ Manag 92:1837–1848
Mulligan KB, Brown C, Yang YCE, Ahlfeld DP (2014) Assessing groundwater policy with coupled economic-groundwater hydrologic modeling. Water Resour Res 50(3):2257–2275
Naghavi S, Ebrahimi-Khusfi Z, Mirzaei A (2021) Decoupling pollution-agricultural growth and predicting climate change impacts on decoupling index using Bayesian network in different climatic regions. Environ Sci Pollut Res 29:1–18
Nature Climate Change (2019) The CMIP6 landscape. Nat Clim Change 9:727–727
Ndebele T (2009) Economic non-market valuation techniques: Theory and application to ecosystems and ecosystem services. Ph.D. thesis, Massey University, Palmerston North, New Zealand
Ndebele T, Forgie V (2017) Estimating the economic benefits of a wetland restoration program in New Zealand: a contingent valuation approach. Econ Anal Policy 55:75–89
Newlin BD, Jenkins MW, Lund JR, Howitt RE (2002) Southern California water markets: potential and limitations. J Water Resour Plann Manag – ASCE 128(1):21–32
Nhamo L, Mabhaudhi T, Mpandeli S, Dickens C, Nhemachena C, Senzanje A, Naidoo D, Liphadzi S, Modi AT (2020) An integrative analytical model for the water-energy-food nexus: South Africa case study. Environ Sci Pol 109:15–24
Nie S, Fu S, Cao W, Jia X (2020) Comparison of monthly air and land surface temperature extremes simulated using CMIP5 and CMIP6 versions of the Beijing Climate Center climate model. Theor Appl Climatol 140(1):487–502
Nikolic VV, Simonovic SP, Milicevic DB (2013) Analytical support for integrated water resources management, a new method for addressing spatial and temporal variability. Water Resou Manag 27:401–417
Nikoo MR, Kerachian R, Karimi A, Azadmia AA (2013) Optimal water and waste-load allocations in rivers using a fuzzy transformation technique: a case study. Environ Monit Assess 185(3):2483–2502
Nikouei A, Ward FA (2013) Pricing irrigation water for drought adaptation in Iran. J Hydrol 503:29–46
Nikouei A, Zibaei M, Ward FA (2012) Incentives to adopt irrigation water saving measures for wetlands preservation: an integrated basin scale analysis. J Hydrol 464–465:216–232
Noel JE, Howitt RE (1982) Conjunctive multi-basin management-an optimal control approach. Water Resour Res 18(4):753–763
Noel JE, Gardner BD, Moore CV (1980) Optimal regional conjunctive water management. Am J Agric Econ 62(3):489–498
Obropta CC, Niazi M, Kardos JS (2008) Application of an environmental decision support system to a water quality trading program affected by surface water diversions. Environ Manag 42:946–956
OECD (ed) (2006) Water and agriculture sustainability, markets and policies. OECD Publishing
Ongley ED, Xiaolan Z, Tao Y (2010) Current status of agricultural and rural non-point source pollution assessment in China. Environ Pollut 158(5):1159–1168
Orubu CO (2006) Water resources, environment and sustainable development in Nigeria. J Hum Ecol 19(3):169–181
Pande CB, Moharir K (2015) GIS based quantitative morphometric analysis and its consequences: a case study from Shanur River Basin, Maharashtra India. Appl Water Sci, Springer Journal, ISSN 2190-5487, Volume-7, Number-2 Published online 23 June 2015
Pande CB, Moharir KN (2021) Estimation of crop and forest biomass resources in semi – arid region using satellite data and GIS. J Saudi Soc Agric Sci. Elsevier. 2021 Source Normalized Impact per Paper (SNIP): 3.560. https://doi.org/10.1016/j.jssas.2021.03.0021658-077X/_2021
Pande CB, Moharir KN, Singh SK, Varade AM (2019) An integrated approach to delineate the groundwater potential zones in Devdari watershed area of Akola district, Maharashtra, Central India. Environ Dev Sustain, Springer Journal, Impact Factor: 1.67. https://doi.org/10.1007/s10668-019-00409-1

Parker DC, Manson SM, Janssen MA, Hoffmann MJ, Deadman P (2003) Multi-agent systems for the simulation of land-use and land-cover change: a review. Ann Assoc Am Geogr 93(2):314–337

Parsapour-Moghaddam P, Abed-Elmdoust A, Kerachian R (2015) A heuristic evolutionary game theoretic methodology for conjunctive use of surface and groundwater resources. Water Resour Manag 29(11):3905–3918

Pastor AV, Palazzo A, Havlik P, Biemans H, Wada Y, Obersteiner M, Ludwig F (2019) The global nexus of food-trade-water sustaining environmental flows by 2050. Nat Sustain 2(6):499–507

Peck DE, Mcleod DM, Hewlett JP, Lovvorn JR (2004) Irrigation dependent wetlands versus instream flow enhancement, economics of water transfer from agriculture to wildlife uses. Environ Manag 34(6):842–855

Pedroso C, Freitas H, Domingos T (2007) Testing for the survey mode effect on contingent valuation data quality: a case study of web based versus in-person interview. Ecol Econ 62:388–398

Pueyo-Ros J, Garcia X, Ribas A, Fraguell RM (2018) Ecological restoration of a coastal wetland at a mass tourism destination. Will the recreational value increase or decrease? Ecol Econ 148:1–14

Pulido-Velazquez M, Andreu J, Sahuquillo A (2006) Economic optimization of conjunctive use of surface water and groundwater at the basin scale. J Water Resour Plan Manag 132(6):454–467

Purkey DR, Joyce B, Vicuna S, Hanemann MW, Dale LL, Yates D, Dracup JA (2008) Robust analysis of future climate change impacts on water for agriculture and other sectors: a case study in the Sacramento Valley. Clim Chang 87(S1):109–122

Ramsar Convention on Wetlands, FAO, International Water Management Institute (2014) Wetlands and agriculture: partners for growth. Accessed 19 Jan 2018

Raskin P, Hansen E, Zhu Z, Stavisky D (1992) Simulation of water supply and demand in the Aral Sea region. Water Int 17(2):55–67

Rawat KS, Singh SK (2017) Estimation of surface runoff from semi-arid ungauged agricultural watershed using SCS-CN method and earth observation data sets. Water Conserv Sci Eng 1(4):233–247

Rawat KS, Singh SK, Szilard S (2021) Comparative evaluation of models to estimate direct runoff volume from an agricultural watershed. Geol Ecol Landsc 5(2):94–108

Rogers P, Smith DV (1970) The integrated use of ground and surface water in irrigation project planning. Am J Agric Econ 52(1):13–24. https://doi.org/10.2307/1238158

Ringler C, Cai X (2006) Valuing fisheries and wetlands using integrated economic–hydrologic modeling Mekong River Basin. J Water Resour Plan Manag 132(6):480–487

Ringler C, Huy NV (2004) Water allocation policies for the Dong Nai River Basin in Vietnam: an integrated perspective. International Food Policy Research Institute

Rochdane S, Reichert B, Messouli M, Babqiqi A, Khebiza MY (2012) Climate change impacts on water supply and demand in Rheraya watershed (Morocco), with potential adaptation strategies. Water 4:28–44

Rong Q, Cai Y, Chen B, Yue W, Yin X, Tan Q (2017) An enhanced export coefficient-based optimization model for supporting agricultural nonpoint source pollution mitigation under uncertainty. Sci Total Environ 580:1351–1362

Rosegrant MW, Ringler C, McKinney DC, Cai X, Keller A, Donoso G (2000) Integrated economic-hydrologic water modeling at the basin scale: the Maipo River basin. Agric Econ 24(1):33–46

Russi D, ten Brink P, Farmer A, Badura T, Coates D, Förster J et al (2013) The economics of ecosystems and biodiversity for water and wetlands. IEEP, London/Brussels, p 78

Sadeghi SH, Moghadam ES, Delavar M, Zarghami M (2020) Application of water-energy-food nexus approach for designating optimal agricultural management pattern at a watershed scale. Agric Water Manag 233:106071

Salamon LM (2002) The new governance and the tools of public action: an introduction. In: Salamon LM (ed) The tools of government. Oxford University Press, New York

Salehi S, Chizari M, Sadighi H, Bijani M (2018) Assessment of agricultural groundwater users in Iran: a cultural environmental bias. Hydrogeol J 26(1):285–295

Satti S, Zaitchik B, Siddiqui S (2015) The question of Sudan: a hydro-economic optimization model for the Sudanese Blue Nile. Hydrol Earth Syst Sci 19(5):2275–2293
Shen Z, Liao Q, Hong Q, Gong Y (2012) An overview of research on agricultural non-point source pollution modelling in China. Sep Purif Technol 84:104–111
Shen Z, Zhong Y, Huang Q, Chen L (2015) Identifying non-point source priority management areas in watersheds with multiple functional zones. Water Res 68C:563–571
Shortle JS, Horan RD (2001) The economics of nonpoint pollution control. J Econ Surv 15(3):255–289
Shortle JS, Horan RD, Abler DG (1998) Research issues in nonpoint pollution control. Environ Resour Econ 11(3–4):571–585
Sieber J, Purkey D (2011) WEAP, water evaluation and planning system. User Guide, Stockholm Environment Institute, U.S. Center, Somerville
Siebert S, Burke J, Faures JM, Frenken K, Hoogeveen J, Döll P, Portmann FT (2010) Groundwater use for irrigation-a global inventory. Hydrol Earth Syst Sci 14:1863–1880
Simonovic SP, Fahmy H (1999) A new modeling approach for water resources policy analysis. Water Resour Res 35(1):295–304
Srivastava A, Grotjahn R, Ullrich PA (2020) Evaluation of historical CMIP6 model simulations of extreme precipitation over contiguous US regions. Weather Clim Extremes 29:100268
Stacke T, Hagemann S (2012) Development and evaluation of a global dynamical wetland's extent scheme. Hydrol Earth Syst Sci 16(8):2915–2933
Steffen W, Richardson K, Rockström J, Cornell SE, Fetzer I, Bennett EM, Biggs R, Carpenter SR, Vries WD, Wit CA, Folke C, Gerten D, Heinke J, Mace GM, Persson LM, Ramanathan V, Reyers B, Sörlin S (2015) Planetary boundaries: guiding human development on a changing planet. Science 347(6223):1259855
Strauch M, Lima JE, Volk M, Lorz C, Makeschin F (2013) The impact of best management practices on simulated streamflow and sediment load in a Central Brazilian catchment. J Environ Manag 127:S24–S36
Strokal M, Kroeze C, Li L, Luan S, Wang H, Yang S, Zhang Y (2015) Increasing dissolved nitrogen and phosphorus export by the Pearl River (Zhujiang): a modeling approach at the sub-basin scale to assess effective nutrient management. Biogeochemistry 125:221–242
Su B, Huang J, Mondal SK, Zhai J, Wang Y, Wen S, Gao M, Yanran L, Jiang S, Jiang T, Li A (2021) Insight from CMIP6 SSP-RCP scenarios for future drought characteristics in China. Atmos Res 250:105375
Tamene L, Le QB, Vlek PLG (2014) A landscape planning and management tool for land and water resources management, an example application in Northern Ethiopia. Water Resour Manag 28(2):407–424
Thomas JS, Durham B (2003) Integrated water resource management: looking at the whole picture. Desalination 156(1–3):21–28
Tisdell J (2010) Acquiring water for environmental use in Australia: an analysis of policy options. Water Resour Manag 24(8):1515–1530
Tol RSJ (2002) New estimates of the damage costs of climate change, part I: benchmark estimates. Environ Resour Econ 21:47–73
Trenholm R, Haider W, Lantz V, Knowler D, Haegeli P (2017) Landowner preferences for wetlands conservation programs in two Southern Ontario watersheds. J Environ Manag 200:6–21
Turner K (1991) Economics and wetland management. Ambio 20:59–63
Turner RK, Morse-Jones S, Fisher B (2010) Ecosystem valuation. Ann NY Acad Sci 1185(1):79–101
UN (2015) World population prospects: the 2015 revision. Department of Economic and Social Affairs, Population Division, New York. http://esa.un.org/unpd/wpp/
UN (2017) World population prospects: the 2017 revision. Department of Economic and Social Affairs, Population Division, New York. http://esa.un.org/unpd/wpp/
United Nations World Water Development Report (2015) Water for a sustainable World, the 2015 edition of the United Nations World Water Development Report (WWDR 2015, on March 20)

United States Department of Agriculture, Farm Service Agency (USDA-FSA) (2007) Conservation reserve program monthly survey July 2007. USDA, Washington, DC. Available at: http://www.fsa.usda.gov/Internet/FSA_File/jul2007.pdf. Accessed 24 Aug 2007

Van Meter KJ, Van Cappellen P, Basu NB (2018) Legacy nitrogen may prevent achievement of water quality goals in the Gulf of Mexico. Science 360(6387):427–430

Ventrella D, Charfeddine M, Moriondo M, Rinaldi M, Bindi M (2012) Agronomic adaptation strategies under climate change for winter durum wheat and tomato in southern Italy: irrigation and nitrogen fertilization. Reg Environ Chang 12:407–419

Villamizar ML, Brown CD (2016) Modelling triazines in the valley of the River Cauca, Colombia, using the annualized agricultural non-point source pollution model. Agric Water Manag 177:24–36

Vinten A, Kuhfuss L, Shortall O, Stockan J, Ibiyemi A, Pohle I et al (2019) Water for all: towards an integrated approach to wetland conservation and flood risk reduction in a lowland catchment in Scotland. J Environ Manag 246:881–896

Volk M, Hirschfeld J, Dehnhardt A, Schmidt G, Bohn C, Liersch S, Gassman PW (2008) Integrated ecological-economic modelling of water pollution abatement management options in the upper Ems River basin. Ecol Econ 66(1):66–76. S0921800908000402. https://doi.org/10.1016/j.ecolecon.2008.01.016

Vorosmarty CJ, McIntyre PB, Gessner MO, Dudgeon D, Prusevich A, Green P, Glidden S, Bunn SE, Sullivan CA, Reidy Liermann C, Davies PM (2010) Global threats to human water security and river biodiversity. Nature 467:555–561

Wang Q, Jiang R, Li R (2018) Decoupling analysis of economic growth from water use in City: a case study of Beijing, Shanghai, and Guangzhou of China. Sustain Cities Soc 41:86–94

Ward FA (2014) Economic impacts on irrigated agriculture of water conservation programs in drought. J Hydrol 508:114–127

Ward FA, Lynch TP (1996) Integrated river basin optimization: modeling economic and hydrologic interdependence. Water Resour Bull 32(6):1127–1138

Ward FA, Pulido-Velazquez M (2009) Water conservation in irrigation can increase water use. Proc Natl Acad Sci 105:18215–18220

Wattage P, Mardle S (2007) Total economic value of wetland conservation in Sri Lanka identifying use and non-use values. Wetland Ecol Manag 16(5):359–369

Wetzstein ME, Centner TJ (1992) Regulating agricultural contamination of groundwater through strict liability and negligence legislation. J Environ Econ Manag 22:1–11

White PCL, Lovett JC (1999) Public preferences and willingness-to-pay for nature conservation in the North York Moors National Park UK. J Environ Manag 55:1–13

Wilhite DA (2005) Drought and water crises science, technology and management issues. CRC Press/Taylor & Francis Group

Wooldridge MJ, Jennings NR (1995) Intelligent agents, theory and practice. Knowl Eng Rev 10(2):115–152

Wu J, Chang I, Bina O, Lam K, Xu H (2011) Strategic environmental assessment implementation in China d five-year review and prospects. Environ Impact Assess Rev 31(1):77–84

WWAP (United Nations World Water Assessment Programme/UN-Water) (2018) The United Nations world water development report 2018: nature-based solutions for water. UNESCO, Paris

WWAP (World Water Assessment Programme) (2012) The United Nations world water development report 4: managing water under uncertainty and risk. UNESCO, Paris

Yaqob EY, Sorial G, Sudian M (2015) Simulation of transboundary wastewater resource management scenarios in the Wadi Zomer watershed, using a WEAP model. Int J Basic Appl Sci 4(1):27

Yaqubi M, Shahraki J, Sabouhi Sabouni M (2016) On dealing with the pollution costs in agriculture: a case study of paddy fields. Sci Total Environ 556:310–318

Yates D, Sieber J, Purkey D, Huber-Lee A (2005) WEAP21 – a demand-, priority-, and preference-driven water planning model. Part 1: model characteristics. Water Int 30(4):487–500

Yuan XC, Wei YM, Pan SY, Jin JL (2014) Urban household water demand in Beijing by 2020, An agent-based model. Water Resour Manag 28(10):2967–2980
Zargar PR, Noorzad A (2010) A conceptual model of integrated water resource management for national water security. Iran Water Resour Res 5(3):86–88
Zechman EM (2011) Agent-based modeling to simulate contamination events and evaluate threat management strategies in water distribution systems. Risk Anal 31:758–772
Zhang L, Yin X, Xu Z, Zhi Y, Yang Z (2016) Crop planting structure optimization for water scarcity alleviation in China. J Ind Ecol 20(3):435–445
Zhao J, Cai X, Wang Z (2013) Comparing administered and market-based water allocation systems through a consistent agent-based modeling framework. J Environ Manag 123:120–130
Zhongmin X, Guodong C, Zhiqiang Z, Zhiyong S, Loomis J (2003) Applying contingent valuation in China to measure the total economic value of restoring ecosystem services in Ejina region. Ecol Econ 44:345–358
Zhou P, Zhou X, Fan LW (2014) On estimating shadow prices of undesirable outputs with efficiency models: a literature review. Appl Energy 130:799–806
Zhu Z, Wang H, Xu H, Bai H (2010) An alternative approach to institutional analysis in strategic environmental assessment in China. JEAPM 12(02):155–183
Zou Y, Duan X, Xue Z, Mingju E, Sun M, Lu X et al (2018) Water use conflict between wetland and agriculture. J Environ Manag 224:140–146

Chapter 23
Isotopic Proxy to Identify Climate Change During the Anthropocene

Manpreet Singh and Prosenjit Ghosh

Abstract Stable isotopes are widely used in past climate reconstruction studies. They find a wide range of applications in climatology, and isotopic values in tree rings, ice cores, and marine sediments enable us to decipher past climatic conditions at the global scale. Since the onset of the industrial revolution in the eighteenth century, the burning of fossil fuels had accentuated the rate of CO_2 rise and exacerbated global warming. The CO_2 uptake by plants is reflected in ^{13}C variations in the atmosphere and helps us in understanding how plants responded to past climatic conditions. However, climatic reconstruction using tree rings is an invasive sampling technique, and hence this chapter attempts to check whether paper samples obtained from trees may also preserve the climate record or not. Therefore, using paper samples from 1832 to 1880, an attempt has been made to reconstruct the climate record using ^{13}C variations in that period. Our results show that paper samples may act as a significant archive for climatic reconstruction especially in Anthropocene due to the prolific growth of the printing industry in that period. Our results further show that there is a net positive trend in ^{13}C values from 1832 to 1880. The paper sample is a more cost-effective method and does not require field-intensive sampling for taking samples of tree rings. Therefore, it may act as an important substitute for tree rings for climatic reconstruction in Anthropocene.

Keywords Anthropocene · Carbon isotopes · Climate record · Paper samples · Tree rings

M. Singh (✉)
Forest Research Institute Deemed to be University, Dehradun, Uttarakhand, India

P. Ghosh
Center for Earth Sciences, Indian Institute of Science, Bengaluru, Karnataka, India

C. B. Pande et al. (eds.), *Climate Change Impacts on Natural Resources, Ecosystems and Agricultural Systems*, Springer Climate,
https://doi.org/10.1007/978-3-031-19059-9_23

Introduction

Since the onset of the industrial revolution, the concentration of atmospheric CO_2 has been increasing due to natural and anthropogenic factors. The burgeoning impacts that human activities have on the planet led scientists to coin the new term "Anthropocene." The term denotes the transition of the Holocene epoch to the Anthropocene in the nineteenth century, which is characterized by the strong driving forces led by humankind and their tremendous impact on planet Earth and its processes (Steffen et al. 2011; Crutzen and Stoermer 2000; Voir Crutzen 2002). In the nineteenth century, the industrial revolution saw the prolific growth of manufacturing units and a large-scale industrial boom. This large-scale industrial explosion exacerbated the dependency on fossil fuels. Thus, fossil fuel burning caused unprecedented and catastrophic damage to the atmospheric fluxes and further disrupted the equilibrium between different atmospheric processes. Anthropogenic sources of CO_2 emissions include deforestation, emissions from industrial units, intensified agriculture farming systems, burning of solid waste, dependency on fossil fuels for different activities, etc. (Wuebbles and Jain 2001). Land use changes, soil degradation, human respiration, vehicular emissions, and airplane emissions are some of the other anthropogenic sources of CO_2, especially in urban metropolitan areas (Koerner and Klopatek 2002). However, the burning of fossil fuels like coal, oil, natural gas, etc., is the single most important and largest contributor to overall atmospheric CO_2 emissions (Yoro and Daramola 2020). Especially, coal combustion is the largest contributor to CO_2 emissions among fossil fuel-based power generation plants (Yoro and Daramola 2020; Tian and Yang 2016). The natural sources of CO_2 emissions include decaying vegetation matter and decomposition of other biomass, volcanic emissions, wildfires, soil effluxes, and outgassing from oceans, and even ruminant animals (Cloy and Smith 2018; Fischer et al. 2019; Guo et al. 2019; Lacroix et al. 2020). Many scientists in the second half of the twentieth century speculated that the rising atmospheric CO_2 values, due primarily to fossil fuel burning, might lead to an increase in temperature by the end of that century (Manabe and Wetherald 1975). The global warming is attributed to many drivers by scientific community such as greenhouse gas emissions (CO_2, CH_4, N_2O, etc.), change in energy fluxes due to radiative forcing, and ocean circulation (Chen et al. 2014; Piao et al. 2011; Toggweiler and Russell 2008; Van Gennip et al. 2017; Zhu et al. 2017; Bellouin et al. 2020). However, among these, the role of CO_2 emissions in global warming got considerable attention from researchers (Chen et al. 2014; Piao et al. 2011). With the help of modeling, researchers predicted the response of temperature to increase in CO_2 concentration (Manabe and Wetherald 1975; Snyder et al. 2002). With the help of the RegCM2.5 model, Snyder et al. (2002) reported an increase of 1.4–3.8 °C in temperature over California with a doubling of CO_2 concentration. However, there are still uncertainties in predicting the response of climate change to changing atmospheric CO_2 levels (Reilly et al. 2001; Murphy et al. 2004; Stainforth et al. 2005). The accurate monitoring of atmospheric CO_2 only started in the late 1950s, and thus the accurate atmospheric CO_2 values are only 72 years old.

Moreover, the monitoring of atmospheric ^{13}C started only in the 1990s (Yakir 2011). Therefore, all the past climatic records have been reconstructed using different proxies, that is, tree rings and ice cores. Tree rings are a widely used proxy mechanism for reconstructing past climatic conditions. The dendrochronology studies using stable isotope analyses of carbon, hydrogen, and oxygen in tree rings have increased manifold since past few decades. Not only living trees but also dead trees or tree rings from fossils are being extensively used for climatic reconstruction with high annual resolution and precision (Zhang 2015). Although some of the tree ring-based chronologies are 1000 years old, they are few. The interaction of temperature and CO_2 also affects the growth of plants (Morison and Lawlor 1999). The techniques employing stable isotopes helped us tremendously in advancing our knowledge about plant-climate interactions and the drivers that shape these interactions (Dawson et al. 2002). Hence, carbon isotopes in tree rings are important indicators of climatic fluctuations or the response of plants to temperature variability. After atmospheric assimilation of CO_2 through stomata in tree leaves, fractionation of CO_2 takes place by virtue of diffusion, in which CO_2 fractionates in favour of the lighter isotope ^{12}C compared to ^{13}C. In addition, photosynthesis, by virtue of producing sugars via carboxylation, also contributes to the fractionation of CO_2 in favour of ^{12}C over ^{13}C. The net effect of fractionation dictates if the consumption rate of CO_2 due to photosynthetic uptake of leaves is greater than the replenishment rate. If yes, then the ^{12}C reservoir would decline, and hence, fractionation against ^{13}C would decrease, which means, $\delta^{13}C$ value would be high (Farquhar and Lloyd 1993; Loader et al. 2007). This differential rate of CO_2 consumption and replenishment in the form of $\delta^{13}C$ values helps us understand the climatic fluctuations and changes over time.

This can be summed up in the following equation given by Farquhar et al. (1982):

$$\Delta 13C \cong a + \left(b - a\right)\left(\frac{C_i}{C_a}\right)$$

Here, symbol a denotes the fractionation of CO_2 due to diffusion in tree leaves, and symbol b denotes the net fractionation due to photosynthetic uptake of tree leaves. Whereas C_i denotes the intercellular partial pressure of CO_2 within leaves and, C_a denotes the ambient partial pressure of the leaves.

The literature is inundated with studies of using stable isotopes in tree rings as a means for reconstructing climatic parameters like atmospheric CO_2, precipitation, etc. (Danis et al. 2006; Loader et al. 2007; Young et al. 2015; Sidorova et al. 2013; Rinne et al. 2013; Buajan et al. 2016). Schubert and Jahren (2012) showed how atmospheric CO_2 might affect the fractionation process of carbon isotopes in plants. Using close chamber experiments and employing different environmental control factors, Schubert and Jahren (2012) showed the potential of $\delta^{13}C$ in reconstructing past atmospheric CO_2 values. Danis et al. (2006) studied the reconstruction of precipitation using $\delta^{18}O$ through tree ring data from oak trees in France. Many studies in the past few years have advanced our understanding of climate response,

adaptability, and drought stress tolerance of forests using stable isotopes (Cernusak and English 2015; Hartl-Meier et al. 2015; Belmecheri et al. 2018; Belmecheri and Lavergne 2020; van Mantgem et al. 2020). Pu et al. (2021) studied the determinants of tree line formation by comparing stable isotopes in the tree rings of high and low elevation trees. Thus, apart from reconstructing these climatic parameters, there has been a paradigm shift in recent years towards using the stable isotopes in tree rings to find the forests's response to climatic fluctuations over time.

Although climate reconstruction using tree ring as a proxy is well studied and extensively documented in the available literature (Loader and Switsur 1996; Loader et al. 2007; McCarroll and Loader 2004; Planells et al. 2009; Aguilera et al. 2011; Gebrekirstos et al. 2009; Zhang et al. 2020; Szejner et al. 2021; Lukač et al. 2021), our research tries to demonstrate that stable isotopes in paper samples from trees can also act as a substitute for a climatic archive, as suggested by Yakir (2011). Especially prior to 1958, we did not have any reliable and accurate atmospheric CO_2 monitoring systems in place. Therefore, to understand how the onset of the industrial revolution exacerbated climatic fluctuations and atmospheric CO_2 levels, we have to rely on proxies. In addition, paper production involves the utilization of material from many trees, and hence, stable isotopes in paper samples may not help us in species-level identification (Yakir 2011). However, the advantage in disguise may be that for studies focusing on climatic trends, running mean values of ^{13}C in different tree species' wood may help us achieve the ultimate objective of deciphering the climatic record. Although tree rings provide high-resolution annual data, they do so at the cost of invasive sampling techniques. Therefore, the major objective of this article is to determine, despite all the limitations, whether the climatic trend through ^{13}C values is preserved in paper samples or not.

We have tried to compare our $\delta^{13}C$ results with those from Beck (2007) and Etheridge et al. (1996). Interestingly, Beck (2007) has compiled the atmospheric CO_2 measurement data from the independent observations made by investigators in the last two centuries using chemical analysis techniques. Beck (2007) is of the view that although these CO_2 measurements are on a local scale only, they are still of paramount importance to fit into the global CO_2 curve of the last two centuries. He argues that all the 138 CO_2 measurements that he has compiled are in congruence with other phenomena such as sunspot cycles, moon phases, etc. He further iterates that the researchers ignored most of the historical records of atmospheric CO_2 surreptitiously because these did not fit into their hypotheses and, most importantly, to further promulgate and fit their findings into the global CO_2 curve. Etheridge et al.'s (1996) data, which is from Law Dome ice cores, showed very few fluctuations because it is a 20-year smoothed data. Given the fact that our study spans over 49 years (if we exclude the few measurements of the eighteenth century), a 20-year smoothed data does not capture the small-scale temporal fluctuations and hence does not afford us much leeway to draw parallels from the Etheridge et al.'s (1996) data.

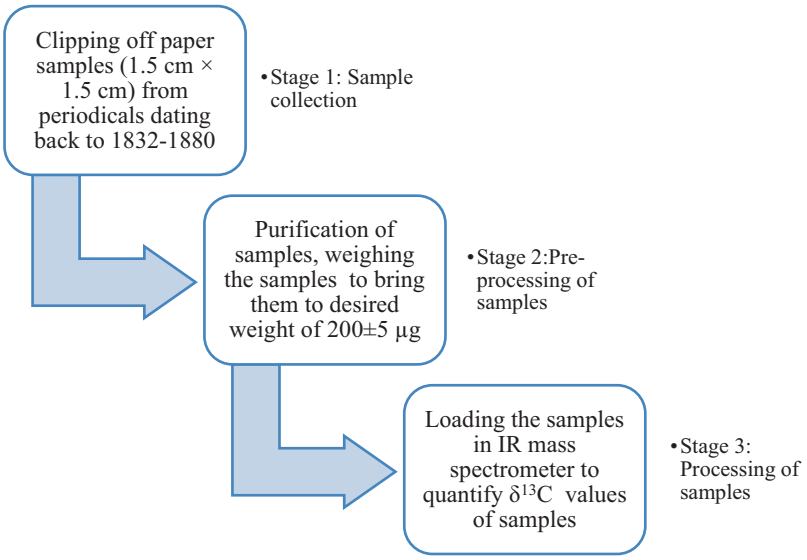

Fig. 23.1 Flow diagram of the sampling methodology followed for the calculation of $\delta^{13}C$ values of paper samples

Materials and Methods

For ease of understanding, the methods are here split into three parts, that is, sample collection, preprocessing of the data, and processing the samples. The flow diagram of methodology is briefed in Fig. 23.1.

Sample Collection

Paper samples were obtained from 12 different periodicals, for which we had access to the archives from 1832 to 1880. Samples were obtained from the National Forest Library and Information Centre, FRI Dehradun, which houses one of the oldest collections of periodicals. We used samples from publications dated between 1832 and 1880, along with some miscellaneous samples dating back to 1775, 1792, 1793, etc. It is due to the reason that, from 1775 to 1832, we did not have access to the journals from each year, and thus only six samples were taken in that time period. For each year, samples from two journals were clipped off. Therefore, two samples per year were taken and two series of samples were formed. The names of the journals from which samples were taken are listed in Table 23.1.

The origin of publication of these journals was confined to London, Edinburgh, or Paris, so the origin of publication does not differ much. The care was taken to not deliberately incorporate periodicals published in other continents or different parts

Table 23.1 Details of the journals from which the paper samples have been clipped off

Sr. no.	Name of journal	Total no. of samples	Year range	Place of publication
1.	*Annales de la Societe Entomologique de France*	23	1832–1850 and 1853–1856	Paris
2.	*Proceedings of Zoological Society of London*	27	1834–1848, 1850–1852, 1854–1861, 1863, and 1865	London
3.	*Transactions of the Entomological Society of London*	19	1849, 1851–1853, 1858, 1861, 1864, 1866–1870, 1873–1877, and 1879–1880	London
5.	*Journal of the Proceedings of the Linnean society*	3	1857, 1859, and 1863	London
6.	*The Annals and Magazine of Natural History*	2	1860 and 1862	Paris
7.	*Transactions of the Scottish Arboricultural society*	1	1862	Edinburgh
8.	*The Record of Zoological Literature*	17	1864–1880	London
9.	*Journal of Chemical Society*	1	1871	London
10.	*Transactions of the Highland and Agricultural Society of Scotland*	2	1872 and 1878	Edinburgh
11.	*Entomologia systematica emendata et aucta*	6	1775, 1781, and 1792–1794	Paris
12	*Species Insectarium*	1	1781	London

of the world so that variability arising due to regional climatic factors could be kept as minimum as possible. However, as these sources of origin are quite distant from each other, it is not surprising to see huge scatter in data. In all, 103 non-inked samples from the bottom-left margin of a page in a journal were clipped off. All the paper samples measured 1.5 cm × 1.5 cm. Special care was taken to cut off the paper samples in such a way that hands did not come in direct contact with the paper because sweaty hands may damage the sample and alter the carbon isotopic values of paper samples. Once cut, paper samples were picked up with a tweezer and placed carefully in zip lock bags. All the zip lock bags were labelled according to the year and series number.

Preprocessing of Samples

All the paper samples were purified using alcohol and then dried up for further processing in the isotope ratio mass spectrometer. From these paper samples, small subsamples were cut off and put into capsules. These capsules were weighed on a weighing machine to ensure that the weight of the sample remains within the limit of 200 ± 5 μg.

Processing the Samples

These sample-containing capsules were then combusted for quantification of $^{13}C/^{12}C$ values in an IR mass spectrometer. The carbon isotopic ratios of samples were then converted to international standards by measuring the ratios of the samples relative to those of a standard (Coplen 1994), as given below:

$$\delta 13C = \left(\frac{R_{\text{sample}}}{R_{\text{standard}}} - 1 \right) \times 1000‰$$

R_{sample} denotes the isotopic ratio of the sample, and R_{standard} denotes the isotopic ratio of the standard. Delta notation is expressed in parts per mill (‰). In an IR mass spectrometer, the gases of a standard and an unknown sample is made to pass through the capillary tubes, from where they enter the source region, and the ionization of gases takes place. Deflection of ions depends upon the charge-mass ratio where heavy ions do not deflect as strongly as the lighter ions do. Hence, intensities of the ion beams correspond to their respective abundance of isotopologues. Further, delta values from isotopic ratios are calculated in the digital machine attached to the IR mass spectrometer (Sharp 2017). We have used the Vienna Pee Dee Belemnite (VPDB) standard for converting the isotopic ratios to international isotopic scales. The atmospheric CO_2 data was taken from two sources:

(i) Beck (2007) who has compiled the atmospheric CO_2 data of 1812–1961 from 138 literature articles like Buch (1948), Kreutz (1941), Scholander (1947), and Lockhart and Court (1942).
(ii) Etheridge et al. (1996) data which they sourced from Law Dome ice cores.

Results and Discussion

We have used two samples per year to calculate the ^{13}C value of paper samples. We have designated them as Series 1 and Series 2. There were 54 paper samples in Series 1 and 49 paper samples in Series 2. The carbon isotopic ratio of samples in both series is given in Table 23.2. The ^{13}C values of both series are also depicted in the scatter plot given in Fig. 23.2. Although the continuous data from periodicals was available only from 1832 to 1880, a few samples have been additionally chosen, that is, 1775, 1781, and 1792–1794, to extend the time series to date back in Anthropocene as far as possible. This is because the continuity from 1775 to 1832 was not possible due to access to very few periodicals in this time duration. There is a 57% correlation between Series 1 and Series 2, which is not unanticipated due to the huge variation in data arising from different sources of origin. It may be noted here that the Series 1 and Series 2 paper samples for a year are from the different periodicals and hence causing large variation in data, as can be seen from scatter

Table 23.2 Carbon isotopic ratio of paper samples from Series 1 and Series 2 and the weight of sample combusted (μg)

Year	Amount μg (series 1)	$\delta^{13}C$ (series 1)	Amount μg (series 2)	$\delta^{13}C$ (series 2)
1775	205	−25.2	–	–
1781	200	−25.5	195	−25.4
1792	198	−24.8	–	–
1793	202	−24.8	205	−25.1
1794	203	−25.2	–	–
1832	195	−25.1	–	–
1833	203	−24.8	–	–
1834	205	−25.6	198	−25.2
1835	205	−21.5	200	−25.4
1836	205	−25.4	205	−25.3
1837	202	−24.8	200	−25.0
1838	197	−25.4	201	−25.7
1839	205	−25.4	203	−25.1
1840	196	−26.0	205	−25.3
1841	200	−25.1	200	−25.2
1842	195	−24.8	199	−25.4
1843	203	−25.6	203	−24.7
1844	202	−26.0	205	−24.6
1845	205	−25.1	205	−25.3
1846	202	−25.5	203	−24.9
1847	198	−25.3	201	−25.3
1848	202	−25.3	205	−20.9
1849	196	−25.1	205	−24.8
1850	203	−25.3	201	−25.1
1851	205	−21.5	203	−23.8
1852	205	−24.2	198	−25.0
1853	199	−25.6	198	−25.3
1854	202	−25.1	197	−25.3
1855	195	−25.6	205	−25.5
1856	204	−24.9	205	−24.7
1857	205	−24.4	204	−25.5
1858	201	−24.7	205	−24.7
1859	196	−25.0	198	−25.2
1860	195	−25.0	205	−25.2
1861	205	−24.7	204	−24.7
1862	201	−25.5	200	−25.3
1863	204	−24.9	195	−25.2
1864	195	−24.9	202	−25.0
1865	200	−23.2	205	−24.6
1866	201	−25.2	198	−25.0
1867	203	−23.5	205	−23.5

(continued)

Table 23.2 (continued)

Year	Amount μg (series 1)	$\delta^{13}C$ (series 1)	Amount μg (series 2)	$\delta^{13}C$ (series 2)
1868	205	−23.8	205	−24.3
1869	201	−24.1	204	−24.9
1870	197	−23.2	205	−24.3
1871	200	−24.4	195	−24.4
1872	205	−22.3	200	−24.1
1873	200	−22.2	199	−21.1
1874	195	−22.2	195	−23.2
1875	203	−21.6	205	−23.3
1876	205	−22.7	195	−23.0
1877	205	−21.8	198	−20.8
1878	200	−21.1	195	−22.6
1879	202	−20.7	203	−25.5
1880	200	−20.9	205	−21.4

plots of series 1 and series 2. The minimum value of ^{13}C in Series 1 is −20.7 in the year 1879, and the maximum value of ^{13}C in Series 2 is −26, which occurs twice in the time series, that is, 1840 and 1844. For Series 2, the minimum value is −20.8 which occurs in 1877, and the maximum value is −25.7, which occurs in 1838. On average, the ^{13}C value increased 0.0875 ± 0.024 for Series 1 and 0.082 ± 0.029 for series 2. If we look at both Series 1 and Series 2, we can see that until 1865, ^{13}C values remain stable; however, there is an abrupt increase in carbon isotopic values from 1865 onward, although it is expected that ^{13}C values would decline over time with a corresponding increase in atmospheric CO_2 values (Yakir 2011). However, due to a sudden rise in ^{13}C values around 1865, this peak could be the reason behind the overall net positive increase of ^{13}C values in this time period. In addition, there are some outliers in the data, which could be due to a variations in the sources of origin or other reasons and hence, need more investigation. There are two outliers in Series 1 and Series 2, that is, 1835 and 1851 in Series 1 and 1848 and 1879 in Series 2.

Yakir (2011) has tried to reconstruct the climate since the Industrial Revolution (1880–2000) using ^{13}C in paper samples. He has observed declining ^{13}C values over this period with a corresponding increase in atmospheric CO_2 levels. He also attributed the large variability and scatter in data to the various sources of origin. Compared with our results, we find that $\delta^{13}C$ values remain stable until 1865 and then increase suddenly, although Yakir (2011) has also correlated the $\delta^{13}C$ values of original paper samples with $\delta^{13}C$ values of cellulose extracted from paper samples. Cellulose extraction although may be helpful to decouple the effects arising from paper production and environmental signal, but nevertheless it is a time-consuming process and is not generally suggested if the emphasis is on temporal trend of climatic record (Yakir 2011). Furthermore, in the study of Yakir (2011), the slope of correlation between the ^{13}C values of the cellulose extracted and the original paper samples was near 1. Therefore, we did not incorporate cellulose purification as a part of this

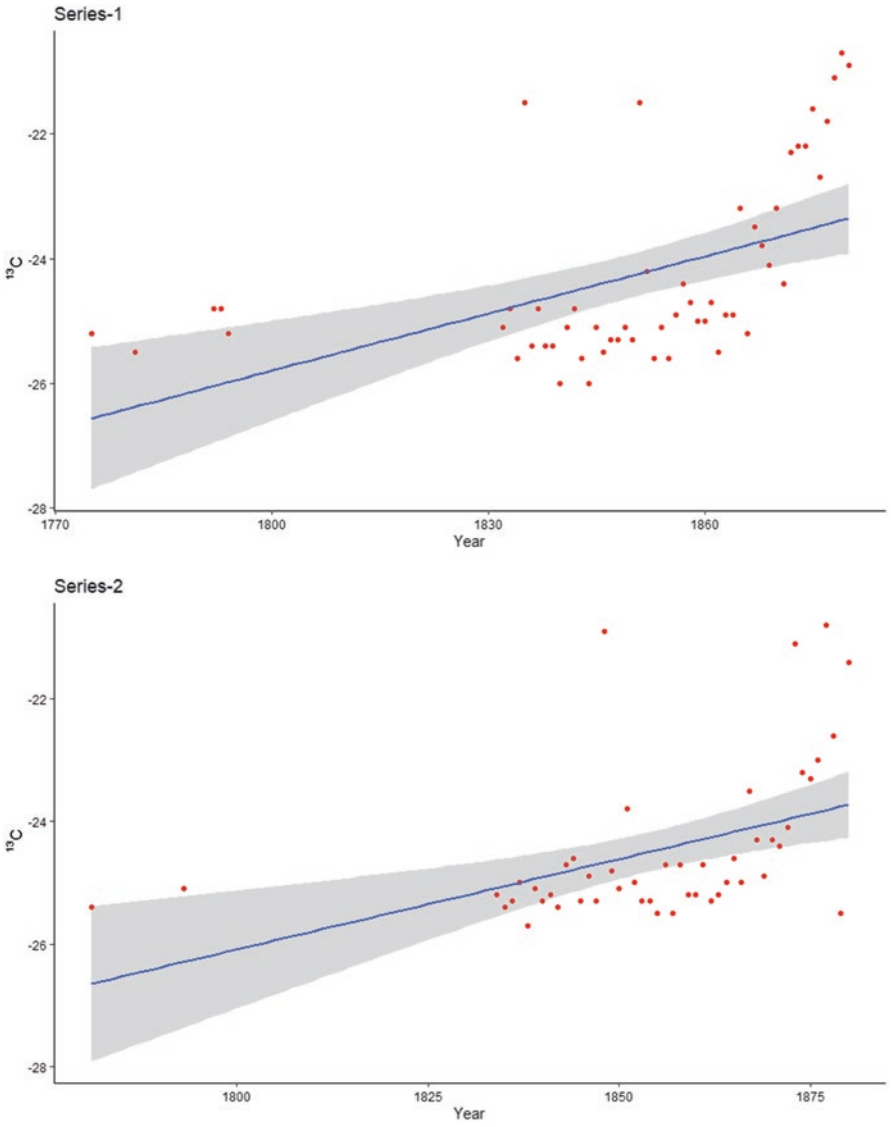

Fig. 23.2 $\delta^{13}C$ values of paper samples from Series 1 (above) and Series 2 (below). The trend line indicates the overall net positive direction over the time period from 1775 to 1880. The gaps of data points from 1775 to 1832 are due to inaccessibility of paper samples in that time period

research because our focus is on the temporal trend of the climate record deciphered from ^{13}C paper sample data. We tried to compare the $\delta^{13}C$ values of paper samples with the atmospheric CO_2 trend from two sources, that is, Beck (2007) and Etheridge et al. (1996) (Fig. 23.3). There is an upward trend in atmospheric CO_2 data from Etheridge et al. (1996), which is sourced from Law Dome ice cores. However,

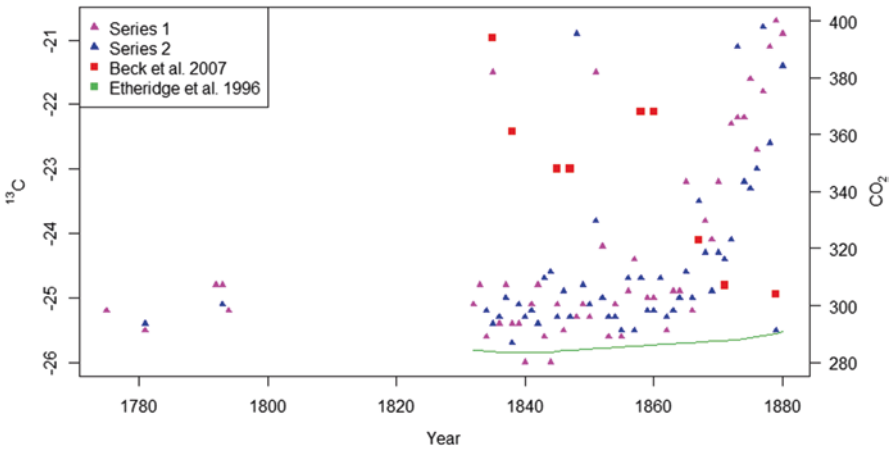

Fig. 23.3 Comparing the $\delta^{13}C$ values from paper samples of periodicals with atmospheric CO_2 (ppm) data from available literature (Beck 2007; Etheridge et al. 1996, 2001). While the atmospheric CO_2 trend from Beck (2007) fluctuates vigorously, there is a negative downward trend corresponding to an increase in $\delta^{13}C$. However, study by Etheridge et al. (1996), on the contrary, shows an upward trend in atmospheric CO_2 with an increase in $\delta^{13}C$ values.

the study of Beck (2007), on the contrary, shows a downward trend in the data with fluctuations from 1832 to 1880. In the data of Beck (2007), there is one maxima in CO_2 concentration around 1857, which is quite congruent with the abrupt upward trend in ^{13}C values of our results from 1860 onward. It may be worth mentioning here that the data from Etheridge et al. (1996) is a 20-year smoothed data, whereas the data from Beck (2007) is an 11-year smoothed data. Hence, the small fluctuations are not visible in the curves shown in Fig. 23.3. Friedli et al. (1986) in their study, which deciphered the atmospheric CO_2 trend in the nineteenth and twentieth centuries from ice core data, reported $\delta^{13}C$ (PDB standard) value of −6.43‰ in 1791, which remains stable until 1854, that is, 6.48‰ in 1854 (with minor fluctuations between 1791 and 1854), and then increases from −6.51‰ in 1847 to −6.42‰ in 1887. With a few exceptions, our results seem to be in good agreement with the results of Friedli et al. (1986); however, due to the disparate standards used in both of the studies (PDB and VPDB), it does not allow us to make any concrete comparisons.

There is still not much research effort directed towards the temporal ^{13}C signal in paper samples as a means to advance our understanding of past climate change, although the results of our study are in contradiction with Yakir (2011), who observed declining ^{13}C values in paper samples with increasing atmospheric CO_2 trend over temporal scale. However, the time period of his study was different (1880–2000) compared to our study (1832–1880). Most importantly, our results are congruent with the nineteenth-century atmospheric CO_2 trend of Beck (2007). Moving forward, future research could be extended to incorporate the drivers and different contributing factors of climatic fluctuations in this time period (1832–1880)

as seen from the ^{13}C trend. The primary focus of this study was to check the feasibility of paper samples in archiving climate record through ^{13}C trend, and the results though show optimistic premise but due to a lack of studies centering on ^{13}C trend in paper samples do not afford us any reliable interpretation.

Conclusion

Tree rings and ice cores are widely used proxies for the reconstruction of the Anthropocene climate. The documentation of the paper trail for archiving climate trends is available in the literature for the time since the industrial revolution (1880–2000). However, to the best of our knowledge, the use of chapter samples for the reconstruction of climate change in the Anthropocene remains neglected by climatologists. Hence, it is a well-guided effort in this direction to corroborate the Anthropocene climate with studies from available literature. We have observed a net positive and upward trend in ^{13}C values over time. It could be due to two reasons. First, there is a huge scatter in the data due to different sources of origin. Second, the abrupt upsurge in ^{13}C values around 1857 culminated in the overall positive trend. Comparing ^{13}C values with records of atmospheric CO_2 from the available literature yielded different conclusions. The one outcome indicates an increase in ^{13}C values over time with a corresponding increase in atmospheric CO_2, and the other outcome shows an increase in ^{13}C values with a decline in the atmospheric CO_2 trend over time. Although our results, despite the scatter in data due to variability in the source of origin, point toward the potential of paper samples to archive past climate record, there is still a need for more research in this direction to bolster this claim.

Recommendations

Although this is a novel effort toward understanding the Anthropocene climate using paper samples, there is still some contention among scientists about the reliability of proxies for past climatic reconstruction. So, future studies should be aimed at understanding the Anthropocene climatic records using different methods for better precision, efficiency, and statistical inference. In addition, efforts should be directed toward extending the application of stable isotopes in paper samples to plant physiology studies.

Acknowledgments We would like to acknowledge the National Forest Library and Information Centre, FRI Dehradun, for giving access to periodicals for paper samples. The valuable inputs of Dr. Rahul Peethambaram merit acknowledgment. We would also like to thank Dr. Ritika Kaushal for her suggestions.

References

Aguilera M, Ferrio JP, Araus JL, Tarrús J, Voltas J (2011) Climate at the onset of western Mediterranean agriculture expansion: evidence from stable isotopes of sub-fossil oak tree rings in Spain. Palaeogeogr Palaeoclimatol Palaeoecol 299(3–4):541–551

Beck EG (2007) 180 years of atmospheric CO_2 gas analysis by chemical methods. Energy Environ 18(2):259–282

Bellouin N, Quaas J, Gryspeerdt E, Kinne S, Stier P, Watson-Parris D et al (2020) Bounding global aerosol radiative forcing of climate change. Rev Geophys 58(1):e2019RG000660

Belmecheri S, Lavergne A (2020) Compiled records of atmospheric CO_2 concentrations and stable carbon isotopes to reconstruct climate and derive plant ecophysiological indices from tree rings. Dendrochronologia 63:125748

Belmecheri S, Wright WE, Szejner P, Morino KA, Monson RK (2018) Carbon and oxygen isotope fractionations in tree rings reveal interactions between cambial phenology and seasonal climate. Plant Cell Environ 41(12):2758–2772

Buajan S, Pumijumnong N, Li Q, Liu Y (2016) Oxygen isotope ($\delta^{18}O$) of teak tree-rings in North-West Thailand. J Trop For Sci 28:396–405

Buch E (1948) Der Kohlendioxydgehalt der Luft als Indikator der Meteorologischen Luftqualitat. Geophysica 3:63–79

Cernusak LA, English NB (2015) Beyond tree-ring widths: stable isotopes sharpen the focus on climate responses of temperate forest trees. Tree Physiol 35(1):1–3

Chen Y, Li B, Li Z, Shi X (2014) Quantitatively evaluating the effects of CO_2 emission on temperature rise. Quat Int 336:171–175

Cloy JM, Smith KA (2018) Greenhouse gas sources and sinks, vol 2. Encyclopedia of the Anthropocene, p 391

Coplen TB (1994) Reporting of stable hydrogen, carbon, and oxygen isotopic abundances (technical report). Pure Appl Chem 66(2):273–276

Crutzen PJ, Stoermer EF (2000) The Anthropocene, Global change newsletter. 41, 17–18. International Geosphere–Biosphere Programme (IGBP)

Danis PA, Masson-Delmotte V, Stievenard M, Guillemin MT, Daux V, Naveau P, Von Grafenstein U (2006) Reconstruction of past precipitation δ18O using tree-ring cellulose δ18O and δ13C: a calibration study near Lac d'Annecy, France. Earth Planet Sci Lett 243(3–4):439–448

Dawson TE, Mambelli S, Plamboeck AH, Templer PH, Tu KP (2002) Stable isotopes in plant ecology. Annu Rev Ecol Syst 33(1):507–559

Etheridge DM, Steele LP, Langenfelds RL, Francey RJ, Barnola JM, Morgan VI (1996) Natural and anthropogenic changes in atmospheric CO_2 over the last 1000 years from air in Antarctic ice and firn. J Geophys Res Atmos 101(D2):4115–4128

Etheridge DM, Steele LP, Langenfelds RL, Francey RJ, Barnola JM, Morgan VI (2001) Law dome atmospheric CO_2 data. Data contribution series, 83

Farquhar GD, Lloyd J (1993) Carbon and oxygen isotope effects in the exchange of carbon dioxide between terrestrial plants and the atmosphere. In: Stable isotopes and plant carbon-water relations. Academic, pp 47–70

Farquhar GD, O'Leary MH, Berry JA (1982) On the relationship between carbon isotope discrimination and the intercellular carbon dioxide concentration in leaves. Funct Plant Biol 9(2):121–137

Fischer TP, Arellano S, Carn S, Aiuppa A, Galle B, Allard P et al (2019) The emissions of CO_2 and other volatiles from the world's subaerial volcanoes. Sci Rep 9(1):1–11

Friedli H, Lötscher H, Oeschger H, Siegenthaler U, Stauffer B (1986) Ice core record of the 13 C/12 C ratio of atmospheric CO_2 in the past two centuries. Nature 324(6094):237–238

Gebrekirstos A, Worbes M, Teketay D, Fetene M, Mitlöhner R (2009) Stable carbon isotope ratios in tree rings of co-occurring species from semi-arid tropics in Africa: patterns and climatic signals. Glob Planet Chang 66(3–4):253–260

Guo M, Li J, Wen L, Huang S (2019) Estimation of CO_2 emissions from wildfires using OCO-2 data. Atmos 10(10):581

Hartl-Meier C, Zang C, Büntgen ULF, Esper JAN, Rothe A, Göttlein A et al (2015) Uniform climate sensitivity in tree-ring stable isotopes across species and sites in a mid-latitude temperate forest. Tree Physiol 35(1):4–15

Koerner B, Klopatek J (2002) Anthropogenic and natural CO_2 emission sources in an arid urban environment. Environ Pollut 116:S45–S51

Kreutz W (1941) Kohlensäure Gehalt der unteren Luftschichten in Abhangigkeit von Witterungsfaktoren. Angew Bot 2:89–117

Lacroix F, Ilyina T, Hartmann J (2020) Oceanic CO_2 outgassing and biological production hotspots induced by pre-industrial river loads of nutrients and carbon in a global modeling approach. Biogeosciences 17(1):55–88

Loader NJ, Switsur VR (1996) Reconstructing past environmental change using stable isotopes in tree-rings. Bot J Scotl 48(1):65–78

Loader NJ, McCarroll D, Gagen M, Robertson I, Jalkanen R (2007) Extracting climatic information from stable isotopes in tree rings. Terrestrial Ecol 1:25–48

Lockhart E, Court A (1942) Oxygen deficiency in Antarctic air. Mon Weather Rep 70(5):93–96

Lukač L, Mikac S, Urban O, Kolář T, Rybníček M, Ač A et al (2021) Stable isotopes in tree rings of Pinus heldreichii can indicate climate variability over the eastern Mediterranean region. Forests 12(3):350

Manabe S, Wetherald RT (1975) The effects of doubling the CO_2 concentration on the climate of a general circulation model. J Atmos Sci 32(1):3–15

McCarroll D, Loader NJ (2004) Stable isotopes in tree rings. Quat Sci Rev 23(7–8):771–801

Morison JIL, Lawlor DW (1999) Interactions between increasing CO_2 concentration and temperature on plant growth. Plant Cell Environ 22(6):659–682

Murphy JM, Sexton DM, Barnett DN, Jones GS, Webb MJ, Collins M, Stainforth DA (2004) Quantification of modelling uncertainties in a large ensemble of climate change simulations. Nature 430(7001):768–772

Piao S, Ciais P, Lomas M, Beer C, Liu H, Fang J et al (2011) Contribution of climate change and rising CO_2 to terrestrial carbon balance in East Asia: a multi-model analysis. Glob Planet Chang 75(3–4):133–142

Planells O, Gutiérrez E, Helle G, Schleser GH (2009) A forced response to twentieth century climate conditions of two Spanish forests inferred from widths and stable isotopes of tree rings. Clim Chang 97(1):229–252

Pu X, Wang X, Lyu L (2021) Tree-ring isotopes provide clues for sink limitation on Treeline formation on the Tibetan plateau. Atmosphere 12(5):540

Reilly J, Stone PH, Forest CE, Webster MD, Jacoby HD, Prinn RG (2001) Climate change. Uncertainty and climate change assessments. Science 293(5529):430–433

Rinne KT, Loader NJ, Switsur VR, Waterhouse JS (2013) 400-year May–August precipitation reconstruction for Southern England using oxygen isotopes in tree rings. Quat Sci Rev 60:13–25

Scholander PF (1947) Analyzer for accurate estimation of respiratory gases in one-half cubic centimeter samples. J Biol Chem 167(1):235–250

Schubert BA, Jahren AH (2012) The effect of atmospheric CO_2 concentration on carbon isotope fractionation in C3 land plants. Geochim Cosmochim Acta 96:29–43

Sharp Z (2017) Principles of stable isotope geochemistry. Pearson Prentice Hall

Sidorova OV, Siegwolf RTW, Myglan VS, Ovchinnikov DV, Shishov VV, Helle G et al (2013) The application of tree-rings and stable isotopes for reconstructions of climate conditions in the Russian Altai. Clim Chang 120(1):153–167

Snyder MA, Bell JL, Sloan LC, Duffy PB, Govindasamy B (2002) Climate responses to a doubling of atmospheric carbon dioxide for a climatically vulnerable region. Geophys Res Lett 29(11):9–1

Stainforth DA, Aina T, Christensen C, Collins M, Faull N, Frame DJ et al (2005) Uncertainty in predictions of the climate response to rising levels of greenhouse gases. Nature 433(7024):403–406

Steffen W, Grinevald J, Crutzen P, McNeill J (2011) The Anthropocene: conceptual and historical perspectives. Philos Trans R Soc A Math Phys Eng Sci 369(1938):842–867

Szejner P, Belmecheri S, Babst F, Wright WE, Frank DC, Hu J, Monson RK (2021) Stable isotopes of tree rings reveal seasonal-to-decadal patterns during the emergence of a megadrought in the Southwestern US. Oecologia 197:1–16

Tian ZH, Yang ZL (2016) Scenarios of carbon emissions from the power sector in Guangdong Province. Sustainability 8(9):863

Toggweiler JR, Russell J (2008) Ocean circulation in a warming climate. Nature 451(7176):286–288

Van Gennip SJ, Popova EE, Yool A, Pecl GT, Hobday AJ, Sorte CJ (2017) Going with the flow: the role of ocean circulation in global marine ecosystems under a changing climate. Glob Chang Biol 23(7):2602–2617

Van Mantgem PJ, Kerhoulas LP, Sherriff RL, Wenderott ZJ (2020) Tree-ring evidence of forest management moderating drought responses: implications for dry, coniferous forests in the southwestern United States. Front For Glob Change 3:41

Voir Crutzen PJ (2002) Geology of mankind: the Anthropocene. Nature 415:23

Wuebbles DJ, Jain AK (2001) Concerns about climate change and the role of fossil fuel use. Fuel Process Technol 71(1–3):99–119

Yakir D (2011) The paper trail of the ^{13}C of atmospheric CO_2 since the industrial revolution period. Environ Res Lett 6(3):034007

Yoro KO, Daramola MO (2020) CO_2 emission sources, greenhouse gases, and the global warming effect. In: Advances in carbon capture. Woodhead Publishing, pp 3–28

Young GH, Loader NJ, McCarroll D, Bale RJ, Demmler JC, Miles D et al (2015) Oxygen stable isotope ratios from British oak tree-rings provide a strong and consistent record of past changes in summer rainfall. Clim Dyn 45(11):3609–3622

Zhang Z (2015) Tree-rings, a key ecological indicator of environment and climate change. Ecol Indic 51:107–116

Zhang R, Qin L, Shang H, Yu S, Gou X, Mambetov BT et al (2020) Climatic change in southern Kazakhstan since 1850 C.E. inferred from tree rings. Int J Biometeorol 64:1–11

Zhu P, Zhuang Q, Ciais P, Welp L, Li W, Xin Q (2017) Elevated atmospheric CO_2 negatively impacts photosynthesis through radiative forcing and physiology-mediated climate feedback. Geophys Res Lett 44(4):1956–1963

Chapter 24
Estimation of Land Surface Temperature for Rahuri Taluka, Ahmednagar District (MS, India), Using Remote Sensing Data and Algorithm

J. Rajesh and Chaitanya B. Pande

Abstract As an outcome of the global warming influence on the atmosphere, India faces grave problem like the rest of the globe. Land surface temperature (LST) is more significant for urban LULC (land use/land cover), climate change, crop water requirement, temperature measurement studies and other essential input materials that contribute to atmosphere models. LANDSAT satellite data have provided many opportunities to use remote sensing and GIS (geographic information system) methods to study the Earth's surface analysis. This study showed that topography, in an extra to human activity, also significantly impacts on the land surface temperature. Such type of research has provided the automated LST developed by LANDSAT-8 images based on algorithms. The majority of climate modelling and analytic applications require this. Remote sensing and geographic information systems suggest many possible uses in climate change assessments when they have been used to calculate LST. The results are presented in that area, where the standard deviation calculated was 4.83 °C LST, as the NDVI (normalized difference vegetation index) values have attained by red and near-infrared bands. Thermal infrared bands were utilized to determine land surface emissivity (LSE). The NDVI, LSE and LST studies have given sufficient accuracy for understanding the temperature variability. Results of study area show the lowest temperature in between 26.65 and 32.31 °C (1.85%), tolerance of 37.73–40.64 °C (24.05%) and deeply below at 43.47–47.89 °C (32.05%) during April 2019.

J. Rajesh
Centre for Advance Agricultural Science and Technology on Climate-Smart Agriculture and Water Management, Mahatma Phule Krishi Vidyapeeth, Rahuri, Maharashtra, India

C. B. Pande (✉)
Indian Institute of Tropical Meteorology (IITM), Pune, Maharashtra, India
e-mail: chaitanay45@gmail.com

C. B. Pande et al. (eds.), *Climate Change Impacts on Natural Resources, Ecosystems and Agricultural Systems*, Springer Climate,
https://doi.org/10.1007/978-3-031-19059-9_24

Keywords Land surface temperature (LST) · NDVI · Near air surface · Temperature data

Introduction

On national and global levels, land surface temperature (LST) is a fundamental parameter in land–surface physical interactions, and it has been broadly utilized for hydrology, meteorology and the surface energy balance. At regional and global levels, remote sensing is a distinctive method of collecting the LST. Many LST outputs generated from various satellite data have been commonly applied in urban ecology, water management and natural disasters (Wan and Dozier 1996; Shahid et al. 2021). Surface temperature of land is a better predictor of energy availability on the Earth's surface, the essential components of large-scale and global terrestrial–surface processes in the physical sciences. The consequences of surface–atmosphere interfaces and energy flow with cloud and the ground have been intergraded (Sellers et al. 1988; Mosammam et al. 2017). A global temperature is directly related to the measurement tool (most measured in Kelvin). The LST is a wood-burning hearth of crust in which warmth and radiation from the sun have been engrossed, redirected and directed. Land surface temperature changes due to climate change and artificial actions, where direct expectations become a challenge. Surface temperature has been recovered from thermal band information based on the particular infrared channel technique or the divided window process and the total bands utilized (Pu et al. 2006). Urban sprawl has been measured as one of the maximum critical changes in climate (McCarthy et al. 2010) and is the main reason for numerous ecological problems (Fathi et al. 2021; Kandekar et al. 2021; Pande 2022; Pande et al. 2022). Continuous urbanization has shown more variation in the LULC classes entirely in the previous two times (Weng 2007; McCarthy et al. 2010; Turkoglu 2010; Pande et al. 2018, 2021a).

Ground surveys would make land-use cover accurate but laborious and expensive and make remote sensing a definite and desirable one (Pande et al. 2021a). Recognized and considered LST varies regionally because of changes in the width of the distributed Earth's and other atmospheric elements. Decreasing urban heat island (UHI) is often dependent on it (Jayaraman and Chokkalingam 2021). Moderate spatial resolution data from LANDSAT-7 and LANDSAT-8 is appropriate for ground cover or vegetation coverage at the village level. The operational land imager (OLI) and thermal infrared sensor (TIRS) are both instruments aboard LANDSAT-8 (Pande et al. 2021b; Pande 2022). OLI assembles data with eight bands. These satellite data cover a wide variety of wavelengths in the electromagnetic spectrum, including visible, near and shortwave infrared and a panchromatic band with a spatial resolution of 15 metres (Pande et al. 2021b; Gulhane et al. 2022). TIRS detects TIR radiation at spatial resolution of 100 metres in both bands positioned between 10 and 12 metres in the atmosphere (Candy et al. 2017; Reddy et al. 2017; Wang et al. 2015; Barsi et al. 2014; Gallo et al. 2011; Liu & Zhang 2011).

The main aim of this chapter is to estimate LST based on the algorithm and remote sensing data. However, data have been utilized for crop water requirement during three periods.

Study Area

The Rahuri taluka is situated in the Ahmednagar district of Maharashtra in India. The area is between 19.38° N and 74.65° E″. As per the GPS average, the elevation of the mean sea level (MSL) is 511 m of the area. The weather of the Rahuri taluka is regularly dry, especially in regions characterized by medium precipitation taking inconsistent spreading, exceeding daytime and yearly temperatures, high humidity, sunshine and wind velocity. According to the 2011 Census India, Rahuri taluka has 64,707 households, with a total population of 3,22,823. The population of children whose age range is 0–6 is 41,564, which is 12.88% of the total population. The literacy rate of Rahuri taluka is 69.48%, out of which 75.58% males are literate and 62.94% females are literate. The rainfall of the study area is found to be 450–600 m overall every year, when this is facing problems of drought, crop damage and drinking water availability; in over the areas, basaltic rocks are found in this area. The total area of Rahuri is 1017.49 sq. km, with a population density of 317 per sq. km. Out of the total population, 78.38% of the population live in urban areas and 21.62% live in rural areas (Fig. 24.1).

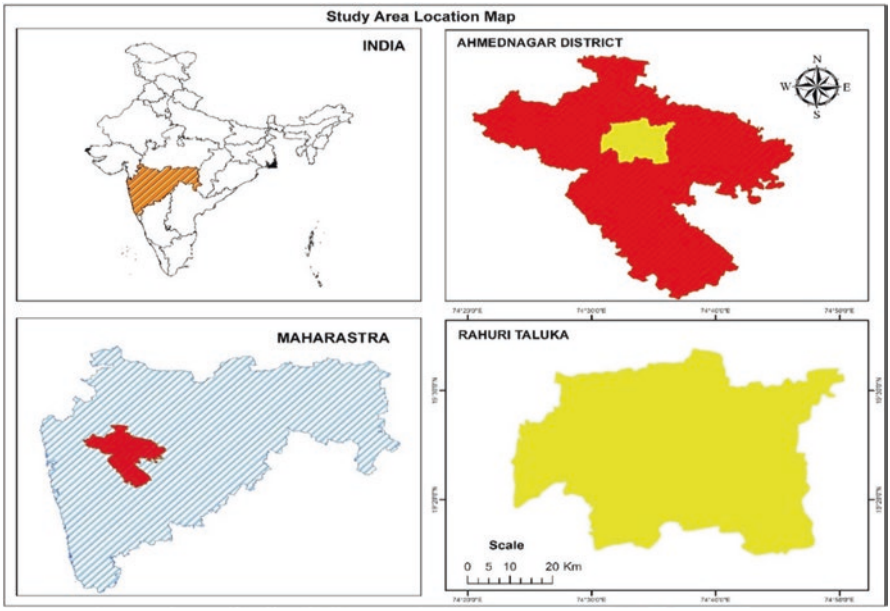

Fig. 24.1 Location map of study area

Methodology

Materials and Methods

LANDSAT-8 data is accessible on the Earth Explorer platform by USGS (US Geological Survey) site; it is an open-source data to study Earth's surface and atmosphere (Sun et al. 2009; Weng et al. 2004; Rajeshwari and Mani 2014; USGS 2013). LANDSAT-8 satellite images are at 16-day time intervals. It is entirely based on remote sensing images with different indices estimated using raster calculator tool in ArcGIS software (Mani et al. 2014; Latif et al. 2014). The algorithm was constructed using LANDSAT-8 data, including the thermal infrared sensor (band 10). Several approaches and measurements were used to compute the return of ground surface temperature. TIR band 10 was utilized to assess the Earth's temperature, vegetation ratio and NDVI for this study region, while bands 4 and 5 have used to calculate the NDVI. In addition, satellite data has been utilized in this investigation for April 2019. LANDSAT-8 contains group metadata such as fixed exchanges, feature value recovery and other features that have been used with an LST algorithm (Fig. 24.2).

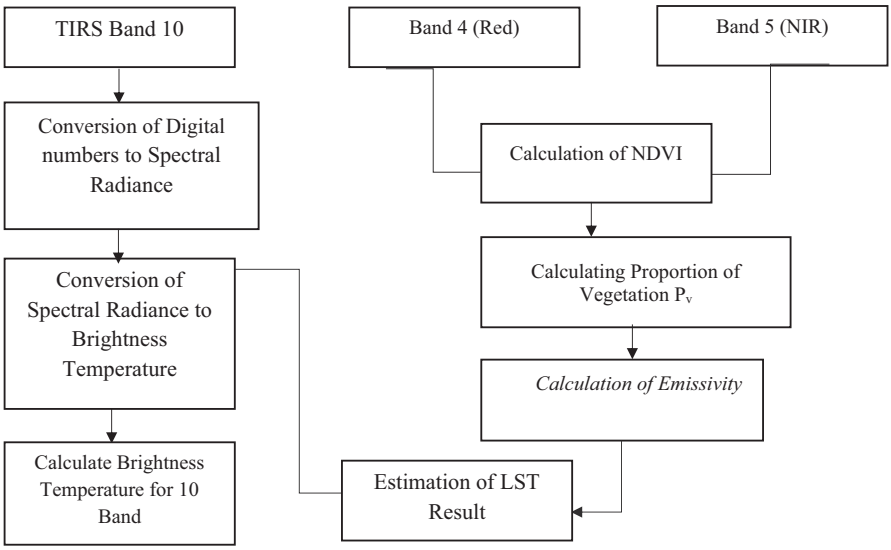

Fig. 24.2 Flow chart of method

Top-of-Atmosphere (TOA) Radiance

The radiance recalibration parameter has been used to translate digital infrared thermal data to TOA spectral data:

$$L\lambda = ML^{*}\,\mathrm{Qcal} + AL \tag{24.1}$$

where:

$L\lambda$, spectral radiance; ML, multiplicative band; AL, add band; and Qcal, quantized and calibrated value.

Top-of-Atmosphere (TOA) Brightness Temperature

The constant thermal values in the metadata file are utilized to transform spectral radiance observations to the maximum air brightness temperature. The following equations are used to study land surface temperature (Eqs. 24.2 and 24.5):

$$BT = K2 / \ln\left(k1 / L\lambda + 1\right) - 272.15 \tag{24.2}$$

$$PV = \left[\left(\mathrm{NDVI} - \mathrm{NDVI\,min}\right) / \left(\mathrm{NDVI\,max} + \mathrm{NDVI\,min}\right)\right]^{2} \tag{24.3}$$

$$E = 0.004^{*}\,PV + 0.986 \tag{24.4}$$

$$\mathrm{LST} = \left(BT / 1\right) + W^{*}\left(BT / 14380\right)^{*} \ln\left(E\right) \tag{24.5}$$

where:

BT, upper of atmosphere brightness hotness (°C); W, wavelength; and E, land surface emissivity.

Results and Discussion

LST refers to the air temperature measured within one-metre Earth's surface in an open area. The exchange of radiation from the ground to the atmosphere heats the air. The LST was always higher than the ambient temperature, depending on the meteorological conditions and the relationship and disparity between air and land surface temperatures.

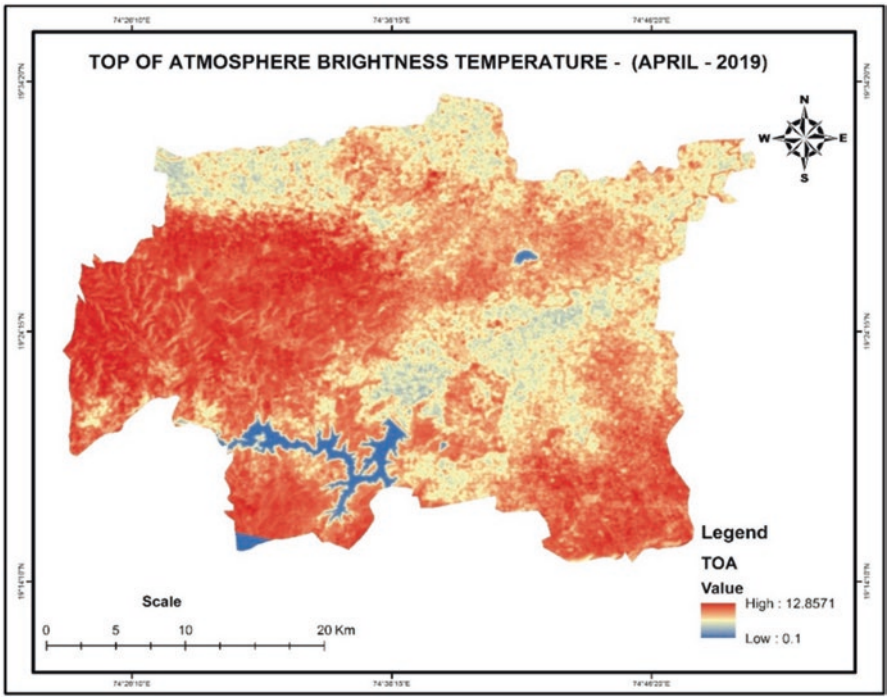

Fig. 24.3 Top-of-atmosphere brightness temperature

Top-of-Atmosphere Brightness Temperature

The TOA map has been shown to be in the range between 0.1 and 12.85 during the month of April. This map is enclosed in Fig. 24.3.

Land Surface Emissivity

The LSE map is shown to be in the range between 0.98 and 0.98 in April 2019 (Fig. 24.4).

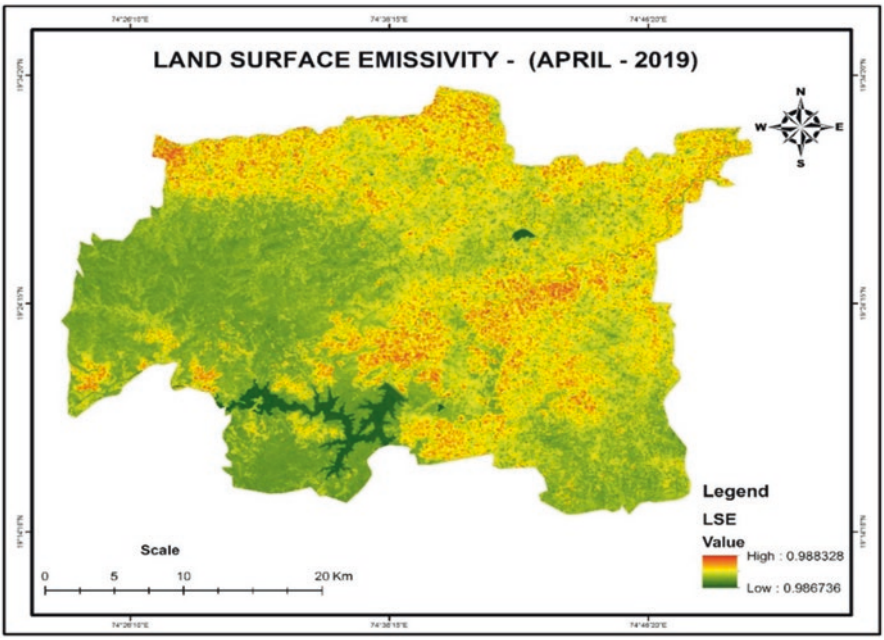

Fig. 24.4 Land surface emissivity

Normalized Difference Vegetation Index

The NDVI map was prepared based on LANDSAT-8 OLI (April 2019) data used in the ArcGIS software to observe the vegetation changes. These map values show the condition of vegetation on the Earth's surface. It is used for the identification of vegetation thickness based on satellite data. The technique separates the substantial rise in reflectance from visible to near-infrared wavelengths. The NDVI equation is

$$\mathrm{NDVI} = (\mathrm{NIR} - \mathrm{RED}) / (\mathrm{NIR} + \mathrm{RED})$$

Bands have changed from DN (digital number) value of raw to reflectance of solar electromagnetic energy. The method uses an only band data set with frequencies between 1 and +1, with higher numbers representing more vegetation and lower values showing water bodies (Fig. 24.5).

Figure 24.5 shows NDVI values to be between – 0.14 and 0.52 in April 2019.

The Proportion of Vegetation

Figure 24.6 shows the range value to be between 0.18 and 0.58 in April 2019.

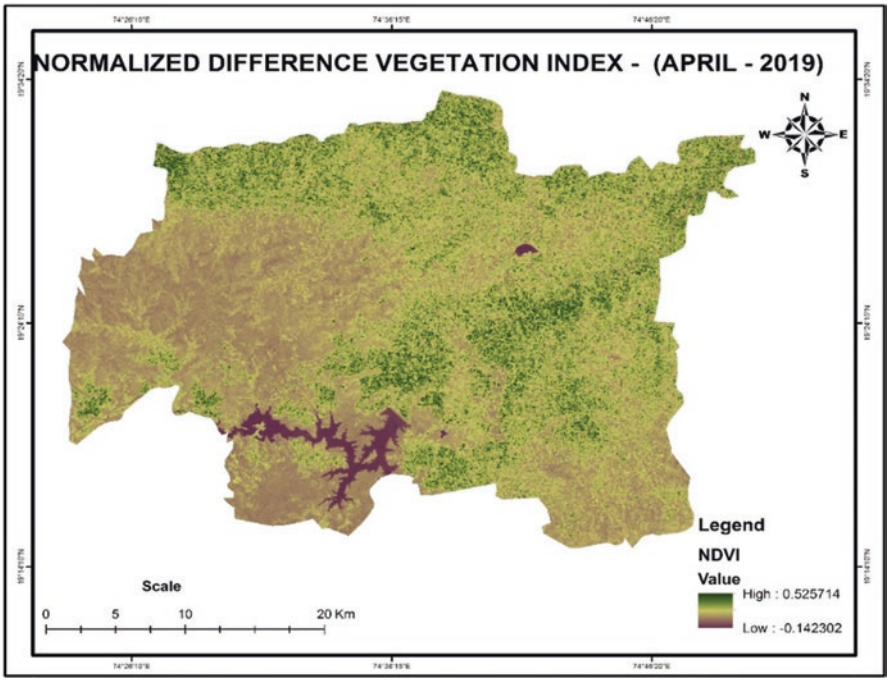

Fig. 24.5 Normalized difference vegetation index

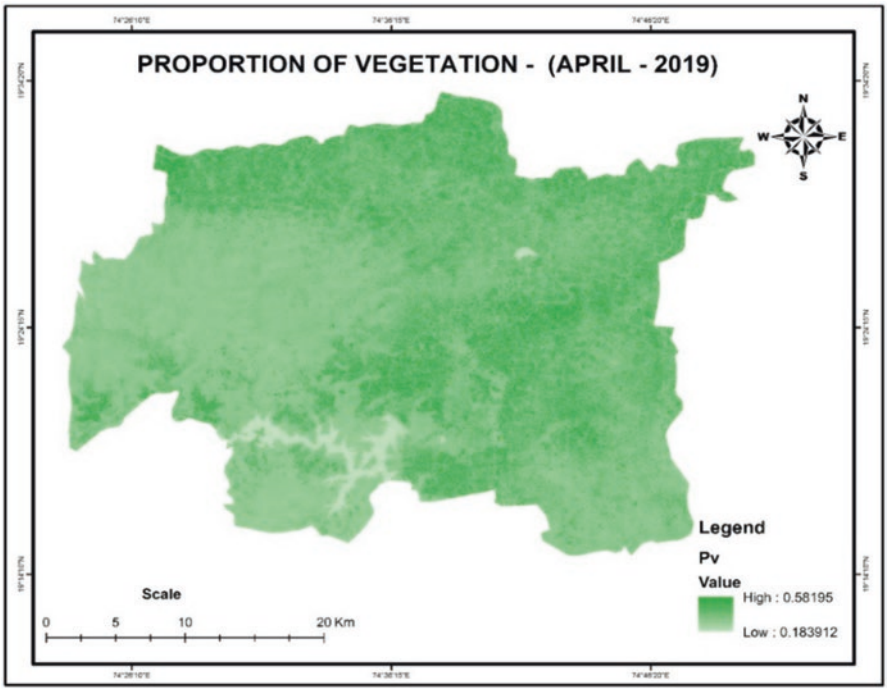

Fig. 24.6 The proportion of vegetation

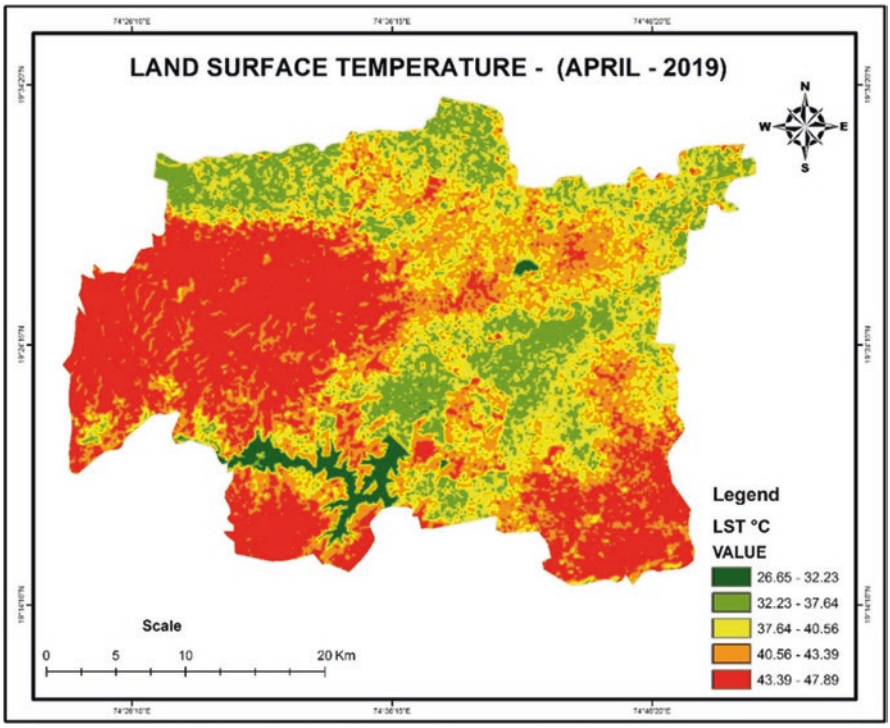

Fig. 24.7 Land surface temperature

Table 24.1 Details of LST in April 2019

Temperature in °C	Area in sq. km	Area in %
26.65–32.31 °C	19.59	1.85
32.31–37.73 °C	170.32	16.07
37.73–40.64 °C	254.88	24.05
40.64–43.47 °C	275.27	25.98
43.47–47.89 °C	339.58	32.05
Total area in sq. km	1059.64	100.00

This map has been derived from the brightness of temperature and land surface emissivity. The land surface temperature ranged between 26.65 and 47.89 °C for April 2019, and this is depicted in Fig. 24.7 (Table 24.1).

Table 24.2 Details of the MPKV (Mahatma Phule Krishi Vidyapeeth), Rahuri near-surface temperature data in the month of April 2019

Station	Month/year	Week	Date	Temperature	
				Max °C	Min °C
Rahuri	April 2019	First	02-04-2019	39.6	18.3
			03-04-2019	39.8	19.4
			04-04-2019	39.4	19.9
			05-04-2019	40.8	23.9
			06-04-2019	39.4	19.9
			07-04-2019	39.0	18.9
			08-04-2019	40.0	19.4
		Second	09-04-2019	40.2	18.9
			10-04-2019	40.0	17.9
			11-04-2019	40.8	19.9
			12-04-2019	41.0	20.9
			13-04-2019	40.2	21.9
			14-04-2019	40.4	22.9
			15-04-2019	40.5	25.9
		Third	16-04-2019	37.4	21.4
			17-04-2019	34.4	18.4
			18-04-2019	35.8	14.9
			19-04-2019	36.0	18.9
			20-04-2019	39.0	18.4
			21-04-2019	38.6	22.9
			22-04-2019	38.8	19.5
		Fourth	23-04-2019	38.4	20.9
			24-04-2019	40.0	22.9
			25-04-2019	40.8	24.4
			26-04-2019	42.0	23.4
			27-04-2019	42.2	25.9
			28-04-2019	43.0	24.9
			29-04-2019	42.4	25.5
		Average temperature (°C)		**39.6 °C**	**21.1 °C**

Near-Surface Air Temperature in April 2019

The monthly average temperature has been observed to be at 39.6 °C. The minimum and maximum temperatures of 21.1 °C and 41.3 °C were recorded in the fourth week of April 2019. A minimum temperature of 37.1 °C was recorded in the second week of April 2019. In the fourth week, the temperature was observed to be higher than all other weeks, due to the lack of monsoon, anthropogenic activities and dense population pressure in the area with moderate land surface temperature (Table 24.2).

LST Validation

The comparison has been made with a near-surface air temperature that is varied and often can lead to significant variations as the LANDSAT-8 30 m resolution and thermal band 100 m included in this study. The pixel of LST, while climate station was placed, was calculated and recorded. Depending on the weather and other conditions, the changes can be rather significant. It is substance noting that the LST and the near-surface airborne temperature differ by 1.1–2 m, implying that temperature discrepancies are typical and expected.

Evaluation of LST Validation with Result

The available data has been selected to compare the findings of Rahuri taluka by taking the remote sensing image at http://earthexplorer.usgs.gov/. Surface temperatures were derived by using an algorithm using ArcGIS. In this area, only one meteorological station has been identified, and the contrast between the recovered LSTs and near-surface airborne temperatures is shown, and the station details are shown in Tables 24.1 and 24.2.

Conclusion

The landscape impact on the LST has been created from satellite data; it is a calculation performed on ArcGIS10. The thermal radiation recorded by TIRS band 10 of LANDSAT-8 was helpful for the development of algorithm. The standard deviation for this field estimated based on the weather stations was 4.83∘C in the Rahuri taluka. It is described that perhaps the variance between the air temperature near the surface and the LST can be changed significantly, we connect the different temperatures in this area. The estimated LST values reveal that in the month of April 2019, a low amount of the land surface temperature lies in the range of 26.65–32.31 °C (1.85%) and moderately 37.73–40.64 °C (24.05%) and highly 43.47–47.89 °C (32.05%). LST measurements should be used to develop the instrument for future investigations. In future, temperature can be increased due to pollution, The study area results may help in planning the use of water for agriculture and the effect of climate changes in semiarid regions.

References

Barsi JA, Schott JR, Hook SJ, Raqueno NG, Markham BL, Radocinski RG (2014) Landsat-8 thermal infrared sensor (TIRS) vicarious radiometric calibration. Remote Sens 6(11):11607–11626

Candy RW et al (2017) The impact of satellite-derived land surface temperatures on numerical weather prediction analyses and forecasts. J Geophys Res Atmos 122(18):9783–9802

Fathi S, Hagen JS, Matanó A, Nogueira GEH (2021) Review of GIS multi-criteria decision analysis for managed aquifer recharge in semi-arid regions. In: Pande CB, Moharir KN (eds) Groundwater resources development and planning in the semi-arid region. Springer, Cham. https://doi.org/10.1007/978-3-030-68124-1_2

Gallo K, Hale R, Tarpley D, Yu Y (2011) Evaluation of the relationship between air and land surface temperature under clear and cloudy-sky conditions. J Appl Meteorol Climatol 50(3):767–775

Gulhane VA, Rode SV et al. (2022) Correlation Analysis of Soil Nutrients and Prediction Model Through ISO Cluster Unsupervised Classification with Multispectral Data. Multimed Tools Appl. https://doi.org/10.1007/s11042-022-13276-2

Jayaraman R, Chokkalingam L (2021) Correlation between land surface temperature and vegetation cover of Nagapattinam Coastal Zone, Tamil Nadu, using geospatial techniques. In: Pande CB, Moharir KN (eds) Groundwater resources development and planning in the semi-arid region. Springer, Cham. https://doi.org/10.1007/978-3-030-68124-1_12

Kandekar VU, Pande CB, Rajesh J et al (2021) Surface water dynamics analysis based on sentinel imagery and Google Earth Engine Platform: a case study of Jayakwadi dam. Sustain Water Resour Manag 7:44. https://doi.org/10.1007/s40899-021-00527-7

Latif MS et al (2014) LST retrival of Landsat-8 data using split window algorithm – a case study of Ranchi District. Int J Eng Res Dev 2(4):3840–3849

Liu L, Zhang YZ (2011) Urban heat island analysis using the Landsat TM data and ASTER data: a case study in Hong Kong. Remote Sens 3(7):1535–1552

Mani ND et al (2014) Estimation of LST of Dindigul district using LANDSAT 8 data. Int J Adv Res Innov Technol 03(05):122–126

McCarthy MP, Best MJ, Betts RA (2010) Climate change in cities due to global warming and urban effects. Geophys Res Lett 37:L09705

Mosammam HM, Nia JT, Khani H, Teymouri A, Kazemi M (2017) Monitoring land use change and measuring urban sprawl based on its spatial forms: the case of Qom city. Egypt J Remote Sens Space Sci 20(1):103–116

Narayana Reddy S et al (2017) Land surface temperature retrieval from LANDSAT data using emissivity estimation. Int J Appl Eng 12(20):9670–9687

Pande CB, Moharir KN, Khadri SFR et al (2018) Study of land use classification in an arid region using multispectral satellite images. Appl Water Sci 8:123. https://doi.org/10.1007/s13201-018-0764-0

Pande CB, Moharir KN, Khadri SFR (2021a) Assessment of land-use and land-cover changes in Pangari watershed area (MS), India, based on the remote sensing and GIS techniques. Appl Water Sci 11:96. https://doi.org/10.1007/s13201-021-01425-1

Pande CB, Moharir KN, Singh SK, Varade AM, Elbeltagie A, Khadri SFR, Choudhari P (2021b) Estimation of crop and forest biomass resources in a semi-arid region using satellite data and GIS. Journal of the Saudi Society of Agricultural Sciences 20(5):302–311

Pande CB (2022) Land use/land cover and change detection mapping in Rahuri watershed area (MS), India using the google earth engine and machine learning approach. Geocarto International. https://doi.org/10.1080/10106049.2022.2086622

Pande CB, Kadam SA, Jayaraman R, Gorantiwar S, Shinde M (2022) Prediction of soil chemical properties using multispectral satellite images and wavelet transforms methods. Journal of the Saudi Society of Agricultural Sciences 21(1):21–28

Pu R, Gong P, Michishita R, Sasagawa T (2006) Assessment of multi-resolution and multi-sensor data for urban surface temperature retrieval. Remote Sens Environ 104:211–225

Rajeshwari, Mani N (2014) Estimation of the land surface temperature of Dindigul district using landsat 8 data. Int J Res Eng Technol 3(5):122–126

Sellers PJ, Hall FG, Asrar G, Strebel DE, Murphy RE (1988) The first ISLSCP Field Experiment (FIFE). Bull Am Meteorol Soc 69:22–27

Shahid M, Rahman KU, Haider S et al (2021) Quantitative assessment of regional land use and climate change impact on runoff across Gilgit watershed. Environ Earth Sci 80:743. https://doi.org/10.1007/s12665-021-10032-x

Sun QQ, Tan JJ, Xu YH (2009) An ERDAS image processing method for retrieving LST and describing urban heat evolution a case study in the Pearl River Delta Region in South China. Environ Earth Sci 59(5):1047–1055

Turkoglu N (2010) Analysis of urban effects on soil temperature in Ankara. Environ Monit Assess 169(1–4):439–450

USGS (2013). http://landsat.usgs.gov/Landsat8UsingProduct.php

Wan Z, Dozier J (1996) A generalized split-window algorithm for retrieving land-surface temperature from space. IEEE Trans Geosci Remote Sens 34:892–905

Wang F, Qin Z, Song C, Tu L, Karnieli A, Zhao S (2015) An improved mono-window algorithm for land surface temperature retrieval from landsat-8 thermal infrared sensor data. Remote Sens 7(4):4268–4289

Weng YC (2007) Spatiotemporal changes of landscape pattern in response to urbanization. Landsc Urban Plan 81(4):341–353

Weng QH, Lu DS, Schubring J (2004) Estimation of land surface temperature-vegetation abundance relationship for urban heat island studies. Remote Sens Environ 89(4):467–483

Chapter 25
Analytical Hierarchy Process (AHP) Based on the Spatial Assessment of an Endangered Alpine Medicinal Herb *Aconitum heterophyllum* in the Western Himalayan Environment

Arun Pratap Mishra, Naveen Chandra, Juan James Mandy, S. K. Dwivedi, Ali Alruzuq, and Chaitanya B. Pande

Abstract Rare and endemic species comprise globally a priority conservation concern in view of being at a higher risk of extinction. Recording the occurrence data for such species, especially in hardly accessible alpine habitats, is a rather challenging task. Modeling serves as an effective tool for predicting habitat suitability as well as in practicing artificial introductions for such species with encouraging conservation implications. *A. heterophyllum* is a critically endangered and endemic medicinal herb that is distributed along 2400–4500 m in Western Himalayas. The excessive demand for *Aconitum heterophyllum* in the herbal and pharmaceutical industry due to the biologically active compounds (aconitine) has led to extensive exploitation of the species from the wild, which has made its survival in its natural habitat miserable. In the present communication, effective criteria were identified in determining suitable areas for the *Aconitum heterophyllum*, which include the eight

A. P. Mishra (✉)
Department of Habitat Ecology, Wildlife Institute of India, Dehradun, Uttarakhand, India

N. Chandra · S. K. Dwivedi
Uttarakhand Space Application Centre, Upper Aamwala Nalapani, Dehradun, Uttarakhand, India

J. J. Mandy
Indian Institute of Remote Sensing, Indian Space Research Organization, Dehradun, Uttarakhand, India

A. Alruzuq
Department of Geography and Department of Civil Engineering, University of Florida, Gainesville, FL, USA

C. B. Pande
Indian Institute of Tropical Meteorology (IITM), Pune, Maharashtra, India

C. B. Pande et al. (eds.), *Climate Change Impacts on Natural Resources, Ecosystems and Agricultural Systems*, Springer Climate,
https://doi.org/10.1007/978-3-031-19059-9_25

criteria of precipitation, temperature, slope, aspect, elevation, topographic wetness index (TWI), vegetation type, and soil texture based on the purpose of the study, regional characteristics, field surveys, local information, and expert opinions. The analytical hierarchy process (AHP), a pair comparison method, was used to determine the incompatibility rate of the criteria based on the questionnaire.

Keywords Site suitability · Multicriteria analysis · *A. heterophyllum* · Alpine regions · Analytical hierarchy process (AHP)

Introduction

Himalaya is well known for its rich plant biodiversity since ancient times and supports the growth of an umpteen number of medicinal and aromatic plant species. The wide phytogeography and peculiar climatic conditions of the area provide a conducive environment for the development of a myriad of signature plant species endowed with lifesaving vital secondary metabolites (Singh and Hajra 1996). The Indian Himalayan Region (IHR) is considered as a biodiversity hotspot with over 8000 species of vascular plants (Samant et al. 1998), out of which 1740 species of MAPs (medicinal and aromatic plants) and around 964 species of medicinal plants are known to occur in this small Himalayan state of India. As per the estimates of Kala (2010), about 1740 species of medicinal and aromatic plants (MAPs) from IHR are used in traditional and modern therapeutic systems. The state of Uttarakhand is endowed with a rich diversity of MAPs, and around 964 species of medicinal plants are known to occur in this small Himalayan state of India (Rau 1975). The plant diversity of the Himalayan region is facing surmounting threats due to various anthropogenic activities in the region, and several plant species of the region are facing the risk of extinction in the imminent future (Ved et al. 2003). The number of such threatened species is increasing every year, due to the unsustainable exploitation of natural resources. *Aconitum heterophyllum* Wall. ex Royle is a signature species of the Himalayan region, facing various threats in the wild, and has been assigned by the International Union for Conservation of Nature (IUCN) threatened species status (Kaul 1997).

A. heterophyllum Wall. is a highly medicinal herb distributed in the high-altitude regions of Western Himalayas and extends to Eastern Himalayas at an altitude range of 2400–4500 m. The species is commonly known as “Atees” or “Patis” and is used for the treatment of various ailments by local people including fever, gastric disorders, and general debility. It is also used by local inhabitants of the Himalayan region for the treatment of gastric clutters, fever, and toothache. An extract of the root is taken as a tonic and also as a substitute for quinine (IUCN 1993). The low regeneration of this species mobilized with the high exploitation rate has rendered the species into a critically endangered status (Nautiyal et al. 2002; Goraya and Ved

2017; Feizizadeh et al. 2014). Observing the present urge of time, it has become imperative to adopt sustainable methods for the use of our natural resources and apply modern scientific techniques for their proper conservation and cultivation as well. The analytical hierarchical process (AHP) is utilized as a decision-making tool for the identification of suitable sites. AHP is one of the multicriteria decision-making methods that were originally developed by Prof. Thomas L. Saaty in 1980. As a multicriteria decision-making strategy, the AHP has been applied for tackling a wide assortment of problems that involve complex criteria over distinctive levels, where the interaction among criteria is common (Boroushaki and Malczewski 2008). In short, it is a method to derive ratio scales from paired comparisons. The input can be obtained from actual measurements such as price and weight or from subjective opinion such as satisfaction feelings and preference. AHP allow some small inconsistency in judgment because human is not always consistent. Weighted overlay besides the AHP gives exceptionally promising results for the location suitability analysis of the endangered and endemic plant species. It can be utilized to multilevel hierarchical structure on different criteria and obliges (Lal et al. 1991).

In view of the critically endangered status and unsustainable exploitation of *A. heterophyllum* from its natural habitat, the use of modern tools and techniques for the effective conservation of this high value medicinal herb is the need of hour. AHP studies for the habitat suitability analysis of the species are urgently required for effective conservation, management, and designing future conservation policy for this high-value medicinal herb.

Therefore, the present investigation is intended for predicting spatial extent and most suitable sites for *A. heterophyllum* in Alpine region of Uttarakhand. Findings of the study might be helpful in conducting species-specific recovery programs through habitat rehabilitation and reintroduction for *A. heterophyllum* (Fig. 25.1).

Study Area

The study was conducted in the alpine area of Uttarakhand above 2700 m between 28° 53′ to 31° 27′ N scopes and 77° 34′ to 81° 02′ E longitudes (Fig. 25.2). The alpine area is bordered by the Tibet (China) in the north, Himachal Pradesh in the west and northwest, and Nepal in the east. The alpine landscape (locally known as Bugyal or meadows) contributes almost 24.11% of the topographical region of the state over 2700 m asl (Sahani 2020). A total of 82 alpine meadows are reported from this region (Singh and Hajra 1996). The physiognomic unit of elevated vegetation is stunted forest, alpine scrub, alpine meadows, and pioneer communities on scree slopes and moraines. Based on elevation, aspect, moisture accessibility, and length of the developing season, six types of alpine meadows are recognized within the region (Singh and Hajra 1996).

Fig. 25.1 Habitat of *A. heterophyllum*

Materials and Methods

In the present study multi-criterion analysis and site suitability were developed to appropriate sites for *A. heterophyllum* based on different criteria. Depending on their importance and significance, eight diverse constraints and criteria were chosen. The identification of diverse criteria depended on the most extreme limitation strategy that impacts the *A. heterophyllum* which includes temperature, rainfall, topographic wetness index (TWI), soil texture, forest type, aspect, elevation, and slope (Table 25.1). These criteria have been selected since temperature and rainfall could briefly cover the influence of climatic parameters on the species. This is since the distribution of the species throughout a region is very much dependent on optimum temperature and rainfall conditions. Further, soil texture could be indicative of soil fertility and the kind of support system that is available for the plant species. The forest type present in the surrounding plays a very critical role as it influences the vegetation pattern as well as the presence and absence of certain species based on its compatibility with the dominant species variety. Finally, terrain indices such as TWI, aspect, elevation, and slope are indicative of amount of sunlight received, sun duration, other climatic factors, etc. These highly influential parameters were believed to be a representative that could cover the multitude of factors that

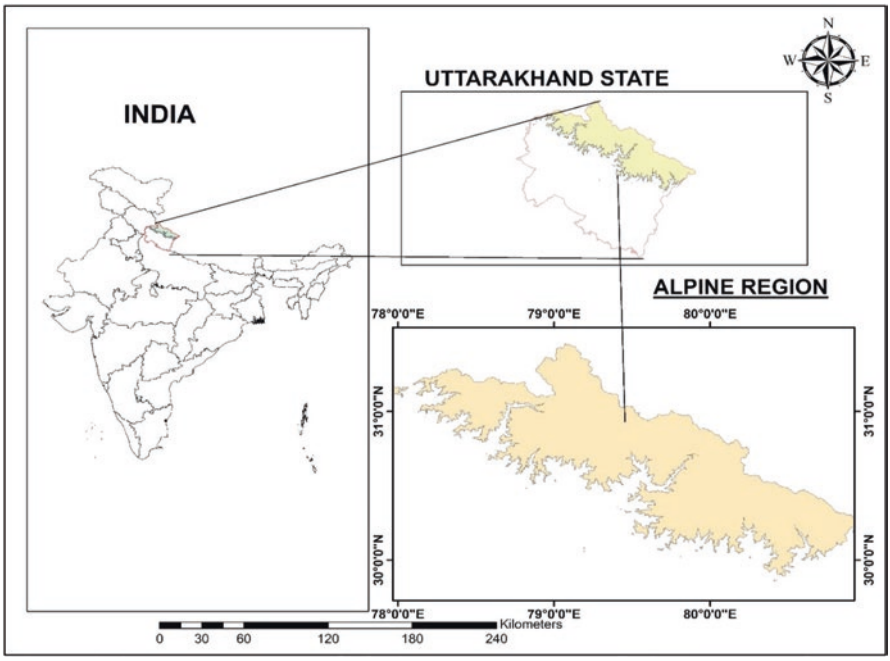

Fig. 25.2 Location map of the study area

Table 25.1 Details of the parameter used in the site suitability analysis

Datasets	Source	Link
Temperature	Wordclim 30 arc second (1 km)	www.worldclim.org
Rainfall	Wordclim 30 arc second (1 km)	www.worldclim.org
Soil texture	FAO Soils Portal	http://www.fao.org/soils-portal/data-hub/soil-maps-and-databases/en/
Forest type (supervised classification using Sentinel-2)	USGS (Earth Explorer)	https://earthexplorer.usgs.gov/
Aspect, elevation, slope, and TWI	Generated from DEM	https://earthexplorer.usgs.gov/

influence the presence of a vegetative species and its distribution. Additionally, weights for each selected criterion were assessed utilizing AHP, and after that, weighted overlay method was received to set up the suitability map. Schematic representation of the methodology for present study is shown in Fig. 25.3. The equation to generate TWI is also stated here as follows:

$$\mathrm{TWI} = \ln\left(a / \tan b\right)$$

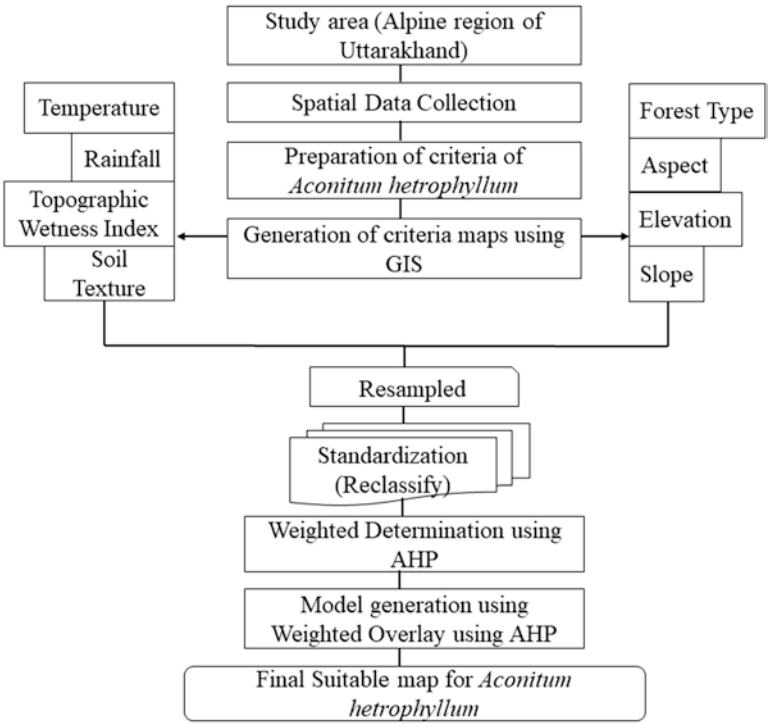

Fig. 25.3 Schematic representation of the methodology

where:

a = upslope contributing area (m^2)
b = slope in radians

Generation of Criterion Maps Using Geospatial Techniques

Shuttle Radar Topography Mission (SRTM) Digital Elevation Model (DEM) was used to generate slope, aspect, elevation, and TWI. Supervised classification technique was used for image classification, in order to prepare the forest type of Alpine region. This was carried out with the help of a classified map of Forest Survey of India using Sentinel-2 imagery that was obtained from the United States Geological Survey (USGS). Rainfall and temperature data with 30 arc second (1 km) spatial resolution were downloaded from Worldclim dataset (www.worldclim.org). Soil texture data was taken from the FAO Digital Soil Map of the World (DSMW) (www.fao.org). Erdas 14 and ArcGIS 10.3 were used to create the spatial data layers

(Pande et al. 2021a). Finally, all the data were resampled into the spatial resolution of satellite imagery in order to facilitate raster analysis using nearest neighbor resampling technique.

Standardization of Selected Criteria Maps

All the chosen criteria have different units. Hence, to execute weighted overlay strategy, they have to be kept in the same units and consequently have to be standardized. Standardization procedures change over the estimation to uniform units, and the resultant score lose their measurement in conjunction with their estimation unit of all criteria (Miller et al. 1998). The vector layers of all criteria maps were converted to the raster layer, and all the raster layers were reclassified and utilized for the input information to the weighted overlay method which finally makes the suitability outline for *A. heterophyllum.* Reclassified strategy in the spatial analyst toolbox of ArcGIS program standardizes the value of all selected criteria for the investigation of comparative centrality.

Calculation of Weight for Each Criterion

AHP is one of the most significant multicriteria decision-making techniques. The method is applied to a set of criteria or sub-criteria to set up a distinct leveled structure by giving the weight of each model (Kiker et al. 2005). The weight analyzes the relative centrality of individual criterion and subsequently needs to be chosen purposely. AHP offers a structural ground for quantifying the strong comparison of design criteria and elements in a pairwise technique and thus decreases the complexity of the decision-making process (Satty 1977, 2008; Rajesh et al. 2021; Pande et al. 2021b). The method decides the weight values by pairwise comparison method by the relative significance of criteria, taken two at a time (Garfi et al. 2009; Satty 1980). Utilizing the pairwise comparison matrix, the analytic hierarchy process calculates the weights for the individual model by taking the eigenvalue and comparing it to the most noteworthy eigenvector of the completed matrix and normalizing the whole of the variables to solidarity (Malczewski 1999). Utilizing the AHP over the pairwise comparison matrix was calculated using a scale of 1–9, where 9 shows extraordinary importance and 1 shows the break-even with the importance of the in-between basis of the network (Malczewski 1999; Satty 1990 and Boroushaki and Malczewski 2008). The comparison framework primarily has the criteria of correspondence which is scientifically communicated as $n\ (n-1)/2$ for n number of components in a pairwise comparison matrix (Akıncı et al. 2013; Garcia and Zimmermann 2014). After the computation of the pairwise framework, relative weights/eigenvectors are calculated utilizing Saaty's strategy. Additionally, AHP also distinguishes and calculates the irregularities of decision-makers which is one

of the critical characteristics (Boroushaki and Malczewski 2008; Cengiz and Akbulak 2009). The effectiveness criteria of AHP are evaluated by consistency relationship (CR) which is measured by Eq. 25.1:

$$\mathrm{CR} = \mathrm{CI} / \mathrm{RI} \tag{25.1}$$

Condition 1 represents the CR where CI shows the consistency index and RI shows the random index. Consistency relationship encourages the assurance of conceivable events and measures coherent irregularities of the decision-makers/judgments (Chen et al. 2012; Girvan et al. 2003). It represents the probability where the network judgments were shaped arbitrarily. The CR primarily depends on the consistency index and random index:

$$\text{Consistency index}\left(\mathrm{CI}\right) = \left(\lambda \max - n\right) / \left(n - 1\right) \tag{25.2}$$

Equation 25.2 indicates the consistency index (CI) when λmax is the principle or highest eigenvector of the computed matrix and *n* denotes the order of the matrix.

The weighted overlay method is compelling to resolve spatial complexity in suitability analysis and site selection based on a common estimation of contrasting and differing impacts (Parimala and Lopez 2012). AHP decides the influential variables within the pecking order of chosen divergent inputs to weighted overlay investigation (Mojid et al. 2009; Mishra et al. 2022). Chosen raster layers were overlaid by recognizing their cell values to the same scale, giving weight to the person model, and coordinating the weight cell values together (Eq. 25.1). The cell values of each raster layer are moreover duplicated by their weight esteem (Pamucar et al. 2021; Parmesan and Yohe 2003 and Chen et al. 2012) utilizing the show builder toolbox of Arc-GIS 10.3:

$$\mathrm{LS} = \sum_{n}^{i=1} \mathrm{WiXi} \tag{25.3}$$

where LS demonstrates the whole suitability score, Wi indicates the weight of the chosen suitability criteria, xi demonstrates the allowed sub-criteria score of i suitability criteria, and *n* indicates the overall number of capability criteria (Fig. 25.4; Tables 25.2 and 25.3).

Step 1: Two criteria are assessed at a time in terms of their relative significance. Index values from 1 to 9 are utilized. On the off chance that model A is precisely as imperative as basis B, this combination gets a record of 1. In case A is much more vital than B, the record is 9. All degrees are conceivable in between. For a "less imperative" relationship, the divisions 1/1–1/9 are accessible: in case A is much less critical than B, the rating is 1/9. The values are entered row by row into a cross-matrix. The diagonal of the matrix contains as it were values of 1. To begin with, the correct upper half of the matrix is filled until each criterion has been compared to the other one. In the event that A to B was evaluated with the relative significance of n, B to A has got to be evaluated with 1/*n*.

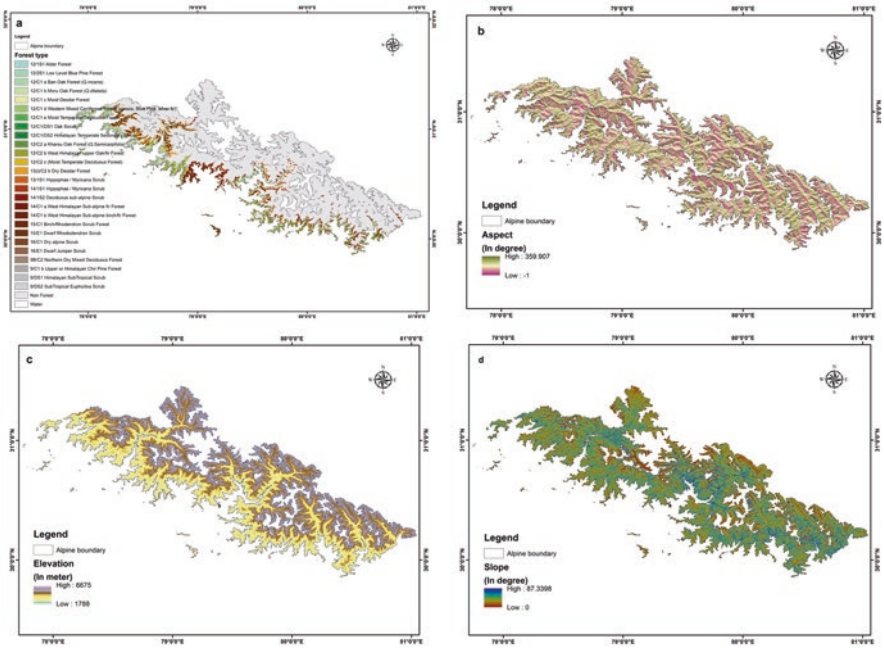

Fig. 25.4 Parameters used for suitable site identification: (**a**) annual mean temperature, (**b**) annual mean rainfall, (**c**) topographic wetness index, (**d**) soil texture, (**e**) forest type, (**f**) aspect, (**g**) elevation, and (**h**) slope

Table 25.2 Explanation of scale and degree of preference

Scale	Degree of preference	Explanation
1	Equally	Two activities contribute equally to the objective
3	Moderately	Experience and judgment slightly to moderately favor one activity over another
5	Strongly	Experience and judgment strongly or essentially favor one activity over another
7	Very strongly	An activity is strongly favored over another and its dominance is showed in practice
9	Extremely	The evidence of favoring one activity over another is of the highest degree possible of an affirmation
2, 4, 6, and 8	Intermediate values	Used to represent compromises between the references in weights 1, 3, 5, 7, and 9
Reciprocals	Opposite	Used for inverse comparison

Source: Saaty and Vargas (1980). Completion of the pairwise comparison framework

Step 2: The weights of the individual criteria are calculated. To begin with, a normalized comparison matrix is made: each esteem within the framework is divided by the sum of its column. To urge the weights of the person criteria, the mean of each row of this second matrix is decided. These weights are as of now normalized; their entirety is 1.

Table 25.3 Pairwise comparison matrix for multi-criteria decision problems for *A. heterophyllum*

Class	Temperature	Rainfall	TWI	Soil texture	Vegetation type	Aspect	Elevation	Slope
Temperature	1	2	3	5	6	7	8	9
Rainfall	1/2	1	2	4	5	6	7	8
TWI	1/3	1/2	1	3	4	5	6	7
Soil texture	1/5	1/4	1/3	1	2	3	4	5
Forest type	1/6	1/5	1/4	1/2	1	2	3	4
Aspect	1/7	1/6	1/5	1/3	1/2	1	2	3
Elevation	1/8	1/7	1/6	1/4	1/3	1/2	1	2
Slope	1/9	1/8	1/7	1/5	1/4	1/3	1/2	1

Table 25.4 The synthesized matrix for all criteria decision-making

Class	Temperature	Rainfall	TWI	Soil texture	Forest type	Aspect	Elevation	Slope
Temperature	0.3876	0.4566	0.4231	0.3501	0.3145	0.2819	0.2540	0.2308
Rainfall	0.1938	0.2283	0.2821	0.2801	0.2621	0.2416	0.2222	0.2051
TWI	0.1292	0.1142	0.1410	0.2101	0.2096	0.2014	0.1905	0.1795
Soil texture	0.0775	0.0571	0.0470	0.0700	0.1048	0.1208	0.1270	0.1282
Forest type	0.0646	0.0457	0.0353	0.0350	0.0524	0.0805	0.0952	0.1026
Aspect	0.0554	0.0381	0.0282	0.0233	0.0262	0.0403	0.0635	0.0769
Elevation	0.0484	0.0326	0.0235	0.0175	0.0175	0.0201	0.0317	0.0513
Slope	0.0431	0.0285	0.0201	0.0140	0.0131	0.0134	0.0159	0.0256

Synthesized Matrix

The pairwise comparison matrix was then synthesized by dividing each element of the matrix by its column total. The priority vector can be obtained by finding the row averages (Table 25.4).

Consistency Ratio Calculation

Then, the appropriate value of average random consistency index (RI) for a matrix size of eight is 1.41. The consistency ratio (CR) is calculated as

$$\begin{aligned} \mathrm{CR} &= \mathrm{CI} / \mathrm{RI} \\ &= 0.05182 / 1.41 \\ &= 0.036752 \end{aligned}$$

As the value of CR was less than 0.1, the above calculation was acceptable (Table 25.5).

Table 25.5 Average random consistency index (RI)

Size of matrix	1	2	3	4	5	6	7	8	9	10
Random consistency	0	0	0.58	0.9	1.12	1.24	1.32	1.41	1.45	1.49

Results and Discussion

Habitat Suitability of A. heterophyllum

In the present study, the six main criteria of precipitation, temperature, slope, altitude, soil texture, and orientation were used to localize *A. heterophyllum* using AHP. AHP results revealed that a total of 567 km^2 area was predicted as highly suitable and about 485 km^2 area is suitable and 914 km^2 area is moderately suitable, while the rest of the area that is 6282 km^2 was not suitable for the species (Fig. 25.5). Most of the highly suitable sites are close to 3000–4000 m elevation. The predicted suitable sites for *A. heterophyllum* lie in grassy slopes and most of the suitable areas fall in the northern aspect. On the basis of our analysis, it has been found that temperature, rainfall, and moisture have a high impact on its distribution. Suitable site identification and multicriteria-based modeling based on their ecological knowledge on its natural sites suggested that *A. heterophyllum* prefers north-facing and grassy slopes in sub-alpine and alpine areas of Uttarakhand Himalaya. *A. heterophyllum* commonly grows in alpine meadows on partly shaded grassy slopes and along the edges of *Betula utilis* (Bhoj Patra) forest between 3000 and 4000 m elevation in Uttarakhand alpine areas.

Discussion

A previous study had used the machine learning algorithm (MaxEnt) to determine the potential sites of threatened MAPs in the region (Chandra et al. 2021; Singh et al. 2020). The present study identified the habitat suitability of *A. heterophyllum* in high-altitude regions of Uttarakhand through AHP using different environmental parameters including temperature, rainfall, TWI, soil texture, vegetation type, aspect, elevation, and slope. Since temperature influences most plant processes, including photosynthesis, transpiration, respiration, germination, and flowering, therefore it was given first criteria. Rainfall plays a critical character in deciding the vegetation of a place. The different characteristics of the vegetation of a place are imposing on numerous geological factors. Rainfall is one of the foremost vital geological components which influence the development of the vegetation in a region. Based on the ecology of *A. heterophyllum* in alpine region, we choose the rainfall as the second criterion. TWI is a highly useful index in vegetation ecology (Zinko et al. 2006), and the index could be a work of both the slope and the upstream contributing zone per unit width orthogonal to the flow direction. Due to the specialty of TWI

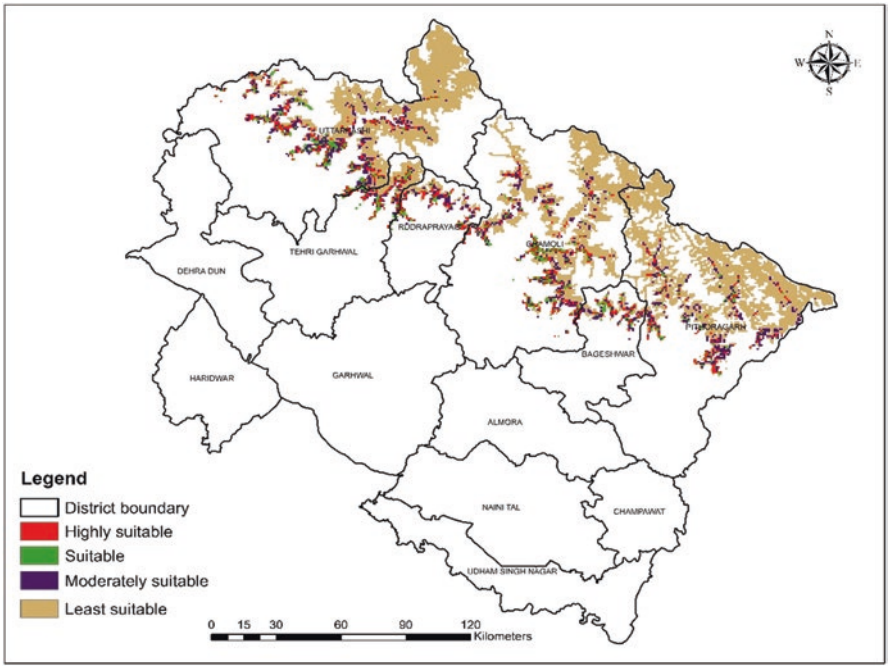

Fig. 25.5 Suitability map of the *A. heterophyllum* in alpine areas of Uttarakhand

index, we choose it as the third criteria. The texture of the soil is imperative since it decides soil characteristics that influence plant growth. So, this was part of our fourth criterion. Major grassland was found to be most suitable for the suitable sites of *A. heterophyllum*, so vegetation types were the fifth criterion. Aspect plays a critical role in influencing vegetation pattern in alpine areas. It was part of the sixth critical criterion. As the seventh criterion, elevation map showed the height variation of the study area. As the eighth and last criterion, slope plays a critical role to differentiate species composition and vegetation pattern. In this study all the criteria are selected based on their importance. The weighted value of selected parameter calculated in AHP and a designated score of sub-criteria were used in weighted overlay analysis to generate the suitable site for *A. heterophyllum* in alpine region of Uttarakhand. Rare and endemic species have acquired top priority for conservation worldwide because these species are at high risk of extinction. Mapping potential habitats for rare and endemic species can aid in conservation planning and management. It is recommended that the species should be reintroduced for conservation in the predicted suitable habitats. Cultivation of target species can reduce the pressure in its natural habitat and may lead to its conservation and sustainable use in the future. This approach will provide more chances to species survival and management easier and more efficient than other practices. Model predictions and field assessments reveal that *A. heterophyllum* has a limited potential distribution. Majority of the predicted habitats are also highly affected by livestock grazing and

human activities like overexploitation, habitat fragmentation, and road construction The increasing demand for this compound in herbal medicines and health-care compounds has led to overharvesting of the tubers, resulting in rapid depletion of the natural stocks of this valuable plant (Pandey et al. 2020). Thus, there is an immediate need to go for in situ and ex situ conservation measures. The predicted suitable areas encompass habitats including alpine grassy slope, dry slope, and shrubbiest and subalpine forest (*Rhododendron campanulatum*). Grassy slope and shrubbiest habitats are among high probability areas for the species; hence, these areas could be used for in situ conservation of the species. Reintroduction of the target species in the predicted habitats would help a great deal in rehabilitating the species population and in improving conservation status, hence in conserving the overall biodiversity of the region.

Climate change, especially global warming, not only causes temperature changes in different regions but also alters the distribution pattern of precipitation. When the change of these climatic factors is close to plant growth, it will lead to the migration of their distribution (Parmesan and Yohe 2003). The increasing demand for this compound in herbal medicines and health-care compounds has led to overharvesting of the tubers, resulting in rapid depletion of the natural stocks of this valuable plant (Pandey et al. 2020). Water availability has a significant impact on physiological responses. Thus, precipitation can constrain species distribution and influence distribution in various ways (Harsch and HilleRisLambers 2016). The increase of precipitation during the driest month results in a longer growing season and helps species migrate to more suitable habitats within their distribution (Vaganov et al. 1999). In addition, extreme high and low temperatures also have a significant influence on plant growth. The decrease of the minimum temperature of the coldest month results in premature freezing injuries to plants, and long-term low temperatures will lead to the death of plants at the distribution limit. Field investigations and modal output revealed that moist meadows, grassy slope, and shrubbies encountered as preferable habitat for the species. Local communities should be encouraged to cultivate the species in such sites and their fellow lands. Involvement of farmers, both indigenous and migrant, and community-based nongovernment organization will be helpful in cultivation of the species that reduce the pressure in the wild. These sites/locations should be managed as in situ conservation sites linking with the Biodiversity Management Committee (BMC) at Gram Panchayat level.

Conclusion

The study was focused on the identification of suitable sites for critically endangered *A. heterophyllum* in the study area. AHP framework with the integration of GIS is utilized for the investigation in which eight diverse criteria were considered. The suitable areas identified in the present study for *A. heterophyllum* would not only help in eco-restoration of degraded forests and habitats, where the species had existed before but also in rehabilitating the species population and improving its

conservation status. Therefore, the findings would be quite useful in sustainable management of the species and conserving overall biological diversity in the region. The integration of informative layers was done using GIS. The results showed that the temperature, rainfall, and TWI were the first, second, and third priority to locate *A. heterophyllum* in the area. A total 567 km^2 area in the alpine zone of Uttarakhand is suitable for the species. Using all these criteria, the most suitable sites for *A. heterophyllum* were predicted. The findings of this study further can be complemented with the species recovery programs through habitat rehabilitation and reintroduction. Moreover, the findings can be useful for initiating farming of this valuable commercial crop in the remote villages and tribal pockets of the state, thereby preventing their migration. Thus, the scope of present study is having both socioeconomic and ecological impacts. The final result can be adopted for the reintroduction and conservation purposes in the study area.

References

Akıncı H, Ozalp AY, Turgut B (2013) Agricultural land use suitability analysis using GIS and AHP technique. Comput Electron Agric 97:71–82

Boroushaki S, Malczewski J (2008) Implementing an extension of the analytical hierarchy process using ordered weighted averaging operators with fuzzy quantifiers in *Arc GIS*. Comput Geosci 34(4):399–410

Cengiz T, Akbulak C (2009) Application of analytical hierarchy process and geographic information systems in land-use suitability evaluation: a case study of Dümrek village (Çanakkale, Turkey). Int J Sustain Dev World Ecol 16(4):286–294

Chandra N, Singh G, Lingwal S, Jalal JS, Bisht MS, Pal V, Rawat B, Tiwari LM (2021) Ecological niche modeling and status of threatened alpine medicinal plant Dactylorhiza Hatagirea D. Don in Western Himalaya. J Sustain For:1–17. https://doi.org/10.1080/10549811.2021.1923530

Chen SM, Yang MW, Lee LW, Yang SW (2012) Fuzzy multiple attributes group decision-making based on ranking interval type-2 fuzzy sets. Expert Syst Appl 39(5):5295–5308

Feizizadeh B, Roodposhti MS, Jankowski P, Blaschke T (2014) A GIS-based extended fuzzy multi-criteria evaluation for landslide susceptibility mapping. Comput Geosci 73:208–221

Garcia K, Zimmermann SD (2014) The role of mycorrhizal associations in plant potassium nutrition. Front Plant Sci 5:337

Garfi M, Tondelli S, Bonoli A (2009) Multi-criteria decision analysis for waste management in Saharawi refugee camps. Waste Manage 29(10):2729–2739

Girvan MS, Bullimore J, Pretty JN, Osborn AM, Ball AS (2003) Soil type is the primary determinant of the composition of the total and active bacterial communities in arable soils. Appl Environ Microbiol 69(3):1800–1809

Goraya GS, Ved DK (2017) Medicinal plants in India: an assessment of their demand and supply. Ministry of Ayush, Dehradun

Harsch MA, HilleRisLambers J (2016) Climate warming and seasonal precipitation change interact to limit species distribution shifts across Western North America. *PloS one 11*(7):e0159184

IUCN (1993) IUCN parks for life: report of the IVth world congress on national parks and protected areas. IUCN, Gland

Kala CP (2010) Assessment of availability and patterns in collection of Timroo (*Zanthoxylum armatum* DC.): a case study of Uttarakhand Himalaya. Med Plants Int J Phytomed Relat Ind 2(2):91–96

Kaul MK (1997) Medicinal plants of Kashmir and Ladakh: temperate and cold arid Himalaya. Indus Publishing
Kiker GA, Bridges TS, Varghese A, Seager TP, Linkov I (2005) Application of multicriteria decision analysis in environmental decision making. Integr Environ Assess Manag Int J 1(2):95–108
Lal JB, Gulati AK, Bist MS (1991) Satellite mapping of alpine pastures in the Himalayas. Int J Remote Sens 12(3):435–443
Malczewski J (1999) Visualization in multicriteria spatial decision support systems. Geomatica 53(2):139–147
Miller CC, Burke LM, Glick WH (1998) Cognitive diversity among upper-echelon executives: implications for strategic decision processes. Strateg Manage J 19(1):39–58
Mishra AP, Singh S, Jani M, Singh KA, Pande CB, Varade AM (2022) Assessment of water quality index using Analytic Hierarchy Process (AHP) and GIS: a case study of a struggling Asan River. Int J Environ Anal Chem:1–13. https://doi.org/10.1080/03067319.2022.2032015
Mojid MA, Mustafa SMT, Wyseure GCL (2009) Growth, yield and water use efficiency of wheat in silt loam-amended loamy sand. J Bangladesh Agric Univ 7(2):403–410
Nautiyal S, Rao KS, Maikhuri RK, Negi KS, Kala CP (2002) Status of medicinal plants on way to Vasuki Tal in Mandakini Valley, Garhwal Himalaya, Uttaranchal
Pamucar D, Yazdani M, Montero-Simo MJ, Araque-Padilla RA, Mohammed A (2021) Multicriteria decision analysis towards robust service quality measurement. Expert Syst Appl 170:114508
Pande CB, Moharir KN, Singh SK, Varade AM, Ahmed Elbeltagie SFR, Khadri PC (2021a) Estimation of crop and forest biomass resources in a semi-arid region using satellite data and GIS. J Saudi Soc Agric Sci 20(5):302–311
Pande CB, Moharir KN, Panneerselvam B et al (2021b) Delineation of groundwater potential zones for sustainable development and planning using analytical hierarchy process (AHP), and MIF techniques. Appl Water Sci 11:186. https://doi.org/10.1007/s13201-021-01522-1
Pandey A, Arunachalam K, Thadani R, Singh V (2020) Forest degradation impacts on carbon stocks, tree density and regeneration status in banj oak forests of Central Himalaya. Ecol Res *35*(1):208–218
Parimala M, Lopez D (2012) Decision making in agriculture based on land suitability–spatial data analysis approach 1. J Theor Appl Inf Technol 46(1):17–23. Asian Research Publishing Network (ARPN). ISSN:19928645
Parmesan C, Yohe G (2003) A globally coherent fingerprint of climate change impacts across natural systems. Nature 421(6918):37–42
Rajesh J, Pande CB, Kadam SA et al (2021) Exploration of groundwater potential zones using analytical hierarchical process (AHP) approach in the Godavari river basin of Maharashtra in India. Appl Water Sci 11:182. https://doi.org/10.1007/s13201-021-01518-x
Rau MA (1975) High altitude flowering plants of West Himalaya
Saaty TL (1977) A scaling method for priorities in hierarchical structures. J Math Psychol 15(3):234–281
Saaty TL (1980) Multicriteria decision making: the analytic hierarchy process. McGraw-Hill, New York. (2nd impr. 1990, RSW Publishing, Pittsburgh)
Saaty TL (1990) How to make a decision: the analytic hierarchy process. Eur J Oper Res 48(1):9–26
Saaty TL (2008) Relative measurement and its generalization in decision making why pairwise comparisons are central in mathematics for the measurement of intangible factors the analytic hierarchy/network process. RACSAM-Revista de la Real Academia de Ciencias Exactas, Fisicas y Naturales. Serie A. Matematicas 102(2):251–318
Saaty TL, Vargas LG (1980) Hierarchical analysis of behavior in competition: prediction in chess. Behav Sci 25(3):180–191
Sahani N (2020) Application of analytical hierarchy process and GIS for ecotourism potentiality mapping in Kullu District, Himachal Pradesh, India. Environ Dev Sustain 22(7):6187–6211
Samant SS, Dhar U, Palni LMS (1998) Medicinal Plants of Indian Himalaya: diversity, distribution, potential value. GyanodayaPrakashan, Nainital

Singh DK, Hajra PK (1996) Floristic diversity. In: Changing perspectives of biodiversity status in the Himalaya. British High Commission Publication, pp 23–38

Singh G, Chandra N, Lingwal S, Bisht MPS, Tiwari LM (2020) Distribution and threat assessment of an endemic and endangered species Angelica glauca in high ranges of western Himalaya. J Herbs Spices Med Plants *26*(4):394–404

Vaganov EA, Hughes MK, Kirdyanov AV, Schweingruber FH, Silkin PP (1999) Influence of snowfall and melt timing on tree growth in subarctic Eurasia. Nature 400(6740):149–151

Ved DK, Kinhal GA, Ravikumar K, Prabhakaran V, Ghate U, Shankar VR, Indresha JH (2003) CAMP report: conservation assessment and management prioritization for medicinal plants of Himachal Pradesh, Jammu, and Kashmir, and Uttarakhand. In: Workshop FRLHT. Shimla, Himachal Pradesh, Bangalore, India

Zinko U, Dynesius M, Nilsson C, Seibert J (2006) The role of soil pH in linking groundwater flow and plant species density in boreal forest landscapes. Ecography 29(4):515–524

Chapter 26
Land Use and Cover Variations and Problems Associated with Coastal Climate in a Part of Southern Tamil Nadu, India, Using Remote Sensing and GIS Approach

B. Santhosh Kumar, J. Rajesh, Chaitanya B. Pande, and Abhay Varade

Abstract Land use is an important factor in planning and managing land resources. Increasing pressure due to population and human resources in the world's resources to meet growing needs contributes to significant land reform in various land uses. Remote sensing and GIS (geographic information system) techniques have been used to study land use change and land cover on the Tuticorin coast in Tamil Nadu. This study examines land use and land cover (LULC) changes from 2001 to 2017 for the coast of Tuticorin. The main objective of this study was to assess changes under the NRSC (National Remote Sensing Center) classification using Landsat ETM + and OLI images using visual interpretation with the help of image interpretation keys. The digitized land use and land cover features are categorized as aquaculture, built-up land, water bodies, cropland, fallow land, forest, a forest plantation, industrial area/mining, mangrove/swamp area, plantation, salt-affected land, salt-pan, sandy areas, land with scrub, land without scrub, and waterlogged area. Apparently the whole study from 2001 to 2017 found that built-up land (+20.44 sq. km) and industrial/mining activities (+5.78 sq. km) were increased and cropland (−8.04 sq. km) and plantation (−7.62 sq. km) were decreased. The ground truth verification of the LULC features performed is made with an effective assessment

B. Santhosh Kumar · J. Rajesh
Department of Remote Sensing, Bharathidasan University, Trichy, Tamil Nadu, India

Indian Institute of Tropical Meteorology (IITM), Pune, Maharashtra, India

C. B. Pande (✉)
Indian Institute of Tropical Meteorology (IITM), Pune, Maharashtra, India
e-mail: chaitanay45@gmail.com

A. Varade
Department of Geology, RTM Nagpur University, Nagpur, Maharashtra, India

C. B. Pande et al. (eds.), *Climate Change Impacts on Natural Resources, Ecosystems and Agricultural Systems*, Springer Climate,
https://doi.org/10.1007/978-3-031-19059-9_26

of the changes. This study shows a significant environmental impact in the study area. In addition, it is crucial to strongly monitor the land use/land cover changes to maintain sustainable growth and in-depth coastal management requirements that can be taken to protect human health and property.

Keywords Environmental issue · Land use/land cover · Remote sensing and GIS · Coastal zone · Change detection

Introduction

Recent developments in global demand for food and fuel bioenergy exchanges, which are directly linked to food and energy prices and volatility, have generated issues about LUCC transformation's influence on biodiversity and other environmental issues. In addition, LUCC change could lead to the depletion of natural resources, affecting the poorest because they rely heavily on natural resources (Mishra et al. 2022). Since the World Summit in 1992, the international community, individual states, communities, civil society, and businesses have been aware of the environmental impact of LUCC change (van Lier 2002). Land cover (LC) is an essential parameter for monitoring and tracking changes to the Earth's surface on a local, regional, and worldwide scale. Climate change, food security, environmental studies, conservational strategies, hydrology, and landscape planning have all used it as a critical variable (Pande et al. 2021a, b; Liu et al. 2021; Verburg et al. 2011). A technique for assessing land use and land cover (LULC) changes is the long-term Earth's observation data record (Ban et al. 2015; Shahid et al. 2021; Pande 2022). Remote sensing has proven to be an effective tool for researching LC patterns at a lower cost and less effort. Satellite imageries have made it feasible to examine LC patterns on a regional and global scale, which would have been difficult, if not impossible, without them (Hansen et al. 2013; Pande et al. 2021a). The foundation of LC is image classification, which involves assigning LC classes to a multiband raster image. Pixel-wise classification, sub-pixel-wise classification, and object-based image classification are the three methods of image classification used in remote sensing. Pixel-wise classification considers each pixel to be pure and assigns it to a single land use-land cover type based on the spectral signature and dependents such as vegetation indices (Gulhane et al. 2022), further separated into unsupervised and supervised classification (Li et al. 2014; Pande et al. 2021a). Geographic information systems and remote sensing approaches provide an opportunity to complete the visions like the changes of land use and land cover maps with spatiotemporal data. However, these approaches have been proven for land use change classes, resulting in better and vastly processing satellite datasets to any natural resources applications by scientific communities (Pande et al. 2021a; Orimoloye et al. 2022). Five ongoing developments were made during the World Summit on Sustainable Development held in Johannesburg in 2002: water, energy, health, agriculture, and biodiversity management. All of the above share the interdependence of the Earth and its use. The land management process determines land use and land cover and

their changes in patterns to processes. Otherwise, without understanding only the effectiveness of land management practices, we will not understand land use decisions or predict the outcome of policy interventions. Land management practices include many factors such as land division, land resource status and suitability, land use potential, policy interventions social and economic practices and enforcement, science, and technology. The various approaches help formulate an integrated land use policy to reduce land degradation, ensure biomass production and food security, expand social and economic benefits to people and their livelihoods and environmental sustainability, and monitor global health (Gautam and Narayanan 1983; Pande et al. 2021b; Mishra et al. 2021).

Coastal regions are the most important and densely populated region in the world. Coastal properties have been subject to severe constraints, and transformation is one of the key factors in land reform (Xiubin 1995; Santhiya et al. 2010). Rapid population growth and coastal migration associated with uncontrolled coastal assets have increased exposure to coastal areas (industry, housing, hospitals, universities, military bases) and increased the effects of extreme incidents (Brown et al. 2011). Globally, approximately more than 60% of the population living in the nearby coastal area has been affected by coastal ecosystems. The Intergovernmental Panel on Climate Change (IPCC) has reported that climate change and rising sea levels will significantly impact the environment and human society in coastal areas (IPCC 2007). Global temperatures have skyrocketed over the past century, while global warming over the past three decades is set at 0.6 °C at 0.2 °C over a decade (Hansen et al. 2006; IPCC 2007; Rosenzweig et al. 2008; Wood 2008). Changes in land redistribution and land use are spatial, unique, and more extreme, leading to global thinking (Lambin et al. 2006). People have been moving the cover of land since early history by removing land parcels of agriculture and livestock (de Sherbinin 2002; Pande et al. 2021b). Land use change information is essential to revitalize land cover maps and good management and planning of sustainable development resources (Alphan 2003; Muttitanon and Tripathi 2005). The essential objective of this paper was to enclose the assessment of land use/land cover changes and issues related to coastal climate in part of southern Tamil Nadu, India.

Study Area Description

An integrated study was done in the area from 77° 48′31.035″ E to 78° 22′24.481″ in longitude and 8° 18′51.239″ N to 9° 10′28.263″ N in latitude. The study area (part of Tuticorin District) lies in Tamil Nadu's southern region. It covers a distance of about 163.5 km and a study area of 1630.32 sq. km (Fig. 26.1). It is bordered on the north by Virudhunagar and Ramanathapuram, on the south by Tirunelveli, and on the east by the Mannar Gulf. The climate in the Tuticorin District is tropical, with extremely hot summers and mild winters. The region experienced 645 mm of annual rainfall in 2011, with a high temperature of 35.7 °C and a low temperature of 24.4 °C. In the coastline sector, Tuticorin has the highest humidity. Rainfall in the Tuticorin region is visible during periods of heavy rainfall in the southwest and

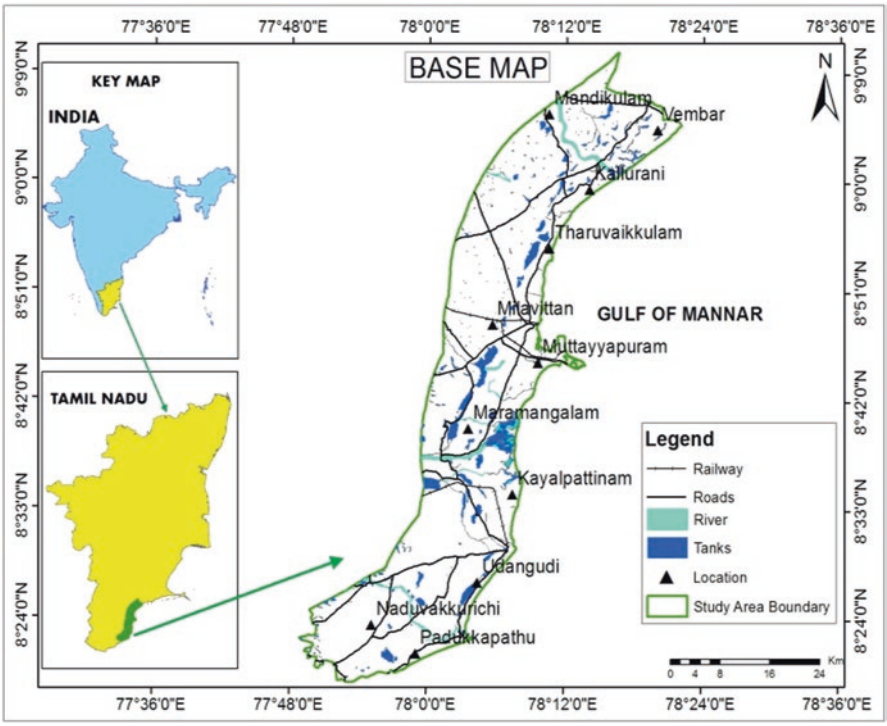

Fig. 26.1 Location map

northeast. The summer season starts in March and lasts until the end of May (CGWB 2009; Anitha Parthasarathy 2015). There are eight taluks in the Tuticorin District. The taluks are further divided into 12 districts and 462 chunks (CGWB 2009). The district's water supply network is controlled by the river, which originates in the Western Ghats and Tamil Nadu areas. A few streams originate in the region's hillocks and flow directly into the sea after a 10–20-mile journey. The primary rivers that pour into the district are the Vaipar, Tambraparni, and Karamanayar. Black soil, red soil, and sandy soil are the three main soil types. Pipes, tanks, and canals are used to irrigate the district. Tuticorin is responsible for 70% of Tamil Nadu's total salt production and 30% of India. Tamil Nadu is India's second largest salt producer, after Rajasthan.

Methodology

Landsat satellite data photos with no clouds were taken for 2001, 2009, and 2017, and topographical maps from the Survey of India were also obtained. To find a land use/land cover mapping, 58k/4, 58k/8, 58L/1, 58L/2, 58L/3, 58H/14, and 58H/15

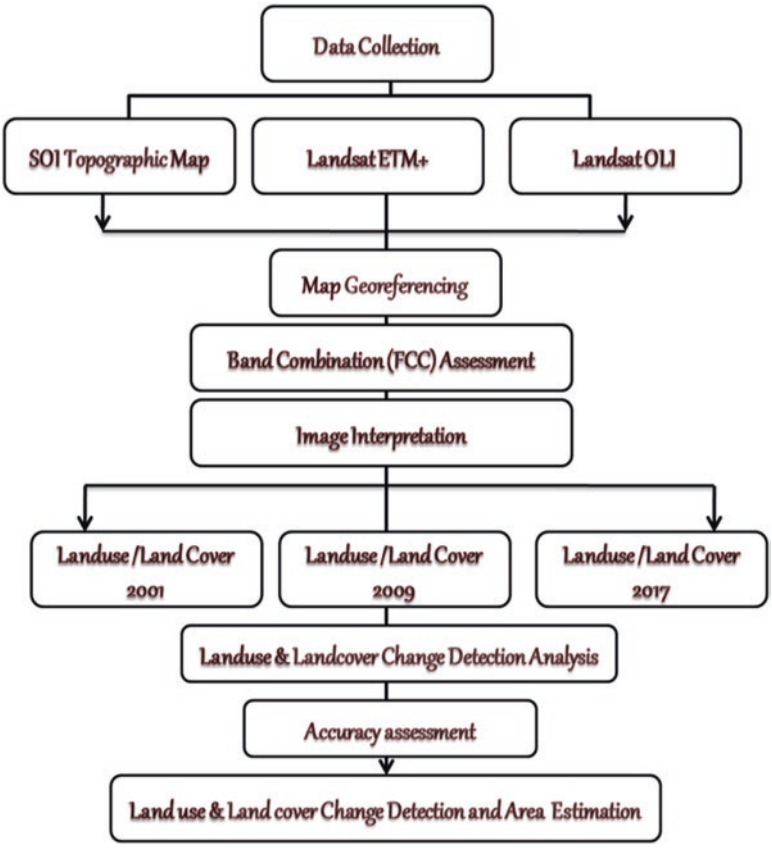

Fig. 26.2 Methodology of flow chart

were employed, along with extensive ground truth verifications. The global land cover facility (GLCF) (http://glcfapp.glcf.umd.edu:8080/esdi/) and the Earth's exploration site (http://earthexplorer.usgs.gov/) provided satellite data for the research area. The satellite data was georeferenced and regionally corrected using the Survey of India (SOI) topographic maps as a ground control point. The World Geodetic System (WGS) 84 and the Universal Transverse Mercator (UTM) were utilized. Because the human brain is an excellent picture translator, visual translation is still one of the most extensively utilized methods of detecting, recognizing, and distinguishing aspects of space in an image. Definitions are based on the visual translation key derived from satellite data as well as changes in the Earth's surface and cover. With the help of the Global Positioning System, a dubious location can be assured for field trips (Fig. 26.2).

Change Detection

Land use change detection and analysis plotting and mapping have been done based on the land use maps of 2001, 2009, and 2017 in the ArcGIS 10.3 software (Pande et al. 2018). Pixels and spectral reflectance of features are used to classify from satellite images. These approaches were completely reliant on pixels or grids within a specific class. These possibilities, equivalent to different input bands, were approved as part of the basic principle. However, these strategies took a long time to compute since they rely heavily on regular data categorization in each input band to over-categorize signatures with large covariance matrix values (Owojori and Xie 2005; Yuan et al. 2005; Pande et al. 2018). Therefore, 16 land use and land cover classes are carried out such as built-up land, industrial area, crop land, plantation, fallow, forest, forest plantation, salt-affected land, land with scrub, land without scrub, sandy areas, swamp/mangroves, waterlogged area, saltpan, river/tank/canal, and aquaculture during 2001, 2009, and 2017, respectively. The adopted methodology is presented in Fig. 26.2.

Results and Discussion

Land Use/Land Cover Changes During 2001–2017

Now a days, costal regions is so much facing problems related to land use changes due to climate changes and man made activities, this regions is so much important for ecosystem and view of maintaining the climate on the earth surface. In this view, we are focus on the land use changes particularly in the coastal. So many important vegetation are presented in the coastal part. The land use/land cover study was conducted for 17 years, from 2001 to 2017, and data was obtained from satellite images and toposheet. The images of 2001, 2009 (Landsat ETM +), and 2017 (Landsat 8 OLI) were used to analyze actual land use/land cover changes in the study area. Remotely sensed satellite images are georeferenced using ERDAS image processing software based on rectified toposheets. After that, geometrically adjusted satellite imagery is calibrated to radiometric and spatial adjustments to minimize error in data. ArcGIS 10.2.1 software is used to prepare the study area's land use/land cover. The NRSC level two classification is adopted for the methodology. After the mapping, the change detection of every class is analyzed. Land use and land cover are divided into 16 different categories, namely, aquaculture, built-up land, water bodies, cropland, fallow land, forest, a forest plantation, industrial area/mining, mangrove/swamp area, plantation, salt-affected land, saltpan, sandy areas, land with scrub, land without scrub, and waterlogged area. The land use and land cover maps are prepared with the help of image interpretation keys such as location, size, shape, pattern, height/depth and site, situation, and association. Analysis of the findings shows significant changes in the huge alteration in the

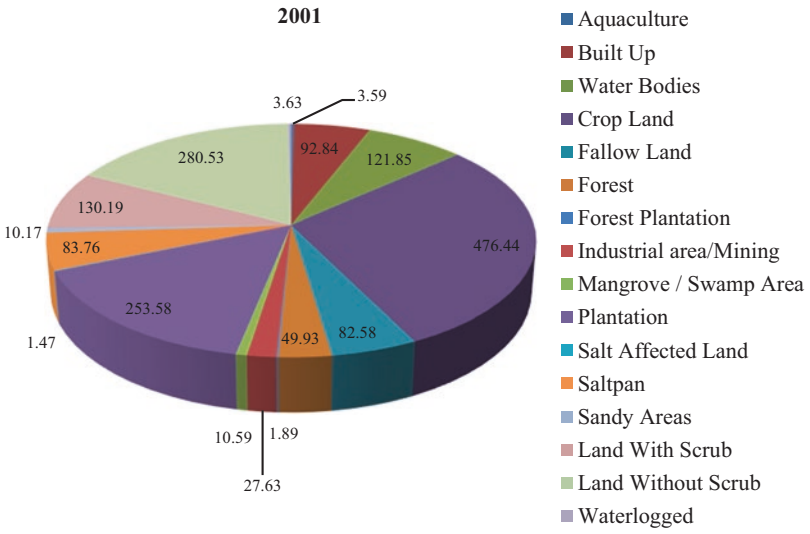

Fig. 26.3 Land use/land cover distribution of the year 2001

built-up land, rapid population and industrial activities, and the consequence of mining activities along the study area. It is evident that the population of the settlement/hamlet increased to 92.84 in 2001, 102.68 in 2009, and 113.28 in 2017. The coastal area of Tuticorin is densely populated in terms of salt products and other activities. Industrial/mining activities have been gradually increasing to 27.63 (2001), 31.27 (2009), and 33.41 (2017). The plantation areas decreased slightly to 253.58 (2001), 249.39 (2009), and 245.96 (2017) due to urban growth development. The land with scrub has gradually decreased to 130.19 (2001), 126.27 (2009), and 119.63 (2017). It is clear that aquaculture was 3.51 in 2001 and increased to 5.11 in 2017. Water bodies covered an estimated 121.85 in 2001 and 119.69 in 2009 and reduced by 119.16 in 2017 based on intervention in this study area (Figs. 26.3, 26.4, and 26.5). The cropland areas covered approximately 476.44 in 2001 and then 471.59 in 2009 and reduced to 468.4 in 2017 based on urban development and coastal infrastructure. It is evident that the fallow land covered 82.58 in 2001 and then 84.49 in 2009 and increased to 86.55 in 2017 (Table 26.1). Improper land reform greatly affects the natural environment of the area. This method can be used to efficiently categorize and map LULC statistics and changes over time. The A value of LULC maps in 2001, 2009, and 2017 and their average are higher than 90%, according to the thematic accuracy assessment (Figs. 26.6, 26.7, 26.8, 26.9, and 26.10).

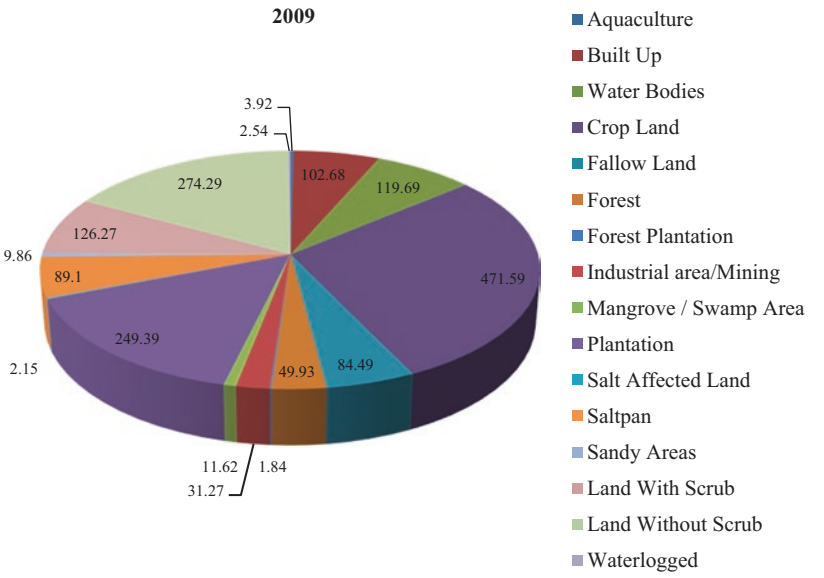

Fig. 26.4 Land use/land cover distribution of the year 2009

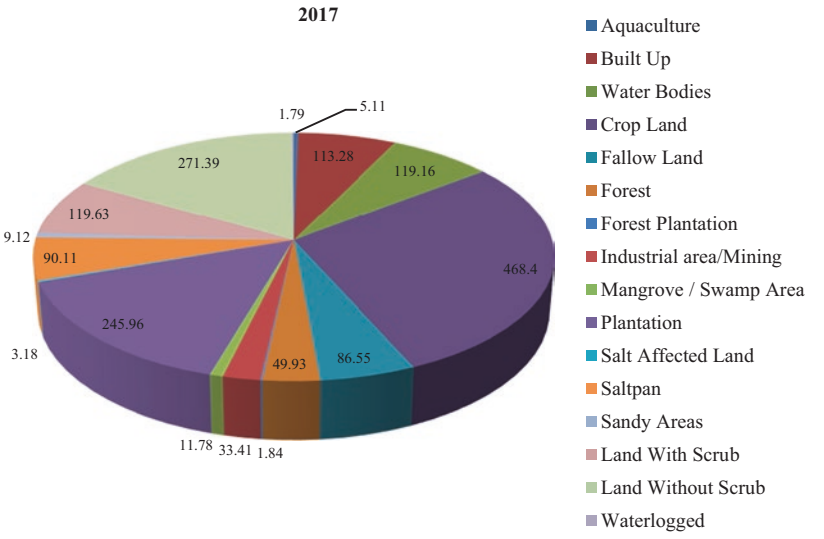

Fig. 26.5 Land use/land cover distribution of the year 2017

Table 26.1 Land use/land cover changes during 2001–2017

Classes	Area in sq. km			Changes					
				2001–2009		2009–2017		2001–2017	
	2001	2009	2017	Sq. km	%	Sq. km	%	Sq. km	%
Built-up land	92.84	102.68	113.28	9.84	10.60	10.6	10.32	20.44	22.02
Industrial area	8.63	9.27	11.46	0.64	7.42	2.19	23.62	2.83	32.79
Crop land	476.44	471.69	468.5	−4.75	−1.00	−3.19	−0.68	−7.94	−1.67
Plantation	221.16	219.18	217.21	−1.98	−0.90	−1.97	−0.90	−3.95	−1.79
Fallow	240.68	244.8	249.96	4.12	1.71	5.16	2.11	9.28	3.86
Forest	49.93	49.93	49.88	0	0.00	−0.05	0.00	−0.05	−0.10
Forest plantation	1.89	1.84	1.89	−0.05	−2.65	0.05	2.72	0	0.00
Salt-affected land	1.47	2.15	3.18	0.68	46.26	1.03	47.91	1.71	116.33
Land with scrub	130.19	126.27	118.59	−3.92	−3.01	−7.68	−6.08	−11.6	−8.91
Land without scrub	180.43	174.16	167.12	−6.27	−3.48	−7.04	−4.04	−13.31	−7.38
Sandy areas	10.17	9.86	9.12	−0.31	−3.05	−0.74	−7.51	−1.05	−10.32
Swamp/ mangroves	3.59	3.15	2.91	−0.44	−12.26	−0.24	−7.62	−0.68	−18.94
Waterlogged area	3.63	2.54	1.79	−1.09	−30.03	−0.75	−29.53	−1.84	−50.69
Saltpan	83.76	89.1	91.11	5.34	6.38	2.01	2.26	7.35	8.78
River/tank/canal	121.85	119.69	119.16	−2.16	−1.77	−0.53	−0.44	−2.69	−2.21
Aquaculture	3.59	3.92	5.11	0.33	9.19	1.19	30.36	1.52	42.34

Environmental Problems Due to the Changes in Tuticorin Coastal Region

Population Pressure

The land has been transformed into a thriving human settlement, resulting in which large amounts of garbage are being produced. For business and subsistence purposes, people migrate to the coast, which has resulted in solid waste disposal, the dumping of solid waste generated by domestic wastewater mixed with seawater, and affects the coastal environment. The population density and household distribution are increasing due to population pressure at local to global scales. However, these activities have directly affected the environmental and land use and land cover mapping. In this context, LULC studies are important for understanding the environmental problems due to the changes in Tuticorin coastal region (Figs. 26.11, 26.12, and 26.13).

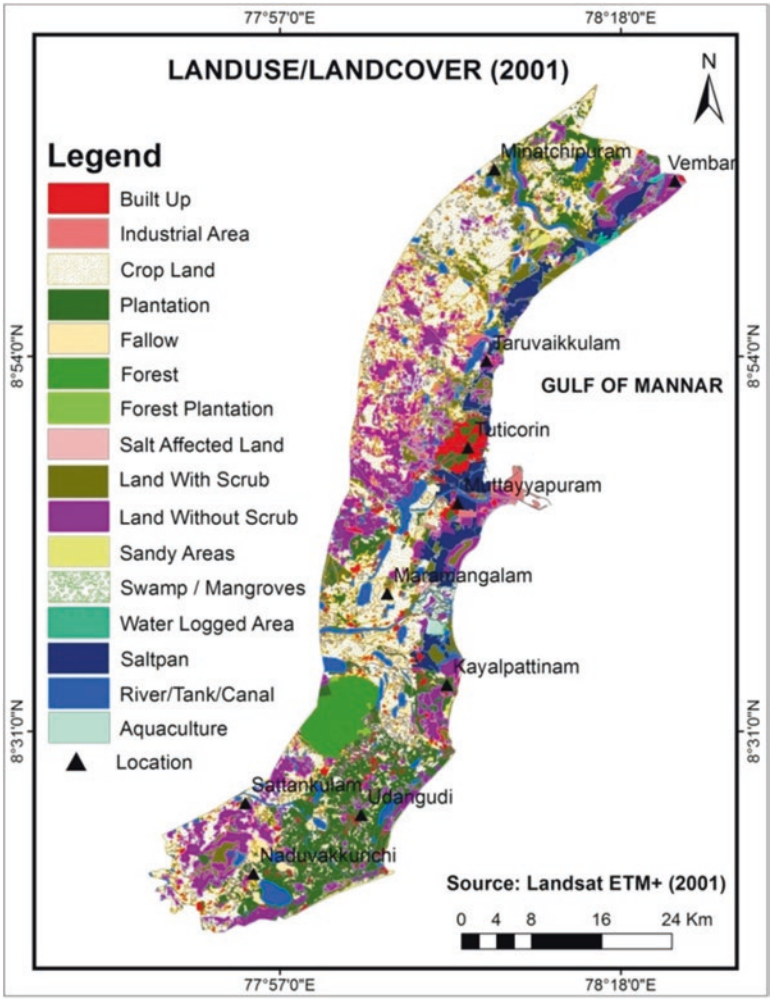

Fig. 26.6 Land use/land cover map of 2001

Industrial/Mining Activities on Nearby Coastal Area

The coastal area of Tuticorin has industries such as the salt industry, the thermal power station, the Sterlite industry, and other related industries. Heavy metals and other toxic chemicals that attract directly to coastal waters are coastal industries, as they affect the coastal environment and the environment (Figs. 26.14 and 26.15).

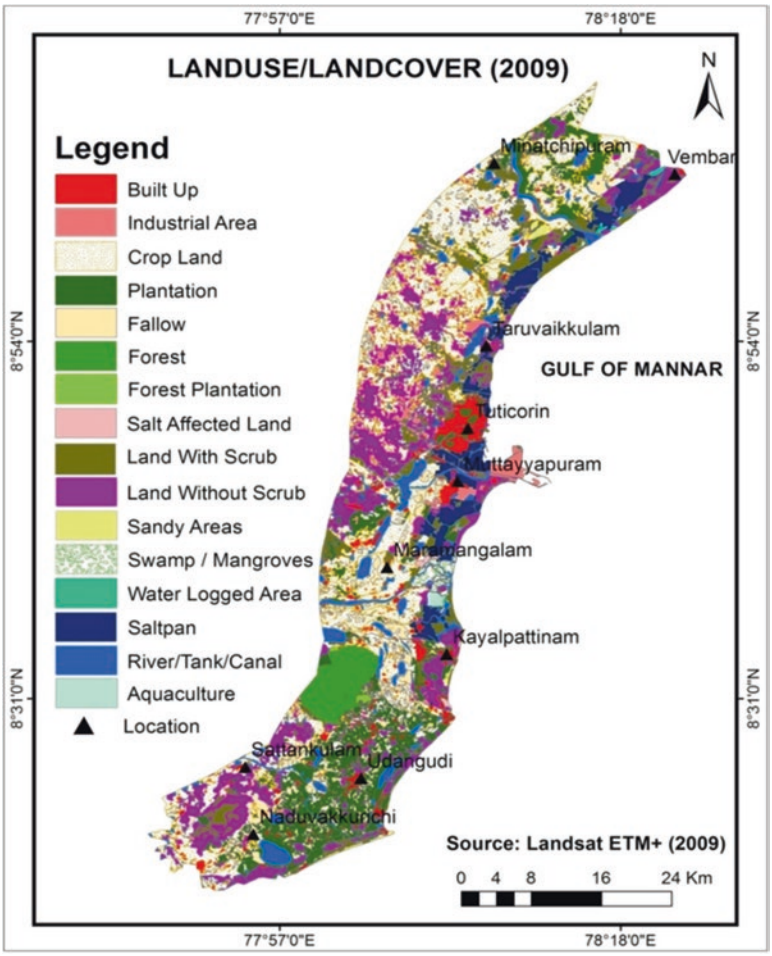

Fig. 26.7 Land use/land cover map of 2009

Conclusion

The above study results indicate that there has been a change in the land use pattern and land cover in the study area. Some changes are good and some are unnatural. Satellite remote sensing and GIS are powerful tools for mapping, monitoring, and monitoring land use and land cover changes. Visual interpretation is essential for the effective analysis of changes. Significant changes in the coastal area of Tuticorin are mainly due to population growth and urbanization. The map shows major changes

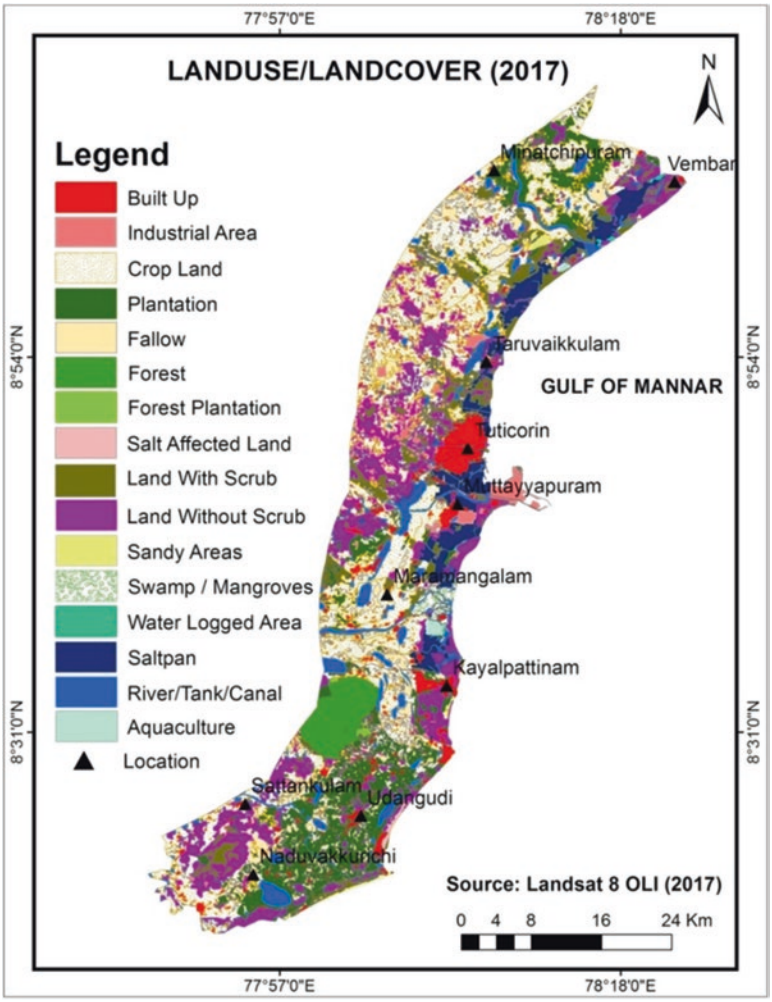

Fig. 26.8 Land use/land cover map of 2017

in coastal structures, namely, an increase in built-up land, industries, salt-affected land, and saltpan. On the other hand, cropland, land with and without scrub, and waterlogged land decreased. National governments are using the results provided in the study to develop flexibility programs and appropriate policies to avoid future losses. This study will help prevent environmental degradation and raise awareness of environmental issues and the importance of coastal ecosystems.

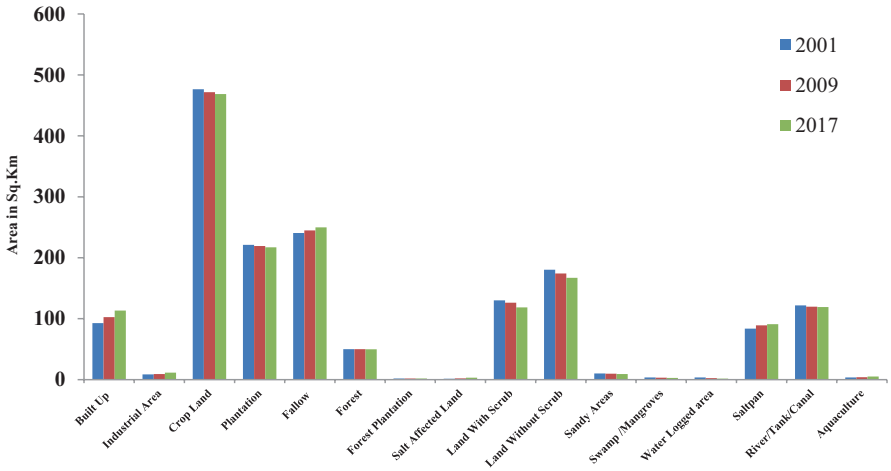

Fig. 26.9 Land use/land cover changes during 2001–2017

Fig. 26.10 The above pictures are taken in Tuticorin coastal region during field investigations. (**a**) Salt pan activities, (**b**) land with scrub, (**c**) waterlogged area, and (**d**) mangrove species

Fig. 26.11 (**a**) Sewage pipes are contaminating the Tuticorin coastal area. (**b**) Mela Arasadi people's search for freshwater

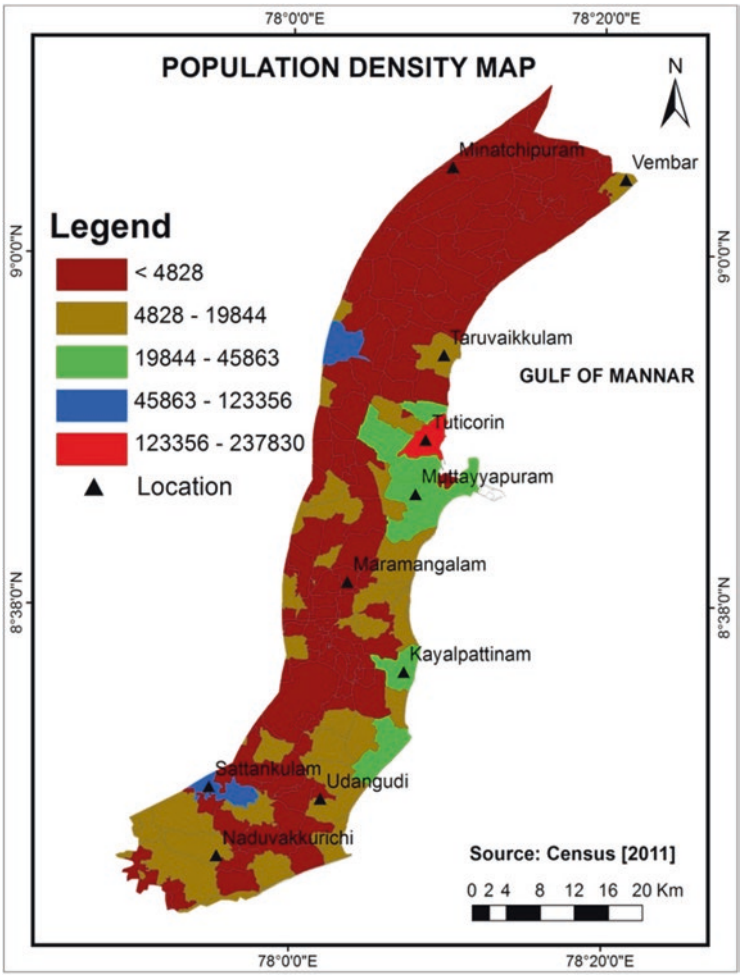

Fig. 26.12 Population density

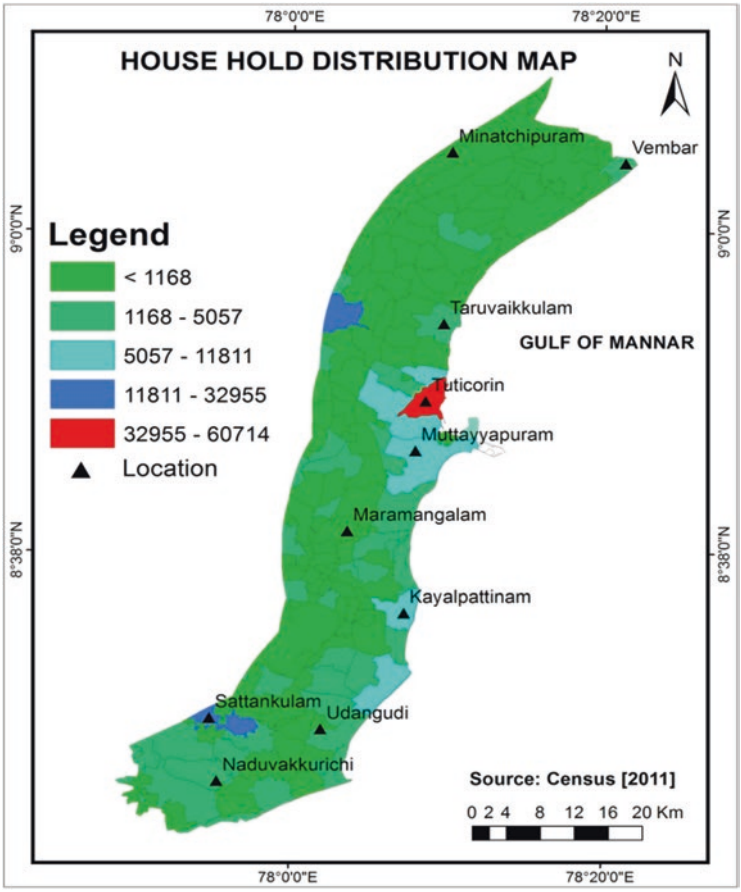

Fig. 26.13 Map showing the household distribution along the Tuticorin coast

Fig. 26.14 Industrial activities in the nearby coastal area

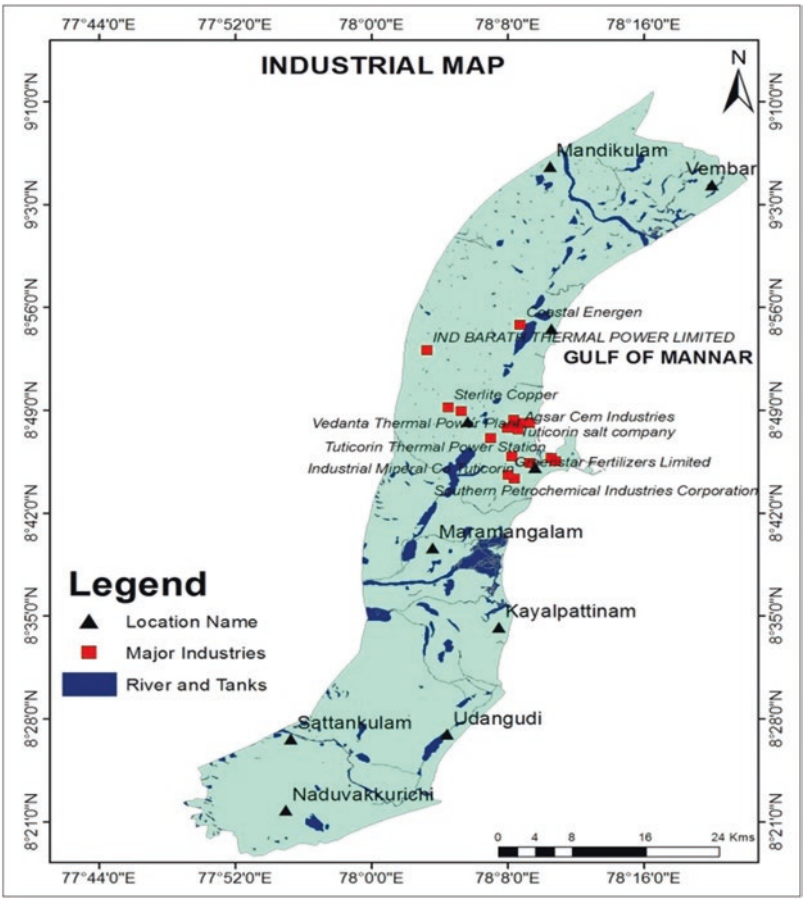

Fig. 26.15 Map showing the major industries along the Tuticorin coast

References

Alphan H (2003) Land use change and urbanization in Adana, Turkey. Land Degrad Dev 14:575–586

Anitha Parthasarathy UN (2015) Coastal vulnerability assessment: a case study on erosion and coastal change along Tuticorin, Gulf of Mannar. Nat Hazards 75(2):1713–1729. https://doi.org/10.1007/s11069-014-1394-y

Ban Y, Gong P, Giri C (2015) Global land cover mapping using Earth observation satellite data: recent progresses and challenges. ISPRS J Photogramm Remote Sens 103:1–6

Brown S, Kebede AS, Nicholls RJ (2011) Sea-level rise and impacts in Africa, 2000 to 2100. University of Southampton, Southampton

Central Ground Water Board (CGWB) (2009) South Eastern Coastal Region Chennai, Government of India, Ministry off Water Resources, District Groundwater Brochure Thoothukudi District, Tamil Nadu, p 1–19

de Sherbinin A (2002) A CIESIN Thematic Guide to Land Use and Land-Cover Change (LUCC), Center for International Earth Science Information Network (CIESIN). Columbia University Palisades, NY, USA, pp 1–67

Gautam NC, Narayanan LRA (1983) Landsat MSS data for land use/land cover inventory and mapping: a case study of Andhra Pradesh. J Indian Soc Remote Sens 11(3):1528

Gulhane VA, Rode SV et al (2022) Correlation Analysis of Soil Nutrients and Prediction Model Through ISO Cluster Unsupervised Classification with Multispectral Data. Multimed Tools Appl. https://doi.org/10.1007/s11042-022-13276-2

Hansen J, Sato M, Ruedy R, Lo K, Lea DW, Medina-Elizade M (2006) Global temperature change. PNAS 103(39):14288–14293

Hansen MC, Potapov PV, Moore R, Hancher M, Turubanova SA, Tyukavina A, Thau D, Stehman SV, Goetz SJ, Loveland TR et al (2013) High-resolution global maps of 21st-century forest cover change. Science 342:850–853

IPCC (2007) Climate Change 2007: mitigation. Contribution of Working Group III to the fourth Assessment Report of the Intergovernmental Panel on Climate Change, Cambridge: Cambridge University Press.

Lambin EF, Geist H, Rindfuss RR (2006) Introduction: local processes with global impacts, Land-use and land-cover change: local processes and global impacts. Springer, Berlin, pp 1–8

Li M, Zang S, Zhang B, Li S, Wu C (2014) A review of remote sensing image classification techniques: the role of spatio-contextual information. Eur J Remote Sens 47:389–411

Liu L, Zhang X, Gao Y, Chen X, Shuai X, Mi J (2021) Finer-resolution mapping of global land cover: recent developments, consistency analysis, and prospects. J Remote Sens 2021:1–38

Mishra AP, Khali H, Singh S et al (2021) An Assessment of In-situ Water Quality Parameters and its variation with Landsat 8 Level 1 Surface Reflectance datasets. Int J Environ Anal Chem. https://doi.org/10.1080/03067319.2021.1954175

Mishra AP, Singh S, Jani M et al (2022) Assessment of water quality index using Analytic Hierarchy Process (AHP) and GIS: a case study of a struggling Asan River. Int J Environ Anal Chem. https://doi.org/10.1080/03067319.2022.2032015

Muttitanon W, Tripathi NK (2005) Land use/cover changes in the coastal zone of Bay Don Bay, Thailand using Landsat 5 TM data. Int J Remote Sens 26(11):2311–2323

Orimoloye IR, Olusola AO, Belle JA et al (2022) Drought disaster monitoring and land use dynamics: identification of drought drivers using regression-based algorithms. Nat Hazards. https://doi.org/10.1007/s11069-022-05219-9

Owojori A, Xie H (2005) Landsat image-based LULC changes of San Antonio, Texas using advanced atmospheric correction and object-oriented image analysis approaches. Paper presented at the 5th international symposium on remote sensing of urban areas, Tempe, AZ

Pande CB (2022) Land use/land cover and change detection mapping in Rahuri watershed area (MS). India using the google earth engine and machine learning approach. Geochem Int. https://doi.org/10.1080/10106049.2022.2086622

Pande CB, Moharir KN, Khadri SFR, Patil S (2018) Study of land use classification in an arid region using multispectral satellite images. Appl Water Sci 8:123. https://doi.org/10.1007/s13201-018-0764-0

Pande CB, Moharir KN, Khadri SFR (2021a) Assessment of land-use and land-cover changes in Pangari watershed area (MS), India, based on the remote sensing and GIS techniques. Appl Water Sci 11:96

Pande CB, Moharir KN, Kumar Singh S, Varade AM, Elbeltagie A, Khadri SFR, Choudhari P (2021b) Estimation of crop and forest biomass resources in a semi-arid region using satellite data and GIS. J Saudi Soc Agric Sci 20(5):302–311

Rosenzweig C, Karoly D, Vicarelli M, Neofotis P, Wu Q, Casassa G, Menzel A, Root TL, Estrella N, Seguin B, Tryjanowski P, Liu C, Rawlins S, Imeson A (2008) Attributing physical and biological impacts to anthropogenic climate change. Nature 453:15. https://doi.org/10.1038/nature06937

Santhiya G, Lakshumanan C, Muthukumar S (2010) Mapping of landuse/landcover changes of chennai coast and issues related to coastal environment using remote sensing and GIS. Int J Geomat Geosci 1(3):563–576

Shahid M, Rahman KU, Haider S et al (2021) Quantitative assessment of regional land use and climate change impact on runoff across Gilgit watershed. Environ Earth Sci 80:743. https://doi.org/10.1007/s12665-021-10032-x

van Lier H (2002) Planning for sustainable rural land-use systems. Sustain Rural Syst 66:189–210

Verburg PH, Neumann K, Nol L (2011) Challenges in using land use and land cover data for global change studies. Glob Chang Biol 17:974–989

Wood R (2008) Natural ups and downs. Nature 453:43–45

Xiubin L (1995) A review of the international researches on land use/cover change. Acta Geograph Sin 51(6):553

Yuan F, Sawaya KE, Loefelholz B, Bauer ME (2005) Land cover classification and change analysis of the Twin Cities (Minnesota) Metropolitan Area by multi-temporal Landsat remote sensing. Remote Sens Environ 98:317–328

Chapter 27
Classification of Vegetation Types in the Mountainous Terrain Using Random Forest Machine Learning Technique

Raj Singh, Arun Pratap Mishra, Manoj Kumar, and Chaitanya B. Pande

Abstract Classification of vegetation into appropriate classes is important for management and conservation planning. Field-based observations are now extensively supported with remote sensing-based observations for such classifications. We demonstrate here the application of a machine learning technique using the random forest (RF) to classify Landsat imageries in the mountainous terrain of the Indian Western Himalayas. The region represents a mega-diverse area having a wide variation in climate and vegetation types with a varied topography. In mountainous regions, vegetation classification is crucial to identify the natural resources for its conservation and management planning. Normalized difference vegetation index (NDVI) using near infra-red and red bands was created for the period 2013–2019. As the imageries are available at a temporal resolution of 16 days, a Fourier transformation was done to compress a large amount of data. To achieve a better accuracy of classification, topographic variables of elevation and slope together with climate variables of temperature and precipitation were considered while implementing the classification algorithm. We successfully characterized the mountainous terrain into the classes of non-forest, evergreen needle leaf trees, evergreen broadleaf trees, moist deciduous trees, dry deciduous trees, shrub, and agriculture with an overall accuracy of 80%. We compared the classified maps with existing vegetation type maps to see inconsistency in mapping with the demonstrated approach. The methodology demonstrated in this study can be used for clas-

R. Singh
GITAM Deemed to be University, Visakhapatnam, Andhra Pradesh, India

Dr. K. N. Modi University, Rajasthan, India

A. P. Mishra (✉)
Department of Habitat Ecology, Wildlife Institute of India, Dehradun, Uttarakhand, India

M. Kumar
GIS Centre, Forest Research Institute (FRI), Dehradun, Uttarakhand, India

C. B. Pande
Indian Institute of Tropical Meteorology (IITM), Pune, Maharashtra, India

C. B. Pande et al. (eds.), *Climate Change Impacts on Natural Resources, Ecosystems and Agricultural Systems*, Springer Climate,
https://doi.org/10.1007/978-3-031-19059-9_27

sifying the landscape into distinct classes with improved accuracy for various purposes.

Keywords Forest type · Indian Western Himalaya · Land use/land cover · NDVI · Remote sensing

Introduction

The potential for using space-based remote sensing measurements to monitor natural resources has grown exponentially in recent decades (Banko 1998; Pal 2005). The classification of vegetation into appropriate types is one of the essential requirements for conservation planning and addressing research-related queries (Martin et al. 1998). The methods used to classify vegetation into various types are dependent upon the field-based observations that can be supplemented with remote sensing-based observations (Pande et al. 2018, 2021a, b). Field-based observations are usually time-consuming and costly and may not be easy for difficult terrain such as mountains (Banko 1998; Martin et al. 1998). Remote sensing has widely been used in vegetation mapping using multiple approaches and using different data sets (Clerici et al. 2012; Han et al. 2004; Jin et al. 2016, 2017; Kumar et al. 2019a, 2021; Singh et al. 2020a, b; Stibig et al. 2003; Mishra et al. 2021). With remote sensing-based observations, it is easy to trace the spatial and temporal changes in a forested landscape as observations are available at planetary scales with repeated observations ranging from days to months. Observation related to the plant structure and its habitat and functional behaviors can be monitored using remote sensing (Clerici et al. 2012; Ivanova et al. 2019; Kumar et al. 2019b, 2021; Shouse et al. 2012; Singh et al. 2020c; Zhang et al. 2019). Among various available approaches to classify remote sensing images, nowadays, the machine learning-based approach has gained wider attention (Anchang et al. 2020; Carreiras et al. 2006; Praticò et al. 2021; Orimoloye et al. 2022). Random forest-based classification is one of the machine learning techniques that is based on the ensemble of decision trees to vote for a particular class with greater probability (Breiman 2001). Various researchers have used multiple remote sensing data to process them using machine learning techniques to classify forest, agriculture, and other land use types (Clerici et al. 2012; Ghazaryan et al. 2018; Htitiou et al. 2019; Li et al. 2019; Mohite et al. 2019; Shelestov et al. 2017; Srinet et al. 2020). Until recently, researchers used standalone software like ArcGIS, ERDAS, Q-GIS, and ENVI to analyze huge data sets (Pande 2022; Gulhane et al. 2022). However, Google has created and released "Google Earth Engine" (GEE), a cloud-based platform for processing remote sensing data (Gorelick et al. 2017). GEE is a powerful tool that can be used to analyze petabyte-scale archives of remote sensing data (Olokeogun and Kumar 2020). GEE has a Java code editor web interface and a Python application programming

interface for quickly building geospatial processes (Kandekar et al. 2021). A web-based interactive development environment (IDE) and Internet-accessible application programming interface (API) allow researchers to utilize freely available data from numerous satellite agencies, topography, land cover, and socioeconomic, environmental, and climatic sources. GEE supports image categorization, multi-temporal land use mapping, numerical and array/matrix operations, machine learning, per-pixel operations, and image-based operations. In this study, we attempt to classify the mountainous terrain of the Indian Western Himalaya to test the applicability of Google Earth Engine in implementing a machine learning-based algorithm (random forest) into various vegetation classes. The major objectives of the study are (i) retrieval of NDVI time-series observation to distinguish vegetation types; (ii) utilization of NDVI along with topographic variables of elevation and slope, and climatic variables of temperature and precipitation to achieve better accuracy of classification; and (iii) comparison of vegetation type maps created by us with existing vegetation maps.

Materials and Methods

Study Area

The study region represents part of the Indian Western Himalaya in the state of Uttarakhand (Fig. 27.1). The region is a hilly terrain having undulating elevation and varying slopes forming distinct habitats to host a wide range of floral and faunal communities. The region receives monsoon rainfall starting in July till September. The annual rainfall in the outer region is 1500–1750 mm, the mid-altitude receives rainfall of 750–1000 mm, and in the alpine region, the average annual rainfall is about 1600 mm. The average summer temperature is approximately 30 °C, and winter temperature is approximately 18 °C. Southern foothills make subtropical climate where average summer temperature is approximately 25 °C. Higher and the middle region has average summer temperature in the range of 15–18 °C, whereas winter temperature is often subzero. The region is dominated by five major forest types: (1) tropical forests, (2) subtropical forests, (3) temperate forests, (4) subalpine forests, and (5) alpine vegetation (Hajra and Rao 1990). The Himalayan moist temperate forest is the major dominant vegetation type (Champion and Seth 1968) in the region whereas the dominant broadleaved species are *Rhododendron arboreum*, *Betula utilis* (Bhojpatra), *Quercus semecarpifolia* (Kharsu oak), *Q. dilatata* (Mohru oak), *Q. incana*, *Q. leucotrichophora*, and *Q. oblongata* (Ban Oak). Dominant coniferous species of the region are *Abies pindrow* (fir), *Picea smithiana* (spruce), *Cedrus deodara* (deodar), and *Pinus roxburghii* (chir pine).

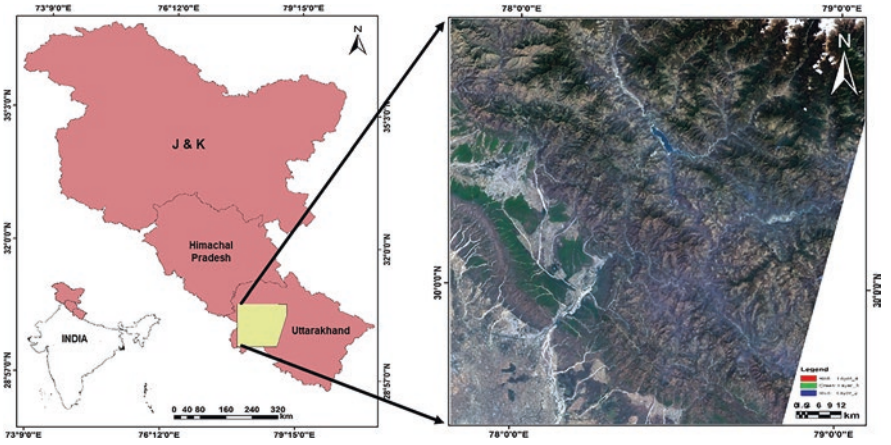

Fig. 27.1 Study region in the state of Uttarakhand representing part of the Indian Western Himalayas

Data Sources and Their Description

We used Landsat 8 data to create time series of NDVI for the study region. The Landsat 8 (synchronous satellite) satellite data comprises of Thermal Infrared Sensor and Operational Land Imager which are available in 11 spectral bands with a revisit time of 16 days. Landsat 8 data is available in tiff format. In this study, Landsat 8 data was used from 2013 to 2019 for NDVI time-series analysis, which was later compressed using Fourier transform before implementing random forest algorithm in the GEE. We used WorldClim climatic variables of temperature and precipitation in this study which was downloaded from the website https://www.worldclim.org/data/index.html. Advanced Spaceborne Thermal Emission and Reflection Radiometer (ASTER) Global Digital Elevation Model (GDEM) (https://asterweb.jpl.nasa.gov/gdem.asp) was used to obtain the elevation of the study region. ASTER GDEM was further processed to obtain the slope map of the region using ArcGIS spatial analyst tool. Landsat 8 satellite imagery was used to compile the NDVI series for the period 2013–2019 at 16-day intervals. The periodicity of phenological evolution shown in the NDVI time-series data helped visualize a specific forest type. Fourier transform was applied on Landsat 8 NDVI data to obtain its sine and cosine components. Each point in the Fourier transformed image reflects the specific frequency of the spatial domain image (Li 2014). Mean pixel values of time series were also obtained using GEE. Field-based ground control points were obtained to provide the signature of different classes for classification using random forest. The final classified maps were compared with available vegetation class maps of ISRO (Indian Space Research Organization) (Roy et al. 2015) and the MODIS (Moderate Resolution Spectroradiometer)-derived plant functional type maps obtained from the archives of LPDAAC (Land Processes Distributed Active Archive Center) (https://lpdaac.usgs.gov). The methodological procedures used to accomplish the goals of this research are shown in Fig. 27.2.

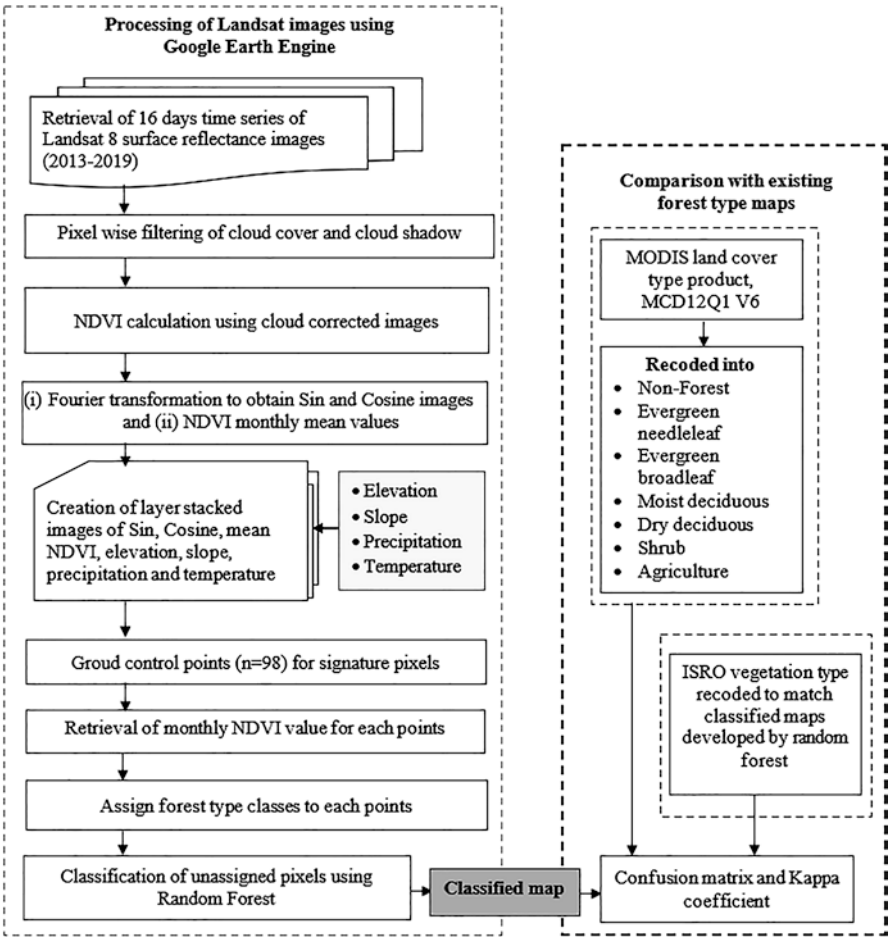

Fig. 27.2 Flow chart of methodological steps implemented to classify vegetation types using random forest algorithm in Google Earth Engine

Fourier Transform

The Fourier transform is of fundamental importance in (McAndrew 2004) image processing. Fourier transform is a classical method to convert image from space domain to frequency domain, and it is also the foundation of image processing titled as the second language for image description. It provides another perspective for image observation and images to frequency distribution characteristics. The Fourier transform among other things provides a power for alternate to linear spatial filtering. It is more efficient to use the Fourier transform than a spatial filter. For a large filter, the Fourier transform also allows us to isolate and process particular image frequencies and from low pass and high pass with a great degree of precision. The

image processing often tends to do corresponding transformation for image by converting domain when facing problems that are complex and hard to deal with (Baharuddin et al. 2011). The Fourier transform is an important image processing tool which is used to decompose an image into its sine and cosine components. The output of the transformation represents the image in the Fourier or frequency domain, while the input image is the spatial domain equivalent. In the Fourier domain image, each point represents a particular frequency contained in the spatial domain image. The Fourier transform is used in a wide range of applications, such as image analysis, image filtering, image reconstruction, and image compression.

Random Forest Approach

An ensemble classification algorithm, RF, consists of a group of tree-based classifiers {h(x, Hk, k = 1,…)}, where x is the input vector and Hk are independent and identically distributed random vectors (Breiman 2001; Hastie et al. 2009). RF uses bootstrapping with replacement to enhance the diversity of classification trees, which allocate each pixel to a class in accordance with the maximum number of votes from the collection of trees. This method, although it has shown high accuracy and ability to model complex interactions among variables, is a "black box" because the individual trees cannot be estimated separately (Prasad et al. 2006). To run the RF model, it was necessary to define several important adjustable parameters. The primary parameters are the number of predictors at each decision tree node split (mtry) and the number of decision trees to run (ntree). Liaw and Wiener (2002) report that mtry = 1 can give good performance. Rodriguez-Galiano et al. (2012) showed that reducing mtry weakens each tree of the model, but it also reduces the correlation among individual trees, which increases the model accuracy. Oliveira et al. (2012) reported that an increase in values of mtry would result in a higher predictive performance of the model and attribution of higher importance to fewer variables. In consideration of these points, it is necessary to optimize the parameters mtry and ntree to maximize the model accuracy. First, to evaluate the model performance, all data were divided with stratified random sampling ranging from 10% (11,781 pixels) to 90% (105,994 pixels) in increments of 10% for test data, left out of the training data. The set of test data, which is an independent validation set, was used only for the model evaluation. Moreover, the remaining training dataset was divided to 75% (training dataset) and 25% (validation dataset) for the sake of a repeated leave-group-out cross-validation (LGOCV) strategy. This procedure is repeated ten times to estimate robust prediction performance. Each datum of the validation data and test data is used to compute accuracies and error rates averaged over all predictions and to estimate each variable's importance in the classification. To reduce data redundancy and to assist the model interpretation and the absolute values of pairwise correlation coefficients were considered. Predictors with near-zero variance values were removed. If two variables are highly correlated (>0.75), then the variable with the largest mean absolute correlation is automatically removed

from the model. In previous studies and recommendations and pretests from our dataset, we have selected 100 trees, while mtry was set to the default value (Zhu 2013; Mishra et al. 2021).

Results and Discussion

The terrain of the study region has undulating land features having a minimum elevation of 187 m and the highest elevation ranges of 4780 m (Fig. 27.3a). Temperature ranges between −2 and 24 °C (Fig. 27.3c), while the region receives an average annual sum of rainfall ranging between 87 and 197 cm (Fig. 27.3d). The various input layers that were used in mapping forest classes and their spatial variation are shown in Fig. 27.3. The temporal evolution of NDVI for the different vegetation classes is shown in Fig. 27.4. The majority of the region is dominated by dry deciduous vegetation followed by evergreen needle leaf, evergreen broadleaf, moist deciduous, and shrub vegetation. The final classified forest type map of the study region using random forest classification is shown in Fig. 27.5. The classified maps

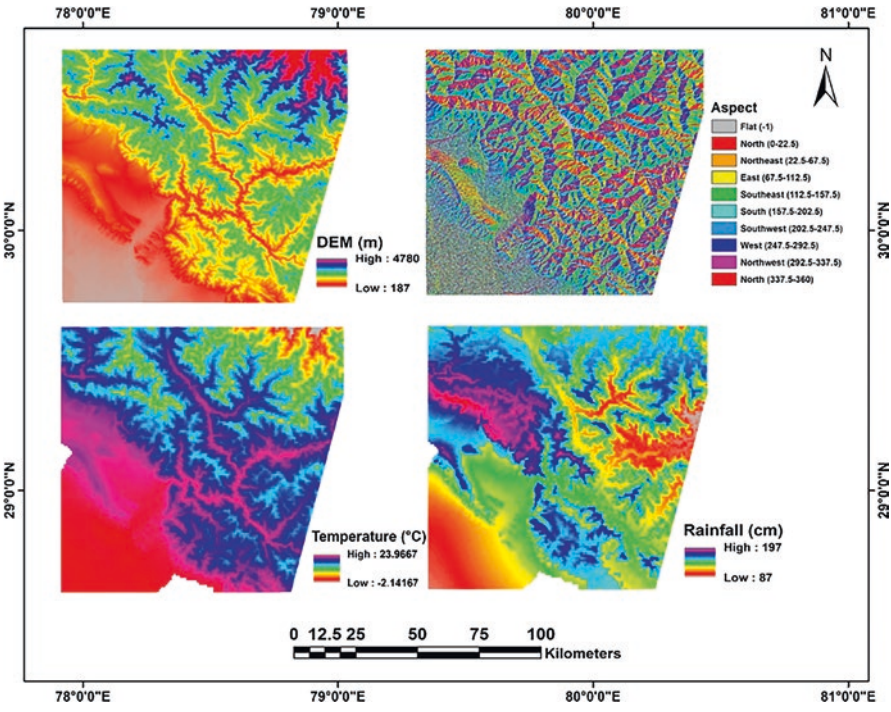

Fig. 27.3 Topographic and climatic variables used for classifying forest types using random forest algorithm: (**a**) elevation layer, (**b**) aspect layer, (**c**) temperature layer, (**d**) rainfall layer, (**e**) Fourier transformed sin value layer, and (**f**) Fourier transformed cosine value layer

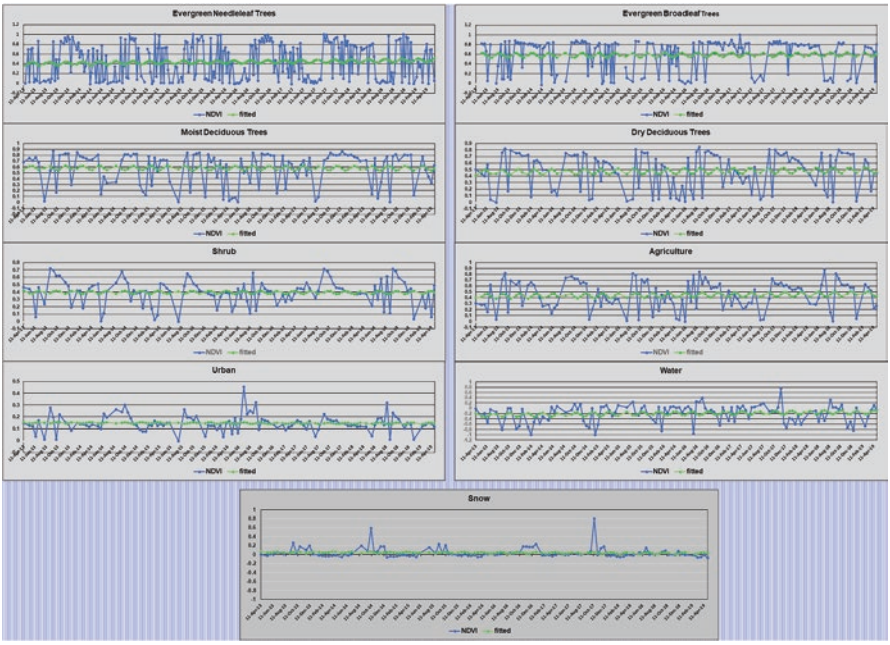

Fig. 27.4 Evolution of time-series average value of NDVI for the period 2013–2019: (**a**) evergreen needle leaf, (**b**) evergreen broadleaf, (**c**) moist deciduous, (**d**) dry deciduous, (**e**) shrub, and (**f**) agriculture

are comparable with the land use cover maps of ISRO and MODIS-derived maps shown in Fig. 27.6. The mapping accuracy of moist deciduous and agriculture classes was low with user accuracy of 50 and 66.67%, respectively. However, for the rest of the classes, user accuracy was more than 80% (Table 27.1). The overall accuracy for all the classes was 75.49%, with a Kappa statistic of 0.80.

Discussion

The research utilized Landsat images and Google Earth Engine to map the vegetation classes representing seven distinct classes of evergreen needle leaf, evergreen broadleaf, moist deciduous, dry deciduous, shrub, agriculture, and nonvegetation classes. It was observed that the use of GEE greatly lowers the processing time for processing a large collection of images. Unlike the traditional approach of downloading individual images and then processing them using paid software of image processing like Erdas, GEE is a freely available platform that can be used to classify remotely sensed images. The validation and accuracy evaluation of the classified vegetation map derived from this research was carried out utilizing established vegetation and land cover maps of MCD12Q1 and ISRO. The method provided in this

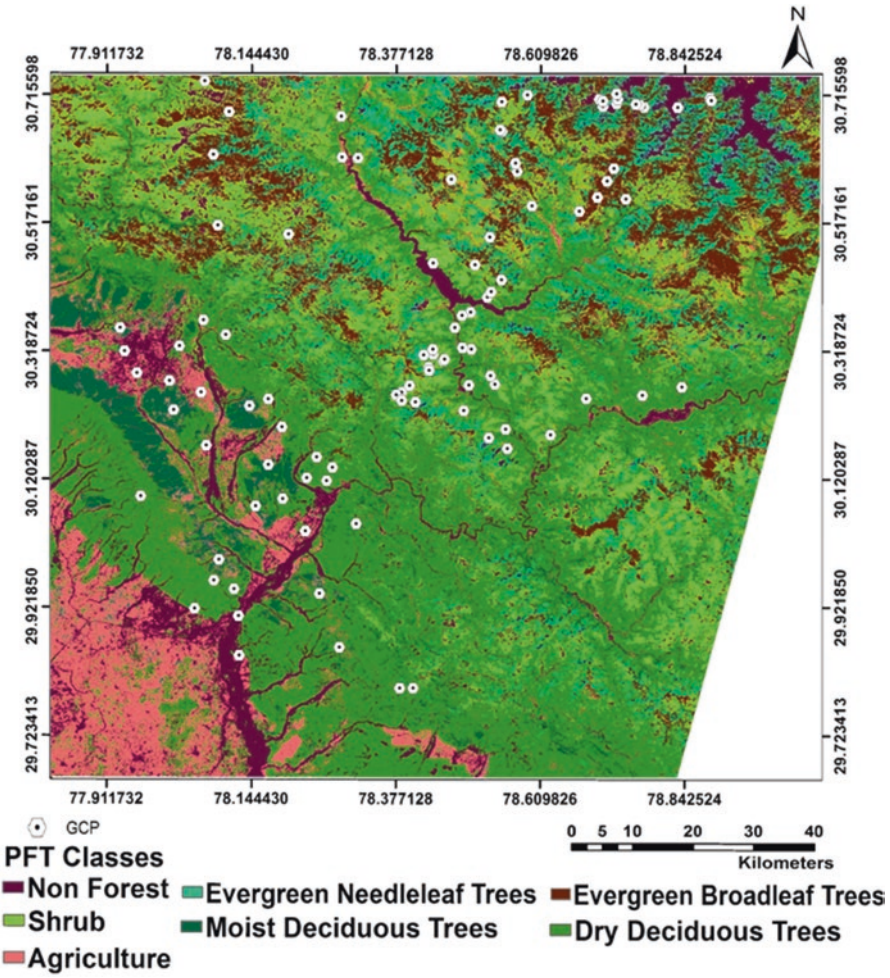

Fig. 27.5 Vegetation classes of study region mapped using random forest algorithm in Google Earth Engine

study shows that vegetation of the study region is mapped effectively, and the findings are similar to the products currently utilized by researchers such as MCD12Q1 and ISRO vegetation class map. The analysis of land cover changes in the area over a period of time can be achieved easily by using a similar approach as demonstrated by us. The demonstrated methodology will help the researcher to visualize changes over a period of time by easily implementing a similar approach in GEE. While it's possible that during this time period, some land classes may have changed from one to another, such as the conversion of agricultural land into built-up class or the loss of forest cover area due to forest fire, we processed images of 2013–2019 to obtain vegetation classes. Hence, while considering any long period images for

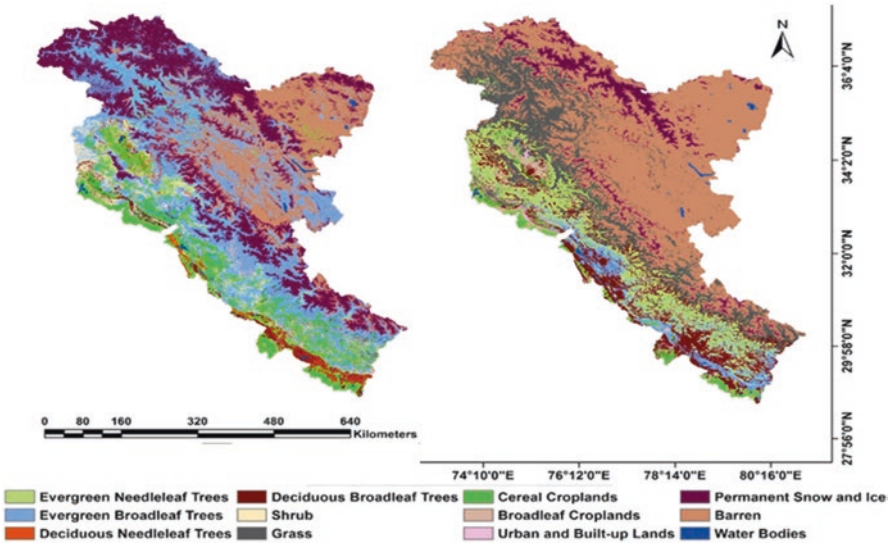

Fig. 27.6 Land cover type map of the study region: land cover map developed by Indian Space Research Organization (left panel) and MODIS land cover type product MCD12Q1 (right panel)

Table 27.1 Accuracy assessment of classified vegetation type map

Class name	Producer's accuracy (%)	User accuracy (%)
Non-forest	92.00	83.64
Evergreen needleleaf	84.16	81.14
Evergreen broadleaf	66.67	80.00
Moist deciduous	71.43	50.00
Dry deciduous	83.33	83.33
Shrub	62.50	87.00
Agriculture	40.00	66.67

Overall accuracy = 75.49%; Kappa coefficient (k) = 0.80

classification, one needs to be careful. The accuracy of classification in such cases would certainly be affected. Srinet et al. (2020) classified vegetation of the same region with an overall accuracy of 66% while we were able to achieve better accuracy in the range of ≥80% for the majority of classes except for agriculture and moist deciduous class. Greater accuracy in our case might have been attributed due to the lesser area mapped by us compared to the area mapped by Srinet et al. (2020). The lower accuracy for agriculture and moist deciduous class would have been due to the variation in NDVI values due to various growing seasons of crops with harvesting period in case of agriculture, while in the case of the moist deciduous forest, leaf shading period has low NDVI value attributing inconsistent value range. The vegetation map classified by us when compared with MCD12Q1 (Fig. 27.6) showed

an overall accuracy of 72% with a Kappa coefficient (k) of 0.68. The producer's accuracy for evergreen needle leaf, evergreen broadleaf, moist deciduous, dry deciduous, shrub, and agriculture was 81.61, 62.56, 71.43, 80.30, 65.50, and 45.00%, respectively, while the user's accuracy for the respective classes was found to be 79.33, 58.02, 69.25, 78.26, 62.00, and 42.91%, respectively. The classified map by us when compared with ISRO vegetation cover map (Fig. 27.6) showed an overall accuracy of 68.58% with a Kappa coefficient (k) of 0.70. The producer's accuracy for evergreen needle leaf, evergreen broadleaf, moist deciduous, dry deciduous, shrub, and agriculture was 80.51, 58.62, 69.71, 82.55, 68.75, and 54.00%, respectively, while the user's accuracy for the respective classes was found to be 78.79, 56.82, 64.20, 77.86, 60.00, and 52.89%, respectively.

Conclusion

Classification of the land cover into its appropriate classes requires field-based observations to classify remotely sensed images. However, once the ground control points are available, it becomes very much easy to classify satellite images to obtain a vegetation class map of a region with reasonable accuracy. The accuracy of mapping depends upon the algorithm used and the variation in the reflectance behavior of the class of interest. The separability of one class from another influences classification accuracy. While mapping vegetation classes, one needs to test various available approaches and algorithm to achieve better accuracy. The classification accuracy is usually improved if additional layers such as topographical variables or climate-related parameters are considered. Likewise, an attempt should be made to identify possible additional layers that could be used to achieve better accuracy of mapping. This requires further study to effectively incorporate different factors that would improve the mapping accuracy. Using available newer machine learning techniques and the formulation of new algorithms to improve vegetation classification is another research area leveraging the utility of remote sensing images.

Conflict of Interest None of the authors of this chapter has a financial or personal relationship with other people or organizations that could inappropriately influence or bias the content of the chapter. It is specifically to mention and declare that "No competing interests are at stake and there is No Conflict of Interest" with other people or organizations that could inappropriately influence or bias the content of the chapter.

References

Anchang JY, Prihodko L, Ji W, Kumar SS, Ross CW, Yu Q, Lind B, Sarr MA, Diouf AA, Hanan NP (2020) Toward operational mapping of Woody Canopy cover in Tropical Savannas Using Google Earth Engine. Front Environ Sci 8. https://doi.org/10.3389/fenvs.2020.00004

Baharuddin AS, Rahman NAA, Shan UK, Hassan MA, Wakisaka M, Shirai Y (2011) Evaluation of pressed shredded empty fruit bunch (EFB)-palm oil mill effluent (POME) anaerobic sludge based compost using Fourier transform infrared (FTIR) and nuclear magnetic resonance (NMR) analysis. Afr J Biotechnol 10(41):8082–8289

Banko G (1998) A review of assessing the accuracy of classifications of remotely sensed data and of methods including remote sensing data in forest inventory

Breiman L (2001) Random forests. Mach Learn 45:5–32

Carreiras JMB, Pereira JMC, Shimabukuro YE (2006) Land-cover Mapping in the Brazilian Amazon Using SPOT-4 vegetation data and machine learning classification methods. Photogramm Eng Remote Sens 72:897–910

Champion HG, Seth SK (1968) A revised survey of the forest types of India. Government of India Publication, New Delhi

Clerici N, Weissteiner CJ, Gerard F (2012) Exploring the use of MODIS NDVI-based phenology indicators for classifying forest general habitat categories. Remote Sens 4:1781–1803. https://doi.org/10.3390/rs4061781

Ghazaryan G, Dubovyk O, Löw F, Lavreniuk M, Kolotii A, Schellberg J, Kussul N (2018) A rule-based approach for crop identification using multi-temporal and multi-sensor phenological metrics. Eur J Remote Sens 51:511–524. https://doi.org/10.1080/22797254.2018.1455540

Gorelick N, Hancher M, Dixon M, Ilyushchenko S, Thau D, Moore R (2017) Google Earth Engine: planetary-scale geospatial analysis for everyone. Remote Sens Environ 202:18

Gulhane VA, Rode SV et al (2022) Correlation analysis of soil nutrients and prediction model through ISO cluster unsupervised classification with multispectral data. Multimed Tools Appl. https://doi.org/10.1007/s11042-022-13276-2

Hajra PK, Rao RR (1990) Distribution of vegetation types in northwest Himalaya with brief remarks on phytogeography and floral resource conservation. Proc Plant Sci 100:263–277

Han K, Champeaux J-L, Roujean J-L (2004) A land cover classification product over France at 1 km resolution using SPOT4/VEGETATION data. Remote Sens Environ 92:52–66

Hastie T, Tibshirani R, Friedman J (2009) Random forests. In: The elements of statistical learning. Springer, New York, pp 587–604

Htitiou A, Boudhar A, Lebrini Y, Hadria R, Lionboui H, Elmansouri L, Tychon B, Benabdelouahab T (2019) The performance of random forest classification based on phenological metrics derived from Sentinel-2 and Landsat 8 to Map crop cover in an irrigated semi-arid region. Remote Sens Earth Syst Sci 2:208–224. https://doi.org/10.1007/s41976-019-00023-9

Ivanova Y, Kovalev A, Yakubailik O, Soukhovolsky V (2019) The use of satellite information (MODIS/Aqua) for phenological and classification analysis of plant communities. Forests 10. https://doi.org/10.3390/f10070561

Jin Y, Sung S, Lee DK, Biging GS, Jeong S (2016) Mapping deforestation in north korea using phenology-based multi-index and random forest. Remote Sens 8:1–15. https://doi.org/10.3390/rs8120997

Jin S, Yang L, Zhu Z, Homer C (2017) A land cover change detection and classification protocol for updating Alaska NLCD 2001 to 2011. Remote Sens Environ 195:44–55. https://doi.org/10.1016/j.rse.2017.04.021

Kandekar VU et al (2021) Surface water dynamics analysis based on sentinel imagery and Google Earth Engine Platform: a case study of Jayakwadi dam. Sustain Water Resour Manag 7(44). https://doi.org/10.1007/s40899-021-00527-7

Kumar M, Padalia H, Nandy S, Singh H, Khaiter P, Kalra N (2019a) Does spatial heterogeneity of landscape explain the process of plant invasion? A case study of Hyptis suaveolens from Indian Western Himalaya. Environ Monit Assess 191:794. https://doi.org/10.1007/s10661-019-7682-y

Kumar M, Savita SH, Pandey R, Singh MP, Ravindranath NH, Kalra N (2019b) Assessing vulnerability of forest ecosystem in the Indian Western Himalayan region using trends of net primary productivity. Biodivers Conserv 28:2163–2182

Kumar M, Kalra N, Singh H, Sharma S, Rawat PS, Singh RK, Gupta AK, Kumar P, Ravindranath NH (2021) Indicator-based vulnerability assessment of forest ecosystem in the Indian Western Himalayas: an analytical hierarchy process integrated approach. Ecol Indic 125:107568

Li Z (2014) Fast Fourier transformation resampling algorithm and its application in satellite image processing. J Appl Remote Sens 8:83683

Li H, Jia M, Zhang R, Ren Y, Wen X (2019) Incorporating the plant phenological trajectory into mangrove species mapping with dense time series Sentinel-2 imagery and the Google Earth Engine platform. Remote Sens 11. https://doi.org/10.3390/rs11212479

Liaw A, Wiener M (2002) Classification and regression by random forest. R News 2(3):18–22

Martin ME, Newman SD, Aber JD, Congalton RG (1998) Determining forest species composition using high spectral resolution remote sensing data. Remote Sens Environ 65:249–254

McAndrew A (2004) An introduction to digital image processing with Matlab Notes for SCM2511 Image Processing 1 Semester 1, 2004

Mishra AP, Rai ID, Pangtey D, Padalia H (2021) Vegetation characterization at community level using sentinel-2 satellite data and random forest classifier in western Himalayan Foothills, Uttarakhand. J Indian Soc Remote Sens 49(4):759–771

Mohite JD, Sawant SA, Rana S, Pappula S (2019) Wheat area mapping and phenology detection using synthetic aperture radar and multi-spectral remote sensing observations. Int Arch Photogramm Remote Sens Spat Inf Sci ISPRS Arch 42:123–127. https://doi.org/10.5194/isprs-archives-XLII-3-W6-123-2019

Oliveira S, Oehler F, San-Miguel-Ayanz J, Camia A, Pereira JM (2012) Modeling spatial patterns of fire occurrence in Mediterranean Europe using multiple regression and random forest. For Ecol Manag 275:117–129

Olokeogun OS, Kumar M (2020) An indicator-based approach for assessing the vulnerability of riparian ecosystem under the influence of urbanization in the Indian Himalayan city. Ecol. Indic, Dehradun. https://doi.org/10.1016/j.ecolind.2020.106796

Orimoloye IR, Olusola AO, Belle JA et al (2022) Drought disaster monitoring and land use dynamics: identification of drought drivers using regression-based algorithms. Nat Hazards. https://doi.org/10.1007/s11069-022-05219-9

Pal M (2005) Random forest classifier for remote sensing classification. Int J Remote Sens 26:217–222

Pande CB (2022) Land use/land cover and change detection mapping in Rahuri watershed area (MS), India using the google earth engine and machine learning approach. Geocarto Int. https://doi.org/10.1080/10106049.2022.2086622

Pande CB, Moharir KN, Khadri SFR et al (2018) Study of land use classification in an arid region using multispectral satellite images. Appl Water Sci 8:123. https://doi.org/10.1007/s13201-018-0764-0

Pande CB, Moharir KN, Khadri SFR (2021a) Assessment of land-use and land-cover changes in Pangari watershed area (MS), India, based on the remote sensing and GIS techniques. Appl Water Sci 11:96. https://doi.org/10.1007/s13201-021-01425-1

Pande CB, Moharir KN, Kumar Singh S, Varade AM, Elbeltagie A, Khadri SFR, Choudhari P (2021b) Estimation of crop and forest biomass resources in a semi-arid region using satellite data and GIS. J Saudi Soc Agric Sci 20(5):302–311

Prasad AM, Iverson LR, Liaw A (2006) Newer classification and regression tree techniques: bagging and random forests for ecological prediction. Ecosystems 9(2):181–199

Praticò S, Solano F, Di Fazio S, Modica G (2021) Machine learning classification of mediterranean forest habitats in Google Earth Engine based on Seasonal Sentinel-2 time-series and input image composition optimisation. Remote Sens 13:586

Rodriguez-Galiano VF, Chica-Olmo M, Abarca-Hernandez F, Atkinson PM, Jeganathan C (2012) Random Forest classification of Mediterranean land cover using multi-seasonal imagery and multi-seasonal texture. Remote Sens Environ 121:93–107

Roy PS, Behera MD, Murthy MSR, Roy A, Singh S, Kushwaha SPS et al (2015) New vegetation type map of India prepared using satellite remote sensing: comparison with global vegetation maps and utilities. Int J Appl Earth Obs Geoinf 39:142–159

Shelestov A, Lavreniuk M, Kussul N, Novikov A, Skakun S (2017) Large scale crop classification using Google earth engine platform. International Geoscience and Remote Sensing Symposium 2017 July, p 3696–3699. https://doi.org/10.1109/IGARSS.2017.8127801

Shouse M, Liang L, Fei S (2012) Identification of understory invasive exotic plants with remote sensing: in urban forests. Int J Appl Earth Obs Geoinf 21:525–534

Singh RK, Sinha VSP, Joshi PK, Kumar M (2020a) A multinomial logistic model-based land use and land cover classification for the South Asian Association for Regional Cooperation nations using Moderate Resolution Imaging Spectroradiometer product. Environ Dev Sustain 23:1–22

Singh RK, Sinha VSP, Joshi PK, Kumar M (2020b) Modelling Agriculture, Forestry and Other Land Use (AFOLU) in response to climate change scenarios for the SAARC nations. Environ Monit Assess 192:1–18

Singh RK, Sinha VSP, Joshi PK, Kumar M (2020c) Mapping of agriculture productivity variability for the SAARC Nations in Response to Climate Change Scenario for the Year 2050. In: Remote sensing and GIScience. Springer, Cham, pp 249–262

Srinet R, Nandy S, Padalia H, Ghosh S, Watham T, Patel NR, Chauhan P (2020) Mapping plant functional types in Northwest Himalayan foothills of India using random forest algorithm in Google Earth Engine. Int J Remote Sens 41:1–14. https://doi.org/10.1080/01431161.2020.1766147

Stibig H-J, Beuchle R, Achard F (2003) Mapping of the tropical forest cover of insular Southeast Asia from SPOT4-Vegetation images. Int J Remote Sens 24:3651–3662. https://doi.org/10.1080/0143116021000024113

Zhang M, Gong P, Qi S, Liu C, Xiong T (2019) Mapping bamboo with regional phenological characteristics derived from dense Landsat time series using Google Earth Engine. Int J Remote Sens 40:9541–9555. https://doi.org/10.1080/01431161.2019.1633702

Zhu X (2013) Land cover classification using moderate resolution satellite imagery and random forests with post-hoc smoothing. J Spat Sci 58(2):323–337

Chapter 28
Water Conservation Structure as an Unconventional Method for Improving Sustainable Use of Irrigation Water for Soybean Crop Under Rainfed Climate Condition

Chaitanya B. Pande, Kanak N. Moharir, and Abhay Varade

Abstract Rainwater harvesting through water conservation structures and techniques is playing a vital role under the rainfed agriculture conditions of the Vidarbha region in Maharashtra. Soil and water conservation activity is one of the most important components for agronomy practices in rainfed conditions. In view of that, the Department of Agriculture (M.S.) is undertaking various projects with the objective of developing rainwater harvesting structures for sustainable use of harvested rainwater for mitigating the need for protective irrigation to the rainfed crops grown at the Akola District. That is utilized for protective irrigation during prolonged dry spells to the kharif crops grown in the vicinity of existing drainage line developed under high surface runoff area. During the *kharif* seasons 2016 and 2017, ten demonstrations in watershed were conducted under rainfed condition. Protective irrigation has resulted in significant increase in yield as compared to rainfed condition/without irrigation at the watershed area. There was a 19.14–33% increase in yield during the kharif season of 2017–2018 as compared to 2016–2017. It was observed due to protective irrigation provided during the critical growth stage and dry spells. The results of study area should be more helpful for agriculture crops and what impacts of groundwater level and that is directly an impact on farmer's income and production yields under different climatologically factors. All of these factors have been considered for dryland conditions based on rainwater conserved in the

C. B. Pande (✉)
Indian Institute of Tropical Meteorology (IITM), Pune, Maharashtra, India
e-mail: chaitanay45@gmail.com

K. N. Moharir
Department of Earth Science, Banasthali University, Aliyabad, Rajasthan, India

A. Varade
Department of Geology, RTM Nagpur University, Nagpur, Maharashtra, India

C. B. Pande et al. (eds.), *Climate Change Impacts on Natural Resources, Ecosystems and Agricultural Systems*, Springer Climate,
https://doi.org/10.1007/978-3-031-19059-9_28

rainwater harvesting structures for protective irrigation for agronomy crops under water stress situations.

Keywords Water · Conservation · Rainfed · Rainfall

Introduction

"Dryland agriculture" means raising of agriculture crops totally under rainfed conditions. In global, 6510 million hectares (m ha) of agriculture land is under rainfed agriculture of which about 60% is in the developing countries. India's position is first among the dryland agricultural countries in the world. Out of every three hectares of cultivated land in India, nearly about two hectares is under the influence of rainfed conditions. Dryland areas occupy an area of 91.0 million hectares out of a total 142.1 m ha cultivated areas in India, and it is predicted that about 60% of our population still depend upon dryland agriculture and rainfed conditions (Anonymous 1997). The irregular climatic conditions in dryland in India consist of aberrant weather conditions such as late onset of the monsoon, prolonged dry spells, early withdrawal of monsoon, early midseason, and terminal droughts. Rainfed agriculture is facing several problems such as resowing of crops, moisture stress during critical growth stages, unavailability of lifesaving irrigation, and efficient fertilizer use (Sharmila Zilve 2013). Most of the food crops are grown in rainfed areas, which plays a key part in food production and poverty decrease (Rockström et al. 2007a, b). The major number of poor people in the world depends on rainfed agriculture conditions for food and earnings and thus livelihood security (FAO 2002). The consequence of rainfed agriculture changes regionally, but most food for poor societies in the developing countries are formed under rainfed agriculture (Elke Noellemeyer et al. 2013). Scarcity of irrigation water has now been globally the main constraint for raising the crops with good productivity (Pande and Moharir 2017; Pande et al. 2020; Pande et al. 2021; Elbeltagi et al. 2022). Availability of sufficient harvested rainwater for irrigation is the preventive measure for reduction in the productivity of agriculture crops in many parts of the world (Gutiérrez-Gómeza et al. 2018). The scarcity of water for agriculture is increasing not only because the sources are reducing but also because the quality of water is failing (Elliott et al. 2015; Crosson 1994; Nagavallemma et al. 2005). Freshwater insufficiency is commonly discussed around the world. Over recent years, freshwater consumption has grown at two times the rate of human population enlargement, and there are an increasing number of areas experiencing constant freshwater shortages (UNESCO 2012). Dalin et al. (2017) state that a quick nonrenewable depletion of aquifers is due to an excessive extraction of water that is used for irrigation in many crop-producing regions worldwide, which threatens the sustainability of water use and food production (Vidya et al. 2021; Pande et al. 2022), not only in the producing regions but also globally due to the international food trade. In the last decades, new terms have been introduced to determine the efficiency and sustainability of water use. Hoekstra and

Hung (2002) introduced the water footprint concept (Lovarelli et al. 2016). The impact of rainwater and groundwater development methods as water harvesting and conservation can be used for increasing productivity and water use efficiency of different agronomical crops during 2016–2017 and 2017–2018 *kharif* seasons.

Material and Methods

Study Area Description

The Kajaleshwar watershed area is situated between 20° 13′59″ N latitude and 77° 13′23″ E longitude and at mean sea level elevation of 337 m and is having an average annual rainfall of 735–855 mm (Fig. 28.1). This area is under basaltic hard rock

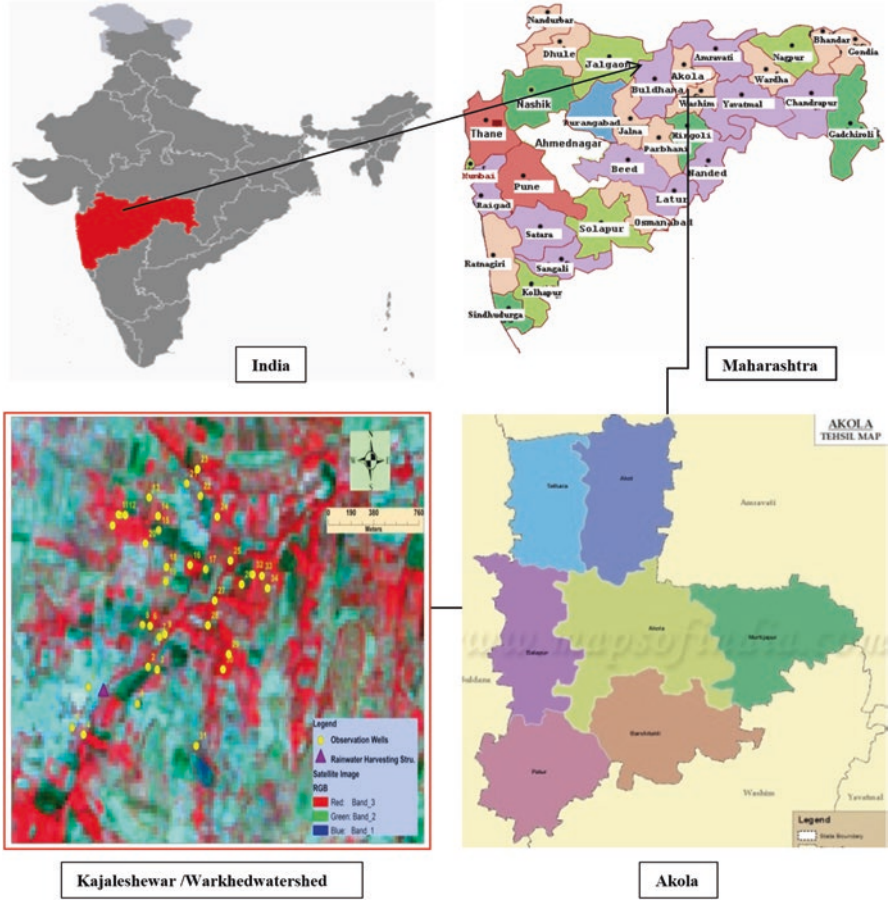

Fig. 28.1 Location map of study area

terrain (Deccan trap), and most of the watershed areas were covered by unconsolidated sediments, black cotton soil, red soils, and basaltic rock of Deccan Traps.

Impact of Rainwater Conservation Activities on the Soybean Crop

The site selection for rainwater harvesting structure was done on drainage line, and it was finalized with agriculture engineering. In this watershed, water conservation structures developed with the widening and deepening work on the existing drainage line under the watershed programmed. It has been used for rainwater management strategy through water conservation structures at watershed area. The digging work of the drainage deepening and widening was done, and the CNB was repaired during summer season 2012–2014. The catchment area of the rainwater conservation structures was in the vicinity of demonstrations conducted during *kharif* seasons 2016–2017 and 2017–2018 in the dryland condition in soybean crop (Fig. 28.4b). The rainwater and runoff water were collected in the water conservation structure, and the stored water has been used for protective irrigation applied during dry spells for sustainable crop production. The water conservation structure is helpful for the development of groundwater regime (Rajesh et al. 2021) and significant increase in crop productivity. It was observed that surrounding groundwater level is increasing due to drainage deepening and widening work on the drainage line at watershed area. The excess runoff water from upper, middle, and lower layers was collected on a daily basis and rainwater stored in the rainwater harvesting structure during *kharif* seasons 2016–2017 and 2017–2018 (Figs. 28.2 and 28.3). The total cumulative quantity of the stored water was measured using water level indicator, and the total quantity of water available in the drainage widening and deepening work was obtained during every month (Table 28.1). Before the initiation of project,

Fig. 28.2 Rainwater storage in deepened and widened drainage and CNB during *kharif* season 2016–2017

Fig. 28.3 Rainwater storage in deepened and widened drainage and CNB during *kharif* season 2017–2018

Table 28.1 Yield of soybean crop during 2016–2017

Plot no.	Yield of soybean q/ha (without irrigation)	Yield of soybean q/ha (one protective irrigation at pod filling stage from water stored in widened and deepened drainage/CNB)	% increase in yield
1	9.37	12.40	32.33
2	8.50	11.10	30.50
3	11.60	15.25	31.40
4	6.25	8.75	40.00
5	7.20	8.50	18.05
6	8.35	10.25	22.75
7	8.95	12.20	36.31
8	11.10	13.20	18.92
9	9.50	12.30	29.47
10	8.20	11.35	38.41

the area was suffering from various aberrant weather conditions such as high percolation, evaporation and seepage rates, and high runoff, as a result of which there is severe loss in moisture conservation leading to declined productivity of crop. But after the construction rainwater harvesting structure on lower layer, the moisture availability in bottom toposequence was increased due to the seepage water, and the soybean crop yield is significantly increased due to protective irrigations provided during the dry spells (Fig. 28.4a). The soybean yield data was recorded from the demonstration plots conducted in the participatory action research mode with farmers.

a b

Fig. 28.4 (**a**) Stored rainwater and protective irrigation applied to soybean crop. (**b**) View of soybean demonstration plots

Result and Discussion

The study area is situated in the Akola District, that is, Vidarbha region of Maharashtra state in which major crops are grown in the rainfed conditions. In this study area, dry spells even during the monsoon periods are not uncommon, resulting in low crop yield. In these areas, it would be wise to harvest the runoff water, store the water, and reuse it for sustainable production of agronomical crops by establishing and developing rainwater structures in the rainfed areas. It is very useful and lifesaving device for rainfed crops in the watershed area which is characterized by low and erratic rainfall due to climate change and ecological imbalance. Protective irrigations to soybean demonstration plots during the prolonged dry spells were applied to soybean crop at critical growth and pod stages. The annual rainfall received during the *kharif* seasons 2016–2017 and 2017–2018 and is below normal, along with the early midseason and terminal droughts responsible for severe decline in the productivity of soybean. Periodically the groundwater level monitoring would be done during pre-post monsoons. Throughout the country, there has been a severe need for conserving rainwater and thereby increasing the groundwater which is beneficial for agriculture, industry, and domestic purposes in rainfed area (Barai and Patil 1991; Abuj et al. 2010).

Rainfall Analysis

The rainfall data was collected from rain gauge established in the study area. In this study area, 707 mm and 428.2 mm rainfall were recorded during the *kharif* seasons 2016–2017and 2017–2018, respectively (Fig. 28.5). During 2016–2017, the amount

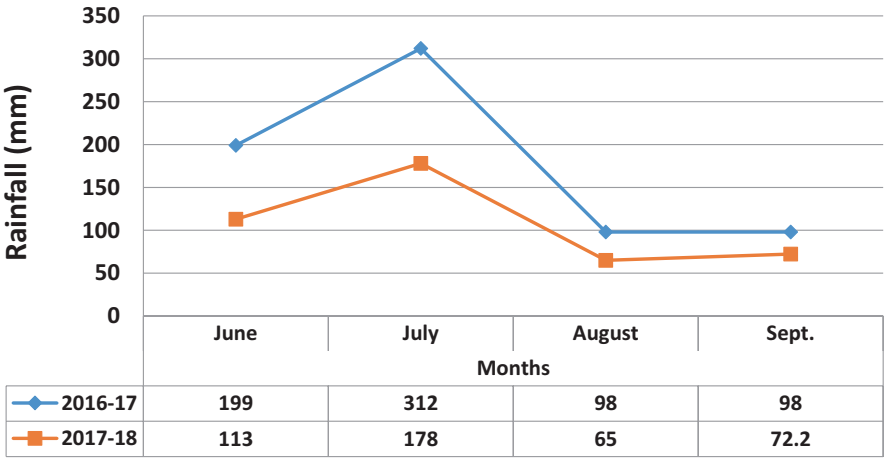

Fig. 28.5 Rainfall differences during 2016–2017 and 2017–2018

of rain received was good compared to *kharif* 2017–2018, and during 2016–2017, it was the highest amount of rainwater collected in the water conservation structure as compared to *kharif* 2017–2018. The stored water is of significant use for demonstration plots during the dry spells due to lack of irrigation sources at the watershed area. Similar water conservation structure work has been suggested in the rainfed area for groundwater regime development. The annual rainfall received was deficient by 34% during the year 2017–2018.

Soybean Yield in 2016–2017

During *kharif* season 2016–2017, ten soybean demonstration plots were conducted in the adjacent vicinity of rainwater harvesting structure at watershed area. The rainwater harvesting work developed an irrigation source to the rainfed area. During the baseline survey conducted in the village, it was observed that most of farmers are in marginal and small category with minimum land holding, and hence the productivity of crop is a very crucial issue for the small landholding farmers. Stored water was used for providing protective irrigations to soybean crop during the one-month dry spell from 13 August to 13 September 2016, at which the soybean is at pod filling stage. This dry spell of one month severely affected the soybean pod filling resulting in very poor yields of soybean in dryland conditions. One protective irrigation during this dry spell from stored water resulted in significant increase in yield as compared to rainfed condition, that is, without irrigation. An increase of 18.05–40% in yield was observed due to protective irrigation provided during the critical growth stage of pod filling in soybean (Table 28.1).

Soybean Yield in 2017–2018

During *kharif* season, the stored water is utilized for soybean crop as a lifesaving irrigation during dry spells which occurred at vegetative and pod filling stages in soybean. The work of drainage widening and deepening was done under this project, and the existing Cement Nalla Bandh (CNB) structure has been repaired for irrigation purpose and groundwater development. The study was undertaken to analyze the impact of rainwater harvesting structure on groundwater seasonal fluctuations at watershed area of Taluka Barshitakli, Akola District, Maharashtra. The annual rainfall received during the year 2017 was deficient by 34%. Due to rainwater harvesting structure, the significant rainwater was harvested in the drainage with CNB (Table 28.2). The stored water was utilized as a protective irrigation during *kharif* as well as *rabi* season for different agronomical crops grown in the vicinity of the demonstrations conducted. Protective irrigation has resulted in significant increase in yield as compared to rainfed condition/without irrigation at the Kajaleshwar watershed. 19.14–33% increase in yield during *kharif* season was observed due to protective irrigation provided during the critical growth stage and dry spells (Fig. 28.6 and Table 28.2).

Rainwater Management During *Kharif* Seasons

The survey data was integrated with existing drainage line suitable for the sustainable use of irrigation and groundwater regime within watershed area. During the years 2015–2016, water conservation work was started on the existing drainage line, the widening and deepening work of about 100 m has been done, and the storage of rainwater has been monitored. During 2016–2017, stored water is sufficient for soybean plots because annual rainfall intensity during 2016–2017 was good as

Table 28.2 Yield of soybean crop during 2017–2018

Plot no.	Yield of soybean q/ha (without irrigation)	Yield of soybean q/ha (one protective irrigation at pod filling stage from water stored in widened and deepened drainage/CNB)	% increase in yield
1	11.30	13.6	20.35
2	09.40	11.2	19.14
3	10.70	13.1	22.42
4	09.80	12.2	24.48
5	10.60	13.2	24.52
6	12.20	14.7	20.49
7	11.60	14.8	27.58
8	13.40	16.5	23.13
9	11.70	14.1	20.51
10	10.30	13.7	33.00

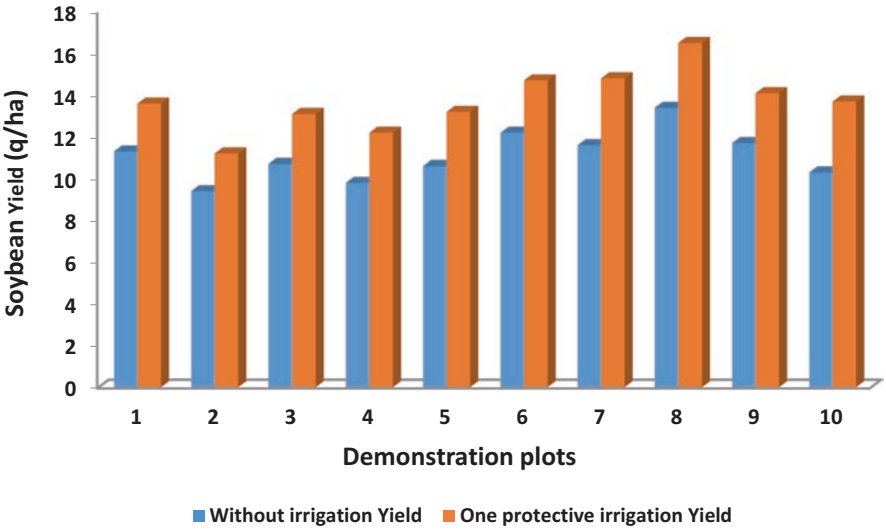

Fig. 28.6 Soybean yield (q/ha) during kharif 2017–2018

compared to 2017–2018. The wells were periodically monitored and there is significant increase in water level. The farmers having wells have been contacted, and the importance of the artificial recharge has been explained to them; the impact has been analyzed using land use and land cover mapping during *kharif* and *rabi* crops. The farmers without well or any other irrigation source but having their fields adjacent to the rainwater harvesting demonstration site were contacted, and as per the availability of stored water and need during *kharif* season, the crop planning was done. The rainwater storage data was collected in the drainage and CNB during 2017–2018 is presented in Tables 28.3 and 28.4. During the months of June and July due to less rainfall, there is very low accumulation of harvested rainwater as there is not a single runoff event during these two months of 2017–2018.

Impact of Water Conservation Structure on Groundwater Table

Surface Water

In this study we measured the stored rainwater in the water conservation structure during two seasons of 2016–2017 and 2017–2018 (Tables 28.3 and 28.4). In this area, more farmers are familiar with the soybean crop or rainfed crops, but nowadays, dry spell increases the time interval which has a direct impact on the soybean crop. In this view, we studied the impact on the soybean crop in the *rainfed* area for two years. It is very important to study if in drought conditions such type of water

Table 28.3 Rainwater storage in the drainage with CNB during kharif season (2016–2017)

S. N.	Month	Initial water vol. (m^3)	Rainwater stored vol. (m^3)	Total available water during this period vol. (m^3)	Water usage (m^3)	Remarks
1	15-May-2016–15-June-2016	0	500	500	200	Usage
2	15-June-2016–15-July-2016	500	1800	2300	0	–
3	15-July-2016–15-Aug-2017	2300	617	2917.20	0(full)	Overflow
4	15-Aug-2016–15-Sept.-2016	2917.20	2917.20	2917.20	0 (full)	Overflow
5	15-Sept.-2016–15-Oct.-2016	2917.20	2545.20	2545.20	372.00	Usage
6	15-Oct.-2016–15-Nov.-2016	2545.20	2100.00	2100.00	445.20	Usage
7	15-Nov.-2017–15-Dec.-2017	2100.00	1530.00		570.00	Usage

Table 28.4 Rainwater storage in the drainage with CNB during 2017–2018

S. N.	Months	Initial water vol. (m^3)	Rainwater stored vol. (m^3)	Total available water during this period vol. (m^3)	Water usage (m^3)	Remarks
1	15-May-2017–15-June-2017	0	–	0	0	Dry
2	15-June-2017–15-July-2017	–	–	–	–	Dry
3	15-July-2017–15-Aug-2017	–	–	–	–	Dry
4	15-Aug-2017–15-Sept.-2017	0	1425.00	1425.00	525.00	Usage, seepage, and other losses
5	15-Sept.-2017–15-Oct.-2017	900.00	735.00	1635.00	430.00	Usage, seepage, and other losses
6	15-Oct.-2017–15-Nov.-2017	1205.00	757.20	1962.20	1060.00	Usage
7	15-Nov.-2017–15-Dec.-2017	902.20	–	902.20	480.00	Usage

conservation structures plays a major role in the sustainable crop yield production and improves farmers' practice during drought situations and climate variation.

Groundwater Table

The study was undertaken to analyze the impact of rainwater harvesting structure on groundwater seasonal fluctuations at watershed area of Taluka Barshitakli, Akola District, Maharashtra. Impact of water conservation structure on groundwater table has been analyzed using graphical representations. Two years of groundwater levels data was collected from 35 observation wells in study area. The groundwater fluctuation level (2015–2017) graph has been prepared. The groundwater level fluctuation values are helpful for knowing the impact of rainwater harvesting on aquifer properties surrounding watershed area. The groundwater fluctuation graph has been useful for further analysis of water levels. From the monitored of groundwater level data for the year 2015 pre-monsoon (before completion of rainwater harvesting structure) and for the year 2017 pre-monsoon (after completion of the rainwater harvesting structure) in the watershed, it has been observed that due to rainwater harvesting structure and its recharge, the groundwater levels of all the wells during 2017 have been increased as compared to the groundwater levels of wells during 2015. The further insufficiency of water for various agricultural production systems should be essential for sustainable water for agriculture crops and the food security using soil and water conservation and management practices. Moreover, the strategy decisions on water management are more essential for groundwater resource management and also impact assessment on groundwater regime efficient method in any country level. In this study, during the year 2017, groundwater level is high as compared to 2015 due to rainwater harvesting structures. In study area, stored water may be affected for groundwater level and are helpful for observation wells recharging in dryland area.

Conclusion

In our work, an evaluation of the impact of water conservation structure which was implanted in watershed area was made with different climatic conditions faced in rainfed areas. Soybean is commonly known as golden bean and occupies coveted place with top rank among oilseed crops of India as well as Maharashtra. The soybean demonstration plots were conducted on farmer's field during *kharif* seasons 2016–2017 and 2017–2018. These demonstration plots are proposed suitable sites near water conservation structure at the watershed area. In *kharif* seasons rainwater was not conserved in any rainwater harvesting structure, as a result of which the groundwater level decreases and agriculture production also decreases before drainage deepening and widening work. During the *kharif* seasons 2016–2017 and

2017–2018, soybean yields were recorded as 31–40% and 19.14–33% under rainfed condition. In the year 2016 soybean crop yield was increased due to sufficient rainfall as compared to 2017. However, the store water was utilization during dry spell period as per plan to soybean-based cropping systems from the water available in drainage and recharged of observation wells for sustainable irrigation in the rainfed condition. The results showed that farmer's crop yield production increased after adopting soil and water conservation practices for rainfed areas.

References

Abuj MD, Magar AP, Bombale VT, Popale PG (2010) Performance evaluation of soil and water conservation structures in Darakwadi Watersheds. J Agri Eng 3(1):73–76

Anonymous (1997) Vision, 2002: CRIDA perspective Plan. Central Research Institute for Dryland Agriculture, Hyderabad, p 80

Barai UN, Patil BM (1991) Effect of conservation practices on soil moisture and crop yield. Indian J Soil Cons 17(2):55–57

Crosson (1994) Degradation of resources on threat to sustainable agriculture. Paper presented at First World Congress of Professionals of Agronomy, 5–8 September, 1994, Satiago, Chille

Dalin C, Wada Y, Kastner T, Puma MJ (2017) Letter 543, Nature Publishing Group, p 700–704

Elbeltagi A, Pande CB, Kouadri S et al (2022) Applications of various data-driven models for the prediction of groundwater quality index in the Akot basin, Maharashtra. India Environ Sci Pollut Res 29:17591–17605. https://doi.org/10.1007/s11356-021-17064-7

Elliott J, Müller C, Deryng D, Chryssanthacopoulos J, Boote KJ, Büchner M, Foster I, Glotter M, Heinke J, Iizumi T, Izaurralde RC, Mueller ND, Ray DK, Rosenzweig C, Ruane AC, Sheffield J (2015) The global gridded crop model inter comparison: data and modeling protocols for Phase 1 (v1.0). Geosci Model Dev 8:261–277. https://doi.org/10.5194/gmd-8-261-2015

FAO (2002) the State of Food Insecurity in the World 2001. Food and Agricultural Organization, Rome

Gutiérrez-Gómeza C, Carrillo-Avilab E, Landeros-Sánchezc C, Coh-Méndezb D, Monsalvo-Espinosab A, Arreola-Enríquezb J, Pimentel-Ópez J (2018) Soil moisture tension as an alternative for improving sustainable use of irrigation water for habanero chilies (Capsicum Chinense Jacq.). Agric Water Manag 204:28–37

Hoekstra AY, Hung PQ (2002) Virtual Water Trade: a quantification of virtual water flows between nations in relation to international crop trade, value of water research report series no. 11. UNESCO-IHE institute for water education, Delft

Lovarelli D, Bacenetti J, Fiala M (2016) Science of the total environment water footprint of crop productions: a review. Sci Total Environ 548–549:236–251

Nagavallemma KP, Wani SP, Reddy MS, Pathak P (2005) Effect of land form and soil depth on productivity of soybean based cropping system and erosion losses in VerticInceptisols. Indian J Soil Cons 33(2):132–136

Noellemeyer E, Fernández R, Quiroga A (2013) Crop and tillage effects on water productivity of dryland agriculture in Argentina. Agriculture 3:1–11. https://doi.org/10.3390/agriculture-3010001

Pande CB, Moharir K (2017) GIS based quantitative morphometric analysis and its consequences: a case study from Shanur River basin, Maharashtra India. Appl Water Sci 7:861–871. https://doi.org/10.1007/s13201-015-0298-7

Pande CB, Moharir KN, Singh SK et al (2020) An integrated approach to delineate the groundwater potential zones in Devdari watershed area of Akola district, Maharashtra, Central India. Environ Dev Sustain 22:4867–4887. https://doi.org/10.1007/s10668-019-00409-1

Pande CB, Moharir KN, Panneerselvam B et al (2021) Delineation of groundwater potential zones for sustainable development and planning using analytical hierarchy process (AHP), and MIF techniques. Appl Water Sci 11:186. https://doi.org/10.1007/s13201-021-01522-1

Pande CB, Kadam SA, Jayaraman R, Gorantiwar S, Shinde M (2022) Prediction of soil chemical properties using multispectral satellite images and wavelet transforms methods. J Saudi Soc Agric Sci 21(1):21–28

Rajesh J, Pande CB, Kadam SA et al (2021) Exploration of groundwater potential zones using analytical hierarchical process (AHP) approach in the Godavari river basin of Maharashtra in India. Appl Water Sci 11:182. https://doi.org/10.1007/s13201-021-01518-x

Rockström J, Lannerstad M, Falkenmark M (2007a) Assessing the water challenge of a new green revolution in developing countries. Proc Natl Acad Sci USA 104:6253–6260. https://doi.org/10.1073/pnas.0605739104

Rockström J, Hatibu N, Oweis TY, Wani S, Barron J, Bruggeman A, Farahani J, Karlberg L, Qiang Z (2007b) Managing water in rainfed agriculture. In: Molden D (ed) Water for food, water for life: a comprehensive assessment of water management in agriculture. Earth scan, London, pp 315–352

Sharmila Zilve (2013) Evaluation of different crops to aberrant weather condition in dry-land semi-arid Vertisols. Thesis submitted in Rajmata Vijayaraje Scindia Krishi Vishwa Vidyalaya, Gwalior

UNESCO (2012) United Nations educational, scientific and cultural organization, managing water under uncertainty and risk, the United Nations World Water Development Report 4 Volume-1, United Nations Educational, Scientific and Cultural Organization 7, place de Fontenoy, 75352 Paris 07 SP, France (Published in 2012)

Vidya UK, Chaitanya B, Pande JR, Atre AA, Gorantiwar SD, Gavit SAKB (2021) Surface water dynamics analysis based on sentinel imagery and Google earth engine platform: a case study of Jayakwadi dam. Sustainable Water Resources Management 7:44. https://doi.org/10.1007/s40899-021-00527-7

Chapter 29
Study of Image Segmentation and Classification Methods for Climate Data Analysis

Ahmed Elbeltagi, Kouadri Saber, Djamal Bengusmia, Behnam Mirgol, and Chaitanya B. Pande

Abstract Artificial intelligence (AI) has revolutionized information technology and has shaped the way we live. AI is a computational model that allows computer to learn out from data and approximate solutions for nonlinear, multi-input functions and doesn't depend upon physical models. Due to their flexibility and robustness, AI has been widely applied in large-scale fields ranging from robotics to airplane flight control. This section of book aims to discuss the advances in all aspect of AI, including machine/deep learning (ML-DL), data mining (DM), computer vision (CV), multi-agent systems (MS), evolutionary computation (EC), and fuzzy logic (FL) methods in image segmentation and classification. This chapter focuses specifically on various applications of AI related to mapping, classification, and segmentation of aerial images, including non-classification-/classification-based methods. Applications of AI are also discussed and showed the importance of AI in performing segmentation and outline extraction on aerial imagery. AI is performing very well on

A. Elbeltagi (✉)
Agricultural Engineering Department, Faculty of Agriculture, Mansoura University, Al Manşūrah, Egypt
e-mail: ahmedelbeltagy81@mans.edu.eg

K. Saber
Laboratory of Water and environment Engineering in Sahara Milieu (GEEMS), Department of Civil Engineering and Hydraulics Faculty of Applied Sciences, Kasdi Merbah University Ouargla, Ouargla, Algeria

D. Bengusmia
Ziane Achour Djelfa University, Djelfa, BP, Algeria

B. Mirgol
Department of Water Engineering, Faculty of Agriculture and Natural Resources, Imam Khomeini International University, Qazvin, Iran

C. B. Pande
Indian Institute of Tropical Meteorology (IITM), Pune, Maharashtra, India
e-mail: chaitanay45@gmail.com

C. B. Pande et al. (eds.), *Climate Change Impacts on Natural Resources, Ecosystems and Agricultural Systems*, Springer Climate,
https://doi.org/10.1007/978-3-031-19059-9_29

the understanding of climate data analysis. Brief introductions of AI with their adaptability for accurate segmentation, classification methods, and outline extraction are also interpreted. Furthermore, we illustrated how the AI tool will help the decision-makers, and developers, in achieving better performance with less computational cost.

Keywords Artificial intelligence · Aerial image · Segmentation · Classification · Outline extraction

Introduction

Man has been known to draw since ancient times, and he used it to express the phenomena that were going on around him and also to record his daily events. Some real-life examples include the drawings on the walls of caves that belong to the oldest civilizations such as the Babylonian civilization, the Pharaonic civilization, the Chinese civilization, and many other civilizations. With the development of man, mankind witnessed the first photograph taken in 1826 by Nappes (Gernheim and Gernheim 1955; Bann 2002). With the development of technology, taking pictures became a daily matter in the life of every human being, so cameras began to come in different shapes and sizes, as well as with variable efficiency from one type to another (Mather and Koch 2011; Medjahed 2015; Nath et al. 2014; Nhamo et al. 2018; Rozenstein and Karnieli 2011; Stanchev et al. 2003). In the early 1940s, the first model of an artificial neural network was developed (Deepan and Sudha 2018; Hölbling et al. 2017; Jain and Singh 2003; Khalid et al. 2014; Kumar and Singh 2013; Lu and Weng 2007), which was inspired by the human nervous system (McCulloch and Pitts 1943; Kouadri et al. 2021). These artificial neural networks were created to solve some problems that are characterized by nonlinearity, which can be described as complex compared to linear regression problems. What we see today in camera technology and merging it with modern techniques such as facial recognition or locating and classifying objects is nothing but a merger of imaging techniques and deep learning techniques. This chapter will include a set of algorithms related to deep learning and its use in the image field, where we will explain how each algorithm works and identify the utility of image segmentation technique in different fields.

Applications of Artificial Intelligence in Image Classification

Classification System

The image classification defines as categorizing all pixels in a particular image into one of several land cover classes which can be used for various applications such as environmental change, agriculture, land use/land planning, urban planning, surveillance, geographic mapping, disaster control, and object detection (Krizhevsky et al.

2012; Abburu and Golla 2015; Pande 2022). In other words, image classification is a pattern recognition method whose aim is to find the features of things on the Earth at the pixels in the satellite images and then tries to identify the most likely class to which the pixel belongs (Al-Doski et al. 2013).

Feature Extraction

Feature extraction is one of the essential fields in artificial intelligence, which consists of extracting an image's most relevant features and assigning them to a label (Salvador et al. 2017). Generally, elements can be labeled as relevant, irrelevant, or redundant (Celebi et al. 2013).

Selecting Good Training Samples

Using a sufficient number of training samples is necessary for successful classification. In this step, a subset from available feature data is selected for the process of a learning algorithm (Pande et al. 2022). Then, the classifier learns its own classification rules from a training set. The classifier decides based on the learning model and its own classification rules to distinguish which class that feature belongs to. The best subset has the least number of dimensions that contribute most to learning accuracy (Chuang et al. 2006; Davis et al. 1975).

Image Preprocessing

Image preprocessing is an essential task to reduce the level of abstraction, which includes radiometric, atmospheric, geometric, and topographic detection and corrections, image enhancement, and initial image clustering (Shahid et al. 2021). Preprocessing aims to improve the image data that suppresses undesired distortions or enhances some image features relevant for further processing and analysis tasks.

Selection of Appropriate Classification Method

In order to obtain reliable information from satellite data, appropriate classification techniques are required. Several classification approaches have been developed over the past decades which each could have its advantages and disadvantages. These methods can be categorized broadly as automatic, manual, and hybrid (Dong et al. 2006). Automated satellite image classification methods are the most common ones

and are classified into supervised and unsupervised classification methods. These methods use algorithms that apply the entire satellite image systematically to gather pixels into specific categories (Pande et al. 2018; Pande et al. 2021a). Manual satellite image classification methods are robust but time-consuming procedures, and users must be familiar with the area covered by the satellite image. The classification accuracy entirely relies on the analyst's knowledge and familiarity with the field of study (Fitzgerald and Lees 1994). The hybrid approach is a combination of automated and manual methods. It uses automated satellite image classification methods to do initial classification; other manual methods are used to refine classification and correct errors (Pande et al. 2021b).

Post-classification Processing

The accuracy of classified areas can be enhanced by post-classification correction so that isolated and noise pixels that appeared after the classification process could be reduced using this procedure (Lin et al. 2015; Gašparović 2020; Geng et al. 2020).

Assessing the Overall Accuracy

In order to evaluate the classification accuracy rate, the overall accuracy percentage computed from the sum of the diagonal elements of the error, confusion, or misclassification matrix resulting from the application of a classifier is expressed. As an excellent measurement, the Kappa test statistic assesses inter-classifier agreement and is applied in determining the classification accuracy of two classifiers.

Applications of Artificial Intelligence in Images Segmentation

Semantic Image Segmentation

The task of classifying the images pixel-wise into a predefined category (or to none of them) is called the semantic segmentation. This kind of problems belongs to supervised learning problems, where a training set of classifiers and a set of labeled pixels will be involved in the process of building the model. Computer vision techniques, one of the promising applications of AI, can be applied for self-driving cars, damage detection, robotic systems, and satellite images to extract the objects embedded in it (Gulhane et al. 2022). Due to rich hierarchical features and an end-to-end trainable framework (Long et al. 2015; Zheng et al. 2015; Yu and Koltun 2015; Lin et al. 2015; Chen et al. 2016), the recent success of deep convolutional

neural network (CNN) models (Krizhevsky et al. 2012; Simonyan and Zisserman 2014; He et al. 2015) has enabled remarkable progress in pixel-wise semantic segmentation tasks. Three of the most used methods in performing semantic segmentation tasks in the state of the art will be discussed in this section, that is, the fully convolutional network (FCN), conditional random fields (CRF), and dilated convolution (DC).

Fully Convolutional Network (FCN)

In FCN, each of the data layers is in the form of a three-dimensional array (h, w, d), where "h" and "w" are the areal dimensions and d is the vertical dimension, which is known as the feature. The image is the first layer in the network, where the image is divided into pixels with dimensions h × w and the color are the dimension d, what we previously called the feature. CFN is based on transferring each pixel from the first layer "image" to the receiving fields statically by means of what is known as a path connected to between each pixel in the image and the receiving field in the final layer. The basic components of CFN depend only on the relative spatial coordinates, and its center of action is at the level of the input area.

Writing x_{ij} for the data vector at location (i, j) in a particular layer, and y_{ij} for the following layer, these functions compute outputs y_{ij} by:

$$y_{ij} = f_{ks}\left(\left\{x_{si} + \delta_i, sj + \delta_j\right\} 0 \le \delta_i, \delta \le k\right)$$

where:
k: kernel size,
s: stride or subsampling factor
f_{ks}: determines the layer type

Layer type could be a matrix multiplication for convolution or average pooling, a spatial max for max pooling, or an element-wise nonlinearity for an activation function and so on for other types of layers.

This functional form is maintained under composition, with kernel size and stride obeying the transformation rule:

$$f_{ks} \circ gk's' = \left(f \circ g\right) / k' + \left(k - 1\right)s', ss'.$$

Whereas general deep networks compute general nonlinear functions, this type of layer-only network computes nonlinear filters called deep filters or fully convolutional networks. The FCN works with inputs of all natural sizes and produces the output of the appropriate (resampled) spatial dimension. The mistake value of loss function configured in the FCN defines the task. If the loss function is the sum of the spatial dimensions of the final layer, $1\left(x;\theta\right) = \sum_{1}^{i} ij1'\left(x_{ij};\theta\right)$, the slope is the sum of

the slopes of each spatial component. Therefore, the "stochastic steepest descent method" calculated for the entire image is the same as the "0" stochastic gradient descent method and uses all end-layer receptive fields for mini-placement. When these fields of acceptance overlap significantly, it is much more efficient to calculate for each layer of the entire image instead of patch-by-patch, independently of feed-forward calculation and selling backward. For pixel-by-pixel forecasts, this output must be reconnected to the pixels. Figure 29.1 presents the FCN process (Long et al. 2015).

Dilated Convolution

The main idea of this method is to create holes (zeroes) between the pixels of the image in a convolutional manner to increase the accuracy of the original image, thus enabling dense feature extraction in deep CNNs. In the semantic segmentation framework, dilated convolution is also used to enlarge the field of convolutional kernels, where this method was developed in the form of an algorithm for wave analysis. Fisher Yu and Vladlen Koltun developed a new convolutional network architecture that systematically uses dilated convolutions for multi-scale context aggregation.

This architecture is driven by the fact that the stretched convolution supports the field of exponentially magnification without loss of resolution and range.

Three equations were involved in the definition of this new method as follows:

Discrete convolution operator
Generalization of operator

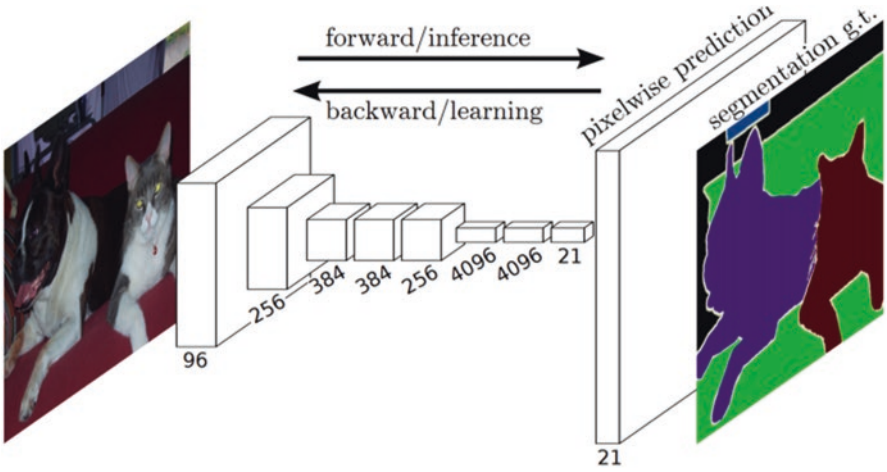

Fig. 29.1 Fully convolutional networks can efficiently learn to make dense predictions for per-pixel tasks like semantic segmentation. (Long et al. 2015)

In a discrete function F: $Z^2 \rightarrow R$.
We found $\Omega r = [-r, r]^2 \cap Z^2$ and k: $\Omega r \rightarrow R$ as a discrete filter of size $(2r + 1)^2$.
The discrete convolution operator $*$ can be defined as

$$(F * k)(p) = \sum_{s+t=p} F(s)k(t) \tag{29.1}$$

$$(F *_l k)(p) = \sum_{s+t=p} F(s)k(t) \tag{29.2}$$

where $*_l$ is the dilated convolution or an *l*-dilated convolution. The familiar discrete convolution $*$ is simply the *1*-dilated convolution.

The dilated convolution operator was called "convolution with dilated filter" in the past. It plays an important role in the "algorithme à trous," which is an algorithm for wavelet decomposition (Holschneider et al. 1987; Shensa 1992). Make it clear that the "extended filter" is set or not displayed.

The convolution operator itself has been modified to use filter parameters differently. The dilated convolution operator can apply the same filter in other ranges using other dilation factors.

Let $F_0, F_1, ..., F_{n-1} : Z^2 \rightarrow R$ be discrete functions and let $k_0, k_1, ..., k_{n-2}$: $\Omega 1 \rightarrow R$ be discrete 3×3 filters.

Consider applying the filters with exponentially increasing dilation:

$$Fi + 1 = Fi * 2i \text{ki for i} = 0, 1, \ldots, n - 2. \tag{29.3}$$

Define the receptive field of an element p in Fi+1 as the set of elements in F0 that modify the value of Fi+1(p). Let the size of the receptive field of p in Fi+1 be the number of these elements. It is easy to see that the size of the receptive field of each element in Fi+1 is $(2i + 2 - 1) \times (2i + 2 - 1)$. The receptive field is a square of exponentially increasing size. This is illustrated in Fig. 29.2, where systematic dilation supports exponential expansion of the receptive field without loss of resolution or coverage. (a) F1 is produced from F0 by a 1-dilated convolution; each element in

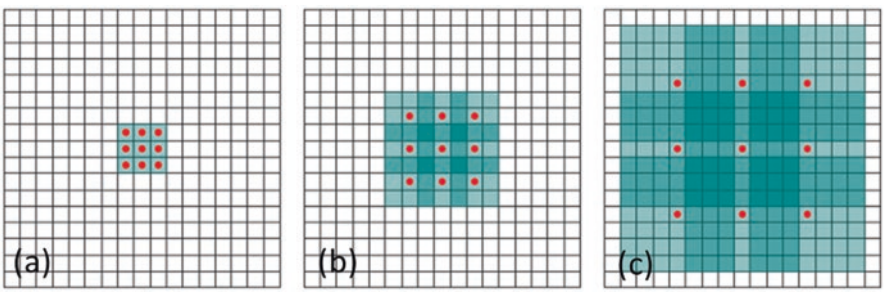

Fig. 29.2 Systematic dilation supports exponential expansion of the receptive field without loss of resolution or coverage

F1 has a receptive field of 3 × 3. (b) F2 is produced from F1 by a 2-dilated convolution; each element in F2 has a receptive field of 7 × 7. (c) F3 is produced from F2 by a 4-dilated convolution; each element in F3 has a receptive field of 15 × 15. The number of parameters associated with each layer is identical. The receptive field grows exponentially while the number of parameters grows linearly.

Conditional Random Fields (CRFs)

Conditional random fields (CRFs) are a class of statistical modeling methods often applied to pattern recognition and machine learning and used in structured prediction. The CRF can consider the context, whereas the CRF predicts the label of a single sample without considering the classifier "neighbor" sample. For this reason, forecasts are modeled as a graphics model that implements the dependencies between forecasts. The type of graph used depends on the application. In image processing, graphs typically connect positions close and/or similar positions to receive similar predictions (Zheng et al. 2015).

For general graphs, the exact inference problem of CRF is awkward. CRF inference problems are basically the same as MRF, and the same claims are maintained (Sutton and McCallum 2006). However, there are special cases where accurate inference is possible.

If the graph is a chain or tree, the message delivery algorithm creates an accurate solution. The algorithm used in such cases is like the forward and Viterbi algorithm for HMMs (hidden Markov models). If the CRF contains only the pair-wise potential and the energy is a submodule, the combined, minimum cut/maximum flow algorithm will calculate the exact solution. If accurate inference is not possible, some algorithms can be used to obtain an approximate solution. These include loopy belief propagation, alpha expansion, mean field inference, and linear programming relaxations.

Parameter ϴ training is generally performed to train the maximum likelihood of $p(Yi \mid Xi;\Theta)$. This optimization is convex if all nodes have an exponential family distribution, and all nodes are observed during training (Sutton and McCallum 2006). It can be solved using the quasi-Newton method, for example, the gradient descent algorithm. On the other hand, if some variables are not observed, you need to solve the inference problem of these variables. Accurate inference is awkward in ordinary graphs, so we use approximate values.

Instance Segmentation

Instance splitting is a combination of two methods: object detection and semantic splitting. One of the most common approaches to solving the problem is to perform the first object detection to split the objects in the box, or vice versa, to split the

image first to detect the objects. It is the combination of various network structures that separate instances (Salvador et al. 2017). Object detection is the assignment of distinguishing objects of interest in the picture and deciding their positions and sizes. This can be addressed as a bouncing box and given a name with the anticipated class of the article inside the crate. There ought to be one box for every item (Salvador et al. 2017). The undertaking of item location was a few stages measured getting the hang of it, including methods, for example, edge discovery and element extraction. The pictures were then contrasted and placed in existing item formats to identify and limit the articles inside the pictures. In later years, the utilization of profound learning has been acquainted with space (Zhao et al. 2019; Fritz 2020).

Image segmentation is the way toward apportioning a picture into numerous sections. These fragments ought to add to a less difficult portrayal of the picture that is simpler to use for additional examination. This is normally used to find objects within the picture. Semantic division is a pixel-level classification, where the items that have a place with a similar class are grouped together. This will differentiate between different classes; however, it doesn't consider the occurrences of numerous objects of a similar class (Xiaolong et al. 2018). There is a scope of utilizations for semantic division, and it is usually utilized in the clinical field (Ronneberger et al. 2015; Fritz 2020). Figure 29.3 presents an original image of a teapot and three cups in section (a); in section (b), we can see that the objects in the photo have been detected, and this is what we called object detection technic where all the objects founded are annotated with a bounding box. The semantic segmentation is presented in section (c), where the different classes have been given a distinct color (teapot is in green and cups are in blue). In section (d), we see that each object has

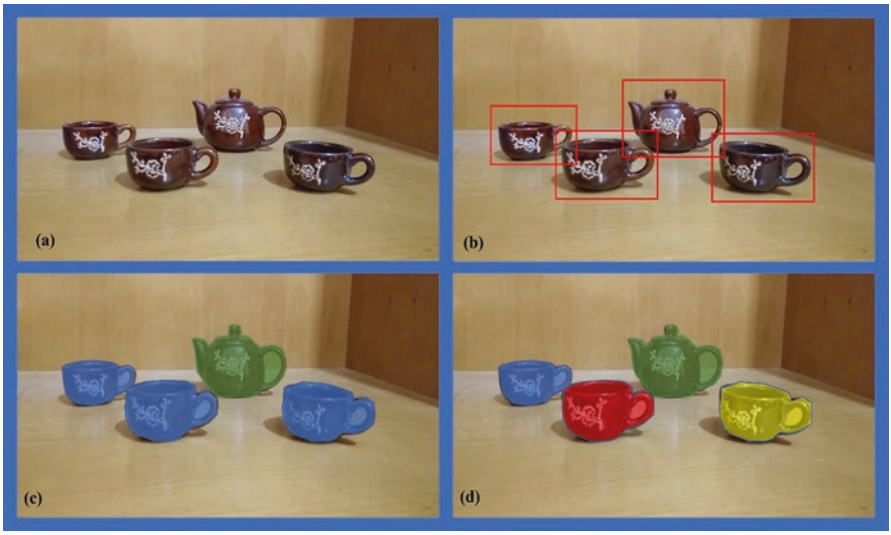

Fig. 29.3 Comparison between original image (**a**), object detection (**b**), semantic segmentation (**c**), and instance segmentation (**d**)

a different color, each cup has its own color in addition to the teapot, and this is the instance segmentation where all pixels are aware of both classes and which instance of that class it belongs to.

Mask R-CNN

As an extension of the faster R-CNN framework (Patil and Shaikh 2016), the Mask R-CNN framework (Fig. 29.4) for object instance segmentation was introduced in 2017 (He et al. 2017). The method recognizes items in an image efficiently while also generating a high-quality segmentation mask for each instance. Faster R-CNN is extended in this framework by adding a branch for predicting segmentation masks alongside the existing branch for bounding box recognition. In COCO challenge 2016, a large-scale object detection, segmentation, and captioning challenge, Mask R-CNN outperformed all current single model entrants on every job. The conventional fastest R-CNN consists of two outputs, a class marker and a bounding box offset for each candidate's object. The Faster R-CNN has two phases. The initial phase of the project is the Regional Proposal Network (RPN). In the second step, Fast R-CNN, the ROI Pool, and classification and bound regression characteristics of each candidate are drawn. The features used in both stages are common for faster deductions. Mask R-CNN utilizes the same two-step approach at a similar initial level. In the second step, however, the Mask R-CNN also releases a binary mask for each RoI parallel to the prediction of the class and box offset. Mask R-CNN is also substituted to a RoI Align, which allows for comparatively precisely created instance segmentation mask, for the rather imprecise RoI Pool operation used in Faster R-CNN. For each sampled RoI, the loss function is specified as L = Lcls + Lbox + Mask, with Lcl's and Lbox equal to those set out in this section 10. The branch has a size of km^2 for each RoI, encoding K binary resolution masks of m to m, one for

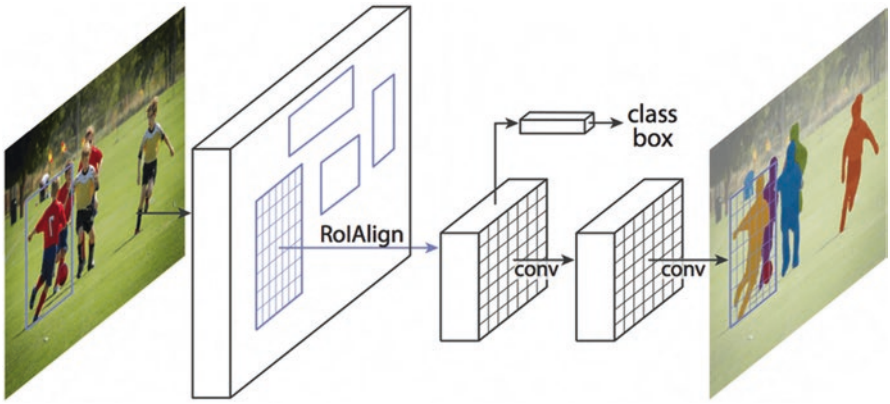

Fig. 29.4 The Mask R-CNN framework for instance segmentation. (He et al. 2017)

every K class. A per-pixel sigmoid is applied, which is described by Lmask as average cross-entropy loss. Lmask is only specified on the kth mask for a RoI in association with the ground-truth class k. Thus, this concept of mask indicates that the network creates masks without rivalry between classes for every class. The classification branch forecasts the class label for the mask to be selected. The mask and class prediction are therefore uncoupled. Figure 29.4 illustrates the Mask R-CNN architecture (He et al. 2017).

Region-Based Segmentation (Threshold Segmentation)

Threshold segmentation is the simplest and most common method of image segmentation. This is a general division algorithm that directly divides the processing of the gradation information of an image based on the gradation values of different targets. Threshold splits can be divided into local threshold methods and global threshold methods. The overall threshold method divides the image into both target and background areas with a single threshold (Davis et al. 1975). The local threshold method requires you to select multiple split thresholds and split the image into multiple thresholds with multiple target areas and backgrounds. The largest interclass variance method (Otsu) (Patil and Shaikh 2016) is the most used threshold segmentation algorithm that selects an optimal solution threshold by boosting the variance between classes. There is also entropy-based segmentation threshold method, the minimum error method, the method of matrix co-occurrence, moment preserving method, simple statistical method, probability relaxation method, fuzzy set method, and threshold methods combined with other methods (Kohler 1981). The benefit of the threshold method is that the estimation is basic and the activity speed is quicker. At the point when the objective and the foundation have high differentiation, the division impact can be gotten. The detriment is that it is hard to acquire exact outcomes for picture division issues where there is no huge dim scale distinction or an enormous crossover of the dim scale esteems in the picture (Yuheng and Hao 2017). Since it just thinks about the dim data of the picture disregarding the spatial data of the picture, it is touchy to clamor and gray scale lopsidedness, driving it frequently joined with different techniques.

Edge Detection Segmentation

The edges of an object are displayed as discrete local features of the image. That is, the most significant parts of the image change the local brightness, such as the gray values of the image. There is always a gray edge between two adjacent areas with different gray values in the image, and the gray values may not be contiguous. These discontinuities can often be detected using derivative operations, and derivative operators can be used to calculate derivatives (Senthilkumaran and Rajesh 2009).

Parallel edge detection is often performed using the space domain derivative operator to perform intricate image segmentation of templates and images. Parallel edge detection is commonly used in image preprocessing methods. The fashionable first derivative operators are the Prewitt operator, the Roberts operator, and the Sobel operator (Kundu and Pal 1986). Two-layer differential operators include nonlinear operators such as the Laplace operator, the Lerk operator, and the Wallis operator.

Sobel Operator

The Sobel operator is a discrete differential operator that is used to determine the approximation of the gradient of the image luminance function. It is mostly utilized for edge detection. The Sobel operator is a standard edge detection operator based on the first derivative. As a result of the operator's introduction of a similar local average operation, the noise has a smooth effect and can effectively eliminate the influence of noise. The influence of the Sobel operator on the position of the pixel is weighted, which is superior to the Prewitt and Roberts operators. In order to achieve the difference between the horizontal, the Sobel operator comprises two sets of 3 × 3 matrices that are cross and longitudinal models with an image plane. The image's edges are detected using the following two templates: horizontal rim detection (Gx) and vertical edge detection (Gy) (Yuheng and Hao 2017).

$$Gx = \begin{bmatrix} -1 & 0 & 1 \\ -2 & 0 & 2 \\ -1 & 0 & 1 \end{bmatrix} \quad Gy = \begin{bmatrix} 1 & 2 & 1 \\ 0 & 0 & 0 \\ -1 & -2 & -1 \end{bmatrix}$$

In order to calculate the gradient size, the horizontal and vertical gradient approximations of each pixel of the image may be combined; the following formula could be used:

$$G = \sqrt[2]{G_x^2 + G_y^2}$$

Laplace Operator

The Laplace operator is a second-order differential operator that is isotropic in nature. It is more appropriate when it is simply concerned with the position of the edge independent of the pixel gray scale difference around it (Haddon 1988). The Laplace operator's reaction to isolated pixels is greater than the edge or line and hence applies exclusively to noise-free pictures. In the presence of noise, the Laplace operator must perform low-pass filtering before identifying the edge. As a result, the standard segmentation method combines the Laplace operator with the smoothing operator to produce a new template. The simplest isotropic differential operator with rotational invariance is the Laplace operator. The Laplace transform of a

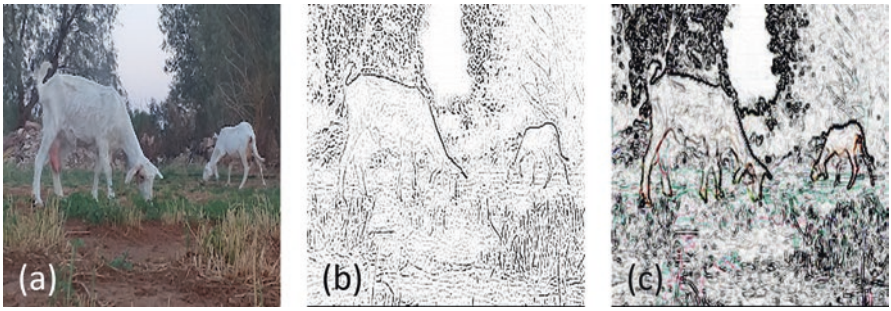

Fig. 29.5 Original image (**a**), Sobel operator, and (**b**) Laplace operator application results

two-dimensional image function is an isotropic second derivative that is better suited for digital image processing, and the pull operator is given in discrete form: because it conforms to the descent model, the Laplace operator is employed to enhance the blurring effect caused by the blurring effect. The diffusion effect occurs often throughout the imaging process. Figure 29.5 presents the outputs of each operator (Yuheng and Hao 2017).

Image Segmentation Based on Clustering

Theory of image segmentation is not all-encompassing. However, since many new theories and techniques from many fields have been introduced, many image segmentation approaches have been coupled with certain particular theories and methodologies. The term "class" refers to a grouping of related elements. Clustering follows specific rules and principles of classification of items in the process (Yuheng and Hao 2017). The feature space clustering method is used to divide pixels in the picture space into feature space points. The feature space is segmented based on their aggregate in the feature space, and the segmentation result is then projected back to the original picture space. One of the most often used clustering algorithms is K-means. The main principle behind K-means is to group data into various clusters based on their distance. The closer the two locations are, the more likely it is that they will obtain compact and independent clusters as clustering targets (Sulaiman and Isa 2010). Figure 29.6 depicts the K-means implementation method.

The approach "K-means clustering" offers quick and easy, highly efficient, and highly skillful solutions for big data sets. The time complexity is likewise almost linear and suitable for large-scale data mining. K-means downside is that it is difficult to estimate its clustering K and does not have specific selection criteria (Chuang et al. 2006). Secondly, the K-means algorithm framework reveals that all the samples are visited by each iteration of the algorithm, which implies the algorithm time is quite costly. The K-means algorithm is also a distance-based partitioning

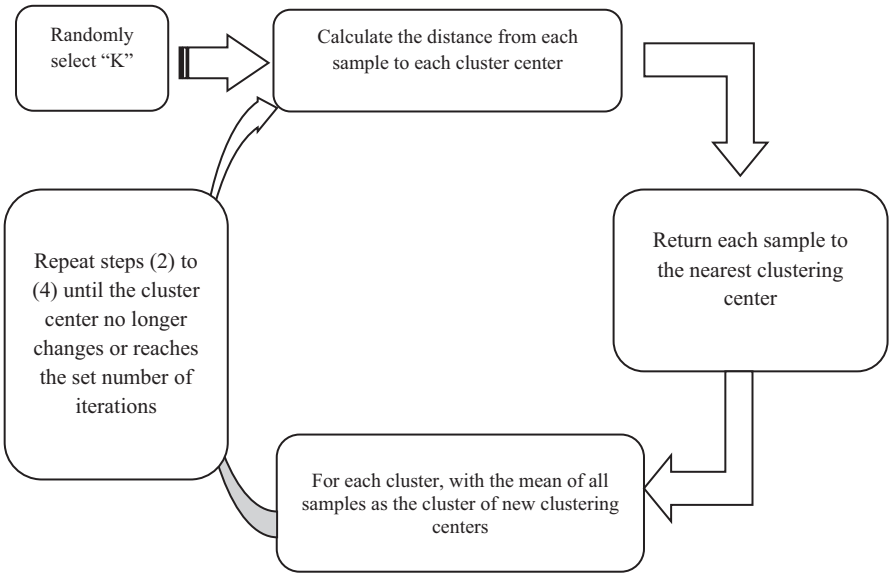

Fig. 29.6 Implantation process of K-means

technique (Celebi et al. 2013). It is only applicable to the data set which is convex and not suitable for clustering nonconvex clusters.

Utility of Different Methods in Our Lives

After a theoretical presentation of each technic in the previous sections, here we will present the utility of each technic in our life by referring to the recent scientific papers including different application domains.

In Medical Field

The diagnosis of Alzheimer's disease is based largely on hippocampal segmentation, cortical thickness, and brain volume of brain MRI scans. By using the well-known LeNet-5 framework in CNNs (Sarraf and Tofighi 2016), trained AD samples for sMRI and fMRI yield 98.84% and 96.85% accuracy, respectively. To make brain tumor detection automated, authors used magnetic resonance imaging (MRI) image segmentation; they have also elaborated the basic concepts involved in segmentation and the image preprocessing steps (Mittal et al. 2020). In a work concerning tooth detection, authors proof that although the Mask R-CNN model mainly considers object detection, object location, and segmentation, it can also have efficient

results for the challenging task of a large number of crowded tooth image segmentation image analyses. Also, the authors founded that the Mask R-CNN seems to be easy to be adapted without the need for several improvements or customization (Guohua Zhu et al. 2020).

In Water Science Field

In a study performed in Poyang Lake (the largest freshwater lake in China), the authors used image segmentation for the aim of detecting the freshwater surface area, where they implement the Otsu method. The results of this study contribute to the update of temporal and spatial variation of Poyang Lake, confirming that its surface water area fluctuated annually and tended to shrink both in the center and boundary of the lake on each January from 2017 to 2020 (Sulong Zhou et al. 2020). In Malaysia, the flood threat is strongly raised. And because of the lack of flood survey data, the protection system against flood won't be developed very well. In the light of the development of new survey technic, the image segmentation methods have been used to extract water information from digital images, which help in providing more information in the development of protection systems against floods (Nur Atirah Muhadi et al. 2020).

In Agricultural Field

Image segmentation is used also in agricultural domain. A new technic has been suggested in order to classify different diseases that affect citrus. The work targeted six different types of diseases, namely, anthracnose, black spot, canker, scab, greening, and melanose. The proposed technique outperforms the existing methods and achieves 89–97% classification accuracy on citrus disease based on data set source (Muhammad Sharif et al. 2018). Another use of this technic was mentioned in the literature. For the aim of the detection of agriculture parcel boundaries, a two-step process followed. First, the segmentation of the images was done using the statistical region merging (SRM) technique (Orimoloye et al. 2022). The boundary information and center of the segmentation were founded out using MATLAB. A match between the extracted boundary information's and the parcel boundaries recorded in revenue registers was noticed (Khadanga and Jain 2020). In order to alleviate the hassle of the task of manually counting ripened chili fruit, as well as helping farmers to plan harvesting, shipping, selling, and postharvest operations, computer vision technology was used to analyze the plant images, which achieved high accuracy results (Nageswararao Naik Bhookya et al. 2020).

Other Uses

In addition to the mentioned fields above, the technic of image segmentation could be used in several other domains like spatial attention for self-driving cars (Sagar and Soundrapandiyan 2020), masked face recognition which is very useful especially in the light of the COVID 19 pandemic extension (Mengyue Geng et al. 2020), forest fire detection (Sharma et al. 2020), and nanotechnology (Zeng et al. 2021).

Conclusion

The technology of image segmentation is widely used in several domains, medical, water science, agricultural field, face recognition, etc. The integration of this technic in our daily life provides us a lot of help like avoiding disasters, predicting disease, developing economics, and finding more information about our environment. This work aims to open the doors of this research field by simplifying the theoretical part of the widely used techniques and also illustrates how this technique can help human beings in their lives.

References

Abburu S, Golla SB (2015) Satellite image classification methods and techniques: a review. Int J Comput Appl 119(8)

Al-Doski J, Mansorl SB, Shafri HZM (2013) Image classification in remote sensing. Department of Civil Engineering, Faculty of Engineering, University Putra, Malaysia, vol 3, no 10

Bann S (2002) Photography, printmaking, and the visual economy in nineteenth-century France. Hist Photogr 26(1):16–25

Bhookya NN, Malmathanraj R, Palanisamy P (2020) Yield estimation of chilli crop using image processing techniques. In: 2020 6th International conference on advanced computing and communication systems (ICACCS), pp 200–204. https://doi.org/10.1109/ICACCS48705.2020.9074257

Celebi ME, Kingravi HA, Vela PA (2013) A comparative study of efficient initialization methods for the kmeans clustering algorithm [J]. Expert Syst Appl 40(1):200–210

Chen L-C, Papandreou G, Kokkinos I, Murphy K, Yuille AL (2016) Deeplab: semantic image segmentation with deep convolutional nets, atrous convolution, and fully connected crfs. arXiv preprint arXiv:1606.00915

Chuang KS, Tzeng HL, Chen S et al (2006) Fuzzy means clustering with spatial information for image segmentation [J]. Comput Med Imaging Graph 30(1):9–15

Davis LS, Rosenfeld A, Weszka JS (1975) Region extraction by averaging and thresholding [J]. IEEE Trans Syst Man Cybernet 3:383–388

Deepan P, Sudha LR (2018) Object detection in remote sensing images: a review. Int J Sci Res Comput Sci Appl Manag Stud. ISSN 23191953

Dong R, Dong J, Wu G, Deng H (2006) Optimization of post-classification processing of high-resolution satellite image: a case study. Sci China Ser E Technol Sci 49(1):98–107

Fitzgerald RW, Lees BG (1994) Assessing the classification accuracy of multisource remote sensing data. Remote Sens Environ 47(3):362–368
Fritz K (2020) Instance segmentation of buildings in satellite images
Gašparović M (2020.)Urban growth pattern detection and analysis. In: Urban ecology. Elsevier, pp 35–48
Geng M, Peng P, Huang Y, Tian Y (2020) Masked face recognition with generative data augmentation and domain constrained ranking. In: Proceedings of the 28th ACM international conference on multimedia, pp 2246–2254
Gernheim H, Gernheim A (1955) The history of photography from the camera obscure to the beginning of the modern era
Gulhane VA, Rode SV, Pande CB (2022) Correlation Analysis of Soil Nutrients and Prediction Model Through ISO Cluster Unsupervised Classification with Multispectral Data. Multimed Tools Appl. https://doi.org/10.1007/s11042-022-13276-2
Haddon JF (1988) Generalised threshold selection for edge detection [J]. Pattern Recogn 21(3):195–203
He K, Zhang X, Ren S, Sun J (2015) Deep residual learning for image recognition. arXiv preprint arXiv:1512.03385
He K, Gkioxari G, Dollár P, Girshick R (2017) Mask r-cnn. In: Proceedings of the IEEE international conference on computer vision, pp 2961–2969
Hölbling D, Eisank C, Albrecht F, Vecchiotti F, Friedl B, Weinke E, Kociu A (2017) Comparing manual and semi-automated landslide mapping based on optical satellite images from different sensors. Geosciences 7(2):37
Holschneider M, Kronland-Martinet R, Morlet J, Tchamitchian P (1987) A real-time algorithm for signal analysis with the help of the wavelet transform. In: Wavelets: time-frequency methods and phase space. Proceedings of the international conference
Jain SK, Singh VP (2003) Water resources systems planning and management. Elsevier, Amsterdam
Khadanga G, Jain K (2020) Agriculture parcel boundary detection from remotely sensed images. In: Chaudhuri B, Nakagawa M, Khanna P, Kumar S (eds) Proceedings of 3rd international conference on computer vision and image processing, Advances in intelligent systems and computing, vol 1022. Springer, Singapore. https://doi.org/10.1007/978-981-32-9088-4_26
Khalid S, Khalil T, Nasreen S (2014) A survey of feature selection and feature extraction techniques in machine learning. In: 2014 science and information conference, pp 372–378. IEEE
Kohler R (1981) A segmentation system based on thresholding [J]. Comput Graphics Image Process 15(4):319–338
Kouadri S, Kateb S, Zegait R (2021) Spatial and temporal model for WQI prediction based on back-propagation neural network, application on EL MERK region (Algerian southeast). J Saudi Soc Agric Sci
Krizhevsky A, Sutskever I, Hinton GE (2012) Imagenet classification with deep convolutional neural networks. In: Advances in neural information processing systems, pp 1097–1105
Kumar S, Singh D (2013) Texture feature extraction to colorize gray images [J]. Int J Comput Appl 63(17)
Kundu MK, Pal SK (1986) Thresholding for edge detection using human psychovisual phenomena [J]. Pattern Recogn Lett 4(6):433–441
Lin G, Shen C, Reid I et al (2015) Efficient piecewise training of deep structured models for semantic segmentation. arXiv preprint arXiv:1504.01013
Long J, Shelhamer E, Darrell T (2015) Fully convolutional networks for semantic segmentation. In: Proceedings of the IEEE conference on computer vision and pattern recognition, pp 3431–3440
Lu D, Weng Q (2007) A survey of image classification methods and techniques for improving classification performance. Int J Remote Sens 28(5):823–870
Mather PM, Koch M (2011) Computer processing of remotely-sensed images: an introduction. Wiley, New York

McCulloch WS, Pitts WH (1943) A logical calculus of the ideas immanent in nervous activity. Bull Math Biophys 5:115–133
Medjahed SA (2015) A comparative study of feature extraction methods in images classification. Int J Image Graphics Signal Process 7(3):16
Mittal M, Arora M, Pandey T, Goyal LM (2020) Image segmentation using deep learning techniques in medical images. In: Verma O, Roy S, Pandey S, Mittal M (eds) Advancement of machine intelligence in interactive medical image analysis. Algorithms for intelligent systems. Springer, Singapore. https://doi.org/10.1007/978-981-15-1100-4_3
Muhadi NA, Abdullah AF, Bejo SK, Mahadi MR, Mijic A (2020) Image segmentation methods for flood monitoring system. Water:12, 1825. https://doi.org/10.3390/w12061825
Nath SS, Mishra G, Kar J, Chakraborty S, Dey N (2014) A survey of image classification methods and techniques. In: 2014 International conference on control, instrumentation, communication and computational technologies (ICCICCT), pp 554–557. IEEE
Nhamo L, Van Dijk R, Magidi J, Wiberg D, Tshikolomo K (2018) Improving the accuracy of remotely sensed irrigated areas using post-classification enhancement through UAV capability. Remote Sens 10(5):712
Orimoloye IR, Olusola AO, Belle JA et al. (2022) Drought disaster monitoring and land use dynamics: identification of drought drivers using regression-based algorithms. Nat Hazards https://doi.org/10.1007/s11069-022-05219-9
Pande CB (2022) Land use/land cover and change detection mapping in Rahuri watershed area (MS), India using the google earth engine and machine learning approach. Geocarto Int. https://doi.org/10.1080/10106049.2022.2086622
Pande CB, Moharir KN, Khadri SFR et al. (2018) Study of land use classification in an arid region using multispectral satellite images. Appl Water Sci 8:123. https://doi.org/10.1007/s13201-018-0764-0
Pande CB, Moharir BN, Singh SK, Varade AM, Elbeltagie A, Khadri SFR, Choudhari P (2021a) Estimation of crop and forest biomass resources in a semi-arid region using satellite data and GIS. J Saudi Soc Agri Sci 20(5):302–311
Pande CB, Moharir KN, Khadri SFR (2021b) Assessment of land-use and land-cover changes in Pangari watershed area (MS), India, based on the remote sensing and GIS techniques. Appl Water Sci 11 96. https://doi.org/10.1007/s13201-021-01425-1
Pande CB, Kadam SA, Jayaraman R, Gorantiwar S, Shinde M (2022) Prediction of soil chemical properties using multispectral satellite images and wavelet transforms methods. J Saudi Soc Agri Sci 21(1):21–28
Patil AB, Shaikh JA (2016) OTSU thresholding method for flower image segmentation. Int J Comput Eng Res IJCER 6(5)
Ronneberger O, Fischer P, Brox T (2015) U-net: convolutional networks for biomedical image segmentation. In: Medical image computing and computer-assisted intervention – MICCAI 2015, pp 234–241
Rozenstein O, Karnieli A (2011) Comparison of methods for land-use classification incorporating remote sensing and GIS inputs. Appl Geogr 31(2):533–544
Sagar A, Soundrapandiyan R (2020) Semantic segmentation with multi scale spatial attention for self-driving cars. arXiv preprint arXiv:2007.12685
Salvador A, Bellver M, Baradad M, Marqués F, Torres J, Gir'o i Nieto X (2017) Recurrent neural networks for semantic instance segmentation. CoRR, abs/1712.00617. http://arxiv.org/abs/1712.00617
Sarraf S, Tofighi G (2016) DeepAD: Alzheimer's disease classification via deep convolutional neural networks using MRI and fMRI. BioRxiv. https://doi.org/10.1101/070441
Senthilkumaran N, Rajesh R (2009) Edge detection techniques for image segmentation–a survey of soft computing approaches [J]. Int J Recent Trend Eng 1(2):250–254
Shahid M, Rahman KU, Haider S et al. (2021) Quantitative assessment of regional land use and climate change impact on runoff across Gilgit watershed. Environ Earth Sci 80:743. https://doi.org/10.1007/s12665-021-10032-x

Sharif M, Khan MA, Iqbal Z, Azam MF, Lali MIU, Javed MY (2018) Detection and classification of citrus diseases in agriculture based on optimized weighted segmentation and feature selection. Comput Electron Agric 150:220–234

Sharma A, Singh PK, Kumar Y (2020) An integrated fire detection system using IoT and image processing technique for smart cities. Sustain Cities Soc 61:102332

Shensa MJ (1992) The discrete wavelet transform: wedding the a trous and Mallat algorithms. IEEE Trans Signal Process 40(10)

Simonyan K, Zisserman A (2014). Very deep convolutional networks for large-scale image recognition. arXiv preprint arXiv:1409.1556

Stanchev P, Green Jr D, Dimitrov B (2003) High level color similarity retrieval

Sulaiman SN, Isa NAM (2010) Adaptive fuzzy-Kmeans clustering algorithm for image segmentation [J]. IEEE Trans Consum Electron 56(4)

Sutton C, McCallum A (2006) An introduction to conditional random fields for relational learning. In: Introduction to statistical relational learning, vol 2, pp 93–128

Xiaolong L, Deng Z, Yang Y (2018) Recent progress in semantic image segmentation. Artif Intell Rev 52(2):1089–1106. https://doi.org/10.1007/s10462-018-9641-3. ISSN 1573-7462

Yu F, Koltun V (2015) Multi-scale context aggregation by dilated convolutions. arXiv preprint arXiv:1511.07122

Yuheng S, Hao Y (2017) Image segmentation algorithms overview. arXiv preprint arXiv:1707.02051

Zeng N, Li H, Wang Z, Liu W, Liu S, Alsaadi FE, Liu X (2021) Deep-reinforcement-learning-based images segmentation for quantitative analysis of gold immunochromatographic strip. Neurocomputing 425:173–180

Zhao Z-Q, Zheng P, Shou-Tao X, Xindong W (2019) Object detection with deep learning: a review. IEEE Trans Neural Netw Learn Syst:1–21. https://doi.org/10.1109/TNNLS.2018.2876865

Zheng S, Jayasumana S, Romera-Paredes B, Vineet V, Su Z, Du D, Huang C, Torr PH (2015) Conditional random fields as recurrent neural networks. In: Proceedings of the IEEE international conference on computer vision, pp 1529–1537

Zhou S, Kan P, Silbernagel J, Jin J (2020) Application of image segmentation in surface water extraction of freshwater lakes using radar data. ISPRS Int J Geo Inf 9(7):424

Zhu G, Piao Z, Kim SC (2020) Tooth detection and segmentation with mask R-CNN. In: 2020 international conference on artificial intelligence in information and communication (ICAIIC). IEEE

Correction to: Climate Change Impacts on Natural Resources, Ecosystems and Agricultural Systems

Chaitanya B. Pande, Kanak N. Moharir, Sudhir Kumar Singh, Quoc Bao Pham, and Ahmed Elbeltagi

Correction to:
C. B. Pande et al. (eds.), *Climate Change Impacts on Natural Resources, Ecosystems and Agricultural Systems*, Springer Climate, https://doi.org/10.1007/978-3-031-19059-9

The original version of the book was inadvertently published with the incorrect affiliation for the co-editor, Quoc Bao Pham. The affiliation has now been updated in the book.

The updated original version for this book can be found at https://doi.org/10.1007/978-3-031-19059-9

C. B. Pande et al. (eds.), *Climate Change Impacts on Natural Resources, Ecosystems and Agricultural Systems*, Springer Climate,
https://doi.org/10.1007/978-3-031-19059-9_30

Index

C. B. Pande et al. (eds.), *Climate Change Impacts on Natural Resources, Ecosystems and Agricultural Systems*, Springer Climate,
https://doi.org/10.1007/978-3-031-19059-9

T